Multiresolution
and
Multirate Signal Processing

Introduction, Principles
and Applications

Multiresolution
and
Multirate Signal Processing

Introduction, Principles and Applications

Vikram M. Gadre
Professor, Department of Electrical Engineering,
IIT Bombay,
Mumbai

Aditya S. Abhyankar
Dean, Faculty of Technology,
and
Professor and Head, Department of Technology,
Savitribai Phule Pune University,
Pune

McGraw Hill Education (India) Private Limited
CHENNAI

McGraw-Hill Education Offices

Chennai New York St Louis San Francisco Auckland Bogotá Caracas
Kuala Lumpur Lisbon London Madrid Mexico City Milan Montreal
San Juan Santiago Singapore Sydney Tokyo Toronto

McGraw Hill Education (India) Private Limited

Published by McGraw Hill Education (India) Private Limited
444/1, Sri Ekambara Naicker Industrial Estate, Alapakkam, Porur, Chennai - 600 116

Multiresolution and Multirate Signal Processing

Print Edition:
ISBN-13: 978-93-5260-144-8
ISBN-10: 93-5260-144-0

Ebook Edition:
ISBN-13: 978-93-5260-145-5
ISBN-10: 93-5260-145-9

Managing Director: *Kaushik Bellani*
Director—Products (Higher Education and Professional): *Vibha Mahajan*
Manager: Product Development: *Koyel Ghosh*
Specialist: Product Development: *Sahil Thorpe*
Head—Production (Higher Education and Professional): *Satinder S Baveja*
Manager—Editorial Services: *Hema Razdan*
Senior Production Manager: *Manohar Lal*
AGM: Product Management (Higher Education and Professional): *Shalini Jha*
Product Manager: *Kartik Arora*
General Manager—Production: *Rajender P Ghansela*
Manager—Production: *Reji Kumar*

Typeset at Chandraprabhu Enterprise Private Limited, Puducherry and printed at

Cover Printer:

Visit us at: www.mheducation.co.in

Foreword

Wavelets and multiresolution analysis created revolution in signal processing nearly three decades ago. Since then the area of research has grown steadily, covering many application areas as well. The topic has had far reaching impact on the way we understand signals, their transforms, and the limitations of time-frequency analysis. These techniques are founded on fundamental principles in mathematics, and at the same time they have great relevance to many practical applications in areas such as audio signal analysis, image processing, medical signal analysis, biological signal processing, and so forth. Wavelet and multiresolution methods have close relation to the theory of multirate filter banks, which also evolved around the same time, nearly three decades ago. For example, the first-order two channel orthonormal filter bank is related to the Haar wavelets through a tree structure, and the more general M-channel orthonormal filter bank can be related to orthonormal wavelets. These connections are also well established in the literature.

This book, authored by Prof. Gadre and Prof. Abhyankar, gives an excellent and up-to-date exposure to the developments in this field. First and foremost, it is written in a reader friendly style. There are many examples throughout the book which motivate the introduction of deep and subtle topics. The authors are careful to make this motivation because, as such, the topic is complicated, and needs this kind of an introduction. The examples chosen here range from simple toy examples to actually practical ones from a wide range of application areas such as image processing, audio, biological signals, and many others. While the book has this attractive style, it also makes sure that the theoretical depth is impressive. Especially in the later chapters, the authors do justice to the detailed and rather intricate theory of multiresolution by providing deeper discussions and derivations, again supplemented with a generous supply of examples. The thoughtful addition of MATLAB codes will be very valuable to students and practicing engineers, as they allow the reader to quickly construct examples and plots that enhance the understanding of the theory just presented. The homework problems at the end of each chapter are thought-provoking and useful.

The introduction of historical anecdotes and notes is an added bonus, and makes it informative for the reader. Any student with an introductory background in signal processing and mathematics will be able to benefit from the book. More advanced readers will also thoroughly enjoy the wealth of material which can motivate further research in the area, and initiate advanced projects in graduate curriculum.

In short, this is a book on a very important and well established topic, which every student and lover of signal processing should learn. It is authored by highly reputed scholars who have taken great pains to present the material in a very welcoming style. It is my great pleasure to welcome this book, which will be a wonderful addition to the literature on signal processing.

Prof. P. P. Vaidyanthan
Department of Electrical Engineering
California Instituite of Technology

Preface

Both of us, as instructors on basic and advanced subjects related to signal processing, have felt the need to strike the delicate balance between inspiring an audience of students to penetrate deep into the subject of multirate signal processing and being 'true to the subject' in terms of rigor and formalism. This has been made possible by making the study and search pleasurable. The subject of wavelets and multiresolution signal processing has posed a major challenge to us, from this point of view. In the numerous opportunities that we have had, to teach or discuss the subject, the audience has always demanded a 'down to earth exposition of the subject', a 'connection to everyday reality', a 'compendium of exercises which will help them understand the theory behind the subject', a 'hands-on experience to feel the subject through implementations' and things of similar nature. This book is a humble endeavour on our part to meet these demands, at least to some measure, based largely on our interaction with Indian audiences.

As authors of this book, we also well appreciate and acknowledge with great respect, the existence of several books on the broad subject of wavelets, multirate and multiresolution signal processing written by experts in the field. Writing this book posed another challenge – to bring just that uniqueness to this, to make it worthy of occupying a place on the shelves on which those other books are kept. We think that the main contribution of this book is twofold – (i) a text written to inspire a beginner in the subject with several guiding examples, illustrations and exercises and (ii) a reference for some advanced topics, explained in a manner that makes them follow smoothly from the more basic ones. The former aspect of the book will make it useful as instructional material, the latter, we hope, makes it attractive to a researcher in the subject.

The book presents a thorough treatment of several concepts, along with simplified mathematical formulas. It also connects these mathematical ideas to the world around, thus giving physical significance to the material. The book also covers the third aspect of helping readers understand implementation strategies of the theory presented, by providing programs and codes, and making these available to readers. We hope that the explanation of concepts supported with many examples, tutorial exercises, codes, historical anecdotes, stories of scientists and demonstrations will make this book a unique reference material for instructors, students as well as researchers.

Today, 'wavelets' has been replacing many traditional mechanisms in multiple applications, spanning several disciplines in engineering and science. For example, the compression standards formulated by the Joint Picture Experts' Group (JPEG) saw an enhancement in the form of JPEG2000. Thus, from the year 2000, for compressing heavy satellite images, critical medical images and standard day-to-day images, JPEG 2000 has gained popularity. JPEG 2000 uses bi-orthogonal wavelet taps in lieu of the conventional DCT (Discrete Cosine Transform). Beyond this example, there are different walks of life where use of wavelets has become a powerful tool. The book starts with basic concepts and the coverage gets extended to latest trends in the field, with the likes of second-generation wavelets, wavelet packets, curvelets, brushlets, ridgelets, and so on.

Chapter 1 introduces the subject to the readers and provides a motivation and foundation for the rest of the book. **Chapters 2–6**, which explains MRA (Multi Resolution Analysis) and exposes readers to Conjugate Quadrature Filters (CQF), in particular, the Haar and Daubechies families. These Chapters provide a detailed explanation with the help of many examples and helps readers understand, how looking at multiple resolutions simultaneously is possible and useful. **Chapters 7–10** uncovers the time-frequency conflict, the uncertainty principle, the time-bandwidth product and allied topics such as the time-frequency plane and tiling in time frequency. **Chapters 11–14** and every chapter is a variant of MRA, viz., Bi-orthogonal filters in Chapter 11, splines in Chapter 12, wavelet packets in Chapter 13 and the lifting scheme in Chapter 14. Whi!le **Chapter 15** gives designs and salient features of about ten wavelet families, **Chapter 16** talks about advanced topics, **Chapter 17** discusses various applications, **Chapter 18** takes the readers beyond the realms of 'traditional ways' in wavelets and the concluding section of Appendix provides extended notes on all chapters. The extended notes are particularly used for topics, which require further extensions to grasp the depth and comprehend the maturity of the topic.

Writing any book is a journey. This journey has been unique in many ways. The thought of collaborating on this project started with Vikram Gadre's course on Multirate Signal Processing and Wavelets, offered under the National Programme on Technology Enhanced Learning (NPTEL) of the Ministry of Human Resource Development (MHRD) Government of India. Aditya Abhyankar was actively associated with this course, initially as a reviewer and later as a Co-Instructor. Since then, we have been expanding the scope of the material through various workshops, interaction with relevant audiences, which included eminent academicians and, importantly, young, bright, enthusiastic students. In particular, when the 'Knowledge Incubation under TEQIP' Initiative of the MHRD (MHRD-TEQIP-KITE) was launched at IIT Bombay, I (Vikram Gadre) was keen that we (I and Aditya Abhyankar) undertake this project as a collaborative endeavour involving IIT Bombay and a reputed University – the S P Pune University, which had reputed TEQIP Institutes like the College of Engineering Pune (COEP) in its circle in Pune. An attempt has been made to create content that will prove useful to the community. For many of the concepts written in this book, the inspiration has been interesting questions posed by colleagues and students in these interactions.

A book, though a manifestation of the thought process of the authors, requires support at many levels from vivid backgrounds and this project has been no exception. We would first like to thank the Almighty, without whose blessings, nothing is possible. We would then like to thank the respective families for the everlasting support provided through this project. Vikram Gadre would like to thank his wife (Kaumudi Gadre), mother, brother and sister-in-law (Nirmala, Rohit and Vaishali Gadre), late father (Manohar Gadre), parents-in-law, brother-, sister-in-law and their daughter (the Pandit family), for their constant support, good wishes and blessings. He would also like to thank his supervisor (Professor R. K. Patney) and several other faculty members at IIT Delhi, who played an important role in shaping his interest and expertise in wavelets. He would also like to thank his colleagues and the administration at IIT Bombay, who then nurtured this interest and expertise further. Aditya Abhyankar would like to thank his father (Vidyavachaspati Shankar Abhyankar), mother (Aparna Abhyankar), brother (CA Jitendra Abhyankar), sister-in-law (Madhura Abhyankar), wife (Arati Abhyankar),

niece (Arundhatee Abhyankar), nephew (Arjun Abhyankar) and son (Advait Abhyankar) for the best of love and support a person could ever ask for. Aditya Abhyankar would also like to thank his PhD advisor Dr Stephanie Schuckers and other professors who have been his source of inspiration. He would also like to thank Professors Raghunath Shevgaonkar and W N Gade, the former and current Vice Chancellors of SP Pune University respectively, for their constant encouragement. The authors would also like to thank many generations of our students at IIT Bombay and at SP Pune University, respectively for their assistance in the creation of digital material. There are just too many names that merit mention in this context but in particular, we would like to mention Gunjan and Sunil, Ph D students of Aditya Abhyankar, for the help in the preparation of the Supplementary Workbook, which was a daunting task. A special thanks to Professor P. P. Vaidyanathan of Caltech, USA, whose contributions to the field of multirate signal processing and wavelets are well known and respected worldwide but whose special role in this book, has been to inspire Vikram Gadre in many ways, to make the project see the light of day. Last but not the least; the authors would like to thank all the students, colleagues, and fellow scholars who have directly or indirectly provided inputs and feedback in making this manuscript more relevant.

Vikram M Gadre

Aditya S Abhyankar

Contents

Chapter 1

Introduction

1.1 | Introduction

This chapter introduces the subject of wavelets and multirate digital signal processing. It provides an inspiration to understand this subject at a greater depth along with broader picture of joint time-frequency analysis (JTFA).

The subject of wavelets follows a basic exposition to subjects like signal analysis, system theory and digital signal processing. It could be considered as an advanced topic on signal processing, however, this does not imply that the concepts introduced in this book are difficult to understand. In fact, the concepts are easier than a basic course on signal analysis. The basic text introduces the idea of abstraction, i.e. abstraction of signals, systems, transforms, analysis in different domains, etc. On the other hand, wavelets bring us closer to reality. We call it a journey from 'romanticism' to 'realism'! Being practical, pragmatic and realistic, use of wavelets not only requires good understanding of fundamentals but also practical constraints. In this sense, the contents covered in this book are very 'hands-on'. Wavelet analysis provides more precise information about signal data than other signal analysis techniques, such as Fourier because of which this branch of signal processing is growing very rapidly. In a basic text on digital signal processing, we assume that the signals last forever, i.e. for infinite duration of time. For example, while calculating the Fourier transform, we represent any signal in terms of basis functions and these basis functions last from $t = -\infty$ to $t = +\infty$, where t denotes time. However, practically no signal in this world can last forever. Thus, we should deal with signals in finite domains.

Example 1.1.1 — Audio signal.

We understand finite domains very well, if that finite domain is the natural domain. To reflect more on this, consider an example of a piece of an audio signal which is finite in time. Here, time is the **natural domain**. From a signal processing perspective, we wish to find the **content** in that audio signal, by enhancing some parts of that signal and suppress others. We may even be interested in characterizing the system. But for doing all these things, we deal with finite time signal and the abstraction of everlasting signals is unnecessary.

Example 1.1.2 — 2D face.

Consider another example, in which we have a picture of a 'face'. In this case, the **natural domain** is space and it is 2-Dimensional. The face has various features like eyebrows, forehead, nose, lips etc. Suppose we wish to isolate a particular feature, say an eye. This requires localization in the spatial domain. Here, again, the amount of data is finite reflecting the finite domain signal. This is shown in Fig. 1.1, where the face image has 3072 columns and 2304 rows and thus 3072 × 2304 number of (finite) pixels per palette. The picture is made up of rows and columns, in other words it gets represented in 2D space and, hence, spatial isolation can be used isolate a particular feature.

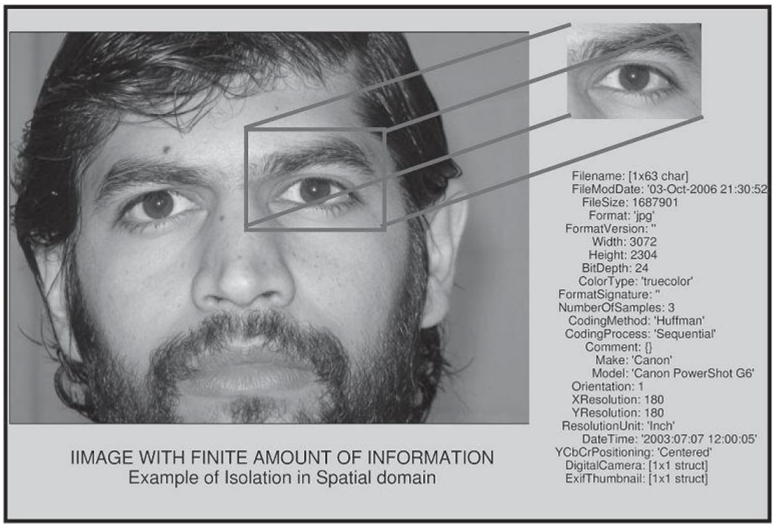

Figure 1.1 | **Face Example: Isolation is spatial domain**

Example 1.1.3 — Musical signal.

Another example which explains localization is a piece of audio in which a number of notes are sung. It may be called as a 'raga' in Indian tradition and the notes may be called as the components of the raga. Now, we aim to make a system that takes the rendition of this 'raga' and identifies the notes that compose it. To achieve this, we need to segment the signal in time. For example, the first note may be played for 1 second, the second note for 0.5 seconds, and so on. This demands segmentation in time. Moreover, we should also understand that all the notes are not of fixed lengths. The length of the time segment is also important. But more important is to understand the concept of 'Notes' in the signal processing context. For example, Notes of raga 'Gujari Todi' are depicted in Fig. 1.2.

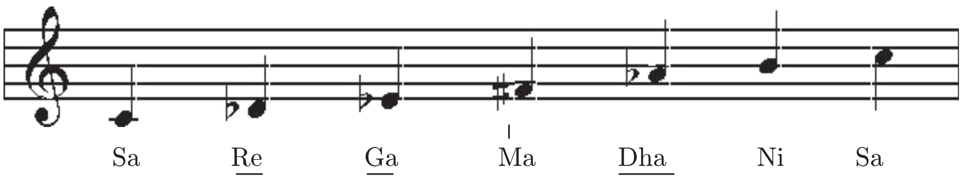

Figure 1.2 | Sample Notation: Frequencies of raga 'Gujari Todi'

In the basic course of "Signals and Systems", we were exposed to the idea of frequency domain. We know that signals have embedded inside them, as collection of sine waves. These sine waves are continuous for continuous time signals while they are sampled for discrete sequences. The continuous signals look for superposition of these sine waves whereas summation of sampled sine waves is observed in discrete case. Thus, most reasonable signals can be thought of as a collection of sine waves. In principle, if the signal is not periodic, its fourier transform comprises infinity of sine waves whose frequency ranges from 0 to ∞. For periodic signals, we have a discrete set of sine waves with possibly finite or infinite range of frequency represented by Fourier series. Thus, a different domain is more useful to analyze the signal. Now if we query about the 'Notes' in the raga, it is equivalent to asking the frequency content in the audio piece, i.e. what points on the frequency axis are occupied by this note? Which are the locations where the transform is prominent? It will also be of interest to analyze to understand exact locations of these frequencies on time-axis. The 'analyzer' often wishes to know at what 'time' which 'frequency' existed. This demands the analysis building blocks to have simultaneous time and frequency localization capabilities. This is one of the most fundamental inspirations to study wavelets, and joint time frequency analysis (JTFA) in broader perspective.

Before continuing with the above example and other concepts, it is worthwhile to introduce the term **'wavelets'**.

1.1.1 Wavelets

Fourier transform deals with sine waves. Sine waves have many important properties. Firstly, they occur naturally. For example, an electrical engineer recognizes sine wave as naturally emerging from an electricity generation system. Secondly, sine waves are the most analytic, the smoothest possible periodic functions. They also have the power to express many other waveforms, i.e. they form a very good basis. Addition of two sine waves of the same frequency but with possibly different amplitudes and phases, gives a sine wave of the same frequency with possibly different amplitude and phase. A sine wave on differentiation or integration is a sine wave of the same frequency. Any linear combination of all these operations on a sine wave results in a sine wave of the same frequency. **But the biggest drawback of sine waves is that they need to last forever**. If the sine wave is truncated (a one sided sine wave, for example), the response to this signal by a system, in general, is different from the response which would be obtained if the signal would be a sine wave from $t = -\infty$ to $t = +\infty$. There would be transients which are not periodic. All the useful properties mentioned above, will then no longer be valid. So, if we need to apply the principles studied in a basic course, we need something unrealistic, i.e. a sine wave which lasts forever. To be **more realistic** in our demands, it is **appropriate to deal with wavelets** rather than waves. **Wavelets are waves that last for a finite time, or more appropriately, they are waves that are not predominant forever. We let the waves die out to create a compactly supported 'wavelet' of finite duration**. They may be significant in a certain region of time and insignificant elsewhere or they might exist only for finite time duration. For example, a sine wave that exists only between $t = 0$ and $t = 1\ \mu\text{sec}$ is, in principle, a wavelet (though not a very good one), a wave that doesn't last forever. Thus, a wavelet is a mathematical function useful in digital signal processing and image compression. In signal processing, wavelets make it possible to recover weak signals from noise.

In subsequent topics we will see that concept of wavelets arose when scientists debated on a serious issue of **"time-frequency localisation"**.

Example 1.1.4 — Musical signal revisited.

Now, we go back to the example of audio clip. The audio clip comprises of many notes of varying time lengths and hence requires time segmentation. On the other hand, identifying notes in a particular time segment, involves segmentation in the frequency domain. Thus we are asking for a **simultaneous localization** in time and frequency domain. But the **uncertainty principle** in nature puts **constraints** on this simultaneous localization beyond a point. In signal processing, we call it **uncertainty in time and frequency domain** i.e. both domains are contrary to each other. Thus, the resolution in the time domain is increased at a compromise in the resolution in the frequency domain. It could be even intuitively argued that, for a shorter audio clip, it is more difficult to identify a note in that time segment than a note played for a longer period of time. But, what is not intuitive from this discussion is that we cannot go down to identifying one particular frequency precisely. So, if we wish to come down to a point on the time axis, we need to spread all over the frequency axis and vice versa. This is the stronger version of this principle. However the weaker version is more subtle. Even if we select a time region on the time axis and ask for the region of frequencies which are predominant in that time region, even then there is a restriction on the simultaneous length or measure of the time and frequency regions. In fact, the more we focus in time, the less we focus in frequency. This could be best explained by examples.

Example 1.1.5 — Mobile system.

Consider a mobile communication system in which a bit stream is transmitted at 1Mbps. If the bit interval is uniform, the time interval for 1 bit is 1 μsec. This indicates segmentation in time. Now, consider that there are two mobile operators operating in a given region. All the users in the region are using mobile from any one of the two operators. To avoid interference or overlapping of these signals, these operators should be separated in some domain. They cannot be separated in the time domain since the users of different operators can use the mobiles at the same time. So the separation could be in frequency domain. Thus, every operator is allocated a particular bandwidth, i.e. a region in the frequency domain so that the users of that operator can operate in that frequency region only without any problem of time coincidence. This is indicative of segmentation in frequency. Thus, in a mobile communication case, there is a desire to localize in time and frequency simultaneously, i.e. transmitting a bit in a time interval of 1 μsec, indicating a localization in time and transmitting in a particular frequency region only indicating localization in frequency. Thus, this example clearly depicts practical need of simultaneous localization in time and frequency.

Example 1.1.6 — Biomedical signal.

Consider another example of a biomedical signal, say ECG signal (electro-cardiographic waveform) in which various features of the ECG signals are analysed. There are various segments in a typical ECG signal which are often indexed by letters say P, Q etc. as shown in Fig. 1.3. These segments are of unequal length, e.g. from Fig. 1.3, it can be seen that interval PR is much shorter than interval QT. In fact, biomedical engineers often talk about what are called as evoked potentials. They give stimulus to a biomedical system and evoke a response and the waveform corresponding to that response is called an evoked potential. An evoked potential typically has both fast and slow-varying parts in the response. Obviously, the slower parts of the response are predominantly located in the lower ranges of the frequency region while the quicker parts of the response are predominantly located in the higher ranges of the frequency. To isolate the quicker parts of the response, is it sufficient to pass the signal through a conventional high pass filter? Here arises the time frequency conflict. Indeed, it is not sufficient. In fact, we need a different perspective on filtering. We need to identify, in different parts of the time axis, which regions of the frequency axis are predominant and then identify different parts of the frequency axis that need to be emphasized in different time ranges. This is yet another example of time frequency conflict. In a basic course, we understand the domains very well because we keep them apart. But one normally needs to consider the two domains together and when we try to do so, there is a fundamental conflict as understood from the uncertainty principle.

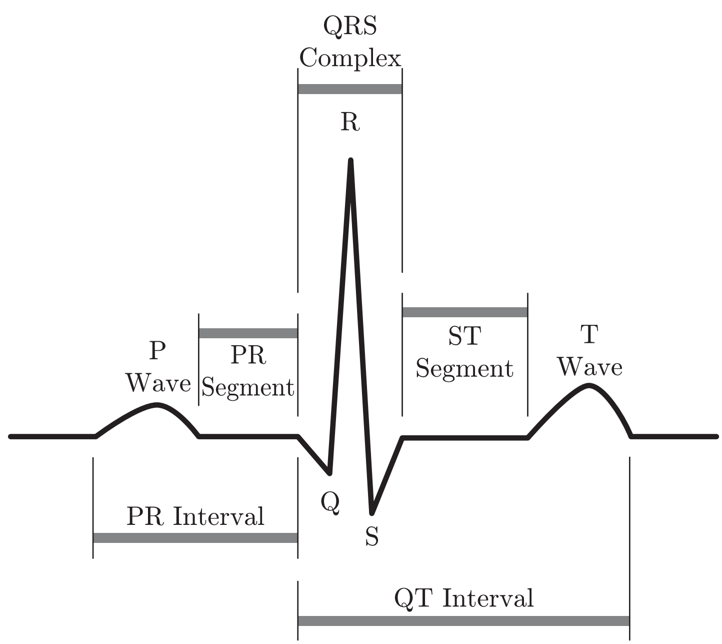

Figure 1.3 | ECG Signal Sample

Struggling with the concept of simultaneous time frequency localisation scientists came to a solution or more like a workaround. Perhaps if a signal is split into components that were not pure sine waves, it would be possible to condense the information in both time and frequency domains. This was the idea which ultimately led to the concept of **wavelets**.

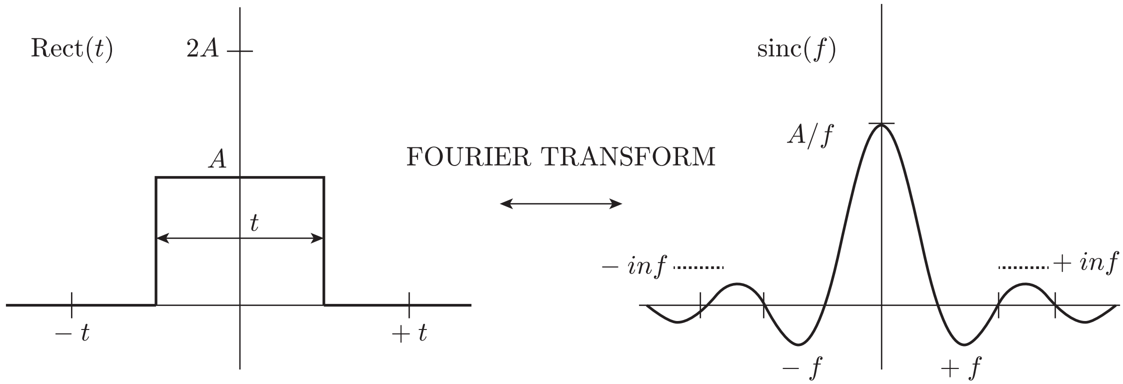

Figure 1.4 | Fourier Transform of Rectangular 'box' type function with crisp and compact time domain presence is a 'sync' function with spread and no isolation in frequency domain

Figure 1.4 clearly depicts the limitation of using sinusoidal basis functions that simultaneous show isolation in time as well as frequency domain is not possible. In fact, as the figure depicts, as the time domain representation is compact in the form of 'box' type rectangular function its Fourier Transform spreads out and has no isolation in frequency domain ('sync' function).

1.2 | Brief Outline of the Book

This book begins with an introduction to the **Haar Multiresolution Analysis** a particular tool to analyze signals; proposed as a dual of the idea of Fourier analysis by Haar, a French mathematician. In Fourier analysis, we represent even discontinuous or non-smooth waveforms into a linear combination of extremely smooth functions, namely, the sine waves. Haar proposed the idea of taking smooth functions and convert them into a linear combination of effectively discontinuous functions. For example, data in a digital communication system, e.g. an audio signal, image, or a video, is transmitted with a large level of discontinuity. To record a digital audio, we first sample the signal followed by digitizing and then recording it. All these are highly discontinuous operations, in which not only forcibly introduce discontinuity in time but also in amplitude. Thus, representing a smooth audio signal into a discontinuous bit stream is very beneficial to digital communication system and a digital recording is even better than an analog recording. Therefore, the first few chapters of this book will look at wavelets and multirate digital signal processing based on the principles that Haar propounded. Understanding Haar multiresolution analysis (MRA) in depth leads to better understanding of many of the principles of wavelets and multirate processing, specifically the two-band processing. After presenting material on Haar MRA, the sequence of presentation in the book would be as follows:

- The Daubechies family of multiresolution analysis (Daubechies is the name of the mathematician who proposed this family of multiresolution analysis).
- The uncertainty principle, fundamentally and in terms of its implications.

- The continuous wavelet transform (CWT). In the Haar multiresolution analysis, we have a certain discretization in the variables associated with the wavelet transform. In the continuous wavelet transform, the variables become continuous.
- Some of the generalisations of the ideas like **'wave packet transform'**, variants of wavelet transforms like next generation wavelets through lifting scheme, etc.
- In the last parts of the book, we shall look at some of the important applications, where wavelets and multirate digital processing provide great advantages.
- A special chapter also provides material on the scope beyond wavelets.

1.3 | Multirate Digital Signal Processing

Let us look at some of the developments in the subject of multirate signal processing. The connection with wavelets will also be seen. Consider the biomedical example discussed previously. The biomedical signal has fast-varying parts and slow-varying parts of the response. The slow-varying parts of the response are likely to last for a longer period of time while the quicker parts of the response are likely to last for a shorter period of time. So, apart from considering localization in time and also in frequency, the localization required for higher frequencies and lower frequencies is also important. Lower frequencies in response have lower time resolution. Resolution means the ability to resolve, the ability to be able to identify specific components. How can the frequency axis be narrowed down? **Frequency resolution** relates to being able to identify the specific frequency components. More appropriately, how much do we need to narrow down? It is often desired (not always) that the higher frequency components be compromised on frequency resolution but not on time resolution. So things that are transient, demand time resolution and things that occupy lower frequency ranges, demand frequency resolution. Hence for increasing frequencies, more frequency resolution is needed opposed to time resolution. This brings the idea of multirate processing. So, if we have higher frequencies, we should use smaller sampling interval and vice versa, in a discrete processing system. This leads to more efficient processing operations. In an evoked potential response, frequent sampling is not required for the lower frequency components. It increases data without any advantage. On the other hand, while handling quicker components, if our sampling rate is less or inadequate, 'aliasing' is introduced. Hence, it is not a good idea to use the same sampling rate for all the frequency components. Unlike a basic course, we deal here with sequences that are obtained with different sampling rates in the same system. This brings the idea of multirate digital signal processing. Thus, in the analysis of same system we need to have different sampling rates according to demand of resolution and the conservation of data.

Another important aspect which triggers use of multirate systems is the way conventional transforms like Fast Fourier Transform (FFT) divides the frequency range. While human ears perceive frequencies in logarithmic sense, FFT provides equal prominence to every frequency bin, thus making frequency segmentation 'linear'.

Example 1.3.1 — Linear segmentation of FFT.

Human hearing is sensitive to typical range of 20 Hz to 20 KHz. Female speech typically ranges from 140 Hz to 500 Hz, male speech typically ranges from 70 Hz to 250 Hz, flute produces frequencies from 260 Hz to 3350 Hz, Violin produces from 200 Hz to 3000 Hz and so on. Often we have to process and analyze various ranges of frequencies. Due to linear segmentation of frequencies using

FFT, to record high frequency data accurately the compromise is made on low frequency resolution. Thus, in general, FFT has excellent high frequency pitch resolution but poor low frequency resolution. For example, let's say we are processing a signal for which Nyquist stability criterion is followed and signal is sampled at appropriate sampling rate. When FFT frame size is divided by sampling rate it gives us frequency window. For a particular signal under analysis, let us assume the frequency window be 50 Hz. This could be very small analysis window for fast moving (high frequency) signal but could be a big window for slow moving (low frequency) signal, which may prevent FFT to capture good details at low frequency. The natural intuitive solution to this is to have different sampling rates for different parts, which leads us to multirate systems.

1.3.1 Filter Banks

Going further, let us construct the idea of filter banks, which is quite important for the analysis and synthesis of the signals. In a biomedical example, to separate components, many different operators have to be simultaneously used. So a system of filters is needed, which has certain individual characteristics as well as collective characteristics. Thus, analysis as well as synthesis is required. In addition to that, we also require localization. So a bank of filters, refers to a set of filters which either have a common input or a common point of output. This concept of a bank of filters, (in fact, two banks of filters) namely analysis and synthesis filter banks, taken together, is very central to multirate signal processing. So a two-band filter bank will be presented in this book at a greater depth. The concept of two-band filter bank is of great importance in constructing wavelets. The subsequent chapters and discussions about Haar multiresolution analysis will bring out the intimate relationship, which exists between the Haar wavelet and a two-band Haar filter bank.

1.4 | Prerequisites

The subject of 'Wavelets' has many interesting features and facets. It uses different approaches for representation of signals and functions than conventional techniques. In this section we will try to build physical significance to bring out concepts from underlying mathematical formulas. The readers who are well versed with the fundamental concepts may skip the reminder of the chapter.

1.4.1 Generalized Vectors

A vector quantity or vector, provides the magnitude as well as the direction of a specific quantity. A two-dimensional vector is generally represented in terms of two co-ordinates along two perpendicular axis. This idea of perpendicularity is intimately related to the idea of independence. Let us look at a system of vector representation:

System representation

When giving directions to a point, it is not enough to say that it is x miles away, but the direction of those x miles must also be provided for the information to be useful. (Note that physical quantities are represented by Scalars, such as temperature, volume and time, etc.)

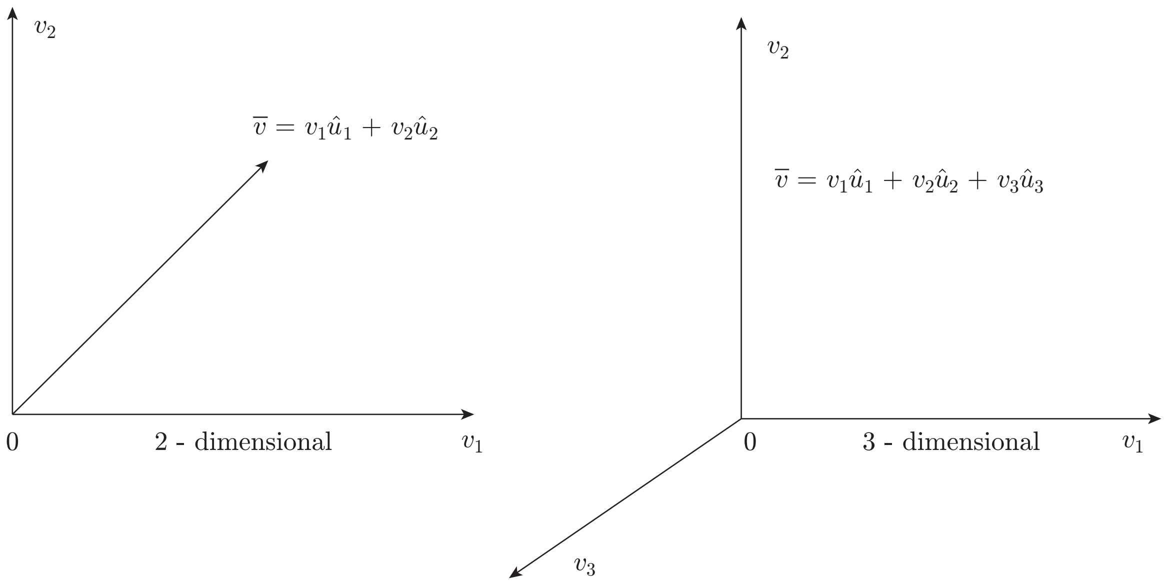

Figure 1.5 | Graphical representation of vectors

Given a coordinate system in three dimensions, a vector may thus be represented by an ordered set of three components, which represent its projections v_1, v_2, v_3 on the three coordinate axes.

$$v = [v_1, v_2, v_3]$$

The three most commonly used coordinate systems are rectangular, cylindrical, and spherical. Alternatively, as shown in Fig. 1.5, a vector may be represented by the sum of the magnitudes of its projections on three mutually perpendicular axes:

$$\overline{v} = v_1\hat{u}_1 + v_2\hat{u}_2 + v_3\hat{u}_3$$

The *n*-dimensional coordinate systems based on the Euclidean space (Cartesian space or *n*-space) represented by R^n or E^n, under *n*-dimensions and *n*-vectors. Usually, the Euclidean space is formed by $(X_1, X_2, X_3, ..., X_n)$ where n is equal to 8.

Example 1.4.1 — Parallelogram law of vector.

Let us take an example. Refer Fig. 1.6, we shall see how we can get the resultant of two vectors by the use of the parallelogram law of vector addition. Given two vectors $\overline{\tilde{v}}_1$ and $\overline{\tilde{v}}_2$, their resultant is given by the diagonal of the parallelogram as shown in the Fig. 1.6.

$$\overline{v} = \overline{\tilde{v}}_1 + \overline{\tilde{v}}_2$$

$$\text{where } \overline{\tilde{v}}_1 = k_1\hat{u}_1$$

$$\text{and } \overline{\tilde{v}}_2 = k_2\hat{u}_2$$

$$\text{then } \overline{v} = k_1\hat{u}_1 + k_2\hat{u}_2$$

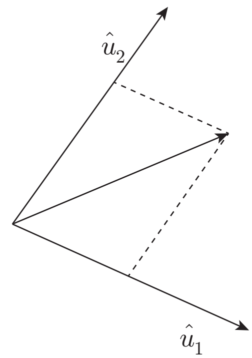

Figure 1.6 | Parallelogram law of vectors

1.4.2 Relationship Between Functions, Sequences, Vectors

As we may recall, one can intimately relate processing of a function to processing of equivalent sequence, and retrieving information from or modifying a function can be done equivalently by processing or modifying that sequence corresponding to function. A sequence is like a vector and each n (corresponding to a value in the sequence) is a different dimension of that vector. Now, once this analogy is clear, it is very easy to extend other ideas of vectors to this context. For example, we can think of vector addition as addition of the sequences point by point, and so on.

An infinite (countably infinite) dimension vector is a sequence $x[n], n \in \mathbb{Z}$, where n is index and $\mathbb{Z}$ is set of integers.

Now, we would like to extend other ideas of vectors to this context of infinite dimension vector.

Dot product of vectors

Let,

$\overline{e}_1 = e_{11}\hat{u}_1 + e_{12}\hat{u}_2$ and $\overline{e}_2 = e_{21}\hat{u}_1 + e_{22}\hat{u}_2$ then dot product is $\overline{e}_1\overline{e}_2 = e_{11}e_{21} + e_{12}e_{22}$.

It can be easily seen that this is nothing but sum of products of corresponding coordinates.

Let two n-dimensional vectors be

$\overline{e}_1 : e_{11}, e_{12}, \ldots, e_{1N}$ and $\overline{e}_2 : e_{21}, e_{22}, \ldots, e_{2N}$

the dot product of these two vectors is

$\langle \overline{e}_1 \overline{e}_2 \rangle = \sum_{k=1}^{N} e_{1k} e_{2k}$. These are also called as orthogonal coordinates.

Let, in two sequences, say $x_1[n], x_2[n], n \in Z$, the 'dot product' or 'inner product' be $\langle x_1, x_2 \rangle$, where

$$\langle x_1, x_2 \rangle = \sum_{n=-\infty}^{+\infty} x_1[n] x_2[n]$$

The word 'magnitude' is generally used in the context of $2-D, 3-D$ space; but in a general $n-D$ space, we will use the word 'norm'. In $L_2(\mathbb{R})$, norm squared represents the energy.

Let vector x: essentially a sequence $x[n], n \in Z$, then the 'norm' of sequence $x = \| x \|$ should be $\langle x_1, x_2 \rangle^{1/2}$

$$\| x \| \geq 0 \text{ and } \| x \| = 0 \text{ iff } x = 0 \text{ i.e. } x[n] = 0 \quad \forall \quad n \in Z$$

If x_1 and x_2 are real,

$$\langle x_1, x_2 \rangle = \sum_{n=-\infty}^{+\infty} x_1[n] x_2[n]$$

$$\langle x, x \rangle = \sum_{n=-\infty}^{+\infty} x^2[n]$$

As long as $x[n]$ is real $\forall n \in \mathbb{Z}$, this will satisfy norm requirements.

A small change will be applied for complex sequences as follows

$$\langle x_1, x_2 \rangle = \sum_{n=-\infty}^{+\infty} x_1[n] \overline{x_2[n]}$$

Properties of Inner product

1. Conjugate commutativity

$$\langle x_1, x_2 \rangle = \overline{\langle x_2, x_1 \rangle}$$

$$= \sum_{n=-\infty}^{+\infty} x_1[n] \overline{x_2[n]}$$

$$= \sum_{n=-\infty}^{+\infty} x_2[n] \overline{x_1[n]}$$

$$\langle x_1, x_2 \rangle = \overline{\langle x_2, x_1 \rangle}$$

2. Linear in first argument

$$\langle a_1 x_1 + a_2 x_2, x_3 \rangle = a_1 \langle x_1, x_3 \rangle + a_2 \langle x_2, x_3 \rangle$$

$$= \sum_{n=-\infty}^{+\infty} (a_1 x_1 + a_2 x_2) x_3$$

$$= \sum_{n=-\infty}^{+\infty} a_1 (x_1 x_3) + a_2 (x_2 x_3)$$

$$\langle a_1 x_1 + a_2 x_2, x_3 \rangle = a_1 \langle x_1, x_3 \rangle + a_2 \langle x_2, x_3 \rangle$$

3. Positive definiteness or non-negativity

$$\langle x, x \rangle = \sum_{n=-\infty}^{+\infty} x[n].x[n]$$

$$\langle x, x \rangle = 0; \quad iff \quad x[n] = 0 \quad \forall n$$

This inner product is also called the 'standard inner product'. In the chapters henceforth when we say inner product of sequences we shall be talking about the 'standard inner product' unless specified.

Extension to uncountably infinite dimension

For any 't', $t \in \mathbb{R}$ is a different dimension and $x(t)$, $t \in \mathbb{R}$, means $x(t)$ for the 't^{th}' coordinate. Then the 'dot product' or 'inner product' between two functions $x(t)$ and $y(t)$ in general is given by

$$\langle x, y \rangle = \int_{-\infty}^{+\infty} x(t)y(t)dt$$

The properties of conjugate commutativity, linearity in the first argument and positive definiteness are also valid for this case and its verification is left as an assignment to the reader.

Parseval's Theorem

The Parseval's theorem states that the inner product of any two functions in time domain is equal to the inner product of those two functions in frequency domain.

Let $x(t)$ be a function then its fourier transform, $\hat{x}(\nu)$ or $\hat{x}(\Omega)$ (in Hz or in radians respectively) is defined as

$$\hat{x}(\nu) = \int_{-\infty}^{+\infty} x(t)e^{-j2\pi\nu t}dt \quad or \quad \hat{x}(\Omega) = \int_{-\infty}^{+\infty} x(t)e^{-j\Omega t}dt \quad \text{where} \quad \Omega = 2\pi\nu$$

From now on we shall use 'Ω' to represent the angular frequency variable in the continuous time and 'ν' to represent the Hertz' frequency variable. What we are referring to shall be clear from the context. Let $y(t)$ be a function and $\hat{y}(\nu)$ or $\hat{y}(\Omega)$ its fourier transform (in Hz or in radians) defined as

$$\hat{y}(\nu) = \int_{-\infty}^{+\infty} y(t)e^{-j2\pi\nu t}dt \quad or \quad \hat{y}(\Omega) = \int_{-\infty}^{+\infty} y(t)e^{-j\Omega t}dt \quad \text{where} \quad \Omega = 2\pi\nu$$

The inner product of these in time domain is

$$\langle x, y \rangle = \int_{-\infty}^{+\infty} x(t)\overline{y(t)}dt$$

and it is equal to the inner product in frequency domain given by

$$\langle \hat{x}, \hat{y} \rangle = \int_{-\infty}^{+\infty} \hat{x}(\nu)\overline{\hat{y}(\nu)}d\Omega$$

That means $\langle x, y \rangle = \langle \hat{x}, \hat{y} \rangle$

The function $x(t)$ can be reconstructed from its frequency components as

$$x(t) = \int_{-\infty}^{+\infty} \hat{x}(\Omega)e^{-j\Omega t}d\Omega$$

Parseval's theorem basically states that the inner product is independent of the co-ordinate system. So, whether we choose to represent two functions in the standard co-ordinate system of 'time' or the slightly less obvious co-ordinate system of 'frequency', their inner product always remains the same.

Example 1.4.2 — Applications of Parseval's theorem.

The Parseval's theorem is often used in many areas like physics and engineering etc, and it is written many of the times as

$$\int_{-\infty}^{+\infty} |x(t)|^2 \, dt = \int_{-\infty}^{+\infty} |\hat{x}(\nu)|^2 \, d\nu$$

where $\hat{x}(\nu)$ represents the continuous Fourier transform of $x(t)$ and ‘TM’ represents the frequency component of x.

From this equation, the theorem states that the total energy contained in a function $x(t)$ **over all time ‘** t **’ is equal to the total energy of the its Fourier Transform** $\hat{x}(\nu)$ **overall frequency ‘**ν**’**.

For discrete time signals, the theorem becomes:

$$\sum_{n=-\infty}^{+\infty} |x[n]|^2 = \frac{1}{2\pi} \int_{-\pi}^{+\pi} |\hat{x}(e^{j\omega})|^2 \, d\omega$$

where $\hat{x}(e^{j\omega})$ is the Discrete-Time Fourier transform (DTFT) of x and ‘ω’ represents the angular frequency (in radians per sample) of x.

For the Discrete Fourier transform (DFT), the relation becomes:

$$\sum_{n=0}^{N-1} |x[n]|^2 = \frac{1}{N} \sum_{k=0}^{N-1} |\hat{x}[k]|^2$$

where $\hat{x}[k]$ is the DFT of $x[n]$ and ‘ N ’ is length of sequence in both domains.

Relation between continuous functions and sequences

Let $x(t)$ be a continuous function and let $\mathbf{f}(t)$ be a unit step function in $[0,1]$ interval, then $x(t)$ can be written as

$$x(t) = ... + C_{-1}\phi(t+1) + C_0\phi(t) + C_1\phi(t-1) + C_2\phi(t-2) + ...$$

It can be graphically represented, as shown in Fig. 1.7.

Through successive approximations as one of the ways of representing signal in interval used, signal $x(t)$ can be represented as sequence $x[n]$ as $x[n] = \{....C_{-1}, C_0, C_1, C_2, ...\}$.

Equivalance between continous funcitons and sequences will be dealt in greater detail in subsequent chapters

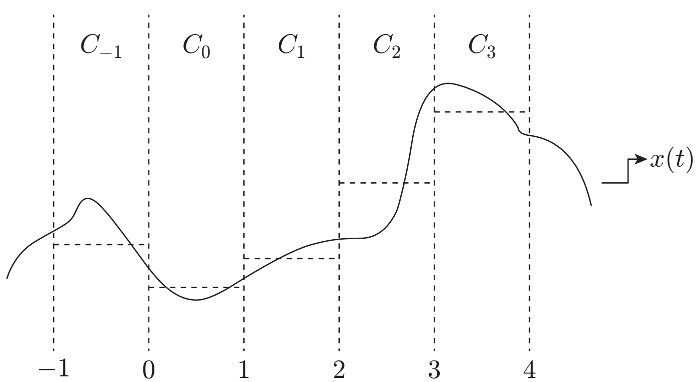

Figure 1.7 | Relation between continous functions and sequences

1.4.3 Need for Transformations

There are many reasons for carrying out a transformation, most siginificant one is convenience. For example, we do not understand music as just few time domain signals with varying voltage, but as sequence of frequencies. Thus, it makes sense to transform musical signal into frequency domain and then the analyzer will be more comfortable dealing with those frequencies. Ultimately, we want to design filters, more pertinently filter banks in the context of wavelets, and it is more convenient to design filter banks in frequency domain compared to time domain or spatial domain.

Wavelet transform is strikingly different than most of the conventional transforms. For all conventional transforms like Laplace transform, Z transform, Fourier Transform and Logarithmic Transform the basis function comes from natural logarithmic base *e*. However, for understanding wavelet transform we have to go beyond the purview of these conventional transforms.

We already know how to analyze Linear Time Invariant (LTI) Systems. For doing so, traditionally, we have two methods,

1. Convolution
2. Difference Equations

Convolution evolves out of the fact that given a signal $x[n]$, we can decompose that signal into scaled and shifted impulse sequences. After doing so, we can write,

$$x[n] = \sum_{k=-\infty}^{\infty} x[k]\delta[n-k] \tag{1.1}$$

This is the scaled summation of shifted impulses. We are able to do this because the system is assumed to be linear and shift invariant. Since the system is linear and thus would follow superposition theorem we are able to add up the products to get $x[n]$. Also, because of time invariance property we are able to shift the impulses without affecting the end result.

Once we do this and understand how the system reacts to impulses as stimulus, we would be able to get the systems impulse response. Now if we call the impulse response as $h[n]$, excite the LTI system with an exponential $e^{j\omega_0 n}$ as an input $x[n]$ and call the output as $y[n]$ we would have,

$$y[n] = \sum_{-\infty}^{\infty} e^{j\omega_0 n} h[n-k] \tag{1.2}$$

However we know by commutative law,

$$y[n] = \sum_{k=-\infty}^{\infty} x[k]h[n-k] = \sum_{-\infty}^{\infty} x[n-k]h[n] \tag{1.3}$$

Thus by putting $e^{j\omega_0 n}$ in place of $x[n]$ we have,

$$y[n] = \sum_{k=-\infty}^{\infty} e^{j\omega_0 [n-k]} h[n] \tag{1.4}$$

This forms an interesting eigen system for LTI analysis. That is because we can split the exponential term from Eq. (1.4) and then the summation happens for variable k and the term $e^{j\omega_0 n}$ can be deduced out of this summation of k terms.

$$y[n] = \sum_{k=-\infty}^{\infty} e^{j\omega_0 [n]} e^{j\omega_0 [-k]} h[n] \tag{1.5}$$

$$y[n] = e^{j\omega_0[n]} \sum_{k=-\infty}^{\infty} e^{j\omega_0[-k]} h[n] \tag{1.6}$$

From Eq. (1.6) we can see that after exciting the system with exponential of frequency ω_0 the result is the same term with something. The term $e^{j\omega_0 n}$ is known to us as eigen function and the multiplying term is known as a eigen value. This eigen value in a broader sense is known to us as a Fourier Transform. The basis function here is exponential e. This fact as discussed earlier in this chapter remains the same for other transforms also, for example in Z transform the basis function Z also equals $e^{j\omega}$.

It would be interesting now to look at from where this constant 'e' comes from.

The constant e was discovered by Dr. Bernoulli in a vague accident for which the story does not have authentic source, it is still very interesting though. Dr. Bernoulli was trying to help his banker friend because his business was not picking up. He gave him a solution based on the formulae for calculation of compound interest. As we know the compound interest formula for investment of a one rupee or one dollar or one euro as principle amount is given as,

$$\left\{1 + \frac{1}{n}\right\}^n$$

Dr. Bernoulli brought in series expansion by applying limit for n terms to infinity,

$$\lim_{n\to\infty} \left\{1 + \frac{1}{n}\right\}^n \tag{1.7}$$

and the constant 'e' came into existence, waiting for Euler to give it meaning! An engineer's perspective is provided in the MATLAB code (Example 1.4.3) for readers to try out the above limit approximation through simulations (rather than solving it actually – may be a mathematician's perspective!) and get convinced that it indeed gives us the constant after few iterations.

**Example 1.4.3 — MATLAB code to approximate constant 'e'. **

```
%************************************************
%************************************************
% MATLAB code to understand calculations for
% Constant 'e': To be accompanied with book on
% Multiresolution and Multirate Signal Processing
% by Dr V M Gadre and Dr A S Abhyankar
%************************************************
%************************************************
clear all;close all;clc;

for n=1:1000000000  % MATLAB doesn't support zero index
                    % we can't take 'n' all the way to infinity
                    % hence some big number 1000000000
```

```
    (1+(1/n))^n     % compound interest formulae
    pause;          % to see the value after every iteration
                    % slowly value saturates to 2.7183
end

% End
```

Jacob Bernoulli

Jacob Bernoulli (1654–1705) was son of Nicolas Bernoulli and elder brother of Johann Bernoulli. Jacob acquired degree in theology to start his formal education as his father was against his children taking up mathematics. In spite of that due to his deep interest and curiosity he became a mathematician. In 1687, he became Professor of mathematics at University of Basel, where he taught till the end of his life. He continued working on the lines of Napier and was able to successfully discover the constant ‘e’. His contributions in the field of calculus are also well known and respected.

Though the story of banker friend of Dr. Bernoulli lacks authenticity, it was certain that around 1889 he published series of articles on theory of infinite series and proposed continuously compounded interest. There were also some series expansions like

$$1+\frac{1}{4}+\frac{1}{9}+\ldots+\frac{1}{k^2}+\ldots$$

for which he could not settle with a converging number and the quest was completed by Dr. Euler when he showed that above infinite summation equates to $\frac{\pi^2}{6}$. Thus in many ways Dr. Euler took Dr. Bernoulli’s work forward. After Dr. Bernoulli invented constant e, Dr. Euler came up with an identity known today as Euler’s Identity which is still regarded as one of the most beautiful of all mathematical discoveries.

$$e^{i\pi}=-1 \tag{1.8}$$

From application perspective more useful version of Euler’s Identity is,

$$e^{i\theta}=\cos(\theta)+j\sin(\theta) \tag{1.9}$$

The interesting thing to note is if we draw a tangent to any point on this exponential curve the y-intercept and slope of this tangent matches. Thus at any point along the curve we can resolve the point into ‘cos’ and ‘sin’ components which are in turn orthogonal in nature. Dr. Euler really gave special meaning to this constant ‘e’ and it’s because of his contribution we get orthognal and energy preserving transforms. It’s because of this unique property of ‘e’, the inverse of the transform also exists.

Leonard Euler

Leonard Euler (1707–1783) was a Swiss mathematician and he was well known for the quality as well as quantity of his work. His contributions in the field of graph theory, number theory and calculus are considered to be outstanding. Born in Basel in 1707, in 1727 he went to St Petersburgh Academy. In 1741 he joined berlin Academy and in 1766 joined back St Petersburgh Academy. He died in 1783. In 1748 he gave a meaning to the constant ‘e’ and gave base to the natural logarithm which then went on to become basis to most of the transforms.

After Dr. Euler gave a powerful meaning to ‘e’, Dr. Fourier worked on analyzing periodic and aperiodic functions and signals. The legacy of transforms is thus result of contribution from these three great scientists. Dr. Fourier gave a systematic way of analyzing periodic as well as aperiodic signals through Fourier series and Fourier Transform framework. For a time domain signal $x(t)$ the corresponding Fourier Transform is given by Eq. (1.10).

$$\hat{X}(\Omega) = \int_{-\infty}^{\infty} x(t)e^{-j\Omega t}\,dt \tag{1.10}$$

Thus, conceptually Fourier description is the inner product between the signal to be analyzed and the basis or kernel function.

Jacob Fourier

Jacob Fourier (1768–1830) was a French mathematician and a well-known scientist with the contributions like Fourier series, Fourier descriptors, Fourier transform etc. Fourier introduced the notion of representing continuous as well as discontinuous functions using continuous basis functions. This was an important and path-breaking research, which also encouraged scientists like Laplace to build their own theories like Laplace transform.

Now, let us look at question why wavelet transform? The wavelet transform decomposes signal into two separate series. One which represents the coarse version which leads to scaling function and other which represents the details or the refined version which leads to wavelet function or the mother wavelet function.

Still two more questions need to be answered: Are not the traditional methods of representing signals good enough? And what is so special about this wavelet transform? We will answer this gradually in this book.

Let us take these questions one at a time. In the traditional methods the most basic representation of signals is with Taylor series.

For example,

Taylor series expansion at $x_0 = 0$,

$$e^x = 1 + \frac{x^1}{1!} + \frac{x^2}{2!} + \frac{x^3}{3!} + \ldots = \sum_{n=0}^{\infty} \frac{x^n}{n!} \tag{1.11}$$

Every single coefficient in the above expression can be looked upon as a decomposed piece and such pieces can be used for reconstructing the corresponding signal or function. If we only make use of finite number of coefficients lets say up to first 5 coefficients and try to reconstruct the signal then the reconstructed signal would look like the signal shown in Fig. 1.8.

Figure 1.8 (b–f) shows Taylor series approximation of exponential function with number of coefficients used to be $N = 1$, $N = 2$, $N = 3$, $N = 4$, and $N = 5$, respectively. It is clear that as the number of coefficients increase the approximation (shown as black dotted line) starts approaching the actual function (shown as black solid line). Thus in Taylor series, cooperation to build better representation is rigid from the perspective of lack of inter-coefficient resolution. Since we have to work with large terms, also scale and translation of every single term is limited. In contrast to this in wavelet analysis the scaling function and its associated wavelet function makes the representation flexible.

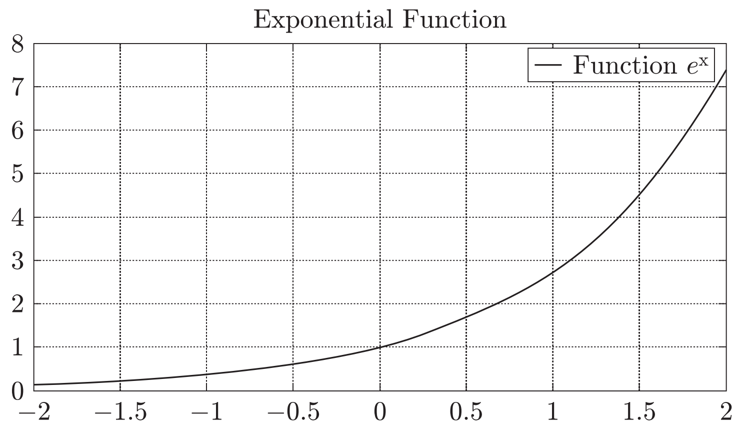

(a) Exponential Function

$y = f(x) = e^x$

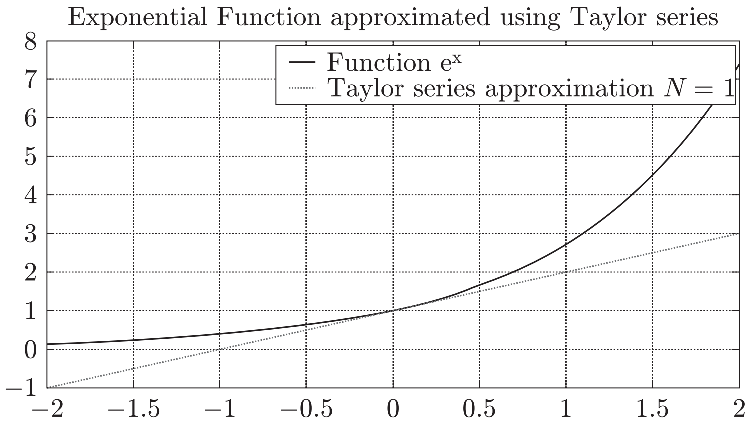

(b) Taylor series approximation using $N = 1$

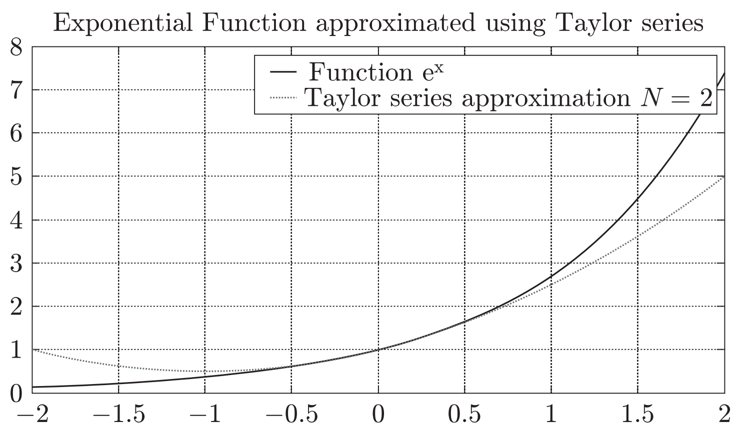

(c) Taylor series approximation using $N = 2$

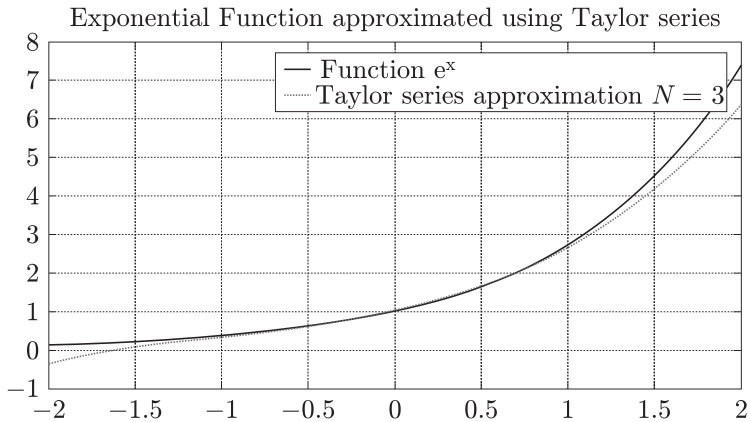

(d) Taylor series approximation using $N = 3$

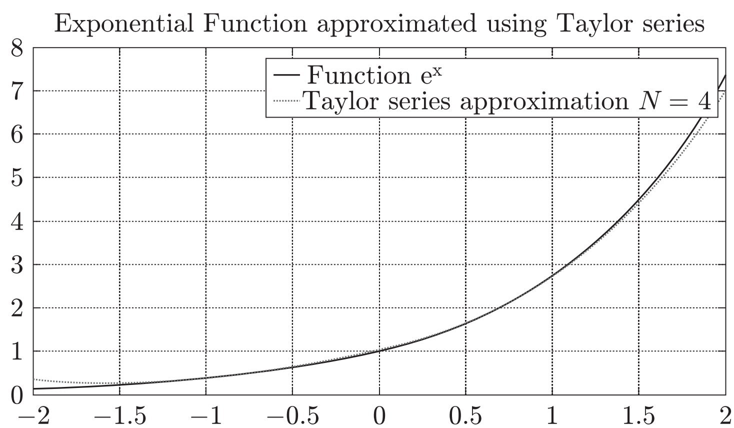

(e) Taylor series approximation using $N = 4$

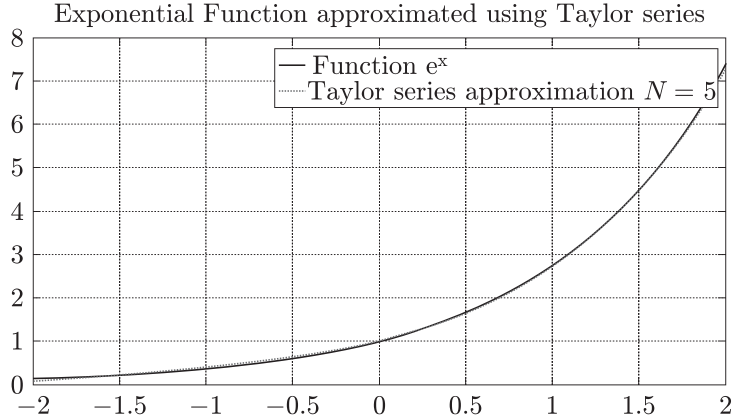

(f) Taylor series approximation using $N = 5$

Figure 1.8 | Approximation of exponential function using up to 5 coefficients from Taylor series

The MATLAB code to try more coefficients out is provided for readers:

Example 1.4.4 — MATLAB code to understand Fourier transform.

```
title('Exponential Function approximated using Taylor
series');

N=5;    % No of coeffs in Taylor series approximation
y_est=0;% Initialize the estimate to zero

for n=0:N
    y_est=y_est + (x.^n)./factorial(n); % Taylor series formulae
end

hold on;

plot(x,y_est,'--r','LineWidth',3) % Plot the approximation as red dotted
legend('Function e^{x}','Taylor series approximation N=5') % legend

% End
```

```
%*********************************************
%*********************************************
% MATLAB code to understand working of Fourier
% Transform: To be accompanied with book on
% Multiresolution and Multirate Signal Processing
% by Dr V M Gadre and Dr A S Abhyankar
%*********************************************
%*********************************************


clear all;close all;clc;

x=-2:0.1:2; % Create x-axis

y=exp(x);   % The exponential function y=e^x

figure(1);
plot(x,y,'b','LineWidth',3); % The function in blue
grid on;
```

In wavelet analysis the scale $\{1/2\}^j$ is dependent upon the analyzer. Thus while sampling a high frequency signal we can bring in a very high value of j. Then a translation $\tau_{j,k} = k/2^j$ can be used to focus on that part. Hence with wavelet analysis we can 'look' into any particular part of the signal.

By changing the scale and translation parameter we have an interesting zoom-in or zoom-out facility of wavelet transform.

Fourier series has a noteworthy advancement over the Taylor series. Since elements of a Taylor series do not necessarily and always form an orthogonal set. However, in case of Fourier series the set $\{1, \cos(nx), \sin(nx)\}_{n=1}^{\infty}$ is always orthogonal on $(-\pi, \pi)$. But still flexibility with scale and translation parameters remains to be explored.

Even though Fourier series is rigid in terms of rotations and translations, we derive some information related to wavelet transformation from it. Fourier series is represented by following equation,

$$f(x) = a_0 + \sum_{k=1}^{\infty}[a_k \cos(kx) + b_k \sin(kx)] \tag{1.12}$$

Where,

$$a_0 = \frac{1}{2\pi}\int_{-\infty}^{\infty} f(x)dx$$

$$a_k = \frac{1}{\pi}\int_{-\infty}^{\infty} f(x)\sin(kx)dx$$

$$b_k = \frac{1}{\pi}\int_{-\infty}^{\infty} f(x)\cos(kx)dx$$

We observe that a special relationship exists between cosine and sine terms of the series. A similar relationship also exists between scaling $\phi(.)$ and wavelet $\psi(.)$ functions. This relationship although trivial is very interesting. Though wavelets are radically different from conventional transforms like Fourier transform, its rise has its roots in the shortcomings of these conventional transforms. To find out what is so different about wavelet representation, let us revisit the Fourier theory briefly.

1.4.4 How Fourier Transform Works?

To answer this question, let us start with Fourier basis function. It is the complex conjugate of known frequency. Euler's theorem allows us to divide this basis into real and imaginary parts as $e^{i\theta} = \cos\theta + i\sin\theta$. The real and imaginary parts of basis function used in Fourier transform are shown in Fig. 1.9.

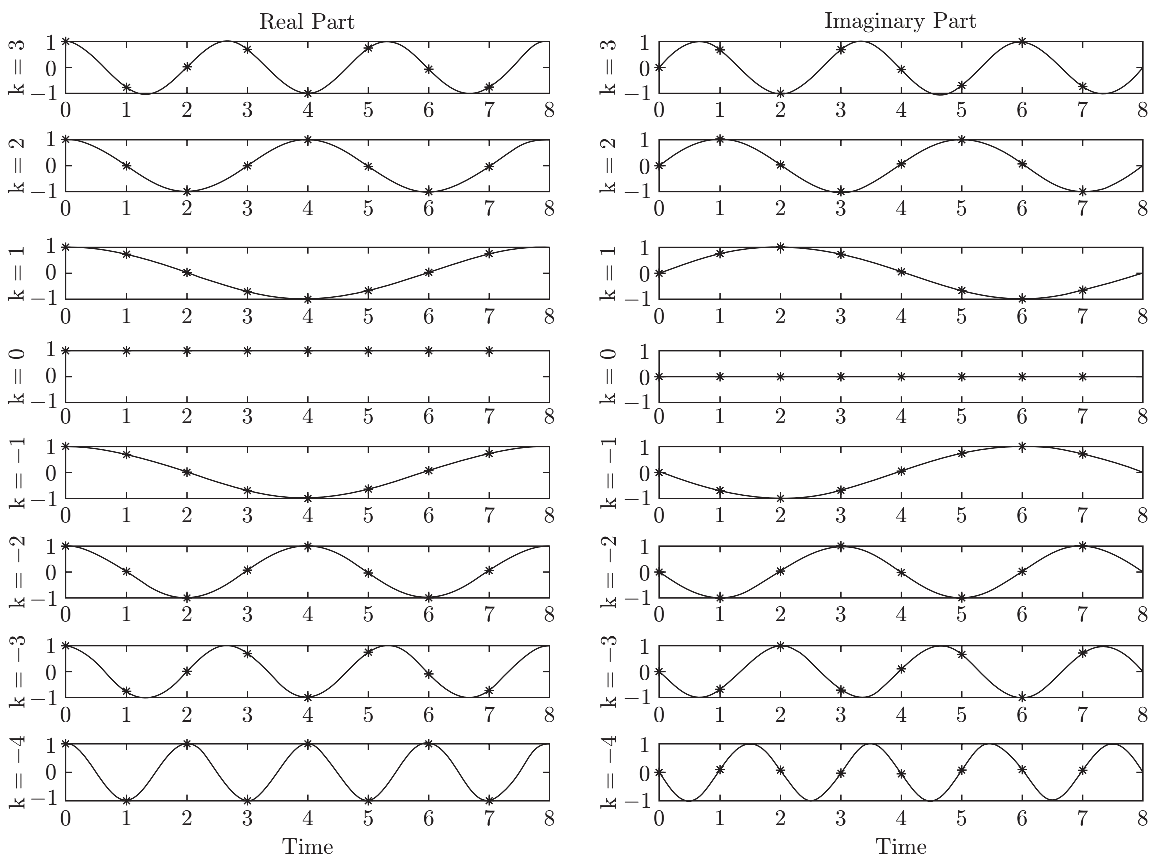

Figure 1.9 | Real and imaginary parts of Fourier basis function

Let us say we want to analyze a stationary signal using Fourier mechanism. Let us also assume that this signal is made up of two frequencies say $\sin(4x)$ and $\cos(7x)$. These are linear frequencies of emerging out of independent variable x and readers should note that $\sin(4x)$ is not 4Hz sinusoidal. We can excite this signal using all the basis functions as in Fig. 1.9 and integration of dot product yields the Fourier domain representation. We know that in Fourier domain this will produce two peaks corresponding to $3x$ and $7x$ coming from sin and cos components respectively in the signal under the probe. The peak generation process comes out of the fact that this mechanism is a dot product or correlation filter mechanism. This can be clearly witnessed from the simulation results below.

Figure 1.10 shows a case when the signal is excited with basis function with different frequency than one of the existing frequency components ($\sin(4x)$ or $\cos(7x)$ in this case). The Fig. 1.10(a) shows the actual signal, Fig. 1.10(b) shows the $\sin(4x)$ basis function superimposed on the signal to be analyzed and Fig. (1.10(c)) demos the effect of dot product in case of excellent correlation. The positive parts when integrated will produce the desired peak at that frequency ($4x$ in this case).

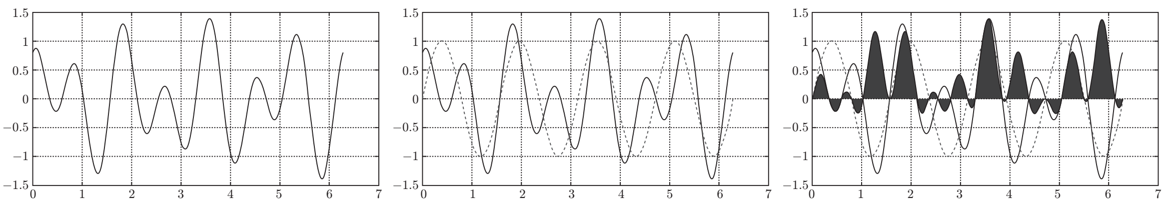

(a) Stationary Signal with sin(4x) and cos (7x) frequencies

(b) Signal super imposed with sin(4x) basis function-good correlation

(c) Dot product of signal with sin(4x) basis giving many positive parts.

Figure 1.10 **When excited with basis frequency which belongs to the signal it produces peak at that frequency**

When the basis uses frequency, which is not part of stationary components of signal, it results in poor correlation and will not produce peak for that frequency.

Figure 1.11 shows a case when the signal is excited with basis function of one of the existing frequency components ($\sin(4x)$ in this case). Figure 1.11(a) shows the actual signal, Fig. 1.11(b) shows the $\sin(7x)$ basis function superimposed on the signal to be analyzed and Fig. 1.11(c) demos the effect of dot product in case of poor correlation. When integrated, the positive parts destroy the negative parts not producing the peak at that frequency ($7x$ in this case as the basis had sin part and signal has cos part. If the signal is excited with $\cos(7x)$ it will certainly produce the peak).
From the simulation we can see that if the basis function contains frequency present in the actual signal on integration of the dot product we will get a peak at that frequency.

This brings the clarity on how exactly Fourier Transform works.

For further clarity readers can run the following MATLAB program and try out different basis examples and bring out conviction on how the dot product helps deploy the thematic of Fourier Transform.

Example 1.4.6 — MATLAB code: Fourier for non-stationary signals.

```
%**************************************************
%**************************************************
% MATLAB code to understand Taylor series approximations
% using different no of coeffs: To be accompanied with book on
% Multiresolution and Multirate Signal Processing
% by Dr V M Gadre and Dr A S Abhyankar
%**************************************************
%**************************************************
clear all;close all;clc;

Ts = 1/40;  % Sampling frequency
time1 = 0:Ts:5; % time for which first frequency exists
time2 = (5+Ts):Ts:10; % time for which second frequency exists
time3 = (10+Ts):Ts:15; % time for which third frequency exists
t = [time1 time2 time3]; % This makes signal non-stationary
```

```
% Let's first create a stationary signal
x1 = (sin(3*pi*t)+sin(12*pi*t)+sin(20*pi*t))/3;
% All the three frequencies are present throughout
% This makes x1 a stationary signal

% Let's now create a non-stationary signal
x2_1 = sin(3*pi*time1); x2_2 = sin(12*pi*time2); x2_3 =
sin(20*pi*time3); x2 = [x2_1 x2_2 x2_3];
% x2 has x2_1 lasting for time1, x2_2 for time2 and x2_3 for time3
% This makes x2 non-stationary

xf1=fft(x1); % This is FFT of stationary signal
xf2=fft(x2); % This is FFT of non-stationary signal
fs = 1/Ts;  % Sampling frequency

% Now let's create frequency axis with
L = (length(x1)-1)/2; f=0:(fs/2)/L:(fs/2);

% Plot the stationary signal
figure(1) subplot(411) plot(t,x1) grid title('Stationary Signal
x_{1}(t)')
% Plot FFT of stationary signal
subplot(412)
plot(f,abs(xf1(1:L+1))) % abs to plot magnitude
grid title('FFT of x_{1}(t)') subplot(413)
% Plot the non-stationary signal
plot(t,x2) grid title('Non Stationary Signal x_{2}(t)')
% Plot FFT of non-stationary signal
subplot(414)
plot(f,abs(xf2(1:L+1))) % abs to plot magnitude
grid title('FFT of x_{2}(t)')

% End
```

Example 1.4.7 — AM-GM inequality.

Further, we will use the result of Young's inequality to get the result (1) i.e. the Hölders Inequality. To do this, consider two real functions $f(t)$ and $g(t)$ in space $L_p(\mathbb{R})$ and $L_q(\mathbb{R})$ respectively. We first normalize these functions by dividing each of them with their respective norms.

Mathematically,

$$f(t) \in L_p(\mathbb{R})$$

$$g(t) \in L_q(\mathbb{R})$$

given that $\frac{1}{p} + \frac{1}{q} = 1$. Now the normalized functions are given as:

$$F(t) = \frac{f(t)}{\| f \|_p}$$

$$G(t) = \frac{g(t)}{\| g \|_q}$$

Where,

$$\| f \|_p = \left(\int_{-\infty}^{+\infty} | f(t) |^p \, dt \right)^{\frac{1}{p}}$$

$$\| g \|_q = \left(\int_{-\infty}^{+\infty} | g(t) |^q \, dt \right)^{\frac{1}{q}}$$

Now using Young's inequality we can point wise state that,

$$\frac{|F^p(t)|}{p} + \frac{|G^q(t)|}{q} \geq |F(t)G(t)|$$

Integrating above equation over real line we get,

$$\int_{-\infty}^{+\infty} \frac{| F(t) |^p}{p} dt + \int_{-\infty}^{+\infty} \frac{| G(t) |^q}{q} dt \geq \int_{-\infty}^{+\infty} | F(t)G(t) | \, dt$$

$$\int_{-\infty}^{+\infty} \frac{|f(t)|^p}{\|f\|_p^p \, p} dt + \int_{-\infty}^{+\infty} \frac{|g(t)^q|}{\|g\|_q^q \, q} dt \geq \int_{-\infty}^{+\infty} \frac{|f(t)g(t)|}{\| f \|_p \| g \|_q} dt$$

$$\frac{1}{p} \frac{\int_{-\infty}^{+\infty} | f(t) |^p \, dt}{\| f \|_p^p} + \frac{1}{q} \frac{\int_{-\infty}^{+\infty} | g(t) |^q \, dt}{\| g \|_q^q} \geq \frac{\int_{-\infty}^{+\infty} | f(t)g(t) | \, dt}{\| f \|_p \| g \|_q}$$

$$\frac{1}{p} + \frac{1}{q} \geq \frac{\int_{-\infty}^{+\infty} | f(t)g(t) | \, dt}{\| f \|_p \| g \|_q}$$

Therefore,

$$\| f \|_p \| g \|_q \geq \int_{-\infty}^{+\infty} | f(t)g(t) | \, dt \tag{1.15}$$

Since,

$$\frac{1}{p} + \frac{1}{q} = 1$$

Example 1.4.5 — MATLAB code to understand Fourier transform.

```
%**********************************************
%**********************************************
% MATLAB code to understand working of Fourier
% Transform: To be accompanied with book on
% Multiresolution and Multirate Signal Processing
% by Dr V M Gadre and Dr A S Abhyankar
%**********************************************
%**********************************************


clear all;close all;clc;
% We will create a signal (y) we wish to analyse
% This signal is stationary signal
% The signal has two frequencies (normalized)
% combination of cos 7x and sin 4x
x = linspace(0,2*pi,5000);
y = 0.6*sin(4*x)+0.8*cos(7*x);
plot(x,y,'r','LineWidth',3);
grid on; hold on; pause;

% yr is the basis function
yr = sin(7*x);
% different basis can be tried out
% examples: sin(1*x), cos(1*x), sin(8*x), cos(8*x),
plot(x,yr,'--g','LineWidth',3);grid on;
% Let's take dot product between signal (y)
% and basis (yr)
hold on; pause;
ymul = y.*yr; area(x,ymul);grid on; hold on;
pause; t = 0:pi/50:10*pi; hold off;

% figure(2);%subplot(121)
% plot3(sin(t),cos(t),t)
% The plots depict original signal y
% basis function (yr)
% correlation (poor/good) can be observed
% between y and yr
% The dot product distructs in case of poor
```

```
% correlation.
% The dot product yields into more positive parts
% in case of good correlation and creates a peak
% at that basis frequency in Fourier domain.
```

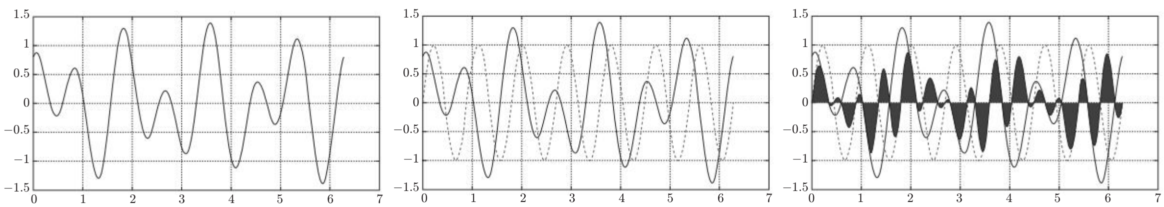

(a) Stationary *Signal* with $sin(4x)$ *and* $cos(7x)$ frequencies

(b) Signal superimposed with $sin(7x)$ basis function-poor correlation

(c) Dot product of signal with $sin(7x)$ basis giving almost equal positive and negative parts.

Figure 1.11 | When excited with basis frequency which does not belong to the signal it produces cancellations

It must be noted, however that Example 1.4.5 shows how Fourier Transform operates effectively for stationary signals. In case of non-stationary signals, Fourier transform fails to provide the information related to at what time which frequency existed. All the real-life signals are non-stationary and Fourier does not provide insight into the time stamps of frequency components to be analyzed. This is a serious limiting factor for many applications and corresponding usage of Fourier.

1.4.5 Fourier Transform and Non-stationary Signals

Stationary signals have all the frequencies existing all the time and because of this exact location of a particular frequency on time axis does not have much meaning for stationary signals. The answer to the question 'At what time instance a particular frequency existed?' will be at every time instance! This does not hold true in case of non-stationary signals and hence exact location of frequency plays vital role. Fourier transform does not capture this and the same is depicted in the MATLAB code Example 1.4.6.

The code creates two signals, $x_1(t)$ is stationary and $x_2(t)$ is non-stationary. As shown in Fig. 1.12 for both these signals the Fourier engine produces similar responses. The exact frequencies are successfully captured by FFT, however, this is not enough for non-stationary signals as the frequencies are present only at pertinent time stamps and not throughout. Interestingly, when inverse Fourier Transform of FFT of non-stationary signal is taken, it produces back stationary signal like $x_1(t)$ in lieu of producing back original non-stationary signal $x_2(t)$.

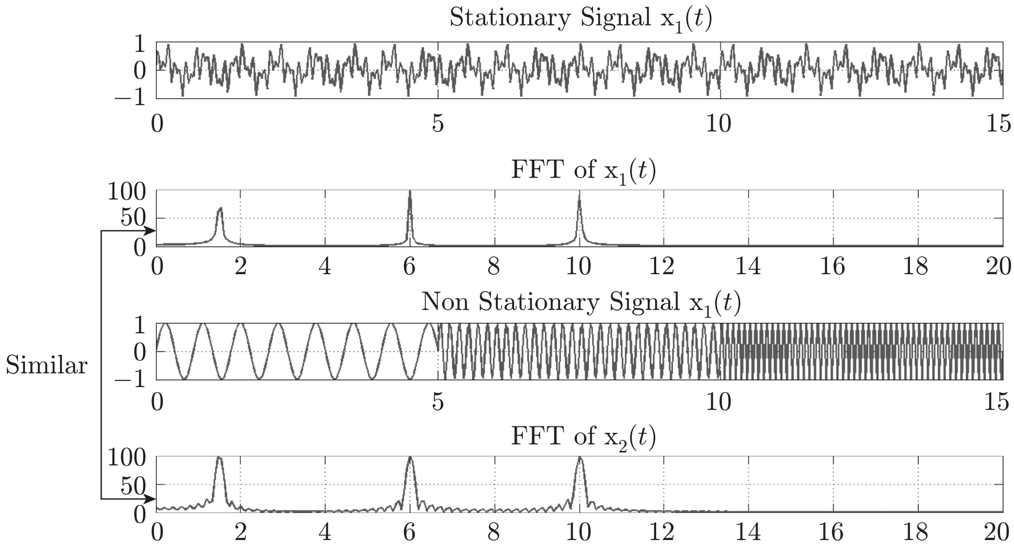

Figure 1.12 | Fourier Transform: difficulty in handling non-stationary signals

Fourier transform can not handle the non-stationary signals because it is governed by 'Uncertainty Principle'. The subsequent sections will bring out this point systematically.

1.4.6 Inability of Simultaneous Time and Band Limitedness

According to the theorem based on the Uncertainty principle of Fourier transform, a non-zero function cannot be both time limited and band limited at the same instance. Basically, this means that a non-zero function cannot be compactly supported in both the domains simultaneously. Now, a function is said to be compactly supported if it has a finite support; for example, a rectangular pulse ranging from point a to b on real line is compactly supported. On the contrary, the Gaussian function which extends throughout the real line is not a compactly supported function. We will prove the result for a class of functions in L_1 space and then extend the proof for a general class L_P where $1 < P < \infty$.

Background of the proof: Let us first recall the basics before we study other tools applied.

Fourier transform

Fourier transform provides a way to look at the signal from its frequency domain. Fourier transform relies on the principle that a signal can be represented by the linear combination of sine waves, and their respective frequencies together constitute the frequency domain of the signal. Further, we can move to complex domain since $\sin(t) = \dfrac{e^{jt} - e^{-jt}}{2j}$. Mathematically, Fourier transform projects the function onto the complex exponentials. Thus, Fourier transform of a function $x(t)$ is given as:

$$X(\Omega) = \int_{-\infty}^{+\infty} x(t)e^{-j\Omega t}\, dt$$

NOTE:

For a function, there exists a Fourier transform only if the function is absolutely integrable i.e. $x(t)$ is said to have a Fourier transform only if $\int_{-\infty}^{+\infty} |x(t)|\, dt$ is finite.

Space $L_P(\mathbb{R})$ and Norm

A function $x(t)$ lies in space $L_P(\mathbb{R})$ if $\left\{\int_{-\infty}^{+\infty} |x(t)|^P\, dt\right\}^{\frac{1}{P}}$ is finite, and the term is called as the L_P norm of the function $x(t)$ where $1 \le P \le \infty$. With the context of our discussion let us see an example of function with finite L_1 norm:

We see that, for above given function the absolute integral of the function is equal to 1 and thus it belongs to space L_1. Also, it can be proved that the function exists in space L_P in general for $1 \le P < \infty$. On the other hand $\sin c$ function does not have a finite absolute integral and, therefore, does not belong to space L_1.

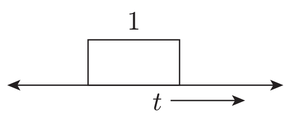

Figure 1.13 | Function belonging to $L_1(\mathbb{R})$

Hölders Inequality

Aforesaid, in this proof we will consider the functions in L_1 space and then extend the proof more general class of functions in spaces L_P where $1 < P \le \infty$. Now, for time to limited functions it can be proved that if a function belongs to L_P where $1 < P \le \infty$ then it also belongs to space L_1 using Hölders Inequality.

Mathematically,

$$f \in L_P,\ for\ \ p \in (1, \infty)$$

$$\Rightarrow f \in L_1$$

Hölders Inequality states that for two functions $f(t)$ and $g(t)$;

$$\int_{-\infty}^{+\infty} f(t)g(t)dt \le \left(\int_{-\infty}^{+\infty} |f(t)|^p\, dt\right)^{\frac{1}{p}} \left(\int_{-\infty}^{+\infty} |g(t)|^q\, dt\right)^{\frac{1}{q}} \tag{1.13}$$

The above condition holds true only if $\frac{1}{p} + \frac{1}{q} = 1$ and $p, q > 0$. The above result of Hölders Inequality can be obtained using Young's Inequality and generalized AM-GM Inequality stated as below.

Young's Inequality

Young's inequality states that, given two positive real numbers a and b,

$$\begin{aligned} a, b &\in \mathbb{R}^+ \\ ab &\le \frac{a^p}{p} + \frac{b^q}{q} \end{aligned} \tag{1.14}$$

Given,

$$\frac{1}{p} + \frac{1}{q} = 1$$

This can be proved using the generalized AM-GM Inequality as explained below.

Arithmetic Mean- Geometric Mean (AM-GM) Inequality

AM-GM inequality states that, given two positive real numbers a and b with weights α_1 and α_2, following equations holds.

$$\frac{\alpha_1 a+\alpha_2 b}{\alpha_1+\alpha_2} \geq \left(a^{\alpha_1} b^{\alpha_2}\right)^{\frac{1}{\alpha_1+\alpha_2}}$$

Now, substituting $a = a^p$, $b = b^q$, $\alpha_1 = p$ and $\alpha_2 = q$ and knowing that $\frac{1}{p}+\frac{1}{q}=1$, we get Eq. (1.14) i.e. Young's inequality.

Thus, using the Hölders Inequality as stated in Eq. (1.13), by selecting appropriate function $g(t)$ we can prove that function $f(t)$ which belongs to $L_p(\mathbb{R})$ also belongs to $L_1(\mathbb{R})$. Now, to prove this consider a function spread over finite interval C which belongs to space L_p, $1 < p < \infty$. Since the function $f(t)$ belongs to space L_p its p^{th} norm is finite i.e. $\left(\int_{-\infty}^{+\infty} |f(t)|^p \, dt\right)^{\frac{1}{p}}$ is finite. The function $f(t)$ can be similar to that shown in Fig. 1.14. We select $g(t)$ as shown in Fig. 1.15 to get the result.

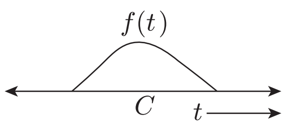

Figure 1.14 | **Function** $f(t)$

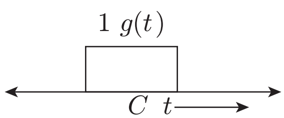

Figure 1.15 | **Function** $g(t)$

Now putting down the Hölders Inequality for these two functions as follows:

$$\begin{aligned}
\|f\|_p \|g\|_q &\geq \int_C |f(t)g(t)| \, dt \\
\int_C |f(t)| \, dt &\leq \left(\int_C |f(t)|^p \, dt\right)^{\frac{1}{p}} \left(\int_C dt\right)^{\frac{1}{q}} \\
\int_C |f(t)| \, dt &\leq \left(\int_C |f(t)|^p \, dt\right)^{\frac{1}{p}} |C|^{\frac{1}{q}}
\end{aligned}$$

Since the right side of the above equation is the product of L_p norm which is finite and another finite quantity the net result on the RHS is finite. Also, since the LHS is less than or equal to RHS we can infer that the L_1 norm of $f(t)$ is finite. Thus, we have proved our statement that if a function belong to space $L_p(\mathbb{R})$, where $1 < p < \infty$, then it also belongs to space L_1.

With this background let us now know some tools which will help us in proving the final result.

Tools for the proof

Fourier transform of *rect*(a)

The Fourier transform of the *rect*(a) function, shown in Fig. 1.16, is

$$\begin{aligned}\mathbb{F}(rect(a)) &= \frac{2}{\Omega}\sin\left(\frac{a\Omega}{2}\right)\\ &= \frac{1}{\pi f}\sin(\pi a f)\\ &= a\sin c(af)\end{aligned}$$

Where, Ω = angular frequency and f = Hertz frequency.

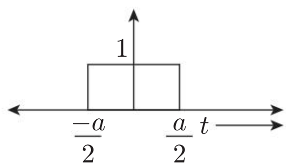

Figure 1.16 | **Function** *rect*(a)

Vandermonde Matrix

A Vandermonde matrix is defined as

$$V_{i,j} = a_i^{j-1}$$

$$V = \begin{bmatrix} 1 & a_1 & a_1^2 & \cdots & a_1^{n-1} \\ 1 & a_2 & a_2^2 & \cdots & a_2^{n-1} \\ \vdots & \vdots & \vdots & \ddots & \vdots \\ 1 & a_m & a_m^2 & \cdots & a_m^{n-1} \end{bmatrix}$$

Where, m and n are the number of rows and columns respectively.

Further, whenever we need to solve any linear equation of the form $A\bar{x} = \bar{y}$, we always look for the invertibility of matrix A so that we can solve for $\bar{x}$ as $\bar{x} = A^{-1}\bar{y}$. Now the Vandermonde matrix have very

**Example 1.4.8 — MATLAB code: Fourier for non-stationary signals. **

```
%**********************************************
%**********************************************
% MATLAB code to understand Taylor series approximations
% using different no of coeffs: To be accompanied with book on
```

```
% Multiresolution and Multirate Signal Processing
% by Dr V M Gadre and Dr A S Abhyankar
%**********************************************
%**********************************************
clear all;close all;clc;

f = 50;  % In India 50Hz is the frequency for Electric Supply
% Let's define what we time we wish to observe the signal
tmin = -0.04; % continuous min time
tmax = 0.04; % continuous max time
t = linspace(tmin, tmax, 400); % Let's create the time axis
% Let's create continuous time domain signal
cont_func = cos(2*pi*f*t);
% Let's plot the continuous function
% In case of no aliasing -- these two will get superimposed
% In case of aliasing -- these two will be different
% Thus aliasing indicates non-unique representation
% Aliasing also indicates incorrect reconstruction from samples.

% End
```

good properties by which it can be shown to be invertible once we know the entries. This is because the determinant of a Vandermonde matrix can be proved to be of the form

$$det(V) = (-1)^{m\frac{m-1}{2}} \cdot \prod_{1 \le i < j \le m} (a_i - a_j)$$

Therefore, until all the entries of a particular row are distinct the value of $det(V)$ will not be equal to zero and V will be invertible.

Review of the proof

Consider a very smooth function which is compactly supported. For example, we can have the following function:

$$\begin{aligned} f(x) &= e^{\frac{-1}{1-x^2}} \qquad |x| \le 1 \\ &= 0 \qquad\qquad else \end{aligned}$$

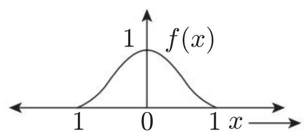

Figure 1.17 | Example of a smooth and compactly supported function

The function has the structure as shown in Fig. 1.17. It can be shown that all the derivatives of $f(x)$ exist in the interval $-1 \le x \le 1$ with all derivatives $f^p(x) \to 0$ as $|x| \to 1$. Now, we need to find if we can have a compactly supported spectrum for such well-behaved time-limited function. Let us look at an existing proof.

For any general well-behaved function in space $L_1(\mathbb{R})$ similar to above example we have the Fourier transform given by:

$$F(\Omega) = \int_{-\infty}^{+\infty} f(t) e^{-j\Omega t} dt$$

```
figure(1); subplot(131); plot(t,cont_func,'b','LineWidth',2)
xlabel('time (seconds)'); ylabel('Continuous Signla (Max Frequency
= 50 Hz)'); title('(a)'); pause;

% Now let's convert the signal into a discrete signal
fs = 110; % Sampling Frequency
% Per Sampling Theorem fs should be >= 100 Hz
Ts = 1/fs; % Sampling time instances
nmin = ceil(tmin / Ts); % Discrete min time
nmax = floor(tmax / Ts); % Discrete max time
n = nmin:nmax; % Discrete instance range
samples = cos(2*pi*f*n*Ts); % Discrete Samples
% Let's plot the samples
figure(1); subplot(132); plot(t,cont_func,'b','LineWidth',2) hold
on plot(n*Ts,samples,'.','LineWidth',3) plot(n*Ts, samples,
'o','LineWidth',3) xlabel('time (seconds)'); ylabel('Sampled
```

```
Signal (fs=110Hz)'); title('(b)'); pause;
% Let's calculate the reconstruction frequency
df=(fs-f); if (df<f)
    df=df;
else if (df == 2*f)
        df=2*f;
    else if (df>f)
            df = f;
        end
    end
end
d_func = cos(2*pi*df*t); %Let's reconstruct using df
%Let's plot the reconstructed signal
figure(1); subplot(133); plot(n*Ts,samples,'.','LineWidth',3) hold
on; plot(t,cont_func,'b','LineWidth',2) plot(n*Ts, samples,
'o','LineWidth',3) plot(t, d_func, 'r','LineWidth',2) xlabel('time
(seconds)'); ylabel('Blue=Signal, Red=Reconstructed, No
Aliasing!'); title('(c)');
%hold on
hold off

% Original signal is plotted in blue
% Reconstructed signal is plotted in red
```

Now, we will also assume that the function is band-limited and show that our assumption will hold only for a zero function. Therefore, with the assumption we have

$$\begin{aligned} |F(\Omega)| &\leq \int_{-\infty}^{+\infty} |f(t)||e^{-j\Omega t}|dt \\ &\leq \int_{-\infty}^{+\infty} |f(t)|\,dt \\ &\leq L_1 \; norm \; of \; f(t) \end{aligned}$$

Now, if we take the derivative of $f(t)$, it can be represented as,

$$f'(t) = j\Omega\int_{-\infty}^{+\infty} f(t)e^{-j\Omega t}dt$$

In the above equation, since function is bounded in both time and frequency, we get a finite bound on the magnitude of $f'(t)$. Similarly, we can show that all the derivatives of $f(t)$ have finite bound on their magnitude. Further, we can express function $f(t)$ in the form of a McLauren series as:

$$f(t) = f(0) + tf'(0) + \frac{t^2}{2!}f''(0) + \cdots$$

Now as per our assumption all the above derivatives of $f(t)$ are finite and therefore above equation is essentially a power series expansion, i.e.

Exercises

Exercise 1.1

Exercise 1.1 What is Short Time Fourier Transform (STFT) and its drawbacks as compared to wavelet transform.
Hint: In STFT, signal is first windowed using different type of window functions like Triangular window, Rectangular window, Gaussian window, etc. Now, Fourier Transform of resulting windowed signal is taken. This gives the STFT of signal for particular time. As window slides along time axis, so basically STFT maps input signal $x(t)$ into two dimensional function in a time-frequency plane or tiling.

So, drawback of STFT is that once a window has been chosen for STFT, then time-frequency resolution is fixed over the entire time-frequency plane or say STFT moves a tile of constant shape in the time-frequency plane. But in case of wavelet transform, the time resolution becomes arbitrarily good at high frequencies, while the frequency resolution becomes arbitrarily good at low frequencies. In other words we can say that CWT moves a tile of variable shape but constant area which is governed by time-bandwidth product.

Exercise 1.2

What is uncertainty principle? Explain it for different domains.
Hint: The basic uncertainty principle also called Heisenberg Uncertainty Principle is that, the position and velocity of an object cannot both be measured exactly, at the same time. Uncertainty principle derives from the measurement problem, the connection between the wave and particle nature of quantum objects. The uncertainty principle is alternatively expressed in terms of particle's momentum and position. the momentum of a particle is equal to the product of its mass times its velocity. The principle applies to other related (conjugate) pair of observables, such as energy and time. Finally, uncertainty principle states that exact knowledge, of complementarity pairs (position, energy/velocity, time) is impossible.

The uncertainty principle for time-frequency pair will be studied further in detail in this course.

Exercise 1.3

What are basis functions? What type of basis function is used in Fourier Transform? How is it different from the basis functions used in Haar multiresolution analysis?
Ans. In mathematics, a basis function is an element of a particular basis for a function space. Every function in the function space can be represented as a linear combination of basis functions, just as every vector in a vector space can be represented as a linear combination of basis vectors.

Complex exponential functions form the basis for Fourier analysis. They are extremely smooth functions. On the other hand, Haar analysis uses discontinuous functions as basis, i.e. every signal is represented as a linear combination of discontinuous functions.

Exercise 1.4

If sum and difference of two vectors $\vec{a}$ and $\vec{b}$ are perpendicular to each other. Find the relation between two vectors.

Hint: The sum $\vec{a}+\vec{b}$ and difference $\vec{a}-\vec{b}$ are perpendicular to each other. Hence, their dot product should be equal to zero.

Exercise 1.5

Find a function $f(t) = a + bt$ that is perpendicular to the another function $g(t) = 1 - t$ in the interval [0,1].

Hint: If the functions are perpendicular to each other, then their dot product is zero.

$$\langle f, g\rangle = \int_0^1 (a+bt)(1-t)dt$$

$$\int_0^1 (a + bt - at - bt^2)dt \quad = 0$$

$$a + \frac{b}{2} - \frac{a}{2} - \frac{b}{3} \quad = 0$$

$$\frac{a}{2} + \frac{b}{6} \quad = 0$$

So, we can take $f(t) = 1 - 3t$

Exercise 1.6

Determine the number of dimensions in the following sequences:

(a) (....,0,0,4,5,3,1,6,0,0....)

(b) (....,0,0,4,0,0,1,0,9,6,0,0....)

Hint:

(a) The dimension of a sequence is the the length of support of a sequence. In this example, a sequence has 5 non-zero samples and hence it has a dimension of 5.

(b) Since the dimension of a sequence is the length of support of a sequence, a sequence has a dimension 7. Note that this also considers the 3 zero samples which have non-zero samples on their either left or right hand sides.

Exercise 1.7

What is Wavelet? How Wavelet transform is different than Fourier transform?
Hint: Refer Section 1.4 of this chapter.

Exercise 1.8

What are orthogonal vectors? How functions, sequences and vectors are relate?
Hint: Refer Chapters 1 and 4 of this book.

Exercise 1.9

What is the concept of dot or inner product? How this product is different than cross or outer product? Describe properties of dot product? What is the significance of dot product in Transforms?
Hint: Refer Section 1.4 of this chapter.

Exercise 1.10

Explain what is uncertainty principle? How this principle revolves around evolution of wavelets from conventional transforms?
Hint: Refer Chapters 7 to 10 of this book.

Exercise 1.11

Exercise 1.11 What is Parseval's Theorem? Explain its applications?
Hint: Refer Section 1.4 of this chapter.

Exercise 1.12

Explain how Fourier Transform produces peaks corresponding to the frequencies present in the signal under consideration? Explain using concept of dot product?
Hint: Refer Section 1.4 of this chapter.

Exercise 1.13

Explain limitations of Fourier Transform in handling non-stationary signals?
Hint: Refer Section 1.4 of this chapter.

Exercise 1.14

What are multirate systems of doing signal analysis? Describe sampling theorem and explain what is the role of sampling theorem in design of multirate systems?
Hint: Refer Section 1.4 of this chapter.

Chapter 2

The Haar Wavelet

Introduction

The Haar wavelet

L_k norms of $x(t)$

Haar MRA (Multi Resolution Analysis)

Axioms of MRA

Theorem of MRA

2.1 | Introduction

In this chapter we shall discuss the Haar Multiresolution Analysis about which we had briefly discussed previously. Haar was a mathematician, who gave a radical idea that any continuous function can be represented in the form of discontinuous functions, and by doing so one can go to any level of continuity that one desires. This is the central idea in the 'Haar way' of representing functions. We start from a very discontinuous function and make it smoother by adding more and more discontinuous functions (which is in a way some additional information) to it until we reach arbitrarily closer to the continuous function that we are trying to approximate. This idea is opposite to the idea of the Fourier transform. One can recall that in Fourier transform the discontinuous function is represented in the form of smooth continuous function.

Alfred Haar

(Hungarian: *Haar Alfréd*; 11 October 1885, Budapest 16 March 1933, Szeged) was a Hungarian mathematician. In 1904 he began to study at the University of *Göttingen*. His doctorate was supervised by David Hilbert. The Haar measure, Haar wavelet, and Haar transform are named in his honor. The Haar sequence is now recognised as the first-known wavelet basis and extensively used as a teaching example.

Representation of the continuous function in the form of discontinuous function has its own importance. Let us look at an example to illustrate this.

Example 2.1.1—Dyadic wavelets picture example.

Information is generally represented in the form of bits. While transmitting an audio piece we convert a extremely smooth audio pattern into a highly discontinuous stream of bits. When these bits are transmitted over a communication channel a discontinuity is introduced every time a bit changes. This discontinuity may be in the function or its derivatives. Thus Haar's way of representation is very useful for us today.

Let us first start building the idea of 'wavelets' or what are more specifically called as 'dyadic' wavelets (explained later). We shall start with the 'Haar' wavelet. For that let us consider how we represent a picture on a screen. Every picture is enclosed by a boundary. Contents of the picture such as a person or a tree are enclosed within the boundary. The natural scene is inherently continuous. In order to represent it in a computer we divide the area of the image into very small subareas. These small rectangular sub-areas are called 'picture elements' or 'pixels'. Now if we make 512 divisions on the vertical and also on the horizontal then we say that we have a '512 × 512' image. We can also have images at other resolutions.

Now consider an image of dimension 204 × 92 pixels. We have 204 divisions on one side and 92 divisions on the other. There exists something called as the piecewise constant representation of the image. What we do is represent each piece (here pixel) by a constant number which represents the average intensity and colour in that area. As we increase the number of divisions the area of each pixel goes on decreasing. Thus as we go from a '512 × 512' image to a '1024 × 1024' image, the area of a pixel becomes one fourth. We introduce more information by increasing the number of divisions. Evidently as we increase the number of pixels, we go closer and closer to the original picture. The effect of changing the resolution of an image can be seen in Fig. 2.1.

Thus one may say that '*the smaller the pixel area the larger the resolution*'. This can be seen easily from the picture below (Fig. 2.1). But the idea that we are trying to build is not quite the idea of the 'Haar MRA'. The Haar MRA does something deeper.

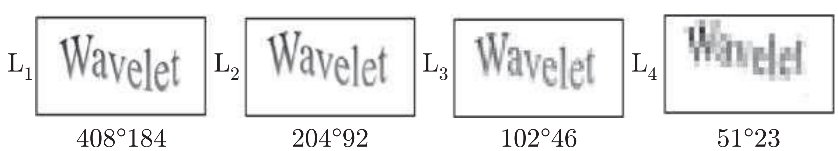

Figure 2.1 | Resolution difference

Example 2.1.2—Audio signal piecewise constants.

The same can be done of an audio signal. Consider an audio output which is a one dimensional signal and can be plotted against time.

Let the output be as shown in Fig. 2.2.

Since this is now '1 dimensional' we divide the time axis in small intervals of size *'T'*. We now represent the function values in each interval by a constant number. Now, it is convenient to choose this number to be the average of the function values in that time interval. By doing so we are trying to represent a continuous function by a discontinuous one. The average C_0 over the strictly open interval $(0,T)$ can be computed as

$$C_0 = \frac{1}{T}\int_0^T x(t)\,dt$$

(Open interval is the interval excluding end points). For any interval of size *T* we have

$$C_n = \frac{1}{T}\int_T x(t)\,dt$$

Similarly, for interval of size *T/2*,

$$C_{n,T/2} = \frac{1}{T/2}\int_{\frac{T}{2}} x(t)\,dt$$

If a time interval of length *'T'* is divided into two time intervals of length *T/2*, we get two averages computed by the above formula. Figure 2.3 clarifies this concept further. Now, consider

$$\begin{aligned} A_T &= \frac{1}{T}\int_0^T x(t)\,dt \\ A_{1,T/2} &= \frac{2}{T}\int_0^{T/2} x(t)\,dt \\ A_{2,T/2} &= \frac{2}{T}\int_{T/2}^{T} x(t)\,dt \end{aligned}$$

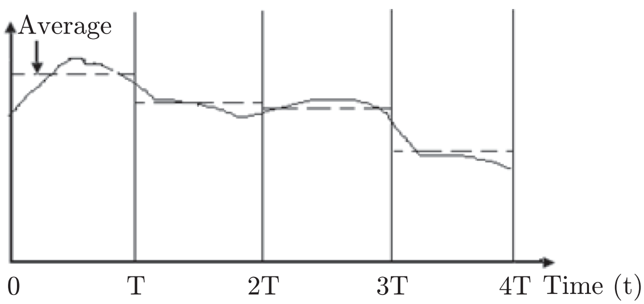

Figure 2.2 | **Audio signal**

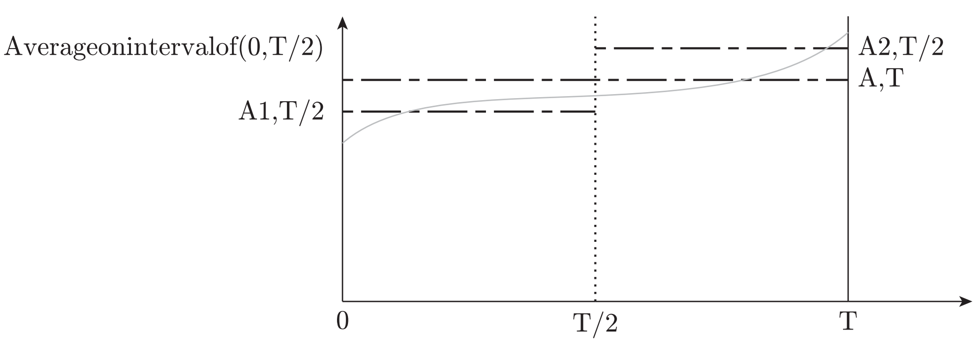

Figure 2.3 | **Average of T and T/2**

A_T is the average of the function on the interval of size 'T' while $A_{1,T/2}$ and $A_{2,T/2}$ are the averages on the two half intervals of size '$\frac{T}{2}$' each. The key concept in Haar multi resolution analysis is to relate these three terms $(A_T, A_{1,T/2}, A_{2,T/2})$ and it is in that relationship that the Haar wavelet is hidden. It can be easily observed that, the average of $A_{1,T/2}$ and $A_{2,T/2}$ gives A_T, i.e.

$$A_T = \frac{A_{1,T/2} + A_{2,T/2}}{2}$$

Thus a function can be approximately represented by addition of **piecewise constant** functions. We can go on reducing the interval by half to whatever degree of accuracy we desire. This is illustrated in the Fig. 2.4.

Each different line (dot dash, dash-dash, bold line with squares) represents a piecewise approximation in its own way, with different resolution. Let the function represented in Fig. 2.4 using dot-dash line be $f_1(t)$ and the bold line with squares be $f_2(t)$ then, the additional information obtained by representing the signal as $f_2(t)$ is given by

$$f_2(t) - f_1(t)$$

which is shown in Fig. 2.5.

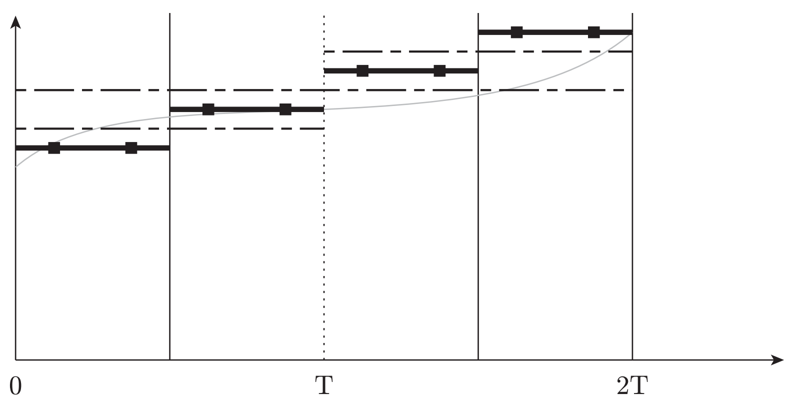

Figure 2.4 | **Intervals of 2T,T and T/2**

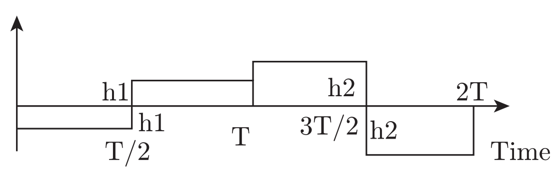

Figure 2.5 | $f_2(t) - f_1(t)$

2.2 | The Haar Wavelet

To understand 'Haar Wavelet', consider the function shown in Fig. 2.6. This function is represented as $\psi(t)$. By usingscalar multiplication and delaying, we can see that $f_2(t)-f_1(t)$ can be reconstructed from $\psi(t)$. Thus,

$$f_2(t)-f_1(t)=-h_1\times\psi(t/T)+h_2\times\psi\left(\frac{t-T}{T}\right)$$

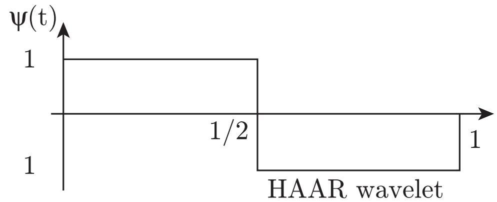

Figure 2.6 | $f_2(t)-f_1(t)$

here h_1 and h_2 are as shown in Fig. 2.5. The function $\psi(t)$ is called the **Haar wavelet**. In general when we start with $\psi(t)$ we can construct a function $\psi\left(\frac{t-\tau}{s}\right)$ as a building block, where *'s'* is positive real and τ should be real. The variable *'s'* dilates $\psi(t)$ and '$/$' translates $\psi(t)$. The variable τ is called the **translation index** and the variable *'s'* is called the **dilation variable**. If we consider time intervals of length *T/2* for piecewise constant approximation then the value of *'s'* is *T/2*, if length of time interval is *T* then $s = T$. It means the single function $\psi(t)$ allows you to bring in resolution step-by-step to any level of detail. Thus, by dividing *T* into smaller subdivisions of *T/2, T/4* and so on, any function $x_a(t)$ can be made **arbitrarily close** to original function $x(t)$. If $x_e(t)$ denotes the error due to approximation, it can be expressed as

$$x_e(t)=x(t)-x_a(t)$$

$$\zeta=\int_{-\infty}^{\infty}|x_e(t)|^2\,dt$$

Where, ζ is the squared error. What we mean by arbitrarily close is that for any fixed value of $\zeta\,(>0)$, we can always find a positive integer **m** such that a piecewise constant approximation of $x(t)$ with an interval of $T/2^m$ satisfies the requirement of ζ.

It must be noted that any signal can be represented in piece wise constant form **if and only if** it has **finite energy**.

2.3 | L_k Norms of $x(t)$

A function with finite energy content implies and is implied by its L_2 norm being finite. So what is this L_2 norm? The L_2 norm of a signal is defined as

$$L_2 \text{ norm of } x(t)=\left[\int_{-\infty}^{\infty}|x(t)|^2\,dt\right]^{\frac{1}{2}}$$

In general, we can define the L_p norm of $x(t)$ as

$$L_p \text{ norm of } x(t)=\left[\int_{-\infty}^{\infty}|x(t)|^p\,dt\right]^{\frac{1}{p}}$$

where p is any real number. The L_∞ norm of $x(t)$ is defined as

$$L_\infty \text{ norm of } x(t) = \lim_{p\to\infty}\left[\int_{-\infty}^{\infty} | x(t) |^p \, dt\right]^{\frac{1}{p}}$$

2.3.1 Significance of L_∞ Norm

As the value of p increases, large values in $x(t)$ are being emphasized. This happens because for a large p, the integral will have a large contribution from higher values in $x(t)$.

$L_2(\mathbb{R})$ is said the to be the space of all **real** functions whose L_2 norm is finite. The word 'space' is used with the intent that if we take a linear combination of two or more functions in that set then we get back a function in that set. As we reduce the size of the individual time intervals previously considered, we said we could as close to the original function as we desire by reducing the error. This clearly means that L_2 norm of the error can be reduced to as small a value as we desire. The Fourier series allows us to do this for a reasonable class of functions.

The same kind of thing is happening here. Just on function $\psi(t)$ is able to take us as close as we desire to the function which we wish to approximate. And this is just one $\psi(t)$. The whole subject of wavelets allows us to build many such $\psi(t)$'s. Each time we improved the resolution by factors of '2' and, hence, the term 'dyadic' which represents steps of two was used in the beginning of the chapter. Thus the Haar wavelet is an example of a dyadic wavelet. In the following chapters we will mostly focus our attention on dyadic wavelets. Dyadic wavelets are the most easily designed, the best and most easily implemented and also the best understood.

After understanding the 'Haar wavelet' and the way in which the Haar MRA is constructed many concepts of multiresolution analysis would become clear. In this chapter, we brought out the idea of the Haar wavelet explicitly. We now know that dialates and traslates of this function can capture information in going from one resolution to the next level of resolution in steps of two each time. So in terms of the spaces we are actually going from one subspace of $L_2(\mathbb{R})$ to the next subspace.

The next task is to see how the dilates and translates of Haar wavelet help us in adding more and more to the subspaces in going from a coarser subspace all the way to $L_2(\mathbb{R})$ on one side and all the way down to a trivial subspace on the other (also referred to as the ladder of subspaces). Further, we will bring out the idea of the basis of these subspaces and how the Haar wavelet helps in capturing the difference subspace.

2.4 | Haar MRA (Multi Resolution Analysis)

As we got a basic instinct about Haar MRA in the previous section, let us understand the fundamental concepts surrounding it in next few sections. The underlying principle of wavelets is to capture incremental or so called additional information in a function. The piecewise constant approximation of a function is a representation of the function at different resolutions.

R For understanding this, consider an example of an onion. Let the outermost shell be of the maximum resolution. Now, the job of wavelet function is to *peel-off* or to take out a particular shell of that onion. Thus, we are essentially peeling-off shell-by-shell using different dilates and translates of a wavelet. Figure 2.7 illustrates the concept of nested subspaces. So, it goes like this,

Different dilates $\xrightarrow{\text{corresponds to}}$ different resolutions.

Different translates $\xrightarrow{\text{takes us along}}$ same resolution corresponding to a given dilate.

The idea of wavelets may be introduced using an example of the Haar wavelet. The Haar wavelet is a dyadic wavelet, i.e. the piecewise constant approximation is defined in steps of powers of two at a time. The wavelet captures the incremental information between two consecutive levels of resolution. In other words, Haar wavelet keeps on retreiving additional information as we move on towards higher and higher resolution.

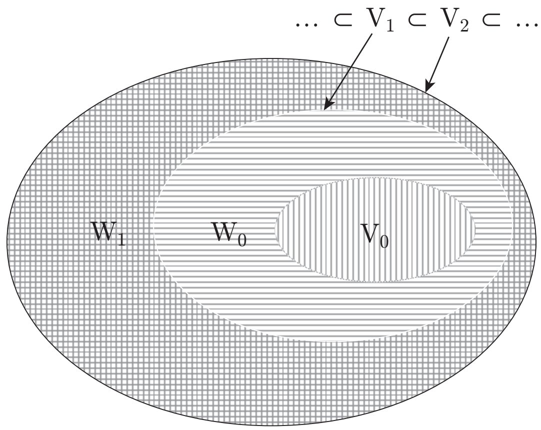

Figure 2.7 | Nested subspaces

Example 2.4.1

The idea of expressing a function at different resolutions may be explained by considering an example. Observe Fig. 2.8, it shows the signal at high resolution in dotted line, its piecewise constant approximation over unit intervals in blue and that over intervals of length 0.5 in green. This piecewise constant approximation is done in the same way as was discussed in the previous lecture, i.e. by taking average value of the function over the dyadic intervals.
The corresponding function which gives the incremental information between the two approximation levels is shown in Fig. 2.9. This was the case of a 1-dimensional function.

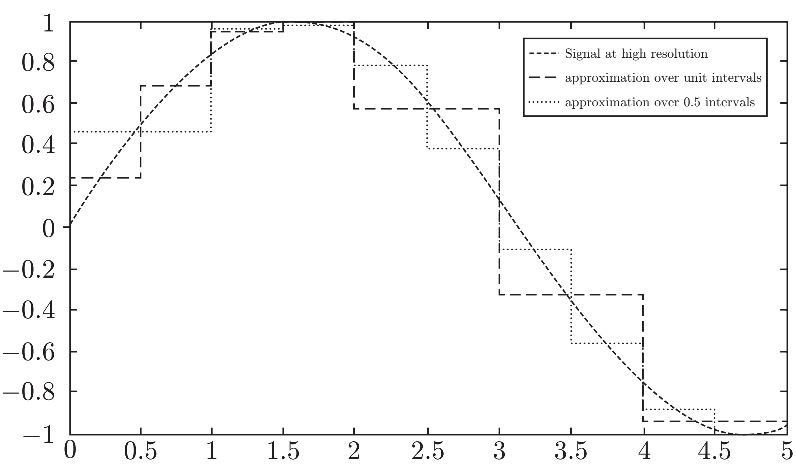

Figure 2.8 | Signal at different resolution

Example 2.4.2

The same idea may be extended to two dimensions as well. In Fig. 2.10, Figure 2.10a is the 2-dimensional image at a certain level of resolution. Figure 2.10b(i) is the image at 0.5 resolution of Fig. 2.10(a). Fig. 2.10b(ii), 2.10b(iii) and 2.10b(iv) gives the additional information in the vertical, horizontal and diagonal directions respectively (also known as 'bands').

Thus, the idea of wavelets is analogous to an object with many shells. Wavelet translates at the maximum resolution, takes out the outermost shell, the next shell is taken out at the next lower resolution and so on. Hence, we are essentially 'peeling off' shell by shell using different dilates and translates of the wavelet function. The dilation takes us to the next level of resolution, while translation takes us along a given resolution. Now, let us look over the focal point for further operations on wavelet to perform.

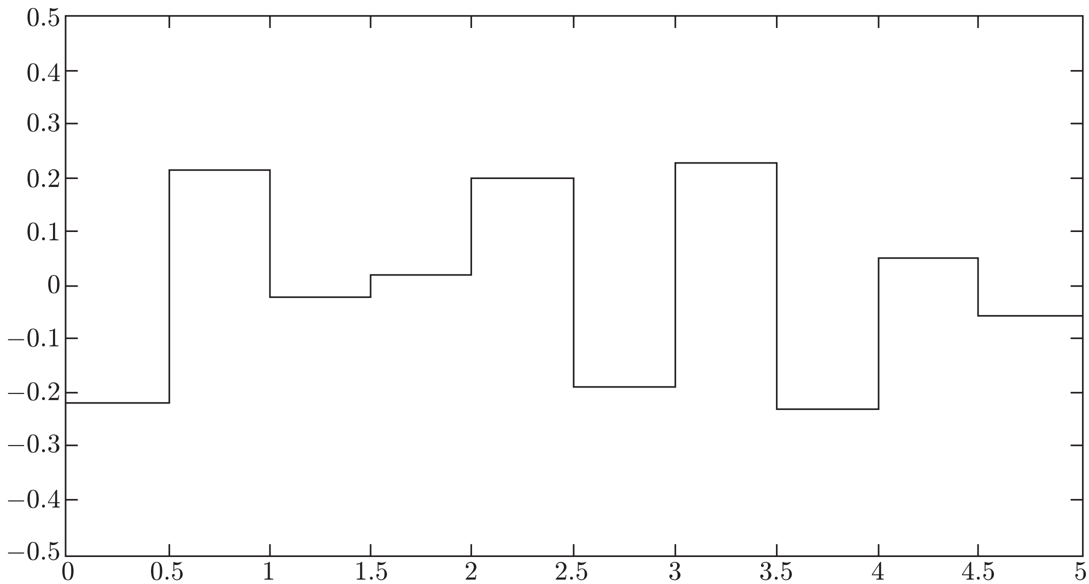

Figure 2.9 | Incremental information

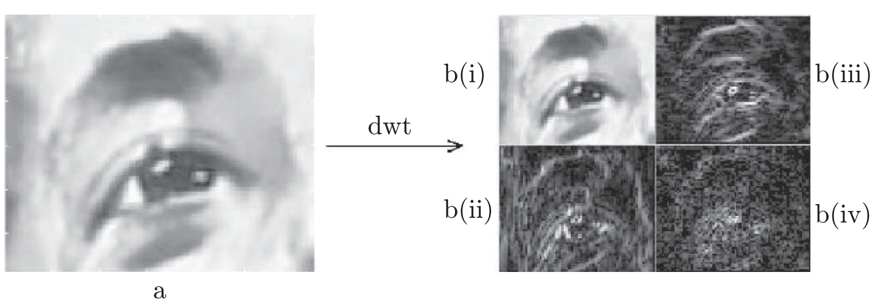

Figure 2.10 | 2D example, showing image 0.5 resolution and incremental information

R **Focal Point:-** Piecewise constant approximation on unit intervals.
Without any loss of generality, let us begin with piecewise constant approximation at a resolution of unit length. The choice of unit interval is entirely one's own choice.

Now a question arises at this point. What function $\phi(t)$ is such that its integer translates can span the space of piecewise constant functions on the standard unit intervals? As we saw in linear algebra or more generally functional analysis, the span of a set of vectors in a vector space is the intersection of all subspaces containing that set. Here, space refers to a linear space of functions, that is, a set of functions which is closed under linear combinations. In other words, the linear combination of these functions belong in the same set/space as of the function itself. Here, we only consider finite linear combinations. The same ideas may be extended for infinite linear combinations.

A set V_0 is defined as follows,

V_0 : { $x(t)$, such that $x(\cdot) \in L_2(\mathbb{R})$ is piecewise constant on interval $]\, n, n+1\, [\, , \forall \quad n \in \mathbb{Z}$ }. The subscript '0' is used for V_0 because of piecewise constancy on interval of size 2^{-0}.

Similarly, V_1 is defined as,

V_1 : { $x(t)$, such that $x(\cdot) \in L_2(\mathbb{R})$ is piecewise constant on all $]\, 2^{-1}n, 2^{-1}(n+1)\, [\, , \forall \quad n \in \mathbb{Z}$ }.

V_1 is the set of functions piecewise constant over the interval of 2^{-1}.

In general V_m is the set of functions which is piecewise constant over the interval of size 2^{-m}.

V_m : { $x(t)$, such that $x(\cdot) \in L_2(\mathbb{R})$ is piecewise constant on all $]\, 2^{-m}n, 2^{-m}(n+1)[\, , \forall \quad n \in \mathbb{Z}$}.

Example 2.4.3—Function.

Function $x(\cdot) \in V_2$. All function belonging to V_2 are piecewise constant over the interval of 2^{-2} i.e. 0.25. Figure 2.11(a) shows a function belonging to V_2. Here $x(t) \in V_2$ means $x(t) \in L_2(\mathbb{R})$. This implies that when squared sum of all the piecewise constant values of the function is carried out, it converge to a finite value.

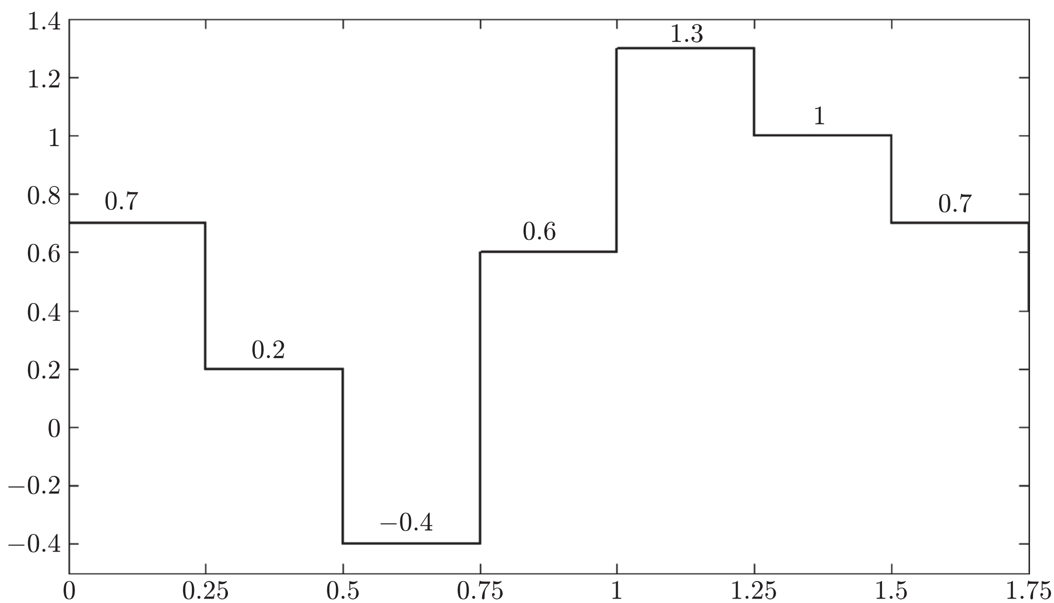

Figure 2.11(a) | **Example of a function belonging to V_2 space**

Example 2.4.4—Function belonging to V_{-1} space.

Any function belonging to V_{-1} is piecewise constant over the interval of length $2^{-(-1)}$ i.e. 2. Figure 2.11(b) shows a function belonging to V_{-1}.

Now, a function which is piecewise constant over the interval of 1 is also piecewise constant on the interval of 0.5 (as that constant value can be divided in two parts). Therefore, a function belonging to space V_0 also belongs to space V_1.

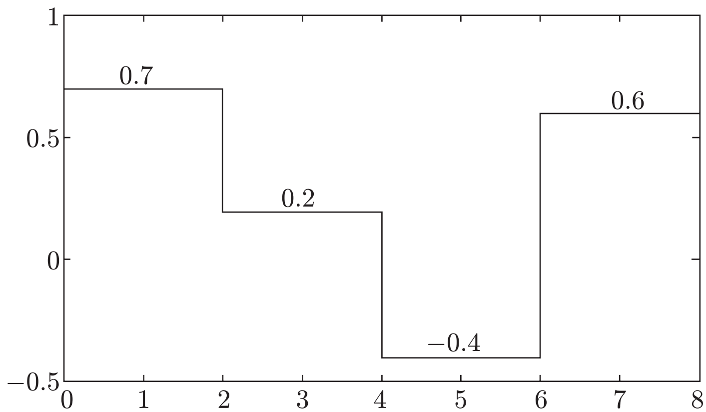

Figure 2.11(b) | Example of a function belonging to V_{-1} space

In general a function which belongs to space V_m also belongs to space V_{m+1}. Hence, a ladder of subspaces is implied as depicted below:

$$\ldots V_{-2} \subset V_{-1} \subset V_0 \subset V_1 \subset V_2 \ldots$$

Intuitively, we can see that as we move towards right, i.e. up the ladder we are moving towards $L_2(\mathbb{R})$

$$\{\overline{\cup V_m}\}_{m \in \mathbb{Z}} = L_2(\mathbb{R})$$

The expression above, if written without the coverline implies that it covers all the interior region whereas with closure (by coverline) ensures the covering of boundary patches too. This talk is not of much importance though but a slight glance at it is necessary.

When we go left towards the ladder? Movement towards leftwards implies, piecewise constant approximation over larger and larger intervals, as m in $2^{-(m)}$ goes more and more negative. Now, consider L_2 norm of function going towards leftwards:

$$\sum_{n=-\infty}^{\infty} |C_m(n)|^2 \, 2^{-m}$$

where $C(\cdot)$ is approximate coefficient at resolution 2^{-m}. Now, as we move towards left m becomes negative and $m \to -\infty$. Therefore L_2 norm is given by

$$2^{|m|}\sum_{n=-\infty}^{\infty}|C_m(n)|^2$$

If we require L_2 norm to converge, however for large $|m|$, $\sum_{n=-\infty}^{\infty}|C_m(n)|^2$ must be zero. That is $C_m(n)=0\ \forall\ n$.

Hence, movement towards left implies movement towards trivial subspace $\{0\}$.

$$\{\cap V_m\}_{m\in\mathbb{Z}}=\{0\}$$

One **important point** to note here is that trivial subspace is different then null subspace as null subspace do not contain any element.

We say that a set of functions $\{f_1, f_2, f_3, \ldots, f_k, \ldots\}$ span a whole space if any function in that space can be represented by the linear combination of these functions.

What is function $\phi(t)$ and how does its integer translates span V_0? We may consider function $\phi(t)$ as shown in Fig. 2.12.

Any function in V_0 can be expressed in the form

$$\sum_{n\in\mathbb{Z}} C_n\phi(t-n)$$

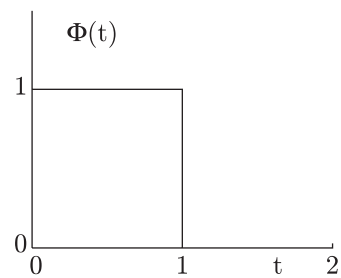

Figure 2.12 | Function $\phi(t)$

where C_n is piecewise approximation constants and $\phi(t-n)$ are the integer translates of $\phi(t)$. Figure 2.13 shows a function belonging to V_0. It can be expressed in terms of translates of $\phi(t)$ as shown below:

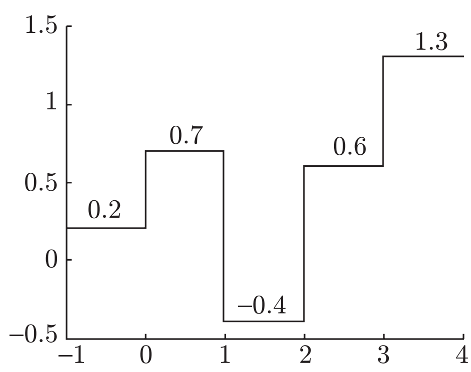

Figure 2.13 | Example of a function belonging to V_0

$$0.2\phi(t+1)+0.7\phi(t)-0.4\phi(t-1)+0.6\phi(t-2)+1.3\phi(t-3)$$

Hence any space V_m can be similarly constructed using a function $\phi(2^m t)$.

$$V_m = span\{\phi(2^m t - n)\}_{n,m\in\mathbb{Z}}$$

$\phi(t)$ is called as **scaling function**(Haar MRA), also known as 'Father function'. The ladder of subspaces

$$...V_{-2} \subset V_{-1} \subset V_0 \subset V_1 \subset V_2...$$

with these properties is called as Multi-Resolution Analysis (MRA).

2.5 | Axioms of MRA

R There exists a ladder of subspaces, $...V_{-2} \subset V_{-1} \subset V_0 \subset V_1 \subset V_2...$ such that

1. $\{\overline{\cup V_m}\}_{m\in\mathbb{Z}} = L_2(\mathbb{R})$
2. $\{\cap V_m\}_{m\in\mathbb{Z}} = \{0\}$
3. There exists $\phi(t)$ such that, $V_0 = span\{\phi(t-n)\}_{n\in\mathbb{Z}}$
4. $\{\phi(t-n)\}_{n\in\mathbb{Z}}$ is an orthogonal set.
5. If $f(t)\in V_m$ then $f(2^{-m}t)\in V_0, \quad \forall m\in\mathbb{Z}$
6. If $f(t)\in V_0$ then $f(t-n)\in V_0, \quad \forall n\in\mathbb{Z}$

2.6 | Theorem of MRA

R Given the axioms, there exists a $\psi(\cdot)\in L_2(\mathbb{R})$, so that $\{\psi(2^m t-n)\}_{m\in\mathbb{Z},n\in\mathbb{Z}}$ spans the $L_2(\mathbb{R})$.

The wavelet function $\Psi(\cdot)$ is also called as 'Mother function'.

Example 2.6.1—Spanning spaces.

In this illustration we will consider the vector space V_j spanned by the discrete scaling functions $\{\phi(2^j x-k)\}$, we use this span of the vector space to project any function say $f(x)$ such that $f_j(x)\in V_j$. The projected function can be mathematically encoded as,

$$f_j(x) = \sum_k \alpha_{j,k} 2^{\frac{j}{2}} \phi(2^j x - k) \tag{2.1}$$

In this equation, $\alpha_{j,k}$ depict the approximation values as it derives the components from the low pass scaling equation as given in equation,

$$\alpha_{j,k} = \int_{-\infty}^{\infty} f(x) 2^{\frac{j}{2}} \phi(2^j x - k) dx \tag{2.2}$$

where the set $\{\phi(2^j x - k)\}$ constitutes the basis. This $f_j(x)$ represents "approximation" of the signal $f(x)$. In most of the denoising applications this finds it's scope, and this set is orthogonal on $(-\infty, \infty)$ with respect to the translation, i.e.,

$$\int_{-\infty}^{\infty} 2^j \phi(2^j x - k)\phi(2^j x - k') = 0,\ k \neq k'$$

Also,

$$\int_{-\infty}^{\infty} \phi^2(2^j x - k) dx = \frac{1}{2^j} \tag{2.3}$$

since,

$$\int_{-\infty}^{\infty} \phi^2(2^j x - k) dx \quad = \frac{1}{2^j} \int_{-\infty}^{\infty} \phi^2(2^j x - k) \frac{1}{2^j} dx \tag{2.4}$$

$$= \frac{1}{2^j} \int_{-\infty}^{\infty} \phi^2(y - k) dy = \frac{1}{2^j} \tag{2.5}$$

where we used the change of variable $y = 2^j x - k$ and the fact that $\int_{-\infty}^{\infty} \phi^2(x) dx = 1$. So, the factor $2^{\frac{j}{2}}$ is for the normalization of $\phi(2^j x - k)$ to be $2^{\frac{j}{2}} \phi(2^j x - k)$, in order that we have,

$$\int_{-\infty}^{\infty} 2^{\frac{j}{2}} \phi(2^j x - k) 2^{\frac{j}{2}} \phi(2^j x - k') dx = \begin{cases} 0, & k \neq k' \\ 1, & k = k \end{cases} \tag{2.6}$$

We mention that the orthogonality of the scaling functions on $(-\infty, \infty)$ with respect to translations, is a very basic requirement in the (usual) definition of the multiresolution analysis.

We know that $V_j \in V_{j+1}$ as depicted in Fig. 2.14, and that V_{j+1} has better refinement than V_j. This "difference" (as only a refinement and not an approximation like $f_j(x)$ in (2.1) of the signal!) is a subset of V_{j+1} spanned by the discrete wavelets of the subspace W_j, $g_j(x) \in W_j$,

$$g_j(x) = \sum_k \beta_{j,k} 2^{\frac{j}{2}} \psi(2^j x - k) \tag{2.7}$$

$$\beta_{j,k} = \int_{-\infty}^{\infty} f(x) 2^{\frac{j}{2}} \psi(2^j x - k) \tag{2.8}$$

The basis $\{\Psi(2^j x - k)\}$ of this vector space W_j are always orthogonal to the scaling functions $\{\phi(2^j x - k)\}$ of V_j on $(-\infty, \infty)$,

$$\int_{-\infty}^{\infty} 2^{\frac{j}{2}} \phi(2^j x - k) 2^{\frac{j}{2}} \psi(2^j x - k') dx = \delta_{k,k'} \tag{2.9}$$

This relation resembles the orthogonality of the cosine functions to the sine functions of the Fourier series.

An example again is that of Haar function and their associated wavelets, where they are orthogonal even when $k = k'$, as can be seen from Fig. 2.15, where their product is, for example $\phi(x-1)\psi(x-2)$ or $\phi(x-1)\psi(x-1)$, is zero on $(-\infty,\infty)$. With this orthogonality of the basis of V_j to those of W_j, we have W_j as the orthogonal complement of V_j in V_{j+1}, $V_{j+1} = V_j \oplus W_j$. This can be done in the same way for $V_j = V_{j-1} \oplus W_{j-1}$, whereas $V_{j+1} = V_{j-1} \oplus W_{j-1} \oplus W_j$. Then this process can be continued until we reach a coarse (or blurred) resolution, for example, such that of V_0 with scale $\frac{1}{2^0} = 1$,

$$V_{j+1} = V_0 \oplus W_0 \oplus W_1 \oplus W_2 \oplus \ldots \oplus W_{j-1} \oplus W_j \tag{2.10}$$

Figure 2.15 shows schematically this relation with the blurred approximation in V_0 of scale $l_0 = 1$, and the refinements that are added to it by W_0, W_1, W_2 and W_3. We must note that, for example, V_1 and W_1 are two subspaces in V_2, where the W_2 basis span the difference between V_2 and V_1.

In the next illustration (Examples 2.6.2 and 2.6.3) we show the decomposition $f_0(x) \in V_0$ of the function $f(x) = x, 0 < x < 3$ as a rough approximation of $f(x)$, then wrote its decomposition (refinement) as $g_0(x) \in W_0$. We showed that the latter decomposition $g_0(x)$ is not an approximation to the function $f(x) = x, 0 < x < 3$, but it represented a helping hand to $f_0(x) \in V_0$ at the scale $l_0 = 1$ where it added to it a bit of a refinement to advance this approximation $f_0(x)$ to the more refined one $f_1(x) \in V_1$ at the smaller scale $l_1 = \frac{1}{2}$. This is the essence of W_0 being the orthogonal complement of V_0 in V_1. Both V_0 and W_0 are subspaces of V_1 and $V_1 = V_0 \oplus W_0$, where the basis of W_1 span the difference between V_1 and V_0. Another way of putting this is that, for having the refinement at the lower scale $l_1 = \frac{1}{2}$, that help us go from V_0 at scale $l_0 = 1$ to V_1 at the scale $\frac{1}{2}$, $V_0 \in V_1$, we can go to the basis of W_0 at the same scale $l_0 = 1$ to span the difference between the spaces V_1 and V_2. This alternative means that while we work with the scale $l_0 = 1$ for V_0 and W_0, we are getting the equivalent refinement of being with the smaller scale $l_1 = \frac{1}{2}$ in V_1. Well, the credit must go to the little details (refinement) in the wavelets series (2.8) versus its associated scaling function series of (2.2) for $j = 0$. This can be seen clearly, where the Haar basic wavelet,

$$\Psi(t) = \begin{cases} 1, & 0 \le x < \frac{1}{2} \\ -1, & \frac{1}{2} \le x < 1 \\ 0, & \text{otherwise} \end{cases} \tag{2.11}$$

has more structure (refinement-details) than that of its associated scaling function,

$$\phi(t) = \begin{cases} 1, & 0 \le x < 1 \\ 0, & \text{otherwise} \end{cases} \tag{2.12}$$

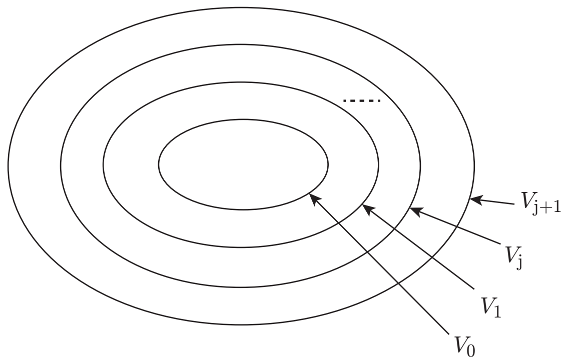

Figure 2.14 | **Nested subspaces spanned by the (discrete) scaling function** $\phi(x),\phi(2x-k),...,\phi(2^j x-k),\phi(2^{j+1} x-k)$

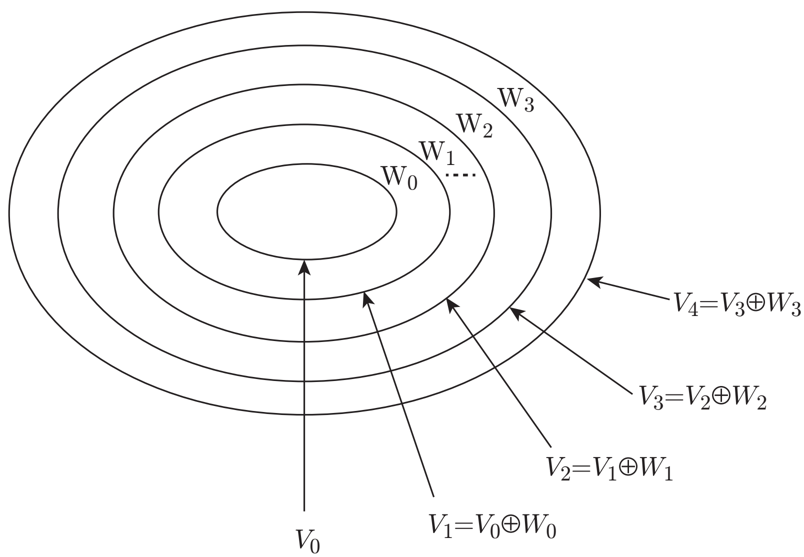

Figure 2.15 | **Wavelets subspaces** W_j **as the orthogonal components of** V_j **in** V_{j+1}, $V_{j+1} = V_j \oplus W_j$

Example 2.6.2—Building multiresolution framework through nested subsets.

In broader perspective wavelet analysis relies on multiresolution framework which gets manifested through nested subsets. While scaling function (father, $\phi(\cdot)$) presents the low pass effect to 'approximately' project the signal to be analysed in some subspace V_j , for the same scale(j) analyser can also use wavelet function (mother, $\psi(\cdot)$) to have high pass effect to produce 'refinements' or 'details', thus projecting the same signal in W_j subspaces. If $f_0(x) \in V_0$ are low pass and $g_0(x) \in W_0$ are high pass projections for scale, then $f_0(x) + g_0(x) = f_1(x) \in V_1$ gives the analyser an opportunity to move from V_0 to V_1 seamlessly. A signal processing perspective of looking at this arrangement is how the frequency content of a signal is measured by the 'dot' product of $< f(\cdot),\phi(\cdot) >$ and $< f(\cdot),\psi(\cdot) >$. Now, Haar scaling function is shown in Figure 2.21 and readers can remember that the frequency representation of a box type function is sync. Thus, Haar $\phi(x)$ produces frequency behaviour of low pass $\cos x$ on $(-\pi,\pi)$, while Haar $\psi(x)$ as shown in Fig. 2.20 produces frequency behaviour of high pass $\sin(x)$ on $(-\pi,\pi)$.

For scale $j=0$ and translation $k=0$, coefficient $\alpha_{0,0}$ will be obtained from dot product $< f(x), \phi(x) >$ and $\beta_{0,0}$ from $< f(x), \psi(x) >$. As $\cos(\omega)|_{\omega=0}=1$ and $\sin(\omega)|_{\omega=0}=0$, $< f(\cdot), \phi(\cdot) >$ indicates frequency content of DC, i.e. zero frequency and $< f(\cdot), \psi(\cdot) >$ indicated the frequency contents of unit frequency.

(IR) Simpler interpretation of this system will be as follows:

For a unit continuous function say *f(x)* on [0,1],

$$< f(x),\phi(x) >= \int_{-\infty}^{\infty} f(x)\cdot\phi(x)\cdot dx = \int_0^1 f(x)\cdot 1\cdot dx \tag{2.13}$$

Equation (2.13) clearly depicts a 'mean' or an 'average' or 'zeroth statistical moment' of *f(x)*. Thus, $< f(x), \phi(x) >$ gives 'coarse' or 'blurred' or 'approximated' or 'low pass' projection of *f(x)* on [0,1]. In case of wavelet basis,

$$\begin{aligned} < f(x),\psi(x) > &= \int_{-\infty}^{\infty} f(x)\cdot\psi(x)\cdot dx \\ &= \int_0^{\frac{1}{2}} f(x)\cdot 1\cdot dx - \int_{\frac{1}{2}}^1 f(x)\cdot 1\cdot dx \end{aligned} \tag{2.14}$$

Equation (2.14) clearly depicts a 'difference' or 'gradient', or 'derivative effect' to *f(x)*. Thus $< f(x),\psi(x) >$ gives 'finer' or 'sharpened', or 'refined' or 'high pass' projection of *f(x)* on [0,1].

Thus where wavelet analysis is very different than a quantizer like successive approximation for example. While $< f(\cdot),\phi(\cdot) >$ gives approximated values, $< f(\cdot),\psi(\cdot) >$ brings in the refinement and ability to add details to improve the resolution, in signal analysis. Blurring of $< f(\cdot),\psi(\cdot) >$ is connected with low pass filtering and detailing of $< f(\cdot),\psi(\cdot) >$ is connected with high pass filtering! This why in DSP we focus on filter design, in wavelet analysis we focus on design of filter 'banks'!

Prior to advent of wavelet theory, electrical engineers used conventional techniques like fourier transform for signal analysis. The measure of frequency content was captured in Fourier coefficients,

$$a_n = \frac{1}{\pi} < f(x), \cos n(x) >, b_n = \frac{1}{\pi} < f(x), \sin n(x) >, -\pi \le x \le \pi$$

Also, for $f(x) \in -\infty,\infty$, Fourier transform is

$$F(\omega) = \frac{1}{2\pi} < f(x), e^{-j\omega x} >=< f(x), e^{-j2\pi fx} >$$

where, 'ω' is frequency in radians per second and '*f*' is frequency in hertz (cycles/second).

In the typical sense of 'highpass filtering',for a given cut-off frequency ω_c, all the frequencies less than ω_c are blocked and higher than ω_c are passed in a given signal. Similarly a typical low pass filter passes all the frequencies lower than a cut-off of ω_c and blocks all the frequencies greater than ω_c. Thus, it makes sense to use high pass philosophy to implement $< f(\cdot),\psi(\cdot) >$ while searching for "details" in the signal, and use low pass philosophy to implement $< f(\cdot),\phi(\cdot) >$ while trying to derive "approximations" from signal.

Implementation strategy: The critical point is how do we implement this moving from one resolution to another? Let us say we have projected signal (with unit range (0,1)) in V_1 such that $f_1 \in V_1$ and scale $= \frac{1}{2^1} = \frac{1}{2}$. We approximate the signal in V_1 with scaling functions $\{\phi_{1,0},\phi_{1,1}\}$ and the corresponding approximation coefficients $\{\alpha_{1,0},\alpha_{1,1}\}$ (Readers should note, as we are in V_1, $j=1$, and since we wish to span unit range and scale is $\frac{1}{2}$, we will require two translations; $k = 0$ & $k = 1$).

Thus $f_1 \in V_1$ gets approximated by $\{\phi_{1,0},\phi_{1,1}\} = \left\{\sqrt{2}\phi(2x-0),\sqrt{2}\phi(2x-1)\right\}$. To add in details we calculate $g_1(x) \in W_1$, which is captured using $\{\psi_{1,0},\psi_{1,1}\} = \left\{\sqrt{2}\psi(2x-0),\sqrt{2}\psi(2x-1)\right\}$ and gets calculated through coefficients $\{\beta_{1,0},\beta_{1,1}\}$. It goes without saying that $\left\{\alpha_{1,0},\alpha_{1,1}\right\}$ is associated with low frequencies and $\{\beta_{1,0},\beta_{1,1}\}$ is associated with higher frequencies.

Schematically this is depicted in Fig. 2.16. If the signal has 'n' samples, then two parallel filters (ϕ :low, ψ :high) add up to produce '$2n$' samples. To maintain same number of samples, we drop every alternate sample at the output of each filter. Thus '$\frac{n}{2}$' samples produces by every filter adds up to maintain 'n' samples. This process of reducing the samples to half is called 'down sampling' and is depicted by $(\downarrow)$; in this particular case 'down sampling by 2' depicted by $(\downarrow 2)$.

From Fig. 2.16, we have averages associated with coefficients $\{\alpha_{1,0},\alpha_{1,1}\}$ of scaling function $\in V_1$, and low pass filter only gives 'blurred' picture of average associated with $\alpha_{0,0}$ of $\phi_{0,0}$ from lower subspace V_0. The details are captured by $\beta_{0,0}$ of wavelet $\psi_{0,0}$ of sub-space W_0. What this leads to in essence is $V_1 = V_0 \oplus W_0$.

What we have shown in Fig. 2.16 is called as 'analysis' or 'decomposition' of signal and what is depicted in Fig. 2.17 is called as 'synthesis' or 'reconstruction' of signal. In decomposition we always move to lower subspaces (e.g. from $V_1 \to V_0$, $V_1 \to W_0$) and in reconstruction we always move towards higher subspaces (e.g. from V_0 and W_0 to V_1).

The two processes above are duals of each other.If 'decomposition' demands downsampling to match up samples,'reconstruction' demands upsampling for the same purpose.In upsampling we insert samples every alternate index and this is called 'upsampling by factor of 2', represented by $(\uparrow 2)$.

A combination of these two is depicted in Fig. 2.18. Together the two operations constitute to what is called 'quadrature mirror filter pair'. Figure 2.18 depicts decomposition (analysis) as well as reconstruction (synthesis) of signal $f_2(x) \in V_2$ via quadrature mirror filter pairs, thus leading us to '2-band filter bank structures'. The first decomposition stage expresses $V_2 = V_1 \oplus W_1$, and second decomposition stage expresses $V_1 = V_0 \oplus W_0$. Thus, $V_2 = V_0 \oplus W_0 \oplus W_1$. This means projections in V_2 are formed by approximations in V_0 with scale =1, orthogonally added to projections of *f(x)* onto wavelet spaces W_0 and W_1 with scales of '1' and '$\frac{1}{2}$' respectively. The analysis can go deeper, e.g. $f_6(x) \in V_6$, and $V_6 = V_0 \oplus W_0 \oplus W_1 \oplus W_2 \oplus W_3 \oplus W_3 \oplus W_5$, with six low and high pass filter pairs for decomposition and same number for reconstruction.

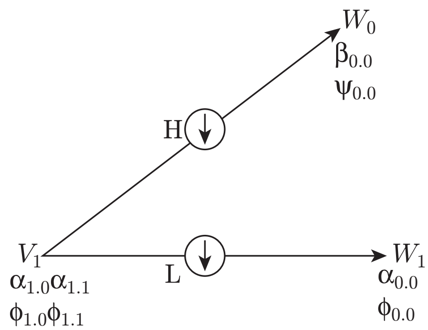

Figure 2.16 **The outputs $f_0(t) \in V_0$ and $g_0(t) \in W_0$ of the low and high pass filters respectively (after down sampling)**

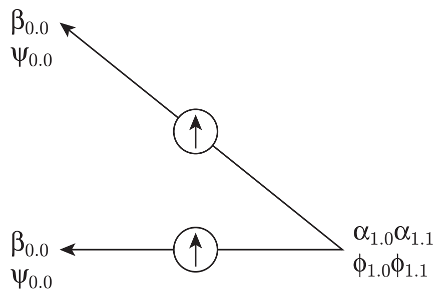

Figure 2.17 **The reconstruction part of the (quadrature mirror) filter pairs to implement the scaling function wavelets reconstruction of the signal $f_1(x) \in V_1$.**

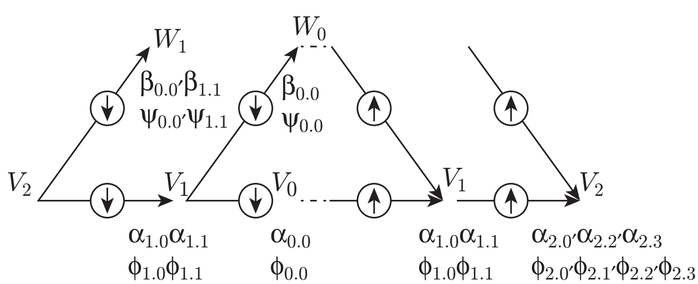

Figure 2.18 **Decomposition and reconstruction of $f_2(x) \in V_2$ – A special case of a "quadrature mirror filter pairs".**

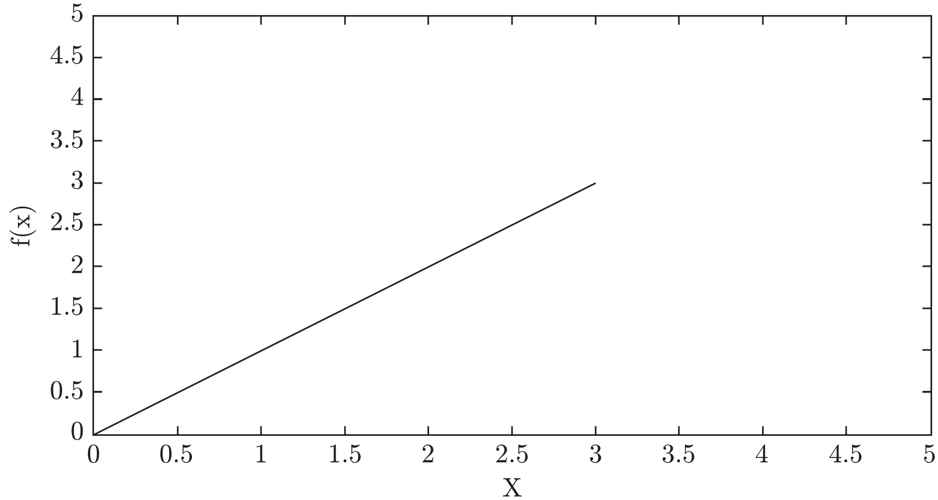

Figure 2.19 | Signal f(x)

Example 2.6.3—Zoom-in and zoom-out.

In this chapter we have seen that wavelet transform decomposes signal into two separate series. One is a single series that represents coarse version, which leads to scaling function, popularly known as the father function. Other is a double series that represents a refined version, which leads to wavelet function, popularly known as mother wavelet. We also got familiarized with the idea of nested subspaces, an MRA and two band filter bank to realize an MRA. The major problem regarding an MRA was that while analyzing a signal we move down the ladder in an MRA. However, in many applications moving up the ladder is desired. Thus, an alternative framework is needed. So let us start defining that framework.

The concept of MRA is in fact based on the idea of nested subspaces. This gives the entire wavelet structure ability to 'zoom-in' and 'zoom-out' of any signal under analysis. We can bring about this essence using two mathematical equations.

1. *Equation of scaling function*

$$\phi(t) = \sqrt{2}\sum_k h_k \phi(2t-k) \tag{2.15}$$

In the above equation we can clearly see that $\phi(t)$ belongs to subspace V_0. Similarly, we can see that $\phi(2t-k)$ belongs to subspace V_1. Thus the idea of nested subspaces is captured in the above equation.

2. *Equation of Wavelet function*

$$\psi(t) = \sqrt{2}\sum_k g_k \phi(2t-k) \tag{2.16}$$

Similar to the case seen above we can see that $\psi(t)$ belongs to subspace W_0 and $\phi(2t-k)$ belongs to V_1.

From the above two equations we can see that,

$$V_j = V_j - 1 \oplus W_j - 1$$

Above equation leads us again to the idea of subspaces. If we start at V_0 and go on adding details then at some stage we would be able to go tantalizingly close to the signal. Let us now see how to achieve that,
Let a function be,

$$f_j(x) \in V_j, \text{ scale} = \frac{1}{2^j}.$$

To span these space V_j the basis function would be $2^{j/2}\phi(2^j x - k)_k$
Here k is the translational parameter and $2^{j/2}$ is the normalizing factor to convert orthogonal basis into an orthonormal basis.
Thus we can write,

$$f_j(x) = \sum_k (\alpha_{j,k} 2^{j/2} \phi(2^j x - k))$$

Alpha can be calculated by as,

$$\alpha_{j,k} = \int_{-\infty}^{+\infty} f_j(x) 2^{j/2} \phi(2^j x - k) dx$$

Similarly, for W subspaces,

$$g_j(x) \in W_j, \text{ scale} = \frac{1}{2^j}$$

The basis would now be,

$$2^{j/2}\psi(2^j x - k)_k$$

Also we can write,

$$g_j(x) = \sum_k (\beta_{j,k} 2^{j/2} \psi(2^j x - k))$$

$$\beta_{j,k} = \int_{-\infty}^{+\infty} g_j(x) 2^{j/2} \psi(2^j x - k) dx$$

β values here would give us the details, which are required to move from one subspace to another.

Now, to understand how the framework so designed is useful in moving up the ladder let us consider a problem.
Consider a signal,

$$f(x) = \begin{cases} x & 0 \le x \le 3, \\ 0 & \text{elsewhere} \end{cases}$$

The function $f(x)$ is shown in Fig. 2.19.

Objectives:
1. To find $f_0(x) \in V_0$
2. To find $g_0(x) \in W_0$

3. To find $f_1(x) \in V_1$ by $f_1(x) = f_0(x) \oplus g_0(x)$. This would be moving up the ladder since we are getting $f_1(x)$ from $f_0(x)$ and $g_0(x)$.
4. Ultimately to prove $V_0 \oplus W_0 = V_1$

Firstly let us find $f_0(x) \in V_0$, $j = 0$ Scale $= \dfrac{1}{2^j} = \dfrac{1}{2^0} = 1$. In, $(2^{j/2}\phi(2^j x - k))_k$, if we put $j = 0$ the basis function would be, $\psi(x-k)_k$. The projection would be,

$$f_0(x) = \sum_{k=0}^{2}(\alpha_{0,k}\phi(x-k))$$

For $k = 0$,

$$\alpha_{0,0} = \int_{-\infty}^{+\infty} f_0(x)\phi(x)dx$$

The interesting thing to note is, here we can choose our own scaling function ϕ which is not the case with Fourier or any other conventional transforms discussed in the last lecture. In the conventional transforms the basis function is fixed and is exponential.

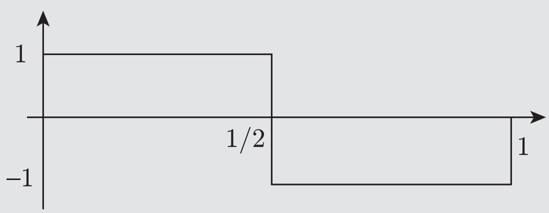

Figure 2.20 | Haar wavelet function

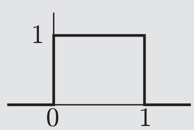

Figure 2.21 | Haar scaling function

Here we would be using Haar scaling and wavelet functions shown in Fig. 2.20, and Fig. 2.21. For $k = 0$ the equation would result in,

$$\alpha_{0,0} = \int_0^1 x dx$$

$$\alpha_{0,0} = \left.\frac{x^2}{2}\right|_0^1$$

$$\alpha_{0,0} = \frac{1}{2}$$

Correspondingly,

$$\alpha_{0,1} = \int_1^2 x\phi(x-1)dx$$

$$\alpha_{0,1} = \int_1^2 xdx$$

$$\alpha_{0,1} = \frac{3}{2}$$

Similarly,

$$\alpha_{0,2} = \int_2^3 x\phi(x-2)dx$$

$$\alpha_{0,2} = \int_2^3 xdx$$

$$\alpha_{0,2} = \frac{5}{2}$$

Now we can write,

$$f_0(x) = \frac{1}{2}\phi(x) + \frac{3}{2}\phi(x-1) + \frac{5}{2}\phi(x-2) \tag{2.17}$$

This is how we can find out projections of signal f in space V_0. The coefficients of $f_0(x)$ represent the approximations of the signal. This can be seen in Fig. 2.22.

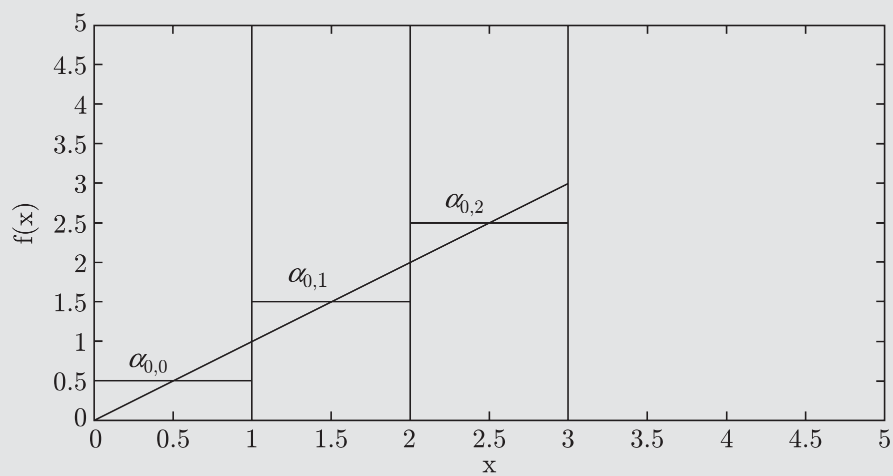

Figure 2.22 | Plotting of $f_0(x)$ coefficients

Now the next task is to find the projections $g_0(x)$ of the signal on W_0. Let, $g_0(x) \in W_0$, scale =1. The basis function would be, $2^{j/2}\psi(2^j x-k)_k$.
We will again make use of Haar wavelet function. Thus as $j = 0$, the basis function would now reduce to, $\psi(x-k)_k$.
Thus we can write,

$$g_0(x) = \sum_k (\beta_{0,k}\psi(x-k))$$

$$\beta_{0,k} = \int_{-\infty}^{+\infty} g_0(x)\psi(x-k)dx$$

As the projections are taken in W_0 subspace these β values will now represent all the details. Similar to the case of α values, from above equation, we can find out corresponding β values as follows,

$$\beta_{0,0} = \int_{-\infty}^{+\infty} g_0(x)\psi(x)dx$$

$$\beta_{0,0} = \int_0^1 x\psi(x)dx$$

$$\beta_{0,0} = \int_0^{1/2} (1)xdx + \int_{1/2}^1 x(-1)dx$$

$$\beta_{0,0} = \frac{1}{8} - \frac{1}{2} + \frac{1}{8}$$

$$\beta_{0,0} = \frac{-1}{4}$$

$$\beta_{0,1} = \int_1^2 x\psi(x-1)dx$$

$$\beta_{0,1} = \int_1^{3/2} (1)xdx + \int_{3/2}^2 x(-1)dx$$

$$\beta_{0,1} = \frac{-1}{4}$$

Similarly,

$$\beta(0,2) = \frac{-1}{4}$$

Thus we can write,

$$g_0(x) = \beta_{0,0}\psi(x) + \beta_{0,1}\psi(x-1) + \beta_{0,2}\psi(x-2)$$

$$g_0(x) = \frac{-1}{4}\psi(x) + \frac{-1}{4}\psi(x-1) + \frac{-1}{4}\psi(x-2) \tag{2.18}$$

Hence, we can see that all the βs have the same value $\frac{-1}{4}$. We will discuss that later in the chapter. The projections $g_0(x)$ are plotted along $f_0(x)$ in Fig. 2.23.

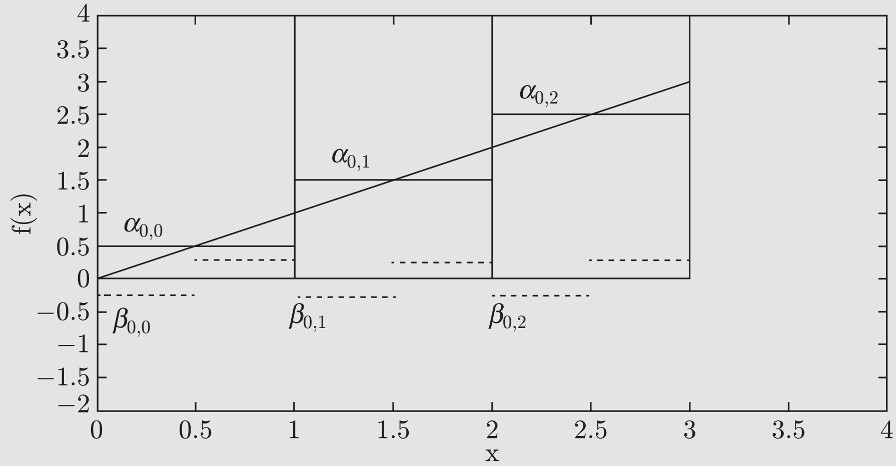

Figure 2.23 | Plotting of $g_0(x)$ and $f_0(x)$ coefficients

Now let us find out projections on V_1 subspace. Let, $f_1(x)\varepsilon V_1$, $j = 1$, scale $= \frac{1}{2^j} = \frac{1}{2}$.

The basis function would now change to, $2^{j/2}\phi(2^j x - k)_k$. As $j = 1$, $\sqrt{2}\phi(2x - k)_k$
Correspondingly, we can write,

$$f_1(x) = \sum_{k=0}^{5}(\alpha_{1,k}\sqrt{2}\phi(2x - k))$$

At this point the α values obtained from above equation should match numerically with the values obtained by orthogonally adding α values in V_0 with β values in W_0. If these values match, we can say that the framework so developed is definitely working and would thus be able to move up the ladder.

So let us now calculate $\alpha_{1,k}$ values.

$$\alpha_{1,0} = \int_{-\infty}^{+\infty} f_1(x)\sqrt{2}\phi(2x)dx$$

$$\alpha_{1,0} = \int_{0}^{1/2} f_1(x)\sqrt{2}\phi(2x)dx$$

$$\alpha_{1,0} = \int_{0}^{1/2} f_1(x)\sqrt{2}\phi(2x)dx$$

From Fig. 2.24,

$$\alpha_{1,0} = \sqrt{2}\int_{0}^{1/2} x(1)dx$$

$$\alpha_{1,0} = \sqrt{2}\frac{1}{8}$$

$$\alpha_{1,0} = \frac{1}{4\sqrt{2}}$$

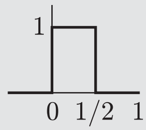

Figure 2.24 | Plotting of function $\phi(2x)$

From Fig. 2.23, we can calculate $\alpha_{1,0}$ as,

$$\alpha_{1,0} = \alpha_{0,0}^{-} + \beta_{0,0}^{-}$$

$$\alpha_{1,0} = \frac{1}{2} - \frac{1}{4}$$

$$\alpha_{1,0} = \frac{1}{4}$$

This matches the previously calculated value with an exception of $\sqrt{2}$ which would eventually get canceled, since we have normalized the basis basis functions. This is seen with the help of following:

$$f_1(x) = \sum_{k=0}^{5} (\alpha_{1,k} \sqrt{2}\phi(2x-k))$$

For $k = 0$,

$$f_1(x) = \alpha_{1,0} \sqrt{2}\phi(2x)$$

$$f_1(x) = \frac{1}{4\sqrt{2}} \sqrt{2}\phi(2x)$$

$$f_1(x) = \frac{1}{4}\phi(x)$$

Similar to $\alpha_{1,0}$ we can calculate other α values.

$$\alpha_{1,1} = \frac{3}{4}$$

$$\alpha_{1,2} = \frac{5}{4}$$

$$\alpha_{1,3} = \frac{7}{4}$$

$$\alpha_{1,4} = \frac{9}{4}$$

$$\alpha_{1,5} = \frac{11}{4}$$

Thus, we can conclude that approximations obtained in V_1 are better than those obtained in V_0. Hence, this is a mechanism through which we can not only think of moving up the ladder but also think of making the choice of the scale and translation parameter and then specifically zoom on to a particular point in the signal or function, which is of greater importance. This framework enables the analyzer to either zoom-in onto a specific part of the signal or zoom-out to understand the big picture. This bigger picture can be illustrated in Fig. 2.25.

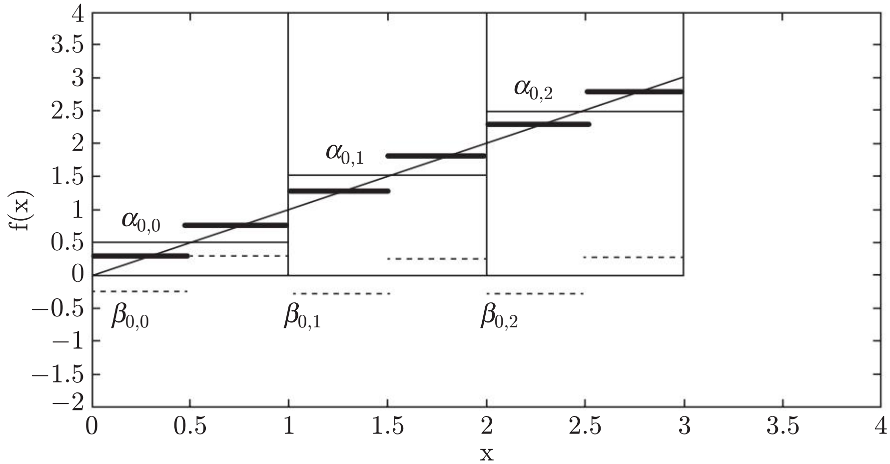

Figure 2.25 | Plotting of α values of $f_1(x)$ [Note - The thick black lines are α values of $f_1(x)$]

The following MATLAB code presents the analysis carried out in the previous illustration.

Example 2.6.4—MATLAB code: Fourier for non-stationary signals.

```
%*************************************************
% MATLAB code to understand MRA (MultiResolution Analysis)
% example: To be accompanied with book on
% Multiresolution and Multirate Signal Processing
% by Dr V M Gadre and Dr A S Abhyankar
%*************************************************
%*************************************************
clear all;close all;clc;

x0=0; % Lower limit of signal
x1=3; % Upper limit of signal


level=9; % Resolution of the signal
x=x0:1/100:x1-1/2^level;

alpha00=1/2;alpha01=3/2; alpha02=5/2;% alpha_0,k values for V0
beta0=1/4; beta1=-1/4; % beta_0,k values for W0

f=x; % The given function
plot(f,x,'k','LineWidth',2); axis([0 4 -1 4]); grid on; hold on;
% Ploting of projections in V0
```

```
plot(x(1:100),alpha00, '+b','LineWidth',8);
plot(x(101:200),alpha01, '+b', 'LineWidth',8);
plot(x(201:300),alpha02, '+b','LineWidth',8); hold on;
% Ploting of projections in W0
plot(x(1:50),beta1, '*g','LineWidth',8); plot(x(51:100),beta0,
'*g','LineWidth',8); plot(x(101:150),beta1, '*g','LineWidth',8);
plot(x(151:200),beta0, '*g','LineWidth',8); plot(x(201:250),beta1,
'*g','LineWidth',8); plot(x(251:300),beta0, '*g','LineWidth',8);
hold on;
alpha10=1/4;alpha11=3/4; alpha12=5/4; % alpha_1,k values for V1
alpha13=7/4;alpha14=9/4; alpha15=11/4;
% Ploting of projections in V1
plot(x(1:50),alpha10, 'or','LineWidth',1); plot(x(51:100),alpha11,
'or','LineWidth',1); plot(x(101:150),alpha12, 'or','LineWidth',1);
plot(x(151:200),alpha13, 'or','LineWidth',1);
plot(x(201:250),alpha14, 'or','LineWidth',1);
plot(x(251:300),alpha15, 'or','LineWidth',1);
title('Multi-Resolution Example');
save test_f.mat f;

% End
```

The saved function can be opened in the wavelet toolebox of MATLAB by typing wavemenu on the command prompt and loading the test signal and doing analysis using wavelet of the reader's choice. The output is shown in the Fig. 2.26.

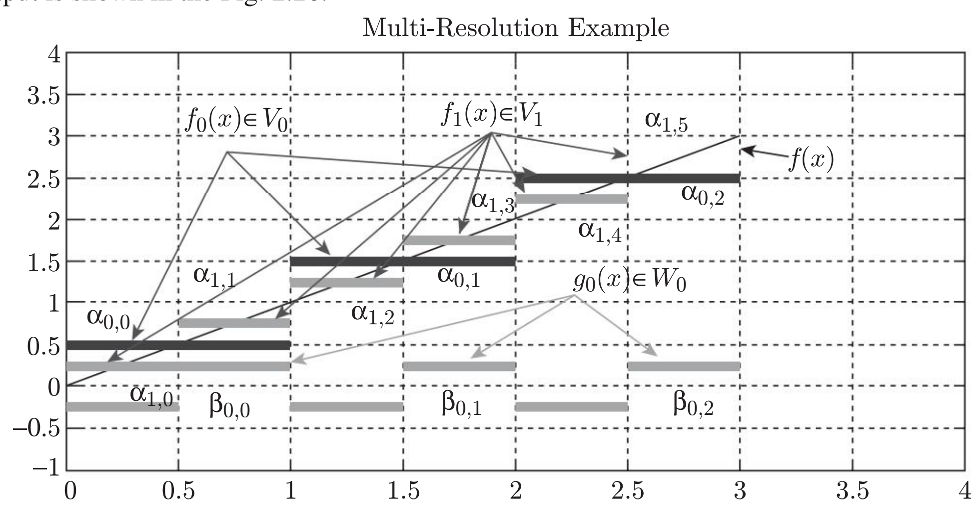

Figure 2.26 **MRA exercise. Black line indicates the function $f(x)$, dotted line projections indicate $f_0(x) \in V_0$, dash-dash line projections indicate** $g_0(x) \in W_0$, red projections indicate $f_1(x) \in V_1$

Question:Use Haar wavelet transform on following signal and solve given objectives:

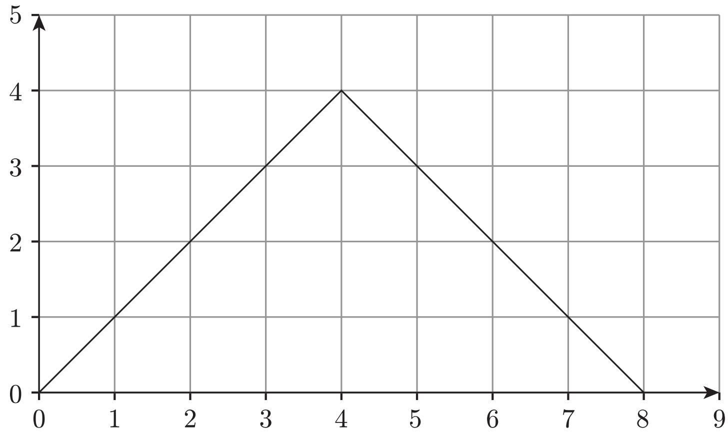

$8-x, 4 \geq x \geq 8$

0, otherwise

1. $f_0(x) \in v_0$
2. $g_0(x) \in w_0$
3. $f_1(x) \in v_1$
4. Prove: $v_1 = v_0 \oplus w_0$

Answer: To solve this problem,we are going to use haar wavelet. The scaling function of Haar wavelet is:

$$f_j(x) \in v_j,\ w_a = \frac{1}{2^j}$$

$$\text{span}\left\{2^{\frac{j}{2}}\phi(2^j x - k)\right\}$$

$$f_j(x) = \sum_k \alpha_{j,k} 2_{\frac{j}{2}} \phi(2^j x - k) \tag{2.19}$$

$$\alpha_{j,k} = \int_{-\infty}^{\infty} f_j(x) 2^{\frac{j}{2}} \phi(2^j x - k) \tag{2.20}$$

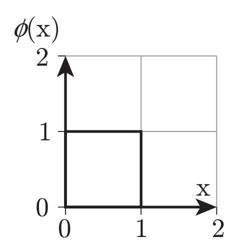

The dilation function of Haar wavelet is: $g_j(x) \in w_j,\ w_a = \frac{1}{2^j}$

$$span\left\{2^{\frac{j}{2}}\psi(2^j x - k)\right\}$$

$$g_j(x) = \sum_k \beta j,k 2^{\frac{j}{2}}\psi(2^j x - k) \tag{2.21}$$

$$\beta j,k = \int_{-\infty}^{\infty} g_j(x) 2^{\frac{j}{2}}\psi(2^j x - k) \tag{2.22}$$

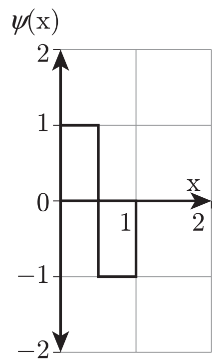

1] $f_0(x) \in v_0 \therefore j = 0$ so $w_a = \frac{1}{2^0} = 1$

$$span\left\{2^{\frac{0}{2}}\phi(2^0 x - k)\right\}$$

$$span\{\phi(x - k)\}$$

From (2),when we put j=0 we get

$$\begin{aligned} f_0(x) &= \sum_k \alpha_{0,k}(2)^{\frac{0}{2}}\phi(2^0 x - k) \\ &= \sum_k \alpha_{0,k}\phi(x - k) \end{aligned} \tag{2.23}$$

$$\begin{aligned} \alpha_{0,k} &= \int_{-\infty}^{\infty} f_0(x) 2^{\frac{0}{2}}\phi(2^0 x - k) \\ &= \int_{-\infty}^{\infty} f_0(x)\phi(x - k) \end{aligned} \tag{2.24}$$

Putting $k = 0$ in Eq. 2.24, we get

$$\begin{aligned} \alpha_{0,0} &= \int_{-\infty}^{\infty} f_0(x)\phi(x - 0)dx \\ &= \int_{-\infty}^{\infty} f_0(x)\phi(x)dx \end{aligned} \tag{2.25}$$

But,

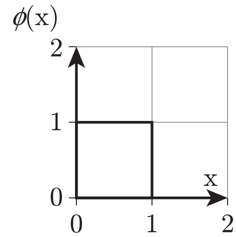

So, scaling function $\phi(x)$ varies from 0 to 1.

$$= \int_0^1 (x)(1)dx$$

$$= \left[\frac{x^2}{2}\right]_0^1$$

$$= \frac{1}{2}$$

$$\boxed{\therefore \alpha_{0,0} = \frac{1}{2}}$$

Putting k=1 in Eq. 2.24, we get

$$\begin{aligned}\alpha_{0,1} &= \int_{-\infty}^{\infty} f_0(x)\phi(x-1)dx \\ &= \int_{-\infty}^{\infty} f_0(x)\phi(x-1)dx \qquad (2.26)\end{aligned}$$

But,

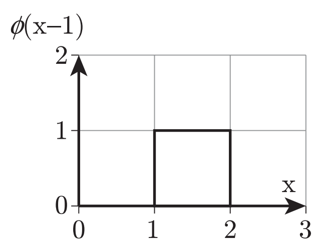

So scaling function $\phi(x-1)$ varies from 1 to 2.

$$= \int_1^2 (x)(1)dx$$

$$= \left[\frac{x^2}{2}\right]_1^2$$

$$= \frac{3}{2}$$

$$\boxed{\therefore \alpha_{0,1} = \frac{3}{2}}$$

Putting $k = 2$ in Eq. 2.24, we get

$$\begin{aligned} \alpha_{0,2} &= \int_{-\infty}^{\infty} f_0(x)\phi(x-2)dx \\ &= \int_{-\infty}^{\infty} f_0(x)\phi(x-2)dx \end{aligned} \tag{2.27}$$

But,

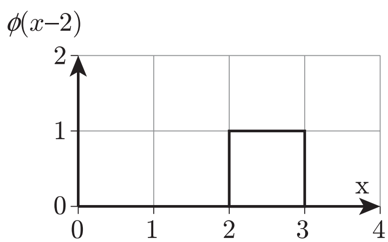

So scaling function $\phi(x-2)$ varies from 2 to 3.

$$= \int_2^3 (x)(1)dx$$

$$= \left[\frac{x^2}{2}\right]_2^3$$

$$= \frac{9}{2} - \frac{4}{2}$$

$$= \frac{5}{2}$$

$$\boxed{\therefore \alpha_{0,2} = \frac{5}{2}}$$

For $k = 3$,

$$\begin{aligned} \alpha_{0,3} &= \int_{-\infty}^{\infty} f_0(x)\phi(x-3)dx \\ &= \int_{-\infty}^{\infty} f_0(x)\phi(x-3)dx \end{aligned} \tag{2.28}$$

But,

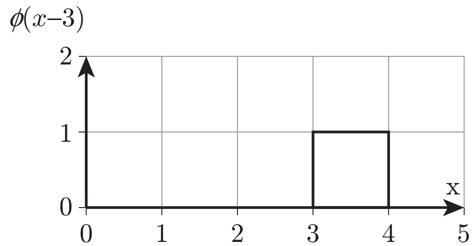

So scaling function $\phi(x-3)$ varies from 3 to 4.

$$= \int_3^4 (x)(1)dx$$

$$= \left[\frac{x^2}{2}\right]_3^4$$

$$= \frac{16}{2} - \frac{9}{2}$$

$$= \frac{7}{2}$$

$$\boxed{\therefore \alpha_{0,3} = \frac{7}{2}}$$

For $k = 4$,

$$\alpha_{0,4} = \int_{-\infty}^{\infty} f_0(x)\phi(x-4)dx$$

$$= \int_{-\infty}^{\infty} f_0(x)\phi(x-4)dx \tag{2.29}$$

But,

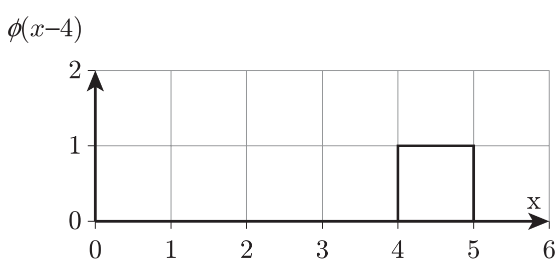

So scaling function $\phi(x-4)$ varies from 4 to 5.

$$= \int_4^5 (8-x)(1)dx$$

$$= \left[8x - \frac{x^2}{2}\right]_4^5$$

$$= \frac{96}{2} - \frac{89}{2}$$

$$= \frac{7}{2}$$

$$\boxed{\therefore \alpha_{0,4} = \frac{7}{2}}$$

For $k = 5$,

$$\alpha_{0,5} = \int_{-\infty}^{\infty} f_0(x)\phi(x-5)dx$$

$$= \int_{-\infty}^{\infty} f_0(x)\phi(x-5)dx \tag{2.30}$$

But,

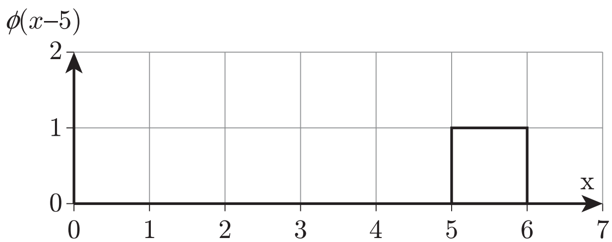

So scaling function $\phi(x-5)$ varies from 5 to 6.

$$= \int_5^6 (8-x)(1)dx$$

$$= \left[8x - \frac{x^2}{2}\right]_5^6$$

$$= \frac{121}{2} - \frac{116}{2}$$

$$= \frac{5}{2}$$

$$\boxed{\therefore \alpha_{0,5} = \frac{5}{2}}$$

For $k = 6$,

$$\alpha_{0,6} = \int_{-\infty}^{\infty} f_0(x)\phi(x-6)dx$$
$$= \int_{-\infty}^{\infty} f_0(x)\phi(x-6)dx \tag{2.31}$$

But,

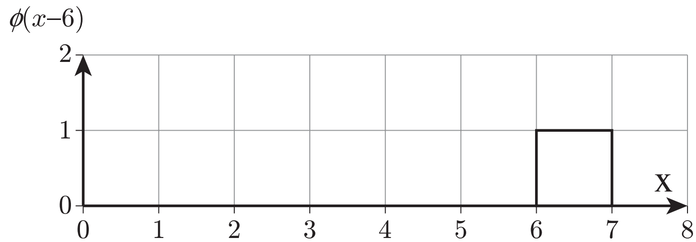

So scaling function $\phi(x-6)$ varies from 6 to 7.

$$= \int_6^7 (8-x)(1)dx$$

$$= \left[8x - \frac{x^2}{2}\right]_6^7$$

$$= \frac{148}{2} - \frac{145}{2}$$

$$= \frac{3}{2}$$

$$\boxed{\therefore \alpha_{0,6} = \frac{3}{2}}$$

For $k = 7$,

$$\alpha_{0,7} = \int_{-\infty}^{\infty} f_0(x)\phi(x-7)dx$$
$$= \int_{-\infty}^{\infty} f_0(x)\phi(x-7)dx \tag{2.32}$$

But,

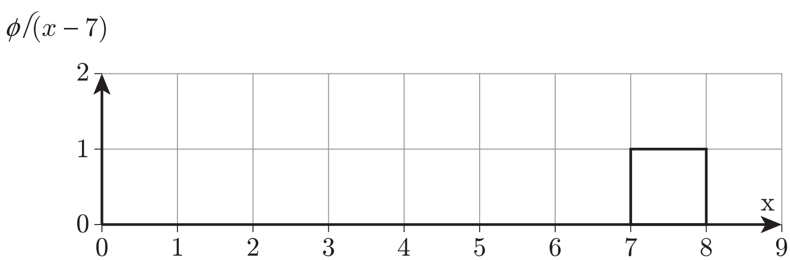

So scaling function $\phi(x-7)$ varies from 7 to 8.

$$= \int_7^8 (8-x)(1)dx$$

$$= \left[8x - \frac{x^2}{2} \right]_7^8$$

$$= \frac{177}{2} - \frac{176}{2}$$

$$= \frac{1}{2}$$

$$\boxed{\therefore \alpha_{0,7} = \frac{1}{2}}$$

Using Eq. 2.23, we can write

$$f_0(x) = \frac{1}{2}\phi(x) + \frac{3}{2}\phi(x-1) + \frac{5}{2}\phi(x-2) + \frac{7}{2}\phi(x-3) + \frac{7}{2}\phi(x-4) + \frac{5}{2}\phi(x-5) + \frac{3}{2}\phi(x-6) + \frac{1}{2}\phi(x-7)$$

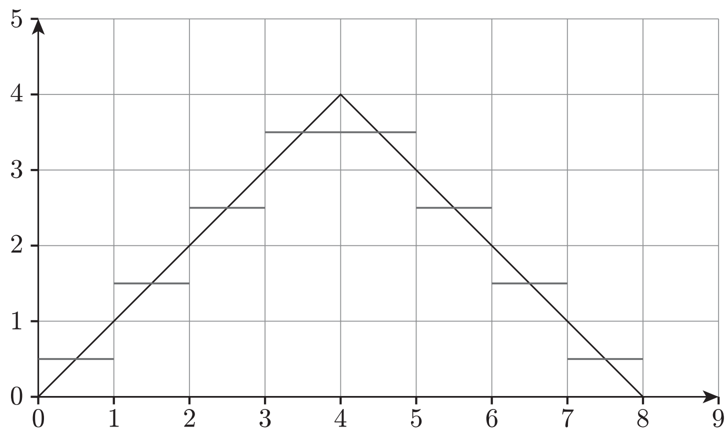

The grey line is showing Wavelet scaling coefficients.

2]$g_0(x) \in g_0 \therefore j = 0$ so $w_a = \frac{1}{2^0} = 1$

$$\text{span}\left\{ 2^{\frac{0}{2}} \psi(2^0 x - k) \right\} \qquad (2.33)$$

$$\text{span}\{\psi(x-k)\}$$

From Eqs. 2.21 and 2.22, when we put $j = 0$

$$\begin{aligned} f_0(x) &= \sum_k \beta_{0,k}(2)^{\frac{0}{2}}\psi(2^0 x - k) \\ &= \sum_k \beta_{0,k}\psi(x-k) \end{aligned} \tag{2.34}$$

$$\begin{aligned} \beta_{0,k} &= \int_{-\infty}^{\infty} f_0(x) 2^{\frac{0}{2}} \psi(2^0 x - k) \\ &= \int_{-\infty}^{\infty} f_0(x)\psi(x-k) \end{aligned} \tag{2.35}$$

For $k = 0$, we have

$$\begin{aligned} \beta_{0,0} &= \int_{-\infty}^{\infty} f_0(x)\psi(x-0)dx \\ &= \int_{-\infty}^{\infty} f_0(x)\psi(x)dx \end{aligned} \tag{2.36}$$

But,

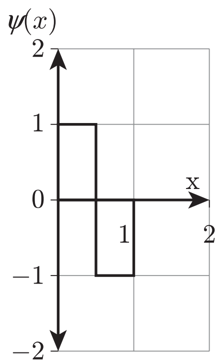

So dilation function $\psi(x)$ varies from 0 to 1.

$$= \int_0^{\frac{1}{2}}(x)(1) + \int_{\frac{1}{2}}^{1}(x)(-1)dx$$

$$= \left[\frac{x^2}{2}\right]_0^{\frac{1}{2}} + \left[-\frac{x^2}{2}\right]_{\frac{1}{2}}^{1}$$

$$= \frac{1}{4} - \frac{1}{2}$$

$$= -\frac{1}{4}$$

$$\boxed{\therefore \beta_{0,0} = -\frac{1}{4}}$$

For $k = 1$, we have

$$\beta_{0,1} = \int_{-\infty}^{\infty} f_0(x)\psi(x-1)dx$$

$$= \int_{-\infty}^{\infty} f_0(x)\psi(x-1)dx \tag{2.37}$$

But,

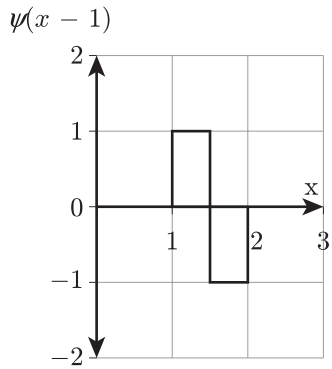

So dilation function $\psi(x-1)$ varies from 1 to 2.

$$= \int_1^{\frac{3}{2}} (x)(1) + \int_{\frac{3}{2}}^{2} (x)(-1)dx$$

$$= \left[\frac{x^2}{2}\right]_1^{\frac{3}{2}} + \left[-\frac{x^2}{2}\right]_{\frac{3}{2}}^{2}$$

$$= \frac{18}{8} - \frac{20}{8}$$

$$= -\frac{1}{4}$$

$$\boxed{\therefore \beta_{0,1} = -\frac{1}{4}}$$

For $k = 2$, we have

$$\beta_{0,2} = \int_{-\infty}^{\infty} f_0(x)\psi(x-2)dx$$

But,

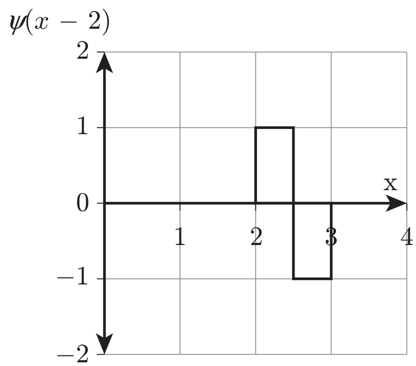

So dilation function $\psi(x-2)$ varies from 2 to 3.

$$= \int_{2}^{\frac{5}{2}} (x)(1) + \int_{\frac{5}{2}}^{3} (x)(-1)dx$$

$$= \left[\frac{x^2}{2}\right]_2^{\frac{5}{2}} + \left[-\frac{x^2}{2}\right]_{\frac{5}{2}}^{3}$$

$$= \frac{50}{8} - \frac{52}{8}$$

$$= -\frac{1}{4}$$

$$\boxed{\therefore \beta_{0,2} = -\frac{1}{4}}$$

For $k = 3$, we have

$$\beta_{0,3} = \int_{-\infty}^{\infty} f_0(x)\psi(x-3)dx$$

But,

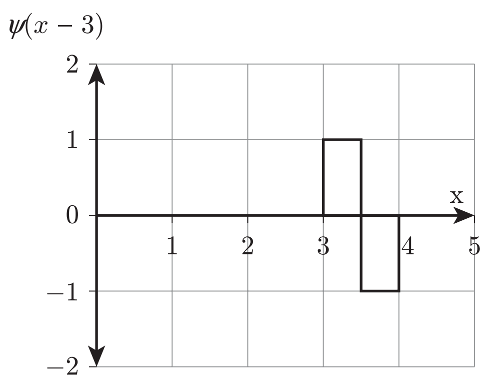

So dilation function $\psi(x-3)$ varies from 3 to 4.

$$= \int_3^{\frac{7}{2}} (x)(1) + \int_{\frac{7}{2}}^{4} (x)(-1)dx$$

$$= \left[\frac{x^2}{2}\right]_3^{\frac{7}{2}} + \left[-\frac{x^2}{2}\right]_{\frac{7}{2}}^{4}$$

$$= \frac{98}{8} - \frac{100}{8}$$

$$= -\frac{1}{4}$$

$$\boxed{\therefore \beta_{0,3} = -\frac{1}{4}}$$

For $k = 4$,

$$\beta_{0,4} = \int_{-\infty}^{\infty} f_0(x)\psi(x-4)dx$$

But,

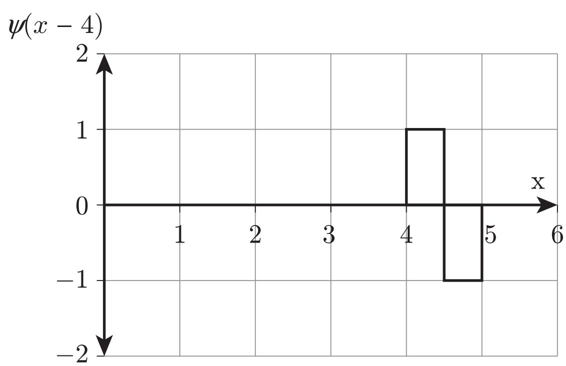

So dilation function $\psi(x-4)$ varies from 4 to 5.

$$= \int_4^{\frac{9}{2}} (x)(1) + \int_{\frac{9}{2}}^{5} (x)(-1)dx$$

$$= \left[\frac{x^2}{2}\right]_4^{\frac{9}{2}} + \left[-\frac{x^2}{2}\right]_{\frac{9}{2}}^{5}$$

$$= \frac{15}{8} - \frac{13}{8}$$

$$= \frac{1}{4}$$

$$\boxed{\therefore \beta_{0,4} = \frac{1}{4}}$$

For $k = 5$, we have

$$\beta_{0,5} = \int_{-\infty}^{\infty} f_0(x)\psi(x-5)dx$$

But,

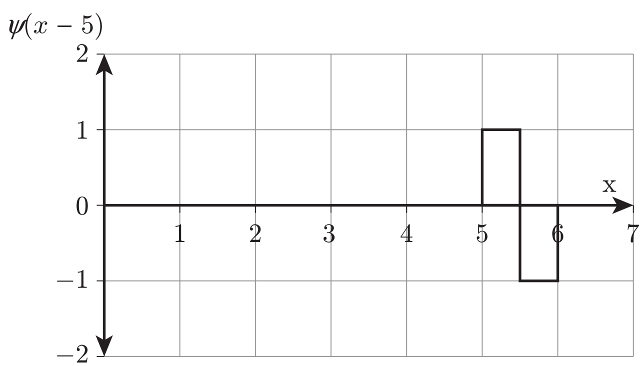

So dilation function $\psi(x-5)$ varies from 5 to 6.

$$= \int_{5}^{\frac{11}{2}} (x)(1) + \int_{\frac{11}{2}}^{6} (x)(-1)dx$$

$$= \left[\frac{x^2}{2}\right]_5^{\frac{11}{2}} + \left[-\frac{x^2}{2}\right]_{\frac{11}{2}}^{6}$$

$$= \frac{11}{8} - \frac{9}{8}$$

$$= \frac{1}{4}$$

$$\boxed{\therefore \beta_{0,5} = \frac{1}{4}}$$

For $k = 6$, we have

$$\beta_{0,6} = \int_{-\infty}^{\infty} f_0(x)\psi(x-6)dx$$

But,

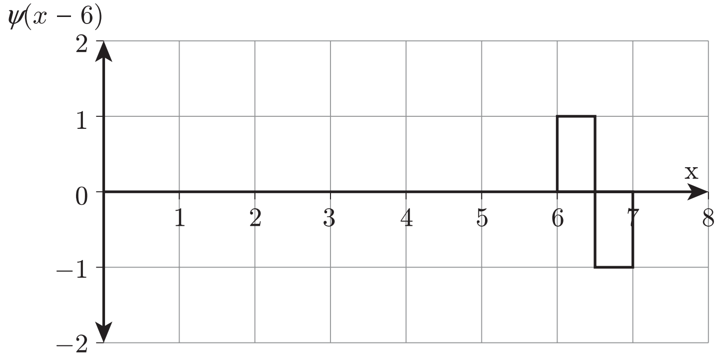

So dilation function $\psi(x-6)$ varies from 6 to 7.

$$= \int_6^{\frac{13}{2}} (x)(1) + \int_{\frac{13}{2}}^{7} (x)(-1)dx$$

$$= \left[\frac{x^2}{2}\right]_6^{\frac{13}{2}} + \left[-\frac{x^2}{2}\right]_{\frac{13}{2}}^{7}$$

$$= \frac{7}{8} - \frac{5}{8}$$

$$= \frac{1}{4}$$

$$\boxed{\therefore \beta_{0,6} = \frac{1}{4}}$$

For $k = 7$, we have

$$\beta_{0,7} = \int_{-\infty}^{\infty} f_0(x)\psi(x-7)dx$$

But,

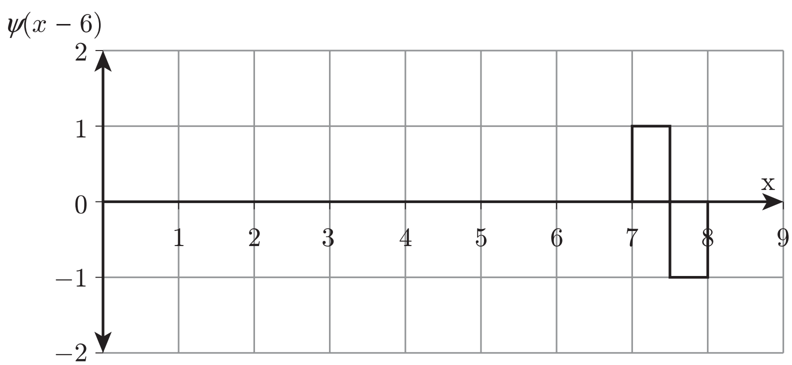

So dilation function $\psi(x-7)$ varies from 7 to 8.

$$= \int_{7}^{\frac{15}{2}} (x)(1) + \int_{\frac{14}{2}}^{8} (x)(-1)dx$$

$$= \left[\frac{x^2}{2}\right]_7^{\frac{15}{2}} + \left[-\frac{x^2}{2}\right]_{\frac{15}{2}}^{8}$$

$$= \frac{3}{8} - \frac{1}{8}$$

$$= \frac{1}{4}$$

$$\boxed{\therefore \beta_{0,7} = \frac{1}{4}}$$

Using Eq. 2.24, we can write

$$g_0(x) = -\frac{1}{4}\psi(x) - \frac{1}{4}\psi(x-1) - \frac{1}{4}\psi(x-2) - \frac{1}{4}\phi(x-3) + \frac{1}{4}\phi(x-4) + \frac{1}{4}\phi(x-5) + \frac{1}{4}\phi(x-6) + \frac{1}{4}\phi(x-7)$$

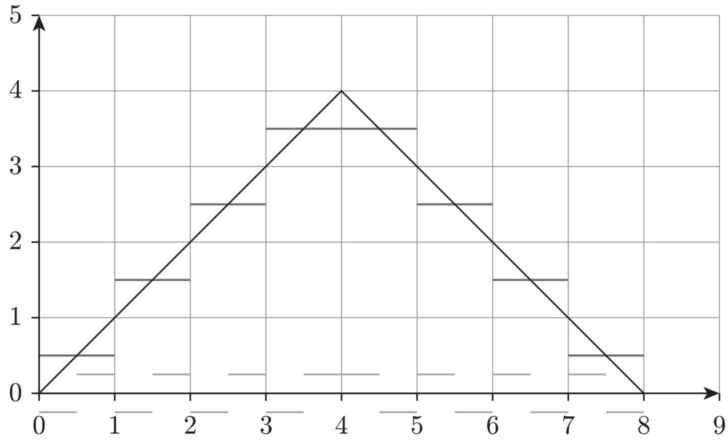

The dark grey line is showing Wavelet scaling coefficients.
The light grey line is showing Wavelet dilation coefficients.

3] $f_1(x) \in v_1 \therefore j = 1$ so $w_a = \frac{1}{2^1} = \frac{1}{2}$

$$\text{span}\left\{2^{\frac{1}{2}}\phi(2^0 x - k)\right\}$$

$$span\left\{\sqrt{2}\phi(2x-k)\right\}$$

From Eq. 2.19, when we put $j = 1$

$$f_1(x) = \sum_k \alpha_{1,k}(2)^{\frac{1}{2}}\phi(2^1 x - k)$$

$$= \sum_k \alpha_{1,k}\sqrt{2}\phi(2x-k)$$

$$\alpha_{1,k} = \int_{-\infty}^{\infty} f_1(x) 2^{\frac{1}{2}}\phi(2^1 x - k)$$

$$\alpha_{1,k} = \int_{-\infty}^{\infty} f_1(x)\sqrt{2}\phi(2x-k) \tag{2.38}$$

For $k = 0$, we have

$$\alpha_{1,0} = \int_{-\infty}^{\infty} f_1(x)\sqrt{2}\phi(2x-0)dx$$

$$= \int_{-\infty}^{\infty} f_1(x)\sqrt{2}\phi(2x)dx$$

But,

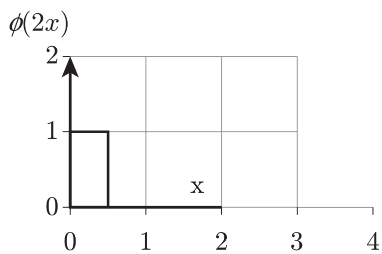

As scaling function $\phi(2x)$ varies from 0 to 0.5.

$$= \int_0^{\frac{1}{2}} \sqrt{2}(x)(1)dx$$

$$= \sqrt{2}\left[\frac{x^2}{2}\right]_{\frac{1}{2}}^{0}$$

$$= \sqrt{2}\cdot\frac{1}{8}$$

$$\boxed{\therefore \alpha_{1,0} = \frac{1}{4\sqrt{2}}}$$

For $k = 1$, we have

$$\alpha_{1,1} = \int_{-\infty}^{\infty} \sqrt{2} f_1(x)\phi(2x-1)dx$$

But,

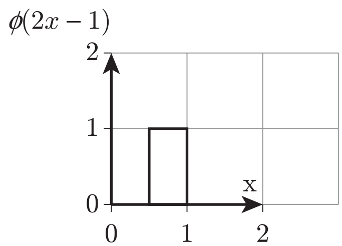

As scaling function $\phi(2x)$ varies from 0.5 to 1.

$$= \int_0^{\frac{0.5}{1}} \sqrt{2}(x)(1)dx$$

$$= \sqrt{2}\left[\frac{x^2}{2}\right]_{\frac{0.5}{1}}^{0}$$

$$= \sqrt{2} \cdot \frac{3}{8}$$

$$\boxed{\therefore \alpha_{1,1} = \frac{3}{4\sqrt{2}}}$$

For $k = 2$, we have

$$\alpha_{1,2} = \int_{-\infty}^{\infty} f_1(x)\sqrt{2}\phi(2x-2)dx$$

But,

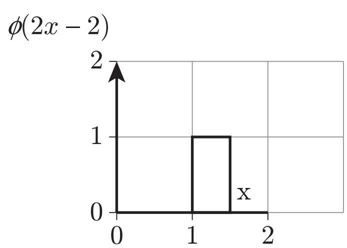

As scaling function $\phi(2x-2)$ varies from 1 to $\frac{3}{2}$.

$$= \int_1^{\frac{3}{2}} \sqrt{2}(x)(1)dx$$

$$= \sqrt{2}\left[\frac{x^2}{2}\right]_{\frac{3}{2}}^{1}$$

$$= \sqrt{2}\cdot\left[\frac{9}{8}-\frac{4}{8}\right]$$

$$= \sqrt{2}\cdot\frac{5}{8}$$

$$\boxed{\therefore \alpha_{1,2} = \frac{5}{4\sqrt{2}}}$$

For $k = 3$, we have

$$\alpha_{1,3} = \int_{-\infty}^{\infty} f_1(x)\sqrt{2}\phi(2x-3)dx$$

But,

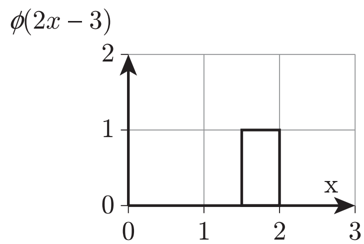

As scaling function $\phi(2x-3)$ varies from 1.5 to 2.

$$= \int_{\frac{3}{2}}^{2}\sqrt{2}(x)(1)dx$$

$$= \sqrt{2}\left[\frac{x^2}{2}\right]_{2}^{\frac{3}{2}}$$

$$= \sqrt{2}\cdot\left[\frac{16}{8}-\frac{9}{8}\right]$$

$$= \sqrt{2}\cdot\frac{7}{8}$$

$$\boxed{\therefore \alpha_{1,3} = \frac{7}{4\sqrt{2}}}$$

For $k = 4$, we have

$$\alpha_{1,4} = \int_{-\infty}^{\infty} f_1(x)\sqrt{2}\phi(2x-4)dx$$

But,

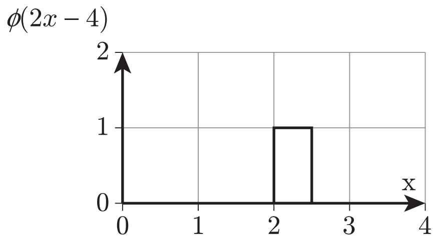

As scaling function $\phi(2x-4)$ varies from 2 to $\frac{5}{2}$.

$$= \int_{2}^{\frac{5}{2}} \sqrt{2}(x)(1)dx$$

$$= \sqrt{2}\left[\frac{x^2}{2}\right]_{\frac{5}{2}}^{2}$$

$$= \sqrt{2}\cdot\left[\frac{25}{8} - \frac{16}{8}\right]$$

$$= \sqrt{2}\cdot\frac{9}{8}$$

$$\boxed{\therefore \alpha_{1,4} = \frac{9}{4\sqrt{2}}}$$

For $k = 5$, we have

$$\alpha_{1,5} = \int_{-\infty}^{\infty} f_1(x)\sqrt{2}\phi(2x-5)dx$$

But,

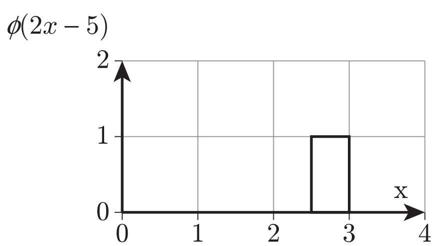

As scaling function $\phi(2x-5)$ varies from $\frac{5}{2}$ to 3.

$$= \int_{\frac{5}{2}}^{6} \sqrt{2}(x)(1)dx$$

$$= \sqrt{2}\left[\frac{x^2}{2}\right]_{\frac{5}{2}}^{3}$$

$$= \sqrt{2} \cdot \left[\frac{36}{8} - \frac{25}{8}\right]$$

$$= \sqrt{2} \cdot \frac{11}{8}$$

$$\boxed{\therefore \alpha_{1,5} = \frac{9}{4\sqrt{2}}}$$

For $k = 6$, we have

$$\alpha_{1,6} = \int_{-\infty}^{\infty} f_1(x)\sqrt{2}\phi(2x-6)dx$$

But,

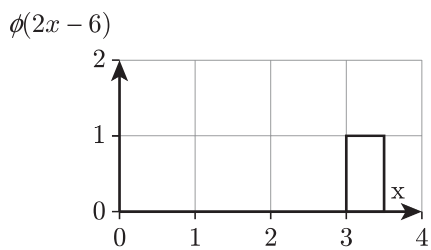

As scaling function $\phi(2x-6)$ varies from 3 to $\frac{7}{2}$.

$$= \int_{3}^{\frac{7}{2}} \sqrt{2}(x)(1)dx$$

$$= \sqrt{2}\left[\frac{x^2}{2}\right]_{\frac{7}{2}}^{3}$$

$$= \sqrt{2} \cdot \left[\frac{49}{8} - \frac{36}{8}\right]$$

$$= \sqrt{2} \cdot \frac{13}{8}$$

$$\boxed{\therefore \alpha_{1,4} = \frac{13}{4\sqrt{2}}}$$

For $k = 7$, we have

$$\alpha_{1,7} = \int_{-\infty}^{\infty} f_1(x)\sqrt{2}\phi(2x-7)dx$$

But,

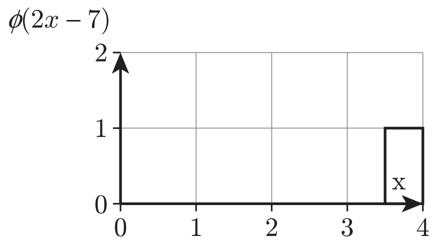

As scaling function $\phi(2x-7)$ varies from $\frac{7}{2}$ to 4.

$$= \int_{\frac{7}{2}}^{4} \sqrt{2}(x)(1)dx$$

$$= \sqrt{2}\left[\frac{x^2}{2}\right]_{\frac{7}{2}}^{4}$$

$$= \sqrt{2}\cdot\left[\frac{64}{8} - \frac{49}{8}\right]$$

$$= \sqrt{2}\cdot\frac{15}{8}$$

$$\boxed{\therefore \alpha_{1,7} = \frac{15}{4\sqrt{2}}}$$

For $k = 8$, we have

$$\alpha_{1,8} = \int_{-\infty}^{\infty} f_1(x)\sqrt{2}\phi(2x-8)dx$$

But,

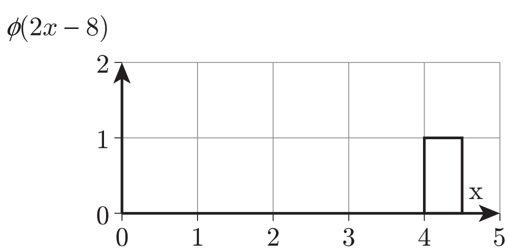

As scaling function $\phi(2x-8)$ varies from 4 to $\frac{9}{2}$

$$= \int_4^{\frac{9}{2}} \sqrt{2}(x)(1)dx$$

$$= \sqrt{2}\left[\frac{x^2}{2}\right]_{\frac{9}{2}}^{4}$$

$$= \sqrt{2}\cdot\left[\frac{352}{8} - \frac{337}{8}\right]$$

$$= \sqrt{2}\cdot\frac{15}{8}$$

$$\boxed{\therefore \alpha_{1,8} = \frac{15}{4\sqrt{2}}}$$

For $k = 9$, we have

$$\alpha_{1,9} = \int_{-\infty}^{\infty} f_1(x)\sqrt{2}\phi(2x-9)dx$$

But,

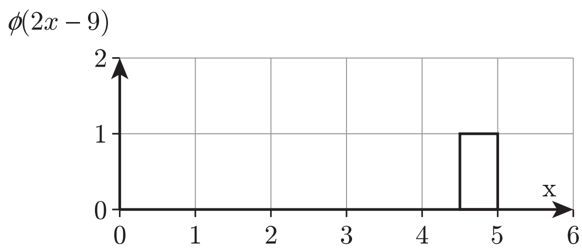

As scaling function $\phi(2x-9)$ varies from $\frac{9}{2}$ to 5

$$= \int_{\frac{9}{2}}^{5} \sqrt{2}(8-x)(1)dx$$

$$= \sqrt{2}\left[8\cdot x - \frac{x^2}{2}\right]_{\frac{9}{2}}^{5}$$

$$= \sqrt{2}\cdot\left[\frac{401}{8} - \frac{388}{8}\right]$$

$$= \sqrt{2} \cdot \frac{13}{8}$$

$$\boxed{\therefore \alpha_{1,9} = \frac{13}{4\sqrt{2}}}$$

For $k = 10$, we have

$$\alpha_{1,10} = \int_{-\infty}^{\infty} f_1(x)\sqrt{2}\phi(2x-10)dx$$

But,

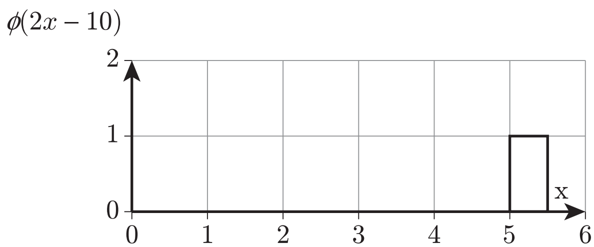

As scaling function $\phi(2x-10)$ varies from 5 to $\frac{11}{2}$.

$$= \int_5^{\frac{11}{2}} \sqrt{2}(8-x)(1)dx$$

$$= \sqrt{2}\left[8 \cdot x - \frac{x^2}{2}\right]_{\frac{11}{2}}^{5}$$

$$= \sqrt{2} \cdot \left[\frac{452}{8} - \frac{441}{8}\right]$$

$$= \sqrt{2} \cdot \frac{11}{8}$$

$$\boxed{\therefore \alpha_{1,10} = \frac{11}{4\sqrt{2}}}$$

For $k = 11$, we have

$$\alpha_{1,11} = \int_{-\infty}^{\infty} f_1(x)\sqrt{2}\phi(2x-11)dx$$

But,

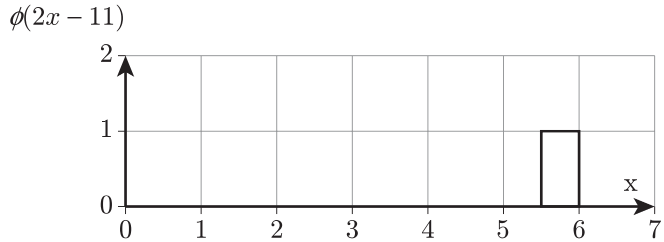

As scaling function $\phi(2x-11)$ varies from $\frac{11}{2}$ to 6.

$$= \int_{\frac{11}{2}}^{6} \sqrt{2}(8-x)(1)dx$$

$$= \sqrt{2}\left[8 \cdot x - \frac{x^2}{2}\right]_{\frac{11}{2}}^{6}$$

$$= \sqrt{2} \cdot \left[\frac{505}{8} - \frac{496}{8}\right]$$

$$= \sqrt{2} \cdot \frac{9}{8}$$

$$\boxed{\therefore \alpha_{1,11} = \frac{9}{4\sqrt{2}}}$$

For $k = 12$, we have

$$\alpha_{1,12} = \int_{-\infty}^{\infty} f_1(x)\sqrt{2}\phi(2x-12)dx$$

But,

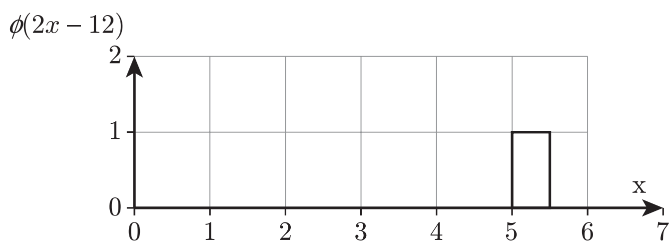

As scaling function $\phi(2x-12)$ varies from 6 to $\frac{13}{2}$

$$\alpha_{1,12} = \int_{6}^{\frac{13}{2}} \sqrt{2}(8-x) \cdot (1) \cdot dx$$

$$= \sqrt{2}\left[8x - \frac{x^2}{12}\right]_6^{\frac{13}{2}} = \sqrt{2}\left[\left(\frac{104}{2} - 48\right) - \left(\frac{169}{8} - \frac{36}{2}\right)\right]$$

$$= \sqrt{2}\left[\frac{8}{2} - \frac{25}{8}\right] = \sqrt{2} \cdot \frac{7}{8}$$

$$= \frac{7}{4\sqrt{2}}$$

$$\boxed{\therefore \alpha_{1,10} = \frac{11}{4\sqrt{2}}}$$

For $k = 13$,

$$\alpha_{1,13} = \int_{-\infty}^{\infty} f_1(x)\sqrt{2}\phi(2x - 13)dx$$

But,

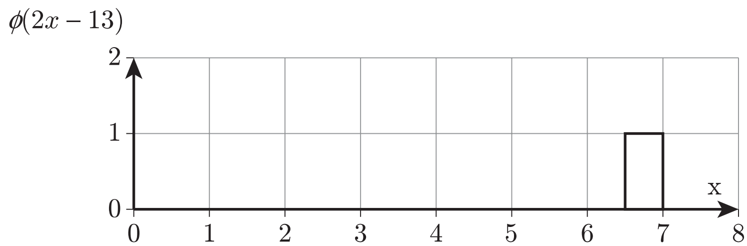

As scaling function $\phi(2x - 13)$ varies from $\frac{13}{2}$ to 7.

$$= \int_{\frac{13}{2}}^{7} \sqrt{2}(8 - x)(1)dx$$

$$= \sqrt{2}\left[8 \cdot x - \frac{x^2}{2}\right]_{\frac{13}{2}}^{7}$$

$$= \sqrt{2} \cdot \left[\frac{617}{8} - \frac{612}{8}\right]$$

$$= \sqrt{2} \cdot \frac{5}{8}$$

$$\boxed{\therefore \alpha_{1,13} = \frac{5}{4\sqrt{2}}}$$

For $k = 14$, we have

$$\alpha_{1,14} = \int_{-\infty}^{\infty} f_1(x)\sqrt{2}\phi(2x-14)dx$$

But,

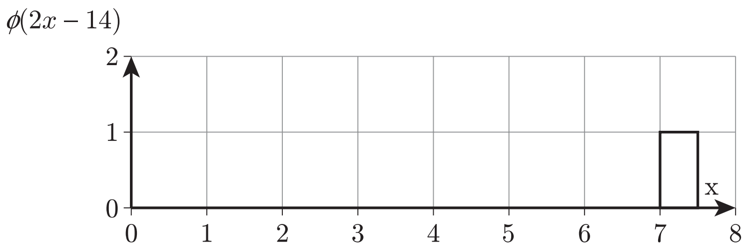

As scaling function $\phi(2x-14)$ varies from 7 to $\dfrac{15}{2}$

$$= \int_{7}^{\frac{15}{2}} \sqrt{2}(8-x)(1)dx$$

$$= \sqrt{2}\left[8\cdot x - \frac{x^2}{2}\right]_{\frac{15}{2}}^{7}$$

$$= \sqrt{2}\cdot\left[\frac{676}{8} - \frac{673}{8}\right]$$

$$= \sqrt{2}\cdot\frac{3}{8}$$

$$\boxed{\therefore \alpha_{1,14} = \frac{3}{4\sqrt{2}}}$$

For $k = 15$,

$$\alpha_{1,15} = \int_{-\infty}^{\infty} f_1(x)\sqrt{2}\phi(2x-15)dx$$

$$= \int_{-\infty}^{\infty} f_1(x)\sqrt{2}\phi(2x-15)dx$$

But,

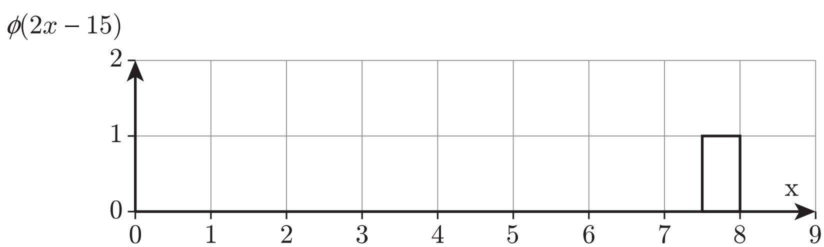

As scaling function $\phi(2x-15)$ varies from $\frac{15}{2}$ to 8.

$$= \int_{\frac{15}{2}}^{8} \sqrt{2}(8-x)(1)dx$$

$$= \sqrt{2}\left[8 \cdot x - \frac{x^2}{2}\right]_{\frac{15}{2}}^{8}$$

$$= \sqrt{2} \cdot \left[\frac{737}{8} - \frac{736}{8}\right]$$

$$= \sqrt{2} \cdot \frac{1}{8}$$

$$\boxed{\therefore \alpha_{1,15} = \frac{1}{4\sqrt{2}}}$$

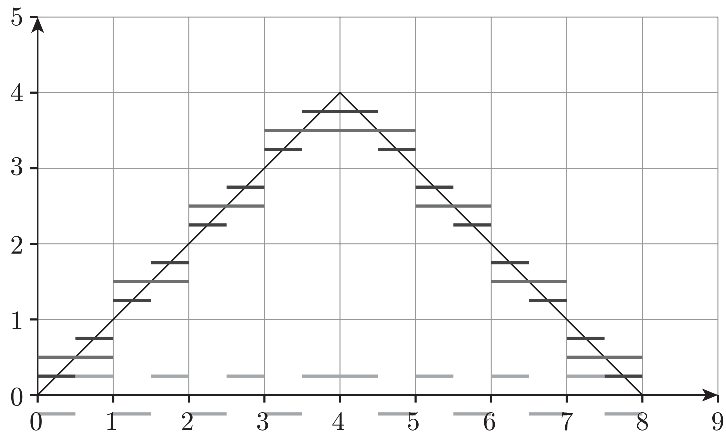

The dark grey line is showing Wavelet scaling coefficients.
The light grey line is showing Wavelet dilation coefficients.
4] Prove: $v_1 = v_0 \oplus w_0$

$$v_0 = \left\{\frac{1}{2}, \frac{3}{2}, \frac{5}{2}, \frac{7}{2}, \frac{7}{2}, \frac{5}{2}, \frac{3}{2}, \frac{1}{2}\right\}$$

$$w_0 = \left\{-\frac{1}{4}, -\frac{1}{4}, -\frac{1}{4}, -\frac{1}{4}, \frac{1}{4}, \frac{1}{4}, \frac{1}{4}, -\frac{1}{4}\right\}$$

$$v_1 = \left\{\frac{1}{4}, \frac{3}{4}, \frac{5}{4}, \frac{7}{4}, \frac{9}{4}, \frac{11}{4}, \frac{13}{4}, \frac{15}{4}, \frac{15}{4}, \frac{13}{4}, \frac{11}{4}, \frac{9}{4}, \frac{7}{4}, \frac{5}{4}, \frac{3}{4}, \frac{1}{4},\right\}$$

Now, take first component of v_0 and first component of w_0 and find out following term,

$$\alpha_{0,1} \cdot \phi(x) + \beta_{0,1} \cdot \psi(k)$$

The scaling function varies from 0 to 1 and the value is 1 overall interval. The dilation function varies from 0 to 1 and the value is 1 for 0 to 0.5 and −1 for 0.5 to 1. So, we will get two values using these two functions.

For $k = 0$

$$\therefore \alpha_{0,0}{}^{(+)} + \beta_{0,0}{}^{(+)}$$

$$= \frac{1}{2} + \frac{-1}{4}$$

$$= \frac{1}{4}$$

This is equal to $\alpha_{1,0}$

Also,

$$\therefore \alpha_{0,0}{}^{(-)} + \beta_{0,0}{}^{(-)}$$

$$= \frac{1}{2} + \frac{1}{4}$$

$$= \frac{3}{4}$$

This is equal to $\alpha_{1,1}$.

For $k = 1$

$$\therefore \alpha_{0,1}{}^{(+)} + \beta_{0,1}{}^{(+)}$$

$$= \frac{3}{2} + \frac{-1}{4}$$

$$= \frac{5}{4}$$

This is equal to $\alpha_{1,2}$.

$$\therefore \alpha_{0,1}{}^{(-)} + \beta_{0,1}{}^{(-)}$$

$$= \frac{3}{2} + \frac{1}{4}$$

$$= \frac{7}{4}$$

This is equal to $\alpha_{1,3}$.

Similarly, we can find values of $\alpha_{0,k}$ and $\beta_{0,k}$ to make a conclusion that addition of these two values will $\alpha_{1,k}$ (k = Total number of coefficients).

Thus, v_1 is formed by combining v_0 and w_0.

Hence,$v_1 = v_0 \oplus w_0$.

Exercises

Exercise 2.1

Verify graphically Mexican hat wavelet function using wavelet dilation equation. Assume compact support of $[0,2)$ for the roof scaling function. State clearly if this pair of scaling and wavelet functions can produce MRA?

Exercise 2.2

Explain which V_j subspace the signal, shown in Fig. 2.27, belongs to and why?

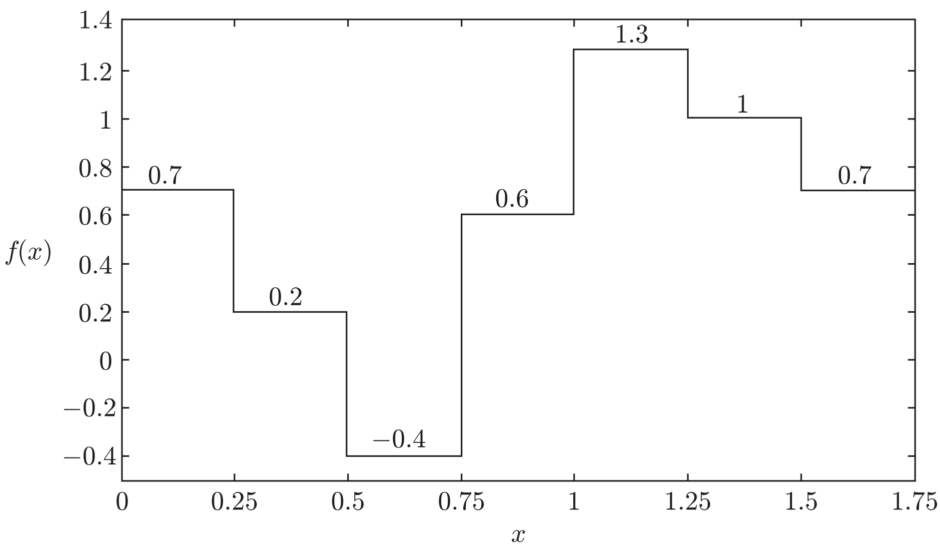

Figure 2.27 | The function $f(x)$. Which V_j subspace it belongs to?

Exercise 2.3

Explain $\{\cap V_m\}_{m\in\mathbb{Z}} = \{0\}$ in detail?

Exercise 2.4

Given,

$$f(x)=\begin{cases}3-x & for\ 0,x,3,\\ 0 & otherwise\end{cases} \tag{2.39}$$

Calculate: $f_0(x)\in V_0$, $g_0(x)\in W_0$ and $f_1(x)\in V_1$,
Prove: $f_0(x)+g_0(x)=f_1(x)\in V_1$

Exercise 2.5

Calculate the L_2 norm of the following function $x(t)$, where $x(t)=1-|t|$ in the interval $[-1,1]$ and zero else where.
Hint: Since the function is symmetric between −1 to 0 and 0 to 1. The norm will be twice that of the value caliculated in any one of the above two intervals.

Hence L_2 norm of $x(t)=[2\int_0^1 |(1-t)|^2\,dt]^{\frac{1}{2}}=[2\int_{-1}^0 |(1+t)|^2\,dt]^{\frac{1}{2}}=\sqrt{2/3}$

Exercise 2.6

Give an example of function which does not exist in $L_2(\mathbb{R})$.
Hint: All the exponential functions having geometric ratio greater than 1 does not exist in $L_2(\mathbb{R})$. For example consider function 2^t for $t>0$. Its L_2 norm does not exist because $\left[\int_0^\infty |2^t|^2\,dt\right]$ does not converge.

Exercise 2.7

Give some examples of functions for the following cases
(a) Function that exists in $L_1(\mathbb{R})$ but does not exist in $L_2(\mathbb{R})$.
(b) Function that exists in $L_2(\mathbb{R})$ but does not exist in $L_1(\mathbb{R})$.
(c) Functions which does not exist in both the spaces.

Hint:
(a) Consider the function $\frac{1}{\sqrt{t}}$ in the interval (0,1] and 0 else where. Its L_1 norm converges but L_2 norm does not converge.
(b) Consider the function $\frac{1}{t}$ in the interval $[1,\infty)$. Its L_2 norm converges, but L_1 norm diverges.
(c) All the periodic functions such as $\sin(t)$ and $\cos(t)$ does not exist in both $L_1(\mathbb{R})$ and $L_2(\mathbb{R})$.

Exercise 2.8

Give the axioms that are to be satisfied by a vector space.
Hint: A real vector space is a set X with a special element 0 called as zero vector, and three operations:
Addition: Given two elements x, y in X, one can form the sum $x + y$, which is also an element of X.
Inverse: Given an element x in X, one can form the inverse $-x$, which is also an element of X.
Scalar multiplication: Given an element x in X and a real number c, one can form the product cx, which is also an element of X.
These operations must satisfy the following axioms
Additive axioms: For every x,y,z in X, we have

(a) $x+y = y+x$.

(b) $(x+y)+z = x+(y+z)$.

(c) $0+x = x+0 = x$.

(d) $(-x) + x = x + (-x) = 0$.

Multiplicative axioms: For every x in X and real numbers c,d, we have

(a) $0x = 0$.

(b) $1x = x$.

(c) $(cd)x = c(dx)$.

Distributive axioms: For every x,y in X and real numbers c,d, we have

(a) $c(x+y) = cx + cy$.

(b) $(c+d)x = cx + dx$. Scalar multiplication: Given an element x in X and a real number c, one can form the product cx, which is also an element of X.

Exercise 2.9

Why in general, only functions in $L_2(\mathbb{R})$ are considered for piecewise constant approximations?
Hint: The L_2 norm signifies the energy of a signal. In general, most of the rea-time signals have finite energy. So we are interested in the signals which have finite energy. So functions in $L_2(\mathbb{R})$ are considered for piecewise constant approximations.

Exercise 2.10

Show that the function $\phi(t)$ is orthogonal to its integer translates.
Hint: Let,

$$\begin{aligned}\phi(t-n) &= 1, \quad n < t < n+1 \\ &= 0, \quad \text{otherwise}\end{aligned}$$

$$\begin{aligned}\phi(t-m) &= 1, \quad m < t < m+1 \\ &= 0, \quad \text{otherwise}\end{aligned}$$

Therefore, their dot product

$$\int_a^b \phi(t-n)\phi(t-m)dt = 0, \ for\, n \neq m$$

Hence $\{\phi(t-n)\}_{n\in\mathbb{Z}}$ are orthogonal.

Exercise 2.11

Explain the effect of dilation and translation of a function $\phi(t)$ in frequency domain.
Hint: Let,

$$\begin{aligned}\phi(t) &= 1, \quad 0 < t < 1\\ &= 0, \quad \text{otherwise}\end{aligned}$$

Fourier Transform of $\phi(t)$ is given as follow,

$$\begin{aligned}\hat{\phi}(\Omega) &= \int_{-\infty}^{+\infty} \phi(t)e^{-j\Omega t}\,dt\\ &= \int_0^1 e^{-j\Omega t}\,dt\\ &= \left[\frac{e^{-j\Omega t}}{-j\Omega}\right]_0^1\\ &= \frac{1-e^{-j\Omega}}{j\Omega}\\ &= \frac{e^{\frac{-j\Omega}{2}}\left[e^{\frac{j\Omega}{2}} - e^{\frac{-j\Omega}{2}}\right]}{j\Omega}\\ &= \frac{2e^{\frac{-j\Omega}{2}}\sin\frac{\Omega}{2}}{\Omega}\\ &= \frac{e^{\frac{-j\Omega}{2}}\sin\frac{\Omega}{2}}{\frac{\Omega}{2}}\end{aligned}$$

Effect of dilation and translation in fourier domain.
Let

$$\begin{aligned}\phi(2^m t - n) &= 1, \quad 2^{-m} n < t < 2^{-m}(n+1)\\ &= 0, \quad \text{otherwise}\end{aligned}$$

By using the scaling and shifting property of Fourier transform we obtain Fourier Transform of $\phi(2^m t - n)$ as

$$= \frac{e^{\frac{-j\Omega 2^{-m}}{2}} e^{-j\Omega n 2^{-m}} \sin(\frac{2^{-m}\Omega}{2})}{\frac{\Omega}{2}}$$

From the Fourier Transform of $\phi(t)$, it can be observed that $\phi(t)$ has a low pass nature and captures a frequency band around zero frequency. Dilation of $\phi(t)$ results in capturing a band of frequencies of varying bandwidth around zero frequency. However, we will see the effect of dilation and translation in detail in subsequent chapters.

Exercise 2.12

Explain the effect of dilation and translation of a function $\psi(t)$ in frequency domain.
Hint: Let

$$\begin{aligned} \psi(t) &= 1 \quad 0 < t < 0.5 \\ &= -1 \quad 0.5 < t < 1 \\ &= 0 \quad \text{otherwise} \end{aligned}$$

Fourier Transform of $\psi(t)$ is given as follow

$$\phi(t) \overset{F.T.}{\leftrightarrow} \hat{\phi}(\Omega)$$

$$\phi(2t) \overset{F.T.}{\leftrightarrow} \frac{1}{2}\hat{\phi}(\frac{\Omega}{2})$$

$$\phi(2t-1) \overset{F.T.}{\leftrightarrow} \frac{1}{2} e^{\frac{-j\Omega}{2}} \hat{\phi}(\frac{\Omega}{2})$$

Using these relationships we get

$$\psi(t) = \phi(2t) - \phi(2t-1)$$

$$\widehat{\psi}(\Omega) = \frac{1}{2}\hat{\phi}\left(\frac{\Omega}{2}\right) - \frac{1}{2} e^{\frac{-j\Omega}{2}} \hat{\phi}\left(\frac{\Omega}{2}\right)$$

$$\psi(\Omega) = \frac{1}{2}\left(1 - e^{\frac{-j\Omega}{2}}\right)\hat{\phi}\left(\frac{\Omega}{2}\right)$$

$$\widehat{\psi}(\Omega) = j e^{\frac{-j\Omega}{2}} \frac{\sin^2\left(\frac{\Omega}{4}\right)}{\frac{\Omega}{4}}$$

Effect of dilation and translation in Fourier domain.
Let

$$\psi(t) \overset{F.T.}{\leftrightarrow} je^{\frac{-j\Omega}{2}} \frac{\sin^2\left(\frac{\Omega}{4}\right)}{\frac{\Omega}{4}}$$

$$\psi(t-n) \overset{F.T.}{\leftrightarrow} e^{-jn\Omega} je^{\frac{-j\Omega}{2}} \frac{\sin^2\left(\frac{\Omega}{4}\right)}{\frac{\Omega}{4}}$$

$$\psi(2^m t-n) \overset{F.T.}{\leftrightarrow} je^{-jn\Omega 2^{-m}} e^{\frac{-j2^{-m}\Omega}{2}} \frac{\sin^2\left(\frac{2^{-m}\Omega}{4}\right)}{\frac{\Omega}{4}}$$

From the Fourier Transform of $\leftarrow(t)$, it can be observed that $\leftarrow(t)$ has a band pass nature and captures a frequency band around certain centre frequency. Dilation of $\leftarrow(t)$ results in capturing a band of frequencies of varying bandwidth around a centre frequency, which itself changes. Again, we will have a detailed discussion on this in subsequent chapters.

Exercise 2.13

Consider the continuous time function $x(t)$ defined as follow.

$$x(t) = 1 - t^2 \quad -1 < t < 1$$
$$= 0$$
otherwise

Compute the piecewise approximation over the subspace V_0 and find the maximum error.
Hint: The given function $x(t)$ is as shown in Fig. 2.28.

$V_0 : x(t)$, such that $x(\cdot) \in L_2(\mathbb{R})$ is piecewise constant on interval$]\, n, n+1\, [$, $\forall \quad n \in Z$ }.

$$]-1,0 \quad [: \int_{-1}^{0} (1-t^2)dt$$

$$= [t - \frac{t^3}{3}]_{-1}^{0}$$

$$= \frac{2}{3}$$

$$]0,1[: \int_{0}^{1} (1-t^2)dt$$

$$= [t - \frac{t^3}{3}]_0^1$$

$$= \frac{2}{3}$$

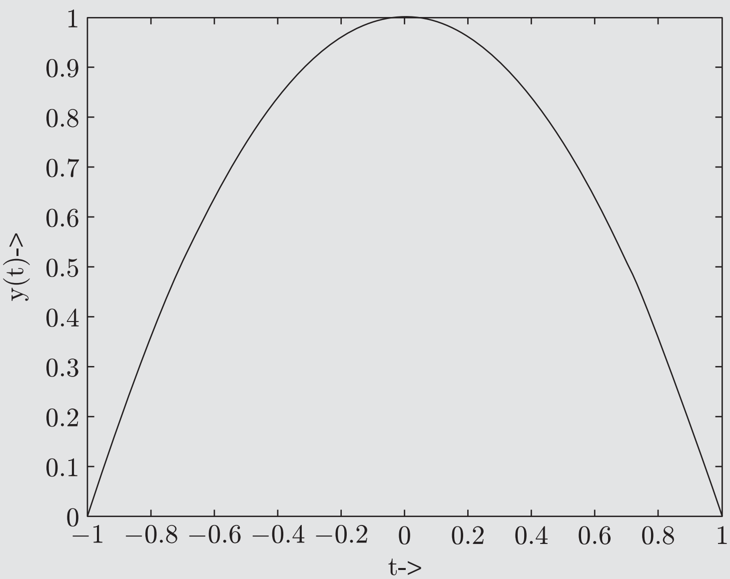

Figure 2.28 | The function $x(t)$

Calculation of maximum error:

$$E = (1 - t^2) - \frac{2}{3}$$

$$\frac{dE}{dt} = -2t$$

$$\frac{d^2E}{dt^2} = -2$$

As second derivative is negative we get maxima so the maximum value is obtained at t=0. So the maximum value is

$$\max(E) = (1 - 0^2) - \frac{2}{3}$$

$$= \frac{1}{3}$$

Chapter 3

The Haar Filter Bank

3.1 | Introduction

In Chapter 2, we saw an equivalence between functions and vectors. We also saw how processing of a function can be related to processing of equivalent sequence w.r.t. inner product and Parseval's theorem. How functions can be considered as generalized vectors? Another dimension of same is replacing work with function, by work with sequence. It is possible to work with sequences in place of functions rather sequences are much easier to deal with as they can be simulated and analysed on computer like in the case of discrete time. If whatever we do with a sequence maps exactly with what we *want* to do with an original continuous time function, then it is an added advantage. This is true for the spaces contained in V_0, in V_1, in V_2, and so on in the $L_2(\mathbb{R})$ ladder shown in Fig. 3.1.

$$\{0\}\ldots \subset V_{-2} \subset V_{-1} \subset V_0 \subset V_1 \subset V_2 \subset \ldots$$

Basis function for V_0 subspace is given by $\{\phi(t-n)\}_{n\in\mathbb{Z}}$. The function $\phi(t-n)$ for $t = n$ is shown below. This is also an orthonormal basis for V_0 because

$$\begin{aligned}\langle \phi(t-n), \phi(t-m)\rangle &= 0, \qquad n \neq m \\ &= 1, \qquad n = m\end{aligned}$$

where $n, m \in \mathbb{Z}$ .This is the primary condition of orthonormality of a function.

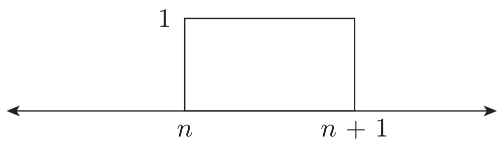

Figure 3.1 | Basis function for V_0

3.2 | Function and Sequence

To have an idea between equivalence of function and sequence, consider the function $x(t) \in V_0$ written in terms of translates of $\phi(t)$.

$$x(t) = \ldots + \left(\frac{1}{2}\right)\phi(t+1) + \left(\frac{-3}{4}\right)\phi(t) + \left(\frac{3}{2}\right)\phi(t-1) + (4)\phi(t-2) + \ldots$$

There is an equivalence between $x(t)$ and sequence. So, the corresponding sequence is

$$x[n] = \left[\ldots, \frac{1}{2}, -\frac{3}{4}, \frac{3}{2}, \underset{\uparrow}{4}, \ldots\right]$$

The downarrow represent the zero'th position of the sequence. Since the function $x(t)$ belongs to $V_0 \in L_2(\mathbb{R})$ thus the sequence $x[n]$ should also belong to a set of square summable sequences. If a function $x(t)$ is square integrable, i.e. $\left(\int_{-\infty}^{\infty} |x(t)|^2\, dt < \infty\right)$ then corresponding sequence is square summable, i.e. $\left(\sum_{n=-\infty}^{\infty} |x[n]|^2 < \infty\right)$. Here, we use a notion that $x(t) \in L_2(\mathbb{R})$ implies $x[n] \in l_2(\mathbb{Z})$. Thus, $l_2(\mathbb{Z})$ is a space of all the discrete sequences which are square summable.
In general, $l_p(\mathbb{Z})$ is a linear space of sequences such that

$$\left(\sum_{n=-\infty}^{\infty} |x[n]|^p < \infty\right)$$

We have just shown a correspondence that if $x(t) \in V_0 \in L_2(\mathbb{R})$ then $x[n] \in l_2(\mathbb{Z})$.
Note: $x[n]$ is the sequence of coefficients of expansion of $x(t)$ with respect to an ORTHONORMAL basis of $x(t)$. If the basis is orthonormal then there is a mapping between inner products of the function and the sequence. For example, suppose $x(t), y(t) \in V_0$, then inner product in continuous time is given by

$$\begin{aligned}\langle x(t), y(t)\rangle &= \int_{-\infty}^{\infty} x(t)\overline{y(t)}dt \\ &= K_0 \sum_{n=-\infty}^{\infty} x[n]\overline{y[n]} \end{aligned} \tag{3.1}$$

where K_0 is a constant.
Therefore, what we do in the context of continuous time function can be equivalently done in the context of discrete domain for corresponding sequence. So, eventually we are leaving behind the continuous function and dealing with the sequence $x[n]$. For example, the concept of pixels or 2-dimensional area in case of an image shows that, we can equivalently replace this continuous intensity of the image in the pixel by 2 sequences ($x[p]$ and $x[q]$) in 2 dimensions. If we want to get some inference from the image, we can look at these sequences and analyse them.
What is the motivation behind this? Our motive is to extract an additional information while going from one subspace to another in a ladder. Now, we will see how to move from one resolution to another and extract the incremental information from the function. Note that this process corresponds to going from lower resolution subspaces to higher resolution in $L_2(\mathbb{R})$ ladder of subspaces.

Example 3.2.1 — Equivalence, decomposition and reconstruction.

Consider $y(t) \in V_1$ i.e.with intervals of length half as shown in Fig. 3.2 and let the corresponding sequence $y[n]$ be

$$[\ldots,4,7,10,\underset{\uparrow}{16},11,3,-1\ldots]$$

The relationship between $y(t)$ and $y[n]$ is

$$y(t) = \sum_{n\in\mathbb{Z}} y[n]\phi(2t-n)$$

where

$$\phi(2t-n) = 1, \quad \frac{n}{2} < t < \frac{n+1}{2}$$
$$= 0, \quad \text{otherwise}$$

Let us move on to another fundamental concept involved here.
Consider the figure shown above. Our next objective is to perform an orthogonal decomposition of a function in V_1 to functions in V_0 and W_0 denoted by

$$V_1 = V_0 \bigoplus W_0$$

where

$$W_0 = \text{span}\{\psi(t-n)\}_{n\in\mathbb{Z}}$$

$$V_0 = \text{span}\{\phi(t-n)\}_{n\in\mathbb{Z}}$$

V_1 is the orthogonal sum of subspaces V_0 and W_0. The idea of orthogonal decomposition states that there is a unique way of taking a vector in V_1 and decomposing this vector into two vectors, one

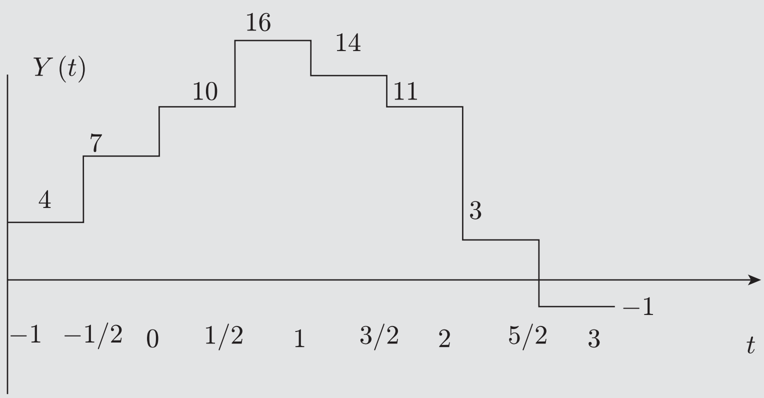

Figure 3.2 | **Function y(t)**

from V_0 and other from W_0 with both being orthogonal to each other, i.e., their inner product is zero. Thus, a linear space is divided into two orthogonal subspaces.

We have seen the equivalence between functions and sequences with respect to square integrability and inner products. Now, consider the angle between two functions or vectors defined in terms of their inner product. An equivalence exists with respect to angles also. As we are considering functions and sequences as generalized vectors, angle between two functions $x(t)$ and $y(t)$ in any subspace can be defined as:

$$\cos(\theta) = \frac{\langle x(t), y(t)\rangle}{\| x \| \| y \|}$$

where θ is the angle between $x(t)$ and $y(t)$ and $x(t), y(t) \in L_2(\mathbb{R})$. Correspondingly we have notion of angle between sequences too.

To check whether it is possible to decompose a sequence in terms of other sequences, consider $x_1(t) \in V_0$ and $x_2(t) \in W_0$ denoted by solid and dashed lines respectively, as shown in Fig. 3.3. Note that $\langle x_1(t), x_2(t)\rangle = 0$ and thus $x_1(t)$ and $x_2(t)$ are orthogonal to each other.

Take any function in V_1 in the open interval $\left[\frac{n}{2}, \frac{n+1}{2}\right]$. It can be written as a summation of function belonging to V_0 and and a function belonging to W_0 from Fig. 3.3. Thus we can decompose a function in V_1 to functions in V_0 and W_0 in a unique way quite easily.

Can we make corresponding construction on the sequences too?

Consider

$$V_1 : p(t) \rightarrow p[n]$$

$$W_0 : q_0(t) \rightarrow q_0[n]$$

$$V_0 : p_0(t) \rightarrow p_0[n]$$

Here $p_0(t)$ and $q_0(t)$ are orthogonally decomposed functions of $p(t)$. Thus, $p(t) = p_0(t) + q_0(t)$ and $p[n]$, $p_0[n]$ and $q_0[n]$ are corresponding sequences. To check whether $p[n] = p_0[n] + q_0[n]$ holds or not, consider the three sequences $p[n]$, $p_0[n]$ and $q_0[n]$ of V_1, V_0 and W_0 subspaces respectively. If the unit interval in V_0 and W_0 subspaces is $[n, n+1]$ then the corresponding interval in V_1 and W_1 subspaces is $[2n, 2n+1]$. The previous example is reconsidered for the corresponding sequences in the Figs. 3.4, 3.5 and 3.6.

Note that function in V_1 has the value C_1 at $2n$ and C_2 at $2n+1$. Thus, $p[2n] = C_1$, $p[2n+1] = C_2$.

Similarly,

$$p_0[n] = \frac{(C1 + C2)}{2}$$

$$q_0[n] = \frac{(C1 - C2)}{2}$$

Note that the relation among $p[n]$, $p_0[n]$ and $q_0[n]$ is not $p[n] = p_0[n] + q_0[n]$, but

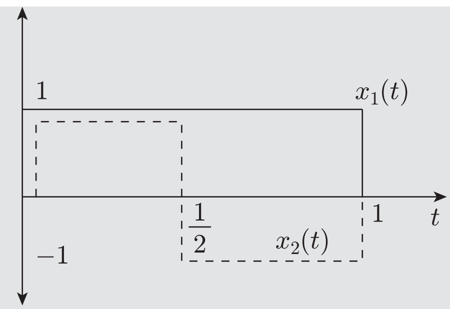

Figure 3.3 | **Functions $x_1(t)$ and $x_2(t)$**

$$p_0[n] = \frac{p[2n] + p[2n+1]}{2} \tag{3.2}$$

$$q_0[n] = \frac{p[2n] - p[2n+1]}{2} \tag{3.3}$$

Looking at these equations, we observe that some filter kind of operations are being done on a set of sequences (i.e above equations) which depict that $p_0[n]$ and $q_0[n]$ are outputs of discrete time filters.

Consider the Discrete time filter with $x[n]$ and $y[n]$ as input and output respectively satisfying:

$$y[n] = \frac{x[n] + x[n+1]}{2} \tag{3.4}$$

This equation looks similar to Eq. 3.2 except that there we have $2n$ as index of the sequence whereas it is n here.Thus we need a new system which satisfies our need, given by the equation:

$$x_{out}[n] = x_{in}[2n]$$

3.3 | Downsampler

In the previous example (Example 3.2.1) if $p[n]$ is the input to the filter given by Eq. 3.4, then output is not $p_0[n]$. For output to be equal to $p_0[n]$, the filter must be driven by a system with input x_{in} and output x_{out} related by $x_{out}[n] = x_{in}[2n]$.

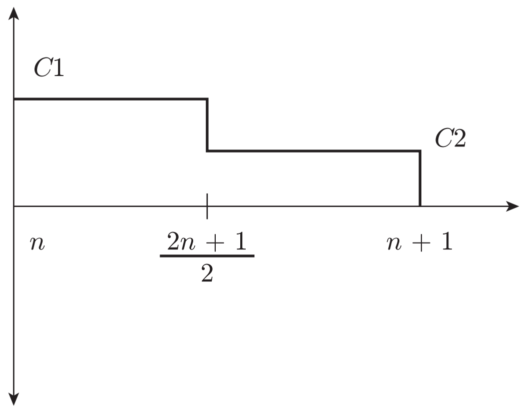

Figure 3.4 | Sequence corresponding to function $p(t) \in V_1$

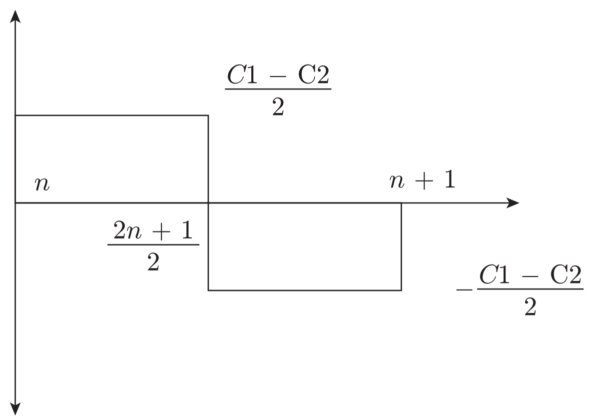

Figure 3.5 | Sequence corresponding to function $q_0(t) \in W_0$

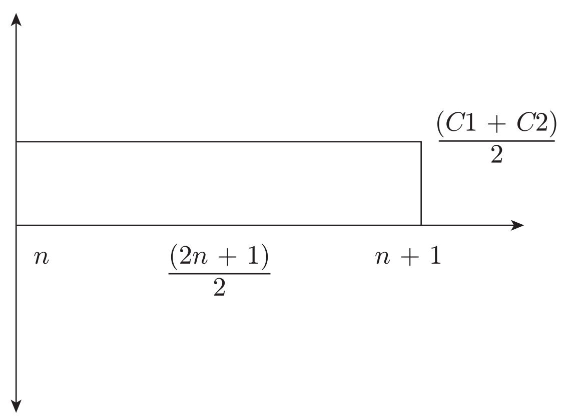

Figure 3.6 | Sequence corresponding to function $p_0(t) \in V_0$

Example 3.3.1 — Downsampler example.

Now, consider the system which does this operation. It retains only the even samples of the input sequence and removes the odd samples. Note that it locates the even samples at half of the original sample number. For example, if $x_{in}[n]=[63527834]$ is the input to this system, then output $x_{out}[n]=[6573]$. Note that $x_{out}[0]$ comes from $x_{in}[0]$, $x_{out}[2]=x_{in}[4]$ and thus $x_{out}[n]=x_{in}[2n]$. Such a system is called **Downsampler** or **Decimator**. Figure. 3.7 shows decimation by 2.

Thus to implement Eq. (3.2) we need a discrete time filter given by Eq. (3.4) followed by a downsampler by two. This helps to construct a sequence $p_0[n]$ from $p[n]$.

Similar kind of filter analysis and decimation process can also be found out for $q_0[n]$.

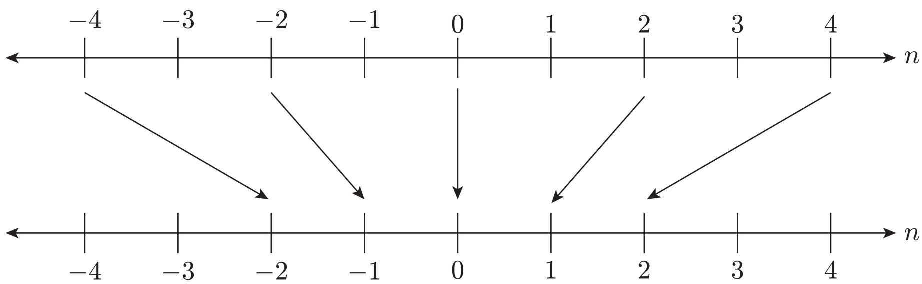

Figure 3.7 | Downsampling by 2

3.4 | The Haar Filter Bank

In this section, we shall continue on the idea of connecting Multi-resolution analysis and a set of filters. Our main aim is to implement Haar MRA using appropriate filter banks. In the analysis part, we decompose a given function in y_{v0} and y_{w0}. Decomposition of corresponding sequence is carried out in terms of wavelet function $\psi(t)$ and scaling function $\phi(t)$. We then explore signal reconstruction using y_{v0} and y_{w0}. Earlier, we have seen that we can divide the real axis (number line) into various equally spaced blocks which then constitute a space. For example, let us split the line into blocks of width *1* as shown in Fig. 3.8.

Corresponding to the figure, we have basis functions of V_0 and W_0. If the same functions were used over a period of half $\left(\frac{1}{2}\right)$, we have the spaces V_1 and W_1, and by halving or doubling the width we achieve the whole range of spaces.

Figure 3.8 | Number Line

$$\{0\} \subset \ldots \subset V_{-2} \subset V_{-1} \subset V_0 \subset V_1 \subset V_2 \subset \ldots$$

3.5 | Analysis Part

Once we have decided the space in which we are operating, we can create a piecewise approximation of a given function.

Example 3.5.1 — Analysis example.

Consider a function $y(t) \in V_1$ defined between [-1, 3]. The number written in between the interval indicates piecewise constant amplitude for that interval (Fig. 3.9).
This continuous function can be associated with the sequence

$$y[-2]=4, y[-1]=7, y[0]=10, y[1]=16, y[2]=14, y[3]=11, y[4]=3, y[5]=-1$$

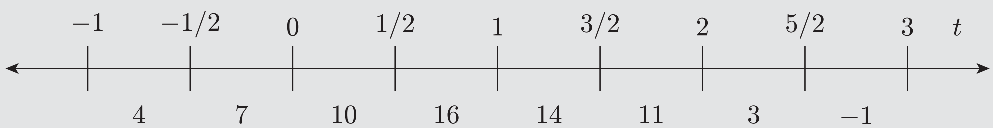

Figure 3.9 | $y(t) \in V_1$

Here it must be noted that -2,-1,0,1... are used as indices for a specific element of the sequence. $y[n]$ is the corresponding sequence of $y(t)$ over a period $\left[\frac{n}{2}, \frac{n+1}{2}\right]$ in the space V_1.
In general, we write

$$y(t) = \sum_{n=-\infty}^{\infty} y[n]\phi(2t-n)$$

where $\phi(2t-n)$ is shifted version of basis function of V_1, as shown in Fig. 3.10.

Now, we decompose space V_1 in two subspaces V_0 and W_0 as

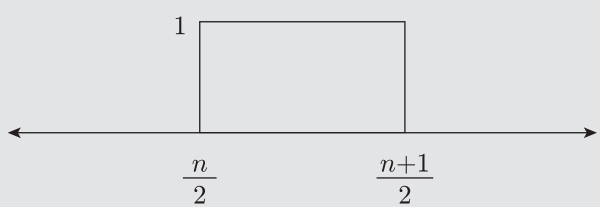

Figure 3.10 | **Basis function of V_1**

$$V_1 = V_0 \bigoplus W_0$$

Corresponding to these subspaces, we obtain two functions y_{v0} and y_{w0}. So, for a given $y(t) \in V_1$, we can split it in two components $y_{v0}(t)$ and $y_{w0}(t)$ which are projections of $y(t)$ on the V_0 and W_0 subspaces, respectively (Fig. 3.11).

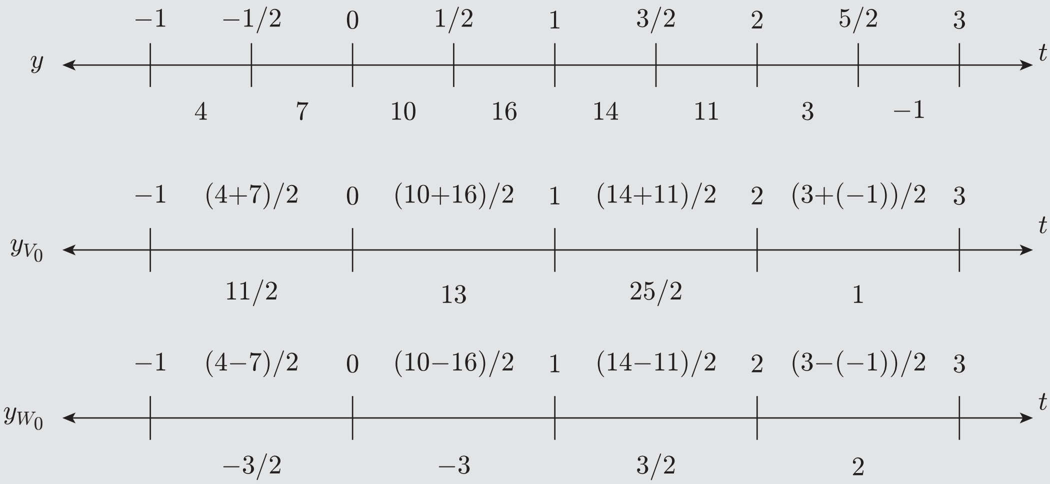

Figure 3.11 | Projection of $y(t)$ over subspaces V_0, W_0

Note that this is after the whole analysis part (after the decimation operation). These functions can be represented as shown in Fig. 3.12.

These representations graphically demonstrate scaled and shifted combinations of the bases to get the original signal (sequence).

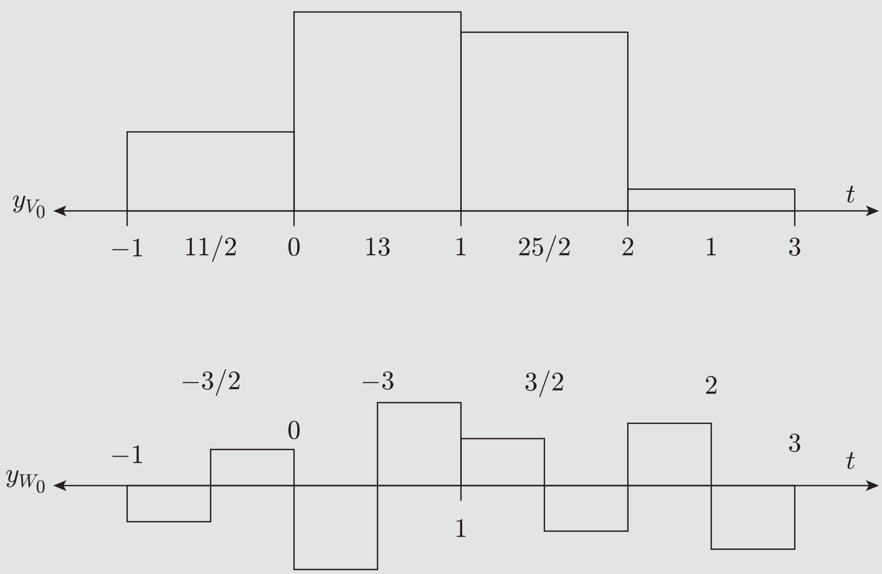

Figure 3.12 | Graphical representation of y_{v0} and y_{w0}

We now, use different notations. We will define $a[n]$ as the input and $b_1[n]$ and $b_2[n]$ as the output of the two filters below as shown in Fig. 3.13.

$$b_1[n] = \frac{1}{2}(a[n] + a[n-1])$$
$$b_2[n] = \frac{1}{2}(a[n] - a[n-1])$$

This is equivalent to

$$b_1[n] = \frac{1}{2}(y[n] + y[n-1])$$
$$b_2[n] = \frac{1}{2}(y[n] - y[n-1])$$

Here, $b_1[n]$ and $b_2[n]$ are sequences having the same length and order as $y[n]$ whereas we want them to be shorted and one order lesser than $y[n]$. $b_1[n]$ and $b_2[n]$ must be modified somehow to get $y_{v0} \in V_0$ and $y_{w0} \in W_0$ respectively. This is performed by decimation (downsampling).
Taking Z-transform on both the sides, we get

$$B_1(Z) = \frac{1}{2}(1 + z^{-1})Y(Z)$$
$$B_2(Z) = \frac{1}{2}(1 - z^{-1})Y(Z)$$

This is followed by the decimation operation to remove unwanted data. The expression of '$\frac{1}{2}(1+z^{-1})$' and '$\frac{1}{2}(1-z^{-1})$' shown in Fig. 3.14 are called the system functions and are obtained by simple algebraic operations on the above two equations. Hence, the Analysis filter bank is as shown in Fig. 3.14.

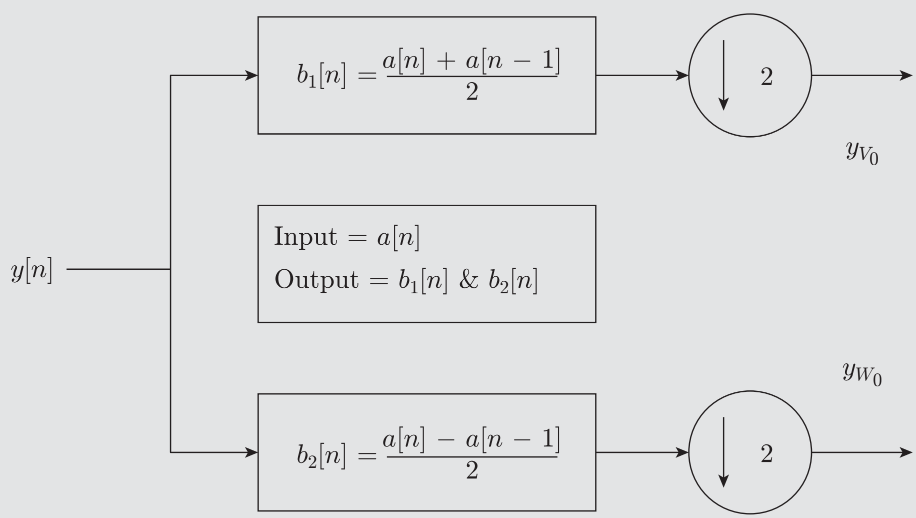

Figure 3.13 | Filter Bank: Analysis part discrete domain

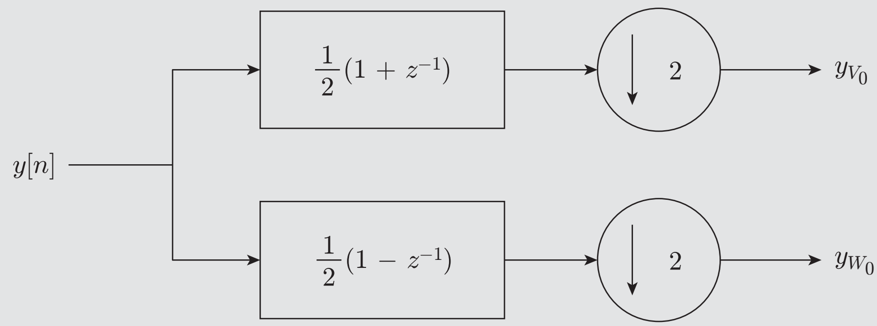

Figure 3.14 | Filter Bank: Analysis part Z domain

3.6 | Synthesis Part

Now, if we have the sequences corresponding to $y_{v0}(t)$ and $y_{w0}(t)$ then what we need to do in order to obtain the original sequence back? We might intuitively realise that we need to 'outdo' the decimation process. So what has the decimation exactly done? It has in some sense halved the n index. It brought the index 4 to index 2, the index 2 to the index 1 and in this sense has reduced the indices by a factor of 2. Thus, to undo this we need to restore the indices back to their original place, which can be done simply by doubling the value of the index. Therefore to construct a Synthesis filter bank or to synthesize $y(t)$ from $y_{v0}(t)$ and $y_{w0}(t)$, in continuous time, we can simply do the following: $y(t) = y_{v0}(t) + y_{w0}(t)$, However, it is not the same in the discrete case. Here we need to work more rigorously.

Example 3.6.1 — Reconstruction example.

So, let us again write all the three sequences,

$$y[n] = \{4, 7, 10, 16, \underset{\uparrow}{14}, 11, 3, -1\}$$

$$y_{v0}[n] = \{\frac{11}{2}, 13, \frac{25}{2}, \underset{\uparrow}{1}\}$$

$$y_{w0}[n] = \{\frac{-3}{2}, -3, \frac{3}{2}, \underset{\uparrow}{2}\}$$

The original sequence $y[n]$ has eight terms and the other two have four each. Therefore, some kind of expansion is required. **Upsampler**: To 'outdo' or 'overcome' decimation operation, we define operation of upsampling by symbol as shown in Fig 3.15.

$$\begin{aligned} x_{out}[n] &= x_{in}\left[\frac{n}{2}\right], && \text{where } n \text{ is multiple of } 2 \\ &= 0, && \text{otherwise} \end{aligned}$$

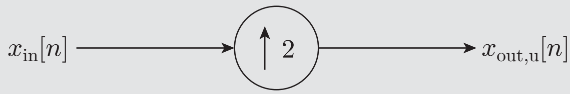

Figure 3.15 | Upsampler

The upsampler, thus, expands the input sequence by adding zero in between successive samples. If $x_{in}[n] = y_{v0}[n]$, then x_{out} is given by

$$x_{out}[n] = \{\frac{11}{2}, 0, 13, 0, \frac{25}{2}, \underset{\uparrow}{0}, 1, 0\}$$

and similarly, $y_{w0}[n]$ on upsampling gives,

$$x_{out}[n] = \{\frac{-3}{2}, 0, -3, 0, \frac{3}{2}, \underset{\uparrow}{0}, 2, 0\}$$

If the sequences obtained after upsampling (y_{v0} and y_{w0}) are added and subtracted alternately, we will get two more sequences. We then alternately allow passage for the elements of the two sequences, i.e. we first pass the first element of the first sequence and then pass the first element of the second sequence. The single sequence so obtained will be the original sequence itself (This will be clarified further if you refer to the Q1 of the Tutorials at the end of this chapter). Figure 3.16 shows how an operation of upsampling. The diagram is called a signal flow graph. Here the circles represent the nodes and the lines with arrows the edges. It is a convenient way of showing computation. When we have a node at which multiple edges come together, the content of the edges is added together and that is the output of the node. Each edge carries information from the source node to the destination node multiplying it by the multiplier of that node and deposits it at the destination node. So if multiple edges come to a node, then all the deposits get added and if they go out of a node then each carries the same value of the node times the multiplier of that edge. In the graph shown in Fig 3.16, each edge has a multiplier of '1' except on edge which has a multiplier of '–1'. We pass the sum branch on one instance (even to be precise) and the difference branch on the next instance (which is odd instance). We can do this by delaying the difference by a unit time period which is as shown by the corresponding operation in the '*Z*' domain. The upsample can commute in the sense that it does not matter whether we first upsample and then add and subtract, or do the reverse. The delay is used to give the output in proper order. The structure that we have thus put down gives us an efficient way of computing the synthesis filter bank.

Figure 3.17 shows the synthesis part of 2-band perfect reconstruction filter bank.

In this way, filter bank is used to implement Analysis and Synthesis aspects of Haar MRA. We shall discuss this in greater depth in the chapters that follow.

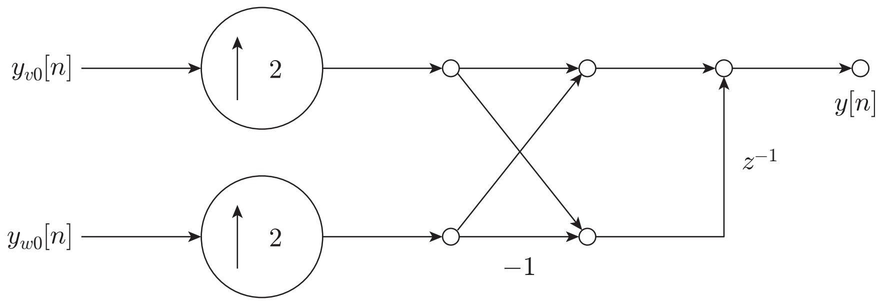

Figure 3.16 | Signal flow diagram with up-sampler by two

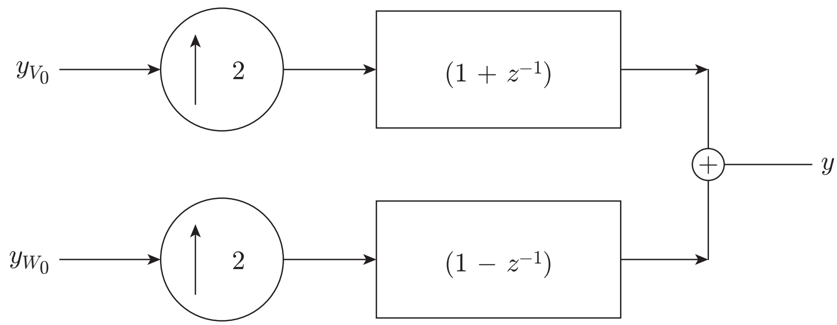

Figure 3.17 | Filter Bank: Synthesis Part

3.7 | Frequency Domain Analysis of Haar Filter Bank

We have looked at the structure of the Haar analysis and synthesis filter bank. In the earlier sections we discussed the Z-transform behaviour of the sequences involved in the filter banks and in this section, the frequency domain behaviour of the Haar MRA filter bank will be explored.

Revising the structure of analysis and synthesis filter bank we obtained the following diagrams (Figs. 3.18 and 3.19).

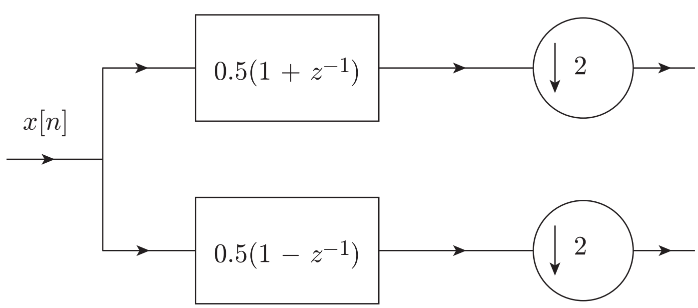

Figure 3.18 | Haar analysis filter bank

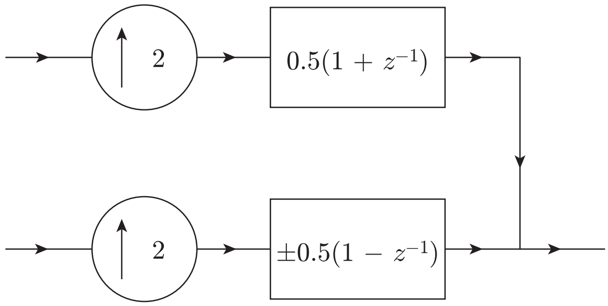

Figure 3.19 | Haar synthesis filter bank

The reason we use ± in the synthesis filter bank is due to a slight ambiguity to determine where to place sum sample and difference sample which will be explored in detail in further chapters. If '+' sign in used, sum sample would get placed at even location and difference sample at odd location. If '-' sign is used, the reverse would happen.

R **Important**: Note the analysis and synthesis filter banks are almost the same (except for the scaling factor). Haar filter banks are not the ideal filter banks. It will soon be understood why. However, understanding Haar filter banks leads us to clarification of many concepts of Multiresolution analysis which will open a new path of processing the images.

3.8 | Frequency Domain Behaviour

Now, let us switch on to the frequency domain. The frequency domain behavior can be determined by substituting $z = e^{j\omega}$. The necessary condition for a system to have a frequency reponse is to ensure that in the Z domain the unit circle lies within the **Region of Convergence (ROC)** of the Z-transform.

3.8.1 Region of Convergence

Typically, the region of convergence of any Z-transform lies within two concentric circles of radius R_1 and R_2 as shown in Fig. 3.20.

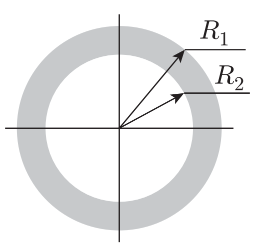

Figure 3.20 | The ROC for any Z-transform

In general, R_1 could be ∞ and R_2 could be 0. The boundary circles may or may not be included in the ROC. If the circle with radius 1, i.e unit circle, is included in the ROC, the system is said to have a frequency response i.e., we say the sequence has a Discrete time fourier transform (DTFT). To determine the frequency response, we substitute $z = e^{j\omega}$. Note that $|z| = 1$, i.e. we are evaluating the Z-transform on the unit circle.

3.8.2 Analysis Filter Bank

Substituting $z = e^{j\omega}$ in $\frac{1+z^{-1}}{2}$, we get

$$\frac{1+e^{-j\omega}}{2} = e^{\frac{-j\omega}{2}} \frac{e^{\frac{j\omega}{2}} + e^{\frac{-j\omega}{2}}}{2}$$

$$= e^{\frac{-j\omega}{2}} cos\left(\frac{\omega}{2}\right) \tag{3.5}$$

Now, consider the magnitude and phase part separately. The magnitude of this response is given by $|\cos\left(\frac{\omega}{2}\right)|$ (because $|e^{\frac{-j\omega}{2}}| = 1$). Similarly the phase response, given by $\frac{-\omega}{2}$ as the $\cos\left(\frac{\omega}{2}\right)$, does not contribute to phase as it is real and positive. The graph of magnitude response is shown in the Fig. 3.21.
Important: Since we have periodicity in the frequency domain with period 2π, thus we need to consider the frequency domain only between -π and +π. We plot only for positive ω noting that magnitude response is an **even function** of ω i.e. magnitude is even-symmetric and, hence, the complete spectrum will also involve a mirror image of the spectrum in figure about the Y-axis. Similarly, the phase response is an odd function of ω or odd-symmetric and thus $\angle H(-\omega_0) = -\angle H(\omega_0)$.

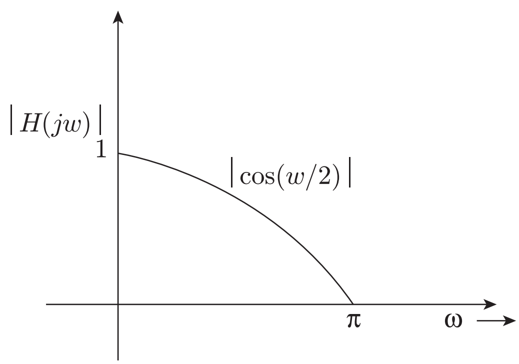

Figure 3.21 | Magnitude response of filter

Looking at the magnitude response, as shown in Fig. 3.21, we observe that this response approximates a **crude low pass filter** (crude imply far from ideal) since it emphasizes lower frequency components. For comparison, the frequency response of an ideal lowpass filter is as shown in Fig. 3.22.
If we plot the phase response of the crude low pass filter, we will get a plot as shown in Fig. 3.23. We observe that the phase response is a **straight line passing through the origin**.

Importance of having a Linear Phase

The frequency response tells us that what happens to a sine wave when it is passed through a system. Let us consider the case in continuous time domain.

If we apply a signal $A_0 cos(\Omega_0 t + \phi_0)$ to a system or a continuous time filter with frequency response given by $H(\Omega)$, then the output is given by

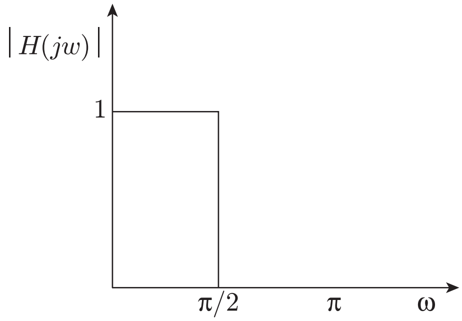

Figure 3.22 | Magnitude response of ideal lowpass D.T. filter with cutoff $\frac{\pi}{2}$

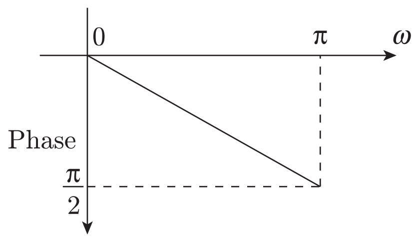

Figure 3.23 | Phase response of ideal lowpass filter

$$\text{Output} = |H(\Omega_0)| A_0 cos(\Omega_0 t + \phi_0 + \angle H(\Omega_0))$$

$$= |H(\Omega_0)| A_0 cos\left[\Omega_0\left(t + \frac{\angle H(\Omega_0)}{\Omega_0}\right) + \phi_0\right] \tag{3.6}$$

where $\angle H(\Omega_0)$ is the angle introduced by system function $H(\Omega_0)$. We see that introduction of this system has resulted in a time shift in the signal, which is dependent on signal frequency Ω_0. Thus, here we see that phase is a **necessary evil**. For a system with no phase response, it would not be a causal. Phase introduces a time shift, which is in general different for different frequencies which we do not desire. Thus if we want to preserve the shape of the waveform, we can at least try that all frequencies are shifted by the same time i.e.

$$\frac{\angle H(\Omega_0)}{\Omega_0} = \tau_0 \text{ (independent of } \Omega_0)$$

τ_0 is a constant independent of Ω_0. This implies that,

$$\angle H(\Omega_0) = \Omega_0 \tau_0$$

This is an equation of a straight line passing through origin, hence called as a **linear phase**. Thus Haar filter bank has the useful property of linear phase.

For the ideal case no $\angle H(\Omega_0)$ is required because of the causality condition, i.e. if casual filters are asked then zero phase condition is unachievable. Also, it is not easy to design filter banks of larger order with linear phase.

3.8.3 Second Filter in Analysis Filter Bank

Substituting $z = e^{j\omega}$ in the expression $\frac{1}{2}(1 - z^{-1})$, we get

$$\frac{1}{2}(1 - e^{-j\omega}) = je^{\frac{-j\omega}{2}} \sin\left(\frac{\omega}{2}\right)$$

The magnitude and phase responses are shown in the Figs. 3.24 and 3.25 respectively.

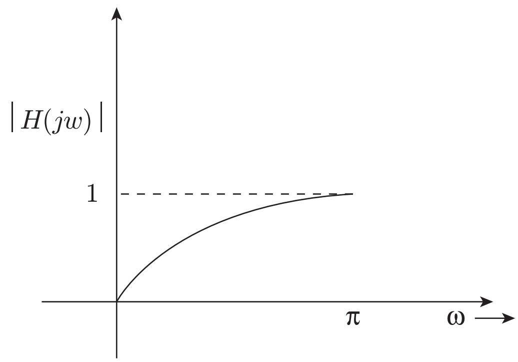

Figure 3.24 | Magnitude response of second analysis filter

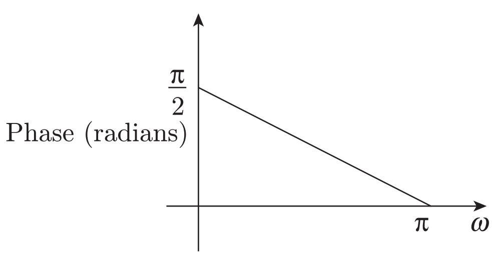

Figure 25 | Phase response of second analysis filter

Note that in calculating phase response we get an extra term of $\frac{\pi}{2}$ due to presence of j. The expression for phase response is thus given by

$$\text{phase}(\omega) = \frac{\pi}{2} - \frac{\omega}{2}$$

It is thus seen that although the graph is still a straight line, it **no longer passes through the origin**. This phase response is thus called **pseudo-linear** response, i.e. it looks similar to linear phase response.

To summarize, we will again see the complete phase and magnitude responses of both filters. Fig. 3.26 shows the response of the first filter and Fig. 3.27 refers to the response of the second filter. The phase response is antisymmetric about origin because the expression is an **odd** function of ω (due to presence of $\sin\left(\frac{\omega}{2}\right)$).

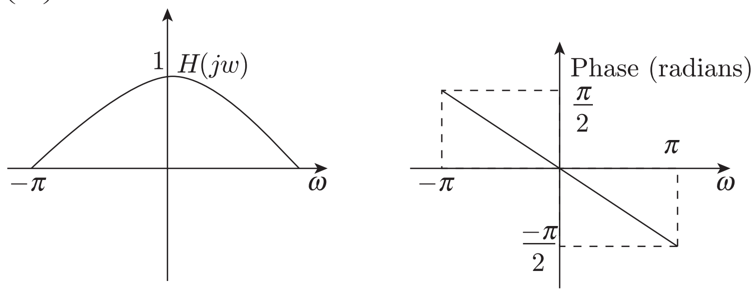

(a) magnitude response (b) phase response

Figure 3.26 | Magnitude and Phase response of first analysis filter

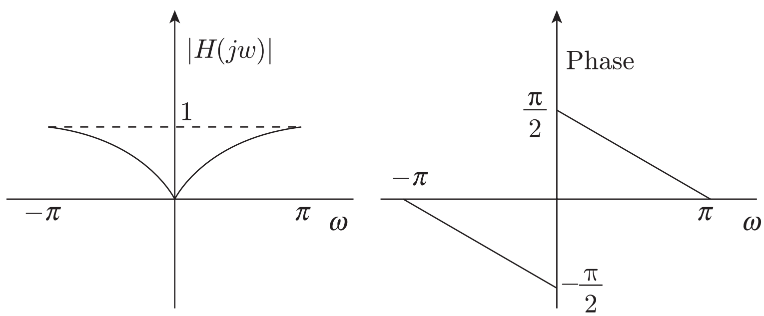

Magnitude response Phase response

Figure 3.27 | Magnitude and Phase response of second analysis filter

Looking at the phase response of the second filter in Fig. 3.27, we observe that at $\omega = 0$ phase has two values namely $-\frac{\pi}{2}$ and $\frac{\pi}{2}$ thus there is an ambiguity. However, since value of magnitude at $\omega = 0$ is zero, the phase response at $\omega = 0$ has no consequence.

Example 3.8.1 — Complementary property.

If we add the functions of both filters, we get

$$\frac{1}{2}(1+z^{-1})+\frac{1}{2}(1-z^{-1})=1$$

The meaning of this result is that if we pass a sine wave through both filters and add the filter outputs, we get back the original sine wave. This property is called the **Magnitude complementarity** property of the filters.

As we know that if we pass a wave of frequency ω_0 through a filter of transfer function $H(\omega)$, the power output is given by $|H(\omega_0)|^2$. If we add the power outputs of both filters, we get

$$|\cos(\frac{\omega_0}{2})|^2 + |\sin(\frac{\omega_0}{2})|^2 = 1$$

Thus, we see that even the sum of powers from both filters is conserved and on addition of the filter outputs, we get the same power back. This property is known as the **Power complementarity** property. Let us consider the analysis filter bank with frequency response of the upper branch as $H_{\text{upper}}(w)$ and that of lower branch as $H_{\text{lower}}(w)$ then we have

$$H_{\text{upper}}(w) + H_{\text{lower}}(w) = 1$$

as magnitude complementary property and

$$|H_{\text{upper}}(w)|^2 + |H_{\text{lower}}(w)|^2 = 1$$

as the power complementary property '1' here represents the identity function. Similar analysis can be done for synthesis filter bank too.
Thus, we can conclude that filters in filter bank may have individual as well as collective properties. Magnitude and power complimentary properties are the collective properties whereas low pass and high pass nature of the filters depict their individual characteristics.

Exercises

Exercise 3.1

What are basis functions? Write down the bases for spaces V_1, V_{-1} and W_{-1} of Haar MRA.
Hint: Basis functions are the basic building blocks of a function space. Any function in the function space, for example $\mathbb{L}_2(\mathbb{R})$ space, can be represented as linear combination of the basis functions or bases of that space. Bases for spaces V_1, V_{-1} and W_{-1} of Haar MRA are span$\{\phi(2t-n)\}_{n\in\mathbb{Z}}$, span$\left\{\phi\left(\frac{t}{2}-n\right)\right\}_{n\in\mathbb{Z}}$ and span$\left\{\psi\left(\frac{t}{2}-n\right)\right\}_{n\in\mathbb{Z}}$ respectively.

Exercise 3.2

Consider a triangular pulse $x(t)$ as described by

$$\begin{aligned} x(t) &= t, \quad 0 \le t \le 1 \\ &= 2-t, \quad 1 \le t \le 2 \end{aligned}$$

$$= 0, \quad \text{otherwise}$$

Write down a sequence $x[n]$ using dilates and translates of $x(t)$.
Hint: $x(t)$ can be sketched in terms of its own dilates and translates as shown in Fig. 3.28, so corresponding sequence is

$$x[n] = [\frac{1}{2}, \underset{\uparrow}{1}, \frac{1}{2}]$$

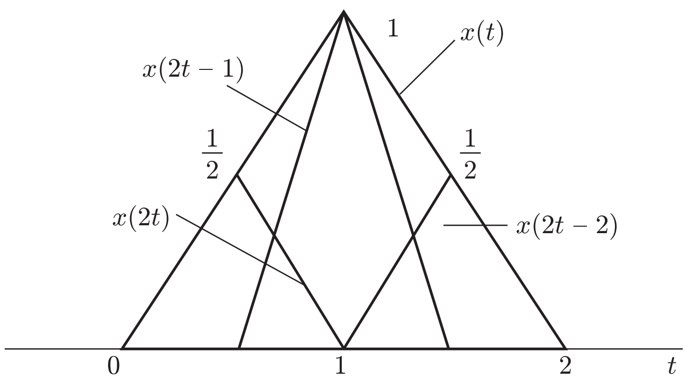

Figure 3.28 | $x(t) = \frac{1}{2}x(2t) + x(2t-1) + \frac{1}{2}x(2t-2)$

Exercise 3.3

In the case of orthogonality and independence of vectors, which is necessary and sufficient condition for the other?
Hint: When two vectors are orthogonal then they are also independent. However, if two vectors are independent then they are not necessarily orthogonal. In other words, orthogonality of vectors is a sufficient condition for the vectors to be independent but independence of vectors is necessary for vectors to be an orthogonal.
Moreover, for two subspaces V_1 and V_2, of vector space V, V_1 and V_2 are said to be orthogonal if every vector in V_1, is orthogonal to every vector in V_2 which implies that bases of subspace V_1 and V_2 are orthogonal. In case of independence, bases of subspace V_1 and V_2 are independent and need not not be orthogonal.

Exercise 3.4

Is orthogonal decomposition unique?
Hint: Orthogonal decomposition is decomposing or splitting the vector space V into the two orthogonal subspaces. Consider a function from V_1 space. Then,

$$V_1 = V_0 \oplus W_0$$

Also, we can write

$$V_0 = V_{-1} \oplus W_{-1}$$

In general,

$$V_{m+1} = V_m \oplus W_m$$

where $m \in \mathbb{Z}$. Hence orthogonal decomposition is not unique but once the subspaces are fixed then the decomposition is unique.
For example, a function from V_1 space can be represented as linear combination of scaling function $\phi(t)$ and wavelet function $\psi(t)$ if space is decomposed into subspaces V_0 and W_0 i.e.

$$f(t) = \sum_{n\in\mathbb{Z}} \phi(t-n) + \sum_{n\in\mathbb{Z}} \psi(t-n)$$

Similarly, the same function can be represented as linear combination of dilates of scaling and wavelet function from subspaces V_{-1}, W_{-1} respectively and wavelet function from space W_0 as

$$f(t) = \sum_{n\in\mathbb{Z}} \phi(\frac{t}{2}-n) + \sum_{n\in\mathbb{Z}} \psi(\frac{t}{2}-n) + \sum_{n\in\mathbb{Z}} \psi(t-n)$$

Exercise 3.5

Comment on the linearity, time-invariant and invertibility property of Upsampler and Downsampler.
Hint: Upsampler: General equation for upsampling by M is given as,

$$\begin{aligned} x_{out}[n] &= x_{in}\left[\frac{n}{M}\right], && \text{where } n \text{ is multiple of } M \\ &= 0, && \text{otherwise} \end{aligned}$$

As, here zeroes are added in between, there is no loss of information during upsampling and we can retrieve the original sequence by passing through the downsampler by M. Hence, it is **Invertible**.
Now, consider,

$$
\begin{aligned}
x_{1out}[n] &= x_{1in}\left[\frac{n}{M}\right], && \text{where } n \text{ is multiple of } M \\
&= 0, && \text{otherwise}
\end{aligned}
$$

$$
\begin{aligned}
x_{2out}[n] &= x_{2in}\left[\frac{n}{M}\right], && \text{where } n \text{ is multiple of } M \\
&= 0, && \text{otherwise}
\end{aligned}
$$

Now, if we apply the combine input x_{1in} and x_{2in}, we get,

$$
\begin{aligned}
x_{out}[n] &= x_{1in}\left[\frac{n}{M}\right] + x_{2in}\left[\frac{n}{M}\right], && \text{where } n \text{ is multiple of } M \\
&= 0, && \text{otherwise}
\end{aligned}
$$

which is same as,

$$
\begin{aligned}
x_{out}[n] &= x_{1out}[n] + x_{2out}[n], && \text{where } n \text{ is multiple of } M \\
&= 0, && \text{otherwise}
\end{aligned}
$$

Hence, it is **Linear**.
Now, again consider our general equation of up-sampler by M. Now, delay the input sequence by k samples.

$$
\begin{aligned}
x_{out}[n] &= x_{in}\left[\frac{n}{M} - k\right], && \text{where } n \text{ is multiple of } M \\
&= 0, && \text{otherwise}
\end{aligned}
\tag{3.7}
$$

Now, replace n by $n-k$ in equation, we get

$$
\begin{aligned}
x_{out}[n] &= x_{in}\left[\frac{n-k}{M}\right], && \text{where } n \text{ is multiple of } M \\
&= 0, && \text{otherwise}
\end{aligned}
\tag{3.8}
$$

Now, Eqs. (3.7) and (3.8) are not equal. Hence, upsampling by M is **Time-variant**.
Downsampler: General equation for downsampling by M is given as,

$$x_{out}[n] = x_{in}[Mn]$$

Here, the samples which are at nonmultiple of M are deleted. Hence, it is not possible to retrieve the deleted samples by passing through upsampler. Hence, it is **Noninvertible**.
Similar to upsampler, we can show that it is **Linear** and **Time-variant**.

Exercise 3.6

A periodic sequence $x[n]$ with a period of 5 is applied at the input of the two-band filter bank shown in Fig. 3.29.

One period of the sequence $x[n]$ is indicated as below:

$$x[n] = \{\underset{\uparrow}{7}, -3, 4, 8, -5\}$$

1. Show that each of the sequences $y_k[n]$, $k = 1,2,3,...,9$ are periodic and obtain each of their periods P_k, $k = 1,2,3,...,9$.
2. For $k = 1,2,3,...,9$, obtain $y_k[n]$, $n = 0,...,(P_k - 1)$.
3. Comment on the relation between the input $x[n]$ and the output $y_9[n]$.

Hint: We can write corresponding sequences as below:

samples: –2 –1 0 1 2 3 4 5 6 7 8 9 10

$x[n]$: 8 −5 7 −3 4 8 −5 7 −3 4 8 −5 7

$x[n-1]$: 4 8 −5 7 −3 4 8 −5 7 −3 4 8 −5

$y_1[n]$: 12 3 2 4 1 12 3 2 4 1 12 3 2

$y_2[n]$: −4 13 −12 10 −7 −4 13 −12 10 −7 −4 13 −12

$y_3[n]$: 4 12 2 1 3 4 12 2 1 3 4 12 2

$y_4[n]$: 10 −4 −12 −7 13 10 −4 −12 −7 13 10 −4 −12

$y_5[n]$: 12 0 2 0 1 0 3 0 4 0 12 0 2

$y_6[n]$: −4 0 −12 0 −7 0 13 0 10 0 −4 0 −12

$y_5[n-1]$: 0 12 0 2 0 1 0 3 0 4 0 12 0

$y_6[n-1]$: 0 −4 0 −12 0 −7 0 13 0 10 0 −4 0

$y_7[n]$: 6 6 1 1 $\frac{1}{2}$ $\frac{1}{2}$ $\frac{3}{2}$ $\frac{3}{2}$ 2 2 6 6 1

$y_8[n]$: −2 2 −6 6 $\frac{-7}{2}$ $\frac{7}{2}$ $\frac{13}{2}$ $\frac{-13}{2}$ 5 −5 −2 2 −6

$y_9[n]$: 4 8 −5 7 −3 4 8 −5 7 −3 4 8 −5

From above, we can easily conclude that, each of the sequences $y_k[n]$, $k = 1,2,3,...,9$ are periodic and their periods P_k, $k = 1,2,3,...,9$ are as below:

$$P_1 = P_2 = P_3 = P_4 = P_9 = 5 \text{ and}$$

$$P_5 = P_6 = P_7 = P_8 = 10.$$

Hence, $y_k[n]$, $n = 0,...,(P_k - 1)$ are written as,

samples:	0	1	2	3	4	5	6	7	8	9
$y_1[n]$:	2	4	1	12	3					
$y_2[n]$:	-12	10	-7	-4	13					
$y_3[n]$:	2	1	3	4	12					
$y_4[n]$:	-12	-7	13	10	-4					
$y_5[n]$:	2	0	1	0	3	0	4	0	12	0
$y_6[n]$:	-12	0	-7	0	13	0	10	0	-4	0
$y_7[n]$:	1	1	$\frac{1}{2}$	$\frac{1}{2}$	$\frac{3}{2}$	$\frac{3}{2}$	2	2	6	6
$y_8[n]$:	-6	6	$\frac{-7}{2}$	$\frac{7}{2}$	$\frac{13}{2}$	$\frac{-13}{2}$	5	-5	-2	2
$y_9[n]$:	-5	7	-3	4	8					

It is seen that, $y_9[n]$ is actually periodic with a period of 5. The period $y_9[n]$, $n: 0 \to 4$ of $y_9[n]$, is essentially the period $x[n]$, $n: 0 \to 4$ of $x[n]$ circularly shifted by 1. This amounts to subjecting $x[n]$ to a delay of 1 sample as expected for this perfect reconstruction system.

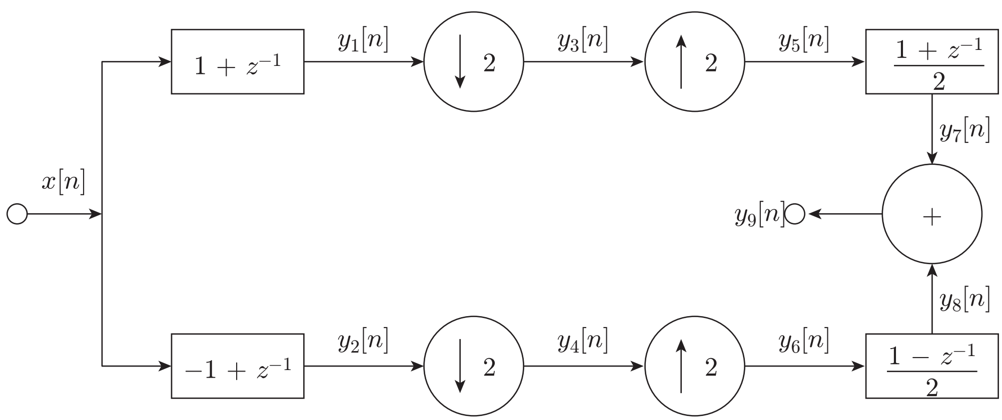

Figure 3.29 | Two-Band Filter Bank

Exercise 3.7

Why is the Haar MRA considered not adequate even though it can give perfect reconstruction?

Hint: The frequency response of the Haar low pass and high pass filter is $\cos\left(\frac{\omega}{2}\right)$ and $\sin\left(\frac{\omega}{2}\right)$ respectively. This leads to poor localization in frequency domain as the filter cutoff is not sharp. Hence, the Haar MRA is not considered adequate.

Exercise 3.8

Why is a filter with a zero phase response necessarily non-causal?
Hint: Consider a filter with transfer function $h(t)$ and Fourier Transform $H(\Omega)$.

$$\begin{aligned} H(\Omega) &= \int_{-\infty}^{\infty} h(t)e^{-j\Omega t}\,dt \\ &= \int_{-\infty}^{\infty} h(t)\cos(\Omega t)dt - j\int_{-\infty}^{\infty} h(t)\sin(\Omega t)dt \end{aligned}$$

For a zero phase response, imaginary part of $H(\Omega)$ is zero. Hence,

$$\int_{-\infty}^{\infty} h(t)\sin(\Omega t)dt = 0$$

Thus $h(t)$ must be an even function of t, i.e. symmetric about zero. Thus it will have values for $t < 0$ and hence will be noncausal.

Exercise 3.9

Why is linear phase important? What is pseudo-linear phase?
Hint: A transfer function is said to have a linear phase if the phase angle is directly proportional to frequency and the graph of angle v/s frequency is a straight line passing through the origin. Linear phase is important because it ensures that the entire waveform is shifted by the same time. In nonlinear phase system, since the different frequency components are delayed by different amounts, the waveform is distorted.
A transfer function is said to have a Pseudo-linear phase if the phase angle ϕ is related to frequency Ω by $\phi = m\Omega + c$, where $c \neq 0$ (**NOTE**: c can be different for different parts of Ω axis). Please refer to figures of magnitude and phase plots in given for further clarification.

Exercise 3.10

Why does 2-D processing NOT require causality as a condition for filter?
Hint: For applications such as image processing, the entire data is already present. Hence, the past, present and future samples are already known. Thus a non-causal filter can be employed for 2-D applications. However, if in 2-D processing, we have 2 different 1-D data streams which have to be operated in real time, then we cannot employ non-causal systems.

Chapter 4

M-Channel Filter Bank

4.1 | Introduction

In this chapter we will learn how to relate $\psi(t)$ and $\phi(t)$ of the MRA to the filter bank by studying the generic structure of the analysis and synthesis filter bank. It is obvious by now that such a connection exists. We built the filter bank out of the idea of multi-resolution analysis with the Haar MRA as an example. Let us first make a few generalizations which will help us to build that relationship more intimately. We will arrive at the general structure of the analysis and the synthesis filter banks based on the study of the Haar MRA.

4.2 | Haar Analysis Filter Bank

We shall discuss a two-band filter bank here as we are speaking of dyadic MRA and dyadic refers to changes by a factor of two. The analysis filter bank is shown in Fig. 4.1 for the case of the Haar MRA. Recall that in the Chapter 3, we had seen that the filter on the top is a crude low pass filter while filter in the bottom is a crude high pass filter. We call them crude in the sense that ideally the pass-band of one filter should not overlap other filter's stop band. We also saw that the filters together satisfy two very important properties, namely

- Magnitude complementarity, i.e. addition of amplitudes from both filters give the original amplitude of the signal.
- Power complementarity, i.e. addition of powers from individual filters gives back the original power of the signal

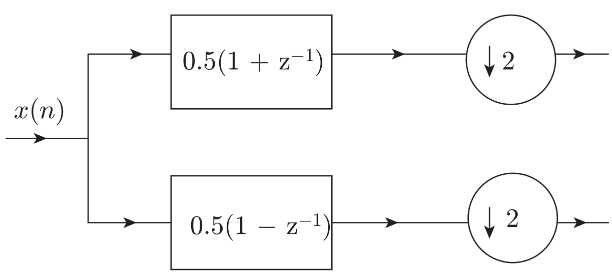

Figure 4.1 | *Haar analysis filter bank*

4.3 | Why is Haar Filter not Ideal?

To understand this, we should ask ourselves, what is the ideal response we would like to have? Let us have a look at both the filter responses of the Haar filter bank. (Fig. 4.2).

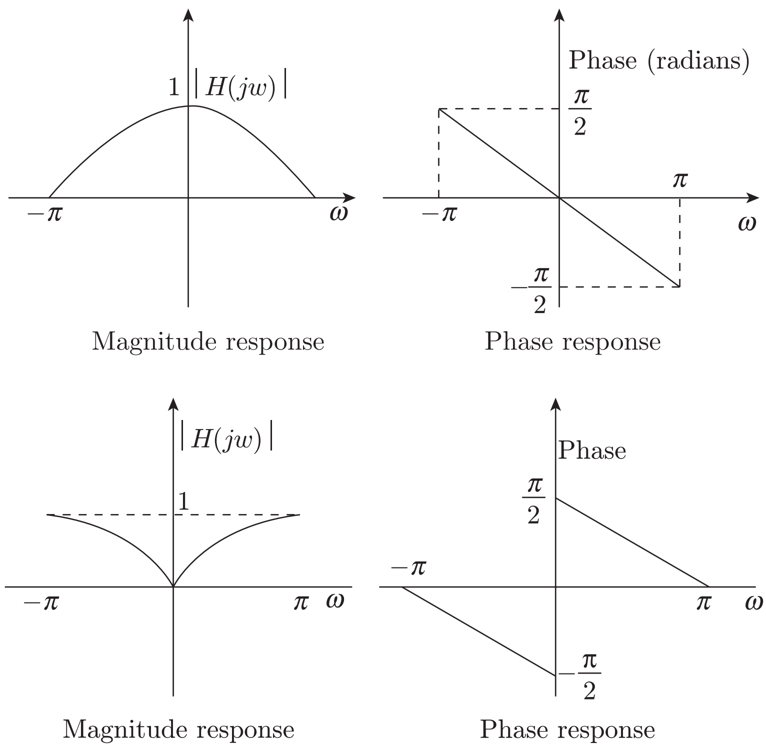

Figure 4.2 | *Magnitude and phase responses of analysis and synthesis filters of the Haar MRA*

The phase response of the high pass filter has a pseudo-linear phase, i.e. it is piecewise linear. The value of magnitude response is same for both the filters at $\omega = \frac{\pi}{2}$. What we ideally want is a perfect high pass and a perfect low pass filter characteristics, as shown in the Fig. 4.3.

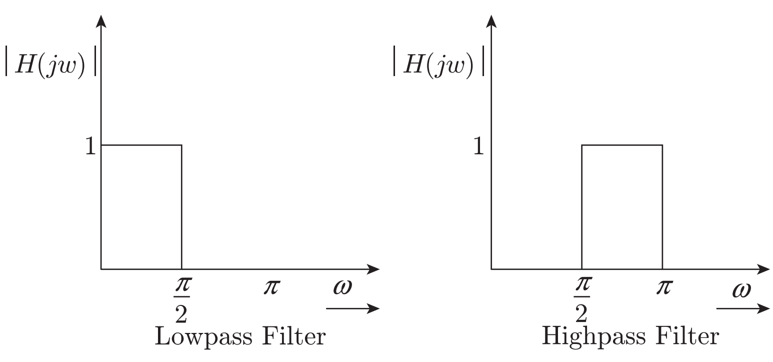

Figure 4.3 | *Ideal filters magnitude response*

It is clearly seen that the Haar filters are far from the desirable ideal filter responses. The ideal filter bank would have a structure similar to that in Fig. 4.4.

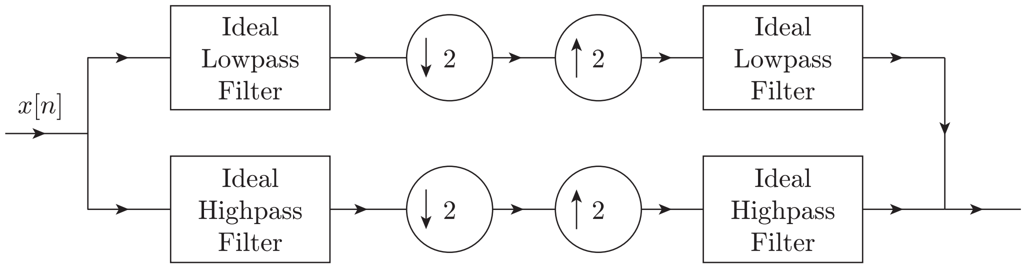

Figure 4.4 | *Ideal filter bank structure*

In ideal filter banks, the filters are identical. However, ideal filters are unrealizable and to reason it out we require the impulse responses of these ideal filters. This is not due to the limitations of technology today but due to the nature of the system. The impulse response $h[n]$ of a filter is obtained by taking the inverse Fourier transform of the filter frequency response as:

$$h_{ideal}[n] = \frac{1}{2\pi}\int_{-\pi}^{\pi} H_{ideal}[\omega] \quad e^{j\omega n}\, d\omega$$

The ideal low pass and high pass filter impulse responses are obtained by solving the above integral. The impulse responses of the ideal low pass and high pass filters are:

$$h_{idealLPF}[n] = \frac{\sin\left(\frac{\pi n}{2}\right)}{(\pi n)}, \quad n \neq 0$$

$$= \frac{1}{2}, \quad n = 0$$

and

$$h_{idealHPF}[n] = \frac{\sin(\pi n) - \sin\left(\frac{\pi n}{2}\right)}{(\pi n)}, \quad n \neq 0$$

$$= \frac{1}{2}, \quad n = 0$$

The above impulse responses show that the ideal filters are:

- *Infinitely noncausal*

The impulse response extends infinitely towards left side, i.e. for the negative values of index n, which makes it noncausal. For finite amount of noncausality, i.e only a finite number of n, Hence the infinite noncausal nature of the ideal filters makes it impossible to realize them.

- *Unstable*

  A linear time invariant system is said to be stable in BIBO (Bounded Input Bounded Output) sense if it produces a bounded output for a bounded input. The condition on the impulse response to attain stability is given as $\Sigma_{n\in\mathbb{Z}} |h[n]| < \infty$ i.e. the absolute sum of the impulse response coefficients should be finite. For ideal filters this absolute sum of impulse response coefficients diverges; *may not* produce a bounded output for a bounded input and are therefore unstable. Intuitively, the system may be stable for many of the known input signal but for some peculiar signal the system may give unbounded output, i.e. the system may become unstable. In other words for a bounded input the system may give unbounded output.

- *Irrational*

  The most important disqualification is that these systems is irrationality. Rationality and irrationality are the characteristics of linear time invariant (LTI) systems which have system function, i.e. their Z-transforms exist in some finite region of convergence. A filter system function is said to be rational if it can be expressed in terms of the ratio of two finite series in powers of z. Ideal filters cannot be expressed as a ratio of two **finite** series in powers of z and are therefore irrational or unrealizable. Non-realizability means that the system cannot be realized by physical means. There are no known techniques to realize irrational filters today, as they require infinite resources. Suppose we want to generate exponential signals they can easily generated by using R-C components. Irrationality must not be confused with stability and causality. Let us see an example of an irrational system function.

  The function $e^{z^{-1}}, |z| > 0$ is irrational and can be expanded as:

  $$e^{z^{-1}} = \sum_{n=0}^{\infty} \frac{(z^{-1})^n}{n!}$$

  Thus, the inverse Z-transform for the above equation can be obtained as

  $$h[n] = \frac{1}{n!} u[n]$$

  This is a convergent sum. Though all irrational systems are not unstable, but it is impossible to realize this as it requires infinite resources. Resources here constitute adders, multipliers and delays. A rational system can be realized by finite resources. However, ideal is often not achievable. But we can go arbitrarily close to the ideal by investing more and more resources. There are several ways of doing it, i.e. the resources can be put to use in different ways. At times investing in one specific method takes us faster to the ideal that some other, but certain aspects need to be compromised for this rate.

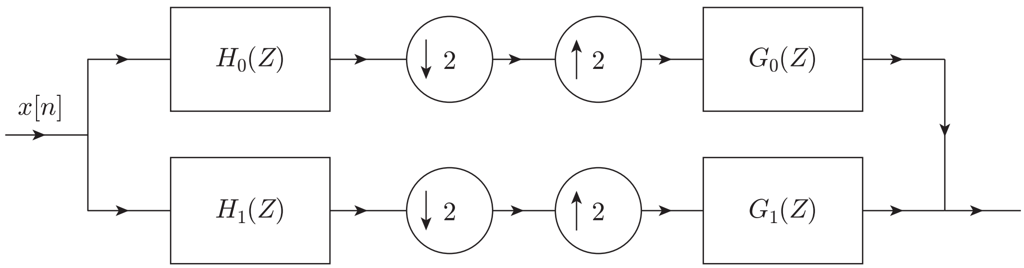

Figure 4.5 | *Haar analysis and synthesis filter banks*

4.4 | Realizable Two Band Filter Bank

Though the ideal filter bank is unachievable we can go quite close to it. We can build a two-band filter bank arbitrarily close to the ideal simply by investing more and more resources. But what does a realizable two-band filter bank look like? Let's say the realizable two-band filter bank looks like the one shown in Fig 4.5. The filter bank is realizable if $H_0(Z), H_1(Z), G_0(Z), G_1(Z)$ are all rational system functions. The filters must not satisfy any of the above-mentioned disqualifications. Hence the system responses $H_0(Z), H_1(Z), G_0(Z), G_1(Z)$ must be rational, stable, finitely causal. $H_0(Z), G_0(Z)$ aspire to be ideal low pass filters with $\omega_c = \frac{\pi}{2}$ and $H_1(Z), G_1(Z)$ aspire to be high pass filters with cutoff frequency $\omega_c = \frac{\pi}{2}$ as ideal filters are not achievable.

4.5 | Relation Between Haar MRA and Filter Bank

In this section, we will try to establish a relation between the functions $\phi(t)$, $\psi(t)$ and the filter banks. Let us focus our attention on Haar MRA. As discussed earlier, the Haar MRA is not ideal. Several concepts can be learned from the shortcomings of Haar MRA, which can be utilized to construct better families of Dyadic Multiresolution analysis.

4.5.1 Relation Between the Function $\phi(t)$ and Filter Banks

For Haar MRA, $\phi(t)$ is the basis of V_0 i.e $\phi(t) \in V_0$. Also, recall that there exists a ladder of spaces in MRA which states that $V_0 \subset V_1$. $\phi(t)$ should, therefore, be expressible in the basis of V_1 i.e. $\phi(2t-n)$, $n \in \mathbb{Z}$.

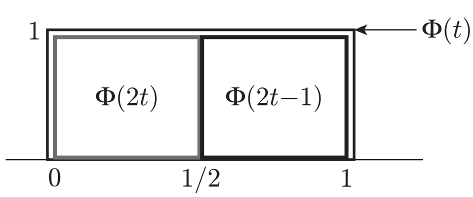

Figure 4.6 | *Expressing $\phi(t)$ in term of dilates and translates*

Example 4.5.1 — Connecting $\phi(t)$ and filter banks.

From the Fig. 4.6 we see that $\phi(t)$ is expressible in its own dilates and translates.

$$\phi(t) = \phi(2t) + \phi(2t-1)$$

The above equation is called the **dilation equation**. If we write down the coefficients of $\phi(2t-n)$ as a sequence, we get the impulse responses corresponding to the Lowpass filter.

$$\begin{array}{cc} 1 & 1 \\ \uparrow & \\ 0 & \end{array}$$

The dilation equation can thus be modified in a generalized way as follows:
If $h[n]$ is the impulse response of the low pass filter in the two band filter bank then,

$$\phi(t) = \sum_{n\in\mathbb{Z}} h[n]\phi(2t-n)$$

4.5.2 Relation Between the Function $\psi(t)$ and Filter Banks

$\psi(t) \in V_0$ should also be expressible in terms of basis of V_1 i.e. $\phi(2t-n), n \in \mathbb{Z}$.

Example 4.5.2 — Connecting $\psi(t)$ and filter banks.

Graphically, from Fig. 4.7, we can see that the dilation equation will be of the form

$$\psi(t) = \phi(2t) - \phi(2t-1)$$

If we write down the coefficients of $\phi(2t-n)$ as a sequence, we get the impulse responses corresponding to the high pass filter.

The dilation equation can thus be modified in a generalized way as follows.
If $g[n]$ is the impulse response of the high pass filter in the two-band filter bank then,

$$\psi(t) = \sum_{n\in\mathbb{Z}} g[n]\phi(2t-n)$$

This implies that, if we know the impulse responses, we can go the reverse way round to generate $\phi(t)$ and $\psi(t)$.
Thus in short,
low pass filter $\rightarrow$ scaling function expansion
high pass filter $\rightarrow$ wavelet expansion
Therefore, we can completely characterize the system $\phi(t)$ and $\psi(t)$ if we know their dilation equation.

$$\begin{array}{cc} 1 & -1 \\ \uparrow & \\ 0 & \end{array}$$

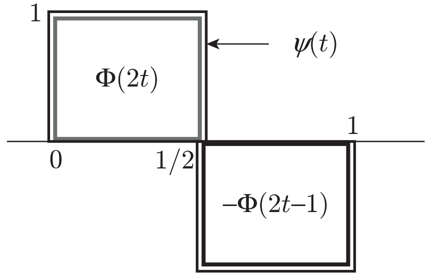

Figure 4.7 | *Expressing $\psi(t)$ in term of dilates and translates*

4.6 | The Strategy for Future Analysis

After obtaining the dilation equations, these equations are used to find the wavelet and the scaling function, given the high pass and the low pass filter responses. This is accomplished in two steps as follows:

- Take Fourier transform on both sides of the dilation equation to get a recursive equation in Fourier domain, which completely characterizes $F\{\phi(t)\}$ in terms of DTFT of $h[n]$.
- Relate Fourier transform of wavelet function to Fourier transform of scaling function by using DTFT of $g[n]$ to obtain the wavelet function.

4.7 | Iterated Filter Banks and Continuous Time MRA

In the last section we deduced certain concepts of the ideal two-band filter bank and studied the frequency response of ideal filter which is obtained for HAAR filter bank. Inspite of certain drawbacks of the ideal nature of filters we then derived the dilation equation, and the sequences related to it showed us a path to move from filter banks to the scaling and wavelet function. In this section, we will study the relation between filter coefficients and the basis vectors. HAAR filter bank case is particularly considered for calculations.

4.8 | Iterating the Filter Bank for $\phi(\cdot)$, $\psi(\cdot)$

The dilation equation relates filter bank to scaling function and also to wavelets.
If $h[n]$: low pass filter impulse response.
Then we can relate the operation of LPF $H(Z)$ on basis of input signal $\phi(t)$ in general as

$$\phi(t) = \sum_{n=-\infty}^{\infty} h[n]\phi(2t-n)$$

$$= \phi(2t) + \phi(2t-1)$$

for the case of HAAR low pass filter.
Dilation equation is a new class of equation, which denotes the relation between wavelets and multirate filter bank.

Example 4.8.1

For analysis let us consider the **Fourier transform of** $\phi(t)$ be $\hat{\phi}(\Omega)$ where Ω represent the analog angular frequency variable.

$$\hat{\phi}(\Omega) = \int_{-\infty}^{+\infty} \phi(t) e^{-j\Omega t} dt$$

$$= \int_{-\infty}^{+\infty} \sum_{n=-\infty}^{\infty} h[n]\phi(2t-n) e^{-j\Omega t} dt$$

$$= \sum_{n=-\infty}^{\infty} h[n] \int_{-\infty}^{+\infty} \phi(2t-n) e^{-j\Omega t} dt$$

$$= \sum_{n=-\infty}^{\infty} h[n] \frac{1}{2} e^{\frac{-j\Omega n}{2}} \int_{-\infty}^{+\infty} \phi(\lambda) e^{-j\Omega \frac{\lambda}{2}} d\lambda$$

$$= \sum_{n=-\infty}^{\infty} h[n] \frac{1}{2} e^{\frac{-j\Omega n}{2}} \hat{\phi}\left(\frac{\Omega}{2}\right)$$

This is via a transformation done by substituting $2\,t$ - $n = \lambda$.
Thus the frequency domain dilation equation can be represented as

$$\hat{\phi}(\Omega) = \frac{1}{2} H\left(\frac{\Omega}{2}\right) \hat{\phi}\left(\frac{\Omega}{2}\right)$$

where

$$\sum_{n=-\infty}^{\infty} h[n] e^{\frac{-j\Omega n}{2}}$$

is DTFT of h[.] at $\frac{\Omega}{2}$.

Recursively we can write,

$$\hat{\phi}\left(\frac{\Omega}{2}\right) = \frac{1}{2} H\left(\frac{\Omega}{4}\right) \hat{\phi}\left(\frac{\Omega}{4}\right)$$

Hence after N recursions,

$$\hat{\phi}(\Omega) = \left\{ \prod_{m=1}^{N} \frac{1}{2} H\left(\frac{\Omega}{2^m}\right) \right\} \hat{\phi}\left(\frac{\Omega}{2^N}\right) \qquad \text{where } N \in \mathbb{Z}$$

As,

$$\lim_{N \to \infty} \frac{\Omega}{2^N} = 0$$

Therefore,

$$\hat{\phi}\left(\frac{\Omega}{2^N}\right) = \hat{\phi}(0)$$

$$\hat{\phi}(\Omega) = \left\{\prod_{m=1}^{N} \frac{1}{2} H\left(\frac{\Omega}{2^m}\right)\right\} \hat{\phi}(0)$$

for finite Ω where $\phi(0)$ = constant. Therefore, we can express the Fourier transform $\hat{\phi}(\Omega)$ completely in terms of product of dilated LPF transfer function $H(\Omega)$ as above.
The product of dilated terms in the frequency domain implies the convolution of impulse response $h[n]$, subject to above dual equation of Fourier transform.

Now, consider the case of HAAR wavelet. When we carry out the same derivation (as above) for the HAAR scaling function ϕ(t) and draw the magnitude response, it appears looks same as the **sinc function** with maximum density around zero frequency and thus depicting the low pass nature.

Figure 4.8 | *h*[*n*] *and* *H*(Ω)

Consider $h[n]$ and its Fourier transform, as shown in Fig. 4.8.

$$\text{As } h[n] = \{1,1\} \overset{F.T}{\Leftrightarrow} H(\Omega) = (1 + e^{-j\Omega n})$$

$$\text{since } h[n] \overset{F.T}{\Leftrightarrow} H(\Omega)$$

$$h\left[\frac{n}{a}\right] \overset{F.T}{\Leftrightarrow} |a|.H(a\Omega)$$

Here $\delta \to 0$ imply moving towards the impulse function.Thus, we have train of impulses corresponding to the impulse response $h[n]$.
Now, consider a term

$$\prod_{m=1}^{N} \frac{1}{2} H\left(\frac{\Omega}{2^m}\right)$$

Let us take first $N = 3$ for our convenience.

$$H\left(\frac{\Omega}{2}\right).H\left(\frac{\Omega}{4}\right).H\left(\frac{\Omega}{8}\right)$$

Now put $\frac{\Omega}{8} = \lambda$.

Hence, the product be $H(4\lambda).H(2\lambda).H(\lambda)$

In time domain $H(4\lambda)$ means $h[n]$ upsampled by 4 and $H(2\lambda)$ is $h[n]$ upsampled by 2.

Now, we have to find out the convolution,
$h[n]$ *($h[n]$ up-sampled by 2)* ($h[n]$ up-sampled by 4).
This process can be carried out by following the steps depicted in plots shown above. We have $h[n]$ shown in Fig. 4.8, ($h[n]$ upsampled by 2) in Fig. 4.9 and convolution of these both, i.e $h[n]$*($h[n]$ upsampled by 2) in Fig. 4.10.

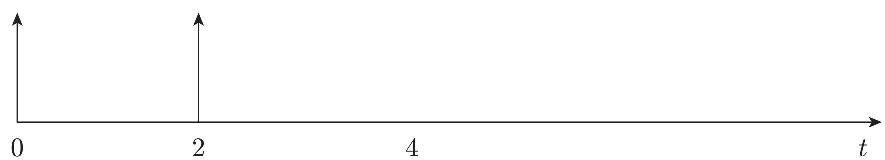

Figure 4.9 | $h[n]$ *upsampled by 2*

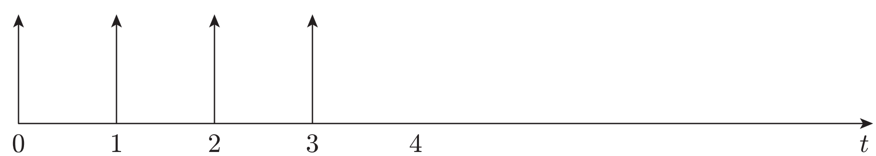

Figure 4.10 | $h[n]$*($h[n]$ *upsampled by 2)*

Now, consider ($h[n]$ upsampled by 4) as shown in Fig. 4.11. The plot shown in the figure convolves with impulse response ($h[n]$ upsampled by 4) to yield Fig. 4.12.

Now, replace $\frac{\Omega}{8} = \lambda$ according to our previous assumption. Since $\frac{\Omega}{8}$ means expansion in the frequency domain, hence we need to contract signal by the same factor in the time domain. Hence, contracting the resulting convolution term by a factor of 8 we get a plot as shown in Fig. 4.13.

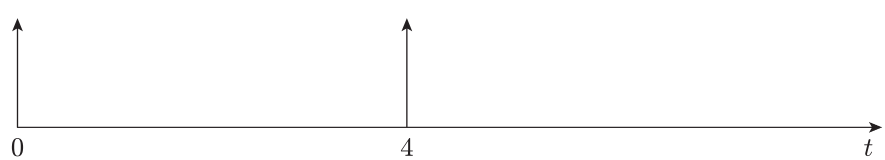

Figure 4.11 | $h[n]$ *upsampled by 4*

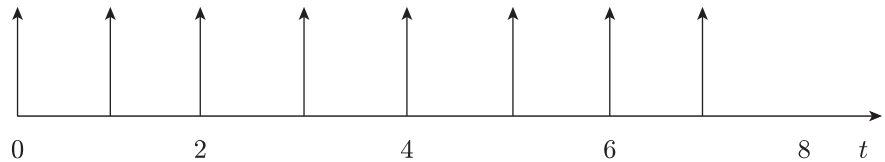

Figure 4.12 | *$h[n]$*($h[n]$ upsampled by 2)*($h[n]$ up-sampled by 4)*

Figure 4.13 | *after substituting* $\frac{\Omega}{8} = \lambda$

If we consider $N = 8$ and the higher indices so on on, i.e., moving towards the infinite iterations, the last of these impulses moves closer and closer to 1. Thus, we are obviously moving towards the continuous signal from 0 to 1 in time domain, as shown in Fig. 4.14, known as scaling function $\phi(t)$.

Similarly, we can construct the wavelet function as it is a function of basis function.

$$\psi(t) = \sum_{n=0}^{\infty} g[n]\phi(2t - n)$$

In terms of Haar wavelet $g[n] = \{1, -1\}$

$$\psi(t) = \phi(2t) - \phi(2t - 1) \quad \text{for } N = 1$$

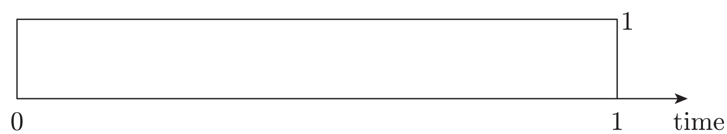

Figure 4.14 | *After infinite iterations*

Example 4.8.2

Let the **Fourier transform** of $\psi(t)$ be $\hat{\psi}(\Omega)$ then we have

$$\hat{\psi}(\Omega) = \int_{-\infty}^{+\infty} \psi(t) e^{-j\Omega t} dt$$

$$= \int_{-\infty}^{+\infty} \sum_{n=0}^{\infty} g[n]\phi(2t-n)e^{-j\Omega t}\,dt$$

$$= \sum_{n=0}^{\infty} g[n] \int_{-\infty}^{+\infty} \phi(2t-n)e^{-j\Omega t}\,dt$$

$$= \sum_{n=0}^{\infty} g[n] \frac{1}{2} e^{\frac{-j\Omega n}{2}} \int_{-\infty}^{+\infty} \phi(\lambda) e^{\frac{-j\Omega\lambda}{2}}\,d\lambda$$

$$= \sum_{n=0}^{\infty} g[n] \frac{1}{2} e^{\frac{-j\Omega n}{2}} \hat{\phi}\left(\frac{\Omega}{2}\right)$$

$$\hat{\psi}(\Omega) = \frac{1}{2} G\left(\frac{\Omega}{2}\right) \hat{\phi}\left(\frac{\Omega}{2}\right)$$

The same transformation in the integral and DTFT of $g[n]$ is being assumed as in the case of derivation of fourier transform of $\phi(t)$.
Recursively we can write,

$$\hat{\psi}\left(\frac{\Omega}{2}\right) = \frac{1}{2} G\left(\frac{\Omega}{4}\right) \hat{\phi}\left(\frac{\Omega}{4}\right)$$

Hence, the recursive equation can be written as,

$$\widehat{\Psi}(\Omega) = \frac{1}{2} G\left(\frac{\Omega}{2}\right) \frac{1}{2} H\left(\frac{\Omega}{4}\right) \frac{1}{2} H\left(\frac{\Omega}{8}\right) .... \hat{\phi}(0)$$

$$\psi(\Omega) = \frac{1}{2} G\left(\frac{\Omega}{2}\right) \{\prod_{m=2}^{N} \frac{1}{2} H\left(\frac{\Omega}{2^m}\right)\} \hat{\phi}(0)$$

Now, let N=3

$$G\left(\frac{\Omega}{2}\right).H\left(\frac{\Omega}{4}\right).H\left(\frac{\Omega}{8}\right)$$

Now put $\frac{\Omega}{8} = \lambda$. Hence the product now transforms to $G(4\lambda).H(2\lambda).H(\lambda)$

In the time domain, $G(4\lambda)$ means $g[n]$ upsampled by 4 and $H(2\lambda)$ signify $h[n]$ upsampled by 2. Now, we need to find out the convolution $h[n]*$ ($h[n]$ upsampled by 2) * ($g[n]$ upsampled by 4) for wavelet function.

This convolution can be carried out in much a similar way as it was in the case of the scaling function convolution.
We have $g[n]$ upsampled by 4 as shown in Fig. 4.15, $h[n]$ upsampled by 2 as shown in Fig. 4.16 and $h[n]$ * ($h[n]$ upsampled by 2) as shown in Fig. 4.17.

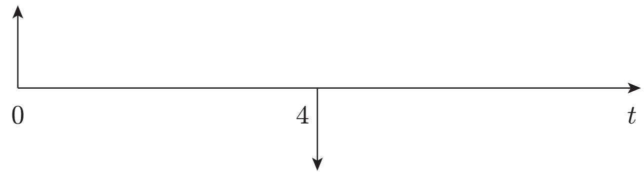

Figure 4.15 | *g[n] upsampled by 4*

Figure 4.16 | *h[n] upsampled by 2*

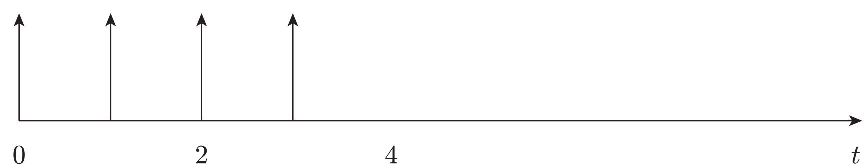

Figure 4.17 | *h[n]*h[n] upsampled by 2*

The convolution output obtained in Fig. 4.16 (i.e, $h[n]*h[n]$ upsampled by 2) is convolved with $g[n]$ upsampled by 4 which is shown in Fig. 4.18.

Now, again considering the assumption $\frac{\Omega}{8} = \lambda$, we contract the signal by factor 8 as explained above. Hence the resulted signal looks as shown in Fig. 4.19, which is achieved after performing the transformation $\frac{\Omega}{8} = \lambda$.

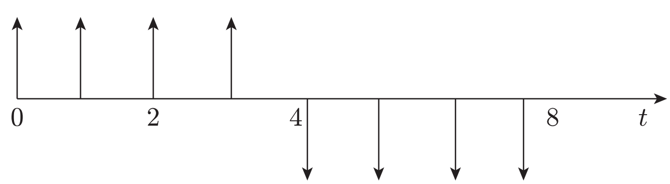

Figure 4.18 | *h[n]*(h[n] upsampled by 2)*(g[n] up-sampled by 4)*

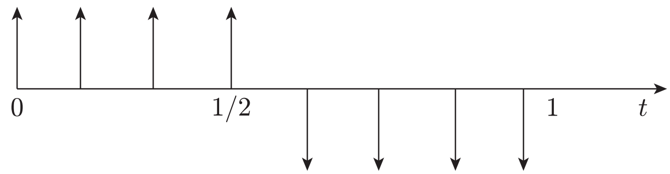

Figure 4.19 | *After substituting* $\frac{\Omega}{8} = \lambda$

Now, when we consider larger number of iterations the function keeps on moving closer to look like wavelet function. Thus, we reconstruct the wavelet function, $\psi(t)$ by performing infinite iterations ($N = \infty$) and get the final plot, as shown in Fig. 4.20.

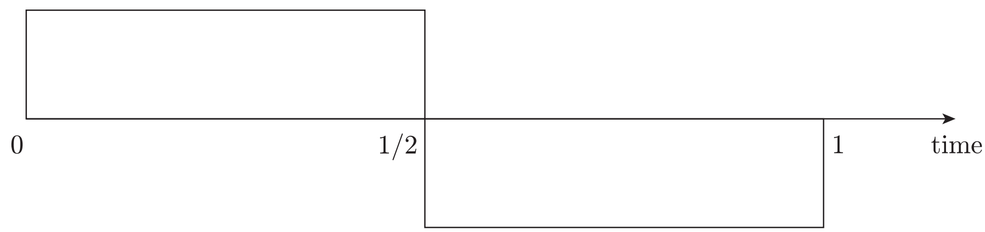

Figure 4.20 | *After infinite iterations*

4.9 | Z-domain Analysis of Multirate Filter Bank

In the few earlier sections we have established a very close relationship between the wavelet functions, the continuous time scaling function and the two channel filter bank. Convincingly, there is an intimate relationship between designing a two-band filter bank and a multiresolution analysis. After knowing the impulse response of the low pass filter in the filter banks, one can obtain the scaling function and hence the wavelet function by iterative convolution. Thus a pertinent reason for studying the two channel filter bank in great depth. We, now need to know how to deal with multi-rate operations. So let us begin with the two-channel filter bank.

4.10 | Two-channel Filter Bank

A two-channel filter bank has an analysis side and a synthesis side, as shown in the Fig. 4.21. On the analysis side we have two filters namely the low pass analysis filter and the high pass analysis filter followed by downsampling operations. On the synthesis side we have the upsampling operation followed by the synthesis low pass filter and the synthesis high-pass filter. The outputs of these got added forming the overall output, as shown in the figure.

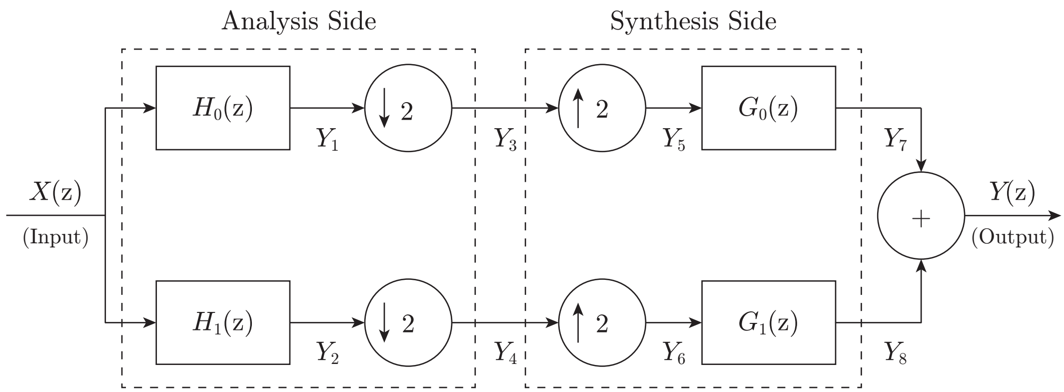

Figure 4.21 | *Two channel filter bank*

$H_0(z)$: Discrete time analysis low pass filter with angular cutoff frequency $\dfrac{\pi}{2}$

$G_0(z)$: Discrete time synthesis low pass filter with angular cutoff frequency $\dfrac{\pi}{2}$

$H_1(z)$: Discrete time analysis high pass filter with angular cutoff frequency $\dfrac{\pi}{2}$

$G_1(z)$: Discrete time synthesis high pass filter with angular cutoff frequency $\dfrac{\pi}{2}$

The signals $X, Y_1, Y_2, Y_5, Y_6, Y_7, Y_8, Y$ are all of sequences of sampling rate x. The signal Y_3, Y_4 are sequences of sampling rate $\dfrac{x}{2}$.

The unusual and new blocks in the above-shown block diagram are the upsampler and downsampler; unusual in the sense that one is not exposed to these while discussing filters.

4.10.1 Analysis of Downsampler Operation

Let us consider the downsampler block in detail. A basic downsampling operation is as follows:

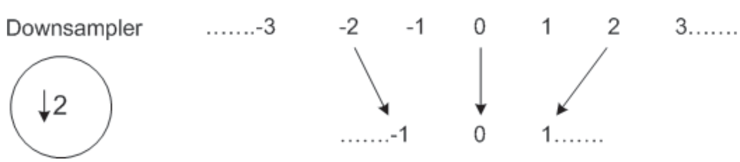

The above sequence of numbers represents the indices of the samples of a signal prior to downsampling, the bottom sequences of numbers represents the resultant indices of the signal after subjecting it to downsampling operation. Hence a downsampling operation can be viewed as the combination of 2 steps as follows:

1. It first “kills” some samples as explained below:

where (.) represent the indices of the samples that are retained without killing and those with no braces represent the ‘killed’ samples of the given sequence.

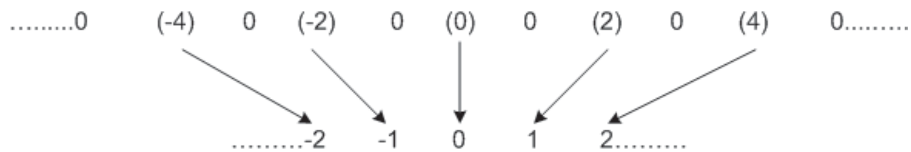

2. Then it compresses the resultant as shown above.

4.10.2 Analysis of Upsampler Operation

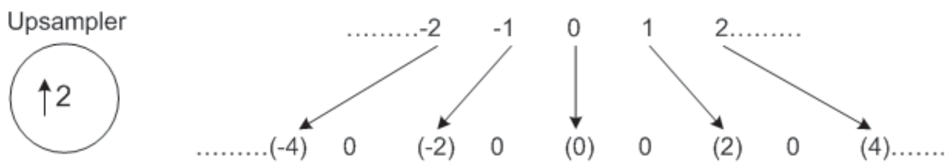

The upsampler outdoes the last ’compression’ step of a downsampler. Hence, it is also called Expander. The upsampler operation is invertible; we can get the original sequence, i.e. the sequence prior the upsampling. It converters a sequence of lower sampling rate to a sequence of higher sampling rate, whereas the downsampling operation is not invertible. The downsampler converts a sequence of higher sampling rate to a sequence of lower sampling rate. Downsampler and upsampler operations are taken care of by clocking rates at different points in the sytem. Consider the downsampling a sequence by M and let $M = 5$, this is as shown below:

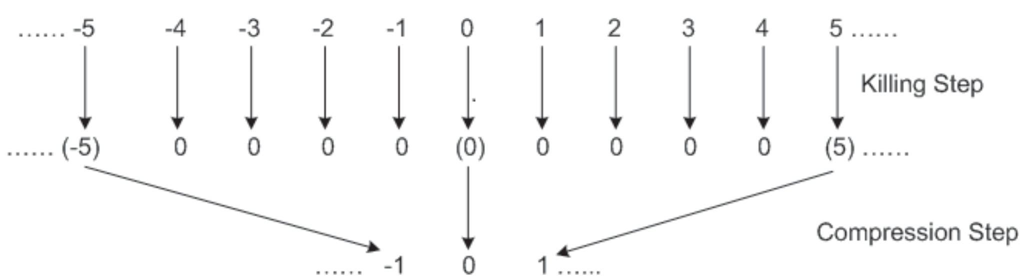

Consider the upsampling operation by M. assume $M = 7$: Then it is as follows:

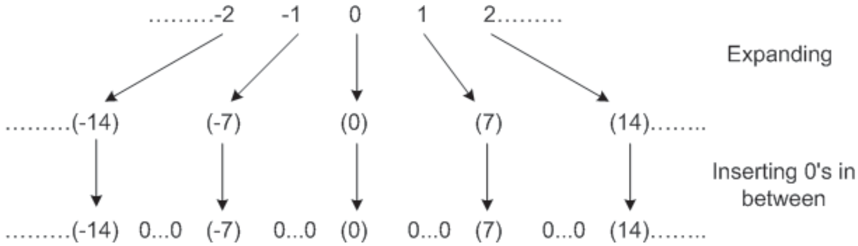

4.10.3 Z-Domain Effect of Upsampling

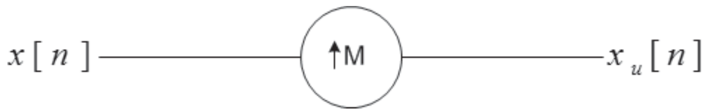

$$X_u[z] = \sum_{-\infty}^{+\infty} x_u[k] z^{Mk}$$

$$X_u[z] = X[z^M]$$

$$X[z] = X_u[z^{\frac{1}{M}}]$$

Therefore, it is evident that the upsampling operation is invertible.

4.10.4 Z-Domain Effect of Downsampling

First "killing step" can be viewed as a "modulation" or "multiplication by killing sequence" (a window). We pass those values through the window which are retained. Window periodic sequence: $P_W[n]$; P represents periodic and W represents windowed.

The process of killing is essentially multiplication by $P_W[n]$ for the appropriate M and it can be written as shown in the figure where the bar on upsampler denotes the inverse upsampling operation.

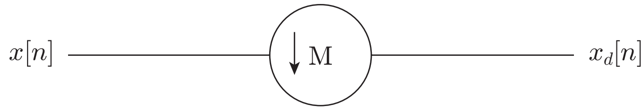

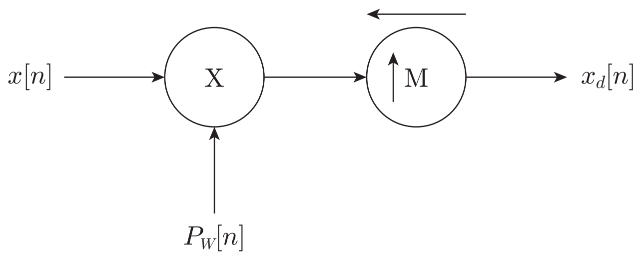

Multiplying a sequence by a sequence in Z-domain is best done by exponentials. So, the noninvertible part of the downsampling operation must be replaced.

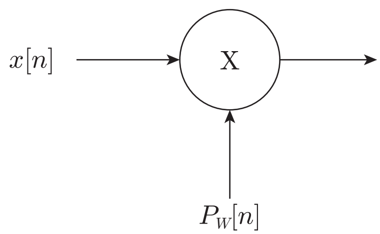

In other words, we need to express $P_W[n] = \sum_{k=1}^{Q} C_k \alpha_k^n$ DFT represents time-limited periodic sequences as the combination of exponentials, i.e., time-limited sequence means $b_0, b_1, ..., b_{N-1}$. Its Discrete Fourier Transform (DFT) is given as:

$$B[k] = \sum_{n=0}^{N-1} b[n] e^{-j\frac{2\pi}{N}nk} \quad \text{where} \quad k = 0, 1, ..., N-1$$

We can reconstruct $b[n]$ by the IDFT equation defined as

$$b[n] = \frac{1}{N} \sum_{k=0}^{N-1} B[k] e^{j\frac{2\pi}{N}nk} \quad \text{where} \quad n = 0, 1, ..., N-1$$

even if reconstructed for $n > N-1$ up to ∞, we can get a sequence periodic in N. The expression $\sum_{k=0}^{N-1} B[k] e^{j\frac{2\pi}{N}nk}$ generates a periodic sequence say $\tilde{b}[n]$.

$$\tilde{b}[n+lN]=\sum_{k=0}^{N-1}B[k]e^{j\frac{2\pi}{N}(n+lN)k}$$

$$=\sum_{k=0}^{N-1}B[k]e^{j\frac{2\pi}{N}nk}.e^{j2\pi l}$$

$$\tilde{b}[n+lN]=\tilde{b}[n]$$

For $M = 2$, we have a periodic sequence ...1 0 1 0 1 0 1 0 1 0 1...

where one period of the sequence is 1 0, taking DFT of the one period 1 0 is given as

$$B[k]=1.e^{-j\frac{2\pi}{2}}+0=1$$

$P_W[N]$ for $M = 2$ is

$$=\frac{1}{2}\sum_{k=0}^{1}B[k]e^{j\frac{2\pi}{2}nk}$$

$$=\frac{1}{2}\sum_{k=0}^{1}1.e^{j\frac{2\pi}{2}nk}$$

$$=\frac{1}{2}[1^n+(-1)^n]$$

Hence

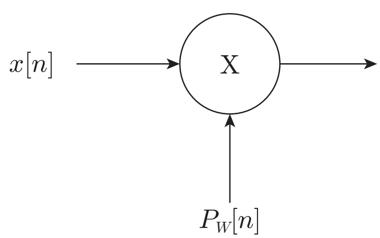

gives Z-transform as

$$=\sum_{n=-\infty}^{+\infty}x[n]\left(\frac{1}{2}[1^n+(-1)^n]\right)z^{-n}$$

$$=\frac{1}{2}\sum_{n=-\infty}^{+\infty}x[n]z^{-n}+\frac{1}{2}\sum_{n=-\infty}^{+\infty}x[n](-z)^{-n}$$

$$=\frac{1}{2}\left(X[z]+X[-z]\right)$$

This is the modulation opereation. So, it is followed by an inverse upsampler operation for the downsampling operation to be completed.

$$X_d[n] = \frac{1}{2}\left(X\left[z^{\frac{1}{2}} \right] + X\left[-z^{\frac{1}{2}} \right] \right)$$

Additional information

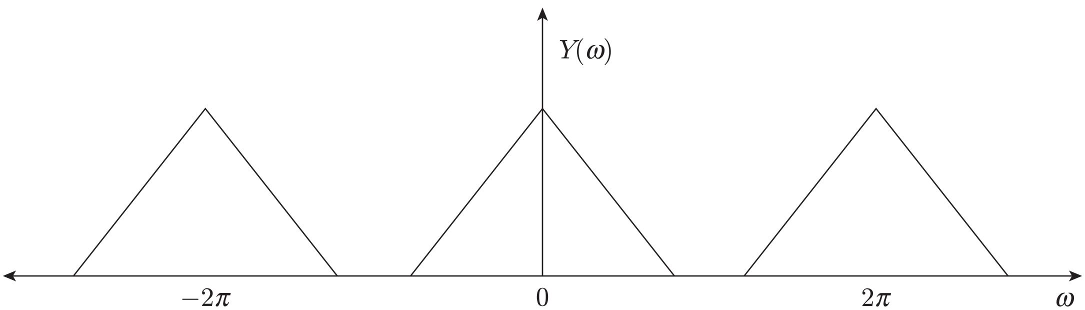

Figure 4.22 | *Signal spectrum before downsampling operation*

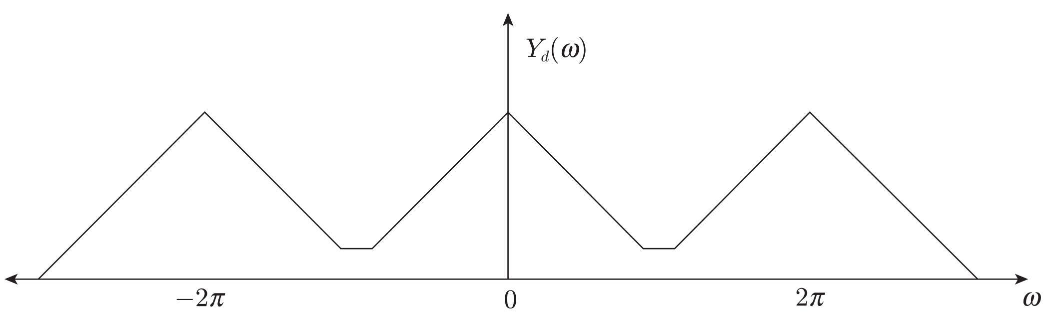

Figure 4.23 | *Signal spectrum after downsampling operation*

Downsampling operation in time domain corresponds to aliasing in the frequency domain unless the given signal is sufficiently bandlimited in time. It can be pictorially explained as shown in Figs. 4.22 and 4.23. Figure 4.22 shows the discrete time fourier transform of a signal without downsampling operation. The signal then subjected to the downsampling operation may result in aliasing in the spectrum of the signal, as shown in Fig. 4.23. It may not be with all downsampling cases as explained below:

Example 4.10.1 — Example: Samplers.

Let $x[n]$ is a discrete time signal given by

$$x_1[n] = [-1,2,1,0,3,-2], \quad n = 0,1,..5$$

$$x_2[n] = [-1,0,1,0,3,0], \quad n = 0,1,..5$$

if the above signals are subjected to downsampling operation by a factor of 2, then the signal $x_1[n]$ will suffer aliasing and signal $x_2[n]$ will not suffer aliasing.
Hence the downsampling operation is not invertible when it result in the aliasing of the spectrum in the frequency domain, while it is invertible when it does not result in aliasing. Whereas the upsampling operation is always invertible.
The aliasing that is noticed in the 2-band filter bank is because of the downsampling operations involved in the process.

In this chapter we have established the Z-transforms of the basic multirate operations in terms of the original Z-transforms of the sequences. We shall continue with this further in the next chapter to carry out the complete analysis of the two-channel filter bank.

4.11 | *M*-band Filter Banks and Looking Ahead

M-band filter banks are generalization of 2-band filter banks. For 2-band filter banks the signal is downsampled and upsampled by a factor of 2 but in the case of generalized *M*-band filter bank, the sequence is sampled by a factor of *M*.
In next few sections a specific case of $M = 3$, called 3-band filter bank, is considered and analyzed in depth, which will help in understanding the generalization to any *M*.

4.12 | 3-band Filter Bank (Ideal)

Similar to 2-band filter banks, we can define 3-band filter banks too. This is shown in Fig 4.24.

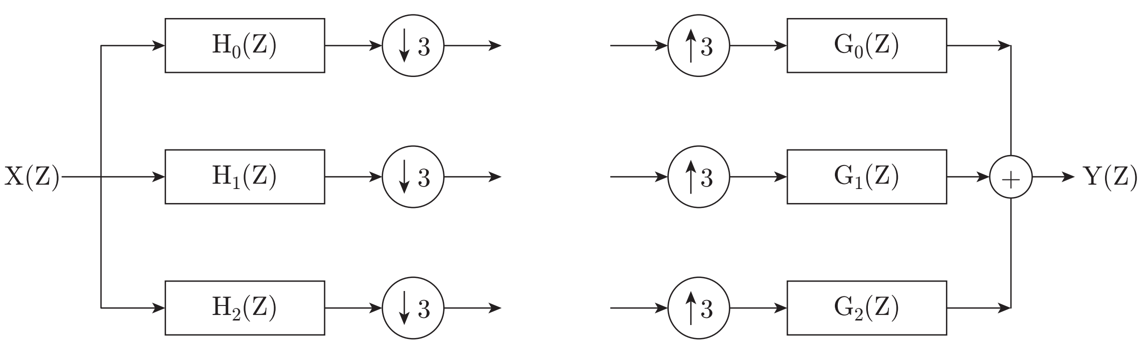

Figure 4.24 | *Analysis side and synthesis side of a 3-band filter bank*

The above filter is true for any uniform 3-band filter bank, i.e., the length of all filters should be equal.
For ideal perfect reconstruction $Y = X$, but in general for perfect reconstruction the output Y can be a scaled or/and delayed function of X, also it can be a version of X with an easily invertible operation.

4.12.1 Analyzing an Ideal 3-band Filter Bank

Conditions for perfect reconstruction:

$$H_0 = G_0$$

$$H_1 = G_1$$

$$H_2 = G_2$$

Frequency responses of the ideal filters

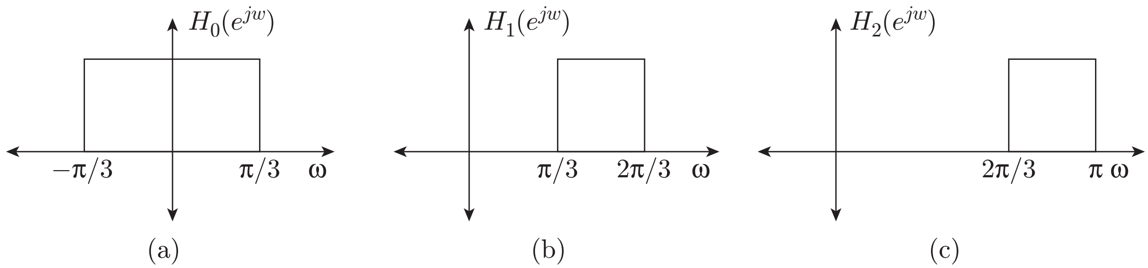

Figure 4.25 | *(a)H_0: a low pass filter, (b)H_1: a band pass filter, (c)H_2: a high pass filter*

Figure 4.25(a–c) shows the frequency responses of the ideal filter banks for a 3-band filter bank. As you can see the frequency axis is divided into three parts from 0 to $\frac{\pi}{3}$, $\frac{\pi}{3}$ to $\frac{2\pi}{3}$ and $\frac{2\pi}{3}$ to π, thereby covering the complete axis.

Frequency effect of Upsampling

$$A(e^{jw}) \longrightarrow \boxed{\uparrow 3} \longrightarrow A(e^{3jw})$$

Figure 4.26 | *Upsampling by 3*

As can be seen there is a compression of frequency axis by a factor of 3. (Fig 4.26).
Suppose we have a spectrum, as shown in Fig. 4.27(a), its upsampled version will be as shown in Fig. 4.27(b) where frequency axis is compressed by a factor of 3.

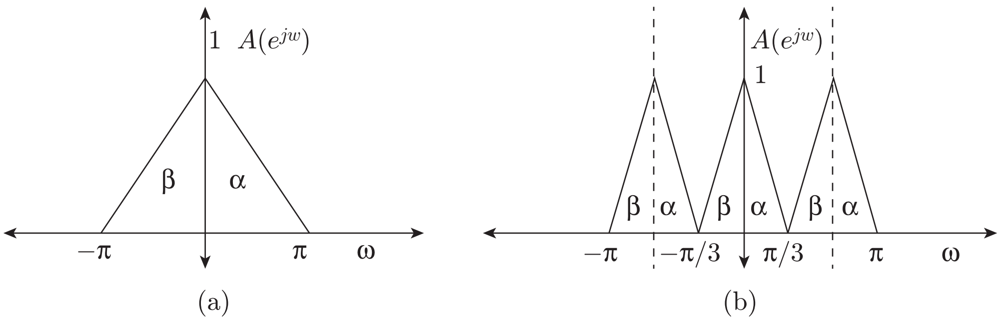

Figure 4.27 | *(a) Original spectrum,(b) Upsampled version by compressing frequency axis by a factor of 3*

Frequency effect of Downsampling

Downsampling by a number creates aliases of the original spectrum, i.e., it will have original spectrum shifted and added. Figure 4.28 shows the downsampling by 3.

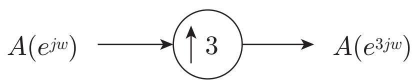

Figure 4.28 | *Downsampling by 3*

Downsampling is effectively multiplying the sequence by ..1001001001.. and then compressing it by throwing away the zeros obtained. Since ..1001001.. is a periodic sequence, it can be expressed in the terms of its IDFT by taking one period, finding its DFT and then IDFT giving us the sequence in form of modulates.

The above periodic sequence can be written as: $\frac{1}{3}\sum_{k=0}^{2} e^{\frac{j2\pi kn}{3}}$. We multiply this expression with the sequence to be downsampled in frequency domain and then reduce the z^3 to z to obtain the final downsampled version.

Effectively,

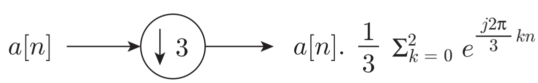

the above equation can be easily analyzed and solved in Z-domain; multiplying it and then replacing Z by $Z^{\frac{1}{3}}$ to get the downsampled sequence.

In Z-domain

$$a[n] \overset{Z-transform}{\rightarrow} A(Z)$$

$$a[n]\frac{1}{3}\sum_{k=0}^{2} e^{\frac{j2\pi kn}{3}} \overset{Z-transform}{\rightarrow} \sum_{k=0}^{2}\frac{1}{3}A(Ze^{\frac{j2\pi k}{3}}) \tag{4.1}$$

now replace Z by $Z^{\frac{1}{3}}$, we get

$$A[z] \longrightarrow \boxed{\downarrow 3} \longrightarrow \sum_{k=0}^{2} \frac{1}{3} A[z^{\frac{1}{3}}. e^{\frac{j2\pi}{3}k}]$$

In sinusoidal frequency domain

$$A[e^{j\omega}] \longrightarrow \boxed{\downarrow 3} \longrightarrow \frac{1}{3} \sum_{k=0}^{2} A[e^{\frac{j(\omega+2\pi)}{3}k}]$$

The last equation in the above section shows that the downsampled version of sequence is obtained by shifting its DTFT on the frequency axis by $\dfrac{2\pi}{3}$ for $k = 0,1,2$ and adding. After adding the shifted DTFTs, scale it vertically by $\dfrac{1}{3}$ and horizontally stretch by a factor of 3 to get the final downsampled by 3 version.

4.12.2 Interpretation of 3-band Filter Bank

Low frequency interpretation

Now, let us analyze the effect of the 3-band filter bank in a low frequency region on a prototype spectrum. Figure 4.29 shows the prototype spectrum to be analyzed. Spreaded over the whole frequency range with a variable amplitude assuming 0 phase.

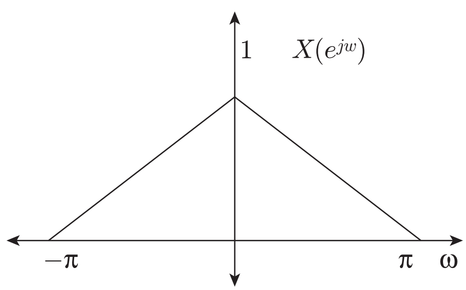

Figure 4.29 | *Prototype spectrum*

Subject this spectrum to the low pass branch in the ideal 3-band filter bank, which has a cut off frequency of $\dfrac{\pi}{3}$ and a downsampler of 3.

Firstly, spectrum obtained after passing it through the low pass filter is shown in Fig. 4.30.

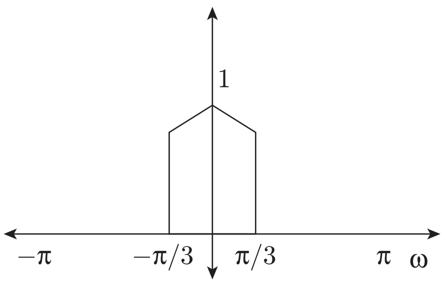

Figure 4.30 | *Low pass spectrum*

Secondly, spectrum obtained after translating to multiples of $\frac{2\pi}{3}$ and adding is shown in Fig. 4.31.

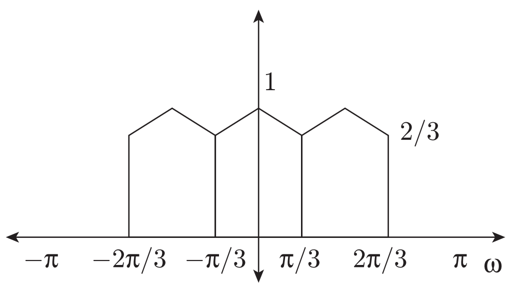

Figure 4.31 | *Translated by multiples of* $\frac{2\pi}{3}$ *and added*

Lastly, the spectrum obtained by scaling vertically by a factor of $\frac{1}{3}$ and horizontally by a factor of 3 is shown in Fig. 4.32.

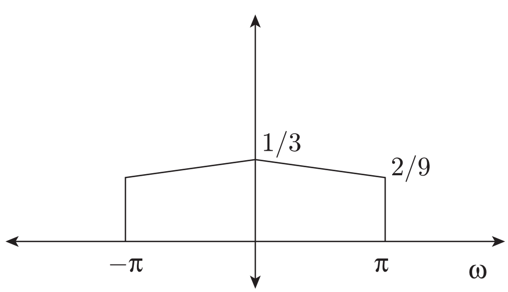

Figure 4.32 | *Spectrum obtained after subjecting to analysis filter bank*

Now, for synthesis we upsample it by 3 and pass it through the synthesis low pass filter. It retains the scaled version of the original filter and destroys the aliases. The spectrum obtained is as shown in Fig. 4.33.

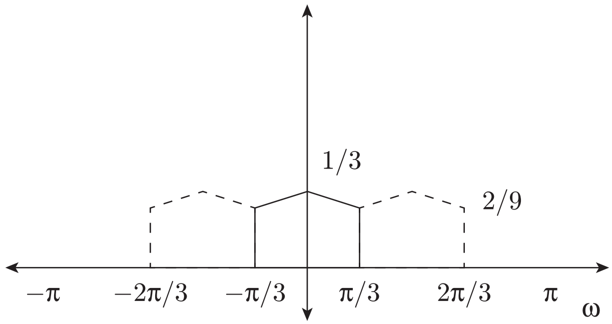

Figure 4.33 | *Spectrum obtained after subjecting the sequence to low frequency branch*

Aliases gets created in between the analysis and synthesis filters, because we wish to retain the total amount of data. The total number of samples per unit time at the input of the analysis filter is reduced to one-third at the outputs of each of the downsamplers. Thus, total amount of information remains the same at any point of time.

Middle branch interpretation

On the analysis side of the middle branch we have a bandpass filter between $\frac{\pi}{3}$ and $\frac{2\pi}{3}$ followed by a downsampler of 3.

Let us take the same prototype spectrum, when subjected to a bandpass filter, we obtain a spectrum as shown in Fig. 4.34.

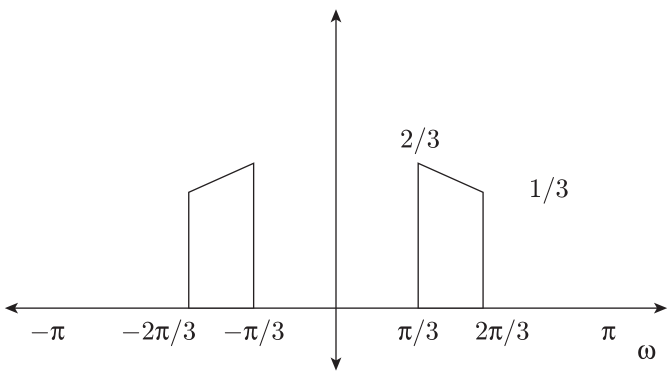

Figure 4.34 | *Band pass version of the signal*

After passing it through the bandpass filter, a downsampler by 3 acts on the spectrum. The spectrum is translated by shifts of multiples of $\frac{2\pi}{3}$ and added as shown in Fig. 4.35. To obtain the final downsampled version, the spectrum is scaled vertically by a factor of $\frac{1}{3}$ and horizontally by a factor of 3. Spectrum obtained is as shown in Fig. 4.36.

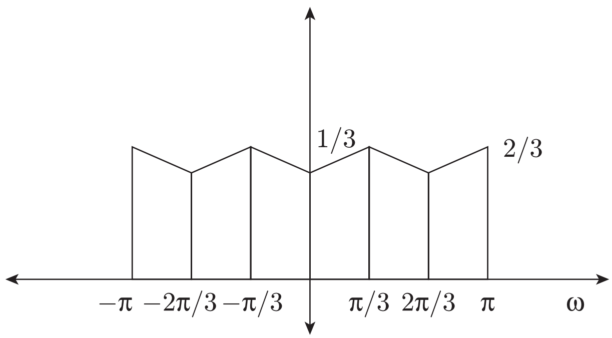

Figure 4.35 | *Translated by multiples of* $\frac{2\pi}{3}$ *and added*

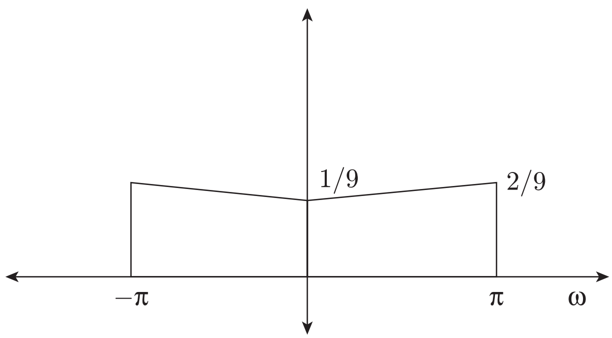

Figure 4.36 | *Middle branch spectrum after subjecting to analysis side*

Now, for synthesis we upsample it by 3 and pass it through the synthesis low pass filter. It retains the scaled version of the original filter and destroys the aliases. The spectrum obtained is as shown in Fig. 4.37.

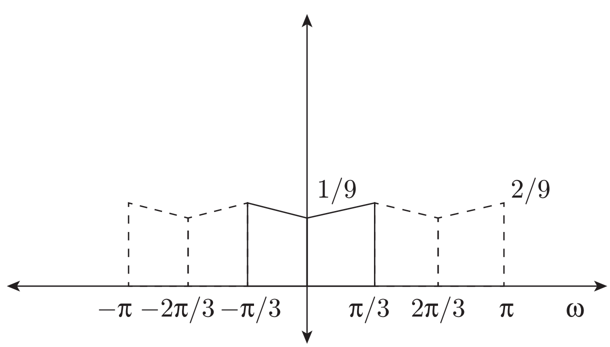

Figure 4.37 | *Reconstructed Middle branch spectrum*

Exercises

Exercise 4.1

Prove that:

$$\sum_{n\in\mathbb{Z}} h[n] = 2$$

and

$$\sum_{n\in\mathbb{Z}} g[n] = 0$$

Where $h[n]$ and $g[n]$ are the impulse responses of the low pass and high pass analysis filters respectively used in MRA.
Hint: The problem can be answered using the two dilation equations of the scaling and the wavelet function used in MRA. The two dilation equations are:

$$\phi(t) = \sum_{n\in\mathbb{Z}} h[n]\phi(2t-n) \tag{4.2}$$

$$\psi(t) = \sum_{n\in\mathbb{Z}} g[n]\phi(2t-n) \tag{4. 3}$$

Integrating Eq. 4.2 with respect to t on both sides we get:

$$\int_{\infty}^{-\infty} \phi(t)dt = \int_{\infty}^{-\infty} \sum_{n\in\mathbb{Z}} h[n]\phi(2t-n)dt$$

$$\int_{\infty}^{-\infty} \phi(t)dt = \sum_{n\in\mathbb{Z}} h[n] \int_{\infty}^{-\infty} \phi(2t-n)dt \tag{4. 4}$$

We will solve the integral term in the above summation:
Substituting $2t - n = k$ in the integral we get:

$$\int_{\infty}^{-\infty} \phi(2t-n)dt = \frac{1}{2}\int_{\infty}^{-\infty} \phi(k)dk \tag{4.5}$$

Now $\int_{\infty}^{-\infty} \phi(k)dk$ is the area under the scaling function which is equal to one, i.e

$$\int_{\infty}^{-\infty} \phi(k)dk = 1 \tag{4.6}$$

Therefore from Eqs. (4.4), (4.5) and (4.6) we get:

$$1 = \sum_{n\in\mathbb{Z}} \frac{h[n]}{2}$$

$$\sum_{n\in\mathbb{Z}} h[n] = 2$$

Similarly, integration dilation equation for the wavelet function, i.e Eq. (4.3) we get

$$\int_{\infty}^{-\infty} \psi(t)dt = \int_{\infty}^{-\infty} \sum_{n\in\mathbb{Z}} g[n]\phi(2t-n)dt$$

$$\int_{\infty}^{-\infty} \psi(t)dt = \sum_{n\in\mathbb{Z}} g[n] \int_{\infty}^{-\infty} \phi(2t-n)dt \tag{4.7}$$

Now $\int_{\infty}^{-\infty} \psi(t)dt = 0$ i.e are under $\psi(t)$
Thus, from Eqs. (4.5), (4.6) and (4.7), we have

$$\sum_{n\in\mathbb{Z}} g[n] = 0$$

Exercise 4.2

Prove that for a causal system the impulse response $h[n] = 0$ for $n < 0$.
Hint: For a system to be causal its output should be independent of the future input, i.e it should be generated or caused as an effect of something (in our case an input). Thus by general sense effect cannot be produced before an event occurs (i.e input), and therefore causal systems are independent of future input values.
Now, consider an impulse response defined for both positive and negative indices, say from -1 to +1, as in Fig.4.38.
Let the output sequence be $y[n]$ and the input be $x[n]$.
The input output relationship in the Z-domain is given as:

$$Y(Z) = H(Z)X(Z)$$

$$Y(Z) = h_{-1}Z + h_0 + h_1 Z^{-1})X(Z)$$

$$Y(Z) = h_{-1}ZX(Z) + h_0 X(Z) + h_1 Z^{-1} X(Z) \tag{4.8}$$

Taking inverse Z-transform of Eq. (4.8), we get

$$y[n] = h_{-1}x[n+1] + h_0 x[n] + h_1 x[n-1].$$

We find that the present output is dependent on future input, i.e $y[n]$ is dependent on $x[n+1]$ which is against our discussion of causality. Thus, to make the system causal, in above case $h_{-1}=0$. Further, we can generalize it as:
For a system to be causal $h[n]=0$ for $n<0$.

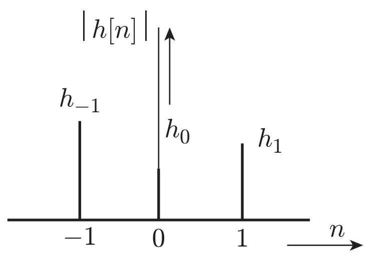

Figure 4.38 | *Impulse response h[n]*

Exercise 4.3

Why the frequency response of $\phi(t)$ should not have zero at $w=0$?

Hint: Frequency response of $\phi(t)$ at $w=0$ is constant because of **low pass** nature of $\phi(t)$.

Exercise 4.4

Prove that if the length of wavelet filter is L then the support of scaling function $\phi(t)$is $L-1$?
Hint: As defined earlier, scaling function is given as,

$$\hat{\phi}(\Omega)=\{\prod_{m=1}^{N}\frac{1}{2}.H\left(\frac{\Omega}{2^m}\right)\}.\hat{\phi}(0).$$

Now, the multiplication in frequency domain corresponds to convolution in time domain.
If we consider two functions $x[n]$ extending from 0 to N and $y[n]$ extending from 0 to M. Now, convolution of $x[n]$ and $y[n]$ will extend from 0 to $N+M$.
Similarly, if we consider wavelet filter $h[n]$ having length L that is extending from 0 to $L-1$.
Now, for each iteration filter support squeezes by a factor $\frac{1}{2}$.
Hence the support of scaling function is the sum of

$$\left(\frac{L-1}{2}\right)+\left(\frac{L-1}{4}\right)+\left(\frac{L-1}{8}\right)+\left(\frac{L-1}{16}\right)+\ldots\ldots\ldots\ldots+\infty.$$

This sums up to $L-1$.

Exercise 4.5

How does the killing step of the downsampling operation is described mathematically?
Hint: Killing is nothing but multiplication of the given signal to be downsampled by a signal termed as windowed periodic sequence $P_W[n]$, which can be described as the combination of the exponentials by means of the DFT (Discrete Fourier Transform) which then simply implies killing step of downsampling is mathematically done by subjecting the given signal to modulation property of the Z-transform.

Exercise 4.6

Are the downsampling and the upsampling operations linear and shift invariant?
Hint: The downsampling and the upsampling operations are linear but not shift invariant, one can easily check the linearity by the principle of superposition. The signals obtained by downsampling the delayed signal will be different from the signal obtained by delaying the downsampled signal, so they are shift variant.

Chapter 5

Conjugate Quadrature Filter Bank

5.1 | Introduction

In the previous chapter we studied Z-domain analysis of two-channel filter bank. This structure is often used in the implementation of discrete wavelet transform. So in this chapter we intend to analyze it completely by relating the Z-transform at every point of following structure and finding relationship between $H_0(Z)$, $H_1(Z)$, $G_0(Z)$ and $G_1(Z)$ which ensures perfect reconstruction at $Y(Z)$. We also aim to enhance our analysis to understand 'conjugate quadrature filter banks'.

Consider two channel filter bank as shown in Fig. 5.1.

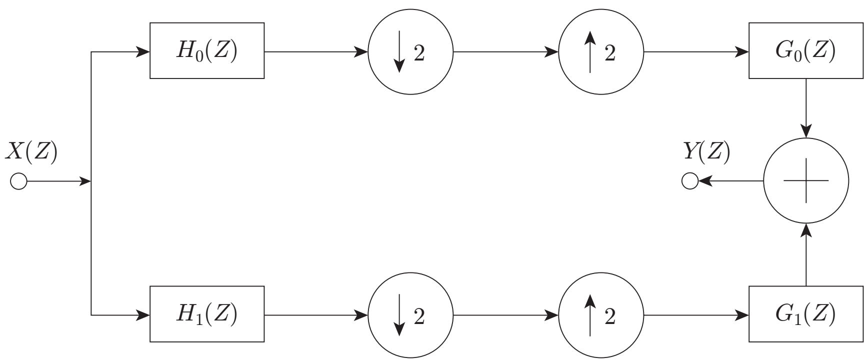

Figure 5.1 | *Two-channel filter bank*

For a two-channel filter bank which realizes the multirate systems effectively, the critical components are upsamplers and downsamplers. In chapter 4 we have seen that for 2-channel structures we use upsampling and downsampling by factor of 2 and for M-channel structures the usage gets extended to upsampling and downsampling by factor of M. In Chapter 4 we have also studies the effect of upsampling and downsampling as:

1. **Effect of Upsampler**

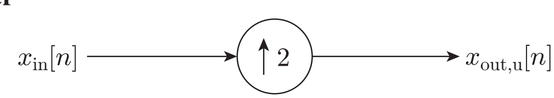

Figure 5.2 | *Upsampler*

$$X_{out,U}(Z) = X_{in}(Z^2) \tag{5.1}$$

2. **Effect of Downsampler**

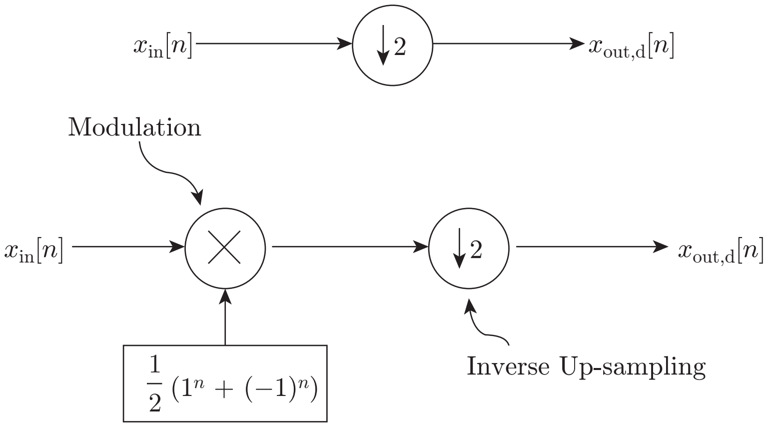

Figure 5.3 | *Downsampler*

In Z-domain,

$$X_{out,D}(Z) = \frac{1}{2}[X_{in}(Z^{\frac{1}{2}}) + X_{in}(-Z^{\frac{1}{2}})] \tag{5.2}$$

As proved earlier, downsampling by factor of 2 operation can be split into modulation by a sequence followed by inverse upsampling by 2. This follows from the fact that, upsampling by any factor is an invertible operation which implies that inverse upsampling is meaningful. Here, $(Z^{\frac{1}{2}})$ appears due to inverse up-sampler. If inverse sampler is not considered, then power of $\frac{1}{2}$ will disappear.

Using this Z-transform, we can get a relation between Z-transform of input and Z- transform of output, provided it exists throughout the process of analysis and synthesis.

5.2 | *Z*-domain Analysis of Filter Bank

To simplify the process, we name the output of each block as shown in Fig. 5.4.

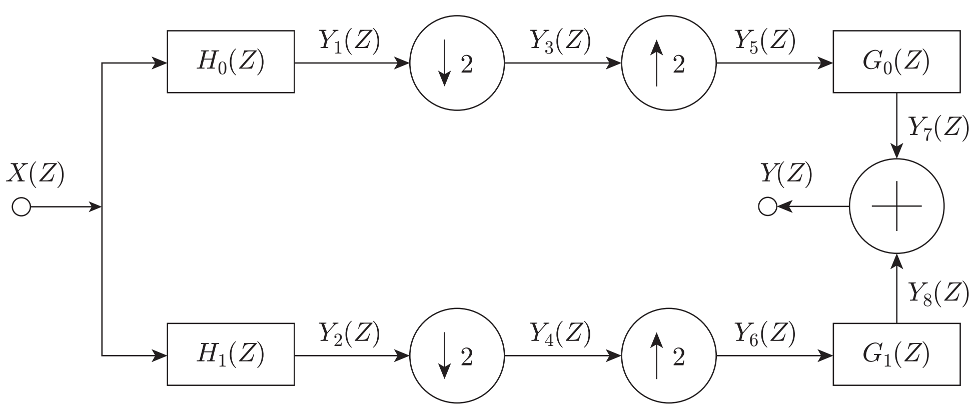

Figure 5.4 | *Filter bank with notations*

With this notations, Z-transform at each point can be written quite easily. It is seen that $Y_1(Z)$ and $Y_2(Z)$ are simply $X(Z)$ passed through filter $H_0(Z)$ and $H_1(Z)$ respectively.

$$Y_1(Z) = H_0(Z)X(Z) \tag{5.3}$$

$$Y_2(Z) = H_1(Z)X(Z) \tag{5.4}$$

We can write the relation between $Y_3(Z)$ and $Y_4(Z)$ in terms of $Y_1(Z)$ and $Y_2(Z)$ respectively. But if we notice the steps for downsampling, then it is clear that inverse upsampling operation needed for downsampling cancels with upsampler leaving only modulation part as a combined effect of downsampling and upsampling. Thus it becomes easy to jump from $Y_1(Z)$ and $Y_2(Z)$ to directly $Y_5(Z)$ and $Y_6(Z)$ respectively (Fig. 5.5). This strategy is quite useful in analyzing multi-rate system particularly when downsampler is followed by upsampler. Thus it follows that,

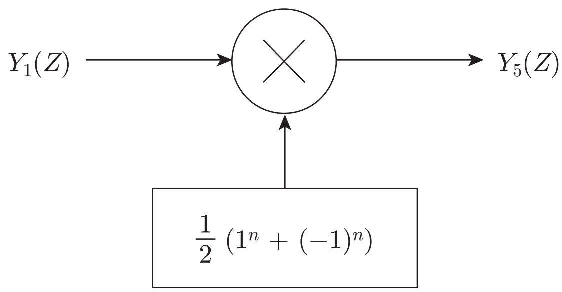

Figure 5.5 | *Jumping across up and down sampler*

$$Y_5(Z) = \frac{1}{2}\{Y_1(Z) + Y_1(-Z)\} \tag{5.5}$$

$$Y_6(Z) = \frac{1}{2}\{Y_2(Z) + Y_2(-Z)\} \tag{5.6}$$

The important point is that from this point on, we have contribution from $X(Z)$ as well as $X(-Z)$. Significance of $X(-Z)$ will be dealt with later on. Once we have $Y_5(Z)$ and $Y_6(Z)$ we can easily go back and write for $Y_3(Z)$ and similarly $Y_4(Z)$ as follows.

$$Y_3(Z) = Y_5(Z^{\frac{1}{2}}) \tag{5.7}$$

$$Y_4(Z) = Y_6(Z^{\frac{1}{2}}) \tag{5.8}$$

Jumping across upsampler and downsampler is useful since it brings us quickly to output. We are only one step away from output which can be easily achieved as

$$Y(Z) = Y_7(Z) + Y_8(Z) \tag{5.9}$$

where $Y_7(Z)$ and $Y_8(Z)$ are given by

$$Y_7(Z) = Y_5(Z)G_0(Z) \tag{5.10}$$

$$Y_8(Z) = Y_6(Z)G_1(Z) \tag{5.11}$$

where

$$Y_2(Z) = H_1(Z)X(Z) \tag{5.12}$$

$$Y_2(-Z) = H_1(-Z)X(-Z) \tag{5.13}$$

In total, we can write

$$Y(Z) = \tau_0(Z)X(Z) + \tau_1(Z)X(Z) \tag{5.14}$$

where

$$\tau_0(Z) = \frac{1}{2}\{G_0(Z)H_0(Z) + G_1(Z)H_1(Z)\} \tag{5.15}$$

$$\tau_1(Z) = \frac{1}{2}\{G_0(Z)H_0(-Z) + G_1(Z)H_1(-Z)\} \tag{5.16}$$

This implies that $Y(Z)$ is a linear combination of $X(Z)$ and $X(-Z)$ in Z-domain. If the term $X(-Z)$ would not have been there, $Y(Z)$ would have simply be the $X(Z)$ passed though a filter with function $\tau_0(Z)$ like a LSI system. Dependence on $X(-Z)$ is what brings the trouble in the equation. To understand this, let us first interpret what the term $X(-Z)$ spectrally means and what it reflects in the frequency domain.

R Effect of $X(-Z)$

To understand effect of $X(-Z)$ let us go back to frequency domain by substituting $z \leftarrow e^{j\omega}$. It implies

$$X(-Z) = X(e^{j(\omega \pm \pi)})$$

i.e. we are shifting the spectrum of $X(e^{j\omega})$ by $+\pi$ or $-\pi$. Due to periodicity on the ω axis of 2π, shifting by $+\pi$ or $-\pi$ is equivalent. The impact of this shift can be best understood by taking an example.

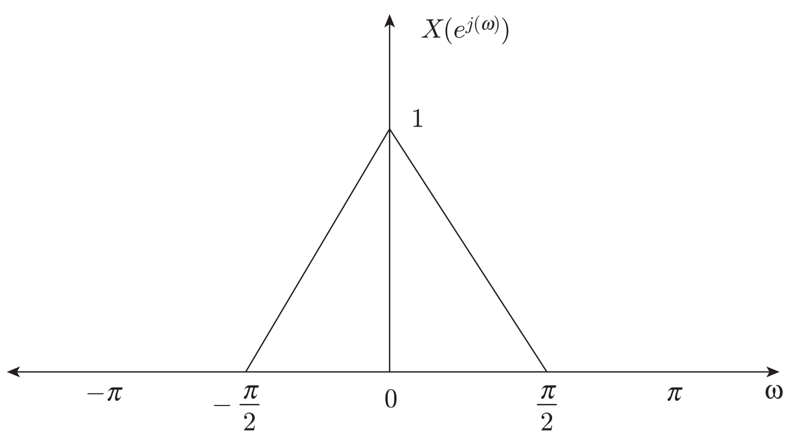

Figure 5.6 | *Spectrum of $X(\omega)$*

Here $X(e^{j\omega})$ is the Fourier transform of some sequence $x[n]$ as shown in Fig. 5.6. But this is just the principal interval of ω axis. Actually, $X(e^{j(\omega)})$ looks as shown in Fig. 5.7.

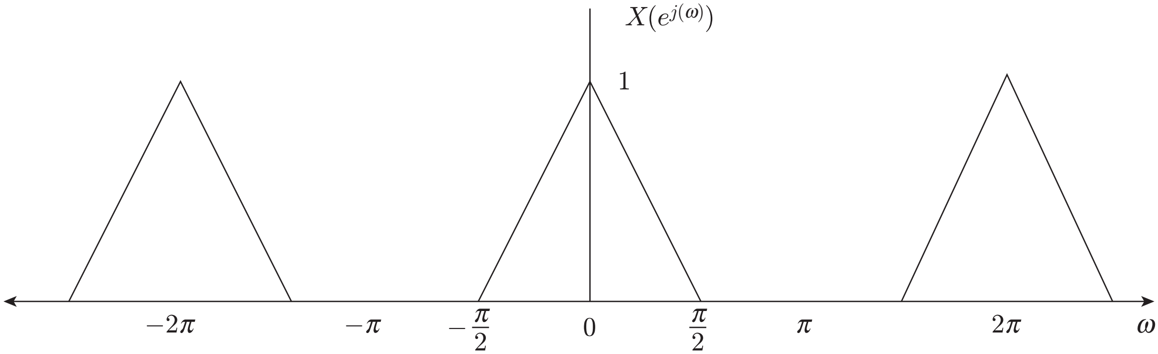

Figure 5.7 | *Periodic nature of spectrum of* $X(\omega)$

After shifting by $+\pi$ or $-\pi$, spectrum becomes, as shown in Fig. 5.8.

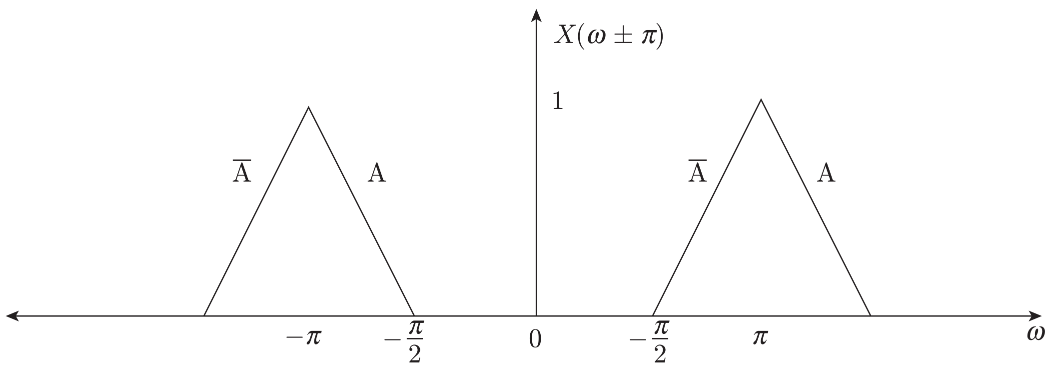

Figure 5.8 | *Spectrum of* $X(\omega)$ *after shift of* $\pm\pi$

Thus it is evident that shifting by $+\pi$ or $-\pi$ is same. Notation A and $\bar{A}$ is justified since for real $x[n]$ which is a general case, $X(e^{j\omega})$ has a conjugate symmetry.

The spectrum can be redrawn by shifting the $X(e^{j\omega})$ by $+\pi$ or $-\pi$. For clarity in future, $X(e^{j\omega})$ is written as $X(\omega)$. We mark the edges of spectrum as A and $\bar{A}$ carefully.

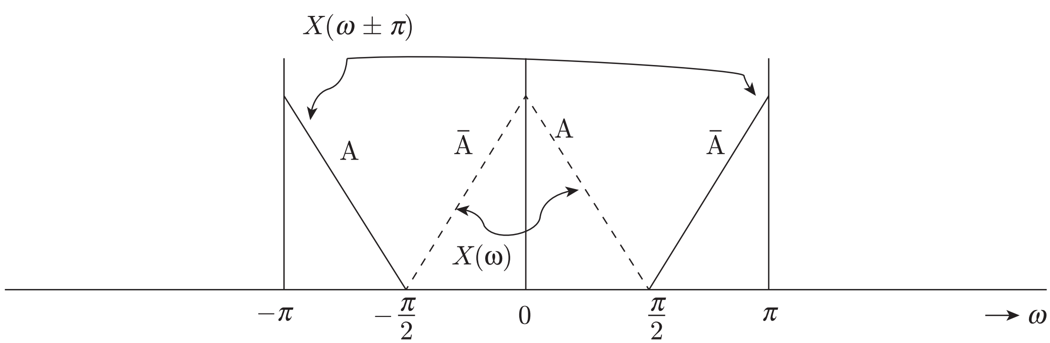

Figure 5.9 | *Spectrum of* $X(\omega)$ *in the principal interval*

A, which has been shifted to region π to $\frac{3\pi}{2}$, is repeated in region $-\pi$ to $-\frac{\pi}{2}$. In Fig. 5.9, solid line represents $X(\omega \pm \pi)$ while dashed line represents original $X(\omega)$. We see clearly from the figure how the position of A and $\bar{\text{A}}$ has been modified from its original position. The so-called negative frequencies between $\frac{-\pi}{2}$ and 0 now appear between $\frac{\pi}{2}$ and π. This results in two changes:

- The order of frequency has been reversed. Frequency, which was initially ordered as 0 to $\frac{-\pi}{2}$ has now been reordered between $\frac{\pi}{2}$ and π. Larger frequency has now become smaller and vice versa. For example frequency $\frac{\pi}{4}$, which was larger than $\frac{\pi}{8}$, appears as a smaller frequency in shifted spectrum.
- The frequency itself has changed. In other words, frequencies have attained a false identity.

This is exactly the same phenomenon as aliasing. It occurs in sampling if the input signal is not sampled with the adequate rate. It has occurred due to the down-sampler used in the process. By using the downsampler, we have allowed the possibility of aliasing. It is due to this fact that term $X(-Z)$ is called aliasing term. In two channel filter bank where we want perfect reconstruction, this aliasing should be absent. Perfect reconstruction means after you analyze (decompose), and finally reconstruct (synthesis), $Y(Z)$ is exact replica of $X(Z)$.This condition is fulfilled when the filters are chosen properly, for example as in case of Haar. Thus in general term $X(-Z)$ is troublemaker. The first step to ensure the prefect reconstruction is to do away with the aliasing term.

5.3 | Aliasing Cancellation

When we say that we do not want aliasing to appear at the output it essentially means that $\tau_1(Z) = 0$. In terms of filter response we want

$$G_0(Z)H_0(-Z) + G_1(Z)H_1(-Z) = 0$$

If we explicitly express the synthesis filter in terms of the analysis filter we can easily ensure that $\tau_1(Z) = 0$. Expressing synthesis filter as required can be done by simply rearranging this equation.

$$\frac{G_1(Z)}{G_0(Z)} = -\frac{H_0(-Z)}{H_1(-Z)} \tag{5.17}$$

Very simple choice for this condition is:

$$G_1(Z) = \pm H_0(-Z)\, G_0(Z) = \mp H_1(-Z) \tag{5.18}$$

This is a simple choice but definitely not the only choice. We can allow the factor common in both numerator as well as denominator, which eventually gets cancelled when we divide them. So more generally,

$$G_1(Z) = \pm R(Z)H_0(-Z) \tag{5.19}$$

$$G_0(Z) = \mp R(Z)H_1(-Z) \tag{5.20}$$

where $R(Z)$ is factor cancelled. Interpretation of $G_1(Z) = \pm H_0(-Z)$ can be shown as follows. Ideally, $H_0(Z)$ is a low pass filter with cutoff frequency of $\frac{\pi}{2}$ and frequency spectrum as shown in Fig. 5.10.

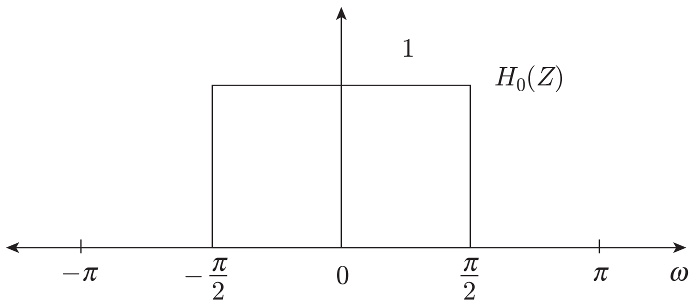

Figure 5.10 | *Spectrum of ideal low pass filter*

Then $H_0(-Z)$ has spectrum as shown in Fig. 5.11.

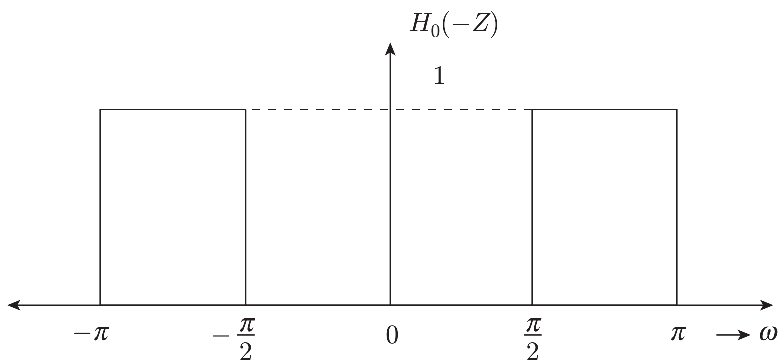

Figure 5.11 | *Spectrum of ideal high pass filter*

This is nothing but a spectrum of ideal high pass filter with cutoff $\frac{\pi}{2}$. Thus relationship $G_1(Z) = +H_0(-Z)$ makes a lot of sense for ideal filter. Same analogy goes for $G_0(Z) = -H_1(-Z)$. Since this is just a magnitude plot, effect of minus sign is not visible here. It only adds additional phase of $\pm\frac{\pi}{2}$ to the system.

Thus, we see that how this simple choice for $G_0(Z)$ and $G_1(Z)$ makes sense for an ideal filter. If we generalize our choice with factor $R(Z)$, there is slightly more modification than just low pass to high pass and vice-versa. With making this choice we have completed the first step towards perfect reconstruction. Next step is to prove the perfect reconstruction property.

5.4 | Perfect Reconstruction: Conjugate Quadrature

In the last few sections we have dealt with two channel filter bank in detail. We had noted the effects of going past a downsampler and an upsampler in the Z-domain. Some of its important points are/noted as follows.

$$\text{Input}: x[n] \xrightarrow{Z} X(Z)$$

$$\text{Output}: y[n] \xrightarrow{Z} Y(Z)$$

Analysis side has low pass filter and high pass filter with system functions $H_0(Z)$ and $H_1(Z)$. Synthesis side has Low Pass Filter and High Pass Filter with system functions $G_0(Z)$ and $G_1(Z)$. Output is

$$Y(Z) = \tau_0(Z)X(Z) + \tau_1(Z)X(-Z) \tag{5.21}$$

X(-Z) is called the 'alias' term and hence $\tau_1(Z)$ is called Alias System Function. We call it a system function, but it is incorrect. The word is a misnomer because when there is an alias term the system is not linear and shift invariant. For alias cancellation we want $\tau_1(Z)$ to be equal to zero. Then system becomes Linear Shift Invariant(LSI).

$$\tau_1(Z) = \frac{1}{2}\{G_0(Z)H_0(-Z) + G_1(Z)H_1(-Z)\} \tag{5.22}$$

For $\tau_1(Z) = 0$

$$\frac{G_1(Z)}{G_0(Z)} = -\frac{H_0(-Z)}{H_1(-Z)} \tag{5.23}$$

Simply equating numerator and denominator we get

$$G_1(Z) = \pm R(Z)H_0(-Z) \tag{5.24}$$

$$G_0(Z) = \mp R(Z)H_1(-Z) \tag{5.25}$$

Here, if $H_1(-Z)$ is a high pass filter, $G_0(Z)$ becomes low pass filter. If $\tau_1(Z)$ becomes zero, the system becomes LSI as $Y(Z) = \tau_0(Z)X(Z)$ with $\tau_0(Z)$ being a system function.

5.5 | Condition for Perfect Reconstruction

We want to decompose a signal and reconstruct it back with ideal case as $X(Z) = Y(Z)$. Even tolerable changes in the output can be accepted.

What could be tolerable or acceptable changes?

In case of time systems, time delays are tolerable since finite time is needed to process the signal at analysis and synthesis side. Even an output multiplied by a constant is acceptable. So, in perfect reconstruction process $\tau_0(Z)$ takes the form of

$$\tau_0(Z) = C_0 z^{-D} \tag{5.26}$$

where C_0 is a constant. Ideally, we would like to have $\tau_0(Z) = 1$ for all z. But this makes the system noncausal. So, a factor Z^{-D} is allowed to take care of causality.

In Haar Filter Bank, shown in Fig. 5.12, we have following

$$\begin{aligned}\tau_1(Z) &= \frac{1}{2}\{G_0(Z)H_0(-Z) + G_1(Z)H_1(-Z)\}\\ &= \frac{1}{2}\left\{(1+z^{-1})\left(\frac{1-z^{-1}}{2}\right) \pm (1-z^{-1})\left(\frac{1+z^{-1}}{2}\right)\right\}\end{aligned} \tag{5.27}$$

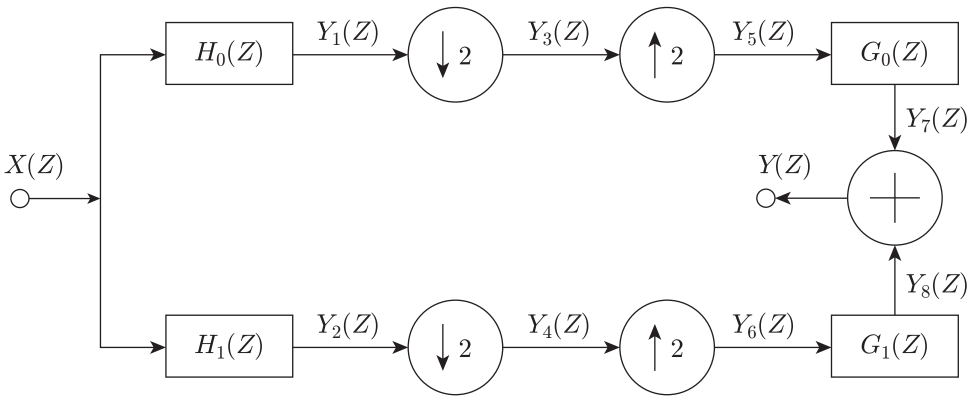

Figure 5.12 | *The haar filter bank*

For alias cancellation we need $\tau_1(z)$ to be equal to zero. This gives $G_1(z) = -(1 - z^{-1})$. System functions of Haar Filter Bank are as follows

$$H_0(Z) = \frac{1 + z^{-1}}{2}$$

$$H_1(Z) = \frac{1 - z^{-1}}{2}$$

$$G_0(Z) = 1 + z^{-1}$$

$$G_1(Z) = -(1 + z^{-1})$$

We find the value of $\tau_0(Z)$

$$\begin{aligned}\tau_0(Z) &= \frac{1}{2}\{G_0(Z)H_0(Z) + G_1(Z)H_1(Z)\} \\ &= \frac{1}{2}\left\{\left(1 + z^{-1}\right)\left(\frac{1 + z^{-1}}{2}\right) - \left(1 - z^{-1}\right)\left(\frac{1 - z^{-1}}{2}\right)\right\} \\ &= z^{-1}\end{aligned} \tag{5.28}$$

This represents a delay of one sample. This delay is required on account of causality. If we try to avoid this delay we must have noncausality either on synthesis side or on analysis side.
Simplest possibilty for alias cancellation is $G_0(Z) = \pm H_1(Z)$. In case of Haar Filter Bank

$$H_1(Z) = \frac{1 - z^{-1}}{2}$$

$$H_1(-Z) = \frac{1 + z^{-1}}{2}$$

Essentially, $G_0(Z) = \pm R(Z)H_1(-Z)$ condition should be satisfied. More generally for alias cancellation we need

$$G_0(Z) = \pm R(Z)H_1(-Z)$$

$$G_1(Z) = \mp R(Z)H_0(-Z)$$

In particular, for Haar case we have chosen $R(Z) = 2$ and $G_1(Z)$ as

$$\begin{aligned} G_1(Z) &= -2H_0(Z) \\ &= \{-2[\frac{1}{2}(1+z^{-1})]\} \\ &= -(1-z^{-1}) \end{aligned}$$

5.6 | Polynomial as an Input

Haar MRA has many hidden concepts. However, we need to study what is the problem associated with Haar MRA. In other words, we should learn how Haar is a beginning of a family of Multiresolution Analysis.

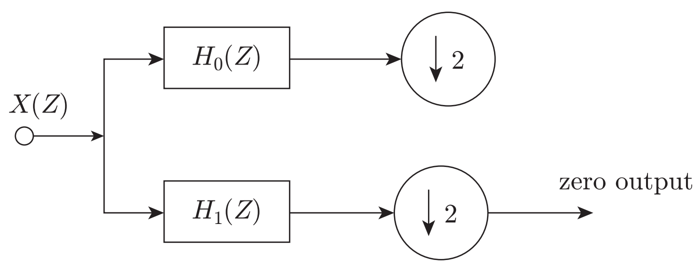

Figure 5.13 | *Output for constant input*

Example 5.6.1 — Effect of splitting on high pass branch.

To have more insight we look at low pass and high pass filters from a different perspective. It can be understood by taking an example of constant sequence as input and noting the output at different points in filter bank.

$$\begin{aligned} x[n] &= C_1 \text{ for all } n \\ H_1(Z) &= \frac{1}{2}(1-z^{-1}) \\ \frac{x[n]-x[n-1]}{2} &= 0 \text{ for all } n \end{aligned}$$

If there is a constant component in the input sequence of Haar filter bank, it is destroyed by high pass filter. This is depicted in Fig 5.13.

In Haar filter bank we have a term $(1-z^{-1})$. What could be the situation in case of multiple or cascaded $(1-z^{-1})$?

If we assume an input having polynomial components, then every instance of $(1-z^{-1})$ reduces degree of polynomial by one. A Taylor series is a polynomial expansion of input and if we subject some terms in the polynomial expansion to $(1-z^{-1})$ we have interpretation like this

$$a_0 n^M + a_1 n^{M-1} + a_2 n^{M-2} + \ldots + a_M = x[n]$$

where $x[n]$ is polynomial input sequence. Every time this is subjected to term $(1-z^{-1})$, what happens is

$$a_0 n^M + a_1 n^{M-1} + a_2 n^{M-2} + \ldots + a_M - \{a_0(n-1)^{M-1} + a_1(n-1)^{M-2} + \ldots + a_M\}$$

When we expand this, coefficient of n^M is $a_0 - a_0$, i.e. zero.
Each time we subject this polynomial to action of $(1-z^{-1})$, we are reducing degree by one. For example, consider sequence of polynomial degree one (say $3n+5$)

$$\begin{aligned} output &= (3n+5) - [3(n-1)+5] \\ &= 3n+5-3n+3-5 \\ &= 3 \quad \text{for all } n \end{aligned}$$

Hence coefficient of highest power of n vanishes. These terms are $(1-z^{-1})$ on high pass branch and can not be on low pass branch. We build up whole family of MRA with more and more $(1-z^{-1})$ terms on high pass branch. That is what is called as **Daubechies family of MRA**.

Figure 5.14 | *Cascade system*

As we increase seniority in this family, there are more and more $(1-z^{-1})$ terms on high pass branch. Effectively, we are reducing degree of higher order polynomial on high pass branch. We are killing them on high pass branch, i.e. we are transferring them on low pass branch. We are thus retaining more smoothness on low pass branch. In addition to this we want the same filters on analysis and synthesis side of filter bank. This gives us a class of filter bank known as Conjugate Quadrature Filter bank. Describing equations of these filter banks is very simple.We start from aliasing cancellation condition

$$G_0(Z) = \pm H_1(Z)$$
$$G_1(Z) = \mp H_0(Z)$$

We choose (inspired by Haar)

$$G_0(Z) = -H_1(-Z)$$
$$G_1(Z) = -H_0(-Z)$$

Here we keep away a factor of 2 that can be absorbed by constant C_0. We need $\tau_1(Z) = 0$ (by construction) and $\tau_0(Z)$ as

$$\tau_0(Z) = \frac{1}{2}\{H_1(-Z)H_0(Z) + (-H_0(-Z))H_1(Z)\} \tag{5.29}$$

As $H_1(Z)$ is a high pass filter (in synthesis side) $H_1(-Z)$ becomes a low pass filter with cutoff $\frac{\pi}{2}$. Therefore, the first term in above expression (Eq. 5.29) represents cascade of two low pass filters and the second term represents a cascade of two high pass filters with cutoff $\frac{\pi}{2}$.

In case of Haar there is relation between H_0 and H_1. For perfect reconstruction, $\tau_0(Z)$ should be equal to a delay and some multiplying constant. In Haar case,

$$H_1(-Z) = \frac{1+z^{-1}}{2} = H_0(Z)$$

We shall in general note that $H_0(Z)$ should be related to $H_1(-Z)$. Choosing $H_1(Z)$ to be slightly modified from $H_0(-Z)$ as

$$H_1(Z) = z^{-D} H_0(-Z^{-1})$$

For Haar case,

$$z^{-1} H_0(-Z^{-1}) = \frac{Z^{-1}-1}{2}$$

In general case for $H_1(Z) = z^{-D} H_0(-Z^{-1})$, $\tau_0(Z)$ becomes

$$\tau_0(Z) = \frac{1}{2}\{H_0(Z)((-Z)^{-D})H_0(Z^{-1}) - H_0(-Z)(Z^{-D})H_0(-Z^{-1})\}$$

$$= \frac{1}{2}\{H_0(Z)(Z^{-D})H_0(Z^{-1})(-1^{-D}) - H_0(-Z)(Z^{-D})H_0((-Z)^{-1})\} \tag{5.30}$$

In Eq. (5.30), we choose value of D and put condition on H_0, then this becomes perfect reconstruction situation, which we shall discuss in more detail in the next section.

5.7 | Conjugate Quadrature Filter Bank

We continue in this section to build upon the particular class of filter bank, which we have introduced earlier called a Conjugate Quadrature Filter (CQF) bank. For the perfect reconstruction system we must first do away aliasing. The alias cancellation equation for the two-band filter bank is given by

$$G_0(Z)H_0(-Z) + G_1(Z)H_1(-Z) = 0 \tag{5.31}$$

$$\frac{G_1(Z)}{G_0(Z)} = -\frac{H_0(-Z)}{H_1(-Z)} \tag{5.32}$$

Equating the numerator and denominator we get the relation between $G_0(Z), H_1(-Z), G_1(Z)$ and $H_0(-Z)$ as

$$G_1(Z) = -H_0(-Z) \tag{5.33}$$

$$G_0(Z) = H_1(-Z) \tag{5.34}$$

The relation between the analysis HPF (high pass filter) and analysis LPF (low pass filter) called a conjugate quadrature relationship, is given by

$$H_1(Z) = z^{-D} H_0(-Z^{-1}) \tag{5.35}$$

Here z^{-D} term is used to introduce causality. Putting $Z = e^{j\omega}$ in the Eq. (5.35), we get the frequency response equation as

$$H_1(Z) = z^{-D} H_0(-Z^{-1})|_{Z=e^{j\omega}}$$

$$H_1(e^{j\omega}) = e^{-j\omega D} H_0(-e^{-j\omega})$$

The magnitude response is given by

$$|H_1(e^{j\omega})| = |e^{-j\omega D} H_0(-e^{-j\omega})|$$

$$|H_1(e^{j\omega})| = |e^{-j\omega D}||H_0(-e^{-j\omega})|$$

$$|H_1(e^{j\omega})| = |H_0(-e^{-j\omega})|$$

$H_0(Z)$ is a Low pass filter with a real impulse response (real coefficients), therefore

$$H_0(e^{-j\omega}) = \overline{H_0(e^{j\omega})}$$

The magnitude response of LPF $H_0(Z)$ is symmetric along the magnitude axis and phase response is anti-symmetric along the frequency axis ω.

$$H_0(-e^{-j\omega}) = H_0(e^{-j(\omega \pm \pi)})$$

$$NOTE: (LPF\ with\ cutoff\ frequency \frac{\pi}{2}) \overset{(With\ shift\ by\ \pi\ on\ \omega)}{\rightleftharpoons} (HPF\ with\ cutoff\ frequency \frac{\pi}{2})$$

We have shown,

$$H_1(Z) = z^{-D} H_0(-Z^{-1})$$

For the perfect reconstruction the equation must satisfy,

$$G_0(Z)H_0(Z) + G_1(Z)H_1(Z) = C_0 z^{-D}$$

$$H_1(-Z)H_0(Z) - H_0(-Z)H_1(Z) = C_0 z^{-D}$$

$$(-1)^{-D} z^{-D} H_0(Z^{-1})H_0(Z) - H_0(-Z)z^{-D} H_0(-Z^{-1}) = C_0 z^{-D}$$

We need the following for perfect reconstruction systems,

$$(-1)^{-D} H_0(Z^{-1})H_0(Z) - H_0(-Z)H_0(-Z^{-1}) = C_0$$

If we consider the Haar filter then the relationship between $H_0(Z)$ and $H_1(Z)$ is given by,

$$H_0(Z) = 1 + z^{-1}$$

$$H_0(-Z^{-1}) = 1 - z$$

The above equation is non-causal so to make it causal by inserting delay, we get the below equation,

$$z^{-D} H_0(-Z^{-1}) = z^{-D}(1 - z)$$

Here z^{-D} retains causality.

If D is odd,

$$H_0(Z)H_0(Z^{-1}) + H_0(-Z)H_0(-Z^{-1}) = -C_0$$
$$H_0(Z)H_0(Z^{-1}) + H_0(-Z)H_0(-Z^{-1}) = \text{Constant}$$

Putting $Z = e^{j\omega}$, we get the above equation in the frequency domain as,

$$H_0(e^{j\omega})H_0(e^{-j\omega}) + H_0(-e^{j\omega})H_0(-e^{-j\omega}) = \text{Constant}$$

For real impulse response we have,

$$H_0(e^{-j\omega}) = \overline{H_0(e^{j\omega})}$$
$$H_0(e^{j\omega})\overline{H_0(e^{j\omega})} + H_0(e^{j(\omega\pm\pi)})\overline{H_0(e^{j(\omega\pm\pi)})} = \text{Constant}$$
$$|H_0(e^{j\omega})|^2 + |H_0(e^{j(\omega\pm\pi)})|^2 = \text{Constant}$$

This equation is called the *power complementary equation*.
For perfect reconstruction system,

$$H_0(Z)H_0(Z^{-1}) + H_0(-Z)H_0(-Z^{-1}) = \text{Constant}$$

Lets us assume $\kappa_0(Z) = H_0(Z)H_0(Z^{-1})$

$$\kappa_0(Z) + \kappa_0(-Z) = \text{Constant} \tag{36}$$

We are going to choose even length of $H_0(Z)$, i.e. $D \to$ Odd

$$\underset{n}{\underset{\uparrow}{h_1[n]}}: \quad \underset{0}{\underset{\uparrow}{h_0}}\ h_1\ h_2\ \ldots \underset{D}{\underset{\uparrow}{h_D}}$$

Similarly, $H_0(Z^{-1})$ is given by,

$$\underset{n}{\underset{\uparrow}{h_2[n]}}: \quad \underset{-D}{\underset{\uparrow}{h_D}} \ldots\ h_2\ h_1\ \underset{0}{\underset{\uparrow}{h_0}}$$

Here, $H_0(Z)H_0(Z^{-1})$ corresponds to its convolution in time domain

$$(\underset{0}{\underset{\uparrow}{h_0}}\ h_1\ h_2\ \ldots \underset{D}{\underset{\uparrow}{h_D}}) * (\underset{-D}{\underset{\uparrow}{h_D}} \ldots\ h_2\ h_1\ \underset{0}{\underset{\uparrow}{h_0}})$$

Let the impulse response $h[k]$ be as given below

$$h[k]: \quad \underset{0}{\underset{\uparrow}{h_0}}\ h_1\ h_2\ \ldots \underset{D}{\underset{\uparrow}{h_D}}$$

And impulse response $g[k]$, as given below, which is mirror image of $h[k]$, that means $g[k] = h[-k]$

$$g[k]: \quad \underset{-D}{\underset{\uparrow}{h_D}} \ldots\ h_2\ h_1\ \underset{0}{\underset{\uparrow}{h_0}}$$

Similarly, $g[n-k]$ is given below

$$g[n-k]: \quad \underset{n}{\underset{\uparrow}{h_0}}\ h_1\ h_2\ \ldots \underset{n+D}{\underset{\uparrow}{h_D}}$$

The convolution between $h[k]$ and $g[k]$ is given as

$$\kappa_0[n] = \sum_{k=-\infty}^{k=+\infty} h[k]g[n-k]$$

Here $h[k]$ is causal and filter length is $(D+1)$.
The convolution at the sample n is $\kappa_0[n]$. Shown below is the multiplication of $h[k]$ and $g[-k]$ (which is shifted by n samples)

$$\begin{array}{llllllll}
k_0[n]: & h_0 & h_1 & h_2 \;\ldots\ldots & h_n & h_{n+1} \;\ldots\ldots & h_D & \\
 & \uparrow & & & h_0 & h_1 & & h_2 \\
 & 0 & & & \uparrow & & & \\
 & & & & n & & &
\end{array}$$

In Z-domain $\kappa_0(Z) = H_0(Z)H_0(Z^{-1})$.
The m^{th} sample of the filter $k_0[m]$ is $< h[k], h[k \pm m] >$
Let m be equal to 2 and filter length 4 $(D = 3)$

$$\begin{array}{llllll}
k_0[2]: & h_0 & h_1 & h_2 & h_3 & & \\
 & \uparrow & & h_0 & h_1 & h_2 & h_3 \\
 & 0 & & \uparrow & & & \\
 & & & 2 & & &
\end{array}$$

$$k_0[2] = h_0h_2 + h_1h_3$$

$$\begin{array}{lllllll}
k_0[-2]: & & & h_0 & h_1 & h_2 & h_3 \\
 & h_0 & h_1 & h_2 & h_3 & & \\
 & \uparrow & & \uparrow & & & \\
 & -2 & & 0 & & &
\end{array}$$

If $m = -2$ and filter length 4 $(D = 3)$

$$k_0[-2] = h_0h_2 + h_1h_3$$

That means the convolution between $h[k]$ and $g[k]$, i.e. $\kappa_0[n]$ and $\kappa_0[-n]$ is symmetrical.

$$\kappa_0(Z) + \kappa_0(-Z) = \text{Constant}$$

$$\frac{1}{2}\{\kappa_0(Z) + \kappa_0(-Z)\} = \text{Constant}$$

$\frac{1}{2}\{\kappa_0(Z) + \kappa_0(-Z)\}$ represents nonzero sample value at the even location and zero sample value at the odd location. Let $\kappa_0(Z)$ correspond to the sequence $k_0[n]$, $\frac{1}{2}\{\kappa_0(Z) + \kappa_0(-Z)\}$, an impulse response so obtained is shown below.

$$\begin{array}{l} \quad\text{multiplication} \\ k_0[n] \rightarrow \otimes \rightarrow \text{non}-\text{zero at even \& zero location} \\ \qquad\quad \rangle \\ \ldots\ldots..1\,0\;\;1\;\;0\;\;1\;\;0\;\;1\;\;0\ldots\ldots. \\ \qquad\quad \rangle \\ \qquad\quad 0 \end{array}$$

Consider the equation $\frac{1}{2}\{\kappa_0(Z)+\kappa_0(-Z)\} = \text{constant}$. Taking inverse Z transform on both sides, we obtain impulse at zero location on Right Hand Side (since inverse Z transform of a constant is an impulse),thus we want the nonzero sample value only at zero location and zero sample value for odd and even location.

So, at the even location $m = 2l$ and $m \neq 0$ and ($l \in \mathbb{Z}$), we want zero sample value.

Let Daubechies filter with length 4($D = 3$)

$$h_0[n]: \; \underset{\substack{\uparrow \\ 0}}{h_0} \; h_1 \; h_2 \ldots \underset{\substack{\uparrow \\ 3}}{h_3}$$

In the Haar case, $(1 - z^{-1})$ represents a High pass filter.

Here, we consider the Daubechies filter with length 4, so two $(1 - z^{-1})$ terms in the High pass filter which means $(1 - z^{-1})^2$ factor in HPF.

Similarly, low pass filter has a factor $(1 + z^{-1})^2$.

A Daubechies low pass filter with length 4 is given by

$$H_0(Z) = h_0 + h_1 z^{-1} + h_2 z^{-2} + h_3 z^{-3}$$

We can write this equation in the factor of $(1 + z^{-1})^2$ that is

$$H_0(Z) = (1 + z^{-1})^2 (1 + B_0 z^{-1})$$

In the above equation, we need three zeros.

Two zeros are already chosen at unit circle which are $-1, -1$ and one zero is selected based on the value of B_0. This value can be obtained by comparing the above two equations.

Expanding the above two equations

$$H_0(Z) = (1 + 2z^{-1} + z^{-2})(1 + B_0 z^{-1})$$

$$H_0(Z) = 1 + (2 + B_0)z^{-1} + (1 + 2B_0)z^{-2} + B_0 z^{-3}$$

The dot product of the impulse response of LPF with its even shifts must be zero. We will use this constraint to find the value of B_0 in the next chapter.

Exercises

Exercise 5.1

Consider $H_0(Z)$ to be an ideal Band Pass Filter with cutoffs $\frac{\pi}{4}$ and $\frac{3\pi}{4}$ as shown in Fig. 5.15. Find and sketch the spectrum of $H_0(-Z)$.

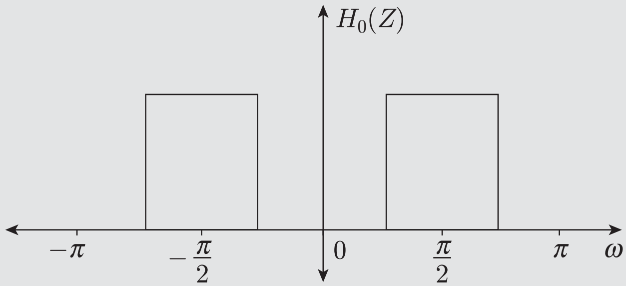

Figure 5.15 | *Spectrum of $H_0(Z)$*

Hint: Replacing Z by $-Z$ in $H_0(-Z)$ implies shifting the spectrum by $+\pi$ or $-\pi$. But, due to the periodicity of ω axis, shifting by $+\pi$ or $-\pi$ are equivalent. Given $H_0(Z)$ is a band pass filter, on shifting its spectrum by $\pm\pi$ will result in a band stop filter as shown in Fig. 5.16 with band stop frequencies $\frac{\pi}{4}$ and $\frac{3\pi}{4}$.

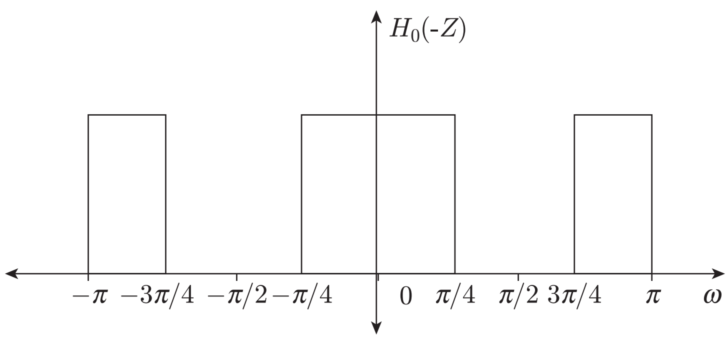

Figure 5.16 | *Spectrum of $H_0(-Z)$*

Exercise 5.2

Find Y_1 to Y_9 in the two channel filter bank after interchanging downsampler and upsampler as shown in Fig. 5.17.

Hint: It can be clearly seen that there is no effect of interchanging on Y_1 and Y_2. To calculate further we will use the Eqs (5.37) and (5.38) previously mentioned in this chapter representing the effects of upsampler and downsampler respectively.

$$Y_1(Z) = H_0(Z)X(Z) \tag{5.37}$$

$$Y_2(Z) = H_1(Z)X(Z) \tag{5.38}$$

now using (5.37),

$$Y_3(Z) = Y_1(Z^2) \tag{5.39}$$

$$Y_4(Z) = Y_2(Z^2) \tag{5.40}$$

now using (5.38),

$$Y_5(Z) = \frac{1}{2}[Y_3(Z^{\frac{1}{2}}) + Y_3(-Z^{\frac{1}{2}})] \tag{5.41}$$

$$Y_6(Z) = \frac{1}{2}[Y_4(Z^{\frac{1}{2}}) + Y_4(-Z^{\frac{1}{2}})] \tag{5.42}$$

substitute $Y_3(Z)$ and $Y_4(Z)$ from (5.39) and (5.40)

$$Y_5(Z) = Y_1(Z) \tag{5.43}$$

$$Y_6(Z) = Y_2(Z) \tag{5.44}$$

$Y_7(Z)$ and $Y_8(Z)$ are given by;

$$Y_7(Z) = G_0(Z)Y_5(Z) = G_0(Z)Y_1(Z) \tag{5.45}$$

$$Y_8(Z) = G_0(Z)Y_6(Z) = G_0(Z)Y_2(Z) \tag{5.46}$$

In total, we can write

$$Y(Z) = Y_7(Z) + Y_8(Z) \tag{5.47}$$

$$Y(Z) = \{H_0(Z)G_0(Z) + H_1(Z)G_1(Z)\}X(Z) \tag{5.48}$$

From the above equations we can infer that there is no effect of a upsampler followed by a downsampler on the signal magnitude or phase.

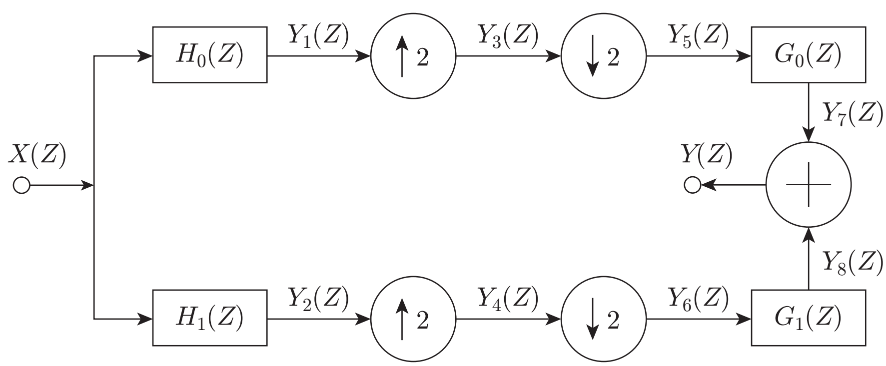

Figure 5.17 | *Modified two-channel filter bank*

Exercise 5.3

Obtain the Z-transform of a general downsampler (down-sampling by a factor of M).
Hint: Downsampler can be broken down into two steps as modulation by a sequence and then inverse upsampling. General sequence for modulation in case of downsampling by a factor of M can be written as:

$$\frac{1}{M}\sum_{l=0}^{M-1} e^{\frac{-j2\pi l}{M}} \tag{5.49}$$

Using this equation, we can write the Z-Transform of downsampler by factor M as:

$$X_{out,d}(Z) = \frac{1}{M}\sum_{l=0}^{M-1} X_{in}(Z^{\frac{1}{M}} \times e^{-j2\pi\frac{l}{M}}) \tag{5.50}$$

Exercise 5.4

Obtain the output of M-channel filter bank.
Hint: Z-transform of M-channel filter bank, which has M analysis filters denoted by $H_0(Z)$, $H_1(Z)$, $\cdots H_{M-1}(Z)$ and corresponding M synthesis filter denoted by $F_0(Z)$, $F_1(Z) \cdots F_{M-1}(Z)$, can be written as follows:

$$X_{out,d}(Z) = \frac{1}{M}\sum_{l=0}^{M-1}(X_{in}(Z \times e^{\frac{-j2\pi l}{M}})\sum_{k=0}^{M-1}(H_k(Z \times e^{\frac{-j2\pi l}{M}}))F_k(Z)) \tag{5.51}$$

(For further reading on filter banks, you can refer *Multirate Systems and Filter Banks* by P.P.Vaidyanathan).

Exercise 5.5

Consider the cascade system given in Fig. 5.14. Input to the system is

$$3n^2 + 5n + 1$$

Find the output and comment on its degree.
Hint: Output y_0 after the first block is:

$$y_0(n) = (3n^2 + 5n + 1) - (3(n-1)^2 + 5(n-1) + 1) \tag{5.52}$$

$$y_0(n) = 6n + 2 \tag{5.53}$$

Final output $y(n)$ will be:

$$y(n) = 6n + 2 - (6(n-1) + 2) = 6 \tag{5.54}$$

Degree of output is lower than input by 2, which is expected as a block of 1-Z^{-1} lowers the degree of polynomial by 1.

Exercise 5.6

Consider the two-channel filter bank, whose two filters are given below:

$$H_0(Z) = 1 + Z^{-1} + Z^{-2}$$

$$H_1(Z) = 1 - Z^{-1} + Z^{-2} - Z^{-3}$$

Find out filters $G_0(Z)$ and $G_1(Z)$ so that alias cancellation occurs.

Hint: For alias cancellation we should have:

$$\tau_1(Z) = \frac{1}{2}\{G_0(Z)H(-Z) + G_1(Z)H_1(-Z)\} = 0 \tag{5.55}$$

$$\frac{G_1(Z)}{G_0(Z)} = -\frac{H_0(-Z)}{H_1(-Z)} \tag{5.56}$$

Hence we get:

$$G_0(Z) = H_1(-Z) = 1 + Z^{-1} + Z^{-2} + Z^{-3}$$

$$G_1(Z) = -H_0(-Z) = -(1 - Z^{-1} + Z^{-2})$$

Exercise 5.7

Consider a two-channel perfect reconstruction filter bank, as shown in Fig. 5.12.

$$H_0 = -(1 + Z^{-1})$$

Find the other three filters, namely $H_1(Z)$, $G_0(Z)$ and $G_1(Z)$

Hint: We know

$$H_1(Z) = Z^{-D} H_0(-Z^{-1})$$

In this simple case, let us take $D = 1$. Therefore, $H_1(Z)$ becomes

$$H_1(Z) = -Z^{-1}(1 - Z) \tag{5.57}$$

$$H_1(Z) = 1 - Z^{-1}$$

$$G_0(Z) = H_1(-Z) \text{ this gives, } G_0(Z) = 1 + Z^{-1}$$

$$G_1(Z) = -H_0(-Z) \text{ this gives, } G_1(Z) = 1 - Z^{-1}$$

It can be verified that this filter bank satisfies both Alias Cancelation and PR condition.

Exercise 5.8

Why $H_1(Z)$ is related to $H_0(-Z)$? Express $H_0(Z)$ in terms of $H_1(Z)$.

Sol. In a perfect reconstruction filter bank, analysis low pass filter and high pass filter are complimentary filters, i.e. frequencies blocked by one filter must pass through another filter so that there is no loss of information and we can get a perfect reconstruction. $H_0(Z)$ is a low pass filter. $H_0(-Z)$ has spectrum of shape similar to that of $H_0(Z)$ but all frequencies shifted by π. It is a high pass filter which is closely related to $H_1(Z)$. The exact mathematical relation is derived as follows:

we know

$$H_1(Z) = Z^{-D} H_0(-Z^{-1})$$

Replacing Z by $-Z^{-1}$, we get

$$H_1(-Z^{-1}) = (-1)^D Z^D H_0(Z)$$

On rearrangement, we get:

$$H_0(Z) = (-1)^D Z^{-D} H_1(-Z^{-1})$$

Assignment

Exercise 5.9

Plot the frequency response (magnitude only) of $(1+Z^{-1})^n$ for $n \in (1,2,3,\ldots)$

Chapter 6

Daubechies Family

6.1 | Introduction

In this chapter we will continue with the discussion of the Daubechies filter bank, which was briefly introduced in Chapter 5. The salient feature of Daubechies filter bank is that its construction depends on addition of polynomial of higher degree in filter transfer function. To be specific, more and more $(1-z^{-1})$ terms are utilized in high pass analysis filter bank.

Ingrid Daubechies

Ingrid Daubechies (born 17 August 1954) is a Belgian physicist and mathematician. Between 2004 and 2011 she was the William R. Kenan, Jr. Professor in the mathematics and applied mathematics departments at Princeton University, New Jersey. In January 2011 she moved to Duke University as a Professor in mathematics. She is the first woman president of the International Mathematical Union (2011–2014). She is best known for her work with wavelets in image compression. At Courant in 1986 she made her best-known discovery: based on quadrature mirror filter-technology she constructed compactly supported continuous wavelets that would require only a finite amount of processing, in this way enabling wavelet theory to enter the realm of digital signal processing.

6.2 | Impulse Response of Daubechies Analysis Low Pass Filter

The first member of the Daubechies family is the Haar filter bank itself. In the second member of Daubechies family the analysis side high pass filter has a factor of $(1-z^{-1})^2$. Now, high pass filter of analysis side is of form $z^{-D}H_0(-z^{-1})$, where $H_0(z)$ is the analysis side low pass filter. So $H_0(z)$ should have a factor of $(1+z^{-1})^2$.

Example 6.2.1 — D2 calculations.

It can be recalled that in the Daubechies family the filter lengths are always even. So, for the second member of the Daubechies family, filter length will be 4 and the order will be 3. So $H_0(z)$ has 3 zeros. Two of them are already specified to be at $z = -1$. The third zero is to be determined to get complete transfer function. The complete transfer function is obtained as follows:

Let the impulse response be,

$$h[n] = [h_0\ h_1\ h_2\ \underset{\uparrow}{h_3}]$$

So $h[n]$ is orthogonal to its even shifts, e.g. shifts of 2,4,6 etc. So the only non-trivial relation is obtained by the dot product of $h[n]$ and $h[n-2]$.

$$h[n] = [h_0\ h_1\ h_2\ \underset{\uparrow}{h_3}]$$

$$h[n-2] = [\ldots\ldots h_0\ \underset{\uparrow\ {\scriptstyle n=2}}{h_1}\ h_2\ h_3]$$

Hence their dot product is $(h_0h_2 + h_1h_3)$ and because of orthogonality of dot product with respect to even shifts,

$$h_0h_2 + h_1h_3 = 0 \tag{6.1}$$

Now, system function can be expressed as,

$$H_0(z) = h_0 + h_1z^{-1} + h_2z^{-2} + h_3z^{-3} \tag{6.2}$$

Also, as $H_0(z)$ has a factor of $(1+z^{-1})^2$, so in general $H_0(z)$ can be written as,

$$H_0(z) = C_0(1+z^{-1})^2(1+B_0z^{-1})$$

where C_0 is a constant.

Here two zeros are constrained at $z = -1$. If we neglect the constant for the time being and then expanding the previous expression, we can write,

$$H_0(z) = 1 + 2z^{-1} + z^{-2} + B_0z^{-1} + 2B_0z^{-2} + B_0z^{-3}$$

$$H_0(z) = 1 + (2+B_0)z^{-}1 + (1+2B_0)z^{-2} + B_0z^{-3} \tag{6.3}$$

Comparing the coefficients of powers of z^{-1} from Eqs. (6.2) and (6.3), we get,

$$h_0 = 1$$

$$h_1 = 2 + B_0$$

$$h_2 = 1 + 2B_0$$

$$h_3 = B_0$$

Putting this value in Eq. (6.1), we get,

$$(1+2B_0)+(2+B_0)B_0=0$$
$$\Rightarrow B_0^2+4B_0+1=0$$

Solving the above quadratic equation, we get,

$$B_0=(-4\pm 2\sqrt{3})/2=-2\pm\sqrt{3} \quad (6.4)$$

Now, the implication of B_0 is that the third zero of $H_0(z)$ is at B_0. For $B_0=-2-\sqrt{3}$, i.e. $B_0=-3.732$, the zero is outside the unit circle in the z-plane. Since $|B_0|>1$, this will not become the minimum phase implementation. The magnitude response being the same as required, there will be more phase delay and group delay in the system which is undesirable. But for $B_0=-2+\sqrt{3}$, i.e. $B_0=-0.268$, the zero is inside the unit circle in the z-plane. Since $|B_0|<1$, the system remains the minimum phase system. We, therefore, choose $B_0=-2+\sqrt{3}$, i.e. $B_0=-0.268$.

So the impulse response of the analysis side low pass filter of length 4 of Daubechies family is as shown in Table 6.1.

In this derivation process we have neglected the constant C_0. To find C_0, let us recall:

$$\kappa_0(z)+\kappa_0(-z)=constant \quad (6.5)$$

where,

$$\kappa_0(z)=H_0(z)H_0(-z^{-1}) \quad (6.6)$$

In order to choose the constant C_0 the easiest option is to do is to make the norm of the impulse response of $H_0(z)$ unity in the sense of l_2 norm. Now, the dot product of a sequence with itself gives the square of its l_2 norm. So the sequence corresponding to $\kappa_0(z)$ at the 0^{th} location is essentially the squared norm in the $l_2(Z)$ of $[h_0\ h_1\ h_2\ h_3]$. So C_0 chosen such as,

$$\begin{aligned} C_0^2(h_0^2+h_1^2+h_2^2+h_3^2) &= 1 \\ C_0^2=1/4.287 &= 0.233 \\ C_0 &= 0.4829 \end{aligned} \quad (6.7)$$

Table 6.1 | Impulse response of the analysis side low pass filter of length 4 of Daubechies family

1	(2 + *B*0)	(1 + *B*0)	*B*0
1	1.732	0.464	-0.268

6.3 | Calculation of Scaling Function

The next step is to calculate $\phi(t)$ and $\psi(t)$ from the calculated impulse response. To calculate the scaling function $\phi(t)$ we have to compress and convolve $h[n]$ iteratively. This is done as follows:

Let us treat $h[n]$ as the set of coefficients of an impulse train containing only 4 impulses in the continuous time domain, such as the function in the continuous time domain is $h(t)$ such as,

$$h(t)=h_0\delta(t)+h_1\delta(t-T)+h_2\delta(t-2T)+h_3\delta(t-3T) \quad (6.8)$$

Accordingly the shape of $h(2t), h(4t), h(8t)$ etc. are shown in Fig. 6.1.

For the iterative convolution, first $h(t)$ is convolved with $h(2t)$ and the result is convolved with $h(4t)$.

h_0	h_1	h_2	h_3
0.4829*1=0.4829	0. 0.4829*1.732=0.8364	0.4829*0.464=0.2241	0.4829*(-0.268)=-0.129

Then the result is convolved with $h(8t)$, and so on. If this convolution process with compressed version of $h(t)$ is carried on infinitely, we will get the scaling function $\phi(t)$.

There is an interesting conclusion of this iterative convolution process. Suppose $h(t)$ has length L, i.e. $h(t) = 0$ for any $t < 0$ and for any $t > L$. So $h(2t)$ has a length $L/2$, $h(4t)$ has a length $L/4$, $h(8t)$ has a length $L/8$, and so on. Now, the convolution of $h(t)$ with $h(2t)$ gives result with length $L + L/2$. This result when convolved with $h(4t)$, it gives a result with length $L + L/2 + L/4$. Continuing this way we can get $\phi(t)$, which is of length $L + L/2 + L/4 + ... = 2L$.

It means $\phi(t)$ is zero for any $t < 0$ and $t > 2L$, i.e. we converge towards a compactly supported scaling function. The independent variable region over which the scaling function is nonzero is finite. This is the most important contribution made by Daubechies. Before Daubechies came up with these set of filter banks, idea of neatly constructing a family of compactly supported multiresolution analysis did not exist in record. So this is a very useful contribution in MRA.

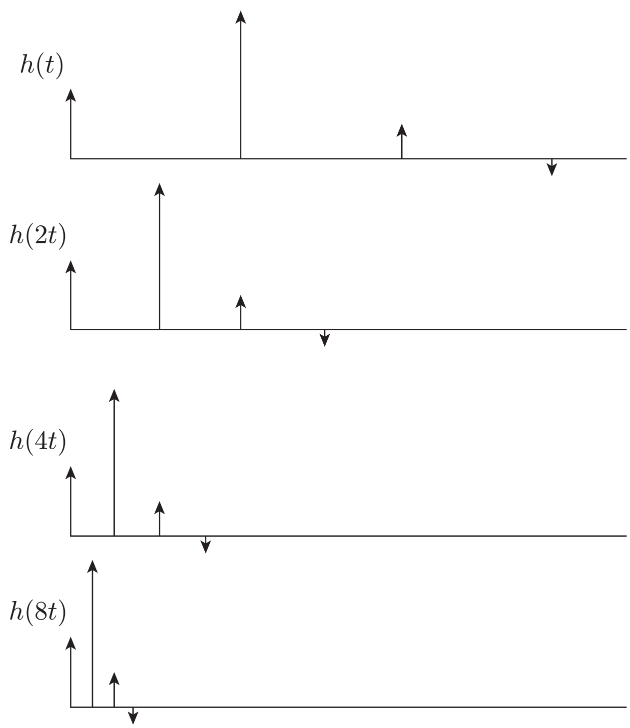

Figure 6.1 | *Shape of* $h(t), h(2t), h(4t)$ *and* $h(8t)$

6.3.1 Interpretation for Daubechies Filter Banks

The theories of wavelets and filter banks developed in parallel. Using filter banks effectively to generate compactly supported scaling function is an important contribution by Daubechies.

A different interpretation can be thought about the Daubechies filter banks. The high pass analysis filter bank essentially reduces the degree of a polynomial input. Suppose there is an input of the form $x[n] = a + bn$, where a and b are constants. So the factor $(1 - z^{-1})$ in the high pass filter reduces the degree of the input. If there had been only this term in the high pass filter, the output would have been in the form of $y[n] = a + bn - a - b(n-1) = b$. If there had been another term of $(1 - z^{-1})$ the output would have become 0. So in Daubechies length 4 (abbreviated as Daub-4) high pass filter bank the polynomial is annihilated. On the other side, in the low pass analysis filter, because of the $(1 + z^{-1})$ term, the output becomes $y[n] = a + bn + a + b(n-1) = 2a + 2bn - b$. It can similarly be extended for another $(1 + z^{-1})$ term. This means that the polynomial form of expression remains in the low pass branch and the high pass branch contains some residual component, thereby retaining a few more smoother terms related to polynomial in the low pass branch and removing them from the high pass branch.

While calculating the iterative convolution we saw that the scaling function thus obtained has a compact support. But it is important to note that had it taken any arbitrary values of h_0, h_1, h_2, h_3 the iterative convolution process might not have converged to a function with finite number of discontinuities. But beauty of Daubechies family is that whatever be the filter length, the convolution always converges to a function with finite number of discontinuities. The specialty that makes the convolution to converge is denoted by a term 'regularity' in Wavelet literature, i.e. the filters need to obey regularity for the iterative convolution to converge. This regularity comes because of the presence of the zeros in the system function. One guaranteed way of forcing regularity is to introduce factors of $(1 + z^{-1})$, i.e. adding zeroes at $z = -1$, i.e. $\omega = \pi$ in the low pass analysis filters. In case of high pass analysis filter the zeros are added at $z = 1$, i.e. $\omega = 0$. So the zeros are put at the extreme high frequency in low pass filter and at the extreme low frequency in high pass filter. In case of different filter banks, the number of zeros are as listed in Table 6.2.

Table 6.2 Daunechies family member and corresponding zeros

Haar	1 zeros
Daub-4	2 zeros
Daub-6	3 zeros

Higher is the filter length more regular is the Daubechies filter. This means the function to which we converge by iterative convolution becomes more and more smooth, i.e. they have more and more derivative which are continuous. In Daubechies-4 there are some issues in the differentiability but in the higher order filters that is also taken care of.

6.3.2 Next Daubechies Family Member Daub-6

The next member of Daubechies family is a length 6 filter of degree 5. In that case $H_0(z)$ can be written as,

$$H_0(z) = C_0(1 + z^{-1})^3(1 + \widetilde{B}_0 z^{-1})(1 + \widetilde{B}_1 z^{-1}) \tag{6.9}$$

here C_0 is a constant. Three zeros are constrained and two are free ($\widetilde{B_0}$ and $\widetilde{B_1}$). Let the impulse response be,

$$h[n] = [h_0\ h_1\ h_2\ h_3\ h_4\ h_5]$$

so $h[n]$ is orthogonal to its even shifts, e.g. shift of 2, 4, 6, etc. The nontrivial relations are obtained by the dot product between $h[n]$ and $h[n-2]$ or $h[n-4]$. Here,

$$h[n] = [h_0\ h_1\ h_2\ h_3\ h_4\ h_5]$$

$$h[n-2] = [\ldots\ldots h_0\ h_1\ h_2\ h_3\ h_4\ h_5]$$
$$\uparrow_{n=2}$$

$$h[n-4] = [\ldots\ldots\ldots\ldots\ldots\ldots h_0\ h_1\ h_2\ h_3\ h_4\ h_5]$$
$$\uparrow_{n=2}$$

$$\Rightarrow h_2h_0 + h_3h_1 + h_4h_2 + h_5h_3 = 0 \tag{6.10}$$

$$\Rightarrow h_4h_0 + h_5h_1 = 0 \tag{6.11}$$

From Eqs. (6.9), (6.10) and (6.11), we can find out the values of $\widetilde{B_0}$ and $\widetilde{B_1}$. Therefrom we can construct the impulse response in a way similar to Daub-4 case.

This type of filter banks are called Conjugate Quadrature filter bank. The reason for this nomenclature is that the low pass and the high pass filter frequency responses are π apart from each other. So the principal equation governing the conjugate quadrature filter is,

$$\kappa_0(z) + \kappa_0(-z) = \text{constant}$$

where,

$$\kappa_0(z) = H_0(z)H_0(z^{-1})$$

$$\kappa_0(e^{j\omega}) = H_0(e^{j\omega})H_0(e^{j\omega})$$

If the frequency response is real, then

$$\left|H_0(e^{j\omega})\right|^2 = \kappa_0(e^{j\omega}) \tag{6.12}$$

This means designing a conjugate quadrature filter bank is essentially designing $\kappa_0(e^{j\omega})$ only. $\kappa_0(z)$ corresponds to a real and even impulse response with the constraints that even samples of the impulse response are all '0' except at the 0th sample.

There are many ways to design such filter banks. Once we have $\kappa_0(z)$ we find its roots. For each root there are pairs of reciprocal roots $H_0(z)$ and $H_0(z^{-1})$. Out of each reciprocal root pair, one root is assigned to $H_0(z)$ and the other automatically gets assigned to $H_0(z^{-1})$. The Daubechies filters are one class of conjugate quadrature filters.

Our future study will aim at what we are looking for out of these filter banks in both time and frequency domains.

6.4 | Daub-4 and Daub-6 Design Details

This aims at using linear algebra and matrices.

we wish to come up with design procedure to construct 'even' length Doubechies filter.

Let

$$h = \{h_0, h_1, \cdots h_L\} \text{ be the LPF coefficients and}$$

$$g = \{g_0, g_1, \cdots g_L\} \text{ be the HPF coefficients and}$$

Let both these filters be finite impulse response filters

For example, if $h = \{h_0, h_1, h_2\} = \left\{\frac{1}{4}, \frac{1}{2}, \frac{1}{4}\right\}$

Then the Fourier series $h(\omega)$ will be

$$H(\omega) = \left(\frac{1}{4} + \frac{1}{2} \cdot e^{j\omega} + \frac{1}{4} \cdot e^{2j\omega}\right) = e^{j\omega} \cdot \frac{1}{2}\left(1 + \cos\omega\right) \tag{6.13}$$

If we plot the magnitude graph over $[0, \pi]$, then

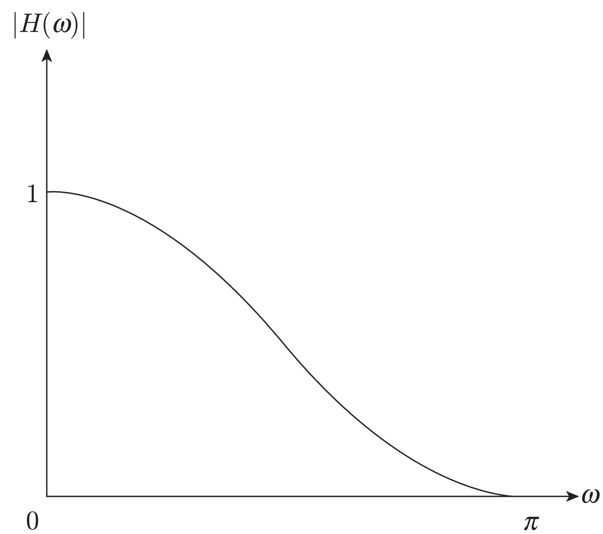

$\therefore$ low pass filter conditions could be

$$H\,|(0)| = \frac{1}{2}(1 + \cos 0) = 1 \quad \text{and}$$

$$H\,|(\pi)| = \frac{1}{2}(1 + \cos\pi) = 0$$

Now,

$$H(\omega) = \sum_{k=0}^{L} h_k \cdot e^{-jk\omega} \tag{6.14}$$

Now if $g = \{g_0, g_1, g_2, \cdots g_L\}$

$$G(\omega) = \sum_{k=0}^{L} g_k \cdot e^{-jk\omega} \tag{6.15}$$

High pass conditions will be $|G(0)| = 0$ and $|G(\pi)| = 1$

To design Daub-4 and Daub-6,

$$L = 3 \ \& \ 5.$$

Now, let us construct system of linear and quadratic equations that coefficient of 'h' show satisfy.

Design 1- Daubechies-4

$$h = \{h_0, h_1, h_2, h_3\}$$

$$g = \{g_0, g_1, g_2, g_3\}$$

Typical output of any filtered is mathematically captured by 'convolution'.

$$x - \boxed{h} - y = x \times h$$

$$y_n = \sum_{k=0}^{L} h_k \cdot x_{n-k} = h_0 \cdot x_n + h_1 \cdot x_n + \cdots \tag{6.16}$$

$\therefore$ For causal system and sequences (i.e. no $y\_1, y\_2, \cdots$ and $x\_1, x\_2, \cdots$ terms)

$$\begin{bmatrix} y_0 \\ y_1 \\ \vdots \\ y_2 \end{bmatrix} = H \cdot \begin{bmatrix} x_0 \\ x_1 \\ \vdots \\ x_2 \end{bmatrix} \tag{6.17}$$

then, 'H' can be written in matrix form as follows:

Upper Triangle $= 0$

$$\begin{bmatrix} h_L & \cdots & \cdots & h_2 & h_1 & h_0 & 0 & 0 & 0 & 0 & 0 & 0 & \cdots \\ 0 & h_L & \cdots & \cdots & h_2 & h_1 & h_0 & 0 & 0 & 0 & 0 & 0 & \cdots \\ 0 & 0 & h_L & \cdots & \cdots & h_2 & h_1 & h_0 & 0 & 0 & 0 & 0 & \cdots \\ \vdots & \vdots & \vdots & \vdots & \vdots & \vdots & \vdots & \vdots & \vdots & \vdots & \vdots & & \ddots \end{bmatrix}$$

Constant Diagonal

Constant Diagonal

Constant Diagonal

Main Diagonal

Important points to note about 'H' matrix:

1. Since it represents a system in matrix form it is a system of linear equations.
2. 'ho's constitute main diagonal.

3. With reference to main diagonal, upper triangle is '0', which suggests, system is causal $\left[H_{ij} = 0\, for\ all\ j > i, i, j \in Z\right]$
4. Since all diagonals are constant, it indicates, system is shift invariant.
5. Therefore, 'H' is a causal LTI system.

Similarly, for high pass filter 'G' matrix can be built. 'H' and 'G' together constitute wavelet matrix 'w', as in wavelets we use filter bank, combination of LPF(H) and HPF(G).

For example, if in case of Haar,

$$h[n] = \left\{\frac{1}{\sqrt{2}}, \frac{1}{\sqrt{2}}\right\} \text{ and } g[n] = \left\{\frac{1}{\sqrt{2}}, \frac{-1}{\sqrt{2}}\right\}$$

'W' matrix will be,

$$W = \begin{bmatrix} H \\ G \end{bmatrix}$$

and would look like

$$W = \sqrt{2} \cdot \begin{bmatrix} 12 & 12 & 0 & 0 \\ 0 & 0 & 12 & 12 \\ -12 & 12 & 0 & 0 \\ 0 & 0 & -12 & 12 \end{bmatrix} \tag{6.18}$$

This is Daub-2 or Haar.

Now, for Daub-4, the filter length will be '4' and W matrix wil be 8×8.

Let us call that as W_{D4}.

$$W_{D4} = \begin{bmatrix} h_3 & h_2 & h_1 & h_0 & 0 & 0 & 0 & 0 \\ 0 & 0 & h_3 & h_2 & h_1 & h_0 & 0 & 0 \\ 0 & 0 & 0 & 0 & h_3 & h_2 & h_1 & h_0 \\ h_1 & h_0 & 0 & 0 & 0 & 0 & h_3 & h_2 \\ - & - & - & - & - & - & - & - \\ g_3 & g_2 & g_1 & g_0 & 0 & 0 & 0 & 0 \\ 0 & 0 & g_3 & g_2 & g_1 & g_0 & 0 & 0 \\ 0 & 0 & 0 & 0 & g_3 & g_2 & g_1 & g_0 \\ g_1 & g_0 & 0 & 0 & 0 & 0 & g_3 & g_2 \end{bmatrix} = \begin{bmatrix} H_{D4} \\ ------ \\ G_{D4} \end{bmatrix} \tag{6.19}$$

Now, for W_{D4} to become a transformation matrix, following conditions should be met:

1. The inverse should exist.
2. W_{D4} should be unitary, i.e. for real values, $W_{D4}^{-1} = W_{D4}^{T}$.
3. W_{D4} should be orthogonal.

Assuming 1^{st} two criteria,
For the orthogonality,

$$W_{D4} \cdot W_{D4}^T = I$$

$$\therefore W_{D4} \cdot W_{D4}^T = \begin{bmatrix} H_{D4} \\ G_{D4} \end{bmatrix} \begin{bmatrix} H_{D4} & G_{D4} \end{bmatrix} = \begin{bmatrix} H_{D4} \cdot H_{D4}^T & H_{D4} \cdot G_{D4}^T \\ G_{D4} \cdot H_{D4}^T & G_{D4} \cdot G_{D4}^T \end{bmatrix} = \begin{bmatrix} I_4 & 0_4 \\ 0_4 & I_4 \end{bmatrix}$$

$$\therefore H_{D4} \cdot H_{D4}^T = I_4$$

$$\therefore \begin{bmatrix} h_3 & h_2 & h_1 & h_0 & 0 & 0 & 0 & 0 \\ 0 & 0 & h_3 & h_2 & h_1 & h_0 & 0 & 0 \\ 0 & 0 & 0 & 0 & h_3 & h_2 & h_1 & h_0 \\ h_1 & h_0 & 0 & 0 & 0 & 0 & h_3 & h_2 \end{bmatrix} \cdot \begin{bmatrix} h_3 & 0 & 0 & h_1 \\ h_2 & 0 & 0 & h_0 \\ h_1 & h_3 & 0 & 0 \\ h_0 & h_2 & 0 & 0 g_0 \\ 0 & h_1 & h_3 & 0 \\ 0 & h_0 & h_2 & 0 \\ 0 & 0 & h_1 & h_3 \\ 0 & 0 & h_0 & h_2 \end{bmatrix} = \begin{bmatrix} 1 & 0 & 0 & 0 \\ 0 & 1 & 0 & 0 \\ 0 & 0 & 1 & 0 \\ 0 & 0 & 0 & 1 \end{bmatrix}$$

Let us work on 1^{st} row, 1^{st} column $\rightarrow$ should lead to '1'
and 1^{st} row, 2^{nd} column $\rightarrow$ should lead to '0'

$\therefore$

$$h_3^2 + h_2^2 + h_1^2 + h_0^2 = 1 \tag{6.20}$$

and

$$h_1 \cdot h_3 + h_0 \cdot h_2 = 0 \tag{6.21}$$

The orthogonality between 'h' and 'g' plays vital role. One way of understanding orthogonality is 'zero' dot product between two vectors. 'Dot' product is element-by-element product. For every 'h', if we create corresponding 'g' by flipping the sequence and making alternate samples go negative, then that will certainly achieve orthogonalization.

For example, if $h = \{1,2,3,4\}$

then $g = \{4,-3,2,-1\}$ is a good candidate to produce orthogonal framework.

$$\langle h \cdot \rangle = \left[1 \times 4 + 2 \times (-3) + 3 \times (2) + 4 \times (-1)\right] = 0!$$

Mathematically, this can be captured using:

$$g_k = (-1)^k \cdot h_{L-k},$$

where, $h = \{h_0, h_1, \cdots, hL\}$ and $g = \{g_0, g_1, \cdots, g_L\}$

This grantees $\langle h, g \rangle = \left[h \cdot g\right] = 0$

$$\therefore g = \{g_0, g_1, g_2, g_3\} = \{h_3, -h_2, h_1, -h_0\}$$

Now,

$$H_{D4} \cdot G_{D4}^{T} = [0]_{4\times 4}$$

$$\therefore \begin{bmatrix} h_3 & h_2 & h_1 & h_0 & 0 & 0 & 0 & 0 \\ 0 & 0 & h_3 & h_2 & h_1 & h_0 & 0 & 0 \\ 0 & 0 & 0 & 0 & h_3 & h_2 & h_1 & h_0 \\ h_1 & h_0 & 0 & 0 & 0 & 0 & h_3 & h_2 \end{bmatrix} \cdot \begin{bmatrix} -h_0 & 0 & 0 & -h_2 \\ h_1 & 0 & 0 & h_3 \\ -h_2 & -h_0 & 0 & 0 \\ h_3 & h_1 & 0 & 0 \\ 0 & -h_2 & -h_0 & 0 \\ 0 & h_3 & h_1 & 0 \\ 0 & 0 & -h_2 & -h_1 \\ 0 & 0 & h_3 & h_2 \end{bmatrix} = \begin{bmatrix} 0 & 0 & 0 & 0 \\ 0 & 0 & 0 & 0 \\ 0 & 0 & 0 & 0 \\ 0 & 0 & 0 & 0 \end{bmatrix}$$

Similarly,

$$G_{D4} \cdot H_{D4}^{T} = [0]_{4\times 4}$$

$$\begin{bmatrix} -h_0 & h_1 & -h_2 & h_3 & 0 & 0 & 0 & 0 \\ 0 & 0 & -h_0 & h_1 & -h_2 & h_3 & 0 & 0 \\ 0 & 0 & 0 & 0 & -h_0 & h_1 & -h_2 & h_3 \\ -h_2 & h_3 & 0 & 0 & 0 & 0 & -h_1 & h_2 \end{bmatrix} \cdot \begin{bmatrix} h_3 & 0 & 0 & h_1 \\ h_2 & 0 & 0 & h_0 \\ h_1 & h_3 & 0 & 0 \\ h_0 & h_2 & 0 & 0g_0 \\ 0 & h_1 & h_3 & 0 \\ 0 & h_0 & h_2 & 0 \\ 0 & 0 & h_1 & h_3 \\ 0 & 0 & h_0 & h_2 \end{bmatrix} = \begin{bmatrix} 0 & 0 & 0 & 0 \\ 0 & 0 & 0 & 0 \\ 0 & 0 & 0 & 0 \\ 0 & 0 & 0 & 0 \end{bmatrix}$$

Also, $G_{D4} \cdot G_{D4}^{'} = I_4$

$$\therefore \begin{bmatrix} -h_0 & h_1 & -h_2 & h_3 & 0 & 0 & 0 & 0 \\ 0 & 0 & -h_0 & h_1 & -h_2 & h_3 & 0 & 0 \\ 0 & 0 & 0 & 0 & -h_0 & h_1 & -h_2 & h_3 \\ -h_2 & h_3 & 0 & 0 & 0 & 0 & -h_1 & h_2 \end{bmatrix} \cdot \begin{bmatrix} -h_0 & 0 & 0 & -h_2 \\ h_1 & 0 & 0 & h_3 \\ -h_2 & -h_0 & 0 & 0 \\ h_3 & h_1 & 0 & 0 \\ 0 & -h_2 & -h_0 & 0 \\ 0 & h_3 & h_1 & 0 \\ 0 & 0 & -h_2 & -h_1 \\ 0 & 0 & h_3 & h_2 \end{bmatrix} = \begin{bmatrix} 1 & 0 & 0 & 0 \\ 0 & 1 & 0 & 0 \\ 0 & 0 & 1 & 0 \\ 0 & 0 & 0 & 1 \end{bmatrix} \tag{6.22}$$

We again confirm,

$$\begin{aligned} h_0^2 + h_1^2 + h_2^2 + h_3^2 &= 1 \\ h_0 h_2 + h_1 h_3 &= 0 \end{aligned}$$

Now,

let us impose conditions so that ‘h’ is truly a low pass filter on $[0,\pi]$

Being a LPF, it should pass frequencies at $\omega = 0$ and block frequencies at $\omega = \pi$.

Let $H(\omega)$ be the Fourier representation of $h(n)$ in the form of series,

$$H(\omega) = h_0 + h_1 \cdot e^{j\omega} + h_2 \cdot e^{2\cdot j\omega} + h_3 \cdot e^{3\cdot j\omega} \tag{6.23}$$

Let us impose first condition to pass frequencies at $w = 0$, and let the magnitude by ‘Unit’ be decided by us.

$$\therefore H(\omega, 0) = h_0 + h_1 \cdot e^0 + h_2 \cdot e^0 + h_3 \cdot e^0 = \text{Unit} \tag{6.24}$$

we choose the unit carefully to normalize orthogonal system, thus making it orthonormal.

Recall the MRA framework we saw, h_k is linked with $\phi(\cdot)$ and s_k is linked with $\psi(\cdot)$. For set $\left\{2^{\frac{j}{2}}\phi(2^j x - k)\right\}$, being orthonormal and linearly independent, it constitutes a basis for vector space V^j at window of analysis $W_a = 12^j$.

This is truly orthonormal on $(-\infty, \infty)$, since

$$\int_{-\infty}^{\infty} 2^{\frac{j}{2}}\phi(2^j x - k)\cdot\phi(2^j x - l)dx = \begin{cases} 0, & k \neq l \\ 1, & k = l \end{cases} \tag{6.25}$$

This is condition for orthogonality,whole makes it orthonormal is normalizing factor of $2^{\frac{j}{2}}$ in $\left\{2^{\frac{j}{2}}\phi(2^j x - k)\right\}$.

If we take norm of $\phi(2^j x - k)$, we get that factor.

$$\|\phi(2^j x - k)\|^2 = \int_{-\infty}^{\infty}\phi^2(2^j x - k)dx = \frac{1}{2^j}\int_{-\infty}^{\infty}\phi^2(2^j x - k)\cdot 2^j\, dx \tag{6.26}$$

Let us put $2^j x - k = a$

Differentiating both sides, we get

$$2^j \cdot dx - 0 = da$$

$$\therefore 2^j dx = da$$

$$\|\phi(2^j x - k)\|^2 = \frac{1}{2^j}\int_{-\infty}^{\infty}\phi^2(a)dx \tag{6.27}$$

Let us prove it for Haar, where

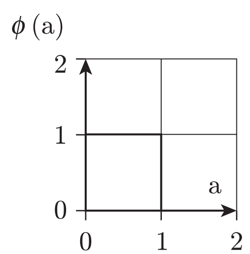

$$\|\phi(2^j x - k)\|^2 = \frac{1}{2^j}\int_0^1 (1)^2 da = \frac{1}{2^j}(1) = \frac{1}{2^j}$$

Taking square root for positives,

$$\| \phi(2^j x - k) \|^2 = \frac{1}{2^j}$$

$\therefore$ We can divide $\phi(2^j x - k)$ by its norm to get orthogonal basis coverted to orthonormal basis,

$$\underline{\phi(2^j x - k)} = 2^{\frac{j}{2}} x - k) = 2^{\frac{j}{2}} \phi(2^j x - k)$$

$$\frac{1}{j^{\frac{j}{2}}}$$

From the point of view of nested subspaces, we have to account for $\sqrt{2}$ every time we move from one subspace to another.

$$\begin{array}{ccccccccccc} \cdots & & \sqrt{2} & & \sqrt{2} & & \sqrt{2} & & \sqrt{2} & & \cdots \\ \cdots & V_{-2} & \subset & V_{-1} & \subset & V_0 & \subset & V_1 & \subset & V_2 & \cdots \end{array}$$

This is a 'dyadic' style of realizing discrete wavelet filters.

$\therefore$ We choose 'Unit' to be '$\sqrt{2}$' to maintain orthogonality.

We will put this in equation (6.23),

$$h_0 + h_1 + h_2 + h_3 = \pm\sqrt{2} \tag{6.28}$$

We will use this as a final check whether the LPF coefficient satisfy this condition or not.

Let us impose second low pass condition of complete attenuation at $w = \pi$.

$$\therefore \qquad H(\pi) = 0 = h_0 + h_1 \cdot e^{j\pi} + h_2 \cdot e^{2j\pi} + h_3 \cdot e^{3j\pi}$$

Using euler's identity $e^{j\pi} = -1$

$$e^2 j\pi = (e^j\pi)^2 = (-1)^2 = 1$$

$$e^3 j\pi = (e^j\pi)^3 = (-1)^3 = -1$$

$$H(\pi) = 0 = h_0 - h_1 + h_2 - h_3 \tag{6.29}$$

'g_k' being a highpass filter, let's impose conditions accordingly,

$$g_k = \{g_0, g_1, g_2, g_3\}$$

$$\therefore \qquad G(\omega) = g_0 + g_1 \cdot e^{j\omega} + g_2 \cdot e^{2j\omega} + g_3 \cdot e^{3j\omega}$$

Put $\{g_0, g_1, g_2, g_3\} = \{{}_+h_3, {}^-h_2, {}_+h_1, {}^-h_0\}$

$\therefore$ $$G(\omega) = h_3 - h_2 \cdot e^{j\omega} + h_1 \cdot e^{2j\omega} - h e^{3j\omega}$$

$G(0) = 0$ -(block low frequencies)

$\therefore$ $$h_3 - h_2 + h_1 - h_0 = 0 \tag{6.30}$$

$$G(\pi) = \text{unit} = \sqrt{2}$$

$$| h_0 + h_1 + h_2 + h_3 | = \sqrt{2} \qquad \text{(another check condition)}$$

Let us combine two orthogonality conditions and one

LPF condition towords finding h_k From Eqs. (6.20), (6.21) and (6.29)

$$\boxed{\begin{array}{l} h_0^2 + h_1^2 + h_2^2 + h_3^2 = 1 \\ h_0 h_2 + h_1 h_3 = 0 \\ h_0 - h_1 + h_2 - h_3 = 0 \end{array}} \text{\_\_\_\_\_\_\_\_\_\_(D1)}$$

These are our design Equations!
let 's start with Eq. (6.21)

$$h_0 + h_2 h_1 h_3 = 0$$

This clearly implies $[h_0\ h_1]^T$ and $[h_2\ h_3]^T$ are orthogonal,

i.e. inner or dot product $< [h_0\ h_1], [h_2\ h_3] >$ suggests

$$h_0 h_2 + h_1 + h_3 \rightarrow \text{going to '0'}$$

For example, $h_0 = 1, h_1 = 1, h_2 = -1,\ h_3 = 1$ ensures

$$[h_o\ h_1]^T \perp [h_2\ h_3]^T$$

We can also prove graphically $[h_2\ h_3]^T \perp c[-h_1\ h_0]^T$

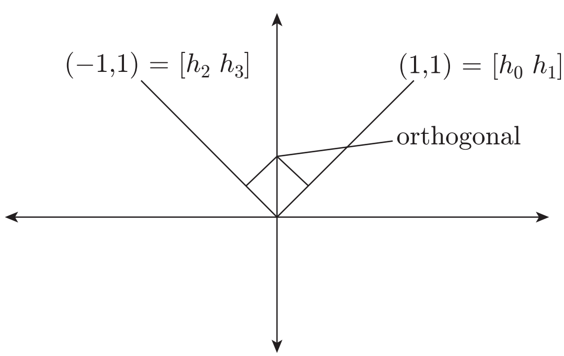

Therefore, it is easy to see that

$$[h_2\ h_3]^T \perp c[-h_1\ h_0]^T \tag{6.31}$$

with $c = 1$ in this case!
For c ≠ 0, if we insert

$$\left[h_2 h_3\right]^T \perp c\left[-h_1 h_0\right]^T \text{ in Eq. (6.21)}$$

We get

$$h_0^2 + h_1^2 = \frac{1}{1+c^2} \tag{6.32}$$

One way of looking at Eq. (6.31) is

$$h_2 = -ch_1 \text{ and } h_3 = ch_0$$

Let's plug these values in Eq. (6.29)

$$\therefore h_0 - h_1 - ch_1 + ch_0 = 0$$

$$\therefore h_0(1-c) + h_1(1+c) = 0$$

$$h_1 = \left(\frac{1-c}{1+c}\right)h_0 = \{c \neq l \tag{6.33}$$

Therefore Eq. (6.32) is clearly a equation of circle of radius $\frac{1}{\sqrt{1+c^2}}$ and Eq. (6.33) is a equation of straight line with slope $\frac{1-c}{1+c}$

Graphically,

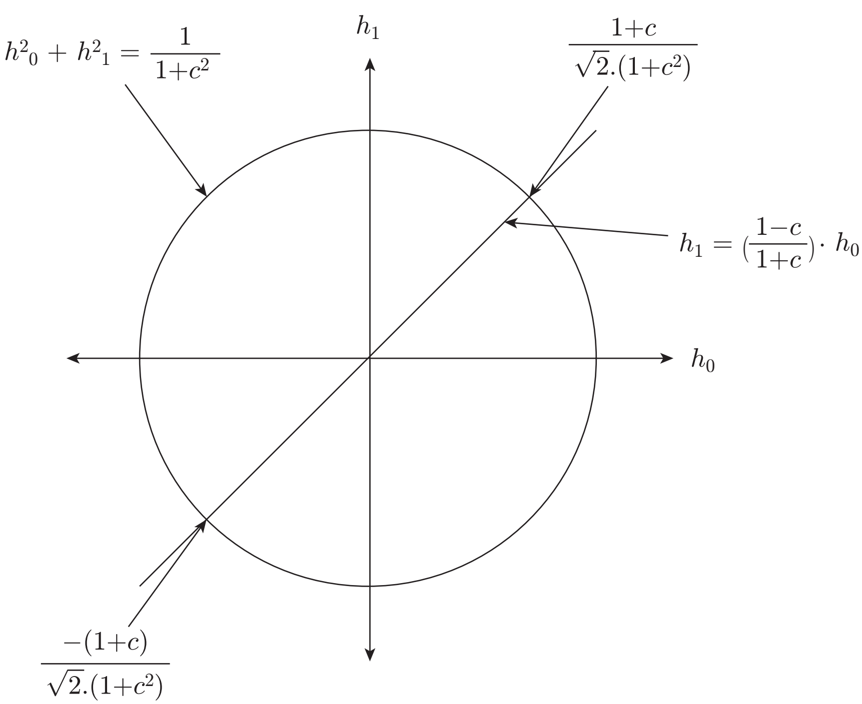

$\therefore$ For any given $c \neq -1$, the line with slope of $\dfrac{1-c}{1+c}$ intersects circle of radius $\dfrac{1}{\sqrt{1+c^2}}$ twice

$\therefore$ For each 'c' there are 2 possible solutions, that will satisfy design conditions D_1.

Let's simplify

$$h_0^2 + h_1^2 = \frac{1}{1+c^2}$$

$$h_0^2 + \left(\frac{1-c}{1+c}\right)^2 \cdot h_0^2 = \frac{1}{1+c^2}$$

$$h_0^2\left(1+\left(\frac{1-c}{1+c}\right)^2\right) = \frac{1}{1+c^2}$$

$$h_0^2\left[\left(\frac{(1+c)^{+}(1-c)^2}{(1+c)^2}\right)\right] = \frac{1}{1+c^2}$$

$$h_0^2\left[\left(\frac{(1+2c+c^2+1-2c+c^2}{(1+c)^2}\right)\right] = h_0^2\left[\frac{2(1+c^2)}{1+c^2}\right]$$

$$\therefore \quad 2h_0^2 = \frac{1}{1+c^2}\cdot\frac{(1+c)^2}{1+c^2}$$

$$\therefore \quad h_0^2 = \frac{1+c^2}{2(1+c^2)^2}$$

$$\therefore \quad h_0 = \pm\frac{1+c}{\sqrt{2}(1+c^2)} \leftrightarrow \text{the 'two' solutions!}$$

Let us choose (+ve)root

$$h_0 = +\frac{1+c}{\sqrt{2}(1+c^2)} \tag{6.34}$$

By plug and solve

$$h_0 = \frac{1-c}{\sqrt{2}(1+c^2)},\ h_2 = +\frac{-c(1-c)}{\sqrt{2}(1+c^2)},\ h_3 = +\frac{-c(1+c)}{\sqrt{2}(1+c^2)}$$

D1 is a system of three equations where we have to figure out four unknowns
Let us add one more LP condition

$$H(\pi) = 0$$

As ideal filtering is not possible, we impose

$$H'(\pi) = 0$$

First-order difference (derivative) will give us,

$$H''(\omega)\,|_{\omega=\pi} = jh_1e^{j\omega} + 2jh_2e^{2j\omega} + 3jh_3e^{3j\omega}\,|_{\omega=\pi}$$

$$0 = j\left(h_1(-1) + 2h_2(-1)^2 + 3h_3(-1)^3\right)$$

$$\therefore h_1 - 2h_2 + 3h_3 = 0 \tag{6.35}$$

Let us add Eq. (6.35) in D1 to get complete set D2

$$\boxed{\begin{aligned} &h_0^2 + h_1^2 + h_2^2 + h_3^2 = 1 \\ &h_0 + h_2 h_1 h_3 = 0 \\ &h_0 - h_1 + h_2 - h_3 = 0 \\ &h_1 - 2h_2 + 3h_3 = 0 \end{aligned}} \text{———————(D2)}$$

Now, let us plug $h_2 = -ch_1$ and $h_3 = ch_0$ in Eq. (6.35)

$$h_1 + 2ch_1 + ch_0 = h_1(1 + 2c) + 3ch_0 = 0$$

$$\therefore \qquad h_1 = -\left(\frac{3c}{(1+2c)\cdot h_0}\right)$$

we already know the slope matches with $\dfrac{1-c}{1+c}$

$$\therefore \qquad \frac{-3c}{1+2c} = \frac{1-c}{1+c}$$

$$\therefore \qquad -3c - 3c^2 = 1 + 2c - c - 2c^2$$

$$\therefore \qquad -3c - 3c^2 = 1 + c - 2c^2$$

$$\therefore \qquad c^2 + 4c + 1 = 0 \tag{6.36}$$

Roots of Eq. (6.36) will be

$$c = -2 \pm \sqrt{3}$$

$c = -2 - \sqrt{3}$ makes system slow and sluggish, as the zero lies outside the unit circle and it ensures max-phase system.

$\therefore$ we choose minimum phase $c = -2 + \sqrt{3}$ solution by backward substitution in D2

$$\boxed{\begin{aligned} h_0 &= \frac{1+\sqrt{3}}{4\sqrt{2}} \qquad & h_1 &= \frac{3+\sqrt{3}}{4\sqrt{2}} \\ h_3 &= \frac{1-\sqrt{3}}{4\sqrt{2}} \qquad & h_2 &= \frac{3-\sqrt{3}}{4\sqrt{2}} \end{aligned}}$$

Now, $g_k = (-1)^k h_3 - k, k = 0,1,2,3$

$$\boxed{\begin{array}{ll} g_0 = h_3 = \dfrac{1-\sqrt{3}}{4\sqrt{2}} & g_1 = -h_2 = -\dfrac{3-\sqrt{3}}{4\sqrt{2}} \\ g_2 = h_1 = \dfrac{3+\sqrt{3}}{4\sqrt{2}} & g_3 = -h_0 - \dfrac{1+\sqrt{3}}{4\sqrt{2}} \end{array}}$$

Now let us repeat this for Daub-6 where

$$h = \{h_0 \cdots h_5\}$$

$$g = \{g_0 \cdots g_5\}$$

$$W_{10} = \begin{bmatrix} h_5 & h_4 & h_3 & h_2 & h_1 & h_0 & 0 & 0 & 0 & 0 \\ 0 & 0 & h_5 & h_4 & h_3 & h_2 & h_1 & h_0 & 0 & 0 \\ 0 & 0 & 0 & 0 & h_5 & h_4 & h_3 & h_2 & h_1 & h_0 \\ h_1 & h_0 & 0 & 0 & 0 & 0 & h_5 & h_4 & h_3 & h_2 \\ h_3 & h_2 & h_1 & h_0 & 0 & 0 & 0 & 0 & h_5 & h_4 \\ - & - & - & - & - & - & - & - & - & - \\ g_5 & g_4 & g_3 & g_2 & g_1 & g_0 & 0 & 0 & 0 & 0 \\ 0 & 0 & g_5 & g_4 & g_3 & g_2 & g_1 & g_0 & 0 & 0 \\ 0 & 0 & 0 & 0 & g_5 & g_4 & g_3 & g_2 & g_1 & g_0 \\ g_1 & g_0 & 0 & 0 & 0 & 0 & g_5 & g_4 & g_3 & g_2 \\ g_3 & g_2 & g_1 & g_0 & 0 & 0 & 0 & 0 & g_5 & g_4 \end{bmatrix} = \begin{bmatrix} H_{D4} \\ --- \\ G_{D4} \end{bmatrix}$$

We can extend D1 conditions directly

$$\boxed{\begin{aligned} h_0^2 + h_1^2 + h_2^2 + h_3^2 + h_4^2 + h_5^2 &= 1 \\ h_0h_2 + h_1h_3 + h_2h_4 + h_3h_5 &= 0 \\ h_0h_4 + h_1h_5 &= 0 \end{aligned}} \quad \text{———————— (D3)}$$

$$g = h_5, h_4, h_3, h_2, h_1, h_0$$

$$\therefore \qquad H_{D10} \cdot H_{D10}{}^T = G_{D10} \cdot G_{D10}{}^T = I_5 \quad \text{and}$$

$$\therefore \qquad H_{D10} \cdot G_{D10}{}^T = G_{D10} \cdot H_{D10}{}^T = 0_5$$

Low pass conditions

$$H(\pi) = 0 = h_0 - h_1 + h_2 - h_3 + h_4 - h_5$$

$$H(0) = \sqrt{2}$$

$$h_0 + h_1 + h_2 + h_3 + h_4 + h_5 = \sqrt{2}$$

additional conditions on $H(\omega)$ will be

$$H'(\pi) = 0$$

and further flatten at $\omega = \pi$ by

$$H'' = 0$$

$$\therefore \quad H(\omega) = h_0 + h_1 e^{j\omega} + h_2 e^{2j\omega} + h_3 e^{3j\omega} + h_4 e^{4j\omega} + h_5 e^{5j\omega}$$

$$\therefore \quad H'(\omega) = j \cdot h_1 e^{j\omega} + 2j \cdot h_2 e^{2j\omega} + 3j \cdot h_3 e^{3j\omega} + 4j \cdot h_4 e^{4j\omega} + 5j \cdot h_5 e^{5j\omega}$$

using $\quad j^2 = (\sqrt{-1})^2 = -1$

$$H''(\omega) = -h_1 e^{j\omega} - 4h_2 e^{2j\omega} - 9h_3 e^{3j\omega} - 16h_4 e^{4j\omega} - 25h_5 e^{5j\omega}$$

let us evaluate @ $\omega = \pi$

$$\therefore \quad H'(\pi) = 0 = h_1 - 2h_2 + 3h_3 - 4h_4 + 5h_5$$

$$\therefore \quad H''(\pi) = 0 = h_1 - 4h_2 + 9h_3 - 16h_4 + 25h_5$$

Therefore, complete set of design equations is:

$$\boxed{\begin{aligned} & h_0^2 + h_1^2 + h_2^2 + h_3^2 + h_4^2 + h_5^2 = 1 \\ & h_0 h_2 + h_1 h_3 + h_2 h_4 + h_3 h_5 = 0 \\ & h_0 h_4 + h_1 h_5 = 0 \\ & h_0 - h_1 + h_2 - h_3 + h_4 - h_5 \\ & h_1 - 2h_2 + 3h_3 - 4h_4 + 5h_5 \\ & h_1 - 4h_2 + 9h_3 - 16h_4 + 25h_5 \end{aligned}} \qquad \text{(D4)}$$

solving we get Daub-6 coefficients

$$h_0 = \frac{\sqrt{2}}{32}\left(1 + \sqrt{10} + \sqrt{5 + 2\sqrt{10}}\right)$$

$$h_1 = \frac{\sqrt{2}}{32}\left(5 + \sqrt{10} + 3\sqrt{5 + 2\sqrt{10}}\right)$$

$$h_2 = \frac{\sqrt{2}}{32}\left(10 - 2\sqrt{10} + 2\sqrt{5 + 2\sqrt{10}}\right)$$

$$h_3 = \frac{\sqrt{2}}{32}\left(10 - \sqrt{10} - 2\sqrt{5 + 2\sqrt{10}}\right)$$

$$h_4 = \frac{\sqrt{2}}{32}\left(5 + \sqrt{10} - 3\sqrt{5 + 2\sqrt{10}}\right)$$

$$h_5 = \frac{\sqrt{2}}{32}\left(1 + \sqrt{10} + \sqrt{5 + 2\sqrt{10}}\right)$$

and
$$g_k = (-1)^k h_5 - k, k = 0, \cdots 5$$
$$g_0 = h_5 = \frac{\sqrt{2}}{32}\left(1+\sqrt{10}+\sqrt{5+2\sqrt{10}}\right)$$
$$g_1 = -h_4 = -\frac{\sqrt{2}}{32}\left(5+\sqrt{10}-3\sqrt{5+2\sqrt{10}}\right)$$
$$g_2 = h_3 = \frac{\sqrt{2}}{32}\left(10-\sqrt{10}-2\sqrt{5+2\sqrt{10}}\right)$$
$$g_3 = -h2 = -\frac{\sqrt{2}}{32}\left(10-2\sqrt{10}+2\sqrt{5+2\sqrt{10}}\right)$$
$$g_4 = h_1 = \frac{\sqrt{2}}{32}\left(5+\sqrt{10}+3\sqrt{5+2\sqrt{10}}\right)$$
$$g_5 = -h_0 = \frac{\sqrt{2}}{32}\left(1+\sqrt{10}+\sqrt{5+2\sqrt{10}}\right)$$

6.5 | Towards Searching Scaling and Wavelets Coefficients

This complete idea of looking at different members and variants of the family takes us to basic approach which aims at searching for scaling and wavelet coefficients.

In Chapter 2, we laid down a framework of multi resolution analysis which gave us the power to move up or down the ladder as required. This made the entire analysis 'scalable'.

This framework led us to two important questions:

1. How do we go about selecting the mother wavelet and scale of analysis?
2. What is the procedure to calculate scaling and wavelet coefficients?

The first question will get answered subsequently.

Now, let us answer the second question here. We have discussed so far Haar and Daubechies wavelets families. The coefficients of low pass and high pass filters for these are well known. However, where exactly we get these coefficients from? Do we have a concrete procedure for finding them? What properties should the scaling equation obey? These are few questions we would try to answer now.

Quest to find scaling equation coefficients

We are familiar with Haar wavelet and scaling function, which is given as,

$$\psi(t) = \begin{cases} 1 & 0 \le x < \frac{1}{2} \\ -1 & \frac{1}{2} \le x < 1 \\ 0 & \text{otherwise} \end{cases}$$

$$\psi(t) = \begin{cases} 1 & 0 \le x < 1 \\ 0 & \text{otherwise} \end{cases}$$

However, important question is where did the above values come from?

The dilation equation in time domain is given as,

$$\phi(t) = \sum_k h_k \sqrt{2}\phi(2t-k) \tag{6.37}$$

$$\psi(t) = \sum_k g_k \sqrt{2}\phi(2t-k) \tag{6.38}$$

From Eqs. (6.37) and (6.38) we can see that $\phi(t) \in V_0$, $\psi(t) \in W_0$, $\phi(2t-k) \in V_1$ and $\psi(2t-k) \in W_1$. Also we know that, $V_1 = V_0 \oplus W_0$. Thus once we know $\phi(2t-k)$ we can find out $\psi(t)$ and $\phi(t)$, hence focus is on finding out scaling equation coefficients.

Now, in order to achieve this let us go through three guiding theorems.

Theorem I:

For the scaling equation $\phi(t) = \sum_k h_k \sqrt{2}\phi(2t-k)$, with nonvanishing coefficients $\{h_k\}_{k=N}^{M}$ only for $N \le k \le M$ its $\phi(x)$ is with a compact support contained in the interval [N,M].

Theorem II:

If the scaling function $\phi(x)$ has compact support on $0 \le x \le N-1$ and if, $\{\phi(x-k)\}$ are linearly independent, then $h_n = h(n) = 0$, for $n < 0$ and $n > N-1$. Hence, N is the length of the sequence.

Theorem III:

If the scaling coefficients $\{h_k\}$ satisfy the condition for existence and orthogonality of $\phi(t)$, then $\psi(x) = \sum_k \sqrt{2}\phi(2x-t)$

where, $g_k = \pm(-1)^k h_{N-k}$

and $\int_{-\infty}^{\infty} \psi(x-l)\phi(x-k)dx = \delta_{1,k} = 0, l \ne k$

From these theorems, we will try to find out coefficients of scaling equation. To do that following are some properties that scaling coefficients have to obey,

1. $\sum h_k = \sqrt{2}$
2. $\sum h_{2k} = \dfrac{1}{\sqrt{2}}$
3. $\sum h_{2k+1} = \dfrac{1}{\sqrt{2}}$
4. $\sum |h_k|^2 = 1$
5. $\sum h_{k-2l} h_k = \delta_{l,0}$
6. $\sum 2h_{k-2l} h_{k-2j} = \delta_{l,j}$

Where exactly do these properties came from? We would first delve on that and then we would solve one example with case study of Haar $\phi(t)$.

Consider property 1 of $\phi(t)$,

$$\sum_k h_k = \sqrt{2}$$

This property is dependent on the kind of normalization we make use of. Rest of the properties are in fact dependent on this property. So we would first understand from where this property comes from.

We know the dilation equation,

$$\phi(t) = \sum_k h_k \sqrt{2}\phi(2t-k)$$

Integrating both the sides,

$$\int_{-\infty}^{\infty} \phi(t)dt = \sum_k h_k \sqrt{2} \int_{-\infty}^{\infty} \phi(2t-k)dt$$

Put, $$2t - k = x \Rightarrow dt = \frac{dx}{2}$$

$$\int_{-\infty}^{\infty} \phi(t)dt = \sum_k h_k \sqrt{2} \frac{1}{2} \int_{-\infty}^{\infty} \phi(t)dt$$

Let, $\int_{-\infty}^{\infty} \phi(t)dt$, which has normalization 1. Then we are left with,

$$1 = \sum_k h_k \sqrt{2} \frac{1}{2}$$

$$\sum_k h_k = \sqrt{2} \tag{6.39}$$

The point to note is that Eq. (6.39) holds true if we consider the normalization to be 1.

At this point, let us assume that property 5 holds true and we would use it to derive the remaining properties. The property number 5 tells us that,

$$\sum_k h_{k-2l} h_k = \delta_{lo}$$

Replacing l by –l we have,

$$\delta_{-lo} = \sum_{k=-\infty}^{\infty} h_{k+2l} h_k$$

Separating 'even' and 'odd' terms,

$$\delta_{-lo} = \sum_{k=-\infty}^{\infty} h_{2k+2l} h_{2k} + \sum_{k=-\infty}^{\infty} h_{2k+1+2l} h_{2k+1}$$

$$\sum_{l=-\infty}^{\infty} \delta_{-lo} = \sum_{l=-\infty}^{\infty} \sum_{k=-\infty}^{\infty} [h_{2k+2l} h_{2k} + h_{2k+1+2l} h_{2k+1}]$$

However, we know that

$$\sum_{l=-\infty}^{\infty} \delta_{-lo} = 1$$

Thus,

$$1 = \sum_{k=-\infty}^{\infty} h_{2k} [\sum_{l=-\infty}^{\infty} h_{2k+2l}] + \sum_{k=-\infty}^{\infty} h_{2k+1} [\sum_{l=-\infty}^{\infty} h_{2k+1+2l}] \tag{6.40}$$

By substituting $l = l - k$ we can write,

$$\sum_{l=-\infty}^{\infty} h_{2k+2l} = \sum_{l=-\infty}^{\infty} h_{2l} = A \tag{6.41}$$

$$\sum_{l=-\infty}^{\infty} h_{2k+1+2l} = \sum_{l=-\infty}^{\infty} h_{2l+1} = B \tag{6.42}$$

From Eqs. (6.40), (6.41) and (6.42) we can write,

$$1 = AA + BB \tag{6.43}$$

$$1 = A^2 + B^2 \tag{6.44}$$

which clearly represents equation of a circle with radius 1. However, there are two unknowns A and B and we have just one equation. So we need another equation. This equation comes out of the first property, i.e.

$$\sum_k h_k = \sqrt{2}$$

Splitting 'even' and 'odd' terms,

$$\sqrt{2} = \sum_k h_{2k} + \sum_k h_{2k+1}$$

$$\sqrt{2} = A + B \tag{6.45}$$

At this point we have an interesting situation, i.e. Eq. (6.44) represents a circle and Eq. (6.45) a line. The situation is as shown in Fig. 6.2.

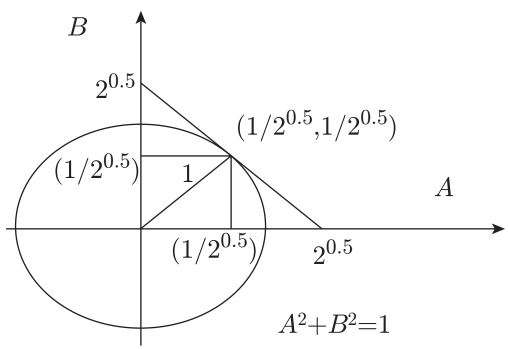

Figure 6.2 | *Scaling function and wavelet function of Daub-4*

Hence from the figure we have,

$$A = \frac{1}{\sqrt{2}}$$

$$B = \frac{1}{\sqrt{2}}$$

Thus by substituting A we have,

$$\sum_k h_{2k} = \frac{1}{\sqrt{2}} \tag{6.46}$$

which gives us property number 2. Also, substituting the value of B we have,

$$\sum_k h_{2k+1} = \frac{1}{\sqrt{2}} \tag{6.47}$$

which gives property number 3.

Now, consider property number 4 we have,

$$\sum_k |h_k|^2 = \sum_k h_k^2 = 1 \tag{6.48}$$

Now let us verify these properties in case of Haar scaling function. We know that in case of Haar $\phi(t)$,

$$h_0 = h_1 = \frac{1}{\sqrt{2}}$$

Putting these values in property 1 we have,

$$\sum_0^1 h_k = h_0 + h_1 = \sqrt{2}$$

Thus property 1 is obeyed.

Similarly, for property 2, 3 and 4,

$$\sum_k h_{2k} = h_0 = \frac{1}{\sqrt{2}}$$

$$\sum_k h_{2k+1} = h_1 = \frac{1}{\sqrt{2}}$$

$$\{\sum_k h_{2k}\}^2 + \{\sum_k h_{2k+1}\}^2 = h_0^2 + h_1^2 = 1$$

Hence, we can clearly see that these properties are obeyed. For property number 5 we have,

$$\sum_k h_{k-2l} h_k = \delta_{0,l}$$

We have only two indices, i.e. 0,1. Let us take the first case,

Case (i)

$$k - 2l = 0 \text{ or } k = 2l$$

if $l \neq 0$, then $k = 2l \geq 2$. Thus sum vanishes unless $l = 0$ and in that case $k = 0$.

Thus we can write,

$$\sum_k h_k - 0h_k = h_0 h_0 = \frac{1}{2} \tag{6.49}$$

Also when $k = 0$, $h_{k-2l} = h_{0-2l}$, which is 0 unless $l = 0$. Thus,

$$\sum_k h_k h_k = h_0^2 = \frac{1}{2} \tag{6.50}$$

From Eqs. (6.49) and (6.50) we can see that the property 5 is obeyed since their results add up to give 1.

Case (ii)

$$k-2l=1,\ k=2l+1$$

if $l \neq 0$, $k \geq 3$. Thus l has to be 0 and $k=1$. Hence we have,

$$\sum_k h_k h_k = h_1^2 = \frac{1}{2} \tag{6.51}$$

Now for $k=1$, $l=0$ hence,

$$\sum_k h_k - 0h_k = h_1 h_1 = \frac{1}{2} \tag{6.52}$$

Similar to case (i), Eqs. (6.51) and (6.52) add up to give 1, hence for case (ii) also property 5 is obeyed. It is important to note that the property 5 gives us idea about the orthogonality and not all the functions obey this property.

Hence, the Haar scaling coefficients obey all these different properties. Also once we find out these scaling coefficients we can find out coefficients of wavelet equation as follows,

$$g_k = (-1)^k h_N - k$$

For $N = 1$ we have,

$$g_k = (-1)^k h_1 - k$$

For $k=0$,

$$g_0 = (-1)^0 h_1 = h_1 = \frac{1}{\sqrt{2}}$$

For $k=1$,

$$g_1 = (-1)^1 h_0 = -h_0 = \frac{-1}{\sqrt{2}}$$

This is how we can find out coefficients of scaling and wavelet equation.

Exercises

Exercise 6.1

What is the condition for a system function to be Minimum Phase System?
Hint: A system function $H(z)$ is said to be a minimum phase if all of its poles and zeros are within the unit circle. Minimum Phase System have property that the system function and its inverse are causal and stable.

Exercise 6.2

Prove that autocorrelation of sequence $h[n]$ has a z-transform of $H(z)H(z^{-1})$.

Hint: Autocorrelation of $h[n]$ is defined as,

$$r_{hh}(l) = \sum_{n=-\infty}^{n=+\infty} h[n]h[n-l] \tag{6.53}$$

Now, put $n-l=-k$ in Eq. (6.53), we get

$$r_{hh}(l)=\sum_{k=-\infty}^{k=+\infty}h[-k+l]h[-k]$$

$$r_{hh}(l)=\sum_{k=-\infty}^{k=+\infty}h[-k]h[l-k] \tag{6.54}$$

RHS of above Eq. (6.54) can be written as convolution from given as follows,

$$h(l)\times h(-l)=\sum_{k=-\infty}^{k=+\infty}h[-k]h[l-k] \tag{6.55}$$

Replacing variable l by n, we can write Eq. (6.55) as follows:

$$h(n)\times h(-n)=\sum_{k=-\infty}^{k=+\infty}h[-k]h[n-k] \tag{6.56}$$

So, from Eqs. (6.53), (6.54) and (6.56), we can say that,

$$r_{hh}(l)=h(n)\times h(-n) \tag{6.57}$$

Now for calculating Z-transform of autocorrelation function. Let z-transform of $h[n]$,

$$h[n]\leftrightarrow H(z) \tag{6.58}$$

So by using property of Z-transforms, Z-transform of $h[-n]$,

$$h[-n]\leftrightarrow H(z^{-1}) \tag{6.59}$$

Also convolution property of Z-transform that is

$$x_1[n]\times x_2[n]\leftrightarrow X_1(z)X_2(z) \tag{6.60}$$

Now taking the Z-transform of Eq. (6.57), and using properties given in Eqs (6.58), (6.59) and (6.60), we can write Z-transform of autocorrelation function,

$$R_{hh}(z)=H(z)H(z^{-1}) \tag{6.61}$$

So, Eq. (6.61) gives the Z-transform of autocorrelation function.

Exercise 6.3

Why are the Daub series analysis LPF impulse responses orthogonal to its even shifted versions?

Hint: The basic equation for designing the analysis side LPF is,

$$\kappa_0(z) + \kappa_0(-z) = C \tag{6.62}$$

where,

$$\kappa_0(z) = H_0(z)H_0(z^{-1}) \tag{6.63}$$

C is constant here. Taking inverse Z-transform of Eq. (6.63), we get,

$$\kappa_0(n) = R(n) \tag{6.64}$$

where $\kappa_0(n)$ is the Z-transform of $\kappa_0(z)$ and $R(n)$ is the autocorrelation of the impulse response of $H_0(z)$. So taking the inverse Z-transform on both sides of Eq. (6.62), we get

$$R(n) + (-1)^n R(n) = C\delta(n) \tag{6.65}$$

This equation implies only for n even, $(n \neq 0)$

$$2R(n) = 0$$

$$R(n) = 0$$

Now $R(n)$ is the dot product of the impulse response of the analysis LPF with its shifted version. So, for even n, $R(n) = 0$ implies that the dot product of the impulse response of the analysis LPF with its even shifted version is zero, i.e. impulse responses of these filters are orthogonal to its even shifted versions.

Exercise 6.4

Why are the Daub series analysis LPF impulse response has even length?

Hint: Let a Daub analysis LPF is of odd length 5. So the impulse response is,

$$h[n] = [h_0\ h_1\ \underset{\uparrow}{h_2}\ h_3\ h_4\ h_5]$$

$$h[n-4] = [\ldots\ldots\ldots\ldots\ldots.h_0\ h_1\ \underset{\uparrow_{n=4}}{h_2}\ h_3\ h_4\ h_5]$$

Now, the dot product of $h[n]$ and $h[n-4]$ should be 0 because of the orthogonality with respect to even shift. For this to be true, $h_0 h_4 = 0$, which means either h_0 or h_4 is zero which effectively means that the filter length is even and our initial assumption was wrong.

Exercise 6.5

Plot the scaling function and wavelet function for Daub-4 MRA.
Low pass filter impulse response:

$$h_0 = 0.4829, h_1 = 0.8364, h_2 = 0.2241, h_3 = 0.129$$

High pass filter impulse response:

$$g_0 = 0.129, g_1 = 0.2241, g_2 = 0.8364, g_3 = 0.4829$$

Hint: Use MATLAB program to generate the plots of scaling function and wavelet function.

Chapter 7

Time-Frequency Joint Perspective

7.1 | Introduction

In Chapter 6 we studied steps required to design conjugate quadrature filter-banks. We set out with the aim to achieve systematic design steps for building higher-order filter banks and learn relationships between analysis and synthesis filters subject to alias cancellation and perfect reconstruction conditions. Such analysis also enabled us to design higher and higher order filters of Daubechies family by incorporating more $(1+z^{-1})$ terms in analysis of low pass filter transfer function for achieving regularity required for convergence.

Till this point, our analysis of scaling and wavelet functions has been either in time domain or in transform domain. However, several tasks require localization in both time and transform domain simultaneously. Wavelet transforms arrive from family of transforms, which provide simultaneous localization known as multi-resolution analysis of the underlying signal. In this chapter, we analyze Haar scaling and wavelet functions for time and frequency localization. We analyze their frequency domain behaviors over the containment ladder. This analysis gives us a reason to move towards ideal aspirations for scaling and wavelet transforms and in turn towards the basic question of bound over simultaneous localization in time and frequency domain also known as the 'uncertainty principle'.

7.2 | Analysis of Haar Scaling Function in Time and Frequency Domain

Consider Haar scaling function as shown in Fig. 7.1.

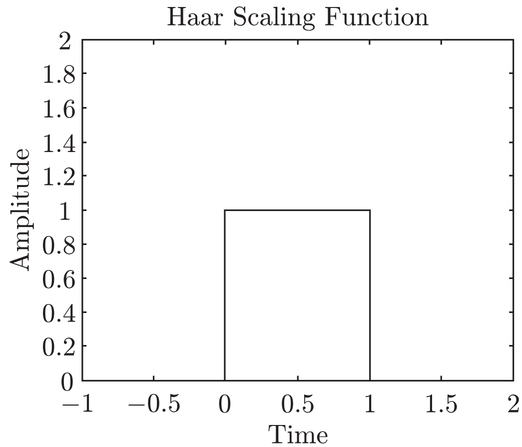

Figure 7.1 | *Haar scaling function*

If we denote Ω as analog angular frequency variable and $\hat{\phi}(\Omega)$ as Fourier transform of scaling function then Fourier transform can be carried out in the following way:

$$\hat{\phi}(\Omega) = \int_{-\infty}^{+\infty} \phi(t) e^{-j\Omega t}\, dt$$

$$\hat{\phi}(\Omega) = \frac{1 - e^{-j\Omega}}{j\Omega}$$

$$\hat{\phi}(\Omega) = e^{\frac{-j\Omega}{2}} \left[\frac{\sin\left(\frac{\Omega}{2}\right)}{\left(\frac{\Omega}{2}\right)} \right]$$

Magnitude for this scaling function is shown in Fig. 7.2. The above analysis of scaling function is applicable to subspace V_0 which is a subspace having piecewise constant approximation over standard unit interval]n, n+1[. Consider a ladder of subspace $\ldots \subset V_{-2} \subset V_{-1} \subset V_0 \subset V_1 \subset V_2 \ldots$. By the scaling property of Fourier transform we have,

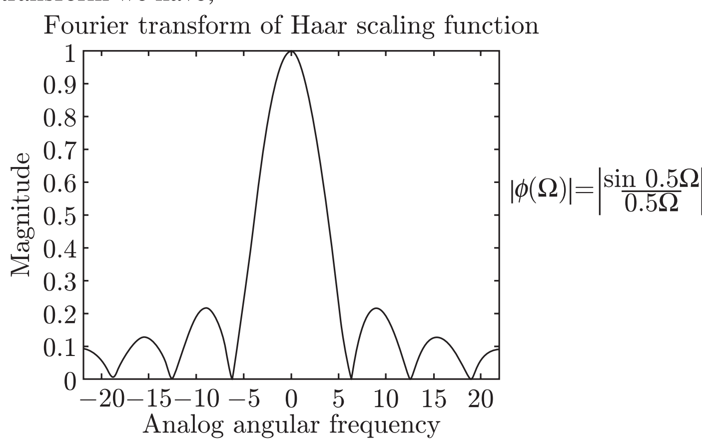

Figure 7.2 | *Magnitude of Fourier transform for haar scaling function*

$$\phi(t) \overset{F.T.}{\leftrightarrow} \hat{\phi}(\Omega)$$

$$\phi(\alpha t) \overset{F.T.}{\leftrightarrow} \frac{1}{|\alpha|}\hat{\phi}\left(\frac{\Omega}{\alpha}\right); \quad \forall \quad \alpha \in \mathbb{R}-\{0\}$$

As translation only affects phase in frequency domain, we consider scaling function without translation in time domain without loss of generality (as our analysis is limited to magnitude only). In this case, above relationship may be represented in the following manner.

$$\phi(t) \overset{F.T.}{\leftrightarrow} |\hat{\phi}(\Omega)|$$

$$\phi(2^m t) \overset{F.T.}{\leftrightarrow} |\frac{1}{|2^m|}\hat{\phi}(\frac{\Omega}{2^m})|$$

Using this relationship, scaling function in time and frequency domain across various subspaces may be sketched as shown in Fig. 7.3.

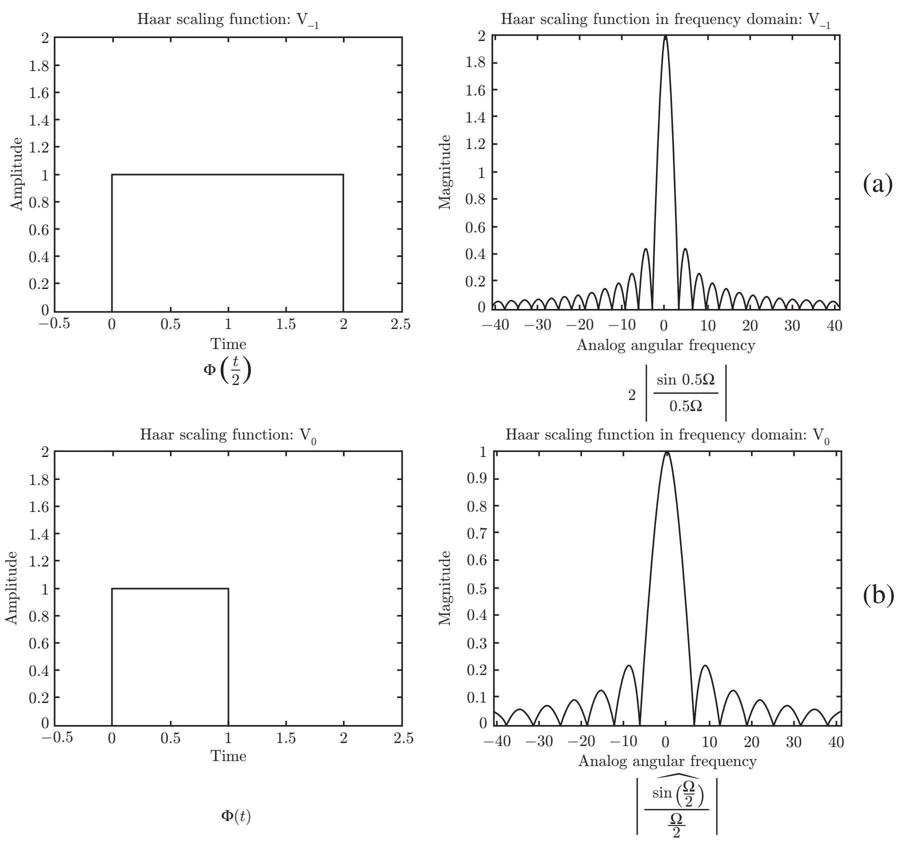

Figure 7.3 | *(Continued)*

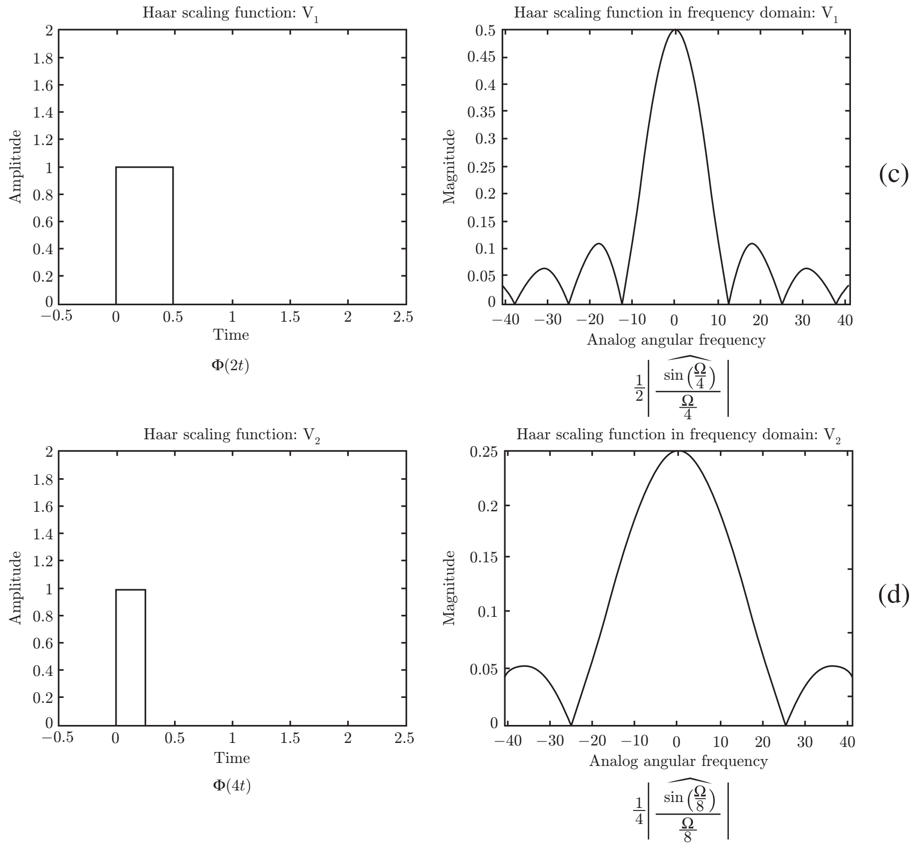

Figure 7.3 | *Haar scaling function at various time and frequency resolutions. Scaling function and frequency domain characteristic in 3(a): V_{-1} subspace, 3(b): V_0 subspace, 3(c): V_1 subspace and 3(d): V_2 subspace. [Note how localization varies across different subspaces starting from coarse subspace V_{-1}.]*

As evident from Fig. 7.3, as we go from subspace V_{-1} towards V_2, subspace localization in time improves by factor of two, i.e. in V_0 subspace scaling function lies in [0 1] interval (nonzero values), whereas in V_1 subspace, scaling function lies in [0 0.5] interval. In this sense, we may say that time localization gets better and better as we move from $V_{-\infty}$ to $V_{+\infty}$. Similarly, localization in frequency gets poorer by factor of two as we go from subspace V_{-1} to V_2, i.e. width of main lobe doubles each time we move to higher subspace. Hence, frequency localization gets poorer as we move from $V_{-\infty}$ to $V_{+\infty}$. This localization affects projection of some signal $x(t) \in L_2(\mathbb{R})$ on various subspaces.

Example 7.2.1 — Orthonormal basis.

For orthonormal basis at some subspace V_m,

$$\left\langle \phi(2^m t - n), \phi(2^m t - l) \right\rangle$$

where, $< a,b >$ represents dot product between functions a and b. As mentioned, when $n \neq l$, scaling functions do not overlap with each other and hence yield zero dot product. We shall now check what happens when $n = l$. Norm of the scaling function is

$$\left\|\phi(2^m \cdot)\right\|_2^2 = \int_0^{2^{-m}} (1)^2\, dt = 2^{-m}$$

where, $\|\cdot\|_2^2$ represents square of L_2 norm and '$\cdot$' represents corresponding argument. Here, argument is used to denote that this relationship is true for any valid translation.
Using *orthonormal* bases we can write

$$V_m = \text{span}\{2^{\frac{m}{2}}\phi(2^m t - n)\} \quad \forall \quad n,m \in \mathbb{Z}$$

Projection of signal $x(t)$ over this subspace may be denoted as $\left\langle x(\cdot), 2^{\frac{m}{2}}\phi(2^m \cdot - n)\right\rangle$.

For understanding relationship between dot product in time and frequency domain we shall interpret what happens when we take Fourier transform and inverse Fourier transform.

If, $x(t) \leftrightarrow \hat{x}(\Omega)$ then $\hat{x}(\Omega) = \int_{-\infty}^{+\infty} x(t)e^{-j\Omega t}dt$. During this process, we take components of $x(t)$ along directions provided by complex exponentials $e^{-j\Omega t}$. Also, inverse Fourier transform gives $x(t)$ back from $\frac{1}{2\pi}\int_{-\infty}^{+\infty}\hat{x}(\Omega)e^{j\Omega t}d\Omega$, which may be interpreted as reconstruction of $x(t)$ from components along $e^{j\Omega t}$.

R Now, from Parseval's theorem:

$$\langle x(t), y(t)\rangle = \langle \hat{x}(\Omega), \hat{y}(\Omega)\rangle$$

i.e. dot product is independent of basis we select and is equal in time and angular frequency domain within a factor of 2π. Using this relationship we may denote the relationship between projection of function $x(t)$ over subspace V_m in the following manner:

$$\left\langle x(t), 2^{\frac{m}{2}}\phi(2^m \cdot - n)\right\rangle = \frac{1}{2\pi}\left\langle \hat{x}(\Omega), 2^{\frac{m}{2}}\widehat{\phi(2^m \cdot - n)}\right\rangle$$

In Fig. 7.4, solid line shows Fourier transform of Haar scaling function and dotted line shows Fourier transform of signal under consideration, namely $x(t)$. Contribution of side lobes towards overall dot product is unsubstantial compared to contribution from main lobe. In other words, frequencies of $x(t)$ inside main lobe of fourier transform of scaling function are emphasized with respect to frequencies outside the main lobe. As we move across the subspace ladder different amount of frequencies are emphasized. To be more precise, as we go from $V_{-\infty}$ to $V_{+\infty}$, more and more frequencies are emphasized as peak always remains on zero frequency.

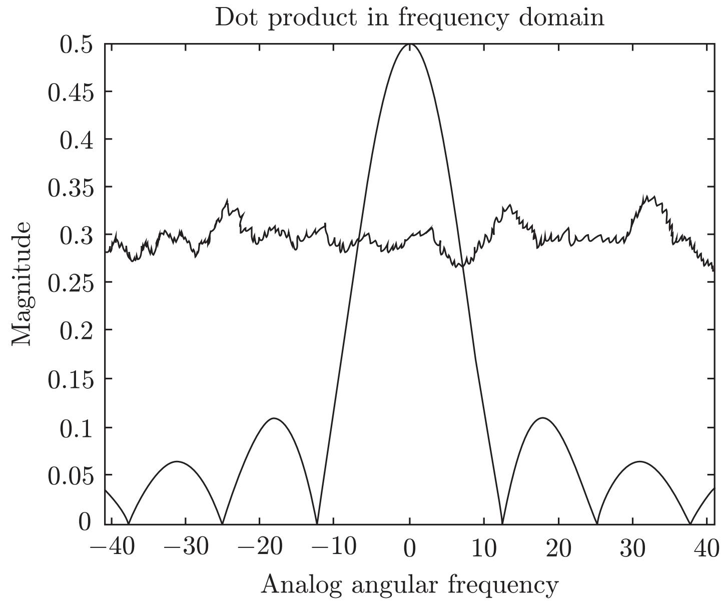

Figure 7.4 | *Pictorial representation of dot product in frequency domain of a signal $x(t)$ with haar scaling function in some subspace*

7.3 | Analysis of Haar Wavelet Function in Time and Frequency Domain

Haar wavelet function is shown in Fig. 7.5. Haar wavelet may also be represented in $\psi(t) = \phi(2t) - \phi(2t-1)$. Fourier transform of Haar wavelet function is

$$\phi(t) \overset{F.T.}{\leftrightarrow} \hat{\phi}(\Omega)$$

$$\phi(2t) \overset{F.T.}{\leftrightarrow} \frac{1}{2}\hat{\phi}\left(\frac{\Omega}{2}\right)$$

$$\phi(2t-1) \overset{F.T.}{\leftrightarrow} \frac{1}{2}e^{\frac{-j\Omega}{2}}\hat{\phi}\left(\frac{\Omega}{2}\right)$$

Using these relationships, we get

$$\psi(t) = \phi(2t) - \phi(2t-1)$$

$$\hat{\psi}(\Omega) = \frac{1}{2}\hat{\phi}\left(\frac{\Omega}{2}\right) - \frac{1}{2}e^{\frac{-j\Omega}{2}}\hat{\phi}\left(\frac{\Omega}{2}\right)$$

$$\hat{\psi}(\Omega) = \frac{1}{2}\left(1 - e^{\frac{-j\Omega}{2}}\right)\hat{\phi}\left(\frac{\Omega}{2}\right)$$

$$\hat{\psi}(\Omega) = 2je^{\frac{-j\Omega}{2}} \frac{\sin^2\left(\frac{\Omega}{4}\right)}{\left(\frac{\Omega}{4}\right)}$$

$$|\hat{\psi}(\Omega)| = \left| 2\frac{\sin^2\left(\frac{\Omega}{4}\right)}{\frac{\Omega}{4}} \right|$$

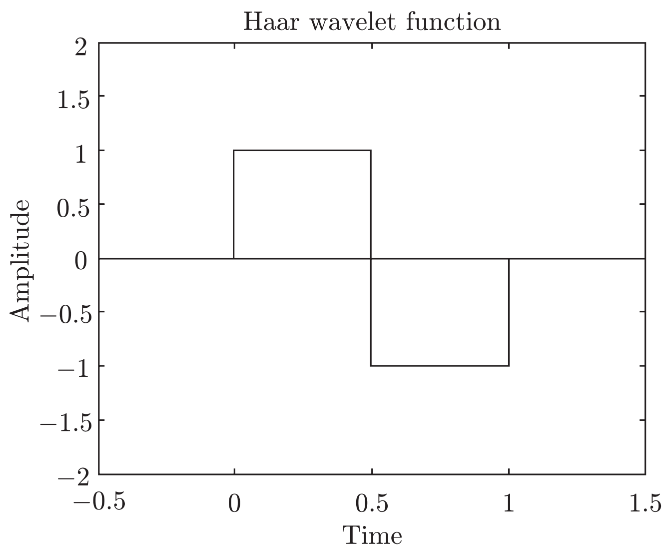

Figure 7.5 | *Haar wavelet function in time domain*

Using this relationship we may plot Haar wavelet function across various subspaces. Figure 7.6 shows Haar wavelet in subspaces W_{-1} to W_2.

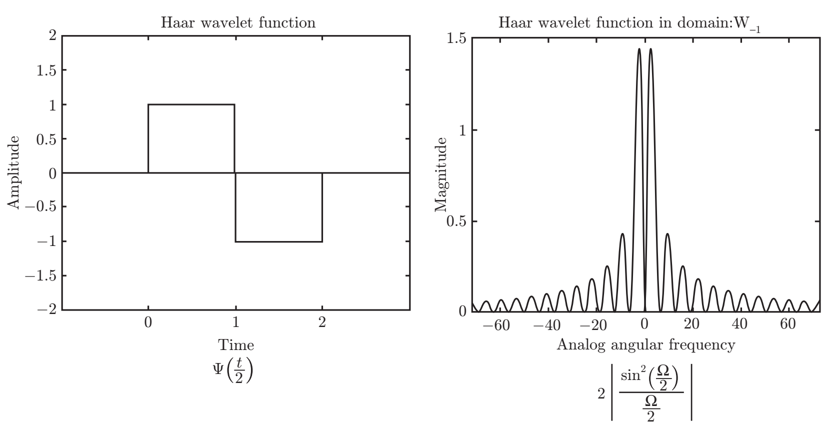

Figure 7.6

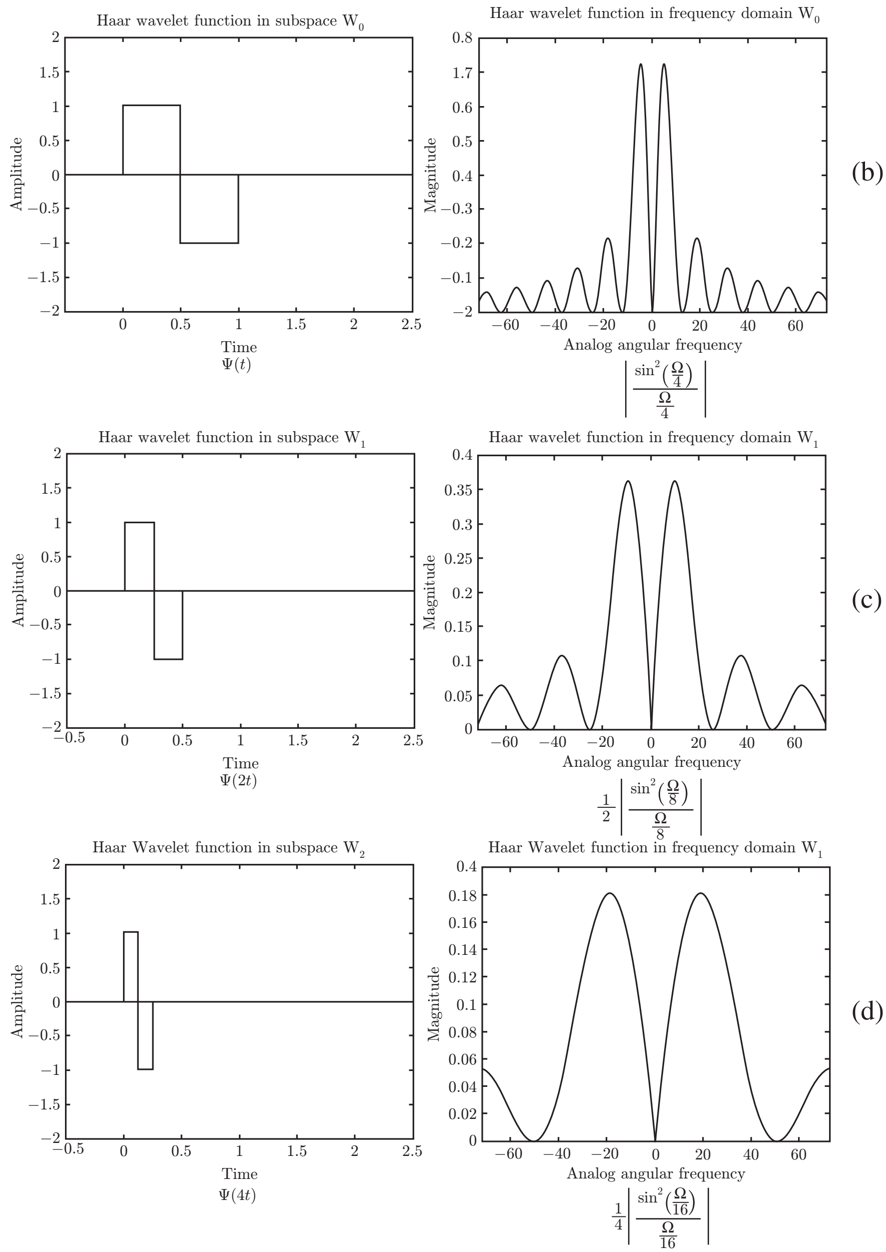

Figure 7.6 | *Haar wavelet function at various time and frequency resolutions. Wavelet function and frequency domain characteristic in 6(a): W_{-1} subspace; 6(b): W_0 subspace; 6(c): W_1 subspace and 6(d): W_2 subspace.*

As in the case of Haar scaling function, here also localization in time improves as we move from W_{-1} to W_2 by factor of two. Similarly, localization in frequency degrades as we go in similar direction by factor of two. However, important thing to note here is along with the bandwidth, centre frequency also shifts, unlike in the case of Haar scaling function. Here different bands with increasing bandwidth are emphasized as we go from $W_{-\infty}$ to $W_{+\infty}$. This characteristic of Haar wavelet function is similar to aspirant band pass filter. Again, similar notion of time and frequency localization applies here as in case of Haar scaling function, namely, localization in time gets better and localization in frequency gets poorer as we go from $W_{-\infty}$ to $W_{+\infty}$.

7.4 | Summary

In this section we analyzed Haar scaling and wavelet functions in detail. Rather than analyzing functions in either time domain or in frequency domain, we consider them in joint domain, i.e. time and frequency domains simultaneously. Analysis reveals that time and frequency domain localization improves and deteriorates respectively as we go from left to right in subspace ladder and vice versa. Also, Haar scaling function aspires to become low pass filter and wavelet function aspires to be band pass filter. Through this analysis we may consider ideal frequency responses of scaling and wavelet functions, which may improve overall response and projections over approximation and detail subspaces (V and W subspaces respectively). Such findings allow us to consider fundamental question of bound over simultaneous localization in time and frequency domain, namely the 'uncertainty principle'.

7.5 | Ideal Time-Frequency Behaviour

In earlier sections we have looked at the Fourier Transform of the scaling function (Father wavelet) $\phi(t)$ and the wavelet function (Mother wavelet) $\psi(t)$ in the Haar Multiresolution Analysis. In next few sections we will see, what is the ideal situation that we are driving towards. We have made some observations about the nature of the magnitude of $\hat{\phi}(\Omega)$ and $\hat{\psi}(\Omega)$. When we take dot product of $x(t)\sqrt{b^2-4ac}$ and a translate of $\phi(t)$, the magnitudes of the Fourier Transforms of $x(\cdot)$ and $\phi(\cdot)$ are getting multiplied. When we cascade two Haar scaling functions it results into Triangular wave function as depicted in Figure 7.7. We have observed that the nature of the Fourier Transform of the $\phi(\cdot)$ and also that of $\psi(\cdot)$ was such that it emphasizes some bands of frequencies of the underlying function $x(t)$.

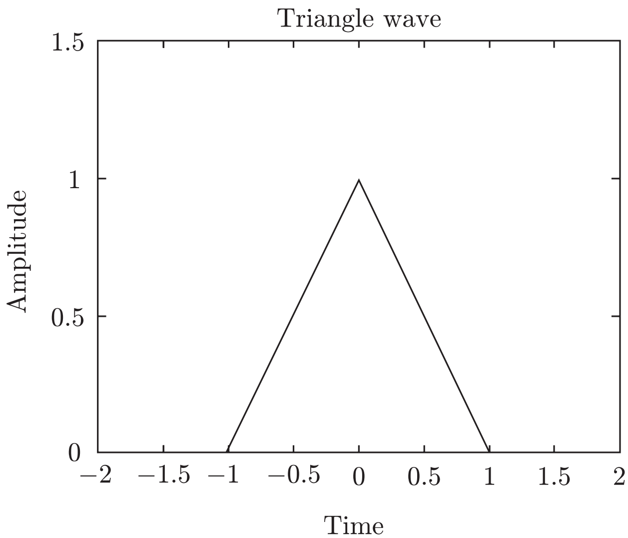

$$x(t) = 1 + t\,; \quad -1 < t < 0$$
$$\quad\;\; = 1 - t\,; \quad 0 < t < 1$$
$$\quad\;\; = 0; \quad \text{otherwise}$$

Figure 7.7 | *Triangular wave in time domain*

7.6 | Frequency Localization by $\phi(t)$ and $\Psi(t)$

The magnitude of Fourier Transform of $\phi(t)$ is shown in Fig. 7.8.

Magnitude of Fourier Transform of $\psi(t)$ is

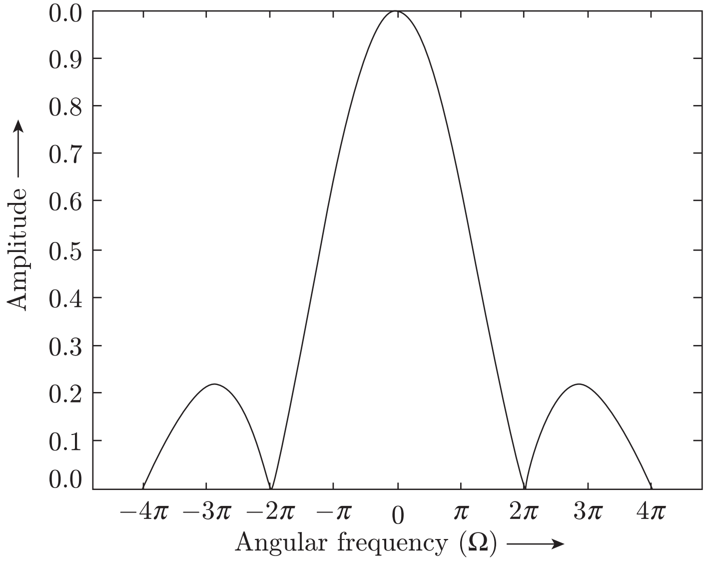

Figure 7.8 | *Magnitude of Fourier transform of* $\phi(t)$

$$|\hat{\psi}(\Omega)| = \frac{\sin^2\left(\frac{\Omega}{4}\right)}{\left(\frac{\Omega}{4}\right)}$$

To sketch its waveform, we first sketch $\dfrac{\sin\left(\frac{\Omega}{4}\right)}{\left(\frac{\Omega}{4}\right)}$ and $\sin\left(\frac{\Omega}{4}\right)$ and then we shall multiply these two waveforms. Function $\left|\sin\left(\frac{\Omega}{4}\right)\right|$ has a monotonically increasing characteristics between 0 and 2π and decreasing characteristics between 2π and 4π. So one cannot possibly have a value of the product of $\left|\sin\left(\frac{\Omega}{4}\right)\right|$ and $\dfrac{\sin\left(\frac{\Omega}{4}\right)}{\left(\frac{\Omega}{4}\right)}$ higher in the range 2π to 4π than the value of it at 2π. The product is zero at $\Omega = 0$ and what is after 2π is less than what is at 2π. So, somewhere in between 0 to 2π that product is having maximum and after that the product monotonically decreases. Also the function is not symmetric in the range 4π to 8π around 6π. So the maximum of the product in 4π to 8π is not at 6π, but somewhere around 6π. Finally, the product would look like, as shown in Fig. 7.9. In range -4π to 4π, $\hat{\phi}(\Omega)$ and $\hat{\psi}(\Omega)$ look like as shown in Fig. 7.10.

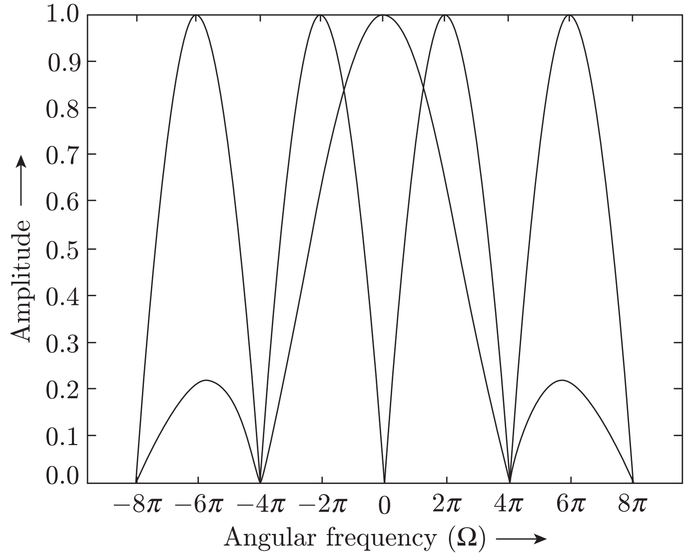

Figure 7.9 | *Magnitude plots of* $\dfrac{\sin\left(\frac{\Omega}{4}\right)}{\left(\frac{\Omega}{4}\right)}$ *(black) and* $\sin\left(\frac{\Omega}{4}\right)$ *(grey)*

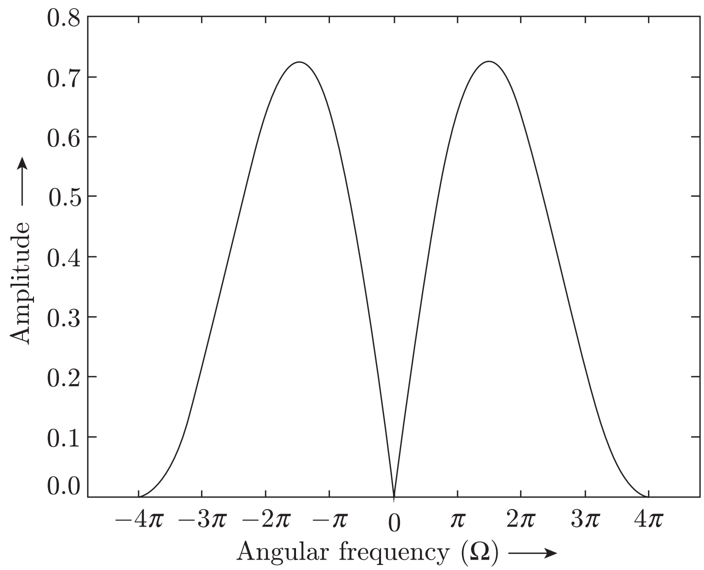

Figure 7.10 | *Magnitude plot of* $\dfrac{\sin^2\left(\frac{\Omega}{4}\right)}{\left(\frac{\Omega}{4}\right)}$

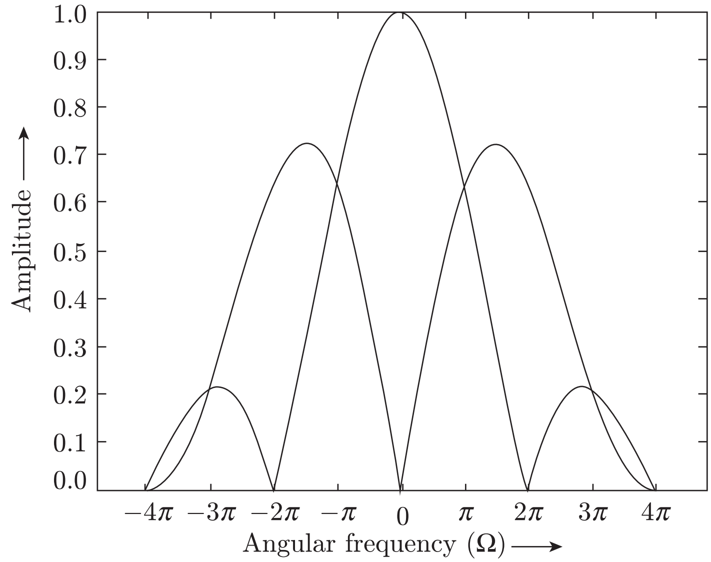

Figure 7.11 | *Magnitude of Fourier Transforms of* $\hat{\phi}(\Omega)$ *(grey) and* $\hat{\psi}(\Omega)$ *(black) in the range* -4π *to* 4π

From Fig. 7.10, it is observed that $\hat{\phi}(\Omega)$ and $\hat{\psi}(\Omega)$ emphasizes those frequencies lying around zero and those frequencies lying around its maximum in the band 0 to 4π respectively and de-emphasizes frequencies on either sides. It is clear that $\hat{\psi}(\Omega)$ has a bandpass characteristic and hence acts as a bandpass function. Magnitude of Fourier Transforms of scaling and wavelet function is as shown in Fig. 7.11. A bandpass function emphasizes frequencies somewhere around its centre frequency, where its value is maximum and de-emphasizes both sides around zero and around infinity. We note that when we contract scaling or wavelet function in time, we go up the ladder in Haar MRA and when we expand, we go down the ladder. Thus, when we go up the ladder, we are expanding in frequency domain and contracting in time domain. And when we go down the ladder, we are expanding in time and, therefore, contracting in frequency.

Example 7.6.1 — Quality factor.

When we go down the ladder, we are contracting in frequency and we are emphasizing smaller and smaller frequency band around zero and also, as we are contracting $\hat{\psi}(\cdot)$, we are emphasizing frequencies around smaller and smaller centre frequency. The centre frequency of $\hat{\psi}(\cdot)$ decreases geometrically or logarithmically as we go down the ladder in the Haar MRA and width of the band of $\hat{\psi}(\cdot)$ also decreases geometrically or logarithmically. Here the ratio of bandwidth to centre frequency remains constant. We call this as constant quality factor. For a bandpass filter or bandpass function the quality factor can be defined as

$$\text{Quality Factor} = \frac{\text{centre frequency}}{\text{bandwidth}}$$

Typically, the term bandwidth is used to denote that range of frequencies within which the magnitude remains within a certain percentage of maximum magnitude. More specifically, we often use half power bandwidth, where the magnitude falls to $\frac{1}{\sqrt{2}}$ of its maximum value, is considered as the cut-off point of that signal. The ratio $\frac{1}{\sqrt{2}}$ has a significance, at that point, where magnitude is $\frac{1}{\sqrt{2}}$ of maximum, power of a sine wave falls to $\frac{1}{2}$ of the maximum value.

R Therefore two important observations can be made

- The ratio of bandwidth to centre frequency of $|\hat{\psi}(\cdot)|$ remains constant.
- As we go up the ladder of MRA, we deal with $|\hat{\psi}(\cdot)|$ having higher centre frequency and larger bandwidth. Similarly, as we go down the ladder, $|\hat{\psi}(\cdot)|$ possesses lower centre frequency and smaller bandwidth.

7.7 | Time Localization and Frequency Localization

Now, we use bandwidth as a measure of the range of frequencies that are emphasized by the function. This is because in finding dot product of $x(t)$ with and translate of $\psi(t)$ or any stretched or compressed version of it, Parseval's theorem says that we are, in fact multiplying Fourier transform of $x(t)$ and Fourier Transform of particular translate or dilate of $\psi(t)$ in frequency domain. The same argument is valid for $\phi(t)$ also.

Now, the translate does not have any effect on magnitude, but dilate does. Thus, when we take dot product of $\psi(t)$ and $x(t)$, we are multiplying the part of $|\hat{x}(\Omega)|$ which lies within the band, by a larger number and other parts by a smaller number. So in effect a filtering effect is also being observed. Effectively $\phi(t)$ is doing a low pass filtering operation and $\psi(t)$ is doing a bandpass filtering operation.

If we take $\phi(\cdot)$ itself and we focus on main lobe of Fourier Transform then, we are emphasizing on signals ranging between $0-2\pi$, and we are doing it by an operation in time domain. $\phi(\cdot)$ and $\psi(\cdot)$ are very precisely localized in time. So the product of $\phi(\cdot)$ and $\psi(\cdot)$ or any of their dilate or translate with $x(t)$ is also localized in time.

In signal processing, we observe conflict between time and frequency. In this case, time localization is precise, but localization in frequency is somewhat suspended. We can roughly say that (focusing on the main lobe) these are in some sense localized. But there are side lobes also.

Ideally, we would like to have precise time as well as frequency localization simultaneously. Now lets consider the dot product of $x(\cdot)$ with particular integer translates of $\phi(\cdot)$ as a sampling problem

So the product is (assuming both functions are real):

$$\int_{-\infty}^{\infty} x(t)\phi(t+\tau)dt$$

From Parseval's theorem

$$\int_{-\infty}^{\infty} x(t)\phi(t+\tau)dt = \frac{1}{2\pi}\int_{-\infty}^{\infty} \hat{x}(\Omega)\widehat{\phi(t+\tau)}d\Omega$$

$$\int_{-\infty}^{\infty} x(t)\phi(t+\tau)dt = \frac{1}{2\pi}\int_{-\infty}^{\infty} \hat{x}(\Omega)\hat{\phi}(\Omega)e^{j\Omega\tau}d\Omega$$

This is the inverse Fourier Transform of $\hat{x}(\Omega)\hat{\phi}(\Omega)$ at the point τ .

So when we multiply by $\hat{\phi}(\Omega)$, we are in effect doing some kind of low-pass filtering operation and when we take Inverse Fourier Transform, we are taking what comes out of the crude low-pass filter whose impulse response is very closely related to $\phi(t)$.

Now, we sample this, at $\tau = n$ where $n \in \mathbb{Z}$. i.e., if we take a function $y(t)$ and sample it ideally for $n \in \mathbb{Z}$, its fourier transform would look like

$$C_0 \sum_{k\in\mathbb{Z}} \hat{y}(\Omega + 2\pi k)$$

C_0 is a constant which relates to the sampling process. We can ignore this constant for this moment. So, in order to reconstruct $y(t)$ from its samples these translates must not interfere with the original. So, we have to ensure that these $\hat{y}(\Omega + 2\pi k)$ are nonoverlapping with the original and that is ensured by ensuring that the low pass filter cuts off at $\Omega = \pi$. Had $\hat{\phi}(\Omega)$ been an ideal low pass function with a cut off of π, then this 'aliasing' $C_0 \sum_{k\in\mathbb{Z}} \hat{y}(\Omega + 2\pi k)$ would leave $\hat{y}(\Omega)$ unaffected. This is the ideal situation we are looking for.

Now, we need to look at what is the ideal towards which we are driving, as far as $\psi(t)$ goes. When we go from V_0 to V_1, we have noted that V_1 is just like V_0, but compressed by a factor of 2 in time and, therefore, expanded by a factor of 2 in frequency domain. So for V_1 (Haar MRA ladder), we expanded by two 2 in frequency, that means we are asking for a low pass filter whose cut off is 2π, instead of π. Now we have interpretation for incremented subspace. Obviously, V_0 is going to contain information between 0 and π and V_1 between 0 and 2π. Then W_0 will contain information between π and 2π. This is shown in Fig. 7.12.

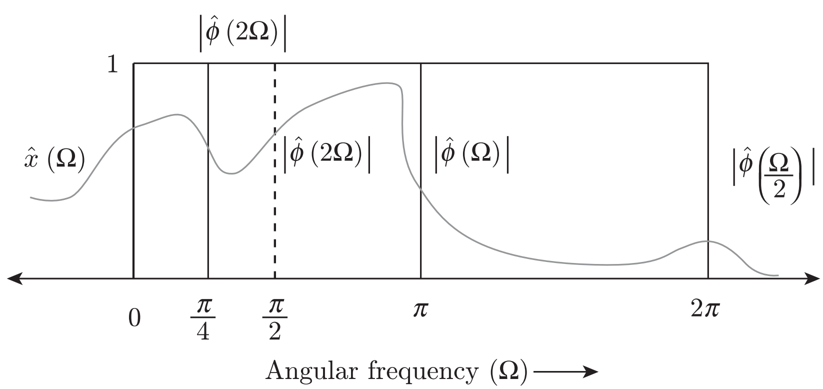

Figure 7.12 | $\phi(\cdot)$ *aspires to become low pass function. Ideally, information captured by it in different subspaces* V_{-1}*(dotted line),* V_0*(black) and* V_1*(solid grey)*

So $\psi(\cdot)$ is aspiring to be a bandpass function between π and 2π. Similarly, while going V_{-1} to V_0, we use corresponding dilate of $\psi(\cdot)$ that aspires to be a bandpass function between $\frac{\pi}{2}$ and π and when we go from V_1 to V_2, we use dilate of $\psi(\cdot)$ that aspires to be a bandpass function between 2π and 4π, and so on. This is illustrated in Fig. 7.13. Now, we want to confine ourselves in a certain region of time and also want to focus or confine on a particular region of frequency. The first question that arises is, whether it is possible or not. Can we be compactly supported in time and frequency simultaneously? The answer is no. We cannot be compactly supported in both the domains(time and frequency).

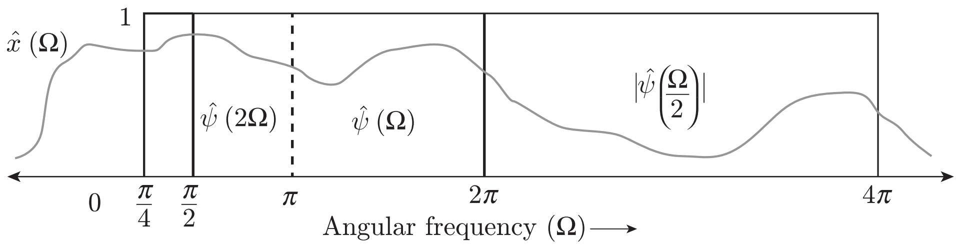

Figure 7.13 | $\psi(\cdot)$ *aspires to become band pass function. Ideally, information captured by it in different subspaces* W_{-1} *(dotted line),* W_0 *(black) and* W_1 *(solid grey)*

However, if we do not ask for compact support in both domains, it is possible to have a function most of whose energy is contained in the finite interval over time as well as frequency. Such functions can be said to have a compact support in a weaker sense. $\phi(\cdot)$ and $\psi(\cdot)$ are bounded in both domains in a weaker sense as we focus on main lobe. Main lobe has certain amount of energy. Then $\phi(\cdot)$ and $\psi(\cdot)$ are localized in time and frequency both. Variance is an important statistical property that is very useful in calculating spread of a given function, which is indicative of concentration of energy of a function within certain band (in time as well as frequency domain).

The question arises that is it possible to have finite variances in both frequency as well as time domain simultaneously? The answer is yes. We can have both the variances to be of finite value. Now, how small can these variances be? To answer this question we introduce time-frequency uncertainty. In case of Haar wavelet, it is somewhat concentrated in frequency, but well-concentrated in time.For the Daubechies function, as we go to higher orders, we get a somewhat better filtering operation that gives us a better frequency localization.

In Chapter 8 we shall investigate the concept of uncertainty deeply.

Exercises

Exercise 7.1

Consider the problem of finding projection of triangular wave shown in Fig. 7.7 over approximation subspaces V_{-1}, V_0, V_1, V_2 and over detail subspaces W_{-1}, W_0, W_1. Through this example one might show that projections of triangular wave over such subspaces follow time and frequency localization discussion carried out in this chapter. That is, one might show that localization in both time and frequency is limited by time and frequency resolutions of dilated Haar scaling and wavelet functions, which enable us to analyze signal by looking at separate frequency bands.

Hint: In order to prove the mentioned claim, we shall first find projection of $x(t)$ over various approximation (V subspaces) and detail subspaces (W subspaces). After finding such projections, we might take Fourier transform of projections and by observation fulfill the claim. However, first let us look at the Fourier transform of triangular wave, which may be given in the following manner. We only consider magnitude response here as we are not interested in phase response at this level of analysis.

$$|x(t)| \overset{F.T.}{\longleftrightarrow} \left| \frac{\sin\left(\frac{\Omega}{2}\right)}{\frac{\Omega}{2}} \right|^2$$

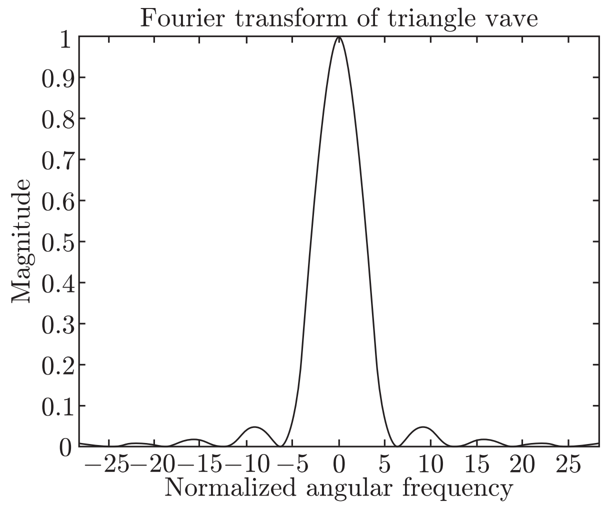

Figure 7.14 | *Fourier transform of Triangular wave*

This relationship easily follows from convolution of two unit pulses, which renders to multiplication in Fourier domain. The frequency domain representation is shown in Fig. 7.14.

Projection of $x(t)$ over positive approximation subspaces ($V_k, k \geq 0$) may be found in the following way:

$$
\begin{aligned}
C(k,l) &= 2^k \int_{2^{-k}l}^{2^{-k}(l+1)} (1-t)dt \\
&= 2^{k-1}(2t - t^2)\Big|_{2^{-k}l}^{2^{-k}(l+1)} \\
&= 1 - 2^{-k}(l + 0.5); \quad k \geq 0
\end{aligned}
$$

where, $C(k,l)$ is an approximation coefficient at k^{th} subspace with scaling function translated by l units in time. Note that triangular wave is symmetric, which allows us to compute coefficients on one side of the symmetry axis and mirror on the other side. For subspaces with $k < 0$, we may find coefficients in the following manner:

$$
\begin{aligned}
C(k,l) &= 2^k \int_0^1 (1-t)dt \\
&= 2^{k-1}(2t - t^2)\Big|_0^1 \\
&= 2^{k-1}; \quad k < 0
\end{aligned}
$$

Projections of $x(t)$ over subspaces V_{-1}, V_0, V_1, V_2 along with respective Fourier transforms are shown in Fig. 7.16.

As evident from Fig. 7.16, localization in time improves as we go to finer subspaces. On the other hand, localization in frequency domain deteriorates increasingly as we move to finer

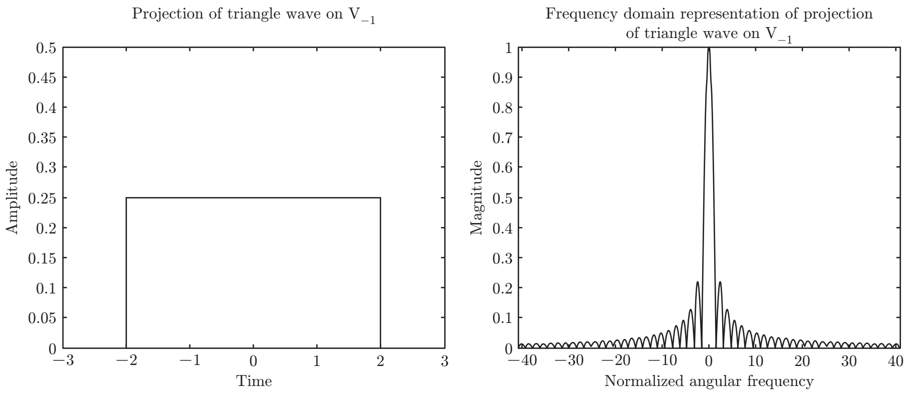

(a) Projection on V_0 and corresponding frequency domain representation

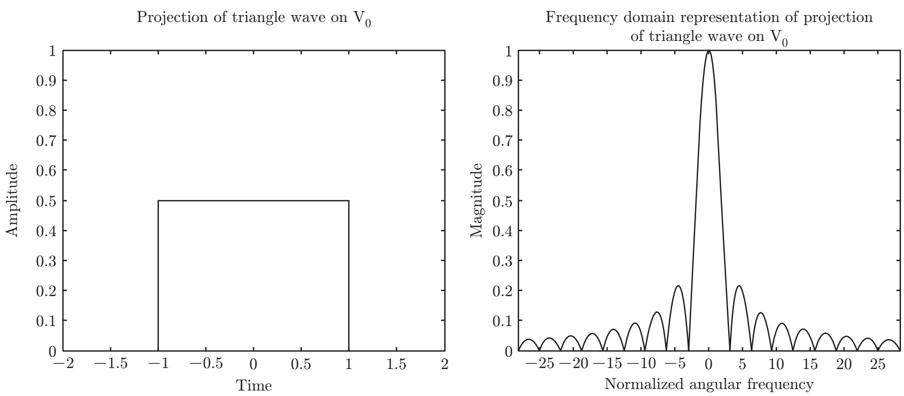

(b) Projection on V_0 and corresponding frequency domain representation

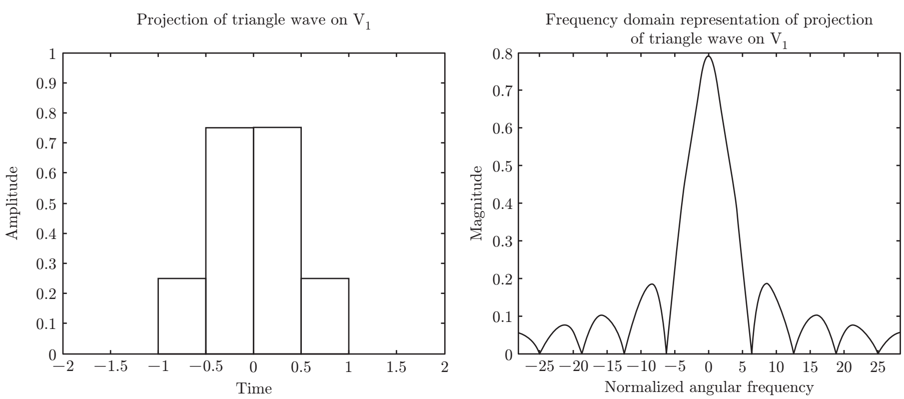

(c) Projection on V_1 and corresponding frequency domain representation

Figure 7.15 | *(Continued)*

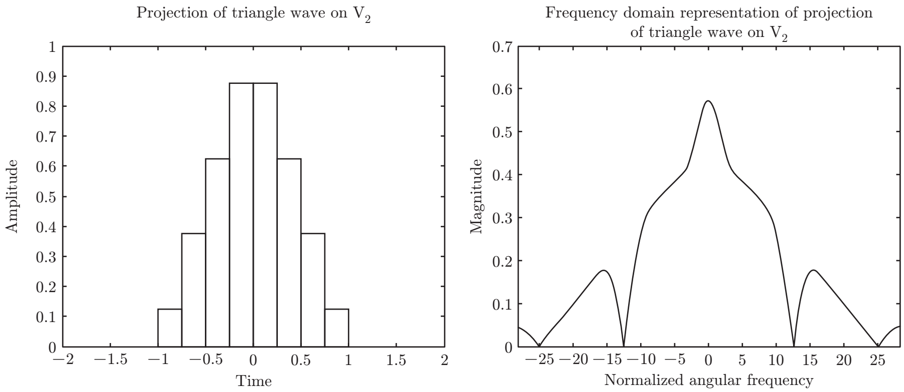

(d) Projection on V_2 and corresponding frequency domain representation

Figure 7.15 *Projections of triangular wave over different approximation subspaces and their corresponding Fourier transforms. [See how localization in time and frequency domain changes as we go from coarser subspace to finer and finer subspaces.]*

subspaces. Localization in time is governed by duration of corresponding scaling function in time, whereas, frequency localization is governed by frequency response of scaling function in that subspace. In V_0, for example, maximum frequency content is upper-bounded by frequency content of scaling function in this subspace. Similar conclusion holds for projection in all other subspaces.

Projections of $x(t)$ over detail subspaces may be found in the following manner:

$$\begin{aligned} d(k,l) &= c(k+1,2l) - c(k,l) \\ &= 1 - 2^{-k-1}(2l+0.5) - 1 + 2^{-k}(l+0.5) \\ &= 2^{-k-2}; \quad k \geq 0 \end{aligned}$$

where, $d(k,l)$ depicts coefficients of detail subspace W_k when wavelet function is shifted by l units in time. As all approximation projections are symmetric, detail projections are also symmetric. For negative detail subspaces, coefficients may be found in the following way:

$$\begin{aligned} d(k,l) &= c(k+1,2l) - c(k,l) \\ &= 2^{k} - 2^{k-1} \\ &= 2^{k-1}; \quad k < 0 \end{aligned}$$

Projections and corresponding frequency domain representations of triangular wave over W_{-1}, W_0 and W_1 are depicted in Fig. 7.16.

Again, it is evident from the figure that time and frequency details are not well localized simultaneously. As resolution in one domain improves, resolution in other domain is bound to deteriorate and vice versa. Also, frequency domain resolution is bounded by bandpass nature of wavelet function. As we move from W_{-1} to W_1, centre frequency shifts away from zero frequency and band gets wider and wider. This leads to condition similar to constant-Q analysis in which ratio of centre frequency and band around it remain approximately constant throughout the analysis.

Exercise 7.2

In continuation to the numerical example depicted, in Exercise 7.1 consider the signal

$$
\begin{aligned}
x(t) &= 1 - |t|^r; \quad && r \in R+ \text{ and } 0 \le |t| \le 1 \\
&= 0; && \text{otherwise}.
\end{aligned}
$$

Explain how projections and corresponding Fourier transforms evolve as r goes to infinity.

Hint: As r goes to infinity, $x(t)$ approaches a rectangular pulse in $-1 \le t \le 1$ interval. Hence, in limit $x(t)$ will be in V_0 subspace. In this case, projections on V_0 to $V_{+\infty}$ will be the same, which explicitly implies no components of $x(t)$ in W_0 to $W_{+\infty}$. By induction, we may say that as r increases components in V_+, subspaces become more and more similar and components in W_+ subspaces become smaller and smaller. In this case, frequency domain representations will also follow similar trend, namely frequency responses of V_+ subspaces will become more similar and frequency responses of W_+ subspaces tend to vanish.

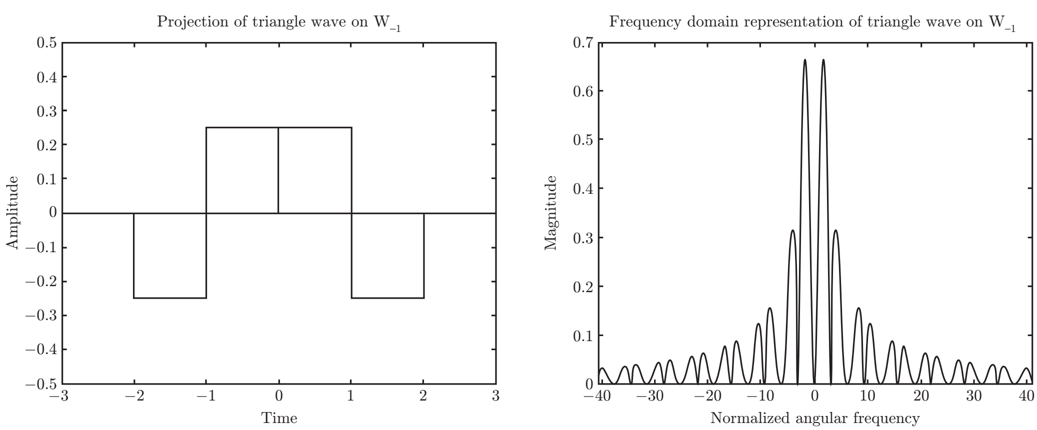

(a) Projection on W_{-1} and corresponding frequency domain representation

Figure 7.16 | *(Continued)*

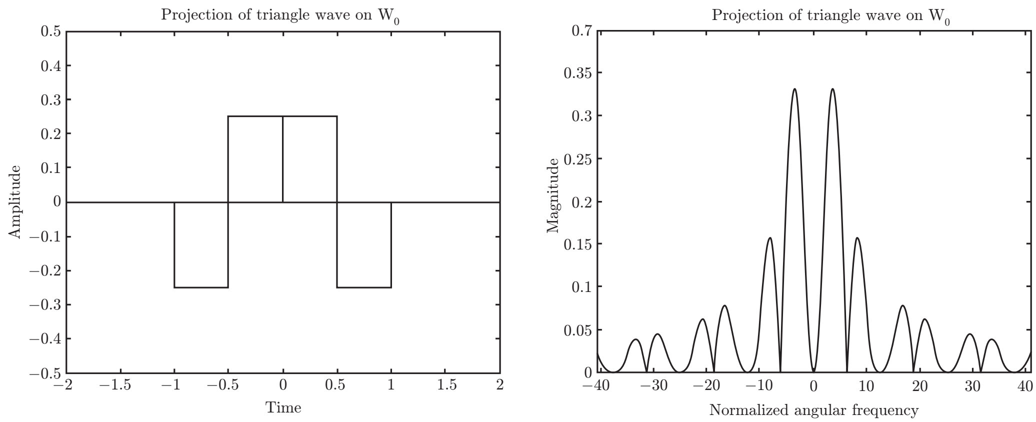

(b) Projection on W_0 and corresponding frequency domain representation

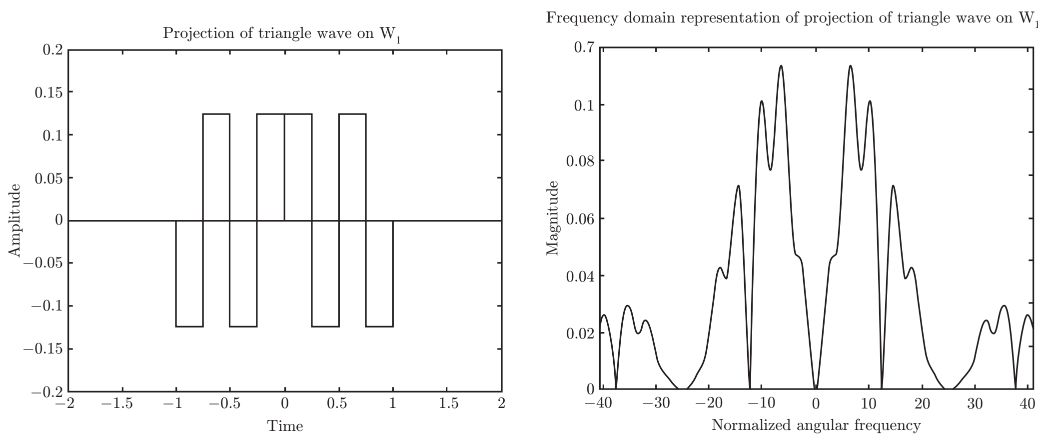

(c) Projection on W_1 and corresponding frequency domain representation

Figure 7.16 | *Projections of triangle wave over different detail subspaces and their corresponding Fourier transforms. [See how localization in time and frequency domain changes as we go from coarser subspace to finer and finer subspaces.]*

Exercise 7.3

Briefly comment about Haar scaling and wavelet functions as analysis tools for joint time-frequency domain representation of a signal.

Hint: Haar scaling and wavelet functions have excellent time localization property as evident from Fig 7.3 and Fig 7.6. However, both have poor frequency localization property as both have frequency responses which are not compactly supported (zero outside some finite range). Hence, according to Parseval's theorem, dot product in frequency domain contains contribution from all frequency components, which contributes to degradation in frequency localization. This very fact provides motivation to question whether simultaneous localization in time and frequency is possible or not, which is answered by the uncertainty principle to be discussed in following set of lectures.

Exercise 7.4

The coefficient of Daub-4, Daub-6, are given, find the frequency response (magnitude only) of corresponding LPF.

$$\text{Daub-4} = \left[\frac{1+\sqrt{3}}{4\sqrt{2}}, \frac{3+\sqrt{3}}{4\sqrt{2}}, \frac{3-\sqrt{3}}{4\sqrt{2}}, \frac{1-\sqrt{3}}{4\sqrt{2}},\right]$$

Daub-6 =

$$\left[\frac{1+\sqrt{10}+\sqrt{5+2\sqrt{10}}}{16\sqrt{2}}, \frac{5+\sqrt{10}+3\sqrt{5+2\sqrt{10}}}{16\sqrt{2}}, \frac{10-\sqrt{10}+2\sqrt{5+2\sqrt{10}}}{16\sqrt{2}}, \frac{10-2\sqrt{10}-\sqrt{5+2\sqrt{10}}}{16\sqrt{2}},\right.$$

$$\left.\frac{5+\sqrt{10}-3\sqrt{5+2\sqrt{10}}}{16\sqrt{2}}, \frac{1+\sqrt{10}-\sqrt{5+2\sqrt{10}}}{16\sqrt{2}}\right]$$

Hint: The frequency responses are as shown in Fig. 7.17.

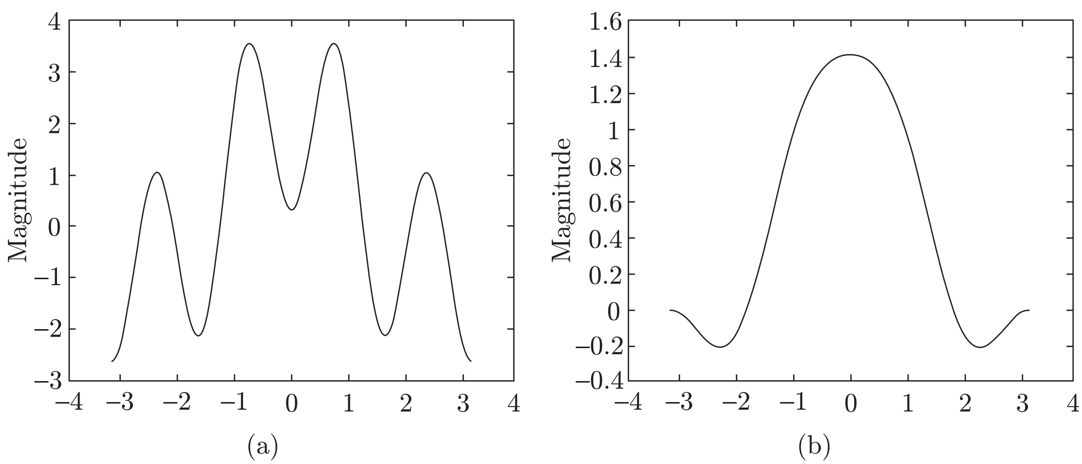

Figure 7.17 | *Magnitude Frequency Response; (a): Daub-4 LPF magnitude frequency responce; (b): Daub-6 LPF magnitude frequency responce.*

Exercise 7.5

Prove that a time-limited signal can not be band limited or vice versa, i.e. a signal can not be time-limited and band-limited simultaneously.

Hint: Assume that a continuous signal $f(t)$ is band-limited and nonzero over a finite interval of time. Let $f(t)$ be zero in interval (a,b). So, we can write

$$f(t) = 0,\ t \in (a,b)$$

Let Fourier transform of $f(t)$ be $F(f)$ which is zero outside the interval $(-f_0, f_0)$ (assuming $f(t)$ to be a real signal.)

We can write for $t \in (a,b)$ as

$$\begin{aligned} f(t) &= 0 \\ &= \int_{-\infty}^{\infty} F(f) e^{j2\pi ft} df \\ &= \int_{-f_0}^{f_0} F(f) e^{j2\pi ft} df \end{aligned}$$

Repeatedly differentiating the above expression with respect to *t*, we get

$$\begin{aligned} f(t) &= 0 \\ &= (2\pi j)^n \int_{-f_0}^{f_0} F(f) f^n e^{j2\pi ft} df \end{aligned}$$

Picking $t_0 \in (a,b)$, we have

$$0 = (2\pi j)^n \int_{-f_0}^{f_0} F(f) f^n e^{j2\pi ft_0} df \tag{7.1}$$

Now, for any t we can write (t need not be in the interval (a,b)) ,

$$\begin{aligned} f(t) &= \int_{-f_0}^{f_0} F(f) e^{j2\pi ft} df \\ &= \int_{-f_0}^{f_0} F(f) e^{j2\pi f(t-t_0)} e^{j2\pi ft_0} df \\ &= \int_{-f_0}^{f_0} \sum_{n=0}^{\infty} \frac{(2\pi jf(t-t_0))^n}{n!} e^{j2\pi ft_0} F(f) df \\ &= \sum_{n=0}^{\infty} \frac{(2\pi jf(t-t_0))^n}{n!} \int_{-f_0}^{f_0} F(f) f^n e^{j2\pi ft_0} df \\ &= \sum_{n=0}^{\infty} \frac{(2\pi jf(t-t_0))^n}{n} .0 \\ &= 0 \end{aligned}$$

Note that, we have made use of Eq. (7.1), in step 3 above which we have already derived. Thus, $f(t)$ is essentially zero for any value of t. So, we can extend interval (a,b) to cover entire time axis i.e. $(-\infty, +\infty)$. Hence, $f(t)$ is zero function and can not be any other time-limited function. So, a function cannot be time-limited as well as band-limited simultaneously.

Chapter 8

The Uncertainty Principle

8.1 | Introduction

We build in this chapter a very important principle, which is infact at the heart of the subject of Wavelets and Time frequency methods, namely, the uncertainty principle. The whole chapter is devoted to a discussion of uncertainty principle; laying the foundation of what the uncertainty means first, and then proceeding to obtain certain numerical bounds in two domains simultaneously.

8.2 | Non-formal Introduction to the Idea of Containment

As we discussed in previous chapter, there is of course a very tight or strong notion of containment. Is it possible to have compact support in both time domain and frequency domain? So, both in the time and in frequency, we demand the function to be non-zero only over a finite part of the independent variable or the real axis; a very strong demand and of course that cannot be met. It is related to the fact that if the function was finitely supported (compactly supported) in the real axis, there were certain properties of that function, specifically the existence of an infinite number of derivatives, which make it impossible for the function to be compactly supported or be non-zero only over a finite interval of the independent variable in the natural domain. Natural domain can mean time, space or any other domain. But we had asked whether a weaker notion of containment could be admitted. So to be on the finite interval of the independent variable, which indexes it and simultaneously in the transformed domain, i.e. the frequency domain, we insisted that most of the content be in a finite interval of the frequency axis. This seems like more reasonable requirement and to a certain extent can be met too. Finally the focus remains on how much we can contain in the two domains simultaneously. There are several steps to reach this destination:

The *first step* is to put down in a nonformal way, what do we mean by 'containment'? What do we mean by 'most of the content being in certain finite range?' The approach that we would take to do this has been discussed briefly in the previous chapter. There are two possible approaches to doing this. We should think of the magnitude-squared of the function and the magnitude-squared of the Fourier transform as a one-dimensional object and then we could talk about the centre of that object or "centre of mass". We could talk about the spread of the object around the centre of mass, using the notion of "radius of gyration" or probability density, built from the squared magnitude of the function and another density built from the squared magnitude of the Fourier transform. We could then look at the "mean" and "variance" of these densities. The variances are indicative of the spread. So this was a nonformal introduction.

8.3 | Formalization of the Idea of Containment

We are going to work in $L_2(\mathbb{R})$. In fact, we must mention that sometimes we are actually going to work in the intersection of the space of square integrable functions and absolutely integrable functions.

$$x(t) \in L_2(\mathbb{R}) \cap L_1(\mathbb{R})$$

Now, as the function belongs to $L_2(\mathbb{R})$, its Fourier transform also belongs to $L_2(\mathbb{R})$. Let, $x(t)$ have the fourier transform $\hat{x}(\Omega)$. Then, $\hat{x}(\Omega) \in L_2(\mathbb{R})$ as well. So, we first define a density or a "one dimensional mass".

$$\int_{-\infty}^{\infty} |x(t)|^2 \, dt = \|x(t)\|_2^2$$

which is finite. Therefore, we define the density as,

$$p_x(t) = \frac{|x(t)|^2}{\|x(t)\|_2^2}$$

which is a probability density, because of the following reasons:

1. $p_x(t) \geq 0 \ \forall \ t$ (It is a density in t)
2. $\int_{-\infty}^{\infty} p_x(t) dt = 1$ (from definition)

Similarly, let us define a density in the angular frequency domain.

$$p_{\hat{x}}(\Omega) = \frac{|\hat{x}(\Omega)|^2}{\|\hat{x}(\Omega)\|_2^2}$$

This is also a probability density, because of the following reasons:

1. $p_{\hat{x}}(\Omega) \geq 0 \ \forall \ \Omega$ (It is a density in Ω)
2. $\int_{-\infty}^{\infty} p_{\hat{x}}(\Omega) d\Omega = 1$ (from definition)

Now we have taken the probability density perspective, but we could as well take the so-called one-dimensional mass perspective, i.e. we could think of the $p_x(t)$ as a one-dimensional mass in t and similarly $p_{\hat{x}}(\Omega)$ as one-dimensional mass in Ω. So, here, we have a simplified situation. We have a mass in one-dimensional space, which can be the space of t or the space of Ω.

If we choose the "mass" perspective, consider the "centre of mass" and the "spread around the centre". Spread around the centre in mechanics can be measured by a quantity called the "Radius of gyration". If we choose the "probability density" perspective, we have the notion of "mean" and "variance".

Now, we must assume that these quantities can be calculated. It is possible that the variance can be infinity, so we are not always guaranteed of a finite variance. Let us find a lower limit as to where these quantities go in the two domains simultaneously.

Considering the function $x(t)$, we prefer to take the probability density perspective. So we think of $p_x(t)$ and $p_{\hat{x}}(\Omega)$ as the probability densities and now we shall write down the "mean".

Let, $p_x(t)$ have the mean t_0.

$$t_0 = \int_{-\infty}^{\infty} t p_x(t) dt$$

Recognizing the definition to hold good for the "centre of mass" here, essentially, we are calculating the moment by choosing the fulcrum to be zero and, therefore, getting a different fulcrum or a point at which the moments are balanced.

Similarly, let $p_{\hat{x}}(\Omega)$ have the mean Ω_0.

$$\Omega_0 = \int_{-\infty}^{\infty} \Omega p_{\hat{x}}(\Omega) d\Omega$$

Further, we assume the "means" are finite and normally they should be. In some deviant situations, we may have a problem. So, assuming these "means" are finite, let us look at the "variances".

So, the variance in t is defined as,

$$\sigma_t^2 = \int_{-\infty}^{\infty} (t - t_0)^2 p_x(t) dt$$

And similarly, the variance in angular frequency is defined as,

$$\sigma_\Omega^2 = \int_{-\infty}^{\infty} (\Omega - \Omega_0)^2 p_{\hat{x}}(\Omega) d\Omega$$

Once again, we are assuming the variances to be finite. Even if the variances are infinite, we will accept it. If we choose to think of these as one-dimensional masses, it is very clear that the variance is an indication of the spread. So larger the variance, the more the density is said to have spread around the "mean" and the smaller the variance; the more the density or the mass is said to be concentrated around the mean. So, now we have a formal way to define containment.

We can say that the containment in a given domain refers to the variance in that domain. So containment in time is essentially σ_t^2, and containment in angular frequency domain is essentially σ_Ω^2 quantity. How small can we make any one of these quantities for a valid function?

To justify this point, we will take the Haar scaling function as an example and calculate its variance.

Example 8.3.1 — Calculate mean and variance for the Haar scaling function.

We can see that the Haar scaling function $\phi(t)$ is one between zero and one and zero elsewhere (Fig. 8.1). Its probability density is given as,

$$p_\phi(t) = \frac{|\phi(t)|^2}{\|\phi(t)\|_2^2}$$

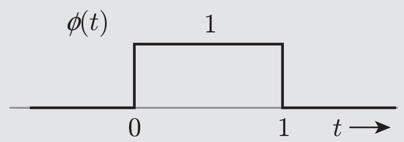

Figure 8.1 | *Haar scaling function*

Now,

$$\|\phi(t)\|_2^2 = \int_{-\infty}^{\infty} |\phi(t)|^2 \, dt = \int_0^1 1 dt = 1$$

Hence, $p_\phi(t)$ is as shown in Fig. 8.2.

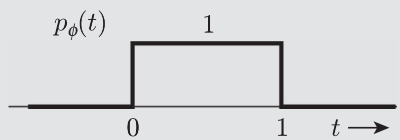

Figure 8.2 | *Probability density function in time*

Now, we will find the "mean". In fact, even before finding the mean formally, we can find it graphically. The mean is going to be at the centre of 0 and 1, i.e, at $\frac{1}{2}$. Let us do it formally,

$$\begin{aligned} t_0 &= \int_{-\infty}^{\infty} t p_\phi(t) dt \\ &= \int_0^1 t dt \\ &= \frac{t^2}{2} \Big|_0^1 \\ &= \frac{1}{2} \end{aligned}$$

Hence, mean is shown as shown in Fig. 8.3.

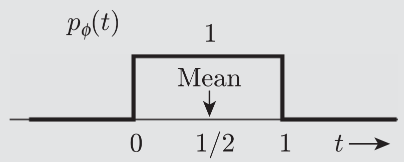

Figure 8.3 | *Mean of $p_\phi(t)$*

Now, we will find the "variance".

$$\sigma_t^2 = \int_{-\infty}^{\infty} (t - t_0)^2 \, p_\phi(t) dt$$

$$= \int_{-\infty}^{\infty} (t - \frac{1}{2})^2 \, p_\phi(t) dt$$

$$= \int_0^1 (t - \frac{1}{2})^2 \, dt$$

Let, $$t - \frac{1}{2} = \lambda,$$

$$\Rightarrow dt = d\lambda.$$

As limits of t are 0 to 1, we get limits of λ as $\frac{-1}{2}$ to $\frac{1}{2}$. Hence, integral becomes

$$\sigma_t^2 = \int_{\frac{-1}{2}}^{\frac{1}{2}} \lambda^2 d\lambda$$

$$= \frac{\lambda^3}{3} \Big|_{\frac{-1}{2}}^{\frac{1}{2}}$$

$$= \frac{1}{3}(\frac{1}{8} + \frac{1}{8})$$

$$= \frac{1}{12}$$

Therefore, taking positive square root, we get

$$\sigma_t = \frac{1}{2\sqrt{3}}$$

As we can be seen that, σ_t is less than $\frac{1}{2}$. In a certain sense, we do not really use the number half to denote the spread of $\phi(t)$ around its mean. The variance does not say it goes all the way to half. It says the spread is a number slightly less than half. Most of the energy is contained in that region around the mean captured by the variance. In fact, to be very specific, the fraction of the energy contained here would be, i.e. the energy contained in $[t_0 - \sigma_t, t_0 + \sigma_t]$ would essentially be given by,

$$\int_{t_0 - \sigma_t}^{t_0 + \sigma_t} p_\phi(t) dt$$

We are not looking for 100% of the energy, in lieu we are considering the significant part of it. Now, we will calculate this value. Substituting the values, the integral becomes,

$$\int_{t_0-\sigma_t}^{t_0+\sigma_t} p_\phi(t)dt = \int_{\frac{1}{2}-\frac{1}{2\sqrt{3}}}^{\frac{1}{2}+\frac{1}{2\sqrt{3}}} 1dt$$

$$= (\frac{1}{2}+\frac{1}{2\sqrt{3}})-(\frac{1}{2}-\frac{1}{2\sqrt{3}})$$

$$= \frac{1}{\sqrt{3}}$$

$$= 0.577$$

It is certainly not a large fraction like 90%, but it is more than 50%. This fraction varies for different functions and depends on the density. Hence, we can say that, the variance is an accepted measure of spread, and very often the variance actually tells us where most of the function is concentrated. Even in this case, if we look at it carefully, part of this function is between $\left(\frac{1}{2}-\frac{1}{2\sqrt{3}}\right)$ and $\left(\frac{1}{2}+\frac{1}{2\sqrt{3}}\right)$.

Now, we will calculate the variance in the frequency domain of this same function. So, let us look at $\hat{\phi}(\Omega)$. Actually, we are interested in $|\hat{\phi}(\Omega)|^2$. And that is of the form,

$$|\hat{\phi}(\Omega)|^2 = \left|\frac{\sin(\frac{\Omega}{2})}{(\frac{\Omega}{2})}\right|^2$$

We could integrate this. Indeed we know that,

$$\|\phi(t)\|_2^2 = \int_{-\infty}^{\infty} |\phi(t)|^2\, dt = \frac{1}{2\pi}\int_{-\infty}^{\infty} |\hat{\phi}(\Omega)|^2\, d\Omega$$

which is equal to 1. Hence,

$$\|\hat{\phi}(\Omega)\|_2^2 = \int_{-\infty}^{\infty} |\hat{\phi}(\Omega)|^2\, d\Omega = 2\pi$$

Hence, $p_{\hat{\phi}}(\Omega)$ is given as,

$$p_{\hat{\phi}}(\Omega) = \frac{|\hat{\phi}(\Omega)|^2}{\|\hat{\phi}(\Omega)\|_2^2} = \frac{|\hat{\phi}(\Omega)|^2}{2\pi}$$

It has an appearance as shown in Fig. 8.4.

Now, it is very easy to see that the mean of this function is zero. This function is symmetrical around $\Omega = 0$. For all real functions $x(t)$, $\hat{x}(\Omega)$ is magnitude symmetric. Therefore, the mean $\Omega_0 = 0$.

Now, let us find the variance. So, the variance of $\hat{\phi}(\Omega)$ is given as,

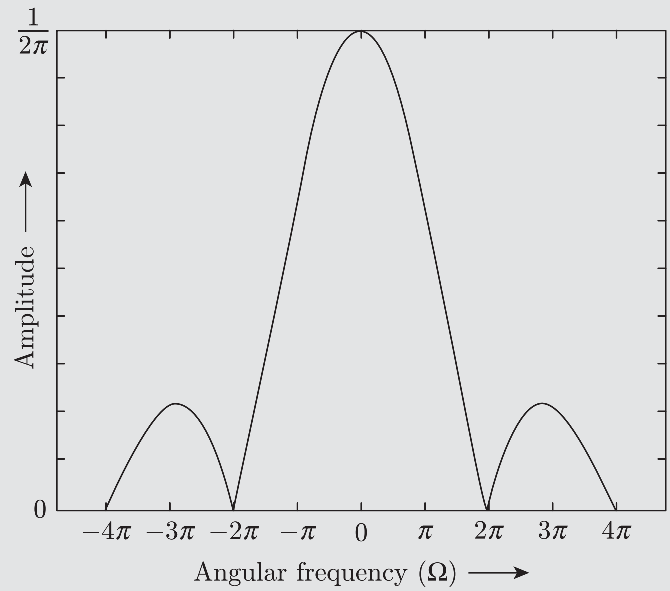

Figure 8.4 | *Waveform of* $p_{\hat{\phi}}(\Omega)$

$$\begin{aligned}
\sigma_{\Omega}^2 &= \int_{-\infty}^{\infty} (\Omega - \Omega_0)^2 p_{\hat{\phi}}(\Omega) d\Omega \\
&= \int_{-\infty}^{\infty} \Omega^2 \frac{|\hat{\phi}(\Omega)|^2}{2\pi} d\Omega \\
&= \int_{-\infty}^{\infty} \frac{\Omega^2}{2\pi} \left| \frac{\sin\left(\frac{\Omega}{2}\right)}{\left(\frac{\Omega}{2}\right)} \right|^2 d\Omega \\
&= \int_{-\infty}^{\infty} \frac{4}{2\pi} \left| \sin\frac{\Omega}{2} \right|^2 d\Omega
\end{aligned}$$

The constant $\frac{4}{2\pi}$ is not important, but $\left|\sin\left(\frac{\Omega}{2}\right)\right|^2$ is very important. We are trying to integrate the $\left|\sin\left(\frac{\Omega}{2}\right)\right|^2$ function, which is a periodic function with period 2π. We are trying to integrate a periodic function from $-\infty$ to $+\infty$, and obviously the integral is going to diverge. So the apprehension comes out to be true in the very simple case of scaling function that we know. The variance of $\hat{\phi}(\Omega)$ is infinite! In other words, $\phi(t)$ is not at all confined in the frequency domain, at least in this sense. When we discussed time and frequency together we had been concerned about presence of these side lobes. Besides, it is feasible to look at the main lobe and talk about the presence in the main lobe. However, these side lobes are falling off by the factor of $\frac{1}{\Omega}$ in magnitude and have created the problem after multiplication of Ω^2 in the calculation of variance. The side lobe creates a periodic function, which is to be integrated, and that causes the trouble.

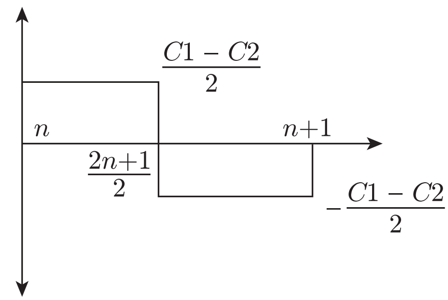

Figure 8.5 | *Waveform of* $|\sin(\frac{\Omega}{2})|^2$

This explains why we have to look much beyond the Haar and can't be contented with the Haar multi-resolution analysis. If we look at the scaling function in the Haar multi-resolution analysis, its variance in the frequency domain analysis is infinite. It is not at all contained in the frequency domain in this sense. The question is what makes the variance infinity? Why did we have a divergent variance? In fact we can answer these questions, if we only make a slight adjustment of the expression of variance. The variance of $\hat{\phi}(\Omega)$ is given as,

$$\begin{aligned}\sigma_\Omega^2 &= \int_{-\infty}^{\infty} \Omega^2 \frac{|\hat{\phi}(\Omega)|^2}{\|\hat{\phi}(\Omega)\|_2^2} d\Omega \\ &= \frac{1}{\|\hat{\phi}(\Omega)\|_2^2} \int_{-\infty}^{\infty} \Omega^2 |\hat{\phi}(\Omega)|^2 \, d\Omega \\ &= \frac{1}{\|\hat{\phi}(\Omega)\|_2^2} \int_{-\infty}^{\infty} |j\Omega\hat{\phi}(\Omega)|^2 \, d\Omega\end{aligned}$$

Now, $j\Omega\hat{\phi}(\Omega)$ has some significance and is essentially the Fourier transform of $\frac{d\phi(t)}{dt}$. Hence, energy in the derivative function is given as,

$$\int_{-\infty}^{\infty} \left|\frac{d\phi(t)}{dt}\right|^2 dt = \frac{1}{2\pi}\int_{-\infty}^{\infty} |j\Omega\hat{\phi}(\Omega)|^2 \, d\Omega$$

Hence, the variance of $\hat{\phi}(\Omega)$ is given as,

$$\begin{aligned}\text{Variance of } \hat{\phi}(\Omega) &= \frac{2\pi(\text{Energy in derivative})}{\|\hat{\phi}(\Omega)\|_2^2} \\ &= \frac{2\pi(\text{Energy in derivative})}{2\pi(\text{Energy in function})}\end{aligned}$$

For a real $x(t)$, the frequency variance, i.e. the Ω variance is,

$$\sigma_\Omega^2 = \frac{\text{Energy in } \frac{dx(t)}{dt}}{\text{Energy in function } x(t)} = \frac{\left\|\frac{dx(t)}{dt}\right\|_2^2}{\|x(t)\|_2^2}$$

As we can see, $\phi(t)$ is discontinuous. So, when its derivative is considered, there are impulses in the derivative, which are not square integrable. So, the numerator diverges. The moment we have a discontinuous function, we have an infinite frequency variance. With this note, we realize that, if we want to get some meaningful uncertainty, some meaningful bound, we must at least consider continuous functions.

8.4 | Self Evaluation Quiz Examples

Example 8.4.1 — What is the difference between $|x(t)|^2$ and $\|x(t)\|_2^2$?

Ans. $\|x(t)\|_2^2$ is the $\mathcal{L}_2$ norm of function $x(t)$ and it is given as,

$$\|x(t)\|_2^2 = \int_{-\infty}^{\infty} |x(t)|^2 \, dt$$

$\|x(t)\|_2^2$ is the scalar quantity, whereas $|x(t)|^2$ is squared magnitude of function $x(t)$.

Example 8.4.2 — Why the frequency centre for real function is zero?

Ans. For real functions, its Fourier transform is magnitude symmetric. Therefore, frequency centre is zero for real function.

Example 8.4.3 — What operations are needed to shift the time centre and frequency centre without affecting its shape?

Ans.

1. Time translation (Frequency domain modulation)
2. Frequency translation (Time domain modulation)

With these operations, we can shift the time centre and frequency centre without affecting the time and frequency variance, i.e. without affecting its shape.

8.5 | The Time-bandwidth Product

In this and next few sections, we will study the time bandwidth product, and the effect of simple signal transformation on the time bandwidth product.

Let us revise some basic formulae that we have.

8.5.1 The Time Centre t_0

The time centre of any waveform $x(t)$ is given by

$$t_0 = \frac{\int_{-\infty}^{\infty} t\,|x(t)|^2\,dt}{\int_{-\infty}^{\infty} |x(t)|^2\,dt} \tag{8.1}$$

Which has already been introduced.

The quantity $\int_{-\infty}^{\infty} |x(t)|^2\,dt$ is often represented as $\|x\|_2^2$ to indicate that it is the squared $\mathbb{L}_2$ norm of $x(t)$.

8.5.2 The Time Variance σ_t^2

The time variance of a function $x(t)$ is defined as

$$\sigma_t^2 = \frac{\int_{-\infty}^{\infty} (t-t_0)^2\,|x(t)|^2\,dt}{\|x\|_2^2} \tag{8.2}$$

8.5.3 The Frequency Centre Ω_0

The frequency centre of $\hat{x}(\Omega)$, where $\hat{x}(\Omega)$ is the Fourier transform of $x(t)$, is given by

$$\Omega_0 = \frac{\int_{-\infty}^{\infty} \Omega\,|\hat{x}(\Omega)|^2\,d\Omega}{\int_{-\infty}^{\infty} |\hat{x}(\Omega)|^2\,d\Omega} \tag{8.3}$$

As before, the quantity $\int_{-\infty}^{\infty} |\hat{x}(\Omega)|^2\,d\Omega$ is expressed as $\|\hat{x}\|_2^2$. For real signals, $|\hat{x}(\Omega)|^2$ is an even function of Ω and hence $\Omega_0 = 0$ due to symmetry.

8.5.4 The Frequency Variance σ_Ω^2

The frequency variance of a signal spectrum $\hat{x}(\Omega)$ given by

$$\sigma_\Omega^2 = \frac{\int_{-\infty}^{\infty} (\Omega-\Omega_0)^2\,|\hat{x}(\Omega)|^2\,d\Omega}{\|\hat{x}\|_2^2} \tag{8.4}$$

8.6 | Signal Transformations

In this section, we shall study the effect of some common signal transformations on the four quantities mentioned above.

Example 8.6.1 — Shifting in time domain.

Let the signal $x(t)$, with time centre t_0 be shifted in time by amount t_1, i.e.

$$y(t) = x(t - t_1) \tag{8.5}$$

Effect on time centre

Since we are only shifting in time and not changing the magnitude, the $\mathbb{L}_2$ norm square in the denominator will remain unchanged. The new time centre will be given as

$$t_{0(new)} = \frac{\int_{-\infty}^{\infty} t\,|\,x(t - t_1)\,|^2\,dt}{\|\,x\,\|_2^2} \tag{8.6}$$

Now, substitute $t - t_1 = u$. Thus

$$dt = du$$

and

$$t = u + t_1$$

The limits of integration remain unchanged. Thus, the new integral will be

$$\begin{aligned}
t_{0(new)} &= \frac{\int_{-\infty}^{\infty} (u + t_1)\,|\,x(u)\,|^2\,du}{\|\,x\,\|_2^2} \\
&= \frac{\int_{-\infty}^{\infty} u\,|\,x(u)\,|^2\,du}{\|\,x\,\|_2^2} + \frac{\int_{-\infty}^{\infty} t_1\,|\,x(u)\,|^2\,du}{\|\,x\,\|_2^2} \\
&= t_0 + t_1 \frac{\int_{-\infty}^{\infty} |\,x(u)\,|^2\,du}{\|\,x\,\|_2^2} \\
t_{0(new)} &= t_0 + t_1 \qquad (8.7)
\end{aligned}$$

because,

$$\int_{-\infty}^{\infty} |\,x(u)\,|^2\,du = \|\,x\,\|_2^2$$

Effect on time variance

From the new time centre, we can write the expression for the time variance as

$$\sigma_{t(new)}^2 = \frac{\int_{-\infty}^{\infty} (t - t_0 - t_1)^2\,|\,x(t - t_1)\,|^2\,dt}{\|\,x\,\|_2^2}$$

substitute

$$t - t_1 = u$$

Thus,

$$\sigma^2_{t(new)} = \frac{\int_{-\infty}^{\infty} (u - t_0)^2 \,|\, x(u) \,|^2 \, du}{\| x \|_2^2}$$

$$\sigma^2_{t(new)} = \sigma^2_t \tag{8.8}$$

Thus, the time variance is unaffected by a shift in time.

Effect on frequency domain

$$\begin{aligned} & y(t) = x(t - t_1) \\ \Rightarrow \quad & \hat{y}(\Omega) = e^{-j\Omega t_1} \hat{x}(\Omega) \\ \Rightarrow \quad & |\, \hat{y}(\Omega) \,| = |\, \hat{x}(\Omega) \,| \\ \Rightarrow \quad & \| \hat{y} \|_2^2 = \| \hat{x} \|_2^2 \end{aligned} \tag{8.9}$$

Since the magnitude of $\hat{y}(\Omega)$ is same as $\hat{x}(\Omega)$, the frequency centre and frequency variance will remain same. The only change is in phase, which is of no consequence in calculating Ω_0 and σ^2_Ω.

Example 8.6.2 — Shifting in frequency domain (or modulation in time domain).

Shifting in frequency domain implies multiplication by a complex exponential in time domain. Thus,

$$\begin{aligned} & y(t) = e^{j\Omega_1 t} x(t) \\ \Rightarrow \quad & \hat{y}(\Omega) = \hat{x}(\Omega - \Omega_1) \end{aligned} \tag{8.10}$$

Students may take it as an exercise to prove that frequency centre is shifted by $+\Omega_1$ and frequency variance is unchanged. Also note that, since

$$|\, y(t) \,| = |\, x(t) \,|$$

time centre and time variance also remain unchanged.The product $\sigma_t^2 \sigma_\Omega^2$ remains unchanged by all these operations. This product is called the **Time-Bandwidth Product** and it is a characteristic (though not unique) of a waveform.

Example 8.6.3 — Multiplication by a constant.

Let

$$\begin{aligned} y(t) &= C_0 x(t) \quad (C_0 \neq 0) \\ \Rightarrow \quad |y(t)|^2 &= |C_0|^2 |x(t)|^2 \\ \Rightarrow \quad |\hat{y}(\Omega)|^2 &= |C_0|^2 |\hat{x}(\Omega)|^2 \end{aligned} \tag{8.11}$$

Substituting $y(t)$ in Eqs. (8.1), (8.2), (8.3), and (8.4), we can see that the term $|C_0|^2$ will come outside the integration in both denominator and numerator and will get cancelled, thus leaving both centres and variances unchanged.

Example 8.6.4 — Scaling of independent variable.

Let

$$\begin{aligned} y(t) &= x(\alpha t) \quad (\alpha \in \mathbb{R}, \alpha \neq 0) \\ \Rightarrow \quad \hat{y}(\Omega) &= \frac{1}{|\alpha|}\hat{x}\left(\frac{\Omega}{\alpha}\right) \end{aligned} \tag{8.12}$$

Effect in time domain

The new time centre is given by

$$t_{0(new)} = \frac{\int_{-\infty}^{\infty} t\,|x(\alpha t)|^2\,dt}{\int_{-\infty}^{\infty} |x(\alpha t)|^2\,dt}$$

Put

$$\begin{aligned} \lambda &= \alpha t \\ \Rightarrow d\lambda &= \alpha dt \\ \Rightarrow t_{0(new)} &= \frac{\frac{1}{\alpha^2}\int_{-\infty}^{\infty} \lambda\,|x(\lambda)|^2\,d\lambda}{\frac{1}{\alpha}\int_{-\infty}^{\infty} |x(\lambda)|^2\,d\lambda} \\ \Rightarrow t_{0(new)} &= \frac{1}{\alpha} t_0 \end{aligned} \tag{8.13}$$

Using similar reasoning, it can be proved that

$$\sigma_{t(new)}^2 = \frac{1}{\alpha^2}\sigma_t^2 \tag{8.14}$$

Note that even if α is negative, the limits of integration would still remain same as there would be reversal of limits twice.

Effect in frequency domain

Starting with $\hat{x}\left(\frac{\Omega}{\alpha}\right)$ it can be proved that

$$\Omega_{0(new)} = \alpha\,\Omega_0 \tag{8.15}$$

$$\sigma^2_{\Omega(new)} = \alpha^2\sigma^2_\Omega \tag{8.16}$$

The multiplier $\left(\frac{1}{\alpha}\right)$ is not considered as it neither affects centre nor the variance. The students should verify the above results as an exercise.

Effect on time bandwidth product

The new time bandwidth product will be given by

$$\begin{aligned}\sigma^2_{t(new)}\sigma^2_{\Omega(new)} &= \left(\frac{1}{\alpha^2}\sigma_t^2\right)\left(\alpha^2\sigma^2_\Omega\right)\\ &= \sigma_t^2\sigma^2_\Omega\end{aligned} \tag{8.17}$$

Thus, the time-bandwidth product is invariant to scaling of the independent variable.

8.7 | Properties of theTime Bandwidth Product

Thus, to summarize, the time bandwidth product is invariant to the following operations

- Shifting waveform in time
- Shifting waveform in frequency(modulation in time)
- Multiplying the function by a constant
- Scaling of independent variable

The time bandwidth product is thus a robust measure of combined time and frequency spread of a signal. It is essentially a property of the **shape** of the waveform.

R **Challenge:** Can two differently shaped waveforms have the same time bandwidth product?
In the last chapter, we had noted that the time-bandwidth product of the Haar scaling function was ∞. The above results prove that the time-bandwidth product of **any** gate/rectangular function is ∞. The next fundamental question which comes to mind is **what is the minimum value of this product?**

8.7.1 Simplification of the Time-bandwidth Formula

Without loss of generality,we can assume that a function has both time and frequency centre zero (because that does not affect the time bandwidth product).

$$\sigma_t^2\sigma_\Omega^2 = \frac{\int_{-\infty}^{\infty} t^2 \mid x(t) \mid^2 \, dt}{\| x \|_2^2} \frac{\int_{-\infty}^{\infty} \Omega^2 \mid \hat{x}(\Omega) \mid^2 \, d\Omega}{\| \hat{x} \|_2^2} \tag{8.18}$$

Now, we simplify the numerator of the frequency variance.

$$\int_{-\infty}^{\infty} \Omega^2 \mid \hat{x}(\Omega) \mid^2 \, d\Omega = \int_{-\infty}^{\infty} \mid j\Omega\hat{x}(\Omega) \mid^2 \, d\Omega$$

We know that if $x(t) \xrightarrow{\mathbb{F}} \hat{x}(\Omega)$

$$\frac{dx(t)}{dt} \xrightarrow{\mathbb{F}} j\Omega\hat{x}(\Omega) \tag{8.19}$$

By Parseval's theorem, $\| \hat{x}(\Omega) \|_2^2 = 2\pi \| x(t) \|_2^2$

$$\| j\Omega\hat{x}(\Omega) \|_2^2 = 2\pi \left\| \frac{dx(t)}{dt} \right\|_2^2$$

Using above results in Eq. (8.18), we get

$$\begin{aligned} \sigma_t^2\sigma_\Omega^2 &= \frac{\| tx(t) \|_2^2}{\| x \|_2^2} \frac{\left\| \frac{dx(t)}{dt} \right\|_2^2}{\| x \|_2^2} \\ &= \frac{\| tx(t) \|_2^2 \cdot \left\| \frac{dx(t)}{dt} \right\|_2^2}{\| x \|_2^4} \end{aligned} \tag{8.20}$$

The next step is to minimize this product, which will be discussed in the next subsequent sections.

8.8 | Evaluating and Bounding the Time-bandwidth Product

We have so far been working on how to evaluate a measure for the joint resolution of time and frequency. Given a wavelet function, the product of the time and frequency variances could give us a precise idea as to how well we can focus in both the domains simultaneously. This time-bandwidth product is invariant to translation and modulation in time domain. Also, the time-bandwidth product is invariant to scaling of the dependent and the independent variable and is a direct function of the shape. We have derived the necessary expressions for the time and frequency variances and will try to evaluate it further and find out the constraint induced by nature on this time-bandwidth product. We will essentially try to find the lower bound on the time-bandwidth product. This will also give us a mathematical proof of the uncertainty that exists in nature when we try to focus in both the domains simultaneously.

8.9 | Evaluation of Time-bandwidth Product $\sigma_t^2\sigma_\Omega^2$

Let us recall the expressions for the time and frequency variances which are given as:

$$\sigma_t^2 = \frac{\int_{-\infty}^{+\infty} t^2 \mid x(t) \mid^2 \, dt}{\int_{-\infty}^{+\infty} \mid x(t) \mid^2 \, dt} \tag{8.21}$$

$$= \frac{\|tx(t)\|_2^2}{\|x(t)\|_2^2} \tag{8.22}$$

$$\sigma_\Omega^2 = \frac{\int_{-\infty}^{+\infty} \left|\frac{d}{dt}x(t)\right|^2 dt}{\int_{-\infty}^{+\infty} |x(t)|^2\, dt}$$

$$= \frac{\|\frac{d}{dt}x(t)\|_2^2}{\|x(t)\|_2^2} \tag{8.23}$$

The time-bandwidth product can therefore be obtained from Eqs (8.21) and (8.23) as:

$$\text{Time band width product} = \frac{\|tx(t)\|_2^2}{\|x(t)\|_2^2}\frac{\|\frac{d}{dt}x(t)\|_2^2}{\|x(t)\|_2^2} \tag{8.24}$$

NOTE:

R While stating the above equations we have put $t_0 = 0$ and $\sigma_0 = 0$. We could do this because the time-bandwidth product is invariant to time and frequency domain shifts. Thus, without the loss of generality we can always obtain a function centred at origin in both the domains either by shifting or by modulation.

Let us now evaluate the numerator first:

$$\text{Numerator} = \|tx(t)\|_2^2 \left\|\frac{d}{dt}x(t)\right\|_2^2 \tag{8.25}$$

To simplify it further, we need to interpret the functions $tx(t)$ and $\frac{d}{dt}x(t)$ as vectors $\vec{v}_1$ and $\vec{v}_2$ respectively. Now, as per the basic principle of inner product of two vectors:

$$\langle \vec{v}_1, \vec{v}_2 \rangle = |\vec{v}_1||\vec{v}_2|\cos\theta \qquad (\theta = \text{angle between the two vectors})$$

$$|\langle \vec{v}_1, \vec{v}_2 \rangle|^2 = |\vec{v}_1|^2 |\vec{v}_2|^2 \cos^2\theta$$

$$\text{Therefore, } |\langle \vec{v}_1, \vec{v}_2 \rangle|^2 \le |\vec{v}_1|^2 |\vec{v}_2|^2 \qquad (\text{as } \cos^2\theta \le 1)$$

This principle can be generalized to the functions viewed as vectors and in fact is a very important theorem in functional analysis called **Cauchy-Schwarz inequality**. The theorem states that if there are two functions say f_1 and f_2 such that $f_1, f_2 \in L_2(\mathbb{R})$ then,

$$|\langle f_1, f_2 \rangle|^2 \le |f_1|^2 |f_2|^2 \tag{8.26}$$

Thus, from Eq. (8.26) the numerator in Eq. (8.24) can be written as:

$$\text{Numerator} \ge \left|\left\langle tx(t), \frac{d}{dt}x(t) \right\rangle\right|^2 \tag{8.27}$$

NOTE:
As per the inequality we are assuming that the functions belong to space $L_2(\mathbb{R})$. Therefore to ensure validity of this inequality in our time-bandwidth evaluation it is important to choose $x(t)$ such that $tx(t) \in L_2(\mathbb{R})$ and $\frac{d}{dt}x(t) \in L_2(\mathbb{R})$. If this condition is not satisfied then the integral diverges and there cannot be a lower bound.

To illustrate the above condition let us consider an example as in Fig. 8.6:
Consider,

$$x(t) = 1 \qquad 0 \le t \le 1$$

The function $\frac{d}{dt}x(t)$ will look like in Fig. 8.2.

Now the function in Fig. 8.7 is not square integrable because it contains two impulses which have infinite energy. This can be well understood by zooming the view a bit on the impulse. The zoomed view of the impulse will be as in Fig. 8.8.

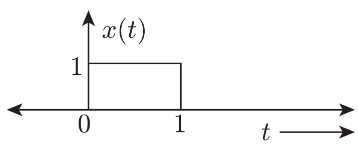

Figure 8.6 | *Function belonging to $L_2(\mathbb{R})$*

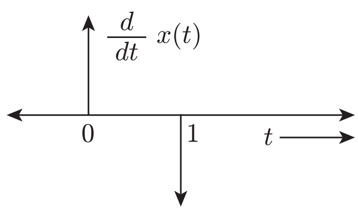

Figure 8.7 | *Function $\frac{d}{dt}x(t)$*

Now,

$$\lim_{\Delta \to 0} \int_{-\infty}^{+\infty} \delta_\Delta^2(t)\,dt$$

diverges.
Therefore, for the time-bandwidth product to have a lower bound the function and its derivative both should belong to $L_2(\mathbb{R})$.

The RHS of Eq. (8.27) can be written as:

$$\left| \left\langle tx(t), \frac{d}{dt}x(t) \right\rangle \right|^2 = \left| \int_{-\infty}^{+\infty} tx(t) \overline{\frac{d}{dt}x(t)}\,dt \right|^2 \tag{8.28}$$

Now, for any complex number Z we have the following relation:

$$|Z|^2 \geq |Re\{Z\}|^2$$

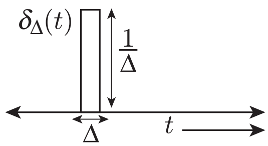

Figure 8.8 | *Delta function*

Therefore from Eqs. (8.27) and (8.28)

$$\text{Numerator} \geq \left| Re\left\{ \int_{-\infty}^{+\infty} tx(t) \overline{\frac{d}{dt}x(t)dt} \right\} \right|^2 \tag{8.29}$$

R REMARK:

t being a real variable $\overline{\frac{d}{dt}x(t)} = \frac{d}{dt}\overline{x(t)}$

Thus,

$$\text{Numerator} \geq \left| Re\left\{ \int_{-\infty}^{+\infty} tx(t) \frac{d}{dt}\overline{x(t)}dt \right\} \right|^2$$

$$\geq \left| \int_{-\infty}^{+\infty} tRe\left\{ x(t) \frac{d}{dt}\overline{x(t)} \right\} dt \right|^2 \tag{8.30}$$

Now,

$$Re\left\{ x(t)\frac{d}{dt}\overline{x(t)} \right\} = \frac{1}{2}\left\{ x(t)\frac{d}{dt}\overline{x(t)} + \overline{x(t)}\frac{d}{dt}x(t) \right\}$$

$$= \frac{1}{2}\frac{d}{dt}\{x(t)\overline{x(t)}\}$$

$$= \frac{1}{2}\frac{d}{dt}|x(t)|^2 \tag{8.31}$$

Therefore from Eqs. (8.30) and (8.31)

$$\text{Numerator } \geq \left| \frac{1}{2}\int_{-\infty}^{+\infty} t\frac{d}{dt}|x(t)|^2\ dt \right|^2 \tag{8.32}$$

Solving the integral term by parts we get

$$\int_{-\infty}^{+\infty} t\frac{d}{dt}|x(t)|^2\ dt = [t|x(t)|^2]_{-\infty}^{+\infty} - \int_{-\infty}^{+\infty} |x(t)|^2\ dt \tag{8.33}$$

$$= -\int_{-\infty}^{+\infty} |x(t)|^2\ dt$$

NOTE:

We have agreed that $\int_{-\infty}^{+\infty} t^2 \mid x(t) \mid^2 \, dt$ should be finite for a bound to exist. Therefore for the integral to converge the function $t^2 \mid x(t) \mid^2$ should decay to zero value as $t \to +\infty$ and $t \to -\infty$. $t^2 \mid x(t) \mid^2 \to 0$ guarantees $t \mid x(t) \mid^2 \to 0$ as $t \to +\infty$ and $t \to -\infty$. Thus, the term $[t \mid x(t) \mid^2]_{-\infty}^{+\infty}$ in Eq. (8.33) becomes zero.

Therefore

$$\int_{-\infty}^{+\infty} t \frac{d}{dt} \mid x(t) \mid^2 \, dt = -\| x \|_2^2 \tag{8.34}$$

Finally from Eqs. (8.32) and (8.34) we get;

$$\text{Numerator of the time bandwidth product} \geq \left| \frac{1}{2} (-\| x \|_2^2) \right|^2$$

$$\geq \frac{1}{4} \| x \|_2^2 \| x \|_2^2 \tag{8.35}$$

Substituting the value of the numerator in Eq. (8.24) of the time bandwidth product we get;

$$\text{Time bandwidth product} \geq \frac{\frac{1}{4} \| x \|_2^4}{\| x \|_2^4}$$

$$\geq \frac{1}{4} \tag{8.36}$$

CONCLUSION:

The time-bandwidth product can never be less than 0.25. The result is fundamental to signal processing and has no relation with the technology and tools available at a particular time. The result tells us that, no matter what we do, we can never get a function with finite energy confined beyond a certain range in both time and frequency simultaneously.

Now, the optimal function in the sense of time-bandwidth product means that the Cauchy-Schwarz inequality becomes an equality. Recall that the inequality essentially arises due to the $\cos^2 \theta$ term in the vectorial interpretation of the functions. Thus to attain equality $\cos^2 \theta = 1$, i.e. we need the vectors $tx(t)$ and $\frac{d}{dt} x(t)$ to be collinear.

NOTE:

Two vectors being collinear means that they should be linearly dependent i.e. one of the two vectors should be a multiple of other.

Thus to get the optimal solution we need to satisfy the given condition:

$$\frac{d}{dt} x(t) = \gamma_0 . t . x(t) \qquad (\gamma_0 = \text{constant})$$

Therefore, solving the above equation

$$\ln x = \gamma_0 . \frac{t^2}{2} + c_0 \qquad (c_0 = \text{constant of integration})$$

$$e^{\ln x} = e^{\gamma_0 \frac{t^2}{2} + c_0}$$

$$x(t) = e^{c_0} . e^{\gamma_0 \frac{t^2}{2}}$$

$$x(t) = c.e^{\gamma_0 \frac{t^2}{2}} \qquad (c = \text{constant}) \tag{8.37}$$

R **REMARK**:

For the function $x(t)$ to be in $L_2(\mathbb{R})$, $|e^{c_0}|^2 . |e^{\gamma_0 \frac{t^2}{2}}|^2$ should be integrable. This is possible only if γ_0 has a negative real part.

Thus, one optimal function with time bandwidth product 0.25 can be of the form $\mathbf{e}^{-\frac{t^2}{2}}$; the Gaussian. Here $\eta_0 = -1$ and $\mathbf{c} = \mathbf{1}$ as in Eq. (8.37).

8.10 | Self Evaluation Quiz Examples

Example 8.10.1 — Verify $\overline{\frac{d}{dt} x(t)} = \frac{d}{dt} \overline{x(t)}$, where $x(t)$ is any complex function and t is real.

Ans. Let $x(t) = a(t) + ib(t)$ be a complex function.

$$\frac{d}{dt} x(t) = \frac{d}{dt}(a(t) + ib(t))$$

$$\overline{\frac{d}{dt} x(t)} = \overline{\frac{d}{dt}(a(t) + ib(t))}$$

$$= \overline{a'(t) + jb'(t)} \qquad \{a'(t) = \frac{d}{dt} a(t) \text{ and } b'(t) = \frac{d}{dt} b(t) \tag{8.38}$$

$$\overline{\frac{d}{dt} x(t)} = a'(t) - jb'(t) \tag{8.39}$$

$$\frac{d}{dt} \overline{x(t)} = \frac{d}{dt} \overline{a(t) + jb(t)}$$

$$= \frac{d}{dt}a(t) - jb(t)$$

$$\frac{d}{dt}\overline{x(t)} = a'(t) - jb'(t) \qquad \{a'(t) = \frac{d}{dt}a(t) \text{ and } b'(t) = \frac{d}{dt}b(t)\} \tag{8.40}$$

Therefore from Eqs. (8.38) and (8.39) we get;

$$\overline{\frac{d}{dt}x(t)} = \frac{d}{dt}\overline{x(t)} \qquad \text{(proved)}$$

Example 8.10.2 — Does $\delta_\Delta(t)$ belong to $L_1(\mathbb{R})$ or $L_2(\mathbb{R})$?

Ans. The function $\delta_\Delta(t)$ looks as in Fig. 8.8.

For a function $x(t)$ to be in $L_1(\mathbb{R})$, $\int_{-\infty}^{+\infty} |x(t)|\, dt$ should be finite.
Now,

$$\lim_{\Delta\to 0}\int_{-\infty}^{+\infty}\delta_\Delta(t)dt = \lim_{\Delta\to 0}\int_0^{+\Delta}\frac{1}{\Delta}dt$$
$$= 1$$

Therefore, $\delta_\Delta(t)$ belong to $L_1(\mathbb{R})$.

For a function $x(t)$ to be in $L_2(\mathbb{R})$, $\int_{-\infty}^{+\infty} |x(t)|^2\, dt$ should be finite.

$$\lim_{\Delta\to 0}\int_{-\infty}^{+\infty}\delta_\Delta^2(t)dt = \lim_{\Delta\to 0}\int_0^{+\Delta}\frac{1}{\Delta^2}dt$$

The above integral does not converge, therefore, $\delta_\Delta(t)$ does not belong to $L_2(\mathbb{R})$.

Example 8.10.3 — What should be the constraint on function $x(t)$ so that the integral $\int_{-\infty}^{+\infty} t\,|x(t)|^2\, dt$ converge?

Ans. For the integral to converge the function $|x(t)|^2$ should decay to a zero value as $t \to +\infty$ and $t \to -\infty$, i.e.

$$\lim_{t\to\pm\infty}|x(t)|^2 = 0$$

Exercises

Exercise 8.1

Calculate the time variance and frequency variance for the function given in Fig. 8.9.

Hint: (i) Here, $x(t)$ is given as, $x(t) = 1 - |t|$, for $-1 \le t \le 1$. Hence,

$$\| x(t) \|_2^2 = \int_{-\infty}^{\infty} | x(t) |^2 \, dt$$

$$= 2\int_0^1 (1-t)^2 \, dt$$

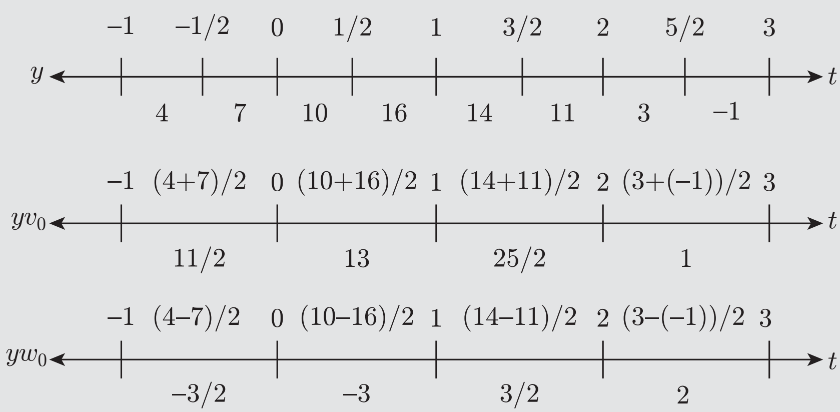

Figure 8.9 | *Functions for Q*

Let, $1 - t = \lambda$

$\Rightarrow dt = -d\lambda$ and

limits are given as, $x : 0$ to $1 \Rightarrow \lambda : 1$ to 0.

$$\| x(t) \|_2^2 = 2\int_0^1 (1-t)^2 \, dt$$

$$= -2\int_1^0 \lambda^2 \, d\lambda$$

$$= 2\int_0^1 \lambda^2 \, d\lambda$$

$$= 2\frac{\lambda^3}{3} \Big|_0^1$$

$$= \frac{2}{3}$$

Now, mean is given as

$$t_0 = \int_{-\infty}^{\infty} t p_x(t) dt$$

$$= \int_{-\infty}^{\infty} \frac{t\,|\,x(t)\,|^2}{\|\,x(t)\,\|_2^2}\,dt$$

By looking at the figure it can be assumed that, the mean would be at the centre of −1 and 1, i.e. at zero. Therefore, mean is given as

$$t_0 = 0$$

Now, we will find the time variance.

$$\sigma_t^2 = \int_{-\infty}^{\infty} (t - t_0)^2\, p_x(t)\,dt$$

$$= \int_{-\infty}^{\infty} t^2 \frac{|\,x(t)\,|^2}{\|\,x(t)\,\|_2^2}\,dt$$

$$= \int_{-\infty}^{\infty} t^2 \frac{|\,x(t)\,|^2}{\frac{2}{3}}\,dt$$

$$= 2 \times \frac{3}{2} \int_0^1 t^2 (1 - t)^2\,dt$$

$$= 3 \int_0^1 (t^2 - 2t^3 + t^4)\,dt$$

$$= 3 \left[\frac{t^3}{3} - \frac{2t^4}{4} + \frac{t^5}{5} \right]_0^1$$

$$= 3 \left[\frac{1}{3} - \frac{1}{2} + \frac{1}{5} \right]$$

$$= 3 \left[\frac{1}{30} \right]$$

$$= \frac{1}{10}$$

$$= 0.1$$

Now, we will find the angular frequency variance.

$$\sigma_\Omega^2 = \int_{-\infty}^{\infty} (\Omega - \Omega_0)^2\, p_{\hat{x}}(\Omega)\,d\Omega$$

$$= \frac{\left\| \frac{dx(t)}{dt} \right\|_2^2}{\|\,x(t)\,\|_2^2}$$

Now, $\frac{dx(t)}{dt}$ is shown in Fig. 8.10

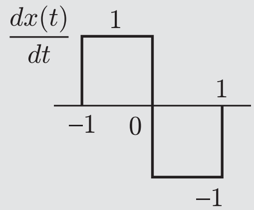

Figure 8.10 | $\frac{dx(t)}{dt}$ *for Exercise 8.1(i)*

$$\left\|\frac{dx(t)}{dt}\right\|_2^2=\int_{-\infty}^{\infty}\left|\frac{dx(t)}{dt}\right|^2 dt$$
$$=2\int_0^1 1dt$$
$$=2$$

Hence, the angular frequency variance is given as,

$$\sigma_\Omega^2=\frac{\left\|\frac{dx(t)}{dt}\right\|_2^2}{\|x(t)\|_2^2}$$
$$=\frac{2}{\frac{2}{3}}$$
$$=3$$

(ii) Here, $x(t)$ is given as, $x(t)=\sin(\pi t)$, for $-1\le t\le 1$. Hence,

$$\|x(t)\|_2^2=\int_{-\infty}^{\infty}|x(t)|^2\,dt$$
$$=2\int_0^1\sin^2(\pi t)\,dt$$
$$=2\int_0^1\frac{1-\cos(2\pi t)}{2}\,dt$$
$$=\left[t-\frac{\sin(2\pi t)}{2\pi}\right]_0^1$$
$$=1-0$$
$$=1$$

Now, mean is given as,

$$t_0=\int_{-\infty}^{\infty}tp_x(t)dt$$
$$=\int_{-\infty}^{\infty}\frac{t\,|x(t)|^2}{\|x(t)\|_2^2}\,dt$$

By looking at the diagram, the mean is assumed to be at the centre of -1 and 1, i.e. at zero. Therefore, mean is given as

$$t_0 = 0$$

Now, we will find the time variance.

$$\begin{aligned}
\sigma_t^2 &= \int_{-\infty}^{\infty}(t-t_0)^2 p_x(t)dt \\
&= \int_{-\infty}^{\infty} t^2 \frac{|x(t)|^2}{\|x(t)\|_2^2} dt \\
&= \int_{-\infty}^{\infty} t^2 \frac{|x(t)|^2}{1} dt \\
&= 2\int_0^1 t^2 \sin^2(\pi t)dt \\
&= 2\int_0^1 t^2 \frac{1-\cos(2\pi t)}{2} dt \\
&= \left[\frac{t^3}{3}\right]_0^1 - \int_0^1 t^2 \cos(2\pi t)dt \\
&= \frac{1}{3} - \left[t^2 \frac{\sin(2\pi t)}{2\pi}\Big|_0^1 - \int_0^1 2t \frac{\sin(2\pi t)}{2\pi} dt\right] \\
&= \frac{1}{3} - 0 + \int_0^1 t \frac{\sin(2\pi t)}{\pi} dt \\
&= \frac{1}{3} + \left[\frac{-t}{\pi}\frac{\cos(2\pi t)}{2\pi}\right]_0^1 + \int_0^1 \frac{\cos(2\pi t)}{2\pi^2} dt \\
&= \frac{1}{3} + \frac{1}{2\pi^2} - \frac{1}{2\pi^2}\frac{\sin(2\pi t)}{2\pi}\Big|_0^1 \\
&= \frac{1}{3} + \frac{1}{2\pi^2}
\end{aligned}$$

Now, we will find the angular frequency variance.

$$\begin{aligned}
\sigma_\Omega^2 &= \int_{-\infty}^{\infty}(\Omega-\Omega_0)^2 p_{\hat{x}}(\Omega)d\Omega \\
&= \frac{\left\|\frac{dx(t)}{dt}\right\|_2^2}{\|x(t)\|_2^2}
\end{aligned}$$

Now, $\frac{dx(t)}{dt} = \pi\cos(\pi t)$ is shown in Fig. 8.11

$$\left\|\frac{dx(t)}{dt}\right\|_2^2 = \int_{-\infty}^{\infty}\left|\frac{dx(t)}{dt}\right|^2 dt$$

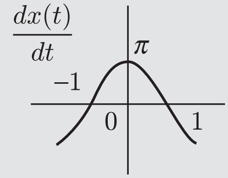

Figure 8.11 | $\frac{dx(t)}{dt}$ *for Exercise 8.1(ii)*

$$= 2\pi^2 \int_0^1 \cos^2(\pi t)dt$$

$$= 2\pi^2 \int_0^1 \frac{1+\cos(2\pi t)}{2} dt$$

$$= \pi^2 \int_0^1 (1+\cos(2\pi t))dt$$

$$= \pi^2 \left[t + \frac{\sin(2\pi t)}{2\pi} \right]_0^1$$

$$= \pi^2 \times 1$$

$$= \pi^2$$

Hence, the angular frequency variance is given as,

$$\sigma_\Omega^2 = \frac{\| \frac{dx(t)}{dt} \|_2^2}{\| x(t) \|_2^2}$$

$$= \frac{\pi^2}{1}$$

$$= \pi^2$$

(iii) Here, $x(t)$ is given as

$$x(t) = 1, \text{ for } 0 \le t \le \frac{1}{2}$$

$$= -1, \text{ for } \frac{1}{2} \le t \le 1$$

Hence,

$$\| x(t) \|_2^2 = \int_{-\infty}^{\infty} | x(t) |^2 \, dt$$

$$= \int_0^1 1 dt$$

$$= 1$$

Now, mean is given as

$$t_0 = \int_{-\infty}^{\infty} t p_x(t) dt$$

$$= \int_{-\infty}^{\infty} \frac{t\,|\,x(t)\,|^2}{\|\,x(t)\,\|_2^2} dt$$

$$= \int_0^1 t dt$$

$$= \left[\frac{t^2}{2}\right]$$

$$= \frac{1}{2}$$

Therefore, mean $t_0 = \frac{1}{2}$.

Now, we will find the time variance.

$$\sigma_t^2 = \int_{-\infty}^{\infty} (t - t_0)^2 p_x(t) dt$$

$$= \int_{-\infty}^{\infty} (t - t_0)^2 \frac{|\,x(t)\,|^2}{\|\,x(t)\,\|_2^2} dt$$

$$= \int_{-\infty}^{\infty} (t - \frac{1}{2})^2 \frac{|\,x(t)\,|^2}{1} dt$$

$$= \int_0^1 (t - \frac{1}{2})^2 dt$$

Let, $t - \frac{1}{2}$ be $= \lambda$

$\Rightarrow dt = d\lambda$ and

limits are given as, $x: 0$ to $1 \Rightarrow \lambda : \frac{-1}{2}$ to $\frac{1}{2}$.

Hence, integral becomes

$$\sigma_t^2 = \int_{\frac{-1}{2}}^{\frac{1}{2}} \lambda^2 d\lambda$$

$$= \left[\frac{\lambda^3}{3}\right]_{\frac{-1}{2}}^{\frac{1}{2}}$$

$$= \frac{1}{3}\left[\frac{1}{8} + \frac{1}{8}\right]$$

$$= \frac{1}{3} \times \frac{1}{4}$$

$$= \frac{1}{12}$$

Now, we will find the angular frequency variance.

$$\sigma_\Omega^2 = \int_{-\infty}^{\infty} (\Omega - \Omega_0)^2 \, p_{\hat{x}}(\Omega) d\Omega$$

$$= \frac{\| \frac{dx(t)}{dt} \|_2^2}{\| x(t) \|_2^2}$$

Now, $\frac{dx(t)}{dt}$ is shown in Fig. 8.12

As, impulses are not square integrable, we get

$$\| \frac{dx(t)}{dt} \|_2^2 = \int_{-\infty}^{\infty} \left| \frac{dx(t)}{dt} \right|^2 dt$$

$$= \infty$$

Hence, the angular frequency variance becomes ∞.

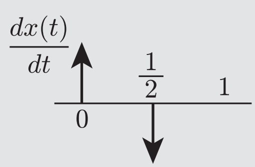

Figure 8.12 | $\frac{dx(t)}{dt}$ *for Exercise 8.1(iii)*

Exercise 8.2

Probability density function is given as,

$$p_x(t) = \frac{| x(t) |^2}{\| x(t) \|_2^2}$$

Show that, it is satisfying all the properties of PDF.

Hint: It satisfies the properties of PDF are as below:

1. $p_x(t) \geq 0 \; \forall \; t$ (It is a density in t).
2. $\int_{-\infty}^{\infty} p_x(t)dt = \int_{-\infty}^{\infty} \frac{|x(t)|^2}{\|x(t)\|_2^2} dt = \frac{\int_{-\infty}^{\infty} |x(t)|^2 \, dt}{\|x(t)\|_2^2} = \frac{\|x(t)\|_2^2}{\|x(t)\|_2^2} = 1.$

Exercise 8.3

Is it possible for two differently shaped waveforms to have the same time-bandwidth product?

Hint: Yes. It is possible for two different shaped waveforms to have the same time-bandwidth product. It is due the **duality property** of Fourier transform. The property states that

$$\begin{aligned} &\text{If} \quad x(t) \xrightarrow{\mathbb{F}} \hat{x}(\Omega) \\ &\text{then} \\ &\hat{x}(t) \xrightarrow{\mathbb{F}} 2\pi x(-\Omega) \end{aligned} \tag{8.39}$$

Thus, if instead of $x(t)$, the input signal is $\hat{x}(t)$, the time bandwidth product will be given by

$$\begin{aligned} \sigma_t^2 \sigma_\Omega^2 &= \frac{\int_{-\infty}^{\infty} t^2 |\hat{x}(t)|^2 \, dt}{\int_{-\infty}^{\infty} |\hat{x}(t)|^2 \, dt} \frac{\int_{-\infty}^{\infty} \Omega^2 (2\pi)^2 |x(-\Omega)|^2 \, d\Omega}{\int_{-\infty}^{\infty} (2\pi)^2 |x(-\Omega)|^2 \, d\Omega} \\ &= \frac{\int_{-\infty}^{\infty} t^2 |\hat{x}(t)|^2 \, dt}{\int_{-\infty}^{\infty} |\hat{x}(t)|^2 \, dt} \frac{\int_{-\infty}^{\infty} \Omega^2 |x(-\Omega)|^2 \, d\Omega}{\int_{-\infty}^{\infty} |x(-\Omega)|^2 \, d\Omega} \\ &\text{now, substitute } t = \lambda \text{ and } -\Omega = t \\ &= \frac{\int_{-\infty}^{\infty} \lambda^2 |\hat{x}(\lambda)|^2 \, d\lambda}{\int_{-\infty}^{\infty} |\hat{x}(\lambda)|^2 \, d\lambda} \frac{\int_{\infty}^{-\infty} t^2 |x(t)|^2 \, dt}{\int_{\infty}^{-\infty} |x(t)|^2 \, dt} \\ &\text{note reversal of limits} \\ &= \frac{\int_{-\infty}^{\infty} \lambda^2 |\hat{x}(\lambda)|^2 \, d\lambda}{\int_{-\infty}^{\infty} |\hat{x}(\lambda)|^2 \, d\lambda} \frac{\int_{-\infty}^{\infty} t^2 |x(t)|^2 \, dt}{\int_{-\infty}^{\infty} |x(t)|^2 \, dt} \\ &\text{limit reversed again, sign unchanged} \end{aligned} \tag{8.40}$$

We see that Eq. (8.40) is same as Eq. (8.18) thus proving that the time bandwidth product is unchanged. Thus the time bandwidth product of $x(t)$ and $\hat{x}(t)$ is same.

Exercise 8.4

Find the time bandwidth product of the following functions

- $e^{-|t|}$
- $\dfrac{1}{1+t^2}$
- $(1-|t|)[u(t+1)-u(t-1)]$, where $u(t)$ is the Heaviside step function.
- $\left(\dfrac{\sin(t)}{t}\right)^2$
- $\dfrac{1}{\sqrt{2\pi}}e^{\frac{-x^2}{2}}$

Hint: (1) $f(t)=e^{-|t|}$

$$\begin{aligned}\|f\|_2^2 &= \int_{-\infty}^{\infty}|f(t)|^2\,dt\\ &= \int_{-\infty}^{\infty}e^{-2|t|}dt\\ &= 2\int_0^{\infty}e^{-2t}dt\\ &= 2\left[\frac{e^{-2t}}{-2}\right]_0^{\infty}\\ &= 2\left(\frac{1}{2}\right) \qquad = 1\end{aligned} \tag{8.41}$$

Calculating the numerator,

$$\int_{-\infty}^{\infty}t^2e^{-2|t|}dt \quad = \int_0^{\infty}t^2e^{-2t}dt$$

integrating by parts repeatedly, we get

$$\begin{aligned}&=2\left(\left[t^2\frac{e^{-2t}}{-2}\right]_0^{\infty}+\left[t\frac{e^{-2t}}{-2}\right]_0^{\infty}+\frac{1}{2}\left[\frac{e^{-2t}}{-2}\right]_0^{\infty}\right)\\ &=2\left(\frac{1}{4}\right)\end{aligned}$$

t^2e^{-2t} and $te^{-2t}\rightarrow 0$ as $t\rightarrow\infty$ because

e^{-2t} decays faster than increase of t^2 and t (8.42)

Calculating the second term of numerator,

$$\begin{aligned}\int_{-\infty}^{\infty}\left|\frac{dx(t)}{dt}\right|^2 dt &= \int_{-\infty}^{\infty}\left|\frac{d}{dt}e^{-|t|}\right|^2 dt \\ &= 2\int_0^{\infty} e^{-2t}\,dt \\ &= 2\left[\frac{e^{-2t}}{-2}\right]_0^{\infty} \\ &= 1\end{aligned} \tag{8.43}$$

Thus, the time bandwidth product will be given by

$$\sigma_t^2\sigma_\Omega^2 = \frac{\frac{1}{2}\cdot 1}{1} = \frac{1}{2} \tag{8.44}$$

(2) $f(t) = \dfrac{1}{1+t^2}$

The Fourier transform of $e^{-|t|}$ is $\dfrac{2}{1+t^2}$. Thus, by use of duality property, the time bandwidth product of $\dfrac{2}{1+t^2}$ will be same as that of $e^{-|t|}$. Also, since multiplying by a constant does not affect the product, the time-bandwidth product of $\dfrac{1}{1+t^2}$ will be same as $\dfrac{2}{1+t^2}$. Hence, the time bandwidth product

$$\text{TBW product}\left(\frac{1}{1+t^2}\right) = \frac{1}{2}$$

(3) $f(t) = \left(1-|t|\right)[u(t+1)-u(t-1)]$

The waveform of such a function is as shown in Fig. 8.13.
Calculating the numerator terms

$$\begin{aligned}\int_{-\infty}^{\infty}\left|\frac{dx(t)}{dt}\right|^2 dt &= \int_{-1}^{0}(1)dt + \int_0^1(-1)dt \\ &= [1]+[1] = 2\end{aligned} \tag{8.45}$$

$$\begin{aligned}\int_{-1}^{1} t^2(1-|t|)^2\,dt &= 2\int_0^1 t^2(1-t)^2\,dt \\ &= 2\int_0^1 (t^2-2t^3+t^4)dt \\ &= 2\left(\left[\frac{t^3}{3}\right]_0^1 - 2\left[\frac{t^4}{4}\right]_0^1 + \left[\frac{t^5}{5}\right]_0^1\right) \\ &= \frac{1}{15}\end{aligned} \tag{8.46}$$

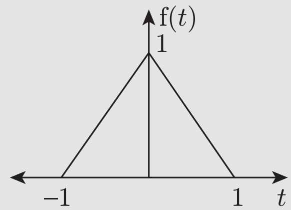

Figure 8.13 | $f(t)=1-|t|$

Calculating norm-squared of the function

$$\begin{aligned}\int_{-\infty}^{\infty}|f(t)|^2\,dt &= 2\int_0^1 (1-t^2)dt \\ &= 2\left([1]-2\left[\frac{t^2}{2}\right]_0^1+\left[\frac{t^3}{3}\right]_0^1\right) \qquad (8.47) \\ &= \frac{2}{3}\end{aligned}$$

Therefore, the time-bandwidth product is given by

$$\sigma_t^2\sigma_\Omega^2 = \frac{2\times\frac{1}{15}}{\frac{2}{3}\times\frac{2}{3}} = 0.3 \qquad (8.48)$$

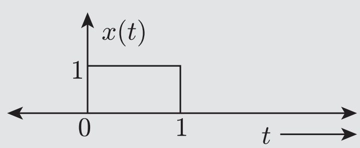

Figure 8.14 | $x(t)=1$

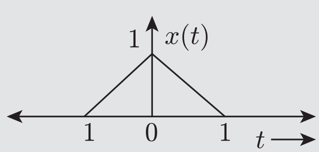

Figure 8.15 | $x(\mathrm{t})=1-|x|$

Exercise 8.5

Find the time-bandwidth product of the functions given by Eqs (8.21), (8.23) and (8.24) graphically shown in Figs 8.14, 8.15 and 8.16 respectively;

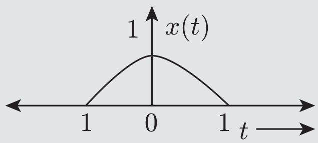

Figure 8.16 | $x(t) = 1 - x^2$

find which one is close to the optimum value of 0.25.

$$x(t) = 1 \qquad 0 \le t \le 1 \tag{8.49}$$

$$x(t) = 1 - |x| \qquad -1 \le t \le 1 \tag{8.50}$$

$$x(t) = 1 - x^2 \qquad -1 \le t \le 1 \tag{8.51}$$

Hint: The time-bandwidth product of a function can be found out as mentioned in Eq. 8.21 i.e.

$$\text{Time bandwidth product} = \frac{\| tx(t) \|_2^2}{\| x(t) \|_2^2} \frac{\| \frac{d}{dt} x(t) \|_2^2}{\| x(t) \|_2^2}$$

(i) For the function in Fig. 8.9, as discussed the term $\| \frac{d}{dt} x(t) \|_2^2$ do not converge since it is an impulse with infinite energy. Therefore the function in Fig. 8.11 has no bound on the time-bandwidth product and its time-bandwidth product tends to ∞.

(ii) For the function in Fig. 8.10

$$\| x(t) \|_2^2 = \int_{-1}^{1} (1 - |t|)^2 \, dt$$

$$= 2\int_0^1 (1-t)^2 \, dt$$

$$= \frac{2}{3}$$

$$\| tx(t) \|_2^2 = \int_{-1}^{1} t^2 (1 - |t|)^2 \, dt$$

$$= 2\int_0^1 t^2 (1-t)^2 \, dt$$

$$= \frac{1}{15}$$

$$\| \frac{d}{dt} x(t) \|_2^2 = \int_{-1}^{1} (\frac{d}{dt}(1 - |t|))^2 \, dt$$

$$= \int_{-1}^{1} (-1)^2 \, dt$$

$$= 2$$

Therefore, the time band width product is given by:

$$\text{Time-bandwidth product} = \frac{\| tx(t) \|_2^2}{\| x(t) \|_2^2} \frac{\| \frac{d}{dt} x(t) \|_2^2}{\| x(t) \|_2^2} = 0.3$$

iii) For the function in Fig. 8.11

$$\| x(t) \|_2^2 = \int_{-1}^{1} (1 - t^2)^2 \, dt$$

$$= 2\int_{0}^{1} (1 - t^2)^2 \, dt$$

$$= \frac{16}{15}$$

$$\| tx(t) \|_2^2 = \int_{-1}^{1} t^2 (1 - t^2)^2 \, dt$$

$$= 2\int_{0}^{1} t^2 (1 - t^2)^2 \, dt$$

$$= \frac{16}{105}$$

$$\| \frac{d}{dt} x(t) \|_2^2 = \int_{-1}^{1} \left(\frac{d}{dt}(1 - t^2)\right)^2 dt$$

$$= \int_{-1}^{1} (-2t)^2 \, dt$$

$$= 8\int_{0}^{1} t^2 \, dt$$

$$= \frac{8}{3}$$

Therefore, the time-bandwidth product is given by:

$$\text{Time-bandwidth product} = \frac{\| tx(t) \|_2^2}{\| x(t) \|_2^2} \frac{\| \frac{d}{dt} x(t) \|_2^2}{\| x(t) \|_2^2} = 0.357$$

Thus, from the results of (i), (ii) and (iii) we can conclude that the function in Fig. 8.10, i.e. $x(t) = 1 - | x |$, where $-1 \le t \le 1$ having its time-bandwidth product equal to 0.3 is close to the optimum.

Chapter 9

Time Frequency Plane and Tilings

9.1 | Introduction

Conclusions drawn from Chapter 8 are as follows:

- Time-bandwidth product= time variance (σ_t^2) × frequency variance (σ_Ω^2)
- Time-bandwidth product $\sigma_t^2\,\sigma_\Omega^2$ for any function $x \in L_2(\mathbb{R}) \geq 0.25$.
- We also showed that Gaussian function $x(t) = e^{-t^2/2}$ is an example of an optimal function in sense of time-bandwidth product. Other optimal functions can be obtained by modulating this $x(t)$ with a term of the form $e^{j\alpha t^2}$.
- A more general optimal function is of the form $e^{\gamma_0 t^2/2}$, where $Re(\gamma_0)$ is negative. γ_0 can be complex in general.
- We know that the Gaussian is optimal. It brings us both good and bad news. Good news is that we were able to find an optimal function, i.e. Gaussian. Bad news is that Gaussian is unrealisable in exact sense in a physical system.

R **Why do we say that the Gaussian is physically unrealisable?** Take for example the exponential time waveform or the exponential time waveform modulated by a sinusoid. These are easily realizable. Circuits which comprise of resistors, inductors, capacitors when excited say with a step or a sinusoid give us either exponentially decaying sinusoids or exponentially decaying transients and therefore those are easy to generate with physical system. Unfortunately there is no meaningful physical system that can generate the Gaussian waveform. So Gaussian is good news in statistical density but bad news as far as the functions in time domain are concerned. In the field of digital communication when one talks of Gaussian mean shift keying or Gaussian minimum shift keying, the word Gaussian there refers to a Gaussian pattern in the impulse response whether it is phase or amplitude. But there again it is really hard to realize a Gaussian filter. So it is difficult to realize in a physical system and can only be approximated.

Now next question arises **if not Gaussian, then, can we use a cascade of two simple systems to realize a function which is close to optimal?**

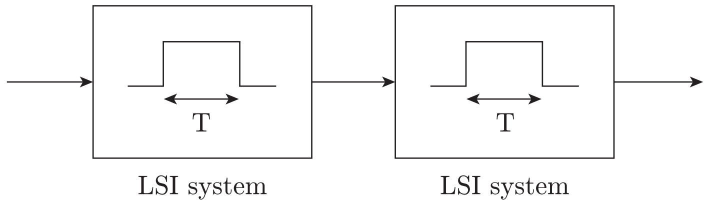

Figure 9.1 | *Cascade of two LSI system*

In other words when we started with Haar we had a terrible time bandwidth product which was infinite. **Now can we do a little better?**. Suppose we took a cascade of two systems each of whose impulse response is essentially a pulse of width T, i.e., instead of taking one pulse take a cascade of them as shown in Fig. 9.1. This together forms a composite LSI system. The impulse response of this composite LSI system is the convolution of the two pulses which will result in a triangular pulse as shown in Fig. 9.2.

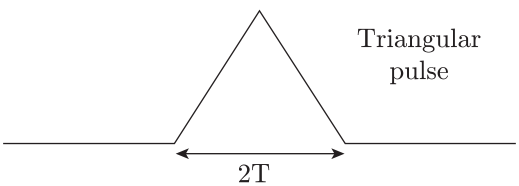

Figure 9.2 | *Triangular pulse obtained by convolution of two pulses*

R The **physical interpretation** is as follows:
When we have an LSI system with an impulse response equal to a pulse what we are essentially doing is a 'sample and hold process'. So if an impulse results in a pulse we are essentially sampling a point and holding it for the duration of the pulse. So if we have two such sample and hold then we are effectively talking about a triangular impulse response.

Now the natural question to ask is **what can we say about the time-bandwidth product of this triangular pulse and how good or bad is it compared to the Gaussian?**
The time bandwidth product of $x(t) = 1-|t|$, where $0 \le t \le 1$ as shown in Fig. 9.3.

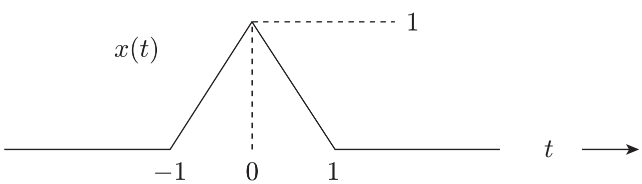

Figure 9.3 | *Triangular pulse centred at 0*

We don't need to worry where this triangular pulse lies. So we can as well make its centre = 0. We don't need to worry how wide this triangular pulse is as long as we have kept it symmetric. So we can put this from −1 to +1. And we don't need to worry what the height is, so we could as well make the height = 1.

All these are because of the invariance property of the time-bandwidth product. It is invariant to **scaling of the dependent as well as independent variable and translation**.

Now let us find the time-bandwidth product of this triangular pulse.

Let us call this a function of t. It is essentially $x(t) = 1 - |t|$, where $0 \le t \le 1$.

We shall first obtain the time variance:

$$\frac{\| tx(t) \|_2^2}{\| x(t) \|_2^2}$$

since $x(t)$ is centred at zero.

Let us begin by calculating the norm $\| x(t) \|_2^2$ first, as we will require it frequently.

$$\| x(t) \|_2^2 = 2\int_0^1 (1-t)^2\, dt$$

The factor of 2 comes due to symmetry around $t = 0$. So, essentially the area on the negative and positive sides are same.

Now, substitute $\lambda = 1 - t$ in the above equation. Hence, $d\lambda = -dt$, evaluating the integral

$$\| x(t) \|_2^2 = (2)(-)\int_1^0 (\lambda)^2\, d\lambda$$

$$= 2\int_0^1 \lambda^2\, d\lambda = \frac{2}{3}$$

Let us evaluate the norm $\| tx(t) \|_2^2$. Here again we will use symmetry.

$$\| tx(t) \|_2^2 = 2\int_0^1 t^2 (1-t)^2\, dt$$

$$= 2\int_0^1 t^2 (1 - 2t + t^2) dt$$

$$= 2\int_0^1 (t^2 - 2t^3 + t^4) dt$$

$$= 2\{\frac{t^3}{3} - \frac{2t^4}{4} + \frac{t^5}{5}\}_0^1$$

$$= 2\{\frac{1}{3} - \frac{2}{4} + \frac{1}{5}\}$$

$$= 2\frac{10 - 15 + 16}{2 \times 15}$$

$$= \frac{1}{15}$$

$$\text{Time variance} = \frac{\| tx(t) \|_2^2}{\| x(t) \|_2^2} = \frac{1/15}{2/3} = \frac{1}{15} \times \frac{3}{2} = 0.1$$

Frequency variance is given by

$$\frac{\| \frac{dx(t)}{dt} \|_2^2}{\| x(t) \|_2^2}$$

and $\frac{dx(t)}{dt}$ is a simple function to evaluate as shown in Fig. 9.4.

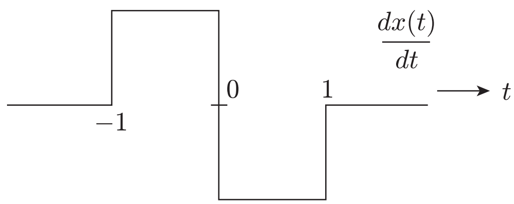

Figure 9.4 | $\frac{dx(t)}{dt}$

From Fig. 9.4 it can be seen that $\frac{dx(t)}{dt}$ has the appearance of a Haar wavelet.
Energy is given by

$$\| \frac{dx(t)}{dt} \|_2^2 = 1^2 \times 1 + 1^2 \times 1 = 2$$

We know $\|x(t)\|_2^2 = \frac{2}{3}$.
Therefore the frequency variance $= \frac{2}{2/3} = 3$.
Now time-bandwidth product = time variance × frequency variance $= 0.1 \times 3 = 0.3$.

This is good news as we know the minimum we can reach is 0.25 and we have come all the way from ∞ to 0.3 just by cascading the system with itself once again. But again we have bad news. The bad news is that if we want to go from 0.3 to 0.25 we must work really hard! i.e., to get closer to the uncertainty principle is not difficult but going any closer is very difficult. In fact one way to go closer to it is to repeatedly convolve the pulse with itself. So now we take cascade of 3 such LSI systems each of whose impulse response is essentially a pulse as shown in Fig. 9.5.

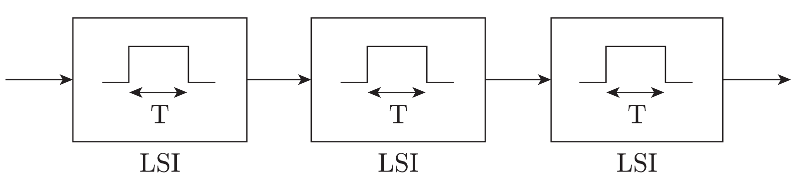

Figure 9.5 | *Cascade of 3 LSI system*

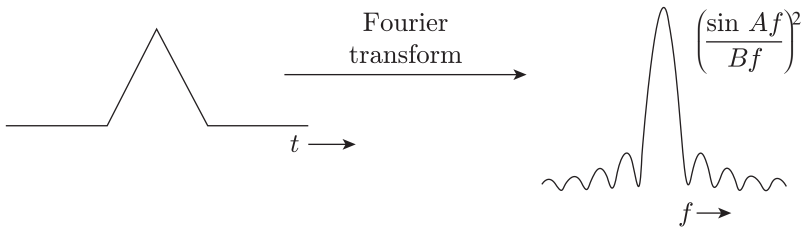

Figure 9.6 | *Fourier transform of the triangular pulse*

Let us make one more remark. It is not just a compactly supported function like this one that has a time bandwidth product of 0.3. We can use a simple argument to show that the same result can come from non-compactly supported function. For that we use the principle of Fourier duality. Figure 9.6 shows the fourier transform of the triangular pulse. Here A, B are constants. Now important question to ask is what is the fourier transform if the time function is of this form and that is what fourier duality will give us as shown in Fig. 9.7. So what we are calling time variance for triangular function becomes the frequency variance for this function and vice versa as is clear from the Fig. 9.7.

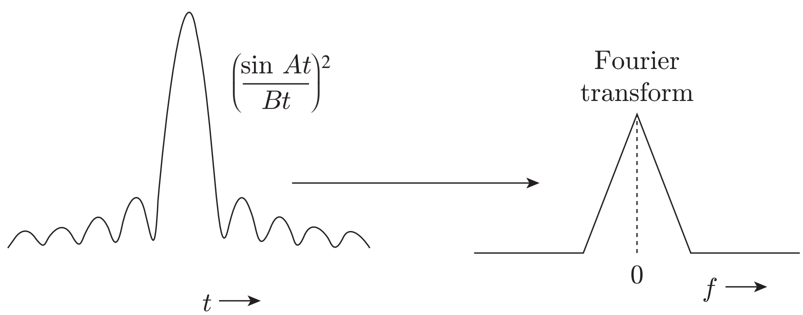

Figure 9.7 | *Fourier duality*

In other words if we take Fourier transform of a function and ask what is its time-bandwidth product, the time-bandwidth product is the same as that of the function!

That is, for the function $\left(\frac{\sin Af}{Bf}\right)^2$ the time variance = frequency variance of $x(t)=1-|t|$ and frequency variance = time variance of $x(t)=1-|t|$.

Therefore time-bandwidth product can easily be calculated. It is 0.3.

Now we have a partial answer for the question that we asked previously. Can you change the shape and maintain the same time-bandwidth product? The answer is Yes.

In fact, this brings up many different conclusions:

(1) We have discovered one more kind of invariance of time bandwidth product. The time bandwidth product is invariant to Fourier transformation.

(2) One more conclusion that we have drawn from this example is that we can have two functions one compactly supported and another NOT compactly supported to have same time-bandwidth product $\sigma_t^2\sigma_\Omega^2$. With this remark we would like to take the idea of time-bandwidth product further. Now that we have identified the two domains, let us put the 2 domains together and bring out a

new domain which is a two-variable domain. So, we shall henceforth talk of what is called a **'time-frequency plane'** as shown in Fig. 9.8.

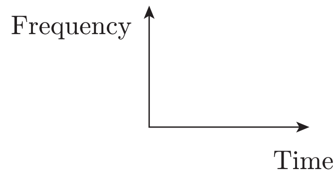

Figure 9.8 | *Time frequency plane*

It is essentially a plane in which one axis, say horizontal axis represents time and other axis say vertical, represents frequency. 'Occupancy' of $x(t) \in L_2(\mathbb{R})$ in time-frequency plane can be thought as being from t_0, the centre in time, to $t_0 + \sigma_t$ on one side and $t_0 - \sigma_t$ on the other side on the horizontal axis. On the vertical axis, we would like to centre it at Ω_0, namely, the frequency centre and we would spread it to $\Omega_0 - \sigma_\Omega$ below $\Omega_0 + \sigma_\Omega$ above as shown in Fig. 9.9. So we could think of the function $x(t)$ as being located in a rectangle which is centred. at t_0, Ω_0 and which has a horizontal width of $2\sigma_t$ and vertical spread of $2\sigma_\Omega$, as shown in Fig. 9.9.

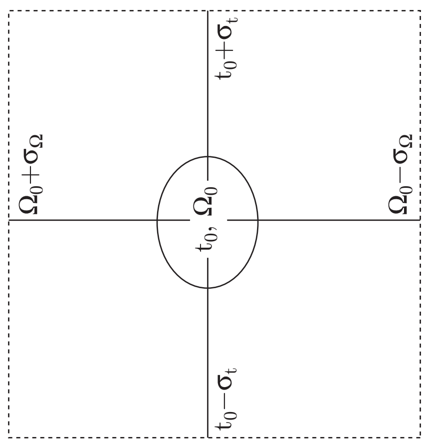

Figure 9.9 | *Time frequency plane centred at t_0 and Ω_0*

A function in $L_2(\mathbb{R})$ occupies a certain area in the time-frequency plane and what the uncertainty principle says is that, this area cannot be smaller than a certain number.

Uncertainty Principle

The rectangle area cannot be smaller than $2\sigma_t \times 2\sigma_\Omega$

$$= 4\sigma_t \sigma_\Omega \geq 4\sqrt{0.25}$$

$$= 4 \times 0.5 = 2 \text{ units}$$

The area of the rectangle cannot be smaller than 2 units. Within limitations we can change the width and height which is the positive side of the uncertainty principle. Now we can talk of what is called as the tiling of the time frequency plane as shown in Fig. 9.10.

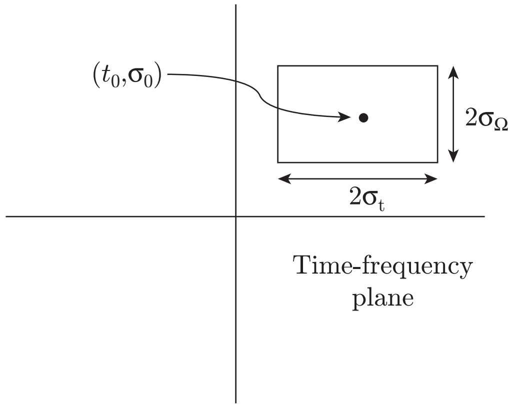

Figure 9.10 | *Tiling the time-frequency plane*

Tiling the time-frequency plane

What this essentially means is covering this plane with rectangular tiles corresponding to such functions. Let us take any other function to be analyzed: $y(t)$. "Tool" function = $x(t)$. From Parseval's theorem,

$$\int_{-\infty}^{+\infty} y(t)\overline{x(t)}dt = \frac{1}{2\Pi}\int_{-\infty}^{+\infty} Y(\Omega)\overline{X(\Omega)}d\Omega$$

Physical interpretation:

R If we take the projection of the function $y(t)$ on such a " Tool" function $x(t)$ in time, we are essentially extracting information about $y(t)$ in the time region between $t_0+\sigma_t$ and $t_0-\sigma_t$. Parseval's theorem says that simultaneously we are also extracting information of the Fourier transform of $y(t)$ in a region captured between $\Omega_0-\sigma_\Omega$ and $\Omega_0+\sigma_\Omega$. So this is the minimum rectangular area over which we can view $y(t)$. There is a minimum resolution and we cannot go finer than that resolution when we look at the two domains together. But the good news is that there are many different ways in which you can look at the small domain when you are within that uncertainty limit.
But tiling has a different interpretation. If we wish to analyze a function we think of the function in the time and frequency domain together. Essentially we are viewing the function in the joint domain and we wish to see how the function looks in the joint domain.

Example 9.1.1 — 'Chirp' function.

Let us take an example, consider "Chirp" function. The chirp function is named after the sound of the birds. When birds chirp crudely the chirp waveform has a pattern with a continuously changing instantaneous frequency in time. It is of the form = $\sin\Omega(t).t$ where Ω is instantaneous frequency.

An important question in analyzing the chirp function that one encounters sometimes in RADAR or SONAR is, trace this variation of the instantaneous frequency in time and there the uncertainty principle hits hard.

In the time frequency plane suppose $\Omega(t) = a$ constant function of time, then we can graphically represent it as follows (see Fig. 9.11).

Suppose $\Omega(t)$ is a linear function of time which is often true, then graphically what we do with the tool is to try to trace this pattern and that is where the uncertainty principle hits us. It says, we can only put rectangles which look, like the ones in Fig. 9.12 and we can never really trace what is happening within the rectangle.

Suppose, we think of putting many rectangles in this time frequency plane and see that these shaded rectangles are " lighted up". In other words, if we looked at the dot product of these functions, $y(t)$, which has the linear chirp nature, with this set of tiles, the tiles in which the function essentially is prominent would be " lighted up". It means that the magnitude of the dot product will be large. So it will show us the discrete points.

Example: If we look into the time frequency plane, each of these rectangles would correspond to a single point here. So it would show points that lie on the line as lighted up.

But we cannot go closer than that. We wouldn't know what has happened between these points. That is what the uncertainty principle says. We cannot get instantaneous frequency as a function of time exactly. But we could do it as closely as we desire by taking smaller rectangles and, the smaller the area we take, the better we can make this estimate. This is one of the meanings of the time-frequency plane and its tiling.

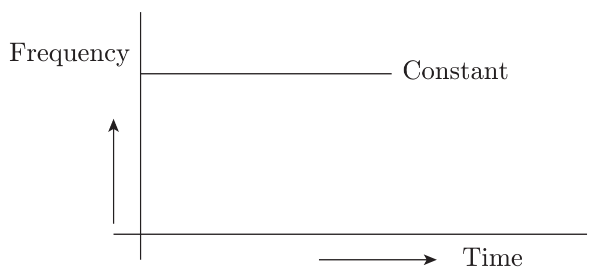

Figure 9.11 | *Chirp function*

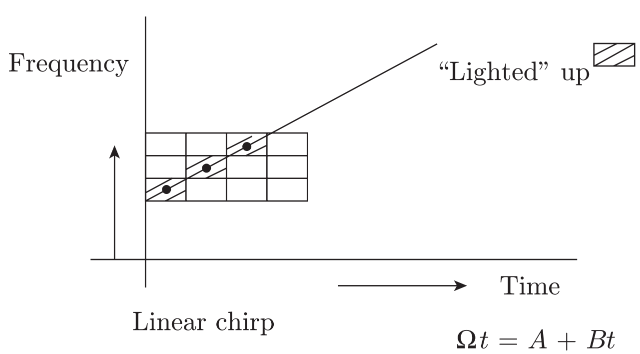

Figure 9.12 | $\Omega(t) = A + Bt$

9.2 | Short Time Fourier Transform (STFT) and Wavelets

The short time Fourier transform, we begin with choosing an appropriate window function: $v(t)$. What we desire from the window function is finite time variance and finite frequency variance. This is required to make a t-f tile of finite area in the t-f plane as will be seen later (Fig. 9.13).

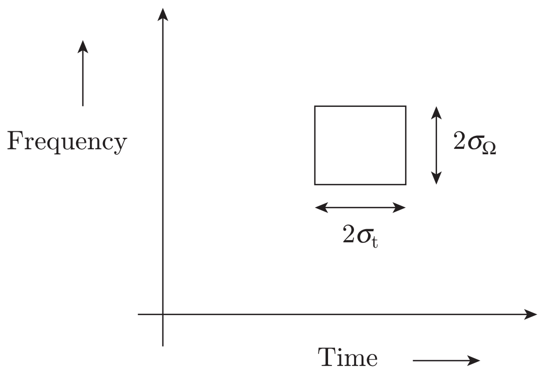

Figure 9.13 | *Tiling of time-frequency plane*

For finite time variance we know that

$$tv(t) \in L_2(R)$$

given $v(t) \in L_2(R)$
also for finite frequency variance

$$\frac{dv(t)}{dt} \in L_2(R)$$

given $v(t) \in L_2(R)$
The simplest window that can be chosen is a rectangular window. Such a window immediately disqualifies as it does not have finite frequency variance.

Example 9.2.1 — Examples of window function that have finite variance in time and frequency

- Triangular Window: $v(t) = 1 - |t|$
- Gaussian Window: $v(t) = e^{\frac{-t^2}{2}}$
- Raised Cosine Window: $v(t) = 1 + \cos(t)$

The idea in the short time Fourier transform is to create a continuum of dot products of such a window function modulated by a sinusoid with the input function. Let,

$$x(t) \in L_2(R) \tag{9.1}$$

Then the STFT (short time Fourier transform) is given as

$$\text{STFT}(X,V)(t_0,\Omega_0) = \text{dot product of } x(t) \text{ with } v(t-t_0)e^{j\Omega_0 t} \tag{9.2}$$

The arguments in the first bracket are the secondary arguments namely X, V and the second bracket holds the primary arguments. Writing the STFT in equation format:

$$\text{STFT}(X,V)(\tau_0,\Omega_0) = \int_{-\infty}^{\infty} x(t)\overline{v(t-\tau_0)e^{j\Omega_0 t}}\,dt \tag{9.3}$$

The bar represents complex conjugation.

Hence the STFT extracts a piece of the function and takes its Fourier transform. Invoking the Parseval's theorem, the above expression has an equivalent in the frequency domain i.e., the product of the Fourier transforms of $x(t)$ and $v(t-\tau_0)e^{j\Omega_0 t}$ respectively, integrated from $-\infty$ to $+\infty$.

The Fourier transform of $v(t-\tau_0)e^{j\Omega_0 t}$:

$$\int_{-\infty}^{\infty} v(t-\tau_0)e^{j\Omega_0 t}e^{-j\Omega t}\,dt \tag{9.4}$$

Let $t-\tau_0 = k$

$$= \int_{-\infty}^{\infty} v(k)e^{j(\Omega_0-\Omega)(k+\tau_0)}\,dk \tag{9.5}$$

$$= e^{j(\Omega_0-\Omega)\tau_0}V(\Omega-\Omega_0) \tag{9.6}$$

$V(\Omega)$ denotes the Fourier transform of the function $v(t)$, putting in the Parseval's theorem expression

$$\frac{1}{2\pi}\int_{-\infty}^{\infty} X(\Omega)\overline{V(\Omega-\Omega_0)e^{j(\Omega_0-\Omega)\tau_0}}\,d\Omega \tag{9.7}$$

$$\frac{e^{-j\Omega_0\tau_0}}{2\pi}\int_{-\infty}^{\infty} X(\Omega)\overline{V(\Omega-\Omega_0)e^{j\Omega\tau_0}}\,d\Omega \tag{9.8}$$

the above expression looks like the inverse Fourier transform evaluated at τ_0.

9.2.1 Duality Interpretation of Fourier Transform

The frequency interpretation term:

$$\frac{e^{-j\Omega_0\tau_0}}{2\pi}\int_{-\infty}^{\infty} X(\Omega)\overline{V(\Omega-\Omega_0)e^{j\Omega\tau_0}}\,d\Omega \tag{9.9}$$

The time interpretation term:

$$\int_{-\infty}^{\infty} x(t)\overline{v(t-\tau_0)e^{j\Omega_0 t}}\,dt \tag{9.10}$$

The STFT creates fixed shape tiles, where τ_0 is the movement along time and Ω_0 is the movement along frequency.

So far we have seen only dyadic DWT and translations happen in unit steps in V_0. The continuous version of the wavelet transform is essentially an inner product of $x(t)$ with translates and dilates of the wavelet $\psi\left(\frac{t-\tau_0}{s_0}\right)$.

Continuous wavelet transform (CWT)

$$< x(t), \frac{1}{\sqrt{s_0}}\psi\left(\frac{t-\tau_0}{s_0}\right) >= \frac{1}{\sqrt{s_0}}\int_{-\infty}^{\infty} x(t)\,\overline{\psi\left(\frac{t-\tau_0}{s_0}\right)}dt$$

Problem of normalization is caused due to change in the norm of the wavelet function upon dilation, hence the factor of $\frac{1}{\sqrt{s_0}}$ is required to normalize it. Interpreting in the frequency domain using the Parseval's relationship implies that the above expression is equivalent to inner product of $X(\Omega)$ with Fourier transform of $\psi(\frac{t-\tau_0}{s_0})$. Fourier transform of $\psi(\frac{t-\tau_0}{s_0})$, first taking care of the dilation, since

$$\frac{1}{\sqrt{s_0}}\psi\left(\frac{t}{s_0}\right) \rightarrow \xrightarrow{\text{FourierTransform}} \rightarrow \sqrt{s_0}\,\Psi(s_0\Omega) \tag{9.11}$$

Hence, the Fourier transform of

$$\frac{1}{\sqrt{s_0}}\psi\left(\frac{t-\tau_0}{s_0}\right) \rightarrow \xrightarrow{\text{FourierTransform}} \rightarrow \sqrt{s_0}\,\Psi(s_0\Omega)e^{-j\Omega\tau_0}$$

The continuous wavelet transform (CWT) is both a function of τ_0 and s_0 with $\tau_0 \in \mathbb{R}$ and $s_o \in \mathbb{R}^+$

$$\text{CWT}(x,\psi)(\tau_0, s_0) = \int_{-\infty}^{\infty} \frac{x(t)}{\sqrt{s_0}}\,\overline{\psi\left(\frac{t-\tau_0}{s_0}\right)}dt \tag{9.12}$$

or using the Parseval's relation

$$\text{CWT}(x,\psi)(\tau_0, s_0) = \frac{\sqrt{s_0}}{2\pi}\int_{-\infty}^{\infty} X(\Omega)\overline{\Psi(s_0\Omega)}e^{j\Omega\tau_0}\,d\Omega$$

- Provided we recall the nature of the Fourier transform for ψ, considering the Haar case the magnitude pattern
- We are multiplying X by a bandpass function and taking the inverse Fourier transform, hence, we are extracting the frequency component of CWT which corresponds to the dilates of Ψ.
- If we accept that Ψ is a bandpass function, then

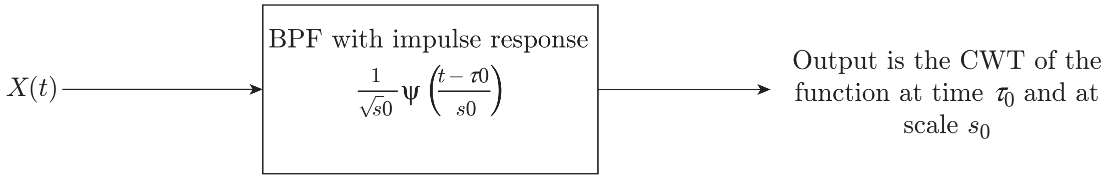

- There is a continuum of such filters.

9.3 | Reconstruction and Admissibility

We have devised Short Time Fourier Transform (STFT) and Continuous Wavelet Transform(CWT) to analyze a signal simultaneously in time and frequency domain. Basically STFT is taking the Fourier transform of the signal multiplied with a tempered weighted function (the window function) shifted in time and modulated in frequency. CWT is taking the Fourier transform of the signal multiplied with normalized wavelet.

In the following sections, we will study reconstruction methods of the signal from its STFT and CWT.

9.4 | Reconstruction from STFT

- How do we reconstruct a signal from its STFT?

STFT of a signal $x(t)$ with a window function $v(t)$ at time τ and frequency Ω is defined by

$$\mathrm{STFT}(x,v)(\tau,\Omega)=\int_{-\infty}^{\infty}x(t)\overline{v(t-\tau)e^{j\Omega t}}\,dt \tag{9.13}$$

But this is equivalent to a dot product of the signal $x(t)$ with a translated and modulated window.

Or in other words, this operation is finding out the component of the signal along something. (May be some sort of space spanned by the window function)

With this idea, we try to reconstruct by taking each component multiplied with the unit vector in its direction and then summing it up.

$$\int_{-\infty}^{\infty}\int_{-\infty}^{\infty}\mathrm{STFT}(x,v)(\tau,\Omega)v(t-\tau)e^{j\Omega t}\,d\tau d\Omega \tag{9.14}$$

Expanding

$$\int_{-\infty}^{\infty}\int_{-\infty}^{\infty}\int_{-\infty}^{\infty}x(y)\overline{v(y-\tau)e^{j\Omega y}}dy\,v(t-\tau)e^{j\Omega t}\,d\tau d\Omega \tag{9.15}$$

Now consider the integral on Ω first

$$\int_{-\infty}^{\infty}e^{-j\Omega y}e^{j\Omega t}d\Omega=\frac{1}{2\pi}\int_{-\infty}^{\infty}2\pi e^{j\Omega(t-y)}\,d\Omega \tag{9.16}$$

which is inverse Fourier transform of a function which is constant ($=2\pi$) for all Ω

$$= 2\pi\delta(y-t) \tag{9.17}$$

$\delta(.)$ being continuous impulse function. So the original triple integral turns into

$$2\pi\int_{-\infty}^{\infty}\int_{-\infty}^{\infty} x(y)\overline{v(y-\tau)}\,v(t-\tau)\delta(y-t)\,d\tau dy \tag{9.18}$$

which gives (using the property of delta function $\int_{-\infty}^{\infty} f(x)\delta(x-a)dx = f(a)$)

$$= 2\pi\int_{-\infty}^{\infty} x(t)\overline{v(t-\tau)}v(t-\tau)d\tau \tag{9.19}$$

$$= 2\pi x(t)\int_{-\infty}^{\infty} |\, v(t-\tau)\,|^2 \; d\tau \tag{9.20}$$

$$= 2\pi \; x(t)\int_{-\infty}^{\infty} |\, v(z)\,|^2 \; dz \tag{9.21}$$

$$= 2\pi \; x(t) \| \, v \, \|^2 = \text{constant} \times x(t) \tag{9.22}$$

where $\| \, v \, \|^2 = < v, v > = L_2$ norm of the window function v.

So we have reconstructed $x(t)$ from its STFT.

But STFT or CWT are continuous transforms which are performed over all values of time and frequency.

This means the choice is made among a continuum of time and frequency centres and the integral is calculated for each such function which is highly impractical.

R Hence comes the natural question:
Can we discretize τ and ω?
Answer is *yes*. It will become evident as we go along.

9.5 | Time Frequency Tiling: Comparison of STFT and CWT

Now, let us compare properties of STFT and CWT tiling of the time-frequency plane:

The STFT moves a tile of constant shape in the time-frequency plane (see Fig. 9.14). The minimum possible area of this STFT tile is governed by the time-bandwidth product which is limited by a bound (= 0.25) as we have seen in Uncertainty Principle.

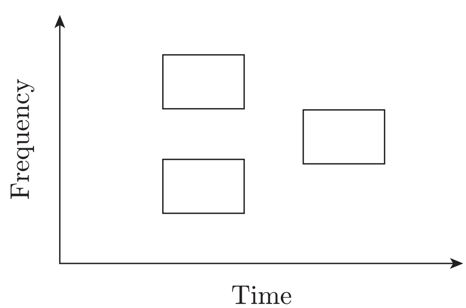

Figure 9.14 | *STFT tiling of time frequency plane*

On the other hand, the CWT tiling is of a different kind. The tile is of a variable shape but constant area which is also governed by time-bandwidth product. The parameters defining the tiling are time centre τ and scaling parameter s_0. When we increase s_0 we are effectively expanding in time and compressing in frequency; while when we decrease s_0 we are effectively compressing in time and expanding in frequency. Movement along the frequency happens because the centre frequency is nonzero. The shape of tile remains rectangular but it keeps changing continuously with change in scaling parameter s_0. This is shown in Fig 9.15.

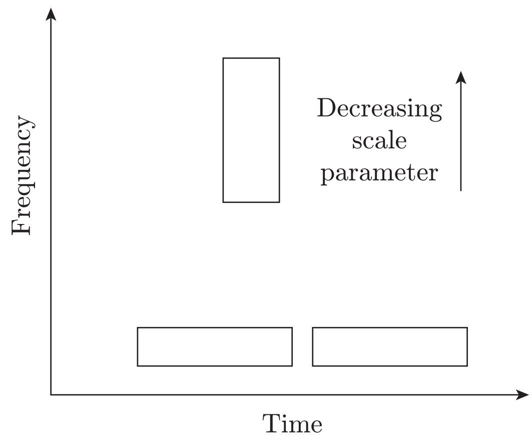

Figure 9.15 | *CWT tiling of time frequency plane*

We can clearly see that τ - time centre determines the location of tile on time frequency plane in a direct manner, but this is not true for scaling parameter s_0. So we can not reconstruct similar to what we did for STFT but after allowing a scale factor (which depends on s_0) reconstruction is achievable as presented in next section.

9.6 | Reconstruction from CWT

Reconstruction of $x(t)$ from CWT $(x, \psi)(\tau, s_0)$ should be:

$$\int_{s_0=0}^{\infty}\int_{-\infty}^{\infty} \mathrm{CWT}(x,\psi)(\tau,s_0)\frac{1}{\sqrt{s_0}}\psi\left(\frac{t-\tau}{s_0}\right)f(s_0)\,d\tau ds_0 \tag{9.23}$$

where $f(s_0)$ is a weight factor which is dependent only on s_o as discussed earlier.

In Chapter 21, we used Parsevel's Theorem to arrive at the following expression of CWT:

$$\mathrm{CWT}(x,\psi)(\tau,s_0) = \frac{1}{2\pi}\int_{-\infty}^{\infty}\sqrt{s_0}\,\widehat{X}(\Omega)\overline{\hat{\Psi}(s_0\Omega)}\,e^{j\Omega\tau}\,d\Omega \tag{9.24}$$

where $\widehat{X}(\Omega)$ is Fourier Transform of $x(t)$. Substituting this in the reconstruction formula we get a triple integral:

$$\frac{1}{2\pi}\int_{s_0=0}^{\infty}\int_{-\infty}^{\infty}\int_{-\infty}^{\infty}\sqrt{s_0}\,\widehat{X}(\Omega)\overline{\hat{\Psi}(s_0\Omega)}\,e^{j\Omega\tau}\,\frac{1}{\sqrt{s_0}}\psi\left(\frac{t-\tau}{s_0}\right)f(s_0)\,d\Omega\,d\tau\,ds_0 \tag{9.25}$$

Let's solve the τ integral first:

Let's say

$$I=\int_{-\infty}^{\infty}\psi\left(\frac{t-\tau}{s_0}\right)e^{j\Omega\tau}\,d\tau \tag{9.26}$$

$$\text{substituting}\ \frac{t-\tau}{s_0}=\lambda$$

$$d\tau=-s_0\,d\lambda$$

$$I=\int_{-\infty}^{\infty}\psi(\lambda)\,e^{j\Omega(t-s_0\lambda)}\,s_0\,d\lambda \tag{9.27}$$

$$I=e^{j\Omega t}s_0\int_{-\infty}^{\infty}\psi(\lambda)\,e^{j\Omega(-s_0\lambda)}\,d\lambda \tag{9.28}$$

which on observation (that integral is a Fourier integral) gives:

$$I=e^{j\Omega t}s_0\hat{\Psi}(s_0\Omega) \tag{9.29}$$

Putting this back in the triple integral we get:

$$\frac{1}{2\pi}\int_{s_0=0}^{\infty}\int_{-\infty}^{\infty}\widehat{X}(\Omega)\overline{\hat{\Psi}(s_0\Omega)}\,f(s_0)\,e^{j\Omega t}\,s_0\hat{\Psi}(s_0\Omega)\,d\Omega\,ds_0 \tag{9.30}$$

Let us now solve and do away with s_0 integral:

$$I_1=\int_{s_0=0}^{\infty}\overline{\hat{\Psi}(s_0\Omega)}\,f(s_0)\,s_0\,\hat{\Psi}(s_0\Omega)\,ds_0 \tag{9.31}$$

$$I_1=\int_{s_0=0}^{\infty}|\hat{\Psi}(s_0\Omega)|^2\,f(s_0)\,s_0\,ds_0 \tag{9.32}$$

If we can make this integral I_1 independent of Ω then we will be done with the reconstruction since rest of the term is Inverse Fourier Transform giving $x(t)$. So the only objective left is to make the integral independent of Ω and that is where the freedom to choose $f(s_0)$ comes in handy.

If we could make

$$s_0\,f(s_0)\,ds_0=\frac{ds_0}{s_0}\ \text{ or }\ f(s_0)=\frac{1}{s_0^2}$$

we get a valid weight function which non negative for all values of s_0.

say $s_1 = \Omega s_0$ which implies $\dfrac{ds_1}{s_1} = \dfrac{ds_0}{s_0} (\Omega \neq 0)$ when Ω is positive, limits of the integral I_1 are 0 to ∞ and when Ω is negative, limits of the integral I_1 are 0 to $-\infty$. In both cases, integral is independent of Ω and hence can be treated as a constant further. Remaining integral becomes:

$$\text{constant} \times \int_{-\infty}^{\infty} \frac{1}{2\pi} \widehat{X}(\Omega) e^{j\Omega t}\, d\Omega \tag{9.33}$$

where the constant is $\int_0^{\infty} |\hat{\Psi}(s_1)|^2 \dfrac{ds_1}{s_1}$ for $\Omega > 0$ Or $\int_0^{-\infty} |\hat{\Psi}(s_1)|^2 \dfrac{ds_1}{s_1}$ for $\Omega < 0$.

These two integrals must be finite for perfect reconstruction. We will take this idea (called *admissibility*) further in next few sections.

9.7 | Admissibility in Detail and Discretization of Scales

In earlier sections we built up the idea of decomposition and reconstruction in STFT and CWT. The central theme in decomposition and reconstruction was to project the function to be decomposed on the basis of vectors and to reconstruct that function from its component by multiplying each component by the vector in that direction. STFT was indexed by translation and modulation while CWT was indexed by translation and scale. Translation can be dealt with easily but for scale we need an additional weighing factor to deal with whole reconstructing.

9.8 | Admissibility

Important steps in reconstructing $x(t)$ from $\text{CWT}(x,\psi)(\tau,s)$: In this, the most important step is to evaluate the triple integral involved. The innermost integral involved is called component corresponding to $\text{CWT}(x,\psi)(\tau,s)$ and is given by

$$\frac{1}{2\pi} \int \widehat{X}(\Omega) \sqrt{s}\, \overline{\hat{\Psi}(s\Omega)} e^{j\Omega\tau}\, d\Omega \tag{9.34}$$

The two outer integral take care of translation and scale parameters. The triple integral is as follows:

$$\int_{s=0}^{\infty} \int_{\tau=-\infty}^{\infty} \text{CWT}(x,\psi)(\tau,s) \frac{1}{\sqrt{s}} \psi\left(\frac{t-\tau}{s}\right) f(s)\, ds\, d\tau \tag{9.35}$$

Here, $\text{CWT}(x,\psi)(\tau,s)$ is the component, $\dfrac{1}{\sqrt{s}} \psi\left(\dfrac{t-\tau}{s}\right)$ is a unit vector and $f(s)$ is the weighing function to deal with the scale. Writing all together, the triple integral becomes.

$$\frac{1}{2\pi} \int_{s=0}^{\infty} \int_{\tau=-\infty}^{\infty} \int_{\Omega=-\infty}^{\infty} \widehat{X}(\Omega) \sqrt{s}\, \overline{\hat{\Psi}(s\Omega)}\, e^{j\Omega\tau} \frac{1}{\sqrt{s}} \psi\left(\frac{t-\tau}{s}\right) f(s)\, ds\, d\Omega\, d\tau \tag{9.36}$$

The approach used to evaluate this integral is that we take $d\tau$ first, ds second and $d\Omega$ in the last. After taking care of $\int_{-\infty}^{\infty} d\tau$, what was left, by choosing $f(s) = \dfrac{1}{s^2}$ is

$$\frac{1}{2\pi}\int_{-\infty}^{\infty}\widehat{X}(\Omega)\int_{0}^{\infty}|\hat{\Psi}(s\Omega)|^2\frac{ds}{s}e^{j\Omega t}d\Omega \tag{9.37}$$

We can observe that $\int_0^\infty |\hat{\Psi}(s\Omega)|^2 \frac{ds}{s}$ is independent of Ω, it becomes a constant and comes out of the integral, hence we get

$$\frac{1}{2\pi}C_\psi\int_{-\infty}^{\infty}\widehat{X}(\Omega)e^{j\Omega t}d\Omega \tag{9.38}$$

This C_ψ tells us the factor by which $x(t)$ is multiplied in the reconstruction. Now, consider the integral $\int_0^\infty |\hat{\Psi}(s\Omega)|^2 \frac{ds}{s}$. Put $s\Omega = \alpha$

Case-I: $\Omega > 0, \alpha : 0 \to +\infty$ when $s : 0 \to +\infty$

$$d\alpha = \Omega ds, \alpha = \Omega s. \text{ Therefore } \frac{d\alpha}{\alpha} = \frac{ds}{s}$$

$$\int_0^\infty |\hat{\Psi}(s\Omega)|^2\frac{ds}{s} = \int_0^\infty |\hat{\Psi}(\alpha)|^2\frac{d\alpha}{\alpha} \tag{9.39}$$

We can see that the right hand side of the above equation is based on the function ψ and independent of Ω.

Case-II: $\Omega < 0, \alpha : 0 \to -\infty$ when $s : 0 \to +\infty$ so the integral becomes $\int_0^{-\infty}|\hat{\Psi}(\alpha)|^2\frac{d\alpha}{\alpha}$, substitute $\alpha = -\beta$ we get

$$\int_{-\infty}^{0}|\hat{\Psi}(s\Omega)|^2\frac{ds}{s} = \int_0^\infty |\hat{\Psi}(-\beta)|^2\frac{d\beta}{\beta} \tag{9.40}$$

Now making integral (on s) independent Ω means:

$$\int_0^\infty |\hat{\Psi}(\alpha)|^2\frac{d\alpha}{\alpha} = \int_0^\infty |\hat{\Psi}(-\beta)|^2\frac{d\beta}{\beta} < \infty \tag{9.41}$$

The above integral must be positive as as the integration is on nonnegative integrands.

If $\psi(t)$ is real then, $\hat{\Psi}(-\beta) = \overline{\hat{\Psi}(\beta)}$. Therefore,

$$|\hat{\Psi}(-\beta)|^2 = |\hat{\Psi}(\beta)|^2 \tag{9.42}$$

However, if $\psi(t)$ is a complex wavelet then we need separately to take control of positive and the negative part of the spectrum.

If we use complex wavelet and insist that spectrum is one-sided then we must ensure the signal as no component on other side, therefore, in that case the particular condition can be removed. For example, we take a complex wavelet where we do not take care of the negative part of the spectrum, so the condition which involves $|\hat{\Psi}(-\beta)|^2$ is not obeyed, then we may only deal with such 'x' which has nonzero components and therefore 'x' must be complex having non-zero components on the positive part of the spectrum i.e., $\Omega > 0$. Conversely, for $\Omega < 0$ original spectrum should have no part on positive side.

Remark

Admissibility allows the function to be called a wavelet. It is the condition required for Reconstruction.

$$\int_0^\infty |\hat{\Psi}(\alpha)|^2 \frac{d\alpha}{\alpha} = \int_0^\infty |\hat{\Psi}(-\beta)|^2 \frac{d\beta}{\beta} < \infty \tag{9.43}$$

9.9 | Case-III $\Omega = 0$ and Case-IV $\Omega = \infty$

Let take $\Omega > 0$ (with real ψ this is enough). Now, according to admissibility condition $\int_0^\infty |\hat{\Psi}(\alpha)|^2 \frac{d\alpha}{\alpha}$ must be finite. We will, now, have a look at $\Omega = 0$ and $\Omega = \infty$

Example 9.9.1—$\Omega = 0$ and $\Omega = \infty$. Consider $|\hat{\Psi}(\alpha)|^2$ to be like:

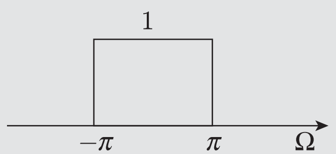

It is obvious that it cannot be a wavelet as:

$$\int_0^\infty |\hat{\Psi}(\alpha)|^2 \frac{d\alpha}{\alpha} = \int_0^\pi 1.\frac{d\alpha}{\alpha} \tag{9.44}$$

$$\int_0^\pi \frac{d\alpha}{\alpha} = \ln\alpha \,|_0^\pi \tag{9.45}$$

The above integral diverges. This trouble comes from region around $\Omega = 0$
Let us take another *e.g.*

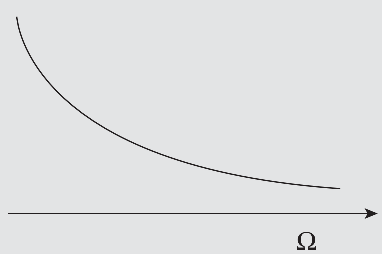

Here $|\hat{\Psi}(\alpha)|^2$ will be a constant (say C_0) as $\alpha \to \infty$, therefore

$$\int_{Large\,value}^\infty |\hat{\Psi}(\alpha)|^2 \frac{d\alpha}{\alpha} \approx \int_{Large\,value}^\infty C_0 \frac{d\alpha}{\alpha} = \ln\alpha \,|_{Large\,value}^\infty \tag{9.46}$$

Here, also we observe that the integral diverges. This time the trouble comes from the region around $\Omega \approx \infty$.

Point to remember: One should not have a spectrum giving a significant contribution around $\Omega = 0$ as well as $\Omega \approx \infty$. The spectrum therefore should get vanish at zero and infinite frequency.

Can we allow following $|\hat{\Psi}(\Omega)|^2$?

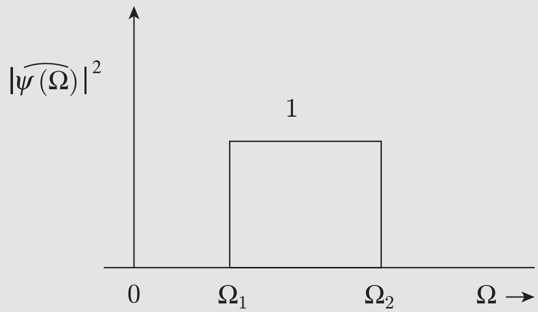

$$\int_0^\infty |\hat{\Psi}(\alpha)|^2 \frac{d\alpha}{\alpha} = \int_{\Omega_1}^{\Omega_2} 1.\frac{d\alpha}{\alpha} = \ln\frac{\Omega_2}{\Omega_1} \tag{9.47}$$

This is finite and therefore acceptable.

A bandpass function is what we can accept for an admissible wavelet.

9.10 | Analysis of Gaussian Function

A important property of Gaussian function is that Gaussian in time domain is also a Gaussian in frequency domain.

Example 9.10.1 — Gaussian analysis.

Lets us consider the function:

$$\frac{1}{\sqrt{2\pi}} e^{\frac{-t^2}{2}} \tag{9.48}$$

Fourier transform of Gaussian function will be of form $e^{-\Omega^2}$ which is also Gaussian.

The question which arises is whether Gaussian is admissible?

The answer is *No*.

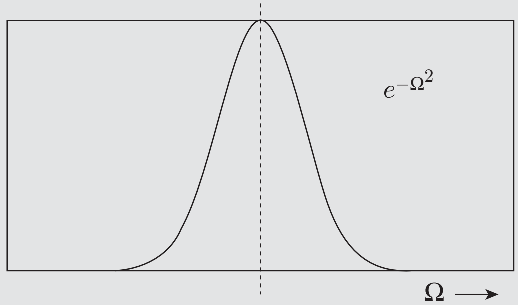

As we can see from the graph, at zero frequency the graph does not vanish, therefore, even for a small area near zero frequency let us say, The integral

$$\int_0^1 |e^{-\Omega^2}|^2 \frac{d\Omega}{\Omega} \tag{9.49}$$

diverges and hence Gaussian is not admissible.
Now, take the derivative of the Gaussian,

$$\frac{d}{d\Omega}(e^{-\Omega^2}) = -2\Omega e^{-\Omega^2} \approx \Omega e^{-\Omega^2} \quad (\text{For consideration}) \tag{9.50}$$

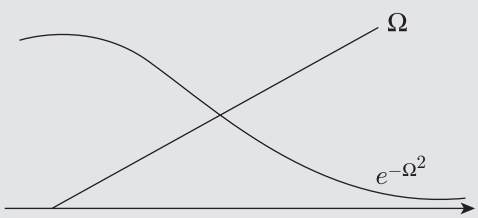

Their product will look like

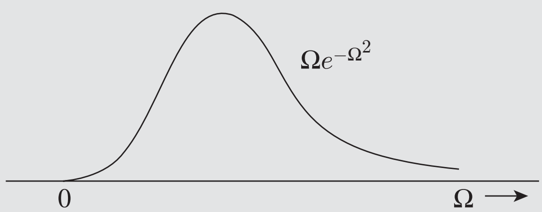

This is admissible as:

$$\int_0^\infty |\Omega e^{-\Omega^2}|^2 \frac{d\Omega}{\Omega} \Rightarrow \int_0^\infty \Omega^2 e^{-2\Omega^2} \frac{d\Omega}{\Omega}$$

$$\Rightarrow \int_0^\infty \Omega e^{-2\Omega^2}\, d\Omega$$

Put $\Omega^2 = \lambda$, therefore $d\lambda = 2\Omega d\Omega$, hence

$$\int_0^\infty e^{-2\lambda}\frac{1}{2}d\lambda \tag{9.51}$$

We observe that this integral converges. Hence derivative of Gaussian is an admissible function. But this function is no longer optimal in the sense of time bandwidth product.

Now, $\dfrac{d}{d\Omega}$ is equivalent to multiply by t. The inverse Fourier transform of $\Omega e^{-\Omega^2}$ has the same form.
(Try to show this as an exercise)
Try doing the same for the second derivative. The second derivative of Gaussian is known as Mexican Hat function.

9.11 | Discretization of Scale

Admissibility is adequate when we talk about reconstructing from CWT. But its a difficult thing to do numerically, to construct a 2-dimensional continuous parameter (τ, s) with 1-dimensional function $x(t)$. Hence we discretize the scale.

9.11.1 Condition of Scale Discretization

When we build CWT,

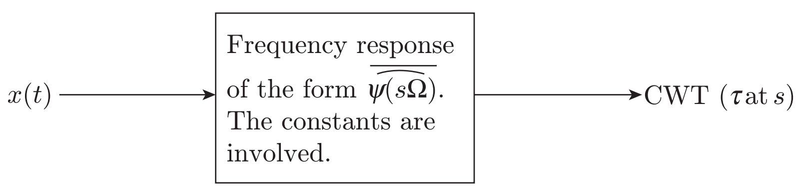

Ideal Band Pass function,

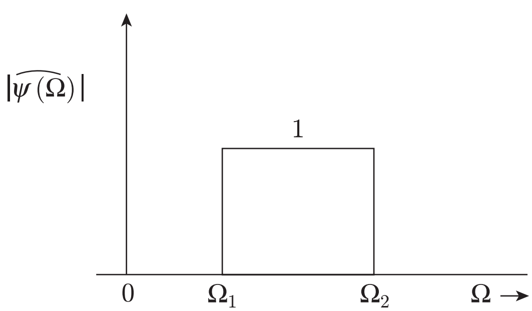

Therefore the graph of $\hat{\Psi}(s\Omega)$ will go from $\frac{\Omega_1}{s}$ to $\frac{\Omega_2}{s}$.

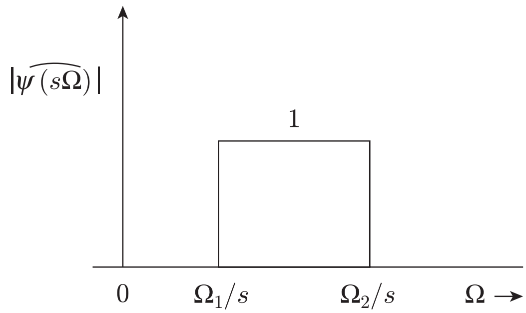

We know that $\Omega_1 > 0$ and $\Omega_2 > 0$, therefore $\frac{\Omega_1}{s}$ and $\frac{\Omega_2}{s}$ will also be greater than Zero. With change of 's', the band of Band Pass Filter will move along the positive part of the spectrum. Therefore the natural condition to discretize the scale parameter is to ensure that we are covering the whole spectrum. When we scale by the factor of 's' we are also scaling the centre frequency and the band. So, there is logarithmic change. So the natural kind of discretization to consider for parameter is Logarithmic discretization. We could in general allow:

$$s = a_0^k \quad ; \quad k \in \mathbb{Z} \quad ; a_0 > 1 \tag{9.52}$$

Exercises

Exercise 9.1

Find impulse response of 3 cascaded LSI systems and find its time-bandwidth product?

Ans. Figure 9.16 shows cascade of 3 systems each of whose impulse response is essentially a pulse of width T. Now consider T = 1, each pulse is extending from 0 to 1. This together form a composite LSI system whose impulse response is given by convolution of 3 pulses. When we convolve first two unit width pulses we get a triangular pulse of width 2 as shown in Fig. 9.17.

Now, the triangular pulse is again convolved with the pulse of unit width to get the impulse response of 3 cascaded system. On convolving we get.

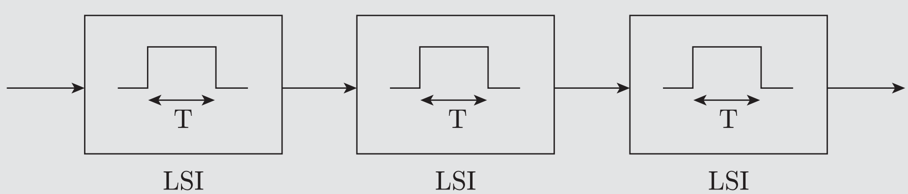

Figure 9.16 | *3 cascaded LSI systems*

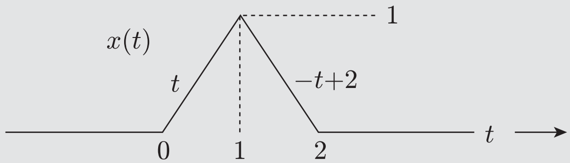

Figure 9.17 | *Result obtained by convolving 2 pulses of unit width*

$$
\begin{aligned}
x(t) &= \frac{t^2}{2} \qquad 0 \le t \le 1 \\
&= -t^2 + 3(t - \frac{1}{2}) \quad 1 < t \le 2 \\
&= \frac{t^2}{2} - 3(t - \frac{3}{2}) \quad 2 < t \le 3
\end{aligned}
$$

the impulse response is shown in Fig. 9.18.
Now, let us first calculate time variance given by $\dfrac{\|(t-t_0)\times x(t)\|_2^2}{\|x(t)\|_2^2}$.

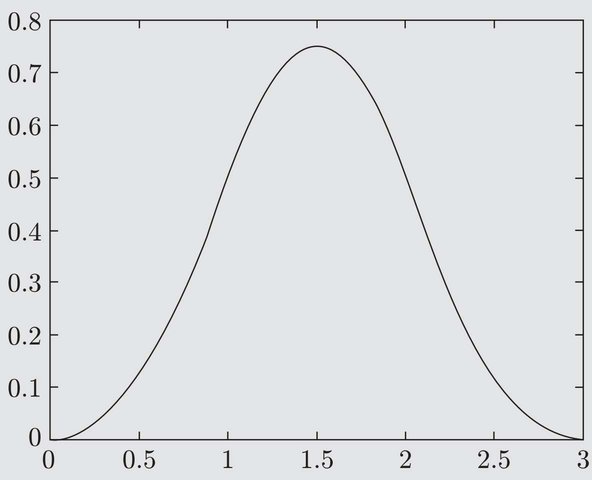

Figure 9.18 | *Impulse response of 3 cascaded system*

From Figure 9.15, time centre t_0 can be seen as $\dfrac{3}{2}$.

$$
\|(t-t_0)\times x(t)\|_2^2 = \int_0^1 (t - \frac{3}{2})\frac{t^2}{2}\,dt + \int_1^2 (t - \frac{3}{2})\{-t^2 + 3(t - \frac{1}{2})\}dt
$$

$$+\int_2^3 (t-\frac{3}{2})\{\frac{t^2}{2}-3(t-\frac{3}{2})\}dt$$

$$= 0.023 + 0.0232 + 0.0303$$

$$= 0.07657$$

$$\|x(t)\|_2^2 = \int_0^1 (\frac{t^2}{2})^2\, dt + \int_1^2 \{-t^2 + 3(t-\frac{1}{2})\}^2\, dt + \int_2^3 \{\frac{t^2}{2}-3(t-\frac{3}{2})\}^2\, dt$$

$$= 0.05 + 0.45 + 0.05$$

$$= 0.55$$

so time variance $= \dfrac{0.07657}{0.55}$

Now frequency variance is given by $\dfrac{\| \frac{d}{dt} x(t) \|_2^2}{\| x(t) \|_2^2}$

$$\| \frac{d}{dt} x(t) \|_2^2 = \int_0^1 (\frac{d}{dt}\frac{t^2}{2})^2\, dt + \int_1^2 \frac{d}{dt}\{-t^2 + 3(t-\frac{1}{2})\}^2\, dt + \int_2^3 \frac{d}{dt}\{\frac{t^2}{2}-3(t-\frac{3}{2})\}^2\, dt$$

$$= 0.333 + 0.333 + 0.333$$

$$= 0.9990$$

Now frequency variance $= \dfrac{0.9990}{0.55}$

therefore time bandwidth product $= \dfrac{0.07657}{0.55} \times \dfrac{0.9990}{0.55} = 0.2529$

Exercise 9.2

Why is Gaussian not realizable and why cant we approximate it by truncating?

Ans. Gaussian is defined for all time ($-\infty$ to ∞) and it don't tends to zero as $t \to (\infty, -\infty)$. Unfortunately there is no physical system which can generate such a waveform and so the Gaussian is not realizable. We have chosen a Gaussian because of its optimality in terms of time-bandwidth product but when we approximate it by truncating, its derivative goes to ∞, therefore, frequency variance becomes ∞ and time-bandwidth product also becomes ∞.

Exercise 9.3

Find the time and frequency variance of raised cosine wave $1+\cos(t)$, $t \in [-\pi, \pi]$ and compare its time bandwidth product to that of Gaussian wave.

Ans. Since, we already know that Gaussian is an optimal function hence its time bandwidth product is 0.25 (also calculated in previous lectures), now let us calculate time bandwidth product of raised cosine wave defined as:

$$x(t) = 1 + \cos(t), -\pi \leq t \leq \pi$$

First, we shall obtain the time variance defined as

$$\frac{\| tx(t) \|_2^2}{\| x(t) \|_2^2}$$

$$=> \frac{\int_{-\pi}^{\pi} t^2 (1+\cos(t))^2 \, dt}{\int_{-\pi}^{\pi} (1+\cos(t))^2 \, dt}$$

$$=> \frac{2\int_{0}^{\pi} t^2 (1+\cos(t))^2 \, dt}{2\int_{0}^{\pi} (1+\cos(t))^2 \, dt} \text{ by symmetry}$$

after solving and putting the limits we get,

$$=> \frac{\pi^3}{3\pi}$$

$$=> \frac{\pi^2}{3}$$

Time variance $= \frac{(3.14)^2}{3} = 3.29$

Now let us obtain the frequency variance of raised cosine wave, which is defined as

$$\frac{\| \frac{dx(t)}{dt} \|_2^2}{\| x(t) \|_2^2}$$

$$=> \frac{\int_{-\pi}^{\pi} (-\sin(t))^2 \, dt}{\int_{-\pi}^{\pi} (1+\cos(t))^2 \, dt}$$

$$=> \frac{2\int_{0}^{\pi} (-\sin(t))^2 \, dt}{2\int_{0}^{\pi} (1+\cos(t))^2 \, dt} \text{ by symmetry}$$

after solving and putting the limits we get,

$$=> \frac{\pi}{3\pi}$$

Frequency variance $= \frac{1}{3} = 0.333$

Thus, time bandwidth product of raised cosine wave is:

$$\sigma_t^2 \sigma_\Omega^2 = 0.333 \times 3.29 = 1.1 > 0.25$$

Time bandwidth product for raised cosine, as can be seen, is greater than that of Gaussian which is an optimal function.

Exercise 9.4

What is the significance of Ω_0 and τ_0 in the STFT expression?

Ans. In the STFT expression τ_0 represents translation along time axis and the quantity Ω_0 represents dilation. We choose τ_0 and Ω_0 and place the window, according to the time and frequency around which we want to take the Fourier transform.

Exercise 9.5

Explain filter bank interpretation of CWT.

Ans. Continuous Wavelet Transform (CWT) of a function is a dot product of the function $x(t)$ with dilated and translated versions of the wavelet function $\psi(t)$.

$$W_s^{\psi} x(\tau, s) = \frac{1}{\sqrt{s}} \int x(t) \psi\left(\frac{t-\tau}{s}\right) dt$$

The wavelet function $\psi(t)$ must obey admissibility condition to analyze and perfectly reconstruct the signal without any loss of information i.e.

$$\int_0^{\infty} \frac{|\psi(\omega)|^2}{|\omega|} d\omega < +\infty$$

This implies that the Fourier transform of the wavelet function goes to zero at 0 and ∞ frequency, hence wavelet function must have a band pass nature.

Filter bank implementation of CWT

At a particular time τ, the dot product can be interpreted as series of filter banks dilated by $s^x \omega$ as shown in the fig. 9.19. Here, since $s \in \mathbb{R}$ hence the number of filters required will be infinite. Though CWT provides high time resolution for high frequencies and low time resolution for low frequencies, it cannot be realized and cannot be used on real data due to its infinite size. In order to achieve the above, it is necessary to discretize the dilation parameter.

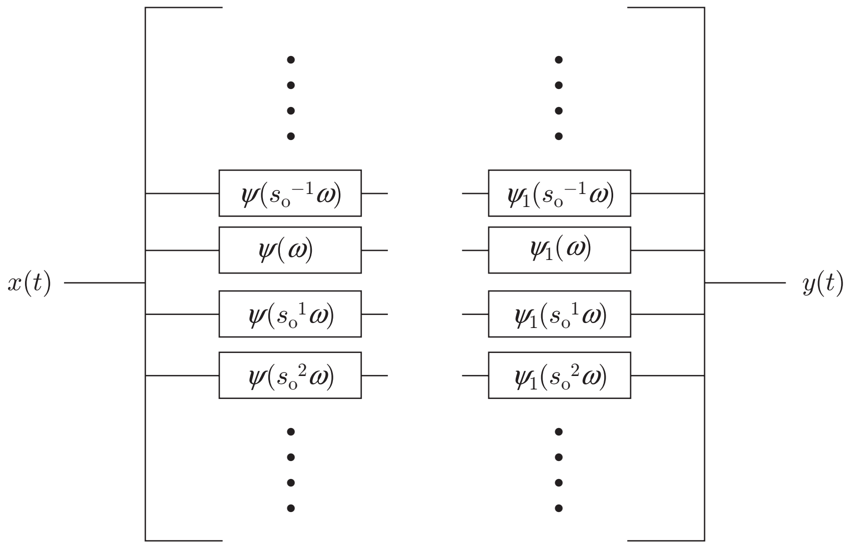

Figure 9.19 | *Dilated filter banks for implementation of CWT*

Exercise 9.6 — Scale Factor $f(s_0)$].

Why do we need scale factor $f(s_0)$ while reconstructing from CWT?
Ans. The scale factor of s is responsible for bringing in dilation to produce multi-resolution effect. Hence scale factor is essential to create multi-resolution effect.

Exercise 9.7 — Constraint of Window Function.

What is the constraint on the window function for reconstruction from STFT ?
Ans. We can see in Eq. (9.22), while reconstructing from STFT we get $\|v\|^2 \times x(t)$, which will give perfect reconstruction only if L_2 norm of window function $v(t)$ is finite i.e. $v(t)\,\varepsilon\, L_2(R)$

Exercise 9.8

Prove by mathematical induction, that the 'n^{th}' derivative of the Gaussian function is a polynomial of degree 'n' multiplied by the Gaussian function itself.

Ans. Let us consider the Gaussian function to be e^{-x^2}.

Now $n=1$ i.e., the first derivative will be $-2xe^{-x^2}$ which is a polynomial of degree 1 multiplied by the Gaussian function itself.

Let us now assume that the 'n^{th}' derivative is also a polynomial of degree 'n' multiplied by a Gaussian itself. Hence, it will be of form $x^{n-1}e^{-x^2}$.
Now we can see that '$(n+1)^{th}$' derivative will be:

$$(-2x^2+(n-1)x^{n-2})e^{-x^2} \tag{9.53}$$

We observe that the above expression is polynomial of degree '$n+1$' multiplied by the Gaussian. Hence by mathematical induction, we can say that the 'n^{th}' derivative of the Gaussian is a polynomial of degree n multiplied by Gaussian itself.

Exercise 9.9

Is the linear combination of two admissible wavelets also admissible?
Ans. Yes, the linear combination of two admissible wavelets is also admissible.
Let ψ_1 and ψ_2 be two admissible wavelets, there linear combination ψ is:

$$\psi = a_1\psi_1 + a_2\psi_2 \tag{9.54}$$

The admissible integral for ψ is:

$$\int_0^\infty |\hat{\Psi}(\omega)|^2 \frac{d\omega}{\omega} = a_1^2 \int_0^\infty |\hat{\Psi}_1(\omega)|^2 \frac{d\omega}{\omega} + a_2^2 \int_0^\infty |\hat{\Psi}_2(\omega)|^2 \frac{d\omega}{\omega} + 2a_1^2 a_2^2 \int_0^\infty |\hat{\Psi}_1(\omega)||\hat{\Psi}_2(\omega)| \frac{d\omega}{\omega} \tag{55}$$

Now we see that the first two terms on the right hand side are finite as ψ_1 and ψ_2 are admissible. The third term consists of the product. Since the wavelet will be bounded in frequency domain, therefore, their product is also finite, hence the third term is finite. Therefore, admissible integral on ψ becomes finite. Hence it is an admissible wavelet.

Exercise 9.10

Is admissibility a sufficient condition to construct filter bank MRA?
Ans. No. Admissibility is a 'Necessary' condition but not a 'Sufficient' condition to construct a filter bank MRA. For example, Mexican Hat Wavelet.

Exercise 9.11

Given the spectrum of the complex wavelet function as in below figure, find the value of C_0 (height) for it to be admissible.

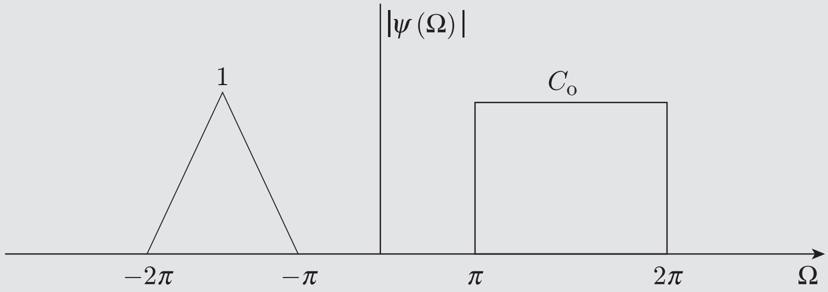

Ans. Now apply the condition of admissibility:
For positive frequency, we get

$$\int_{\pi}^{2\pi} C_0^2 \frac{d\Omega}{\Omega} = C_0^2 \ln 2 \tag{9.56}$$

For negative frequency we get:

$$\int_{\pi}^{\frac{3}{2}\pi} \left| \frac{-2}{\pi}(-\Omega+\pi) \right|^2 \frac{d\Omega}{\Omega} + \int_{\frac{3}{2}\pi}^{2\pi} \left| \frac{2}{\pi}(-\Omega+2\pi) \right|^2 \frac{d\Omega}{\Omega} \tag{9.57}$$

Therefore, on equating them, we get

$$0.1219 + 0.1029 = C_0^2 \ln 2 \Rightarrow C_0 = 0.569 \tag{9.58}$$

Chapter 10

Dyadic MRA

10.1 | Introduction

In Chapter 9, we discussed the admissibility condition for the continuous wavelet transform (CWT) in depth. The admissibility condition was essentially the condition for the ability to reconstruct a signal from its continuous wavelet transform. The continuous wavelet transform was extremely redundant. To use a continuous scale and a continuous translation, that means a two-dimensional representation for a one-dimensional entity, is extremely redundant. Therefore, we exploit the possibilities of discretization of scale as well as the translation parameter. This chapter deals with discretization of the scale parameter. It deals with Logarithmic Discretization (in general) and Dyadic Discretization (in particular). The continuous wavelet transform operates like a filter both on the synthesis side as well as on the analysis side.

The continuous wavelet transform at scale 's' is a filtering operation with a frequency response $\widehat{\Psi}(s\Omega)$ as shown in Fig. 10.1 (with some constants which are ignored).

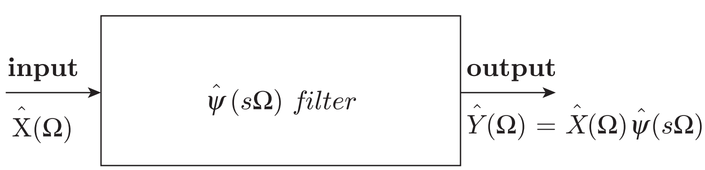

Figure 10.1 | *CWT as filtering operation*

The output independent variable 'τ' here can be interpreted as the translation. If we take an ideal filter or an ideal wavelet (real), the $\widehat{\Psi}(\Omega)$ corresponding to that wavelet is essentially an ideal bandpass filter with cutoff frequencies $\Omega 1$ and $\Omega 2$, as shown in the Fig. 10.2. Only the positive side of the frequency response is shown.

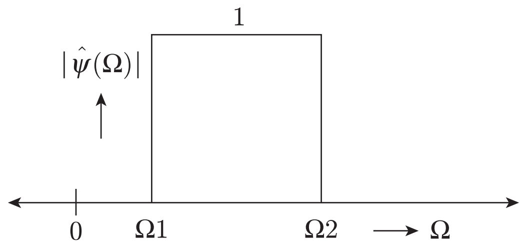

Figure 10.2 | *Ideal wavelet bandpass response*

Now, if we take the dilation of this band pass function, we again get a band pass function. So, for any $s > 0$, $\widehat{\Psi}(\Omega)$ would essentially be as shown in Fig. 10.3.

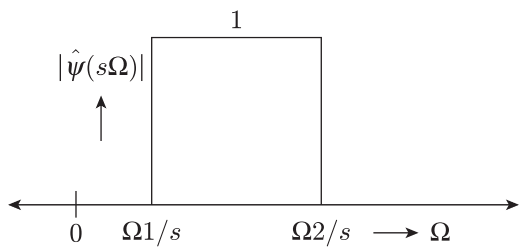

Figure 10.3 | *Dilated wavelet response*

Thus, there is contraction or expansion in both the band as well as the centre frequency. Now, logarithmic discretization means, the parameter 's' should be discretized as

$$s = a_0^k$$

where 'k' runs through the set of all integers and $a_0 > 1$.

Since, we are taking 'k' so as to run through the set of all integers (positive as well as negative), it is obvious that we need not consider the possibility of a_0 to be less than 1. Now for each such 'k', we have a filter. In the ideal condition (we shall study ideal conditions initially and then degrade to the nonideal conditions eventually), the k^{th} filter would have a frequency response as shown in Fig. 10.4.

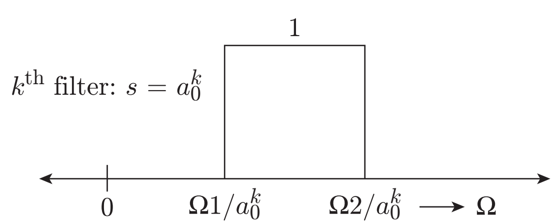

Figure 10.4 | *k^{th} ideal filter responce*

Now, if we pass a signal $x(t)$ through this ideal filter and obtain the CWT, the reconstruction should also be done using the same process. In fact, $x(t)$ could be obtained, as shown in the Fig. 10.5.

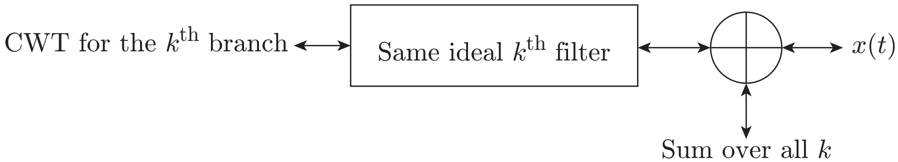

Figure 10.5 | *Reconstruction of* $x(t)$

Thus, each particular k^{th} branch extracts a particular band on the frequency axis and it is obvious that each branch should have a separate nonoverlapping band. This could be explained by an example.

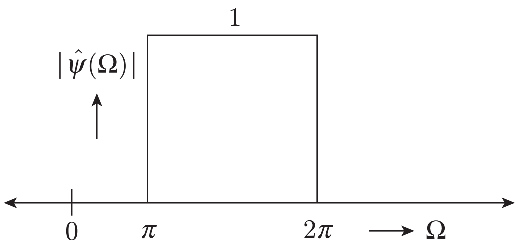

Figure 10.6 | *Ideal* $\widehat{\Psi}(\Omega)$ *with '+' side of* Ω *axis*

Example 10.1.1—Consider a wavelet having ideal frequency response $\widehat{\Psi}(\Omega)$ as shown in Fig .10.6.

Then, if $a_0 = 2$, then the k^{th} branch would be the following:

Thus for different integers k, these bands would be nonoverlapping as shown in Figs. 10.7 and 10.8.

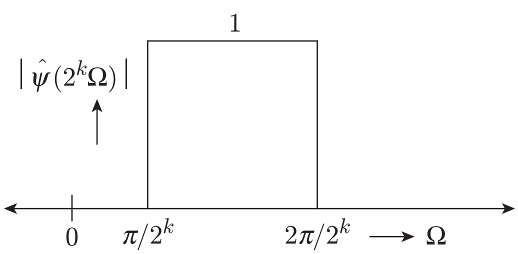

Figure 10.7 | $\widehat{\Psi}(2^k\Omega)$ *with '+' side of* Ω

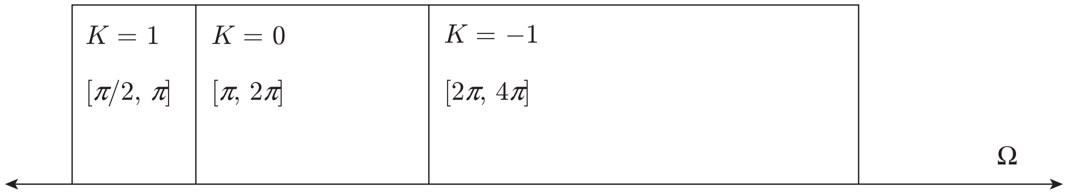

Figure 10.8 | *Nonoverlapping bands with different 'k'*

Now, the question is whether we obtain such discretization in the frequency domain by time-limited functions or not, and the answer is '*NO*' because of the uncertainty principle.

This discretization of the scale parameter also explains the notion of filter banks. In fact, it is equivalent to constructing a filter bank. A filter bank is a collection of filters either with a common input or with all the outputs summed together to get a common output and of course, more subtly, the filters are interrelated. All these qualities are satisfied in the k^{th} branch filters that we are considering here. Now, we look at the analysis and synthesis side. The analysis side is the one that creates the CWT. It is shown below, ignoring the constants

Thus on the analysis and synthesis side, as shown in Figs 10.9 and 10.10.

$$\begin{aligned}
&\text{Output of the } k^{\text{th}}\ \hat{X}(\Omega) \text{ analysis branch} && = \hat{X}(\Omega)(\text{conjugate of } \hat{\Psi}(a_0^k\Omega) = \hat{X}(\Omega)(\overline{\hat{\Psi}(a_0^k\Omega)})\\
&\text{Output from the } k^{\text{th}} \text{ synthesis branch} && = \hat{X}(\Omega)\,|\hat{\Psi}(a_0^k\Omega)|^2\\
&\text{Overall output by summing over all '}k\text{'} && = \hat{X}(\Omega)\sum_{k=-\infty}^{\infty}|\hat{\Psi}(a_0^k\Omega)|^2
\end{aligned}$$

Ideally, $\sum_{k=-\infty}^{\infty}|\hat{\Psi}(a_0^k\Omega)|^2 = 1$ for all Ω indicating a perfect reconstruction. The challenge here is to obtain $\sum_{k=-\infty}^{\infty}|\hat{\Psi}(a_0^k\Omega)|^2 = 1$ for all Ω using time-limited functions.

To meet this challenge, we need to relax in the frequency domain. The first step towards this is not to consider it as a constant. In fact, we can consider it to be lying between two strictly positive constants $c1$ and $c2$. Therefore for designability, we consider

$$0 < c1 \le \sum_{k=-\infty}^{\infty}|\hat{\Psi}(a_0^k\Omega)|^2 \le c2 < \infty$$

Thus $0 < c1 \le c2 < \infty$. Thus instead of this term being strictly constant we allow this term to lie between two constants $c1$ and $c2$. Of course, the term cannot go negative as it is obvious from the expression. Note that $c1$ is strictly greater than 0 and $c2$ is strictly less than ∞. By using this condition, we can make a small change on the synthesis filter as follows and obtain a perfect reconstruction. We define another function $\hat{\hat{\psi}}(\Omega)$ in the frequency domain from $\hat{\psi}(\Omega)$ as

$$\hat{\hat{\Psi}}(\Omega) = \frac{\hat{\Psi}(\Omega)}{\sum_{k=-\infty}^{\infty}|\hat{\Psi}(a_0^k\Omega)|^2} \tag{10.1}$$

Since the condition of $c1$ is imposed on the denominator, it cannot go to 0. Hence, we can define such a function. We aim to show that $\widehat{\Psi}(\Omega)$ could be used on the analysis side while $\widehat{\widehat{\Psi}}(\Omega)$ can be used on the synthesis side. Before proving this, we first show Ψ is automatically admissible (Ψ is real). As discussed earlier, we consider the following integral for admissibility

$$\Rightarrow \int_0^\infty |\widehat{\Psi}(\alpha)|^2 \frac{d\alpha}{\alpha}$$

Let us break this integral as

$$\int_0^\infty |\widehat{\Psi}(\alpha)|^2 \frac{d\alpha}{\alpha} = \sum_{k=-\infty}^{\infty} \int_{a_0^k}^{a_0^{k+1}} |\widehat{\Psi}(\alpha)|^2 \frac{d\alpha}{\alpha} \tag{10.2}$$

Put $\alpha = a_0^k \beta$

$$\Rightarrow \int_{a_0^k}^{a_0^{k+1}} |\widehat{\psi}(\alpha)|^2 \frac{d\alpha}{\alpha} = \int_1^{a_0} |\widehat{\psi}(a_0^k \beta)|^2 \frac{d\beta}{\beta} \tag{10.3}$$

$$\Rightarrow \int_0^\infty |\widehat{\Psi}(\alpha)|^2 \frac{d\alpha}{\alpha} = \int_1^{a_0} \{ \sum_{k=-\infty}^{\infty} |\widehat{\Psi}(a_0^k \beta)|^2 \} \frac{d\beta}{\beta} \tag{10.4}$$

From Eqs. (10.2), (10.3) and (10.4) reversing the order of summation and integration. Since the limits of integration are finite and the argument of integration is also upper bounded by $c2$, integral is indeed convergent and hence $\widehat{\Psi}(\Omega)$ is admissible. In fact, the admissibility integral is upper bounded by,

$$\int_1^{a_0} c2 \frac{d\beta}{\beta} = c2 ln(a_0)$$

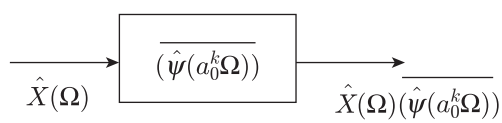

Figure 10.9 | *Analysis filters*

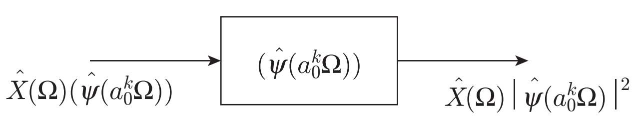

Figure 10.10 | *Synthesis filters*

10.2 | Sum of Dilated Spectra (SDS)

The quantity

$$\sum_{k=-\infty}^{\infty} |\widehat{\Psi}(a_0^k\Omega)|^2$$

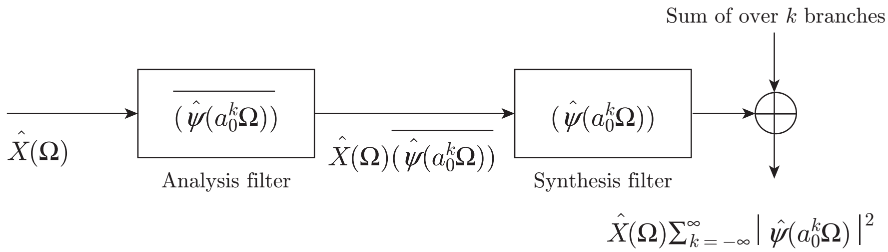

Figure 10.11 | *Overall filter*

is called as Sum of Dilated Spectra (SDS). SDS has primary as well as secondary arguments, where primary arguments a_0, k are those which are important and change in a given context and the secondary argument 'ψ ' is used for the construction of continuous wavelet transform. The overall filter is shown in Fig 10.11. Therefore,

$$\mathrm{SDS}(\Psi, a_0)(\Omega) = \sum_{k=-\infty}^{\infty} |\widehat{\Psi}(a_0^k\beta)|^2 \tag{10.5}$$

where

$$0 < c1 \leq \mathrm{SDS}(\Psi, a_0)(\Omega) \leq c2 < \infty$$

and $c2$ guarantees admissibility.

Now, let us check the admissibility condition for $\hat{\hat{\psi}}(\Omega)$. From Eqs. (10.1) and (10.5),

$$\widehat{\widehat{\Psi}}(\Omega) = \frac{\widehat{\Psi}(\Omega)}{\mathrm{SDS}(\Psi, a_0)(\Omega)} \tag{10.6}$$

For this purpose, we need to consider $\mathrm{SDS}(\widetilde{\psi}, a_0)$

$$|\widehat{\widehat{\Psi}}(a_0^k\Omega)|^2 = \frac{|\widehat{\Psi}(a_0^k\Omega)|^2}{\{\sum_{k=-\infty}^{\infty} |\widehat{\Psi}(a_0^l a_0^k\Omega)|\}^2} \tag{10.7}$$

$$|\widehat{\widehat{\Psi}}(a_0^k\Omega)|^2 = \frac{|\widehat{\Psi}(a_0^k\Omega)|^2}{\{\mathrm{SDS}(\Psi, a_0)(\Omega)\}^2} \tag{10.8}$$

$$\mathrm{SDS}(\widetilde{\Psi}, a_0)(\Omega) = \frac{\sum_{k=-\infty}^{\infty} |\widehat{\Psi}(a_0^k\Omega)|^2}{\{\mathrm{SDS}(\Psi, a_0)(\Omega)\}^2} \tag{10.9}$$

$$\mathrm{SDS}(\widetilde{\Psi}, a_0)(\Omega) = \frac{\mathrm{SDS}(\Psi, a_0)(\Omega)}{\{\mathrm{SDS}(\Psi, a_0)(\Omega)\}^2} \tag{10.10}$$

Cancellation from the numerator and denominator is valid because of the bounds $c1$, $c2$.

$$\mathrm{SDS}(\widetilde{\Psi}, a_0)(\Omega) = \frac{1}{\mathrm{SDS}(\Psi, a_0)(\Omega)} \tag{10.11}$$

We know that, $0 < c1 \le \mathrm{SDS}(\Psi, a_0)(\Omega) \le c2 < \infty$, hence

$$\infty > \frac{1}{c1} \ge \frac{1}{\mathrm{SDS}(\Psi, a_0)(\Omega)} \ge \frac{1}{c2} > 0$$

i.e.,

$$0 < \frac{1}{c2} \le \mathrm{SDS}(\widehat{\Psi}, a_0)(\Omega) \le \frac{1}{c1} < \infty$$

So, $\widetilde{\Psi}$ is also an admissible wavelet.

Using $\widetilde{\Psi}$ on the synthesis side, as shown in Fig 10.12, we have, for the k^{th} branch,

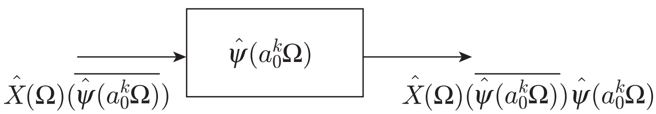

Figure 10.12 | *Synthesis filter with* $\widehat{\widehat{\Psi}}(t)$

the output of the analysis and synthesis filters together can be written as

$$= \hat{x}(\Omega) \times \sum_k \overline{\widehat{\Psi}(a_0^k\Omega)} \times \widehat{\widehat{\Psi}}(a_0^k\Omega)$$

$$= \hat{x}(\Omega) \times \sum_k \overline{\widehat{\Psi}(a_0^k\Omega)} \times \frac{\widehat{\Psi}(a_0^k\Omega)}{\mathrm{SDS}(\Psi, a_0)(\Omega)}$$

$$= \hat{x}(\Omega) \times \frac{\mathrm{SDS}(\Psi, a_0)(\Omega)}{\mathrm{SDS}(\Psi, a_0)(\Omega)}$$

Because of the $c1$ and $c2$, we can cancel the second term for all Ω

$$= \hat{x}(\Omega)$$

This gives perfect reconstruction.

This gives us a new dimension. If we allow $\mathrm{SDS}(\Psi, a_0)(\Omega)$ to lie between two constants $c1$ and $c2$, we need to generalize the notion of analysis and synthesis filters i.e., by allowing a different wavelet on the analysis side and on the synthesis side. Thus we have 'Ψ' on the analysis side and '$\widetilde{\Psi}$' on the synthesis side. We are in fact slowly leading to a different paradigm in the context of filter banks. Earlier, we presumed that the wavelet on the analysis side and on the synthesis side was the same. Now, we are allowing them to be different to relax the condition on SDS for designability.

R Important Note

If $c1 = c2$ then Ψ , $\widetilde{\Psi}$ are the same, that gives us orthogonal filter banks. However, here, we have not yet discretized the translation parameter. We have discretized only the scale. So it does not follow that Haar wavelet has SDS as a constant because the translation parameter is discrete in the Haar case. In particular, if $a_0 = 2$, we get a dyadic orthogonal filter bank.

10.3 | The Theorem of (Dyadic) MRA

As we had seen earlier, we are moving from continuous scaling and translation parameter to discrete scaling and translation. Till now, discretization of the scaling parameter has been discussed; the translation parameter is still continuous. The scaling parameter had been discretized logarithmically. More specifically, our aim is discretizing the translation parameter considering that the wavelet transform is discretized with scaling parameter in powers of two.

Before proceeding to the discretization of translation parameter in the powers of two (i.e. in dyadic scale manner) let us see in short, what we had done earlier.

10.4 | Bi-orthogonal Filter Bank

Filter banks with different analysis and synthesis wavelets and scaling functions are called **Bi-orthogonal Filter Banks**. When we talk about a filter bank given over here, there should be perfect reconstruction.

In general, the k^{th} analysis branch takes input $x(t)$ and subjects it to filter $\overline{\hat{\Psi}(a_0^k\Omega)}$, where $a_0 > 1$ and k runs over all integer. Output of k^{th} analysis branch given as input to k^{th} synthesis branch whose frequency response is $\hat{\widetilde{\Psi}}(a_0^k\Omega)$.

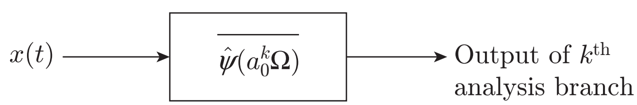

Figure 10.13 | *Analysis branch*

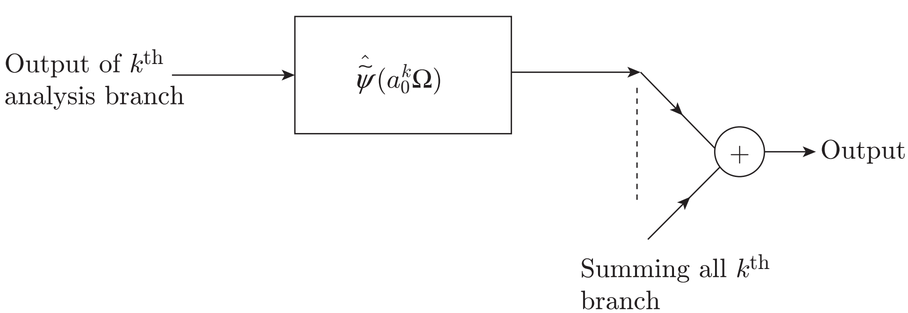

Figure 10.14 | *Synthesis branch*

All synthesis branches are added together to get the output.

We have $\widehat{\widehat{\Psi}}(a_0^k\Omega)$ in frequency domain as

$$\widehat{\widehat{\Psi}}(\Omega) = \frac{\widehat{\Psi}}{\mathrm{SDS}(\Psi, a_0)(\Omega)}$$

Where, SDS is the sum of dilated spectra.

$$\mathrm{SDS}(\Psi, a_0)(\Omega) = \sum_{k=-\infty}^{+\infty} |\widehat{\Psi}(a_0^k\Omega)|^2$$

This SDS is bounded by $C1$ and $C2$ so that

$$0 < C1 \leq \mathrm{SDS}(\Psi, a_0)(\Omega) \leq C2 < \infty$$

We had guaranteed Ψ is admissible because of $C1$. $\widehat{\widehat{\Psi}}$ was meaningful because of upper and lower bound. $\widetilde{\Psi}$ is also admissible and the bound on SDS of $\widetilde{\Psi}$ is $\frac{1}{C1}, \frac{1}{C2}$. In case $\mathrm{SDS}(\psi, a_0)(\Omega)$ is a constant for all Ω then it is called an orthogonal filter bank.

10.5 | Orthogonal Filter Bank

When filters on analysis side and synthesis side are the same (i.e. same wavelet function with same scaling parameter) then these are called **Orthogonal Filter Bank**.

10.5.1 Construction of Orthogonal Filter Bank

Example 10.5.1 — Orthogonal Filter Design.

Let us define $\widehat{\widehat{\widehat{\Psi}}}(\Omega)$ as

$$\widehat{\widehat{\widehat{\Psi}}}(\Omega) = \frac{\widehat{\Psi}(\Omega)}{+\sqrt{\mathrm{SDS}(\Psi, a_0)(\Omega)}}$$

Same as earlier, because of upper and lower bound there is meaning of putting $\mathrm{SDS}(\psi, a_0)(\Omega)$ in denominator.

$$0 < \sqrt{C1} \leq \sqrt{\mathrm{SDS}(\Psi, a_0)(\Omega)} \leq \sqrt{C2} < \infty$$

With above observation let us prove that the $\approx{\psi}$ is admissible, to prove it take $\mathrm{SDS}(\overset{\approx}{\psi}, a_0)(\Omega)$

$$\mathrm{SDS}(\overset{\approx}{\Psi}, a_0)(\Omega) = \frac{\sum_{k=-\infty}^{+\infty} |\widehat{\Psi}(a_0^k\Omega)|^2}{\mathrm{SDS}(\Psi, a_0)(\Omega)}$$

Sum of dilated spectra is independent of the scaling parameter a_0^k, let us replace Ω by $a_0^k\Omega$. It does not affect the value of SDS i.e.

$$\mathrm{SDS}(\Psi, a_0)(\Omega) = \mathrm{SDS}(\Psi, a_0)(a_0^m\Omega)$$

Proof (in general):

$$\mathrm{SDS}(\Psi, a_0)(a_0^m \Omega) = \sum_{k=-\infty}^{+\infty} |\widetilde{\Psi}(a_0^k a_0^m \Omega)|^2$$

$$= \sum_{k=-\infty}^{+\infty} |\widetilde{\Psi}(a_0^{k+m} \Omega)|^2$$

Here, m is a constant integer. Therefore, as k runs over all integers, $k+m$ will also run over all integers i.e.

$$\mathrm{SDS}(\widetilde{\widetilde{\Psi}}, a_0)(\Omega) = \frac{\sum_{k=-\infty}^{+\infty} |\widehat{\Psi}(a_0^k \Omega)|^2}{\mathrm{SDS}(\widetilde{\Psi}, a_0)(\Omega)}$$

$$=1$$

for all Ω.

We have a constant SDS in case of $\widetilde{\widetilde{\Psi}}$. So, $\widetilde{\widetilde{\Psi}}$ can be used as wavelet on both analysis side and synthesis side because $\widetilde{\widetilde{\Psi}}$ is an admissible and orthogonal wavelet.

$\widetilde{\widetilde{\Psi}}$ is admissible and its SDS has upper bound equal to lower bound and that is equal to one. Here, we have constructed an orthogonal wavelet function from a bi-orthogonal wavelet. But still the translation parameter is continuous.

For example in the HAAR wavelet, it does not satisfy the condition of upper bound being equal to lower bound. This is because, in case of HAAR the orthogonality is with respect to discrete shifts in time, not continuous shifts. This is a weaker requirement. However, this is desirable in implementation, as we do not want to retain the whole continuous translation parameter. Now, we are going to accept a wavelet Ψ which has the property of admissibility and reconstructibility, i.e. it has a finite nonzero $C1$ and $C2$, and we are going to ask, can we discretize the translation parameter taking the dyadic case i.e. $a_0 = 2$ to construct a dyadic multiresolution analysis.

10.6 | Dyadic Multiresolution Analysis

Examples of dyadic MRA constitute HAAR MRA, Daubechies MRA. These are essentially the special case of $a_0 = 2$. The wavelet obeys the requirement

$$0 < C1 \leq \mathrm{SDS} \leq C2 < \infty, \text{for all } \Omega$$

The wavelet may not obey this requirement for all a_0, but it obeys this requirement for $a_0 = 2$. So these bounds, in general, depend on a_0. Also, the wavelet admits discretizing the translation parameter. Now, the question is *should we discretize the translation parameter in the same way in all the branches, or do it differently?*

Let us look at the k^{th} branch. On the k^{th} analysis branch, the output is broadly a bandpass function, that is, it is significant in a certain band of frequencies, not around zero. For different values of k, there is a logarithmic variation of the band. We invoke a generalization of the sampling theorem for bandpass functions and illustrate it with an example.

Consider a bandpass function where the band on Ω lies between π and 2π (Fig. 10.15).

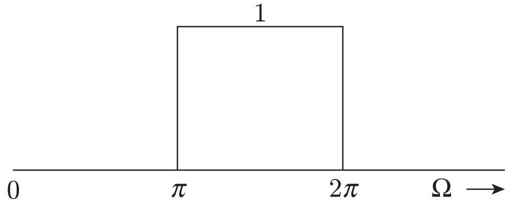

Figure 10.15 | *Bandpass function*

Discretizing the translation parameter basically talks about sampling the output of the k^{th} analysis branch and feeding these samples to the k^{th} synthesis branch, instead of the continuous function. So "*How do we sample the output of the k^{th} branch so that we do not lose anything*", is equivalent to the question "*How do we discretize the translation parameter?*"

We have two options:

1. To sample the signal following the Nyquist criteria, and considering 2π as the highest frequency.
2. To sample it presuming that the band between o and π is blank and signal occupancy is only between π and 2π.

In the second case, we can use a sampling rate twice the band occupancy.

Here band occupancy = π

Therefore, we could use a sampling rate = 2π

If we simply use the Nyquist criteria, we should have sampling frequency f_s such that

$$2\pi f_s = 4\pi, \Rightarrow f_s = 2$$

But we can also do with a sampling frequency f_s such that

$$\begin{aligned} 2\pi f_s &= 2 \text{ times the band occupancy} \\ &= 2\pi \end{aligned}$$

therefore,

$$f_s = 1$$

Suppose we do use a sampling frequency of 1. Then we are adding all the aliases, which are shifts of the original spectrum by $2\pi k$, for all integer k. Figure 10.16 shows the original spectrum along with the aliases due to shifting the spectrum by 2π and -2π.

The translations by 2π and -2π do not affect the original spectrum. Similarly, translations by 4π and -4π leave the original spectrum 'unpolluted'. For higher translations of the original spectrum, the aliases move further away from the original spectrum, and hence insignificant. The original part of the signal is, therefore, unaffected. The original signal can be retrieved by putting a bandpass filter between π and 2π. This is, therefore, the bandpass sampling which cannot, however, be generalized for any

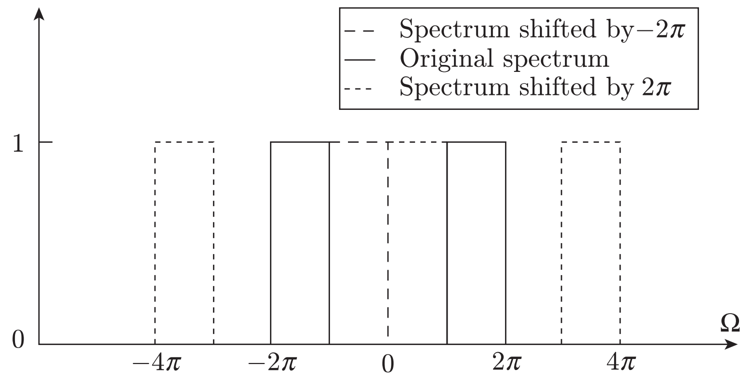

Figure 10.16 | *Frequency spectrum of bandpass function*

position of the frequency band, i.e. wherever a band of π is put, a sampling rate of 2π may be used, this is not true in general but depends on the position of the band. That is why, the Bandpass Sampling theorem is a little more complicated than the conventional low-pass sampling theorem. It certainly is more economical. In fact, in the dyadic MRA, we are essentially invoking the Bandpass Sampling theorem.

The same principle is applicable for bands between 2π and 4π, 4π and 8π, and so on. So for different branches on the analysis side, we would need to use different sampling frequencies, which will also be related logarithmically. That is exactly what happens in Dyadic MRA. When we go from V_0 to V_1, or from V_1 to V_2, number of points are doubled. Going from V_0 to V_{-1}, number of points is halved. All these are essentially manifestations of the Bandpass Sampling Theorem.

Let us now focus on $a_0 = 2$. We need to use a logarithmic change of the form $2k$ of sampling. On the k^{th} branch, the sampling rate relates to $2k$. This is automatically ensured by the Dyadic MRA axioms.

10.6.1 Axioms of a Dyadic MRA

1. **Ladder axiom**

$$\ldots V_{-2} \subset V_{-1} \subset V_0 \subset V_1 \subset V_2 \subset \ldots$$

   V_0 is the subspace where the functions are bandpass in a certain band, V_1 is the subspace where functions are bandpass in the next higher band, V_2 the next higher band and so on. Each time the frequency occupancy is doubled. As we go downwards, the frequency occupancy is halved. So, as we go upwards the sampling frequency is doubled, and as we go downwards the sampling frequency is halved.

2. **Axiom of perfect reconstruction**

$$\overline{\bigcup_{m\in\mathbb{Z}} V_m} = L_2(\mathbb{R})$$

   When all the incremental subspaces are collected together, we go back to the original input signal.

3. We will remain in $L_2(\mathbb{R})$ so as we go downwards we are going towards smaller and smaller bands and finally we are going to reach a band with zero power.

$$\bigcap_{m\in\mathbb{Z}} V_m = \{0\}$$

4. If

$$x(t) \in V_0$$

then

$$x(2^m t) \in V_m$$

Implicitly, this provides for logarithmic sampling. More specifically, logarithmic sampling with a order of 2.

5. **Axiom of translation**
If

$$x(t) \in V_0$$

then

$$x(t-n) \in V_0, \text{for all } n \in Z$$

It essentially says that we have a uniform sampling.

6. **Axiom of orthogonal basis**
There exists a $\Phi(t)$ such that $\{\Phi(t-n)\}_{n\in\mathbb{Z}}$ is a basis for V_0. Given axioms 4 and 5, we have a corresponding basis for each of the V_m. This axiom gives us a way to reconstruct the function from samples. The coefficients in the expansion of the function with respect to $\{\Phi(t-n)\}_{n\in\mathbb{Z}}$ are like generalized samples of the function after filtering.

Now, V_0 is a collective subspace and we are sampling a collective subspace, not an incremental subspace. The theorem of multiresolution analysis would give us an incremental subspace.

10.7 | Theorem of Multiresolution Analysis

R Given axioms 1 to 6, there exists a function $\Psi(t)$ ($\Psi(t) \in L_2(\mathbb{R})$ and $\Psi(t) \in V_1$) such that $\{\Psi(2^m t - n)\}_{m\in\mathbb{Z}, n\in\mathbb{Z}}$ forms an orthogonal basis for $L_2(\mathbb{R})$.

10.8 | Proof of Theorem of Dyadic MRA

In the last section, we conclude that one of the ways to interpret the whole question of discretization of the translation parameter is to raise the issue of sampling. But in generalized sampling note that we dealt with the High-Pass function instead of a band limited function and we also noted in brief that if we look into the discretization of the translation parameter, in space V ($V_0, V_1, V_2, \ldots$ ladder) it amounted to a version of the band-limited sampling theorem. Because if we look into the spaces of V_0 contained in V_1, V_1 contained in V_2, and so on, in the ladder, we are talking of a band-limited function with the band doubling each time but the bands are around zero frequency, so it is all inclusive bank up to a certain frequency, then double, then four times and eight times as you go up the ladder. Obviously, the sampling frequency needs to be doubled.

On the other hand, we looked at the ideal case of the Bandpass function and we said that if the band was strategically placed for example, if we look at the band between π and 2π, and sampled such a bandpass signal contained in this band at a sampling rate of $2\times(\pi)$ instead of $2\times(2\pi)$. We got the bandpass version of the sampling theorem.

We saw that the translates of spectrum created by sampling the bandpass function at the angular sampling frequency of two times band (2π) instead of (4π), which is the highest frequency, we still get dilates of the original spectrum not overlapping with the original frequency spectrum. Therefore, we can put a Bandpass filter and reconstruct the signal even after sampling.

Now, the sampling functions in ideal sense, i.e. ideal Bandpass reconstruction filter has an impulse response, which is unrealizable and therefore, the use of wavelets is a way of bandpass sampling and reconstruction practically.

10.9 | Proof of Theorem of Dyadic MRA

Example 10.9.1

Look at the typical function $f(t)$ in the incremental subspace W_0.

Characteristics of the function $f(t)$:

1. $f(t)$ is orthogonal to every translate of $\phi(t)$ i.e. $\phi(t-m)$, where $m \in \mathbb{Z}$.
2. $f(t-m) \in V_1$. $f(t)$ can be expressed or expanded in terms of $\phi(2t-n)$, where $n \in \mathbb{Z}$.

Combining these two properties and coming up with some interesting results.

Let $f(t) = \sum_{n=-\infty}^{+\infty} f[n]\phi(2t-n)$ where $f[n]$ are the coefficients of expansion.

$$\phi(t) \in V_0 \in V_1$$

$$\phi(t) \text{ can be expanded in terms of } \phi(2t-n)$$

$$\phi(t) = \sum_{n=-\infty}^{+\infty} h[n]\phi(2t-n)$$

where $h[n]$ is the low-pass impulse response coefficient.

$$\phi(t-m) = \sum_{n=-\infty}^{+\infty} h[n]\phi(2t-2m-n)$$

Using the orthogonality property:

$$\langle f(t), \phi(t-m)\rangle = 0$$

$$\left\langle \sum_n f[n]\phi(2t-n), \sum_l h[l]\phi(2t-2m-1) \right\rangle = 0 \quad \forall m$$

We now invoke the orthogonality of $\phi(t)$ with its own translates:

$$\langle \phi(2t-k_1), \phi(2t-k_2)\rangle = \int_{-\infty}^{+\infty} \phi(2t-k_1)\overline{\phi(2t-k_2)}dt$$

Put $2t = \lambda$

$$\langle \phi(\lambda-k_1), \phi(\lambda-k_2)\rangle = \frac{1}{2}\int_{-\infty}^{+\infty} \phi(\lambda-k_1)\overline{\phi(\lambda-k_2)}d\lambda = \frac{1}{2}\delta[k_1-k_2]$$

Thus,

$$\langle f(t), \phi(t-m)\rangle = \sum_n \sum_l f[n]\overline{h[l]}\langle \phi(2t-n), \phi(2t-2m-l)\rangle = 0$$

Only $n = 2m + l$ survives.

$$\langle f(t), \phi(t-m) \rangle = \frac{1}{2} \sum_l f[2m+l]\overline{h[l]}$$

We are essentially looking at the cross-correlation of the sequences $f[\cdot]$ and $h[\cdot]$. Cross-correlation is often denoted by:

$$r_{fh}[p] = \sum_l f[p+l]\overline{h[l]}$$

Therefore, $r_{fh}[p]_{p-2m} = 0 \quad \forall \quad m \in \mathbb{Z}$

The cross-correlation of $f[\cdot]$ and $h[\cdot]$ is evaluated at all even shifts. This is the orthogonality requirement. We know how to deal with the situation when we want to look at an even location; in fact, we know the operator that does that (downsampling by 2). So if you were to take notionally this cross-correlation sequence and down sample by 2, you will get an all-zero sequence, this is depicted in the figure below:

$$r_{fh}[p] \longrightarrow \boxed{\downarrow 2} \longrightarrow \text{Zero sequence}$$

$$r_{fh}[p] \longrightarrow \boxed{\downarrow 2} \longrightarrow \boxed{\uparrow 2} \longrightarrow \text{All zero sequence}$$

In Z-domain

$$r_{fh}[p] \to R_{fh}(z)$$

$$r_{fh}[p] \longrightarrow \boxed{\downarrow 2} \longrightarrow \boxed{\uparrow 2} \xrightarrow{\text{Z-Transform}} \frac{1}{2}\{\mathrm{R}_{fh}(\mathrm{Z}) + \mathrm{R}_{fh}(-\mathrm{Z})\}$$

$$R_{fh}(z) + R_{fh}(-z) = 0$$

$$F(z)H(z^{-1}) + F(-z)H(-z^{-1}) = 0$$

$$\frac{F(z)}{F(-z)} = -\frac{H(-z^{-1})}{H(z^{-1})}$$

This typical function F belongs to the incremental subspace. In the ratio $\dfrac{F(z)}{F(-z)}$, we have managed to cancel which is specific to $F(z)$. So, $F(z)$ must be of form:

$$F(z) = -\Lambda(z)H(-z^{-1}) \tag{10.12}$$

$$F(-z) = \Lambda(z)H(z^{-1}) \tag{10.13}$$

Put $z = -z$ in Eq. (10.12), we get:

$$F(-z) = -\Lambda(-z)H(z^{-1}) \tag{10.14}$$

Comparing Eqs. (10.13) and (10.14) we have:

$$\Lambda(z) = -\Lambda(-z)$$

$$\Lambda(z) + \Lambda(-z) = 0$$

In terms of sequences, if $\Lambda(z)$ is the Z-transform of a sequence, then sequence should be zero at all even locations. Sequence could have been obtained by upsampling another sequence and shifting by one place. By upsampling by 2, zeros get introduced at odd positions. For making a zero sequence, shift by odd number of samples.

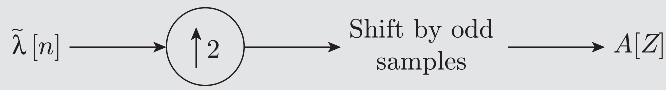

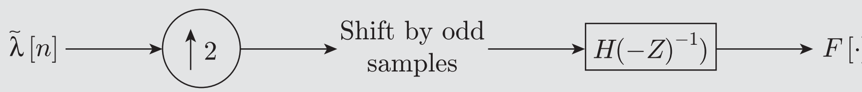

We could in particular choose odd number of samples: $L-1$, where L = Low Pass Analysis Filter length.

Recall that $z^{-(L-1)}H(-z^{-1})$ is essentially the analysis High-Pass Filter (HPF).

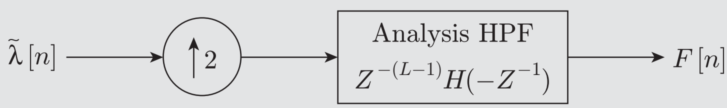

$$f(t) = \sum_{n=-\infty}^{+\infty} f[n]\phi(2t-n)$$

Let $g[n]$ be inverse Z-transform of $z^{-(L-1)}H(-z^{-1})$.

Essentially $g[n]$: impulse response of the analysis HPF.

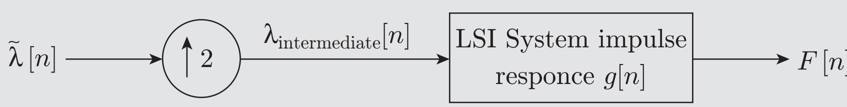

$$\begin{aligned} f[n] &= \lambda_{\text{intermediate}}[n] * g[n] \\ &= \sum_{k=-\infty}^{+\infty} \lambda_{\text{intermediate}}[k]g[n-k] \end{aligned}$$

$\lambda_{\text{intermediate}}[k]$ is nonzero only at $2k$ (even).

$$
\begin{aligned}
f[n] &= \sum_{k=-\infty}^{+\infty} \lambda_{\text{intermediate}}[2k]g[n-2k] \\
&= \sum_{k=-\infty}^{+\infty} \tilde{\lambda}[k]g[n-2k] \\
f(t) &= \sum_{n=-\infty}^{+\infty} \sum_{k=-\infty}^{+\infty} \tilde{\lambda}[k]g[n-2k]\phi(2t-n) \\
&= \sum_{k=-\infty}^{+\infty} \tilde{\lambda}[k] \sum_{n=-\infty}^{+\infty} g[n-2k]\phi(2t-n)
\end{aligned}
$$

Substitute $n-2k=q$

$$
\begin{aligned}
f(t) &= \sum_{k=-\infty}^{+\infty} \tilde{\lambda}[k] \sum_{q=-\infty}^{+\infty} g[q]\phi(2t-q-2k) \\
&= \sum_{k=-\infty}^{+\infty} \tilde{\lambda}[k] \sum_{q=-\infty}^{+\infty} g[q]\phi(2(t-k)-q)
\end{aligned}
$$

Here, $(t-k)$ denotes shift in continues variable t by k. Now, let us define

$$
\psi(t) = \sum_{q \in \mathbb{Z}} g[q]\phi(2t-q)
$$

It follows that $\phi(\cdot) \in V_1$. Thus, effectively we have,

$$
f(t) = \sum_{k} \tilde{\lambda}[k]\psi(t-k)
$$

The importance of this equation is that we have proved that this prototype function $f(t)$ is in the orthogonal complement of V_0 in V_1, i.e. W_0 is expressible in terms of integer translates of function $\psi(t)$ and that is exactly the goal. If you could capture single function $\psi(t)$ and its entire integer translate forms, this basis could span W_0, i.e. $(\psi(t-k))_{k\in\mathbb{Z}}$ spans W_0.

The proof is almost complete except to demonstrate

1. $(\psi(t-k))_{k\in\mathbb{Z}}$ forms orthogonal set.
2. $\langle \psi(t-k), \phi(t-k) \rangle = 0 \quad \forall k, m \in \mathbb{Z}$.

This will be taken up in the Chapter 11.

Exercises

Exercise 10.1

The Fourier Transform $|\widehat{\psi}(s\Omega)|$ of a real, continuous time, square integrable function $\psi(t)$ has the squared magnitude shown only for the positive side of angular frequency axis, in Fig. 10.17. Show that $\psi(t)$ is admissible as a wavelet and that it admits for dyadic discretization of its scale parameter.

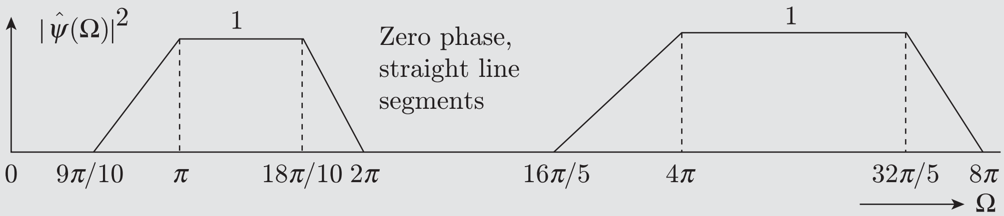

Figure 10.17 | $|\widehat{\psi}(\Omega)|^2$ *(for '+' Ω axis)*

Hint: Clearly $\int_0^\infty |\widehat{\psi}(\alpha)|^2$ is upper bounded by

$$\int_{9\pi/10}^{2\pi} 1.\frac{d\Omega}{\Omega} + \int_{16\pi/5}^{8\pi} 1.\frac{d\Omega}{\Omega} = ln(\frac{2\pi}{9\pi/10}) + ln(\frac{8\pi}{16\pi/5})$$

which is finite. Hence $\psi(t)$ is admissible.

$$|\widehat{\psi}(\Omega)|^2 = |\widehat{\psi_1}(\Omega)|^2 + |\widehat{\psi_1}(\Omega)|^2$$

where $|\widehat{\psi_1}(\Omega)|^2$ is the part of the spectrum between $9\pi/10$ and 2π, $|\widehat{\psi_2}(\Omega)|^2$ between $16\pi/5$ and 8π. We need to consider,

$$\sum_{k=-\infty}^{\infty} |\widehat{\psi}(2^k\Omega)|^2 = \sum_{k=-\infty}^{\infty} |\widehat{\psi_1}(2^k\Omega)|^2 + \sum_{k=-\infty}^{\infty} |\widehat{\psi_2}(2^k\Omega)|^2$$

only over a logarithmic interval of 2.
From Fig. 10.18,

$$\sum_{k=-\infty}^{\infty} |\widehat{\psi_1}(2^k\Omega)|^2 = 1$$

everywhere.
From Fig. 10.19,

$$\sum_{k=-\infty}^{\infty} |\widehat{\psi_2}(2^k\Omega)|^2 = 1$$

everywhere.
Thus $\sum_{k=-\infty}^{\infty} |\widehat{\psi}(2^k\Omega)|^2 = 2$ everywhere which satisfies the condition for dyadic discretization.

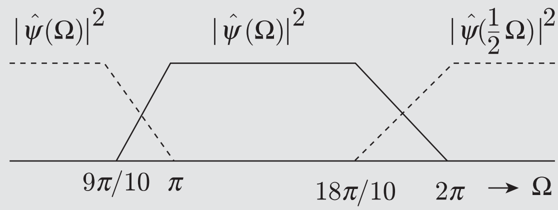

Figure 10.18 | *Dilated spectra of* $|\widehat{\psi_1}(\Omega)|^2$

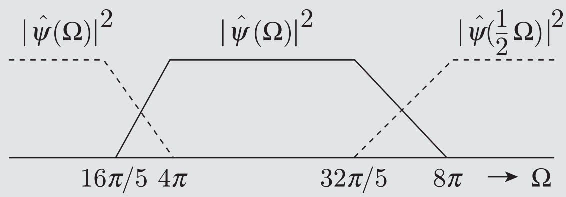

Figure 10.19 | *Dilated spectra of* $|\widehat{\psi_2}(\Omega)|^2$

Exercise 10.2

The Fourier Transform $\widehat{\Phi}(\Omega)$ of a real, continuous time, square integrable function $\Phi(t)$ has the squared magnitude shown only for the positive side of angular frequency axis, in Fig. 10.20. Establish that the set $\{\Phi(t-n)$, for all integers n$\}$ is orthogonal for some condition(s) on Δ_1 and Δ_2 assuming that Δ_1 and Δ_2 are both nonnegative real numbers between 0 and π. Obtain the condition(s).

Hint: We consider $\sum_{k=-\infty}^{\infty}|\hat{\phi}(\Omega+2\pi k)|^2$ over interval of 2π as shown in Fig. 10.21.
On adding the spectral components shown, we find that the sum is a constant if and only if $\Delta_1=\Delta_2$.

Hence the condition is $\Delta_1=\Delta_2$ for which $\sum_{k=-\infty}^{\infty}|\hat{\phi}(\Omega+2\pi k)|^2$ is a constant, whereupon $\{\phi(t-n)\}_{n\varepsilon Z}$ is an orthogonal set.

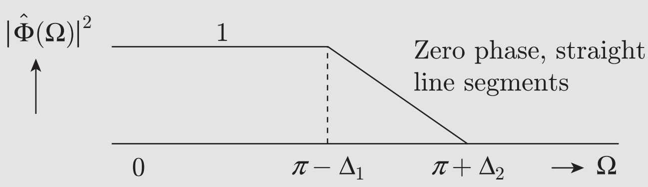

Figure 10.20 | *Spectra of* $|\widehat{\Phi}(\Omega)|^2$

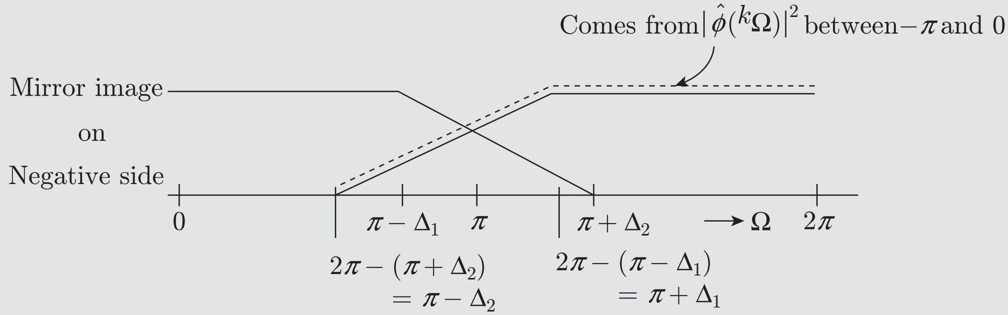

Figure 10.21 | *Dilated spectra of* $|\widehat{\Phi}(\Omega)|^2$

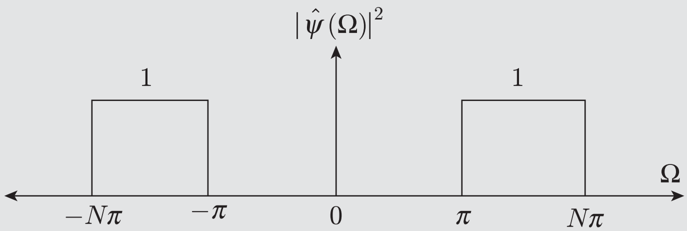

Figure 10.22 | $|\widehat{\psi}(\Omega)|^2$

Exercise 10.3

The Fourier Transform $\widehat{\psi}(\Omega)$ of a real, continuous time, square integrable function $\Phi(t)$ has the squared magnitude shown in Fig. 20.22. Find the maximum value of 'a_0' for the discretization of scale so that the dilates cover entire spectrum for N ε Z and N $\geq$ 2.

Hint: We consider 3-cases for the discretization of scale $s = a_0^k$, i.e. $a_0 = N$, $a_0 < N$ and $a_0 > N$. The dilated spectra for these 3-cases considering the positive Ω axis are shown in Figs. 10.23, 10.24 and 10.25 respectively.

By observing the dilated spectra it is obvious that for $a_0 > N$ holes are created in the spectrum, hence the maximum range of 'a_0' is N.

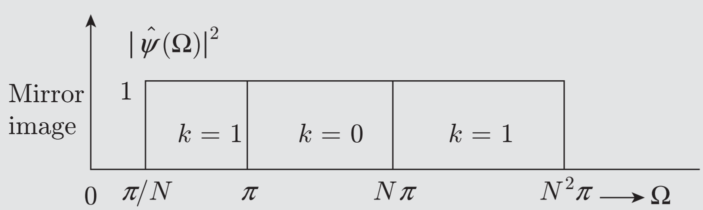

Figure 10.23 | $|\widehat{\psi}(\Omega)|^2$ *for* $a_0 = N$

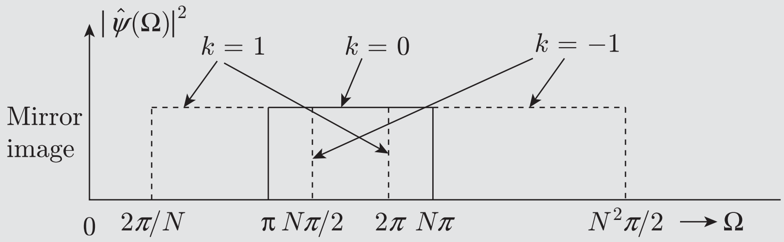

Figure 10.24 | $|\widehat{\psi}(\Omega)|^2$ *for* $a_0 < N$ *with a specific case of* $a_0 = N/2$

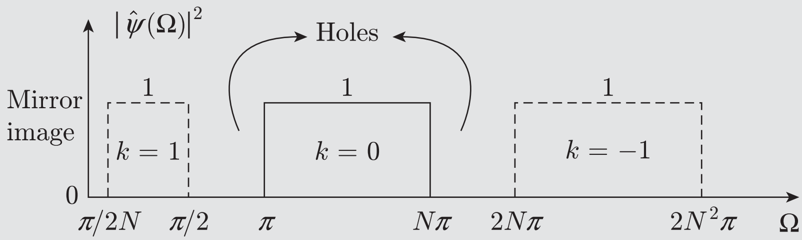

Figure 10.25 | $|\widehat{\psi}(\Omega)|^2$ *for* $a_0 > N$ *with a specific case of* $a_0 = 2N$

Exercise 10.4

For the Haar Wavelet $\psi(t)$, shown in Fig. 10.26. Show that

$$0 < c1 \le SDS(\psi, a_0)(\Omega) \le c2 < \infty$$

(**Hint:** The upper bound $c2$ could be obtained from the admissibility condition of Haar while the lower bound $c1$ is a bit tricky).

The Fourier transform $\widehat{\psi}(\Omega)$ of $\psi(t)$ can be obtained as

$$\widehat{\psi}(\Omega) = \int_0^{\frac{1}{2}} e^{-j\Omega t}\,dt - \int_{\frac{1}{2}}^{1} e^{-j\Omega t}\,dt$$

$$\widehat{\psi}(\Omega) = j.e^{\frac{-j\Omega}{2}} \frac{\sin^2 \frac{\Omega}{4}}{\frac{\Omega}{4}}$$

Therefore $|\widehat{\psi}(\Omega)|^2$ is of the form,

$$\widehat{\psi}(\Omega)^2 = \frac{\sin^4 \frac{\Omega}{4}}{\left(\frac{\Omega}{4}\right)^2}$$

Now consider the admissibility integral,

$$\Rightarrow \int_0^\infty |\widehat{\psi}(\Omega)|^2 \frac{d\Omega}{\Omega}$$

$$\int_0^\infty |\widehat{\psi}(\Omega)|^2 \frac{d\Omega}{\Omega} = \int_0^\infty \frac{\sin^4 \frac{\Omega}{4}}{\left(\frac{\Omega}{4}\right)^2} \frac{d\Omega}{\Omega}$$

$$\int_0^\infty |\widehat{\psi}(\Omega)|^2 \frac{d\Omega}{\Omega} = \int_0^\Delta \frac{\sin^4 \frac{\Omega}{4}}{\left(\frac{\Omega}{4}\right)^2} \frac{d\Omega}{\Omega} + \int_\Delta^\infty \frac{\sin^4 \frac{\Omega}{4}}{\left(\frac{\Omega}{4}\right)^2} \frac{d\Omega}{\Omega}$$

where $\Delta > 0$.

It is easy to show that the above integral is convergent, hence the upper bound $c2$ is finite.

The $|\widehat{\psi}(\Omega)|^2$ is, as shown in Fig. 10.27.

The dilated spectra moves the nulls of $|\widehat{\psi}(\Omega)|^2$, in order to satisfy the lower bound $c1$, these nulls should not coincide.

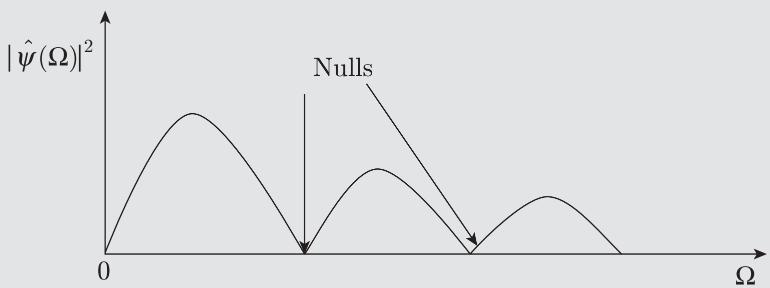

Figure 10.27 | $|\widehat{\psi}(\Omega)|^2$

Exercise 10.5

Establish a procedure for Bandpass Sampling. Construct the spectrum after sampling (Fig. 10.28) with Bandpass Function with sampling frequency $f_s = 2 \times$ Bandwidth. Is there any aliasing?

Hint: Suppose we consider a Bandpass Function where the band on Ω lies between π and 2π (Fig. 10.29).

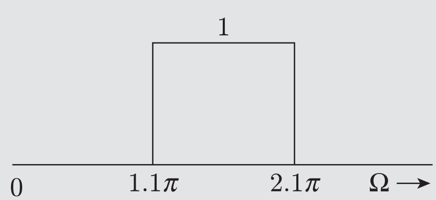

Figure 10.28 | *Bandpass function*

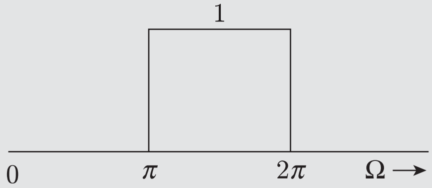

Figure 10.29 | *Bandpass function*

What could be the sampling rate when we talk about discretizing the translation parameter. We are essentially talking about sampling the output of this filter on the k^{th} analysis branch and feeding those samples instead of continuous function to the input of k^{th} synthesis branch.

How do we sample in such a way that we don't loose something. How do we discretize the translation parameter?

Band occupancy is π.

If we simply use Nyquist criteria and sampling frequency as f_s.

Then $2\pi f_s = 4\pi$.

Therefore, $f_s = 2$.

But we can also do with a sampling rate

$$2\pi f_s = 2 \times \text{band occupancy} = 2\pi$$

Therefore, $f_s = 1$.

In Bandpass sampling theorem, we decide the sampling frequency by looking at the bandpass occupancy and not the maximum frequency.

Suppose we use a sampling rate of 1. We are essentially adding all aliases, which are shifts of the original spectrum by $(2\pi \times 1 \times k)$ for all integer k.

Take the original spectrum, shift it by all multiples $(2\pi \times 1 \times k)$ for all integer k and add up these translates.

We can retrieve the original signal by putting any filter between π and 2π. However, we can not generalize this. Whenever there is a band occupancy of π we can not use sampling rate of 2π (i.e. twice the band and not the maximum frequency). It is true, depending on the location of the band as well. That is why Bandpass Sampling theorem is more complicated than the conventional Low-Pass Sampling Nyquist theorem.

For the Bandpass function given in the question (Fig. 10.29), band occupancy is π. If we use the sampling rate as (2 × band occupancy) i.e. 2π. We will get the following spectrum as shown in Fig 10.30.

From the above spectrum it is clear that there will be aliasing and we cannot retrieve the original signal.

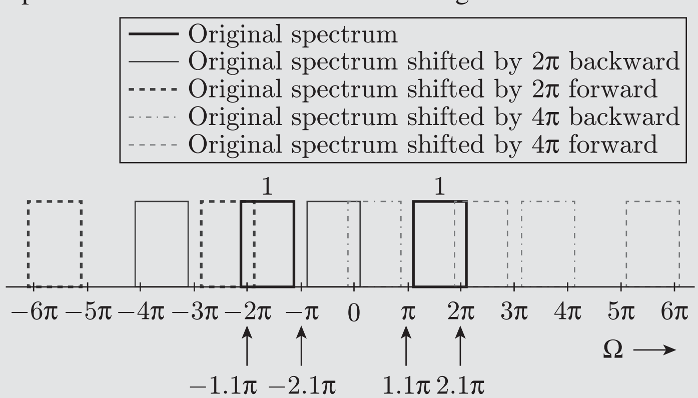

Figure 10.30 | *Sampling of bandpass function*

Exercise 10.6

Explain the concept of log periodicity. Prove that sum of dilated spectra is log periodic.

Hint: Generally in Ω axis the translates are shifted by multiples of some frequency (a parameter). Consider $(k \times \pi)$, where k can take any integer value. Therefore, the shifts will be $\pi, 2\pi, 3\pi$, and so on.

But if we consider the $(a^k \times \pi)$, where a is any constant and k can take any integer value. Then shifts will be of the multiples of a^k times π. i.e. $a\pi, a^2\pi, a^3\pi, a^4\pi$.

Log periodic signal means the signal whose period is power of some constant, like a^k where a is constant and k can take any integer value.

To prove that the Sum of Dilated Spectra (SDS) is log-periodic. i.e.

To show that,

$$\mathrm{SDS}(\Psi, a_0)(\Omega) = \mathrm{SDS}(\Psi, a_0)(a_0^m \Omega)$$

Proof (in general):

$$\begin{aligned}\mathrm{SDS}(\Psi, a_0)(a_0^m \Omega) &= \sum_{k=-\infty}^{+\infty} |\widetilde{\Psi}(a_0^k a_0^m \Omega)|^2 \\ &= \sum_{k=-\infty}^{+\infty} |\widetilde{\Psi}(a_0^{k+m} \Omega)|^2\end{aligned}$$

Here m is a constant integer. Therefore, as k runs over all integers, $k+m$ will also run over all integers.

Exercise 10.7

What is the significance of closure in the Union Axiom of MRA?

Hint: Union Axiom

$$\overline{\bigcup_{m \in \mathbb{Z}} V_m} = L_2(\mathbb{R})$$

This is essentially an Axiom of perfect reconstruction. When all incremental subspaces are combined together, we get the whole input back.

Union over V_m should cover the entire space on $L_2(\mathbb{R})$. But in some cases it may leave some patches on the boundary. While taking the closure also ensure covering the entire boundary as well.

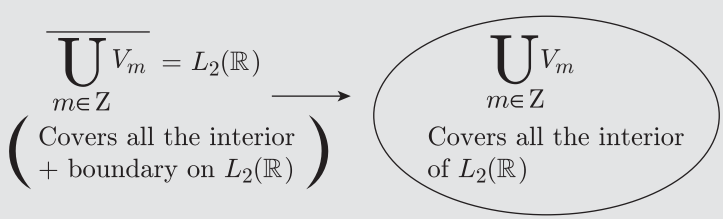

Figure 10.31 | *Closure on union of V_m*

Exercise 10.8

$\lambda[n] = (1, 2, 4, 2, 1)$

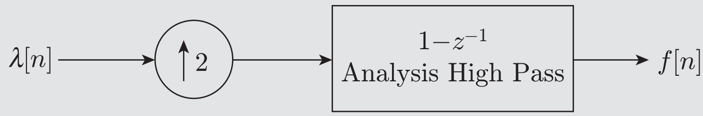

Find $f[n]$ and plot $f(t)$, show that $f(t) = \sum_n f[n]\phi(2t-n)$ lies in W_0

Hint: $\lambda_{\text{intermediate}}(z) = 1 + 2z^{-2} + 4z^{-4} + 2z^{-6} + z^{-8}$

So $F(z)$ can be expressed as product of $\lambda_{\text{intermediate}}(z)$ with the Analysis High-Pass Filter.

$$\begin{aligned}
F(z) &= (1 - z^{-1})(\lambda_{\text{intermediate}}(z)) \\
&= (1 - z^{-1})(1 + 2z^{-2} + 4z^{-4} + 2z^{-6} + z^{-8}) \\
&= 1 - z^{-1} + 2z^{-2} - 2z^{-3} + 4z^{-4} - 4z^{-5} + 2z^{-6} - 2z^{-7} + z^{-8} - z^{-9} \\
f[n] &= (1, -1, 2, -2, 4, -4, 2, -2, 1, -1)
\end{aligned}$$

Now $f(t) = \sum_n f[n]\phi(2t-n)$, so $f(t)$ can be plotted as follows

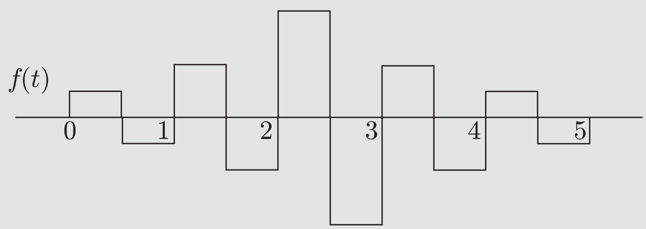

Again $f(t)$ can be expressed as a function of $\psi(t)$ as follows

$$f(t) = \psi(t) + 2\psi(t-1) + 4\psi(t-2) + 2\psi(t-3) + \psi(t-4)$$

and $\psi(t)$ lies in W_0 and so as $f(t)$.

Chapter 11

MRA Variant 1: Bi-orthogonal Filters

11.1 | Introduction

In this chapter we need to explore some more avenues of the concept of MRA. First let us complete few details of the proof of the theorem of MRA attempted in earlier chapters and then introduce different variants of MRA.

11.2 | Inner Product of Wavelet Function $\psi(t)$ and Scaling Function $\phi(t-m)$

We had already shown that, $\psi(t) \in V_1$ and $\psi(t)$ can be expanded as,

$$\psi(t) = \sum_{n \in Z} g[n]\phi(2t - n)$$

Where $g[n]$ is the impulse response of the analysis high-pass filter and corresponds to the inverse Z-transform of $z^{-(L-1)}H(-z^{-1})$, where $H(z)$ is analysis low-pass filter. Expressing $\phi(t)$ in terms of the basis of the V_1 involves coefficients of low-pass analysis filter. Expressing wavelet $\psi(t)$ in terms of the basis of the V_1 involves coefficients of high-pass analysis filter.

Example 11.2.1 — High-pass filter impulse response.

For example, in the Haar case, High-pass filter impulse response is given as,

$$[1 \; -1]$$
$$\uparrow$$

And, accordingly Haar wavelet is given as,

$$\psi_{\text{Haar}}(t) = 1.\phi(2t) - 1.\phi(2t-1)$$

The wavelet and scaling functions in general are given as,

$$\psi(t) = \sum_{n \in Z} g[n]\phi(2t-n)$$

$$\phi(t-m) = \sum_{n_1 \in Z} h[n_1]\phi(2t-2m-n_1)$$

The inner product between wavelet function $\psi(t)$ and scaling function $\phi(t)$ shifted by m is given as,

$$<\psi(t), \phi(t-m)> = \sum_{n}\sum_{n1} g[n]\overline{h[n_1]} < \phi(2t-n), \phi(2t-2m-n_1) > \tag{11.1}$$

The inner product term on the right hand side can be evaluated as,

$$<\phi(2t-n), \phi(2t-2m-n_1)> = \int_{-\infty}^{+\infty} \phi(2t-n)\overline{\phi(2t-2m-n_1)}dt$$

Let $2t$ be $= \lambda$. It gives $2dt = d\lambda$ and $t: -\infty \to +\infty \Rightarrow \lambda = -\infty \to +\infty$ With this substitution the above integral turns out to be,

$$<\phi(2t-n), \phi(2t-2m-n_1)> = \frac{1}{2}\int_{-\infty}^{+\infty} \phi(\lambda-n)\overline{\phi(\lambda-2m-n_1)}d\lambda$$

$$<\phi(2t-n), \phi(2t-2m-n_1)> = \frac{1}{2}\delta[n-(2m+n_1)]$$

Putting the value in Eq. (11.1) we get,

$$<\psi(t), \phi(t-m)> = \frac{1}{2}\sum_{n}\sum_{n1} g[n]\overline{h[n_1]}\delta[n-(2m+n_1)]$$

Dropping $\sum_n$, we get

$$<\psi(t), \phi(t-m)> = \frac{1}{2}\sum_{n1} g[2m+n_1]\overline{h[n_1]} \tag{11.2}$$

Equation (11.2) is the cross-correlation of $g[.]$ and $h[.]$ evaluated at $2m$, $\forall m \in Z$. So the Z-transform of the cross-correlation of $g[.]$ and $h[.]$ is,

$$G(z)H(z^{-1}) = z^{-(L-1)}H(-z^{-1})H(z^{-1}) \tag{11.3}$$

Since $G(z) = z^{-(L-1)}H(-z^{-1})$. For simplicity, let us assume that the impulse response is real. Consider which gives us

$$z^{-(L-1)}H(-z^{-1})H(z^{-1}) + z^{-(L-1)}H(-z^{-1})H(z^{-1})|_{z \leftarrow -z}$$

$$z^{-(L-1)}H(-z^{-1})H(z^{-1}) + (-1)^{L-1}z^{-(L-1)}H(z^{-1})H(-z^{-1}) = 0$$

This happens because L is even. The cross-correlation of $g[.]$ and $h[.]$ is zero for all $2m$. So

$$<\psi(t), \phi(t-m)> = 0 \forall m \in Z \tag{11.4}$$

Similarly, the inner product between scaling function and its translate by n is given as

$$< \phi(t), \phi(t-m) > = \frac{1}{2}\sum_{n} h[2m+n]\overline{h[n]}$$

The above expression shows the auto-correlation of impulse response of low-pass filter in the analysis side. Now, the design equations for an orthogonal filter bank ensures that

$$H(z)H(z^{-1}) + H(-z)H(-z^{-1}) = \text{constant}$$

Autocorrelation sequence is '0' at all even locations $2m$ except when $m = 0$.

11.3 | Variants of MRA

To know the variants of MRA, we need to ask certain questions regarding some other avenues of MRA.

1. Should we have essentially the same analysis and synthesis filters?

   The answer is 'No', because JPEG-2000 standard for data compression employs bi-orthogonal filter banks in which the analysis and synthesis filter banks are different.
2. Do the filters in filter banks need to be finite impulse response filters?

   The answer is 'No, not necessarily'.
3. Should we always iterate on the low-pass branch?

   The answer is again 'No, not always'. In wave-packet transform we also iterate on the high-pass branch.

By Discrete wavelet transform generally we make a wavelet tree that looks like as in Fig. 11.1.

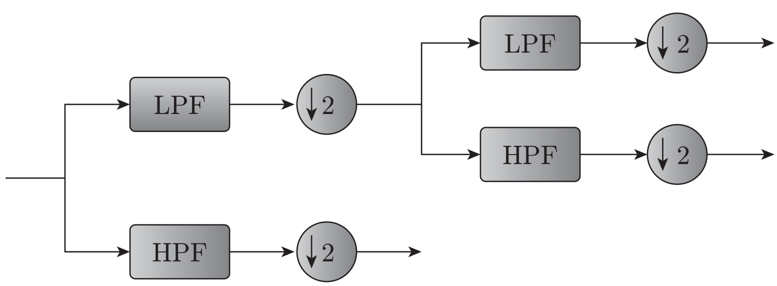

Figure 11.1 | *Discrete wavelet transform*

While iterating on the high-pass branch as well, which is used in wavelet packet transform, it looks like as in Fig. 11.2.

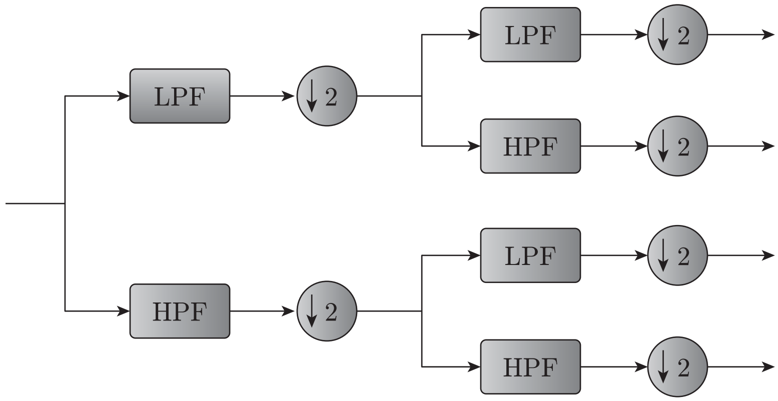

Figure 11.2 | *Wavelet packet transform*

11.4 | Introduction of Bi-orthogonal Filter Banks

Now, let us try to look for an elaborate answer for the first question using the Haar MRA. In the case of Haar, the dilation equation for $\phi_0(t)$,

$$\phi_0(t) = \phi_0(2t) + \phi_0(2t-1)$$

This can be seen in Fig. 11.3.

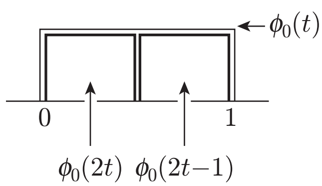

Figure 11.3 | *Dilation equation for* $\phi_0(t)$

Now, we want to calculate $\phi_0(t) \times \phi_0(t)$. Given that $h(t) \times g(t) = r(t)$ then what is $h(at+b) \times g(at+c)$? For same scaling $a \in R$(real),

$$h(at+b) \times g(at+c) = \int_{-\infty}^{+\infty} h(a\lambda + b) g[a(t-\lambda)+c]\, d\lambda$$

Let $a\lambda + b = \gamma$, $a \neq 0$ and $a \in R$. If $a > 0$,

$$d\gamma = a d\lambda, \text{ and } \lambda : -\infty \to +\infty \Rightarrow \gamma = -\infty \to +\infty$$

If $a < 0$,

$$d\gamma = a d\lambda, \text{ and } \lambda : -\infty \to +\infty \Rightarrow \gamma = +\infty \to -\infty$$

In general,

$$\int_{-\infty}^{+\infty} h(a\lambda + b) g[a(t-\lambda) + c] d\lambda = \frac{1}{|a|}\int_{-\infty}^{+\infty} h(\gamma) g(-\gamma + at + b + c) d\gamma$$

$$\int_{-\infty}^{+\infty} h(a\lambda + b) g[a(t-\lambda) + c] d\lambda = \frac{1}{|a|}\int_{-\infty}^{+\infty} h(\gamma) g(at + b + c - \gamma) d\gamma$$

$$\int_{-\infty}^{+\infty} h(a\lambda + b) g[a(t-\lambda) + c] d\lambda = \frac{1}{|a|} h \times g \,|_{(at+b+c)}$$

Using this equation and denoting $\phi_0(t) \times \phi_0(t) = \phi_1(t)$, as shown in Fig. 11.4.

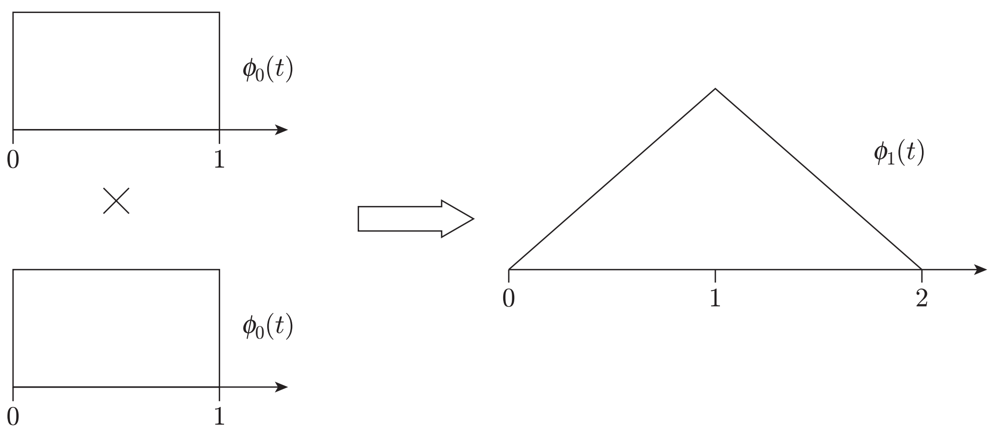

Figure 11.4 | *Convolution of $\phi_0(t)$ with itself gives $\phi_1(t)$*

The dilation equation of $\phi_1(t)$ is,

$$\phi_1(t) = \frac{1}{2}[\phi_1(2t) + 2\phi_1(2t-1) + \phi_1(2t-2)]$$

Also,

$$\phi_0(2t) \times \phi_0(2t-1) = \phi_0(2t-1) \times \phi_0(2t) = \frac{1}{2}\phi_1(2t-1)$$

This dilation equation is also shown in Fig. 11.5.

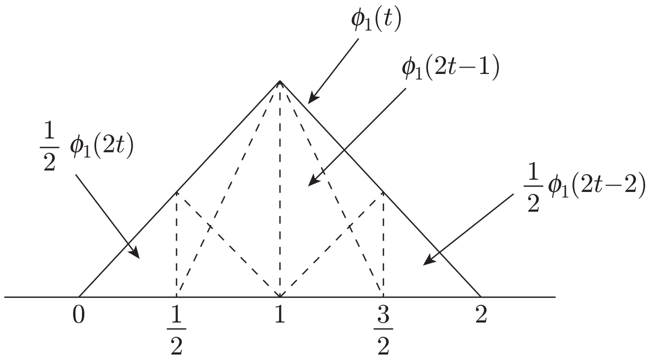

Figure 11.5 | *Dilation equation of $\phi_1(t)$*

Coefficients in dilation equation: $\phi_1(t) = \frac{1}{2}\phi_1(2t) + \phi_1(2t-1) + \frac{1}{2}\phi_1(2t-2)$ are

$$\left[\frac{1}{2} 1 \frac{1}{2}\right]$$

And the corresponding filter is

$$H(z) = \frac{1}{2} + 1.z^{-1} + \frac{1}{2}.z^{-2}$$

$$H(z) = \frac{1}{2}(1+z^{-1})^2$$

But this scaling function is not orthogonal to all its integer translates.

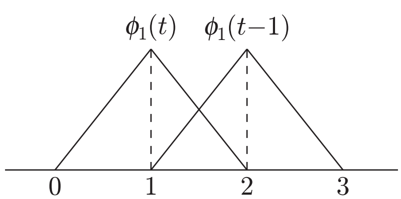

Figure 11.6 | *$\phi_1(t)$ is not orthogonal to its translate by 1*

Figure 11.6 shows that $\phi_1(t)$ is not orthogonal to its translate by 1, i.e the axiom of orthogonality is not obeyed.

11.5 | JPEG 2000 5/3 Filter-bank and Spline MRA

We have already been introduced to variants of multi-resolution analysis (MRA). In particular, MRA with different analysis and synthesis filters such as, bi-orthogonal filter-banks in perfect reconstruction framework, MRA with infinite impulse response (IIR) and MRA which iterates on high-pass branch along with the low-pass branch were discussed. In this, and the subsequent sections, we discuss these variants in detail. We start with bi-orthogonal filter-banks utilized in Joint Photographic Experts Group 2000 (JPEG 2000) image compression standard. We use piece-wise linear function as a scaling function at synthesis side and apply alias cancellation and perfect reconstruction requirements to achieve transfer functions of the filters involved. This filter-bank differs from orthogonal MRA in nonorthogonality of scaling function to its integer translates. In this chapter, we see how JPEG 2000 filter-bank is derived for spline type (piece-wise linear with desirable interpolation characteristics) scaling function. In subsequent chapters, extension to orthogonal MRA for piece-wise linear functions has been discussed, which explicitly reveals the simplicity offered by biorthogonal filter-banks by sacrificing orthogonality requirement of scaling and wavelet functions.

11.6 | Description

Dilation equation for Haar scaling function is given as:

$$\phi_0(t) = \phi_0(2t) + \phi_0(2t-1) \tag{11.5}$$

Convolution of this function with itself yields another piece-wise linear function, which may be represented in the following manner (Eq. 11.6):

$$\phi_1(t) = \frac{1}{2}\phi_1(2t) + \phi_1(2t-1) + \frac{1}{2}\phi_1(2t-2) \tag{11.6}$$

Clearly, this results in a triangular function, as shown in Fig. 11.7.

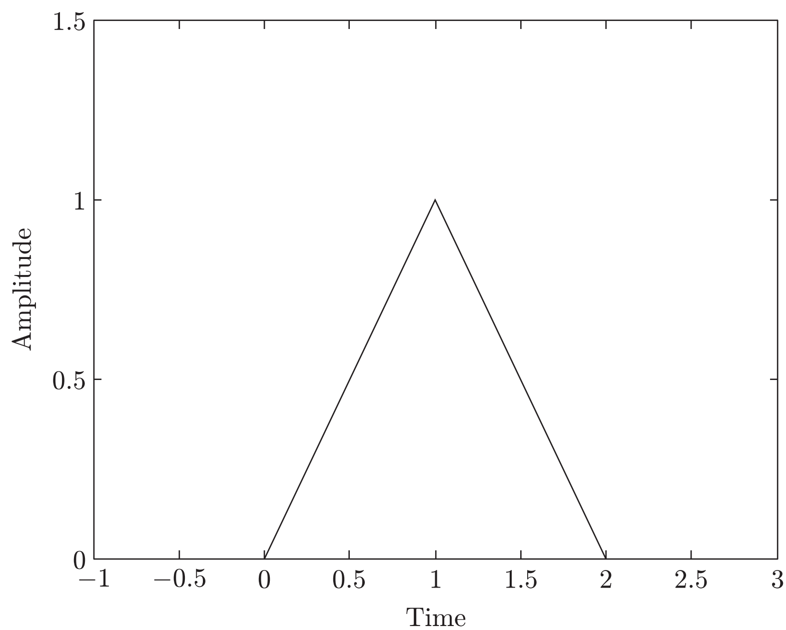

Figure 11.7 | *Triangular wave resulting from convolution of haar scaling function with itself*

This function comes from the class of piece-wise polynomial interpolants, also called as 'Splines'. Z-transform of this function may be depicted in the following manner:

$$\Phi(Z) = (1 + Z^{-1})^2 \tag{11.7}$$

Here, we can note that $\phi_1(t)$ is a piece-wise linear function and is not orthogonal to its integer translates. However, it is orthogonal to all its translates $\phi_1(t-m)$ for $m > 2$. We need to obtain the following filter-bank structure (Fig. 11.8) for this scaling function, which should be similar to orthogonal MRA.

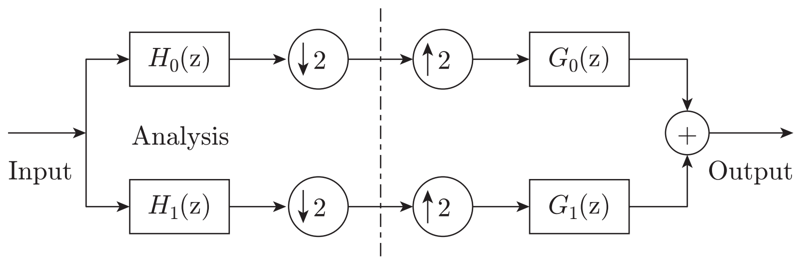

Figure 11.8 | *Desired filter-bank structure from piecewise linear function*

Example 11.6.1 — Bi-orthogonal coefficients.

Without the loss of generality, let us select $G_0(Z) = (1 + Z^{-1})^2$. At this point, we may note that once the alias cancellation and perfect reconstruction conditions are met, we may interchange analysis and synthesis filters. Alias cancellation condition is given as:

$$H_0(-Z)G_0(Z) + H_1(-Z)G_1(Z) = 0 \tag{11.8}$$

If we replace Z by $-Z$, we get:

$$H_0(Z)G_0(-Z) + H_1(Z)G_1(-Z) = 0 \tag{11.9}$$

which is indeed a requirement of alias cancellation for analysis and synthesis filters interchanged. Also, perfect reconstruction condition is given as:

$$H_0(Z)G_0(Z) + H_1(Z)G_1(Z) = C_0 Z^{-D} \tag{11.10}$$

If we replace G_0 by H_0 and G_1 by H_1 or vice versa, we get the same condition back, which indicates that perfect reconstruction condition is also satisfied for this new filter-bank. Hence, we may say that once the filter-bank satisfies alias cancellation and perfect reconstruction conditions, analysis and synthesis filters can be interchanged to get a new 2-band perfect reconstruction filter-bank. However, if there are two separate scaling functions at analysis and synthesis side, then the 'smoother' scaling function is preferred at the reconstruction side for more 'appealing' reconstruction.

Let us continue with the construction of bi-orthogonal MRA from $G_0(Z) = (1+Z^{-1})^2$. Using alias cancellation condition for this case, relationship between various filter transfer functions can be obtained. Such a relationship is shown below:

$$H_0(-Z)G_0(Z) + H_1(-Z)G_1(Z) = 0$$

On rearranging, we get:

$$\frac{G_0(Z)}{G_1(Z)} = -\frac{H_1(-Z)}{H_0(-Z)} \tag{11.11}$$

For the simplest analysis, we equate the numerators and denominators and arrive at the following:

$$G_0(Z) = -H_1(-Z) \tag{11.12}$$

$$G_1(Z) = H_0(-Z) \tag{11.13}$$

Taking the perfect reconstruction condition into consideration, we can get an important relationship to obtain the analysis low-pass filter transfer function from the synthesis low-pass transfer function. From the perfect reconstruction condition, we have:

$$H_0(Z)G_0(Z) + H_1(Z)G_1(Z) = C_0 Z^{-D} \tag{11.14}$$

However, $G_1(Z) = H_0(-Z)$ and $G_0(Z) = -H_1(-Z)$. Substituting these value in Eq. (11.14), we have:

$$H_0(Z)G_0(Z) - G_0(-Z)H_0(-Z) = C_0 Z^{-D} \tag{11.15}$$

Let us denote $\kappa_0(Z) = G_0(Z)H_0(Z)$. Now, we have the following relationship:

$$\kappa_0(Z) - \kappa_0(-Z) = C_0 Z^{-D} \tag{11.16}$$

This relationship indicates that we 'kill' all the even samples in the inverse Z-transform of $\kappa_0(Z)$ and out of the remaining odd samples, we find that only one sample (namely, the D^{th} sample) has a nonzero value (equal to C_0). If we want the same degree of regularity (or smoothness) at analysis and synthesis sides, we may select $H_0(Z)$ to have two zeros at $Z = -1$. In other words, we select $H_0(Z)$ to have $(1+Z^{-1})^2$ factor in its transfer function.

In order to have a linear phase characteristics, we need symmetry in the transfer function. Taking note of this and without considering the effect of causality, we may parsimoniously extend $H_0(Z)$ by introducing a factor $(1 + h_0 Z^{-1} + Z^{-2})$. We may note that by introducing this factor along with the factor $(1+Z^{-1})^2$, we have retained symmetry and only one degree of freedom is introduced in terms of the parameter h_0.

$$H_0(Z) = (1+Z^{-1})^2(1 + h_0 Z^{-1} + Z^{-2}) \tag{11.17}$$

In retaining symmetry, we could have used some constant, say h_1, for coefficients of Z^0 and Z^{-2} and retained h_0 as coefficient of Z^{-1}. Apparently, we would have had two degrees of freedom in such a case. However, the factor introduced here essentially scales the whole filter transfer function by a constant. Scale factor for a transfer function is not really important for magnitude and phase characteristics. Hence, scaling can also be taken care of at the time of normalization.

In other words, we introduce only as many degrees of freedom as required to get something novel in terms of nature of frequency response and not in terms of overall scaling, which can always be adjusted while normalizing the impulse response. Therefore, keeping only one degree of freedom, let us now impose the condition on $G_0(Z)H_0(Z)$, which may be depicted as:

$$G_0(Z)H_0(Z) = (1+Z^{-1})^2(1+Z^{-1})^2(1+h_0Z^{-1}+Z^{-2})$$

$$G_0(Z)H_0(Z) = (1+4Z^{-1}+6Z^{-2}+4Z^{-3}+Z^{-4})(1+h_0Z^{-1}+Z^{-2}) \tag{11.18}$$

which is in fact the convolution, as shown here

$$\underset{\substack{\uparrow\\0}}{1} \quad 4 \quad 6 \quad 4 \quad 1 \quad \times \quad \underset{\substack{\uparrow\\0}}{1} \quad h_0 \quad 1$$

Thus giving the following sequence:

$$\underset{\substack{\uparrow\\0}}{1} \quad (4+h_0) \quad (7+4h_0) \quad (8+6h_0) \quad (7+4h_0) \quad (4+h_0) \quad 1 \tag{11.19}$$

As discussed above, we do not have any knowledge about the even samples as they were 'killed' (according to Eq. 11.16). However, we have some information about the nature of odd samples. Accordingly, we need to retain only one sample out of them. Note that if we remove the two $(4+h_0)$ samples, we would achieve what we wanted. In other words, if we make $(4+h_0)=0$, we retain only one sample out of all the odd samples. Therefore, we select $h_0 = -4$.

Hence,

$$H_0(Z) = (1+Z^{-1})^2(1-4Z^{-1}+Z^{-2}) \tag{11.20}$$

Again for expansion, if we want to denote $H_0(Z)$ as a series, we can denote the relationship (Eq. 11.20) in terms of convolution of two series, given by:

$$\underset{\substack{\uparrow\\0}}{1} \quad 2 \quad 1 \quad \times \quad \underset{\substack{\uparrow\\0}}{1} \quad -4 \quad 1$$

Carrying out this convolution gives the following sequence:

$$1 \quad -2 \quad -6 \quad -2 \quad 1 \tag{11.21}$$

Therefore,

$$H_0(Z) = 1-2Z^{-1}-6Z^{-2}-2Z^{-3}+Z^{-4} \tag{11.22}$$

which is a low-pass filter of the analysis side. We note that length of this filter is 5. Hence, we started out with

$$G_0(Z) = 1+2Z^{-1}+Z^{-2}$$

and obtained

$$H_0(Z) = 1-2Z^{-1}-6Z^{-2}-2Z^{-3}+Z^{-4}$$

Here, $G_0(Z)$ is of length 3 and $H_0(Z)$ is of length 5. This filter-bank is known as the JPEG 5/3 filter bank, where, 5/3 refers to lengths of impulse responses.

11.7 | Note

R JPEG-2000 compression standard admits two kinds of filter banks: a 5/3 filter-bank and a 9/7 filter-bank. As we have seen, 5/3 refers to lengths of impulse responses in a 5/3 filter-bank. Similarly, 9/7 also refers to lengths of impulse responses of a 9/7 filter-bank.

Lengths of impulse responses in the JPEG 2000 5/3 filter bank may be represented, as shown in Fig. 11.9.

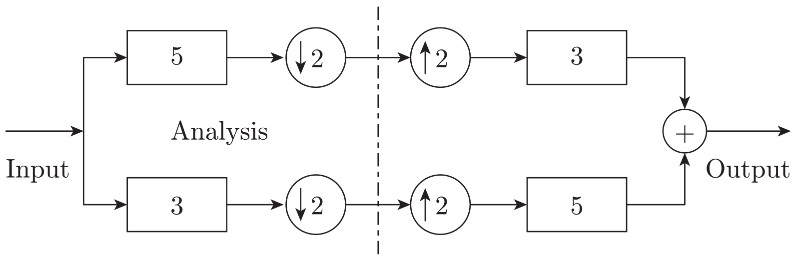

Figure 11.9 | *JPEG 2000 5/3 filter-bank*

We may use the above noted relationships between various filter transfer functions to get the transfer functions of all the filters involved in JPEG 2000 5/3 filter bank. Now,

$$G_0(Z) = -H_1(-Z) \Rightarrow H_1(Z) = -G_0(-Z) = -(1-Z^{-1})^2 \tag{11.23}$$

Further,

$$G_1(Z) = H_0(-Z) \Rightarrow G_1(Z) = 1 + 2Z^{-1} - 6Z^{-2} + 2Z^{-3} + Z^{-4} \tag{11.24}$$

Filter transfer functions for JPEG 2000 may be summarized in the following manner:

$$H_0(Z) = 1 - 2Z^{-1} - 6Z^{-2} - 2Z^{-3} + Z^{-4} \tag{11.25}$$

$$G_0(Z) = 1 + 2Z^{-1} + Z^{-2} \tag{11.26}$$

$$H_1(Z) = -G_0(-Z) = -(1-Z^{-1})^2 \tag{11.27}$$

$$G_1(Z) = 1 + 2Z^{-1} - 6Z^{-2} + 2Z^{-3} + Z^{-4} \tag{11.28}$$

We may note that the individual sums of coefficients of high-pass filters on analysis and synthesis sides are zero. This simply indicates the presence of zero (null) at zero frequency. In fact, in both $H_1(Z)$ and $G_1(Z)$, there is a factor of $(1-Z^{-1})^2$, which indicates the presence of two zeros at zero frequency. This substantiates our intuition that both filters should be high-pass filters in nature.

As evident from our discussion throughout this chapter, our major aim was to achieve a perfect reconstruction filter-bank from a scaling function, which does not form an orthogonal basis set with its integer translates. Due to such a property, orthogonal MRA is not possible using such a scaling function.

In such a case, we could still achieve a perfect reconstruction filter-bank, however, we ended up getting different scaling functions at analysis and synthesis sides. In perfect reconstruction framework, such an MRA is known as bi-orthogonal MRA. Idea of a bi-orthogonal basis vectors may be explained more lucidly in a 2-D vector space, as explained next.

Consider a set of vectors consisting of $\hat{u}_1$ and $\hat{u}_2$, which are orthogonal to each other, i.e., their inner product is zero. One such representation is shown in Fig. 11.10.

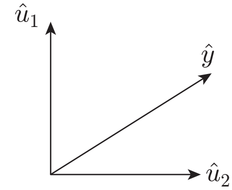

Figure 11.10 | *Orthogonal basis vectors ($\hat{u}_1$ and $\hat{u}_2$)*

In this case, representing any other vector in this vector space involves projecting that vector over $\hat{u}_1$ and $\hat{u}_2$ by taking inner products with respect to such basis vectors. If vectors $\hat{u}_1$ and $\hat{u}_2$ are linearly independent but not orthogonal to each other, even then they form a basis set for the corresponding vector space. However, the ease of representation of vector $\hat{y}$ with respect to such basis vectors is lost. This can be seen from Fig. 11.11, which denotes two linearly independent vectors in a 2-D vector space.

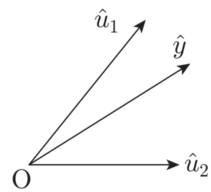

Figure 11.11 | *Non-orthogonal basis vectors ($\hat{u}_1$ and $\hat{u}_2$)*

We can note here that it is not impossible to obtain such a representation. In fact, one may solve a set of linear equations and come up with such representation. However, the ease with which coordinates may be obtained from orthogonal basis vectors (simply by taking inner products) is lost.

Bi-orthogonal basis vectors can help in such a case to restore the ease of representation. We want $\hat{y}$ to be represented in terms of $c_1\hat{u}_1 + c_2\hat{u}_2$. Consider a set of vectors $\tilde{u}_1$ and $\tilde{u}_2$, selected such that $\tilde{u}_1$ is orthogonal to $\hat{u}_1$ and $\tilde{u}_2$ is orthogonal to $\hat{u}_2$. Further, $<\hat{u}_1, \tilde{u}_1>= 0$ and $<\hat{u}_2, \tilde{u}_2>= 0$. These vectors may be represented as shown in Fig. 11.12.

We can now take the inner product of $\hat{y}$ with $\tilde{u}_1$ and obtain its projection over $\hat{u}_2$. Similarly, inner product of $\hat{y}$ with $\tilde{u}_2$ yields projection over $\hat{u}_1$. In this way, we can obtain representation of $\hat{y}$ in terms of linearly independent basis vectors $\hat{u}_1$ and $\hat{u}_2$. This idea is extended to the generation of a bi-orthogonal filter-bank. We may compare similarity by noting that in biorthogonal filter-bank, two scaling functions and two corresponding wavelet functions exist; one each at analysis and synthesis sides. However, neither of them (scaling functions) form an orthogonal set with its integer translates.

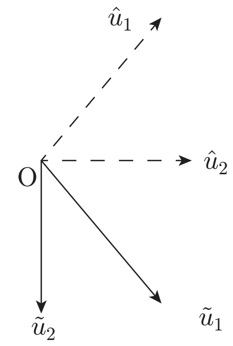

Figure 11.12 | *Idea of bi-orthogonal basis vectors*

11.8 | 5/3 tap in Nutshell

In last few sections, we started with the piece-wise linear scaling function obtained by convolving Haar scaling function with itself. Such scaling function is a member of the broad class of functions known as splines. However, due to its nonorthogonality with its integer translates, we could not build orthogonal MRA. By imposing alias cancellation and perfect reconstruction properties, we came up with a filter-bank known as JPEG 2000 5/3 filter-bank, which is biorthogonal in nature. In this specific MRA, both synthesis and analysis filters have different impulse response lengths, unlike in the case of orthogonal MRA. Apparently, we dropped orthogonality requirement from MRA and could construct perfect reconstruction bi-orthogonal MRA. One of the advantages of such MRA is the possibility of achieving nontrivial linear phase filters, which is not possible to achieve in orthogonal MRA (except in the case of simplest Haar MRA). In practice one may start with piece-wise linear scaling function and come up with an orthogonal MRA, which require infinite impulse response (IIR) filters for spline (piece-wise linear) type of scaling functions. However, it is computationally quite involved to construct such an MRA. This will be precisely dealt with in subsequent chapters. Such an exercise will lucidly indicate the advantages of bi-orthogonal MRA in context of perfect reconstruction filter-banks.

11.9 | Filter Design Strategy

Haar filter is the only finite length, symmetric, orthogonal filter whose Fourier representation $[H(\omega)]$ satisfies zero derivative conditions at $\omega = \pi$, as was explained by Daubechies.

Researchers across the globe have confirmed that having symmetric filters is advantageous in multiple ways for many real-life applications.

Another important characteristics of filters is orthogonality.It guarantees energy preservation and inverse of wavelet transform matrix. For orthogonal filter 'h' that gives orthogonal transform matrix W_N, the implementation is straightforward.This is because W_N is 'unitary' which guarantees that for all real valued W_N, $W_N^{-1} = W_N^T$. This simple transpose gives us the inverse, which is really crucial in inverse calculations as as 'separable' multidimensional calculations.

For 'non-orthogonal' filters, however, one desirable strategy to build the system could be to ensure that inverse of transform matrix is transpose of another transformation matrix.

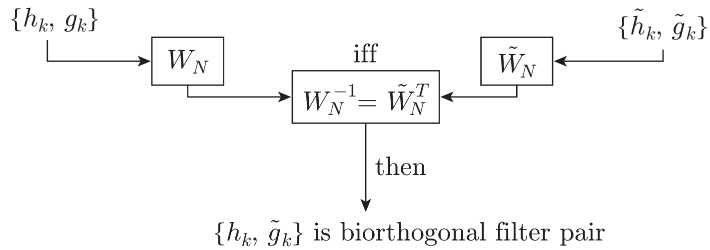

Haar, though orthogonal, finite length and symmetric, has its own drawback, which we have already brought out. Going beyond filter length of '2', we need to give up 'orthogonality' as requirement, which comes as filter constraint.

Let us try constructing $\frac{5}{3}$ normalized tap:

Design problem:

1. From symmetric h_k and g_k
2. Construct wavelet transform W_N
3. When inverse W_N^{-1} is calculated.
4. W_N^{-1} should also be a transform matrix!
5. Find such $\tilde{g}_k$ & $\tilde{h}_k$ (symmetric)!

Let 'H_B' be $\frac{N}{2} \times N$ matrix from h_k.

Let 'G_B' be $\frac{N}{2} \times N$ matrix from g_k.

Let '$\widetilde{G}_B$' be $\frac{N}{2} \times N$ matrix from $\tilde{g}_k$.

Let '$\widetilde{H}_B$' be $\frac{N}{2} \times N$ matrix from $\tilde{h}_k$.

Forward wavelet matrix can be written as:

$$W_B = \begin{bmatrix} H_B \\ G_B \end{bmatrix}$$

For synthesis part, similarly,

$$\widetilde{W}_B = \begin{bmatrix} \widetilde{H}_B \\ \widetilde{G}_B \end{bmatrix}$$

keeping in mind, we want to create dual filters in semi-orthogonal sense,

$$W_B \cdot \widetilde{W}_B^T = I_{N\times N} \tag{11.29}$$

Now, $W_B \cdot \widetilde{W}_B^T = \begin{bmatrix} H_B \\ G_B \end{bmatrix} \cdot \begin{bmatrix} \widetilde{H}_B^T & \widetilde{G}_B^T \end{bmatrix} = \begin{bmatrix} H_B \cdot \widetilde{H}_B^T & H_B \cdot \widetilde{G}_B^T \\ G_B \cdot \widetilde{H}_B^T & G_B \cdot \widetilde{G}_B^T \end{bmatrix}$

Here,

$$\begin{aligned} H_B \cdot \widetilde{H}_B^T &= G_B \cdot \widetilde{G}_B^T = I_{N\times N} \\ H_B \cdot \widetilde{G}_B^T &= G_B \cdot \widetilde{H}_B^T = 0_{N\times N} \end{aligned} \tag{11.30}$$

Now, $h_k = \{h_{-2}, h_{-1}, h_0, h_1, h_2\}$ & $\tilde{h}_k = \{\tilde{h}_{-1}, \tilde{h}_0, \tilde{h}_1\}$ in the spirit of $\frac{5}{3}$ tap.

Therefore, analysis low-pass filter has 5 coefficients and
synthesis low-pass filter has 3 coefficients,
as '5' is the bigger of the two

let $\frac{N}{2} = 5, \therefore N = 10$

$$\therefore H_B = \begin{bmatrix} h_0 & h_1 & h_2 & 0 & 0 & 0 & 0 & 0 & h_{-2} & h_{-1} \\ h_{-2} & h_{-1} & h_0 & h_1 & h_2 & 0 & 0 & 0 & 0 & 0 \\ 0 & 0 & h_{-2} & h-1 & h_0 & h_1 & h_2 & 0 & 0 & 0 \\ 0 & 0 & 0 & 0 & h_{-2} & h_{-1} & h_0 & h_1 & h_2 & 0 \\ h_2 & 0 & 0 & 0 & 0 & 0 & h_{-2} & h_{-1} & h_0 & h_1 \end{bmatrix}$$

$$\widetilde{H}_B = \begin{bmatrix} \tilde{h}_0 & \tilde{h}_1 & 0 & 0 & 0 & 0 & 0 & 0 & 0 & \tilde{h}_{-1} \\ 0 & \tilde{h}_{-1} & \tilde{h}_0 & \tilde{h}_1 & 0 & 0 & 0 & 0 & 0 & 0 \\ 0 & 0 & 0 & \tilde{h}_{-1} & \tilde{h}_0 & \tilde{h}_1 & 0 & 0 & 0 & 0 \\ 0 & 0 & 0 & 0 & 0 & \tilde{h}_{-1} & \tilde{h}_0 & \tilde{h}_1 & 0 & 0 \\ 0 & 0 & 0 & 0 & 0 & 0 & 0 & \tilde{h}_{-1} & \tilde{h}_0 & \tilde{h}_1 \end{bmatrix}$$

Now, $H_B \cdot \widetilde{H}_B^T = I_{5\times 5}$

$$\begin{bmatrix} h_0 & h_1 & h_2 & 0 & 0 & 0 & 0 & 0 & h_{-2} & h_{-1} \\ h_{-2} & h_{-1} & h_0 & h_1 & h_2 & 0 & 0 & 0 & 0 & 0 \\ 0 & 0 & h_{-2} & h-1 & h_0 & h_1 & h_2 & 0 & 0 & 0 \\ 0 & 0 & 0 & 0 & h_{-2} & h_{-1} & h_0 & h_1 & h_2 & 0 \\ h_2 & 0 & 0 & 0 & 0 & 0 & h_{-2} & h_{-1} & h_0 & h_1 \end{bmatrix} \cdot \begin{bmatrix} \tilde{h}_0 & 0 & 0 & 0 & 0 \\ \tilde{h}_1 & \tilde{h}_{-1} & 0 & 0 & 0 \\ 0 & \tilde{h}_0 & 0 & 0 & 0 \\ 0 & \tilde{h}_1 & \tilde{h}_{-1} & 0 & 0 \\ 0 & 0 & \tilde{h}_0 & 0 & 0 \\ 0 & 0 & \tilde{h}_1 & \tilde{h}_{-1} & 0 \\ 0 & 0 & 0 & \tilde{h}_0 & 0 \\ 0 & 0 & 0 & \tilde{h}_1 & \tilde{h}_{-1} \\ 0 & 0 & 0 & 0 & \tilde{h}_0 \\ \tilde{h}_{-1} & 0 & 0 & 0 & \tilde{h}_1 \end{bmatrix} = I_{5\times5}$$

$1^{st}\ row \times 1^{st}\ column, 1^{st}\ row \times 2^{nd}\ column$ and $1^{st}\ row \times last\ column$ will give us three equations,

$$h_0 \cdot \tilde{h}_0 + h_1 \cdot \tilde{h}_1 + h_{-1} \cdot \tilde{h}_{-1} = 1 \tag{11.31}$$

$$h_0 \cdot \tilde{h}_1 + h_2 \cdot \tilde{h}_0 = 0 \tag{11.32}$$

$$h_{-2} \cdot \tilde{h}_0 + h_{-1} \cdot \tilde{h}_1 = 0 \tag{11.33}$$

Equation (11.31) can be written as,

$$\sum_{K=-1}^{1} h_k \cdot \tilde{h}_k = 1 \tag{11.34}$$

Equations (11.32) and (11.33) can be written as,

$$\sum_{K=-1}^{1} h_{k-2m} \cdot \tilde{h}_k = 0, m = -1, 1 \tag{11.35}$$

Similarly, $G_B \cdot \widetilde{G}_B^T = I_{5\times5}$
Here,

$$g_k = \{ g_{-1}, g_0, g_1 \} \ \& \ \tilde{g}_k = \{ g_{-2}, g_{-1}, g_0, g_1, g_2 \}$$

Therefore, analysis high-pass filter has ‘3’ coefficients,
synthesis high-pass filter has ‘5’ coefficients

$$\frac{N}{2} = 5, \therefore N = 10$$

$$G_B = \begin{bmatrix} g_0 & g_1 & 0 & 0 & 0 & 0 & 0 & 0 & 0 & g_{-1} \\ 0 & g_{-1} & g_0 & g_1 & 0 & 0 & 0 & 0 & 0 & 0 \\ 0 & 0 & 0 & g_{-1} & g_0 & g_1 & 0 & 0 & 0 & 0 \\ 0 & 0 & 0 & 0 & 0 & g_{-1} & g_0 & g_1 & 0 & 0 \\ 0 & 0 & 0 & 0 & 0 & 0 & 0 & g_{-1} & g_0 & g_1 \end{bmatrix}$$

$$\widetilde{G}_B = \begin{bmatrix} \tilde{g}_0 & \tilde{g}_1 & \tilde{g}_2 & 0 & 0 & 0 & 0 & 0 & \tilde{g}_{-2} & \tilde{g}_{-1} \\ \tilde{g}_{-2} & \tilde{g}_{-1} & \tilde{g}_0 & \tilde{g}_1 & \tilde{g}_2 & 0 & 0 & 0 & 0 & 0 \\ 0 & 0 & \tilde{g}_{-2} & \tilde{g}_{-1} & \tilde{g}_0 & \tilde{g}_1 & \tilde{g}_2 & 0 & 0 & 0 \\ 0 & 0 & 0 & 0 & \tilde{g}_{-2} & \tilde{g}_{-1} & \tilde{g}_0 & \tilde{g}_1 & \tilde{g}_2 & 0 \\ \tilde{g}_2 & 0 & 0 & 0 & 0 & 0 & \tilde{g}_{-2} & \tilde{g}_{-1} & \tilde{g}_0 & \tilde{g}_1 \end{bmatrix}$$

Now, $G_B \cdot \widetilde{G}_B^T = I_{5\times 5}$

$$\begin{bmatrix} g_0 & g_1 & 0 & 0 & 0 & 0 & 0 & 0 & 0 & g_{-1} \\ 0 & g_{-1} & g_0 & g_1 & 0 & 0 & 0 & 0 & 0 & 0 \\ 0 & 0 & 0 & g_{-1} & g_0 & g_1 & 0 & 0 & 0 & 0 \\ 0 & 0 & 0 & 0 & 0 & g_{-1} & g_0 & g_1 & 0 & 0 \\ 0 & 0 & 0 & 0 & 0 & 0 & 0 & g_{-1} & g_0 & g_1 \end{bmatrix} \cdot$$

$$\begin{bmatrix} \tilde{g}_0 & \tilde{g}_{-2} & 0 & 0 & \tilde{g}_2 \\ \tilde{g}_1 & \tilde{g}_{-1} & 0 & 0 & 0 \\ \tilde{g}_2 & \tilde{g}_0 & \tilde{g}_{-2} & 0 & 0 \\ 0 & \tilde{g}_1 & \tilde{g}_{-1} & 0 & 0 \\ 0 & \tilde{g}_2 & \tilde{g}_0 & \tilde{g}_{-2} & 0 \\ 0 & 0 & \tilde{g}_1 & \tilde{g}_{-1} & 0 \\ 0 & 0 & \tilde{g}_2 & \tilde{g}_0 & \tilde{g}_{-2} \\ 0 & 0 & 0 & \tilde{g}_1 & \tilde{g}_{-1} \\ \tilde{g}_2 & 0 & 0 & \tilde{g}_2 & \tilde{g}_0 \\ \tilde{g}_{-1} & 0 & 0 & 0 & \tilde{g}_1 \end{bmatrix} = I_{5\times 5}$$

$$g_0 \cdot \tilde{g}_0 + g_1 \cdot \tilde{g}_1 + g_{-1} \cdot \tilde{g}_{-1} = 1 \tag{11.36}$$

$$g_0 \cdot \tilde{g}_{-2} + g_1 \cdot \tilde{g}_{-1} = 0 \tag{11.37}$$

$$g_0 \cdot \tilde{g}_2 + g_{-1} \cdot \tilde{g}_1 = 0 \tag{11.38}$$

$\therefore$ Equation (11.36) get written as:

$$\sum_{K=-1}^{1} g_k \cdot \tilde{g}_k = 1 \tag{11.39}$$

Equation (11.37) and (11.38) becomes

$$\sum_{K=-1}^{1} g_{K-2m} \cdot \tilde{g}_k = 0, m = -1, 1 \tag{11.40}$$

Now, design aspect demands $H_B \cdot \widetilde{\widetilde{H}}_B^T$ to be an identity matrix, which demands h_k and $\tilde{h}_k$ to be orthogonal.

For two filters to be orthogonal, let us derive the sufficient and necessary condition with, again, an example of Haar wavelet.

For Haar, if

$$h_k = \{h_0, h_1\} = \sqrt{2}\left\{\frac{1}{2}, \frac{1}{2}\right\}$$

$$\therefore H(\omega) = \sqrt{2}\left(\frac{1}{2} + \frac{1}{2} \cdot e^{j\omega}\right) = \sqrt{2} \cdot e^{\frac{j\omega}{2}} \cdot \cos(\frac{\omega}{2})$$

$$\therefore |H(\omega)| = \sqrt{2} \cdot \cos(\frac{\omega}{2}) \cdots \text{ (\textit{Note:} Magnitude of } e^{j\omega} = 1 \text{ on interval of } [-\pi, \pi])$$

We have already seen that when $H(z)$ becomes H(-z), the frequency band gets shifted by π amount, which can be represented as: $H(\omega + \pi)$

$$\therefore |H(\omega + \pi)| = \sqrt{2} \cdot \cos(\frac{\omega + \pi}{2})$$

Now, if we add squared magnitudes of $H(\omega)$ and $H(\omega + \pi)$, we get

$$|H(\omega)|^2 = 2 \cdot \cos^2(\frac{\omega}{2}) \tag{11.41}$$

$$|H(\omega + \pi)|^2 = \left(\sqrt{2}\cos\left(\frac{\omega + \pi}{2}\right)\right)^2 = 2 \cdot \cos^2\left(\frac{\omega + \pi}{2}\right)$$

$$\therefore |H(\omega + \pi)| = 2 \cdot \sin^2\left(\frac{\omega}{2}\right) \tag{11.42}$$

Using (11.41) and (11.42),

$$\therefore |H(\omega)^2| + |H\omega + \pi)^2| = 2 \cdot \cos^2\left(\frac{\omega}{2}\right) + 2 \cdot \sin^2\left(\frac{\omega}{2}\right) \tag{11.43}$$

This '2' also comes as we are using normalized filters, in absence of normalization, the sum would be '1'.

Important thing to note is, a constant suggest orthogonality.

Using equations (11.41), (11.42) and (11.43), we can write

$$\overline{H(\omega)}\cdot\widetilde{H}(\omega)+\overline{H(\omega+\pi)}\cdot\widetilde{H}(\omega+\pi)=2 \tag{11.44}$$

When $H(\omega)$ and $(\tilde{\omega})$ satisfy (Eq. 11.44), we have,

$$\sum_{K\in Z} h_k\cdot\tilde{h}_k=1 \tag{11.45}$$

For $m\in Z$, $m\neq 0$,

$$\sum_{K\in Z} h_{K-2m}\cdot\tilde{h}_k=0 \tag{11.46}$$

Similarly,

$$\overline{G(\omega)}\cdot\widetilde{G}(\omega)+\overline{G(\omega+\pi)}\cdot\widetilde{G}(\omega+\pi)=2 \tag{11.47}$$

When $H(\omega)$ and $(\tilde{\omega})$ satisfy Eq. (11.44), we have,

$$\sum_{K\in Z} g_k\cdot\tilde{g}_k=1 \tag{11.48}$$

For $m\in Z$, $m\neq 0$,

$$\sum_{K\in Z} g_{K-2m}\cdot\tilde{g}_k=0 \tag{11.49}$$

To ensure $H_B\cdot\widetilde{G}_B^T=0$

$$\overline{H(\omega)}\cdot\widetilde{G}(\omega)+\overline{H(\omega+\pi)}\cdot\widetilde{G}(\omega+\pi)=0 \tag{11.50}$$

for all $m\in z$,

$$\sum_{K\in Z} h_{K-2m}\cdot\widetilde{g_k}=0 \tag{11.51}$$

To ensure, $G_B\cdot\widetilde{H}_B^T=0$

$$\overline{G(\omega)}\cdot\widetilde{H}(\omega)+\overline{G(\omega+\pi)}\cdot\widetilde{H}(\omega+\pi)=0 \tag{11.52}$$

For all $m\in Z$

$$\sum_{K\in Z} g_{K-sm}\cdot\widetilde{h_k}=0 \tag{11.53}$$

Equations (11.44) to (11.53) give us definition for bi-orthogonal filter pairs. For example, if $H(\omega)$ and $\widetilde{H(\omega)}$ of h_k and $\tilde{h}_k$ respectively follow:

$$H(\omega)\cdot\widetilde{H}(\omega)+\overline{H(\omega+\pi)}\cdot\widetilde{H}(\omega+\pi)=2$$

then, h_k and $\tilde{h}_k$ are called bi-orthogonal filter pair!

From (11.44), (11.47), (11.50) and (11.52)

$G(\omega)=e^{i(n\omega+b}\cdot\overline{\widetilde{H}(\omega+\pi)}$ [Analysis high-pass connected with synthesis low pass] and

$\widetilde{G}(\omega)=e^{i(n\omega+b}\cdot\overline{H(\omega+\pi)}$ [Synthesis high-pass connected with analysis low pass]

Let us confirm this by plugging in

$$\begin{aligned}\overline{G(\omega)}\cdot\widetilde{G}(\omega) &= \overline{e^{j(n\omega)+b}\cdot\overline{\widetilde{H}(\omega+\pi)}}\cdot e^{j(n\omega+b)}\cdot\overline{H(\omega+\pi)}\\ &= e^{-j(n\omega+b)}\cdot\widetilde{H}(\omega+\pi)\cdot e^{j(n\omega+b)}\cdot\overline{H(\omega+\pi)}\\ &= \overline{H(\omega+\pi)}\cdot\widetilde{H}(\omega+\pi)\end{aligned} \tag{11.54}$$

$\therefore$ Since they are equal, together they shall produce '2'!

By replacing 'ω' with '$\omega+\pi$' in Eq. (11.54)

$$\overline{G(\omega+\pi)}\cdot\widetilde{G}(\omega+\pi)=\widetilde{H}(\omega)\cdot\overline{H(\omega)}\quad [As\,these\,are\text{`}2\pi-periodic'\ functions,\therefore\ \overline{\omega+2\pi}=\overline{\omega}] \tag{11.55}$$

Adding Eqs. (11.54) and (11.55),

$$\overline{G(\omega)}\cdot\widetilde{G}(\omega)+\overline{G(\omega+\pi)}\cdot\widetilde{G}(\omega+\pi)=\overline{H(\omega)}\cdot\widetilde{H}(\omega)+\overline{H(\omega+\pi)}\cdot\widetilde{H}(\omega+\pi)=2$$

Now,

$$\begin{aligned}\widetilde{H}(\omega)\cdot\overline{G(\omega)} &= \widetilde{H}(\omega)\cdot\overline{e^{j(n\omega+b)}\cdot\overline{\widetilde{H}(\omega+\pi)}}\\ &= \widetilde{H}(\omega)\cdot e^{-j(n\omega+b)}\cdot\widetilde{H}(\omega+\pi)\end{aligned} \tag{11.56}$$

Let us replace 'ω' by '$\omega+\pi$' in Eq. (11.56)

$$\begin{aligned}\widetilde{H}(\omega+\pi)\cdot\overline{G(\omega+\pi)} &= \widetilde{H}(\omega+\pi)\cdot e^{-j(n\omega+n\pi+b)}\cdot\widetilde{H}(\omega+2\pi)\\ &= \widetilde{H}(\omega+\pi)\cdot e^{-jn\pi}\cdot e^{-j(n\omega+b)}\cdot\widetilde{H}(\omega)\\ &= (-1)^n\cdot\widetilde{H}(\omega+\pi)\cdot e^{-j(n\omega+b)}\cdot\widetilde{H}(\omega)\\ &= -\widetilde{H}(\omega+\pi)\cdot e^{-}j(n\omega+b)\cdot(\tilde{\omega})\cdots\cdots[\text{`}n\text{' being odd },(-1)^n=-1]\end{aligned} \tag{11.57}$$

Adding Eqs. (11.56) and (11.57),

$$\widetilde{H}(\omega)\cdot\overline{G(\omega)}+\widetilde{H}(\omega+\pi)\cdot\overline{G(\omega+\pi)}=0$$

Readers should note, g_k is connected with $\tilde{h}_k$ and $\tilde{g}_k$ is connected with h_k!
b can be '0' or π to keep filter real values and for $n = 1$,

$$g_k = (-1)^K \cdot \tilde{h}_{1-K} \tag{11.58}$$

$$\widetilde{g_k} = (-1)^K \cdot h_{1-K} \tag{11.59}$$

Let us confirm this for normalized $\frac{5}{3}$ tap.

$$h = \{h_{-2}, h_{-1}, h_0, h_1, h_2\} = \left\{-\frac{1}{2}, 1, \frac{3}{4}, -\frac{1}{2}, \frac{1}{4}\right\} \cdot \sqrt{2} \tag{11.60}$$

and

$$\tilde{h} = \{\tilde{h}_{-1}, \tilde{h}_0, \tilde{h}_1\} = \left\{\frac{1}{4}, \frac{1}{2}, \frac{1}{4}\right\} \cdot \sqrt{2} \tag{11.61}$$

Plugging (11.60) and (11.61) in (11.58) and (11.59), we get,

$$\begin{aligned} \tilde{g} &= \{\tilde{g}_{-1}, \tilde{g}_0, \tilde{g}_1, \tilde{g}_2, \tilde{g}_3\} \\ &= \{h_2, h_1, -h_0, h_{-1}, h_{-2}\} \\ &= \left\{-\frac{1}{4}, -\frac{1}{2}, -\frac{3}{4}, 1, \frac{1}{2}\right\} \cdot \sqrt{2} \end{aligned} \tag{11.62}$$

Similarly,

$$\begin{aligned} g &= \{g_0, g_1, g_2\} \\ &= \{\widetilde{h_1}, -\tilde{h}_0, \tilde{h}_{-1}\} \quad = \left\{\frac{1}{4}, -\frac{1}{2}, \frac{1}{4}\right\} \cdot \sqrt{2} \end{aligned} \tag{11.63}$$

Let us approve these filters:

$$H(\omega) = -\frac{\sqrt{2}}{2} \cdot e^{-2j\omega} + \sqrt{2} \cdot e^{-j\omega} + \frac{3\sqrt{2}}{4} - \frac{\sqrt{2}}{2} \cdot e^{j\omega} + \frac{\sqrt{2}}{4} \cdot e^{2j\omega} \tag{11.64}$$

$$\widetilde{H}(\omega) = \frac{\sqrt{2}}{4} \cdot e^{-j\omega} + \frac{\sqrt{2}}{2} + \frac{\sqrt{2}}{4} \cdot e^{j\omega} \tag{11.65}$$

Let us evaluate Eqs. (11.64) and (11.65), for $\omega = 0$ and $\omega = \pi$

$$H(\omega)|_{\omega=0} = \sqrt{2}\left(-\frac{1}{2} + 1 + \frac{3}{4} - \frac{1}{2} + \frac{1}{4}\right) = \sqrt{2}$$

$$H(\omega)|_{\omega=\pi} = 0$$

Similarly,

$$\widetilde{H}(\omega)\,|_{\omega=0} = \sqrt{2}\ \&\ \widetilde{H}(\omega)\,|_{\omega=\pi} = 0$$

Conjugating $H(\omega)$ we get,

$$\overline{H(\omega)} = \frac{\sqrt{2}}{4}\cdot e^{-2j\omega} - \frac{\sqrt{2}}{2}\cdot e^{-j\omega} + \frac{3\sqrt{2}}{4} + \sqrt{2}\cdot e^{j\omega} - \frac{\sqrt{2}}{2}\cdot e^{2j\omega}$$

$$\begin{aligned}\therefore \widetilde{H}(\omega)\cdot\overline{H\omega} &= \left(\frac{\sqrt{2}}{4}\cdot e^{-j\omega} + \frac{\sqrt{2}}{2} + \frac{\sqrt{2}}{4}\cdot e^{j\omega}\right)\times\left(\frac{\sqrt{2}}{4}\cdot e^{-2j\omega} - \frac{\sqrt{2}}{2}\cdot e^{-j\omega} + \frac{3\sqrt{2}}{4} + \sqrt{2}\cdot e^{j\omega} - \frac{\sqrt{2}}{2}\cdot e^{2j\omega}\right)\\ &= \frac{1}{8}\cdot e^{-3j\omega} + 1 + \frac{9}{8}\cdot e^{j\omega} - \frac{1}{4}\cdot e^{3j\omega}\end{aligned} \tag{11.66}$$

Replacing 'ω' by '$\omega+\pi$' in Eq. (11.66)

$$\begin{aligned}&\widetilde{H}(\omega+\pi)\cdot\overline{H(\omega+\pi)}\\ &= \frac{1}{8}\cdot e^{-3j(\omega+\pi)} + 1 + \frac{9}{8}\cdot e^{j(\omega+\pi)} - \frac{1}{4}\cdot e^{3j(\omega+\pi)}\\ &= \frac{1}{8}\cdot e^{-3j\omega}\cdot e^{-3j\pi} + 1 + \frac{9}{8}\cdot e^{j\omega}\cdot e^{j\pi} - \frac{1}{4}\cdot e^{3j\omega}\cdot e^{3j\pi}\end{aligned}$$

Note, $e^{3j\pi} = e^{-3j\pi} = e^{j\pi} = e^{-j\pi} = -1$ (Euler's identity)

$$\therefore \widetilde{H}(\omega+\pi)\cdot\overline{H(\omega+\pi)} = -\frac{1}{8}\cdot e^{-3j\omega} + 1 - \frac{9}{8}\cdot e^{j\omega} + \frac{1}{4}\cdot e^{3j\omega} \tag{11.67}$$

Now let us create wavelet transformation matrix for bio-orthogonal 5/3 tap let us call it $\omega_{5/3}$

$$\omega_{5/3} = \begin{bmatrix} h_0 & h_1 & h_2 & 0 & 0 & 0 & h_{-2} & h_{-1} \\ h_{-2} & h_{-1} & h_0 & h_1 & h_2 & 0 & 0 & 0 \\ 0 & 0 & h_{-2} & h_{-1} & h_0 & h_1 & h_2 & 0 \\ h_2 & 0 & 0 & 0 & h_{-2} & h_{-1} & h_0 & h_1 \\ - & - & - & - & - & - & - & - \\ g_0 & g_1 & g_2 & 0 & 0 & 0 & 0 & 0 \\ 0 & 0 & g_0 & g_1 & g_2 & 0 & 0 & 0 \\ 0 & 0 & 0 & 0 & g_0 & g_1 & g_2 & 0 \\ g_2 & 0 & 0 & 0 & 0 & 0 & g_0 & g_1 \end{bmatrix}$$

$$= \sqrt{2}\begin{bmatrix} 3/4 & -1/2 & 1/4 & 0 & 0 & 0 & -1/2 & 1 \\ -1/2 & 1 & 3/4 & -1/2 & 1/4 & 0 & 0 & 0 \\ 0 & 0 & -1/2 & 1 & 3/4 & -1/2 & 1/4 & 0 \\ 1/4 & 0 & 0 & 0 & -1/2 & 1 & 3/4 & -1/2 \\ - & - & - & - & - & - & - & - \\ 1/4 & -1/2 & 1/4 & 0 & 0 & 0 & 0 & 0 \\ 0 & 0 & 1/4 & -1/2 & 1/4 & 0 & 0 & 0 \\ 0 & 0 & 0 & 0 & 1/4 & -1/2 & 1/4 & 0 \\ 1/4 & 0 & 0 & 0 & 0 & 0 & 1/4 & -1/2 \end{bmatrix}$$

$$\text{Similarly,}\quad \tilde{\omega}_{5/3} = \begin{bmatrix} \tilde{h}_0 & \tilde{h}_1 & 0 & 0 & 0 & 0 & 0 & \tilde{h}_{-1} \\ 0 & \tilde{h}_{-1} & \tilde{h}_0 & \tilde{h}_1 & 0 & 0 & 0 & 0 \\ 0 & 0 & 0 & \tilde{h}_{-1} & \tilde{h}_0 & \tilde{h}_1 & 0 & 0 \\ 0 & 0 & 0 & 0 & 0 & \tilde{h}_{-1} & \tilde{h}_0 & \tilde{h}_1 \\ - & - & - & - & - & - & - & - \\ \tilde{g}_0 & \tilde{g}_1 & \tilde{g}_2 & \tilde{g}_3 & 0 & 0 & 0 & \tilde{g}_{-1} \\ 0 & \tilde{g}_{-1} & \tilde{g}_0 & \tilde{g}_1 & \tilde{g}_2 & \tilde{g}_3 & 0 & 0 \\ 0 & 0 & 0 & \tilde{g}_{-1} & \tilde{g}_0 & \tilde{g}_1 & \tilde{g}_2 & \tilde{g}_3 \\ \tilde{g}_2 & \tilde{g}_3 & 0 & 0 & 0 & \tilde{g}_{-1} & \tilde{g}_0 & \tilde{g}_1 \end{bmatrix}$$

$$\therefore \tilde{\omega}_{5/3} = \sqrt{2}\begin{bmatrix} 1/2 & 1/4 & 0 & 0 & 0 & 0 & 0 & 1/4 \\ 0 & 1/4 & 1/2 & 1/4 & 0 & 0 & 0 & 0 \\ 0 & 0 & 0 & 0 & 1/4 & 1/2 & 1/4 & 0 \\ 0 & 0 & 0 & 0 & 0 & 1/4 & 1/2 & 1/4 \\ - & - & - & - & - & - & - & - \\ -1/2 & -3/4 & 1 & 1/2 & 0 & 0 & 0 & -1/4 \\ 0 & -1/2 & -1/2 & -3/4 & 1 & 1/2 & 0 & 0 \\ 0 & 0 & 0 & -1/4 & -1/2 & -3/4 & 1 & 1/2 \\ 1/2 & 0 & 0 & 0 & -1/4 & -1/2 & -3/4 & 1 \end{bmatrix}$$

it is clear, that

$$\boxed{\tilde{\omega}_{5/3}^{-1} = \tilde{\omega}_{5/3}^{T}}$$

an extension:

using this approach different bi-orthogonal taps can be studied.

For example, let us design 6/2 tap tp produce $\omega_{6/2}$ and $\tilde{\omega}_{6/2}$

Here,

$$h_k = \{h_{-2}, h_{-1}, h_0, h_1, h_2, h_3\} \text{ line of symmetry;}$$

$$\tilde{h}_k = \{\tilde{h}_0, \tilde{h}_1\} \text{ (1.9,0.5) line of symmetry;}$$

as the filters are symmetric, for $\tilde{h}_k$, $\tilde{h}_0 = \tilde{h}_1$
for $h_k, h_0 = h_1, h_{-1} = h_2, h_{-2} = h_3$

$$\widetilde{H}\omega = h_0 + h_1.e^{j\omega} = h_0 + h_0.e^{j\omega} \tag{11.68}$$

and

$$\begin{aligned} H(\omega) &= h_{-2}.e^{-2j\omega} + h_{-1}.e^{-j\omega} + h_0 + h_1.e^{j\omega} + h_2.e^{2j\omega} + h_3.e^{3j\omega} \\ &= h_3.e^{-2j\omega} + h_2.e^{-j\omega} + h_1 + h_1.e^{j\omega} + h_2.e^{2j\omega} + h_3.e^{3j\omega} \end{aligned} \tag{11.69}$$

from Eq. (11.68)

Now $\widetilde{H}(\omega)|_{\omega=0} = 2h_0 = \sqrt{2}$

$$\therefore \qquad h_0 = h_1 = \frac{\sqrt{2}}{2} \qquad \text{(Haar!)}$$

for h_k, let us force low-pass conditions on $H(\omega)$.

$$H(\omega)|_{\omega=0} = \sqrt{2}$$

let us plug $\omega = 0$ in Eq. (11.69)

$$\therefore 2h_1 + 2h_2 + 2h_3 = \sqrt{2} \therefore h_1 + h_2 + h_3 = \frac{\sqrt{2}}{2}$$

similarly,

$$H(\omega)|_{\omega=\pi} = 0 \therefore h_3 - h_2 + h_1 - h_1 + h_2 - h_3 = 0 \text{ -(holds good)}$$

Using Eq. (11.45)

$$h_0.\tilde{h}_0 + h_1.\tilde{h}_1 = 1$$

$$\therefore \frac{\sqrt{2}}{2}h_0 + \frac{\sqrt{2}}{2}h_1 = 1, \text{ but } h_0 = h_1!$$

$$\sqrt{2}h_0 = 1$$

$\therefore h_0 = h_1 = \dfrac{1}{\sqrt{2}}$ from Eq. (11.46),

$h_0.\tilde{h}_{-2} + h_1.\tilde{h}_{-1} = 0$

$\therefore \dfrac{z}{2}h_3 + \dfrac{z}{2}h_2 = 0, \ \therefore h_2 = h_3,$

$h_2 = h_3 = h_{-1} = h_{-2} = \times$ (some real no.)

$\therefore h_k = \left\{x, -x, \dfrac{2}{2}, \dfrac{2}{2}, -x, x\right\}$

and $\tilde{h}_k = \left\{\dfrac{\sqrt{2}}{2}, \dfrac{\sqrt{2}}{2}\right\}$

Readers are encougraged to complete following steps:

1. calculate $\tilde{g}_k[1\times 6]$ from h_k
2. calculate $g_k[1\times 2]$ from $\tilde{h}_k$
3. calculate $\omega_{6/2}$ and $\tilde{\omega}_{6/2}$ from $h_k, \tilde{h}_k, h_k, \tilde{h}_k$

Exercises

Exercise 11.1

Prove that $<\phi(t), \phi(t-m)> = \dfrac{1}{2} r_{hh}[2m]$

Hint: As we know that, scaling function $\phi(t)$ can written as follows,

$$\phi(t) = \sum_{n\in Z} h[n]\phi(2t-n)$$

Similarly, $\phi(t-m)$ can be written as,

$$\phi(t-m) = \sum_{n_1\in Z} h[n]\phi(2t-2m-n_1)$$

So dot product of $\phi(t)$ and $\phi(t-m)$ is given by,

$$<\phi(t), \phi(t-m)> = \sum_n \sum_{n1} h[n]\overline{h[n_1]} <\phi(2t-n), \phi(2t-2m-n_1)> \tag{11.70}$$

The inner product term on the right hand side can be evaluated as,

$$<\phi(2t-n), \phi(2t-2m-n_1)> = \int_{-\infty}^{+\infty} \phi(2t-n)\overline{\phi(2t-2m-n_1)}dt$$

Let $2t = \lambda$. It gives $2dt = d\lambda$ and $t : -\infty \to +\infty \Rightarrow \lambda = -\infty \to +\infty$. With this substitution the above integral turns out to be,

$$<\phi(2t-n),\phi(2t-2m-n_1)> = \frac{1}{2}\int_{-\infty}^{+\infty}\phi(\lambda-n)\overline{\phi(\lambda-2m-n_1)}d\lambda$$

$$<\phi(2t-n),\phi(2t-2m-n_1)> = \frac{1}{2}\delta[n-(2m+n_1)]$$

Putting value in Eq. (11.70) we get,

$$<\phi(t),\phi(t-m)> = \frac{1}{2}\sum_{n}\sum_{n1}h[n]\overline{h[n_1]}\delta[n-(2m+n_1)] \tag{11.71}$$

Dropping $\sum_n$, we get

$$<\phi(t),\phi(t-m)> = \frac{1}{2}\sum_{n1}h[2m+n_1]\overline{h[n_1]} \tag{11.72}$$

The above expression is the autocorrelation of $h[.]$ evaluated at $2m$, $\forall m \in Z$. We can write Eq. (11.72) as,

$$<\phi(t),\phi(t-m)> = \frac{1}{2}r_{hh}[2m]$$

Exercise 11.2

Show that $\sum_{k\in Z}\left|\hat{\psi}(\Omega+2\pi k)\right|^2 = \text{Constant}$

Given that $\left|G(e^{j\Omega})\right|^2 + \left|G(e^{j(\Omega+\pi})\right|^2 = \text{Constant}$

and $\sum_{k\in Z}\left|\hat{\phi}(\Omega+2\pi k)\right|^2 = \text{Constant}$

Here, G is analysis high-pass filter.

Hint: We know, the dilation equation for $\psi(t)$ is given as,

$$\psi(t) = \sum_{n\in Z}g[n]\phi(2t-n) \tag{11.73}$$

Taking Fourier transform both side in Eq. (11.73)

$$\hat{\psi}(\Omega) = \int_{-\infty}^{+\infty}\sum_{n\in Z}g[n]\phi(2t-n)e^{-j\Omega t}dt \tag{11.74}$$

First evaluate term $\int_{-\infty}^{+\infty}\phi(2t-n)e^{-j\Omega t}dt$

Put $2t-n=\lambda$, It gives $2dt=d\lambda$ and $t:-\infty\to+\infty \Rightarrow \lambda=-\infty\to+\infty$

$$\int_{-\infty}^{+\infty}\phi(2t-n)e^{-j\Omega t}dt=\frac{1}{2}\int_{-\infty}^{+\infty}\phi(\lambda)e^{-j\Omega(\frac{\lambda+n}{2})}d\lambda$$

$$=\frac{1}{2}e^{-j\frac{\Omega}{2}n}\hat{\phi}(\frac{\Omega}{2})$$

Putting value of term $\int_{-\infty}^{+\infty}\phi(2t-n)e^{-j\Omega t}dt$ in Eq. (11.74), we get

$$\hat{\psi}(\Omega)=\sum_{n\in Z}\frac{1}{2}g[n]e^{-j\frac{\Omega}{2}n}\hat{\phi}(\frac{\Omega}{2})$$

$$\hat{\psi}(\Omega)=\frac{1}{2}[\sum_{n\in Z}g[n]e^{-j\frac{\Omega}{2}n}]\hat{\phi}(\frac{\Omega}{2})$$

$$\hat{\psi}(\Omega)=\frac{1}{2}G(e^{j\frac{\Omega}{2}})\hat{\phi}(\frac{\Omega}{2}) \tag{11.75}$$

Now if we take term $\sum_{k\in Z}\left|\hat{\psi}(\Omega+2\pi k)\right|^2$ and evaluate using Eq. (11.75), we get

$$\sum_{k\in Z}\left|\hat{\psi}(\Omega+2\pi k)\right|^2=\sum_{k\in Z}\frac{1}{2}^2\left|G(e^{j(\frac{\Omega}{2}+\pi k)})\right|^2\left|\hat{\phi}(\frac{\Omega}{2}+\pi k)\right|^2 \tag{11.76}$$

Above equation 11.76 can be also written as,

$$\sum_{k\in Z}\left|\hat{\psi}(\Omega+2\pi k)\right|^2=\sum_{k\in Z}(\frac{1}{2})^2\left|G(e^{j(\frac{\Omega}{2}+2\pi k)})\right|^2\left|\hat{\phi}(\frac{\Omega}{2}+2\pi k)\right|^2+\sum_{k\in Z}(\frac{1}{2})^2\left|G(e^{j(\frac{\Omega}{2}+2\pi k+\pi)})\right|^2\left|\hat{\phi}(\frac{\Omega}{2}+2\pi k+\pi)\right|^2 \tag{11.77}$$

In Eq. (11.77) terms $\left|G(e^{j(\frac{\Omega}{2}+2\pi k)})\right|^2$ and $\left|G(e^{j(\frac{\Omega}{2}+2\pi k+\pi)})\right|^2$ are periodic. Also, terms $\left|\hat{\phi}(\frac{\Omega}{2}+2\pi k)\right|^2$ and $\left|\hat{\phi}(\frac{\Omega}{2}+2\pi k+\pi)\right|^2$ are constant as given in question.

Let the constant be denoted by C_0. So, now, Eq. (11.77) can be written as,

$$\sum_{k\in Z}\left|\hat{\psi}(\Omega+2\pi k)\right|^2=\frac{C_0}{4}\left|G(e^{j(\frac{\Omega}{2})})\right|^2+\frac{C_0}{4}\left|G(e^{j(\frac{\Omega}{2}+\pi)})\right|^2$$

$$\sum_{k\in Z}\left|\hat{\psi}(\Omega+2\pi k)\right|^2=\frac{C_0}{4}\left(\left|G(e^{j(\frac{\Omega}{2})})\right|^2+\left|G(e^{j(\frac{\Omega}{2}+\pi)})\right|^2\right) \tag{11.78}$$

But also in question given that power complementary property, i.e $\left|G(e^{j\Omega})\right|^2+\left|G(e^{j(\Omega+\pi)})\right|^2=$ Constant(C_1). So by using this property RHS of Eq. (11.78) become a constant. Now we can write,

$$\sum_{k\in Z}\left|\hat{\psi}\ (\Omega+2\pi k)\right|^2=\frac{C_0C_1}{4}=\text{Constant}$$

Exercise 11.3

Find the dilation equation of $\phi_2(t)=\phi_0(t)\times\phi_0(t)\times\phi_0(t)$. Here $\phi_0(t)$ is the Haar Scaling function.

Hint: For solving this question we are using property that has already been discussed in this chapter and is now given here also,

$$h(at+b)\times g(at+c)=\frac{1}{|a|}h\times g\,|_{(at+b+c)} \tag{11.79}$$

Dilation equation for $\phi_0(t)$ is given as,

$$\phi_0(t)=\phi_0(2t)+\phi_0(2t-1) \tag{11.80}$$

Let $\phi_1(t)=\phi_0(t)\times\phi_0(t)$, Using property of Eq. (11.79) dilation equation of $\phi_1(t)$ can be written as,

$$\phi_1(t)=(\phi_0(2t)+\phi_0(2t-1))\times(\phi_0(2t)+\phi_0(2t-1))$$

$$\phi_1(t)=\frac{1}{2}[\phi_1(2t)+2\phi_1(2t-1)+\phi_1(2t-2)] \tag{11.81}$$

Now $\phi_2(t)=\phi_1(t)\times\phi_0(t)$, so dilation equation of $\phi_2(t)$ given as,

$$\phi_2(t)=\frac{1}{2}[\phi_1(2t)+2\phi_1(2t-1)+\phi_1(2t-2)]\times\phi_0(2t)+\phi_0(2t-1))$$

$$\phi_2(t)=\frac{1}{4}[\phi_2(2t)+\phi_2(2t-1)+\phi_2(2t-2)+\phi_2(2t-1)+\phi_2(2t-2)+\phi_2(2t-3)]$$

$$\phi_2(t)=\frac{1}{4}\phi_2(2t)+\frac{1}{2}\phi_2(2t-1)+\frac{1}{2}\phi_2(2t-2)+\frac{1}{4}\phi_2(2t-3) \tag{11.82}$$

Equation (11.82) gives the dilation equation of $\phi_2(t)$.

Exercise 11.4

Explain, why Linear phase is not possible for Daubechies family other than Haar?

Hint: Linear phase means that phase response of filter is the linear function of frequency. This means delay introduced by filter is same at all frequency.

Linear phase requires symmetry in impulse response of filter. That means any filter in linear phase requires that its coefficients are symmetrical around the centre coefficients, i.e. first coefficients is same as last coefficients; second is the same as second last, and so on. One other way to seeing this that zeros must be occur in reciprocal pairs.

So in Daubechies family this type of symmetry is not occurred so it does not give the linear phase.

Exercise 11.5

The two-band filter bank shown in Fig. 11.13, is the 5/3 filter bank used in JPEG 2000 standards. The filters are defined as follows:

$$H_0(Z) = \frac{1}{8}(-1 + 2Z^{-1} + 6Z^{-2} + 2Z^{-3} - Z^{-4})$$

$$H_1(Z) = -\frac{1}{2}(1 - Z^{-1})^2$$

$$G_0(Z) = \frac{1}{2}(1 + 2Z^{-1} + Z^{-2})$$

$$G_1(Z) = \frac{1}{8}(1 + 2Z^{-1} - 6Z^{-2} + 2Z^{-3} + Z^{-4})$$

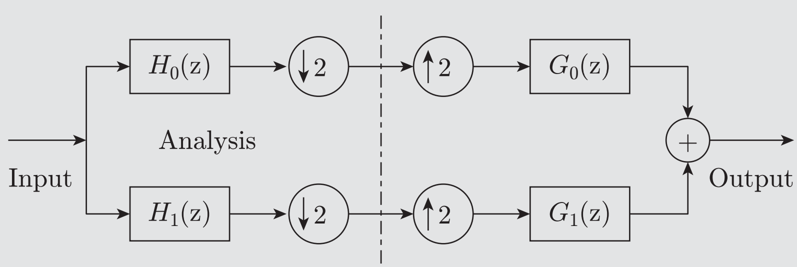

Figure 11.13 | *Two-band filter bank*

(a) Obtain and sketch the magnitude and frequency responses of the low-pass synthesis and the high-pass analysis filters.
(b) Obtain scaling and wavelet functions corresponding to synthesis filter bank.

Hint: (a) Low-pass synthesis filter transfer function:

$$G_0(Z) = \frac{1}{2}(1 + 2Z^{-1} + Z^{-2})$$
$$= \frac{1}{2}Z^{-1}\left(Z^{\frac{1}{2}} + Z^{-\frac{1}{2}}\right)^2$$

Put $Z = e^{jw}$, hence frequency response is as follows:

$$= \frac{1}{2}e^{-jw}\left(e^{\frac{jw}{2}} + e^{-\frac{jw}{2}}\right)^2$$
$$= 2e^{-jw}\cos^2\left(\frac{w}{2}\right)$$

Magnitude response is shown in Fig. 11.14.

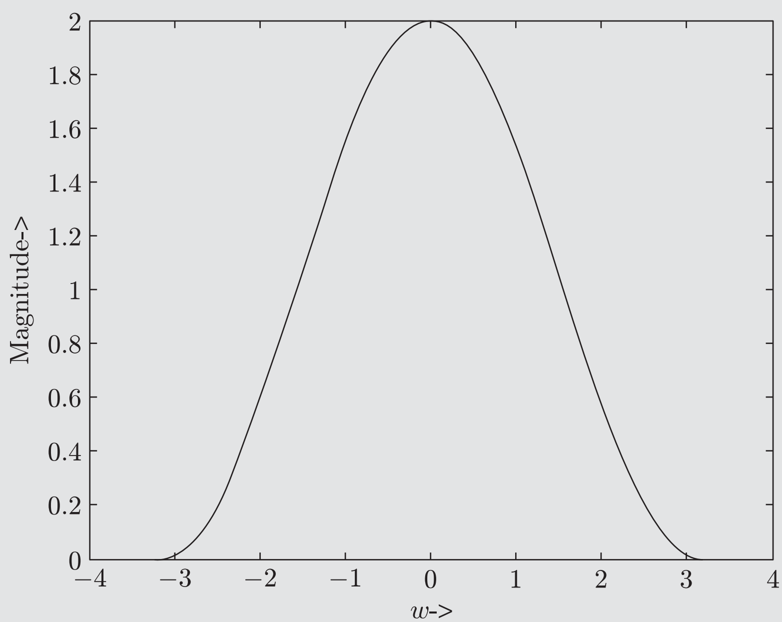

Figure 11.14 | *Magnitude response of low-pass filter*

$$|G_0(Z)| = \left|2e^{-jw}\cos^2(\frac{w}{2})\right|$$
$$= \left|2\cos^2(\frac{w}{2})\right|$$
$$= |1+\cos w| \angle |G_0(Z)|$$
$$= -w$$

High-pass analysis filter transfer function:

$$H_1(Z) = -\frac{1}{2}(1 - 2Z^{-1} + Z^{-2})$$
$$= -\frac{1}{2}Z^{-1}(Z^{\frac{1}{2}} - Z^{-\frac{1}{2}})^2$$

Put $Z = e^{jw}$, hence frequency response is as follows:

$$= -\frac{1}{2}e^{-jw}\left(e^{\frac{jw}{2}} - e^{-\frac{jw}{2}}\right)^2$$
$$= 2e^{-jw}\sin^2\left(\frac{w}{2}\right)$$

Magnitude and phase of the above frequency response are shown in Fig. 11.15 and in Fig. 11.16.

$$|H_1(Z)| = \left|2e^{-jw}\sin^2\left(\frac{w}{2}\right)\right|$$
$$= |1 - \cos w| \angle |H_1(Z)| = -w$$

Hint: (b) The scaling function satisfies the dilation equation:

$$\phi(t) = \frac{1}{2}(\phi_1(t) + 2\phi_1(t-1) + \phi_1(t-2))$$

The wavelet function obtained from synthesis highpass filter impulse response:

$$\frac{1}{8}(\underset{\substack{\uparrow \\ 0}}{-1} \quad -2 \quad 6 \quad -2 \quad -1)$$

The wavelet function is given by following expression and shown in Fig. 11.17.

$$\frac{1}{8}(-\phi_1(t) - 2\phi_1(t-1) + 6\phi_1(t-2) - 2\phi_1(t-3) - \phi_1(t-4))$$

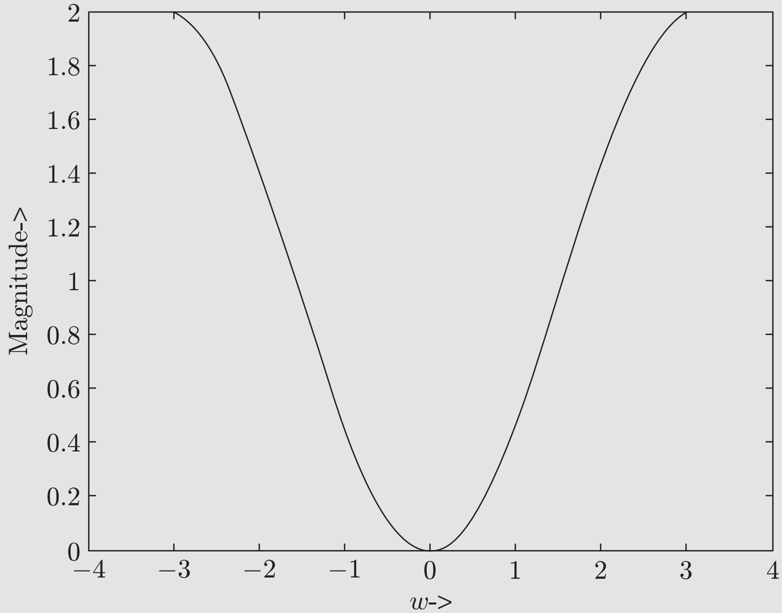

Figure 11.15 | *Magnitude response of high pass filter*

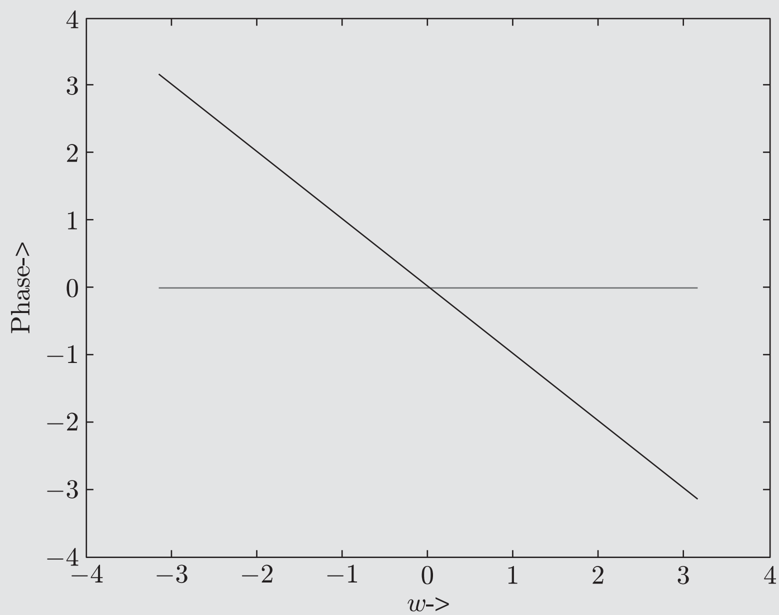

Figure 11.16 | *Phase response*

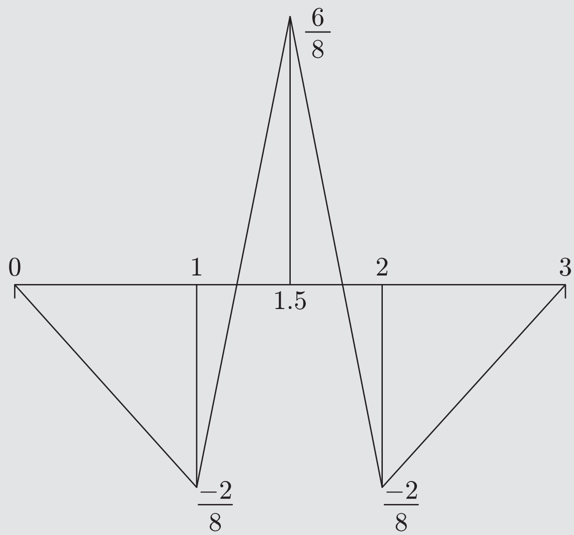

Figure 11.17 | *Wavelet function for synthesis filter bank*

Chapter 12

MRA Variant 2: Splines

12.1 | Introduction

In this chapter, we shall continue to discuss one more variant on the idea of MRA. In earlier chapters, we had built an idea on the orthogonal or perfect reconstruction with one filter and also extended it to biorthogonal or perfect reconstruction with two filters. We had taken the example of a 5/3 filter bank in JPEG 2000. When we extend the MRA to 2 filters, it involved building a filter bank and not really the MRA. So, we had essentially built a perfect reconstruction filter bank where the filters were of unequal lengths. But we saw that we could get the advantage of linear phase and symmetry in the impulse response. Further, we could extend what we did in the Haar case to a piece-wise linear function. So, if we take 5/3 filter bank and if we look at the 3 length LPF, the filter has an impulse response of $(1+z^{-1})^2$. It would essentially give us the triangular function as the scaling function. The disadvantage with the triangular function was that it was not orthogonal to all its integer translates; it was orthogonal when translated by two units or more, but it was not orthogonal when translated by one unit. Thus, we had to venture to other areas by looking at variants of the filter banks that we had already discussed and bring in the idea of a biorthogonal filter bank.

Now, in this chapter we shall take the same $(1+z^{-1})^2$ again; the length 3 LPF that we have seen in the 5/3 filter bank. But we shall deal with it in a slightly different way, which would bring us to the idea of orthogonal MRA with splines. Here, we need to make a compromise in the nature of the scaling and the wavelet function that we construct and also in the nature of the filter bank that we would build. In fact, as a consequence of our demanding an orthogonal MRA we shall have to go from finite length to infinite length filters.

12.2 | 5/3 Filter Bank

If we look at the length-3 Low-pass filter in the 5/3 filter bank, it essentially has $\frac{1}{2}(1+z^{-1})^2$ as the system function. We know that the corresponding scaling function is $\phi_1(t)$ and it obeys the dilation equation:

$$\phi_1(t)=\frac{1}{2}\phi_1(2t)+\phi_1(2t-1)+\frac{1}{2}\phi_1(2t-2) \tag{12.1}$$

$\phi_1(t)$ has an appearance as shown in Fig. 12.1.

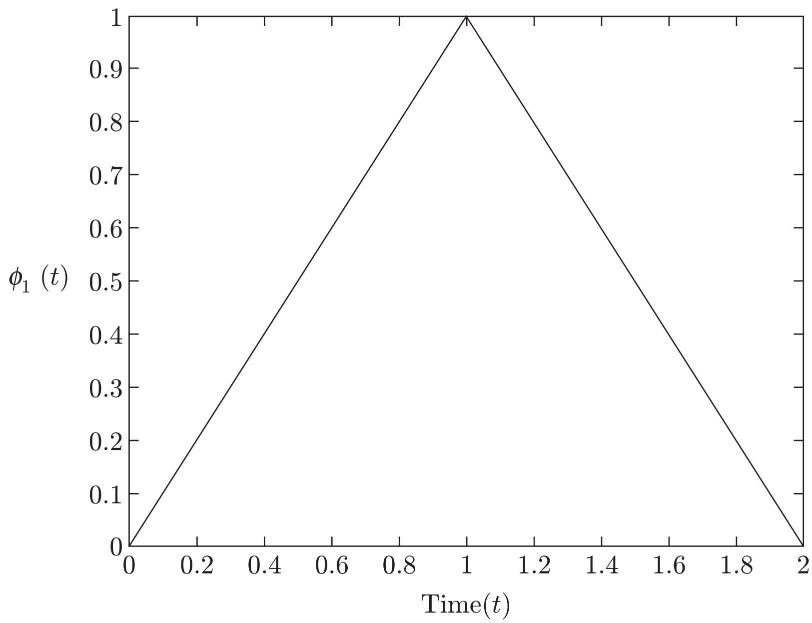

Figure 12.1 | *The scaling function*

Now, our main problem and the reason as to why we need to go for a bi-orthogonal filter bank, as opposed to an orthogonal filter bank, is that this scaling function is not orthogonal to its translates by unity. So, if we translate this by unity and take the dot product essentially between $\phi_1(t)$ and $\phi_1(t-1)$, i.e., if we consider these two dot products,

$$\ll \phi_1(t), \phi_1(t-1) \gg \text{and} \ll \phi_1(t), \phi_1(t+1) \gg \tag{12.2}$$

we find that these two are nonzero. This was our main goal of contention because of which we would not be satisfied with this $\phi_1(t)$ to construct an orthogonal MRA out of it. Now, we wish to explore that possibility. Even though $\phi_1(t)$ is not orthogonal to its own integer translates, we wish to construct an orthogonal MRA from a function that looks similar to $\phi_1(t)$, or in other words, out of a function that is piece-wise linear. We would build an orthogonal MRA with scaling functions, which are piece-wise linear even though not exactly $\phi_1(t)$. So, what we are saying is, *Can we build a multi-resolution analysis with a piece-wise linear function for ϕ and ψ?* We shall try to answer the question in this chapter and for that we must relax the requirement of orthogonality.

12.3 | Derivation of Orthogonal MRA

The notion of orthogonality of $\phi(t)$ to its integer translates, is expressed in terms of the autocorrelation of ϕ, i.e. the autocorrelation function of $\phi(t)$ at all the integers except at '0' is 0, i.e. $R_{\phi\phi}(\tau) = 0$ for all $\tau \in \mathbb{Z}$ except for $\tau = 0$, where $R_{\phi\phi}(\tau)$ is the autocorrelation function of $\phi(t)$. This is the basic principle of a function being orthogonal to its integer translates.

Example 12.3.1

Let the scaling function be $\phi(t)$ and it is orthogonal to its integer translates $\phi(t-m)$, where $m \in \mathbb{Z}$. Essentially, we mean to say that the autocorrelation function $R_{\phi\phi}(\tau)$ when sampled at $\tau = m, m \in \mathbb{Z}$ (i.e., we sample at all integers, or at a sampling rate of 1) gives an impulse sequence. Mathematically, the sequence is a discrete impulse sequence. Now, we need to deal with it in the frequency domain. So, when we sample it, the Fourier transform of the autocorrelation function gets aliased. In fact, we know that the Fourier transform of the autocorrelation function is $|\hat{\phi}(\Omega)|^2$ where $\hat{\phi}(\Omega)$ is the Fourier transform of the scaling function $\phi(t)$. In other sense, we can say that the Fourier transform of the autocorrelation function is the power spectral density of the scaling function in the frequency domain. Now sampling $R_{\phi\phi}(\tau)$ at $\tau = m$ for $m \in \mathbb{Z}$, means summing up all the aliases of $|\hat{\phi}(\Omega)|^2$ in the Fourier domain. In other words, constructing the sum,

$$K_0 \sum_{k=-\infty}^{\infty} |\hat{\phi}(\Omega + 2\pi k)|^2, \text{ where } K_0 \text{ is a constant.} \tag{12.3}$$

Recall that when we sample a continuous function, its Fourier transform shifts on the frequency axis by every multiple of the sampling frequency and adds up all these translates or aliases. In a way, the sequence $R_{\phi\phi}(\tau)|_{\tau=m}$ is an impulse sequence, then its DTFT must be a constant. And, therefore, we now have a clear cut criterion in the frequency domain. In order that the $\phi(t)$ is orthogonal to its integer translates, we require that the quantity, sum of aliases of the power spectral density must be a constant. In other words, $K_0 \sum_{k=-\infty}^{\infty} |\hat{\phi}(\Omega + 2\pi k)|^2$ is a constant. We shall call $K_0 \sum_{k=-\infty}^{\infty} |\hat{\phi}(\Omega + 2\pi k)|^2$ as the sum of translated spectra of $\phi(.)$. We shall abbreviate sum of translated spectra by STS. STS $(\phi, 2\pi)(\Omega)$ has Ω as the primary argument and ϕ, 2π as secondary arguments. In general,

$$\text{STS } (\phi, T)(\Omega) = K_0 \sum_{k=-\infty}^{\infty} |\hat{\phi}(\Omega + Tk)|^2 \tag{12.4}$$

With this little notational introduction, we take the same strategy as we did when we relaxed the condition for the sum of dilated spectra. We know that when we discretize the scale, we need to essentially relax the requirement of sum of dilated spectra to be a constant, where it is between two positive constants. If one gets the sum of dilated spectra to be a constant, we shall be happy if it is between two positive (strictly non zero and finite) constants. Similar will be true for this case. In fact now, we also bring out a relationship between relaxation of this requirement in the τ domain or shift domain and frequency domain. Now, if we look back, it is easier to start from the ϕ domain. Next, we take the function $\phi_1(t)$ which is as shown in Fig. 12.1. The dot product of $\phi_1(t)$ with its integer translates is zero only when the translates are greater than 2. Hence, we need a relaxation when the translate is equal to 1 and –1. The relaxation that we are asking for is that the dot product is zero. We can even actually calculate the dot product. The dot product of ϕ with itself would have certain value and it is equal to the energy of the function. And if we take the dot product of ϕ with its translates by 1 and –1, they are expected intuitively to have a smaller value. So in other words the relaxation we are asking for is that the auto correlation of this function is not quite as an impulse, but close to an impulse. This means it is a nonzero for very few values around $n = 0$ and that manifests in the frequency domain as the STS, which is not a constant but between two positive constants. We shall calculate these quantities now and prove mathematically. So, for $\phi_1(t)$, by looking at Fig. 12.1, we can observe that,

$$R_{\phi_1\phi_1}(1) = R_{\phi_1\phi_1}(-1) \tag{12.5}$$

Let us now find $\int_{-\infty}^{\infty}\phi_1(t)\phi_1(t-1)dt$. In fact, this quantity can be easily calculated by shifting both the functions to left by 1 unit as shown in Fig. 12.2. Equation (12.5) now becomes,

$$\int_0^1 t(1-t)dt = \frac{1}{6}$$

Now, in a similar way $R_{\phi_1\phi_1}(0)$ can be calculated,

$$\begin{aligned} R_{\phi_1\phi_1}(0) &= \int_0^2 \phi_1^2(t)dt \\ &= \frac{2}{3} \end{aligned}$$

Therefore,
$$R_{\phi_1\phi_1}(\tau)|_{\tau=m,m\in\mathbb{Z}} = \left\{\frac{1}{6}, \underset{\uparrow}{\frac{2}{3}}, \frac{1}{6}\right\}$$

Therefore, DTFT of $R_{\phi_1\phi_1}(\tau)|_{\tau=m,m\in\mathbb{Z}} = \frac{1}{6}e^{j\Omega} + \frac{2}{3} + \frac{1}{6}e^{-j\Omega}$. From this equation we can infer that

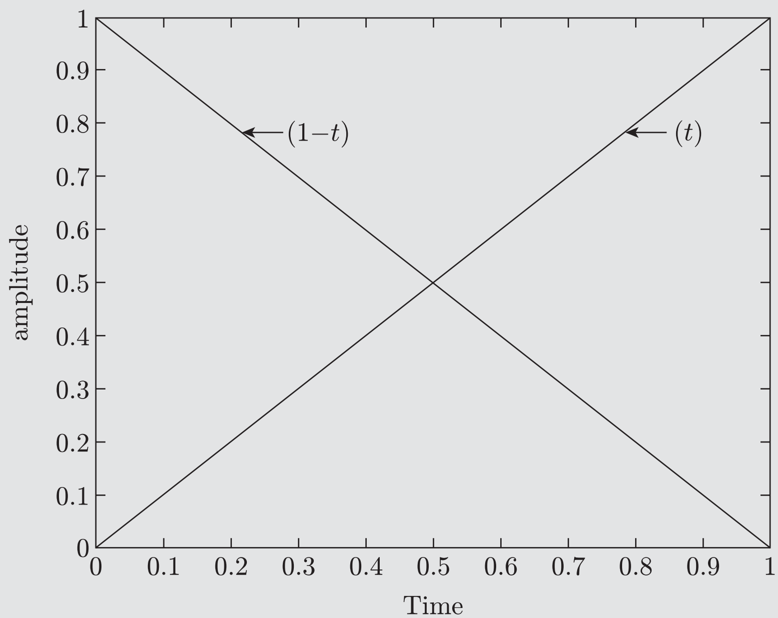

Figure 12.2 | *Graphical representation of dot product between* $\phi_1(t)$ *and* $\phi_1(t-1)$

$$K_0 \sum_{k=-\infty}^{\infty} |\hat{\phi}(\Omega + 2\pi\ k)|^2 \quad = \frac{1}{6}e^{j\Omega} + \frac{2}{3} + \frac{1}{6}e^{-j\Omega} \quad = \frac{2}{3}(1 + \frac{1}{2}\cos(\Omega)) \tag{12.6}$$

As expected, this sum is strictly positive and lies between two positive constants and it can be observed that the constants are $\frac{1}{3}$ and 1, i.e.

$$\frac{1}{3} \le \frac{2}{3}(1 + \frac{1}{2}\cos(\Omega)) \le 1 \tag{12.7}$$

So relaxation of the requirement in time domain has also led to a corresponding relaxation in the frequency domain. And, now, we can employ the same strategy (as we did when we relaxed the requirement of the sum of dilated spectrum). We can see that the sum of translated spectrum lies between two positive bounds. We could say that even though $\phi_1(t)$ by itself gives us a multi-resolution analysis. The question arises, can we construct another function $\tilde{\phi}_1(t)$ out of $\phi_1(t)$ by using the sum of translated spectrum in such a way that $\tilde{\phi}_1(t)$ gives us an orthogonal MRA. Let us strategically define such a $\tilde{\phi}_1(t)$, as we did while taking inspiration from sum of dilated spectrum. So, let us define $\tilde{\phi}_1(t)$ in terms of its Fourier transform. Therefore,

$$\hat{\tilde{\phi}}_1(\Omega) = \frac{\hat{\phi}_1(\Omega)}{+\sqrt{\mathrm{STS}(\phi_1, 2\pi)(\Omega)}} \tag{12.8}$$

Let us justify this definition by noting that the denominator is between two positive bounds. Denominator is known to be between 1/3 and 1. So, this division will not go up towards infinity and neither it will go to zero. Now, consider the denominator, i.e., $\mathrm{STS}(\phi_1, 2\pi)(\Omega)$. This exhibits an important property of periodicity with period 2π, i.e.,

$$\begin{aligned}
\mathrm{STS}(\phi, 2\pi)(\Omega) &= \mathrm{STS}(\phi, 2\pi)(\Omega + 2\pi) \quad \forall \Omega \\
\mathrm{STS}(\phi, 2\pi)(\Omega + 2\pi) &= \sum_{k=-\infty}^{\infty} |\hat{\phi}(\Omega + 2\pi + 2\pi\ k)|^2 \\
&= \sum_{k=-\infty}^{\infty} |\hat{\phi}(\Omega + 2\pi(k+1))|^2
\end{aligned} \tag{12.9}$$

As, k runs from $-\infty$ to ∞, $k+1$ also has the same limits. Hence, the summation in Eq. (12.9) becomes $\mathrm{STS}(\phi, 2\pi)(\Omega)$. Using this result we are going to find $\mathrm{STS}(\tilde{\phi}_1, 2\pi)(\Omega)$.

$$\begin{aligned}
\mathrm{STS}(\tilde{\phi}_1, 2\pi)(\Omega) &= \sum_{k=-\infty}^{\infty} \frac{|\hat{\phi}_1(\Omega + 2\pi\ k)|^2}{\mathrm{STS}(\hat{\phi}_1, 2\pi)(\Omega + 2\pi\ k)} \\
&= \frac{1}{\mathrm{STS}(\phi_1, 2\pi)(\Omega)} \sum_{k=-\infty}^{\infty} |\hat{\phi}_1(\Omega + 2\pi\ k)|^2 \\
&= \frac{\mathrm{STS}(\phi_1, 2\pi)(\Omega)}{\mathrm{STS}(\phi_1, 2\pi)(\Omega)} \\
&= 1
\end{aligned}$$

From the above result it is clear that $\mathrm{STS}(\tilde{\phi}_1, 2\pi)(\Omega)$ is constant and is equal to one. Therefore, we can say that the underlying continuous function $\tilde{\phi}_1(t)$ is orthogonal to its integer translates. To characterize $\tilde{\phi}_1(t)$, let us consider its Fourier domain. We have,

$$\hat{\tilde{\phi}}_1(\Omega) = \frac{\hat{\phi}_1(\Omega)}{+\sqrt{\mathrm{STS}(\phi_1, 2\pi)(\Omega)}} \tag{12.10}$$

Substituting the value of $\mathrm{STS}(\phi_1, 2\pi)(\Omega)$ from Eq. (12.6), we get

$$\hat{\tilde{\phi}}_1(\Omega) = \frac{\hat{\phi}_1(\Omega)}{\sqrt{\frac{2}{3}\left(1 + \frac{1}{2}\cos(\Omega)\right)}} \tag{12.11}$$

Expanding Eq. (12.11) in the form of binomial expansion, i.e.,

$$\hat{\tilde{\phi}}_1(\Omega) = \hat{\phi}_1(\Omega)\left(\frac{2}{3}\right)^{-\frac{1}{2}}\left(1 + \frac{1}{2}\cos(\Omega)\right)^{-\frac{1}{2}} \tag{12.12}$$

This equation is of the form $(1+\lambda)^R, R \in \mathbb{R}$, we know that

$$(1+\lambda)^R = 1 + R.\lambda + \frac{R(R-1)}{2!}\lambda^2 + \frac{R(R-1)(R-2)}{3!}\lambda^3 + \ldots \tag{12.13}$$

Comparing Eqs. (12.12) and 12.13 and expanding Eq. (12.12) gives a typical p^{th} term, which can be represented as follows,

$$K_p \lambda^p = K_p (\cos(\Omega))^p \left(\frac{1}{2}\right)^p \tag{12.14}$$

We know that, $\cos(\Omega)^p = \left(\frac{e^{j\Omega} + e^{-j\Omega}}{2}\right)^p$. Using this result in Eq. (12.14) and expanding it, we get a final expression which looks like

$$\hat{\tilde{\phi}}_1(\Omega) = \sum_{k=-\infty}^{\infty} \tilde{C}_k e^{j\Omega k} \hat{\phi}_1(\Omega) \tag{12.15}$$

Now, from Eq. 12.15 we can find the Inverse DTFT to get $\tilde{\phi}_1(t)$ easily. We know that multiplication by the term $e^{j\Omega k}$ in Fourier domain shifts the signal by k in time domain. Therefore, $\tilde{\phi}_1(t)$ turns out to be,

$$\tilde{\phi}_1(t) = \sum_{k=-\infty}^{\infty} \tilde{C}_k \phi_1(t+k) \tag{12.16}$$

From Eq. (12.16), $\tilde{\phi}_1(t)$ turns out to be a linear combination of $\phi_1(t)$ shifted by integer translates. When we shift a piece-wise linear function by integer translates and add them, we still get a piece-wise linear function. Hence, $\tilde{\phi}_1(t)$ is a piece-wise linear function.

In subsequent chapters we shall study the nature of $\tilde{C}_k$'s and know how to construct an MRA out of $\tilde{\phi}_1(t)$.

12.4 | Building Piece-wise Linear Scaling Function, Wavelet

In earlier sections, we began with building piece-wise linear MRA. We also saw the piece-wise linear function obtained by convolving the Haar Scaling function with itself, as shown in Fig. 12.3.

$$\phi_1(t) = \phi_0(t) \times \phi_0(t) \tag{12.17}$$

This $\phi_1(t)$ is not orthogonal to its integral translates. This led to Sum of Translated Spectra (STS) not being a constant. It was only 1 and -1 which were problematic translates. But as expected, the STS was a constant within two positive bounds. As a result, one could extract from $\phi_1(t)$ another function, which was orthogonal to its own translates. This new function can be used to build MRA based on piece-wise linear scaling function and wavelets.

12.5 | Building of Piece-wise Linear Scaling Function

We saw that:

$$\text{STS}(\phi_1, 2\pi)(\Omega) = \sum_{K=-\infty}^{\infty} |\,\phi_1(\Omega + 2\pi\, K)\,|^2 \tag{12.18}$$

This is not a constant as required but it lies between two positive bounds.

$$0 < A \leq \text{STS}(\phi_1, 2\pi)(\Omega) \leq B < \infty \tag{12.19}$$

$$\frac{B}{A} = 3 \tag{12.20}$$

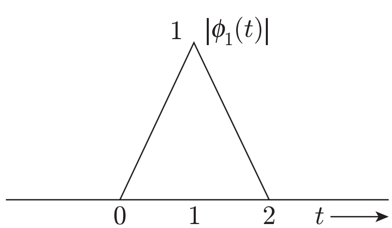

Figure 12.3 | *The linear scaling function*

If we scale a function by a constant, the STS is scaled by the square of that constant.

In Chapter 11, we had already discussed that we can define a function $\tilde{\phi}_1(\Omega)$ as:

$$\hat{\tilde{\phi}}_1(\Omega) = \frac{\tilde{\phi}_1(\Omega)}{+\sqrt{\text{STS}(\phi_1, 2\pi)(\Omega)}} \tag{12.21}$$

$$\text{STS}(\tilde{\phi}_1, 2\pi)(\Omega) = \frac{\text{STS}(\phi_1, 2\pi)(\Omega)}{\text{STS}(\phi_1, 2\pi)(\Omega)} = 1(\text{Constant}) \tag{12.22}$$

Both numerator and denominator are greater than 0 and less than ∞ and hence cancellation is possible.

Therefore, $\tilde{\phi}_1(t)$ is orthogonal to all its integer translates, i.e.,

$$< \tilde{\phi}_1(t), \tilde{\phi}_1(t-m) > = 0 \quad \forall \quad m \in Z \tag{12.23}$$

Now, we saw that it is of the form,

$$\hat{\tilde{\phi}}_1(\Omega) = \frac{\tilde{\phi}_1(\Omega)}{+\sqrt{\frac{2}{3}\left(1 + \frac{1}{2}\cos\Omega\right)}} \tag{12.24}$$

Using binomial expansion or Taylor series expansion, i.e., $(1+\gamma)^R, \quad R \in \mathbb{R}, \quad |\gamma| < 1$

$$(1+\gamma)^R = 1 + R\gamma + \frac{R(R-1)}{2!}\gamma^2 + \frac{R(R-1)(R-2)}{3!}\gamma^3 + \ldots \tag{12.25}$$

Therefore, we get

$$\hat{\tilde{\phi}}_1(\Omega) = \frac{\tilde{\phi}_1(\Omega)}{\sqrt{2/3}}\left(1 + \frac{1}{2}\cos\Omega\right)^{-\frac{1}{2}} \tag{12.26}$$

Now, $\cos^N\Omega = \left(\dfrac{e^{j\Omega} + e^{-j\Omega}}{2}\right)^N$

Therefore,

$$\hat{\tilde{\phi}}_1(\Omega) = \sum_{l=-\infty}^{\infty} \tilde{C}_l \quad e^{j\Omega l}\hat{\phi}_1(\Omega) \tag{12.27}$$

The calculation of $\tilde{C}_l$ is cumbersome as for each $\tilde{C}_l$ we have to write a series.

Now, $\tilde{C}_l = \tilde{C}_{-l}$ from symmetry in expanding $(\cos\Omega)^l$. Therefore, if we take the Inverse Fourier transform of Equation 12.27, we get,

$$\tilde{\phi}_1(t) = \sum_{l=-\infty}^{\infty} \tilde{C}_l \quad \phi_1(t+l) \tag{12.28}$$

Therefore, $\tilde{\phi}_1(t)$ is a linear combination of $\phi_1(t)$ and its integer translates, as shown in Fig. 12.4.

This shows that $\tilde{\phi}_1(t)$ is piece-wise linear. For further clarity, one can calculate few $\tilde{C}_l$, may be for $l = 0, \quad \pm 1, \quad \pm 2$ and we will see that $\tilde{C}_l$ and $\tilde{C}_{-l}$ decay as $l \to +\infty$.

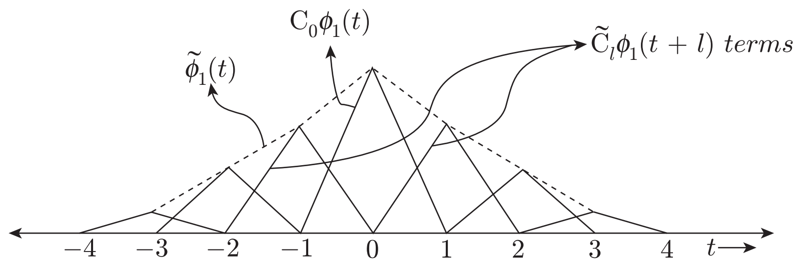

Figure 12.4 | *Representing $\tilde{\phi}_1(t)$ as a piecewise linear function*

Example 12.5.1 — Properties of $\tilde{\phi}_1(t)$:

1. Piecewise linear: A sum of piecewise linear functions.
2. $\phi_1(t)$ should be orthogonal to all its integer translates, i.e.

$$< \phi_1(t-m), \phi_1(t-n) >= 0; \quad \forall m, n \in Z; \quad m \neq n \tag{12.29}$$

3. $\tilde{\phi}_1(\cdot)$ obeys the dilation equation.

Property 3 is critical for MRA because it is this dyadic dilation equation which ensures that $\tilde{\phi}_1(t)$, when dilated by a factor of 2 and then translated by all the integers, constructs a basis for next subspace, V_0. This subspace V_0 is spanned by $\phi_1(t)$ and its integer translates and then we have a subspace which is spanned by $\tilde{\phi}_1(t)$ contracted by a factor of 2 and its integer translates.

We shall use the frequency domain to prove this. Time domain dyadic equation for a general scaling function $\phi(\cdot)$:

$$\phi(t) = \sum_{k=-\infty}^{\infty} h[k] \quad \phi(2t-k) \tag{12.30}$$

Taking Fourier transform:

$$\hat{\phi}(\Omega) = \frac{1}{2} H\left(\frac{\Omega}{2}\right)\hat{\phi}\left(\frac{\Omega}{2}\right) \tag{12.31}$$

where $H(\cdot)$ is the DTFT of $h[k]$.

To establish a dyadic dilation equation on $\hat{\hat{\phi}}_1(\cdot)$ we essentially need to consider $\dfrac{\hat{\hat{\phi}}_1(\Omega)}{\hat{\hat{\phi}}_1\left(\frac{\Omega}{2}\right)}$, and show that this is of the form $\frac{1}{2}H\left(\frac{\Omega}{2}\right)$ where:

$$H(\Omega) = \sum_{k=-\infty}^{\infty} h[k]\, e^{-jk\Omega} \tag{12.32}$$

Essentially, we need to establish that $\dfrac{\hat{\hat{\phi}}_1(\Omega)}{\hat{\hat{\phi}}_1\left(\frac{\Omega}{2}\right)}$ is a DTFT. That is, it is

(i) Periodic with period 2π

(ii) It is bounded on any interval of 2π, so that its IDTFT can be calculated.

Boundedness is needed, therefore:

$$\frac{1}{2\pi}\int f(\Omega)\, e^{j\Omega n}\, d\Omega \,\text{must converge,}$$

where

$$f(\Omega) = \frac{\hat{\hat{\phi}}_1(\Omega)}{\hat{\hat{\phi}}_1\left(\frac{\Omega}{2}\right)} \tag{12.33}$$

$$\frac{\hat{\hat{\phi}}_1(\Omega)}{\hat{\hat{\phi}}_1\left(\frac{\Omega}{2}\right)} = \frac{\hat{\phi}_1(\Omega)\ \left(\frac{2}{3}\left(1+\frac{1}{2}\cos\frac{\Omega}{2}\right)\right)^{1/2}}{\left(\frac{2}{3}\left(1+\frac{1}{2}\cos\Omega\right)\right)^{1/2}\ \hat{\phi}_1\left(\frac{\Omega}{2}\right)} \tag{12.34}$$

Now, we focus on the term inside the square root, i.e., $\left[\dfrac{\frac{2}{3}\left(1+\frac{1}{2}\cos\frac{\Omega}{2}\right)}{\frac{2}{3}\left(1+\frac{1}{2}\cos\Omega\right)}\right]^{1/2}$. This is a function of Ω, and hence it is periodic. This is definitely of the form $\frac{1}{2}H\left(\frac{\Omega}{2}\right)$ with properties of $H(\cdot)$ desired. Now, if we replace Ω by 2Ω in Eq. (12.34) (term inside the root), we get,

$$\left[\frac{\frac{2}{3}\left(1+\frac{1}{2}\cos\Omega\right)}{\frac{2}{3}\left(1+\frac{1}{2}\cos 2\Omega\right)}\right]^{1/2} \tag{12.35}$$

In this expression, the numerator is periodic with period 2π and the denominator is periodic with period π and hence the overall expression is periodic with period 2π. **Therefore the periodicity is established**.

Now, we look at the boundedness. Let us say that in the expression(inside the root):

$$0 < A \le \text{Numerator} \le B < \infty \tag{12.36}$$

and

$$0 < A \le \text{Denominator} \le B < \infty \tag{12.37}$$

Therefore, we can say that the fraction is also between two positive bounds as:

$$0 < \frac{A}{B} \le \frac{\text{Numerator}}{\text{Denominator}} \le \frac{B}{A} < \infty \tag{12.38}$$

So, let us write Equation 12.33 as:

$$\frac{\hat{\tilde{\phi}}_1(\Omega)}{\hat{\tilde{\phi}}_1\left(\frac{\Omega}{2}\right)} = \frac{\hat{\phi}_1(\Omega)}{\hat{\phi}_1\left(\frac{\Omega}{2}\right)}(Q) \tag{12.39}$$

where Q already obeys periodicity and boundedness as required.

Now, we know that the ratio $\dfrac{\hat{\tilde{\phi}}_1(\Omega)}{\hat{\tilde{\phi}}_1\left(\frac{\Omega}{2}\right)}$ obeys the requirement.

Hence $\tilde{\phi}_1(\cdot)$ must obey a dyadic dilation equation:

$$\tilde{\phi}_1(t) = \sum_{k=-\infty}^{\infty} \tilde{h}[k] \quad \tilde{\phi}_1(2t-k) \tag{12.40}$$

$$\tilde{h}[k] \xrightarrow{DTFT} \tilde{H}(\Omega) \tag{12.41}$$

i.e.,

$$\tilde{H}[\Omega] = \sum_{k=-\infty}^{\infty} h[k]e^{-jk\Omega} \tag{12.42}$$

Therefore,

$$\frac{1}{2}\tilde{H}\left(\frac{\Omega}{2}\right) = \frac{\hat{\tilde{\phi}}_1(\Omega)}{\hat{\tilde{\phi}}_1\left(\frac{\Omega}{2}\right)} = \frac{\tilde{\phi}_1(\Omega)}{\tilde{\phi}_1\left(\frac{\Omega}{2}\right)}Q = \frac{1}{2}C_o\left(1+2e^{-j\frac{\Omega}{2}}+e^{-j2\frac{\Omega}{2}}\right)\left[\frac{\frac{2}{3}\left(1+\frac{1}{2}\cos\frac{\Omega}{2}\right)}{\frac{2}{3}\left(1+\frac{1}{2}\cos\Omega\right)}\right]^{1/2} \tag{12.43}$$

12.6 | Summary

We have now established the existence as well as the method to calculate $\tilde{H}[k]$, though the calculation is highly cumbersome. If we have $\tilde{H}[k]$, we have the impulse response of the low-pass filter in orthogonal MRA. Once we have the dyadic dilation equation, the coefficients of the equation give the low-pass filter response. Once we have the analysis low-pass filter, we can construct all the other filters.

We can observe that IDTFT of $\tilde{H}[k]$ will be of ∞ length, will be infinitely noncasual and also irrational. This makes this a nonrealizable filter. So in general, we can say that to get an orthogonal piece-wise linear MRA, one requires an unrealizable filter.

Once we know impulse response of the low-pass filter of analysis side, we also know how to construct the wavelet because analysis high-pass filter impulse response coefficients will construct the wavelet from the scaling function.

Exercises

Exercise 12.1

Prove that Fourier transform of autocorrelation of a real function $\phi(t)$ is the power spectral density function of $\phi(t)$ in frequency domain.

Hint: We have, by definition,

$$R_{\phi\phi}(\tau) = \int_{-\infty}^{\infty} \phi(t)\phi(t+\tau)dt, \text{ Now substituting } t+\tau = k, \text{ we get}$$

$$R_{\phi\phi}(\tau) = \int_{-\infty}^{\infty} \phi(k)\phi(k-\tau)dk$$

$$= \int_{-\infty}^{\infty} \phi(k)\phi(-(\tau-k))dk$$

By observing the above equation, we can see that $R_{\phi\phi}(\tau)$ is the convolution of $\phi(t)$ with $\phi(-t)$. We know that convolution in time domain is multiplication in frequency domain. Let the Fourier transform of $\phi(t)$ be $\hat{\phi}(\Omega)$, then the Fourier transform of $\phi(-t)$ is $\hat{\phi}(-\Omega)$. Therefore, Fourier transform of $R_{\phi\phi}(\tau)$ is,

$$\hat{R}_{\phi\phi}(\Omega) = \hat{\phi}(\Omega)\hat{\phi}(-\Omega)$$

$$= |\hat{\phi}(\Omega)|^2$$

$|\hat{\phi}(\Omega)|^2$ is essentially the power spectral density function of $\phi(t)$ in frequency domain. Hence proved.

Exercise 12.2

Prove that autocorrelation of any function $\phi(t)$ is symmetric and has a maximum value at $t = 0$.

Hint: In Question 1, we have made an important observation that autocorrelation of a function $\phi(t)$ is convolution of $\phi(t)$ with $\phi(-t)$, i.e.

$$R_{\phi\phi}(\tau) = \phi(\tau)\times\phi(-\tau), \text{which implies}$$

$$R_{\phi\phi}(-\tau) = \phi(-\tau)\times\phi(\tau)$$

We know that convolution follows commutative property. Therefore, the above two equations have the same values. Therefore,

$$R_{\phi\phi}(\tau) = R_{\phi\phi}(-\tau)$$

Hence, symmetry is proved. Now, $R_{\phi\phi}(0)$ is the area under the curve $|\hat{\phi}(\Omega)|^2$ which is always positive. Therefore, $R_{\phi\phi}(0) \geq 0$ for any function ϕ. Now, consider a new function $\phi_1(t)$ where,

$$\phi_1(t) = \phi(t) - \phi(t+\tau)$$

Now $R_{\phi_1\phi_1}(0) \geq 0$

$$\Rightarrow R_{\phi_1\phi_1}(0) = \int_{-\infty}^{\infty} \phi_1(t)\phi_1(t)dt \geq 0$$
$$\Rightarrow \int_{-\infty}^{\infty} (\phi(t) - \phi(t+\tau))(\phi(t) - \phi(t+\tau))dt \geq 0$$
$$\Rightarrow \int_{-\infty}^{\infty} \phi(t)^2\,dt + \int_{-\infty}^{\infty} \phi(t+\tau)^2\,dt - 2\int_{-\infty}^{\infty} \phi(t)\phi(t+\tau)dt \geq 0$$
$$\Rightarrow R_{\phi\phi}(0) + R_{\phi\phi}(0) - 2R_{\phi\phi}(\tau) \geq 0$$
$$\Rightarrow R_{\phi\phi}(0) \geq R_{\phi\phi}(\tau)$$

Hence proved.

Exercise 12.3

Prove that if $\mathrm{STS}(\phi, 2\pi)(\Omega)$ is constant, then $\phi(t)$ is orthogonal to its integer translates.

Hint: Given $\mathrm{STS}(\phi, 2\pi)(\Omega)$ is constant

$$\Rightarrow \sum_{k=-\infty}^{\infty} |\hat{\phi}(\Omega + 2\pi\,k)|^2 = K, \text{where } K \text{ is a constant}$$

Now, Fourier transform of $R_{\phi\phi}(\tau)|_{\tau=m}\ m \in \mathbb{Z}$ is the Fourier transfom of $R_{\phi\phi}(\tau)$ shifted by multiples of 2π and added, i.e.,

$$\sum_{k=-\infty}^{\infty} |\hat{\phi}(\Omega + 2\pi\,k)|^2$$

But it is given as a constant. Therefore, Fourier transform of $R_{\phi\phi}(\tau)|_{\tau=m}\ m \in \mathbb{Z}$ is a constant which implies $R_{\phi\phi}(\tau)|_{\tau=m}\ m \in \mathbb{Z}$ is a discrete impulse sequence, which indeed implies $\phi(t)$ is orthogonal to its integer translates.

Exercise 12.4

We have $\tilde{\phi}_1(t) = \sum_{k=-\infty}^{\infty} \tilde{C}_k \phi_1(t+k)$, then write down the series for $\tilde{C}_0$.

Hint: We have from equation (12.12),

$$\hat{\tilde{\phi}}_1(\Omega) = \hat{\phi}_1(\Omega)\left(\frac{2}{3}\right)^{-\frac{1}{2}}\left(1+\frac{1}{2}\cos(\Omega)\right)^{-\frac{1}{2}}$$

Consider the term $\left(1+\frac{1}{2}\cos(\Omega)\right)^{-\frac{1}{2}}$ in the above equation

$$\left(1+\frac{1}{2}\cos(\Omega)\right)^{-\frac{1}{2}} = 1-\frac{1}{2}\cos(\Omega)+\frac{1.3}{2.2.2!}\left(\frac{\cos(\Omega)}{2}\right)^2+\dots$$

Using the expansion $\cos(\Omega)^p = \left(\frac{e^{j\Omega}+e^{-j\Omega}}{2}\right)^p$, and substituting in the above equation we get the constant term only from the even powers of p, i.e.

$$\tilde{C}_0 = \left(\frac{2}{3}\right)^{-\frac{1}{2}}\left(1+\frac{1.3}{2.2.2!.2^2}.\left(\frac{2}{1}\right)+\frac{1.3.5.7}{2^4.4!.2^4}.\left(\frac{4}{2}\right)+\dots\right)$$

$$= \left(\frac{2}{3}\right)^{-\frac{1}{2}}\left(1+\frac{1.3}{2^4}+\frac{1.3.5.7}{2^8.(2!)^2}+\frac{1.3.5.7.9.11}{2^{12}.(3!)^2}+\dots+\frac{1.3..(2n+1)}{2^{4n}.(n!)^2}\right)$$

R (NOTE: In a similar way, series for $\tilde{C}_1$ can be found. It is left as an exercise to the readers).

Exercise 12.5

$f(t) = \sum_k a_k \quad \phi_1(t-k)$. Given $a_k = \{1,2,0,1,2\}$, find $f(t)$ for ϕ_0 and ϕ_1. Plot $f(t)$

Hint:

1. For ϕ_0

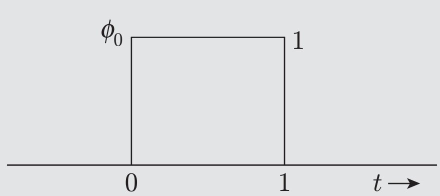

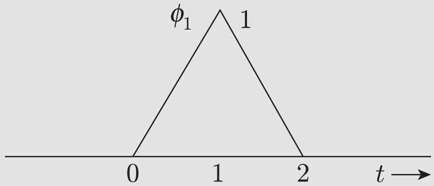

2. For ϕ_1

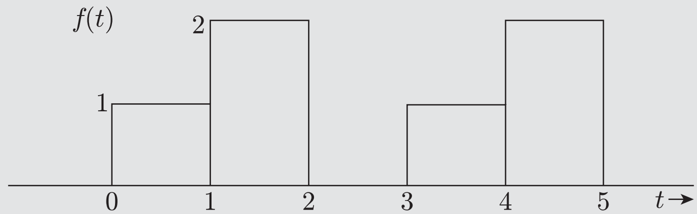

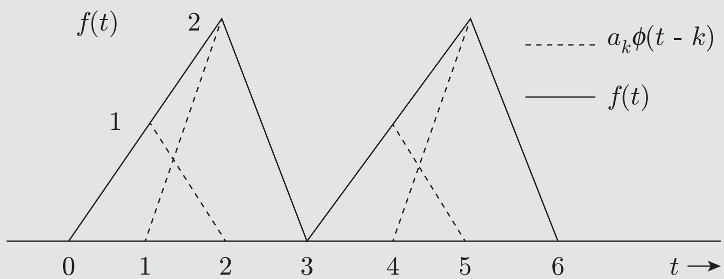

Exercise 12.6

Two function $x(t)$, $y(t)$ are periodic with period t_1 and t_2 respectively. t_1 and t_2 are rational nonzero numbers. Prove that x/y is also periodic and find its period.

Hint: We know that, $x(t+t_1) = x(t)$ and $y(t+t_2) = y(t)$. Let

$$g(t) = \frac{x(t)}{y(t)} \tag{12.44}$$

Assume the $g(t)$ to be periodic with period t_3, therefore,

$$g(t+t_3) = \frac{x(t+t_3)}{y(t+t_3)} = g(t) \tag{12.45}$$

Now, if t_3 is equal to LCM of t_1 and t_2 and both $x(t+t_3)$ and $y(t+t_3)$ equal to $x(t)$ and $y(t)$ respectively, hence $g(t)$ will be periodic with period t_3 where t_3 is LCM of t_1 and t_2.

Chapter 13

MRA Variant 3: Wave Packets

13.1 | Introduction

In the earlier chapters, we discussed the variants of the wavelet transform or of time-frequency analysis. We have so far discussed the short time Fourier transform (STFT) and continuous wavelet transform (CWT). We have also seen the discretization of CWT in scale and then in translation. We have studied the specific case of dyadic discretization ($a_0 = 2$) of scale and a corresponding uniform discretization of the translation parameter. Following that, we have brought in the possibility of bi-orthogonal multiresolution analysis (bi-orthogonal MRA) and we took inspiration for biorthogonal MRA by considering the need to construct **'splines'** (piece-wise polynomial functions). Essentially, we looked at the possibility of piece-wise polynomial interpolation. When we moved from piece-wise constant, which gave us the Haar Multiresolution Analysis, to piecewise linear, we came across two options; either we use the same analysis and synthesis filters (i.e. same scaling and wavelet functions at analysis and synthesis side) or we make synthesis side different from the analysis side.

In Chapters 10 and 11, we realized that insisting on constructing in orthogonal MRA with piece-wise linear scaling functions and wavelets, puts a very difficult task before us. Indeed, it is achievable but it is extremely cumbersome to construct those scaling functions and wavelets. Moreover, these being of infinite length, there are chances of losing the compact support. If we wish to stick to compactly supported scaling functions and wavelets or rather we wish to stick correspondingly to the finite impulse response filters on the analysis and synthesis side, then we need to bring in a variant of the multiresolution analysis called **'Bi-orthogonal MRA'**. We have so far introduced the bi-orthogonal MRA only from the perspective of the filter bank and we intend to maintain the stand for the time being. Later, we shall look at its implication in continuous time or in iteration. In this lecture,we wish to look at one more variant of multiresolution analysis, but this time it is variant on the iteration of the filter bank, this is called a 'Wave packet transform' and, therefore, this chapter is appropriately titled, **'The Wave Packet Transform'**.

13.2 | The Wave Packet Transform

The idea behind the Wave Packet transform is very simple. Till now, when constructing the dyadic discrete wavelet transform (DWT), the focus has been an decomposing the so-called approximation subspace. Let us put this notion graphically called ladder of subspaces about which we are speaking very often as shown in Fig. 13.1, every time we have pilled off an incremental subspace.

In the wave packet transform our objective is to get around this limitation, by decomposing the incremental subspace (i.e. detail subspace) as we do the approximation subspace. For example, we decompose V_1 into V_0 and W_0, we also intend to decompose W_0 in the next step.

R In one sentence the idea behind the Wave Packet transform is:

Idea:
Decompose the incremental or detail subspace also.

Towards this objective, the simplest approach would be to look at the filter bank structure, instead of starting from the basis or the continuous time functions.

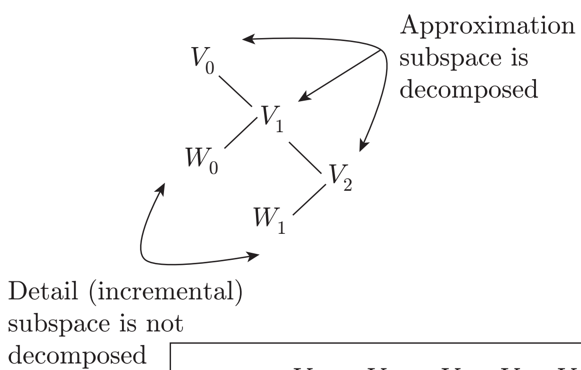

$$.....V_{-2} \subset V_{-1} \subset V_0 \subset V_1 \subset V_2.....$$

Ladder of subspaces

Figure 13.1 | *Notion of decomposition of subspaces in DWT*

Let us assume that you have a sequence representing the function in an approximation subspace. For simplicity, let us take the subspace V_2, i.e. it is a sequence of coefficients in the expansion of given function in $L_2(R)$ in terms of basis of V_2. The filter bank operates on these coefficients and creates coefficients of expansion in V_1 and W_1 using the low-pass and high-pass analysis filters. The filter bank is iterated on the low-pass branch and suppose we also choose to iterate the filter bank on the high-pass branch. Essentially, what is acquired is so-called Wave packet transform.

Let us first investigate from the ideal i.e. ideal frequency behaviour of the filter bank. In the DWT, as shown in Fig. 13.2, consider a sequence of coefficients, which is subjected to analysis low-pass and high-pass filters (ideal with cutoff $\frac{\pi}{2}$) and followed by a downsampling operation. At point 'A', we get coefficients in the lower approximation subspace and at point 'B' in the detail subspace.

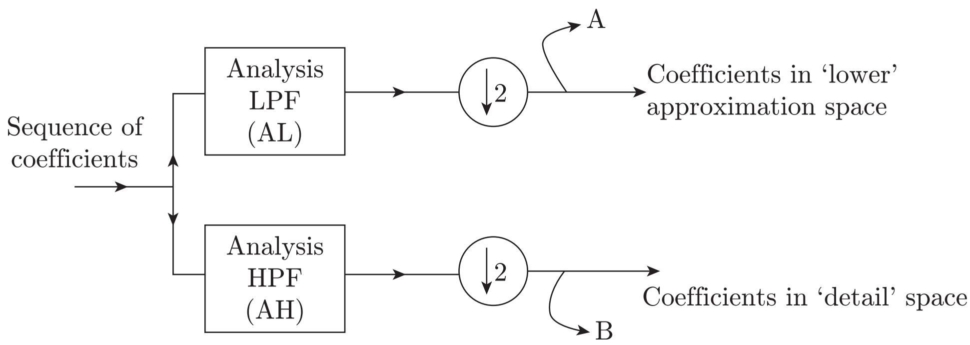

Figure 13.2 | *One-level of DWT*

Now, the next time we will take the entire structure of Fig. 13.2 and will put at point 'A' to get two-level DWT as shown in Fig. 13.3. This gives us the two-level DWT, note that here the high-pass branch is not iterated.

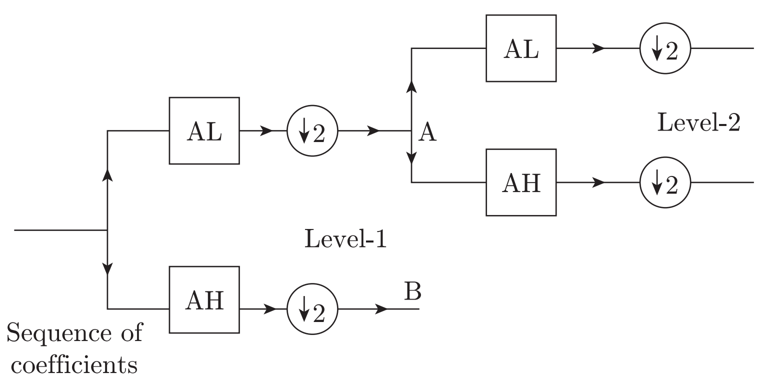

Figure 13.3 | *Two-level of DWT*

What we will get is Wavepacket transform if high-pass branch is also iterated as shown in Fig. 13.4. Now, whatever we will get will be additional which we want to investigate. Consider that all the filters are ideal. Let '**IAL**' and '**IAH**' be ideal analysis low-pass and ideal analysis high pass filters with cutoff

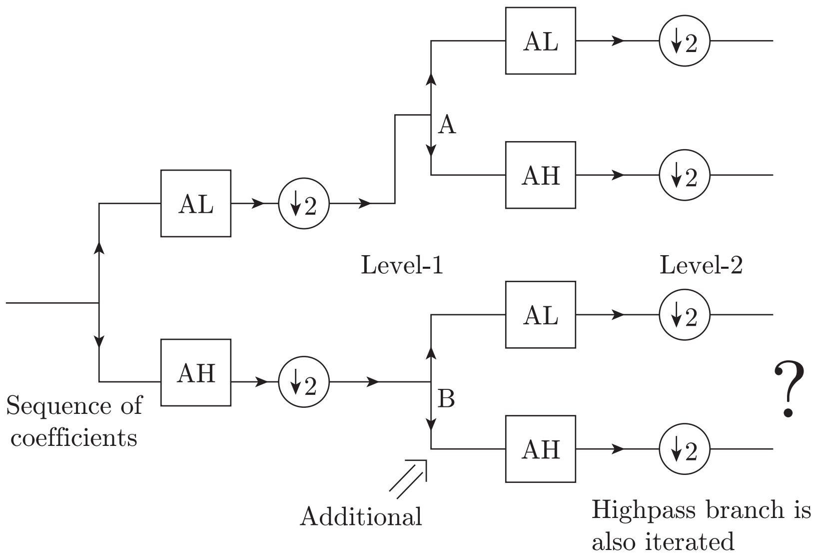

Figure 13.4 | *Wave packet transform*

$\pi / 2$ respectively. Let us analyze the above filter bank structure with ideal prototype spectrum X_0 where we can see clearly the spectrum at every point (Fig. 13.5). The Spectra at points X_{11} and X_{21} are as shown in Fig. 13.6. Note that the Spectra X_{11} and X_{21} are periodic with period 2π.

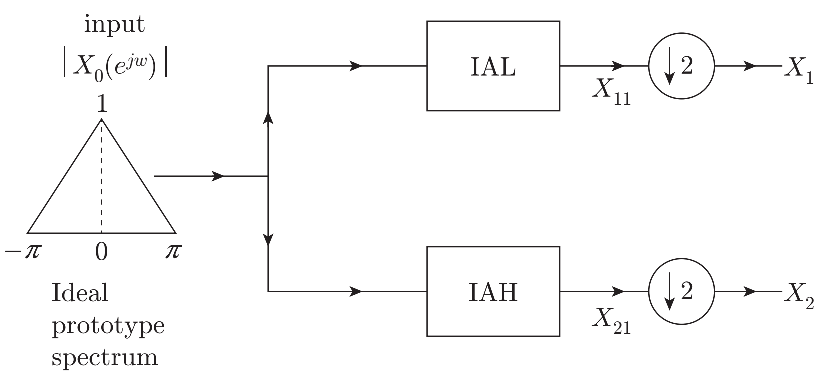

Figure 13.5 | *Ideal filter bank with prototype i/p spectrum*

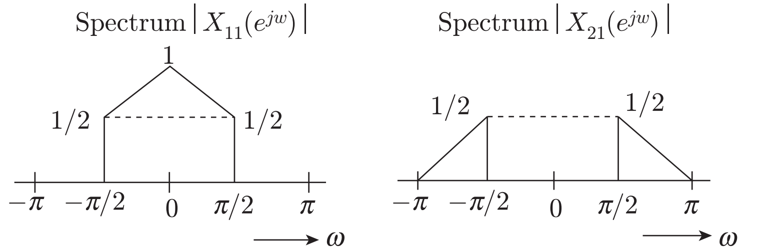

Figure 13.6 | *Spectrum at X_{11} and X_{21}*

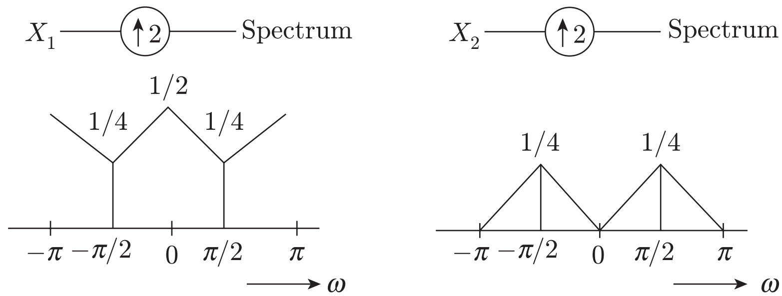

Figure 13.7 | *Upsampled spectra of X_1 and X_2*

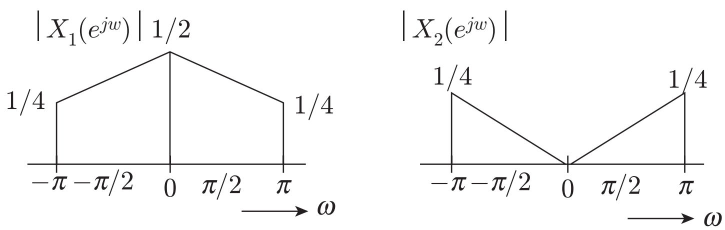

Figure 13.8 | *Spectra at X_1 and X_2*

Now, it is important to emphasize at this stage that we need to establish a correspondence between the segments of original spectrum X_0 and the spectra X_1 and X_2. Let us divide the spectrum X_0 into four segments as

$$\alpha = (\pi / 2 \Rightarrow \pi)$$
$$\beta = (0 \Rightarrow \pi / 2)$$
$$\beta'' = (-\pi / 2 \Rightarrow 0)$$
$$\alpha'' = (-\pi \Rightarrow -\pi / 2)$$

The segments are marked as shown in Fig. 13.9 and corresponding segments are marked in X_1 and X_2 as shown in Fig. 13.10.

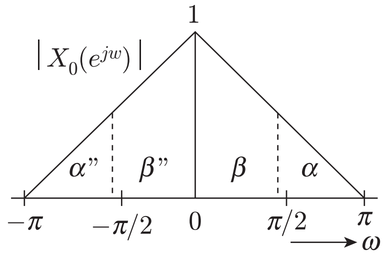

Figure 13.9 | *Segments of spectrum X_0*

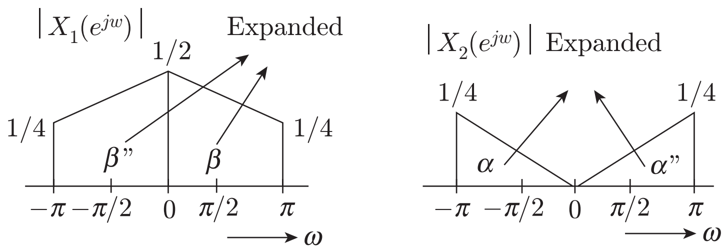

Figure 13.10 | *Segments of spectra X_1 and X_2*

13.3 | Notion of Frequency Inversion in Highpass Filtering

Frequency inversion means the reversal of order of frequencies. We notice that high-pass segments $\alpha,\ \alpha''$ has gone to high-pass branch, but there is a frequency inversion. In original input spectrum X_0 as we move from $\pi / 2$ to π, correspondingly in X_2 it is from π to 0; While in original input spectrum X_0 as we move from 0 to $\pi / 2$, correspondingly in X_1 we are moving from 0 to π. The decomposition of input spectrum at each stage is shown Figs. 13.11 to 13.13. Figure 13.14 shows the summary of band distribution.

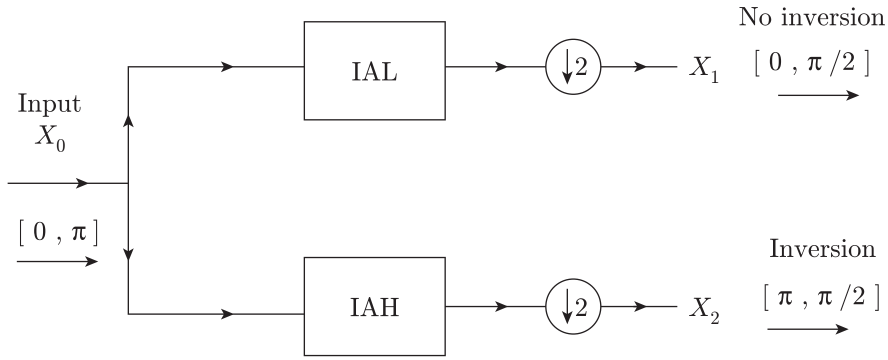

Figure 13.11 | *Decomposition of* X_0

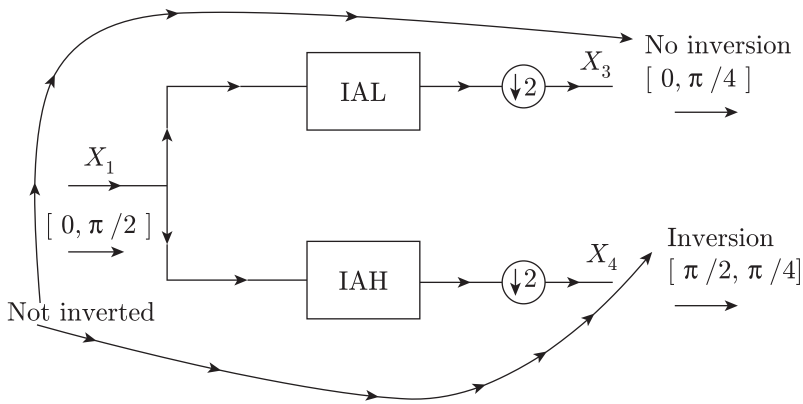

Figure 13.12 | *Decomposition of* X_1

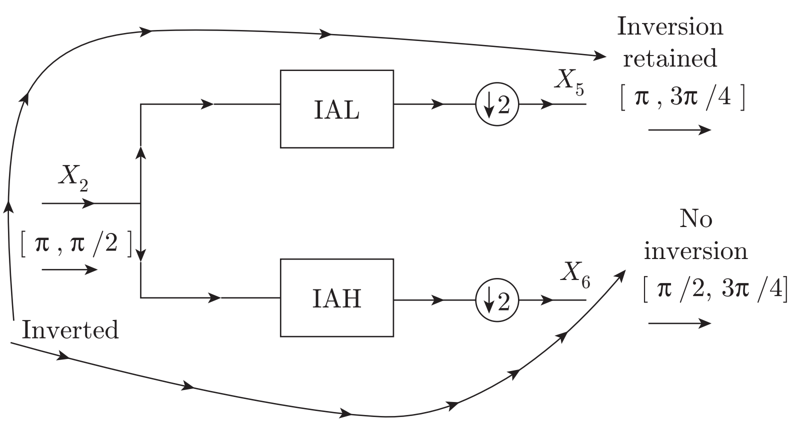

Figure 13.13 | *Decomposition of* X_2

X_3 : $[0, \pi/4]$ $\Rightarrow$ Not inverted

X_4 : $[\pi/2, \pi/4]$ $\Rightarrow$ Inverted

X_5 : $[\pi, 3\pi/4]$ $\Rightarrow$ Inverted

X_6 : $[\pi/2, 3\pi/4]$ $\Rightarrow$ Not inverted

Figure 13.14 | *Band distribution of spectra X_3 to X_6*

13.4 | Reconstruction of Input x_0 from Wave Packet Transform

In reconstruction we can use the same ideal filters (i.e. not separate synthesis filters) as synthesis filters along with upsampling operations. Even if it is not ideal and if we have a perfect reconstruction synthesis filters then also reconstruction is possible. The reconstruction steps are as shown in Figs. 13.15, 13.16 and 13.17.

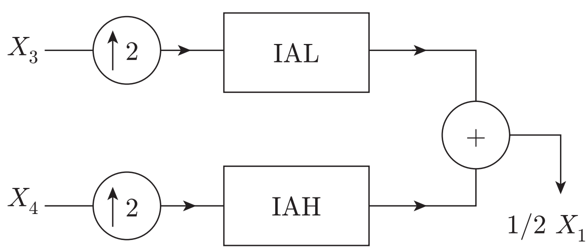

Figure 13.15 | *Reconstruction of X_1*

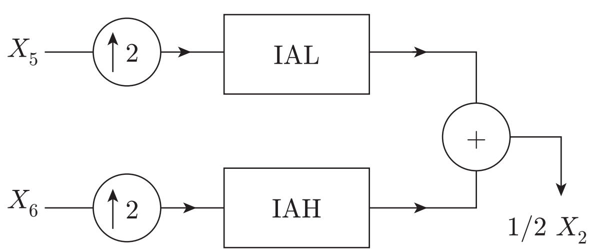

Figure 13.16 | *Reconstruction of X_2*

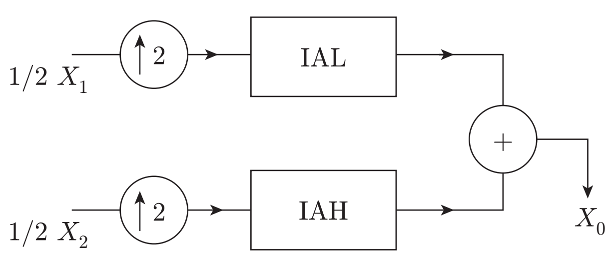

Figure 13.17 | *Reconstruction of X_0*

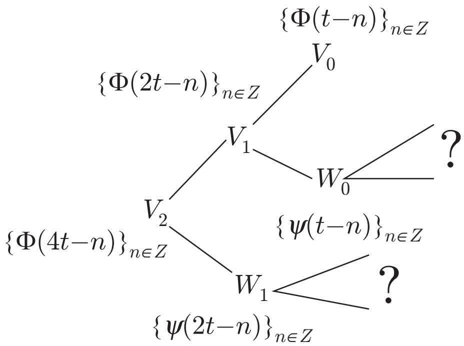

Figure 13.18 | *Basis functions for decomposed subspaces*

Now, let us see carefully what happens if we apply this structure to Haar MRA. We will consider the Fig. 13.18 to explain this, which shows the basis functions for respective subspaces. If we decompose W_0 and W_1 as in wave packet transform marked by question mark in Fig. 13.18, following are the few questions that need to be answered:

1. What are the basis functions for W_0 and W_1?
2. Can those basis functions, obtained from a single function, be called as generating function?
3. Can we generalize this if we decompose the incremental subspaces?

We shall answer them later.

13.5 | Noble Identities

In the preceding sections, we have introduced the idea of wavepacket transform. In wavepacket transform, along with low-pass branch of filter bank, high-pass branch is also further decomposed. This decomposition of high-pass branch has some counter intuitive observations in frequency domain. Being observed Wavepacket transform in ideal filter bank, in this section we will see Haar Wavepacket transform. Along with this, a concept of Noble Identities is also discussed in great detail.

Noble Identities occur frequently when we want to iterate the filter bank in which case we are often required to combine down- and up-samplers and different filters. Noble Identities are useful in dealing with cascade of sampling rate changes and cascade of filters.

Example 13.5.1 — Noble identity for downampler.

Consider a down-sampler by 2 followed by a filter, as shown in Fig. 13.19.

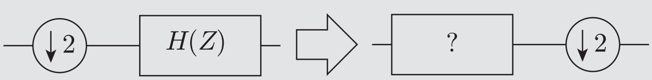

Figure 13.19 | *Interchanging the positions of down-sampler and filter to get noble identity*

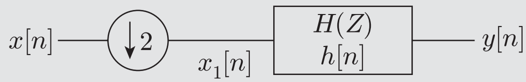

Figure 13.20 | *Output sequence as convolution of input sequence and impulse response*

Noble identity illustrates how to interchange the positions of down-sampler and filter. When the positions of filter and down-sampler are interchanged, what will be the nature of new filter? In order to get the answer, consider Fig. 13.20, in which output $y[n]$ is convolution of impulse response $h[n]$ of filter and sequence $x_1[n]$. Sequence $x_1[n]$ is related to input sequence $x[n]$ as $x_1[n] = x[2n]$ for $\forall n \in \mathbb{Z}$.

We can write,

$$y[n] = x_1[n] \times h[n]$$

$$= \sum_{k=-\infty}^{\infty} x_1[k]h[n-k] \tag{13.1}$$

$$= \sum_{l=-\infty}^{\infty} h[l]x_1[n-l] \tag{13.2}$$

Equation (13.1) can be rewritten as

$$y[n] = \sum_{k=-\infty}^{\infty} x[2k]h[n-k] \tag{13.3}$$

Here, we are trying to get an equivalent system in which, a filter is followed by a down-sampler and which will give the expression given by Eq. (13.3). Also, we can write Eq. (13.2) as

$$y[n] = \sum_{l=-\infty}^{\infty} h[l]x[2n-2l] \tag{13.4}$$

In Eq. (13.4), the index '$2n$' is due to downsampling operation. If '$2n$' is replaced by 'n', we arrive at a point after a filter in an equivalent system. So, we have expression

$$\sum_{l=-\infty}^{\infty} h[l]x[n-2l] \tag{13.5}$$

which is a convolution in which $h[l]$ is located at '$2l'^{th}$ points and at other places it is zero.

$$h_1[n] = 0 \quad n \text{ is odd}$$

$$= h[\frac{n}{2}] \quad \text{Otherwise}$$

Hence,

$$y[n] = \sum_{l=-\infty}^{\infty} h_1[l]x[2n-l] \tag{13.6}$$

This indicates that impulse response of an equivalent filter before downsampler is the impulse response of original filter but upsampled by two. This is shown in Fig. 13.21.

This is called as a Noble identity for down-sampler.

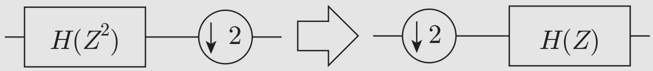

Figure 13.21 | *Noble identity for down-sampler by 2*

This equivalent structure, however, has disadvantage over the previous structure in terms of number of computations. In the new structure, the samples obtained after convolution are discarded by down-sampler which results in wastage of computations carried out during convolution process. However, in original structure, as down-sampling is done first, there is no question of wastage in number of computations in convolution.

Example 13.5.2 — Noble identity for upsampler.

The Noble Identity for Upsampler can be derived through the concept of 'transposition'. In case of signal flow graph (with no up- and down-sampler), its transpose is obtained by reversing the direction of each arrow and keeping constant multiplier the same. The summing point and branching points in previous graph become branching points and summing points respectively. The similar operation can be done if signal flow graph contains up and down-sampler with only change, that down-sampler in original graph becomes up-sampler in transposed graph with same factor and vice versa.

So applying the rules of transposition to Noble identity of down-sampler, we get Noble identity for up-sampler as shown in Fig. 13.22.

According to noble identity of upsampler the operation of filtering followed by upsampling is same as the operation of upsampling followed by filtering (with impulse response of this filter being upsampled version of impulse response of original filter).

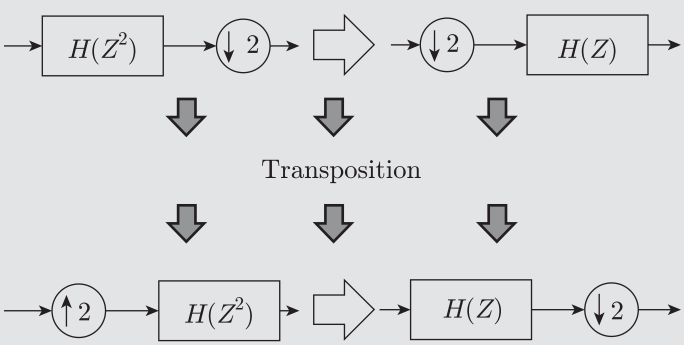

Figure 13.22 | *Noble identity for upsampler*

13.6 | Haar Wavepacket Transform

With the introduction of Noble identities, we will employ them in the Haar Wavepacket transform. Figure 13.23 shows filter bank corresponding to Haar Wavepacket transform. Now, considering one branch at a time, e.g. upper branch and applying Noble Identity we get an equivalent branch as shown in Fig. 13.24. In Fig. 13.24, we note that downsampler by 4 is the result of two cascaded downsamplers by two.

So, there are four filters highlighted in the process of Wavepacket transform. Figure 13.25 shows that during the process subspace V_2 is decomposed into subspaces V_1 and W_1; V_1 is decomposed into V_0 and W_0; and the important feature is that W_1 is also further decomposed into subspaces say W_{10} and W_{11}.

Let us look at the filter on the upper branch. Use of Noble Identity results in a filter as

$$(1+z^{-1})(1+z^{-2}) = 1+z^{-1}+z^{-2}+z^{-3}$$

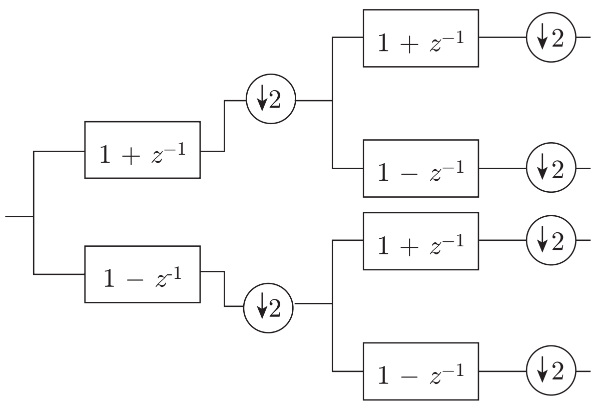

Figure 13.23 | *Filter bank employing Haar wavepacket transform*

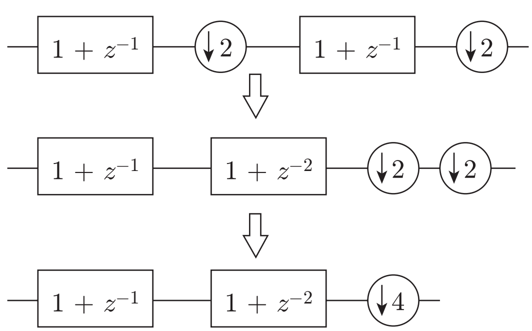

Figure 13.24 | *Application of noble identity for downsampler on the branch of Haar filter bank*

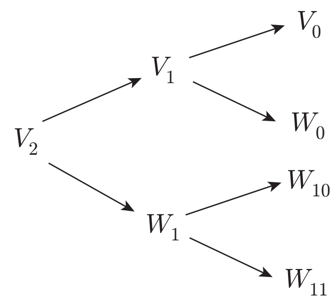

Figure 13.25 | *Decomposition of subspaces in wavepacket transform*

The sequence corresponding to above expression, i.e. [1,1,1,1] tells us how to express the basis of V_0 in terms of bases of V_2. In other words, $\phi(t)$ (basis of V_0) can be expressed as linear combination of $\phi(4t)$ (basis of V_2). Note that, down-sampling by 4 results in dilation of $\phi(t)$ by factor of 4, which effectively results in going from V_0 to V_2. So, we can write this as,

$$\phi(t) = \phi(4t) + \phi(4t-1) + \phi(4t-2) + \phi(4t-3)$$

Similarly, we can write expressions for other filters such that corresponding sequences represent bases of W_0,W_{10} and W_{11} in terms of bases of V_2.

13.7 | Wavelet Packets: Framework

In this section, we present framework of wavelet packets to understand how the analysis and synthesis is done systematically using packet technique. For this we shall use Wavelet Haar packets on following signal $x[n]$ to perform following operations:

(1) Decomposition or Analysis
(2) Reconstruction or Synthesis

$$x[n] \in V_3 = \{1,2,3,4,5,6,7,8\} \tag{13.7}$$

The Wavelet packet transformation can be captured in mathematical formulas as follows:

$$W^{[2n]}(t) = \sqrt{2}\sum_k h[k]\cdot W^{[n]}(2t-k) \tag{13.8}$$

$$W^{[2n+1]}(t) = \sqrt{2}\sum_k g[k]\cdot W^{[n]}(2t-k) \tag{13.9}$$

These equations are governed by the typical dilation principles that we have demonstrated at various places in this book.

Here the normalized low ($h[k]$) and high ($g[k]$) pass filters used are,

$$h[k] = \left\{\frac{1}{\sqrt{2}}, \frac{1}{\sqrt{2}}\right\} \tag{13.10}$$

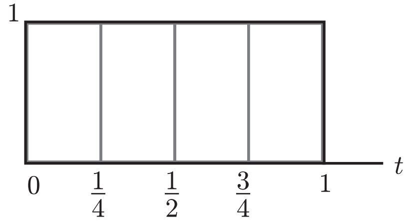

$$V_2 \to V_1 \to V_0$$
$$(1+z^{-1})(1+z^{-2}) = 1+z^{-1}+z^{-2}+z^{-3}$$
$$\textit{The sequence} = [1,1,1,1]$$
$$\uparrow$$
$$\text{Basis for } V_0 = \phi(4t) + \phi(4t-1) + \phi(4t-2) + \phi(4t-3)$$

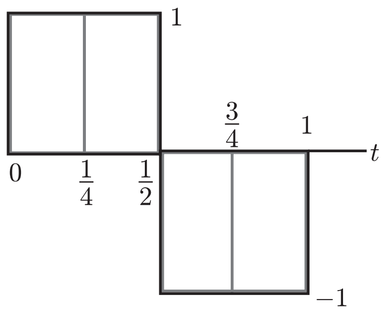

$$V_2 \to V_1 \to W_0$$
$$(1+z^{-1})(1+z^{-2}) = 1+z^{-1}-z^{-2}-z^{-3}$$
$$\textit{The sequence} = [1,1,-1,-1]$$
$$\uparrow$$
$$\text{Basis for } W_0 = \phi(4t) + \phi(4t-1) + \phi(4t-2) + \phi(4t-3)$$
(i.e Haar Wavelet)

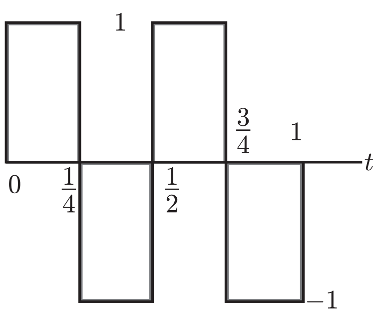

$$V_2 \to W_1 \to W_{10}$$
$$(1-z^{-1})(1+z^{-2}) = 1-z^{-1}+z^{-2}-z^{-3}$$
$$\textit{The sequence} = [1,-1,1,-1]$$
$$\uparrow$$
$$\text{Basis for } W_{10} = \phi(4t) - \phi(4t-1) + \phi(4t-2) + \phi(4t-3)$$

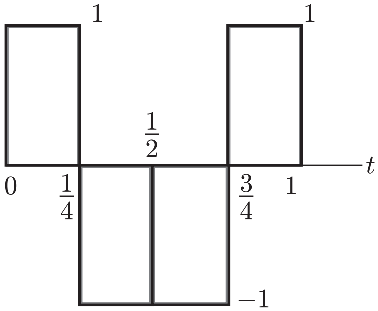

$$V_2 \to W_1 \to W_{11}$$
$$(1-z^{-1})(1-z^{-2}) = 1-z^{-1}-z^{-2}+z^{-3}$$
$$\textit{The sequence} = [1,-1,-1,1]$$
$$\uparrow$$
$$\text{Basis for } W_{11} = \phi(4t) - \phi(4t-1) - \phi(4t-2) + \phi(4t-3)$$

Figure 13.26 | *Bases for V_0, W_0, W_{10} and W_{11}. Basis for V_2 and its translations are shown in grey*

$$g[k]=\left\{\frac{1}{\sqrt{2}},\frac{-1}{\sqrt{2}}\right\} \tag{13.11}$$

Now, for Haar Wavelet

$$W^{[0]}(t)=\phi(t) \tag{13.12}$$

$$W^{[1]}(t)=\psi(t) \tag{13.13}$$

From the earlier framework of MRA we recall,

$$f_j(x)\in V_j \tag{13.14}$$

$$f_j(x)=\sum_k \alpha_{j,k}\cdot 2^{\frac{j}{2}}\,\phi(2^j x-k) \tag{13.15}$$

However, in wavelet packets we go beyond the realms of simple MRA style wavelet analysis. We note that every time we go pass a sub-space a normalizing factor of $\sqrt{2}$ gets added up. Thus, during transition from V_3 to V_0 a total factor of $\sqrt{2}\times\sqrt{2}\times\sqrt{2}=2\sqrt{2}$ gets added up. This is captured in equations below,

As $x[n]\in V_3\, j=3$

$$x[n]=\sum_k \alpha_{3,k}\cdot 2^{\frac{3}{2}}\,\phi(2^3 x-k)=2\sqrt{2}\sum_k \alpha_{3,k}\,\phi(8x-k) \tag{13.16}$$

therefore

$$\begin{aligned}x[n]=\{&2\sqrt{2}\,\phi(8t)+4\sqrt{2}\phi(8t-1)+6\sqrt{2}\phi(8t-2)+8\sqrt{2}\phi(8t-3)\\&+12\sqrt{2}\phi(8t-5)+14\sqrt{2}\phi(8t-6)+16\sqrt{2}\phi(8t-7)\}\end{aligned} \tag{13.17}$$

Now, we shall evolve the basis to create bases in order to move across the sub-spaces. Readers should remember that these bases are essential as we shall split on the

for $n=1$

$$W^{[2]}(t)=W^{[1]}(2t)+W^{[1]}(2t-1) \tag{13.18}$$

$$W^{[3]}(t)=W^{[1]}(2t)-W^{[1]}(2t-1) \tag{13.19}$$

for $n=2$

$$W^{[4]}(t)=W^{[2]}(2t)+W^{[2]}(2t-1) \tag{13.20}$$

$$W^{[5]}(t)=W^{[2]}(2t)-W^{[2]}(2t-1) \tag{13.21}$$

for $n=3$

$$W^{[6]}(t)=W^{[3]}(2t)+W^{[3]}(2t-1) \tag{13.22}$$

$$W^{[7]}(t)=W^{[3]}(2t)-W^{[3]}(2t-1) \tag{13.23}$$

Using Eqs. (13.18) to (13.23) we will get values of *W* as follows (Graphically):

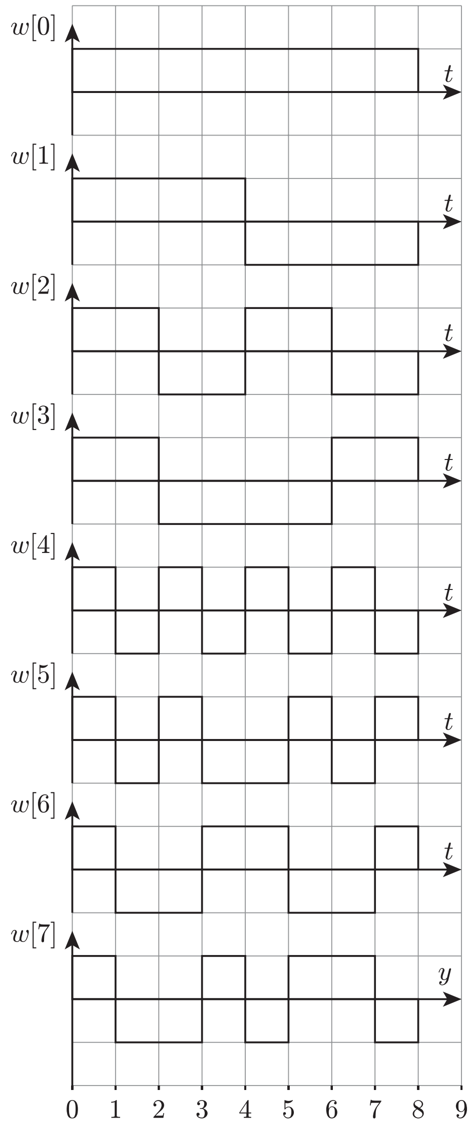

Now, Let us decompose the given signal.

1. **Decompositition**

Decomposition is shown in Fig. 13.27.

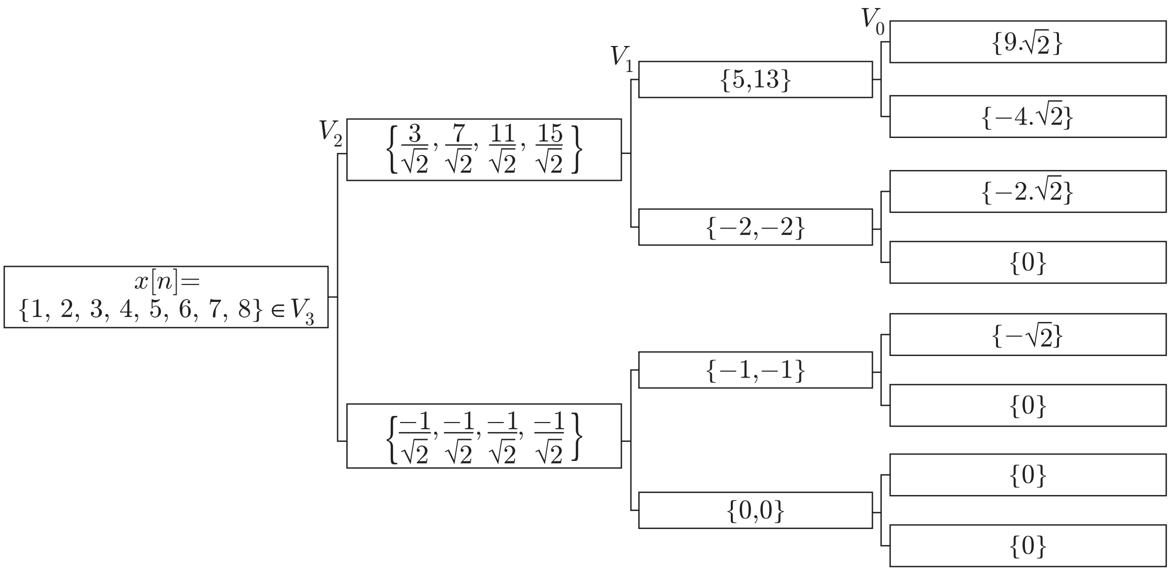

Figure 13.27 | *Decomposition of $x[n] \in V_3$ using wavelet packets*

We have decomposed the signal till we get single value (here $\in V_0$).

2. **Reconstruction**

Using decomposed coefficients,We have to reconstruct original signal. We have the decomposed signal single leaf values $\in V_0$ and we also evolved bases; using a combination of these two, Let us reconstruct the original signal back now.

We begin with the reconstruction of the very first coefficient. Since the signal $x[n] \in V_3$ the first coefficient lasts from 0 to $\frac{1}{8}$. We shall consider only this first interval:

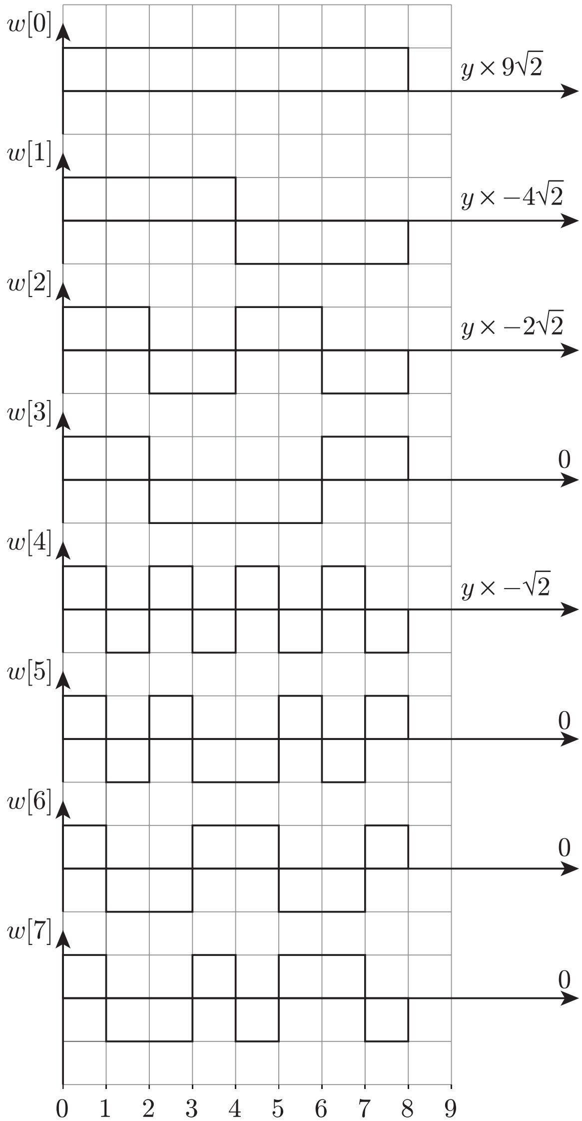

$$\therefore 9\sqrt{2}\times 1 - 4\sqrt{2}\times 1 - 2\sqrt{2}\times 1 + 0\times 1 - \sqrt{2}\times 1 + 0\times 1 + 0\times 1 + 0\times 1 = 2\cdot\sqrt{2}$$
$$= \alpha_{3,0}$$

Similarly, for the second coefficient let us consider the second interval:

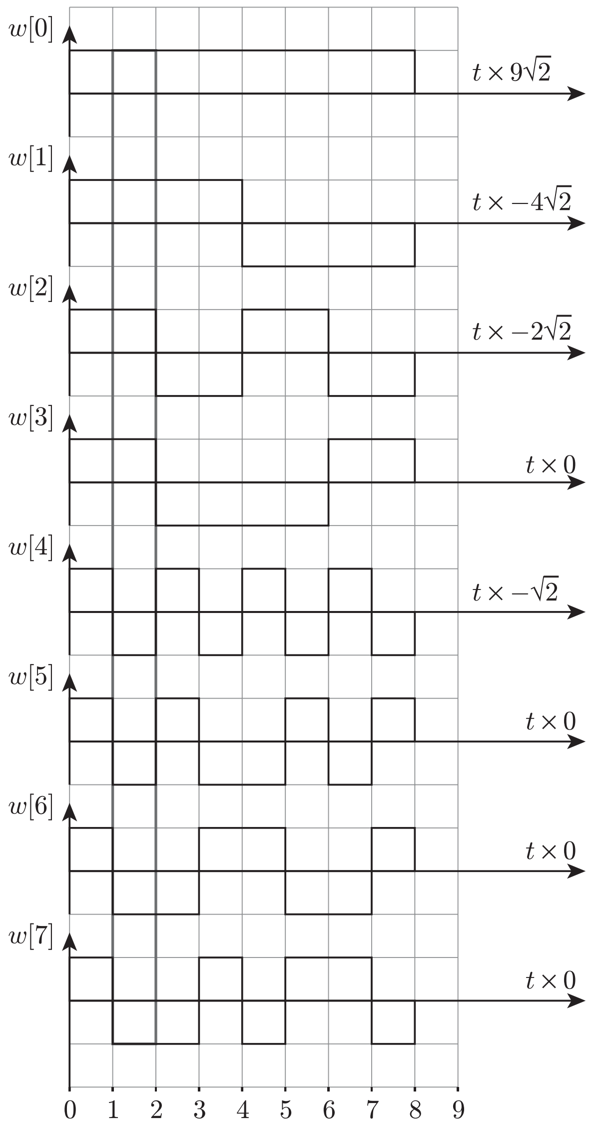

$$9\sqrt{2}\times 1 - 4\sqrt{2}\times 1 - 2\sqrt{2}\times 1 + 0\times -1 - \sqrt{2}\times -1 + 0\times -1 + 0\times -1 + 0\times -1 = 4\cdot\sqrt{2}$$
$$= \alpha_{3,1}$$

Similarly, for the third coefficient the third interval and it continues....

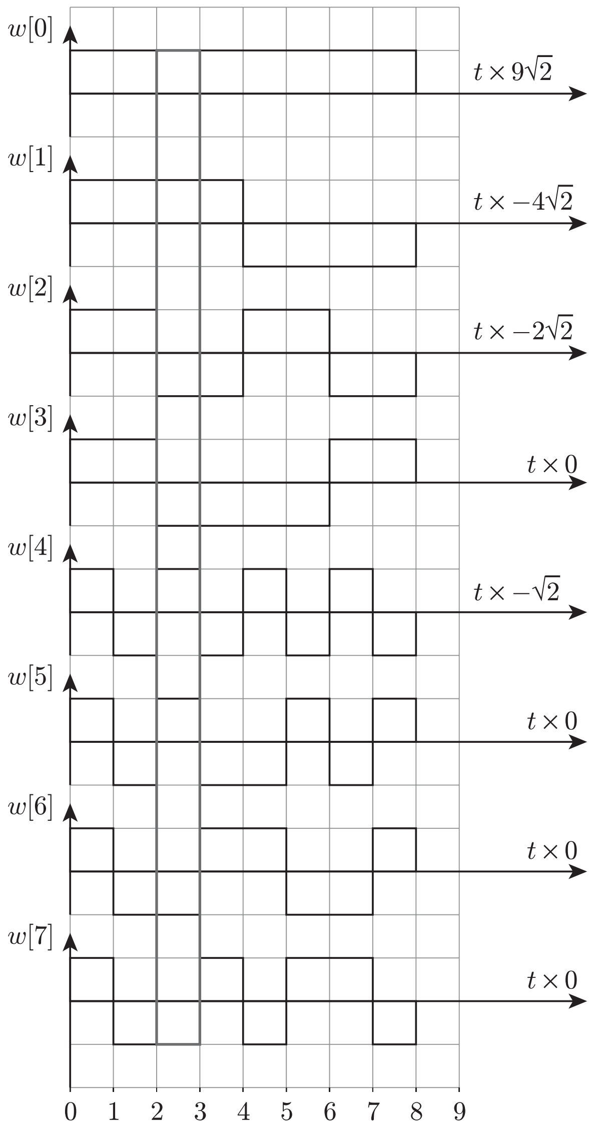

$$9\sqrt{2}\times 1 - 4\sqrt{2}\times 1 - 2\sqrt{2}\times -1 + 0\times -1 - \sqrt{2}\times 1 + 0\times 1 + 0\times -1 + 0\times -1 = 6\cdot\sqrt{2}$$
$$=\alpha_{3,2}$$

For all the intervals, the reconstructed coefficients will look as follows:

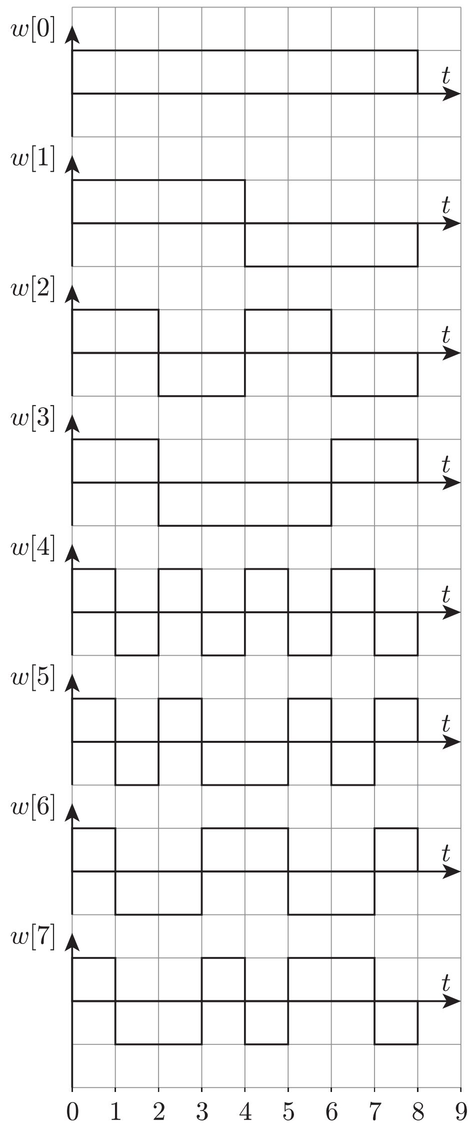

$$2\sqrt{2} \quad 4\sqrt{2} \quad 6\sqrt{2} \quad 8\sqrt{2} \quad 10\sqrt{2} \quad 12\sqrt{2} \quad 14\sqrt{2} \quad 16\sqrt{2}$$

Thus, all the coefficients match with the projected values as depicted in Eq. (13.17). This clearly shows that the evolved bases were able to capture the packet decomposition and, thus, we get complete reconstruction of the decomposed signal using wavelet packets.

Exercises

Exercise 13.1

For the 2-level wave packet transform with ideal analysis lowpass and highpass filters with cut-off $\pi / 2$, draw the spectra of X_1, X_2, X_3, X_4, X_5 and X_6 if the input spectrum is as shown below in Fig 13.28.

Hint: The spectra X_1 to X_6 for a 2-level wave packet transform shown in figure 13.29 for the given input spectrum X_0 are as shown in figure 5. The X_{11} and X_{21} are the just outputs of lowpass and highpass filters respectively (Fig 13.30). But here the output of downsampler is tricky. In general downsampling operation by a factor of '**M**' mathematically is given by,

Downsampling by a factor of M

$$Y(e^{jw}) = \frac{1}{M}\sum_{k=0}^{M-1} X(e^{\frac{j(w-2\pi k)}{M}})$$

where $k = 0,1,2...M-1$.

This can be graphically interpreted as:

1. Original spectrum $X(e^{jw})$ is translated by $\frac{2\pi}{M}k$ where $k = 0,1,..,M-1$.
2. These translates are added and resulting spectrum is multiplied by $\frac{1}{M}$
3. Frequency axis is stretched by factor of M.

Using the above steps, the spectra from X_1 to X_6 are as shown in Fig 13.31.

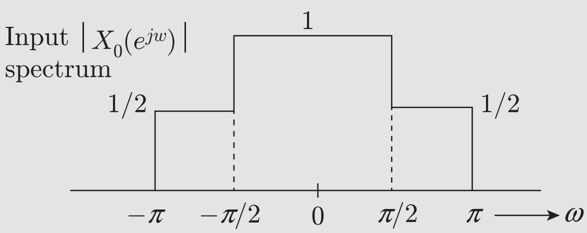

Figure 13.28 | *Input spectrum X_0*

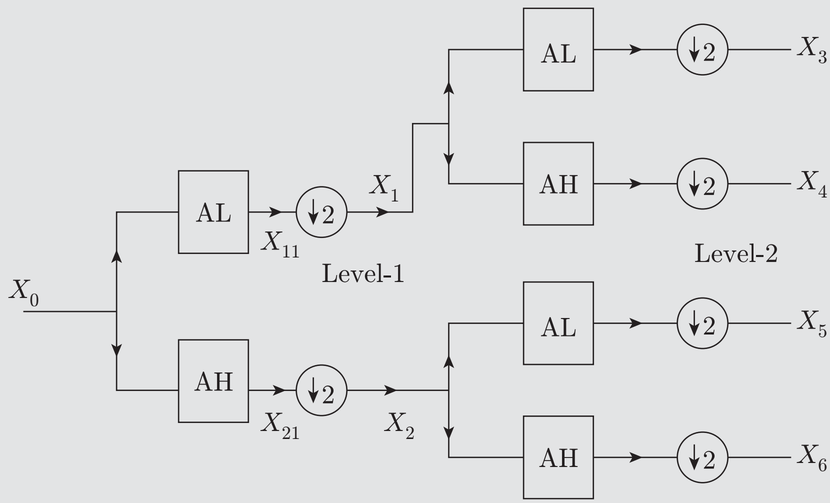

Figure 13.29 | *Two-level wave packet transform*

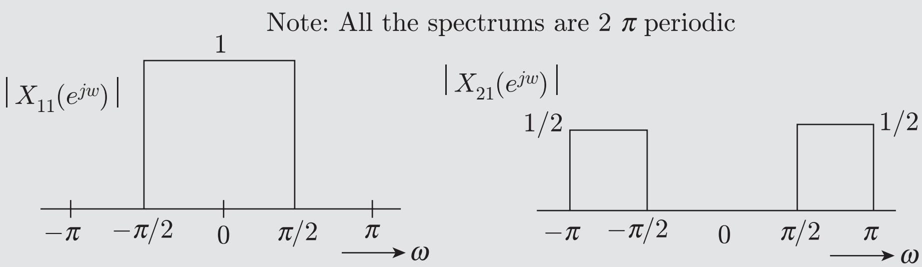

Figure 13.30 | *Spectra of X_{11} and X_{21}*

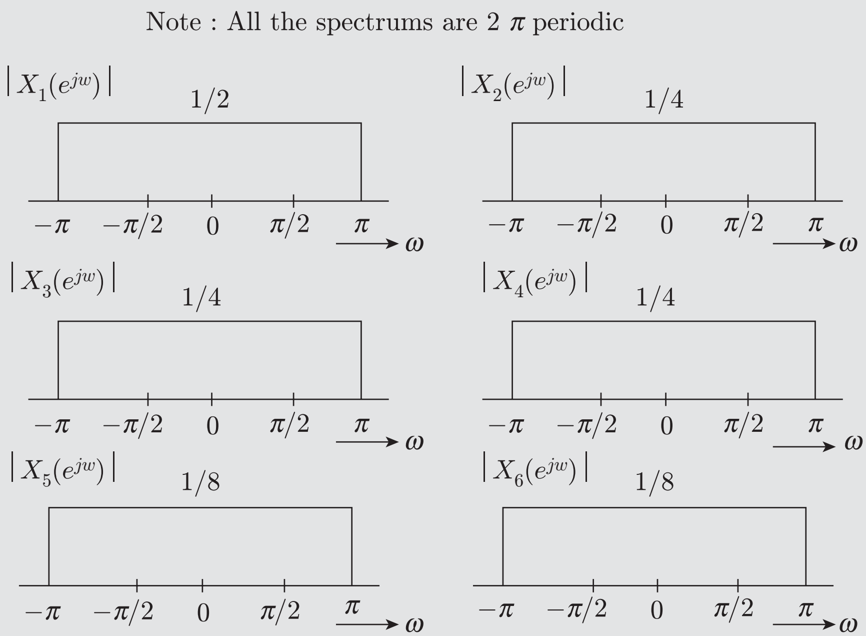

Figure 13.31 | *Spectra of X_1 to X_6*

Exercise 13.2

Simplify the following system, shown in Fig. 13.32, using Noble Identities for up- and down-sampler.

Hint: Given system can be simplified using Noble identities for up and downsampler as shown in Fig. 13.33. In Step 1, the first downsampler of factor 2 is brought ahead of filter (given by $1 + z^{-2} + z^{-4}$) and combined with second downsampler of factor 2 to give downsampler of factor 4. In Step 2, upsampler of factor 4 is brought all the way to the end and the filters are changed according to Noble identities. Finally, up-sampler of factor 4 followed by down-sampler of factor 4 cancel each other, as shown in Step 3.

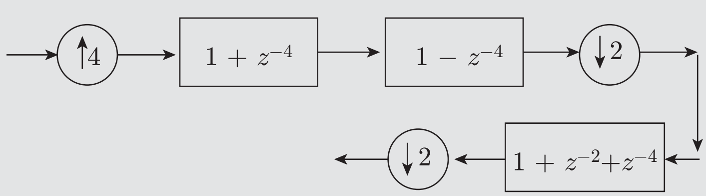

Figure 13.32 | *Tutorial 32.1: Given system*

Exercise 13.3

Construct the basis functions for the subspaces V_{0000}, V_{0001}, V_{0010}, V_{0011}, V_{0100}, V_{0101}, V_{0110}, V_{0111} as shown in Fig. 13.34 which are nonzero in an interval [0,8]

Hint: For each of the spaces we need to construct 'defining system function' using Noble identities.

$$V_{0000} : (1+z^{-1}) \rightarrow\downarrow 2 \rightarrow (1+z^{-1}) \rightarrow\downarrow 2 \rightarrow (1+z^{-1}) \rightarrow\downarrow 2$$
$$\Rrightarrow (1+z^{-1})(1+z^{-2})(1+z^{-4}) \rightarrow\downarrow 8$$

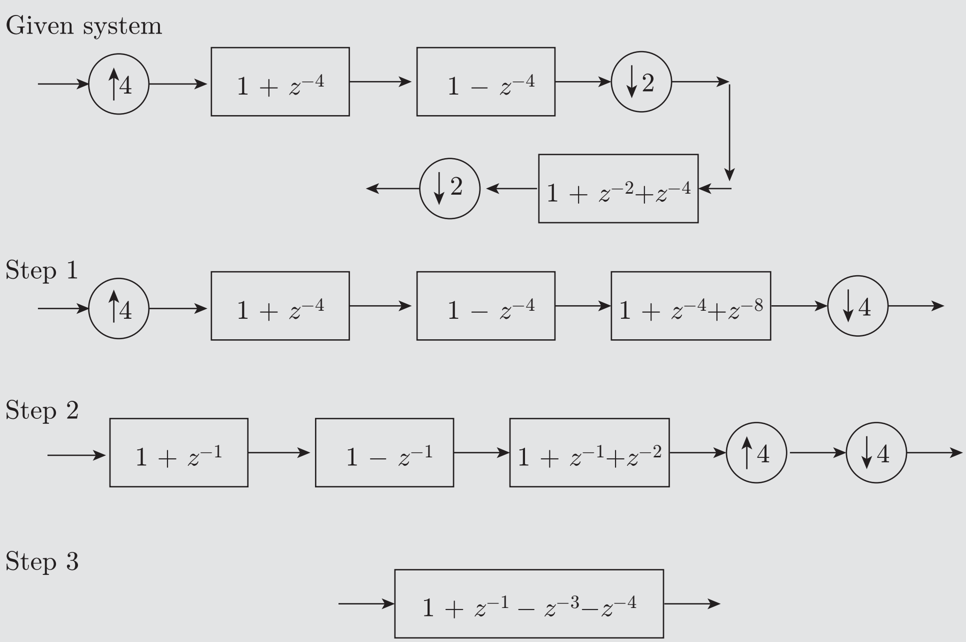

Figure 13.33 | *Tutorial 32.1: Simplification of a given system using Noble identities for up and downsampler*

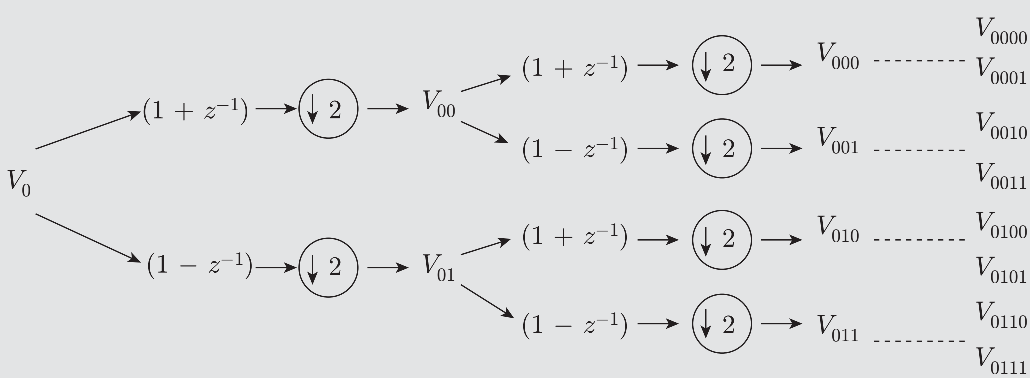

Figure 13.34 | *Tutorial 32.2: 3 level Haar Wavepacket Transform*

So, defining system function is:

$$(1+z^{-1}+z^{-2}+z^{-3}+z^{-4})(1+z^{-4})$$
$$1+z^{-1}+z^{-2}+z^{-3}+z^{-4}+z^{-5}+z^{-6}+z^{-7}$$

Corresponding primary basis function which is nonzero in interval]0,8[is shown in Figure 13.35. Similarly, basis functions for other subspaces are as follows.

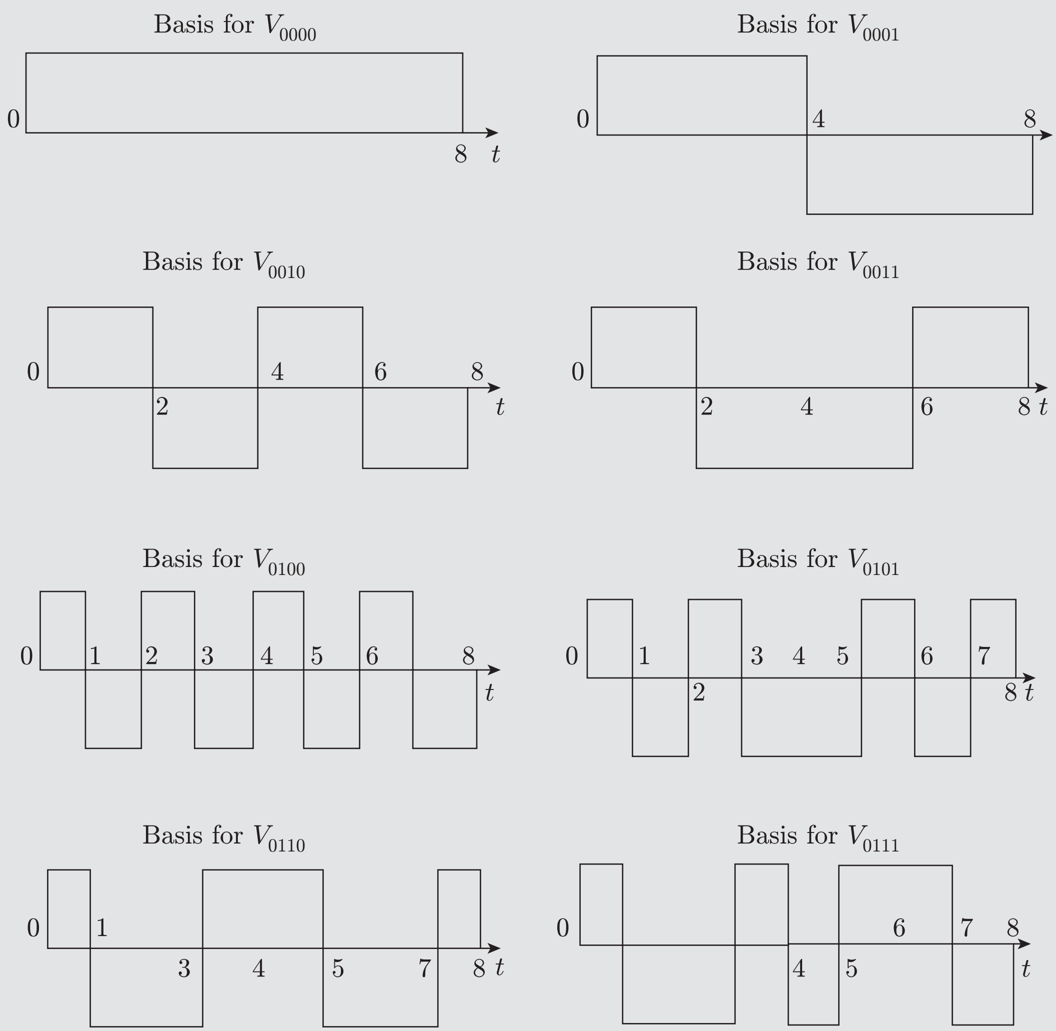

Figure 13.35 | *Tutorial 32.2: Basis functions*

$$V_{0001}:(1+z^{-1})(1+z^{-2})(1-z^{-4})$$
$$V_{0010}:(1+z^{-1})(1-z^{-2})(1+z^{-4})$$
$$V_{0011}:(1+z^{-1})(1-z^{-2})(1-z^{-4})$$
$$V_{0100}:(1-z^{-1})(1+z^{-2})(1+z^{-4})$$
$$V_{0101}:(1-z^{-1})(1+z^{-2})(1-z^{-4})$$
$$V_{0110}:(1-z^{-1})(1-z^{-2})(1+z^{-4})$$
$$V_{0111}:(1-z^{-1})(1-z^{-2})(1-z^{-4})$$

Figure 13.35 Shows basis function for different subspaces.

Exercise 13.4

Prove the Noble identities for up and downsampler for general case of any positive integer *M*.

Hint: Let us look at Noble identity for downsampler first. Consider downsampler by *M* as shown in Fig. 13.36.

We can write,

$$y[n] = p[n]\times h[n]$$

$$= \sum_{k=-\infty}^{\infty} p[k]h[n-k]$$

$$= \sum_{l=-\infty}^{\infty} h[l]p[n-l] \tag{13.24}$$

$$y[n] = \sum_{l=-\infty}^{\infty} h[l]x[Mn-Ml] \tag{13.25}$$

In Eq. (13.25), the index '*Mn*' is due to down-sampling operation. If '*Mn*' is replaced by '*n*', we arrive at a point after a filter in an equivalent system. So, we have expression

$$w[n] = \sum_{l=-\infty}^{\infty} h[l]x[n-Ml]$$

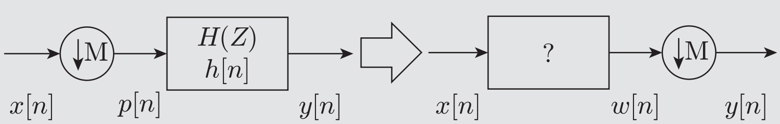

Figure 13.36 | *Tutorial 32.3: Noble identity for downsampler by M*

which is a convolution in which $h[l]$ is located at 'Ml^{th}' points and at other places it is zero.

$$h_1[n] = 0 \quad n \text{ is not a multiple of } M$$

$$= h[\frac{n}{M}] \quad n \text{ is a multiple of } M$$

Hence,

$$y[n] = \sum_{l=-\infty}^{\infty} h_1[l]x[Mn-l] \tag{13.26}$$

This indicates that impulse response of an equivalent filter before downsampler is the impulse response of original filter but upsampled by M. This is shown in Fig. 13.37.

Now, let us see Noble identity for Upsampler. We will prove this Noble Identity using Z-transform. Consider Fig. 13.38, in which a filter is followed by an upsampler of factor M. We have to find a system function $H_1(Z)$ for a filter, which comes after an upsampler of factor M.

In Z-domain we can write output of a system in which a filter is followed by down-sampler by M as

$$Y(Z) = X_1(Z^M)$$

$$Y(Z) = X(Z^M)H(Z^M)$$

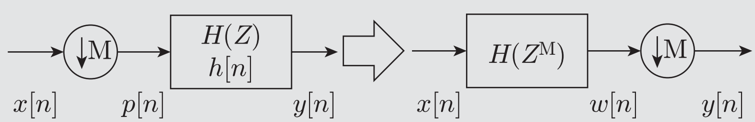

Figure 13.37 | *Tutorial 32.3: Noble identity for downsampler by M*

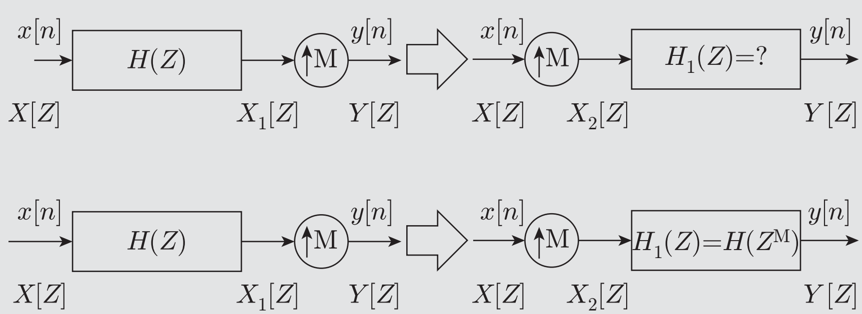

Figure 13.38 | *Tutorial 32.3: Noble identity for upsampler by M*

Also, for a system in which down-sampler by M is followed by a filter, output is given by

$$Y(Z) = X_2(Z)H_1(Z)$$

$$Y(Z) = X(Z^M)H_1(Z)$$

In order to have both systems equivalent, system function of a new filter must be $H_1(Z) = H(Z^M)$. Thus, Noble identity of up sampler tells that the operation of filtering followed by upsampling is same as the operation of up-sampling followed by filtering, with impulse response of this filter being upsampled version of impulse response of original filter.

Chapter 14

MRA Variant 4: Lifting Scheme

14.1 | Introduction

In this chapter we need to explore another variant of MRA, in fact the variant 4, the lifting scheme. We have already discussed Bi-orthogonal filter, splines and wave packets in preceding chapters. First we need to understand the lattice structure for orthogonal filter banks.

14.2 | The Lattice Structure for Orthogonal Filter Banks

Let us begin with Haar analysis filter bank (Fig. 14.1). The low-pass filter is given as

$$H_{low}(Z) = 1 + Z^{-1}$$

and the highpass filter is given as

$$Z^{-1}H_{low}(-Z^{-1}) = Z^{-1}(1 - Z) = -1 + Z^{-1}$$

Here, we perform convolution first and then pass through downsampler. Hence, actually, we are “wasting” half computation. Here, we are unnecessarily calculating odd samples which are finally washed off.

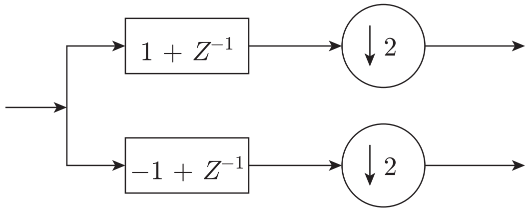

Figure 14.1 | *Haar analysis filter bank*

Hence, we must look for a more efficient structure, which downsamples first and then computes the convolution. We must invoke the "noble" identities and recast the analysis filters.

We can redraw the Haar analysis filter bank, as shown in Fig. 14.2.

The down-samplers $\downarrow 2$ can "jump" across adders, constant multipliers and branch points. Hence, we can obtain structure as shown in Fig. 14.3. This is computationally efficient structure.

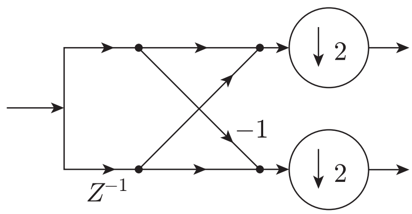

Figure 14.2 | *Lattice structure for the Haar analysis filter bank*

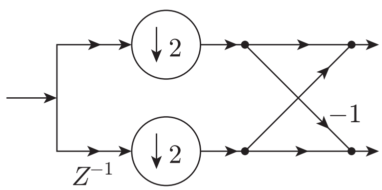

Figure 14.3 | *Efficient structure for the Haar analysis filter bank*

Let us generalize this structure (Fig. 14.4). This is the one stage or one module of lattice.

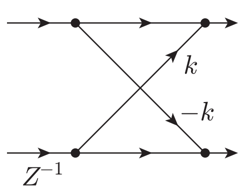

Figure 14.4 | *One stage of lattice in generalized form*

Inductive Assumption

A conjugate quadrature pair has been created at the input of this module. It's first stage is as shown in Fig. 14.5.

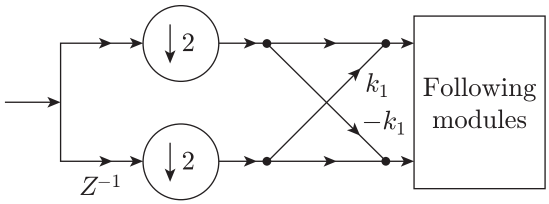

Figure 14.5 | *First stage*

and its l^{th} stage is as shown in Fig. 14.6.

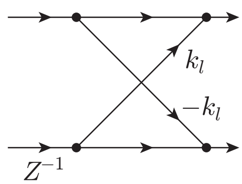

Figure 14.6 | *l^{th} stage*

Inductive Step

The inductive step is essentially to prove that,

$$B(Z) = Z^{-(L+2-1)} A(-Z^{-1})$$

Here, $Z^{-(L+2-1)}$ indicates length of filter is increased by 2. Here, we will use noble identities to prove this (Fig. 14.7).

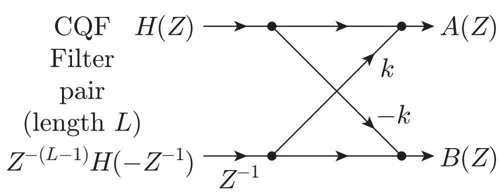

Figure 14.7 | *Inductive step*

By, applying noble identity of down-samplers, we get, (Fig 14.8 (a & b))

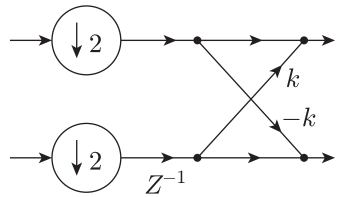

(a) Noble identity of down sampler

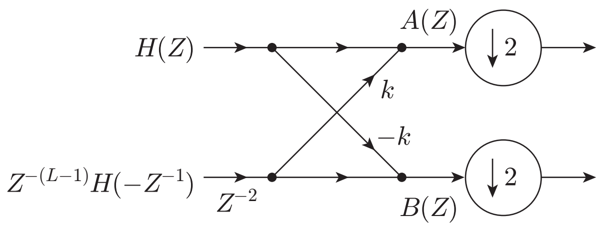

(b) Noble identity of down sampler inductive step

Figure 14.8 | *Inductive step - noble identity of down sampler*

Now,

$$\begin{aligned} A(Z) &= H(Z) + kZ^{-2}Z^{-(L-1)}H(-Z^{-1}) \\ &= H(Z) + kZ^{-(L+2-1)}H(-Z^{-1}) \end{aligned}$$

$$\begin{aligned} B(Z) &= -kH(Z) + Z^{-2}Z^{-(L-1)}H(-Z^{-1}) \\ &= -kH(Z) + Z^{-(L+2-1)}H(-Z^{-1}) \end{aligned}$$

We, essentially, need to consider $A(Z)$ is low-pass filter and find $Z^{-(L+2-1)}A(-Z^{-1})$. Hence, it can given as,

$$\begin{aligned} Z^{-(L+2-1)}A(-Z^{-1}) &= Z^{-(L+2-1)}\{H(-Z^{-1}) + k(-Z)^{L+2-1}H(Z)\} \\ &= Z^{-(L+2-1)}H(-Z^{-1}) + k(-1)^{L+2-1}H(Z) \end{aligned}$$

By inductive assumption, L is even. Hence,

$$\begin{aligned} Z^{-(L+2-1)}A(-Z^{-1}) &= Z^{-(L+2-1)}H(-Z^{-1}) - kH(Z) \\ &= B(Z) \end{aligned}$$

The inductive step is complete. Hence,

$$B(Z) = Z^{-(L+2-1)}A(-Z^{-1})$$

Basis Step

We need to study the relation between the two outputs in the Fig 14.9.

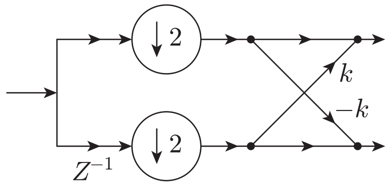

Figure 14.9 | *Downsampler by factor of 2*

By applying noble identity, we can obtain, (Fig 14.10)

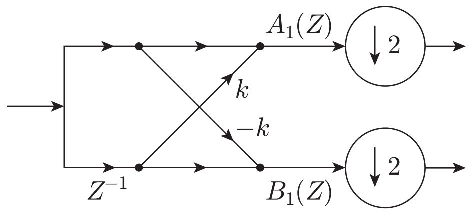

Figure 14.10 | *Noble identity applied to downsampler*

Here,

$$A_1(Z) = 1 + kZ^{-1}$$
$$B_1(Z) = -k + Z^{-1}$$

And, indeed,

$$B_1(Z) = Z^{-1}A_1(-Z^{-1})$$

Basis step is also complete. Therefore, it is proved that the given structure generates the CQF on analysis side, by mathematical induction.

Now, $(m+1)^{th}$ stage is given as

$$H_m(Z) \qquad \Rightarrow \begin{cases} H_{m+1}(Z) \\ \tilde{H}_{m+1}(Z) \end{cases}$$
$$\tilde{H}_m(Z)$$
$$= Z^{-(2m-1)}H_m(-Z^{-1})$$

Here

$$\begin{aligned} H_{m+1}(Z) &= H_m(Z) + Z^{-2}k\tilde{H}_m(Z) \\ &= H_m(Z) + kZ^{-2}Z^{-(2m-1)}H_m(-Z^{-1}) \\ &= H_m(Z) + kZ^{-(2m+2-1)}H_m(-Z^{-1}) \end{aligned}$$

and

$$\begin{aligned}\tilde{H}_{m+1}(Z) &= -kH_m(Z) + Z^{-2}\tilde{H}_m(Z) \\ &= -kH_m(Z) + Z^{-2}Z^{-(2m-1)}H_m(-Z^{-1}) \\ &= -kH_m(Z) + Z^{-(2m+2-1)}H_m(-Z^{-1})\end{aligned}$$

Our objective in synthesis or construction is,

$$\begin{matrix} H_{m+1}(Z) \\ \\ \tilde{H}_{m+1}(Z) \end{matrix} \quad \Rightarrow \begin{cases} H_m(Z) \\ \tilde{H}_m(Z) \end{cases}$$

Now,

$$H_{m+1}(Z) = H_m(Z) + kZ^{-2}Z^{-(2m-1)}H_m(-Z^{-1})$$

Here, $H_m(Z)$ is of length $2m$. Hence,

$$H_m(Z) = h_0 + h_1 Z^{-1} + \cdots + h_{2m-1}Z^{-(2m-1)}$$

Hence, $\tilde{H}_m(Z)$ is essentially,

$$\tilde{H}_m(Z) = h_{2m-1} + h_{2m-2}Z^{-1} + \cdots + h_0 Z^{-(2m-1)}$$

Therefore, $h_0 k$ is the coefficient of the highest power of Z^{-1} in $H_{m+1}(Z)$.

Now, we have a mechanism to obtain k. Once we have k, we should have a mechanism to peel off the last stage. We will complete the construction of lattice stage later.

14.3 | Lattice Structure and Its Variants

In the last section, we saw that we can construct a modular lattice structure for implementing a filter bank. Repetition of the modules will lead to an increase of order by 2 for every module. In this section and subsequent sections, the idea is to go the opposite way, i.e. if we know the final filter response, is it possible to peel off the modules to know earlier system functions in order to construct the lattice structure.

14.4 | The Lattice Module

A single lattice stage is shown in Fig. 14.11.

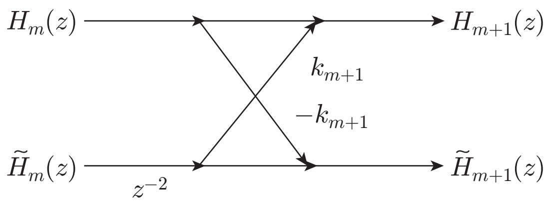

Figure 14.11 | *A stage in lattice structure*

We have shown that the conjugate quadrature relationship is preserved, i.e. given that

$$\widetilde{H}_m(z) = z^{-(2m-1)} H_m(-z^{-1}) \tag{14.1}$$

we have

$$\widetilde{H}_{m+1}(z) = z^{-(2(m+1)-1)} H_{m+1}(-z^{-1})$$

In constructing a lattice structure, we have to go the other way, i.e.

$$\begin{matrix} H_{m+1}(z) & & H_m(z) \\ & \rightarrow & \\ \widetilde{H}_{m+1}(z) & & \widetilde{H}_m(z) \end{matrix} \tag{14.2}$$

14.5 | Inductive (Recursive) Lattice Relation

The inductive lattice relation is given by

$$H_{m+1}(z) = H_m(z) + k_{m+1} z^{-2} \widetilde{H}_m(z) \tag{14.3}$$

$$\widetilde{H}_{m+1}(z) = z^{-2} \widetilde{H}_m(z) - k_{m+1} H_m(z) \tag{14.4}$$

We will determine $H_m(z)$ in terms of $H_{m+1}(z)$ and $\widetilde{H}_{m+1}(z)$ by solving Eqs. (14.3) and (14.4) for $H_m(z)$. Solving, we get $H_m(z)$ as given in Eq. (14.5)

$$H_m(z) = \frac{H_{m+1}(z) - k_{m+1} \widetilde{H}_{m+1}(z)}{1 + k_{m+1}^2} \tag{14.5}$$

14.5.1 Obtaining k_{m+1}

In Eq. (14.3), $H_{m+1}(z)$ is of length $2(m+1)$ and $H_m(z)$ is of length $2m$. The z^{-2} term increases length by 2. Now, we shall inductively show that the coefficient of z^0 in $H_m(z)$ is 1.

Basis step

The system function of first module of lattice is given as

$$H_1(z) = 1 + k_1 z^{-1} \tag{14.6}$$

$$\widetilde{H}_1(z) = -k_1 + z^{-1} \tag{14.7}$$

Thus, the coefficient of z^0 is 1 in $H_1(z)$. Now, let it also be true for $H_m(z)$. According to Eq. (14.3), the z^0 can come only from $H_m(z)$ as the lowest power of z in the second term would be z^{-2}. The the coefficient of z^0 is "carried forward" from $H_m(z)$ to $H_{m+1}(z)$. Thus, it is proved by induction that coefficient of z^0 in $H_{m+1}(z)\ \forall m \in \mathbb{N}$ is 1. From Eq. (14.1), if

$$H_m(z) = 1 + h_1^m z^{-1} + h_2^m z^{-2} + \cdots + h_{2m+1}^m z^{-(2m-1)} \tag{14.8}$$

then $\widetilde{H}_m(z)$ is given by

$$\widetilde{H}_m(z) = -h_{2m+1}^m + \cdots - h_1^m z^{-2m} + z^{-(2m-1)} \tag{14.9}$$

Thus, coefficient of highest power of z, *i.e* $z^{-(2m-1)}$ is 1. The highest negative power of z will come from the second term on the RHS of Eq. (14.3). Since k_{m+1} is the multiplier in this term, it is obvious that the coefficient of the highest negative power of z in the filter Z-transform is k_{m+1}. Thus the last coefficient directly gives the value of k_{m+1}. Once we know k_{m+1}, we can peel off one module. Since H_{m+1} is known, we can construct $\widetilde{H}_{m+1}(z)$. Thus we can determine $H_m(z)$ from Eq. (14.5).

Example 14.5.1 — An example.

Consider the example of length 4 Daubechies filter with coefficients 1, $h1$, $h2$, $h3$. We have a 2-stage lattice structure to implement this filter. The analysis structure is shown in Fig. (14.12).

Given the length 4 filter, we have Eq. (14.10)

$$\begin{aligned} k_2 &= h_3 \\ H_2(z) &= 1 + h_1 z^{-1} + h_2 z^{-2} + h_3 z^{-3} \\ \widetilde{H}_2(z) &= -h_3 + h_2 z^{-1} - h_1 z^{-2} + z^{-3} \end{aligned} \tag{14.10}$$

We can calculate $H_1(z)$ from Eq. (14.5) as

$$\begin{aligned} H_1(z) &= \frac{H_2(z) - k_2 \widetilde{H}_2(z)}{1 + k_2^2} \\ &= \frac{H_2(z) - h_3 \widetilde{H}_2(z)}{1 + h_3^2} \end{aligned}$$

Consider the numerator only

$$= 1 + h_3^2 + (h_1 - h_2 h_3) z^{-1} + (h_2 + h_1 h_3) z^{-2} \tag{14.11}$$

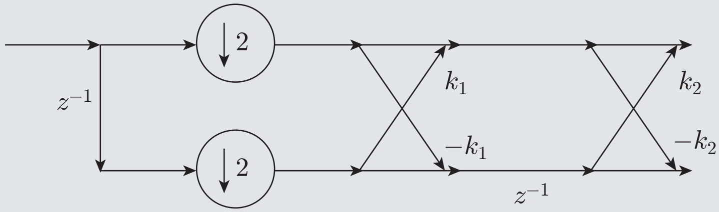

Figure 14.12 | *Lattice structure for Daubechies length 4 filter*

The Daubechies filter bank impulse response is orthogonal to its even translates, i.e., the product of

$$\begin{array}{cccccc} 1 & h_1 & h_2 & h_3 & & \\ & & 1 & h_1 & h_2 & h_3 \end{array}$$

would be zero, i.e

$$h_2 + h_1 h_3 = 0$$

Hence,

$$\begin{aligned} H_1(z) &= \frac{1+(h_1 - h_2 h_3)z^{-1} + (h_2 + h_1 h_3)z^{-2}}{1+h_3^2} \\ &= \frac{(1+h_3^2)+(h_1 - h_2 h_3)z^{-1}}{1+h_3^2} \\ &= 1 + \frac{h_1 - h_2 h_3}{1+h_3^2} z^{-1} \end{aligned} \tag{14.12}$$

This also gives us the value of k_1.

$$k_1 = \frac{h_1 - h_2 h_3}{1+h_3^2}$$

The backward recursion in Eq. (14.5) is effected by

- k_{m+1} is the coefficient of highest power of z^{-1}.
- As long as this coefficient is real, the denominator $1+k_{m+1}^2$ poses no problem.
- The length of $H_m(z)$ is reduced by 2, one due to cancelation of highest order coefficient, and one due to the orthogonality of the filter response to its even translates.

14.6 | The Synthesis Variant

The synthesis side of the lattice structure is essentially the transpose of analysis side. Hence for the first stage, shown in Fig. 14.13.

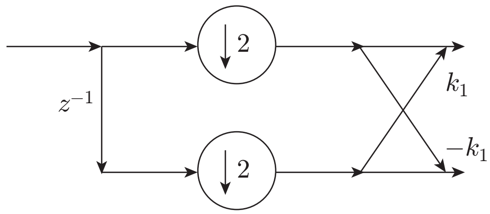

Figure 14.13 | *Analysis lattice structure first stage*

The corresponding synthesis stage is shown in Fig. 14.14.

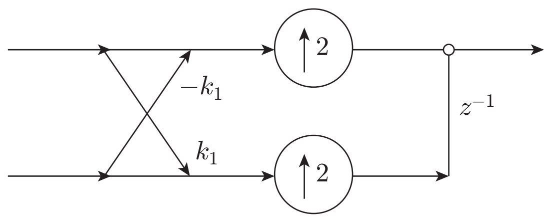

Figure 14.14 | *Synthesis lattice structure first stage*

The inductive analysis stage is shown in Fig. 14.15.

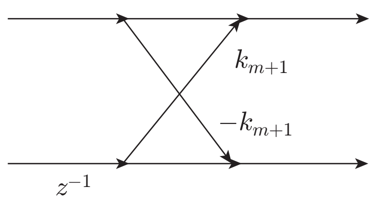

Figure 14.15 | *Inductive analysis lattice structure stage*

The corresponding inductive synthesis stage is shown in Fig. 14.16.

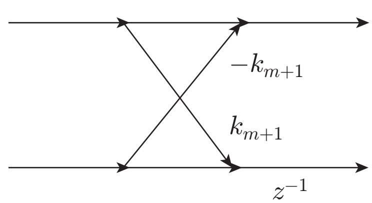

Figure 14.16 | *Inductive synthesis lattice structure stage*

14.7 | Efficient Deployment Schemes for Lifting Structures

In the last section we derived a computationally efficient structure to realize orthogonal filter banks, this structure are called as lattice.

Lattice is a periodic repetition of uniform modular piece. We also saw that complexity was more on the lattice structure, as it simultaneously works on two inputs to give two outputs.

For computationally efficient realization of orthogonal filter banks, we will go for further simplification of lattice structure, i.e., we are going to decompose lattice stages into two sub stages which have more elementary operation that is called as lifting structure and this will lead to the idea of polyphase matrices.

14.8 | The Lifting Structures and Polyphase Matrices

Figure 14.17 shows a simple lattice stage.

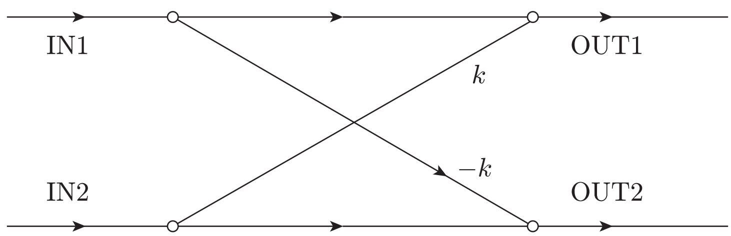

Figure 14.17 | *Lattice stage*

Here K is known as lattice parameter. It distinguishes one stage from the other. From Fig. 14.17 it is clear that two computations are performed simultaneously so basically a criss-cross is involved here.

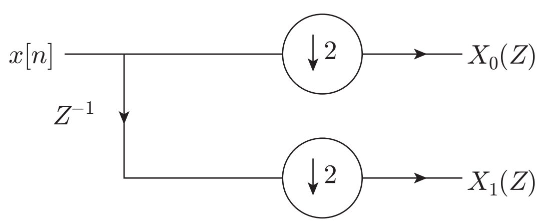

Figure 14.18 | *Operations performed in a lattice stage*

Let us now relate IN1 and IN2 with OUT1 and OUT2 by method of a 2 × 2 matrix known as polyphase matrix.

Let us introduce the idea of **polyphase matrices**.

At the beginning of every lattice stage, operation, as shown in Fig. 14.18, is performed. Now, we seek a relation between $X(Z)$, $X_0(Z)$, $X_1(Z)$.

Graphically

$$x_{-n} \cdots\cdots\cdots\cdots x_{-2}\, x_{-1}\, x_0\, x_1 \cdots\cdots$$

The subscripts here represents the value of n.

On the X_0 branch,

$$x_0[n] \text{ we have } ....x_{-4}\ x_{-2}\ x_0\ x_2\ x_4........$$

On the X_1 branch,

$$x_1[n] \text{ we have } ....x_{-3}\ x_{-1}\ x_1\ x_3\ x_5........$$

$x[n]$ is obtained by interleaving the sequence on x_0 branch and than on x_1 branch and continue this further.

$$x_0[n] = x[2n] \quad \forall n \in \mathbb{Z}$$

$$x_1[n] = x[2n+1] \quad \forall n \in \mathbb{Z}$$

It is easy to see

$$X(z) = \sum_{n=-\infty}^{n=\infty} x[n]z^{-n}$$

can be decomposed into following two summations.

$$= \sum_{n=-\infty}^{n=\infty} x[2n]z^{-2n} + \sum_{n=-\infty}^{n=\infty} x[2n+1]z^{-(2n+1)}$$

$$= \sum_{n=-\infty}^{n=\infty} x_0[n](z^2)^{-n} + \sum_{n=-\infty}^{n=\infty} x_1[n]z^{-1}(z^2)^{-n}$$

$x_0[n]$ and $x_1[n]$ are called the polyphase components of $x[n]$, which means switching from one phase to another phase for one sample and the other phase for another sample and this continues for other coming samples for constructing $x_0[n]$ and $x_1[n]$.

$$X(z) = X_0(z^2) + z^{-1}X_1(z^2)$$

So the above equation gives a relationship between Z-transform of polyphase components and Z-transform of sequence.

Lattice performs operation on this polyphase components, therefore, we can say that the whole of analysis and synthesis filter bank is essentially a operation on polyphase components instead of an operation on sequence. It can be thought of as operation on 2×2 sequence.

So, each stage of lattice is 2×2 matrix operation on polyphase components.

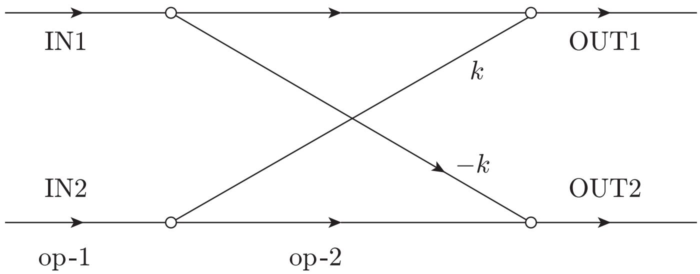

Figure 14.19 | *Operation 1*

Matrix corresponding to op-1 or operation 1 is shown in Fig. 14.19.

$$\begin{bmatrix} 1 & 0 \\ 0 & z^{-1} \end{bmatrix} \begin{bmatrix} IN1 \\ IN2 \end{bmatrix} = \begin{bmatrix} Int1 \\ Int2 \end{bmatrix}$$

Here, Int1 and Int2 stands for intermediate stages 1 and 2, respectively.
Matrix corresponding to op-2 or operation 2, as shown in Fig. 14.19,

$$\begin{bmatrix} 1 & k \\ -k & 1 \end{bmatrix} \begin{bmatrix} Int1 \\ Int2 \end{bmatrix} = \begin{bmatrix} OUT1 \\ OUT2 \end{bmatrix}$$

$$\begin{bmatrix} OUT1 \\ OUT2 \end{bmatrix} = \begin{bmatrix} 1 & k \\ -k & 1 \end{bmatrix} \begin{bmatrix} 1 & 0 \\ 0 & z^{-1} \end{bmatrix} \begin{bmatrix} IN1 \\ IN2 \end{bmatrix}$$

$$\begin{bmatrix} 1 & k \\ -k & 1 \end{bmatrix} \begin{bmatrix} 1 & 0 \\ 0 & z^{-1} \end{bmatrix}$$

is known as a polyphase matrix.

$$\begin{bmatrix} 1 & 0 \\ 0 & z^{-1} \end{bmatrix}$$

cannot be further simplified.
But we can think of simplifying

$$\begin{bmatrix} 1 & k \\ -k & 1 \end{bmatrix}$$

into an upper triangular matrix and a lower triangular matrix for reducing computational complexity.

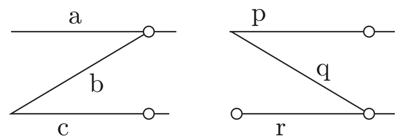

Figure 14.20 | *Upper Δ and lower Δ computations*

$$\begin{bmatrix} 1 & k \\ -k & 1 \end{bmatrix} = \begin{bmatrix} a & b \\ 0 & c \end{bmatrix} \begin{bmatrix} p & 0 \\ q & r \end{bmatrix}$$

Figure 14.20 shows the computation involve in upper Δ and lower Δ.
On solving matrix we get,

$$\begin{bmatrix} 1 & k \\ -k & 1 \end{bmatrix} = \begin{bmatrix} ap+bq & br \\ cq & cr \end{bmatrix}$$

On equating both sides,

$$\begin{aligned} ap+bq &= 1 \\ br &= k \\ cq &= -k \\ cr &= 1 \end{aligned}$$

We exploit degree of freedom by choosing very simple variable.

$p = 1, r = 1$ where upon

$$\begin{aligned} a+bq &= 1 \\ cq &= -k \\ b &= k \\ c &= 1 \\ q &= -k \\ a &= 1+k^2 \end{aligned}$$

So finally we get the following matrix. Structure is represented in Fig. 14.21.

$$\begin{bmatrix} 1 & k \\ -k & 1 \end{bmatrix} = \begin{bmatrix} 1+k^2 & k \\ 0 & 1 \end{bmatrix} \begin{bmatrix} 1 & 0 \\ -k & \end{bmatrix}$$

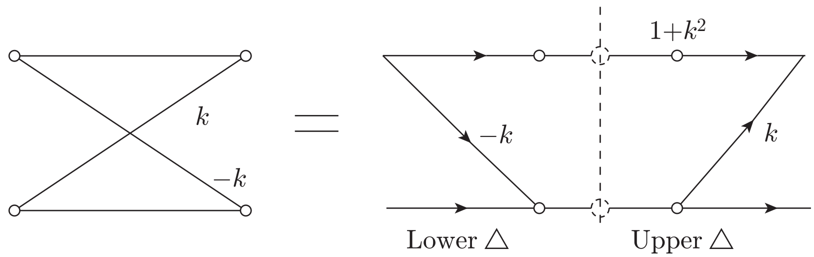

Figure 14.21 | *Resulting structure after solving matrices*

On redrawing and including delay factor as shown in Fig. 14.22.

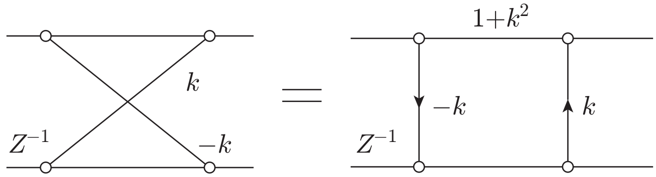

Figure 14.22 | *Lifting stage*

The idea of lifting is to lift from no-transform to a meaningful transform in case of up-samplers and down-samplers, as shown in Fig. 14.22.

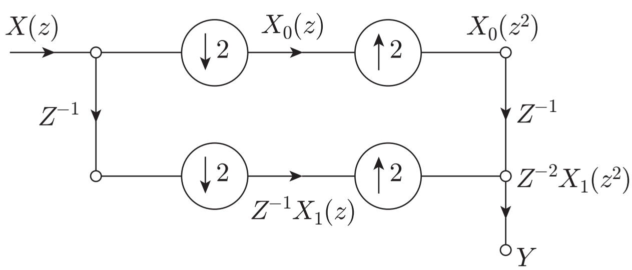

Figure 14.23 | *Lazy wavelet transform*

This is called a lazy wavelet transform and has no action at all if no lattice stages are present. The structure is as shown in Fig. 14.23. So from a structure which does nothing at all a stage-by-stage structure, which has meaningful frequency response, is built. Lifting is used because it lifts the inefficient wavelet transform to a transform which does great deal in time and frequency.

14.9 | The Polyphase and the Modulation Approach

In earlier few sections we have discussed briefly the idea of polyphase decomposition. We will use it to construct different kinds of structure to carry out computation efficiency in a filter bank. In the reminder of this chapter we will put down formally the approach based on polyphase components for perfect reconstruction.

We will discuss two approaches for perfect reconstruction:

1. The Polyphase Approach
2. The Modulation Approach

And we will generalized it for M-bank filter bank.

14.10 | Towards Building Polyphase Structures

Consider two-bank filter bank.

$$x[n] \underset{Z-Transform}{\rightarrow} X(Z)$$

The Polyphase decomposition of order two is given as,

$$\begin{aligned} n &= 2m \\ &= 2m+1, \text{ for all integer } m \end{aligned}$$

Example 14.10.1 — Order 3.

To generalize it, consider the order 3.

$$\begin{aligned} n &= 3m \\ &= 3m+1 \\ &= 3m+2, \text{ for all integer } m \end{aligned}$$

Example 14.10.2 — Order M.

In general, for order M

$$\begin{aligned} n &= Mm \\ &= Mm+1 \\ &\vdots \\ &= Mm+(M-1), \text{ for all integer } m \end{aligned}$$

So now let us put down explicitly the mechanism for the decomposition of $X(Z)$, the Z-transform of $x[n]$, into the Z-transform of the polyphase component of the order M. For that we need to spilt the index M.

To decompose $X(Z)$ using polyphase decomposition of the order M.

$$X(Z) = \sum_{n=-\infty}^{+\infty} x[n]Z^{-n}$$

$$\sum_{n=-\infty}^{+\infty} \cdots (n) \text{ variation as a function of } n$$

Now splitting $\sum_n$ into

$$\sum_{l=0}^{M-1} \sum_{m=-\infty}^{+\infty} \cdots (Mm+l) \text{ variation as a function of } (Mm+l)$$

$$X(Z) = \sum_{l=0}^{M-1} \sum_{m=-\infty}^{+\infty} x[Mm+l] Z^{-(Mm+l)}$$

$$X(Z) = \sum_{l=0}^{M-1} Z^{-l} \left\{ \sum_{m=-\infty}^{+\infty} x[Mm+l] Z^{-(Mm)} \right\}$$

The term $\sum_{m=-\infty}^{+\infty} x[Mm+l]Z^{-(Mm)}$ is the Z-transform of all those points which lie at multiples of $(M+l)$.

For example, $l=0$ represents the Z-transform of all those points which lie at multiples of M. $l=1$ refers to all those points which lie at multiples of $(M+1)$ displaced by 1 from multiples of M. This can go up to $(M-1)$ and after this l again becomes zero.

We break $X(Z)$ into M disjoint parts.

$$X(Z) = \sum_{l=0}^{M-1} Z^{-l} \left\{ \sum_{m=-\infty}^{+\infty} x[Mm+l] Z^{-(Mm)} \right\}$$

The term $\sum_{m=-\infty}^{+\infty} x[Mm+l]Z^{-(Mm)}$ can be represented by $X_{l,M}(Z^M)$. M^{th} order polyphase component and l^{th} of those component with the argument given by Z^M is,

$$X_{l,M}(Z) = \sum_{m=-\infty}^{+\infty} x[Mm+l] Z^{-m}$$

$X_{l,M}(Z)$ is essentially the Z-transform of l^{th} polyphase component of sequence $x[\cdot]$, order M.

Two important points order of decomposition and the component number. There will be as many components as the order.

When $M=2$ then $l=0$ or 1 When $M=3$ then $l=0,1$ or 2, and so on.

Relationship between Z-transform of the original sequence and Z-transform of its polyphase component is given as,

$$X(Z) = \sum_{l=0}^{M-1} Z^{-l} X_{l,M}(Z^M)$$

This is the manifestation of the polyphase decomposition in the Z-domain.

Now, we would like to see how polyphase decomposition works when we have analysis and synthesis side. A general relationship may be put down for analysis and synthesis polyphase components and their interaction, to give perfect reconstruction.

General analysis branch in M-Bank filter bank is as shown in Fig 14.24 and synthesis branch is as shown in Fig 14.25.

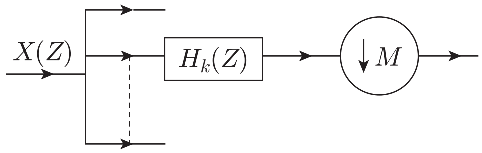

Figure 14.24 | *Analysis branch*

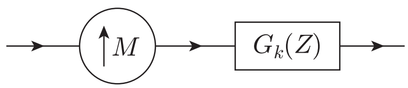

Figure 14.25 | *Synthesis branch*

In a given M-Bank filter bank the number of analysis branches and synthesis branches must be same.

B is the number of branches and its value can be different from M as depicted in Fig 14.26.

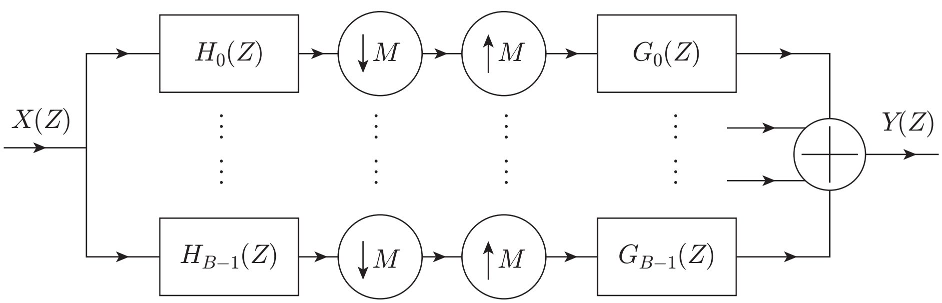

Figure 14.26 | *M-bank filter bank structure*

$B = M$: critically sampled M-Bank filter bank

$B < M$: under sampled M-Bank filter bank

$B > M$: over sampled M-Bank filter bank

14.11 | Polyphase Approach

Decompose the filters, both analysis and synthesis, into polyphase components and decompose the input and output also into its polyphase component of order M. Order of the polyphase decomposition is the same as the down- and up-sampling factors.

Consider the k^{th} branch, as shown in Fig 14.27.

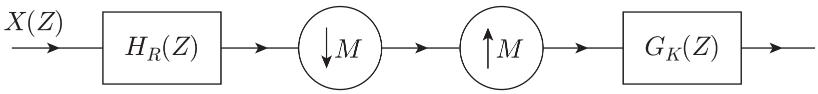

Figure 14.27 | *k^{th} branch in M-bank filter bank*

Z domain analysis,

$$X(Z) = \sum_{l=0}^{M-1} Z^{-l} X_{l,M}(Z^M)$$

Similarly,

$$H_k(Z) = \sum_{l=0}^{M-1} Z^{-l} H_{k,l,M}(Z^M)$$

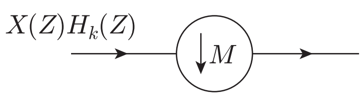

Figure 14.28 | 0^{th} *Polyphase component of order M*

$$X(Z)H_k(Z) = \sum_{l_1=0}^{M-1}\sum_{l_2=0}^{M-1} Z^{-l_1} Z^{-l_2} X_{l_1,M}(Z^M) H_{k,l_2,M}(Z^M)$$

The 0^{th} polyphase component, as shown in Fig 14.28, results when $Z^{-l_1}.Z^{-l_2} = Z^{-(l_1+l_2)}$ contributes $(Z^M)^{l_0}$, $l_0 \in \mathbb{Z}$.

Considering l_1 and l_2, when l_1 is zero, l_2 is also zero. When l_1 is 1, l_2 is $M-1$. Likewise, when l_1 is $M-1$ l_2 is 1.

With one l_1 there is one unique l_2. The relation for the l_2 is,

$$l_2 = (M - l_1) \text{ modulo } M$$

So, when $X(Z)H_k(M)$ is down-sampled with M, we will get

$$X_{0,M}(Z)H_{k,0,M}(Z)+\left\{\sum_{l=1}^{M-1}X_{l,M}(Z)H_{k,M-1,M}(Z)\right\}Z^{-1}$$

Except for the first case (i.e. when l_1 and l_2, both are zero) (l_1+l_2) gives M as so after down-sampling by M, we get Z^{-M} as Z^{-1}.

The k^{th} row, as in Fig. 14.29, in the matrix (Fig. 14.30) is

$$k^{th}\ \ row = H_{k,0,M}(\cdot).Z^{-1}.H_{k,M-1,M}(\cdot)\ldots Z^{-1}H_{k,1,M}(Z)$$

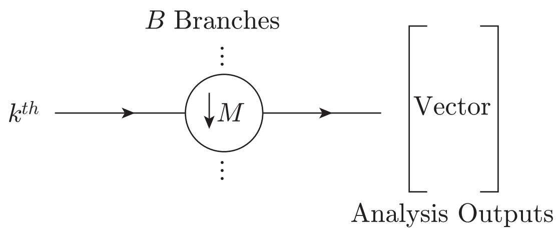

Figure 14.29 | *Analysis outputs of k^{th} branches*

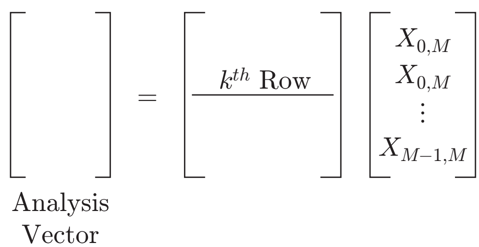

Figure 14.30 | *Analysis polyphase matrix*

The size of the polyphase matrix will be as many branches times the polyphase decomposition $B \times M$.

Let us consider what happens to the k^{th} branch after up-sampling by M followed by filtering by G, as shown in Fig 14.31.

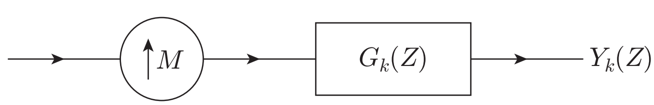

Figure 14.31 | *k^{th} Synthesis branch*

Decomposing $Y_k(Z)$ into its polyphase components.

$$Y_k(Z) = \sum_{l=0}^{M-1} Z^{-l} Y_{k,l,M}(Z^M)$$

$$G_k(Z) = \sum_{l=0}^{M-1} Z^{-l} G_{k,l,M}(Z^M)$$

Therefore,

$$Y_{k,l,M}(Z^M) = G_{k,l,M}(Z^M).\{\text{ Output of the } k^{th} \text{ up sampler}\}$$

Output of the k^{th} up-sampler can be given, as given in Fig. 14.32.

$$\begin{bmatrix} \\ k^{th} \text{ row of analysis} \\ \text{polyphase matrix} \\ \\ \end{bmatrix} \begin{bmatrix} X_{0,M} \\ X_{1,M} \\ \vdots \\ X_{M-1,M} \end{bmatrix}$$

Figure 14.32 | *Output of the* k^{th} *up sampler*

Because of the up-sampler Z has been replaced by Z^M.

This is the polyphase approach to analyze the overall M-Bank filter Bank. We have seen the k^{th} branch output is

$$Y(Z) = \sum_{k=1}^{B} Y_k(Z) \qquad \text{where, } B \text{ is the Number of branches}$$

$$Y_{l,M}(Z^M) = \sum_{k=1}^{B} G_{k,l,M}(Z^M)(\text{Output of the k}^{\text{th}} \text{ up-sampler})$$

We can write down the output of the polyphase vector component and input polyphase component and relate them (Fig. 14.33)

l^{th} Row of synthesis polyphase matrix is

$$[G_{0,l,M}(Z^M)\cdots G_{B-1,l,M}(Z^M)]$$

Now, we have M such rows and each row has B elements. Whereas in analysis polyphase matrix we have B rows and M elements in each row.

$$\underset{\substack{\text{Output}\\ \text{Polyphase}\\ \text{Components}}}{\begin{bmatrix} Y_{0},M \\ Y_{1},M \\ \vdots \\ Y_{M-1,M} \end{bmatrix}} = \underset{\substack{\text{Synthesis Polyphase}\\ \text{Matrix}}}{\begin{bmatrix} M \times B \text{ polyphase} \\ \text{components of } G_k \end{bmatrix}}$$

Figure 14.33 | *Synthesis polymer matrix equated to output polyphase components*

The overall analysis of M-Bank filter bank with B-branches in terms of the polyphase components as be shown, as shown in Fig. 14.34.

$$\underset{M \times 1}{\begin{bmatrix} \text{Output} \\ \text{Polyphase} \\ \text{Vector} \\ (Z^M) \end{bmatrix}} = \underset{M \times B}{\begin{bmatrix} \text{Polyphase} \\ \text{Synthesis} \\ \text{Matrix} \\ (Z^M) \end{bmatrix}} \underset{B \times M}{\begin{bmatrix} \text{Polyphase} \\ \text{Analysis} \\ \text{Matrix} \\ (Z^M) \end{bmatrix}} \underset{M \times 1}{\begin{bmatrix} \text{Input} \\ \text{Polyphase} \\ \text{Matrix} \\ (Z^M) \end{bmatrix}}$$

Figure 14.34 | *M-bank filter bank in terms of polyphase components*

14.12 | Modulation Approach

In this approach we treat down sampling as a sum of modulations. Consider an example of $M = 2$.

$$x[n] \longrightarrow \boxed{\downarrow 2} \longrightarrow \boxed{\uparrow 2} \longrightarrow y[n]$$

The output $y[n]$ obtained after first down-sampling the input $x[n]$ by 2 and then up-sampling by 2 can be considered as the multiplication of the input $x[n]$ sequence by $\cdots 101010 \cdots$. Here, 1 is at every multiple of 2.

In general, for any positive integer M, the effect of first down-sampling by M and then up-sampling by M is same as multiplication by a sequence given below:

$$\ldots \quad \underset{\text{Multiples of } M}{\underline{1}} \quad \underbrace{0\ 0\ \cdots\ 0}_{(M-1)}\ 1\ 0\ 0\ \cdots 0 \ldots$$

In the modulation approach, the idea is instead of decomposing the sequence in time we essentially treat the sequence as a sum of modulations. And we combine the down- and up-sampler when we treat it thus as a sum.

Next, we shall go further and learn modulation approach and contrast it with the polyphase approach, bringing out the differences and the similarities between the two and establish condition for the perfect reconstruction based on both these approaches.

14.13 | Modulation Analysis and 3-band Filter Bank, Application

In the previous section we have discussed one way to analyze the general system with analysis and synthesis filters, namely the approach of polyphase decomposition. Essentially, polyphase decomposition is a time decomposition approach where we recognize all sequences in question; whether the input sequence, the output sequence, filter impulse response, could be thought of comprising of as many subsequence as the number by which the sequence is decimated and interpolated, i.e., down-sampling factor and up-sampling factor. For example, if we have down-sampling and up-sampling by 2, we think of odd and even number points on all sequence of interest. Based on this decomposition we identify relation between output polyphase and input polyphase component through filter polyphase component.

Naturally, this is difficult to do in time domain, hence we use Z-domain. We also noted that condition of perfect reconstruction amounts to a condition on product of polyphase matrix corresponding to analysis and synthesis side.

14.14 | Final Step in Polyphase Approach

$$\begin{bmatrix} \text{Output Polyphase} \\ \text{Vector} \end{bmatrix} = \begin{bmatrix} \text{Synthesis} \\ \text{polyphase} \\ \text{Matrix} \end{bmatrix} \begin{bmatrix} \text{Analysis} \\ \text{Polyphase} \\ \text{Matrix} \end{bmatrix} \begin{bmatrix} \text{Input} \\ \text{Polyphase} \\ \text{vector} \end{bmatrix}$$

All the matrices are of order M, which is the factor of down-sampling and up-sampling. Product of synthesis and analysis polyphase matrices of order M is equal to square matrix of size $M \times M$.

Question to be answered is that what should this matrix be for a perfect reconstruction.

For a perfect reconstruction we require:

$$Y(Z) = C_0 Z^{-D} X(Z) \tag{14.13}$$

If we decompose $Y(Z)$ and $X(Z)$ we get,

$$Y(Z) = \sum_{K=0}^{M-1} Z^{-K} \quad Y_{K,M}(Z^M) \tag{14.14}$$

$$X(Z) = \sum_{K=0}^{M-1} Z^{-K} \quad X_{K,M}(Z^M) \tag{14.15}$$

Therefore,

$$\sum_{K=0}^{M-1} Y_{K,M}(Z^M) Z^{-K} = C_0 Z^{-D} \sum_{K=0}^{M-1} X_{K,M}(Z^M) Z^{-K} = C_0 \sum_{K=0}^{M-1} Z^{-(D+K)} X_{K,M}(Z^M) \tag{14.16}$$

We need to separate $D+K$: D is fixed for all K, $D+K$ essentially carries out a rearrangement of polyphase component.

For example, $M=3$, $D=5$.

K	K+D	
0	5	$\equiv 2$
1	6	$\equiv 0$
2	7	$\equiv 1$

Therefore 0^{th} number polyphase component of input is mapped to 2^{nd} number polyphase component of the output. Similarly, 1^{st} and 2^{nd} number polyphase component of input are mapped to 0^{th} number and 1^{st} number polyphase component of the output, respectively.

What we have is the cyclic rearrangement of the polyphase component and, therefore, if we look at product matrix what we require is that every row and column must have only one nonzero entry, i.e., if we take every row and every column, there is exactly one nonzero entry and that is identical. The constant factor in each of the entry is C_0 and the additional delay depends on D.

14.14.1 Summary of the Method

For perfect reconstruction,

synthesis matrix × Analysis matrix = (following form) Each row and column has exactly one entry of the form $C_0 Z^{-L}$.

where, L depends on D.

For example, $D=5$, $M=3$

Polyphase matrices written in Z^3 , then $L=3$.

Polyphase matrices written in Z , then $L=1$.

Think about: If we have to obtain perfect reconstruction but if the analysis–synthesis system together becomes linear shift invariant system, that means one can equivalently treat output as a result of input been acted upon by a LSI system with a certain transfer function. What can we say about the entries of this product matrix when this LSI invariance is present in overall analysis–synthesis structure? Can we attribute a certain structure to this product matrix?

14.15 | Modulation Approach

It is frequency domain approach. Consider one of the branch:

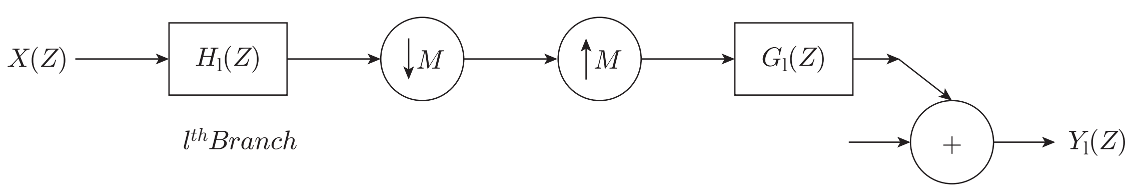

We wish to establish a relation across this branch. All these branches with different $G_l(Z)$ will come together in summation to form $Y_0(Z)$. Now look at

$$\longrightarrow \boxed{\downarrow M} \longrightarrow \boxed{\uparrow M} \longrightarrow$$

This is essentially a multiplication by a periodic sequence $P_M[n]$

$$\begin{aligned} P_M[n] &= 1, \quad n \text{ is a multiple of } M \\ &= 0, \quad \text{else} \end{aligned}$$

Now, in modulation approach we think of the process of down-sampling followed by up-sampling as modulation by sequence and that sequence is broken into its component sequences each of which is exponential.

Consider one period i.e., $P_M[n]$ restricted to $0,1,...(M-1)$. Obtain its DFT.

$$\tilde{P}_M[k] = \sum_{n=0}^{M-1} P_M[n] W_M^{-nk} \quad ; W_M = e^{j\frac{2\pi}{M}} \tag{14.17}$$

This $\tilde{P}_M[k]$ is dot product of one period of the sequence with the exponential.

$$\tilde{P}_M[k] = 1, \quad k = 0,1,.....(M-1) \tag{14.18}$$

Take inverse Fourier transform.

$$P_M[k] = \frac{1}{M} \sum_{k=0}^{M-1} 1.W_M^{nk} \quad ; \forall n \tag{14.19}$$

Now,

$$X(Z) \rightarrow \left[H_l(Z)\right] \rightarrow X(Z)H_l(Z) \overset{Modulated\, by}{\rightarrow} \frac{1}{M} \sum_{k=0}^{M-1} W_M^{nk} \tag{14.20}$$

When we modulate a sequence by α^n, $Z \leftarrow Z\alpha^{-1}$ in the Z-transform. Using this property repeatedly we note that Z-transform is the linear operator

$$X(Z)H_l(Z) \longrightarrow \boxed{\downarrow M} \longrightarrow \boxed{\uparrow M} \longrightarrow \frac{1}{M} \Sigma_{k=0}^{M-1} \; X(ZW_M^{-k}) \; H(ZW_M^{-k})$$

So we have M modulates of input being acted upon by corresponding M modulates of analysis filter.

$$Y_l(Z) = G_l(Z)\sum_{k=0}^{M-1} X(ZW_M^{-k})H_l(ZW_M^{-k}) \tag{14.21}$$

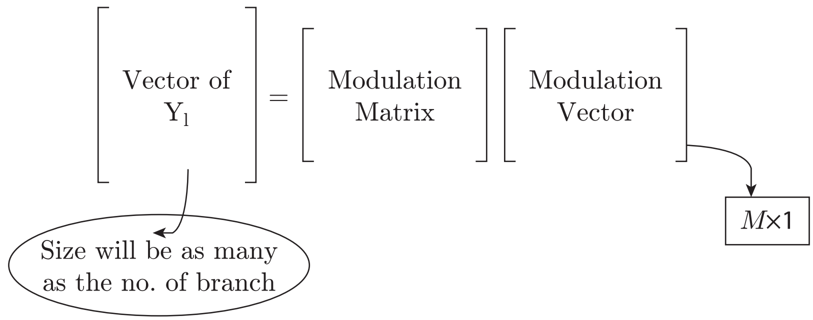

l^{th} row of modulation matrix =

$$G_l(Z)[H_l(ZW_M^{-0}).H_l(ZW_M^{-1}).H_l(ZW_M^{-2})......H_l(ZW_M^{-(M-1)})] \tag{14.22}$$

For perfect reconstruction, we first want alias cancellation.

Alias cancellation means, no contribution from $X(ZW_M^{-k})$, $k \neq 0$.

Essentially, we ask for: First column of modulation matrix is the only nonzero column. This is very stringent requirement. It is sufficient but not necessary. A more general condition is:

Sum of columns in the modulation matrix = 0 $\forall k \neq 0$.

Example: $M = 3$ and 3 channels.

$$\begin{bmatrix} G_0(Z) & 0 & 0 \\ 0 & G_1(Z) & 0 \\ 0 & 0 & G_2(Z) \end{bmatrix} = \begin{bmatrix} H_0(Z) & H_0(ZW_3^{-1}) & H_0(ZW_3^{-2}) \\ H_1(Z) & H_1(ZW_3^{-1}) & H_1(ZW_3^{-2}) \\ H_2(Z) & H_2(ZW_3^{-1}) & H_2(ZW_3^{-2}) \end{bmatrix}$$

What we need is this:

$$\sum_{l=0}^{2} G_l(Z)H_l(ZW_3^{-k}) = 0, \quad k = 1,2 \tag{14.23}$$

R

Think about: Consider the ideal 3-band 3-channel filter bank where analysis and synthesis filters are each triple band filter. So lowpass filter is ideal filter with passband from 0 to $\frac{\pi}{3}$, the middle filter is bandpass filter with passband from $\frac{\pi}{3}$ to $\frac{2\pi}{3}$ and last is ideal highpass filter with passband from $\frac{2\pi}{3}$ to π. Work out modulation terms explicitly.

Exercises

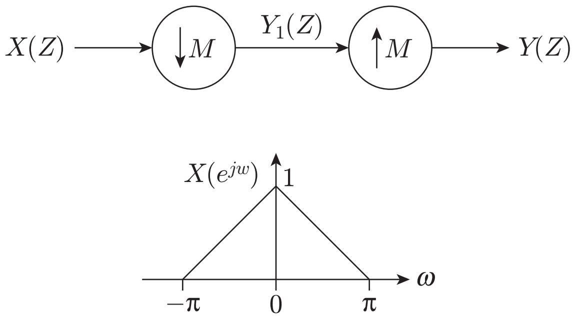

Figure 14.35 | *X(Z) for Q* 1.

Exercise 14.1

For Fig. 14.35, show that,

$$Y_1(Z) = \frac{1}{M}\sum_{k=0}^{M-1} X\left(Z^{\frac{1}{M}} e^{-j\frac{2\pi}{M}k}\right)$$

For $M = 3$, obtain the output waveform of $Y_1(Z)$ and $Y(Z)$, for the following $X(Z)$.

Hint: The down-sampling by M, followed by up-sampling by M is essentially equivalent to multiplication by a periodic sequence, $p_M[n]$, which is given as

$$\begin{aligned} p_M[n] &= 1, \quad \text{where } n \text{ is multiple of } M \\ &= 0, \quad \text{elsewhere} \end{aligned}$$

Consider one period of $p_M[n]$ restricted to 0 to $M-1$. Hence, obtain its Discrete Fourier Transform(DFT).

$$\begin{aligned} \tilde{P}_M[k] &= \sum_{n=0}^{M-1} p_M[n] e^{\frac{-j2\pi kn}{M}} \\ &= 1 \quad \text{for } k = 0 \text{ to } M-1 \end{aligned}$$

Take Inverse Discrete Fourier transform (IDFT).

$$p_M[n] = \frac{1}{M}\sum_{k=0}^{M-1} \tilde{P}_M[k] e^{\frac{j2\pi kn}{M}}$$

$$= \frac{1}{M}\sum_{k=0}^{M-1} e^{\frac{j2\pi kn}{M}}$$

Consider, $x[n]$, $y_1[n]$ and $y[n]$ has Z-transform $X(Z)$, $Y_1(Z)$ and $Y(Z)$, respectively. The translates of $X(Z)$ are shown in Fig 14.36. Hence,

$$\begin{aligned} y[n] &= x[n] \times p_M[n] \\ &= x[n]\{\frac{1}{M}\sum_{k=0}^{M-1} e^{\frac{j2\pi kn}{M}}\} \\ &= \frac{1}{M}\sum_{k=0}^{M-1} x[n](e^{\frac{j2\pi k}{M}})^n \end{aligned}$$

Using modulation property, we can obtain Z-transform of $y[n]$ as,

$$\begin{aligned} Y(Z) &= \frac{1}{M}\sum_{k=0}^{M-1} X(\frac{Z}{e^{\frac{j2\pi k}{M}}}) \\ &= \frac{1}{M}\sum_{k=0}^{M-1} X(Ze^{\frac{-j2\pi k}{M}}) \end{aligned}$$

Using noble identity for up-sampler by M, we can obtain $Y_1(Z)$ as follows,

$$\begin{aligned} Y_1(Z) &= Y(Z^{-M}) \\ &= \frac{1}{M}\sum_{k=0}^{M-1} X(Z^{-M} e^{\frac{-j2\pi k}{M}}) \end{aligned}$$

For $M = 3$, $Y(Z)$ can be obtained as,

$$\begin{aligned} Y(Z) &= \frac{1}{3}\sum_{k=0}^{2} X(Ze^{\frac{-j2\pi k}{3}}) \\ &= \frac{1}{3}\{X(Z) + X(Ze^{\frac{-j2\pi}{3}}) + X(Ze^{\frac{-j4\pi}{3}})\} \end{aligned}$$

On adding these translates, we get, $Y(Z)$, and by stretching ω-axis, we can obtain $Y_1(Z)$, as shown in Fig. 14.37.

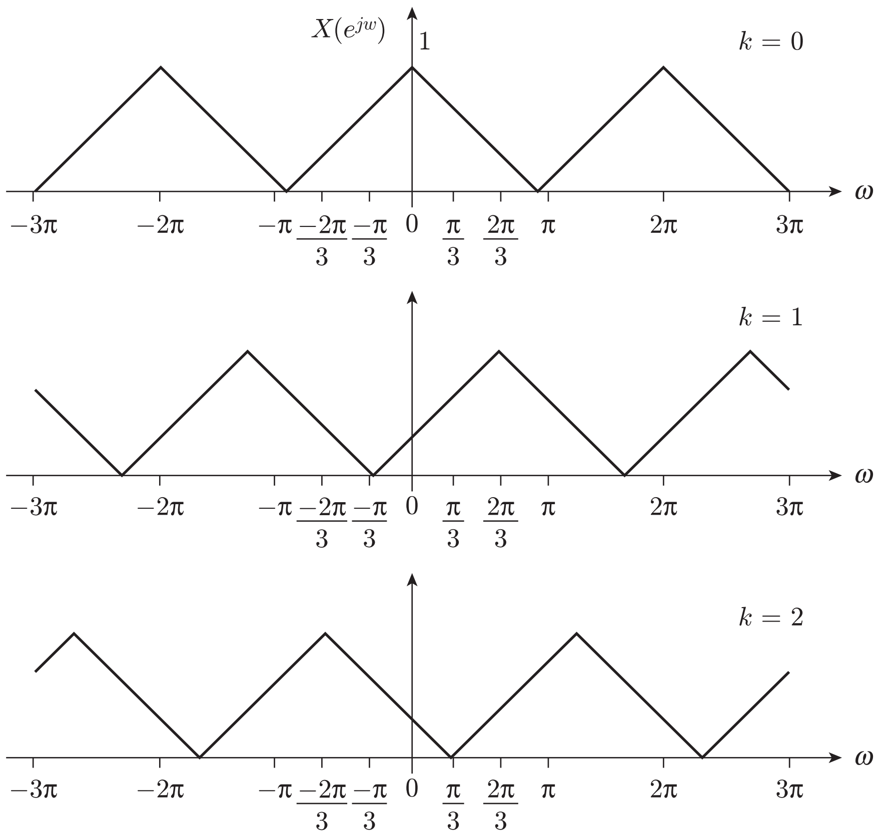

Figure 14.36 | *Translates of* $X(Ze^{\frac{-j2\pi k}{3}})$ *for* $k = 0,1,2$ *respectively*

Exercise 14.2

Find lattice coefficients k_1 and k_2 for Daubechies family length 4 filter, given that the filter coefficients are $1, \sqrt{3}, -3 + 2\sqrt{3}, \sqrt{3} - 2$.

Hint: As discussed above, the last coefficient of the filter directly reveals k_2. Hence

$$k_2 = \sqrt{3} - 2$$

We have also calculated

$$
\begin{aligned}
k_1 &= \frac{h_1 - h_2 h_3}{1 + h_3^2} \\
&= \frac{\sqrt{3} - (-3 + 2\sqrt{3})(\sqrt{3} - 2)}{1 + (\sqrt{3} - 2)^2} \\
&= \frac{\sqrt{3} - (-3\sqrt{3} + 2\sqrt{3} + 6 - 4\sqrt{3})}{1 + (3 - 4\sqrt{3} + 4)} \\
&= \frac{6\sqrt{3} - 6}{8 - 4\sqrt{3}} \\
&= \frac{3\sqrt{3} - 3}{4 - 2\sqrt{3}}
\end{aligned} \tag{14.24}
$$

The Daubechies 4 filter analysis side is shown in Fig. 14.38

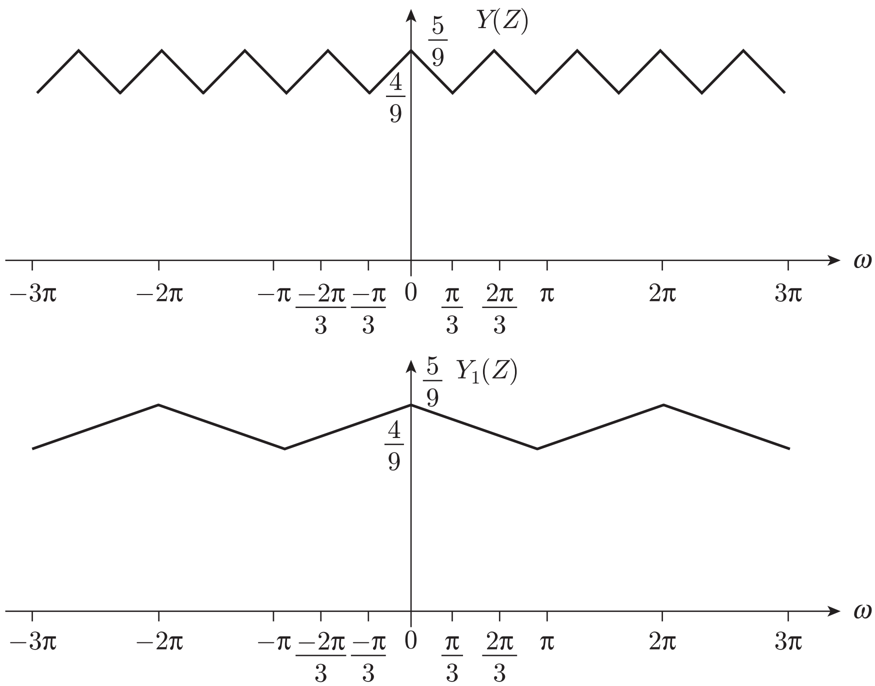

Figure 14.37 | $Y(Z)$ *and* $Y_1(Z)$

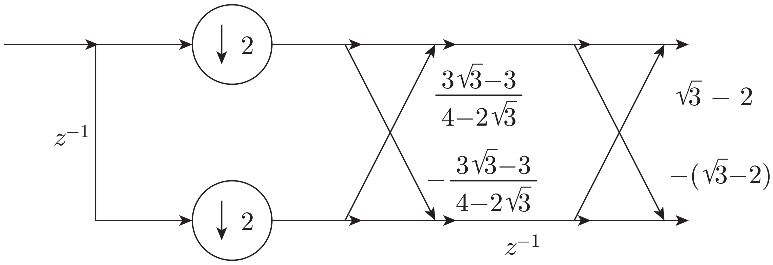

Figure 14.38 | *Daubechies 4 filter analysis lattice structure*

Exercise 14.3

Work out the recursive relations for synthesis lattice structure.

Hint: A lattice stage is after moving upsampler location prior to $H_m(z)$ is shown in Fig. 14.39. Thus, the recursive relations work out as follows

$$H_m(z) = H_{m+1}(z) - k_{m+1}\widetilde{H}_{m+1}(z) \tag{14.25}$$

$$\widetilde{H}_m(z) = z^{-2}(\widetilde{H}_{m+1}(z) + k_{m+1}H_{m+1}(z)) \tag{14.26}$$

(R) (NOTE: The readers should verify that $H_m(z)$ length indeed decreases by 2 as compared to length of $H_{m+1}(z)$ and $\widetilde{H}_{m+1}(z)$ by taking example of Daub 4 filter).

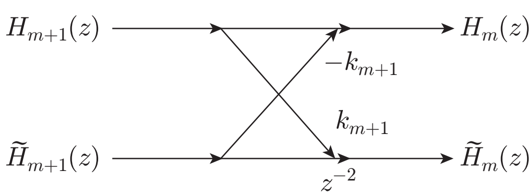

Figure 14.39 | *Synthesis lattice stage*

Chapter 15

Other Wavelet Families

15.1 | Introduction

In this book, we have predominantly used the Daubechies N wavelets, specifically Daub 1 (the Haar) and Daub 2 wavelets and few other higher order members in Daubechies family. The main reason behind illustrating with Haar was its simple form which brings out clarity in the computations. More global reason for using general Daub N scaling functions and corresponding wavelets is the inherent orthonormal nature which suits the multiresolution analysis framework. This has been the scenario till Chapter 10.

In Chapters 11 and 12 we illustrated with the splines scaling functions as examples of bases that are not orthogonal and looked at the bi-orthogonal tap structures as well.

We illustrated the splines with the linear roof (triangular) function and the quadratic B-spline. In this chapter we wish to go beyond the splines and by virtue of doing *orthogonalization* we intend to make these splines orthogonal, which are known to us as the B-spline Battle-Lemaire scaling functions and wavelets.

In fact, in this chapter we wish to expose readers to following different families of wavelets:

- Coiflets (Extended vanishing moments)
- Symlets (Nearly Symmetrical Wavelets)
- Morlets (No scaling function $\phi(.)$ only $\psi(.)$)
- Mexican Hat (belongs to derivation of gaussian wavelets)
- Mayer (Wavelet and scaling functions defined in frequency domain)
- Battle-Lemaire (Orthogonalized splines)

- Gabor wavelet
- Shannon wavelet (example of Complex Wavelets)
- Bi-orthogonal Filters

All these wavelet families have their own special characteristics and we shall bring those characteristics out systematically.

15.2 | Coiflets

In this section we present a very important set of orthonormal scaling functions and wavelets, namely, the Coiflets.

The Coiflets can be understood by its very important characteristics of vanishing higher moments for the scaling functions $\phi(.)$. In Chapter 18 while discussing interesting wavelet applications we shall demonstrate importance of the vanishing high number of moments for a wavelet $\psi(.)$ function. A wavelet function with more and more vanishing moments is important for building applications like compression, denoising, detection of discontinuities to name a few. By the admissibility condition the zeroth moment (zeroth moment m_0 is the mean value, any wavelet when integrated over its compact support produces a zero) of any wavelet always vanishes. The key lies in design of the filter to make higher moments vanish. For example, if a particular wavelet has $m_0 = m_1 = m_2 = m_3 = m_4 = 0$, then it has five vanishing moments. This indicates that up to fifth order derivative the analysis using such mother wavelet is possible and so decomposition does happen at these derivatives. As a consequence this mother wavelet does not per say “sense” these derivatives in the decomposed version of the signal and these very small values can be ignored at the time of reconstruction or synthesis of the signal. This, thus results into energy compaction thus providing compression.

Now, if we pose the question if the same rationale can be applied for the scaling function coefficients. Here, of course, we have $\int_{-\infty}^{\infty}\phi(t)dt = 1 = M_0$, so the zeroth moment of a typical scaling function does not vanish. This also has strong connection to the fact that scaling function is the ‘low pass filter’ and hence the zeroth moment will not vanish. However, we may follow up on vanishing higher moments

$$M_n = \int_{-\infty}^{\infty} t^n \phi(t)dt$$

for $n = 1, 2$, as an example.

This concept of allowing higher moments of scaling function to vanish was proposed by Prof. R. Coifman of Yale University in 1989. This idea was taken up by Dr. Ingrid Daubechies who not only very convincingly proposed solution to this intriguing problem but also came up with neat implementation scheme. She was gracious enough in constructing these wavelets and named these wavelets, after Coifman, as ‘coiflet’!

The readers may wonder what serious advantages these coiflets will have over traditional wavelets, say Daubechies family, and how these advantages are tangible in vivid applications. To understand this, let us recollect the framework of multiresolution that was introduced in Chapter 2 and has been used in subsequent chapters to explain various concepts. The framework suggests:

For function $f_j(x) \in v_j$, and for window of analysis $w_a = \dfrac{1}{2^j}$

the span of the function using the orthonormal scaling function will be *span* $\left\{2^{\frac{j}{2}}\phi(2^j x - k)\right\}$

The function can be represented as:

$$f_j(x) = \sum_k \alpha_{j,k} 2^{\frac{j}{2}} \phi(2^j x - k) \tag{15.1}$$

where, the $\alpha_{j,k}$ values are approximated values and are calculated as:

$$\alpha_{j,k} = \int_{-\infty}^{\infty} f_j(x) 2^{\frac{j}{2}} \phi(2^j x - k) \tag{15.2}$$

The zeroth moment of scaling function never vanishes, hence the emphasis is on higher order moments of the scaling function getting vanished. Here for a scaling function with $M_1 = M_2 = 0$, it is sufficient to consider only the first term $f(2^{-j}k)$ in the above formula of $\alpha_{j,k}$.

Thus, with such scaling functions, the scaling coefficients

$$\alpha_{j,k} = \int_{-\infty}^{\infty} f(t) 2^{\frac{j}{2}} \phi(2^j t - k) dt$$

can be approximated at the scale level $j = J$ by

$$\int_{-\infty}^{\infty} f(2^{-J}k) 2^{\frac{J}{2}} \phi(2^J t) dt = 2^{\frac{J}{2}} f(2^{-J}k) \int_{-\infty}^{\infty} \phi(2^J t) dt$$

$$= 2^{\frac{J}{2}} f(2^{-J}k) \int_{-\infty}^{\infty} \frac{1}{2^J} \phi(2^J t) d(2^J t),$$

$$\alpha_{J,k} \approx 2^{-\frac{J}{2}} f(2^{-J}k)(1)$$

These equations can be written as functions of some independent variable, it could be x or t or any other variable of our choice. This means that such scaling functions do not 'perceive' the second- and third-order derivatives.

Thus, as was suggested by Coifman, for a scaling function with vanishing higher moments, an advantage exists. It is for $\alpha_{J,k}$, instead of using the samples of the signal in the integral, it is sufficient to use only the fine scale coefficients $\alpha_{J,k} \approx 2^{-\frac{J}{2}} f(2^{-J}k)$ with samples at $\frac{k}{2^J}$. The consequence of this, is that we have a "close match" between the average (trend) of the signal and the signal itself. This is so, since, here the scaling coefficients are found in terms of the more refined samples $f\left(\frac{k}{2^J}, J\right)$ of the signal. Here J could be any value more than 1, and larger this value gets closer we approach the actual signal in our quest to go 'tantalizingly' close to the signal under analysis.

The Coiflet scaling functions coefficients can be produced in a closed form. For example, those for Coif1 are

$$h_0 = \frac{1 - \sqrt{7}}{16\sqrt{2}}$$

$$h_1 = \frac{5+\sqrt{7}}{16\sqrt{2}}$$

$$h_2 = \frac{14+2\sqrt{7}}{16\sqrt{2}}$$

$$h_3 = \frac{14-2\sqrt{7}}{16\sqrt{2}}$$

$$h_4 = \frac{1-\sqrt{7}}{16\sqrt{2}} \text{ and}$$

$$h_5 = \frac{3+\sqrt{7}}{16\sqrt{2}}$$

The coefficients $g_n, n = 0,1,2,...,$ for constructing the Coif1 wavelets are related to h_n of the associated scaling functions as

$$g_n = (-1)^n h_{5-n}$$

$$\psi(t) = \sum_k g_k \sqrt{2}\phi(2t-k)$$

$$g_0 = h_5$$

$$g_1 = -h_4$$

$$g_2 = h_3$$

$$g_3 = -h_2$$

$$g_4 = h_1$$

$$g_5 = -h_0$$

We have already seen in Chapters 3 and 4 the close relationship between the analysis filters to construct scaling and wavelet functions using iterative approach. The same approach can be used to construct these functions. This is depicted in Fig. 15.1.

In Coiflets, $coifN$ nomenclature is used where N is the number of vanishing moments for both scaling as well as wavelet function. Another nomenclature makes use of the filter length to refer to these filters as $3N$.

As more moments vanish, though more filter coefficients are required to be invested, it results into more regular scaling and wavelet filters. As more moments vanish they also 'perceive' more derivatives in the smoother parts of the signals thus producing better compression.

Figure 15.2 captures the analysis low and high pass filters along with Scaling $(\phi(.))$ and wavelet $(\psi(.))$ functions of $Coif5$. The Scaling $(\phi(.))$ and wavelet $(\psi(.))$ are smoother and more regular.

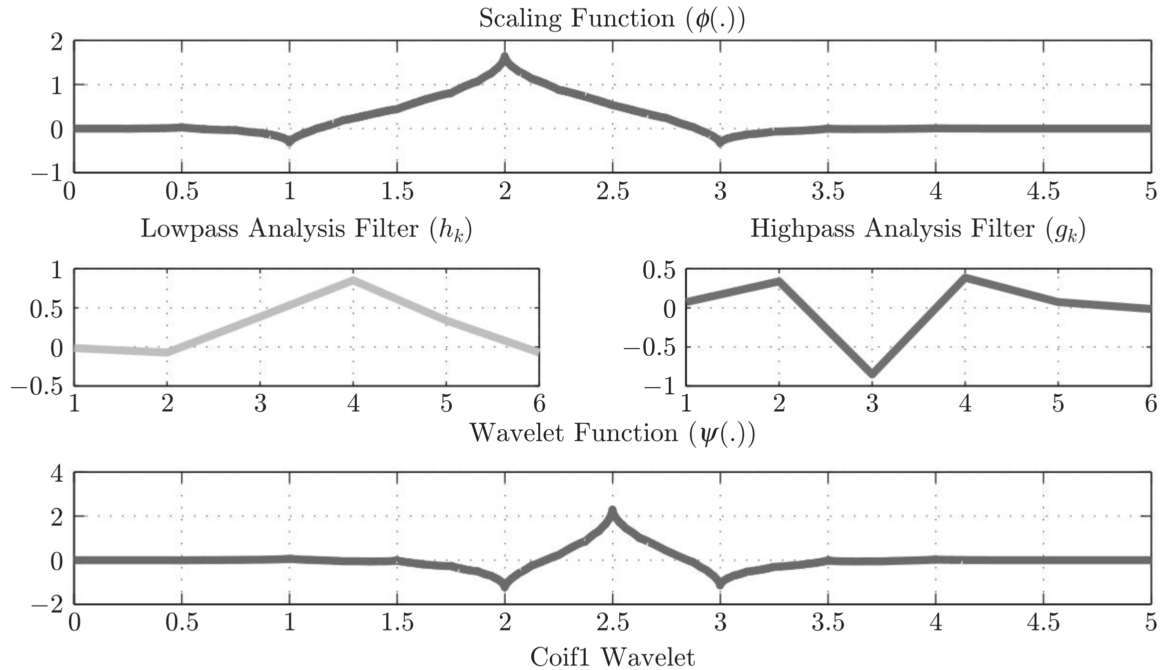

Figure 15.1 *Coif1 Wavelet. Analysis Low and High pass filters along with Sacling* (ϕ(.)) *and wavelet* (ψ(.)) *functions*

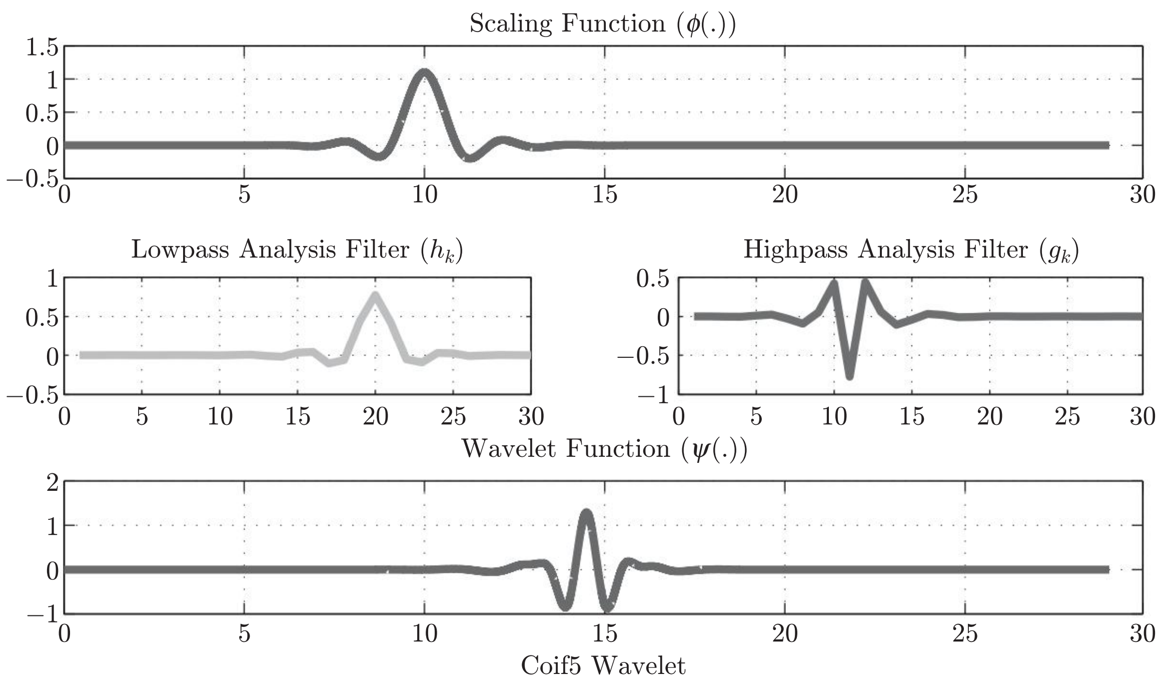

Figure 15.2 *Coif5 Wavelet. Analysis Low and High pass filters along with Sacling* (ϕ(.)) *and wavelet* (ψ(.)) *functions*

Ronald Coifman

Ronald Raphael Coifman is the Phillips Professor of Mathematics at Yale University. Coifman graduated from the University of Geneva in 1965. Coifman is a member of the American Academy of Arts and Sciences, the Connecticut Academy of Science and Engineering, and the National Academy of Sciences, Washington, USA. He is a recipient of the 1996 DARPA Sustained Excellence Award, the 1996 Connecticut Science Medal, the 1999 Pioneer Award of the International Society for Industrial and Applied Science, and the 1999 National Medal of Science.

15.2.1 Design Strategy for Coiflet Filters

We have already studied design of Daub-4 and Daub-6 filters. We used combinations of conditions coming from W_N and lowpass conditions imposed on fourier representation $H(\omega)$ of h[n]

Therefore, for filter $h = h_0, h_1 \cdots h_l$

$$\begin{aligned} &H^{(m)}(\pi) = 0 \\ &\text{where} \quad m = 0, \cdots, \frac{L-1}{2} \end{aligned} \tag{15.3}$$

Higher order helps in more and more suppression @ $\omega = \pi$ orthogonality conditions gave us

$$\sum_{k=0}^{L} h_k^2 = 1 \tag{15.4}$$

and

$$\sum_{k=2m}^{L} h_k \cdot h_{k-2m} = 0 \ , m = 1, 2, \cdots, \frac{L-1}{2}. \tag{15.5}$$

R. Coifman of yale university was also particularly interested in maximizing vanishing movements of scaling function $\phi(.)$

Dr. Ingrid Daubechies proposed solution to impose derivative conditions on $H(\omega)$, at $\omega = 0$, thus optimizing the low pass band as well.

Therefore, design focuses on constructing orthogonal filter 'h' such that

$$H^{(m)} = 0, \ m = 1, 2, \cdots$$

Now, typically binomial coefficient is defined as:

$$\binom{a}{b} = \frac{a!}{b!(a-b)!} \tag{15.6}$$

Ingrid Daubechies used in Eq. (15.6) through an interesting identity:

$$\cos^{2k}\left(\frac{\omega}{2}\right)\sum_{j=0}^{k-1}\binom{k-1+j}{j}\sin^{2j}\left(\frac{\omega}{2}\right) + \sin^{2k}\left(\frac{\omega}{2}\right)\sum_{j=0}^{k-1}\binom{k-1+j}{j}\cos^{2j}\left(\frac{\omega}{2}\right) = 1 \tag{15.7}$$

An informal proof of this identity is provided in Appendix (Chapter 19) using above identity, Let k = 1,2,... and define the 2π -periodic $H(\omega)$ as

$$H(\omega) = \sqrt{2}\cos^{2k}\left(\frac{\omega}{2}\right) \cdot \left(\sum_{j=0}^{k-1}\binom{k-1+j}{j}\sin^{2j}\left(\frac{\omega}{2}\right) + \sin^{2k}\left(\frac{\omega}{2}\right)\sum_{j=0}^{2k-1} a_l \cdot e^{jl\omega}\right) \tag{15.8}$$

then,

$H(0) = \sqrt{2}$ (orthogonal unit chosen).

$H^{(m)}(0) = 0, m = 0,1,\cdots,2k-1$

$H^{(m)}(\pi) = 0, m = 0,1,\cdots,2k-1$

also,

$|H(\omega)|^2 + |H(\omega+\pi)|^2 = 2$

The complete proof is given by Daubechies, however, we shall try and bring out only those parts which are intuitively important for signal processing.

To understand, $H^{(m)}(\pi) = 0, m = 0,1,\cdots,2k-1$

$$\cos\left(\frac{\omega}{2}\right) = \frac{e^{j\frac{\omega}{2}} + e^{-j\frac{\omega}{2}}}{2} = \frac{1}{2}e^{-j\frac{\omega}{2}}\left(e^{j\frac{\omega}{2}} + 1\right) \tag{15.9}$$

We put Eqs (15.9) in (15.8)

$$H(\omega) = \frac{\sqrt{2}}{2^{2k}e^{-jk\omega}}\left(1 + e^{j\omega}\right)^{2k} \cdot \left(\sum_{j=0}^{k-1}\binom{k-1+j}{j}\sin^{2j}\left(\frac{\omega}{2}\right) + \sin^{2k}\left(\frac{\omega}{2}\right)\sum_{j=0}^{2k-1} a_l \cdot e^{jl\omega}\right) \tag{15.10}$$

Since this equation has $(1+e^{j\omega})^{2k}$ factor, it has roof multiplicity at least 2K @ $\omega=\pi$.
Rewriting Eq. (15.10)

$$H(\omega)=\sqrt{2}+\sqrt{2}\sin^{2k}\left(\frac{\omega}{2}\right)$$
$$\cdot\left(-\sum_{j=0}^{k-1}\binom{k-1+j}{j}\sin^{2j}\left(\frac{\omega}{2}\right)+\sin^{2k}\left(\frac{\omega}{2}\right)\sum_{j=0}^{2k-1}a_l\cdot e^{jl\omega}\right) \tag{15.11}$$

again,

$$\sin\left(\frac{\omega}{2}\right)=\frac{e^{j\frac{\omega}{2}}-e^{-j\frac{\omega}{2}}}{2j}=\frac{1}{2j}e^{j\frac{\omega}{2}}\left(e^{j\frac{\omega}{2}}-1\right)=\frac{j}{2}e^{-j\frac{\omega}{2}}\left(1-e^{j\omega}\right) \tag{15.12}$$

putting Eq. (15.12) into Eq. (15.11), we get

$$H(\omega)=\sqrt{2}+\sqrt{2}\left(\frac{j}{2}\right)^{2k}e^{jk\omega}\left(1-e^{j\omega}\right)^{(2k)}$$
$$\cdot\left(-\sum_{j=0}^{k-1}\binom{k-1+j}{j}\sin^{2j}\left(\frac{\omega}{2}\right)+\sin^{2k}\left(\frac{\omega}{2}\right)\sum_{j=0}^{2k-1}a_l\cdot e^{jl\omega}\right) \tag{15.13}$$

if $\phi(\omega)=H(\omega)-\sqrt{2}$, we see

$Q(\omega)$ has $(1-e^{j\omega})^{(2k)}$ factor!

Therefore, has roof multiplicity atleast $2k$ @ $\omega=0$; $Q^{(m)}=0$, for $m = 0, 1, ..., 2k - 1$
for $m = 0$

$$Q(0) = H(0) - \sqrt{2} = 0$$

$\therefore$ $$H(0)=\sqrt{2}$$

For $m=1,\cdots\cdots,2K-1$

$$Q^{(m)}=H^{m}(w)$$

$\therefore$ $$H^{(m)}(0)=0!$$

coiflet filter for $K = 1$
from and for $K = 1$

$$\begin{aligned} H(\omega) &= \sqrt{2}\cos^2\left(\frac{\omega}{2}\right)\left(1+\sin^2\left(\frac{\omega}{2}\right)\sum_{l=0}^{1} a_l \cdot e^{jl\omega}\right) \\ &= \sqrt{2}\left(\cos^2\left(\frac{\omega}{2}\right)+\cos^2\left(\frac{\omega}{2}\cdot\right)\sin^2\left(\frac{\omega}{2}\right)\left(a_0+a_1\cdot e^{j\omega}\right)\right) \\ &= \sqrt{2}\left(\cos^2\left(\frac{\omega}{2}\right)+\frac{\sin^2(\omega)}{4}\left(a_0+a_1\cdot e^{j\omega}\right)\right) \end{aligned} \tag{15.14}$$

$$\sin(2\theta) = 2\cdot\sin(\theta)\cdot\cos(\theta)$$

$$\text{Also, } \cos^2\left(\frac{\omega}{2}\right) = \frac{1}{4}\left(e^{j\omega}+2+e^{-j\omega}\right)$$

$$\sin^2\left(\frac{\omega}{2}\right) = \frac{1}{4}\left(-e^{2j\omega}+2=e^{-2j\omega}\right)$$

we put thus in Eq. (15.14),

$$\begin{aligned} H(\omega) &= \sqrt{2}\left(\frac{1}{4}\left(e^{j\omega}+2+e^{-j\omega}\right)+\frac{1}{16}\left(-e^{2j\omega}+2-e^{-2j\omega}\right)\cdot\left(a_0+a_1\cdot e^{j\omega}\right)\right) \\ &= \frac{\sqrt{2}}{16}\left(-a_0\cdot e^{-2j\omega}+\left(4\cdot a_1\right)\cdot e^{-j\omega}+(8+2\cdot a_0)+(4+2\cdot a_1)\cdot e^{j\omega}-a_0\cdot e^{2j\omega}-a_1\cdot e^{3j\omega}\right) \end{aligned} \tag{15.15}$$

$$\boxed{\therefore h_{-2} = \frac{-\sqrt{2}\cdot a_0}{16}, h_{-1} = \frac{4-a_1}{16}, h_0 = \frac{\sqrt{2}(8+2\cdot a_0)}{16}, h_1 = \frac{\sqrt{2}(4+2\cdot a_1}{16}, h_{-2} = \frac{-\sqrt{2}\cdot a_0}{16}} \tag{15.16}$$

These filter coefficients suggest support from $[-2,3]$

Therefore, filter in non-causal,which can be made causal by introducing a delay train of two elements, in sense of convolution.

Let’s impose orthogonality conditions,

$$h_{-2}^2+h_{-1}^2+h_0^2+h_1^2+h_2^2+h_3^2 = \text{Unit} = 1(\text{say}) \tag{15.17}$$

$$h_{-2}\cdot h_0+h_{-1}\cdot h_1+h_0\cdot h_2+h_1\cdot h_3 = 0 \tag{15.18}$$

$$h_{-2}\cdot h_2+h_{-1}\cdot h_3 = 0 \tag{15.19}$$

Solving for unknown G_0 and a_1,

We get by plugin t_1 in Eqs (15.17, 15.18, and 15.19)

$$\begin{aligned} &16\cdot a_0+3\cdot a_0^2+4\cdot a_1+3\cdot a_1^2 = 16 \\ &4-4\cdot a-a_0^2-a_1^2 = 0 \\ &-4\cdot a_1+a_0^2+a_1^2 = 0 \end{aligned}$$

Simplifying we get

1. $a_0 = \frac{1}{2}\left(\sqrt{7}-1\right), a_1 = \frac{1}{2}\left(3-\sqrt{7}\right)$
2. $a_0 = \frac{-1}{2}\left(\sqrt{7}+1\right), a_1 = \frac{1}{2}\left(3+\sqrt{7}\right)$

For 1, we get the following coefficient values,

$$h_{-2} = \frac{1}{16\cdot\sqrt{2}}(1-\sqrt{7}), \qquad h_{-1} = \frac{1}{16\cdot\sqrt{2}}(5+\sqrt{7})$$

$$h_0 = \frac{1}{8\cdot\sqrt{2}}(7+\sqrt{7}), \qquad h_1 = \frac{1}{8\cdot\sqrt{2}}(7-\sqrt{7})$$

$$h_2 = \frac{1}{16\cdot\sqrt{2}}(1-\sqrt{7}), \qquad h_3 = \frac{1}{16\cdot\sqrt{2}}(-3+\sqrt{7})$$

Strategy

This strategy is exactly similar to the one we saw in finding the $h+k$ for Daub-6. This strategy imposes orthogonality and low and high pass conditions, along with flattening stop frequencies at $\omega = \pi$ by taking first and second order of derivatives of $H(\omega)$.

This gives us following equations to be solved.

$$h_{-2}^2 + h_{-1}^2 + h_0^2 + h_1^2 + h_2^2 + h_3^2 = 1$$

$$h_{-2}\cdot h_0 + h_{-1}\cdot h_1 + h_0\cdot h_2 + h_1\cdot h_3 = 0$$

$$h_{-2}\cdot h_2 + h_{-1}\cdot h_3 = 0$$

$$h_{-2} + h_{-1} + h_0 + h_1 + h_2 + h_3 = \sqrt{2}$$

$$h_{-2} - h_{-1} + h_0 - h_1 + h_2 - h_3 = 0$$

$$-2\cdot h_{-2} - h_{-1} + h_1 + 2\cdot h_2 + 3\cdot h_3 = 0$$

$$-2\cdot h_{-2} + h_{-1} - h_1 + 2\cdot h_2 - 3\cdot h_3 = 0$$

Readers are encouraged to use symbolic math toolbox of MATLAB to solve above system of equations.

Wavelet constructions for Coiflet

Since, $(2K-1)$ will always remain an odd integer, we use

$$g_k = (-1)^K h_{(2K-1)-K}$$

When $K = 1$,

$$g_k = (-1)^K h_{1-K}$$

$\therefore g_{-2}=h_3, g_{-1}=-h_2, g_0=h_1, g_1=-h_0, g_2=h_1, g_3=-h_2$ (Plug in actual values too)

Wavelet transform matrix of Coiflet filter will look like:

$$W_{12}=\begin{bmatrix} h_3 & h_2 & h_1 & h_0 & h_{-1} & h_{-2} & 0 & 0 & 0 & 0 & 0 & 0 \\ 0 & 0 & h_3 & h_2 & h_1 & h_0 & h_{-1} & h_{-2} & 0 & 0 & 0 & 0 \\ 0 & 0 & 0 & 0 & h_3 & h_2 & h_1 & h_0 & h_{-1} & h_{-2} & 0 & 0 \\ 0 & 0 & 0 & 0 & 0 & 0 & h_3 & h_2 & h_1 & h_0 & h_{-1} & h_{-2} \\ h_{-1} & h_{-2} & 0 & 0 & 0 & 0 & 0 & 0 & h_3 & h_2 & h_1 & h_0 \\ h_1 & h_0 & h_{-1} & h_{-2} & 0 & 0 & 0 & 0 & 0 & 0 & h_3 & h_2 \\ - & - & - & - & - & - & - & - & - & - & - & - \\ -h_2 & h_1 & -h_0 & h_1 & -h_2 & h_3 & 0 & 0 & 0 & 0 & 0 & 0 \\ 0 & 0 & -h_2 & -h_1 & -h_0 & h_1 & -h_2 & h_3 & 0 & 0 & 0 & 0 \\ 0 & 0 & 0 & 0 & -h_2 & h_1 & -h_0 & h_1 & -h_2 & h_3 & 0 & 0 \\ 0 & 0 & 0 & 0 & 0 & 0 & -h_2 & h_1 & -h_0 & -h_1 & -h_2 & -h_3 \\ -h_2 & h_3 & 0 & 0 & 0 & 0 & 0 & 0 & -h_2 & h_1 & -h_0 & h_1 \\ -h_0 & h_1 & -h_2 & h_3 & 0 & 0 & 0 & 0 & 0 & 0 & -h_2 & h_1 \end{bmatrix} \tag{15.20}$$

15.3 | Symlet Filters

We have already seen in Chapters 2 to 6 how Daubechies filters got evolved and from Haar which is also the first member of Daubechies family $(db-1)$ we saw filters designs of few higher members with the likes of $(db-2)$ and $(db-3)$. Daubechies filters are orthogonal filters and they have compact support which makes them a natural choice for many practical applications. We have also seen the importance of filter coefficients being even. If the scaling coefficients are represented as $h_0, h_1, ..., h_{2p-1}$, then the normalized version of it will be $\sqrt{2}\times h_0, h_1, ..., h_{2p-1}$. In chapter 4 we have also shown that by double shift of these coefficients $\sum_n \overline{h_n} h_{n-2k} = \delta_k$ the orthogonality os maintained. The Haar case is depicted by $p=1$, where filter length is 2 with only one vanishing moment. The function becomes smoother as p increases, however length of the filter also increases thus demanding more hardware to be invested. These Daubechies filters with $2p$ filter length have p vanishing moments and are orthogonal and depict compact support. These filters, however, lack symmetry for $p>1$. Haar filter are symmetric, however they have some inherent drawbacks and as we move higher in the family, the higher members lack symmetry. This is precise where 'symlets' play important role and they produce symmetric or near symmetric filters, thus producing scaling function $\phi(.)$ to be linear phase or nearly linear phase. Since these filters are 'symmetric' they are called as 'symlets'.

Example 6.2.1 – D2 Calculations from Chapter 6 depicts the complete design of the D2 filter. It derives the h_k components from B_0 and in Eq. (6.4) we have explained choice made by Daubechies to select $B_0=-2+\sqrt{3}$. This value keeps it inside the unit circle and when all the zeros are inside unit circle, such systems are called as minimum phase systems. These filters, however are very asymmetric and it can be shown that these filters have their energy concentrated close to the starting coefficients of the filter. Daubechies has shown that Haar filter is the only filter to have linear support though it belongs to the compactly supported conjugate mirror family. The 'symmlets' are obtained by selecting the B_0

value for obtaining near linear phase. The resulting $\psi(.)$ has a minimum support $[-p+1, p]$ with p vanishing moments, however they are near symmetric. The filters are depicted in Fig. 15.3.

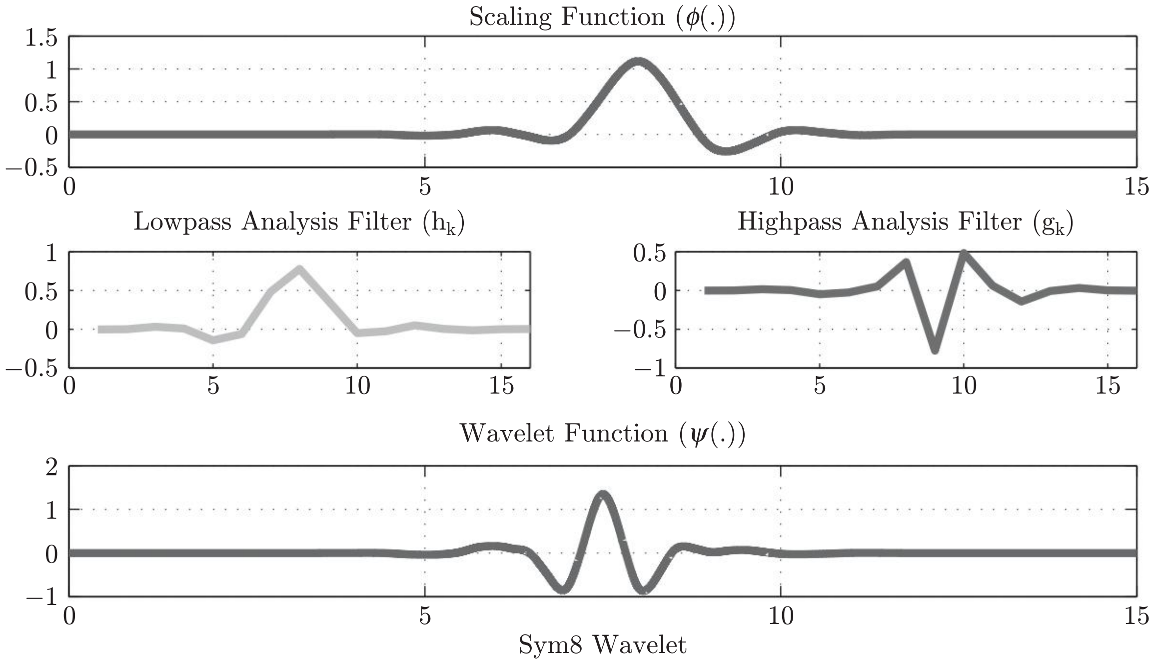

Figure 15.3 | *Symlet Wavelet (sym8). Analysis Low and High pass filters along with Sacling* $(\phi(.))$ *and wavelet* $(\psi(.))$ *functions*

Figure 15.4 has three parts. (A) shows h as analysis low pass filter, g as analysis high pass filter, rh as synthesis low pass filter and rg as synthesis high pass filter. (B) shows the magnitude response of all the four filters and (C) shows the phase response of these filters. From (C) it is clear that the 'symmlets' have near linear phase and near symmetric scaling and wavelet equations emerging out of h_k and g_k.

Following MATLAB example depicts generation of discrete wavelet kernels, which is used for different diagrams in this chapter.

Example 15.3.1 — MATLAB code: Discrete wavelet families. \\

```
%**********************************************
%**********************************************
% MATLAB code to Wavelet Families with
% examples: To be accompanied with book on
% Multiresolution and Multirate Signal Processing
% by Dr V M Gadre and Dr A S Abhyankar
```

```
%**********************************************
%**********************************************
clc; clear all; close all;

wfam='sym8'; figure(1); title('Symlet Wavelet'); [LoD,HiD,LoR,HiR]
= wfilters(wfam); subplot(3,2,3) plot(LoD,'g', 'LineWidth',3);grid
on; title('Lowpass Analysis Filter (h_{k})'); subplot(3,2,4)
plot(HiD,'r', 'LineWidth',3); grid on; title('Highpass Analysis
Filter (g_{k})');
% subplot(3,2,7)
% plot(LoR); grid on;
% title('Lowpass Synthesis Filter');
% subplot(3,2,8)
% plot(HiR); grid on;
% title('Highpass Synthesis Filter');

[phi,psi,xval] = wavefun(wfam,10);
%figure(1);
subplot(3,2,[1 2]) plot(xval,phi, 'LineWidth',3);grid on;
title('Scaling Function (\phi(.))'); subplot(3,2,[5 6])
plot(xval,psi, 'LineWidth',3);grid on;
title('Wavelet Function (\psi(.))');
```

15.4 | Morlet Filters

Jean Morlet

J. Morlet (born 13 January 1931) is French geophysicist. He is considered to be the one who invented the term 'wavelet'. In 1981 he worked with Grossman to develop what is known to us as 'wavelet transform'. He was awarded in 1997 with the Reginald Fessenden Award for his contributions in the field of wavelets.

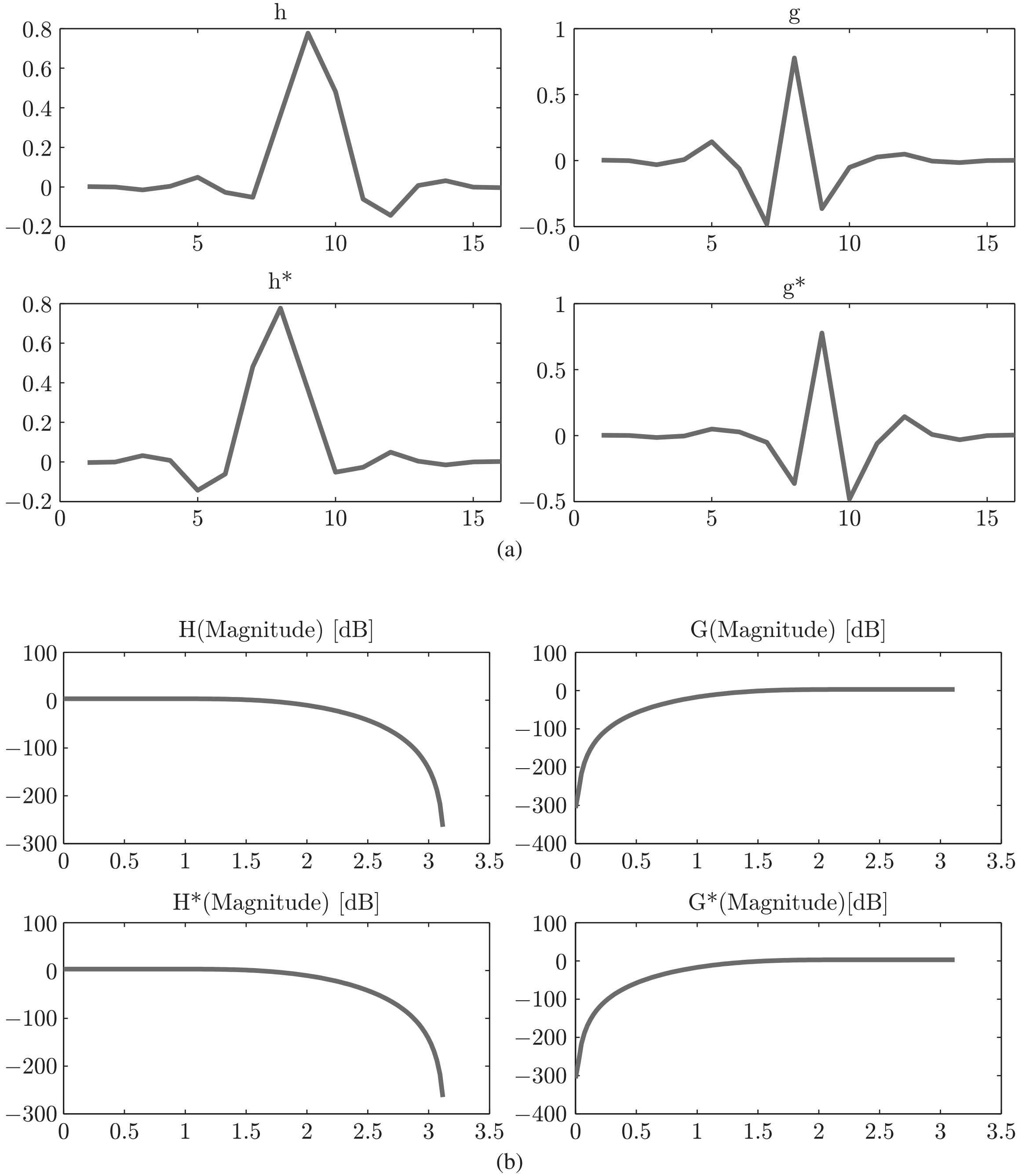

Figure 15.4 | *Symlet filters and filter responses (Continued)*

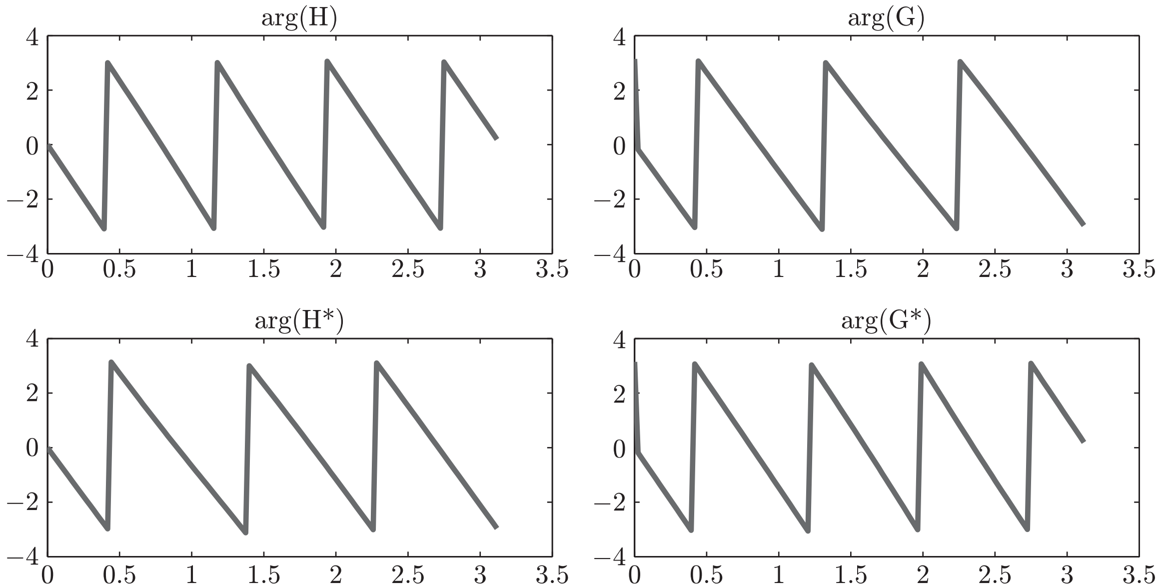

(c)

Figure 15.4 | *(Continued)*

J. Morlet for doing analysis of seismic data proposed the 'Morlet Filters' in 1983. This is a different mother basis function than what we have discussed so far. This mother wavelet does NOT have the corresponding scaling function and is a kernel meant for a typical continuous domain processing. This book emphasizes more on the Discrete Wavelet Transform (DWT) and seldom we have touched upon the Continuous Wavelet Transform (CWT). This is because the modern signal processing is predominantly digital or discrete in treating the signals for the numerous advantages of digital domain over analog, which are discussed in depths in basic texts on signal processing and hence we shall not discuss it here.

In DWT the signals are sampled and hence are discrete, thus $f \in l^2(\mathbb{Z})$ (for non-periodic signals for whom we seek transform solutions). In DWT the dilation and translation parameters are also discrete. There is no harm, thematically at least, in keeping the dilation and translation parameters continuous. If we call these parameters as a and b respectively, then the the wavelets formulae is CWT sense can be written as:

$$\psi_{a,b}(t) = \sqrt{|a|}\psi(a(t-b)), \quad a \neq 0, \; a,b \in \mathbb{R} \tag{15.21}$$

with $\psi \in \mathrm{L}^2$.

Morlet function is used in CWT analysis. This function does not have corresponding $\phi(.)$ scaling function and the $\psi(.)$ function satisfies the admissibility condition only approximately.

One way of looking at the Morlet function is it's a modulated version of the Gaussian kernel. Mathematically it is represented as: $\psi(t) = e^{i\alpha t}e^{-t^2/2}$, where the α parameter needs to be chosen carefully. This wavelet does **NOT** satisfy the condition $\hat{\psi}(0) = 0$, however for $\alpha \geq 5.5$ the conditions gets almost satisfied with negligible error.

The filters are depicted in Fig. 15.5(a).

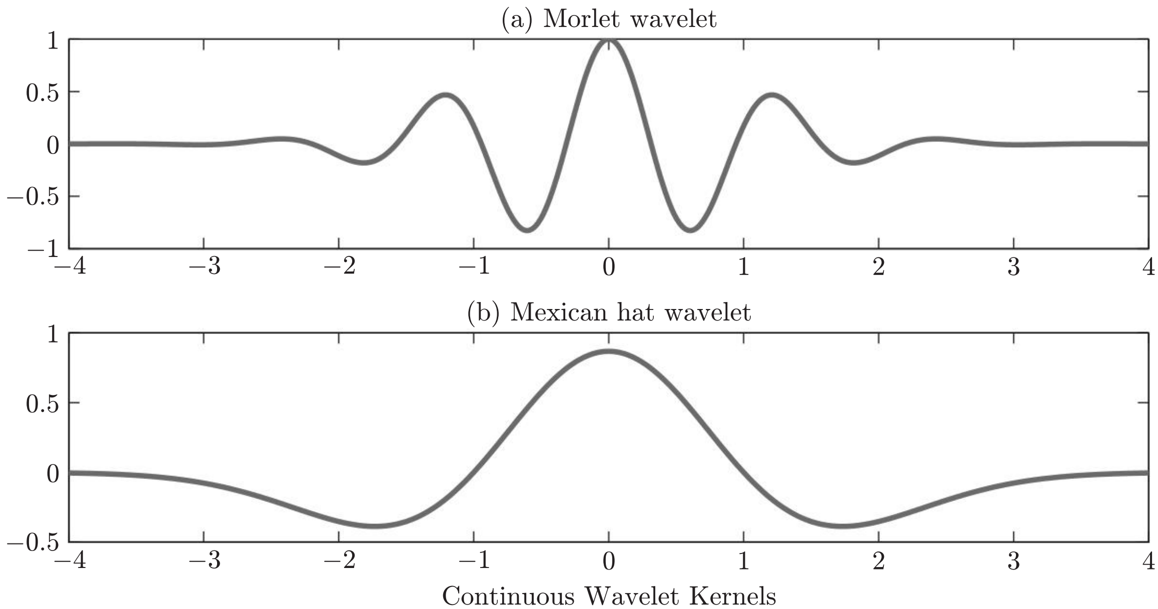

Figure 15.5 | *Continuous Wavelet Kernels. (a) depicts Morlet Wavelet and (b) depicts Mexican Hat Wavelet*

Following MATLAB example demos continuous wavelet kernels.

Example 15.4.1 — MATLAB code: Morlet and Mexican Hat Kernels. \\

```
%*********************************************
%*********************************************
% MATLAB code to Continuous Wavelet Families with
% examples: To be accompanied with book on
% Multiresolution and Multirate Signal Processing
% by Dr V M Gadre and Dr A S Abhyankar
%*********************************************
%*********************************************
clc; clear all; close all;

% Set effective support and grid parameters.
lb = -4; ub = 4; n = 1000;
```

```
% Compute and plot Morlet wavelet.
[psi,x] = morlet(lb,ub,n); figure(1); title('Continuous Wavelet
Kernels');grid on; subplot(211);grid on; plot(x,psi),
title('Morlet wavelet')


% Set effective support and grid parameters.
lb = -4; ub = 4; n = 1000;

% Compute and plot Mexican hat wavelet.
[psi,x] = mexihat(lb,ub,n); subplot(212);grid on; plot(x,psi),
title('Mexican hat wavelet')
```

15.4.1 Morlet Wavelet Design Strategy

Morlet wavelet is a kernel for CWT. CWT $W_x(b,a)$ of a continuous-time function $x(t)$ is defined as:

$$W_x(b,a) = |a|^{-\frac{1}{2}} \int_{-\infty}^{\infty} x(t) \cdot \psi^*\left(\frac{t-b}{a}\right) \cdot dt \tag{15.22}$$

Therefore, CWT is an 'inner' or 'dot' product between the signal to be analyzed $x(t)$ & scaled and translated version of mother wavelet $\psi(t)$. The 'a' scales the wavelet function and 'b' shifts or translates it.

One way of understanding CWT is to consider $\psi(t)$ to be a bandpass impulse response and then CWT becomes a bandpass analysis. This Δ change in $a := \Delta a$ will directly affect bandwidth and central frequency (first two statistical parameters) of the bandpass.

For fixed values of 'a', the transform in Eq. (15.22) becomes time-reversed and scaled wavelet function convolved with the function $x(t)$.

$$W_x(t,a) = |a|^{-\frac{1}{2}} x(t) * \psi_a(t), \psi_a(t) = \psi^*\left(\frac{-t}{a}\right) \tag{15.23}$$

Factor $|a|^{-\frac{1}{2}}$ is the normalizing factor and it makes the basis orthonormal. This ensures $\forall |a|^{-\frac{1}{2}} \psi^*\left(\frac{-t}{a}\right)$ with a $\in$ IR the energy remains same. For wavelet transform,while doing effective representations of signal $x(t)$, it is important to ensure perfect reconstruction from the representations.

Mathematically,

$$C_{\psi} = \int_{-\infty}^{\infty} \frac{|\Psi(\omega)|^2}{|\omega|} \cdot d\omega < \infty \tag{15.24}$$

where,

$$\psi(t) \xrightarrow{F.T} \Psi(\omega)$$

To Satisfy Eq. (15.24)

$$\Psi(0) = \int_{-\infty}^{\infty} \psi(t) \cdot dt = 0 \tag{15.25}$$

This is known to us as 'admissibility condition' of wavelet $\psi(t)$. The $|\Psi(\omega)|$ must decrease rapidly for $|\omega| \to 0$ approaching $|\omega| \to \infty$. Therefore, $\psi(t)$ must have bandpass impulse response, which results into a small wave or a compactly supported 'wavelet'.

One example of such type of wave is complex Morlet wavelet, which is nothing else but a plane wave modulated by a Gaussian envelope.

$$\psi(t) = e^{i\alpha t} \cdot e^{-\frac{t^2}{2}} \tag{15.26}$$

Here, parameter 'α' is the wavenumber associated with Morlet wavelet. 'α' is connected with the number of oscillations of morlet mother wavelet.

The Fourier transform of Eq. (15.26) will be,

$$\hat{\psi}(\Omega) = \sqrt{2\pi} \cdot e^{-\frac{1}{2}(2\pi\Omega - \alpha)^2} \tag{15.27}$$

For admissibility condition to get fulfilled at $\Omega = 0$,

Eq. (15.27) should be '0'.

It is easy to see, however, that Eq. (15.27) doesn't satisfy admissibility condition of wavelet.

$\therefore$ The zeroth moment doesn't vanish!.

In order to make this a wavelet, we enforce the admissibility condition by setting

$$\widehat{\psi}(\Omega = 0) = 0 \tag{15.28}$$

If we evaluate Eq. (15.27) at $\Omega = 0$, then it gives an additional factor of $e^{-\frac{\alpha^2}{2}}$ because of which the admissibility is not met.

To compensate for the same, Eq. (15.27) can be modified as follows:

$$\hat{\psi}(\Omega) = \sqrt{2\pi} \left[e^{-\frac{1}{2}(2\pi\Omega - \alpha)^2} - e^{-\frac{1}{2}\alpha^2} \cdot e^{-\frac{1}{2}(2\pi\Omega)^2} \right] \tag{15.29}$$

Factor to contract admissibility

When above Eq. (15.29) is evaluated at $\Omega = 0$, it gives us

$$\widehat{\psi}(\Omega)|_{\Omega=0} = \sqrt{2\pi}\left[e^{\frac{-\alpha^2}{2}} - e^{\frac{-\alpha^2}{2}} \cdot e^0\right] = 0 \tag{15.30}$$

The correction factor of $e^{-\frac{\alpha^2}{2}}$ is important and also modifies the representation in time domain accordingly. The Morlet wavelet adjusted for admissibility thus becomes,

$$\psi(t) = \left(e^{i\alpha t} - e^{\frac{-\alpha^2}{2}}\right) \cdot e^{\frac{-t^2}{2}} \tag{15.31}$$

The admissibility is achieved as in Fourier domain (Eq. (15.29)) the correction decrease rapidly as we move away from $\Omega = 0$ point on Ω-axis.

For the wavelet to have compact support at given dilation 'a', it's frequency gets centered at: $\Omega = \dfrac{\Omega_\psi}{2\pi a}$,

where

$$\Omega_\psi = \frac{\int_0^\infty \Omega\,|\hat{\psi}(\Omega)|\cdot d\Omega}{\int_0^\infty |\hat{\psi}(\Omega)|\cdot d\Omega} \tag{15.32}$$

For Complex Morlet, center frequency is controlled by 'α'.

$$\therefore \qquad \Omega_\psi = \alpha \tag{15.33}$$

Following MATLAB example depicts creation of the Morlet kernel.

Example 15.4.2 — MATLAB code: Morlet Kernel calculation. \\

```
%***********************************************
%***********************************************
% MATLAB code to understand Morlet Wavelet
% To be accompanied with book on
% Multiresolution and Multirate Signal Processing
% by Dr V M Gadre and Dr A S Abhyankar
%***********************************************
%***********************************************

clc; clear all; close all; N=16;
```

```
a=0.1329; %Normalization factor
alpha = 6; % The alpha value should be > 5.55
k = [1:N/2-1]; k = [0 k -N/2 -fliplr(k)]; delta = 1/N;
fk = k/N/delta; % frequency spread
k = fk;
k = a*k; % scaling using dilation parameter 'a'
fmo =
sqrt(2*pi)*(exp(-(2*pi*k-alpha).^2/2)-exp(-alpha^2/2)*exp(-(2*pi*k).^2/2));
fmo = sqrt(a)*fmo; % denormalization of scales

x = [-N/2:N/2 - 1]*(1/N); % x-axis spread
xs = x/a; % scaling using dilation parameter 'a'
mo = ( exp(i*alpha*xs) - exp(-alpha^2/2) ) .* exp(-xs.^2/2);
mo = (1/sqrt(a))*mo; % denormalization of scales
figure(1);title('Morlet wavelet'); grid on; plot(xs,mo)
```

The outcome of the code above is shown in Fig. 15.6.

15.5 | Mexican Hat Filters

This basis function is used in CWT analysis just like Morlet basis. Though the function and it's Fourier transform do not have compact support in strict sense, the wavelet function satisfies the admissibility condition (unlike Morlet) and has two vanishing moments associated with it. The Mexican Har wavelet filter is depicted in Fig. 15.5(b).

This function in its appearance looks like a 'Mexican Hat' and hence has been named likewise. The Mexican hat basis function is derived from Gaussian function and in fact is second order derivative of $e^{\frac{-t^2}{2}}$.

The wavelet has mathematical form as follows:

$$\psi(t) = (t^2 - 1)e^{\frac{-1}{2}t^2} \tag{15.34}$$

The Fourier transform of Eq. (15.34) will be

$$\psi(\omega) = (i\omega)^2 F(e^{-t^2/2}) = -\omega^2 e^{\frac{-\omega^2}{2}} \tag{15.35}$$

From Eqs. (15.34) and (15.35) it can be observed that neither the wavelet function nor its Fourier representation has compact support. Good news, however is, they both decay rapidly outside finite width. If Eq. (15.35) is evaluated at $\omega = 0$, it becomes 0, which ensures that this wavelet basis follows admissibility condition. We encourage the readers to solve the zeroth and first moments and confirm that they both vanish for Mexican Hat Wavelet function.

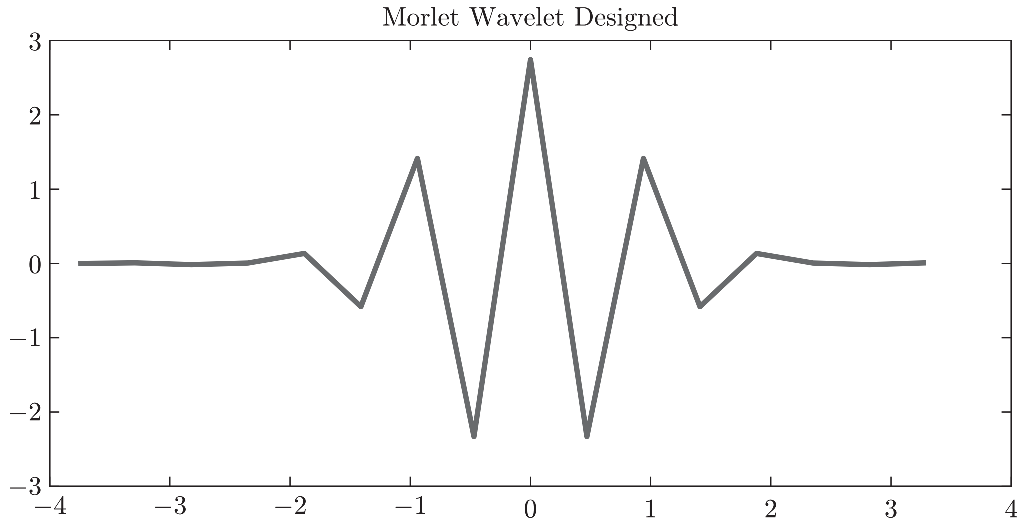

Figure 15.6 | *Designed Morlet Wavelet*

15.6 | Meyer Filters

Yves Meyer

Y. Meyer (born 19 July 1939) is French mathematician and scientist. He along with Mallat gave the framework of multiresolution analysis. The wavelet constructed by him are named after his as 'Meyer Wavelet filters'. He is currently Professor Emeritus at the Ecole Normale Superieure de Cachan and has won many prestigious awards like 2010 Gauss award.

Yves Meyer was able to construct smooth orthogonal wavelet basis using the design strategy in Fourier domain.He was able to come with neat representation of Fourier transform ($\hat{\phi}(\omega)$) of scaling function ($\phi(t)$) as:

$$\hat{\phi}(\omega) = \begin{cases} 1 & \text{if } |\omega| \le \frac{2}{3}\pi \\ \cos\left[\frac{\pi}{2} x \left(\frac{3}{4\pi} \,|\, \omega \,|\, -1\right)\right] & \text{if } \frac{2}{3}\pi \le |\omega| \le \frac{4}{3}\pi \\ 0 & \text{otherwise} \end{cases} \tag{15.36}$$

Where $x(\cdot)$ is a smooth function and

$$x(t) = \begin{cases} 0, & \text{if } t \le 0 \\ 1, & \text{if } t \ge 1 \end{cases} \tag{15.37}$$

With another property

$$x(t) + x(1-t) = 1 \tag{15.38}$$

In Chapters 2 to 6,we have understood that in orthogonal filters, $\psi(\cdot)$ can be calculated from $\phi(\cdot)$. Therefore, Fourier representation of ψ will be,

$$\begin{aligned} \psi(\omega) &= e^{\frac{i\omega}{2}} \sum_{l \in Z} \phi(\omega + 2\pi(2l+1)) \cdot \phi\left(\frac{\omega}{2}\right) \\ &= e^{\frac{i\omega}{2}} \left[\phi(\omega + 2\pi) + \phi(\omega - 2\pi)\right] \cdot \phi\left(\frac{\omega}{2}\right) \end{aligned} \tag{15.39}$$

Inverse of Eq. (15.39) gives us $\psi(t)$, as Eq. (15.39) is compactly supported.

The filters are depicted in Fig. 15.7.

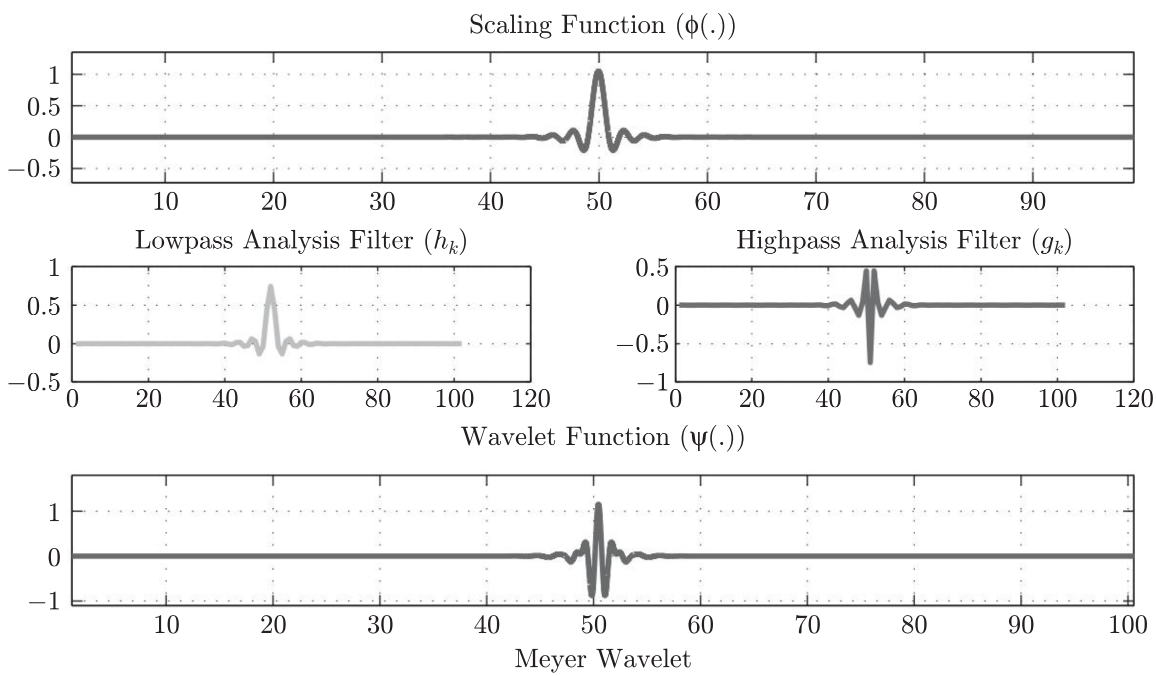

Figure 15.7 | *Meyer's Wavelet. Analysis Low and High pass filters along with Scaling $(\phi(.))$ and wavelet $(\psi(.))$ functions*

15.7 | Battle-Lemarie Wavelets – Orthogonalization of the B-Splines

We have already seen the roof scaling function in Chapter 12, which is a special case of an important family of scaling functions, namely, the B-splines. In Chapter 12 we have mentioned that the roof function is a linear spline, which can be constructed as a self convolution of the gate function (spline of degree zero). In general, the Rth convolution $(p_a \star \ldots^{R} \star p_a(t)$ of the gate function $p_a(t)$ is a B-spline of degree $R+1$, and it is written as $\phi_{R+1}(a(R+1),t), -(R+1)a \le t \le (R+1)a$. It is identically zero outside this interval and provides, what we are seeking, a compact support. So, the roof function is $\phi_2(2a,t), -2a \le t \le 2a$, and the gate function $p_a(t)$ is $\phi_1(a,t), -a < t < a$. The roof function is defined on the four subintervals: $(-\infty,-2a],[-2a,0],[0,2a]$, and $[2a,\infty)$. We also note that at the boundary points $t=-2a,0$, and $2a$ between these four subintervals, the first derivative has a jump discontinuity. These points are called the *knots* of this B-spline. It turned out that $\phi_{R+1}(a(R+1),t)$ is defined on $R+2$ subintervals with continuous derivatives up to the order $R-1$ at the knots. In the case of the roof function with $R=1$, only the zeroth derivative, i.e., the function itself is continuous.

Another example of the quadratic B-spline could be $\phi_3\left(\frac{3}{2},t\right)$, as the three times self convolution of the gate function or the haar scaling function $p_{\frac{1}{2}}(t)$ with $a=\frac{1}{2}$,

$$\phi_3\left(\frac{3}{2},t\right)=\begin{cases}\frac{1}{2}\left(t+\frac{3}{2}\right)^2, & -\frac{3}{2}\le t\le -\frac{1}{2}\\ \frac{3}{4}-t^2, & -\frac{1}{2}\le t\le \frac{1}{2}\\ \frac{1}{2}\left(t-\frac{3}{2}\right)^2, \frac{1}{2}\left(t-\frac{3}{2}\right)^2, & \frac{1}{2}\le t\le \frac{3}{2}\\ 0, & \text{otherwise}\end{cases}$$

This $\phi_3\left(\frac{3}{2},t\right)$ appears to be a smooth function, and as if it is a Gaussian like function. If we, however take its first order derivative we can easily see the sharp corners at the four knots $t=-\frac{3}{2},-\frac{1}{2},\frac{1}{2}$, and $\frac{3}{2}$.

$$\frac{d\phi_3}{dt}=\begin{cases}t+\frac{3}{2}, & -\frac{3}{2}\le t\le -\frac{1}{2}\\ -2t, & -\frac{1}{2}\le t\le \frac{1}{2}\\ t-\frac{3}{2}, & \frac{1}{2}\le t\le \frac{3}{2}\\ 0, & \text{otherwise}\end{cases}$$

Differentiating again (i.e. the second order derivative of the original function), we see the jump discontinuities of its second derivative at these four knots.

$$\frac{d^2\phi_3}{dt^2} = \begin{cases} 1, & -\frac{3}{2} \le t \le -\frac{1}{2} \\ -2, & -\frac{1}{2} \le t \le \frac{1}{2} \\ 1, & \frac{1}{2} \le t \le \frac{3}{2} \\ 0, & \text{otherwise} \end{cases}$$

Note the symmetry of $\phi_3\left(\frac{3}{2},t\right)$ around the origin with its knots at $-\frac{3}{2},-\frac{1}{2},\frac{1}{2}$, and $\frac{3}{2}$.

As it is the case with the roof function, it is a usual practice that we translate the spline function such that the knots fall at integer multiples. In this case we translate (shift) $\phi_3\left(\frac{3}{2},t\right)$ to the right by $t_0 = \frac{1}{2}$ to have

$$\phi_3\left(\frac{3}{2},t-\frac{1}{2}\right) = \begin{cases} \frac{1}{2}(t+1), & -1 \le t \le 0 \\ \frac{3}{4}(t-\frac{1}{2})^2, & 0 \le t \le 1 \\ \frac{1}{2}(t-2)^2, & 1 \le t \le 2 \\ 0, & \text{otherwise} \end{cases}$$

From the convolution theorem we get,

$$\mathcal{F}\left\{\phi_3\left(\frac{3}{2},t\right)\right\} = \left[\frac{\sin\frac{\lambda}{2}}{\frac{\lambda}{2}}\right]^2,$$

and with the translation property of the Fourier transform, we have

$$\Phi_3(\lambda) = \mathcal{F}\left\{\phi_3\left(\frac{3}{2},t-1\right)\right\} = e^{-\frac{i\lambda}{2}}\left[\frac{\sin\frac{\lambda}{2}}{\frac{\lambda}{2}}\right]^2$$

In Chapter 12 we showed that the roof function (B-spline of degree 1) satisfies the scaling equation with scaling coefficients $h_0 = \frac{1}{2}, h_1 = 1, h_2 = \frac{1}{2}$. Here, we can do the same verification for $\phi_3\left(\frac{3}{2},t-\frac{1}{2}\right)$ with its four non-vanishing scaling coefficients $h_0 = \frac{1}{4}, h_1 = \frac{3}{4}, h_2 = \frac{3}{4}$ and $h_3 = \frac{1}{4}$. We leave this part to readers for further investigation and confirmations of the details mentioned above.

15.7.1 Battle-Lemarie Design Details

In Chapter 12 we have shown that the B-splines make good scaling functions, with their important property of compact support. Yet, as we had illustrated for the roof function, they are not orthogonal with respect to their translation by integers. Simplest way to understand this is when we translate the function by factor of 1 and take the dot product with the original function, it does NOT produce zero. Thus, they can not comply with the usual multiresolution analysis (MRA) framework, where the orthogonality is at the core. The design question is can they be made orthogonal. This brings us to the (orthogonal) Battle-Lemarie scaling functions that are constructed using the B-splines.

While such new scaling functions are orthogonal with respect to translations by integers (including the shift by 1), they on the other hand, lose on account of having a compact support. The final result of the method for modifying the B-spline is to become the Battle-Lemarie (orthogonal) scaling functions.

This modification method relies heavily on the Fourier transform of $\Phi_{R+1}(\omega)$ of the $\phi_{R+1}(t)$ -B-spline, and the sum of the squares of its translates by $2\pi k, \sum_k |\Phi_{R+1}(\omega + 2\pi k)|^2$. The method starts by modifying the $\Phi_{R+1}(\omega)$ to $\tilde{\Phi}_{R+1}(\omega)$ as,

$$\tilde{\Phi}_{R+1}(\omega) = \Phi_{R+1}(w)\left[2\pi \sum_k |\Phi_{R+1}(\omega_2 \pi k)|^2\right]^{-\frac{1}{2}} \tag{15.40}$$

Then it is important to find the inverse Fourier transform of $\tilde{\Phi}_{R+1}(w)$ as $\tilde{\phi}_{R+1}(t)$, which is the desired orthogonal Battle-Lemarie scaling function.

As an example from Ten lectures by Daubechies, with the Fourier transform $\Phi_2(\omega)$ of the linear B-spline in Eq. (15.40), it is found that:

$$2\pi \sum_k |\Phi_2(\omega + 2\pi k)|^2 = \frac{2}{3} + \frac{1}{3}\cos\omega = \frac{1}{3}(1 + 2\cos^2\frac{\omega}{2}) \tag{15.41}$$

That gives us,

$$\tilde{\Phi}_2(\omega) = \sqrt{3}(2\pi)^{-\frac{1}{2}} \frac{4\sin^2\frac{\lambda}{2}}{\lambda^2\left[1 + 2\cos^2\frac{\lambda}{2}\right]^{\frac{1}{2}}} \tag{15.42}$$

What remains is to find $\tilde{\phi}_2(t)$, the inverse Fourier transform of this $\tilde{\Phi}_2(\omega)$. This works for having an orthogonal Battle-Lemarie scaling function. The next design quest is to find its scaling coefficients, more over their relation to coefficients of constructing the associated wavelet. The interested readers can divulge deeper into this and this certainly forms a very good topic to research on.

The filters are depicted in Fig. 15.8.

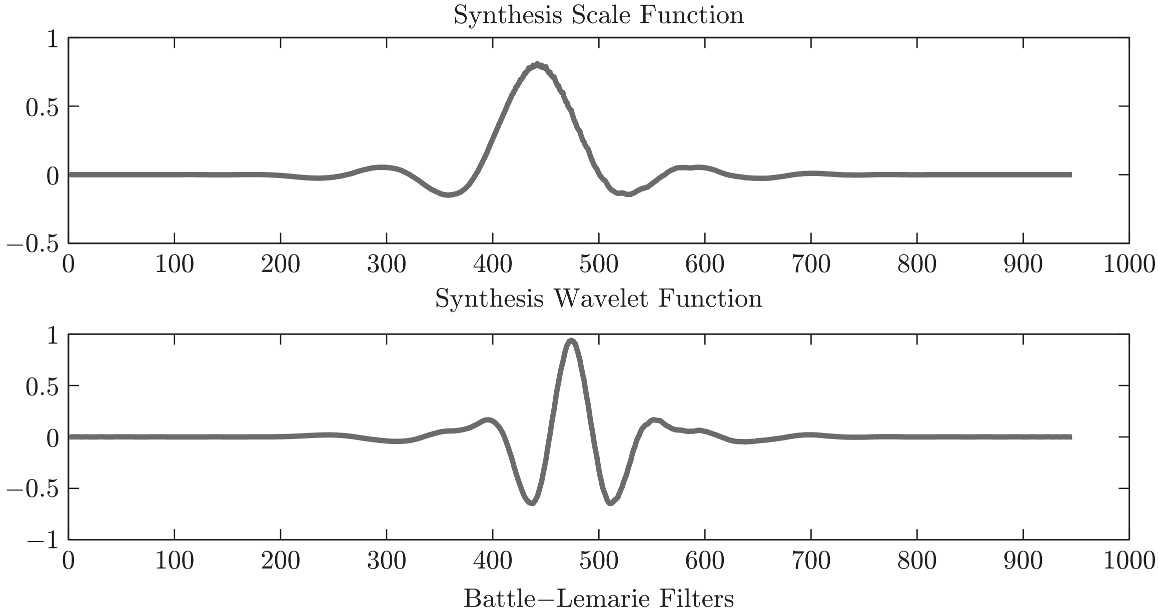

Figure 15.8 | *Battle-Lemarie Wavelet. Synthesis Sacling* $(\phi(.))$ *and wavelet* $(\psi(.))$ *functions*

15.8 | Gabor Filters

Gabor wavelets were invented by Denis Gabor. They are well known for their ability to capture oriented information from the signal or image to be analyzed. This salient feature makes them more useful in analysis of oriented images like fingerprint images. $2D$ Gabor kernel can be looked upon as Gaussian kernel function modulated by sinusoidals (sin and cos waves).

The formulae for Gabor filters in $2D$ sense is given as:

$$G_c[i,j] = C_1 e^{\frac{-(i^2+j^2)}{2\sigma^2}} \cos(2\pi f(i\cos\theta + j\sin\theta)) \tag{15.43}$$

$$G_s[i,j] = C_2 e^{\frac{-(i^2+j^2)}{2\sigma^2}} \sin(2\pi f(i\cos\theta + j\sin\theta)) \tag{15.44}$$

Where, C_1 and C_2 are used for normalization. Variation in θ helps an engineer in analyzing the oriented information in a particular direction.

15.9 | Shannon Filters

Shannon wavelet is also called an ‘Sinc’ wavelet.

Its Fourier transform $H(\omega)$ is:

$$H(\omega)=\begin{cases}\sqrt{2}, |\omega| \le \dfrac{\pi}{2} \\ 0, |\omega| > \dfrac{\pi}{2}\end{cases} \tag{15.45}$$

This is nothing else but an ideal low pass filter!

This leads the solution to normalizing factor of $\sqrt{2\pi}$

e.g. if

$$C(\omega)=\begin{cases}1, |\omega| \le \dfrac{\pi}{2} \\ 0, |\omega| > \dfrac{\pi}{2}\end{cases} \quad \text{and} \quad \phi(\omega)=\begin{cases}1, |\omega| \le \pi \\ 0, |\omega| > \pi\end{cases} \tag{15.46}$$

Then, dilation equation $\phi(2\omega)=c(\omega)\cdot\phi(\omega)$ gets satisfied.

In time domain,

$$\psi(t)=\sum_K g_k \cdot \psi(2t-K) \tag{15.47}$$

If $g_0 = 1$ and $g_{2K}=0$

and
$$g_{2K+1}=(-1)^K \frac{2}{(2K+1)\pi}$$

then,

$$\psi(t)=\sqrt{2\pi}\cdot\frac{\sin(\pi t)}{\pi t} \tag{15.48}$$

Since Eq. (15.45) is normalized, it's time domain representation will be

$$h(t)=\frac{\sin(\pi t)}{\pi t} \tag{15.49}$$

This is sinc form of solution, Therefore, this filter is also called sinc wavelet.

The filter coefficients will be (normalized),

$$h_0=\frac{1}{\sqrt{2}}, h_{2n}=0, n \ne 0$$

$$h_{2n+1} = \frac{(-1)^n \sqrt{2}}{(2n+1)\pi}$$

Wavelet function gets derived from corresponding high pass filter

$$G(\omega) = \begin{cases} \sqrt{2}, |\omega| \geq \dfrac{\pi}{2} \\ 0, |\omega| < \dfrac{\pi}{2} \end{cases} \tag{15.50}$$

Therefore, filter coefficients will be,

$$g_0 = \frac{1}{\sqrt{2}}, g_{2n} = 0, n \neq 0$$

$$g_{2n+1} = \frac{(-1)^{n+1} \sqrt{2}}{(2n+1)\pi}$$

This gives us

$$\boxed{\psi(t) = 2h(2t) - h(t) = \frac{\sin(2\pi t) - \sin(\pi t)}{\pi t}} \tag{15.51}$$

The filters are depicted in Fig. 15.9.

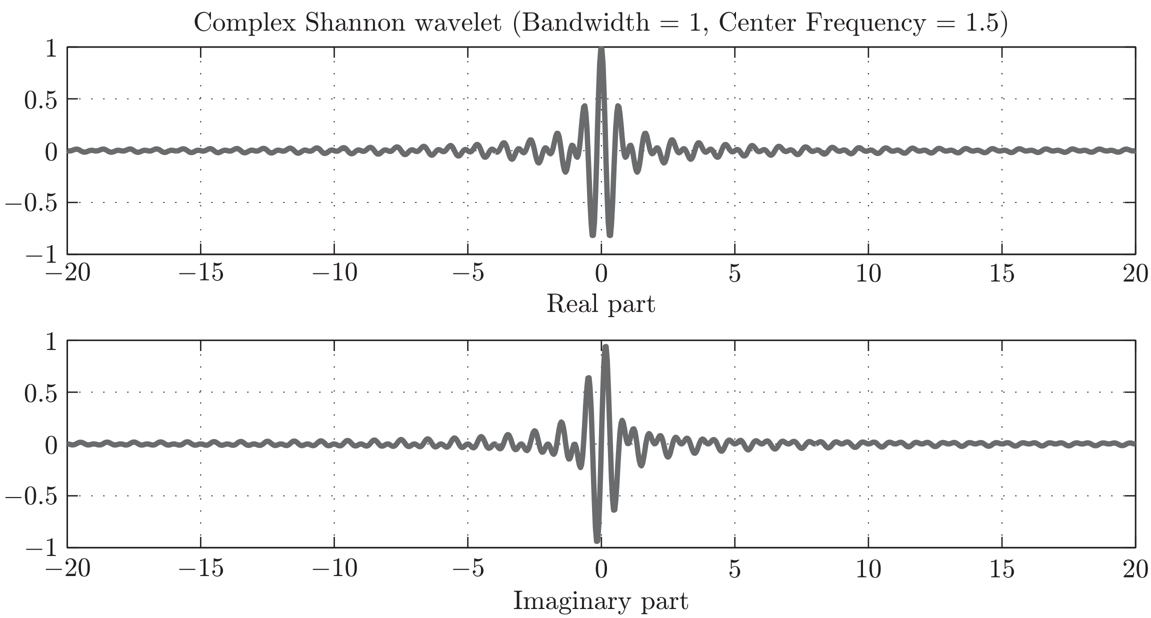

Figure 15.9 *Shannon wavelet. Analysis low and high pass filters along with Scaling ($\phi(.)$) and wavelet ($\psi(.)$) functions*

15.10 | Bi-orthogonal Filters

The design strategy could be as under.

Haar filter is the only finite length, symmetric, orthogonal filter whose Fourier representation [$H(\omega)$] satisfies zero derivative conditions at $\omega = \pi$, as was explained by Daubechies.

Researchers across the globe have confirmed that having symmetric filters is advantageous in multiple ways for many real life applications.

Another important characteristics of filters is orthogonality. It guarantees energy preservation and inverse of wavelet transform matrix. For orthogonal filter 'h' that gives orthogonal transform matrix W_N, the implementation is straight forward. This is because W_N is 'unitary' which guarantees that for all real valued W_N, $W_N^{-1} = W_N^T$. This simple transpose gives us the inverse,which is very crucial in inverse calculations as as 'separable' multidimensional calculations.

For 'non-orthogonal' filters, however, one strategy to build the system we desire could be to ensure that inverse of transform matrix is transpose of another transformation matrix.

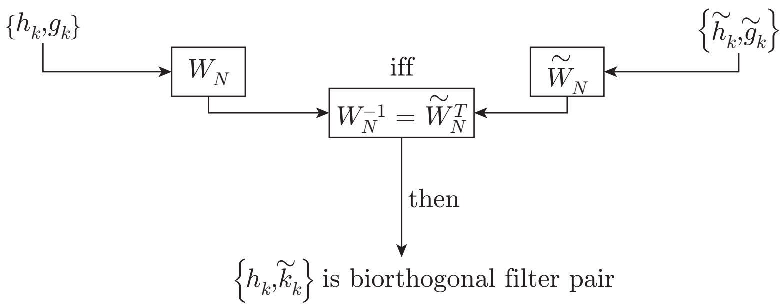

Haar, though orthogonal, finite length and symmetric, has its own drawback the we have already brought out. Going beyond filter length of '2',we shall give up 'orthogonality' as requirement coming as filter constraint.

Let us try constructing $\frac{5}{3}$ normalized tap:

Design problem:

1. From symmetric h_k and g_k
2. Construct wavelet transform W_N
3. When inverse W_N^{-1} is calculated.
4. W_N^{-1} should also be a transform matrix!
5. Find such $\tilde{g}_k$ and $\tilde{h}_k$ (symmetric)!

Let 'H_B' be $\frac{N}{2} \times N$ matrix from h_k.

Let 'G_B' be $\frac{N}{2} \times N$ matrix from g_k.

Let '$\widetilde{G}_B$' be $\frac{N}{2} \times N$ matrix from $\tilde{g}_k$.

Let '$\widetilde{H}_B$' be $\frac{N}{2} \times N$ matrix from $\tilde{h}_k$.

Forward wavelet matrix can be written as:

$$W_B = \begin{bmatrix} H_B \\ G_B \end{bmatrix}$$

For synthesis part, similarly,

$$\widetilde{W}_B = \begin{bmatrix} \widetilde{H}_B \\ \widetilde{G}_B \end{bmatrix}$$

keeping in mind,we want to create dual filters in semi-orthogonal sense,

$$W_B \cdot \widetilde{W}_B^T = I_{N\times N} \tag{15.52}$$

Now, $W_B \cdot \widetilde{W}_B^T = \begin{bmatrix} H_B \\ G_B \end{bmatrix} \cdot \begin{bmatrix} \widetilde{H}_B^T & \widetilde{G}_B^T \end{bmatrix} = \begin{bmatrix} H_B \cdot \widetilde{H}_B^T & H_B \cdot \widetilde{G}_B^T \\ G_B \cdot \widetilde{H}_B^T & G_B \cdot \widetilde{G}_B^T \end{bmatrix}$

Here,

$$\begin{gathered} H_B \cdot \widetilde{H}_B^T = G_B \cdot \widetilde{G}_B^T = I_{N\times N} \\ H_B \cdot \widetilde{G}_B^T = G_B \cdot \widetilde{H}_B^T = 0_{N\times N} \end{gathered} \tag{15.53}$$

Now, $h_k = \{h_{-2}, h_{-1}, h_0, h_1, h_2\}$ and $\tilde{h}_k = \{\tilde{h}_{-1}, \tilde{h}_0, \tilde{h}_1\}$ in the spirit of $\frac{5}{3}$ tap.

$\therefore$ Analysis low pass filter has 5 coefficients and Synthesis low pass filter has 3 coefficients as '5' is bigger of them,

Let $\frac{N}{2} = 5,\ \therefore N = 10$

$$\therefore H_B = \begin{bmatrix} h_0 & h_1 & h_2 & 0 & 0 & 0 & 0 & 0 & h_{-2} & h_{-1} \\ h_{-2} & h_{-1} & h_0 & h_1 & h_2 & 0 & 0 & 0 & 0 & 0 \\ 0 & 0 & h_{-2} & h_{-1} & h_0 & h_1 & h_2 & 0 & 0 & 0 \\ 0 & 0 & 0 & 0 & h_{-2} & h_{-1} & h_0 & h_1 & h_2 & 0 \\ h_2 & 0 & 0 & 0 & 0 & 0 & h_{-2} & h_{-1} & h_0 & h_1 \end{bmatrix}$$

$$\widetilde{H}_B = \begin{bmatrix} \tilde{h}_0 & \tilde{h}_1 & 0 & 0 & 0 & 0 & 0 & 0 & 0 & \tilde{h}_{-1} \\ 0 & \tilde{h}_{-1} & \tilde{h}_0 & \tilde{h}_1 & 0 & 0 & 0 & 0 & 0 & 0 \\ 0 & 0 & 0 & \tilde{h}_{-1} & \tilde{h}_0 & \tilde{h}_1 & 0 & 0 & 0 & 0 \\ 0 & 0 & 0 & 0 & 0 & \tilde{h}_{-1} & \tilde{h}_0 & \tilde{h}_1 & 0 & 0 \\ 0 & 0 & 0 & 0 & 0 & 0 & 0 & \tilde{h}_{-1} & \tilde{h}_0 & \tilde{h}_1 \end{bmatrix}$$

Now, $H_B \cdot \widetilde{H}_B^T = I_{5\times5}$

$$\begin{bmatrix} h_0 & h_1 & h_2 & 0 & 0 & 0 & 0 & 0 & h_{-2} & h_{-1} \\ h_{-2} & h_{-1} & h_0 & h_1 & h_2 & 0 & 0 & 0 & 0 & 0 \\ 0 & 0 & h_{-2} & h_{-1} & h_0 & h_1 & h_2 & 0 & 0 & 0 \\ 0 & 0 & 0 & 0 & h_{-2} & h_{-1} & h_0 & h_1 & h_2 & 0 \\ h_2 & 0 & 0 & 0 & 0 & 0 & h_{-2} & h_{-1} & h_0 & h_1 \end{bmatrix} \cdot \begin{bmatrix} \tilde{h}_0 & 0 & 0 & 0 & 0 \\ \tilde{h}_1 & \tilde{h}_{-1} & 0 & 0 & 0 \\ 0 & \tilde{h}_0 & 0 & 0 & 0 \\ 0 & \tilde{h}_1 & \tilde{h}_{-1} & 0 & 0 \\ 0 & 0 & \tilde{h}_0 & 0 & 0 \\ 0 & 0 & \tilde{h}_1 & \tilde{h}_{-1} & 0 \\ 0 & 0 & 0 & \tilde{h}_0 & 0 \\ 0 & 0 & 0 & \tilde{h}_1 & \tilde{h}_{-1} \\ 0 & 0 & 0 & 0 & \tilde{h}_0 \\ \tilde{h}_{-1} & 0 & 0 & 0 & \tilde{h}_1 \end{bmatrix} = I_{5\times5}$$

1^{st} *row* $\times$ 1^{st} *column*, 1^{st} *row* $\times$ 2^{nd} *column* and 1^{st} *row* $\times$ *last column* will give us three equations,

$$h_0 \cdot \tilde{h}_0 + h_1 \cdot \tilde{h}_1 + h_{-1} \cdot \tilde{h}_{-1} = 1 \tag{15.54}$$

$$h_0 \cdot \tilde{h}_1 + h_2 \cdot \tilde{h}_0 = 0 \tag{15.55}$$

$$h_{-2} \cdot \tilde{h}_0 + h_{-1} \cdot \tilde{h}_1 = 0 \tag{15.56}$$

Equation (15.54) can be written as,

$$\sum_{K=-1}^{1} h_k \cdot \tilde{h}_k = 1 \tag{15.57}$$

Equation (15.55) and (15.56) can be written as,

$$\sum_{K=-1}^{1} h_{k-2m} \cdot \tilde{h}_k = 0, m = -1, 1 \tag{15.58}$$

Similarly, $G_B \cdot \widetilde{G}_B^T = I_{5\times5}$
Here,

$$g_k = \{g_{-1}, g_0, g_1\} \text{ and } \tilde{g}_k = \{g_{-2}, g_{-1}, g_0, g_1, g_2\}$$

Therefore, analysis high pass filter has '3' coefficients,
synthesis high pass filter has '5' coefficients

$$\frac{N}{2} = 5, \ \therefore N = 10$$

$$G_B = \begin{bmatrix} g_0 & g_1 & 0 & 0 & 0 & 0 & 0 & 0 & 0 & g_{-1} \\ 0 & g_{-1} & g_0 & g_1 & 0 & 0 & 0 & 0 & 0 & 0 \\ 0 & 0 & 0 & g_{-1} & g_0 & g_1 & 0 & 0 & 0 & 0 \\ 0 & 0 & 0 & 0 & 0 & g_{-1} & g_0 & g_1 & 0 & 0 \\ 0 & 0 & 0 & 0 & 0 & 0 & 0 & g_{-1} & g_0 & g_1 \end{bmatrix}$$

$$\widetilde{G}_B = \begin{bmatrix} \tilde{g}_0 & \tilde{g}_1 & \tilde{g}_2 & 0 & 0 & 0 & 0 & 0 & \tilde{g}_{-2} & \tilde{g}_{-1} \\ \tilde{g}_{-2} & \tilde{g}_{-1} & \tilde{g}_0 & \tilde{g}_1 & \tilde{g}_2 & 0 & 0 & 0 & 0 & 0 \\ 0 & 0 & \tilde{g}_{-2} & \tilde{g}_{-1} & \tilde{g}_0 & \tilde{g}_1 & \tilde{g}_2 & 0 & 0 & 0 \\ 0 & 0 & 0 & 0 & \tilde{g}_{-2} & \tilde{g}_{-1} & \tilde{g}_0 & \tilde{g}_1 & \tilde{g}_2 & 0 \\ \tilde{g}_2 & 0 & 0 & 0 & 0 & 0 & \tilde{g}_{-2} & \tilde{g}_{-1} & \tilde{g}_0 & \tilde{g}_1 \end{bmatrix}$$

Now, $G_B \cdot \widetilde{G}_B^T = I_{5\times 5}$

$$\begin{bmatrix} g_0 & g_1 & 0 & 0 & 0 & 0 & 0 & 0 & 0 & g_{-1} \\ 0 & g_{-1} & g_0 & g_1 & 0 & 0 & 0 & 0 & 0 & 0 \\ 0 & 0 & 0 & g_{-1} & g_0 & g_1 & 0 & 0 & 0 & 0 \\ 0 & 0 & 0 & 0 & 0 & g_{-1} & g_0 & g_1 & 0 & 0 \\ 0 & 0 & 0 & 0 & 0 & 0 & 0 & g_{-1} & g_0 & g_1 \end{bmatrix} \cdot$$

$$\begin{bmatrix} \tilde{g}_0 & \tilde{g}_{-2} & 0 & 0 & \tilde{g}_2 \\ \tilde{g}_1 & \tilde{g}_{-1} & 0 & 0 & 0 \\ \tilde{g}_2 & \tilde{g}_0 & \tilde{g}_{-2} & 0 & 0 \\ 0 & \tilde{g}_1 & \tilde{g}_{-1} & 0 & 0 \\ 0 & \tilde{g}_2 & \tilde{g}_0 & \tilde{g}_{-2} & 0 \\ 0 & 0 & \tilde{g}_1 & \tilde{g}_{-1} & 0 \\ 0 & 0 & \tilde{g}_2 & \tilde{g}_0 & \tilde{g}_{-2} \\ 0 & 0 & 0 & \tilde{g}_1 & \tilde{g}_{-1} \\ \tilde{g}_2 & 0 & 0 & \tilde{g}_2 & \tilde{g}_0 \\ \tilde{g}_{-1} & 0 & 0 & 0 & \tilde{g}_1 \end{bmatrix} = I_{5\times 5}$$

$$g_0 \cdot \tilde{g}_0 + g_1 \cdot \tilde{g}_1 + g_- \cdot \tilde{g}_{-1} = 1 \tag{15.59}$$

$$g_0 \cdot \tilde{g}_{-2} + g_1 \cdot \tilde{g}_{-1} = 0 \tag{15.60}$$

$$g_0 \cdot \tilde{g}_2 + g_{-1} \cdot \tilde{g}_1 = 0 \tag{15.61}$$

Therefore, equation (15.59) get written as:

$$\sum_{K=-1}^{1} g_k \cdot \tilde{g}_k = 1 \tag{15.62}$$

Equations (15.60) and (15.61) becomes

$$\sum_{K=-1}^{1} g_{K-2m} \cdot \tilde{g}_k = 0, m = -1,1 \tag{15.63}$$

Now, Design aspect demands $H_B \cdot \widetilde{H}_B^T$ to be an identity matrix which demands h_k and $\tilde{h}_k$ to be orthogonal.

For two filters to be orthogonal, let us derive the sufficient & necessary condition with again an example of Haar wavelet.

For Haar, if

$$h_k = \{h_0, h_1\} = \sqrt{2}\left\{\frac{1}{2}, \frac{1}{2}\right\}$$

$$\therefore \qquad H(\omega) = \sqrt{2}\left(\frac{1}{2} + \frac{1}{2} \cdot e^{j\omega}\right) = \sqrt{2} \cdot e^{\frac{j\omega}{2}} \cdot \cos\left(\frac{\omega}{2}\right)$$

$\therefore \ |H(\omega)| = \sqrt{2} \cdot \cos\left(\frac{\omega}{2}\right) \cdots$ (Note: Magnitude of $e^{j\omega} = 1$ on interval of $[-\pi, \pi]$)

We have already seen that when $H(z)$ becomes $H(-z)$, the frequency band gets shifted by π amount, which can be represented as: $H(\omega + \pi)$

$$\therefore \qquad |H(\omega + \pi)| = \sqrt{2} \cdot \cos\left(\frac{\omega + \pi}{2}\right)$$

Now, if we add squared magnitudes of $H(\omega)$ and $H(\omega + \pi)$, we get

$$|H(\omega)|^2 = 2 \cdot \cos^2\left(\frac{\omega}{2}\right) \tag{15.64}$$

$$|H(\omega + \pi)^2 = \left(\sqrt{2}\cos\left(\frac{\omega + \pi}{2}\right)\right)^2 = 2 \cdot \cos^2\left(\frac{\omega + \pi}{2}\right)$$

$$\therefore \qquad |H(\omega + \pi)| = 2 \cdot \sin^2\left(\frac{\omega}{2}\right) \tag{15.65}$$

Using Eqs. (15.64) and (15.65),

$$\therefore \qquad |H(\omega)^2| + |H(\omega + \pi)^2| = 2 \cdot \cos^2\left(\frac{\omega}{2}\right) + 2 \cdot \sin^2\left(\frac{\omega}{2}\right) \tag{15.66}$$

This ‘2’ also comes as we are using normalized filters, in absence of normalization, the sum would be ‘1’.

Important thing to note is, a constant suggest orthogonality.

Using Eqs. (15.66) and (15.52), we can write

$$\overline{H(\omega)} \cdot \widetilde{H}(\omega) + \overline{H(\omega+\pi)} \cdot \widetilde{H}(\omega+\pi) = 2 \tag{15.67}$$

When $H(\omega)$ and $(\tilde{\omega})$ satisfy Eq. (15.67), we have,

$$\sum_{K \in Z} h_k \cdot \tilde{h}_k = 1 \tag{15.68}$$

For $m \in Z, m \neq 0$,

$$\sum_{K \in Z} h_{K-2m} \cdot \tilde{h}_k = 0 \tag{15.69}$$

Similarly,

$$\overline{G(\omega)} \cdot \widetilde{G}(\omega) + \overline{G(\omega+\pi)} \cdot \widetilde{G}(\omega+\pi) = 2 \tag{15.70}$$

When $H(\omega)$ and $(\tilde{\omega})$ satisfy Eq. (15.67), we have,

$$\sum_{K \in Z} g_k \cdot \tilde{g}_k = 1 \tag{15.71}$$

For $m \in Z, m \neq 0$,

$$\sum_{K \in Z} g_{K-2m} \cdot \tilde{g}_k = 0 \tag{15.72}$$

To ensure $H_B \cdot \widetilde{G}_B^T = 0$

$$\overline{H(\omega)} \cdot \widetilde{G}(\omega) + \overline{H(\omega+\pi)} \cdot \widetilde{G}(\omega+\pi) = 0 \tag{15.73}$$

for all $m \in z$,

$$\sum_{K \in Z} h_{K-2m} \cdot \widetilde{g}_k = 0 \tag{15.74}$$

To ensure, $G_B \cdot \widetilde{H}_B^T = 0$

$$\overline{G(\omega)} \cdot \widetilde{H}(\omega) + \overline{G(\omega+\pi)} \cdot \widetilde{H}(\omega+\pi) = 0 \tag{15.75}$$

For all $m \in Z$

$$\sum_{K \in Z} g_{K-sm} \cdot \widetilde{h}_k = 0 \tag{15.76}$$

Equations (15.67) to (15.76) give us definition for bi-orthogonal filter pairs. e.g. If $H(\omega)$ and $\widetilde{H(\omega)}$ of h_k and $\tilde{h}_k$ respectively follow:

$$H(\omega)\cdot\widetilde{H}(\omega)+\overline{H(\omega+\pi)}\cdot\widetilde{H}(\omega+\pi)=2$$

Then, h_k and $\tilde{h}_k$ are called bi-orthogonal filter pair!
From Eqs. (15.67), (15.70), (15.73) and (15.75)

$G(\omega)=e^{i(n\omega+b}\cdot\overline{\widetilde{H}(\omega+\pi)}$ [Analysis high pass connected with synthesis low pass] and

$\widetilde{G}(\omega)=e^{i(n\omega+b}\cdot\overline{H(\omega+\pi)}$ [Synthesis high pass connected with analysis low pass]

Let's confirm this by pluggin in

$$\begin{aligned}\overline{G(\omega)}\cdot\widetilde{G}(\omega) &= \overline{e^{j(n\omega)+b}\cdot\overline{\widetilde{H}(\omega+\pi)}}\cdot e^{j(n\omega+b)}\cdot\overline{H(\omega+\pi)}\\ &= e^{-j(n\omega+b)}\cdot\widetilde{H}(\omega+\pi)\cdot e^{j(n\omega+b)}\cdot\overline{H(\omega+\pi)}\\ &= \overline{H(\omega+\pi)}\cdot\widetilde{H}(\omega+\pi)\end{aligned}\tag{15.77}$$

Since they are equal, together they shall produce '2'!
By replacing 'ω' with '$\omega+\pi$' in Eq. (15.77)

$$\overline{G(\omega+\pi)}\cdot\widetilde{G}(\omega+\pi)=\widetilde{H}(\omega)\cdot\overline{H(\omega)}\quad [Astheseare`2\pi-periodic'\ functions.\therefore\ \overline{\omega+2\pi}=\overline{\omega}]\tag{15.78}$$

Adding Eqs. (15.77) and (15.78),

$$\overline{G(\omega)}\cdot\widetilde{G}(\omega)+\overline{G(\omega+\pi)}\cdot\widetilde{G}(\omega+\pi)=\overline{H(\omega)}\cdot\widetilde{H}(\omega)+\overline{H(\omega+\pi)}\cdot\widetilde{H}(\omega+\pi)=2$$

Now,

$$\begin{aligned}\widetilde{H}(\omega)\cdot\overline{G(\omega)} &= \widetilde{H}(\omega)\cdot\overline{e^{j(n\omega+b)}\cdot\overline{\widetilde{H}(\omega+\pi)}}\\ &= \widetilde{H}(\omega)\cdot e^{-j(n\omega+b)}\cdot\widetilde{H}(\omega+\pi)\end{aligned}\tag{15.79}$$

Let's replace 'ω' by '$\omega+\pi$' in Eq. (15.79)

$$\begin{aligned}\widetilde{H}(\omega+\pi)\cdot\overline{G(\omega+\pi)} &= \widetilde{H}(\omega+\pi)\cdot e^{-j(n\omega+n\pi+b)}\cdot\widetilde{H}(\omega+2\pi)\\ &= \widetilde{H}(\omega+\pi)\cdot e^{-jn\pi}\cdot e^{-j(n\omega+b)}\cdot\widetilde{H}(\omega)\\ &= (-1)^n\cdot\widetilde{H}(\omega+\pi)\cdot e^{-j(n\omega+b)}\cdot\widetilde{H}(\omega)\\ &= -\widetilde{H}(\omega+\pi)\cdot e^{-}j(n\omega+b)\cdot\tilde{(\omega)}\cdots\cdots[`n`\text{ being odd, }(-1)^n=-1]\end{aligned}\tag{15.80}$$

Adding Eqs. (15.79) and (15.80),

$$\widetilde{H}(\omega)\cdot\overline{G(\omega)}+\widetilde{H}(\omega+\pi)\cdot\overline{G(\omega+\pi)}=0$$

It should be noted that, g_k is connected with $\tilde{h}_k$ and $\tilde{g}_k$ is connected with h_k !
b can be '0' or π to keep filter real values and for $n = 1$,

$$g_k = (-1)^K \cdot \tilde{h}_{1-K} \tag{15.81}$$

$$\widetilde{g_k} = (-1)^K \cdot h_{1-K} \tag{15.82}$$

Let's confirm this for normalized $\frac{5}{3}$ tap.

$$h = \{h_{-2}, h_{-1}, h_0, h_1, h_2\} = \left\{-\frac{1}{2}, 1, \frac{3}{4}, -\frac{1}{2}, \frac{1}{4}\right\} \cdot \sqrt{2} \tag{15.83}$$

and

$$\tilde{h} = \{\tilde{h}_{-1}, \tilde{h}_0, \tilde{h}_1\} = \left\{\frac{1}{4}, \frac{1}{2}, \frac{1}{4}\right\} \cdot \sqrt{2} \tag{15.84}$$

Plugging Eqs. (15.82) and (15.83) in (15.80) and (15.81), we get,

$$\begin{aligned} \tilde{g} &= \{\tilde{g}_{-1}, \tilde{g}_0, \tilde{g}_1, \tilde{g}_2, \tilde{g}_3\} \\ &= \{h_2, h_1, -h_0, h_{-1}, h_{-2}\} \\ &= \left\{-\frac{1}{4}, -\frac{1}{2}, -\frac{3}{4}, 1, \frac{1}{2}\right\} \cdot \sqrt{2} \end{aligned} \tag{15.85}$$

Similarly,

$$\begin{aligned} \tilde{g} &= \{g_0, g_1, g_2\} \\ &= \{\tilde{h}_1, -\tilde{h}_0, \tilde{h}_{-1}\} \quad = \left\{\frac{1}{4}, -\frac{1}{2}, \frac{1}{4}\right\} \cdot \sqrt{2} \end{aligned} \tag{15.86}$$

Let's approve these filters:

$$H(\omega) = -\frac{\sqrt{2}}{2} \cdot e^{-2j\omega} + \sqrt{2} \cdot e^{-j\omega} + \frac{3\sqrt{2}}{4} - \frac{\sqrt{2}}{2} \cdot e^{j\omega} + \frac{\sqrt{2}}{4} \cdot e^{2j\omega} \tag{15.87}$$

$$\widetilde{H}(\omega) = \frac{\sqrt{2}}{4} \cdot e^{-j\omega} + \frac{\sqrt{2}}{2} + \frac{\sqrt{2}}{4} \cdot e^{j\omega} \tag{15.88}$$

Let's evaluate Eqs. (15.87) and (15.88), for $\omega = 0$ and $\omega = \pi$

$$H(\omega)|_{\omega=0} = \sqrt{2}\left(-\frac{1}{2} + 1 + \frac{3}{4} - \frac{1}{2} + \frac{1}{4}\right) = \sqrt{2}$$

$$H(\omega)|_{\omega=\pi} = 0$$

Similarly,

$$\widetilde{H}(\omega)\,|_{\omega=0} = \sqrt{2} \text{ and } \widetilde{H}(\omega)\,|_{\omega=\pi} = 0$$

Conjugating $H(\omega)$ we get,

$$\overline{H(\omega)} = \frac{\sqrt{2}}{4}\cdot e^{-2j\omega} - \frac{\sqrt{2}}{2}\cdot e^{-j\omega} + \frac{3\sqrt{2}}{4} + \sqrt{2}\cdot e^{j\omega} - \frac{\sqrt{2}}{2}\cdot e^{2j\omega}$$

$$\begin{aligned}\therefore \widetilde{H}(\omega)\cdot\overline{H\omega} &= \left(\frac{\sqrt{2}}{4}\cdot e^{-j\omega} + \frac{\sqrt{2}}{2} + \frac{\sqrt{2}}{4}\cdot e^{j\omega}\right)\times\left(\frac{\sqrt{2}}{4}\cdot e^{-2j\omega} - \frac{\sqrt{2}}{2}\cdot e^{-j\omega} + \frac{3\sqrt{2}}{4} + \sqrt{2}\cdot e^{j\omega} - \frac{\sqrt{2}}{2}\cdot e^{2j\omega}\right)\\ &= \frac{1}{8}\cdot e^{-3j\omega} + 1 + \frac{9}{8}\cdot e^{j\omega} - \frac{1}{4}\cdot e^{3j\omega}\end{aligned} \tag{15.89}$$

Replacing 'ω' by '$\omega+\pi$' in Eq. (15.89)

$$\begin{aligned}&\widetilde{H}(\omega+\pi)\cdot\overline{H(\omega+\pi)}\\ &= \frac{1}{8}\cdot e^{-3j(\omega+\pi)} + 1 + \frac{9}{8}\cdot e^{j(\omega+\pi)} - \frac{1}{4}\cdot e^{3j(\omega+\pi)}\\ &= \frac{1}{8}\cdot e^{-3j\omega}\cdot e^{-3j\pi} + 1 + \frac{9}{8}\cdot e^{j\omega}\cdot e^{j\pi} - \frac{1}{4}\cdot e^{3j\omega}\cdot e^{3j\pi}\end{aligned}$$

Note, $e^{3j\pi} = e^{-3j\pi} = e^{j\pi} = e^{-j\pi} = -1$ (Euler's identity)

$$\therefore \qquad \widetilde{H}(\omega+\pi)\cdot\overline{H(\omega+\pi)} = -\frac{1}{8}\cdot e^{-3j\omega} + 1 - \frac{9}{8}\cdot e^{j\omega} + \frac{1}{4}\cdot e^{3j\omega} \tag{15.90}$$

Now let's create wavelet transormation matrix for bio-orthogonal $\frac{5}{3}$ tap let's call it $\omega_{\frac{5}{3}}$

$$\omega_{\frac{5}{3}} = \begin{bmatrix} h_0 & h_1 & h_2 & 0 & 0 & 0 & h_{-2} & h_{-1} \\ h_{-2} & h_{-1} & h_0 & h_1 & h_2 & 0 & 0 & 0 \\ 0 & 0 & h_{-2} & h_{-1} & h_0 & h_1 & h_2 & 0 \\ h_2 & 0 & 0 & 0 & h_{-2} & h_{-1} & h_0 & h_1 \\ - & - & - & - & - & - & - & - \\ g_0 & g_1 & g_2 & 0 & 0 & 0 & 0 & 0 \\ 0 & 0 & g_0 & g_1 & g_2 & 0 & 0 & 0 \\ 0 & 0 & 0 & 0 & g_0 & g_1 & g_2 & 0 \\ g_2 & 0 & 0 & 0 & 0 & 0 & g_0 & g_1 \end{bmatrix}$$

$$= \sqrt{2}\begin{bmatrix} \frac{3}{4} & \frac{-1}{2} & \frac{1}{4} & 0 & 0 & 0 & \frac{-1}{2} & 1 \\ \frac{-1}{2} & 1 & \frac{3}{4} & \frac{-1}{2} & \frac{1}{4} & 0 & 0 & 0 \\ 0 & 0 & \frac{-1}{2} & 1 & \frac{3}{4} & \frac{-1}{2} & \frac{1}{4} & 0 \\ \frac{1}{4} & 0 & 0 & 0 & \frac{-1}{2} & 1 & \frac{3}{4} & \frac{-1}{2} \\ - & - & - & - & - & - & - & - \\ \frac{1}{4} & \frac{-1}{2} & \frac{1}{4} & 0 & 0 & 0 & 0 & 0 \\ 0 & 0 & \frac{1}{4} & \frac{-1}{2} & \frac{1}{4} & 0 & 0 & 0 \\ 0 & 0 & 0 & 0 & \frac{1}{4} & \frac{-1}{2} & \frac{1}{4} & 0 \\ \frac{1}{4} & 0 & 0 & 0 & 0 & 0 & \frac{1}{4} & \frac{-1}{2} \end{bmatrix}$$

Similarly, $$\widetilde{\omega}_{\frac{5}{3}} = \begin{bmatrix} \tilde{h}_0 & \tilde{h}_1 & 0 & 0 & 0 & 0 & 0 & \tilde{h}_{-1} \\ 0 & \tilde{h}_{-1} & \tilde{h}_0 & \tilde{h}_1 & 0 & 0 & 0 & 0 \\ 0 & 0 & 0 & \tilde{h}_{-1} & \tilde{h}_0 & \tilde{h}_1 & 0 & 0 \\ 0 & 0 & 0 & 0 & 0 & \tilde{h}_{-1} & \tilde{h}_0 & \tilde{h}_1 \\ - & - & - & - & - & - & - & - \\ \tilde{g}_0 & \tilde{g}_1 & \tilde{g}_2 & \tilde{g}_3 & 0 & 0 & 0 & \tilde{g}_{-1} \\ 0 & \tilde{g}_{-1} & \tilde{g}_0 & \tilde{g}_1 & \tilde{g}_2 & \tilde{g}_3 & 0 & 0 \\ 0 & 0 & 0 & \tilde{g}_{-1} & \tilde{g}_0 & \tilde{g}_1 & \tilde{g}_2 & \tilde{g}_3 \\ \tilde{g}_2 & \tilde{g}_3 & 0 & 0 & 0 & \tilde{g}_{-1} & \tilde{g}_0 & \tilde{g}_1 \end{bmatrix}$$

$$\therefore \widetilde{\omega}_{\frac{5}{3}} = \sqrt{2}\begin{bmatrix} \frac{1}{2} & \frac{1}{4} & 0 & 0 & 0 & 0 & 0 & \frac{1}{4} \\ 0 & \frac{1}{4} & \frac{1}{2} & \frac{1}{4} & 0 & 0 & 0 & 0 \\ 0 & 0 & 0 & 0 & \frac{1}{4} & \frac{1}{2} & \frac{1}{4} & 0 \\ 0 & 0 & 0 & 0 & 0 & \frac{1}{4} & \frac{1}{2} & \frac{1}{4} \\ - & - & - & - & - & - & - & - \\ -1/2 & \frac{-3}{4} & 1 & \frac{1}{2} & 0 & 0 & 0 & \frac{-1}{4} \\ 0 & \frac{-1}{2} & \frac{-1}{2} & \frac{-3}{4} & 1 & \frac{1}{2} & 0 & 0 \\ 0 & 0 & 0 & \frac{-1}{4} & \frac{-1}{2} & \frac{-3}{4} & 1 & \frac{1}{2} \\ 1/2 & 0 & 0 & 0 & \frac{-1}{4} & \frac{-1}{2} & \frac{-3}{4} & 1 \end{bmatrix}$$

it is clear, that

$$\boxed{\widetilde{\omega}_{\frac{5}{3}}^{-1} = \widetilde{\omega}_{\frac{5}{3}}^{T}}$$

an extension:
using this approach different biorthogonal taps can be studied.

E.g let's design $\frac{6}{2}$ tap tp produce $\omega_{\frac{6}{2}}$ and $\widetilde{\omega}_{\frac{6}{2}}$

Here,

$$h_k = \{h_{-2}, h_{-1}, h_0 \mid h_1, h_2, h_3\}$$

–nodeline of symmetry; (– 0.3,1)node

$$\tilde{h}_k = \{\tilde{h}_0, \mid \tilde{h}_1\}$$

– (1.9,0.5)[red]nodeline of symmetry;

as the filters are symmetric, for $\tilde{h}_k$, $\tilde{h}_0 = \tilde{h}_1$
for $h_k, h_0 = h_1, h_{-1} = h_2, h_{-2} = h_3$

$$\widetilde{H}\omega = h_0 + h_1.e^{j\omega} = h_0 + h_0.e^{j\omega} \tag{15.91}$$

and

$$\begin{aligned} H(\omega) &= h_{-2}.e^{-2j\omega} + h_{-1}.e^{-j\omega} + h_0 + h_1.e^{j\omega} + h_2.e^{2j\omega} + h_3.e^{3j\omega} \\ &= h_3.e^{-2j\omega} + h_2.e^{-j\omega} + h_1 + h_1.e^{j\omega} + h_2.e^{2j\omega} + h_3.e^{3j\omega} \end{aligned} \tag{15.92}$$

from Eq. (15.91)

Now $\widetilde{H}(\omega)|_{\omega=0} = 2h_0 = \sqrt{2}$

$$\therefore \qquad h_0 = h_1 = \frac{\sqrt{2}}{2} \qquad \text{(Haar!)}$$

for h_k, let's force low pass conditions on $H(\omega)$.

$$H(\omega)|_{\omega=0} = \sqrt{2}$$

let's plug $\omega = 0 \text{ in} (15.92)$

$$\therefore \qquad 2h_1 + 2h_2 + 2h_3 = \sqrt{2} \qquad \therefore h_1 + h_2 + h_3 = \frac{\sqrt{2}}{2}$$

similarly,

$$H(\omega)|_{\omega=\pi} = 0 \qquad \therefore h_3 - h_2 + h_1 - h_1 + h_2 - h_3 = 0 \text{ -(holds good)}$$

using Eqs. (15.68) and (15.69)

$$h_0.\tilde{h}_0 + h_1.\tilde{h}_1 = 1$$

$$\therefore \qquad \frac{\sqrt{2}}{2}h_0 + \frac{\sqrt{2}}{2}h_1 = 1, \text{ but } h_0 = h_1!$$

$$\sqrt{2}h_0 = 1$$

$$\therefore \qquad h_0 = h_1 = \frac{1}{\sqrt{2}} \text{ from Eq. (15.69),}$$

$$h_0.\tilde{h}_{-2} + h_1.\tilde{h}_{-1} = 0$$

$$\therefore \qquad \frac{z}{2}h_3 + \frac{z}{2}h_2 = 0, \qquad \therefore h_2 = h_3,$$

$$h_2 = h_3 = h_{-1} = h_{-2} = \times \text{ (some real no.)}$$

$$\therefore \qquad h_k = \left\{ x, -x, \frac{2}{2}, \frac{2}{2}, -x, x \right\}$$

and

$$\tilde{h}_k = \left\{ \frac{\sqrt{2}}{2}, \frac{\sqrt{2}}{2} \right\}$$

Readers are encougraged to complete following steps:

1. calculate $\tilde{g}_k[1\times 6]$ from h_k
2. calculate $g_k[1\times 2]$ from $\tilde{h}_k$
3. calculate $\omega_{\frac{6}{2}}$ and $\tilde{\omega}_{\frac{6}{2}}$ from $h_k, \tilde{h}_k, h_k, \tilde{h}_k$

15.11 | Summary

We saw many interesting wavelet families in this chapter. We can now take a look at bird's eye view and try and understand big picture by bringing out peculiarities of every family design. We can probably understand different wavelet families from the perspective of parameters like orthogonality, compact support, symmetry, smoothness, interpolation, regularity, rational coefficients, linearity of filters etc.

- Haar
  (a) Orthogonal
  (b) Linear phase filters0
  (c) Compact support
  (d) Scaling function symmetric
  (e) Wavelet function anti-symmetric
  (f) One vanishing moment (admissible)
  (g) Only one to be linear, compactly supported, orthogonal and has symmetry.
- Daubechies
  (a) Most successful wavelet family
  (b) Orthogonal
  (c) Compactly supported
  (d) Only first member (Haar) is symmetric
  (e) Higher members are NOT symmetric
  (f) For filter length of $2N$, N moments vanish
  (g) For filter length of $2N$, support width is $2N-1$
  (h) Regularity of around $0.2N$ for large N They also have bi-orthogonal form
- Coifleets
  (a) Orthogonal
  (b) Compactly supported
  (c) Almost asymmetric
  (d) Scaling function exhibit vanishing moments too
  (e) In *coifN* filter, N is number of vanishing moments for both ψ as well as ϕ
  (f) Typical filter length is $6N$, for which ψ has $2N$ and ϕ has $2N-1$ vanishing moments
- Symlets
  (a) Orthogonal
  (b) The filters have adjusted symmetry
  (c) Compactly supported
  (d) For filter length of $2N$, ψ has N vanishing moments
  (e) ϕ is nearly linear phase
  (f) Also called Daubechies' least asymmetric wavelets
  (g) For filter length of $2N$, support width is $2N-1$
  (h) They also have bi-orthogonal form

- Morlet
  (a) Does not technically satisfy admissibility condition
  (b) Real-valued and complex-valued versions possible
  (c) Used in continuous analysis
  (d) The filters are symmetric
  (e) Though the effective support is from [– 4 4], the support width is infinite
- Mexican Hat
  (a) Continuous function
  (b) Satisfies admissibility condition
  (c) Two vanishing moments
  (d) Special case of DoG (Derivative of Gaussian) class of filters
  (e) No scaling function associated with this wavelet
  (f) These filters have infinite support width
- Meyer
  (a) Orthogonal
  (b) Scaling function is symmetric
  (c) Wavelet function is symmetric
  (d) Infinite support (decays faster than sinc though)
  (e) Both scaling and wavelet functions are defined in frequency domain
  (f) The wavelet is infinitely differentiable
  (g) The derivatives don't have finite support but decay fast
  (h) Not compactly supported, yet approximation leads to good FIR type implementation
  (i) These filters are band-limited
- Battle-Lemarie
  (a) These are based on B-splines
  (b) Compact support
  (c) Filter coefficients are smooth
  (d) Orthogonality is enforced
  (e) Typically obtained by convolution of zero order splines (box functions) and then made orthogonal
  (f) Compactly supported splines are feasible only when orthogonality is relaxed to bi-orthogonality
- Gabor
  (a) Capable of capturing oriented information
  (b) Obtained from Gaussian kernel
  (c) More useful in $2D$ applications
  (d) Variants like log-Gabor are popular
- Shannon
  (a) Orthogonal
  (b) Scaling function is symmetric
  (c) Wavelet function is symmetric
  (d) Finitely infinite support (lacks compact support)
  (e) Slowly decaying IIR type filters
  (f) Non-causal and hence difficult to deploy
  (g) Theoretically infinite vanishing moments

- Bi-orthogonal
  (a) Bi-orthogonal is nature
  (b) Compactly supported
  (c) Symmetric filters possible
  (d) Arbitrary number of vanishing moments
  (e) Scaling function exists
  (f) Deployment as FIR filters
  (g) Perfect reconstruction possible

Exercises

Exercise 15.1

Consider the signal $f(t) = 10t^2(1-t)^2 \cos 8\pi t, 0 < t < 1$ on the interval (0,1).

We use the Wavelets Tool Box to compute the scaling levels a_1 and a_2 over the interval (0,1), for the Coif 6 and the Daub 2 scaling functions coefficients. We will compare the maximum error on the interval (0,0.2) between the above Coif 6 approximation and the exact sample values. The same is done with Daub 2 computing the error between its corresponding scaling coefficients and the above estimation, it is found that for level 1, the maximum error for the Coif 6 is an order of magnitude less, and the same is for level 2. It is left for an exercise to check this accuracy at higher levels, where it is expected to decrease.

Exercise 15.2

As we did for the other scaling functions and wavelets, we call $\{h_n\}$ the scaling coefficients, let us call $h_1(n)$ as the corresponding wavelets coefficients. Show that the Coif 6 scaling coefficient satisfy the following equality,

$$\sum_{n=0}^{5} h_n^2 = 1$$

Give the interpretation of this result in terms of the energy of the Coif 6 wavelet. Show that Coif 6 scaling function satisfies the (new) relation,

$$-2h_0 - h_1 + h_3 + 2h_4 + 3h_5 = 0$$

while ϕ_{D2} does not.

Exercise 15.3

For Example, consider the signal

$$f(t) = 20t^2(1-t)^4 \cos 12\pi t, 0 < t < 3$$

Compute the scaling functions coefficients for Coif 6 and Daub 2, and compare the maximum error as done in Example 15.1 at the levels 1, 2, 3 and 4. Use very small scales of l_{10} then l_{14}, and make your conclusion.

For the same problem try Coif 12 and Daub 3.

Chapter 16

Advanced Topics

16.1 | Introduction

In this chapter we shall introduce advanced concepts in the field of 'Wavelet Analysis'. First few sections will focus on the effective implementation strategies like 'Fast Wavelet Transform (FWT)', 2 dimensional and going beyond M dimensional wavelet transform. We shall also discuss few interesting concepts like non-separable basis, self similar structures, regularity etc.

16.2 | Fast Wavelet Transform

To bring out the Fast Wavelet Transform structure we shall need the multiresolution framework that we introduced in chapter 2 and have used it throughout this text.

As we had discussed already in Chapters 2 to 6, we shall use α values to denote approximations emerging out of low pass filtering and β values to denote the details emerging out of high pass filtering. Recollect this framework:

Let a function be,

$$f_j(x) \in V_j,\ \text{scale} = \frac{1}{2^j}.$$

To span these space V_j the basis function would be $2^{\frac{j}{2}}\phi(2^j x - k)_k$

Here k is the translational parameter and $2^{\frac{j}{2}}$ is the normalizing factor to convert orthogonal basis into an orthonormal basis.

Thus we can write,

$$f_j(x) = \sum_k (\alpha_{j,k} 2^{\frac{j}{2}} \phi(2^j x - k))$$

Alpha can be calculated by as,

$$\alpha_{j,k} = \int_{-\infty}^{+\infty} f_j(x) 2^{\frac{j}{2}} \phi(2^j x - k) dx$$

Similarly for W subspaces,

$$g_j(x) \in W_j \text{, scale} = \frac{1}{2^j}$$

The basis would now be,

$$2^{\frac{j}{2}} \psi(2^j x - k)_k$$

Also we can write,

$$g_j(x) = \sum_k (\beta_{j,k} 2^{\frac{j}{2}} \psi(2^j x - k))$$

$$\beta_{j,k} = \int_{-\infty}^{+\infty} g_j(x) 2^{\frac{j}{2}} \psi(2^j x - k) dx$$

β values here would give us the details which are required to move from one subspace to another.

Let's start with 2^n samples $\vec{s} = \{s_0, s_1, s_2, ...s_{2^n-1}\} = \{f_k\}_{k=0}^{2^n-1}$ and with the necessary periodic or aperiodic extensions (padding) we will have $2 \cdot 2^n = 2^{n+1}$ samples to represent the function under consideration. The Fast Wavelet Transform (FWT) uses the coefficients $\{\alpha_k\}$ in approximating the signal $\tilde{f}(t)$,

$$\tilde{f}(t) = \sum_{k=0}^{2 \cdot 2^n - 1} a_k \phi(t - k) \tag{16.1}$$

Now, $\{\alpha_k\}_{k=0}^{2 \cdot 2^n - 1}$ will be calculated as,

$$\alpha_k = \sum_k f_i \phi(i - k) \tag{16.2}$$

Equation (16.2) is the discrete version of calculating α values from framework given in Chapter 2.

The translations in $\phi(k - j)$ may extend the span and scope of scaling functions beyond the length of the samples sequence. The extension of the sequence can be done:

1. artificially by adding zeros to its both ends (or in one end)
2. extending the sequence periodically, or as a mirror image

The extrapolation of some order leads to spline like solution.

These $2\cdot 2^n$ sample coefficients (after extension) $\{\alpha_k\}_{k=0}^{2^{n+1}-1}$ can be looked upon as the output of the first low pass filter in the filter bank (corresponding to the scaling function). Let the low pass function is represented with following system function:

$$H(\omega)=\begin{cases}1, & -a\le\omega\le a\\ 0, & \text{otherwise.}\end{cases} \tag{16.3}$$

Now, let's try and understand the periodicity and orthogonal addition across the scales to bring out the 'twiddle' like factor to create the transform matrix.

The approximated values $\{\alpha_k\}$, corresponding to scaling functions $\{\phi(t-k)\}$ with scale $l_0=1$, is in multiresolution sense an input to two parallel low pass and high pass filters at the larger scale $l_{-1}=2$. This we have already seen in 2-band filter bank structures and we extended the philosophy to M-band filter bank structures. These correspond to the slower moving parts captured by the scaling function and the fast moving parts captured by the wavelet function, respectively in the lower sub-space. From the MRA (Multiresolution Analysis) axioms from Chapters 2 and 3, after down sampling, these parts add up to the same approximated signal:

$$\tilde{f}(t)=\sum_{k=0}^{2^n-1}a_{k,n-1}\phi\left(\frac{t}{2}-k\right)+\sum_{k=0}^{2^n-1}b_{k,n-1}\psi\left(\frac{t}{2}-1-k\right) \tag{16.4}$$

The instance of $n-1$ samples in $\alpha_{k,n-1},\beta_{k,n-1}$ indicates exactly twice the scale in $\alpha_{k,n}$. The sampling rate plays vital role in multirate systems and it should be observed that the total samples of the scaling and wavelets series is $2^n+2^n=2\cdot 2^n=2^{n+1}$, which is for same as those for the scaling coefficients $\{\alpha_k\}_{k=0}^{2^{n+1}-1}$ of (16.2). This is in line with transition while moving from V_j to V_{j-1}. Here the number of samples should be double as input to two parallel filters with input of 2^{n+1} samples produce an output of 2^{n+1} each, a total of 2^{n+2}. To bring this number to the original inputting number 2^{n+1}, we use *down sampler* on these two outputs, where usually every odd indexed outputted sample is thrown away for down-sampling with factor of 2. In simpler words if we have *n* samples in V_j, then we get $\frac{n}{2}$ samples at the output of two parallel filters, and low pass filter produces $\frac{n}{2}$ samples of V_{j-1} subspace and high pass filter produces $\frac{n}{2}$ samples of W_{j-1} subspace. The normalized, cyclic and periodic version of the low pass filter modified from Eq. (16.3) will be,

$$H(\omega)=\begin{cases}1, & -\pi\le\omega\le\pi\\ 0, & \text{otherwise.}\end{cases} \tag{16.5}$$

This low pass filter blocks all higher frequencies outside its band $-\pi\le w\le\pi$.

In contrast to this, a high(band) pass filter, passes higher frequencies than those of the low pass filter. Mathematically it can be encoded as:

$$G(\omega) = \begin{cases} 0, & -\infty \le \omega < -2\pi \\ 1, & -2\pi \le \omega \le -\pi \\ 0, & -\pi \le \omega < \pi \\ 1, & \pi \le \omega < 2\pi \\ 0, & 2\pi < \omega < \infty. \end{cases} \tag{16.6}$$

$H(\omega)$ and $G(\omega)$ are shown in Figs 16.1 and 16.2 respectively.

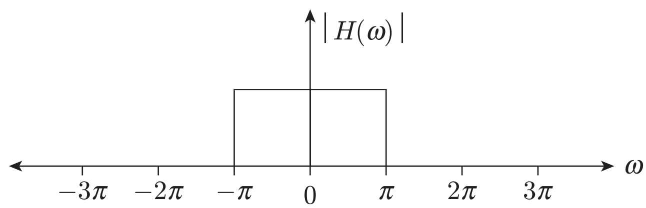

Figure 16.1 | *Low pass filter* $H(\omega)$

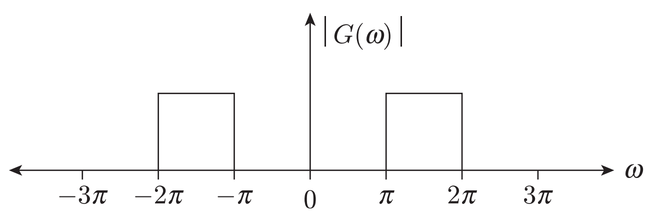

Figure 16.2 | *High pass filter* $G(\omega)$

These two filters truly complement each other on the frequency band $(-2\pi, 2\pi)$. If we look at only positive frequencies, low pass filter $H(\omega)$ passes low frequencies from $(0, \pi)$ and high pass filter $G(\omega)$ passes higher frequencies from $(\pi, 2\pi)$. Thus the two filters are dual of each other and can together form a complete band structure.

16.3 | The Daubechies Fast Wavelet Transform (FDWT) and its Inverse (IFDWT)

In this book, we have used Haar filters multiple times to bring out the conceptual parts in crisp manner. The Fast Discrete Wavelet Transform (FDWT) has its trick in appropriate creation of the transform matrix using the filter coefficients.

For the FDWT illustration, in lieu of Haar in this chapter we choose Daubechies scaling function ϕ_{D2} with its four coefficients $h_0 = \frac{1+\sqrt{3}}{4\sqrt{2}}$, $h_1 = \frac{3+\sqrt{3}}{4\sqrt{2}}$, $h_2 = \frac{3-\sqrt{3}}{4\sqrt{2}}$, $h_3 = \frac{1-\sqrt{3}}{4\sqrt{2}}$, and its associated wavelet ψ_{D2} with its coefficients $h_0' = h_3 = \frac{1-\sqrt{3}}{4\sqrt{2}}$, $h_1' = -h_2 = -\frac{3-\sqrt{3}}{4\sqrt{2}}$, $h_2' = h_1 = \frac{3+\sqrt{3}}{4\sqrt{2}}$, $h_3' = -h_0 = -\frac{1+\sqrt{3}}{4\sqrt{2}}$, which are the building blocks of the associated scaling functions ϕ_{D2}. Readers can note that the presence of $\sqrt{2}$ in the denominator of above eight coefficients is cumbersome. We shall use the adjusted coefficients as: $p_0 = \sqrt{2}h_0 = \frac{1+\sqrt{3}}{4}$, $p_1 = \sqrt{2}h_1 = \frac{3+\sqrt{3}}{4}$, $p_2 = \sqrt{2}h_2 = \frac{3-\sqrt{3}}{4}$, and $p_3 = \sqrt{2}h_3 = \frac{1-\sqrt{3}}{4}$. We have already shown in chapter 6 that h_0, h_1, h_2, h_3 correspond to the normalized scaling functions of $\{\sqrt{2}\phi(2t-k)\}$ through iterative procedure in the scaling dilation equation,

$$\phi(t) = \sqrt{2}\sum_k h_k(\phi(2t-k)) \tag{16.7}$$

The modified coefficients p_0, p_1, p_2 and p_3 correspond to the use of the not normalized scaling functions $\phi(2t-k)\}$ in the same scaling dilation equation,

$$\phi(t) = \sum_k p_k(\phi(2t-k)) \tag{16.8}$$

So, in order not to avoid nuisance of $\sqrt{2}$ in the computations for the fast Daubechies wavelet transform, we shall adopt the notation of $\{p_k\}$ as given in equation (16.8), however for our own convenience we will keep calling them $\{h_k\}$ with understanding that the $\phi(2t-k)$ used are not normalized. We stay with the use of $\{h_k\}$ because the nomenclature symbolizes the filter structure, such as $\{h_0, h_1, h_2, h_3\}$ and $\{h_3, -h_2, h_1, -h_0\}$, for the Daubechies 2 low pass and high pass filters, respectively.

The output produced by the coefficients $\{\alpha_{k,n}\}$ of the first low pass filter at the scale $l_n = \frac{1}{2^n}$ gets to those $\{\alpha_{k,n-1}, \beta_{k,n-1}\}$ of the next sub-level low pass and high pass filters outputs at the scale l_{n-1}. We have 2^{n+1} samples for coefficients $\{\alpha_{k,n}\}$ and the total samples together of the $\{\alpha_{k,n-1}, \beta_{k,n-1}\}$ coefficients, after downsampling, will also be 2^{n+1}.

Let us remember that for the averaging or low pass process with

$$\alpha_{k,0} = \sum_{i=0}^{2^n-1} f(i)\phi(i-k)$$

We had extended the samples to have them match the given values of the scaling functions. We will assume here a periodic extension. So, if we start with four samples, for example, we have a period of 4, so that $f_4 = f_0, f_5 = f_1, f_6 = f_2$, and $f_7 = f_3$. (In case of Haar we would have cared for periodicity of only 2!)

The linear equation takes us from $\{\alpha_{k,n}\}$ to $\{\alpha_{k,n-1}, \beta_{k,n\cdot 1}\}$ thus creating a matrix system where input is column vector of $\{\alpha_{k,n}\}$ and output results into alternate columns of $\{\alpha_{k,n-1}\}$ and $\{\beta_{k,n-1}\}$. This ensures the matrix Ω as square transformation matrix is sparse. From Chapter 6, we can now collect important properties of scaling coefficient of Daub-2.

$$h_0^2 + h_1^2 + h_2^2 + h_3^2 = 2 \tag{16.9}$$

$$h_2 h_0 + h_3 h_1 = 0 \tag{16.10}$$

The sparse nature of Ω is captured via how, the inverse matrix Ω^{-1} is related to Ω as follows:

$$\Omega^{-1} = \frac{1}{2}\Omega^{T} \tag{16.11}$$

This inverse matrix will be needed for the reconstruction (synthesis) process of the signal as we construct from $\{\alpha_{k,n-1}, \beta_{k,n-1}\}$ to $\{\alpha_{k,n}\}$. This is also in compliance with the fact that transform matrix should be a Unitary matrix and hence for real valued matrix A the condition that needs to be fulfilled thematically is $A^{-1} = A^{T}$.

Note that had we used the coefficients from Eq. (16.9) with a normalized scaling function in their scaling dilation equation. The summation in Eq. (16.9) becomes 1 because of the $\frac{1}{\sqrt{2}}$ in the denominator of our usual expressions for these coefficients.

In the next few examples we shall demonstrate that $\Omega\Omega^{T} = I$. This will be the foundation for the fast wavelet constructs through the matrix calculations.

Example 16.3.1 — Decomposition (analysis) matrix Ω and its reconstruction (synthesis) matrix Ω^{-1}.

The transformation matrix of the scaling functions kernel associated with scale l_0 to those of the scaling functions-wavelets associated with scale l_{-1} is given as below:

$$\Omega = \begin{pmatrix} h_0 & h_1 & h_2 & h_3 & 0 & 0 & 0 & 0 \\ h_3 & -h_2 & h_1 & -h_0 & 0 & 0 & 0 & 0 \\ 0 & 0 & h_0 & h_1 & h_2 & h_3 & 0 & 0 \\ 0 & 0 & h_3 & -h_2 & h_1 & -h_0 & 0 & 0 \\ 0 & 0 & 0 & 0 & h_0 & h_1 & h_2 & h_3 \\ 0 & 0 & 0 & 0 & h_3 & -h_2 & h_1 & -h_0 \\ 0 & 0 & 0 & 0 & 0 & 0 & h_0 & h_1 \\ 0 & 0 & 0 & 0 & 0 & 0 & h_3 & -h_2 \end{pmatrix}. \tag{16.12}$$

The transpose Ω^{T} of this matrix is

$$\Omega^{T} = \begin{pmatrix} h_0 & h_3 & 0 & 0 & 0 & 0 & 0 & 0 \\ h_1 & -h_2 & 0 & 0 & 0 & 0 & 0 & 0 \\ h_2 & h_1 & h_0 & h_3 & 0 & 0 & 0 & 0 \\ h_3 & -h_0 & h_1 & -h_2 & 0 & 0 & 0 & 0 \\ 0 & 0 & h_2 & h_1 & h_0 & h_3 & 0 & 0 \\ 0 & 0 & h_3 & -h_0 & h_1 & -h_2 & 0 & \\ 0 & 0 & 0 & 0 & h_2 & h_1 & h_0 & h_3 \\ 0 & 0 & 0 & 0 & h_3 & -h_0 & h_1 & -h_2 \end{pmatrix}. \tag{16.13}$$

Now we shall calculate,

$$\Omega\Omega^T = \begin{pmatrix} h_0 & h_1 & h_2 & h_3 & 0 & 0 & 0 & 0 \\ h_3 & -h_2 & h_1 & -h_0 & 0 & 0 & 0 & 0 \\ 0 & 0 & h_0 & h_1 & h_2 & h_3 & 0 & 0 \\ 0 & 0 & h_3 & -h_2 & h_1 & -h_0 & 0 & 0 \\ 0 & 0 & 0 & 0 & h_0 & h_1 & h_2 & h_3 \\ 0 & 0 & 0 & 0 & h_3 & -h_2 & h_1 & -h_0 \\ 0 & 0 & 0 & 0 & 0 & 0 & h_0 & h_1 \\ 0 & 0 & 0 & 0 & 0 & 0 & h_3 & -h_2 \end{pmatrix}$$

$$\times \begin{pmatrix} h_0 & h_3 & 0 & 0 & 0 & 0 & 0 & 0 \\ h_1 & -h_2 & 0 & 0 & 0 & 0 & 0 & 0 \\ h_2 & h_1 & h_0 & h_3 & 0 & 0 & 0 & 0 \\ h_3 & -h_0 & h_1 & -h_2 & 0 & 0 & 0 & 0 \\ 0 & 0 & h_2 & h_1 & h_0 & h_3 & 0 & 0 \\ 0 & 0 & h_3 & -h_0 & h_1 & -h_2 & 0 & \\ 0 & 0 & 0 & 0 & h_2 & h_1 & h_0 & h_3 \\ 0 & 0 & 0 & 0 & h_3 & -h_0 & h_1 & -h_2 \end{pmatrix}$$

$$= \begin{pmatrix} h_0^2 + h_1^2 + h_2^2 + h_3^2 & h_0h_3 - h_1h_2 + h_1h_2 - h_0h_3 & h_0h_2 + h_1h_3 & .... \\ h_0h_3 - h_1h_2 + h_1h_2 - h_0h_3 & h_0^2 + h_1^2 + h_2^2 + h_3^2 & h_0h_1 - h_0h_1 & .... \\ h_0h_2 + h_1h_3 & h_0h_1 - h_0h_1 & h_0^2 + h_1^2 + h_2^2 + h_3^2 & ... \\ h_3h_2 - h_3h_2 & h_1h_3 + h_0h_2 & h_0h_3 - h_1h_2 + h_1h_2 - h_0h_3 & ... \\ 0 & 0 & 0 & .. \\ .. & .. & .. & .. \end{pmatrix}$$

$$= 2\begin{pmatrix} 1 & 0 & 0 & .. \\ 0 & 1 & 0 & .. \\ 0 & 0 & 1 & .. \\ .. & .. & .. & .. \\ 0 & .. & .. & 1 \end{pmatrix} = 2I,$$

Thus,

$$\Omega\Omega^T = 2I \tag{16.14}$$

$$\frac{\Omega\Omega^T}{2} = I \tag{16.15}$$

Hence,

$$\Omega^{-1} = \frac{1}{2}\Omega^T \tag{16.16}$$

It is understood again that the constant of 2 in Eq. (16.14) is the result of using $h_0 = \frac{1+\sqrt{3}}{4}, h_1 = \frac{3+\sqrt{3}}{4}, h_2 = \frac{3-\sqrt{3}}{4}, h_3 = \frac{1-\sqrt{3}}{4}$ instead of normalized coeffs with an added $\frac{1}{\sqrt{2}}$ factor.

This provides the basic foundation to carry out the fast calculations. Equations (16.14) to (16.16) confirm the **unitary** nature of transformation matrix which guarantees energy compaction and preservation.

To better illustrate the fast wavelet transform, we concentrate on the Daubechies, using Daubechies 2 scaling functions and wavelets. We are considering the Daubechies scaling function $\phi_{D2}(t)$ and the wavelet ψ_{D2} with the four scaling coefficients $h_0, h_1, h_2,$ and h_3 with the $\frac{1}{\sqrt{2}}$ factor of our usual notation missing to simplify the illustration.

Example 16.3.2 — Decomposition and reconstruction with FDWT.

The FDWT emerges out of the scaling dilation equation,

$$\phi(t) = h_0\phi(2t) + h_1\phi(2t-1) + h_2\phi(2t-2) + h_3\phi(2t-3) \tag{16.17}$$

and constructing the associated wavelet from the scaling functions using wavelet dilation equation,

$$\psi(t) = -h_0\phi(2t-1) + h_1\phi(2t) - h_2\phi(2t+1) + h_3\phi(2t+2) \tag{16.18}$$

In the decomposition (analysis) process we move towards the coarser scales. For example, in the first parallel low pass and high pass filters, we move from $\phi(t)$ to $\phi\left(\frac{t}{2}\right)$ and $\psi\left(\frac{t}{2}\right)$ and their translations. This is obtained from Eqs (16.17) and (16.18) by changing t to $\frac{t}{2}$,

$$\phi\left(\frac{t}{2}\right) = h_0\phi(t) + h_1\phi(t-1) + h_2\phi(t-2) + h_3\phi(t-3) \tag{16.19}$$

$$\psi\left(\frac{t}{2}\right) = -h_0\phi(t-1) + h_1\phi(t) - h_2\phi(t+1) + h_3\phi(t+2) \tag{16.20}$$

The rest of the scaling functions translations are manifested towards wavelet series. Here $\psi\left(\frac{t}{2}-1\right) = \psi\left(\frac{t-2}{2}\right)$ is obtained from $\psi\left(\frac{t}{2}\right)$ above by changing t to $t-2$,

$$\psi\left(\frac{t}{2}-1\right) = \psi\left(\frac{t-2}{2}\right) = -h_0\phi(t-2-1) + h_1\phi(t-2)$$

$$- h_2\phi(t-2+1) + h_3\phi(t-2+2)$$
$$= -h_0\phi(t-3) + h_1\phi(t-2) - h_2\phi(t-1) + h_3\phi(t).$$

By virtue of placing the terms of this series in the same order as for $\phi\left(\frac{t}{2}\right)$ in (16.17) with the term $\phi(t)$ being the first, we have

$$\psi\left(\frac{t}{2}-1\right) = h_3\phi(t) - h_2\phi(t-1) + h_1\phi(t-2) - h_0\phi(t-3) \tag{16.21}$$

Similarly,

For $\phi\left(\frac{t}{2}-1\right) = \phi\left(\frac{t-2}{2}\right)$, we have

$$\phi\left(\frac{t}{2}-1\right) = \phi\left(\frac{t-2}{2}\right) = h_0\phi(t-2) + h_1\phi(t-2-1)$$
$$+ h_2\phi(t-2-2) + h_3\phi(t-2-3)$$
$$= h_0\phi(t-2) + h_1\phi(t-3) + h_2\phi(t-4) + h_3\phi(t-5)$$

We can again write $\phi\left(\frac{t}{2}-1\right)$ in the same way and continue to $\phi\left(\frac{t}{2}-k\right)$,

Where k denotes translation

$$\phi\left(\frac{t}{2}-k\right) = h_0\phi(t-2k) + h_1\phi(t-2k-1) + h_2\phi(t-2k-2) + h_3\phi(t-2k-3) \tag{16.22}$$

Similarly,

$$\psi\left(\frac{t}{2}-1-1\right) = \psi\left(\frac{t-4}{2}\right) = h_3\phi(t-2) - h_2\phi(t-3) + h_1\phi(t-4) - h_0\phi(t-5) \tag{16.23}$$

and

$$\psi\left(\frac{t}{2}-k-1\right) = \psi\left(\frac{t-2k-2}{2}\right) = h_3\phi(t-2k) - h_2\phi(t-2k-1)$$
$$+ h_1\phi(t-2k-2) - h_0\phi(t-2k-3)$$

What we have in Eqs (16.22) and (16.23) is the scaling functions $\left\{\phi\left(\frac{t}{2}-k\right)\right\}$ and the wavelets $\left\{\psi\left(\frac{t}{2}-1-k\right)\right\}$ respectively with the coarser scale $l_{-1} = 2$ (projection in v_{-1}, hence scale $= \frac{1}{2^{-1}} = 2$) as a linear combination of the scaling functions $\{\phi(t-j)\}$ only at the smaller scale $l_0 = 1$ (projections in v_0, hence scale $= \frac{1}{2^0} = 1$) .

The approximate input signal,

$$\tilde{f}(t) = \sum_k \alpha_{k,n} \phi(t-k) \tag{16.24}$$

is also at the finer scale of 1, where we associate the coefficients $\{\alpha_{k,n}\}$ with this scale. In comparison, the coefficients $\alpha_{k,n-1}$ and $\beta_{k,n-1}$ of the low and high pass filters in Eq. (16.4) are associated with the coarser scale of 2 via the two series expansions in Eqs (16.22) and (16.23) in terms of $\psi\left(\frac{t}{2}-1-k\right)$.

The crux of the Daubechies 2 fast wavelet transform starts with concentrating on Eqs (16.22) and (16.23). As already explained we see that we are expressing the bases at the scale 2 in terms of the scaling functions $\{\phi(t-j)\}$ at the scale 1.

The scaling coefficients $\alpha_{k,n}$ were obtained as a linear combination of $\{\phi(t-j)\}$ in Eq. (16.2). We are after the coefficients $\{\alpha_{k,n-1}\}$ and $\{\beta_{k,n-1}\}$, where their linear combination is used, respectively to represent. So, we look at Eqs (16.19) and (16.20) for giving us the transformation of the bases $\{\phi(t-j)\}$. Finding this transformation will lead to transforming the coefficients $\{\alpha_{k,n}\}$ to $\{\alpha_{k,n-1}, \beta_{k,n-1}\}$.

Equations (16.19) and (16.20) can be represented in a compact form as a matrix equation:

$$\begin{pmatrix} \phi\left(\frac{t}{2}\right) \\ \cdots \\ \cdots \\ \\ \end{pmatrix} = \begin{pmatrix} h_0 & h_1 & h_2 & h_3 & 0 & 0 & \cdots & \\ h_3 & -h_2 & h_1 & -h_0 & 0 & 0 & \cdots & \\ 0 & 0 & h_0 & h_1 & h_2 & h_3 & \cdots & \\ 0 & 0 & h_3 & -h_2 & h_1 & -h_0 & \cdots & \\ 0 & 0 & 0 & 0 & h_0 & h_1 & h_2 & \cdots \\ 0 & 0 & 0 & 0 & h_3 & -h_2 & h_1 & \cdots \\ \cdots & \cdots & \cdots & \cdots & \cdots & \cdots & \cdots & \cdots \\ \cdots & \cdots & \cdots & \cdots & \cdots & \cdots & \cdots & \cdots \end{pmatrix} \begin{pmatrix} \phi(t) \\ \phi(t-1) \\ \phi(t-2) \\ \phi(t-2) \\ \phi(t-3) \\ \phi(t-4) \\ \phi(t-5) \\ \phi(t-6) \\ \phi(t-7) \\ \cdots \\ \cdots \end{pmatrix} \tag{16.25}$$

For example, from the first row we get $\phi\left(\frac{t}{2}\right) = h_0\phi(t) + h_1\phi(t-1) + h_2\phi(t-2) + h_3\phi(t-3)$ and from the second row we get $\psi = h_3\phi(t) - h_2\phi(t-1) + h_1\phi(t-2) - h_0\phi(t-3)$ and so forth. Stick to use Ω for the Daubechies coefficients square matrix with $\vec{\phi} = [\phi(t), \phi(t-1), \ldots.]^T$, $\vec{\omega} = \left[\phi\left(\frac{t}{2}\right), \psi \ldots.\right]^T$ as two column matrices, we may write the above matrix equation as $\vec{\omega} = \Omega\vec{\phi}$. Since the basis $\vec{\phi}$ are used for coefficients $\vec{a}_n = [\alpha_{0,n}, \alpha_{1,n}, ...]^T$ and the basis $\vec{\omega}$ for $\vec{d}_{n-1} = [\alpha_{0,n-1}, \beta_{0,n-1}, \alpha_{1,n-1}, ...]^T$. We can use the above transformation to have $\vec{d}_{n-1} = \Omega\vec{a}_n$, i.e., Ω will transform the coefficients $\{\alpha_{0,n}, \alpha_{1,n}, ...\}$ at the scale l_n to $\{\alpha_{0,n-1}, \beta_{0,n-1}, \alpha_{1,n-1}, \beta_{1,n-1} .....\}$ at the lower scale l_{n-1}.

This transformation is for the decomposition (analysis) process. What we also need is a transformation from $\vec{d}_{n-1}$ back to $\vec{a}_n$ for the reconstruction (synthesis) process, i.e., an inverse transform or the inverse of the matrix Ω.

We have already derived following properties of the Daubechies scaling coefficients,

$$h_0^2 + h_1^2 + h_2^2 + h_3^2 = 1 \tag{16.26}$$

$$h_2 h_0 + h_3 h_1 = 0 \tag{16.27}$$

We have also brought out that the inverse matrix Ω^{-1} is related in a very simple way to Ω as $\Omega^{-1} = \frac{1}{2}\Omega^T$, i.e., as half its transpose. Intuitively it makes sense as the transformation matric is unitary nature and factor of 1/2 suggests normalization of $\sqrt{2}$ while moving from some scale into lower scale $\ln^{-1}$ and vice versa.

Analytically, the above coefficients relations can be verified easily by a simple substitution. With the existence of this inverse matrix, we can transform the basis $\vec{\omega} = \left[\phi\left(\frac{t}{2}\right), \psi\left(\frac{t}{2} - 1\right), ...\right]^T$ back to $\vec{\phi} = [\phi(t), \phi(t-1), ...]^T$, $\vec{\phi} = \Omega^{-1}\vec{\omega} = \frac{1}{2}\Omega^T\vec{\omega}$. In terms of the coefficients $\vec{a}_n = [\alpha_{0,n}, \alpha_{1,n}, ...]^T$ and $\vec{d}_{n-1} = [\alpha_{0,n}, \beta_{0,n-1}, \alpha_{1,n-1}, \beta_{1,n-1}, ...]$, we use the matrix Ω to go from $\vec{a}_n$ to $\vec{d}_{n-1} = \Omega\vec{a}_n$,

$$\vec{d}_{n-1} = \begin{pmatrix} \alpha_{0,n-1} \\ \beta_{0,n-1} \\ \alpha_{1,n-1} \\ \beta_{1,n-1} \\ \cdots \\ \cdots \\ \cdots \\ \cdots \\ \cdots \\ \cdots \end{pmatrix} = \Omega\vec{a}_n \tag{16.28}$$

$$\vec{d}_{n-1} = \begin{pmatrix} h_0 & h_1 & h_2 & h_3 & 0 & 0 & \dots & \\ h_3 & -h_2 & h_1 & -h_0 & 0 & 0 & \dots & \\ 0 & 0 & h_0 & h_1 & h_2 & h_3 & \dots & \\ 0 & 0 & h_3 & -h_2 & h_1 & -h_0 & \dots & \\ 0 & 0 & 0 & 0 & h_0 & h_1 & h_2 & \dots \\ 0 & 0 & 0 & 0 & h_3 & -h_2 & h_1 & \dots \\ \dots & \dots & \dots & \dots & \dots & \dots & \dots & \dots \\ \dots & \dots & \dots & \dots & \dots & \dots & \dots & \dots \end{pmatrix} \begin{pmatrix} \alpha_{0,n} \\ \alpha_{1,n} \\ \alpha_{2,n} \\ \alpha_{3,n} \\ \dots \\ \dots \\ \dots \\ \dots \\ \dots \\ \dots \\ \dots \end{pmatrix}, \tag{16.29}$$

and to go back from $\vec{d}_{n-1}$ to $\vec{a}_n$ via $\vec{a}_n = \Omega^{-1}\vec{d}_{n-1} = \Omega^T \vec{d}_{n-1}$,

$$\vec{a}_n = \begin{pmatrix} \alpha_{0,n} \\ \alpha_{1,n} \\ \alpha_{2,n} \\ \alpha_{3,n} \\ \dots \\ \dots \\ \dots \\ \dots \end{pmatrix} = \Omega^{-1}\vec{d}_{n-1} = \frac{1}{2}\Omega^T \vec{d}_{n-1} \tag{16.30}$$

$$\vec{a}_n = \frac{1}{2} \begin{pmatrix} h_0 & h_3 & 0 & 0 & 0 & 0 & 0 & 0 \\ h_1 & -h_2 & 0 & 0 & 0 & 0 & 0 & 0 \\ h_2 & h_1 & h_0 & h_3 & 0 & 0 & 0 & 0 \\ h_3 & -h_0 & h_1 & -h_2 & 0 & 0 & 0 & 0 \\ 0 & 0 & h_2 & h_1 & h_0 & h_3 & 0 & 0 \\ 0 & 0 & h_3 & -h_0 & h_1 & -h_2 & 0 & \\ 0 & 0 & 0 & 0 & h_2 & h_1 & h_0 & h_3 \\ 0 & 0 & 0 & 0 & h_3 & -h_0 & h_1 & -h_2 \end{pmatrix} \begin{pmatrix} \alpha_{0,n-1} \\ \beta_{0,n-1} \\ \alpha_{1,n-1} \\ \beta_{1,n-1} \\ \dots \\ \dots \\ \dots \\ \dots \\ \dots \\ \dots \end{pmatrix}. \tag{16.31}$$

If we refer to our nomenclature of h_2, h_1, h_0, h_3 with the $\frac{1}{\sqrt{2}}$ factor, the $\frac{1}{2}$ factor in Eq. (16.31) becomes unity, i.e. 1. With this understanding of normalization factor we will not carry the factor of $\frac{1}{2}$ in Eq. (16.31). Let us recall that the string of coefficients in the above matrices $[h_0, h_1, h_2, h_3]$ and

$[h_3, -h_2, h_1, -h_0]$ are those associated with the Daubechies ϕ_{D2} and ψ_{D2}, respectively. In the filters implementation of this wavelet transform, we refer to them as the low and high pass filters, respectively.

What we should note here is that in the decomposition (matrix) equation $\vec{d}_{n-1} = \Omega \vec{a}_n$ of Eq. (16.29) we have the two full strings of the above coefficients in the first and second rows of Ω, followed by their translations to the right by two positions, and so on. So, the multiplication of $\Omega \vec{a}_n$ proceeds as expected. However, for the inverse transformation $\vec{a}_n = \Omega^{-1} \vec{d}_{n-1}$ in Eq. (16.31), we first, and expect as we are doing construction with Ω^{-1} versus decomposition with Ω, see that we have the two strings of these coefficients in different order in their elements from those of the direct transformation. Second, they start as complete set of two filters in the third and fourth rows, then shifted by two instances to the right, and so on. The serious, apparent problem here is with the first two rows of Ω^{-1}, where the first two elements of the above two strings of coefficients are missing. The resolution of this problem, fortunately, is achieved by the periodicity of the coefficients, as we shall attend to the next.

Let us assume that we have the eight coefficients $\{\alpha_{0,0}, b_{0,0}, \alpha_{1,0}, \beta_{1,0}, \alpha_{2,0}, \beta_{2,0}, \alpha_{3,0}, \beta_{3,0}\}$ in Eq. (16.31), and we extend them periodically with period 8. Then, we see in the above matrix Eq. (16.31) the first complete pair of filters $\{h_2, h_1, h_0, h_3\}$ and $\{h_3, -h_0, h_1, -h_2\}$ use the first four elements $\alpha_{0,0}, \beta_{0,0}, \alpha_{1,0}, \beta_{1,0}$ in their matrix multiplication. The second full pair also uses $\alpha_{1,0}, \beta_{1,0}, \alpha_{2,0}, \beta_{2,0}$. The third full pair uses $\alpha_{2,0}, \beta_{2,0}, \alpha_{3,0}, \beta_{3,0}$ and so does the fourth full pair.

Then we see in the matrix multiplication of Eq. (16.31) that the inner product of the first complete pair of filters $\{h_2, h_1, h_0, h_3\}$ and $\{h_3, -h_0, h_1, -h_2\}$ with the coefficients $\{\alpha_{0,n-1}, \beta_{0,n-1}, \alpha_{1,n-1}, \beta_{1,n-1}\}$ give following.

We shall also make a quick change for the simplicity of the notation. Let $a = \alpha$ and $b = \beta$ and then,

$$
\begin{aligned}
a_{2,n} &= h_2 a_{0,n-1} + h_1 b_{0,n-1} + h_0 a_{1,n-1} + h_3 b_{1,n-1}, \\
a_{3,n} &= h_3 a_{0,n-1} - h_0 b_{0,n-1} + h_1 a_{1,n-1} - h_2 b_{1,n-1}.
\end{aligned}
$$

In the same manner we get $a_{4,n}$ and $a_{5,n}$ from the inner product of the two complete filters, shifted by two positions, and the coefficients $\{a_{1,n-1}, b_{1,n-1}, a_{2,n-1}, b_{2,n-1}, c_{2,n-1}\}$,

$$
\begin{aligned}
a_{4,n} &= h_2 a_{1,n-1} + h_1 b_{1,n-1} + h_0 a_{2,n-1} + h_3 b_{2,n-1}, \\
a_{5,n} &= h_3 a_{1,n-1} - h_0 b_{1,n-1} + h_1 a_{2,n-1} - h_2 b_{2,n-1},
\end{aligned}
$$

a_6 and a_7 are obtained, similarly, after shifting filters coefficients by two positions to the right

$$
\begin{aligned}
a_{6,n} &= h_2 a_{2,n-1} + h_1 b_{2,n-1} + h_0 a_{3,n-1} + h_3 b_{3,n-1}, \\
a_{7,n} &= h_3 a_{2,n-1} - h_0 b_{2,n-1} + h_1 a_{3,n-1} - h_2 b_{3,n-1}.
\end{aligned}
$$

What is left is $a_{0,n}$ and $a_{1,n}$, in the first two rows of $\vec{a}_n$, because of the incomplete filters in the first two rows of the inverse matrix Ω^{-1} in Eq. (16.31). Thus, we are left with finding $a_{0,n}$ and $a_{1,n}$ to complete the first period for the eight numbers sequence $\{a_{0,n}, a_{1,n}, a_{2,n}, a_{3,n}, a_{4,n}, a_{5,n}, a_{6,n}, a_{7,n}\}$.

The next period uses, $\{a_{0,n-1}, b_{0,n-1}, a_{1,n-1}, b_{1,n-1}, a_{2,n-1}, b_{2,n-1}, a_{3,n-1}, b_{3,n-1}\}$, and that leads us to solution.

If we extend the size of the matrix from 8×8 to 10×12 and the column $\vec{d}_{n-1}$ to 12×1, we can compute the first two elements $a_{8,n}$ and $a_{9,n}$ of the second period.

$$a_{8,n} = h_2 a_{3,n-1} + h_1 b_{3,n-1} + h_0 a_{0,n-1} + h_3 b_{0,n-1},$$
$$a_{9,n} = h_3 a_{3,n-1} - h_0 b_{3,n-1} + h_1 a_{0,n-1} - h_2 b_{0,n-1}.$$

But, by the periodicity with period 8, $a_{8,n} = a_{0,n}$ and $a_{9,n} = a_{1,n}$. So

$$a_{0,n} = h_2 a_{3,n-1} + h_1 b_{3,n-1} + h_0 a_{0,n-1} + h_3 b_{0,n-1},$$
$$a_{1,n} = h_3 a_{3,n-1} - h_0 b_{3,n-1} + h_1 a_{0,n-1} - h_2 b_{0,n-1}.$$

This is also equivalent to filling the first and second row of the sqaure matrix by the first halves of their filters, $\{h_2, h_1\}$ and $\{h_3, -h_0\}$, at the far end of theirs first two rows, respectively, which we illustrate here for period $8 = (2)\,2^n$, $n = 2$:

$$\begin{pmatrix} a_{0,2} \\ a_{1,2} \\ a_{2,2} \\ a_{3,2} \\ a_{4,2} \\ a_{5,2} \\ a_{6,2} \\ a_{7,2} \end{pmatrix} = \begin{pmatrix} h_0 & h_3 & 0 & 0 & 0 & 0 & h_2 & h_1 \\ h_1 & -h_2 & 0 & 0 & 0 & 0 & h_3 & -h_0 \\ h_2 & h_1 & h_0 & h_3 & 0 & 0 & 0 & 0 \\ h_3 & -h_0 & h_1 & -h_2 & 0 & 0 & 0 & 0 \\ 0 & 0 & h_2 & h_1 & h_0 & h_3 & 0 & 0 \\ 0 & 0 & h_3 & -h_0 & h_1 & -h_2 & 0 & \\ 0 & 0 & 0 & 0 & h_2 & h_1 & h_0 & h_3 \\ 0 & 0 & 0 & 0 & h_3 & -h_0 & h_1 & -h_2 \end{pmatrix} \begin{pmatrix} a_{0,1} \\ b_{0,1} \\ a_{1,1} \\ b_{1,1} \\ a_{2,1} \\ b_{2,1} \\ a_{3,1} \\ b_{3,1} \end{pmatrix}, \tag{16.32}$$

$$a_{0,2} = h_0 a_{0,1} + h_3 b_{0,1} + h_2 a_{3,1} + h_1 b_{3,1},$$
$$a_{1,2} = h_1 a_{0,1} - h_2 b_{0,1} + h_3 a_{3,1} - h_0 b_{3,1}.$$

This is for period $8 = (2)2^2$, $n = 2$. For period $4 = (2)2^1$, $n = 1$, we generate a period 8 from extending the union of $\{a_{0,0}, a_{1,0}\}$ and $\{b_{0,0}, b_{1,0}\}$ periodically with period 4 as $\{a_{1,0}, b_{1,0}, a_{0,0}, b_{0,0}, a_{1,0}, b_{1,0}, a_{0,0}, b_{0,0}\}$. Here we appeal to $a_{4,n}$ and $a_{5,n}$, which are the same as $a_{0,n}$ and $a_{1,n}$,

$$a_{0,n} = h_2 a_{3,n-1} + h_1 b_{3,n-1} + h_0 a_{0,n-1} + h_3 b_{0,n-1},$$
$$a_{1,n} = h_3 a_{3,n-1} - h_0 b_{3,n-1} + h_1 a_{0,n-1} - h_2 b_{0,n-1}.$$

This is obtained, in a similar way for the modified inverse matrix,

$$\begin{pmatrix} a_{0,1} \\ a_{1,1} \\ a_{2,1} \\ a_{3,1} \end{pmatrix} = \begin{pmatrix} h_0 & h_3 & h_2 & h_1 \\ h_1 & -h_2 & h_3 & -h_0 \\ h_2 & h_1 & h_0 & h_3 \\ h_3 & -h_0 & h_1 & -h_2 \end{pmatrix} \begin{pmatrix} a_{0,1} \\ b_{0,1} \\ a_{1,1} \\ b_{1,1} \end{pmatrix}. \tag{16.33}$$

For example,

$$a_{0,1} = h_0 a_{0,1} + h_1 b_{0,1} + h_2 a_{1,1} + h_1 b_{1,1},$$
$$a_{1,1} = h_1 a_{0,1} - h_2 b_{0,1} + h_3 a_{1,1} - h_0 b_{1,1},$$

This also means raising the last two elements $\{a_{1,1}, b_{1,1}\}$ to the top of the column had we used the usual order of the first filter as $\{h_2, h_1, h_{0,}, h_3\}$ and the second filter as $\{h_3, -h_0, h_1, -h_2\}$. Readers can note and appreciate that these filters are dual of each other, which we will explore further in next section.

For period $N = 16$, as another example, we look for the 18×20 matrix, using the periodicity of the coefficients with period 16, where $\{h_2, h_1\}$ and $\{h_3, -h_0\}$ appear after $12 = N - 4$ positions for $N = 16$ of translations for the preceding rows. Thus, in the first modified two rows we see the first halves of the top two rows in the matrix appear after 12 positions of translations for the preceding rows. Hence, we must have $\{h_2, h_1\}$ and $\{h_3, -h_1\}$ separated from their respective second halves at the beginning of the first two rows by 12 zeros. Equivalently, we need only to place them at the end of the first two rows, respectively. Of course, in an application such as signal (or spikes) detection, we shall need high resolution. So, period 16 is very modest, and we may have to go to a resolution of scale $l_j = \dfrac{1}{2^8} = \dfrac{1}{256}$, which needs 256 coefficients. However, a simple computer program with the above clear instructions should do it.

Another form for the inverse matrix

Another equivalent way to modify Eq. (16.31), which gives the same result, is to fill the first two rows as $\{h_2, h_1, h_0, h_3\}$ and $\{h_3, -h_0, h_1, -h_2\}$, move $a_{3,n-1}$ and $b_{3,n-1}$ from the bottom of their column to the top, but shift the remaining second, third, and so on, pairs of the filter's two succeeding positions to the right. For our example with period $2 \cdot 2^n = 2 \cdot 2^2 = 8$ with $n = 2$, this alternative is

$$\begin{pmatrix} a_{0,2} \\ a_{1,2} \\ a_{2,2} \\ a_{3,2} \\ a_{4,2} \\ a_{5,2} \\ a_{6,2} \\ a_{7,2} \end{pmatrix} = \begin{pmatrix} h_2 & h_1 & h_0 & h_3 & 0 & 0 & 0 & 0 & 0 & \\ h_3 & -h_0 & h_1 & -h_2 & 0 & 0 & 0 & 0 & 0 & \\ 0 & 0 & h_2 & h_1 & h_0 & h_3 & 0 & 0 & 0 & \\ 0 & 0 & h_3 & -h_0 & h_1 & h_2 & 0 & 0 & 0 & \\ 0 & 0 & 0 & 0 & h_2 & h_1 & h_0 & h_3 & 0 & 0 \\ 0 & 0 & 0 & 0 & h_3 & -h_0 & h_1 & -h_2 & 0 & 0 \\ 0 & 0 & 0 & 0 & 0 & 0 & h_2 & h_1 & h_0 & h_3 \\ 0 & 0 & 0 & 0 & 0 & 0 & h_3 & -h_0 & h_1 & -h_2 \end{pmatrix} \begin{pmatrix} a_{3,1} \\ b_{3,1} \\ a_{0,1} \\ b_{0,1} \\ a_{1,1} \\ b_{1,1} \\ a_{2,1} \\ b_{2,1} \\ a_{3,1} \\ b_{3,1} \end{pmatrix}. \tag{16.34}$$

Clearly, the first choice in Eq. (16.32) is better, even though both choices emphasize the importance of the periodicity of the coefficients (which is at the heart of fast computation).

16.4 | Low and High Pass Effects: Dual Filters

For the matrix Ω in Eq. (16.29), we should note that the pair of sets of coefficients $\{h_0, h_1, h_2, h_3\}$ and $\{h_3, -h_2, h_1, -h_0\}$ in the first two rows do averaging (CLPF) and differencing (HPF), respectively, on the column $\vec{a}_n$ to obtain the corresponding elements of the column $\vec{d}_{n-1}$. For example, by preforming the multiplication of the first row and the second row with the column $\vec{a}_n$, we have

$$a_{0,n-1} = h_0 a_{0,n} + h_1 a_{1,n} + h_2 a_{2,n} + h_3 a_{3,n},$$
$$b_{0,n-1} = h_3 a_{0,n} - h_2 a_{1,n} + h_1 a_{2,n} - h_0 a_{3,n}.$$

The first is definitely an average weighted by the scaling coefficients and is similar to moving average filter with window size of 2. The second row is adding weighted differences for the first two and second two elements of $\vec{a}_n$. Of course, this is much more clear with the shapes of the Haar scaling function and its associated wavelet using their corresponding filters $\left\{\frac{1}{\sqrt{2}}, \frac{1}{\sqrt{2}}\right\}$ and $\left\{\frac{1}{\sqrt{2}}, -\frac{1}{\sqrt{2}}\right\}$ which show the sum and difference, respectively.

The Daubechies 2 coefficients are slightly more difficult to visualize and imagine, however, the + sign for the scaling function filter $\{h_2, h_1, h_0, h_3\}$ and the alternating signs for the wavelet filter $\{h_3, -h_0, h_1, -h_2\}$ suggests averaging and differencing, respectively. In addition, if we look at the shape of ϕ_{D2} and ψ_{D2} in Figures A16.1 and 16.2 if compared with Haar, we see that ϕ_{D2} is more or less positive on almost all its compact support, while ψ_{D2} resembles to an extent that of the differencing in the Haar wavelet.

The above discussion becomes much more clear when we use the Haar scaling coefficients $\{h_0, h_1\} = \left\{\frac{1}{\sqrt{2}}, \frac{1}{\sqrt{2}}\right\}$ for the low pass filter and $\left\{\frac{1}{\sqrt{2}}, -\frac{1}{\sqrt{2}}\right\}$ for the high pass filter. Again, for a better illustration of the usual averaging, we shall normalize these coefficients to $\left\{\frac{1}{2}, \frac{1}{2}\right\}$ and $\left\{\frac{1}{2}, -\frac{1}{2}\right\}$, respectively.

We illustrate this in the following Example 16.4.1 using the Haar coefficients.

Example 16.4.1 — Illustration with the Haar wavelet matrix.

Consider the sequence of coefficients in the column matrix $\{a_{0,2}, a_{1,2}, a_{2,2}, a_{3,2}\} = \vec{a}_2 = [4, 2, 5, -3]^T$.

We are to use $\vec{d}_1 = \Omega \vec{a}_2$, where Ω is the Haar wavelet matrix with $h_0 = h_1 = \frac{1}{2}$,

$$\Omega = \frac{1}{2}\begin{pmatrix} 1 & 1 & 0 & 0 \\ 1 & -1 & 0 & 0 \\ 0 & 0 & 1 & 1 \\ 0 & 0 & 1 & -1 \end{pmatrix}. \tag{16.35}$$

Now,

$$\begin{pmatrix} a_{0,1} \\ b_{0,1} \\ a_{1,1} \\ b_{1,1} \end{pmatrix} = \frac{1}{2}\begin{pmatrix} 1 & 1 & 0 & 0 \\ 1 & -1 & 0 & 0 \\ 0 & 0 & 1 & 1 \\ 0 & 0 & 1 & -1 \end{pmatrix}\begin{pmatrix} 4 \\ 2 \\ 5 \\ -3 \end{pmatrix}$$

$$= \frac{1}{2}\begin{pmatrix} 4+2 \\ 4-2 \\ 5+(-3) \\ 5-(-3) \end{pmatrix} = \begin{pmatrix} \frac{4+2}{2} \\ \frac{4-2}{2} \\ \frac{5+(-3)}{2} \\ \frac{5-(-3)}{2} \end{pmatrix} = \begin{pmatrix} \frac{6}{2} \\ \frac{2}{2} \\ 1 \\ 4 \end{pmatrix} \tag{16.36}$$

$$a_{0,1} = \frac{4+2}{2} = \frac{6}{2}, a_{1,1} = \frac{5+(-3)}{2} = 1\ ;\ b_{0,1} = \frac{4-2}{2} = \frac{2}{2}, b_{1,1} = \frac{5-(-3)}{2} = \frac{8}{2} = 4\ .$$

Hence, the $a_{0,1}$ and $a_{1,1}$ are obtained by averaging the first couple and the second couple of the sequence $\{4, 2, 5, -3\}$. On the other hand, $b_{0,1}$ and $b_{1,1}$ are obtained by taking $\frac{1}{2}$ the difference between the first two elements 4 and 2, and the second two elements 5 and –3, respectively.

Now, we show next that the above Ω, with $h_0 = h_1 = \frac{1}{\sqrt{2}}$, is its own inverse:

$$\Omega\Omega = \frac{1}{2}\begin{pmatrix} 1 & 1 & 0 & 0 \\ 1 & -1 & 0 & 0 \\ 0 & 0 & 1 & 1 \\ 0 & 0 & 1 & -1 \end{pmatrix}\begin{pmatrix} 1 & 1 & 0 & 0 \\ 1 & -1 & 0 & 0 \\ 0 & 0 & 1 & 1 \\ 0 & 0 & 1 & -1 \end{pmatrix}$$

$$= \frac{1}{2}\begin{pmatrix} 1+1 & 1-1 & 0 & 0 \\ 1-1 & 1+1 & 0 & 0 \\ 0 & 0 & 1+1 & 1-1 \\ 0 & 0 & 1-1 & 1+1 \end{pmatrix} = \frac{2}{2}\begin{pmatrix} 1 & 0 & 0 & 0 \\ 0 & 1 & 0 & 0 \\ 0 & 0 & 1 & 0 \\ 0 & 0 & 0 & 1 \end{pmatrix} = I.$$

Hence, $\Omega\Omega = I$, where $\Omega = \Omega^{-1}$, and we say that Ω is self adjoint, i.e., $\Omega^T = \Omega$. This can be seen clearly when we exchange the elements of Ω across the diagonal, which gives Ω^T that results in Ω itself. We show next that for the Haar case $\Omega^{-1} = 2\Omega$ (using $h_0, h_1 = \frac{1}{2}$) where we can use it on the above resulting sequence $\{a_{0,1}, b_{0,1}, a_{1,1}, b_{1,1}\} = [3, 1, 1, 4] = \vec{d}_1$ to recover the original sequence $\{4, 2, 5, -3\} = [a_{0,2}, a_{1,2}, a_{2,2}, a_{3,2}]^T = \vec{a}_2$:

$$\Omega^{-1}\vec{d}_1 = 2\Omega\vec{d}_1 = \frac{2}{2}\begin{pmatrix} 1 & 1 & 0 & 0 \\ 1 & -1 & 0 & 0 \\ 0 & 0 & 1 & 1 \\ 0 & 0 & 1 & -1 \end{pmatrix}\begin{pmatrix} 3 \\ 1 \\ 1 \\ 4 \end{pmatrix}$$

$$= \begin{pmatrix} 3+1 \\ 3-2 \\ 1+4 \\ 1-4 \end{pmatrix} = \frac{2}{2}\begin{pmatrix} 4 \\ 2 \\ 5 \\ -3 \end{pmatrix} = \begin{pmatrix} 4 \\ 2 \\ 5 \\ -3 \end{pmatrix},$$

which is the original sequence.

16.5 | Numerical Computations for the Fast Discrete Wavelets Transform and its Inverse

We now demonstrate the numerical computations of the FDWT process of decomposition and construction. [The Fast Daubechies Wavelet Transform for decomposition (analysis)]

Example 16.5.1 — The fast Daubechies wavelet transform for decomposition (analysis).

We illustrate the decompositions process of the (extended) coefficients using the fast Daubechies wavelet transform of Eq. (16.29). We will use the same sequence of sample $\{s_0, s_1, s_2, s_3\} = \{0,1,2,3\}$. For the latter we will use the mirror image extension around $t = 0$ and $t = 3$ with the slope matching of the sequence and its extensions at $t = 0,3,$. By virtue of this, we shall obtain the extended sequence $\{s_{-4}, s_{-3}, s_{-2}, s_{-1}, s_0, s_1, s_2, s_3, s_4, s_5, s_6, s_7\} = \left\{4, \frac{7}{3}, \frac{2}{3}, -1, 0, 1, 2, 3, 4, \frac{7}{3}, \frac{2}{3}, -1\right\}$ with its period of 8, for example $\left\{0,1,2,3,4,\frac{7}{3},\frac{2}{3},-1\right\}$. From our understanding from previous section, we get, $a_{-2} = -\frac{1+\sqrt{3}}{2}, a_{-1} = \frac{1-\sqrt{3}}{2}, a_0 = \frac{3-\sqrt{3}}{2}, a_1 = \frac{5-\sqrt{3}}{2}$, and $a_2 = \frac{7-\sqrt{3}}{2}$. For the period 8, we will need $\{a_0, a_1, a_2, a_3, a_4, a_5, a_6, a_7\}$. We have $a_6 = a_{-2}$, since by the periodicity of the coefficients with period 8, $a_{-2+8} = a_{-2} = a_6$, $a_6 = -\frac{1+\sqrt{3}}{2}$. Also, $a_7 = a_{-1}$, since $a_{-1+8} = a_{-1} = a_7$, $a_7 = \frac{1-\sqrt{3}}{2}$. For illustration purpose a_3, a_4, and a_5, computations are as follows.

$$a_3 = \sum_{k=3}^{6} f_k \phi(k-3) = f_3\phi(0) + f_4\phi(1) + f_5\phi(2) + f_6\phi(3)$$

$$= (3)(0) + (4)\frac{1+\sqrt{3}}{2} + \left(\frac{7}{3}\right)\frac{1-\sqrt{3}}{2} + \left(\frac{2}{3}\right)(0)$$

$$= \frac{12+12\sqrt{3}+7-7\sqrt{3}}{6} = \frac{19+5\sqrt{3}}{6}$$

$$a_4 = \sum_{k=4}^{7} f_k \phi(k-4) = f_4\phi(0) + f_5\phi(1) + f_6\phi(2) + f_7\phi(3)$$

$$= (4)(0) + \left(\frac{7}{3}\right)\frac{1+\sqrt{3}}{2} + \left(\frac{2}{3}\right)\frac{1-\sqrt{3}}{2} + (-1)(0)$$

$$= \frac{7+7\sqrt{3}+2-2\sqrt{3}}{6} = \frac{9+5\sqrt{3}}{6}$$

$$a_5 = \sum_{k=5}^{8} f_k \phi(k-5) = f_5\phi(0) + f_6\phi(1) + f_7\phi(2) + f_8\phi(3)$$

$$= \left(\frac{7}{3}\right)(0) + \left(\frac{2}{3}\right)\frac{1+\sqrt{3}}{2} + (-1)\frac{1-\sqrt{3}}{2} + (0)(0)$$

$$= \frac{2+2\sqrt{3}-3+3\sqrt{3}}{6} = \frac{-1+5\sqrt{3}}{6}$$

$$a_6 = a_{-2+8} = a_{-2} = -\frac{1+\sqrt{3}}{2}$$

$$a_7 = a_{-1+8} = a_{-1} = \frac{1-\sqrt{3}}{2}$$

With these $(2)2^n = (2)2^2 = 8$ coefficients of period 8, we are at the level $n = 2$ and we designate the first low pass filter coefficients as $\{a_{k,n}\} = \{a_{k,2}\}$. After passing these eight coefficients through the first two parallel low and high pass filters, we end up with eight coefficients each $\{a_{k,1}\}_{k=0}^{7}$ and $\{b_{k,1}\}_{k=0}^{7}$, and after down sampling these become four each.

The interpolated signal, using the eight coefficients $\{a_{k,2}\}_{k=0}^{7}$, weighted by their corresponding translated scaling functions, is

$$\begin{aligned}\tilde{f}(t) = \sum_{k=0}^{7} a_{k,2}\phi(t-k) &= a_{0,2}\phi(t) + a_{1,2}\phi(t-1) + a_{2,2}\phi(t-2)\\ &+ a_{3,2}\phi(t-3) + a_{4,2}\phi(t-4) + a_{5,2}\phi(t-5) + a_{6,2}\phi(t-6)\\ &+ a_{7,2}\phi(t-7).\end{aligned}$$

For our previous computation, we used $a_{k,n} = a_k$:

$$\tilde{f}(t) = \frac{3-\sqrt{3}}{2}\phi(t) + \frac{5-\sqrt{3}}{2}\phi(t-1) + \frac{7-\sqrt{3}}{2}\phi(t-2)$$
$$+\frac{19+5\sqrt{3}}{6}\phi(t-3) + \frac{9+5\sqrt{3}}{6}\phi(t-4) + \frac{-1+5\sqrt{3}}{6}\phi(t-5)$$
$$-\frac{1+\sqrt{3}}{2}\phi(t-6) + \frac{1-\sqrt{3}}{2}\phi(t-7).$$

Now, we substitute the eight coefficients for the column matrix on the right of Eq. (16.29) to obtain the eight coefficients $\{a_{0,1}, b_{0,1}, a_{1,1}, b_{1,1}, a_{2,1}, b_{2,1}, a_{3,1}, b_{3,1}\}$ for the column on the left.

From the matrix multiplication, $a_{0,1}$ for example, is obtained as the inner product of the first row of the matrix Ω and the right column of $\vec{a}_n$,

$$\begin{aligned}
a_{0,1} &= [h_0 \quad h_1 \quad h_2 \quad h_3][a_{0,2} \quad a_{1,2} \quad a_{2,2} \quad a_{3,2}]^T \\
&= \begin{bmatrix} \frac{1+\sqrt{3}}{4\sqrt{2}} & \frac{3+\sqrt{3}}{4\sqrt{2}} & \frac{3-\sqrt{3}}{4\sqrt{2}} & \frac{1-\sqrt{3}}{4\sqrt{2}} \end{bmatrix} \times \\
&\quad \begin{bmatrix} \frac{3-\sqrt{3}}{2} & \frac{5-\sqrt{3}}{2} & \frac{7-\sqrt{3}}{2} & \frac{19+5\sqrt{3}}{6} \end{bmatrix}^T \\
&= \frac{1}{24\sqrt{2}}[(1+\sqrt{3})(9-3\sqrt{3}) + (3+\sqrt{3})(15-3\sqrt{3}) \\
&\quad + (3-\sqrt{3})(21-3\sqrt{3}) + (1-\sqrt{3})(19+5\sqrt{3})] \\
&= \frac{14-4\sqrt{3}}{3\sqrt{2}}
\end{aligned}$$

$$\begin{aligned}
b_{0,1} &= [h_3 \quad -h_2 \quad h_1 \quad -h_0][a_{0,2} \quad a_{1,2} \quad a_{2,2} \quad a_{3,2}]^T \\
&= \begin{bmatrix} \frac{1-\sqrt{3}}{4\sqrt{2}} & -\frac{3-\sqrt{3}}{4\sqrt{2}} & \frac{3+\sqrt{3}}{4\sqrt{2}} & -\frac{1+\sqrt{3}}{4\sqrt{2}} \end{bmatrix} \times \\
&\quad \begin{bmatrix} \frac{3-\sqrt{3}}{2} & \frac{5-\sqrt{3}}{2} & \frac{7-\sqrt{3}}{2} & \frac{19+5\sqrt{3}}{6} \end{bmatrix}^T \\
&= \frac{1}{24\sqrt{2}}[(1-\sqrt{3})(9-3\sqrt{3}) + (-3+\sqrt{3})(15-3\sqrt{3}) \\
&\quad + (3+\sqrt{3})(21-3\sqrt{3}) + (-1-\sqrt{3})(19+5\sqrt{3})] \\
&= \frac{-2}{3\sqrt{2}}
\end{aligned}$$

$$a_{1,1} = [h_0 \quad h_1 \quad h_2 \quad h_3][a_{2,2} \quad a_{3,2} \quad a_{4,2} \quad a_{5,2}]^T$$

$$= \left[\frac{1+\sqrt{3}}{4\sqrt{2}} \quad \frac{3+\sqrt{3}}{4\sqrt{2}} \quad \frac{3-\sqrt{3}}{4\sqrt{2}} \quad \frac{1-\sqrt{3}}{4\sqrt{2}}\right] \times$$

$$\left[\frac{7-\sqrt{3}}{2} \quad \frac{19+5\sqrt{3}}{6} \quad \frac{9+5\sqrt{3}}{6} \quad \frac{-1+5\sqrt{3}}{6}\right]^T$$

$$= \frac{1}{24\sqrt{2}}[(1+\sqrt{3})(21-3\sqrt{3}) + (3+\sqrt{3})(19+5\sqrt{3})$$

$$+ (3-\sqrt{3})(9+5\sqrt{3}) + (1-\sqrt{3})(-1+5\sqrt{3})]$$

$$= \frac{10+8\sqrt{3}}{3\sqrt{2}}$$

$$b_{1,1} = [h_3 \quad -h_2 \quad h_1 \quad -h_0][a_{2,2} \quad a_{3,2} \quad a_{4,2} \quad a_{5,2}]^T$$

$$= \left[\frac{1-\sqrt{3}}{4\sqrt{2}} \quad -\frac{3-\sqrt{3}}{4\sqrt{2}} \quad \frac{3+\sqrt{3}}{4\sqrt{2}} \quad -\frac{1+\sqrt{3}}{4\sqrt{2}}\right] \times$$

$$\left[\frac{7-\sqrt{3}}{2} \quad \frac{19+5\sqrt{3}}{6} \quad \frac{9+5\sqrt{3}}{6} \quad \frac{-1+5\sqrt{3}}{6}\right]^T$$

$$= \frac{1}{24\sqrt{2}}\left[\left(1-\sqrt{3}\right)\left(21-3\sqrt{3}\right) + \left(-3+\sqrt{3}\right)\left(19+5\sqrt{3}\right)\right.$$

$$\left. + \left(3+\sqrt{3}\right)\left(9+5\sqrt{3}\right) + \left(-1-\sqrt{3}\right)\left(-1+5\sqrt{3}\right)\right]$$

$$= \frac{2}{3\sqrt{2}}$$

$$a_{2,1} = [h_0 \quad h_1 \quad h_2 \quad h_3][a_{4,2} \quad a_{5,2} \quad a_{6,2} \quad a_{7,2}]^T$$

$$= \left[\frac{1+\sqrt{3}}{4\sqrt{2}} \quad \frac{3+\sqrt{3}}{4\sqrt{2}} \quad \frac{3-\sqrt{3}}{4\sqrt{2}} \quad \frac{1-\sqrt{3}}{4\sqrt{2}}\right] \times$$

$$\left[\frac{9+5\sqrt{3}}{6} \quad \frac{-1+5\sqrt{3}}{6} \quad -\frac{1+\sqrt{3}}{2} \quad \frac{1-\sqrt{3}}{2}\right]^T$$

$$= \frac{1}{24\sqrt{2}}[(1+\sqrt{3})(9+5\sqrt{3}) + (3+\sqrt{3})(-1+5\sqrt{3})$$

$$+ (3-\sqrt{3})(-3-3\sqrt{3}) + (1-\sqrt{3})(3-3\sqrt{3})]$$

$$= \frac{6+2\sqrt{3}}{3\sqrt{2}}$$

$$b_{2,1}=[h_3 \quad -h_2 \quad h_1 \quad -h_0][a_{4,2} \quad a_{5,2} \quad a_{6,2} \quad a_{7,2}]^T$$

$$=\left[\frac{1-\sqrt{3}}{4\sqrt{2}} \quad -\frac{3-\sqrt{3}}{4\sqrt{2}} \quad \frac{3+\sqrt{3}}{4\sqrt{2}} \quad -\frac{1+\sqrt{3}}{4\sqrt{2}}\right]\times$$

$$\left[\frac{9+5\sqrt{3}}{6} \quad \frac{-1+5\sqrt{3}}{6} \quad -\frac{1+\sqrt{3}}{2} \quad \frac{1-\sqrt{3}}{2}\right]^T$$

$$=\frac{1}{24\sqrt{2}}[(1-\sqrt{3})(9+5\sqrt{3})+(-3+\sqrt{3})(-1+5\sqrt{3})$$
$$+(3+\sqrt{3})(-3-3\sqrt{3})+(-1-\sqrt{3})(3-3\sqrt{3})]$$

$$=\frac{-4\sqrt{3}}{3\sqrt{2}}$$

$$a_{3,1}=[h_0 \quad h_1 \quad h_2 \quad h_3][a_{6,2} \quad a_{7,2} \quad a_{8,2} \quad a_{9,2}]^T$$

$$=\left[\frac{1+\sqrt{3}}{4\sqrt{2}} \quad \frac{3+\sqrt{3}}{4\sqrt{2}} \quad \frac{3-\sqrt{3}}{4\sqrt{2}} \quad \frac{1-\sqrt{3}}{4\sqrt{2}}\right]\times$$

$$\left[-\frac{1+\sqrt{3}}{2} \quad \frac{1-\sqrt{3}}{2} \quad \frac{3-\sqrt{3}}{2} \quad \frac{5-\sqrt{3}}{2}\right]^T$$

$$=\frac{1}{24\sqrt{2}}[(1+\sqrt{3})(-1-\sqrt{3})+(3+\sqrt{3})(1-\sqrt{3})$$
$$+(3-\sqrt{3})(3-\sqrt{3})+(1-\sqrt{3})(5-\sqrt{3})]$$

$$=\frac{2-2\sqrt{3}}{\sqrt{2}}$$

$$b_{3,1}=[h_3 \quad -h_2 \quad h_1 \quad -h_0][a_{6,2} \quad a_{7,2} \quad a_{8,2} \quad a_{9,2}]^T$$

$$=\left[\frac{1-\sqrt{3}}{4\sqrt{2}} \quad -\frac{3-\sqrt{3}}{4\sqrt{2}} \quad \frac{3+\sqrt{3}}{4\sqrt{2}} \quad -\frac{1+\sqrt{3}}{4\sqrt{2}}\right]\times$$

$$\left[-\frac{1+\sqrt{3}}{2} \quad \frac{1-\sqrt{3}}{2} \quad \frac{3-\sqrt{3}}{2} \quad \frac{5-\sqrt{3}}{2}\right]^T$$

$$=\frac{1}{24\sqrt{2}}[(1-\sqrt{3})(-1-\sqrt{3})+(-3+\sqrt{3})(1-\sqrt{3})$$
$$+(3+\sqrt{3})(3-\sqrt{3})+(-1-\sqrt{3})(5-\sqrt{3})]$$

$$=0$$

The resulting four coefficients, $\{a_{0,1}.a_{1,1}, a_{2,1}, a_{3,1}\}$, after down sampling the output of the low pass filter, are with period 4 and we will use this extension. They are passed again to another set of low and high pass filters to result in two samples for each filter. The four output coefficients of the high pass filter $\{b_{0,1}, b_{1,1}, b_{2,1}, b_{3,1}\}$ are not split further in the spirit of MRA.

So, to obtain the two coefficients each of the output of these two filters, we repeat the same matrix multiplication as in Eq. (16.29),

$$
\begin{aligned}
a_{0,0} &= [h_0 \quad h_1 \quad h_2 \quad h_3][a_{0,1} \quad a_{1,1} \quad a_{2,1} \quad a_{3,1}]^T \\
&= \begin{bmatrix} \frac{1+\sqrt{3}}{4\sqrt{2}} & \frac{3+\sqrt{3}}{4\sqrt{2}} & \frac{3-\sqrt{3}}{4\sqrt{2}} & \frac{1-\sqrt{3}}{4\sqrt{2}} \end{bmatrix} \times \\
&\quad \begin{bmatrix} \frac{14-4\sqrt{3}}{3\sqrt{2}} & \frac{10+8\sqrt{3}}{3\sqrt{2}} & \frac{6+2\sqrt{3}}{3\sqrt{2}} & \frac{2-2\sqrt{3}}{\sqrt{2}} \end{bmatrix}^T \\
&= \frac{1}{24}[(1+\sqrt{3})(14-4\sqrt{3}) + (3+\sqrt{3})(10+8\sqrt{3}) \\
&\quad + (3-\sqrt{3})(6+2\sqrt{3}) + (1-\sqrt{3})(6-6\sqrt{3})] \\
&= \frac{23+8\sqrt{3}}{6}
\end{aligned}
$$

$$
\begin{aligned}
b_{0,0} &= [h_3 \quad -h_2 \quad h_1 \quad -h_0][a_{0,1} \quad a_{1,1} \quad a_{2,1} \quad a_{3,1}]^T \\
&= \begin{bmatrix} \frac{1-\sqrt{3}}{4\sqrt{2}} & -\frac{3-\sqrt{3}}{4\sqrt{2}} & \frac{3+\sqrt{3}}{4\sqrt{2}} & -\frac{1+\sqrt{3}}{4\sqrt{2}} \end{bmatrix} \times \\
&\quad \begin{bmatrix} \frac{14-4\sqrt{3}}{3\sqrt{2}} & \frac{10+8\sqrt{3}}{3\sqrt{2}} & \frac{6+2\sqrt{3}}{3\sqrt{2}} & \frac{2-2\sqrt{3}}{\sqrt{2}} \end{bmatrix}^T \\
&= \frac{1}{24}[(1-\sqrt{3})(14-4\sqrt{3}) + (-3+\sqrt{3})(10+8\sqrt{3}) \\
&\quad + (3+\sqrt{3})(6+2\sqrt{3}) + (-1-\sqrt{3})(6-6\sqrt{3})] \\
&= \frac{14-5\sqrt{3}}{6}
\end{aligned}
$$

$$
\begin{aligned}
a_{1,0} &= [h_0 \quad h_1 \quad h_2 \quad h_3][a_{2,1} \quad a_{3,1} \quad a_{4,1} \quad a_{5,1}]^T \\
&= \begin{bmatrix} \frac{1+\sqrt{3}}{4\sqrt{2}} & \frac{3+\sqrt{3}}{4\sqrt{2}} & \frac{3-\sqrt{3}}{4\sqrt{2}} & \frac{1-\sqrt{3}}{4\sqrt{2}} \end{bmatrix} \times \\
&\quad \begin{bmatrix} \frac{6+2\sqrt{3}}{3\sqrt{2}} & \frac{2-2\sqrt{3}}{\sqrt{2}} & \frac{14-4\sqrt{3}}{3\sqrt{2}} & \frac{10+8\sqrt{3}}{3\sqrt{2}} \end{bmatrix}^T
\end{aligned}
$$

$$= \frac{1}{24}[(1+\sqrt{3})(6+2\sqrt{3})+(3+\sqrt{3})(6-6\sqrt{3})$$
$$+(3-\sqrt{3})(14-4\sqrt{3})+(1-\sqrt{3})(10+8\sqrt{3})]$$
$$= \frac{13-8\sqrt{3}}{6}$$

$$b_{1,0} = [h_3 \quad -h_2 \quad h_1 \quad -h_0][a_{2,1} \quad a_{3,1} \quad a_{4,1} \quad a_{5,1}]^T$$
$$= \begin{bmatrix} \frac{1-\sqrt{3}}{4\sqrt{2}} & -\frac{3-\sqrt{3}}{4\sqrt{2}} & \frac{3+\sqrt{3}}{4\sqrt{2}} & -\frac{1+\sqrt{3}}{4\sqrt{2}} \end{bmatrix} \times$$
$$\begin{bmatrix} \frac{6+2\sqrt{3}}{3\sqrt{2}} & \frac{2-2\sqrt{3}}{\sqrt{2}} & \frac{14-4\sqrt{3}}{3\sqrt{2}} & \frac{10+8\sqrt{3}}{3\sqrt{2}} \end{bmatrix}^T$$
$$= \frac{1}{24}[(1-\sqrt{3})(6+2\sqrt{3})+(-3+\sqrt{3})(6-6\sqrt{3})$$
$$+(3+\sqrt{3})(14-4\sqrt{3})+(-1-\sqrt{3})(10+8\sqrt{3})]$$
$$= \frac{-10+\sqrt{3}}{6}$$

The $\{b_{0,0}, b_{1,0}\}$ are not split and to be added to the previous four as

$$\{b_{0,0}, b_{1,0} \mid b_{0,1}, b_{1,1}, b_{2,1}, b_{3,1}\}$$

The $\{a_{0,0}, a_{1,0}\}$ of the low pass filter are now input to the next pair of filters to end up (after down sampling) with one sample output for each of the two filters:

$$a_{0,-1} = [h_0 \quad h_1 \quad h_2 \quad h_3][a_{0,0} \quad a_{1,0} \quad a_{2,0} \quad a_{3,0}]^T$$
$$= \begin{bmatrix} \frac{1+\sqrt{3}}{4\sqrt{2}} & \frac{3+\sqrt{3}}{4\sqrt{2}} & \frac{3-\sqrt{3}}{4\sqrt{2}} & \frac{1-\sqrt{3}}{4\sqrt{2}} \end{bmatrix} \times$$
$$\begin{bmatrix} \frac{23+8\sqrt{3}}{6} & \frac{13-8\sqrt{3}}{6} & \frac{23+8\sqrt{3}}{6} & \frac{13-88\sqrt{3}}{6} \end{bmatrix}^T$$
$$= \frac{1}{24\sqrt{2}}[(1+\sqrt{3})(23+8\sqrt{3})+(3+\sqrt{3})(13-8\sqrt{3})$$
$$+(3-\sqrt{3})(23+8\sqrt{3})+(1-\sqrt{3})(13-8\sqrt{3})]$$
$$= 3\sqrt{2}$$

$$b_{0,-1} = [h_3 \quad -h_2 \quad h_1 \quad -h_0][a_{0,0} \quad a_{1,0} \quad a_{2,0} \quad a_{3,0}]^T$$
$$= \begin{bmatrix} \frac{1-\sqrt{3}}{4\sqrt{2}} & -\frac{3-\sqrt{3}}{4\sqrt{2}} & \frac{3+\sqrt{3}}{4\sqrt{2}} & -\frac{1+\sqrt{3}}{4\sqrt{2}} \end{bmatrix} \times$$

$$\begin{bmatrix} \frac{23+8\sqrt{3}}{6} & \frac{13-8\sqrt{3}}{6} & \frac{23+8\sqrt{3}}{6} & \frac{13-88\sqrt{3}}{6} \end{bmatrix}^T$$

$$= \frac{1}{24\sqrt{2}}[(1-\sqrt{3})(23+8\sqrt{3})+(-3+\sqrt{3})(13-8\sqrt{3})$$

$$+(3+\sqrt{3})(23+8\sqrt{3})+(-1-\sqrt{3})(13-8\sqrt{3})]$$

$$= \frac{5+8\sqrt{3}}{3\sqrt{2}}$$

$b_{0,-1}$ is added to the previous ones to make

$$\{b_{0,-1} \mid, b_{0,0}, b_{1,0} \mid, b_{0,1}, b_{1,1}, b_{2,1}, b_{3,1} \mid\}.$$

The significance of the coefficient $a_{0,-1}$ output of the last low pass filter, that it is very close to the average of the extended sequence. The seven coefficient outputs of the three (in cascade) high pass filters are supposed to give the "details" of the sequence and its mirror image extension.

Now, we write the approximated signal $\tilde{f}$ decomposition in four equivalent ways: (i) V_0, (ii) $V_0 = V_{-1} \oplus W_{-1}$, (iii) $V_0 = V_{-2} \oplus W_{-2} \oplus W_{-1}$, and (iv) $V_0 = V_{-3} \oplus W_{-3} \oplus W_{-2} \oplus W_{-1}$. These correspond to (i) the output of the first low pass filter at scale $l_0 = 1$, (ii) the outputs of the first pair of the filters at scale $l_{-1} = 2$, (iii) the output of the low pass filter at scale $l_{-2} = 4$ in the second filters pair plus the output of the second high pass filter. We add to those what was stored of the output of the first high pass filter. (iv) The output of the low pass filter at scale $\ell_{-3} = 8$ of the third filters pair, plus the output of its parallel high pass filter, and what was stored as the outputs of the high pass filters from the first and second pairs of the filtering operations.

(i) In V_0: We have $a_{k,n}$, with period $N = (2)2^n = (2)2^2 = 8$,

$$\tilde{f}(t) = a_{0,2}\phi(t) + a_{1,2}\phi(t-1) + a_{2,2}\phi(t-2) + a_{3,2}\phi(t-3)$$
$$+ a_{4,2}\phi(t-4) + a_{5,2}\phi(t-5) + a_{6,2}\phi(t-6) + a_{7,2}\phi(t-7).$$

Here we write $a_{k,n}$ for $n = 2$ of the period $N = (2)2^2 = 8$.

(ii) $V_0 = V_{-1} \oplus W_{-1}$: We have $\{a_{k,n-1}\} = \{a_{k,1}\}_{k=0}^{4}$, $\{b_{k,n-1}\} = \{b_{k,1}\}_{k=0}^{4}$ with period $N = (2)\,2^{n-1} = (2)\,2^1 = 4$ for each sequence,

$$\tilde{f}(t) = a_{0,1}\phi\left(\frac{t}{2}\right) + a_{1,1}\phi\left(\frac{t}{2} - 2(1)\right) + a_{2,1}\phi\left(\frac{t}{2} - 2(2)\right) + a_{3,1}\phi\left(\frac{t}{2} - 2(3)\right)$$
$$+ b_{0,1}\psi\left(\frac{t}{2} - 1\right) + b_{1,1}\psi\left(\frac{t}{2} - 1 - 2(1)\right) + b_{2,1}\psi\left(\frac{t}{2} - 1 - 2(2)\right)$$
$$+ b_{3,1}\psi\left(\frac{t}{2} - 1 - 2(3)\right).$$

Note the translation by $2k$ in the above scaling functions and wavelets for the purpose of down sampling. Also, there is an extra translation of the wavelet by 1 to accommodate matching the compact support of the wavelet with its associated scaling function.

(iii) In $V_0 = V_{-2} \oplus W_{-2} \oplus W_{-1}$ we have $\{a_{k,n-2}\} = \{a_{k,0}\}_{k=0}^{1}$, $\{b_{k,n-1}\} = \{b_{k,0}\}_{k=0}^{1}$ with period $N = (2)2^{n-2} =$ $(2)2^0 = 2$ for each sequence,

$$\begin{aligned}\tilde{f}(t) = {} & a_{0,0}\phi\left(\frac{t}{4}\right) + a_{1,0}\phi\left(\frac{t}{2} - 4(1)\right) + b_{0,0}\psi\left(\frac{t}{4} - 1\right) \\ & + b_{1,0}\psi\left(\frac{t}{4} - 1 - 4(1)\right) + b_{0,1}\psi\left(\frac{t}{2} - 1\right) \\ & + b_{1,1}\psi\left(\frac{t}{2} - 1 - 2(1)\right) + b_{2,1}\psi\left(\frac{t}{2} - 1 - 2(2)\right) \\ & + b_{3,1}\psi\left(\frac{t}{2} - 1 - 2(3)\right).\end{aligned}$$

We note here the down sampling again in $V_{-2} \oplus W_{-2}$, of the first four terms, where the translations now are by steps of 4.

(iv) In $V_0 = V_{-3} \oplus W_{-3} \oplus W_{-2} \oplus W_{-1}$ we have $\{a_{k,n-3}\} = \{a_{k,-1}\}_{k=0}$ and $\{b_{k,n-3}\} = \{b_{k,-1}\}_{k=0}$ with period N = $(2)\,2^{n-3} = (2)\,2^{2-3} = (2)\frac{1}{2} = 1$,

$$\begin{aligned}\tilde{f}(t) = {} & a_{0,-1}\phi\left(\frac{t}{8}\right) + b_{0,-1}\psi\left(\frac{t}{8} - 1\right) + b_{0,0}\psi\left(\frac{t}{4} - 1\right) \\ & + b_{1,0}\psi\left(\frac{t}{4} - 1 - 4(1)\right) + b_{0,1}\psi\left(\frac{t}{2} - 1\right) + b_{1,1}\psi\left(\frac{t}{2} - 1 - 2(1)\right) \\ & + b_{2,1}\psi\left(\frac{t}{2} - 1 - 2(2)\right) + b_{3,1}\psi\left(\frac{t}{2} - 1 - 3(2)\right).\end{aligned}$$

The last step is to substitute all coefficients to compute back the signal:

$$\begin{aligned}\tilde{f}(t) = {} & (3\sqrt{2})\phi\left(\frac{t}{8}\right) + \left(\frac{5 + 8\sqrt{3}}{3\sqrt{2}}\right)\psi\left(\frac{t}{8} - 1\right) + \left(\frac{14 - 5\sqrt{3}}{6}\right)\psi\left(\frac{t}{4} - 1\right) \\ & + \left(\frac{-10 + \sqrt{3}}{6}\right)\psi\left(\frac{t}{4} - 1 - 4\right) + \left(\frac{-2}{3\sqrt{2}}\right)\psi\left(\frac{t}{2} - 1\right) \\ & + \left(\frac{2}{3\sqrt{2}}\right)\psi\left(\frac{t}{2} - 1 - 2\right) + \left(\frac{-4\sqrt{3}}{3\sqrt{2}}\right)\psi\left(\frac{t}{2} - 1 - 4\right) \\ & + (0)\psi\left(\frac{t}{2} - 1 - 6\right).\end{aligned}$$

We said that the decomposition in the V_{-3} corresponds to a blurred picture or an average of the signal. This is seen above in the coefficients $a_{0,-1} = 3\sqrt{2}$ of $\phi\left(\frac{t}{8}\right)$.

Example 16.5.2 — Illustrating the inverse Daubechies wavelet transform for reconstruction (synthesis).

For this illustration we follow the reverse process of what we did for the Forward Daubechies wavelet transform. We start with the sequence $\{a_{0,-1}, b_{0,-1}\}$, which is periodic with period 2. We extend it as $\{a_{0,-1}, b_{0,-1}; a_{0,-1}, b_{0,-1}\}$ to fit the matrix multiplication by the (4×4) inverse matrix Ω^{-1} for $\vec{a}_n = \Omega^{-1}\vec{d}_{n-1}$ in Eqs (16.31) and (16.32) for obtaining $a_{0,0}$ and $a_{1,0}$.

$$\begin{pmatrix} a_{0,0} \\ a_{1,0} \\ a_{0,0} \\ a_{1,0} \end{pmatrix} = \begin{pmatrix} h_0 & h_3 & h_2 & h_1 \\ h_1 & -h_2 & h_3 & -h_0 \\ h_2 & h_1 & h_0 & h_3 \\ h_3 & -h_0 & h_1 & -h_2 \end{pmatrix} \begin{pmatrix} a_{0,-1} \\ b_{0,-1} \\ a_{0,-1} \\ b_{0,-1} \end{pmatrix}$$

$$\begin{aligned}
a_{0,0} &= [h_0 \quad h_3 \quad h_2 \quad h_1][a_{0,-1} \quad b_{0,-1} \quad a_{0,-1} \quad b_{0,-1}]^T \\
&= \left[\frac{1+\sqrt{3}}{4\sqrt{2}} \quad \frac{1-\sqrt{3}}{4\sqrt{2}} \quad \frac{3-\sqrt{3}}{4\sqrt{2}} \quad \frac{3+\sqrt{3}}{4\sqrt{2}}\right] \times \\
&\quad \left[3\sqrt{2} \quad \frac{5+8\sqrt{3}}{3\sqrt{2}} \quad 3\sqrt{2} \quad \frac{5+8\sqrt{3}}{3\sqrt{2}}\right]^T \\
&= \frac{1}{24}[(1+\sqrt{3})(18) + (1-\sqrt{3})(5+8\sqrt{3}) \\
&\quad + (3-\sqrt{3})(18) + (3+\sqrt{3})(5+8\sqrt{3})] \\
&= \frac{23+8\sqrt{3}}{6}
\end{aligned}$$

$$\begin{aligned}
a_{1,0} &= [h_1 \quad -h_2 \quad h_3 \quad -h_0][a_{0,-1} \quad b_{0,-1} \quad a_{0,-1} \quad b_{0,-1}]^T \\
&= \left[\frac{3+\sqrt{3}}{4\sqrt{2}} \quad -\frac{3-\sqrt{3}}{4\sqrt{2}} \quad \frac{1-\sqrt{3}}{4\sqrt{2}} \quad -\frac{1+\sqrt{3}}{4\sqrt{2}}\right] \times \\
&\quad \left[3\sqrt{2} \quad \frac{5+8\sqrt{3}}{3\sqrt{2}} \quad 3\sqrt{2} \quad \frac{5+8\sqrt{3}}{3\sqrt{2}}\right]^T \\
&= \frac{1}{24}[(3+\sqrt{3})(18) + (-3+\sqrt{3})(5+8\sqrt{3}) \\
&\quad + (1-\sqrt{3})(18) + (-1-\sqrt{3})(5+8\sqrt{3})] \\
&= \frac{13-8\sqrt{3}}{6}
\end{aligned}$$

These $a_{1,0}, a_{0,0}$ at $n = 0$ are now combined with their respective $b_{1,0}, b_{0,0}$ to make a sequence $\{a_{1,0}, b_{1,0}, a_{0,0}, b_{0,0}\}$ of period 4, and we extend it to find $a_{0,1}$ and $a_{1,1}$ from Eq. (16.32). Here, we will need $a_{1,0}$ and $b_{1,0}$ from the second period since the coefficients of the square matrix are shifted by two positions:

$$\begin{pmatrix} a_{0,1} \\ a_{1,1} \\ a_{2,1} \\ a_{3,1} \end{pmatrix} = \begin{pmatrix} h_0 & h_3 & h_2 & h_1 \\ h_1 & -h_2 & h_3 & -h_0 \\ h_2 & h_1 & h_0 & h_3 \\ h_3 & -h_0 & h_1 & -h_2 \end{pmatrix} \begin{pmatrix} a_{0,0} \\ b_{0,0} \\ a_{1,0} \\ b_{1,0} \end{pmatrix}$$

$$\begin{aligned}
a_{0,1} &= [h_0 \quad h_3 \quad h_2 \quad h_1][a_{0,0} \quad b_{0,0} \quad a_{1,0} \quad b_{1,0}]^T \\
&= \left[\frac{1+\sqrt{3}}{4\sqrt{2}} \quad \frac{1-\sqrt{3}}{4\sqrt{2}} \quad \frac{3-\sqrt{3}}{4\sqrt{2}} \quad \frac{3+\sqrt{3}}{4\sqrt{2}}\right] \times \\
&\quad \left[\frac{23+8\sqrt{3}}{6} \quad \frac{14-5\sqrt{3}}{6} \quad \frac{23+8\sqrt{3}}{6} \quad \frac{14-5\sqrt{3}}{6}\right]^T \\
&= \frac{1}{24\sqrt{2}}[(1+\sqrt{3})(23+8\sqrt{3}) + (1-\sqrt{3})(14-5\sqrt{3}) \\
&\quad + (3-\sqrt{3})(13-8\sqrt{3}) + (3+\sqrt{3})(-10+3\sqrt{3})] \\
&= \frac{14-4\sqrt{3}}{3\sqrt{2}}
\end{aligned}$$

$$\begin{aligned}
a_{1,1} &= [h_1 \quad -h_2 \quad h_3 \quad -h_0][a_{0,0} \quad b_{0,0} \quad a_{1,0} \quad b_{1,0}]^T \\
&= \left[\frac{3+\sqrt{3}}{4\sqrt{2}} \quad -\frac{3-\sqrt{3}}{4\sqrt{2}} \quad \frac{1-\sqrt{3}}{4\sqrt{2}} \quad -\frac{1+\sqrt{3}}{4\sqrt{2}}\right] \times \\
&\quad \left[\frac{23+8\sqrt{3}}{6} \quad \frac{14-5\sqrt{3}}{6} \quad \frac{23+8\sqrt{3}}{6} \quad \frac{14-5\sqrt{3}}{6}\right]^T \\
&= \frac{1}{24\sqrt{2}}[(3+\sqrt{3})(23+8\sqrt{3}) + (-3+\sqrt{3})(14-5\sqrt{3}) \\
&\quad + (1-\sqrt{3})(13-8\sqrt{3}) + (-1-\sqrt{3})(-10+3\sqrt{3})] \\
&= \frac{10+8\sqrt{3}}{3\sqrt{2}}
\end{aligned}$$

$$\begin{aligned}
a_{2,1} &= [h_2 \quad h_1 \quad h_0 \quad h_3][a_{0,0} \quad b_{0,0} \quad a_{1,0} \quad b_{1,0}]^T \\
&= \left[\frac{3-\sqrt{3}}{4\sqrt{2}} \quad \frac{3+\sqrt{3}}{4\sqrt{2}} \quad \frac{1+\sqrt{3}}{4\sqrt{2}} \quad \frac{1-\sqrt{3}}{4\sqrt{2}}\right] \times \\
&\quad \left[\frac{23+8\sqrt{3}}{6} \quad \frac{14-5\sqrt{3}}{6} \quad \frac{23+8\sqrt{3}}{6} \quad \frac{14-5\sqrt{3}}{6}\right]^T
\end{aligned}$$

$$= \frac{1}{24\sqrt{2}}[(3-\sqrt{3})(23+8\sqrt{3})+(3+\sqrt{3})(14-5\sqrt{3})$$
$$+(1+\sqrt{3})(13-8\sqrt{3})+(1-\sqrt{3})(-10+3\sqrt{3})]$$
$$= \frac{6+2\sqrt{3}}{3\sqrt{2}}$$

$$a_{3,1} = [h_3 \quad -h_0 \quad h_1 \quad -h_2][a_{0,0} \quad b_{0,0} \quad a_{1,0} \quad b_{1,0}]^T$$
$$= \left[\frac{1-\sqrt{3}}{4\sqrt{2}} \quad -\frac{1+\sqrt{3}}{4\sqrt{2}} \quad \frac{3+\sqrt{3}}{4\sqrt{2}} \quad -\frac{3-\sqrt{3}}{4\sqrt{2}}\right]\times$$
$$\left[\frac{23+8\sqrt{3}}{6} \quad \frac{14-5\sqrt{3}}{6} \quad \frac{23+8\sqrt{3}}{6} \quad \frac{14-5\sqrt{3}}{6}\right]^T$$
$$= \frac{1}{24\sqrt{2}}[(1-\sqrt{3})(23+8\sqrt{3})+(-1-\sqrt{3})(14-5\sqrt{3})$$
$$+(3+\sqrt{3})(13-8\sqrt{3})+(-3+\sqrt{3})(-10+3\sqrt{3})]$$
$$= \frac{2-2\sqrt{3}}{\sqrt{2}}$$

These $\{a_{0,1}, a_{1,1}, a_{2,1}, a_{3,1}\}$ are now added to the stored $\{b_{0,1}, b_{1,1}, b_{2,1}, b_{3,1}\}$ at the same level n = 1 to make the sequence of period 8: $\{a_{0,1}, b_{0,1}, a_{1,1}, b_{1.1}, a_{2,1}, b_{2,1}, a_{3,1}, b_{3,1}\}$. As we discussed in obtaining Eq. (16.32), the first two rows of the inverse matrix Ω are completed equivalently by adding the first halves $\{h_2, h_1\}$ and $\{h_3, -h_0\}$ of the two filters at the end of the first and second row, respectively.

$$\begin{pmatrix} a_{0,2} \\ a_{1,2} \\ a_{2,2} \\ a_{3,2} \\ a_{4,2} \\ a_{5,2} \\ a_{6,2} \\ a_{7,2} \end{pmatrix} = \begin{pmatrix} h_0 & h_3 & 0 & 0 & 0 & 0 & h_2 & h_1 \\ h_1 & -h_2 & 0 & 0 & 0 & 0 & h_3 & -h_0 \\ h_2 & h_1 & h_0 & h_3 & 0 & 0 & 0 & 0 \\ h_3 & -h_0 & h_1 & -h_2 & 0 & 0 & 0 & 0 \\ 0 & 0 & h_2 & h_1 & h_0 & h_3 & 0 & 0 \\ 0 & 0 & h_3 & -h_0 & h_1 & -h_2 & 0 & 0 \\ 0 & 0 & 0 & 0 & h_2 & h_1 & h_0 & h_3 \\ 0 & 0 & 0 & 0 & h_3 & -h_0 & h_1 & -h_2 \end{pmatrix} \begin{pmatrix} a_{0,1} \\ b_{0,1} \\ a_{1,1} \\ b_{1,1} \\ a_{2,1} \\ b_{2,1} \\ a_{3,1} \\ b_{3,1} \end{pmatrix}$$

$$a_{0,2} = h_0 a_{0,1} + h_3 b_{0,1} + h_2 a_{3,1} + h_1 b_{3,1}$$
$$= \left(\frac{1+\sqrt{3}}{4\sqrt{2}}\right)\left(\frac{14-4\sqrt{3}}{3\sqrt{2}}\right)+\left(\frac{1-\sqrt{3}}{4\sqrt{2}}\right)\left(\frac{-2}{3\sqrt{2}}\right)$$

$$+\left(\frac{3-\sqrt{3}}{4\sqrt{2}}\right)\left(\frac{2-2\sqrt{3}}{\sqrt{2}}\right)+\left(\frac{3+\sqrt{3}}{4\sqrt{2}}\right)(0)$$

$$=\frac{1}{24}\left[(1+\sqrt{3})(14-4\sqrt{3})+(1-\sqrt{3})(-2)+(3-\sqrt{3})(6-6\sqrt{3})+0\right]$$

$$=\frac{3-\sqrt{3}}{2}$$

$$a_{1,2}=h_1a_{0,1}-h_2b_{0,1}+h_3a_{3,1}-h_0b_{3,1}$$

$$=\left(\frac{3+\sqrt{3}}{4\sqrt{2}}\right)\left(\frac{14-4\sqrt{3}}{3\sqrt{2}}\right)-\left(\frac{3-\sqrt{3}}{4\sqrt{2}}\right)\left(\frac{-2}{3\sqrt{2}}\right)$$

$$+\left(\frac{1-\sqrt{3}}{4\sqrt{2}}\right)\left(\frac{2-2\sqrt{3}}{\sqrt{2}}\right)+\left(\frac{1+\sqrt{3}}{4\sqrt{2}}\right)(0)$$

$$=\frac{1}{24}\left[(3+\sqrt{3})(14-4\sqrt{3})+(-3+\sqrt{3})(-2)+(1-\sqrt{3})(6-6\sqrt{3})+0\right]$$

$$=\frac{5-\sqrt{3}}{2}$$

$$a_{2,2}=h_2a_{0,1}+h_1b_{0,1}+h_0a_{1,1}+h_3b_{1,1}$$

$$=\left(\frac{3-\sqrt{3}}{4\sqrt{2}}\right)\left(\frac{14-4\sqrt{3}}{3\sqrt{2}}\right)+\left(\frac{3+\sqrt{3}}{4\sqrt{2}}\right)\left(\frac{-2}{3\sqrt{2}}\right)$$

$$+\left(\frac{1+\sqrt{3}}{4\sqrt{2}}\right)\left(\frac{10+8\sqrt{3}}{3\sqrt{2}}\right)+\left(\frac{1-\sqrt{3}}{4\sqrt{2}}\right)\left(\frac{2}{3\sqrt{2}}\right)$$

$$=\frac{1}{24}\left[(3-\sqrt{3})(14-4\sqrt{3})\right.$$

$$\left.+(3+\sqrt{3})(-2)+(1+\sqrt{3})(10+8\sqrt{3})+(1-\sqrt{3})(2)\right]$$

$$=\frac{7-\sqrt{3}}{2}$$

$$a_{3,2}=h_3a_{0,1}-h_0b_{0,1}+h_1a_{1,1}-h_2b_{1,1}$$

$$=\left(\frac{1-\sqrt{3}}{4\sqrt{2}}\right)\left(\frac{14-4\sqrt{3}}{3\sqrt{2}}\right)-\left(\frac{1+\sqrt{3}}{4\sqrt{2}}\right)\left(\frac{-2}{3\sqrt{2}}\right)$$

$$+\left(\frac{3+\sqrt{3}}{4\sqrt{2}}\right)\left(\frac{10+8\sqrt{3}}{3\sqrt{2}}\right)-\left(\frac{3-\sqrt{3}}{4\sqrt{2}}\right)\left(\frac{2}{3\sqrt{2}}\right)$$

$$= \frac{1}{24}\Big[(1-\sqrt{3})(14-4\sqrt{3})+(-1-\sqrt{3})(-2)$$

$$+(3+\sqrt{3})(10+8\sqrt{3})+(-3+\sqrt{3})(2)\Big]$$

$$= \frac{19+5\sqrt{3}}{6}$$

$$a_{4,2} = h_2 a_{1,1} + h_1 b_{1,1} + h_0 a_{2,1} + h_3 b_{2,1}$$

$$= \left(\frac{3-\sqrt{3}}{4\sqrt{2}}\right)\left(\frac{10+8\sqrt{3}}{3\sqrt{2}}\right)+\left(\frac{3+\sqrt{3}}{4\sqrt{2}}\right)\left(\frac{2}{3\sqrt{2}}\right)$$

$$+\left(\frac{1+\sqrt{3}}{4\sqrt{2}}\right)\left(\frac{6+2\sqrt{3}}{3\sqrt{2}}\right)+\left(\frac{1-\sqrt{3}}{4\sqrt{2}}\right)\left(\frac{-4\sqrt{3}}{3\sqrt{2}}\right)$$

$$= \frac{1}{24}\Big[(3-\sqrt{3})(10+8\sqrt{3})+(3+\sqrt{3})(2)$$

$$+(1+\sqrt{3})(6+2\sqrt{3})+(1-\sqrt{3})(-4\sqrt{3})\Big]$$

$$= \frac{9+5\sqrt{3}}{6}$$

$$a_{5,2} = h_3 a_{1,1} - h_0 b_{1,1} + h_1 a_{2,1} - h_2 b_{2,1}$$

$$= \left(\frac{1-\sqrt{3}}{4\sqrt{2}}\right)\left(\frac{10+8\sqrt{3}}{3\sqrt{2}}\right)-\left(\frac{1+\sqrt{3}}{4\sqrt{2}}\right)\left(\frac{2}{3\sqrt{2}}\right)$$

$$+\left(\frac{3+\sqrt{3}}{4\sqrt{2}}\right)\left(\frac{6+2\sqrt{3}}{3\sqrt{2}}\right)-\left(\frac{3-\sqrt{3}}{4\sqrt{2}}\right)\left(\frac{-4\sqrt{3}}{3\sqrt{2}}\right)$$

$$= \frac{1}{24}\Big[(1-\sqrt{3})(10+8\sqrt{3})+(-1-\sqrt{3})(2)$$

$$+(3+\sqrt{3})(6+2\sqrt{3})+(-3+\sqrt{3})(-4\sqrt{3})\Big]$$

$$= \frac{-1+5\sqrt{3}}{6}$$

$$a_{6,2} = h_2 a_{2,1} + h_1 b_{2,1} + h_0 a_{3,1} + h_3 b_{3,1}$$

$$= \left(\frac{3-\sqrt{3}}{4\sqrt{2}}\right)\left(\frac{6+2\sqrt{3}}{3\sqrt{2}}\right)+\left(\frac{3+\sqrt{3}}{4\sqrt{2}}\right)\left(\frac{-4\sqrt{3}}{3\sqrt{2}}\right)$$

$$+\left(\frac{1+\sqrt{3}}{4\sqrt{2}}\right)\left(\frac{2-2\sqrt{3}}{\sqrt{2}}\right)+\left(\frac{1-\sqrt{3}}{4\sqrt{2}}\right)(0)$$

$$= \frac{1}{24}\Big[(3-\sqrt{3})(6+2\sqrt{3})+(3+\sqrt{3})(-4\sqrt{3})$$
$$+(1+\sqrt{3})(6-6\sqrt{3})+0\Big]$$
$$= -\frac{1+\sqrt{3}}{2}$$

$$a_{7,2} = h_3 a_{2,1} - h_0 b_{2,1} + h_1 a_{3,1} - h_2 b_{3,1}$$
$$= \left(\frac{1-\sqrt{3}}{4\sqrt{2}}\right)\left(\frac{6+2\sqrt{3}}{3\sqrt{2}}\right) - \left(\frac{1+\sqrt{3}}{4\sqrt{2}}\right)\left(\frac{-4\sqrt{3}}{3\sqrt{2}}\right)$$
$$+\left(\frac{3+\sqrt{3}}{4\sqrt{2}}\right)\left(\frac{2-2\sqrt{3}}{\sqrt{2}}\right) - \left(\frac{3-\sqrt{3}}{4\sqrt{2}}\right)(0)$$
$$= \frac{1}{24}\Big[(1-\sqrt{3})(6+2\sqrt{3})+(-1-\sqrt{3})(-4\sqrt{3})$$
$$+(3+\sqrt{3})(6-6\sqrt{3})+0\Big]$$
$$= \frac{1-\sqrt{3}}{2}$$

Interested readers can try out following variations for further insights:

1. (a) Follow above examples to illustrate the Haar wavelet transform and its inverse for the coefficients sequence $\{1,-2,3,5\}$ by showing the decomposition in $V_{-2} = V_1 \oplus W_1$, then the reconstruction to show that you recover the oringinal sequence.
   (b) We note that this sequence in part (a) has a jump at t = 1, and we expect, with good resolution, that it can be detected by the wavelet part of the decomposition. Try $V_2 \oplus W_0 \oplus W_1$ to see if the part in $W_0 \oplus W_1$ shows it better than just the W_1 in $V_2 = V_1 \oplus W_1$ of part (a). If not, try $V_3 = V_0 \oplus W_0 \oplus W_1 \oplus W_2$.
2. Consider the sequence of samples $\{0,1,4,9\}$.
   (a) Use extension with zeros to calculate its eight coefficients, and write its interpolation $\tilde{f}(t) \in V_0$.
   (b) Use the first Daubechies wavelet transform, for the decomposition in:
      (i) $V_0 = V_{-1} \oplus W_{-1}$
      (ii) $V_0 = V_{-2} \oplus W_{-2} \oplus W_{-1}$
      (iii) $V_0 = V_{-3} \oplus W_{-3} \oplus W_{-2} \oplus W_{-1}$
   (c) Use the inverse Daubechies wavelet transform for the construction of the original signal to verify your results.
3. Repeat (2) with the periodic extension with matching slopes at the ends. Compare your results with that of (2). How does the edge effect in (2) affect the comparison?

4. Repeat (2) and (3) for the sequence $\{1,3\}$, using the zeros extension for the Haar scaling function and wavelets.
5. Repeat (2) for the sequence $\{0,1,4,9\}$ with the zeros extension and the Haar scaling functions and wavelets.

16.6 | Multi-dimensional Wavelets

A signal is a 1-D entity and often gets represented using function of independent variable time 't'. We represent images in space as they are 2D entities. If we can extend 1D wavelet analysis to 2D, then we should be able to extend it to M-dimensions.

2D wavelet analysis has two possible methods:

1. An easier approach in which we construct tensor product wavelets which are separable.
2. Little difficult part of wavelet theory in which two variables are not separable in general. This means a wavelet function $\psi(x,y)$ can not be written as product $\psi(x)\cdot\psi(y)$ and requires more attention.

16.6.1 Separable Tensor Product Wavelets

A wavelet transform of M-dimensional vector can be obtained in easiest way by transforming array sequentially to first index,then to second index, going all the way till M^{th} index. The order of indices hardly matters, as by associativity of matrix product, the result remains independent of the order. Each transformation boils down to multiplication with orthogonal matrix. An image is a good example of 2D information representation.

A 2D-wavelet analysis of an image upto scale 2 can be depicted as follows:

(A)

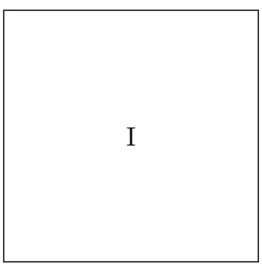

original image

(B)

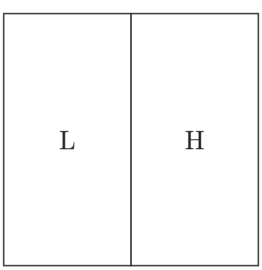

One step of 1D transform on each rows of image I, resulting in low resolution 'L' & high resolution 'H' part.

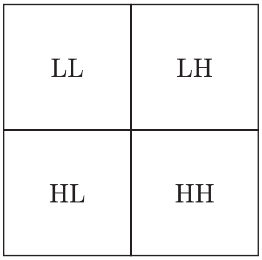

(C)

One step of 1D transform on each of columns of image I, resulting in LL,LH,HL,HH (4 subbands).

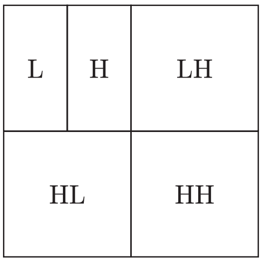

(D)

For next scale,in spirit of MRA we process only energy rich LL band.
1-D transform row-wise.

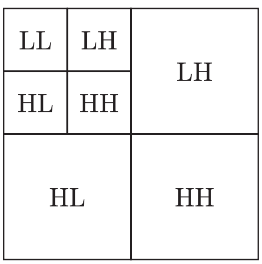

(E)

1-D transform column-wise

⋮

Nomenclature:
LL: Low pass filtering for rows and columns
LH: Low pass filtering for columns and high pass filtering for rows
HL: High pass filtering for columns and low pass filtering for rows
HH: High pass filtering for columns and high pass filtering for rows.

Typically, HH captures diagonal features, HL gives horizontal and LH gives vertical features, LL captures low pass features and has highest energy.

If 'I' is the image to be analyzed and $\tilde{K} = \left[\tilde{H} \quad \tilde{G}\right]$ is the transformation matrix in 1-D wavelet sense, then

$$I^1 = \begin{array}{|c|c|}\hline \mathrm{LL} & \mathrm{LH} \\ \hline \mathrm{HL} & \mathrm{HH} \\ \hline \end{array} = [\tilde{K}^*] \cdot I \cdot [\tilde{K}^*]^T$$

The rectangular transform corresponds to taking 1-D wavelet transform in x and y independently with $\tilde{K}_1$ matrix exactly of half size (downsampled in x as well as y by 2) but of same class of $\tilde{K}$, we get second step,

$$I^2 = \begin{bmatrix} \tilde{K}_1^* & 0 \\ 0 & I \end{bmatrix} \cdot I^1 \cdot \begin{bmatrix} \tilde{K}_1^* & 0 \\ 0 & I \end{bmatrix}^T$$

Rectangular division corresponds to,

$$V_j = \text{span}\{\phi_{j,k}(x)\cdot\phi_{j,l}(y), \phi_{j,k}(x)\cdot\psi_{j,l}(y), \psi_{j,k}(x)\cdot\phi_{j,l}(y) : k,l \in Z\}$$

and

$$W_j = \text{span}\{\psi_{j,k}(x)\cdot\psi_{j,l}(y); k,l \in Z\}$$

Thus,

$$(h \otimes g)(x,y) = h(x)\cdot g(y)$$

$$\therefore I(x,y) = \sum_{m,l}\sum_{j,k} q_{m,j,l,k}(\psi_{ml} \otimes \psi_{jk})(x,y)$$

In MRA, the next step is applied only on LL band.

$\therefore$ Let's take LL band separate and perform $\left[\tilde{K}_1^*\right]\cdot\left[I_{LL}^1\right]\cdot\left[\tilde{K}_1^*\right]^T$ which gives

$$V_j = \text{span}\{\phi_{j,k}(x)\phi_{j,l}(y) : k,l \in z\}$$

(LL square)

W_j is spanned by mixed basis.

$$W_j = \text{span}\left\{\phi_{j,k}(x).\psi_{j,l}(y), \psi_{j,k}(x).\phi_{j,l}(y), \psi_{j,k}(x).\psi_{j,l}(y) : k,l \in z\right\}$$

(HL,LH,HH squares)

There is scaling of 2^{-j} for both x & y directions.

$$\begin{aligned} V_{j+1} &= V_{j+1}^{(x)} \otimes V_{j+1}^{(y)} \\ &= \left[V_j^{(x)} \oplus W_j^{(x)}\right] \otimes \left[V_j^{(y)} \oplus W_j^{(y)}\right] \\ &= \left[V_j^{(x)} \otimes V_j^{(y)}\right] \oplus \left[V_j^{(x)} \otimes W_j^{(y)}\right] \oplus \left[W_j^{(x)} \otimes V_j^{(y)}\right] \oplus \left[W_j^{(x)} \otimes W_j^{(y)}\right] \end{aligned}$$

The calculation of coefficients by recursion in matrix form can be now set:

$$V_{j-1} = \widetilde{H}^* \cdot V_j \cdot \left[\widetilde{H}^*\right]^T \quad \text{(LL sub-band)}$$

$$W_{j-1}^{(x)} = \widetilde{H}^* \cdot V_j \cdot \left[\widetilde{G}^*\right]^T \quad \text{(LH sub-band)}$$

$$W_{j-1}^{(y)} = \widetilde{G}^* \cdot V_j \cdot \left[\widetilde{H}^*\right]^T \quad \text{(HL sub-band)}$$

$$W_{j-1}^{(xy)} = \widetilde{G}^* \cdot V_j \cdot \left[\widetilde{G}^*\right]^T \quad \text{(HH sub-band)}$$

Thus, reconstruction shall be:

$$V_{j+1} = H \cdot V_j \cdot H^T + G \cdot W_j^{(x)} \cdot H^T + H \cdot W_j^{(y)} \cdot G^T + G \cdot W_j^{(xy)} \cdot G^T$$

16.6.2 Non-Separable wavelets

If two variables are not separable then the row-wise and column-wise application in 1D style will not work.

Let's derive this using conventional convolution mechanism.

In 1D sense

$$\xrightarrow{\quad f \quad} \boxed{H} \xrightarrow{\quad g \quad}$$

If 'H' is the impulse response of filter then 'g' is calculated using

$$g = h * f$$

This holds true for 2D filter as well. Let H_2 be the 2D filter with impulse response $h_2 = \{h_{k1,k2} \mid k_1, k_2 \in z\}$, and

$$g_2 = h_2 * f_2$$

$$g_{n1,n2} = \sum_{K_1}\sum K_2 h_{K_1,K_2} f_{n1-k1,n2-k2} \tag{16.37}$$

Convolution in time or sparse becomes multiplication in 'Z' domain.

$$\therefore \quad G(Z) = H(Z) \cdot F(Z)$$

$$\therefore \quad G(Z) = \left(\sum_{K_1,K_2} h_{K_1,K_2} \cdot Z_1^{-K_1} \cdot Z_2^{-K_2}\right) \cdot \left(\sum_{K_1,K_2} f_{K_1,K_2} \cdot Z_1^{-K_1} \cdot Z_2^{-K_2}\right) \tag{16.38}$$

Let 'M' describe subsampling in 2D sense. For separable case 'M' is diagonal, for non-seprable case it's not.

$$(\downarrow M)y(n_1, n_2) = y(M_n) = y(2n_1, 2n_2) \tag{16.39}$$

Equation (16.39) depicts downsampling by 2 ($\downarrow$2) in every direction.

$\therefore$ Only these samples for which $n_1 + n_2 =$ even are retained.

$$\therefore M(Z_1,Z_2) = \begin{bmatrix} H(Z_1,Z_2) & H(-Z_1,-Z_2) \\ G(Z_1,Z_2) & G(-Z_1,-Z_2) \end{bmatrix} \tag{16.40}$$

We choose simplest solution of form

$$M \cdot M^* = 2I \tag{16.41}$$

For Eq. (16.41) to hold, $G(Z_1,Z_2)$ should be an odd delay of $H(-Z_1^{-1},-Z_2^{-1})$ For 1D MRA,with $H(\omega) = \sum_K h_k \cdot e^{-ik\omega}$ the dialation equation was,

$$\phi(t) = \sqrt{2}\sum_K h_k \cdot \phi(2t-K) = \sqrt{2} < h^*, \Phi_0(2t) >_{l^2(Z)} \tag{16.42}$$

we can generalize this to *M-D*

$$\phi(t) = \sqrt{M}\sum_K h_k \cdot \phi(M_t - K) = \sqrt{M} < h^*, \Phi_0(Mt) >_{l^2(Z^2)} \tag{16.43}$$

where, $\Phi_0(t) = (\phi_{0k}(t)) \in l^2(Z^2)$. For variable change of $S = Mt - K$

$$M\iint \phi(Mt-K)\cdot dt_1 - dt_2 = \iint \phi(s)\cdot ds_1 \cdot ds_2 \tag{16.44}$$

There will be $(M-1)$ wavelet functions,

$$\psi^{(m)}(t) = \sqrt{M}\sum_K g_K^{(m)} \cdot \phi(Mt-K) \tag{16.45}$$

$$\psi^{(m)}(t) = \sqrt{M} < g^{*(m)}, \Phi_0(Mt) >_{l^2(Z^2)}, M = 1,\cdots,M-1 \tag{16.46}$$

From Eqs (16.43)-(16.46),

$$V_0 = \text{span}\{\phi_{ok}(t) = \phi(t-K) : K \in Z^2\} \tag{16.47}$$

and orthogonally,

$$W_0 = \text{span}\{\psi_{ok}^{(m)}(t) = \psi^{(m)}(t-k) : m = 1,\cdots,M-1; K \in Z^2\} \tag{16.48}$$

Taking all dilates and translates, of wavelet,

$$\boxed{\psi_{n,K}^{(m)}(t) = M^{\frac{n}{2}}\psi(m)(M^n t - K)}$$

This is the orthonormal basis for entire $L^2(R^2)$ 2-D wavelet examples:

1. Mexican Hat:

$$\psi(t) = (\| t \|^2 - 2)\exp(-\frac{1}{2}\| t \|^2)$$

2. Morlet:

$$\psi(t) = \exp(iK^T t) \cdot \exp\left(-\frac{1}{2}\| At \|^2\right) \cdots (\| K \| > 56 \to \text{admissible})$$

16.7 | The Two-Dimensional Haar Wavelet Transform

In this session we shall demonstrate the separable basis for doing the 2*D* wavelet analysis. We shall keep using Haar basis to ensure the readers will find it easy to grasp the 2*D* analysis steps and that will enable them to understand how to generalize the analysis that can be extended to *M* dimensional analysis.

The Haar wavelet transform, as has been demonstrated throughout the book, does a simple averaging and differential to each pair of a one-dimensional sequence, for example, $\vec{S} = \{s_0, s_1, s_2, s_3\}$. So, now we have an idea about a two-dimensional Haar wavelet transform of a two dimensional sequence, lets take case of the four points in space: $z_0 = f(0,0) = 9, z_1 = f\left(0, \frac{1}{2}\right) = 7, z_2 = f\left(\frac{1}{2}, 0\right) = 5$ and $z_3 = f\left(\frac{1}{2}, \frac{1}{2}\right) = 3$. Even though this is a 2×2 array, we hope that it will give some feeling about what we may expect in dealing with two-dimensional images. Here, we can take the values 9, 7, 5, and 3 can be thought of as a measure of the luminance or chrominance in an image.

These samples are easily interpolated by using a two-dimensional Haar scaling function with an area of $\frac{1}{2} \times \frac{1}{2} = \frac{1}{4}$, when using scale $l_1 = \frac{1}{2}$ in both the x and y directions. With scale $l_0 = 1$, the double Haar scaling function can be written as:

$$\Phi^{(0)}_{(0,0)}(x, y) = \begin{cases} 1, & 0 \le x < 1 \text{ and } 0 \le y < 1 \\ 0, & \text{otherwise} \end{cases} \tag{16.49}$$

as shown in Fig. 16.3,

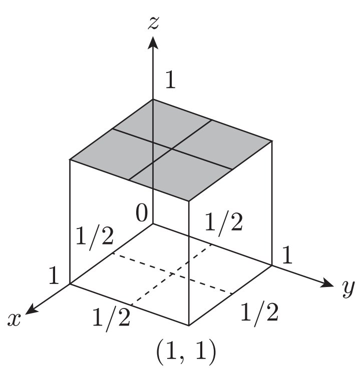

Figure 16.3 | *The Haar wavelet $\Phi^{(0)}_{(0,0)}(x, y)$ (scaling function in two dimensions)*

The expression in Eq. (16.49) we obtain from the tensor product of our usual scaling function,

$$\phi(x) \equiv \varphi^{(0)}_{(0,0)}(x) = \begin{cases} 1, & 0 \le x < 1, 0 \le y < 1 \\ 0, & \text{otherwise} \end{cases} \tag{16.50}$$

and a similar one in the y-direction,

$$\phi(y) \equiv \varphi^{(0)}_{(0,0)}(y) = \begin{cases} 1, & 0 \le y < 1 \\ 0, & \text{otherwise} \end{cases} \tag{16.51}$$

$$\Phi^{(0)}_{(0,0)}(x,y) = \phi^{(0)}_{(0,0)}(x)\phi^{(0)}_{(0,0)}(y) = \begin{cases} 1, & 0 \le x < 1, 0 \le y < 1 \\ 0, & \text{otherwise} \end{cases} \tag{16.52}$$

We will use the subscript (a,b) in $\Phi^{(j)}_{(a,b)}(x,y)$ to indicate the top left corner of its base support in the $x-y$ plane. The superscript (j) is used to indicate the scale l_j (in this case $l_0 = 1$) in both the x and y directions, where we see that the base of the cube is 1×1 in Fig. 16.3.

Reader will note that $\Phi^{(0)}_{(0,0)}(x,y)$ in Eq. (16.52) is asociated with "averaging" in the x and y directions (LL). However, we expect more operations, such as average of differencing (LH), difference of averaging (HL), and difference of differencing (HH). As it may sound, this would involve other Haar wavelet actions in the y, x, and both (namely, diagonal) directions, to which we shall refer as $\Psi^{h}_{(0,0)}(x,y)$, $\Psi^{v}_{(0,0)}(x,y)$, and $\Psi^{d}_{(0,0)}(x,y)$, respectively. The scale used will be spelled out, or we may write ${}_h\Psi^{(1)}_{(0,0)}(x,y)$, ${}_v\Psi^{(1)}_{(0,0)}(x,y)$ and ${}_d\Psi^{(1)}_{(0,0)}(x,y)$ at scale $l_1 = \frac{1}{2}$, for example. Here h and v refer to the horizontal and vertical edges resulting from the differencing caused by the wavelets actions along the perpendicular direction to that particular edge. Such three mixed combinations that involve wavelets, are the reason behind using the symbol Ψ instead of Φ, as the latter is reserved for the pure averaging as in Eq. (16.52).

We note that we are moving to the scale $\frac{1}{2}$ for the four $\frac{1}{2} \times \frac{1}{2}$ squares of the unit square, where we will also involve translations by $\frac{1}{2}$. Reader should note that normalization happens in both the dimensions and squeezing of area is not necessary. For the two-dimensional wavelet, such as $\Psi^{h}_{(0,0)}(x,y)$, if we are to scale it with scale $l_1 = \frac{1}{2}$, and we want to indicate that, we use ${}_h\Psi^{(1)}_{(0,0)}$; the same notation is used for the others. An example of scaling with $l_1 = \frac{1}{2}$ is

$$\Phi^{(1)}_{(0,0)} = \Phi^{(0)}_{(0,0)}(2x,2y) = \begin{cases} 1, & 0 \le x < \frac{1}{2}, 0 \le y < \frac{1}{2} \\ 0, & \text{otherwise} \end{cases} \tag{16.53}$$

which is located at the top-left $\frac{1}{2} \times \frac{1}{2}$ square, $0 \le x \le \frac{1}{2}, 0 \le y \le \frac{1}{2}$ in Fig. 16.3. Its translation by $\frac{1}{2}$ in the y-direction is

$$\Phi^{(1)}_{(0,0)}\left(2x, 2\left(y - \frac{1}{2}\right)\right) \equiv \Phi^{(1)}_{(0,1)}(x,y) = \begin{cases} 1, & 0 \le x < \frac{1}{2}, \frac{1}{2} \le y < 1 \\ 0, & \text{otherwise} \end{cases} \tag{16.54}$$

which is located at the top-right $\frac{1}{2} \times \frac{1}{2}$ square. The same thing is done for the other $\Phi^{(1)}_{(0,0)}$ functions. Illustrative cases will be:

$$\Phi^{(1)}_{(0,0)}(2\left(x - \frac{1}{2}\right), y) \equiv \Phi^{(1)}_{(1,0)}(x,y),$$

$$\Phi^{(0)}_{(0,0)}\left(2x-\frac{1}{2}\right),2\left(y-\frac{1}{2}\right) \equiv \Phi^{(1)}_{(1,1)}(x,y). \tag{16.55}$$

These are shown in Fig. 16.4.

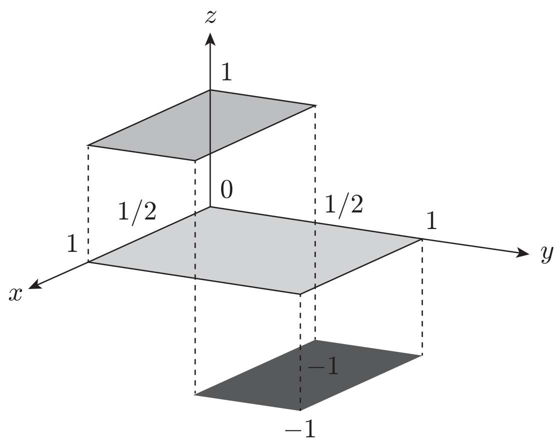

Figure 16.4 | ${}_h\Psi^{(0)}_{(0,0)}(x,y)$ - *The horizontal wavelet*

Two dimensional Haar bases will be written as:

$$\Psi^{h}_{(0,0)} = \phi^{(0)}_{(0,0)}(x)\psi^{(0)}_{(0,0)}(y) = \begin{cases} 1, & 0 \le x < 1, 0 \le y < \dfrac{1}{2} \\ -1, & 0 \le x < 1, \dfrac{1}{2} \le y < 1 \\ 0, & \text{otherwise,} \end{cases} \tag{16.56}$$

as illustrated in Fig. 16.4.

This can be interpreted as the wavelet operation in the *Y*-direction, which results in differences, followed by the scaling function operation in the *X*-direction, which averages these differences. Here, we are using the scale $l_1 = \frac{1}{2}$. So, from Figs 16.3 and 16.4, we may see that ${}_h\Psi^{(0)}_{(0,0)}(x,y)$ can be written in terms of the $\Phi^{(1)}$ basis at this scale as a sum of differences (in the *x*-direction).

$$\Psi^{h}_{(0,0)} \equiv {}_h\Psi^{(0)}_{(0,0)}(x,y) = (\Phi^{(1)}_{(0,0)} - \Phi^{(1)}_{(0,1)}) + (\Phi^{(1)}_{(1,0)} - \Phi^{(1)}_{(1,1)}) \tag{16.57}$$

This is a sum in the x -direction (due to the scaling function) of the differences in the *Y*-direction caused by the wavelet action. The action of differential causes the vertical edges parallel to the x-axis, hence the use of h in ${}_h\Psi^{(0)}_{(0,0)}$ (or $\Psi^{h}_{(0,0)}$). Next, we have ${}_v\Psi^{(0)}_{(0,0)}$ or just,

$$\Psi^{v}_{(0,0)}(x,y)=\psi(x)\phi(y)=\begin{cases}1, & 0\le x<\dfrac{1}{2}, 0\le y<1\\ -1, & \dfrac{1}{2}\le x<1, 0\le y<1\\ 0, & \text{otherwise.}\end{cases} \tag{16.58}$$

Here, the wavelet action in the x-direction causes the vertical edges parallel to the y-axis, as shown in Fig. 16.5.

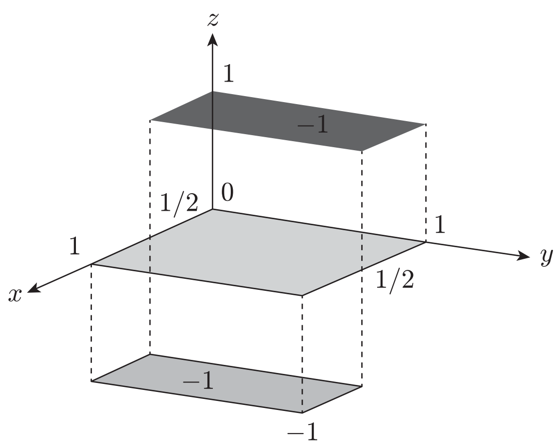

Figure 16.5 | $\Psi^{v}_{(0,0)}(x,y)$ - *The vertical wavelet*

Again we can see from Fig. 16.3 and 16.5 that this $\phi^{v}_{(0,0)}(x,y)$ can be expressed in terms of the $\Phi^{(1)}$ basis as a difference of sums in the y-direction,

$$\Psi^{v}_{(0,0)}=(\Phi^{(1)}_{(0,0)}+\Phi^{(1)}_{(0,1)})-(\Phi^{(1)}_{(1,0)}+\Phi^{(1)}_{(1,1)}), \tag{16.59}$$

which can be seen clearly as we look at the back positive half versus the front negative half in Fig. 16.5.
Next is the diagonal wavelet,

$$_{d}\Psi^{(0)}_{(0,0)}=\psi(x)\psi(y)=\begin{cases}1, & 0\le x<\dfrac{1}{2}; 0\le y<\dfrac{1}{2}\\ -1, & \dfrac{1}{2}\le x<1; 0\le y<\dfrac{1}{2}\\ 1, & \dfrac{1}{2}\le x<1; \dfrac{1}{2}\le y<1\\ -1, & 0\le x<\dfrac{1}{2}; \dfrac{1}{2}\le y<1\\ 0, & \text{otherwise}\end{cases} \tag{16.60}$$

is shown in Fig. 16.6,

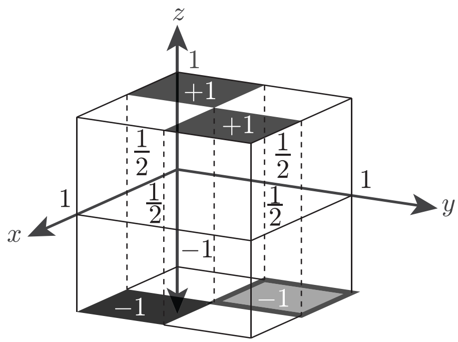

Figure 16.6 | ${}_d\Psi_{(0,0)}$ *- The diagonal wavelet*

where we should be able to verify that it can be expressed as a differences of two differences. Here we have actions of the wavelets in both of the horizontal and vertical directions. So, we expect more edges,

$$
\begin{aligned}
{}_d\Psi^{(0)}_{(0,0)} &= (\Phi^{(1)}_{(0,0)} - \Phi^{(1)}_{(1,0)}) + (\Phi^{(1)}_{(1,1)} - \Phi^{(1)}_{(0,1)}) \\
\Psi^{d}_{(0,0)} &\equiv (\Phi^{(1)}_{(0,0)} - \Phi^{(1)}_{(1,0)}) - (\Phi^{(1)}_{(0,1)} + \Phi^{(1)}_{(1,1)})
\end{aligned}
\tag{16.61}
$$

and we see its action as difference of differences.

The first two terms in (16.51) are due to the wavelet action with scale $l_1 = \frac{1}{2}$ in the x-direction with base as the first back half (extending in the x-direction) of the 1×1 square. The next two terms are due to the wavelet action in the opposite x-direction with base as the right half of the square. As seen in Fig. 16.6, the above two branches are two of the resulting four, the other two are with the same bases but in the opposite direction of the first two, and we left their tops and bottoms blank.

Last, we see from Fig. 16.3 that $\Phi^{(0)}_{(0,0)}(x,y)$ of (16.52),

$$
\Phi^{(0)}_{(0,0)}(x,y) = \Phi^{(0)}_{(0,0)}(x)\Phi^{(0)}_{(0,0)}(y) = \begin{cases} 1, & 0 \le x < 1; 0 \le y < 1 \\ 0, & \text{otherwise} \end{cases}
\tag{16.62}
$$

is the sum of the following four scaling functions $\Phi^{(1)}$ at the four $\frac{1}{2}\times\frac{1}{2}$ squares,

$$
\Phi^{(0)}_{(0,0)} = \Phi^{(1)}_{(0,0)} + \Phi^{(1)}_{(0,1)} + \Phi^{(1)}_{(1,0)} + \Phi^{(1)}_{(1,1)}.
\tag{16.63}
$$

16.7.1 The Basis Transformation

Following our quest for the one-dimensional case, we have a possibility of exploring the relation between the above wavelets $\Phi^{(0)}$ at scale $l_0 = 1$ and those $\Phi^{(1)}$ at scale $l_1 = \frac{1}{2}$. We have already prepared for this in Eqs (16.57), (16.59), (16.61), and (16.64),

$$
\Phi^{(0)}_{(0,0)} = \Phi^{(1)}_{(0,0)} + \Phi^{(1)}_{(0,1)} + \Phi^{(1)}_{(1,0)} + \Phi^{(1)}_{(1,1)}
\tag{16.64}
$$

$$
{}_h\Psi^{(0)}_{(0,0)} = \Phi^{(1)}_{(0,0)} - \Phi^{(1)}_{(0,1)} + \Phi^{(1)}_{(1,0)} - \Phi^{(1)}_{(1,1)}
\tag{16.65}
$$

$$ {}_{v}\Psi^{(0)}_{(0,0)} = \Phi^{(1)}_{(0,0)} + \Phi^{(1)}_{(0,1)} - \Phi^{(1)}_{(1,0)} - \Phi^{(1)}_{(1,1)} \tag{16.66} $$

$$ = (\Phi^{(1)}_{(0,0)} + \Phi^{(1)}_{(0,1)}) - (\Phi^{(1)}_{(1,0)} + \Phi^{(1)}_{(1,1)}) \tag{16.66a} $$

$$ {}_{d}\Psi^{(0)}_{(0,0)} = \Phi^{(1)}_{(0,0)} + \Phi^{(1)}_{(0,1)} - \Phi^{(1)}_{(1,0)} - \Phi^{(1)}_{(1,1)} \tag{16.67} $$

$$ = (\Phi^{(1)}_{(0,0)} + \Phi^{(1)}_{(1,1)}) - (\Phi^{(1)}_{(0,1)} + \Phi^{(1)}_{(1,0)}) \tag{16.67a} $$

We can write these four equations as the following matrix transformation equation:

$$ \begin{bmatrix} \Phi^{(0)}_{(0,0)} \\ \Psi^{h}_{(0,0)} \\ \Psi^{v}_{(0,0)} \\ \Psi^{d}_{(0,0)} \end{bmatrix} = \begin{bmatrix} 1 & 1 & 1 & 1 \\ 1 & -1 & 1 & -1 \\ 1 & 1 & -1 & -1 \\ 1 & -1 & -1 & 1 \end{bmatrix} \begin{bmatrix} \Phi^{(1)}_{(0,0)} \\ \Phi^{(1)}_{(0,1)} \\ \Phi^{(1)}_{(1,0)} \\ \Phi^{(1)}_{(1,1)} \end{bmatrix} $$

which we can rewrite symbolically as

$$ \left(\Phi^{(0)}, \Psi^{(0)}\right) \equiv \Omega \Phi^{(1)} \tag{16.68} $$

with Ω as the above 4×4 square matrix. We can find Ω^{-1}, the inverse, of this matrix Ω so that we can write $\Phi^{(1)} = \Omega^{-1}(\Phi^{(0)}, \Psi^{(0)})$ as follows,

$$ \begin{bmatrix} \Phi^{(1)}_{(0,0)} \\ \Phi^{(1)}_{(0,1)} \\ \Phi^{(1)}_{(1,0)} \\ \Phi^{(1)}_{(1,1)} \end{bmatrix} = \frac{1}{4} \begin{bmatrix} 1 & 1 & 1 & 1 \\ 1 & -1 & 1 & -1 \\ 1 & 1 & -1 & -1 \\ 1 & -1 & -1 & 1 \end{bmatrix} \begin{bmatrix} \Phi^{(0)}_{(0,0)} \\ \Psi^{h}_{(0,0)} \\ \Psi^{v}_{(0,0)} \\ \Psi^{d}_{(0,0)} \end{bmatrix} \tag{16.69} $$

where we can easily show that $\Omega^{-1} = \frac{1}{4}\Omega$

16.7.2 The Decomposition in $2D$ sense

At the scale $l_1 = \frac{1}{2}$, our array $\begin{bmatrix} s_{0,0} & s_{0,1} \\ s_{1,0} & s_{1,1} \end{bmatrix}$ of samples can be used with the mere $\Phi^{(1)}$ scaling functions to approximate the image as

$$ \tilde{f} = s_{0,0}\Phi^{(1)}_{(0,0)} + s_{0,1}\Phi^{(1)}_{(0,1)} + s_{(1,0)}\Phi^{(1)}_{(1,0)} + s_{1,1}\Phi^{(1)}_{(1,1)}, \tag{16.70} $$

as can be seen from Fig. 16.3, where the four cubes of the $\Phi^{(1)}$ are given the $s_{0,0}$, $s_{0,1}$, $s_{1,0}$, and $s_{1,1}$ heights at their respective locations as indicated by the subscripts (m,n) in $\Phi^{(1)}_{(m,n)}, m,n = 0,1$. For example, the array $\begin{bmatrix} 6 & 3 \\ 1 & 2 \end{bmatrix}$ gives the discontinuous surface for $\tilde{f}$ in Fig. 16.7,

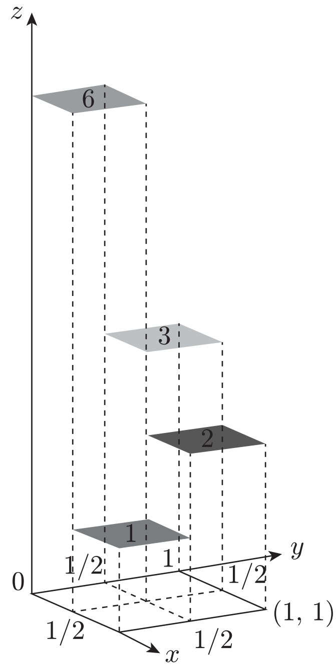

Figure 16.7 | *The array*

$$\tilde{f} = 6\Phi^{(1)}_{(0,0)} + 3\Phi^{(1)}_{(0,1)} + 1\Phi^{(1)}_{(1,0)} + 2\Phi^{(1)}_{(1,1)} \tag{16.71}$$

where we recall from Eq. (16.63) that $\Phi^{(0)}_{(0,0)} = \Phi^{(1)}_{(0,0)} + \Phi^{(1)}_{(0,1)} + \Phi^{(1)}_{(1,0)} + \Phi^{(1)}_{(1,1)}$. However, as we expect, this does not give much information, or, in particular, details about the image (array). It parallels what we used as a one low pass filter in the one-dimensional case.

Now comes the role of the above inverse transformation that gives us the decomposition (analysis) of the image. This is seen, where

$$\Phi^{(1)}_{(0,0)} = \frac{1}{4}[\Phi^{(0)}_{(0,0)} + \Psi^{h}_{(0,0)} + \Psi^{v}_{(0,0)} + \Psi^{d}_{(0,0)}]$$
$$\Phi^{(1)}_{(0,1)} = \frac{1}{4}[\Phi^{(0)}_{(0,0)} - \Psi^{h}_{(0,0)} + \Psi^{v}_{(0,0)} - \Psi^{d}_{(0,0)}]$$
$$\Phi^{(1)}_{(1,0)} = \frac{1}{4}[\Phi^{(0)}_{(0,0)} + \Psi^{h}_{(0,0)} - \Psi^{v}_{(0,0)} - \Psi^{d}_{(0,0)}]$$
$$\Phi^{(1)}_{(1,1)} = \frac{1}{4}[\Phi^{(0)}_{(0,0)} - \Psi^{h}_{(0,0)} - \Psi^{v}_{(0,0)} + \Psi^{d}_{(0,0)}].$$

Thus, the decomposition of the approximate surface $\tilde{f}$ in Eq. (16.70) in terms of $\Phi^{(0)}_{(0,0)}$, $\Psi^{h}_{(0,0)}$, $\Psi^{v}_{(0,0)}$, and $\Psi^{d}_{(0,0)}$ is obtained by substituting in Eq. (16.55) for $\Phi((0,0))^{(1)}, \Phi((0,1))^{(1)}, \Phi((1,0))^{(1)}$, and $\Phi((1,1))^{(1)}$ from the above four equations to have

$$\begin{aligned}
\tilde{f} &= s_{0,0}\Phi^{(1)}_{(0,0)} + s_{0,1}\Phi^{(1)}_{(0,1)} + s_{1,0}\Phi^{(1)}_{(1,0)} + s_{1,1}\Phi^{(1)}_{(1,1)} \\
&= s_{0,0}[\Phi^{(0)}_{(0,0)} + \Psi^{h}_{(0,0)} + \Psi^{v}_{(0,0)} + \Psi^{d}_{(0,0)}] \\
&\quad + s_{0,1}[\Phi^{(0)}_{(0,0)} - \Psi^{h}_{(0,0)} + \Psi^{v}_{(0,0)} - \Psi^{d}_{(0,0)}] \\
&\quad + s_{(1,0)}[\Phi^{(0)}_{(0,0)} + \Psi^{h}_{(0,0)} - \Psi^{v}_{(0,0)} - \Psi^{d}_{(0,0)}] \\
&\quad + s_{1,1}[\Phi^{(0)}_{(0,0)} - \Psi^{h}_{(0,0)} - \Psi^{v}_{(0,0)} + \Psi^{d}_{(0,0)}] \\
&= \frac{1}{4}(s_{0,0} + s_{0,1} + s_{1,0} + s_{1,1})\Phi^{(0)}_{(0,0)} \\
&\quad + \frac{1}{4}(s_{0,0} - s_{0,1} + s_{1,0} - s_{1,1})\Psi^{h}_{(0,0)} \\
&\quad + \frac{1}{4}((s_{0,0} + s_{0,1}) - (s_{1,0} + s_{1,1}))\Psi^{v}_{(0,0)} \\
&\quad + \frac{1}{4}((s_{0,0} - s_{0,1}) - (s_{1,0} - s_{1,1}))\Psi^{d}_{(0,0)}.
\end{aligned} \tag{16.72}$$

Here, we see that the coefficients of $\Phi^{(0)}_{(0,0)}$ gives us the average $\frac{1}{4}(s_{0,0} + s_{0,1} + s_{1,0} + s_{1,1})$ of the four element sequence in the array. The coefficients of $\Psi^{h}_{(0,0)}$ give the sum of the differences in its two rows. The coefficients of $\Psi^{v}_{0,0}$ give the difference between the sums of the two rows, and that of $\Psi^{d}_{0,0}$ gives the difference between the difference of the two elements in the first row and the difference of the two elements in the second row. We can also see the latter as $s_{0,0} - s_{0,1} - s_{1,0} + s_{1,1} = (s_{0,0} + s_{1,1}) - (s_{0,1} + s_{1,0})$, which is the difference between the sums of the two elements along the two diagonals of the array.

Example 16.7.1 — 2D decomposition

For our simple example of $\begin{bmatrix} s_{0,0} & s_{0,1} \\ s_{1,0} & s_{1,1} \end{bmatrix} = \begin{bmatrix} 6 & 3 \\ 1 & 2 \end{bmatrix}$, its decomposition is

$$\begin{aligned}
\tilde{f} &= \left(\frac{6+3+1+2}{4}\right)\Phi^{(0)}_{(0,0)} + \left(\frac{6-3+1-2}{4}\right)\Psi^{h}_{(0,0)} \\
&\quad + \left(\frac{6+3-(1+2)}{4}\right)\Psi^{v}_{(0,0)} + \left(\frac{6-3-1+2}{4}\right)\Psi^{d}_{(0,0)} \\
&= \frac{12}{4}\Phi^{(0)}_{(0,0)} + \frac{2}{4}\Psi^{h}_{(0,0)} + \frac{6}{4}\Psi^{v}_{(0,0)} + \frac{4}{4}\Psi^{d}_{(0,0)}.
\end{aligned} \tag{16.73}$$

The first coefficient $\frac{12}{4}$ in Eq. (16.73) is a large number $\frac{1}{4}(6+3+1+2)$ compared to the others, and it tells about the average of the four samples being large and thus has highest energy. The next coefficient of the small $\frac{2}{4} = \frac{(6-3)+(1-2)}{4}$ tells that there are no drastic changes in the two rows. The third relatively large coefficient of $\frac{6}{4} = \frac{(6+3)-(1+2)}{4}$ tells about a major difference between the sums of the two rows. The last coefficient of $\frac{4}{4} = \frac{(6+2)-(3+1)}{4}$ sees no drastic change between the sums of the two elements $(5+2)$ and $(3+1)$ on the two diagonals, as seen in Eq. (16.67a).

The readers encouraged to look at $\begin{bmatrix} 16 & 4 \\ 3 & -1 \end{bmatrix}$ for drawing similar observations.

Looking at equation Eq. (16.72), we get a sense for the first term being the result of a Haar low pass filter on each of the two rows, as indicated by $\frac{1}{4}(s_{0,0}+s_{0,1})$, and $\frac{1}{4}(s_{1,0}+s_{1,1})$, followed by another low pass filter as indicated by adding $\frac{1}{4}(s_{0,0}+s_{0,1})$ and $\frac{1}{4}(s_{1,0}+s_{1,1})$. The second term can be seen, as a Haar high pass filter on the two rows followed by a low pass filter. The third term would be two low pass filters on the two rows followed by a high pass filter. The fourth term with coefficients written as $(s_{0,0}-s_{1,0})-(s_{0,1}-s_{1,1})$ is a high pass filter on both columns followed by another high pass filter.

What we expect from a double Haar wavelet transform is to filter with its one-dimensional filter in the x-direction and follow it by filtering in the y-direction. This resembles what we do in partial differentiation, coming from the calculus of one variable to that of two or several variables.

Indeed, it turns out that if we operate on the 2×2 array by the Haar filter $\frac{1}{2}\begin{bmatrix} 1 & 1 \\ 1 & -1 \end{bmatrix}$ in the x-direction, then follow it by the same operation in the y-direction for a 2×2 array, we obtain a complete decomposition of the array. It is a bit different for the $2n\times 2n, n>1$ array. For our example of $S=\begin{bmatrix} 6 & 3 \\ 2 & 1 \end{bmatrix}$, the horizontal sweep (of a Haar low pass filter on each of the two rows) gives

$$\begin{bmatrix} 6 & 3 \\ 1 & 2 \end{bmatrix} \xrightarrow{H} \begin{bmatrix} \frac{6+3}{2} & \frac{6-3}{2} \\ \\ \frac{1+2}{2} & \frac{1-2}{2} \end{bmatrix} = \begin{bmatrix} \frac{9}{2} & \frac{3}{2} \\ \\ \frac{3}{2} & -\frac{1}{2} \end{bmatrix}.$$

The vertical sweep (of a Haar low pass filter followed by a high pass filter on each of the two columns) on the above result gives

$$\begin{bmatrix} \frac{9}{2} & \frac{3}{2} \\ \frac{3}{2} & -\frac{1}{2} \end{bmatrix} \xrightarrow{V} \begin{bmatrix} \frac{\frac{9}{2}+\frac{3}{2}}{2} & \frac{\frac{3}{2}-\frac{1}{2}}{2} \\ \\ \frac{\frac{9}{2}-\frac{3}{2}}{2} & \frac{\frac{3}{2}+\frac{1}{2}}{2} \end{bmatrix} = \begin{bmatrix} \frac{12}{4} & \frac{2}{4} \\ \\ \frac{6}{4} & \frac{4}{4} \end{bmatrix}. \tag{16.74}$$

The horizontal sweep followed by a vertical sweep on $S=\begin{bmatrix} s_{0,0} & s_{0,1} \\ s_{1,0} & s_{1,1} \end{bmatrix}$ with the use of the two-dimensional Haar wavelet transform follows. First, let us refer to the horizontal and vertical sweeps by Ω_H and Ω_V operations, respectively, then

$$S = \begin{bmatrix} s_{0,0} & s_{0,1} \\ s_{1,0} & s_{1,1} \end{bmatrix} \xrightarrow{\Omega_H} \frac{1}{2} \begin{bmatrix} s_{0,0} + s_{0,1} & s_{0,0} - s_{0,1} \\ s_{1,0} + s_{1,1} & s_{1,0} - s_{1,1} \end{bmatrix} \tag{16.75}$$

$$S = \begin{bmatrix} s_{0,0} & s_{0,1} \\ s_{1,0} & s_{1,1} \end{bmatrix} \xrightarrow{\Omega_V} \frac{1}{2} \begin{bmatrix} s_{0,0} + s_{1,0} & s_{0,1} + s_{1,1} \\ s_{0,0} - s_{1,0} & s_{0,1} - s_{1,1} \end{bmatrix}. \tag{16.76}$$

So, the horizontal sweep followed by the vertical sweep on S follows from operating with Ω_V on the result in Eq. (16.75),

$$\begin{aligned} &\Omega_V \Omega_H S \\ &= \frac{1}{4} \begin{bmatrix} (s_{0,0} + s_{0,1}) + (s_{1,0} + s_{1,1}) & (s_{0,0} - s_{0,1}) + (s_{1,0} - s_{1,1}) \\ (s_{0,0} + s_{0,1}) - (s_{1,0} + s_{1,1}) & (s_{0,0} - s_{0,1}) - (s_{1,0} - s_{1,1}) \end{bmatrix} \\ &= \frac{1}{4} \begin{bmatrix} s_{0,0} + s_{0,1} + s_{1,0} + s_{1,1} & s_{0,0} - s_{0,1} + s_{1,0} - s_{1,1} \\ s_{0,0} + s_{0,1} - s_{1,0} + s_{1,1} & s_{0,0} - s_{0,1} - s_{1,0} - s_{1,1} \end{bmatrix} \end{aligned} \tag{16.77}$$

which is what we have in Eq. (16.72) with the use of the four wavelets basis, where the four elements of the above matrix $w_{0,0}, w_{0,1}, w_{1,0},$ and $w_{1,1}$ correspond to the coefficients of $\Phi^{(0)}_{(0,0)}, \Phi^{h}_{(0,0)}, \Phi^{v}_{(0,0)}$, and $\Phi^{d}_{(0,0)}$ in Eq. (16.72).

16.7.3 Working with Bigger Arrays (4 4 toy example)

What we did above was for a 2×2 array, where we constructed the two dimensional (Haar) wavelets bases $\Phi^{(0)}_{(0,0)}$, $\Psi^{h}_{(0,0)}$, $\Psi^{v}_{(0,0)}$, and $\Psi^{d}_{(0,0)}$. There, we ended with pure averagings that gave us the average of the samples of the array as the coefficient of the pure two-dimensional low pass filter asociated with $\Phi^{(0)}_{0,0}$.

The problem becomes more involved when we consider a 4×4 array with its 16 elements. First, we go to scale $l_2 = \frac{1}{4}$, and we have to find 16 bases on the sixteen $\frac{1}{4} \times \frac{1}{4}$ squares of the unit square in Fig. 11.1. Second, and most important, when we go to the 4×4 array, the above horizontal and vertical sweeps will not be enough, as we shall discuss in the following sections. This is so since instead of ending with pure averaging (where we stop) at the top left corner of the 2×2 case, we will have four elements of averages mixed with differences at the top left corners of the resulting four 2×2 matrices. These four elements must be operated on by the two sweeps to result in a pure averaging in the top left corner of the resulting 4×4 matrix. The remaining 12 elements of the first two sweeps in the four 2×2 arrays are then distributed to the remaining three 2×2 arrays according to their wavelet operation content. For example, those bottom right elements of the four 2×2 arrays of the first two sweeps have the most differencing, so they are relegated to the bottom right 2×2 array. This will be illustrated with complete details in the following Example 16.7.2.

Example 16.7.2 — The double Haar transform of an array.

In this example we will consider a 4×4 array

$$S = \begin{pmatrix} 9 & 7 & 6 & 2 \\ 5 & 3 & 4 & 4 \\ 8 & 2 & 4 & 0 \\ 6 & 0 & 2 & 2 \end{pmatrix}. \tag{16.78}$$

The Haar wavelet matrix for this 4×4 case is

$$\Omega = \frac{1}{2}\begin{bmatrix} 1 & 1 & 0 & 0 \\ 1 & -1 & 0 & 0 \\ 0 & 0 & 1 & 1 \\ 0 & 0 & 1 & -1 \end{bmatrix} \tag{16.79}$$

The horizontal sweep of this Haar filter matrix on the array S in Eq. (16.78) will average then difference the first two elements of the first row of S, then does the same for next two elements. This is done on the rest of the three rows,

$$\Omega_H S = \Omega_H \begin{pmatrix} 9 & 7 & 6 & 2 \\ 5 & 3 & 4 & 4 \\ 8 & 2 & 4 & 0 \\ 6 & 0 & 2 & 2 \end{pmatrix}$$

$$\rightarrow \begin{pmatrix} \frac{9+7}{2} & \frac{9-7}{2} & \frac{6+2}{2} & \frac{6-2}{2} \\ \frac{5+3}{2} & \frac{5-3}{2} & \frac{4+4}{2} & \frac{4-4}{2} \\ \frac{8+2}{2} & \frac{8-2}{2} & \frac{4+0}{2} & \frac{4-0}{2} \\ \frac{6+0}{2} & \frac{6-0}{2} & \frac{2+2}{2} & \frac{2-2}{2} \end{pmatrix}$$

$$= \begin{pmatrix} 8 & 1 & 4 & 2 \\ 4 & 1 & 4 & 0 \\ 5 & 3 & 2 & 2 \\ 3 & 3 & 2 & 0 \end{pmatrix}. \tag{16.80}$$

This is followed by the vertical sweep as $\Omega_V \Omega_H S$. This averages then differences the first two elements of the first column of the above result of $\Omega_H S$, then does the same for the rest of the three columns,

$$\Omega_V \Omega_H S = \Omega_V \begin{pmatrix} 8 & 1 & 4 & 2 \\ 4 & 1 & 4 & 0 \\ 5 & 3 & 2 & 2 \\ 3 & 3 & 2 & 0 \end{pmatrix}$$

$$= \begin{pmatrix} \frac{8+4}{2} & \frac{1+1}{2} & \frac{4+4}{2} & \frac{2+0}{2} \\ \frac{8-4}{2} & \frac{1-1}{2} & \frac{4-4}{2} & \frac{2-0}{2} \\ \frac{5+3}{2} & \frac{3+3}{2} & \frac{2+2}{2} & \frac{2+0}{2} \\ \frac{5-3}{2} & \frac{3-3}{2} & \frac{2-2}{2} & \frac{2-0}{2} \end{pmatrix}$$

$$= \begin{pmatrix} 6 & 1 & 4 & 1 \\ 2 & 0 & 0 & 1 \\ 4 & 3 & 2 & 1 \\ 1 & 0 & 0 & 1 \end{pmatrix}. \tag{16.81}$$

Let us first note, as we have indicated above, that this result of the two sweeps is not the final one of decomposing the 4×4 array S. The first indication is that the top left corner element 6 is not the average of the array, the latter is $\frac{1}{16}(9+7+6+2+5+3+4+4+8+2+4+0+6+0+2+2) = \frac{64}{16} = 4.$ We note from the middle steps leading to Eqs (16.80) and (16.81) that the four elements $\begin{bmatrix} 6 & 4 \\ 4 & 2 \end{bmatrix}$ at the top left corners of the four 2×2 submatrices are the result of two averagings. We also know from decomposing a 2×2 array that the two sweeps there end with the final decomposition. Thus, we have to decompose this array $\begin{bmatrix} 6 & 4 \\ 4 & 2 \end{bmatrix}$ with the two sweeps,

$$\begin{bmatrix} 6 & 4 \\ 4 & 2 \end{bmatrix} \xrightarrow{H} \frac{1}{2}\begin{bmatrix} 6+4 & 6-4 \\ 4+2 & 4-2 \end{bmatrix} = \begin{bmatrix} 5 & 1 \\ 3 & 1 \end{bmatrix} \tag{16.82a}$$

and

$$\begin{bmatrix} 5 & 1 \\ 3 & 1 \end{bmatrix} \xrightarrow{V} \frac{1}{2}\begin{bmatrix} 5+3 & 1+1 \\ 5-3 & 1-1 \end{bmatrix} = \begin{bmatrix} 4 & 1 \\ 1 & 0 \end{bmatrix}, \tag{16.82b}$$

which gives the numbers 4 as the average of the whole 4×4 array at its top left corner. This submatrix will take the top left corner for our final decomposition of the 4×4 array.

Now, the four top right corners elements in $\begin{bmatrix} 1 & 1 \\ 3 & 1 \end{bmatrix}$ of the four 2×2 submatrices in Eq. (16.81) of the result of the two sweeps are the result of differencing followed by averaging, and will be placed in the top right corner of the final 4×4 matrix as shown below in Eq. (16.83). The bottom left corner elements in $\begin{bmatrix} 2 & 0 \\ 1 & 0 \end{bmatrix}$ of Eq. (16.81) are the result of averaging followed by differencing, and will be relegated to the bottom left corner of the final 4×4 matrix. The bottom right corner elements in $\begin{bmatrix} 0 & 1 \\ 0 & 1 \end{bmatrix}$ of (16.81) are the result of differencing followed by differencing, and will be placed in the bottom right corner of the final 4×4 matrix of the decomposed array. This final result is termed the *two-dimensional Haar wavelet transform* Ω of S,

$$\Omega S = \begin{bmatrix} 4 & 1 & 1 & 1 \\ 1 & 0 & 3 & 1 \\ & & & \\ 2 & 0 & 0 & 1 \\ 1 & 0 & 0 & 1 \end{bmatrix}. \tag{16.83}$$

We note that while the top left corner element 4 gives the average of the array S, the bottom right element small value of 1 indicates that there is not much of a big surprise change $\frac{1}{4}[(9+3+4+2)-(6+2+4+2)] = \frac{1}{4}(18-14) = 1$ along the diagonals of the array S in (11.25). The interpretation of the five resulting zero elements are left for the reader. For example, such zeros indicate a relative smoothness inside of the array. It is also true that the above result in Eq. (16.83) with its many zeros is easier to transmit than the original S array in (16.79). We see here that the elements of the bottom right corner submatrix in Eq. (16.83), are some of the relatively small value elements. The ones there, may be replaced by zeros, which results in compressing the array or image.

We leave it as an exercise to double Haar transform the Letter L as represented inside a 4×4 array with $s_{0,1} = s_{2,1} = s_{3,1} = s_{4,1} = s_{4,2} = s_{4,3} = 1$ and the rest (placed on the $\frac{1}{4} \times \frac{1}{4}$ remaining ten squares) are zeros.

The answer is $\begin{bmatrix} \frac{3}{8} & \frac{1}{4} & \frac{1}{2} & 0 \\ -\frac{1}{4} & 0 & \frac{1}{4} & \frac{1}{4} \\ 0 & 0 & 0 & 0 \\ -\frac{1}{4} & -\frac{1}{4} & -\frac{1}{4} & -\frac{1}{4} \end{bmatrix}$.

We can easily see that $\frac{3}{8}$ gives the average of the element of the array $\frac{6}{16} = \frac{3}{8}$. This may represent an example of double Haar transforming a simple image. The question that remains is how to capture the original L-shaped image. So, we are against finding the transformation involved in such an inverse process.

Of course, we can backtrack what we did in previous Example 16.7.2, starting from the last operation, and undo what was done there followed by undoing the vertical then the horizontal sweep. Keeping track and accounting of this process may not be so easy. One way to resolve this is to use matrices and their familiar operations, which is what we shall attempt to do in the following section.

16.7.4 Inverse Transform: Matrix Notation

We shall need the transpose $A^T = [\alpha_{ji}]$ of the matrix $A = [\alpha_{ij}]$. Also, the fact that $(AB)^T = B^T A^T$. Furthermore, for $A = \begin{bmatrix} \frac{1}{2} & \frac{1}{2} \\ \frac{1}{2} & -\frac{1}{2} \end{bmatrix}$ of the Haar filter, we have $A = A^T$. We will try to represent the full operation of the double Haar wavelet transform, as done in the Example 16.7.2, with the help of the matrix operation.

The horizontal sweep of $S = \begin{pmatrix} s_{0,0} & s_{0,1} \\ s_{1,0} & s_{1,1} \end{pmatrix}$ by the low and high pass filter $\begin{bmatrix} \frac{1}{2} & \frac{1}{2} \\ \frac{1}{2} & -\frac{1}{2} \end{bmatrix}$ can be accomplished via $(AS^T)^T$,

$$(AS^T)^T = (S^T)^T A^T = SA^T = SA \tag{16.84}$$

where we used the fact that $(BC)^T = C^T B^T$, $(B^T)^T = B$, and that we have $A = A^T$, since $\begin{bmatrix} \frac{1}{2} & \frac{1}{2} \\ \frac{1}{2} & -\frac{1}{2} \end{bmatrix}^T = \begin{bmatrix} \frac{1}{2} & \frac{1}{2} \\ \frac{1}{2} & -\frac{1}{2} \end{bmatrix}$.

So, the horizontal sweep becomes

$$SA = \begin{bmatrix} s_{0,0} & s_{0,1} \\ s_{1,0} & s_{1,1} \end{bmatrix} \begin{bmatrix} \frac{1}{2} & \frac{1}{2} \\ \frac{1}{2} & -\frac{1}{2} \end{bmatrix}$$

$$= \begin{bmatrix} \frac{s_{0,0} + s_{0,1}}{2} & \frac{s_{0,0} - s_{0,1}}{2} \\ \frac{s_{1,0} + s_{1,1}}{2} & \frac{s_{1,0} - s_{1,1}}{2} \end{bmatrix} \tag{16.85}$$

which is an averaging followed by differencing on each row. Thus,

$$S = \begin{bmatrix} 9 & 7 \\ 5 & 3 \end{bmatrix} \xrightarrow{H} SA = \begin{bmatrix} 9 & 7 \\ 5 & 3 \end{bmatrix} \begin{bmatrix} \frac{1}{2} & \frac{1}{2} \\ \frac{1}{2} & -\frac{1}{2} \end{bmatrix}$$

$$= \begin{bmatrix} \frac{9+7}{2} & \frac{9-7}{2} \\ \frac{5+3}{2} & \frac{5-3}{2} \end{bmatrix} = \begin{bmatrix} 8 & 1 \\ 4 & 1 \end{bmatrix}. \tag{16.86}$$

We do this with matrices in order to have a chance at the inverse operation, preparation for the inverse double Haar transform. To find S from SA, we multiply SA from the right by A^{-1}, where we can verify that $A^{-1} = \begin{bmatrix} 1 & 1 \\ 1 & -1 \end{bmatrix}$,

$$\begin{aligned} AA^{-1} &= \begin{bmatrix} \frac{1}{2} & \frac{1}{2} \\ \frac{1}{2} & -\frac{1}{2} \end{bmatrix} \begin{bmatrix} 1 & 1 \\ 1 & -1 \end{bmatrix} \\ &= \begin{bmatrix} \frac{1}{2}+\frac{1}{2} & \frac{1}{2}-\frac{1}{2} \\ \frac{1}{2}-\frac{1}{2} & \frac{1}{2}+\frac{1}{2} \end{bmatrix} \\ &= \begin{bmatrix} 1 & 0 \\ 0 & 1 \end{bmatrix} \\ &= I \end{aligned}$$

where I is he identity matrix.

So,

$$\begin{aligned} (SA)A^{-1} &= \begin{bmatrix} 8 & 1 \\ 4 & 1 \end{bmatrix} \begin{bmatrix} 1 & 1 \\ 1 & -1 \end{bmatrix} \\ &= \begin{bmatrix} 8+1 & 8-1 \\ 4+1 & 4-1 \end{bmatrix} = \begin{bmatrix} 9 & 7 \\ 5 & 3 \end{bmatrix} \\ &= S \end{aligned}$$

as the original S array.

For the vertical sweep, its is obtained by

$$
\begin{aligned}
AS &= \begin{bmatrix} \frac{1}{2} & \frac{1}{2} \\ \frac{1}{2} & -\frac{1}{2} \end{bmatrix} \begin{bmatrix} 9 & 7 \\ 5 & 3 \end{bmatrix} \\
&= \begin{bmatrix} \frac{9+5}{2} & \frac{7+3}{2} \\ \frac{9-5}{2} & \frac{7-3}{2} \end{bmatrix} \\
&= \begin{bmatrix} 7 & 5 \\ 2 & 2 \end{bmatrix}.
\end{aligned}
$$

The original array S is recovered via multiplying the above AS by A^{-1} from the left,

$$
\begin{aligned}
S = A^{-1}AS &= \begin{bmatrix} 1 & 1 \\ 1 & -1 \end{bmatrix} \begin{bmatrix} 7 & 5 \\ 2 & 2 \end{bmatrix} \\
&= \begin{bmatrix} 7+2 & 5+2 \\ 7-2 & 5-2 \end{bmatrix} \\
&= \begin{bmatrix} 9 & 7 \\ 5 & 3 \end{bmatrix}
\end{aligned}
\tag{16.87}
$$

as the original S.

So, if we had already done the horizontal then the vertical sweeps, such a result, as shown in Eqs. (16.80), (16.81), and (16.83), amounts to $A(SA)$, and in our example, we have

$$
\begin{aligned}
A(SA) &= \begin{bmatrix} \frac{1}{2} & \frac{1}{2} \\ \frac{1}{2} & -\frac{1}{2} \end{bmatrix} \begin{bmatrix} 8 & 1 \\ 4 & 1 \end{bmatrix} \\
&= \begin{bmatrix} \frac{8+4}{2} & \frac{1+1}{2} \\ \frac{8-4}{2} & \frac{1-1}{2} \end{bmatrix} \\
&= \begin{bmatrix} 6 & 1 \\ 2 & 0 \end{bmatrix}.
\end{aligned}
\tag{16.88}
$$

To recover S, we operate on ASA from the right and left with A^{-1},

$$\begin{aligned} A^{-1}(ASA)A^{-1} &= \begin{bmatrix} 1 & 1 \\ 1 & -1 \end{bmatrix}\left(\begin{bmatrix} 6 & 1 \\ 2 & 0 \end{bmatrix}\begin{bmatrix} 1 & 1 \\ 1 & -1 \end{bmatrix}\right) \\ &= \begin{bmatrix} 1 & 1 \\ 1 & -1 \end{bmatrix}\begin{bmatrix} 7 & 5 \\ 2 & 2 \end{bmatrix} \\ &= \begin{bmatrix} 9 & 7 \\ 5 & 3 \end{bmatrix} \end{aligned} \tag{16.89}$$

as the original array S.

Thus, in summary, our direct two-sweep transformation is accomplished by $ASA = S'$, and the inverse operation $A^{-1}S'A^{-1} = S$ on S' recovers S.

It should be easy to extend this matrix representation of the two horizontal and vertical sweeps to a 4×4 array of samples. In practice, for images we need a large size $2^n \times 2^n$ array, as n that may reach 6 or 7 for high resolution.

Now we return to the complete double Haar transform of the 4×4 array. We know that the top left corner submatix $\begin{bmatrix} 4 & 1 \\ 1 & 0 \end{bmatrix}$ in Eq. (16.82b) of previous example was the result of the two sweeps on the four elements at the top left corners of the four submatrices. So, we must operate on this submatrix with $A^{-1}SA^{-1}$ to recover the original four elements, then return them to their respective four top left corners.

In our example, we have $S' = \begin{bmatrix} 4 & 1 \\ 1 & 0 \end{bmatrix}$,

$$\begin{aligned} S = A^{-1}S'A^{-1} &= \begin{bmatrix} 1 & 1 \\ 1 & -1 \end{bmatrix}\left\{\begin{bmatrix} 4 & 1 \\ 1 & 0 \end{bmatrix}\begin{bmatrix} 1 & 1 \\ 1 & -1 \end{bmatrix}\right\} \\ &= \begin{bmatrix} 1 & 1 \\ 1 & -1 \end{bmatrix}\begin{bmatrix} 5 & 3 \\ 1 & 1 \end{bmatrix} \\ &= \begin{bmatrix} 6 & 4 \\ 4 & 2 \end{bmatrix}. \end{aligned} \tag{16.90}$$

We need to recall that the second submatrix on the first row of the final double Haar transform came from the top right corners elements of the four submatices before transforming the top right submatrix, the same for the remaining three. The third submatrix on the second row came from the bottom left corners elements of the four submatrices, and they should return to their original locations. The same with the fourth submatrix in the second row, where elements come form the original lower left corners of the four submatices.

Thus, we must distribute the elements of $\begin{bmatrix} 6 & 4 \\ 4 & 2 \end{bmatrix}$ to the four top left corners, $\begin{bmatrix} 1 & 1 \\ 3 & 1 \end{bmatrix}$ to the top right corners, $\begin{bmatrix} 2 & 0 \\ 1 & 0 \end{bmatrix}$ to the bottom left corners, and $\begin{bmatrix} 0 & 1 \\ 0 & 1 \end{bmatrix}$ to the bottom right corner to have the result of only the two horizontal followed by a vertical sweeps as ASA,

$$ASA = \begin{bmatrix} 6 & 1 & 4 & 1 \\ 2 & 0 & 0 & 1 \\ 4 & 3 & 2 & 1 \\ 1 & 0 & 0 & 1 \end{bmatrix} \tag{16.91}$$

This ASA in Eq. (16.91) represents the result of the vertical sweep on the result of the horizontal sweep, i.e., $ASA \equiv S_V = AS_H$. So we should first free S_H with $A^{-1}S_V = A^{-1}AS_H = S_H$. Then, for $S_H = SA$, the original array is freed with $S_H A^{-1} = S$,

$$\begin{aligned} S_H &= A^{-1}S_V = A^{-1}(ASA) \\ &= \begin{bmatrix} 1 & 1 & 0 & 0 \\ 1 & -1 & 0 & 0 \\ 0 & 0 & 1 & 1 \\ 0 & 0 & 1 & -1 \end{bmatrix} \begin{bmatrix} 6 & 1 & 4 & 1 \\ 2 & 0 & 0 & 1 \\ 4 & 3 & 2 & 1 \\ 1 & 0 & 0 & 1 \end{bmatrix} \end{aligned} \tag{16.92}$$

$$\begin{aligned} S_H &= \begin{bmatrix} 6+2 & 1+0 & 4+0 & 1+1 \\ 6-2 & 1-0 & 4-0 & 1-1 \\ 4+1 & 3+0 & 2+0 & 1+1 \\ 4-1 & 3-0 & 2-0 & 1-1 \end{bmatrix} \\ &= \begin{bmatrix} 8 & 1 & 4 & 2 \\ 4 & 1 & 4 & 0 \\ 5 & 3 & 2 & 2 \\ 3 & 3 & 2 & 0 \end{bmatrix}. \end{aligned} \tag{16.93}$$

Now,

$$\begin{aligned} S &= S_H A^{-1} \\ &= \begin{bmatrix} 8 & 1 & 4 & 2 \\ 4 & 1 & 4 & 0 \\ 5 & 3 & 2 & 2 \\ 3 & 3 & 2 & 0 \end{bmatrix} \begin{bmatrix} 1 & 1 & 0 & 0 \\ 1 & -1 & 0 & 0 \\ 0 & 0 & 1 & 1 \\ 0 & 0 & 1 & -1 \end{bmatrix} \\ &= \begin{bmatrix} 8+1 & 8-1 & 4+2 & 4-2 \\ 4+1 & 4-1 & 4+0 & 4-0 \\ 5+3 & 5-3 & 2+2 & 2-2 \\ 3+3 & 3-3 & 2+0 & 2-0 \end{bmatrix} \\ &= \begin{bmatrix} 9 & 7 & 6 & 2 \\ 5 & 3 & 4 & 4 \\ 8 & 2 & 4 & 0 \\ 6 & 0 & 2 & 2 \end{bmatrix} \end{aligned} \tag{16.94}$$

which is our original array in Eq. (16.78) of prior example.

Example 16.7.3 — Unitary nature of transform matrix.

For any transformation in signal or image processing, it is important to ensure that the transformation guarantees two things in particular:

(a) Energy compaction
(b) Energy preservation

These important characteristics lead to compression of the data to be processed and also unique representation of the information for processing in further conveniently. The above characteristics are met if the transformation matrix is a 'unitary' matrix,which then results into a unitary transform.

A matrix 'A' is called unitary if $A^{-1} = A^{*T}$, where A^{*T} is conjugate transpose. For real matrix A, it is unitary if $A^{-1} = A^T$.

Let's consider a Haar transformation matrix H_A

$$H_A = \frac{1}{\sqrt{2}}\begin{bmatrix} 1 & 1 \\ -1 & 1 \end{bmatrix} \tag{16.95}$$

For this matrix,

$$H_A^{-1} = \frac{1}{\sqrt{2}}\begin{bmatrix} 1 & -1 \\ 1 & 1 \end{bmatrix} = H_A^T \tag{16.96}$$

∴ Haar matrix is unitary!
Let's now check if this H_A can 'decorrelate' the information and help achieve energy preservation.
Case (I):
Let's say we want to process

$$\vec{x} = \begin{bmatrix} 3 \\ 4 \end{bmatrix} \text{ using } H_A$$

Please note, $\vec{x}$ is highly correlated.
Given,

$$H_A = \frac{1}{\sqrt{2}}\begin{bmatrix} 1 & 1 \\ -1 & 1 \end{bmatrix} \text{ and } \vec{x} = \begin{bmatrix} 3 \\ 4 \end{bmatrix}$$

$$\vec{y} = A \cdot \vec{x} = \frac{1}{\sqrt{2}}\begin{bmatrix} 1 & 1 \\ -1 & 1 \end{bmatrix}\begin{bmatrix} 3 \\ 4 \end{bmatrix} = \frac{1}{\sqrt{2}}\begin{bmatrix} 7 \\ 1 \end{bmatrix} \tag{16.97}$$

Now, let's verify energy preservation.
Energy, i.e $\bar{x}$ will be

$$\| \vec{x} \|^2 = 3^2 + 4^2 = 25 \tag{16.98}$$

Energy in $\bar{y}$ will be,

$$\| \vec{y} \|^2 = \frac{7^2 + 1^2}{2} = 25 \tag{16.99}$$

as (16.98) and (16.100) match H_A preserves energy.

Note that ‘3’ and ‘4’ in $\bar{x}$ are highly correlated and ‘7’ and ‘1’ in $\bar{y}$ are decorrelated. This can help us achieve energy compaction, as ‘1’ is weaker compared to ‘7’ we can drop that and achieve compression.

After dropping ‘1’, energy is $\bar{y}$ will be

$$\| \tilde{y} \|^2 = \frac{7^2}{2} = \frac{49}{2} = 24.5 \tag{16.100}$$

Thus $\| \tilde{x} \|^2 \approx \| \tilde{y} \|^2$ and compression of 50% was achieved as we dropped one out of two elements of $\bar{y}$.

Example 16.7.4 — Demonstration of de-correlation.

Demonstration of de-correlation, energy compaction and energy preservation for 2D case using transformation matrix H_A, for given

$$H_A = \begin{bmatrix} 1 & 2 \\ 3 & 4 \end{bmatrix}$$

It can be easily noted that,all the elements in ‘x’ are highly correlated.

Now,since H_A is ‘separable’ , we shall apply it row-wise and column-wise as ‘x’ is a 2D entity (matrix) and we shall obtain output y as:

$$y = H_A \cdot x \cdot H_A^T = H_A \cdot x \cdot H_A^{-1} \tag{16.101}$$

$$y = \frac{1}{\sqrt{2}} \begin{bmatrix} 1 & 1 \\ -1 & 1 \end{bmatrix} \cdot \begin{bmatrix} 1 & 2 \\ 3 & 4 \end{bmatrix} \cdot \begin{bmatrix} 1 & -1 \\ 1 & 1 \end{bmatrix} \frac{1}{\sqrt{2}} \tag{16.102}$$

$$y = \begin{bmatrix} 5 & -1 \\ -2 & 0 \end{bmatrix} \tag{16.103}$$

$\therefore$ Energy in ‘x’ is:

$$\| x \|^2 = 1^2 + 2^2 + 3^2 + 4^2 = 30$$

Energy in ‘y’ is:

$$\| y \|^2 = 5^2 + (-2)^2 + (-1)^2 + 0^2 = 30$$

$\therefore$ Energy preservation is proven.

If we drop all elements of ‘y’ except ‘5’ then the energy will be 25.

We dropped 3 out of 4 elements and therefore achieved 75% compression and could retain 83.33% energy.

$\therefore$ This decorrelation is useful in energy compaction!

Example 16.7.5 — De-correlation using Hadamard matrix.

Given, $x = \begin{bmatrix} 100 & 98 & 98 & 100 \end{bmatrix}$.

Apply Hadamard transformation matrix to prove decorrelation, energy compaction and preservation.

A Hadmard matrix is named after french mathematician Jacques Hadmard. It is also at times referred as Walsh matrix, named after Jospeh Walsh who proposed it in 1923, and it emerges out of Walsh functions.

The natural ordered Hadmard matrix is governed by a recursive formulae. It is a unique square matrix with dimension of some power of 2, with all entries either +1 or –1 and property of orthogonality by virtue of which dot product of any two distinct rows or columns is zero. Generalized formula for Hadamard matrix is:

$$H(2^K) = \begin{bmatrix} H(2^{K-1}) & H(2^{K-1}) \\ H(2^{K-1}) & -H(2^{K-1}) \end{bmatrix} = H(2) \otimes H(2^{K-2})$$

For $2 \leq K \in N$, where $\otimes$ = Kronecker product.

$\therefore$ Members in family will be,

$$\therefore \qquad H(2^1) = \begin{bmatrix} 1 & 1 \\ 1 & -1 \end{bmatrix} = H_2, H_{2N} = \frac{1}{\sqrt{2}} \cdot H_2$$

(Normalized)

$$H(2^2) = \begin{bmatrix} 1 & 1 & 1 & 1 \\ 1 & -1 & 1 & -1 \\ 1 & 1 & -1 & -1 \\ 1 & -1 & -1 & 1 \end{bmatrix} = H_4, H_{4N} = \frac{1}{2} \cdot H_4$$

(Normalized)

We shall use this H_{4N} to analyze given $\bar{x}$.

Given question is 1D(vector).

$$\bar{y} = H_{4N} \cdot \bar{x} \tag{16.104}$$

$$\therefore \qquad \bar{y} = \frac{1}{2} \begin{bmatrix} 1 & 1 & 1 & 1 \\ 1 & -1 & 1 & -1 \\ 1 & 1 & -1 & -1 \\ 1 & -1 & -1 & 1 \end{bmatrix} \begin{bmatrix} 100 \\ 98 \\ 98 \\ 100 \end{bmatrix} = \begin{bmatrix} 198 \\ 0 \\ 0 \\ 2 \end{bmatrix}$$

It is easy to observe '$\bar{x}$' is highly correlated and $\bar{y}$ is extremely sparse or decorrelated.

Energy in $\bar{x}$

$$\| x \|^2 = 100^2 + 98^2 + 98^2 + 100^2 = 39208$$

Energy in $\bar{y}$

$$\| y \|^2 = 198^2 + 2^2 = 39208$$

If we drop '2' and retain only '198', energy will be 39204.

$\therefore$ By 75% compression, we achieve 99.9898% energy preservation !

Example 16.7.6 — Energy compaction using Hadamard matrix.

Given,

$$x = \begin{bmatrix} 100 & 100 & 98 & 99 \\ 100 & 100 & 94 & 96 \\ 98 & 97 & 99 & 100 \\ 100 & 99 & 97 & 94 \end{bmatrix}$$

We shall use Hadamard transformation matrix

$$\therefore \qquad H_{4N} = \frac{1}{\sqrt{2}} \begin{bmatrix} 1 & 1 & 1 & 1 \\ 1 & -1 & 1 & -1 \\ 1 & 1 & -1 & -1 \\ 1 & -1 & -1 & 1 \end{bmatrix}$$

Since 'x' is a matrix i.e. it is a 2D information and Since H_{4N} is separable, We apply it rowwise and columnwise.

$$\therefore \qquad y = H_{4N} \cdot x \cdot H_{4N}^{T} = H_{4N} \cdot x \cdot H_{4N}^{-1} \tag{16.105}$$

$$y = \begin{bmatrix} 392.75 & 0.25 & 4.25 & 0.75 \\ 2.75 & -0.75 & -4.75 & 0.75 \\ 0.75 & -1.75 & 2.25 & 0.75 \\ 0.75 & 1.25 & 1.25 & -1.25 \end{bmatrix} \tag{16.106}$$

We leave it to readers to verify that if we retain only 392.75 from 'y' from (16.60), and leave out all others:

(a) we achieve huge compression
(b) We retain almost all energy.

This is because:

(a) Transformation matrix is unitary.
(b) y is extremely sparse!

16.8 | Wavelets and Self-Similarity

Wavelets are often used to determine self-similarity amongst signals. This makes sense as Wavelets themselves are structures depicting self-similar nature and hence are the natural choice for such type of applications.

Conventionally signal processing makes use of robust LSI (Linear Shift Invariant) structure for analyzing various types of signals. For particular signals, which are self similar, a different approach is required.

When the signals in local segments are similar in specific way to the entire signal, they are called as self-similar signals. The temporal scaling of such signals produces the signal if it is deterministic else produces statistical characteristics in case of stochastic signals. In literature many examples of self-similar structures have been reported with the likes of Fractional Gaussian noise, homogeneous signals, fractional Brownian motion etc.

Dilation provides the foundation to achieve scale changes in Wavelet analysis. In fact, 'Dilation' and 'Dilation Equations' are truly at the heart of the Multiresolution framework we have seen since chapter 2. It is through the dilation equation we create a linkage to use 2-band or M-band filter bank structure to create the deployment platform for wavelet filters.

For many computer vision problems it is desired to have scale invariance. There could be two different images captured with different zoom or actual physical distance and yet the application may demand correct match and just the difference in the scales should not spoil the show.

Since dilation is inherent in any wavelet transformation, it leads to hidden **self-similarity** and in a way the fractals with self-similar structures lead to scale-invariant systems. One easier way of understanding scale-invariant systems is when an input is scaled by some scale, the output also gets scaled equally. Such scale-invariant systems (SIS) can be represented as:

$$S\left[x\left(\frac{t}{a}\right)\right] = y\left(\frac{t}{a}\right) \tag{16.107}$$

for $a > 0$. The scaling happens with reference to the independent variable, which is time t is this case. Thus, to gain scale-invariance, one has to give up time-invariance.

Let $k(t,\tau)$ be the system kernel which is function of t and τ both and characterizes linear but time varying system. For this kernel function to correspond to linear and time varying system, the necessary and sufficient condition is:

$$k(t,\tau) = a \times k(a \cdot t,\, a \cdot \tau) \tag{16.108}$$

System function can be written as,

$$y(t) = \int_{\tau} k(t,\tau) \cdot x(\tau) d\tau \tag{16.109}$$

Thus, the output is obtained by taking dot product between input and the kernel. For $\tau \neq 0$ the kernel $k(t,\tau)$ gets scaled at every instance, thus giving us,

$$\tau k(t,\tau) = h(t,\tau) \tag{16.110}$$

Given this,

$$y(t) = \int_{-\inf}^{\inf} x(\tau) h\left(\frac{t}{\tau}\right) \frac{d\tau}{\tau} = \int_{-\inf}^{\inf} x\left(\frac{t}{\tau}\right) h(\tau) \frac{d\tau}{\tau} \tag{16.111}$$

For a deterministic signal $x(t)$, it is self-similar if

$$x(t) = a^{-H} x(at) \tag{16.112}$$

OR

$$x\left(\frac{t}{a}\right) = a^{-H} x(t) \tag{16.113}$$

for $a > 0$

A random process $X(t)$, is self-similar if the mean (zeroth moment) $M_X(t)$ and autocorrelation $R_X(t,s)$

$$M_X(t) \equiv E[X(t)] = a^{-H} M_X(at) \tag{16.114}$$

and

$$R_X(t,s) \equiv E[X(t)X(s)] = a^{-2H} R_X(at,as) \tag{16.115}$$

for $a > 0$

In the MRA framework we have already seen the scaling of the wavelet kernel through dilation equation. Through the wavelet dilation equation the wavelet function gets connected with father equation, which is also called as *scaling* equation.

This leads to many hidden structures in every wavelet and its scaling function which are scaled down versions of the bigger signal and make the complete structure self similar. This is illustrated in Fig. 16.8.

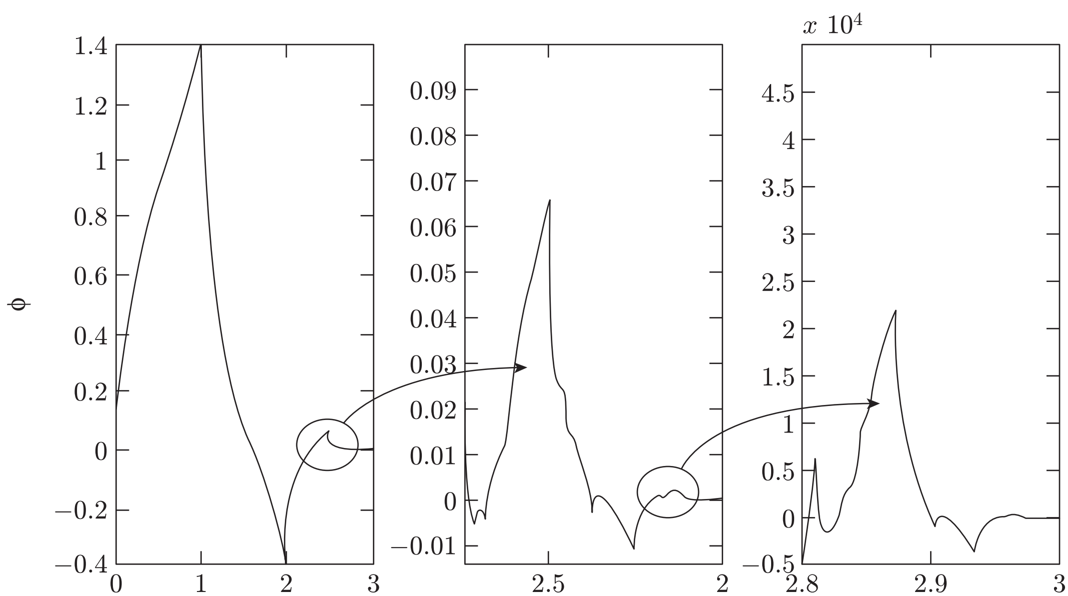

Figure 16.8 | *Daub-4 scaling function with hidden self-similarity.*

Because of this very unique property, scaling and wavelet functions can be used to detect self-similarity in signals. Interested readers can explore this further as this has started gaining importance in research community.

16.9 | Wavelet Transform: In Perspective of Moving from Continuous to Discrete

Historically, continuous wavelet transform (CWT) was discovered first and physicists and seismic analyzers looked at it as an alternative to windowed Fourier Transform.

In CWT of signal $f(t)$,

$$W_\psi f = F(a,b) = \frac{1}{\sqrt{2\pi C_\psi}} \int_{\mathbb{R}} \overline{\psi_{a,b}(t)} f(t)dt \tag{16.116}$$

For the admissibility condition to be satisfied it was necessary to have $0 < C_\psi < \inf$, thus

$$C_\psi = \int \mathbb{R} \,|\, \Psi(\omega) \,|^2 \frac{d\omega}{|\,\omega\,|} < \inf \tag{16.117}$$

which also means,

$$\int_{\mathbb{R}} \psi(t)dt = 0 \tag{16.118}$$

The wavelet transform is an overcomplete representation of the signal $f(t)$. Only if the $\psi(t)$ of the CWT complies with the MRA norms, discretization is possible, but the transform remains redundant.

16.9.1 Overcomplete Wavelet Transform

The approximation of CWT can be understood in the sense of computing it in a subset plane and then the DWT emerges out of evaluating it at dyadic points,

$$(a,b) \in \Gamma_{DWT} = \{(a_n, b_{nm}) : a_n = 2^n, b_{nm} = 2^{-n} m\} \tag{16.119}$$

It is important for Γ to have "regularity". For example, the semilog regular sampling can be $\Gamma(\Delta, a_0) = \{a_0^m\} \times \{n\Delta\}$. The reconstruction is done by using the Riesz basis. When the grid moves from semilog to a complete grid without subsampling, the transform is referred as Redundant Discrete Wavelet Transform (RDWT).

16.10 | Redundant Discrete Wavelet Transform

RDWT differs from Mallat's FWT (Fast Wavelet Transform) in only one aspect and that is it lacks subsampling. There are no downsamplers involved in the analysis part of the structure. RDWT is also called as 'stationary wavelet transform' or more popularly 'trous algorithm'. In RDWT as we double the samples at each step, it produces huge redundancy and computational time for DRWT is $O(N \log N)$ against $O(N)$ for FWT.

Few interesting advantages of DRWT are:

- DRWT is translation invariant, which is not true for FWT
- DRWT is extendable to non-dyadic inputs

One serious limitation of DRWT is being redundant the reconstruction is not unique. Two independent reconstructions are possible at every step.

$$\omega_{nk}^{DRWT} = \frac{2^{\frac{n}{2}}}{\sqrt{2\pi}} \int_{\mathbb{R}} f(t)\tilde{\psi}(2^n t - 2^{n-N} k)dt \tag{16.120}$$

This is again a very active area of research and interested readers can explore this further.

16.11 | Regularity and Convergence

These important topics have a strong connection with the wavelet filter design and we have discussed these in depth in Chapter 15. The best way to implement DWT is through multirate orthogonal perfect reconstruction filters. If we, however, start with filters which guarantee perfect reconstruction by satisfying the necessary conditions and solve the equations across scales, will the solution yield smooth and continuous ψ and ϕ. Well, not necessarily!

16.11.1 Convergence

Orthogonal wavelets will satisfy,

$$|H(\omega)|^2 + |H(\omega+\pi)|^2 = 1 \tag{16.121}$$

If we impose the necessary condition arriving out of dilation condition on filter coefficients we get,

$$H(0) = 1 \tag{16.122}$$

For the solution of n^{th} iteration of the scaling function in frequency domain we have,

$$\Phi_n(\omega) = \Phi_H\left(\frac{\omega}{2^n}\right)\prod_{i=1}^{n} H\left(\frac{\omega}{2i}\right) \tag{16.123}$$

What we check as test for convergence is as $n \to \inf$, whether the function $\Phi_n(\omega)$ converges to a reasonable function.

Regularity

The more critical question is whether the convergence mentioned in the previous subsection is to a smooth and continuous function.

Daubechies has given two crisp necessary conditions for the same:

(i) For point wise convergence $|H(\omega)| \le 1$ for $\omega \ne 0$
(ii) Another requirement is if,

$$H(\omega) = \left(\frac{1+\exp(-j\omega)}{2}\right)^N R(\omega) \tag{16.124}$$

the, $\max|R(\omega)| < 2^{N-1}$.

The second condition stems out of the fact that more zeros at $\omega = \pi$ for $H(\omega)$ more chance for scaling and wavelet function to be smooth.

The smoothness which governs regularity is closely associated with the number of vanishing moments.

If the wavelet function satisfies admissibility such that,

$$\int \psi(t)dt = 0 \tag{16.125}$$

the smoothness of this wavelet increases if it satisfies,

$$\int t^k \psi(t)dt = 0 \tag{16.126}$$

for integer values of k from 0 to K. The wavelet then has K vanishing moments. More the vanishing moments, smoother is the function.

Exercises

Exercise 16.1

Demonstrate de-correlation, energy compaction and energy preservation for 2D case using any orthogonal transformation matrix for given H_A,

$$H_A = \begin{bmatrix} 28 & 29 \\ 32 & 33 \end{bmatrix}$$

Exercise 16.2

Demonstrate de-correlation, energy compaction and energy preservation for 2D case using any orthogonal transformation matrix for given H_A,

$$H_A = \begin{bmatrix} 8 & 9 \\ 7 & 8 \end{bmatrix}$$

Exercise 16.3

Given,

$$\begin{bmatrix} 104 & 110 & 98 & 99 \\ 120 & 110 & 98 & 96 \\ 98 & 98 & 99 & 100 \\ 100 & 99 & 97 & 97 \end{bmatrix}$$

We shall use Hadamard transformation matrix.

Chapter 17

Wavelet Applications

17.1 | Introduction

We have looked at various mechanism for creating the wavelets, implementing and deploying them with conventional as well as modern strategies. In this chapter we expose readers to various applications from different domains to bring out ability of wavelets to solve real challenging problems.

17.2 | Application: Face Recognition Using Wavelet Packet Analysis

It is an application from image processing or in broader sense from computer vision. Face recognition is one of the biometric authentication problems. Face recognition involves extraction of critical features for the system to be able to recognize the face. A transform like wavelet transform, with an ability to look at the information locally as well as globally and create scalable constructs through the MRA framework is an apt choice for such kind of application.

Example 17.2.1 — Face detection in recognition.

Let us say we are looking at Surveillance application in which we have to monitor a particular region in which no person is allowed. In that case if we use face detection and recognition, we can get a very good analytics over a particular region. So we can say if somebody enters at a particular time in that restricted zone and what was he doing, with details like class of activity. This problem can also be looked from activity tracking and abnormality detection.

The basic difference between face detection and face recognition is that in face detection we look of similar features in all the faces while in face recognition we look for features which are different across the faces. In this application we deal with face recognition, so we assume that some region of face which contains image is given.

A typical face contains nose, mouth, etc. These are in focus when we look in different scales in different subspaces because they contain different frequencies as well as facial regions. So we need to go for a decorrelation in spatial as well as frequency domain. Therefore this is the signal where we need to look into time as well as frequency localization and that is why we use wavelets as they give better representation in terms of time and frequency. With wavelet packet analysis we not decompose the low frequency band but also the high frequency band. This gives richer representation of the face image. So there are two things here, we are decorrelating face in time as well as frequency and we are getting better face representation. So given an image we need to decompose it using wave packet analysis and then we can represent it by features and these features are well decorrelated so we can do good classification.

The only problem stands is with the dimensionality. If we decompose this image into multiple subbands (say 10-15 subbands), then the data we have for classification is huge which is difficult to manage. So we go for *moment's based approach* and we take only 1st and 2nd moments, that is mean and variance of feature and then we can classify.

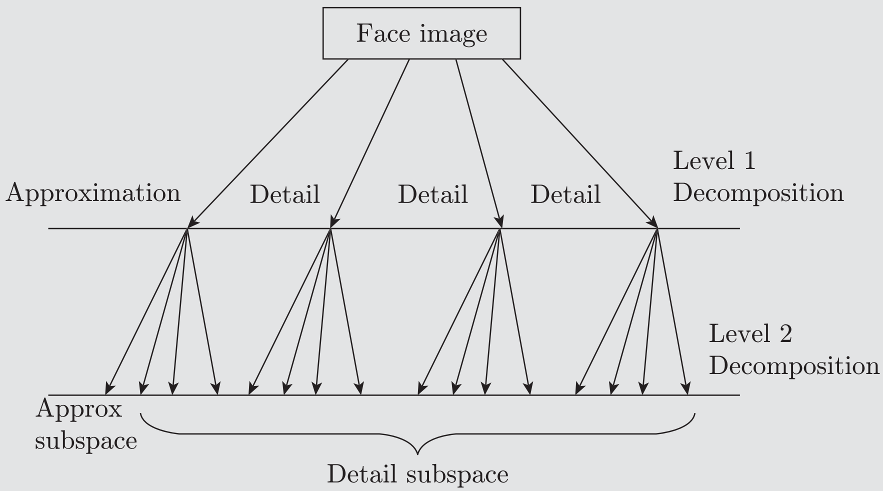

Figure 17.1 | *Two-Level Wavelet packet decomposition*

Face image is decomposed in approximation (Fig. 17.1) and detail subspace in level 1. In level 2 decomposition we can decompose approximation and details of level 1 further and we will get around 16 subspaces in which 1 is approximation subspace and 15 are detail subspace. Now we need to generate features from this, we will use mean and variance only for features representation.

When we utilize euclidean distance we generally have features which are not mean and variance together because we are now looking at probability distribution function rather then individual values. So we need a distance matrix which takes care of mean as well as variance so normal euclidean distance will not perform better in that case.

17.3 | Application of Wavelets in Data Mining

Data mining is ensemble of tool which we use to deal with huge amount of data efficiently for our purpose.

Example 17.3.1 — Data mining.

Data mining involves two things. One is storing the data with the help of efficient data structure and second is the retrieval of data from data structure for own purpose. When we have to store and retrieve the data, the user basically interacts with the data structure by the help of some responses and queries. In practice when we have large amount of time series data, the queries that are generally encountered are not point queries but are spread over some larger duration of time. For example, if data is stock prices of a company for a particular period of time then queries which we encounter are generally like on which month the stock prices had a rising trend or on which week stock prices should deep dip.

In order to get this data we need to do some post processing on the raw data and we get the output of this query. This way we interact with the data structure and get the output.

Wavelet transform on a signal gives us the information at various levels of abstraction and with various translates and various scales. Raw data can be thought of a sequence or signal, i.e. daily stock price as a signal than depending upon the response or queries we can say that we are interested on various translates in the data such as we are interested in the data 2 months back or 6 months back. Also, we are interested in a data at different scales such as we are interested in a weekly data 2 months back; therefore, 2 months become a translates and week becomes a scale. Wavelet can be used efficiently to deal with such problems. In this case, we need very little post-processing to analyze this type of data.

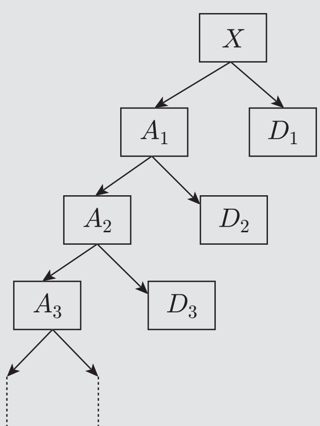

Fig 17.2 | *Trent and surprise abstraction tree*

Figure 17.2 is showing trend and surprise abstraction tree (TSA tree). Where 'X' is original sequence, 'A' and 'D' are are Discrete wavelet transform of the parent node (X).

As we go down this tree, at each level we increase our abstraction by one level and we need a trend or surprise at any level, say at 2^{nd} level, first we need to extract out A_2 node and then do post-processing to get trend information corresponding to this level. Similarly extract D_2 node and post-process to get the surprise information corresponding to that level. The next part is to implement this in memory efficient manner. For this, we need to store the leaf nodes (*i.e.*, D_1, D_2 .... D_n A_{n+1}) and we can extract any other node.

Node dropping and coefficient dropping talk about further compressing the leaf node information to get a better memory efficient implementation of this method.

17.4 | Application of Wavelets in (Big) Data Analysis

Data mining is used for efficient way of representing data. The problem statement is, given a time series data, the time series data may be large, our aim is to improve the efficiency of Multilevel surprise and trend queries. When we have a long time series data, generally we do not encounter point queries.

For example, if we record temperature of a particular city for an year we never ask what is the temperature at this particular day or time. We always ask for the trend how the temperature is varying in a particular month. Such queries are called trend queries. Surprise queries are those which deal with queries like sudden change in the temperature of a particular city in a particular month. Wavelets are effiecient in handling such queries. Multilevel indicates the various levels of abstraction of data whether the data is for a month, or an year, or a decade. So, our first problem is how to represent such a huge amount of data. One of the ways is representing the data in a matrix, i.e.

$$\tilde{X} = M \times N$$

Let $\tilde{X}$ be the whole data to be represented and N for example be the stock prices of a company for a year. Then N will be 365 and let M be the total no.of companies for which we are storing the data. So each row of this matrix represents the stock prices of that particular company. This is how we represent data. Now the first thing we need to do is efficiently store this data. Secondly, we require to retrieve data efficiently and thirdly we require to modify data easily. If these three things could be done easily using wavelets then our job is done.

Firstly, let us see other methods in data mining namely, **Singular Value Decomposition**. We represent $\tilde{X}$ as follows,

$$\tilde{X} = U \Lambda V$$

where U is a column orthogonal matrix with size $M \times r$ and Λ is a diagonal matrix of size $r \times r$ and V is a row orthogonal matrix of size $r \times N$ where r is the rank of the matrix $\tilde{X}$. Now instead of storing data in a large $M \times N$ matrix we are storing it in 3 small matrices out of which one is a diagonal matrix. Suppose now if we want to retrieve a data of particular company, i.e. a row of $\tilde{X}$ the complexity required is of the size V which is $r \times N$. If N corresponds to a decade then it ends up with a huge complexity. One of the other disadvantages of this method is that if we want to modify the data we need to recompute all the three matrices again which is not the case with wavelets. This method is efficient when N is small and there is no need to update data frequently.

Now using wavelets first we take a row X of the matrix $\tilde{X}$ and we decompose it as shown in Fig. 17.3. Initially it is decomposed into approximate and detail subspaces $AX1$ and $DX1$ and then $AX1$ is further decomposed to its corresponding approximate and detail subspaces $AX2$ and $DX2$ and so on to the third level reducing the length of the data by 2 each time.

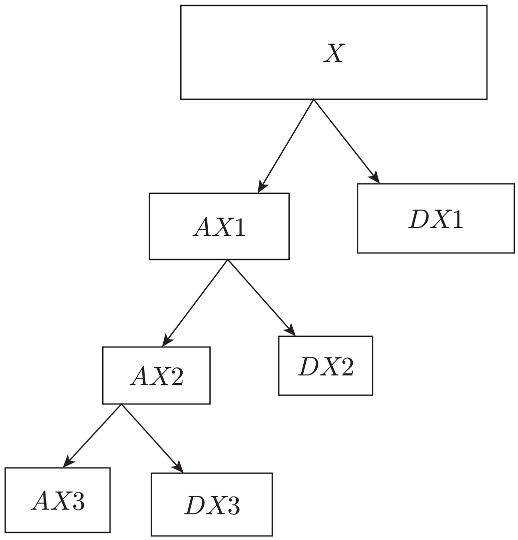

Figure 17.3 | *TSA tree*

This representation is called as TSA (Trend surprise abstraction) tree. The approximate subspaces store the trend data and the detailed subspace store the surprise data. So, wavelets naturally decompose the data into trend and surprise data. This is the main advantage of using wavelets. The split and merge operations of the data, i.e. decomposing into subspaces and reconstructing it from the subspaces is done according to methods we discussed in earlier chapters. Some important properties of this tree are:

1. Perfect reconstruction of the original data using the approximate and detail level subspaces.
2. Power complimentary property, i.e. the power of the signal is preserved as we decompose into lower levels.
3. Size of each node reduces by 2 as we go down by one level.

The nodes which are not decomposed into lower levels are called leaf nodes. For example, in Fig. 17.3 $DX1$, $DX2$, $AX3$ and $DX3$ are leaf nodes. As we see the split and merge operations are of negligible complexity. The Data extraction operation is the costly operation of all and its cost is directly proportional to size of the data. So the third property is very useful in this case. The leaf nodes are sufficient for surprise and trend queries. For example, if we require the trend query we just need the $AX3$ level using which we can go to $AX2$ by passing $AX3$ through lowpass filter and upsampler and now using $AX2$ in the similar way we can go to $AX1$, by which we can get trend queries at different levels. Similarly, if we require surprise queries we use $DX3$ and pass it through a high pass filter and reach at the surprise queries at each level.

An optimal TSF tree is that tree which stores only the leaf nodes and incurs minimum cost and minimum storage. So, there is no need to store other nodes. Now, can we further reduce some of the leaf nodes and still arrive at accurate results? The answer is yes. Wavelets are very good at compression. One of the method is node dropping in which we exploit the property of orthogonality of wavelets. Suppose we remove a leaf node $DX3$ and reconstruct the original signal without $DX3$. Let us call this signal as $\hat{X}$. Now, orthogonality property states the result as follows:

$$\|X - \hat{X}\|^2 = \sum_{DX3} \| \text{node} \|^2$$

which implies that the error between the original and reconstructed signal completely depends on the removed node. Now, we can calculate

$$\frac{\text{norm}^2(\text{node})}{\text{size}(\text{node})}$$

for each leaf node and we store only those nodes which we feel have a significant value in the above equation and rest of the nodes we may drop. The disadvantage of this method is that we may loose some important information in the dropped node. So, we have another method called coefficient dropping.

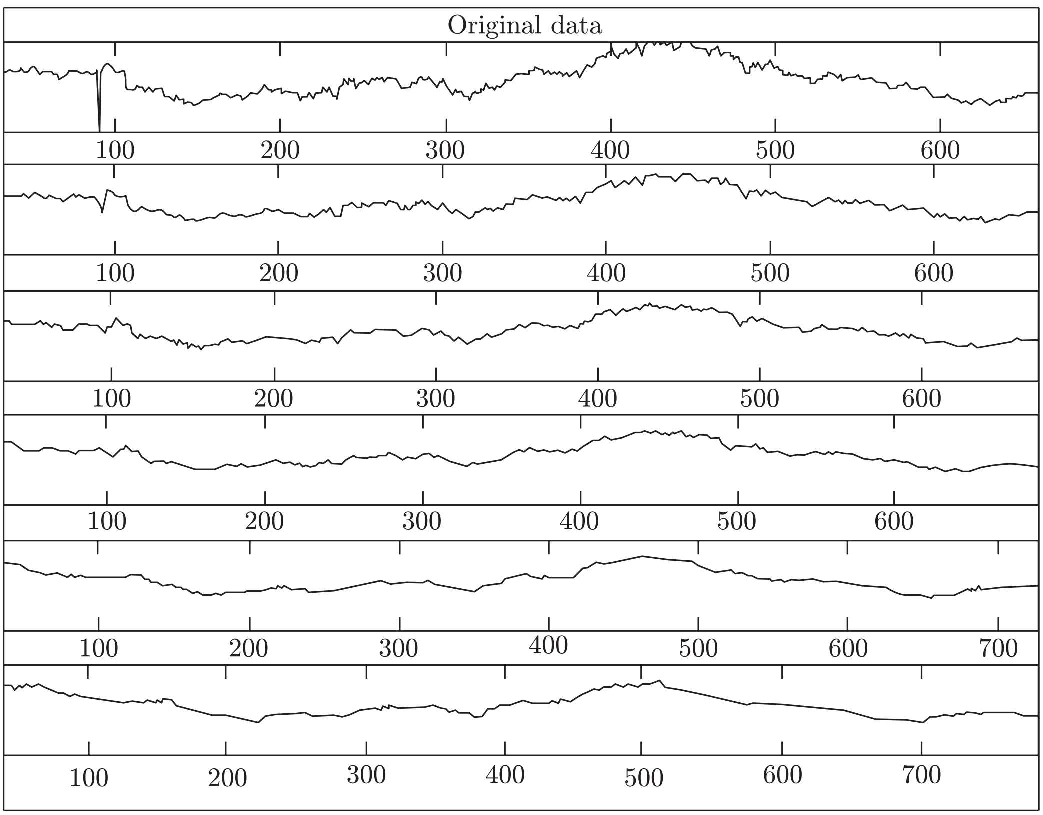

Figure 17.4 | *Results for trend query*

In coefficient dropping method we store the leaf nodes in a sequence such that only significant coefficients are stored. Since we are storing the coefficients we are supposed to store their index also as to identify to which node it belongs. Here we must be careful with the memory constraints because for each coefficient we are storing two values, one is the coefficent and other is its index. So if we do not drop any coefficient in a node it is better to store entire node without their indices. We store indices only when the coefficients and indices together added are less than the size of the entire node. This is about coefficient dropping method.

Let us look at some results. Figure 17.4 shows the trend graphs. The first graph is original data. It is taken from yahoo stock market and it is of SBI's of 2 years. The second graph is of 2 day decomposition level, third graph is 4 day level and so on. As we go down we observe that averaging is increased.

Figure 17.5 shows the results for surprise queries. As we observe, in the original data there is a surprise data which is being averaged out in the subsequent levels. But as we go down subsequent levels we can observe more surprise data which we could not observe in original data.

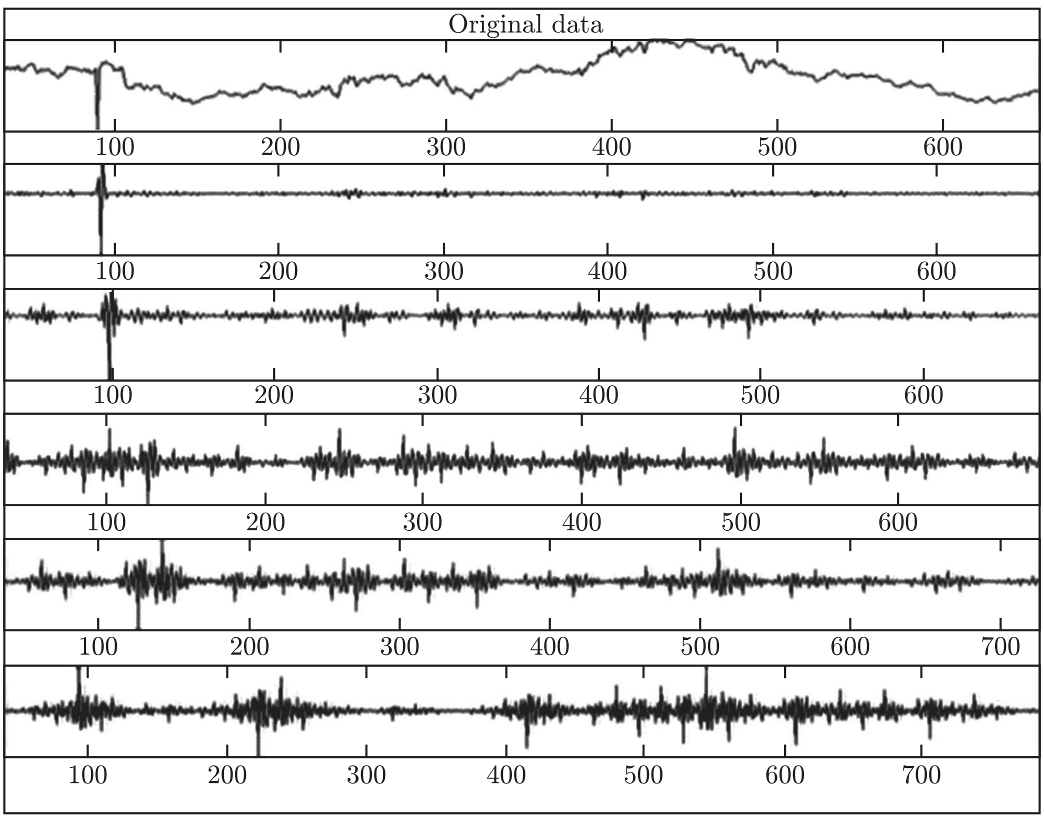

Figure 17.5 | *Results for surprise query*

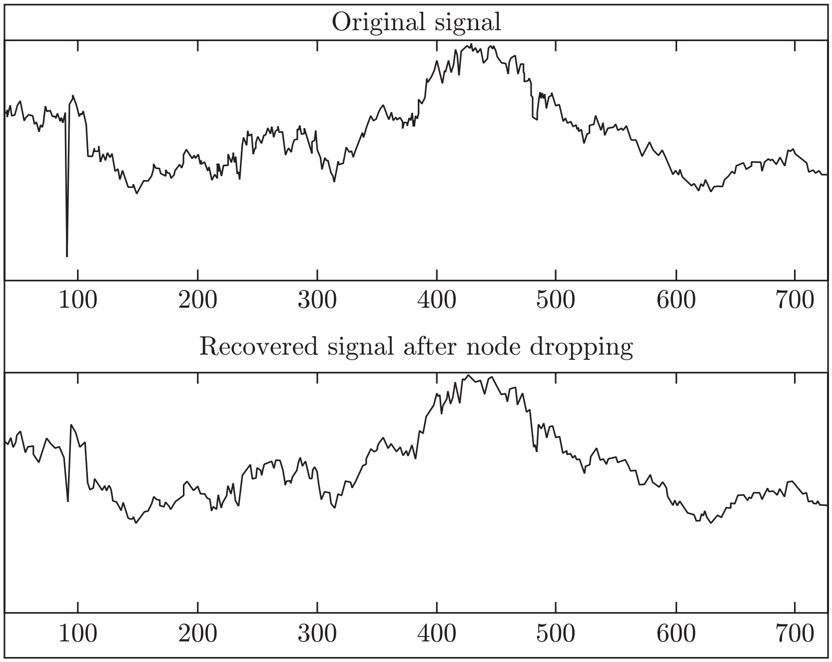

Figure 17.6 | *Results for node dropping method*

Figure 17.6 shows the results for node dropping method. As we observe the recovered data is almost similar to original data except for the small surprise data in the beginning of the original data. Here about 300 coefficients are removed out of 700 and yet we are able to achieve almost our original data.

Figure 17.7 shows the results for coefficent dropping method. Here we can see that even that small surprise data is also retained. Here Daubechies family of filters are used. As we increase the length of the filter the averaging is done more efficiently.

The reference used for this application is C. Shahabi, X. Tian, W. Zhao, TSA tree: A Wavelet-based Approach to Improve Multi-Level Surprise and Trend Queries on Time-Series Data. In Statistical and Scientific Database Management, pages 55-68, 2000.

17.5 | Face Recognition Through Wavepacket Analysis

The two keywords in this presentation are face recognition and another is wave packet analysis. Firstly, why do we need wave packet analysis for face recognition? The answer is, we need decorrelation in spatial domain as well as frequency domain for the task of classification. However, for this wavlets meet the basic requirement. Then why do we go for wavepacket analysis? In wavepacket analysis we decompose detail subspaces not only the approximate subspaces. When we do task of classification we should not miss any information from the underlying signal. The underlying signal here is a face image. The task of face recognition can be accomplished both by wavelets and wavepacket transform. Wavepacket transform is used for richer representation of image.

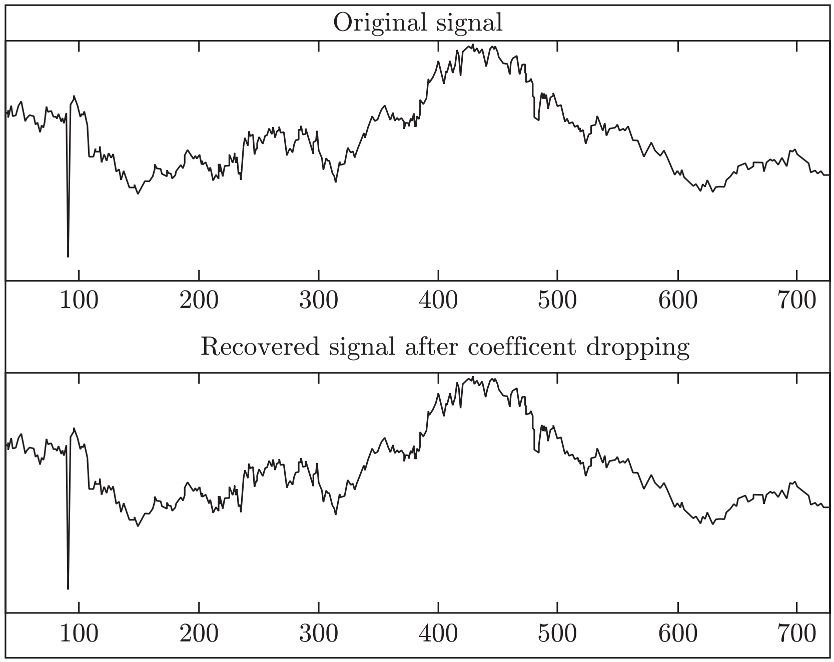

Figure 17.7 | *Results for node dropping method*

Why is face recognition required? One of the answer is for biometric authentication. Face can be easily morphed by covering with sun glasses or by growing a moustache. But some of the images like retina and fingerprints are difficult to be morphed. However, Face recognition is used in surveillance. In task of surveillance we may do activity tracking and recognition and also provide abnormal detection. Also, can be used in videos for automatic character(Actor) Recognition.

There are two approaches used for face recognition, one is geometric approach and the second is feature based recognition. In geometric based approach one goes on detecting basic features like nose, eyes, chin and generate face using those features. The problem here is these features are difficult to extract. So, feature based extraction is used for this application. The basic block diagram of this project is shown in Fig. 17.8.

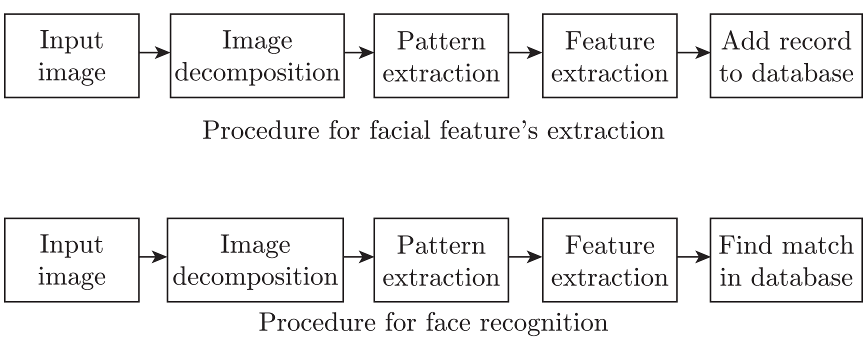

Figure 17.8 | *Block diagram for face recognition*

In this presentation we are not going to discuss about how face detection is done. After face is extracted we do subband decomposition using wavepacket transform. We already store some features in Learnt prototype and then we do matching with a given image. There are two types of applications based on face recognition: content based image retrieval and simple classification of image into different classes. Decomposition of image into subbands is done as shown in Fig. 17.9.

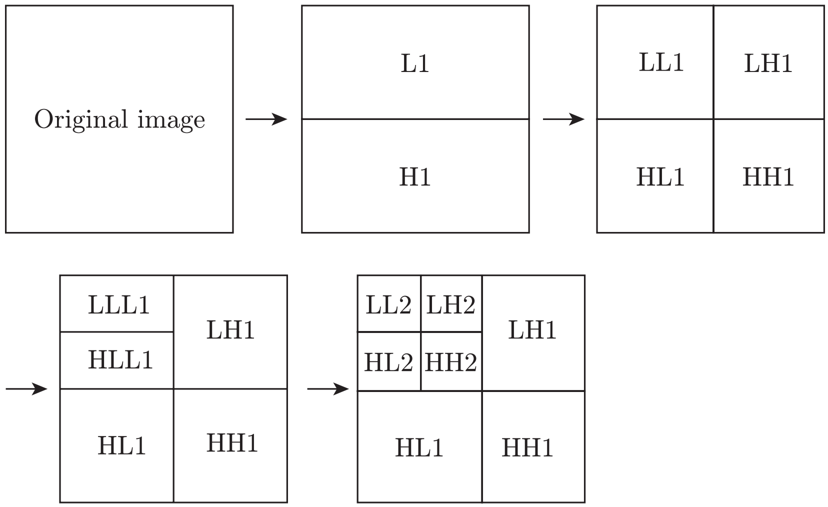

Figure 17.9 | *Decomposition of image into various subbands*

In wavelet analysis we just decompose the LL subband. But in Wavepacket analysis we also decompose the other subbands as well. So, when decompose using Wavepacket transform we get 16 subbands, Whereas in wavelets we just get 4 subbands. Here we are not bothered about perfect reconstruction so our analysis filters need to be good. We need filters which have good feature extraction capabilities. Filters used for this application are shown in Fig. 17.10.

The impulse responses of both LPF and HPF are also shown in the Fig. 17.10. We decompose the image upto two levels. We do not really need to further decompose image because the image becomes smaller and smaller as we decompose into subsequent levels. When we decompose a an approximate subspace we require a LPF and a BPF. Whereas, for decomposing a detail subspace we require a BPF and a HPF. All these filters are separable in nature and can be used for both dimension separately. Altogether we get 16 subspaces after two level decomposition. The Higher frequency features of face such as eyes can be seen when detail subspace is decomposed into its subbands. After all these 16 bands are extracted, we can go for feature extraction. In each of the 16 images there are features required for face recognition. If we go for all the pixels in all 16 images, then our feature extraction vector becomes very large. So, we go for moments like first order moment and second order moment in all the 16 images giving rise to 32 features. But for detailed subspaces we have zero mean. So a 17 dimensional feature vector is sufficient. But, the approximate and detail subspaces are different. Detail subspace have more information compared to approximate subspace. The feature vectors which are extracted are shown in Fig. 17.11.

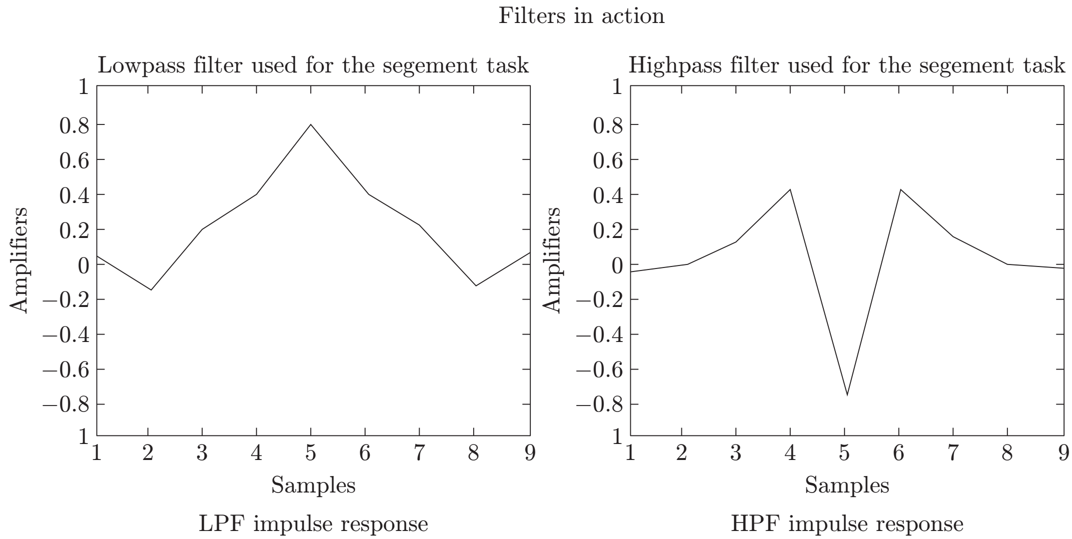

Filter	Impulse responses								
LPF	0.05	−0.15	0.20	0.40	0.80	0.40	0.20	−0.15	0.05
HPF	−0.06	−0.04	0.10	0.40	−0.80	0.40	0.10	−0.04	−0.06

Figure 17.10 | *The filters used for this project – improved figure to follow*

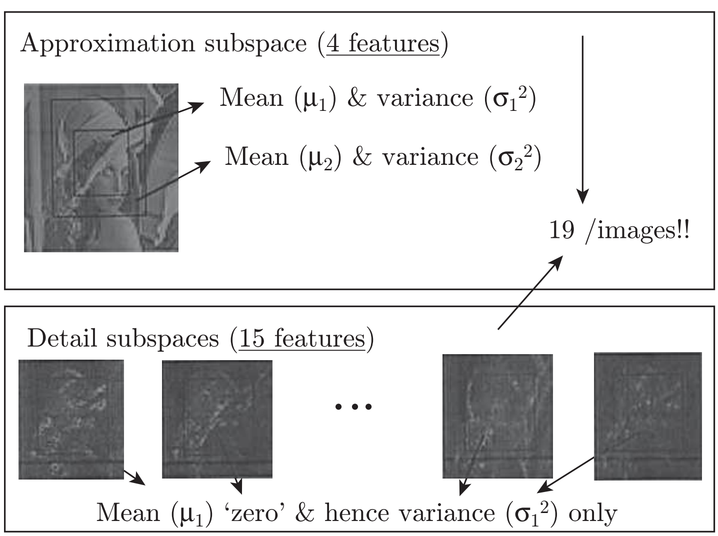

Figure 17.11 | *Feature vectors for different subspaces – improved figure to follow*

We had two boxes in approximate subspace and in each box we can extract mean and variance for each box. For Detail subspace we extract variance and altogether we get 19 feature vectors. We compare these features with already stored feature vectors. We use distance metric for matching. The distance is calculated using Bhattacharya distance for all the feature vectors extracted. The experimental results obtained are shown in Fig. 17.12.

Exp	Number of images used in learning/ class	Total images used in learning	Total number of query images	Number of images matched to the native class	Accuracy ($\pm$1.25%)
1	4	40	80	66	82.5%
2	6	60	80	64	80.0%
3	8	80	80	64	80.0%

Figure 17.12 | *Various experimental results – improved figure to follow*

17.6 | Wavelet Based Denoising – Application

Denoising as the name suggests, is the operation of separation of wanted and unwanted in a mixture of signal and noise.

As expected, normally the noise or perturbation is unwanted and it is often the case when one goes in wavelet domain particularly in the context of biomedical signals, it is easier to separate the wanted signal from unwanted noise. We could have several instances of this, but what we have in this section is essentially a separation of respiratory artifacts described.

17.6.1 Wavelet Based Denoising for Suppression of Respiratory Artifacts in Impedance Cadiogram Signals (ICG)

The technique that is mentioned was developed by Dr. Vinod K Pandey and Prof. P. C. Pandey of IIT Bombay. First of all, let us divulge into what is meant by '**Impedance cardiography**'.

17.6.2 Impedance Cardiography (Definition)

It is a noninvasive technique for monitoring stroke volume (SV) and other cardiovascular indices, thereby obtaining diagnostic information on cardiovascular functioning by sensing variation in the thoracic impedance due to change in blood volume.

17.6.3 Structure and Functioning of Heart

The actual structure of the heart is as shown in Fig. 17.13. It essentially consists of four chambers namely:

1. Right atrium
2. Left atrium

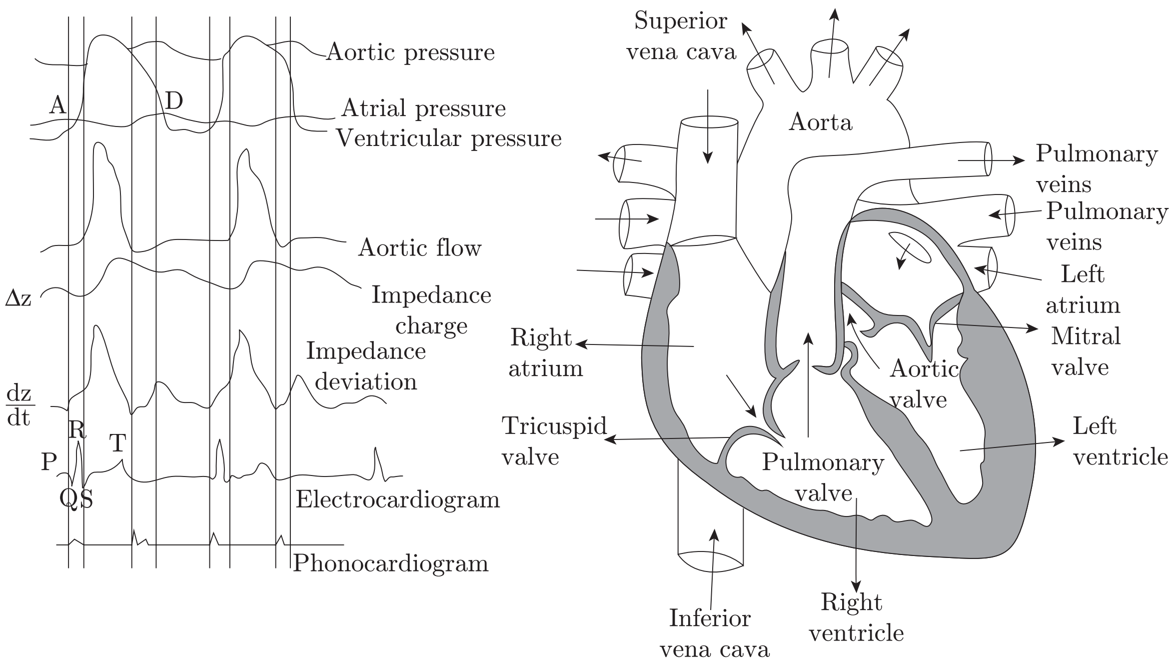

Figure 17.13 | *Structure of Heart*

3. Right ventricle
4. Left ventricle

These four chambers can be visualized as a four pumps similar to mechanical pumps whose function is just pump the blood. The blood from the different part of the body enter into the heart.

There are two major vessels namely:

1. Superior vena cava
2. Inferior vena cava

Superior vena cava will be bringing the blood from the upper part of the body to the heart where as Inferior vena cava will be bringing the blood from the lower part. The names superior and inferior are not due to their functioning but as per their positions.

The right side of the heart deals with the deoxygenated blood and left side of the heart deals with the oxygenated blood. As soon as the right atrium filled with the blood, right atrium will pump the blood to right ventricle. There is valve separating the right atrium and right ventricle known as tricuspid valve. The right ventricle pumps the blood to lungs for getting oxygenated. As we know blood coming from different parts of the body to the heart has carbon-dioxide in it. We need oxygen in the blood for body functioning. Now, this blood will exchange, i.e. carbon-dioxide and oxygen, for that the right ventricle pumps the blood to the lungs through pulmonary artery. During this period pulmonary valve will be open and tricuspide valve will be closed. The blood will come back to the heart in left atrium through pulmonary vein. From this left atrium blood will be pumping in left ventricle. There is a valve separating left atrium and left ventricle known as mitral valve.

Out of the four chambers, left ventricle is the most important part because left ventricle is supplying the blood to all parts of the body. Since our body parts are far away from the heart, left ventricle has to do a lot of work. The left ventricle is contracting with maximum force and will pass through aortic valve to the aorta and blood will be supplied through different branches of aorta to the different parts of the body. Even though if atrium pumps are not working due to some problem, tricuspide valve and mitral valve will be opened due to gravitational force and weight, the 70% of blood will automatically fall in ventricle. So disorders related to atrium are not much dangerous compared to disorders related to ventricle.

Now look at the some waveforms related to heart blood cycle as shown in left side of Fig. 17.13. In the first waveform the upper doted line shows the aortic blood pressure, i.e. when we are measuring blood pressure using pressure meters with the help of doctors, we will be getting this aortic blood pressure (80 to 120 for healthy persons). The related variations of other two pressures namely atrial pressure and ventricular pressure are shown in the same first waveform. The next waveform is aortic flow showing blood flow aorta which is pulsating in nature. The waveform shows electrocardiogram signal (ECG) which is a measure of electrical activities of the heart. The last waveform is phonocardiogram which are actually cardiac sounds of valves.

17.6.4 ICG Signal and Artifacts

In impedance cardiography, the four sensors are placed on the body, the corresponding region is known as thoracic region, as shown in Fig. 17.14.

Experimental setup

Impedance cardiograph Model HIC2000 from Bio-impedance technology

- Sampling frequency 500 Hz
- Signals recorded under
  (a) subject at resting condition and
  (b) subject performing different physical activities

Figure 17.14 | *Experimental setup of 'ICG' recoding*

A high frequency and low amplitude current is passed through upper and lower electrodes and voltage is measured between the two middle electrodes and hence the impedance. As shown in the Fig.17.13, the third waveform $\Delta(Z)$ shows the impedance variation and forth waveform is the time derivative $\left(\dfrac{dZ}{dt}\right)$ of it known as impedance cardiogram signal (ICG).

The stroke volume (SV) is the amount of blood pumped by the heart during one heart bit and is given by,

$$SV = \rho \frac{L^2}{Z_0^2}\left(-\frac{dz}{dt}\right)_{\max} T_{\text{lvet}}$$

where,
SV = Stroke volume (mL)
ρ = Resistivity of the blood (Ω-cm) $\cong$ 150
L = Length of the modeled conductor (cm)
Z_0 = Basal impedance(Ω) $\cong$ 25 (Varies from patient to patient)
$\left(-\frac{dz}{dt}\right)_{\max}$ = Maximum of the derivative of the impedance during the systole (Ω/s)
T_{lvet} = Left ventricle ejection time (s)

Cardiac output = $SV \times HR$ (heart rate)

Basically impedance cardiogram signal (ICG) have few types of artifacts, these are manmade signals which are unnecessary in impedance cardiography point of view. We have two major artifacts, i.e. respiratory and motion artifacts. Respiratory artifacts are very low frequency (0.04 – 2 Hz) and motion artifacts (0.1 – 10 Hz). Figure 17.15 shows ICG signal during exorcize of a normal person. The baseline drift is due to the respiratory artifacts and peaks due to motion artifacts.

As shown, the ICG signal range is 0.8 to 20 Hz, therefore, respiratory and motion artifacts lie within same band. In this presentation particularly we are looking for respiratory artifacts suppression because these create difficulties in calculating stroke volume and other cardiovascular indices.

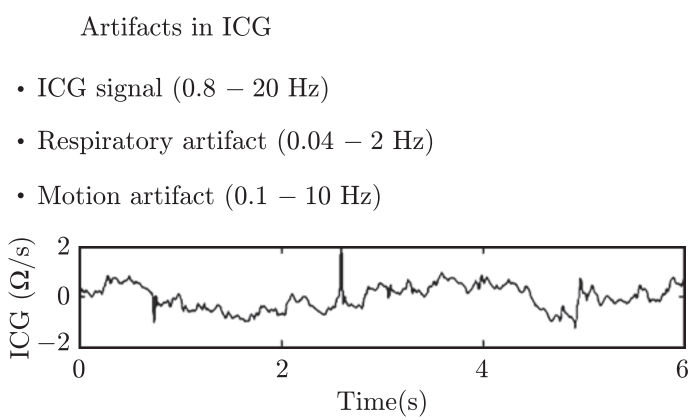

Figure 17.15 | *Artifacts in 'ICG'*

17.6.5 Application Objective

- Investigate the different denoising techniques for the suppression respiratory artifacts.
- Study the wavelet based denoising for artifact suppression.
- Study different wavelets and its applicability in artifact suppression.

There are few techniques of suppression of respiratory artifacts namely:

(a) **Breath Hold:** Respiratory artifacts are because of respiration and the easiest way to suppress these artifacts is to hold the breath. The problem to hold breath is that when we are holding the breath cardiac activity will always go down. Another problem is when we are recording 'ICG' after exercise, it is difficult to hold the breath.

(b) **Ensemble averaging[8]:** The bit-to-bit variability in the 'ICG' will be removed in ensemble averaging technique, so it blur the important points of 'ICG' waveform such as *B*, *X* points. Hence it will introduce errors in calculating stroke volume (SV).

(c) **Adaptive filtering[10]:** Adaptive filtering is always good in biosignal de-noising if we have a reference signal, but obtaining a reference signal is a difficult task.

(d) **Wavelet based level dependent thresholding[5]:** In wavelet based denoising selection of wavelet basis is an important task. In many denoising applications it is observed that if wavelet and waveform has some similar shape, then those wavelets gives better separation of noise and signal. Hence, selection of wavelet basis is an important step in wavelet based denoising. Here, we are using this technique for the suppression of respiratory artifacts in 'ICG' signal.

17.6.6 Wavelet Based Denoising

The basic wavelet decomposition is as shown in Figs 17.16 and 17.17. The original waveform is sampled at 500 Hz. Each detail gives a bandpass signal and each approximation gives a low-pass signal when we are decomposing the signal into different levels. In this method, we are decomposing the signal into different levels and artifacts into different levels and we are seeing up to what levels the signal is present and up to what levels the artifacts are present. We have used different wavelets for decomposition in this project. We have tested different wavelets such as Coif5, db6, demey (discrete meyer wavelet) and symlet wavelet in decomposition of 'ICG' signal. Based on these results we will choose specific wavelets for denoising application.

The 10-level wavelet decomposition of an 'ICG' signal under breath hold condition is as shown in Figs 17.18, 17.19 and 17.20 by using 'Coif5', 'db6' and 'demey' wavelets respectively.

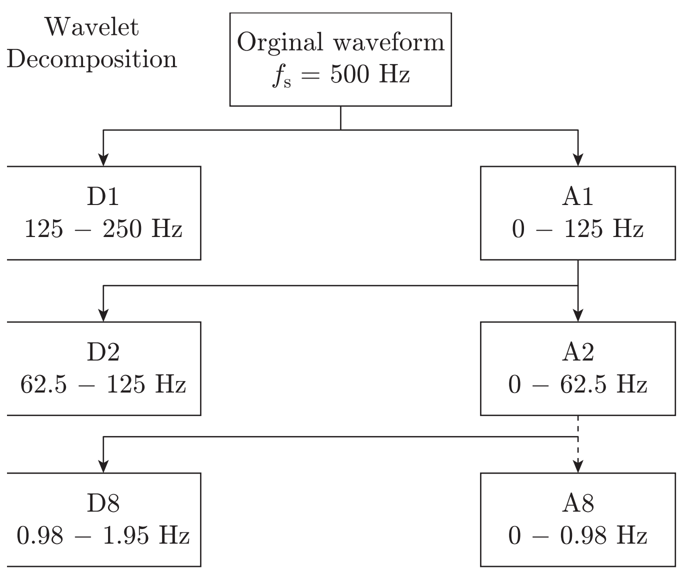

Figure 17.16 | *Wavelet decomposition*

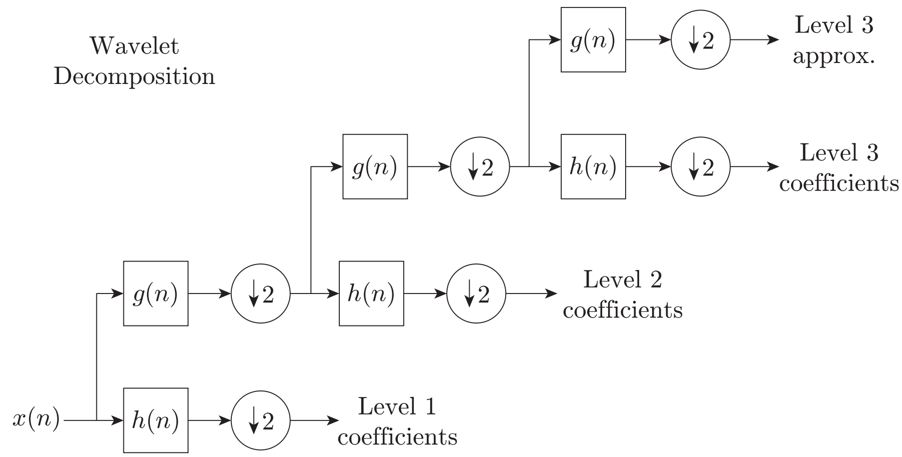

Figure 17.17 | *Block diagram of DWT*

In Fig.17.18, the details D1 to D3 has no signal content because they contains high frequency components and the signal has only components up to 20 Hz. The details D4 to D10 contains the signal content so we can not use this particular wavelet for separation of signal and artifacts since it is not capturing signal components in any particular details. As we can see D8-D9 has signal content and if artifacts are present along with the signal.

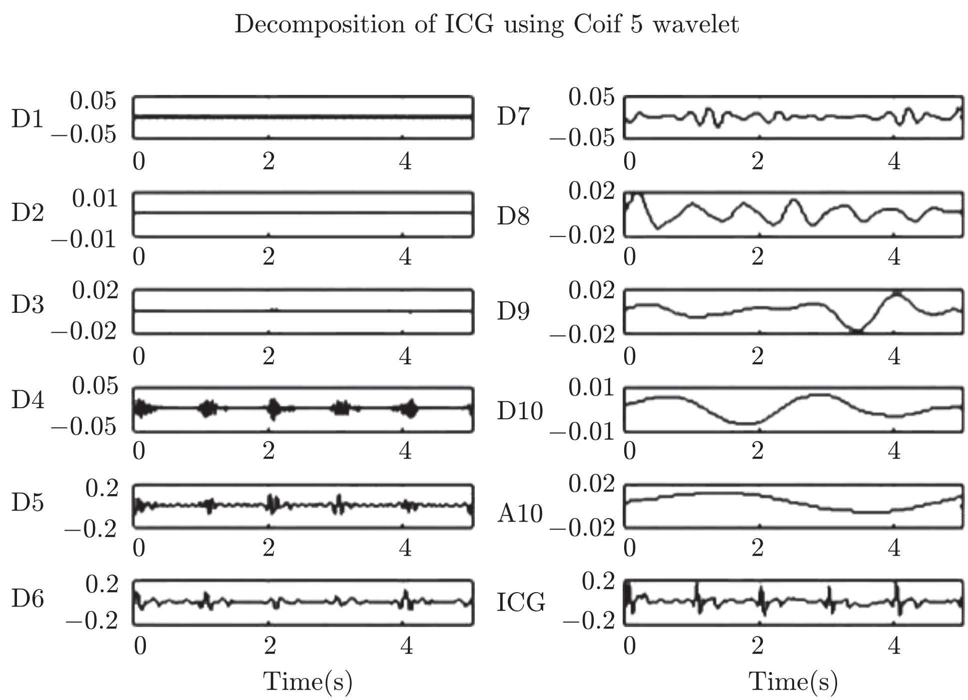

Figure 17.18 | *10-level decomposition of ICG with 'Coif 5' wavelet*

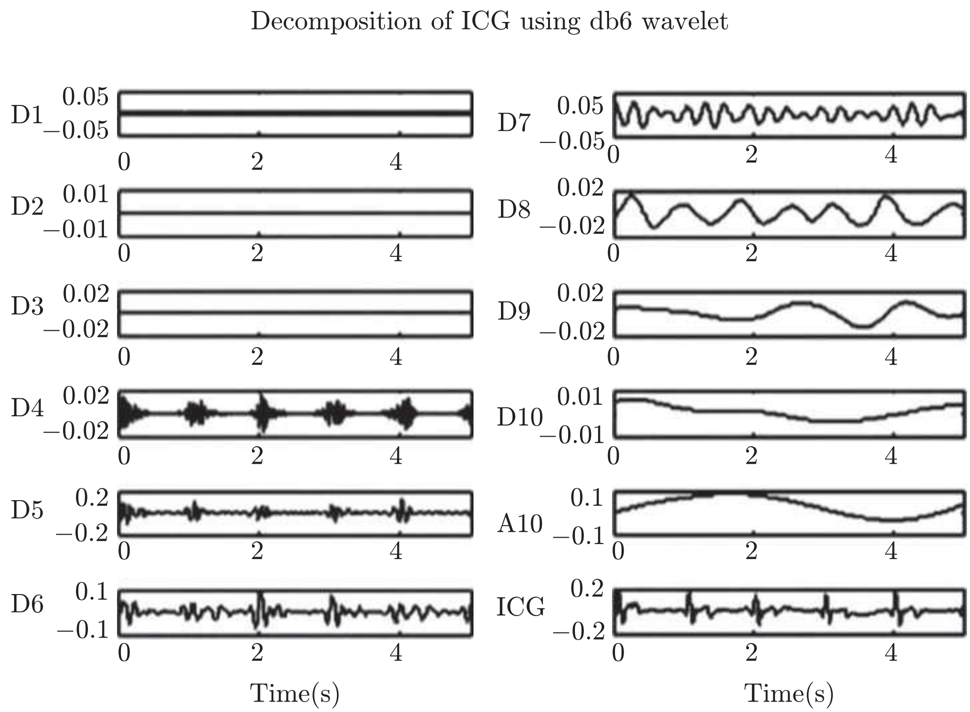

Figure 17.19 | *10-level decomposition of ICG with 'db6' wavelet*

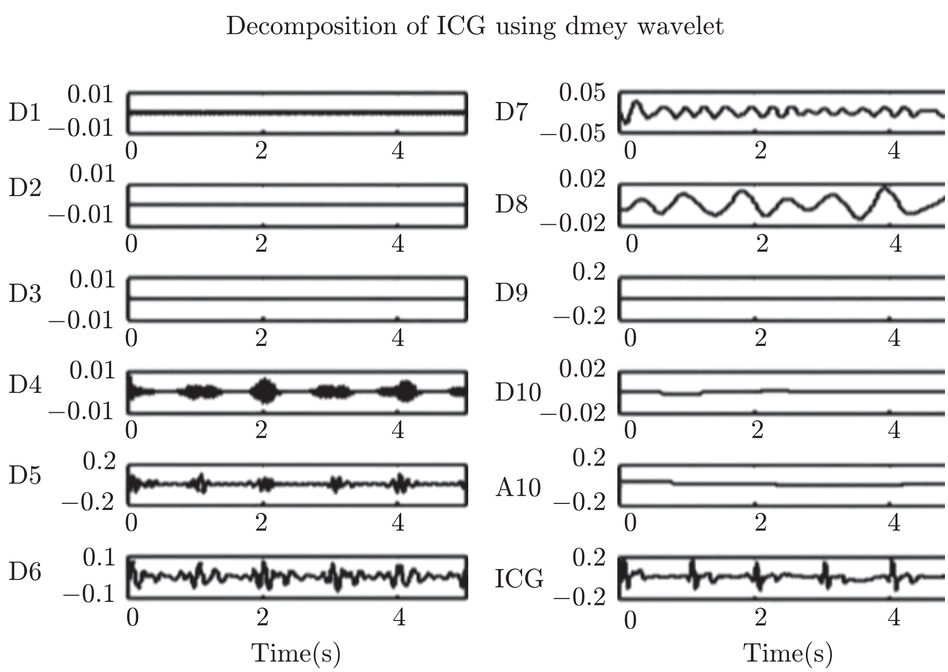

Figure 17.20 | *10-level decomposition of ICG with 'demey' wavelet*

In Fig. 17.19, the same 10-level wavelet decomposition of an 'ICG' signal using Daubechies wavelet (db6), again we can see all the details and approximation contains the signal content, so this wavelet also will not serve the purpose of artifact separation from the 'ICG' signal.

In Fig. 17.20, we can see that there is no signal content in D1 to D3, but D4 to D8 have signal content, but one important observation here is that in D9-D10, we do not have signal components. The D9 details contains frequency components in the range 0 to 0.98 Hz. In our denoising experiment we are adding the details D1 to D8 and removing D9, D10 and A10 for artifacts suppression.

By observing these results, we can see that the choice of wavelet basis plays a critical role for artifacts suppression in 'ICG' signal.

17.6.7 Denoising Results

Further studies at SPI lab EE department at IITB showed that similar results can be achieved by using 'demey' wavelet can also be achieved by using one more wavelet known as 'sym26' wavelet.

The first waveform in Fig. 17.21 is an 'ICG' signal under resting condition but with respiration.

The second waveform in Fig. 17.21 is an denoised 'ICG' signal using 'demey' wavelet, i.e. 'ICG' signal is decomposed with 10-levels and the reconstruction is done using first 8 details. The third waveform is obtained by following the same procedure using 'sym26' wavelet. We can visually see that both the wavelets giving the same performance. The fourth waveform is the artifacts which are extracted from from 'ICG' waveform by using 'demey' wavelet. This is basically first waveform minus second waveform. The last waveform is the artifacts removed by using 'sym26' wavelet. Here, we can observe that both wavelets capturing exactly the same artifacts and same signal.

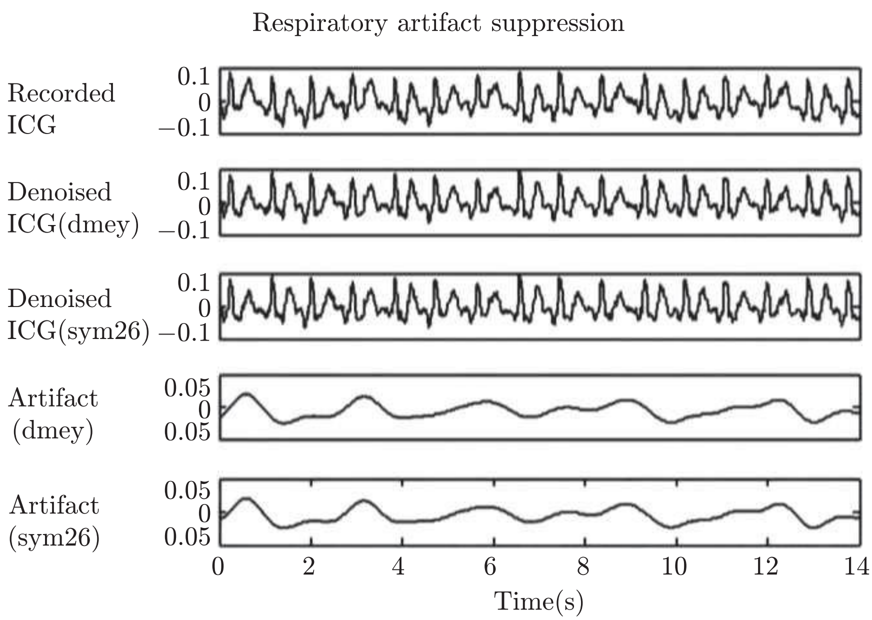

Figure 17.21 | *Respiratory artifact suppression with 'demey' and 'sym26' wavelet*

The question may arise in one's mind that why this is happened. The shapes of wavelet and scaling function of 'demey' and 'sym26' are as shown in Fig.17.22. We can see that both have same shapes and matches with the shape of ICG signal and hence these wavelets gives better artifacts suppression performance over other wavelets. All the de-noising experiments are performed with Matlab using wavelet toolbox.

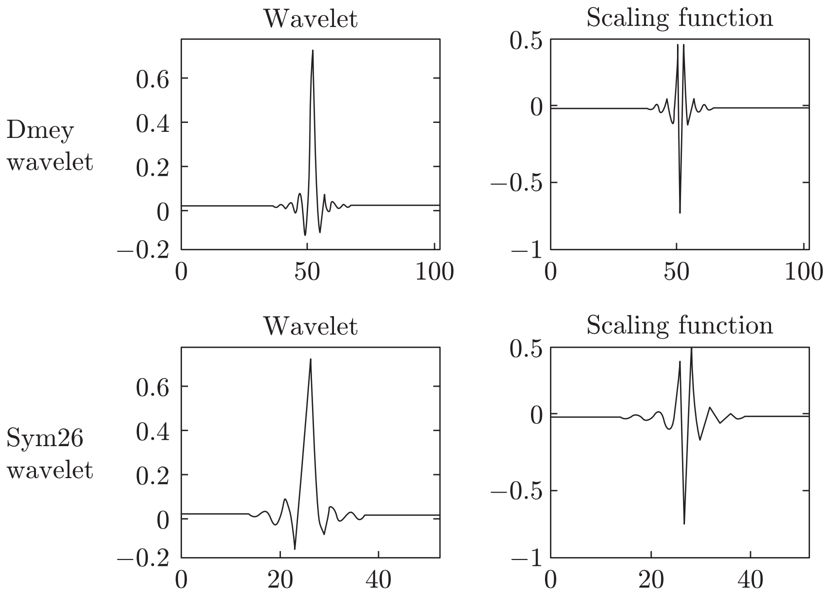

Figure 17.22 | *Wavelet and scaling functions of 'demey' and 'sym26' wavelet*

17.6.8 Possible Embellishments

- 'Sym26' and 'demey' are better than other wavelets for respiratory artifacts suppression.
- 'Sym26' reduces the calculation complexity compared to 'demey' wavelet.
- Study the applicability of wavelet based techniques for motion artifact suppression in 'ICG' signal.
- Study the wavelet based techniques in 'ECG' denoising applications.

17.7 | Finding Hidden Discontinuity – Application

While authors were developing a solution for a mechanical industry to detect cracks in rotating gears, it was realized that the problem at crux was finding hidden discontinuities.

In the following toy example, we will try to find out a hidden discontinuity. Consider the following function (Fig. 17.23),

$$g(t) = \begin{cases} t & 0 \le t \le \dfrac{1}{2}, \\ t-1 & \dfrac{1}{2} \le t < 1 \end{cases}$$

We can see that at $t = 0.5$ there is a clear discontinuity. However such discontinuities are easier to detect, we will slightly complicate the matter. We will smooth out this signal by integrating it.

$$h(t) = \int g(t)dt = \begin{cases} \dfrac{t^2}{2} & 0 \le t \le \dfrac{1}{2}, \\ \dfrac{t^2}{2} - t + \dfrac{1}{2} & \dfrac{1}{2} \le t < 1 \end{cases}$$

We can see that there is still a cusp jump at $t = 0.5$. Thus integrating again,

$$f(t) = \int h(t)dt = \begin{cases} \dfrac{t^3}{6} & 0 \le t \le \dfrac{1}{2}, \\ \dfrac{t^3}{6} - \dfrac{t^2}{2} + \dfrac{t}{2} - \dfrac{1}{8} & \dfrac{1}{2} \le t < 1 \end{cases}$$

This appears absolutely smooth to eye. So we will solve this problem of finding out the discontinuity using wavelets.

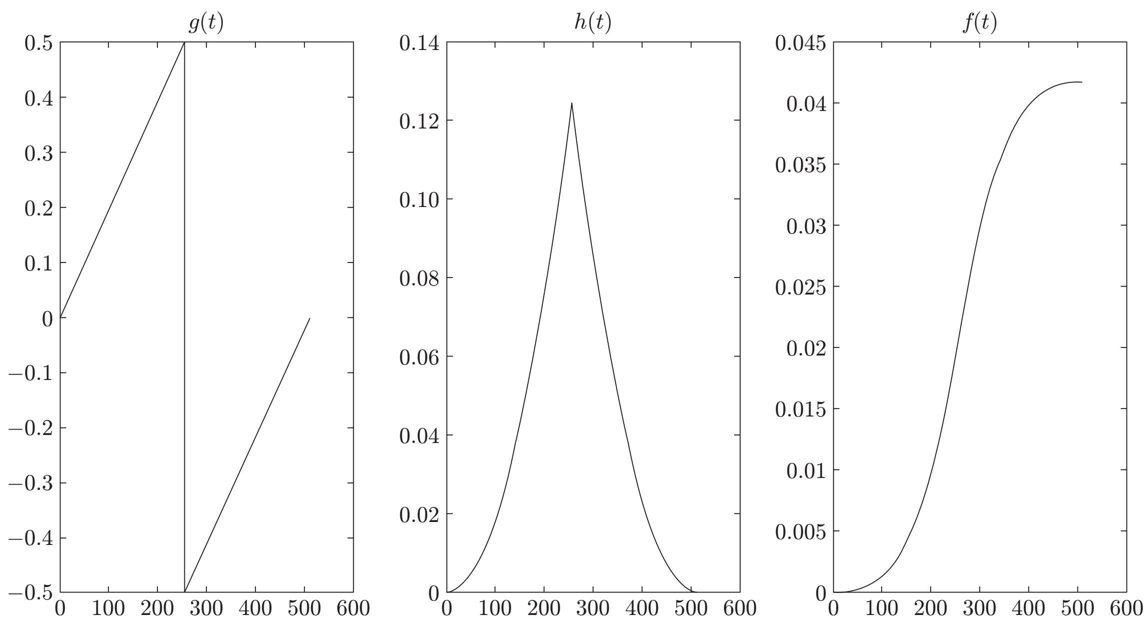

Figure 17.23 | *Plot of functions g(t), h(t), f(t)*

Simulation Results

As can be seen from Fig. 17.24, Haar filter completely missed the discontinuity. This is because Haar has only one vanishing moment and can sense only up to first order derivative.

As can be seen from Fig. 17.25, higher members in Daubechies family can sense and detect the discontinuity. This is because filters like db-2 onwards have at least two vanishing moments and thus can sense up to second order derivative.

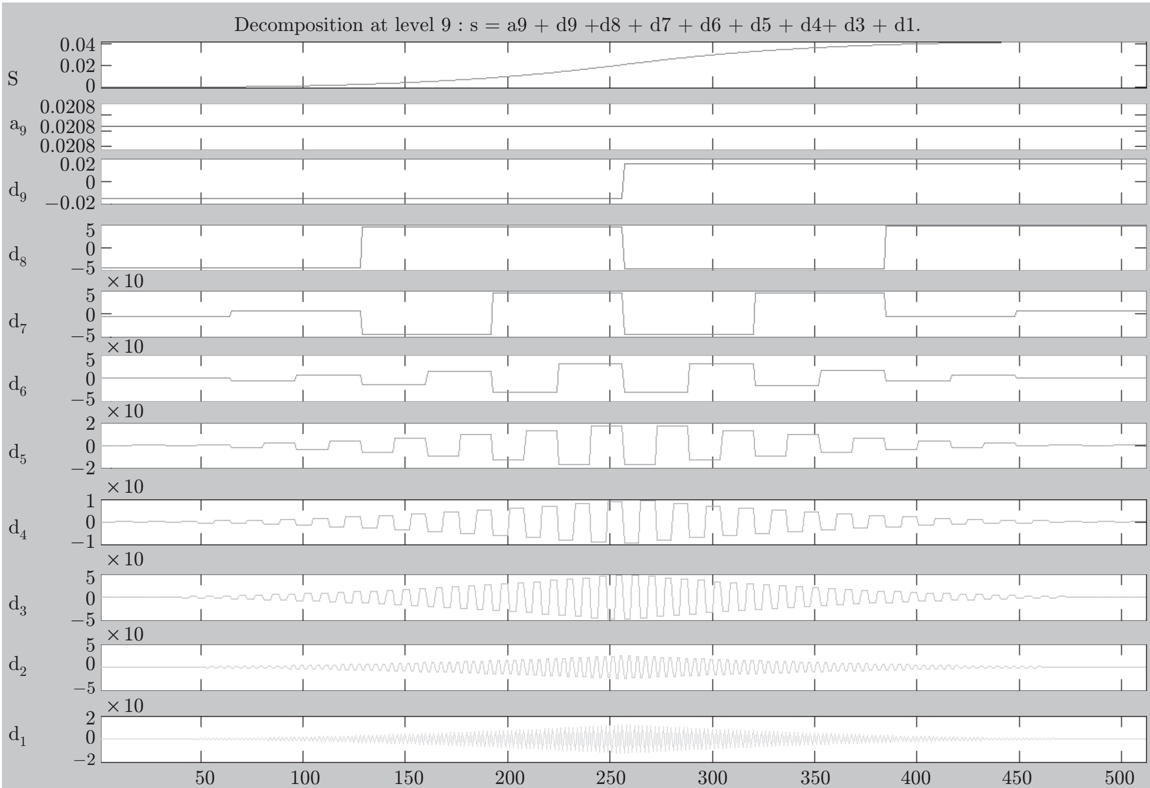

Figure 17.24 | *Haar wavelet completely misses out the hidden discontinuity*

17.8 | Denoising the Underlying Signal – Application

The second applications we would be looking at is suppressing polynomials towards denoising the underlying signal. It is in a way dependent on scaling function ϕ. We would work out this application with the help of a simulation.

Figure 17.26 shows a signal and same signal with noise added to it. The noise added is white Gaussian noise. The signal to noise ratio is 4. Thus a good enough strength disturbs the signal and not all the details are visible. Thus there is a need to clean up the signal to bring out its underlying characteristics. We will try to complete this task using wavelets.

We know that any signal can be looked upon as a polynomial and if we suppose that its degree is two, then daub2 would not be able to do a neat analysis of the signal. This is because the moment corresponding to the second derivative does not vanish. Thus, in Figs. 17.27 and 17.28 we can see that the decomposition with Haar, i.e. db1 and db2 is not satisfactory.

However if we look at the decomposition with db3 wavelet shown in Fig. 17.29, we can see from analysis at d4 and d5 that the noise has started getting suppressed. If this happens we will eventually be left with noise. We can also subtract this noise and get back the original signal as shown in Fig. 17.30. Also, we can see that most of the details present in the original signal are restored. To what level we want to restore the details is once again a question of selecting an appropriate mother wavelet function and corresponding father or scaling function.

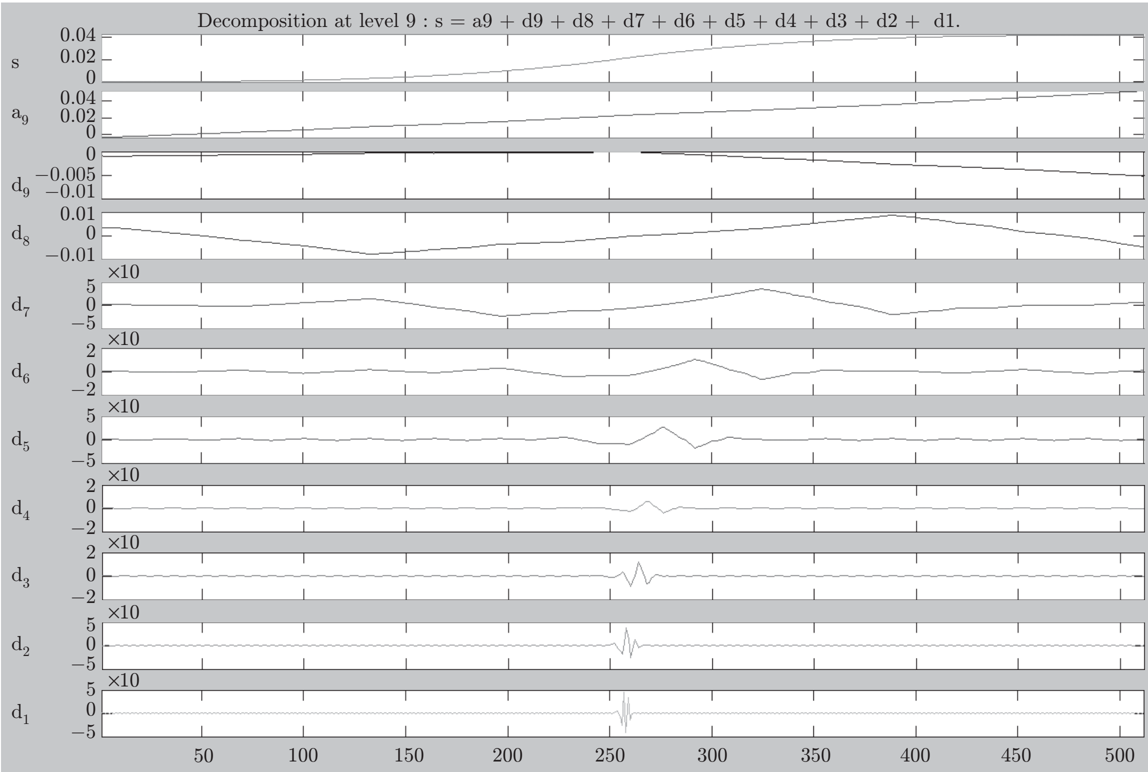

Figure 17.25 | *Db3 successfully detects the hidden discontinuity.*

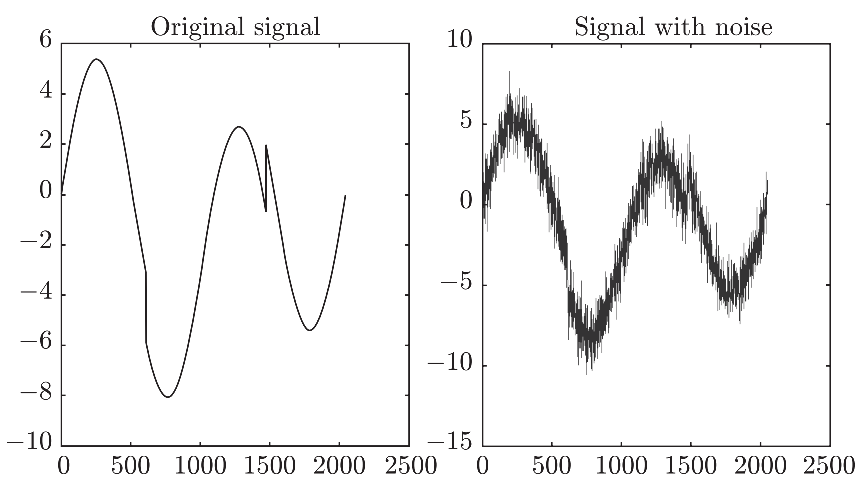

Figure 17.26 | *Original signal and Signal with noise*

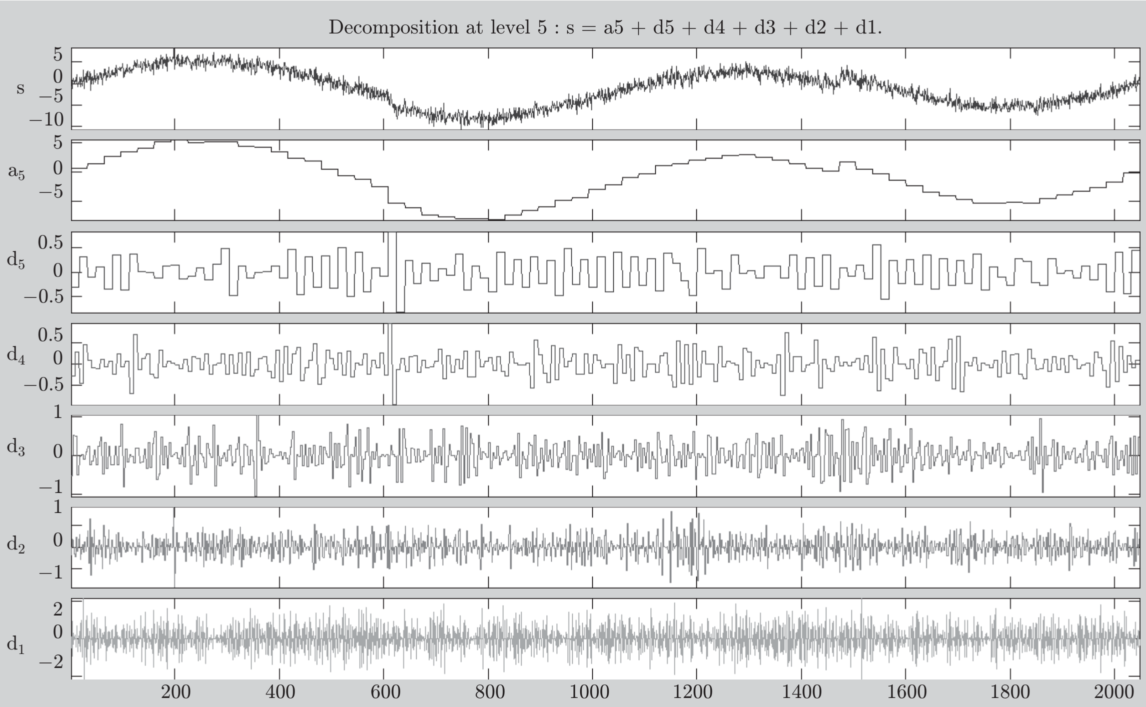

Figure 17.27 | *Decomposition of the signal with Haar*

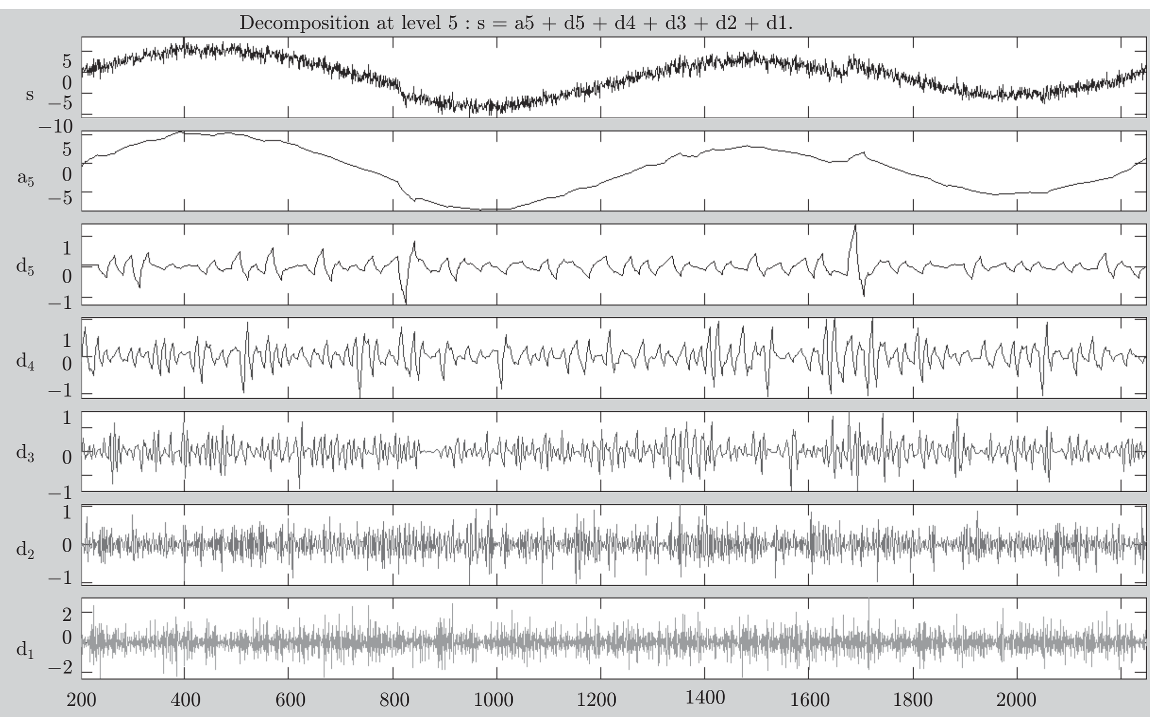

Figure 17.28 | *Decomposition of the signal with db2*

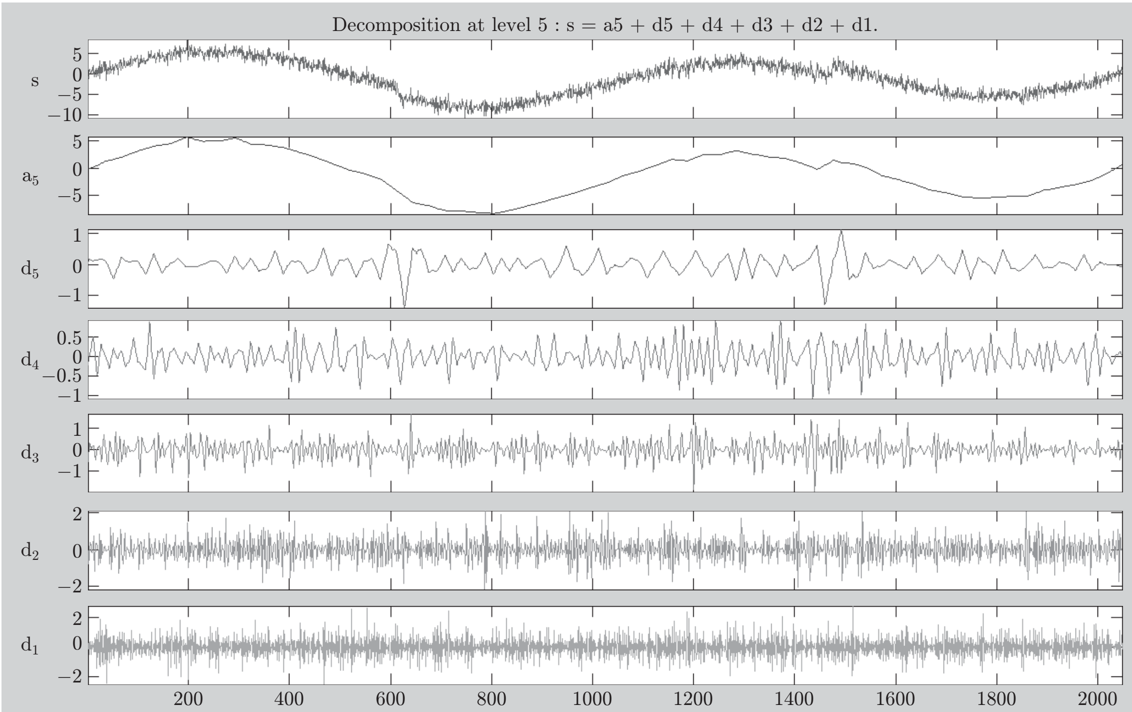

Figure 17.29 | *Decomposition of the signal with db3*

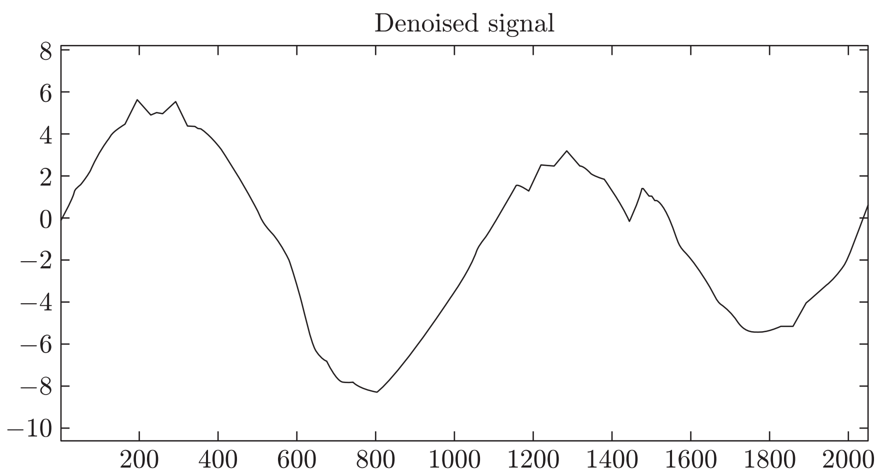

Figure 17.30 | *De-noised Signal*

17.9 | Compression and Pattern Recognition Using Wavelets

Now, let us look at another application. So far we have only dealt with one dimensional applications, now we look at a two-dimensional application. Specifically, we will study compression and pattern recognition using wavelets.

As far as two-dimensional signal or image analysis is concerned typically the basis function should be of unitary nature. Only then we can guarantee two important properties, energy compaction i.e. we must be able to represent the energy we have with us and energy conservation, i.e. we should be able to preserve most of the energy. Only then we can achieve compression.

A matrix A is called unitary if,

$$A^{-1} = A^{*T}$$

For a real matrix A, it is unitary if,

$$A^{-1} = A^{T} \tag{17.1}$$

When the basis matrix is unitary it guarantees de-correlation of the information. Once we de-correlate the information we can guarantee energy conservation and also energy compaction.

Now, let us look at an important question, can we preserve using wavelet transform?

Consider the following signal,

$$x[n] = \{3, 2, 5, 1\} \in V_2$$

Lets use Haar wavelet for analyzing this signal thus,

$$h_0 = h_1 = \frac{1}{\sqrt{2}}$$

$$g_0 = \frac{1}{\sqrt{2}}, g_1 = -\frac{1}{\sqrt{2}}$$

Its approximations would be,

$$a_1 = \left\{\frac{5\sqrt{2}}{2}, 3\sqrt{2}\right\}$$

Its approximations would be,

$$d_1 = \left\{\frac{\sqrt{2}}{2}, 2\sqrt{2}\right\}$$

Now energy in a_1 and d_1 would be,

$$E_{a_1} = \left\{\frac{5\sqrt{2}}{2}\right\}^2 + \left\{3\sqrt{2}\right\}^2 = \frac{61}{2}$$

$$E_{d_1} = \left\{\frac{\sqrt{2}}{2}\right\}^2 + \left\{2\sqrt{2}\right\}^2 = \frac{17}{2}$$

Thus, the energy stored in details is about 22 percent. This is because the signal we have considered has many transitions. Now as against this if we consider a smooth signal,

$$x_1[n] = \{4, 6, 10, 12\} \in V_2$$

Then the details would be,

$$a_1 = \left\{5\sqrt{2}, 11\sqrt{2}\right\}$$

Its details would be,

$$d_1 = \left\{-\sqrt{2}, -\sqrt{2}\right\}$$

Energies would be given as,

$$E_{a_1} = 292$$
$$E_{d_1} = 4$$

Hence, in this case the energy stored in the details is only about 1.4 percent and most of the energy would be stored in approximations. So we can conclude that for smooth looking signals most of the energy would be stored in approximations and for fairly rough looking signals for, e.g. a textured image the energy distribution is in a way even, however most of the energy would still be in approximations. Thus, indeed energy gets preserved in case of wavelet transform.

Now, let us carry out two important tasks, first is de-noising a two-dimensional toy image. Consider the following sample image, let's revisit example 16.7.2 from application perspective.

$$S = \begin{bmatrix} 9 & 7 & 6 & 2 \\ 5 & 3 & 4 & 4 \\ 8 & 2 & 4 & 0 \\ 6 & 0 & 2 & 2 \end{bmatrix}$$

We shall use following unitary Haar transform matrix,

$$A = \frac{1}{2}\begin{bmatrix} 1 & 1 & 0 & 0 \\ 1 & -1 & 0 & 0 \\ 0 & 0 & 1 & 1 \\ 0 & 0 & 1 & -1 \end{bmatrix}$$

We would carry out the analysis in two steps,

1. To find out S in horizontal direction as, $S_H = SA$
2. To find out S in horizontal and vertical direction as, $S_{HV} = AS_H = ASA$.

Consider step 1,

$$S_H = SA$$

$$S_H = \begin{bmatrix} 9 & 7 & 6 & 2 \\ 5 & 3 & 4 & 4 \\ 8 & 2 & 4 & 0 \\ 6 & 0 & 2 & 2 \end{bmatrix} \frac{1}{2}\begin{bmatrix} 1 & 1 & 0 & 0 \\ 1 & -1 & 0 & 0 \\ 0 & 0 & 1 & 1 \\ 0 & 0 & 1 & -1 \end{bmatrix}$$

$$S_H = \begin{bmatrix} 8 & 1 & 4 & 2 \\ 4 & 1 & 4 & 0 \\ 5 & 3 & 2 & 2 \\ 3 & 3 & 2 & 2 \end{bmatrix}$$

Consider step 2,

$$S_{HV} = AS_H$$

This results in,

$$S_{HV} = \begin{bmatrix} 6 & 1 & 4 & 1 \\ 2 & 0 & 0 & 1 \\ 4 & 3 & 2 & 1 \\ 1 & 0 & 0 & 1 \end{bmatrix}$$

Now, consider first 2 × 2 matrix from S_{HV} and S let D and F be these matrices respectively then,

$$D = \begin{bmatrix} 6 & 1 \\ 2 & 0 \end{bmatrix}$$

$$F = \begin{bmatrix} 9 & 7 \\ 5 & 3 \end{bmatrix}$$

If we take the average of elements of F we would get element (1,1) of D, i.e.

$$\frac{1}{4}[9+7+5+3] = 6$$

This is the low pass element. Also consider element (2,1) of D which can be obtained by vertical difference as,

$$\frac{1}{4}[(9-5)+(7-3)] = 2$$

This would be a high pass element since it is obtained by taking an average of difference in rows. Correspondingly we can say that (1,2) element of D i.e. 1 is a high pass element which would be difference in horizontal direction. Also we can observe that element (2,2) of D i.e. 0 is a high pass element obtained by taking a difference in diagonals. Thus, we can conclude that D is actually a decomposed version of F.

These coefficients are of great importance since they help in building the final matrix when it comes to transforming an image into wavelet space. The transformed version in case of the matrix S can be written from S_{HV} by considering all the four 2 × 2 matrices similar to matrix D, obtained by dividing the matrix into four equal parts.

The low pass coefficients in that case would be,

$$S_1 = \begin{bmatrix} 6 & 4 \\ 4 & 2 \end{bmatrix}$$

Now, if we again analyze S_1 using Haar MRA then we would have,

$$S_{I_H} = S_1 A$$

$$S_{I_H} = \begin{bmatrix} 6 & 4 \\ 4 & 2 \end{bmatrix} \frac{1}{2} \begin{bmatrix} 1 & 1 \\ 1 & -1 \end{bmatrix}$$

$$S_{I_H} = \begin{bmatrix} 5 & 1 \\ 3 & 1 \end{bmatrix}$$

Performing analysis also in vertical direction we have,

$$S_{I_{HV}} = AS_{I_H}$$

$$S_{I_{HV}} = \begin{bmatrix} 4 & 1 \\ 1 & 0 \end{bmatrix}$$

Finally, the matrix in the wavelet domain would be,

$$W = \Omega S = \begin{bmatrix} 4 & 1 & 1 & 1 \\ 1 & 0 & 3 & 1 \\ 2 & 0 & 0 & 1 \\ 1 & 0 & 0 & 1 \end{bmatrix}$$

We can see from W that, $\begin{bmatrix} 4 & 1 \\ 1 & 0 \end{bmatrix}$ has the maximum energy and $\begin{bmatrix} 0 & 1 \\ 0 & 1 \end{bmatrix}$ has the minimum energy. Making this part zero, the resulting image would be,

$$W_d = \begin{bmatrix} 4 & 1 & 1 & 1 \\ 1 & 0 & 3 & 1 \\ 2 & 0 & 0 & 0 \\ 1 & 0 & 0 & 0 \end{bmatrix}$$

W_d is called as the denoised version. Using W_d we can calculate the inverse transform. Let B be the first 2×2 matrix of W_d thus,

$$B = \begin{bmatrix} 4 & 1 \\ 1 & 0 \end{bmatrix}$$

We can use $A^{-1}BA^{-1}$ where, $A^{-1}=\begin{bmatrix}1 & 1\\ 1 & -1\end{bmatrix}$ thus we can write,

$$A^{-1}BA^{-1}=\begin{bmatrix}6 & 4\\ 4 & 2\end{bmatrix}$$

This leads us to the denoised version of the image,

$$S_{d_{HV}}=\begin{bmatrix}6 & 1 & 4 & 1\\ 2 & 0 & 0 & 0\\ 4 & 3 & 2 & 1\\ 1 & 0 & 0 & 0\end{bmatrix}$$

Finally, the denoised image can be calculated as,

$$S_d=A^{-1}S_{d_{HV}}A^{-1}=\begin{bmatrix}9 & 7 & 5 & 3\\ 5 & 3 & 4 & 4\\ 8 & 2 & 3 & 1\\ 6 & 0 & 3 & 1\end{bmatrix}$$

If we compare this image with original image S, then we can see that first two rows of S were relatively smooth. However, the last two rows needed denoising. In image S_d we can see that the first two rows are even better and problem is in a way solved for the third row. However, problem still exists for the fourth row. But we know what is the solution; we can go on pursuing this analysis for next couple of scales and probably instead of using Haar wavelet we can use db2 wavelet having three vanishing moments which will give us results much quicker.

So this was one application which showed how the two-dimensional analysis actually works. Next, we would look at an application regarding pattern recognition.

Let us say, we have three letters L, C and U.

$$L=\begin{bmatrix}1 & 0 & 0 & 0\\ 1 & 0 & 0 & 0\\ 1 & 0 & 0 & 0\\ 1 & 1 & 1 & 1\end{bmatrix}$$

$$C=\begin{bmatrix}1 & 1 & 1 & 1\\ 1 & 0 & 0 & 0\\ 1 & 0 & 0 & 0\\ 1 & 1 & 1 & 1\end{bmatrix}$$

$$U = \begin{bmatrix} 1 & 0 & 0 & 1 \\ 1 & 0 & 0 & 1 \\ 1 & 0 & 0 & 1 \\ 1 & 1 & 1 & 1 \end{bmatrix}$$

If we calculate W_L, W_C and W_U and calculate mean squared error (M.S.E.) between all of them, then we would realize that L and C are closer than L and U and C and U. We leave it to the readers to explore further.

17.10 | JPEG 2000 Filter Strategy

Cohen-Daubechies-Feauveau $\frac{9}{7}$ biorthogonal filter pair is popularlty known as CDF97 in literature. It got approved by the committee to becomd part of lossy JPEG 2000 compression standard. CDF97 is not a member of the biorthogonal spline filter pair family. In fact, it works better than $\frac{9}{7}$ tap that can be designed using biorthogonal spline framework we have already seen.

In this filter, length of h_k and $\tilde{g}_k$ is 'g' and $\tilde{h}_k$ & g_k is '7'.

Therefore
$$H(\omega) = \sum_{K=-4}^{4} h_k \cdot e^{jK\omega}$$

and

$$\widetilde{H}(\omega) \sum_{K=-3}^{3} \tilde{h}_k \cdot e^{jK\omega}$$

The filter needs to obey typical LPF conditions.

$$H(\pi) = H^{'}(\pi) = 0$$

Moreover,

$$\widetilde{H}^{(m)}(\pi) = 0, m = 0, \cdots, 5$$

The zeros at $\omega = \pi$ of $H(\omega)$ & $\widetilde{H}(\omega)$ for CDF97 filter pair are equally balanced.

We shall start with condition necessary and sufficient for biorthogonal filters:

$$\widetilde{H}(\omega) \cdot \overline{H(\omega)} + \widetilde{H}(\omega + \pi) \cdot \overline{H(\omega + \pi)} = 2 \tag{17.2}$$

as $h = \{h_{-L}, \cdots, h_L\}$ is odd length and symmetric,

if $h_K = h_{-K}$ then,

$$H(\omega) = \sum_{K=-L}^{L} h_K \cdot e^{jK\omega}$$

is an even function. Furthermore,

$$H(\omega) = h_0 + 2 \cdot \sum_{K=1}^{L} h_k \cdot \cos(\omega_K) \tag{17.3}$$

The trick lies in expressing function $\cos(K\omega)$ as polynomial in $\cos(\omega)$.
For example $\cos(3\omega) = 4 \cdot \cos^3(\omega) - 3 \cdot \cos(\omega)$

Therefore $\cos(3\omega)$ is written by composing $\cos(\omega)$ and polynomial $P(t) = 4 \cdot t^3 - 3 \cdot t$!

For odd length symmetric filters,

$$H(\omega) = \sum_{K=-L}^{L} h_k \cdot e^{jK\omega} \tag{17.4}$$

$$H(\omega) = \sqrt{2} \cdot \cos^{2l}\left(\left(\frac{\omega}{2}\right) \cdot P(\cos(\omega)\right) \tag{17.5}$$

Here, $P(1) = 1$ and $P(-1) \neq 0$
The even solution will be

$$\tilde{H}(\omega) = \sqrt{2} \cdot \cos^{2\tilde{l}}\left(\frac{\omega}{2}\right) \cdot \tilde{p}(\cos(\omega)) \tag{17.6}$$

$\tilde{l}$ = non-negative integer and $\tilde{p}(-1) \neq 0$ and $\tilde{p}(1) = 1$

Equations (17.5) and (17.6) be characterized into,

$$P(\cos(\omega)) \cdot \tilde{p}(\cos(\omega)) = \sum_{j=0}^{K-1} \binom{K-1+j}{j} \sin^{2j}\left(\frac{\omega}{2}\right) \tag{17.7}$$

Where, $K = l + \tilde{l}$ and degree of $p(t) \cdot \tilde{p}(t) < K$
Now, the important step is to choose 'K' and the factor

$$P(t) = \sum_{j=0}^{K-1} \binom{K+j-1}{j} t^j \tag{17.8}$$

CDF97 crux lies in choosing $K = 4$ and $l = \tilde{l} - 2$

Therefore
$$P(t) = \sum_{j=0}^{3} \binom{3+j}{j} t^j = 1 + 4 \cdot t + 10 \cdot t^2 + 20 \cdot t^3 \tag{17.9}$$

Roots of $P(1)$ are,

$$r_1 = -0.3424,\ r_2 - 0.0788 - 0.3733j,\ r_3 = -0.0788 + 0.3733j$$

Biggest coefficient of $P(1) = 20$,

Therefore $$P(t) = 20(t - r_1)(t - r_2)(t - r_3) \tag{17.10}$$

Let us distribute as:

$$\widetilde{P(t)} = a(t - r_1) \text{ and } p(t) = \frac{20}{a}(t - r_2)\cdot(t - r_3)$$

$\tilde{l} = 2$, and $\widetilde{P}(t) = a(t + 0.3424)$

By substituting $t = \sin^2\left(\frac{\omega}{2}\right)$

$$\widetilde{H}(\omega) = \sqrt{2}\cos^4\left(\frac{\omega}{2}\right) a\left[\sin^2\left(\frac{\omega}{3}\right) + 0.3423\right] \tag{17.11}$$

and

$$H(\omega) = \sqrt{2}\cos^4\left(\frac{\omega}{2}\right)\frac{20}{a}\left(\sin^2\left(\frac{\omega}{2}\right) + 0.0786 - 0.3733j\right)\cdot\left(\sin^2\left(\frac{\omega}{2}\right) + 0.0786 - 0.3733j\right) \tag{17.12}$$

As $H(0) = \widetilde{H}(0) = \sqrt{2}$

Solving for $\widetilde{H}$, we get $a = 2.9207$

Solving for Eq.(17.4)

$$\widetilde{H}(\omega) = \sum_{K=-3}^{3} \tilde{h}_K \cdot e^{jK\omega}$$

$$\boxed{\begin{aligned} \tilde{h}_0 &= 0.7884 \\ \tilde{h}_1 &= 0.4181 = \tilde{h}_{-1} \\ h_2 &= -0.0406 = \tilde{h}_{-2} \\ h_3 &= -0.0645 = h_{-3} \end{aligned}} \tag{17.13}$$

and

$$H(\omega) = \sum_{K=-4}^{4} h_k \cdot e^{jK\omega}$$

$$\boxed{\begin{aligned} h_0 &= 0.852 \\ h_1 &= 0.3775 = h_{-1} \\ h_2 &= -0.1106 = h_{-2} \\ h_3 &= -0.0238 = h_{-3} \\ h_4 &= -0.0378 = h_{-4} \end{aligned}} \tag{17.14}$$

$$
\begin{aligned}
\tilde{g}_K &= \left\{\tilde{g}_{-3},\tilde{g}_{-2},\tilde{g}_{-1},\tilde{g}_0,\tilde{g}_1,\tilde{g}_2,\tilde{g}_3\right\} \\
&= (-1)^K \cdot h_{1-K} \\
&= \left\{-h_4,h_3,-h_2,h_1,-h_0,h_1,-h_2,h_0,-h_4\right\} \\
&= \left\{-0.0378,-0.0238,0.1106,0.3774,-0.8526,0.3774,0.1106,-0.0238,-0.0378\right\}
\end{aligned} \tag{17.15}
$$

$$
\begin{aligned}
g_k &= \left\{g_{-2},g_{-1},g_0,g_1,g_2\right\} \\
&= (-1)^K \cdot \tilde{h}_{1-K} \\
&= \left\{\tilde{h}_3,-\tilde{h}_2,\tilde{h}_1,-\tilde{h}_0,\tilde{h}_1,-\tilde{h}_2,\tilde{h}_3\right\} \\
&= \left\{-0.0645,0.0406,0.4180,-0.7884,0.4180,0.0406,-0.0645\right\}
\end{aligned} \tag{17.16}
$$

$g_k,\tilde{g}_K,h_k,\tilde{h}_K$ gives us W_{CDF97} and $\widetilde{W}_{CDF97}$

17.11 | Two Interesting Techniques SPIHT and EZW

For those researchers working in the field of pattern recognition and computer vision, two very effective wavelet based techniques which have made a serious impact on the technological advancement are:

- SPIHT (Set Partitioning in Hierarchical Trees)
- EZW (Embedded Zerotrees of Wavelet transforms)

SPIHT is an image compression algorithm and harps on the ability to exploit inherent similar structures across the sub-bands in a specific hierarchy. This algorithm was developed by Pearlman et.al. and interested readers can explore this further.

EZW is lossy image compression algorithm. At the low bit rates the sub-band coding produces many near-zero coefficients, the subtrees created out of these are called zerotrees. EZW was developed by Shapiro in around 1993, and interested readers can explore this further.

Exercises

Exercise 17.1

Consider the signal $f(t) = 10t^2(1-t)^2 cos 8\pi t, 0 < t < 1$ on the interval (0,1).

We use the Wavelets Tool Box to compute the scaling levels a_1 and a_2 over the interval (0,1), for the Coif 6 and the Daub 2 scaling functions coefficients. We will compare the maximum error on the interval (0,0.2) between the above Coif 6 approximation and the exact sample values. The same is done with Daub 2 computing the error between its corresponding scaling coefficients and the above estimation in. The readers are encouraged to find that for level 1, the maximum error for the Coif 6 is an order of magnitude less, and the same is for level 2. It is left for an exercise to check this accuracy at higher levels, where it is expected to decrease.

Exercise 17.2

As we did for the other scaling functions and wavelets, we call $\{h_n\}$ the scaling coefficients, let us call $h_1(n)$ as the corresponding wavelets coefficients. Show that the Coif 6 scaling coefficient satisfy the following equality,

$$\sum_{n=0}^{5} h_n^2 = 1.$$

Give the interpretation of this result in terms of the energy of the Coif 6 wavelet. Show that Coif 6 scaling function satisfies the (new) relation,

$$-2h_0 - h_1 + h_3 + 2h_4 + 3h_5 = 0$$

while ϕ_{D2} does not.

Exercise 17.3

Consider the signal

$$f(t) = 20t^2(1-t)^4 \cos 12\pi t, 0 < t < 3$$

Compute the scaling functions coefficients for Coif 6 and Daub 2, and compare the maximum error as done in Example 17.1 at the levels 1, 2, 3 and 4. Use very small scales of ℓ_{10} then ℓ_{14}, and make your conclusion.

For the same problem try Coif 12 and Daub 3.

Chapter 18

Going Beyond the Realms

18.1 | Introduction

Classical Wavelets analysis has brought in a fresh perspective all together and yet researchers across the globe face limitations when it comes to using wavelet filters on highly oriented data and particularly in higher dimension. The building blocks of wavelet analysis offer isolation in time and frequency at depths greater than the conventional transforms, but only in rigid sense when it comes to dealing with angular information. Haar being the most primitive of all mother wavelets, represents the analysis in the form of first order difference. This gradient approach typically allows the analyzer to resolve the information at multiple scales along only four angles in the spirit of gradient analysis. As the wavelet filters hold only fixed number of directional elements they struggle in capturing particularly anisotropic parts in images and higher dimensional data. As a consequence, in the last decade or so, we have witnessed orientation-specific multiscale and multiresolution structures, which have manifested themselves into modern transforms with the likes of ridgelets, curvelets, brushlets to name a few. These have led to interesting applications from various domains with different type of data.

A better representation always leads to optimum utilization of memory and resource resulting into compression. In section (16.7) of Chapter 16 and particularly in examples (16.7.3-16.7.6) we have also brought out significance of transformation matrix being unitary. Along with a transformation matrix being unitary, it is equally important for it to be enough sensitive towards relevant information pieces. Only then it leads to sparse representation thus producing compactness. The above mentioned transforms are important from this important perspective.

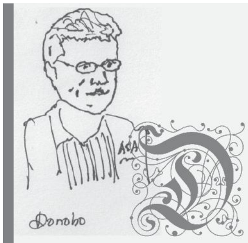

David Donoho

David Donoho (born 5 March 1957) is a professor of statistics at Stanford University. He is very well known for his contributions in the field of multiscale geometric analysis which has led interesting offshoots of wavelet with the likes of ridgelets, curvelets etc. For his outstanding contributions in the field he has won many awards like 2010 Norbert Wiener Prize in Applied Mathematics etc.

18.2 | Ridgelets

We use smooth and univariate function $\psi : \mathbb{R} \to \mathbb{R}$, to define two dimensional continuous ridgelet transform in $\mathbb{R}^2$ with characteristic of a compactly supported function, keeping sufficient decay and to satisfy basic admissibility condition,

$$\int |\hat{\psi}(\omega)|^2 / |\omega|^2 \, d\omega < \infty \tag{18.1}$$

The above equation (18.1) holds true if the basic admissibility condition is met, that is if zeroth statistical moment (mean) vanishes, i.e. $\int \psi(t)dt = 0$. In a typical construct of such kind, a special normalization about ψ is proposed, such that $\int_0^\infty |\hat{\psi}(\omega)|^2 \, \omega^{-2} d\omega = 1$. For a regular wavelet construct the Hallmark features are scaling, translation and dilation. In ridgelets the 'orientations' add the necessary ingredients of the transform.

The bivariate ridgelet $\psi_{a,b,\theta}(X) : \mathbb{R}^2 \to \mathbb{R}$ for every scale $a > 0$, translate $b \in \mathbb{R}$ and orientation $\theta \in [0, 2\pi)$ can be defined as:

$$\psi_{a,b,\theta}(X) = \psi_{a,b,\theta}(x_1, x_2) = a^{/2}.\psi((x_1 \cos\theta + x_2 \sin\theta - b)/a) \tag{18.2}$$

As typical wavelet has consistent pattern along x-axis translations, so does a typical ridgelet along $x_1 \cos\theta + x_2 \sin\theta$. The coefficients are calculated using the dot product concept again,

$$\mathbb{R}_f(a,b,\theta) := < f, \psi_{a,b,\theta} > = \int_{R^2} f(x) \bar{\psi}_{a,b,\theta}(x) dx \tag{18.3}$$

Equation (18.2) and (18.3) depict the transformation in the forward direction. The inverse reconstruction formulae can be worked out as:

$$f(x) = \int_0^{2\pi} \int_{-\inf}^{\inf} \int_0^{\inf} \mathbb{R}_f(a,b,\theta) \, \psi_{a,b,\theta}(x) \frac{da}{b} db \frac{d\theta}{4\pi} \tag{18.4}$$

Parseval relation holds for equation (18.4). The energy analysis, in typical signal processing sense, is possible for functions which are integrable and square integrable.

Hough transform for all the lines, also referred as 'Radon Transform' could be helpful in designing the deployment strategy for Ridgelets. In fact, a wavelet style of analysis of radon domain results into Ridgelet constructs. This has a strong connection with the fact that owing to uncertainty principle a line in an image space (which can be thought of to be made up of number of points) gets represented as a singular point in Hough space; and wavelet transform is known to provide 'sparse' representation for singular points. Hough transform for lines or radon transform of an object f is the collection of line integrals indexed by $(\theta,t) \in [0,2\pi) \times \mathbb{R}$ given by,

$$Rf(\theta,t) = \int_{2} f(x_1,x_2)\delta(x_1 \cos\theta + x_2 \sin\theta - t)\,dx_1 dx_2 \tag{18.5}$$

where, δ is the Dirac distribution function. The reader can very clearly see now that when $1-D$ wavelet transform is to indexed slices of Radon transform for consistent angular variable θ and varying t (producing translates), it gets manifested into a ridgelet transform.

Two step recipe for ridgelet transform:

1. Compute Radon Transform $Rf(t,\theta)$.
2. Apply $1-D$ wavelet transform to the slices $Rf(.,\theta)$.

18.2.1 Digital Ridgelet Transform

There are different ways of constructing digital Ridgelets, however the most conventional one is what is known as 'The RectoPolar Ridgelet transform'.

Owing to the projection-slice-theorem, a faster implementation of the Radon transform is feasible in Fourier domain. The $2D-FFT$ (Fast Fourier Transform) of given image is computed first, and adjustments are made to bring the energy points together (using function like *fftshift* in MATLAB) at the center. The frequency domain representation evaluates the frequency instances in a manner that lead the analysis from origin (where energy is concentrated) spreading out with uniform angular spread. This forms a polar grid like construct, and on the polar grid, each ray depicts a projection and each shift per the angle is marked by every sample on each ray. Through gridding used in Tomography, interpolation gives the way to map from the Cartesian to Polar grid. The readers should note here that interpolation, however, is extremely to sensitive, thus making the entire system less robust and inaccurate. Further radon projections are obtained by applying $1D-IFFT$ (Inverse Fourier Transform) for each ray.

The pragmatic question is how can we implement such circular polar grid in $2D$ discrete sense. The readers will realize that for all $2D$ operations on an image the geometry is mapped in square or rectangular matrices. Any pixel of an image can have maximum 8 neighboring pixels. The structuring elements (SEs) for morphological operations or masks for filtering operations are square geometric with size of 3×3, 5×5, 7×7 etc. The most practical deployment strategy for Fourier based Radon transform is to replace polar-grid with pseudo-polar-grid.

The way pseudo-polar-grid manifests is presented in Fig. 18.1. We had concentric circles with linearly growing radius outwards in polar-grid. In pseudo-polar-grid these circles are replaced by concentric squares of linear outward growing sides. Naturally the outward spread is not angular, but along slope of line slant with prefixed angle. The 'pseudo' constructs of such grid closely resemble the polar nature, and as a consequence one can think of implementing FFT on this grid without interpolation. Thus, we get an interesting radon transform variation where the projection angles are not spaced uniformly. As a penalty, the pseudo-polar FFT should have at least twice as many samples as original image to maintain robustness and stability. The advantage is the nature of grid now being of $2D$ array it can be represented in matrix form, resulting into ease of implementation.

Now, the next step is to apply $1-D$ wavelet transform along radial variable in Radon space to complete the Ridgelet transform in true sense. The circumstances, however give push to use 'band-limited-wavelet' than the 'compactly-supported-wavelet'. It could be decimated wavelet schemes used at critical sampling or hard-thresholds put on wavelet coefficients, we have witnessed (in video coding for example) how time-domain-compactly-supported wavelets when confronted with nonlinear processing, results into artifacts. Owing to 'Uncertainty Principle', compactly supported wavelet kernels do not get isolation or compactness on frequency axis resulting in coarse-scale anomalies manifesting at finer-scale. Hence, we use inverse radon transform to reconstruct Fourier theme. This pushes us to use frequency-domain approach and use of wavelet basis which is 'band-limited' rather than 'compactly-supported'. The wavelet transform algorithm makes use of scaling function ϕ, which has limited band interval $[-\omega_c, \omega_c]$ and vanishes outside. Fourier transform of such scaling function can be re-normalized B3-spline:

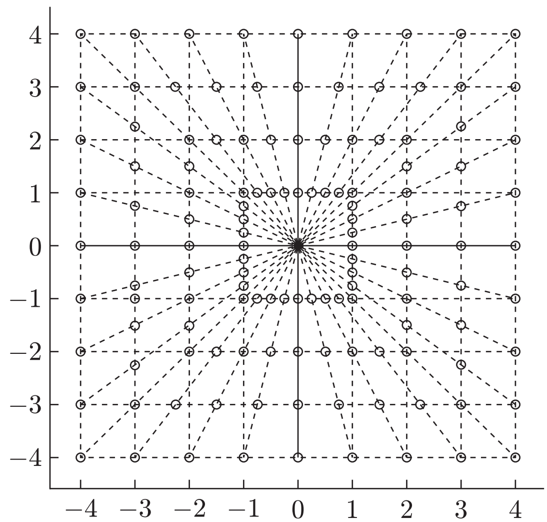

Figure 18.1 | *Illustration of the pseudo-polar grid in the frequency domain for an n by n image ($n = 8$)*

$$\hat{\phi}(\omega) = \frac{3}{2} B_3(4v) \tag{18.6}$$

Consequently, $\hat{\psi}$ can be posed as first order difference between two consecutive scales,

$$\hat{\psi}(2\omega) = \hat{\phi}(\omega) - \hat{\phi}(2\omega) \tag{18.7}$$

Using Sampling Theorem, one can build a pyramid of $n + n/2 + ... + 1 = 2n$ elements for compactly supported $\hat{\psi}$.

Thus the transform depicts following properties:

- The structure has optimum computational complexity. Computations of $1D$ inverse Fourier Transform along each radial line is avoided, and rather wavelet coefficients are directly calculated in Fourier space.

- Perfect reconstruction is guaranteed. Wavelet coefficients can be added to reproduce the original signal and ridgelet coefficients are added to construct Fourier coefficients. For this to hold, it is necessary sample each sub-band above sampling rate prescribed by Shannon-Nyquist-Whittaker (sampling theorem).

Though the transform is computationally not complex, it introduces data redundancy. But, Ridgelets are not meant for data compression, in lieu they are geared up towards accurate data representation, useful for better data analysis. Readers will also recollect that translation invariant over-complete mapping has interesting benefits.

All that has been discussed so far can be put together to form the complete schematic flowchart of discrete ridgelet transform (DRT) as shown in Fig. 18.2. The big picture is ridgelets are capable of sparse representation of images ridges which are not necessarily straight aligned only in known 4 gradient directions. We must also state that ridgelets:

- Guarantee exact reconstruction
- Reconstruction robust against delta changes in coefficients
- Like many intermittent stages, they are irreversible

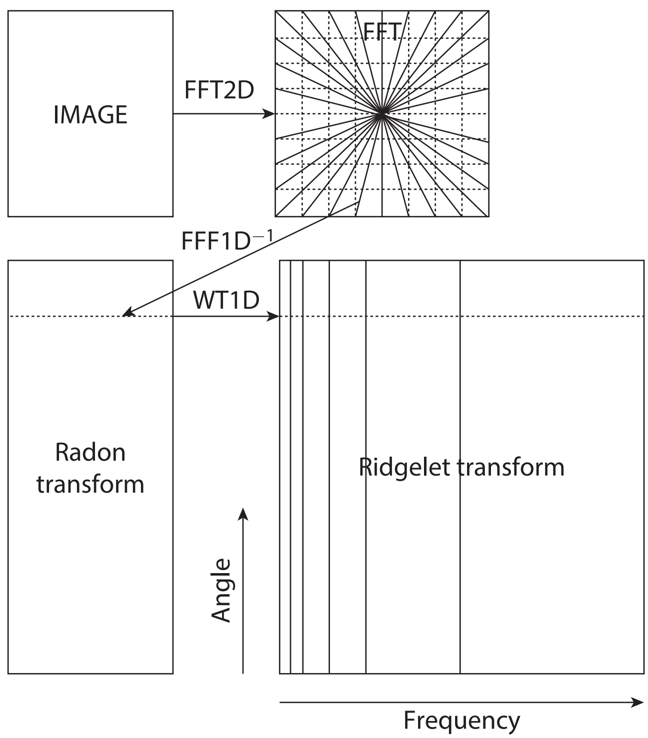

Figure 18.2 | *Discrete ridgelet transform flowchart. Each of the 2n radial lines in the Fourier domain is processed separately. The 1-D inverse FFT is calculated along each radial line followed by a 1-D nonorthogonal wavelet transform. In practice, the one-dimensional wavelet coefficients are directly calculated in the Fourier space*

18.3 | Curvelets

In image processing applications, many times the decisions are based on mapping the objects correctly for detection, identification, tracking and other purposes. Any object is made up of shape, size, color, texture. The first defining characteristics of any object is shape and shape is made up of the boundary, boundary is made of ridges and ridges are made of edges. Most of the times the edges are in the form of curves and not necessarily straight lines. Yet, as engineers many times pose non-linear system as a piecewise linear system, curves can thought of made of very tiny straight lines. Then curves can be captured by deploying Ridgelets at local level of a very small scale. This concept leads us to the first generation curvelets (CurveletG1).

The emphasis of CurveletG1 transform is to use same transform (Ridgelet) at different scales with different block size. The idea behind CurveletG1 is as shown in Fig. 18.3. Local ridgelet transform is applied on every wavelet sub-band after decomposition of an image into sub-bands. Different levels of multiscale ridgelet pyramid are built to use them represent different sub-bands produced by wavelet filter.

In section (18.1), we discussed about importance of anisotropic parts. Taking clue from parabolic-scaling-law, which gives relationship of $width \approx length^2$, during sub-band decomposition elements of critical frames are maintained roughly anisotropic.

The First Generation (G1) Discrete Curvelet Transform of function $f(x)$ uses dyadic scale sequences and by typical use of bandpass filter banks Δ_j can have dense representation in range $[2^{2j}, 2^{2j+2}]$, and,

$$\Delta_j(f) = \Psi_{2j} * f, \Psi_{2j}(\omega) = \hat{\Psi}(2^{-2j}\omega) \tag{18.8}$$

It is only in compliance to use decomposition into dyadic sub-bands $[2^j, 2^{j+1}]$ as per classical wavelet theory. Quite the opposite, in discrete curvelet transform, the sub-bands used have non-dyadic range $[2^{2j}, 2^{2j+2}]$. This range has again its roots in the parabolic-scaling-law.

Curvelet decomposition: pseudo-code

- Sub-band Decomposition: Object f is decomposed into sub-bands.
- Sub-band Partitioning: Each sub-band gets partitioned into "squares" of scale of side-length $\sim 2^{-j}$.
- Ridgelet Step: Each square is subjected to Ridgelet Transform.

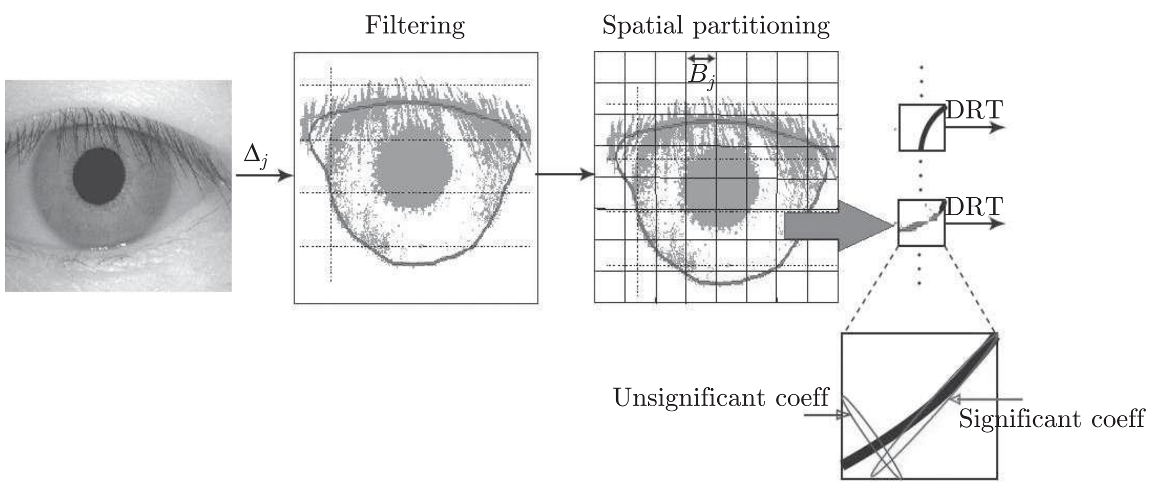

Figure 18.3 | *First generation (G1) discrete curvelet transform*

For digital implementation the algorithm decomposes an n by n image $f[i_1,i_2]$ as a superposition of the form:

$$f[i_1,i_2]=c_J[i_1,i_2]+\sum_{j=1}^{J}\omega_j[i_1,i_2] \tag{18.9}$$

where, c_J is a coarse or smooth version of the original image f and w_j represents 'the details of *f*' at scale 2^{-j}. Thus, the algorithm outputs $J+1$ sub-band arrays of size $n \times n$.

The algorithm snap shot is as follows:

For the given input $n \times n$ image $f[i_1,i_2]$:

1. Apply isotropic $2D$ wavelet transform with J scales
2. Set $B_1 = B_{min}$
3. for $j = 1,....,J$ while
4. Partition the sub-band w_j with a block size B_j and apply the Ridgelet to each block
5. if $j\ modulo\ 2 = 1$ then
6. $B_{j+1} = 2B_j\ else$
7. $B_{j+1} = B_j\ endif$
8. end for

Keeping compliance with fundamental principle of curvelets of having elements of length of $2^{-j/2}$ to be used for the analysis (decomposition) and synthesis (reconstruction) of the has to double its side length at every dyadic sub-band; this also keeps coarse representation of image c_J intact.

18.4 | Brushlets

Images which are rich in oriented textured ridge patterns require special type of filters for efficient feature extraction. E.g. Edges and textures in fingerprint images can exist at vivid possible locations, scales and orientations. The ability to efficiently analyze and extract features from textured patterns is thus of fundamental importance for building robust feature extractor.

The conventional model of patch of periodic and cyclic texture located at (x_0, y_0) is provided by a windowed complex exponential,

$$\omega(x-x_0, y-y_0)e^{i(\xi x+\eta y)} \tag{18.10}$$

where ω is a functional localization around the origin. Local Fourier basis is used to get the most appropriate representation for texture analysis. First, the image is divided into local blocks of same fixed size and then Fourier bases (F) are applied to encode the entire image by virtue of generating Fourier expansion within every block. The basic problems in this easiest approach are as follows:

- The size of the block should be adapted to the image ridge map content. (a large geometric feature should NOT belong to several small blocks etc.)
- The size of the blocks should be adapted to the frequencies of complex exponentials. (shorter blocks for higher frequencies etc.)
- 'Blocking' artifacts at boundaries of blocks
- Difficulty to superimpose blocks of different sizes

To solve these issues we replace Fourier framework with multiresolution framework. Two dimensional wavelet bases are created using tensor product of one dimensional bases. Let ϕ be the scaling function and ψ be the corresponding wavelet function, four wavelet functions can be written as:

$$\psi_k(x,y)=\begin{Bmatrix}\phi(x)\phi(x),\text{if } k=0\\ \phi(x)\psi(x),\text{if } k=1\\ \psi(x)\phi(x),\text{if } k=2\\ \psi(x)\psi(x),\text{if } k=3\end{Bmatrix} \tag{18.11}$$

The corresponding filter banks $m_k(\xi,\eta), k=1,2,3$ can resolve 2.5 directions namely, horizontal, vertical and an undecided diagonal direction. We deploy wavelet packet strategy to adaptively construct an optimum tiling of the plane. The implementation of such scheme and its geometric interpretation, however, becomes very challenging as tensor product of two real valued wavelet packets gets associated with four symmetric peaks in the frequency plane. The main challenge lies with the fact that intensity in the image is either oscillating as a planar wave $e^{i(w_x x+w_y y)}$ or with the conjugate frequency $e^{i(w_x x-w_y y)}$. To remove the conjugate part, following filter is used:

$$m_3(\xi,\eta)=0 \text{ if } \xi>0 \text{ and } \eta<0, \text{or if } \xi<0 \text{ and } \eta>0 \tag{18.12}$$

To be able to construct such filters we use two wavelets ψ_g and ψ_h which form an approximate Hilbert pair:

$$\psi_g(\xi)=\begin{cases}-i\psi_h(\xi),\text{if } \xi>0\\ i\psi_h(\xi),\text{if } \xi<0\end{cases} \tag{18.13}$$

with ϕ_h,ϕ_g being the corresponding scaling functions. To avoid localization of Fourier transform to only one quadrant for tensor product like $\psi_h(x)\,\psi_g(y)$, tensor product for wavelet ψ_h is taken as follows:

$$\begin{aligned}\psi_{h,1}(x,y)&=\phi_h(x)\,\psi_h(y)\\ \psi_{h,2}(x,y)&=\psi_h(x)\,\phi_h(y)\\ \psi_{h,3}(x,y)&=\psi_h(x)\,\psi_h(y)\end{aligned} \tag{18.14}$$

Similar tensor products are used for ψ_g. Sum and difference were calculated as:

$$\begin{aligned}\psi_i(x,y)&=\psi_{h,i}(x,y)+\psi_{g,i}(x,y)\\ \psi_{i+3}(x,y)&=\psi_{h,i}(x,y)-\psi_{g,i}(x,y),\quad i=0,1,2\end{aligned} \tag{18.15}$$

This transform gets resolved into 6 different directions with 4 directions of greater significance. This is further refined using steerable wavelet packets or *brushlets*. Basis functions for four quadrants and four directions is shown in Fig. 18.4.

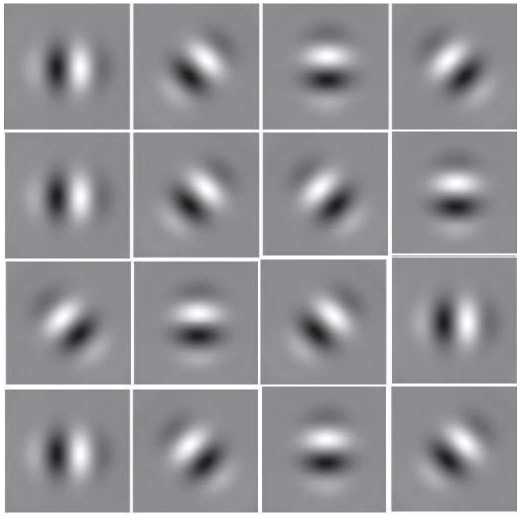

Figure 18.4 | *Brushlets coefficients being antisymmetric with respect to origin, imaginary part of coefficients for each quadrant gets distributed unevenly. As seen, upper right quadrant contains texture with patterns oriented along the direction* $\frac{\pi}{4}$ *; upper left window with patterns oriented along the direction* $\frac{3\pi}{4}$ *etc.*

Biorthogonal bases generation

Let $f \in L^2(\mathbb{R})$ and let $\hat{f}$ be the Fourier transform of f. Cover of the frequency axis will be,

$$\bigcup_{n=-\infty}^{n=\infty}\left[w_n - \frac{l_n}{2}, w_n + \frac{l_n}{2}\right] \tag{18.16}$$

where, w_n is the center of intervals of size l_n. As given in, unitary nature of Fourier transform can be used to obtain new pair of biorthogonal bases by applying inverse Fourier transform on local Fourier basis $u_{n,k}$ and $\tilde{u}_{n,k}$. $\{\psi_{m,j}, \hat{\psi}_{n,k}, \forall\, j,k,m,n \in \mathbb{Z}\}$ being bi-orthogonal bases for $L^2\mathbb{R}$, brushlets $\{\psi_{n,k}\}$ and $\{\tilde{\psi}_{n,k}\}$ are obtained.

$$\begin{aligned}\psi_{n,k}(x) &= \frac{1}{\sqrt{l_n}} e^{2i\pi w_n x}\left\{(-1)^k \hat{b}_n\left(x - \frac{k}{l_n}\right)\right. \\ &\left. -2i\sin(\pi l_n x)\hat{h}\left(x + \frac{k}{l_n}\right)\right\}\end{aligned} \tag{18.17}$$

In Eq. (18.17), $\psi_{n,k}(x)$ is a complex valued function and has a phase component which captures the orientations, k is the translation index and l_n is the analysis scaling factor. This theme is extended to a two dimensional kernel by partitioning the frequency plane through lattice cubes,

$$\bigcup_{n=-\infty}^{\infty}\bigcup_{m=-\infty}^{\infty}\left[\xi_m-\frac{h_m}{2},\xi_m+\frac{h_m}{2}\right]\otimes\left[\eta_n-\frac{l_n}{2},\eta_n+\frac{l_n}{2}\right] \tag{18.18}$$

(ξ_m,η_n) is the center of each rectangle of size $h_m\times l_n$.

18.5 | Contourlets

A special member of the emerging family of multiscale geometric transforms is the contourlet transform which was developed in the last few years in an attempt to overcome inherent limitations of traditional multistage representations such as curvelets and wavelets. For example, biomedical images were typically denoised using firstly wavelet then curvelets and finally contourlets transform and results show that contourlets transform outperforms the curvelets and wavelet transform in terms of signal noise ratio. Interested readers can explore this algorithm in detail from the toolbox developed by the authors who invented contourlets.

18.6 | Bandelets

Bandelets are wavelet style orthonormal basis which are better suited to problems like tracking object boundaries with specific geometric shape etc. Many researchers consider Bandelets as warped wavelet basis. This is an extension of the philosophy proposed in contourlets and curvelets. Smooth functions defined on smoothly bounded domains need the orthogonality mapped irrespective of preservation of compact nature of the problem. Bandelets typically give exciting results under such circumstances.

18.7 | Platelets

Traditional wavelet based methods are out and out parametric. Platelets is a novel approach and provide non-parametric multi-scale algorithms. Platelets are localized functions at various scales, locations, and orientations that are capable of producing piecewise linear image approximations, and a new multiscale decomposition based on these functions. Platelet decompositions of Poisson distributed images or signals are tractable and computationally efficient and hence have started to become popular choice for denoising. In the modern era we have witnessed fast, platelet-based, maximum penalized likelihood methods for image denoising, deblurring and reconstruction problems.

18.8 | (W)Edgelets

While conventional wavelets are good at capturing the point singularities, the Edgelet transform is good at capturing the linear singularities or edges and hence the name. Wedgelet transform takes all dyadic squares into consideration and thus forms wedges, hence the name. In Wedgelet transform the Wedgelet Dictionary is formed and Edgelet can be used for the said purpose. Edgelet chains and Wedgelets are useful in applications like noise removal with edges, scanning for segments, travelling salesman analysis, curve compression to name a few.

18.9 | Shearlets

Anisotropic diffusion plays vital role in noise modelling in image analysis. Shearlets are a multiscale framework which allows to efficiently encode anisotropic features in multivariate problem classes.

Shearlets are constructed by parabolic scaling, shearing and translation applied to a few generating functions and hence the name. This philosophy was introduced in 2006 by Guo et.al.

18.10 | Hilbert-Huang-Transform (HHT)

HHT has become popular for the non-parametric natured problems of late. Though the transform lacks the formal structure and does not necessarily gives the characterization through the properties, due to its applicability it has become preferred choice for few of the applications.

18.10.1 Hilbert-Huang Analysis

Huang et. al. developed a signal analysis method, called as the Empirical Mode Decomposition (EMD) method. This method analyzes the signal under the consideration, by decomposing it into mono-components called Intrinsic Mode Functions (IMF). The empirical nature of the approach may be partially attributed to a subjective definition of the envelope and the intrinsic mode function involved in its sifting process. The EMD method used in conjunction with Hilbert Transform is also known as 'Hilbert-Huang Transform' (HHT). Because of its effectiveness in analyzing a nonlinear, non-stationary signal, the HHT was recognized as one of the most important discoveries in the field of applied mathematics in NASA history. By the EMD method, the obtained signal $f(t)$ can be represented in terms of IMFs as:

$$f(t) = \sum_{i=1}^{n} c_i(t) + r_n \tag{18.19}$$

where, $c_i(t)$ is the i^{th} intrinsic mode function and r_n is the residue.

A set of analytic functions can be constructed for these IMFs. The analytic function $z(t)$ of a typical IMF $c(t)$ is a complex signal having the original signal $c(t)$ as the real part and its Hilbert transform of the signal as its imaginary part. By representing the signal in the polar coordinate form one has

$$z(t) = c(t) + jH[c(t)] = a(t)e^{j\phi(t)} \tag{18.20}$$

where $a(t)$ is the instantaneous amplitude and $\phi(t)$ is the instantaneous phase function. The instantaneous amplitude $a(t)$ and is the instantaneous phase function $\phi(t)$ can be calculated as,

$$a(t) = \sqrt{\{c(t)\}^2 + \{H[c(t)]\}^2} \tag{18.21}$$

$$\phi(t) = \tan^{-1}\left\{\frac{H[c(t)]}{c(t)}\right\} \tag{18.22}$$

The instantaneous frequency of a signal at time t can be expressed as the rate of change of phase angle function of the analytic function obtained by Hilbert Transform of the signal. The expression for instantaneous frequency is given in Eq. (18.23).

$$\omega(t) = \frac{d\phi(t)}{dt} \tag{18.23}$$

Because of a capability of extracting instantaneous amplitude $a(t)$ and instantaneous frequency $\omega(t)$ from the signal, this method can be used to analyze an obtained non-stationary signal. In a special case of a single harmonic signal, the phase angle of its Hilbert transform is a linear function of time and therefore its instantaneous frequency is constant and is exactly equal to the frequency of the harmonic. In general, the concept of instantaneous frequency provides an insightful description as how the frequency content of the signal varies with the time.

The empirical mode decomposition (EMD) method proposed by Huang decomposes a signal into IMFs by an innovative sifting process. The IMF is defined as a function which satisfy following two criterion:

- The number of extrema and the number of zero crossings in the component must either equal or differ at most by one.
- At any point, the mean value of the envelope defined by the local maxima and the envelope defined by local minima is zero.

A sifting process proposed to extract IMFs from the signal process the signal iteratively in order to obtain a component which satisfies above mentioned conditions. An intention behind application of these constraints on the decomposed components was to obtain a symmetrical mono-frequency component to guarantee a well-behaved Hilbert transform. It is shown that the Hilbert transform behaves erratically if the original function is not symmetric with x-axis or there is sudden change in phase of the signal without crossing x-axis.

Although the IMFs are well behaved in their Hilbert Transform, it may not necessarily have any physical significance. For example, an impulse response of a simple linear damped oscillator, which is physically mono-component with a single frequency, may not be necessarily fit the definition of the IMF and envelope function. Moreover the empirical sifting process does not guarantee exact modal decomposition. The EMD method may lead to mode mixture and the analyzing signal needs to pass through a bandpass filter before analysis by EMD method.

The sifting process separates the IMFs with decreasing order of frequency, i.e. it separates high frequency component first and decomposes the residue obtained after separating each IMF till a residue of nearly zero frequency content does not obtained. Till date, there is no mathematical formulation derived for EMD method and the studies done in order to analyze the behaviour of this method in stochastic situations involving broadband noise shows that the method behaves a dyadic filter bank when applied to analyze a fractional Gaussian noise (see Fland). In this sense, the sifting process in the EMD method may be viewed as an implicit wavelet analysis and the concept of the intrinsic mode function in the EMD method is parallel to the wavelet details in wavelet analysis.

The wavelet packet analysis of the signal also can be seen as a filter bank with adjustable time and frequency resolution. It results in symmetrical orthonormal components when a symmetrical orthogonal wavelet is used as a decomposition wavelet. As a signal can be decomposed into symmetrical orthonormal components with wavelet packet decomposition, they also guarantee well behaved Hilbert transform. These facts motivated to formulate a sifting process based on wavelet packet decomposition to analyze a non-stationary signal obtained from the fingerprint images, and it may be used to detect what type fingerprint has generated the said signal.

18.10.2 Wavelet Packet Transform

A wavelet packet is represented as a function, $\psi^{i}_{j,k}$ where i is the modulation parameter, j is the dilation parameter and k is the translation parameter.

$$\psi^{i}_{j,k}(t) = 2^{\frac{-j}{2}}\psi^{i}(2^{-j}t - k) \tag{18.24}$$

Here $i = 1, 2 j^n$ and n is the level of decomposition in wavelet packet tree.

The wavelet packet coefficients $c^i_{j,k}$ corresponding to the signal $f(t)$ can be obtained as,

$$c^i_{j,k} = \int_{-\infty}^{\infty} f(t)\psi^i_{j,k}(t)dt \tag{18.25}$$

The entropy E is an additive cost function such that $E(0) = 0$. The entropy indicates the amount of information stored in the signal, i.e. higher the entropy, more is the information stored in the signal and vice-versa. There are various definitions of entropy in the literature. Among them, two representative ones are used here, i.e. the energy entropy and the Shannon entropy. The wavelet packet node energy entropy at a particular node n in the wavelet packet tree of a signal is a special case of $P = 2$ of the P-norm entropy which is defined as,

$$e_n = \sum_k | c^i_{j,k} |^P \quad (P \geq 1) \tag{18.26}$$

where $c^i_{j,k}$ are the wavelet packet coefficients at particular node of wavelet packet tree. It was demonstrated that the wavelet packet node energy has more potential for use in signal classification as compared to the wavelet packet node coefficients alone. The wavelet packet node energy represents energy stored in a particular frequency band and is mainly used to extract the dominant frequency components of the signal. The Shannon entropy is defined as,

$$e_n = -\sum_k (c^i_{j,k})^2 \log[(c^i_{j,k})^2] \tag{18.27}$$

Note that one can define his own entropy function if necessary. Here the entropy index (EI) is defined as a difference between the number of zero crossings and the number of extrema in a component corresponding to a particular node of the wavelet packet tree as,

$$EI = |\text{No of zero cross} - \text{No of extrama}| \tag{18.28}$$

Entropy index value greater than 1 indicates that the component has a potential to reveal more information about the signal and it needs to be decomposed further in order to obtain simple frequency components of the signal.

18.10.3 Wavelet Based Sieving

The overall algorithm first performs singularity point detection which filters noisy and partial images, and localizes the ridge information for further analysis. Next the localized ridges are interpolated with cubic splines. The interpolated data increases the time resolution of the signal which will in turn increase the regularity of the decomposed components. The cubic spline interpolation assures the conservation of signal data between sampled points without large oscillations.

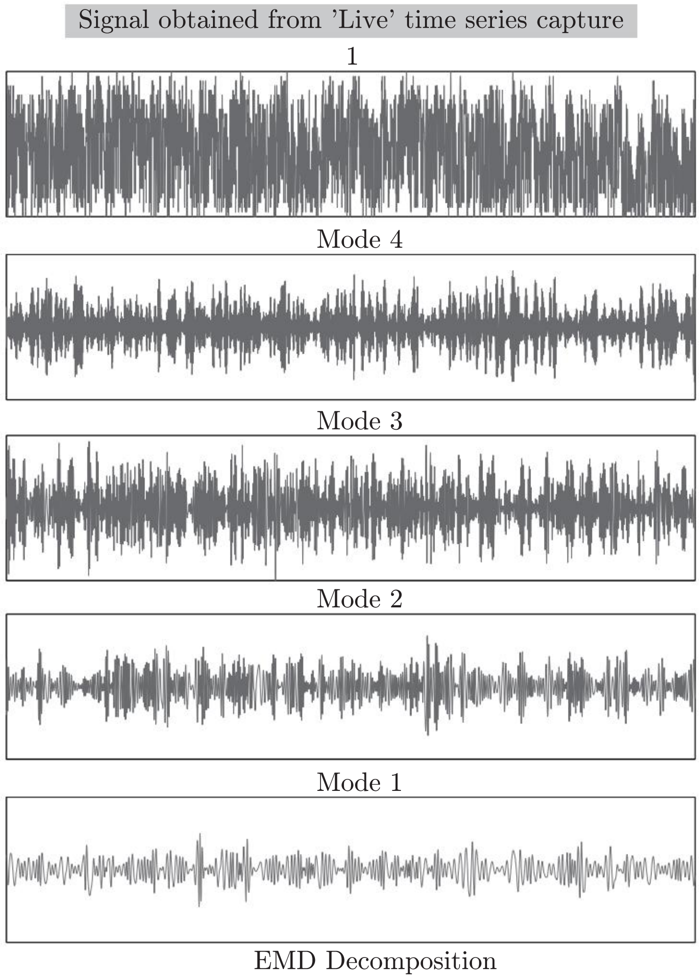

Figure 18.5 | *EMD Decomposition for the live capture*

The interpolated data is decomposed into different frequency components by using wavelet packet decomposition. A shape of the decomposed components by wavelet analysis depends on the shape of the mother wavelet used for decomposition. Daubechies wavelet of higher order (16) shows good symmetry and leads to symmetrical and regular shaped components.

In case of the binary wavelet packet tree, decomposition at level n results in 2^n components. This number may become very large at a higher decomposition level and necessitate increased computational efforts. An optimum decomposition of the signal can be obtained based on the conditions required to be an IMF. A particular node (N) is split into two nodes N_1 and N_2 if and only if the entropy index of the corresponding node is greater than 1 and thus the entropy of the wavelet packet decomposition is kept as least as possible. Other criteria such as the minimum number of zero crossings and the minimum peak value of components can also be applied to decompose only the potential components in the signal.

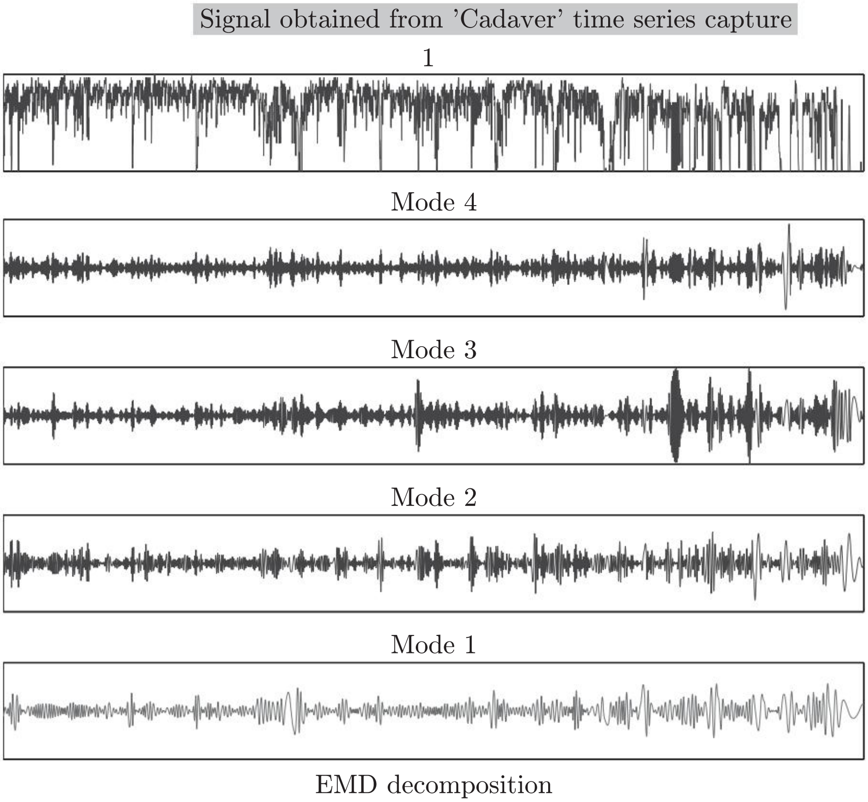

Figure 18.6 | *EMD Decomposition for the Cadaver fingerprint signal*

Once the decomposition is carried out, the mono-frequency components of the signal can be sieved out from the components corresponding to the terminal nodes of the wavelet packet tree. The percentage energy contribution of the component corresponding to each terminal node to the original signal is used as sieving criteria in order to identify the potential components of the signal. This is obtained by summing up the energy entropy corresponding to the terminal nodes of the wavelet packet tree of the signal decomposition in order to get total energy content and then calculating the percentage contribution of energy corresponding to each terminal node to the total energy. Higher the percentage energy contribution, more significant is the component. Note that the decomposition is unique if the mother wavelet in the wavelet packet analysis is given and the sieving criteria are specified. Figures 18.5 and 18.6 depict the EMD decomposition of live and cadaver finger captures. From the various modes it can be seen how EMD is capable of brining out subtle descriptors which are further useful is building decision support systems (DSS).

Readers are left to divulge deeper.

Appendix Extended Notes

This appendix provides extended notes to various discussion pointers across the various chapters in the book.

Extended Notes for Chapter 1

The very first chapter gave us inspirational pointers to study the very subject of ‘Wavelets’. The journey from Fourier transform through the realms of ‘Short term Fourier Transform’ lead us to Wavelets by making us understand the importance of joint time while frequency perspective remains the crux point. The following MATLAB example will bring this point and help enable the readers to go deeper.

Example A1.1 — MATLAB code to simulate spectrograms.

```
%***********************************************
%***********************************************
% MATLAB code to understand STFT (Short Term Fourier
% Transform: To be accompanied with book on
% Multiresolution and Multirate Signal Processing
% by Dr V M Gadre and Dr A S Abhyankar
%***********************************************
%***********************************************
clear all;close all;clc;
N=1000; % No of points
n=0:N;
s=sin(pi*n.*n/N/2); % sin kernel to generate chirp
fs=44000; % sampling frequency
Ts=1/fs;
t=n*Ts; % time sample instances
subplot(2,2,1:2), plot(t,s), axis([0, max(t), -1, 1]),
title('Chirp Signal')

% Spectrograms give joint time frequency perspective

subplot(2,2,3), specgram(s,200,fs,25),%25 samples for DFT
axis([0 0.02 0 2.2e4]), caxis([-70,30]), colorbar, title('25
points')
subplot(2,2,4), specgram(s,200,fs,45),%45 samples for DFT
axis([0 0.02 0 2.2e4]), caxis([-70,30]), colorbar, title('45
points')

% End
```

The above MATLAB code gives following output as shown in Figure A1.1. The figure shows chirp signal which is a perfect case of a non-stationary signal. The two STFTs with different window sizes are plotted. Spectrogram gives us the joint time frequency perspective. The left STFT uses smaller window of 25 points to calculate Fourier coefficients compared to the larger window of 45 points in case of right STFT. The left STFT clearly has better temporal resolution compared to right STFT as can be clearly seen from the figure.

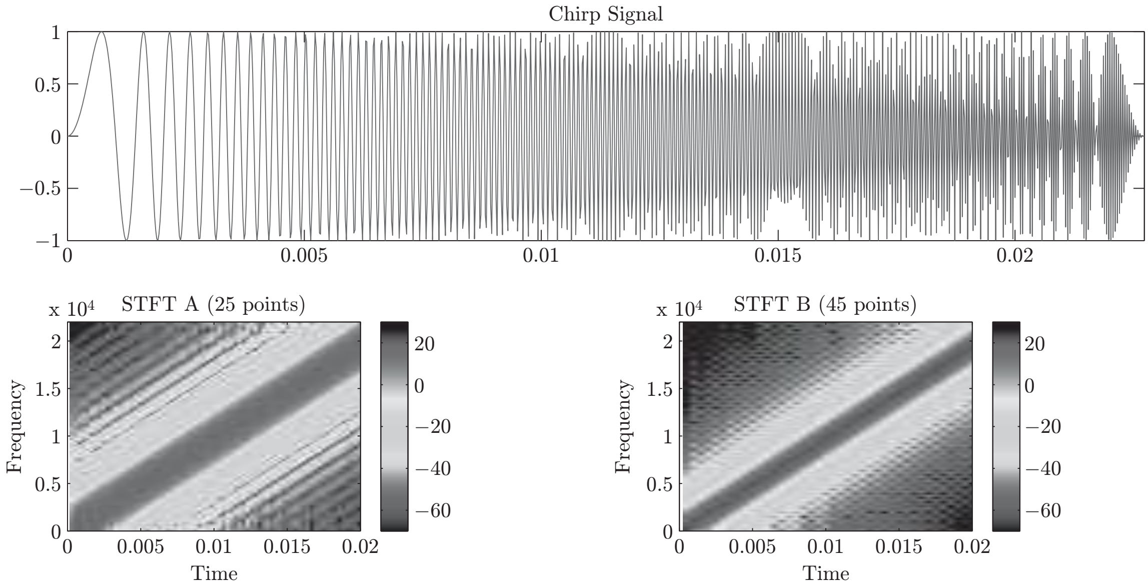

Figure A1.1 *The chirp signal is a non-stationary signal. The STFT with lower window of 25 points and with higher window of 45 points is shown*

Extended Notes for Chapter 2

If $x_1(t) = (1 - t)$ and $x_2(t) = e^{-t}$, then,

Exercise A2.1

Verify that $x_1(t)$ and $x_2(t)$ belong to $L_2(\mathbb{R})$. Also find their norms.
Ans. We will find norms of $x_1(t)$ and $x_2(t)$ and show that they are finite.
norm squared of x_1 in $L_2(\mathbb{R})$ =

$$\int_{-\infty}^{\infty} |x_1(t)|^2 \, dt$$

from symmetry,

$$\| x_1 \|_2^2 = 2\int_0^{\infty} (1-t)^2 \, dt = \frac{2}{3}$$

$$\| x_1 \|_2 = \sqrt{\frac{2}{3}}$$

Similarly,

$$\| x_2 \|_2^2 = \int_0^\infty (e^{-t})^2 \, dt = \frac{1}{2}$$

$$\| x_1 \|_2 = \sqrt{\frac{1}{2}}$$

Since L_2 norm is finite for both functions, they belong to $L_2(\mathbb{R})$.

Exercise A2.2

Obtain the projections of x_1 and x_2 in the space V_0 in the Haar MRA.
Ans. First, let us do the exercise for function x_1.
It is easy to see that non zero projections will only be there in]-1,1[and by symmetry, projection of $x_1(t)$ in]-1,0[= projection of $x_1(t)$ in]0,1[= average of function in each of the intervals which is equal to

$$\int_0^1 (1-t)dt = 0.5$$

We can plot this projection as shown in Figure A2.1. We will denote it by $\mathrm{Proj}_{V_0} x_1$.

Now let us do the same exercise for function x_2. Its projection will be non-zero in only positive half of real axis.
Consider the standard intervals of unit length $]n, n+1[$. Projection of x_2 in this interval will be

$$\int_n^{n+1} e^{-t} dt = e^{-n}(1-e^{-1})$$

Thus, we get exponentially decaying series of constants as depicted in Figure A2.2.

To verify that this projection also belongs to $L_2(\mathbb{R})$, we will show finite value of $\int_{-\infty}^{\infty} |\mathrm{Proj}_{V_0} x_1|^2 \, dt$

$$\int_{-\infty}^{\infty} |\mathrm{Proj}_{V_0} x_1|^2 \, dt = \sum_{n=0}^{\infty} (e^{-n}(1-e^{-1}))^2 \tag{A2.1}$$

$$= (1-e^{-1})^2 \sum_{n=0}^{\infty} e^{-2n} \tag{A2.2}$$

$$= \frac{(1-e^{-1})^2}{(1-e^{-2})} \tag{A2.3}$$

Hence, the projection also belongs to $L_2(\mathbb{R})$.

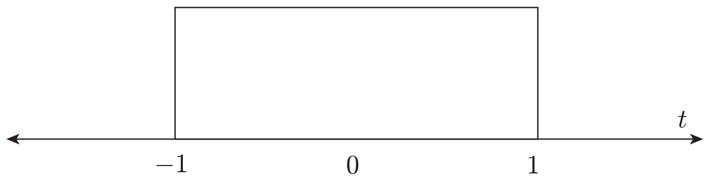

Figure A2.1 | *Projection of x_1 in V_0*

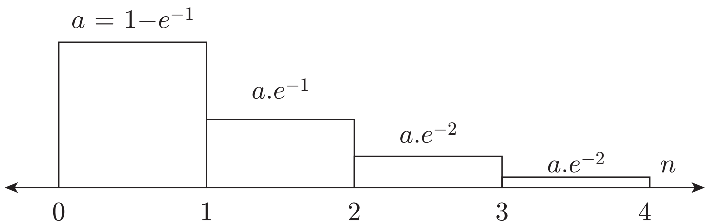

Figure A2.2 | *Projection of x_2 in V_0*

Exercise A2.3

Obtain the projections of the functions x_1 and x_2 on the space V_1 in the Haar MRA.
Ans. We need standard intervals of lenth $2^{-1} = 0.5$ to get projections in space V_1.
By symmetry, We can evaulate only in]0,1[.
In interval]0,0.5[

$$\frac{1}{\frac{1}{2}}\int_0^{0.5}(1-t)dt = 0.75$$

In interval]0.5,1[

$$\frac{1}{\frac{1}{2}}\int_{0.5}^{1}(1-t)dt = 0.25$$

This is denoted by $\text{Proj}_{V_1} x_1$ and is depicted in Figure A2.3.

To get the ideas of projections clear, we draw both $\text{Proj}_{V_1} x_1$ and $\text{Proj}_{V_0} x_1$ (shown in thick grey line) on the same graph in Figure A2.4.

Now, we can find the projection of x_1 in incremental subspace W_0:

$$\text{Proj}_{W_0} x_1 = \text{Proj}_{V_1} x_1 - \text{Proj}_{V_0} x_1$$

This shown in Figure A2.5.

We can observe that

$$Proj_{W_0} x_1 = 0.25\psi(t) - 0.25\psi(t+1)$$

where $\psi(t)$ is Haar Wavelet function.
Now let's do the same for function x_2.
In the interval $]0.5n, 0.5(n+1)[$ where $n \varepsilon \mathbb{Z}$ and $n \geq 0$,

$$Proj_{V_1} x_2 = \frac{1}{2}\int_{0.5n}^{0.5(n+1)} e^{-t}dt$$

$$= 2e^{-\frac{n}{2}}(1 - e^{\frac{-1}{2}})$$

which is an exponential sequence. We can see that exponnential nature of function replicates itself in the projection.
Now we will find $Proj_{W_0} x_2$ in $]n, n+1[$. It will be a multiple of $\psi(t-n)$. The constant by which $\psi(t-n)$ denoted by d_n can be found as following:
d_n = average of x_2 over $]n, n+0.5[$ - average of x_2 over $]n, n+1[$

$$d_n = e^{-n}(1 - e^{\frac{-1}{2}}) - e^{-n}(1 - e^{-1})$$

$$d_n = e^{-n}(e^{-1} - e^{\frac{-1}{2}})$$

Therefore,

$$Proj_{W_0} x_2 = \sum_{n=0}^{\infty} d_n \psi(t-n)$$

For exponentially decaying functions, the projections on V_m $(m \varepsilon \mathbb{Z})$ and the projections on W_m $(m \varepsilon \mathbb{Z})$ are all exponentially decaying piecewise constants.

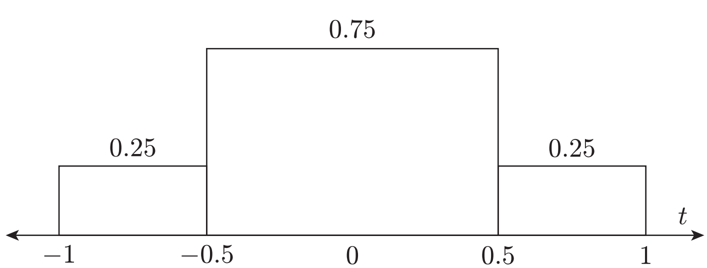

Figure A.2.3 | *Projection of x_1 in V_1*

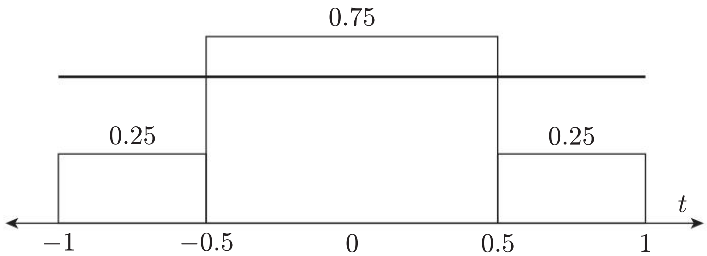

Figure A2.4 | *Projection of x_1 in V_1 and V_0 (shown in thick grey line) in the same graph*

Figure A2.5 | *Projection of x_1 in W_0*

A2.3 | Self Evaluation Quizzes

Q 1. Show that d_n can also be obtained by $< x_2, \psi(t-n) >$.
Ans.

$$< x_2, \psi(t-n) >= \int_n^{n+0.5} e^{-t} dt - \int_{n+0.5}^{n+1} e^{-t} dt$$

$$= e^{-n} - 2e^{-(n+0.5)} + e^{-(n+1)}$$

Extended Notes for Chapter 3

In Section (3.8) we analyzed the analysis filters by looking at their frequency domain behavior. We capture the same in the following MATLAB example.

Example A3.1 — MATLAB code: Haar filter response.

```
%**********************************************
%**********************************************
% MATLAB code to understand Haar Analysis Filter
% Response: To be accompanied with book on
% Multiresolution and Multirate Signal Processing
% by Dr V M Gadre and Dr A S Abhyankar
%**********************************************
%**********************************************
```

```
clear all;close all;clc;

h0=1/2;h1=1/2; % Filter coefficients
figure(1); subplot(221) for w=0:0.005:pi
    y=abs(h0+h1*exp(-i*w)); %Frequency Response
    plot(w,y);
    hold on;
end title('Magnitude Response of Haar Analysis LPF');

h0=1/2;h1=-1/2; figure(1); subplot(222) for w=0:0.005:pi
    y=abs(h0+h1*exp(-i*w)); %Frequency Response
    plot(w,y);
    hold on;
end title('Magnitude Response of Haar Analysis HPF');
%---------------------------------------------------

h0=1/2;h1=1/2; figure(1); subplot(223) for w=0:0.005:pi
    y=angle(h0+h1*exp(-i*w)); %Frequency Response
    plot(w,y);
    hold on;
end title('Phase Response of Haar Analysis LPF (Linear!!!)');

h0=1/2;h1=-1/2; figure(1); subplot(224) for w=0:0.005:pi
    y=angle(h0+h1*exp(-i*w)); %Frequency Response
    plot(w,y);
    hold on;
end title('Phase Response of Haar Analysis HPF (Linear!!!)');

%End of code
```

The outcome of the MATLAB code given above is shown in the Figure A3.1.
From Figure A3.1 following things can be noted:

- X-axis is ω axis and ranges from 0 to 3.1416 which is the value of *pi*.
- The low pass filters can be observed passing lower frequencies and high pass filter can be observed passing higher frequencies.
- The phase of the filter can be observed to be linear

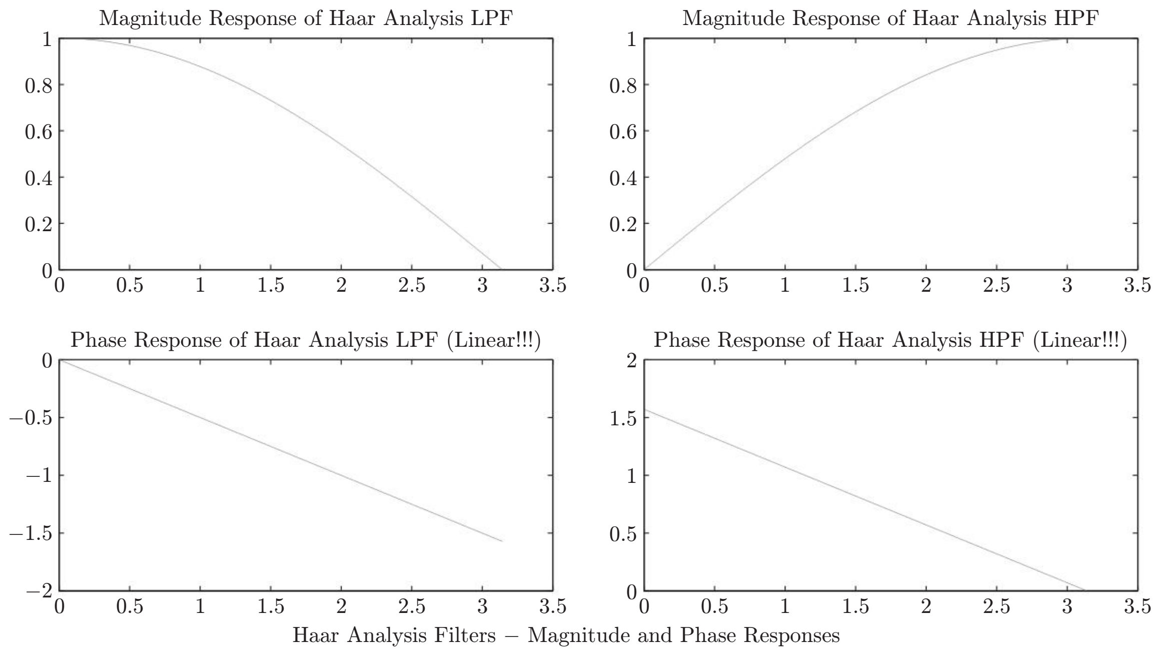

Figure A3.1 | *Magnitude and Phase response of Haar analysis filter*

A3.2 | Three Different Types of Filters

It is important to note that while moving from a subspace to another either higher or lower subspace, we need to take into account factor of $\frac{1}{\sqrt{2}}$. The end result (cumulative result of decomposition or analysis and reconstruction or synthesis) will remain same for all the three different types of filters for a two-band filter bank as depicted below:

To begin with, let the filters be as shown in Table A3.1.

Table A3.1 | *Type (I) filters*

Filter Type	Low Pass	High Pass
Analysis	$\left\{\frac{1}{\sqrt{2}}, \frac{1}{\sqrt{2}}\right\}$	$\left\{\frac{1}{\sqrt{2}}, -\frac{1}{\sqrt{2}}\right\}$
Synthesis	$\left\{\frac{1}{\sqrt{2}}, \frac{1}{\sqrt{2}}\right\}$	$\left\{\frac{1}{\sqrt{2}}, -\frac{1}{\sqrt{2}}\right\}$

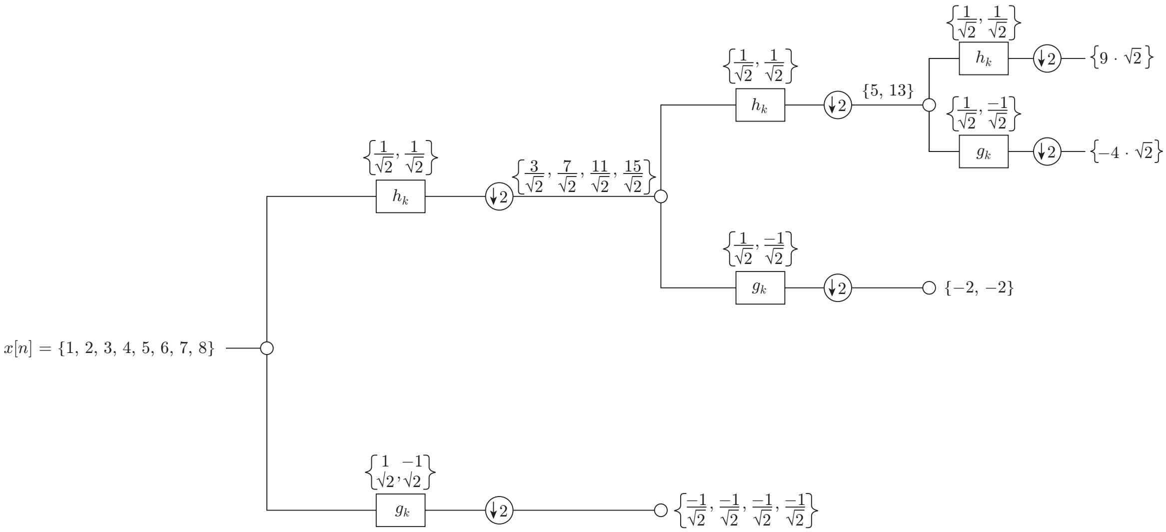

Table A3.2 | *Type (II) filters*

Filter Type	Low Pass	High Pass
Analysis	$\{1,1\}$	$\{1,-1\}$
Synthesis	$\left\{\frac{1}{2},\frac{1}{2}\right\}$	$\left\{\frac{1}{2},-\frac{1}{2}\right\}$

Table A3.3 | *Type (III) filters*

Filter Type	Low Pass	High Pass
Analysis	$\left\{\frac{1}{2},\frac{1}{2}\right\}$	$\left\{\frac{1}{2},-\frac{1}{2}\right\}$
Synthesis	$\{1,1\}$	$\{1,-1\}$

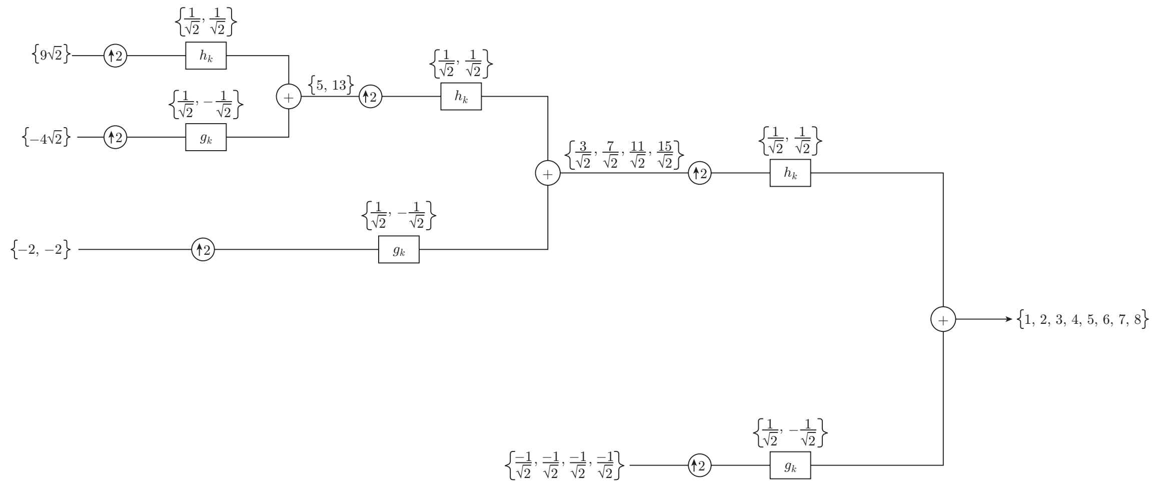

Second, let the filters be as shown in Table A3.2.

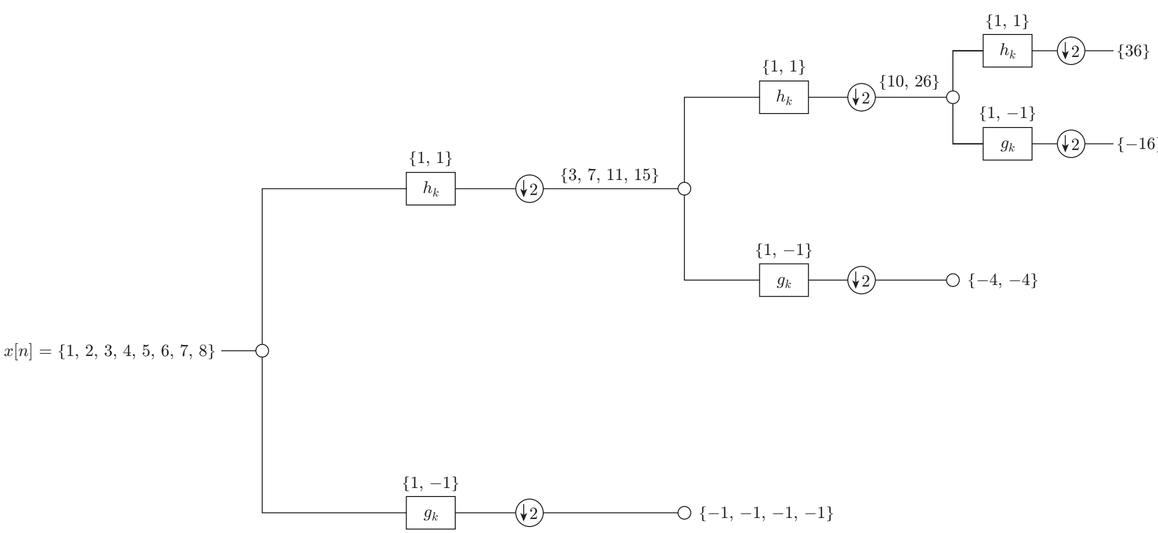

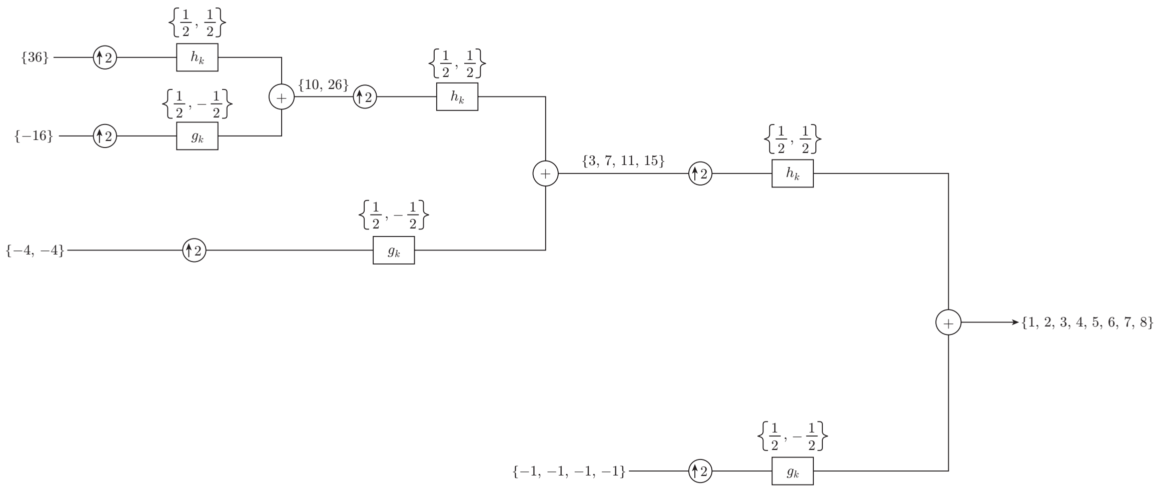

Third, let the filters be as shown in Table A3.3.

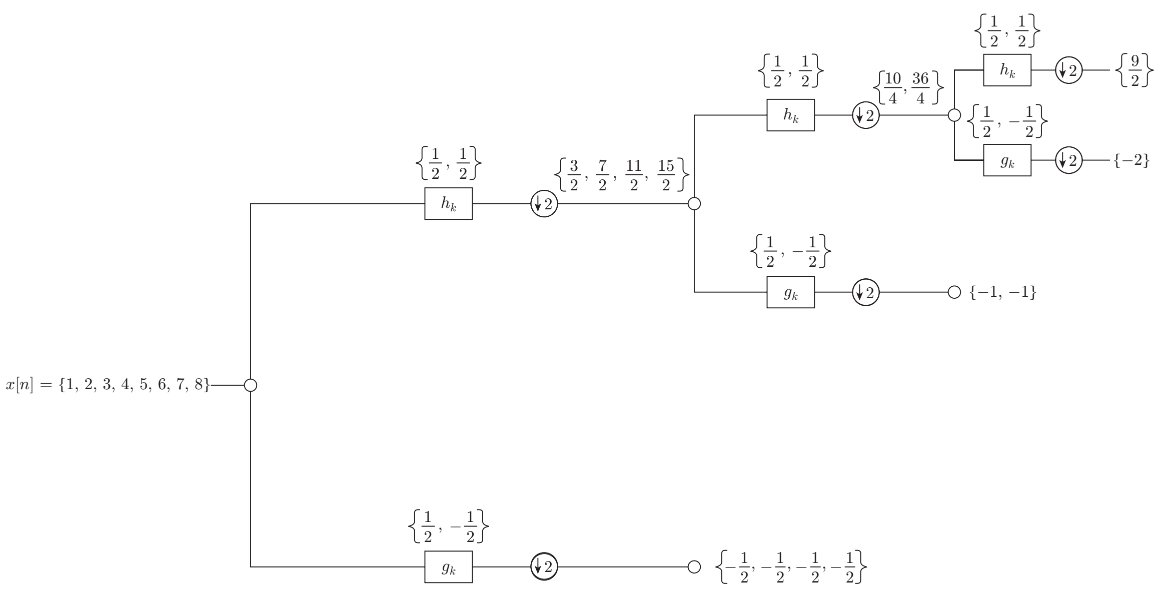

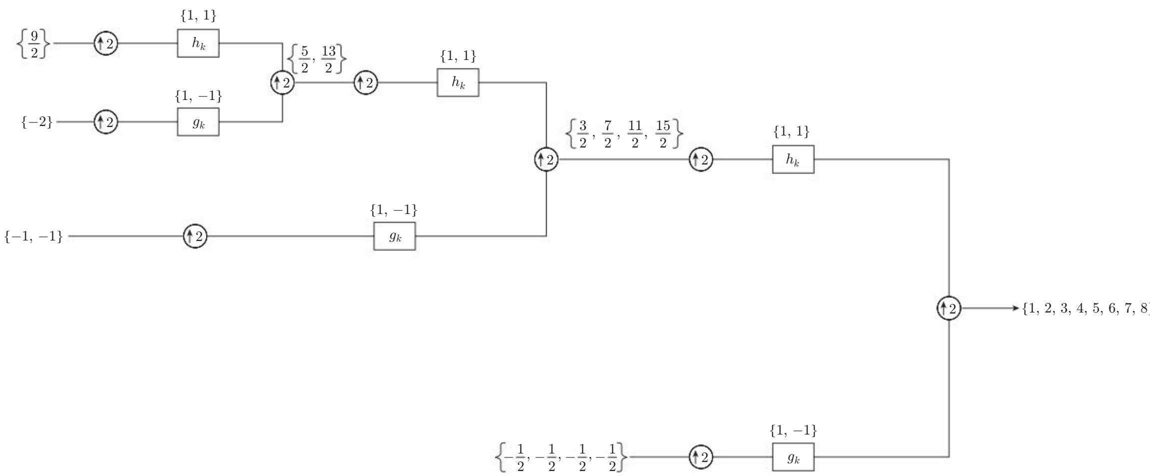

Extended Notes for Chapter 4

In Section (4.8) we saw iterative way of generating scaling function $\phi(.)$ and wavelet function $\psi(.)$. The following section presents the simulation for the same.

A4.1 | Simulation of Iterative Way of Generating Scaling Functions

We use MATLAB to simulate and understand the recursive procedure to generate scaling and wavelet functions.

Example A4.1 — MATLAB code: Haar Recursive Process.

```
%************************************************
%************************************************
% MATLAB code to understand Haar Analysis Filter
% Response: To be accompanied with book on
% Multiresolution and Multirate Signal Processing
% by Dr V M Gadre and Dr A S Abhyankar
%************************************************
%************************************************

h0=1; h1=1; itr=1; t=512; temp=[h0 zeros(1,t-1) h1];
subplot(2,1,1); plot(temp);

title('IMPULSE RESPONSE OF ANALYSIS SIDE LPF');
%axis([-50 3500 -.2 1.2]);
```

```
while (t>1)
t=t/2; % Dilation
h_scaled=[h0 zeros(1,t-1) h1];
temp=conv(temp,h_scaled); % Recursion
subplot(2,1,2); plot(temp);

title('SCALING FUNCTION FOR HAAR FILTER BANK');pause; itr=itr+1;
itr % Iteration number
end

% axis([-50 3500 -.02 .06]);
%
% L=length(temp);
% for i=2:2:L,
%     y_sq(i/2)=temp(i);
% end
% subplot(4,1,3);
% plot(y_sq);
% axis([-50 3500 -.02 .06]);
% title('SCALING FUNCTION SCALED BY 2 IN THE INDEPENDENT VARIABLE');
%
% filter_length=4;
% unit_shift=ceil(L/(2*(filter_length-1)));
%
% ph0=[y_sq zeros(1,3*unit_shift)];
% ph1=[zeros(1,1*unit_shift) y_sq zeros(1,2*unit_shift)];
% ph2=[zeros(1,2*unit_shift) y_sq zeros(1,1*unit_shift)];
% ph3=[zeros(1,3*unit_shift) y_sq];
%
% g0=.129;
% g1=.2241;
% g2=-.8364;
% g3=.4829;
%
% for i=1:1:L,
%     shi(i)=g0*ph0(i)+g1*ph1(i)+g2*ph2(i)+g3*ph3(i);
% end
% subplot(4,1,4);
% plot(shi);
% title('DAUB-4 WAVELET');

%End code
```

The outcome of the MATLAB code given above is shown in the Figures A4.1 – A4.5 given below.

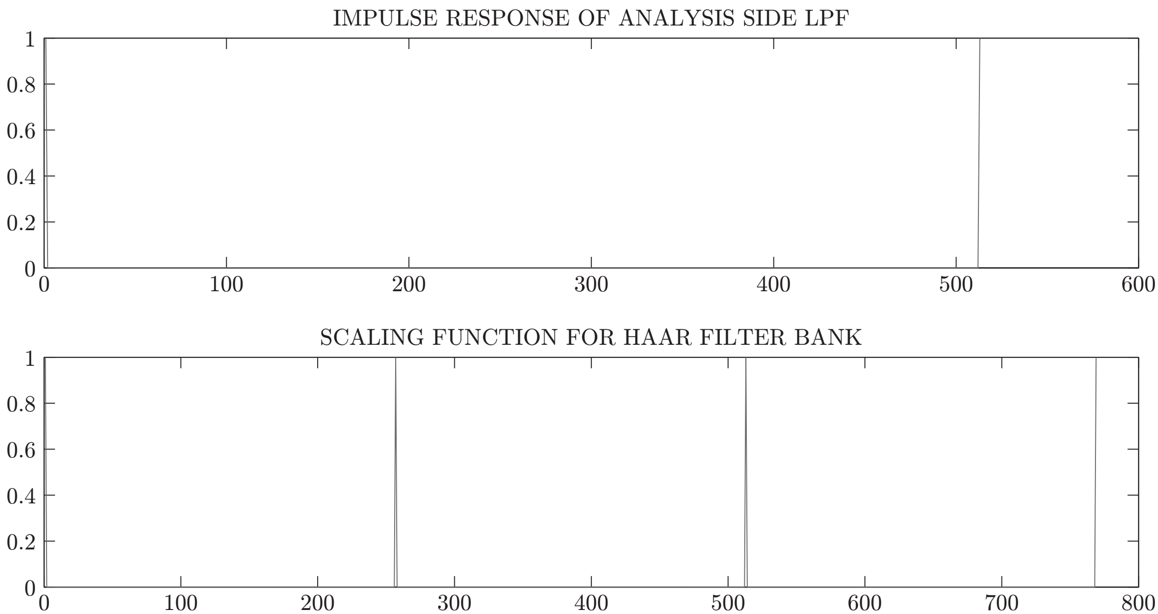

Figure A4.1 | *Haar scaling function after 1 iteration*

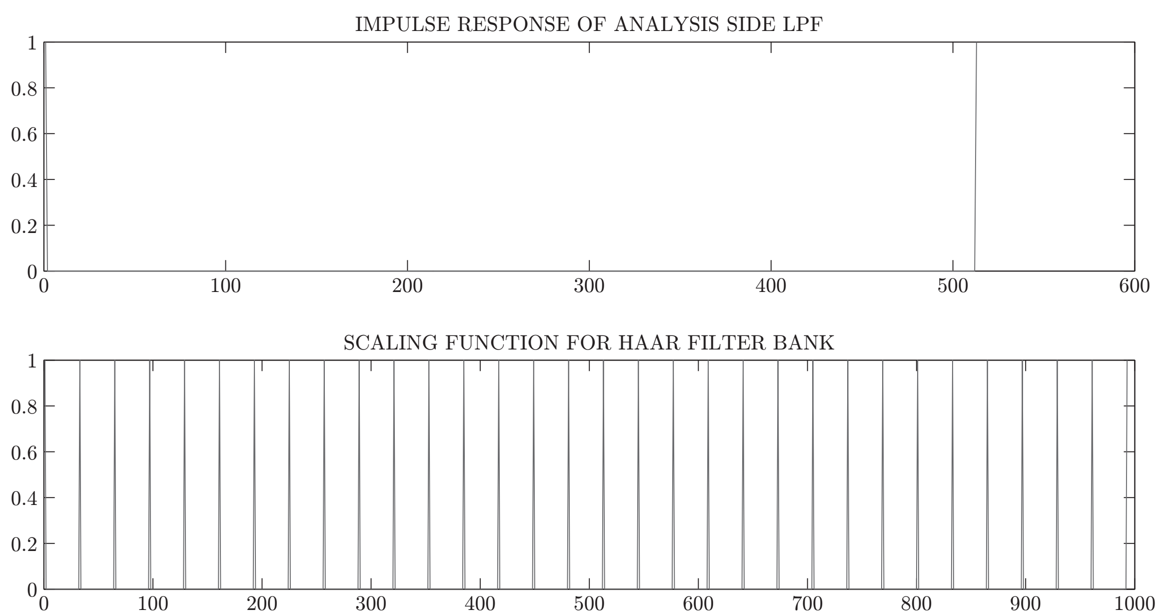

Figure A4.2 | *Haar scaling function after 4 iterations*

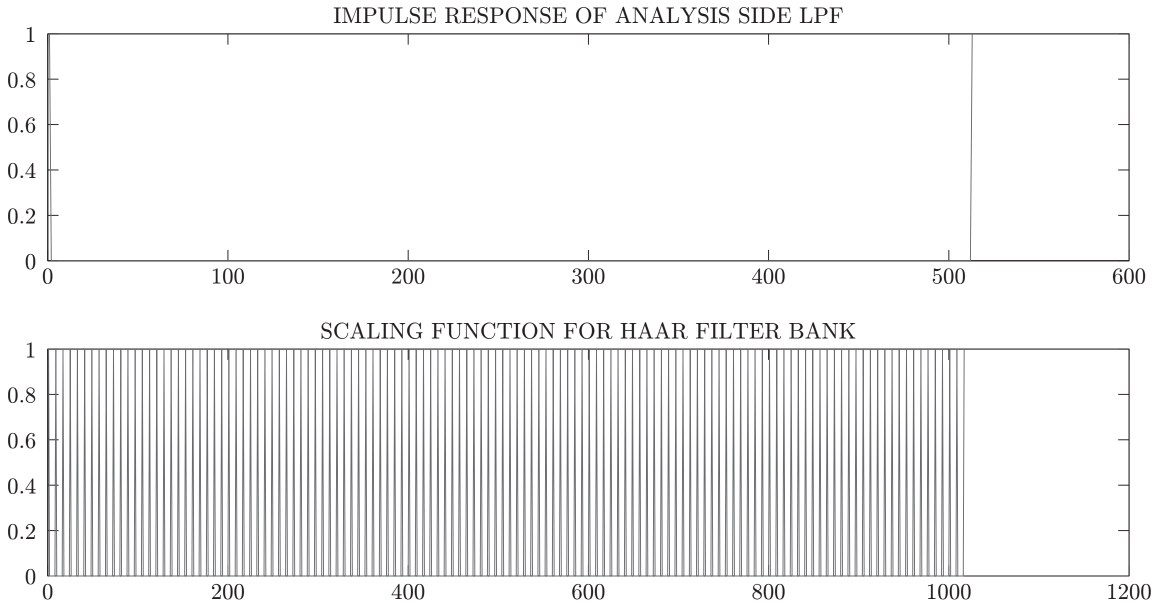

Figure A4.3 | *Haar scaling function after 6 iterations*

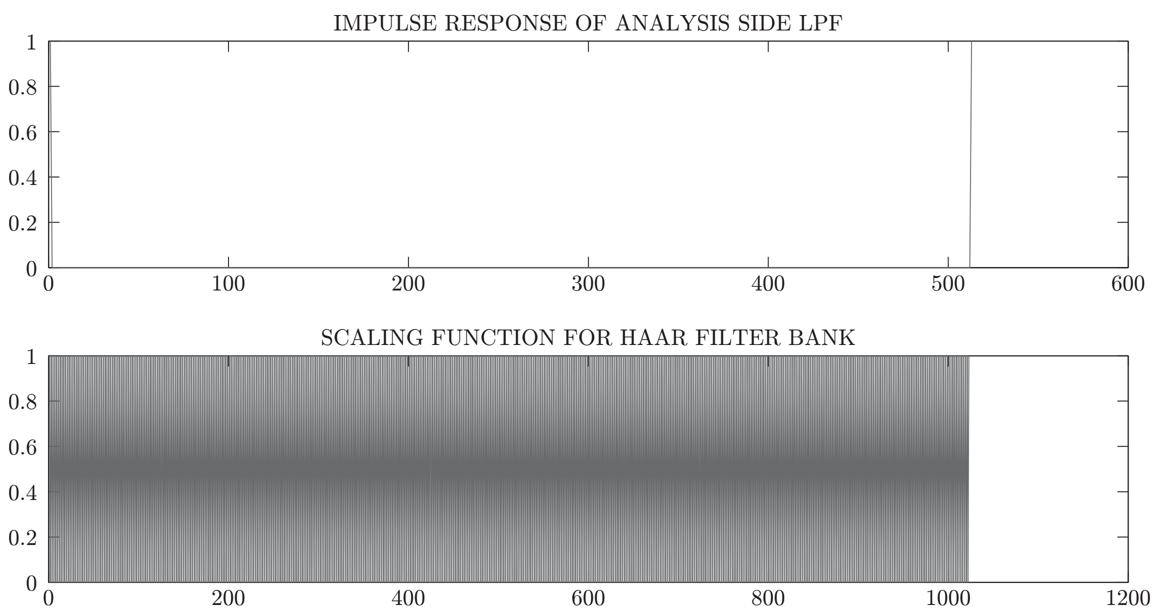

Figure A4.4 | *Haar scaling function after 9 iterations*

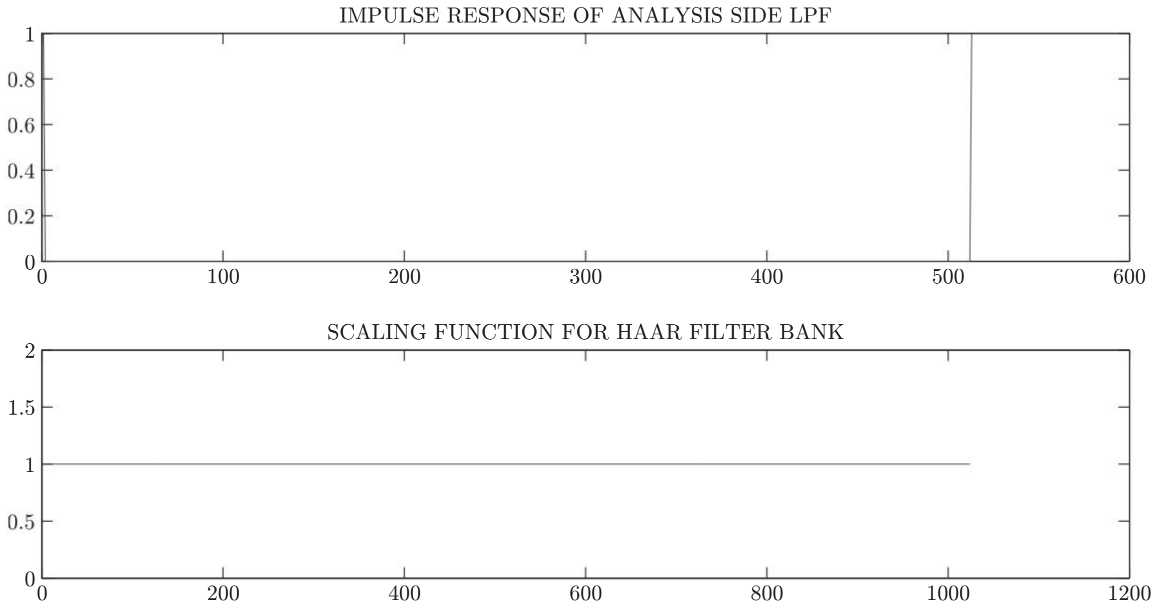

Figure A4.5 | *Haar scaling function after 10 iterations*

The recursive procedure to generate roof scaling function is given in the following MATLAB code.

Example A4.2 — MATLAB code: Roof recursive process.\\

```
%**********************************************
%**********************************************
% MATLAB code to understand Roof Recursive Scaling
% Function: To be accompanied with book on
% Multiresolution and Multirate Signal Processing
% by Dr V M Gadre and Dr A S Abhyankar
%**********************************************
%**********************************************

clc; close all; clear all;

for ct=1:10; h(ct,1)=1/(2*sqrt(2)); h(ct,2)=1/(sqrt(2));
h(ct,3)=1/(2*sqrt(2)); h(ct,4)=0; end;

Fs=1024; Ts=1/Fs; N=4; len=(N-1)*Fs;
```

```
J = 4; t = 0:1/Fs:N-1-Ts; shift = Fs/2; phi = 2*ones(len,1);

figure; pts=0:0.5:3; ptl=1:7; for i = 1:10

scale = 1; phi2 = reshape(phi,2,len/2);
%phi2=phi;
phi = sqrt(2)*(h(i,1)*[phi2(1,:)';zeros(3*shift,1)] +
h(i,2)*[zeros(shift,1);phi2(1,:)';zeros(2*shift,1)]... +
h(i,3)*[zeros(2*shift,1);phi2(1,:)';zeros(shift,1)] +
h(i,4)*[zeros(3*shift,1);phi2(1,:)']); subplot(5,2,i);

plot(phi); title(['Roof Scaling function for iteration=',
num2str(i)]);
%end
end
```

The output produced by MATLAB code above is shown in Figure A4.6.

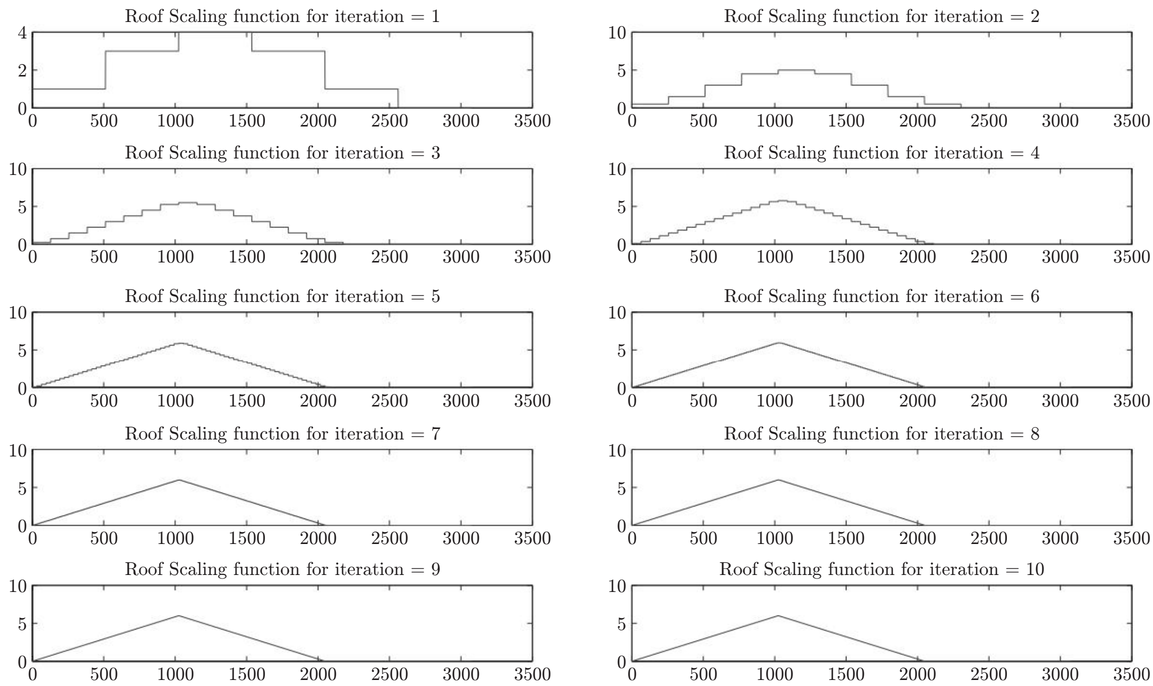

Figure A4.6 | *Roof scaling function: all 10 iterations*

The recursive procedure to generate daub-4 scaling function is given in the following MATLAB code.

Example A4.3 — MATLAB code: Daub-4 recessive process.

```
%************************************************
%************************************************
% MATLAB code to understand Daub4 Recursive Scaling
% Function: To be accompanied with book on
% Multiresolution and Multirate Signal Processing
% by Dr V M Gadre and Dr A S Abhyankar
%************************************************
%************************************************

clc; close all; clear all;
 epsilon = 1e-10; mine = 0.2741*pi;
alpha = [0.1*pi , pi/3 , 0.9*pi, mine ]; N=4;

for ct=1:10; h(ct,1)=(1+sqrt(3))/(4*sqrt(2));
h(ct,2)=(3+sqrt(3))/(4*sqrt(2)); h(ct,4)=(1-sqrt(3))/(4*sqrt(2));
h(ct,3)=(3-sqrt(3))/(4*sqrt(2)); end; for ct=1:10;
    for n=1:N;
        hh(ct,n)=(-1)^(1-n)*h(ct,N+1-n);
    end;end;

Fs=1024; Ts=1/Fs; N=4; len=(N-1)*Fs;
%len=4;

 J = 10;
t = 0:1/Fs:N-1-Ts; shift = Fs/2; phi = 0.1*ones(len,1); figure;
pts=0:0.5:3; ptl=1:7; for i = 1:10 scale = 1; phi2 =
reshape(phi,2,len/2); phi =
sqrt(2)*(h(i,1)*[phi2(1,:)';zeros(3*shift,1)] +
h(i,2)*[zeros(shift,1);phi2(1,:)';zeros(2*shift,1)]... +
h(i,3)*[zeros(2*shift,1);phi2(1,:)';zeros(shift,1)] +
h(i,4)*[zeros(3*shift,1);phi2(1,:)']); subplot(5,2,i);

plot(t,phi); title(['Scaling function for iteration=',
num2str(i)]);
%end
end
```

```
for ct=1:100; h(ct,1)=(1+sqrt(3))/(4*sqrt(2));
h(ct,2)=(3+sqrt(3))/(4*sqrt(2)); h(ct,4)=(1-sqrt(3))/(4*sqrt(2));
h(ct,3)=(3-sqrt(3))/(4*sqrt(2)); end;

% Wavelet Function part
J=1; t = 0:1/Fs:N-1-Ts; shift = Fs/2;

psi=phi;

figure; for scale = 1:J psi2 = reshape(psi,2,len/2); psi =

sqrt(2)*(hh(i,1)*[psi2(1,:)';zeros(3*shift,1)]
+hh(i,2)*[zeros(shift,1);psi2(1,:)';zeros(2*shift,1)]... +
hh(i,3)*[zeros(2*shift,1);psi2(1,:)';zeros(shift,1)] +
hh(i,4)*[zeros(3*shift,1);psi2(1,:)']);

plot(t,psi); title('Daub-4 Wavelet Function'); end
%end
```

The output produced by MATLAB code above is shown in Figure A4.7.
The duab 4 Wavelet produced by the code is as shown in Figure A4.8.

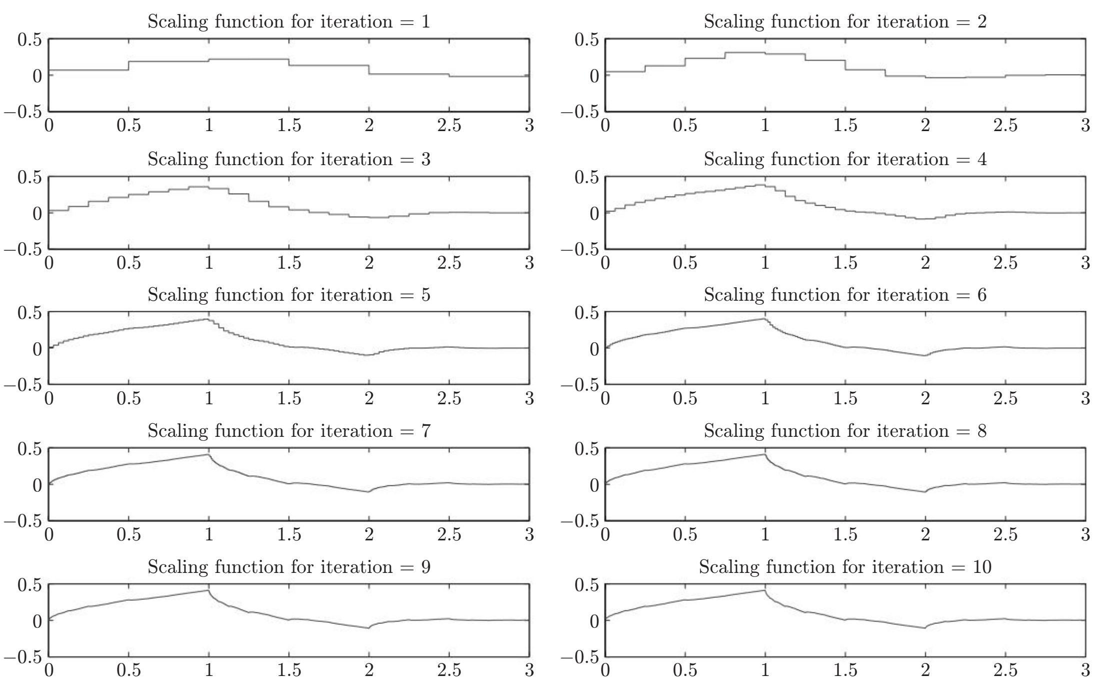

Figure A4.7 | *Daub-4 scaling function: all 10 iterations*

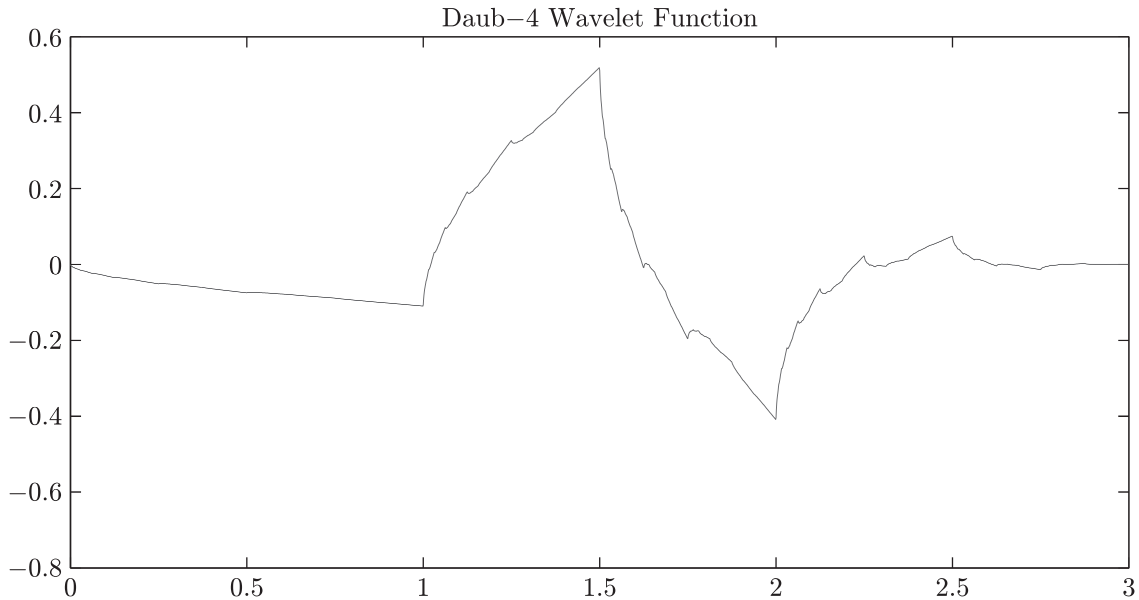

Figure A4.8 | *Daub-4 scaling function: all 10 iterations*

Extended Notes for Chapter 5

A5.1 | Two-Band Filter Bank – Tutorial

The two-band filter bank have two section. The analysis section and the synthesis section.

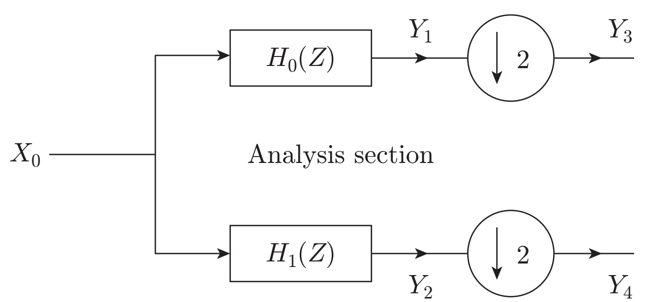

$H_0(Z)$ is a low pass filter with a cut off frequency $\frac{\pi}{2}$ and $H_1(Z)$ is a high pass filter with a cut off frequency $\frac{\pi}{2}$. Analysis section analyzes or breaks down the input in two components.

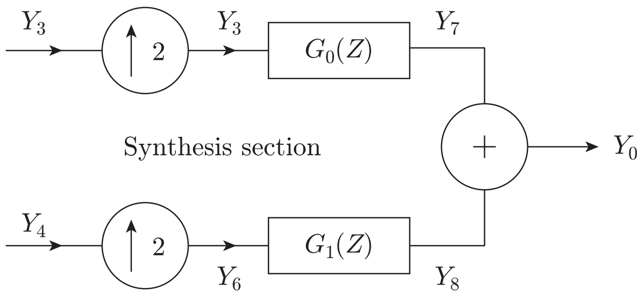

$G_0(Z)$ is a low pass filter with a cut off frequency $\frac{\pi}{2}$ and $G_1(Z)$ is a high pass filter with a cut off frequency $\frac{\pi}{2}$. Synthesis section re-synthesize output from the inputs.

It is impossible situation as we can never reach ideal low pass or high pass filter. Even so, it is possible to build perfect reconstruction structure. For example, if we take Haar 2-band filter bank, we have set of filters H_0, H_1, G_0 and G_1 all of them have impulse response of length 2 which can create perfect reconstruction situation *i.e.*, output Y_0 is same as input X_0 except for a constant multiplier and a shift.

A5.2 | Haar 2-Band Filter Bank

$$H_0(Z) = (1 + Z^{-1}) \tag{A5.1}$$

$$H_1(Z) = (-1 + Z^{-1}) \tag{A5.2}$$

$$G_0(Z) = \frac{(1 + Z^{-1})}{2} \tag{A5.3}$$

$$G_1(Z) = \frac{(1 - Z^{-1})}{2} \tag{A5.4}$$

The factor of $\frac{1}{2}$ can either be on the analysis or synthesis side.

Let us take $x[n]$ be the input to this Haar 2-band filter bank.

$$x[n] = \underset{\underset{0}{\uparrow}}{7} \quad 5 \quad -4 \quad 6 \quad 3 \quad 8$$

Analysis side:

$x[n]$ denotes time domain, $X(Z)$ denotes complex frequency domain.

Now, $H_0(Z) = (1 + Z^{-1})$, therefore corresponding impulse response $h_0(n)$ is

$$h_0(n) = \underset{\underset{0}{\uparrow}}{1} \quad 1$$

Therefore $y_1 = x * h_0$,

$$y_1(n) = \underset{\underset{0}{\uparrow}}{7} \quad 5 \quad -4 \quad 6 \quad 3 \quad 8 \quad * \quad \underset{\underset{0}{\uparrow}}{1} \quad 1$$

$$= \underset{\underset{0}{\uparrow}}{7} \quad 12 \quad 1 \quad 2 \quad 9 \quad 11 \quad 8 \quad = x * h_0$$

Hence, output at point Y_1 is as expected of length 7.

$y_2 = x * h_1$ and $H_1(Z) = (-1 + Z^{-1})$. Hence

$$h_1(n) = -\underset{\underset{0}{\uparrow}}{1} \quad 1$$

Therefore,

$$x * h_1 = -\underset{\underset{0}{\uparrow}}{7} \quad 2 \quad 9 \quad -10 \quad 3 \quad -5 \quad 8$$

Output at Y_2 is as expected of length 7.
After Downsampling by 2:

$$Y_1 \longrightarrow \boxed{\downarrow 2} \longrightarrow Y_3$$

$$Y_3(n) = \underset{\underset{0}{\uparrow}}{7} \quad 1 \quad 9 \quad 8$$

$$Y_2 \longrightarrow \boxed{\downarrow 2} \longrightarrow Y_4$$

$$Y_4(n) = -\underset{\underset{0}{\uparrow}}{7} \quad 9 \quad 3 \quad 8$$

As expected, the result after downsampling are of length 4.

Synthesis side:
After Upsampling by 2:

$$Y_3 \longrightarrow \boxed{\uparrow 2} \longrightarrow Y_5$$

$$Y_5(n) = \underset{\underset{0}{\uparrow}}{7} \quad 0 \quad 1 \quad 0 \quad 9 \quad 0 \quad 8$$

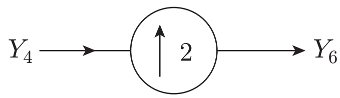

$$Y_6(n) = \underset{\substack{\uparrow\\0}}{-7} \quad 0 \quad 9 \quad 0 \quad 3 \quad 0 \quad 8$$

Again as expected the result after upsample are back to length 7.
Now, Y_5 is subjected to Low Pass Filter.

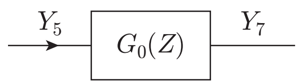

$$G_0(Z) = \frac{(1+Z^{-1})}{2} \tag{A5.5}$$

$$Y_7(n) = \underset{\substack{\uparrow\\0}}{\frac{7}{2}} \quad \frac{7}{2} \quad \frac{1}{2} \quad \frac{1}{2} \quad \frac{9}{2} \quad \frac{9}{2} \quad \frac{8}{2} \quad \frac{8}{2}$$

Y_6 is subjected to High-Pass Filter.

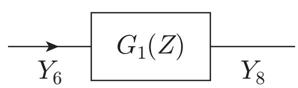

$$G_1(Z) = \frac{(1-Z^{-1})}{2} \tag{A5.6}$$

$$y_8[n] = \frac{y_6[n] - y_6[n-1]}{2} \tag{A5.7}$$

$$Y_8(n) = \underset{\substack{\uparrow\\0}}{-\frac{7}{2}} \quad \frac{7}{2} \quad \frac{9}{2} \quad -\frac{9}{2} \quad \frac{3}{2} \quad -\frac{3}{2} \quad \frac{8}{2} \quad -\frac{8}{2}$$

Now, $Y_0 = Y_7 + Y_8$

$$Y_0(n) = \underset{\substack{\uparrow\\0}}{0} \quad 7 \quad 5 \quad -4 \quad 6 \quad 3 \quad 8 \quad 0$$

We can observe that the output sequence is same as input sequence shifted by one sample. We notice that $y_0[n] = x[n-1]$. The factor of $\frac{1}{2}$ has taken care of the scaling. Delay has occurred on account of causality need. We want filter to be casual. Causality is needed because if we do not allow some delay *i.e.*, time for the processing then we could not have real time processing. Causality is therefore required for a real time processing. We could have done without the delay if we do Non-Casual filtering in at least one of analysis or synthesis side.

A5.3 | Periodizing the Input

The periodic input $\tilde{x}[n]$ is:

$$\tilde{x}[n] = \sum_{k=-\infty}^{\infty} x[n+kN], \quad N \geq 6 \tag{A5.8}$$

For simplicity we will take N=6, so

$$\tilde{x}[n] = \ldots \quad 3 \quad 8 \quad \underset{\underset{0}{\uparrow}}{7} \quad 5 \quad -4 \quad 6 \quad 3 \quad 8 \quad 7 \quad 5 \quad -4\ldots$$

We will analyze the output only in the range (0-5).

$$Y_1 = \ldots \quad \underset{\underset{0}{\uparrow}}{15} \quad 12 \quad 1 \quad 2 \quad 9 \quad 11 \quad 15\ldots$$

$$Y_2 = \ldots \quad \underset{\underset{0}{\uparrow}}{1} \quad 2 \quad 9 \quad -10 \quad 3 \quad -5 \quad 1\ldots$$

Now downsampling:

$$Y_3 = \ldots \quad \underset{\underset{0}{\uparrow}}{15} \quad 1 \quad 9 \quad 15\ldots$$

$$Y_4 = \ldots \quad \underset{\underset{0}{\uparrow}}{1} \quad 9 \quad 3 \quad 1\ldots$$

Period of Y_3 and Y_4 is '3'.
Now Upsampling:

$$Y_5 = \ldots \quad \underset{\underset{0}{\uparrow}}{15} \quad 0 \quad 1 \quad 0 \quad 9 \quad 0 \quad 15\ldots$$

$$Y_6 = \ldots \quad \underset{\underset{0}{\uparrow}}{1} \quad 0 \quad 9 \quad 0 \quad 3 \quad 0 \quad 1\ldots$$

Period of Y_5 and Y_6 is 6.

$$Y_7(n) = \ldots \quad \frac{15}{2} \quad \frac{15}{2} \quad \frac{1}{2} \quad \frac{1}{2} \quad \frac{9}{2} \quad \frac{9}{2} \quad \frac{15}{2}\ldots$$

$$Y_8(n) = \ldots \quad \frac{1}{2} \quad \frac{-1}{2} \quad \frac{9}{2} \quad -\frac{9}{2} \quad \frac{3}{2} \quad -\frac{3}{2} \quad \frac{1}{2}\ldots$$

$$Y_0 = \ldots \quad \underset{\underset{0}{\uparrow}}{8} \quad 7 \quad 5 \quad -4 \quad 6 \quad 3 \quad 8\ldots$$

As expected output is delayed by one sample and is same as input. It it periodically repeated with a period of 6.

A5.4 | Frequency-domain Analysis of Two-band Filter Bank - Tutorial

In the Previous session we have placed before you a tutorial on two-band filter bank from the point of view of the time domain. We want to understand in depth how a signal progress through a different stages of a two-band filter bank and emerges with perfect reconstruction subjected to a delay and some constant multiplication factor.

Now, we will see the frequency domain analysis of two-band filter bank. *How do we see the sinusoidal being treated by different stages of the two-band filter bank? What does the two-band filter bank do in frequency domain?* Now can we illustrate it with a use of a domain for looking a two-band filter bank. Each one of them has advantages and limitations.

The advantage of time domain precisely is to understand what filter bank does to the signal in the natural domain. When we have long-term signal in mind and we wish to look at the sinusoidal content, both at the input and output, it is the frequency characteristics of a two-band filter bank.

A5.5 | Two-band Filter Bank

The deviation from the ideal two-band filter bank is that LPF and HPF are with cutoff $\left(\frac{2\pi}{3}\right)$, as shown in Fig. A5.1.

We will consider the 'Prototype' input as shown in the Fig. A5.1. We consider this input because it's amplitude is linear with the frequency scale.

$$G_{out}(Z) = \frac{1}{2}\{Gin(Z) + Gin(-Z)\}$$

$$\text{In } Z \text{ Domain } Z \leftarrow e^{j\omega}$$

$$G_{out}(Z) = \frac{1}{2}\{Gin(e^{j\omega}) + Gin(e^{j(\omega\pm\pi)})\}$$

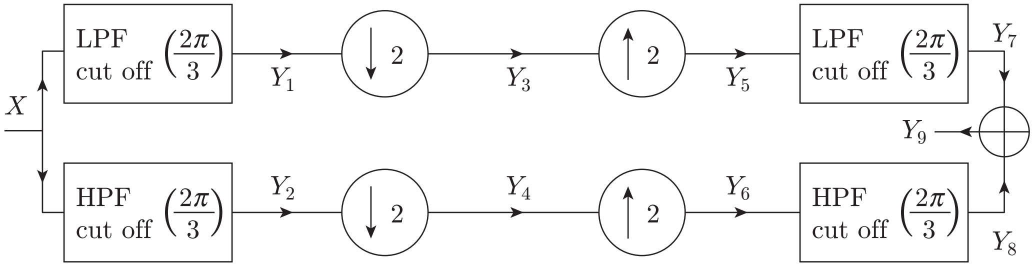

Figure A5.1 | *Two-Band filter Bank*

$$G_{out}(Z) = \frac{1}{2}(\text{Original DTFT}) + \frac{1}{2}(\text{Aliased DTFT})$$

$$Y_6(e^{j\omega}) = \frac{1}{2}\left\{Y_2(e^{j\omega}) + Y_2(e^{j(\omega\pm\pi)})\right\}$$

Essentially multiplication by -1 of variable Z accounts of phase shift by π.

Aliased is obtained by replacing Z by $-Z, \Rightarrow e^{j\omega} \leftarrow -e^{j\omega}$.

Now subjecting to the action of high-pass filters of cutoff $\left(\frac{2\pi}{3}\right)$, it retains the original spectra. HPF with cutoff $\left(\frac{\pi}{3}\right)$ retains $\frac{1}{2}Y_2(e^{j\omega})$ and destroy $\frac{1}{2}Y_2(e^{j(\omega\pm\pi)})$ (aliased), as captured in Figs. A5.3 to A5.6.

$$Y_5(e^{j\omega}) = \frac{1}{2}Y_1(e^{j\omega}) + \frac{1}{2}Y_1(e^{j(\omega\pm\pi)})$$

Now, it illustrates very clearly in the frequency domain what the consequence of non-ideal cut-off is, although the two filters are looked to be complementary because one of the filter did not obey the requirement of aliasing or rather had a passband beyond $\frac{\pi}{2}$ when we observed the aliasing taking place.

As expected the aliasing takes place to the extend that we exceeded the $\frac{\pi}{2}$ band. The excess was from $\frac{\pi}{2}$ to $\frac{2\pi}{3}$ and therefore we have aliasing between $\frac{\pi}{2} + \frac{\pi}{3}$ and $\frac{\pi}{2}$ - $\frac{\pi}{3}$.

Aliasing has occurred in a band of extent $\frac{2\pi}{3} - \frac{\pi}{2} = \frac{\pi}{6}$ on either side of $\frac{\pi}{2}$.

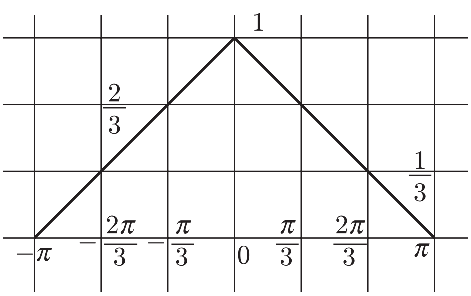

Figure A5.2 | *Prototype Input*

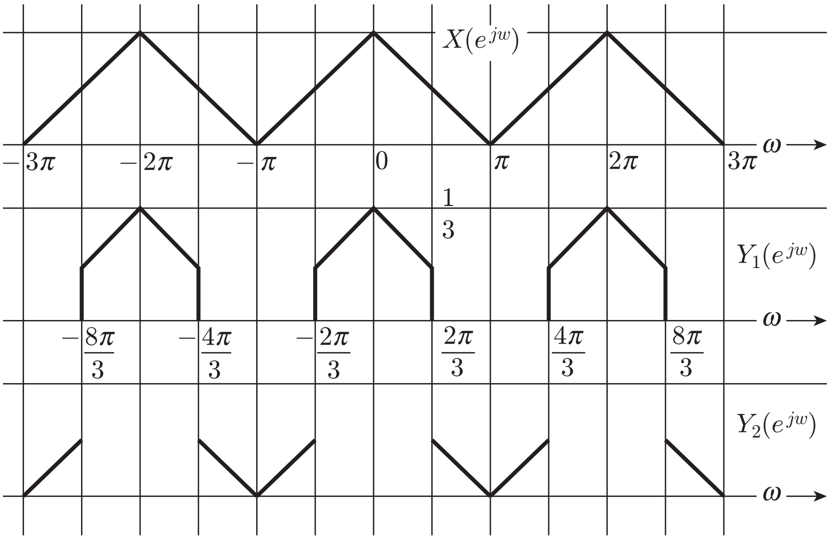

Figure A5.3 | *Output at Y_1 and Y_2 in two-band filter bank*

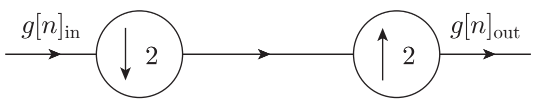

Figure A5.4 | *Intermediate branch of two-band filter bank*

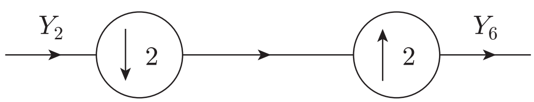

Figure A5.5 | *Intermediate branch of two-band filter bank*

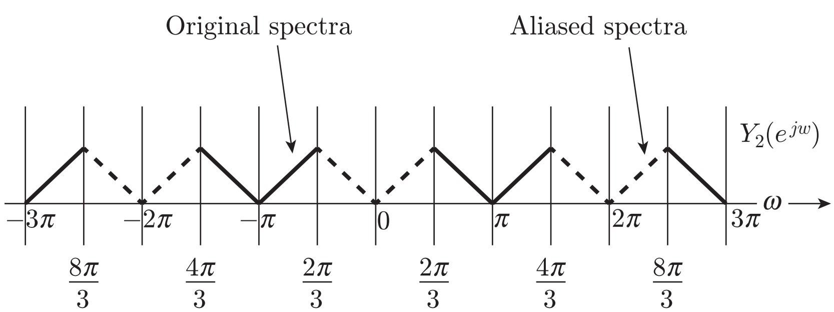

Figure A5.6 | *DTFT spectra*

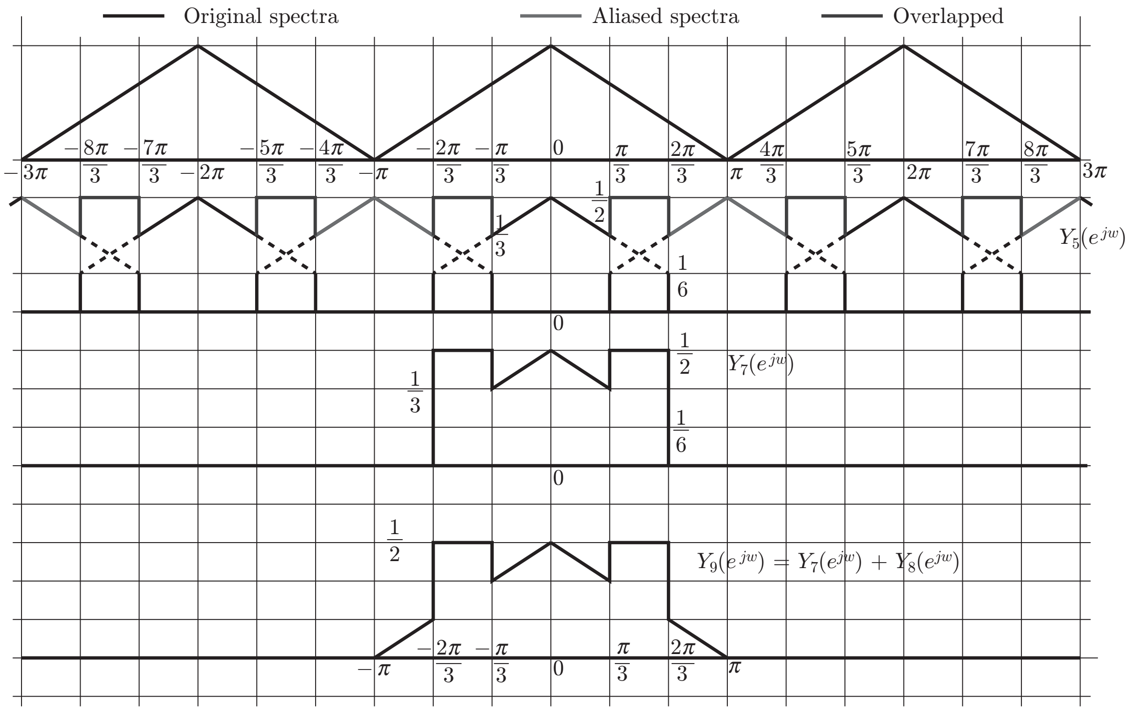

Figure A5.7 | *DTFT spectra*

This is an example of frequency domain behavior where we are not adhering to the requirement of cutoff.

As we can see in the Fig. A5.7 the overlap between the original spectra and the aliased spectra resulted into a straight line.

Extended Notes for Chapter 6

A6.1 | Exact Method for the Daubechies Scaling Coefficients

In Section 6.5, we used the Fourier transform for reducing the scaling equation

$$\phi(t) = \sum_{k=0}^{n} h_k \sqrt{2}\phi(2t-k)$$

to the following algebraic equation in its Fourier transforms $\Phi(w)$ and $\Phi\left(\frac{w}{2}\right)$:

$$\frac{\Phi(w)}{\Phi\left(\frac{w}{2}\right)} = \sum_{k=0}^{n} h_k \sqrt{2} e^{-\frac{iw}{2}k}$$

$$= \sum_{k=0}^{n} h_k \sqrt{2} z^k, z = e^{-\frac{iw}{2}}$$

$$= P_n(z) \tag{A6.1}$$

Here we continue this Fourier analysis with a theorem based on mutiresolution analysis, and an "ingenuous idea", which will lead us to determine the Daubechies scaling coefficients.

We shall first start with the basic theorem. This development will also make very clear the importance of the "vanishing moments" of a wavelet to its quality in the computations.

The following Theorem (A6.1) addresses conditions on the polynomial $P_n(z)$ in (A6.1), among which is the orthogonality of its resulting scaling functions of the scaling equation. So, we will move with $P_n(z)$ minding a strict adherence to all conditions of this theorem. We will see that, in contrast to the attempt in Section 4.7 of the self-convolution of the Haar functions, an "ingenuous" attempt is done to guarantee the second of this theorem's three conditions. This attempt will finally enable us to find the four coefficients of the Daubechies 2 scaling function $\phi_{D2}(t)$. It also extends to those of higher order such as $\phi_{D3}(t)$ and $\phi_{D4}(t)$, etc. For more illustration we will present the details for finding the coefficients of ϕ_{D3} in Example (A6.3)

In (A6.1) we had,

$$P_n(z) = \frac{\Phi(w)}{\Phi\left(\frac{w}{2}\right)} = \sum_k \frac{1}{\sqrt{2}} h_k z^k. \tag{A6.2}$$

We will now state the important guiding theorem. Then we will try to satisfy all its conditions. This theorem will also expose us to its conditions that guarantee the *convergence* of the iterative process for solving the scaling equation that we covered with illustration in Section 4.7. In addition, this convergence will guarantee that the limit of the iterative process,

$$\phi_m(t) = \sum_k h_k \sqrt{2} \phi_{m-1}(2t-k), \tag{A6.3}$$

is the sought-after orthogonal scaling functions, i.e., $\lim_{m\to\infty} \phi_m(t) = \phi(t)$.

Theorem A6.1 *"Consider the polynomial* $P_n(z), z = e^{\frac{-iw}{2}}$ *in (A6.1), which satisfies the following the three conditions*:

$$P_n(1) = 1 \tag{A6.4}$$

$$|P_n(z)|^2 + |P_n(-z)|^2 = 1, \text{ for } |z| = 1 \tag{A6.5}$$

$$|P_n(e^{ix})| > 0, \text{ for } x \le \frac{\pi}{2} \tag{A6.6}$$

To start the iterative method for (A6.3), let $\phi_0(x)$ be the Haar function as its zeroth approximation (in solving the scaling equation),

$$\phi_m(t) = \sum_k \frac{1}{\sqrt{2}} h_k \phi_{m-1}(t-k). \tag{A6.7}$$

Then the sequence $\phi_m(t)$ converges 'point-wise' to a function $\phi(t)$ that is square integrable on $(-\infty,\infty)$, which satisfies the orthonormality of $\{\phi(t-k)\}$, i.e.,

$$\int_{-\infty}^{\infty}\phi(t-k)\phi(t-l)dx = \begin{cases} 0, & k \neq l \\ 1, & k = l \end{cases}$$

Before we try to use this theorem to find scaling functions that are orthonormal on $(-\infty,\infty)$, let us illustrate it with what we know, the Haar scaling function. This will also make a sort of simple review for working with the complex-valued polynomial $P_n(z), z = e^{\frac{-iw}{2}}$.

We note in the theorem that we need, for example, $|P_n(z)|$ the absolute value (amplitude) of this complex-valued $P_n(z)$.

In general, for the complex-valued function $f(z)$ we can write,

$$f(z) = Re\, f(z) + i\, Im\, f(z)$$
$$f(z) = R(x,y) + i\, I(x,y)$$

where we used the real valued $R(x,y)$ and $I(x,y)$ for real $f(z)$ and imaginary $f(z)$, respectively.

As a simple example,

$$f(z) = z^2 = (x+iy)^2 = (x^2 - y^2) + i2xy$$

where $R(x,y) = x^2 - y^2$ and $I(x,y) = 2xy$. The complex conjugation $\overline{f(z)}$ of $f(z)$ amounts to changing every imaginary number i in $f(z)$ to $-i$; so, for example,

$$\overline{f(z)} = \overline{z^2} = \overline{(x^2 - y^2) + i2xy} = (x^2 - y^2) - i2xy$$

Also,

$$|f(z)| = \sqrt{R^2(x,y) + I^2(x,y)}$$

or

$$|f(z)|^2 = R^2(x,y) + I^2(x,y)$$

This can be obtained as

$$|f(z)|^2 = f(z)\overline{f(z)},$$
$$|f(z)|^2 = (R(x,y) + iI(x,y))(R(x,y) - iI(x,y)) = R^2(x,y) + I^2(x,y).$$

In the example of $f(z) = z^2$,

$$|f(z)|^2 = f(z)\overline{f(z)} = (x+iy)^2(x-iy)^2$$
$$= [(x+iy)(x-iy)]^2$$

$$= [x^2 - (iy)^2]^2$$
$$= [x^2 + y^2]^2$$
$$= x^4 + y^4 + 2x^2y^2.$$

This could have been obtained from the direct computation of $|f(z)|^2$ with $f(z) = z^2 = (x^2 - y^2) + i2xy$ above,

$$|f(z)|^2 = (Re\, z^2) + (Im\, z^2) = (x^2 - y^2)^2 + 4x^2y^2$$
$$= x^4 + y^4 - 2x^2y^2 + 4x^2y^2$$
$$= x^4 + y^4 + 2x^2y^2.$$

Example A6.1 Verifying theorem A6.1 for the haar scaling function.

Earlier, we had the polynomial $P_1(z)$, associated with the Haar scaling function, as,

$$P_1(z) = \frac{1}{\sqrt{2}}h_0 + \frac{1}{\sqrt{2}}h_1 z, \quad z = e^{\frac{-iw}{2}} \tag{A6.8}$$

and now we want to verify Theorem (A6.1) for this very special case:

(i)
$$P_1(1) = \frac{1}{\sqrt{2}}h_0 + \frac{1}{\sqrt{2}}h_1 = \frac{1}{\sqrt{2}}\frac{1}{\sqrt{2}} + \frac{1}{\sqrt{2}}\frac{1}{\sqrt{2}} = \frac{1}{2} + \frac{1}{2} = 1 \tag{A6.9}$$

(ii)
$$|P_1(z)|^2 + |P_1(-z)|^2 = |P_1(1)|^2 + |P_1(-1)|^2 \; for\, |z| = 1$$
$$= \left(\frac{1}{2} + \frac{1}{2}\right)^2 + \left(\frac{1}{2} - \frac{1}{2}\right)^2 = 1 - 0 = 1 \tag{A6.10}$$

(iii)
$$|P_1(e^{it})| = \left|\left(\frac{1}{2} + \frac{1}{2}e^{it}\right)\right| = \sqrt{\left(\frac{1}{2} + \frac{1}{2}e^{it}\right)\left(\frac{1}{2} + \frac{1}{2}e^{-it}\right)}$$
$$|P_1(e^{it})| = \frac{1}{2}\sqrt{(1 + e^{it})(1 + e^{-it})}$$
$$= \frac{1}{2}\sqrt{2 + (e^{it} + e^{-it})}$$
$$|P_1(e^{it})| = \frac{1}{\sqrt{2}}\sqrt{1 + \cos t} > 0, \; for \; |t| \leq \frac{\pi}{2} \tag{A6.11}$$

We also know one conclusion of the theorem: the final result of the iterative process is the orthonormal scaling functions $\{\phi(t-k)\}$ on $(-\infty, \infty)$.

In moving towards our goal we shall consider the polynomial

$$p(w) \equiv P(e^{-iw}) = \frac{1+e^{-iw}}{2} \tag{A6.12}$$

instead of

$$P\left(e^{\frac{-iw}{2}}\right) = \frac{1+e^{\frac{-iw}{2}}}{2} \equiv P_1(z), \tag{A6.13}$$

and we explain our reason very shortly.

For this new polynomial $p(w)$ we show next that it satisfies the three conditions of Theorem (A6.1).

(i)
$$p(0) \equiv P(e^{-iw})|_{w=0} = P(1) = \frac{1+e^0}{2} = 1 \tag{A6.14}$$

(ii)
$$
\begin{aligned}
|P(z)|^2 + |P(-z)|^2 &= |p(w)|^2 + |p(w+\pi)|^2 \\
&= \left|\frac{1+e^{-iw}}{2}\right|^2 + |1+e^{-i(w+\pi)}|^2 \\
&= \frac{(1+e^{-iw})(1+e^{iw})}{4} + \frac{(1+e^{-i(w+\pi)})(1+e^{i(w+\pi)})}{4} \\
&= \frac{2+e^{-iw}+e^{iw}}{4} + \frac{2+e^{-i(w+\pi)}+e^{i(w+\pi)}}{4} \\
&= \frac{2+2\cos w}{4} + \frac{2+2\cos(w+\pi)}{4} \\
&= \frac{2+2\cos w+2-2\cos w}{4} \\
&= \frac{4}{4} \\
&= 1,
\end{aligned}
$$

$$|P(z)|^2 + |P(-z)|^2 = 1 \tag{A6.15}$$

(iii)
$$|P(z)| = |p(w)| = \left|\frac{1+e^{-iw}}{2}\right| = \frac{1}{2}\left|e^{-\frac{iw}{2}}\left(e^{\frac{iw}{2}} + e^{-\frac{iw}{2}}\right)\right| = \left|e^{-\frac{iw}{2}}\cos\frac{w}{2}\right|$$

$$|P(z)| = |p(w)| = \left|\cos\frac{w}{2}\right| > 1, \ for \ \frac{-\pi}{2} \le w \le \frac{\pi}{2} \tag{A6.16}$$

As we mentioned above, the question may be raised: why did we move from $P(e^{\frac{-iw}{2}}) = \frac{1}{2}\frac{1+e^{\frac{-iw}{2}}}{2} \equiv P_1(z)$ of Eq. (A6.8) in Example (A6.1) to the present $P(e^{-iw}) \equiv p(w)$? The answer may be seen in having this $p(w)$ written as

$$p(w) = \frac{1}{2}(1+e^{-iw}) = \frac{1}{2}e^{-\frac{iw}{2}}\left(e^{\frac{iw}{2}} + e^{-\frac{iw}{2}}\right) = e^{\frac{-iw}{2}}\cos\frac{w}{2}, \tag{A6.17}$$

where, as we shall see soon, we will be working with this towards the ingenuous step of finding the Daubechies 2 scaling coefficients and more.

We have already indicated that considering the self convolution $p_1(w) * p_1(w)$ of the Haar would result in the continuous roof function; however, its increased compact support to $(0,2)$ denies it the orthogonality

$$\int_{-\infty}^{\infty}\phi(w-k)\phi(w-l)dw = 0,\ k \neq l$$

So, we repeat that our attempt in this direction seeking continuous orthogonal scaling functions failed.

A6.1.1 Determining the Daubechies 2 Scaling Coefficients

We should note at this stage that in moving from the Haar scaling function polynomial

$$P(e^{\frac{-iw}{2}}) = P_1(z) = \frac{1}{2}[1+e^{\frac{-iw}{2}}] \tag{A6.18}$$

to the new one

$$p(w) = P(e^{-iw}) = \frac{1}{2}[1+e^{-iw}] = e^{\frac{-iw}{2}}\cos\frac{w}{2}, \tag{A6.19}$$

results in scaling down by a factor of 2 in the w-frequency space, since we went from $P_1\left(e^{-\frac{iw}{2}}\right)$ to $P\left(e^{-\left(\frac{iw}{2}\right)/\frac{1}{2}}\right) = P(e^{-iw})$ with a smaller scale of $\frac{1}{2}$. This, according to the Fourier transform pair, corresponds to scaling up by a factor of 2 in the time space. Thus, $P(w)$ corresponds to a Haar scaling function with the larger compact support $(0,2)$. Note that this may be in the direction of our development, since, according to Theorem on scaling equation with non-vanishing coefficient, a larger compact support increases the number of non-vanishing coefficients.

A6.1.2 Innovative Step

Now, the other possibility, for aiming at a continuous scaling function or better, is to consider the polynomial,

$$q(w) = p^2(w) = \frac{1}{4}(1+e^{-iw})^2 = e^{-iw}\cos^2\frac{w}{2}. \tag{A6.20}$$

Unfortunately, this polynomial does not satisfy Condition 2 of Theorem 10.4, since, in general, $\left|e^{-iw}\cos^2\frac{w}{2}\right|^2 + \left|e^{\frac{-iw}{2}}\cos^2\frac{-w}{2}\right|^2 = \cos^4\frac{w}{2} + \cos^4\frac{w}{2} = 2\cos^4\frac{w}{2} \neq 1$. This is only true for $p(w)$ itself in (10.40) (as we showed in Example (A6.1)). So, there is no point in going further to consider $p^n(w), n > 1$.

We see from this and the above discussion that the crux of the matter in part of this attempt for satisfying Condition 2 of Theorem (A6.1), is the simple identity:

$$\cos^2\frac{w}{2} + \sin^2\frac{w}{2} = 1,$$

which will ensure Condition 2. At this stage comes the promised crucial step, which is to stay with this identity and try high integer powers of it. For example, we start with cubing both sides of this identity,

$$\begin{aligned}\left[\cos^2\frac{w}{2} + \sin^2\frac{w}{2}\right]^3 &= 1 \\ &= \cos^6\frac{w}{2} + 3\cos^4\frac{w}{2}\sin^2\frac{w}{2} + 3\cos^2\frac{w}{2}\sin^4\frac{w}{2} + \sin^6\frac{w}{2} \\ &= \left[\cos^6\frac{w}{2} + 3\cos^4\frac{w}{2}\sin^2\frac{w}{2}\right] + \left[3\sin^2\left(\frac{w+\pi}{2}\right)\right. \\ &\quad \left.\cos^4\left(\frac{w+\pi}{2}\right) + \cos^6\frac{w+\pi}{2}\right],\end{aligned} \tag{A6.21}$$

after using $\cos\theta = \sin\left(\theta + \frac{\pi}{2}\right)$ and $\sin\theta = -\cos\left(\theta + \frac{\pi}{2}\right)$.

The grouping of two parts in (A6.21) is done in the preparation of the first two terms in parenthesis, as a nominee for a polynomial $Q(w) = |p(w)|^2$, where $p(w)$, and not $|p(w)|$, is the sought polynomial for $P(w)$ of Theorem (A6.1).

$$|p(w)|^2 = Q(w) = \cos^6\frac{\pi}{2} + 3\cos^4\frac{w}{2}\sin^2\frac{w}{2} \tag{A6.22}$$

The second part of two terms in (A6.20) makes the polynomial $Q(w+\pi) = |p(w+\pi)|^2$,

$$|p(w+\pi)|^2 = Q(w+\pi) = 3\sin^2\left(\frac{w+\pi}{2}\right)\cos^4\left(\frac{w+\pi}{2}\right) + \cos^6\left(\frac{w+\pi}{2}\right). \tag{A6.23}$$

This is done to ensure Condition 2 of Theorem (A6.1) is satisfied, in advance, where we have

$$\begin{aligned} Q(w)+Q(w+\pi) &= 1 \\ &= |p(w)|^2 + |p(w+\pi)|^2 = 1. \end{aligned} \tag{A6.24}$$

Condition 3 of Theorem A6.1 requires that $|p(w)|>0$ for $-\frac{\pi}{2}<w<\frac{\pi}{2}$, which is satisfied here, as we shall show next. From Eq. (A6.22), we have

$$|p(w)|^2 = \cos^4\frac{w}{2}\left[\cos^2\frac{w}{2}+3\sin^3\frac{w}{2}\right] \tag{A6.25}$$

where we have $cos\frac{w}{2}\ge\frac{1}{\sqrt{2}}$ for $-\frac{\pi}{2}\le w\le\frac{\pi}{2}$, and the sum of the two terms above is positive. Hence, $|p(w)|>0$ for $-\frac{\pi}{2}\le w\le\frac{\pi}{2}$.

We note that the above choice of $p(w)$ in (A6.22) for $P(e^{-iw})$ allows the latter to be $P(e^{iw})$ since if we change $-iw$ by iw in $Q(w)=|p(w)|^2$ of (10.48) we obtain the same result. Hence, we can speak of $p(w)$ as a function of e^{iw}, which Condition 3 specifies for $P(e^{iw})$.

What remains is Condition 1 of Theorem (A6.1), which requires $p(0)=1$ for the above new polynomial $p(w)$. However, we do not yet have $p(w)$, since in Eq. (A6.22) we only defined its absolute value $|p(w)|$,

$$Q(w)=p(w)|^2=\cos^6\frac{\pi}{2}+3\cos^4\frac{w}{2}\sin^2\frac{w}{2}.$$

We need to find $p(w)$ from $|p(w)|$, where at the end we will show that $p(0)=1$.

Note that we can write a complex number in its polar form,

$$z=x+iy=re^{i\theta}, r=\sqrt{x^2+y^2}=|z|.$$

So, in $|z|=|re^{i\theta}|=r$, we lose the phase factor $e^{i\theta}$, which is what we must recover for $p(w)$ from having $|p(w)|$ in Eq. (A6.22). We shall, for now, allow such a phase factor $\gamma(w)$ for $p(w)=|p(w)|\gamma(w)$ to be determined in the sequel, in such a way that serves our purpose for determining the scaling coefficients.

Now, by factorizing the sum in Eq. (A6.25) and realizing that $|x-iy|=|x+iy|=\sqrt{x^2+y^2}$ that allows us to write $\left|\cos\frac{w}{2}-i\sqrt{3}\sin\frac{w}{2}\right|=\left|\cos\frac{w}{2}+i\sqrt{3}\sin\frac{w}{2}\right|$, we have

$$\begin{aligned} |p(w)|^2 &= \cos^4\frac{w}{2}\left[\cos^2\frac{w}{2}+3\sin^2\frac{w}{2}\right] \\ &= \cos^4\frac{w}{2}\left(\cos\frac{w}{2}+i\sqrt{3}\sin\frac{w}{2}\right)\left(\cos\frac{w}{2}-i\sqrt{3}\sin\frac{w}{2}\right), \end{aligned}$$

$$= \cos^4\frac{w}{2}\left|\cos\frac{w}{2}+i\sqrt{3}\sin\frac{w}{2}\right)\right|^2,$$

$$|p(w)| = \cos^2\frac{w}{2}\left|\cos\frac{w}{2}+i\sqrt{3}\sin\frac{w}{2}\right)\right|. \tag{A6.26}$$

To write $p(w)$, as we mentioned, we must multiply its above absolute value by the phase factor $\gamma(w)$,

$$p(w) = |\,p(w)\,|\,\gamma(w) = \cos^2\frac{w}{2}\left|\cos\frac{w}{2}+i\sqrt{3}\sin\frac{w}{2}\right|\gamma(w)$$

$$= \cos^2\frac{w}{2}\left[\cos\frac{w}{2}+i\sqrt{3}\sin\frac{w}{2}\right] \tag{A6.27}$$

after writing $\left|\cos\frac{w}{2}+i\sqrt{3}\sin\frac{w}{2}\right|\gamma(w) = \left[\cos\frac{w}{2}+i\sqrt{3}\sin\frac{w}{2}\right].$

For the present case of cubing $\cos^2\frac{w}{2}+\sin^2\frac{w}{2}=1$ in (A6.21), for the search of the scaling coefficients of the Daubechies 2 wavelet, the phase factor $\gamma(w)$ in (A6.27) is chosen to make $p(w)$ a polynomial of degree 3. This is to aim at the four coefficients of the polynomial $P_3(z)$ in (A6.33).

We are after the four coefficients of $p(w) = P_3(w) = P_3(w) = \frac{1}{2}[a_0 + a_1 z + a_2 z^2 + a_3 z^3] = \frac{1}{2}[h_0 + h_1 z + h_2 z^2 + h_3 z^3]$ in $z = e^{-iw}$. So, we write the trigonometric functions in (A6.27) in terms of complex exponentials. After this, the phase factor is chosen such that the first term in our result is of degree zero in $z = e^{iw}$,

$$p(w) = \frac{1}{4}\left[e^{\frac{iw}{2}} + e^{-\frac{iw}{2}}\right]^2\left[\left(\frac{e^{\frac{iw}{2}} + e^{-\frac{iw}{2}}}{2}\right) + i\sqrt{3}\left(\frac{e^{\frac{iw}{2}} - e^{-\frac{iw}{2}}}{2i}\right)\right]\gamma(w) \tag{A6.28}$$

$$p(w) = \frac{1}{8}[e^{iw} + e^{-iw} + 2]\left[e^{\frac{iw}{2}} + e^{-\frac{iw}{2}} + \sqrt{3}\left(e^{\frac{iw}{2}} - e^{-\frac{iw}{2}}\right)\right]\gamma(w)$$

$$= \left[\frac{1}{8}\left\{e^{\frac{i3w}{2}} - e^{\frac{iw}{2}} + \sqrt{3}\left(e^{\frac{i3w}{2}} - e^{\frac{iw}{2}}\right)\right\}\right] + \frac{1}{8}\left\{e^{-\frac{iw}{2}} + e^{-\frac{3iw}{2}}\right.$$

$$\left. + \sqrt{3}\left(e^{-\frac{iw}{2}} - e^{-\frac{3iw}{2}}\right)\right\} + \frac{2}{8}\left\{e^{\frac{iw}{2}} + e^{-\frac{iw}{2}} + \sqrt{3}\left(e^{\frac{iw}{2}} - e^{-\frac{iw}{2}}\right)\right\}\Bigg]\gamma(w)$$

$$= \frac{1}{8}\left[\left(e^{\frac{i3w}{2}} + \sqrt{3}e^{\frac{i3w}{2}}\right) + \left(e^{\frac{iw}{2}} + 2e^{\frac{iw}{2}} - \sqrt{3}e^{\frac{iw}{2}} + 2\sqrt{3}e^{\frac{iw}{2}}\right)\right.$$

$$\left. + \left(e^{-\frac{iw}{2}} + \sqrt{3}e^{-\frac{iw}{2}} + 2e^{-\frac{iw}{2}} - 2\sqrt{3}e^{-\frac{iw}{2}}\right) + \left(e^{-\frac{i3w}{2}} - \sqrt{3}e^{-\frac{i3w}{2}}\right)\right]\gamma(w),$$

$$p(w)=\frac{1}{8}\left[\left(1+\sqrt{3}\right)e^{\frac{i3w}{2}}+\left(3+\sqrt{3}\right)e^{\frac{iw}{2}}+\left(3-\sqrt{3}\right)e^{-\frac{iw}{2}}+\left(1-\sqrt{3}\right)e^{-\frac{i3w}{2}}\right]\gamma(w) \tag{A6.29}$$

after grouping the similar terms involving $e^{\frac{i3w}{2}}$, $e^{\frac{iw}{2}}$, $e^{-\frac{iw}{2}}$, and $e^{-\frac{3iw}{2}}$.

Now to have the first term be of degree zero in $z=e^{-iw}$, we choose the phase factor $\gamma(w)=e^{-\frac{i3w}{2}}$,

$$\begin{aligned}p(w)&=\frac{1}{8}\left[\left(1+\sqrt{3}\right)+\left(3+3\sqrt{3}\right)e^{-iw}+\left(3-\sqrt{3}\right)e^{-i2w}+\left(1-\sqrt{3}\right)e^{-3iw}\right]\\&=\frac{1}{2}\left[\frac{1+\sqrt{3}}{4}+\frac{3+\sqrt{3}}{4}e^{-iw}+\frac{3-\sqrt{3}}{2}e^{-i2w}+\frac{1-\sqrt{3}}{4}e^{-3iw}\right]\\&=\frac{1}{2}\left[\frac{1+\sqrt{3}}{4}+\frac{3+\sqrt{3}}{4}z+\frac{3-\sqrt{3}}{2}z^2+\frac{1-\sqrt{3}}{4}z^3\right].\end{aligned} \tag{A6.30}$$

The last step is to equate coefficients of the same powers of z in the above polynomial and $P_3(z)$ in Eq. (A6.2),

$$P_3(z)=\frac{1}{\sqrt{2}}[h_0+h_1z+h_2z^2+h_3^3],$$

to have the Daubechies 2 scaling coefficients

$$h_0=\frac{1+\sqrt{3}}{4\sqrt{2}}, h_1=\frac{3+\sqrt{3}}{4\sqrt{2}}, h_2=\frac{3-\sqrt{3}}{4\sqrt{2}}, \text{and } h_3=\frac{1-\sqrt{3}}{4\sqrt{2}}. \tag{A6.31}$$

A6.1.3 Towards Determining the Daubechies N (or ϕ_N) Scaling Coefficients

For the above case of Daubechies $N=2$, we raised the identity $\cos^2 w+\sin^2 w=1$ to power $2N-1=2(2)-1=3$ for the $2N=2(2)=4$ non-zero coefficients. It is tempting to generalize the above method for finding the scaling coefficients for Daubechies 3, 4, etc., which happened to be the course to follow, as was done by Daubechies. But, before that, let us note for the Haar (Daubechies 1) scaling function, we had a polynomial $P_1(z)$ of degree 1, where the Haar scaling function is discontinuous. For the above Daubechies 2, we have a polynomial $P_3(z)$ of degree 3, and we know that the scaling function $\phi_2(t)$ is continuous.

We must sense from this observation that the higher degree polynomial has something to do with the quality of the scaling function. Indeed, there is another observation that such polynomial $P_{2N-1}(z)$, resulting from raising $\cos^2 w+\sin^2 w=1$ to power $2N-1$ for Daubechies N with $2N$ non-zero coefficients, factorizes as

$$P_{2N-1}(z)=(1+z)^N Q_{N-1}(z), \tag{A6.32}$$

where $Q_{N-1}(z)$ is another polynomial of degree $N-1$, and $Q_{N-1}(-1)\neq 0$.

It is easy to verify (A6.32) for the Haar scaling function with $P_1(z) = \frac{1}{\sqrt{2}}h_0 + \frac{1}{\sqrt{2}}h_1 z = \frac{1}{\sqrt{2}} \cdot \frac{1}{\sqrt{2}} + \frac{1}{\sqrt{2}} \cdot \frac{1}{\sqrt{2}} z = (1+z).\frac{1}{2}$ for $N = 1$, where $Q_{N-1}(z)$ is of degree zero, i.e., $Q_0(z) = \frac{1}{2}$.

Also, by a simple multiplication, we can verify that $P_3(z) = p(z)$ in (A6.30) has the following factorization:

$$P_3(z) = (1+z)^2 Q_1(z) = (1+z)^2 \left(\frac{1+\sqrt{3}}{8} + \frac{1-\sqrt{3}}{8} z \right) \tag{A6.33}$$

as a special case of (A6.32) for $N = 2$ with $Q_1(z) = \frac{1+\sqrt{3}}{8} + \frac{1-\sqrt{3}}{8} z$, and $Q_1(-1) = \frac{\sqrt{3}}{4} \neq 0$.

For Daubechies 3, we can parallel the above computations, done for the four scaling coefficients, by using $\left[\cos^2 \frac{w}{2} + \sin^2 \frac{w}{2} = 1 \right]^5$ to find the six non-zero coefficients, and show that $p(w) = p_5(z)$ factorizes as a special case of (A6.32),

$$P_5(z) = (1+z)^3 Q_2(z). \tag{A6.34}$$

A6.2 | Vanishing Moments of a Wavelet: Towards Embellishment

We know that this Daubechies 3 scaling function is smoother than that of Daubechies 2. Hence, it seems that the factor $(1+z)^N$ in (A6.32) plays a role in this direction. As we shall use it shortly, this role is that $P_{2N-1}(-1) = 0$. Briefly, this will lead us to N "vanishing moments" for the Daubechies N wavelet. We will explain this term soon in the sense that the smoothness of these Daubechies scaling functions and wavelets N increases with the number N of vanishing moments.

In mechanics the integral $\int_{-\infty}^{\infty} x^k \rho(x) dx$ defines the kth moment of the mass distribution $\rho(x), x \in (-\infty, \infty)$. But this term is used for any function $f(x)$, for example, the wavelet $\psi(x)$ with its kth moment on $(-\infty, \infty)$ as

$$M_k = \int_{-\infty}^{\infty} x^k \psi(x) dx. \tag{A6.35}$$

We start with a short cut towards a feeling for how the smoothness of $\psi(x)$ is measured by its vanishing of high-order moments $M_k = \int_{-\infty}^{\infty} x^k \psi(x) dx = 0$ for $k = 0,1,2,...,N-1$, which is the case, as we shall show for the Daubechies N wavelets.

We recall the Fourier transform operational property (A6.36) of reducing derivatives to algebraic operations,

$$F\left\{ \frac{d^n f}{dt^n} \right\} = i^n w^n F(w), \tag{A6.36}$$

$$\frac{d^n f}{dt^n} = i^n F^{-1}\{w^n F(w)\} = \frac{i^n}{2\pi}\int_{-\infty}^{\infty} e^{-iwt} w^n F(w)dw. \quad \text{(A6.37)}$$

From the existence of the above Fourier integral, we have the existence of the nth derivative $\frac{d^n f(t)}{dt^n}$ at $t = 0$, since

$$f^{(n)}(0) = \frac{i^n}{2\pi}\int_{-\infty}^{\infty} w^n F(w)dw = \frac{i^n}{2\pi} M_n. \quad \text{(A6.38)}$$

This indicates the existence of the M_n moment of $F(w)$, which also indicates the smoothness of $f(t)$ about $t_0 = 0$ by ensuring its n^{th} derivative there.

A6.2.1 Vanishing moments: saving in the computations and detecting defects

The question now is why the vanishing of $k = 1,2,...,n$ moments of $f(t)$ is of value. Part of the answer lies in the savings we obtain when computing for $f(t)$ via its Taylor series expansion about $t_0 = 0$, for example,

$$f(t) = f(0) + tf'(0) + \frac{t^2 f''(0)}{2!} + \frac{t^3 f^3(0)}{3!} + \cdots + \frac{t^n f^n(0)}{n!} + \cdots \quad \text{(A6.39)}$$

If t is very small, we may consider only the first four terms. So, if $f(t)$, for example, has vanishing moments of order 0, 1, and 2, the first three terms in the above series vanish, and we compute only the fourth term $\frac{t^3}{3!} f^3(0)$.

We shall illustrate this further in the following example.

Example A6.2 — Vanishing moments: savings in computing the wavelet series coefficients.

We do take advantage of the vanishing moments $M_n, n = 0,1,2,...,N$ for the Daubechies wavelet when we compute its series coefficients $c_{j,k}$ for the signal $f(t)$ at very small scale $l_j = \frac{1}{2^j}$ for high j:

$$f(t) = \sum_k c_{j,k} 2^{\frac{j}{2}} \psi(2^j t - k), \quad \text{(A6.40)}$$

$$c_{j,k} = \int_{-\infty}^{\infty} f(t) 2^{\frac{j}{2}} \psi(2^j t - k)dt. \quad \text{(A6.41)}$$

Let us consider, as an example, the Daubechies 2 wavelet, where for now we assume its vanishing moments of order 0, 1, and 2. The vanishing moment order 0 is clear from the admissibility condition,

$$\int_{-\infty}^{\infty} \psi(t)dt = 0 \quad \text{(A6.42)}$$

The Daubechies 2 wavelet in the integral of (A6.41) has a compact support $[0,3)$,

$$c_{j,k} = \int_0^3 f(t) 2^{\frac{j}{2}} \psi(2^j t - k) dt \tag{A6.43}$$

$$= \int_0^{3-2^{-j}k} f(x + 2^{-j}k) 2^{\frac{j}{2}} \psi(2^j x) dx, \tag{A6.44}$$

after the change of variable $t = x + 2^{-j}k$.

For high value of j, the term $2^{-j}k$ is very small, and if the signal has derivatives up to its second one, we approximate $f(x + 2^{-j}k)$ about $x_0 = 2^{-j}k$ using only the first three terms,

$$\begin{aligned} f(x + 2^{-j}k) &\approx f(2^{-j}k) + (x + 2^{-j}k - x^{-j}k) f'(2^{-j}k) \\ &\quad + \frac{(x + 2^{-j}k - 2^{-j}k)^2}{2} f''(2^{-j}k) \\ &= f(2^{-j}k) + x f'(2^{-j}k) + \frac{1}{2} x^2 f''(2^{-j}k) \end{aligned} \tag{A6.45}$$

in the integral of Eq. (A6.44),

$$c_{j,k} = \int_0^{3 \cdot 2^{-j}} [f(2^{-j}k) + x f'(2^{-j}k) + \frac{1}{2} x^2 f''(2^{-j}k)] 2^{\frac{j}{2}} \psi(2^j x) dx. \tag{A6.46}$$

So, if we have here $\psi_2(2^j x)$ with its two M_0 and M_1 vanishing moments, the above integral over each of the first two terms vanish, and we only evaluate the third integral, which represents a saving in the computations.

In the following section we will discuss the other more important advantage, of the vanishing higher moments of wavelet, in the search for hidden discontinuities, jumps in the derivatives. Examples are the jump discontinuities of the derivatives in the spline functions, or fault in structures such as defect in the rotor of power system.

A6.2.2 Vanishing moments - for Detecting Higher Derivatives

The second and more important advantage of vanishing higher order moments of certain wavelets, lies in the wavelets series detecting or seeing the higher order derivatives in the decomposed signal.

We can tell that from the expression of the wavelets coefficients $c_{j,k}$ in (A6.47),

$$c_{j,k} = \int_{-\infty}^{\infty} f(t) 2^{\frac{j}{2}} \psi(2^j t - k) dt. \tag{A6.47}$$

as the correlation between the wavelet and the signal at the scale level ℓ_j and the position k. After the Taylor series expansion of $f(t)$ in (A6.46) of the above Example (A6.2), we can see that if the wavelet has, for example, vanishing moments $M_0 = M_1 = 0$, then the wavelets coefficient $c_{j,k}$ is a correlation of that wavelet with the second and higher derivatives of the given signal. It also means that such a wavelet does not see the first derivative of the signal or its linear part. This, of course, besides not seeing the zeroth derivative or the flat part of the signal. We can continue this anlysis for a wavelet with $M_0 = M_1 = M_2 = 0$, which will see the third derivative and higher of the signal, and so on.

An example of a function $g(t)$ with jump discontinuity at $t = \frac{1}{2}$ is shown in Figure 17.23. But we can integrate it twice with some matching of its two branches to have a continuous function $f(t)$ as shown in Figure 12.3. So, in the general structure of this smooth looking $f(t)$, we know well that it has "a hidden trouble", namely that its second derivative has a jump discontinuity. This is besides the worse trouble of a third derivative at $t = \frac{1}{2}$, which represents a very steep spike, or a Dirac delta function. Of course, in general, for a given signal, we don't know if it has such a hidden trouble, but often those of much interest do. Indeed, we consider such complexity of the signal as a desirable activity or more information. An example is the signal we receive in searching for oil, which we would like it to carry good activity or fine structure.

In Section 12.2. we also see that for detecting the discontinuity in the second derivative we should use a wavelet with at least $M_1 = 0$. Better yet we may consider one with $M_0 = M_1 = M_2 = 0$, where this one will see the third derivative with its very clear activity as a spike. In the case of using Daubechies wavelets, we know that ψ_N has vanishing moments up to M_{N-1}. So for the above example we should use at least ψ_2 with its four non-vanishing coefficients, or better yet ψ_3 with its six coefficients. It may also become necessary to go to ψ_4, giving attention to better resolution with small scale such as $\ell_7 = \frac{1}{128}$ or $\ell_8 = \frac{1}{256}$ to see the activity around $t = \frac{1}{2}$.

We shall return to this example and show how Matlab or the wavelet tool box is used for very feasible computations. We may add here, that for detecting hidden discontinuities in a signal, we are after "details" and not the general picture of the signal. Hence, we will use only the wavelet series for this application. In contrast, when we decompose an image of a face, for example, we will definitely need the outline of the face which is accomplished by the scaling functions series, plus the details supplied by the wavelet series, to have a satisfactory picture of the face.

A6.2.3 The Daubechies Wavelets Fourier Transform Factorization - for Showing its Vanishing Moments

Now, we return to show the importance of the factorization of the polynomial $P_{2N-1}(z)$ in (A6.32)

$$P_{2N-1}(z) = (1+z)^N Q_{N-1}(z), Q_{N-1}(-1) \neq 0, \tag{A6.48}$$

to the vanishing of the N first moments of the Daubechies N wavelet, $M_k = 0, k = 0,1,2,...,N-1$ in (A6.36).

This will take us back to our original polynomial $P_n(z)$ of (6.49) in the result of Fourier transforming the scaling equation,

$$\Phi(w) = \Phi\left(\frac{w}{2}\right) P_n\left(e^{\frac{-iw}{2}}\right). \tag{A6.49}$$

If we repeat this identity for $\Phi\left(\frac{w}{2}\right)$ on the left side, we have

$$\Phi\left(\frac{w}{2}\right) = \Phi\left(\frac{w}{4}\right)P_n\left(e^{\frac{-iw}{4}}\right) = \Phi\left(\frac{w}{2^2}\right)P_n\left(e^{\frac{-iw}{2^2}}\right),$$

$$\Phi(w) = \Phi\left(\frac{w}{2^2}\right)P_n\left(e^{\frac{-iw}{2^2}}\right)P_n\left(e^{\frac{-iw}{2}}\right).$$

This can be repeated again for $\Phi\left(\frac{w}{2^2}\right)$, then $\Phi\left(\frac{w}{2^3}\right),\ldots,\Phi\left(\frac{w}{2^m}\right)$. It results in a product of m factors for the polynomials $\left\{P_n\left(e^{\frac{-iw}{2^k}}\right)\right\}_{k=1}^{m}$ and one factor $\Phi\left(\frac{w}{2^m}\right)$,

$$\Phi(w) = \Phi\left(\frac{w}{2^m}\right)\cdot P_n\left(e^{\frac{-iw}{2}}\right)P_n\left(e^{-\frac{iw}{2^2}}\right)P_n\left(e^{-\frac{iw}{2^3}}\right)\cdots P_n\left(e^{-\frac{iw}{2^m}}\right) \tag{A6.50}$$

where, symbolically, we write it as a finite product,

$$\Phi(w) = \Phi\left(\frac{w}{2^m}\right)\prod_{k=1}^{m}P_n\left(e^{-\frac{iw}{2^k}}\right) \tag{A6.51}$$

where $\prod$ refers to products as compared to $\sum$ of the sum.

If we let $m \to 0$, $\Phi\left(\frac{w}{2^m}\right) \to \Phi(0) = \int_{-\infty}^{\infty}\phi(t)dt = 1$, and we have the infinite product expression for the Fourier transform of the scaling function $\phi(t)$,

$$\Phi(w) = \prod_{k=1}^{\infty}P_n\left(e^{-\frac{iw}{2^k}}\right). \tag{A6.52}$$

After finding the result of the infinite product, we have $\Phi(w)$, whose inverse Fourier transform gives us the sought scaling function $\phi(w)$. However, we must realize that it is not that easy to work with the infinite products, when compared to the much more familiar infinite series and its available tools and theorems.

For the wavelet $\psi(t)$,

$$\psi(t) = \sum_k(-1)^k h_{1-k}2^{\frac{1}{2}}\phi(2t-k), \tag{A6.53}$$

we can develop a parallel to equation (6.49) of the scaling function by considering a new polynomial $R(z) = -zP_n(-z)$, to have

$$\Psi(w) = \Psi\left(\frac{w}{2}\right) R\left(e^{-\frac{iw}{2}}\right) = \Psi\left(\frac{w}{2}\right) \cdot \left(-e^{-\frac{iw}{2}}\right) P_n\left(-e^{\frac{iw}{2}}\right) \tag{A6.54}$$

where we used the fact that $P_n(z)$ is with real coefficients, thus $\overline{P_n(-z)} = P_n(-\bar{z})$.

To get to the stated results of the vanishing moments $M_k = 0, k = 0,1,2,...,N-1$ of the Daubechies N wavelet, we shall need the results in (A6.52) and (A6.54). So, we should derive the expression of $\Psi(w)$ in (A6.54), since we will need its derivatives $\frac{d^k\Psi(w)}{dw^k}$ to vanish at $w = 0$ for $k = 0,1,2,...,N-1$ to prove the above result of $M_k = 0, k = 0,1,2,..,N-1$ for $\psi(t)$.

From (A6.53), assuming real-valued coefficients, we have the scaling functions series of their associated wavelet

$$\psi(t) = \sum_k (-1)^k h_{1-k} \sqrt{2}\phi(2t-k).$$

The Fourier transform of $\psi(t)$, as we did for the scaling equation, is

$$\begin{aligned}
\Psi(w) &= \sum_k (-1)^k \sqrt{2} h_{1-k} \cdot \frac{1}{2} e^{\frac{-ikw}{2}} \Phi\left(\frac{w}{2}\right) \\
&= \Phi\left(\frac{w}{2}\right) \cdot \frac{1}{2} \sum_k (-1)^k \sqrt{2} h_{1-k} \left(e^{-\frac{iw}{2}}\right)^k \\
&= \Phi\left(\frac{w}{2}\right) \cdot \frac{1}{2} \sum_k (-1)^k \sqrt{2} h_{1-k} z^k \\
&= \Phi\left(\frac{w}{2}\right) \cdot R(z)
\end{aligned} \tag{A6.55}$$

with the new polynomial,

$$R(z) = \frac{1}{2} \sum_k (-1)^k \sqrt{2} h_{1-k} (z)^k. \tag{A6.56}$$

This polynomial is very much related to the polynomial P_n of the scaling equation in (6.49). Indeed, we shall show next that

$$R(z) = -z\overline{P_n(-z)} \tag{A6.57}$$

$$R(z) = \frac{1}{2} \sum_k (-1)^k \sqrt{2} h_{1-k} z^k$$

$$= \frac{1}{2}\sum_j (-1)^{1-j}\sqrt{2}h_j z^{1-j}, \quad j = 1-k$$

$$= -\frac{1}{2}z\sum_j (-1)^{-j}\sqrt{2}h_j z^{-j} = -\frac{1}{2}z\sum_j (-1)^{-j}\sqrt{2}h_j\left(e^{-\frac{iw}{2}}\right)^{-j}$$

$$= -\frac{1}{2}z\sum_j (-1)^{j}\sqrt{2}h_j z^{-j} \tag{A6.58}$$

Now,

$$P(-z) = \frac{1}{2}\sum_k \sqrt{2}h_k(-z)^k,$$

$$\overline{P(-z)} = \frac{1}{2}\sum_k \sqrt{2}h_k(-\bar{z})^k = \frac{1}{2}\sum_k \sqrt{2}h_k(-1)^k\left(e^{\frac{iw}{2}}\right)^k$$

$$= \frac{1}{2}\sum_k \sqrt{2}h_k(-1)^k z^{-k}. \tag{A6.59}$$

Hence, from (A6.59) and (A6.60) we have the sought result (A6.57),

$$R(z) = -z\overline{P_n(-z)}.$$

With this result, (A6.55) becomes

$$\Psi(w) = -\Phi\left(\frac{w}{2}\right)\cdot e^{-\frac{iw}{2}}P_n\left(-e^{-\frac{iw}{2}}\right)$$

or (A6.57),

$$\Psi(w) = \Phi\left(\frac{w}{2}\right)\cdot R\left(e^{-\frac{iw}{2}}\right). \tag{A6.60}$$

We may note from (A6.32) that $P_{2N-1}(-1) = 0$, and when combined with the above result, we have $\Psi(0) = 0 = \int_{-\infty}^{\infty}\psi(t)dt$, which means that such Daubechies N wavelets satisfy the admissibility condition. This also means that we have a vanishing moment $M_0 = 0$. What concerns us is having vanishing moments $M_k = 0$ for $k > 0$. Indeed, it turns out that for $\psi_N(t)$, $M_k = 0, k = 0,1,2,...,N-1$. We shall illustrate this in the following example for $M_1 = 0$, where the same method can be followed to show the rest of the vanishing moments $M_k, k = 2,3,...,N-1$ for the Daubechies $\psi_N(t)$.

Example A6.3 — Vanishing moment M_1 for the Daubechies 2 wavelet.

Showing that $M_1 = \int_{-\infty}^{\infty} t\psi(t)dt = 0$ requires looking at the derivative of the Fourier transform $\Psi(w)$ of $\psi(t)$:

$$\frac{d}{dw}\Psi'(w) = \int_{-\infty}^{\infty} -ite^{-iwt}\psi(t)dt \tag{A6.61}$$

to vanish at $w = 0$, $\Psi'(0) = -i\int_{-\infty}^{\infty} t\psi(t)dt = -iM_1 = 0$.

So, we use $\Psi(w)$ in (A6.54) to find its first derivative,

$$\Psi'(w) = \frac{1}{2}\Psi'\left(\frac{w}{2}\right)\left[-e^{-\frac{iw}{2}}P_n\left(-e^{-\frac{iw}{2}}\right)\right]$$

$$+\Psi\left(\frac{w}{2}\right)\left[\frac{i}{2}e^{-\frac{iw}{2}}P_n\left(-e^{-\frac{iw}{2}}\right) - e^{-\frac{iw}{2}}\left(\frac{i}{2}e^{-\frac{iw}{2}}P_n'\left(e^{-\frac{iw}{2}}\right)\right)\right]$$

Thus,

$$\Psi'(0) = \frac{1}{2}\Psi'(0)[-P_n(-1)] + \Psi(0)[-\frac{i}{2}P_n(-1) - \frac{i}{2}P_n'(-1)] \tag{A6.62}$$

The first term on the right vanishes because of $P_n(-1) = 0$ from (A6.42). The second term vanishes because of $\Psi(0) = 0$, the vanishing of the M_0 moment of $\psi(t)$. In the second term we have $P_n(-1)$ and P_n'(-1) are finite, since $P_n(z)$ is a polynomial of degree n. Hence, $\Psi'(0) = 0$.

A6.3 | Determining the Daubechies 3 Coefficients

To further illustrate the exact method for determining the Daubechies scaling coefficients, which we did in (A6.21)-(A6.31) for ϕ_{D2}, we will do that for ϕ_{D3} in the following example.

Example A6.4 determining the ϕ_{D3} Coefficients.
As was mentioned above, we will start with the expansion of

$$[\cos^2(\omega) + \sin^2(\omega)]^5 = 1$$

From this expansion we will, as we did for ϕ_{D2} in (A6.24)-(A6.25), take one part of the expansion as $Q(\omega) = |\, p(\omega)|^2$; and we see that the other part reduces $Q(\omega + \pi) = |\, p(\omega + \pi)|^2$. This helps to satisfy the basic condition of Theorem (A6.1) in Eq. (A6.5),

$$|\, P_n(z)|^2 + |\, P_n(-z)|^2 = 1,\ for\ |\, z| = 1 \tag{A6.63}$$

with $|\, P_n(z)|^2 = Q(\omega) = |\, p(\omega)|^2,\ z = e^{-\frac{i\omega}{2}}$.

$$1=\left[\cos^2\frac{\omega}{2}+\sin^2\frac{\omega}{2}\right]^5$$

$$=\left(\cos^{10}\frac{\omega}{2}+5\cos^8\frac{\omega}{2}\sin^2\frac{\omega}{2}+10\cos^6\frac{\omega}{2}\sin^4\frac{\omega}{2}\right)$$

$$+\left(10\cos^4\frac{\omega}{2}\sin^6\frac{\omega}{2}+5\cos^2\frac{\omega}{2}\sin^8\frac{\omega}{2}+\sin^{10}\frac{\omega}{2}\right) \tag{A6.64}$$

We let

$$Q(\omega)=|\,p(\omega)\,|^2=\cos^6\frac{\omega}{2}\left[\cos^4\frac{\omega}{2}+5\cos^2\frac{\omega}{2}\sin^2\frac{\omega}{2}+10\sin^4\frac{\omega}{2}\right]$$

$$=\cos^6\frac{\omega}{2}\left[\sin^2\frac{\omega}{2}\left(5\cos^2\frac{\omega}{2}+10\sin^2\frac{\omega}{2}\right)+\cos^4\frac{\omega}{2}\right]. \tag{A6.65}$$

The second part in (6.64) becomes $Q(\omega+\pi)=|\,p(\omega+\pi)\,|^2$, because $\cos^{2n}\left(\frac{\omega+\pi}{2}\right)=(-\sin\omega)^{2n}=$ $\sin^{2n}\omega$, $\sin^{2n}\left(\frac{\omega+\pi}{2}\right)=\cos^{2n}\omega$ for $n=2,3,4$, and 5 in its three terms. Now,

$$|\,p(\omega)\,|^2=\cos^6\frac{\omega}{2}\left[\sin^2\frac{\omega}{2}\left(5\cos^2\frac{\omega}{2}+10\sin^2\frac{\omega}{2}\right)+\cos^4\frac{\omega}{2}\right].$$

Next, we write

$$5\cos^2\frac{\omega}{2}+10\sin^2\frac{\omega}{2}=\left(\sqrt{5}\cos\frac{\omega}{2}+i\sqrt{10}\sin\frac{\omega}{2}\right)\left(\sqrt{5}\cos\frac{\omega}{2}-i\sqrt{10}\sin\frac{\omega}{2}\right) \tag{A6.66}$$

$$=\left|\sqrt{5}\cos\frac{\omega}{2}+i\sqrt{10}\sin\frac{\omega}{2}\right|^2,$$

$$|\,p(w)\,|^2=\cos^6\frac{\omega}{2}\left[\sin^2\frac{\omega}{2}\left|\sqrt{5}\cos\frac{\omega}{2}+i\sqrt{10}\sin\frac{\omega}{2}\right|^2+\cos^4\frac{\omega}{2}\right]. \tag{A6.67}$$

Similar to the way of the above writing of

$$5\cos^2\frac{\omega}{2}+10\sin^2\frac{\omega}{2}=\left|\sqrt{5}\cos\frac{\omega}{2}+i\sqrt{10}\sin\frac{\omega}{2}\right|^2 \tag{A6.68}$$

we can do it for

$$\left|\sqrt{5}\cos\frac{\omega}{2}+i\sqrt{10}\sin\frac{\omega}{2}\right|^2+\cos^4\frac{\omega}{2}=$$

$$\left|i\left|\sqrt{5}\cos\frac{\omega}{2}+i\sqrt{10}\sin\frac{\omega}{2}\right|+\cos^2\frac{\omega}{2}\right|^2 \tag{A6.69}$$

Hence,

$$|\,p(\omega)\,|^2 = \cos^6\frac{\omega}{2}\left[\sin^2\frac{\omega}{2}\left|\left(i\left|\sqrt{5}\cos\frac{\omega}{2}+i\sqrt{10}\sin\frac{\omega}{2}\right|+\cos^2\frac{\omega}{2}\right)\right|^2\right] \tag{A6.70}$$

$$|\,p(\omega)\,| = \cos^3\frac{\omega}{2}\left[\sin\frac{\omega}{2}\left|\left(i\left|\sqrt{5}\cos\frac{\omega}{2}+i\sqrt{10}\sin\frac{\omega}{2}\right|+\cos^2\frac{\omega}{2}\right)\right|\right]. \tag{A6.71}$$

We note here that we have a different situation from the case of ϕ_{D2}, as we move from $|\,p(\omega)\,|$ to the sought $p(\omega)$, since we have two absolute values. One is of the two terms above and the other for the first term there. For the first we will need a phase factor $\gamma(\omega)$ to be decided later. For the other, an $\alpha(\omega)$ phase factor can be applied, and we can choose it to be one, which will not affect the derivation.

So, in order to get $p(\omega)$ from $|\,p(\omega)\,|$ in (A6.71), we have to introduce a phase factor $\alpha(\omega)$ for the inside term, and another phase factor $\gamma(\omega)$ for the whole expresion. This means that we will have two degrees of freedom at our disposal to decide them as we come to equate the coefficients of $p(\omega)$ with those of $P_5(z) = P_5\left(e^{-\frac{i\omega}{2}}\right)$ in Eq. (A6.1).

This is to be compared with the case of ϕ_{D2}, where we had one degree of freedom (phase factor $\gamma(\omega)$) in (A6.27).

In reference to what we did in (A6.16)-(A6.17) for the Haar case, we did not need a phase factor. This means that for the Haar case we have zero degree of freedom. One may make the conclusion as we find $\phi_{DN}, N > 3$ that there will be $N-1$ degrees of freedom.

So,

$$p(\omega) = \cos^3\frac{\omega}{2}\left[i\sin\frac{\omega}{2}\left(\sqrt{5}\cos\frac{\omega}{2}\right.\right.$$
$$\left.\left.+\,i\sqrt{10}\sin\frac{\omega}{2}\right)\alpha(\omega)+\cos^2\frac{\omega}{2}\right]\gamma(\omega) \tag{A6.72}$$

It turns out that we can assign $\alpha(\omega)=1$ without affecting our derivation. The phase factor $\gamma(\omega)$ will be chosen, similar to what we did for $\phi_{D,2}$, to make the first term in the expansion of degree zero in $z = e^{-i\omega}$.

Now, we prepare

$$\cos^3\frac{\omega}{2} = \left(\frac{e^{i\frac{\omega}{2}}+e^{-i\frac{\omega}{2}}}{2}\right)^3$$
$$= \frac{1}{8}\left[e^{3i\frac{\omega}{2}}+3e^{i\frac{\omega}{2}}+3e^{-i\frac{\omega}{2}}+e^{-3i\frac{\omega}{2}}\right] \tag{A6.73}$$

$$\left(\cos^3\frac{\omega}{2}\right)i\sin\frac{\omega}{2} = \cos^3\frac{\omega}{2}\, i\,\frac{e^{i\frac{\omega}{2}} - e^{-i\frac{\omega}{2}}}{2i}$$

$$= \frac{1}{16}\left[e^{3i\frac{\omega}{2}} + 3e^{i\frac{\omega}{2}} + 3e^{-i\frac{\omega}{2}} + e^{-3i\frac{\omega}{2}}\right]\left[e^{i\frac{\omega}{2}} - e^{-i\frac{\omega}{2}}\right]$$

$$= \frac{1}{16}\left[e^{2i\omega} + 3e^{i\omega} + 3 + e^{-i\omega} - e^{i\omega} - 3 - 3e^{-i\omega} - e^{-2i\omega}\right]$$

$$= \frac{1}{16}\left[e^{2i\omega} + 2e^{i\omega} - 2e^{-i\omega} - e^{-2i\omega}\right]. \quad \text{(A6.74)}$$

Next,

$$\left[\sqrt{5}\cos\frac{\omega}{2} + \sqrt{10}i\sin\frac{\omega}{2}\right]\alpha(\omega)$$

$$= \left[\sqrt{5}\,\frac{e^{i\frac{\omega}{2}} + e^{-i\frac{\omega}{2}}}{2} + \sqrt{10}i\,\frac{e^{i\frac{\omega}{2}} - e^{-i\frac{\omega}{2}}}{2i}\right]\alpha(\omega). \quad \text{(A6.75)}$$

From (A6.74) and (A6.75), we have,

$$\cos^3\frac{\omega}{2}\, i\sin\frac{\omega}{2}\left[\sqrt{5}\cos\frac{\omega}{2} + \sqrt{10}i\sin\frac{\omega}{2}\right]$$

$$= \cos^3\frac{\omega}{2}\left[i\sin\frac{\omega}{2}\left(\sqrt{5}\cos\frac{\omega}{2} + \sqrt{10}i\sin\frac{\omega}{2}\right)\alpha(\omega)\right]$$

$$= \frac{1}{32}\left[\sqrt{5}\left(e^{5i\frac{\omega}{2}} + 2e^{3i\frac{\omega}{2}} - 2e^{-i\frac{\omega}{2}} - e^{-3i\frac{\omega}{2}} + e^{3i\frac{\omega}{2}} + 2e^{i\frac{\omega}{2}}\right.\right.$$

$$\left. -2e^{-3i\frac{\omega}{2}} - e^{-5i\frac{\omega}{2}}\right) + \sqrt{10}\left(e^{5i\frac{\omega}{2}} + 2e^{3i\frac{\omega}{2}} - 2e^{-i\frac{\omega}{2}}\right.$$

$$\left.\left. -e^{-3i\frac{\omega}{2}} - e^{3i\frac{\omega}{2}} - 2e^{i\frac{\omega}{2}} + 2e^{-3i\frac{\omega}{2}} + e^{-5i\frac{\omega}{2}}\right)\right]\alpha(\omega). \quad \text{(A6.76)}$$

We still have to add the term $\cos^3\frac{\omega}{2}\cos^2\frac{\omega}{2}$ of (E.8), then multiply by the phase factor $\gamma(\omega)$.

$$\cos^3\frac{\omega}{2}\cos^2\frac{\omega}{2} = \cos^5\frac{\omega}{2} = \left[\frac{e^{i\frac{\omega}{2}} + e^{-i\frac{\omega}{2}}}{2}\right]^5$$

$$= \frac{1}{32}\left[e^{5i\frac{\omega}{2}} + 5e^{3i\frac{\omega}{2}} + 10e^{i\frac{\omega}{2}} + 10e^{-i\frac{\omega}{2}} + 5e^{-3i\frac{\omega}{2}} + e^{-5i\frac{\omega}{2}}\right] \tag{A6.77}$$

after a long multiplication.

Now we add (A6.77) to the result in (A6.76) and multiply by $\gamma(\omega)$ to get $p(\omega)$. During that addition, we collect similar terms involving $e^{5i\frac{\omega}{2}}, e^{3i\frac{\omega}{2}}, e^{i\frac{\omega}{2}}, e^{-i\frac{\omega}{2}},\ e^{-3i\frac{\omega}{2}}$, and $e^{-5i\frac{\omega}{2}}$. We will arrange the result to start with $e^{5i\frac{\omega}{2}}$, then we choose $\gamma(\omega) = e^{-5i\frac{\omega}{2}}$ to have the first term as the coefficient of 1 for the polynomial $P_5(z)$ in Eq. (A6.1); hence, h_0 the first of six coefficients of ϕ_{D3},

$$\begin{aligned} p(\omega) = \frac{1}{2}\Bigg[& \frac{\sqrt{5}+\sqrt{10}+1}{16}e^{5i\frac{\omega}{2}} + \frac{3\sqrt{3}+\sqrt{10}+5}{16}e^{3i\frac{\omega}{2}} + \\ & \frac{2\sqrt{5}-2\sqrt{10}+10}{16}e^{i\frac{\omega}{2}} + \frac{-2\sqrt{5}-2\sqrt{10}-10}{16}e^{-i\frac{\omega}{2}} \\ & + \frac{-3\sqrt{5}+3\sqrt{10}+5}{16}e^{-3i\frac{\omega}{2}} + \frac{-\sqrt{5}+\sqrt{10}+1}{16}e^{-5i\frac{\omega}{2}}\Bigg]\gamma(\omega). \end{aligned} \tag{A6.78}$$

We let $\gamma(w) = e^{-5i\frac{\omega}{2}}$,

$$\begin{aligned} p(\omega) = \frac{1}{2}\Bigg[& \frac{\sqrt{5}+\sqrt{10}+1}{16} + \frac{3\sqrt{3}+\sqrt{10}+5}{16}e^{-2i\frac{\omega}{2}} \\ & + \frac{2\sqrt{5}-2\sqrt{10}+10}{16}e^{-4i\frac{\omega}{2}} + \frac{-2\sqrt{5}-2\sqrt{10}-10}{16}e^{-6i\frac{\omega}{2}} \\ & + \frac{-3\sqrt{5}+3\sqrt{10}+5}{16}e^{-8i\frac{\omega}{2}} + \frac{-\sqrt{5}+\sqrt{10}+1}{16}e^{-10i\frac{\omega}{2}}\Bigg] \end{aligned} \tag{A6.79}$$

$$\begin{aligned} p(\omega) = \frac{1}{2}\Bigg[& \frac{\sqrt{5}+\sqrt{10}+1}{16} + \frac{3\sqrt{3}+\sqrt{10}+5}{16}z \\ & + \frac{2\sqrt{5}-2\sqrt{10}+10}{16}z^2 + \frac{-2\sqrt{5}-2\sqrt{10}-10}{16}z^3 \\ & + \frac{-3\sqrt{5}+3\sqrt{10}+5}{16}z^4 + \frac{-\sqrt{5}+\sqrt{10}+1}{16}z^5\Bigg], \end{aligned} \tag{A6.80}$$

where $z = e^{-i\omega}$.

Now, we equate coefficients of the similar powers of z with $P_5(z)$ of Eq. (A6.1),

$$P_5(z) = \sum_{k=0}^{5} \frac{1}{\sqrt{2}} h_k = \frac{1}{\sqrt{2}}\left[h_0 + h_1 z + h_2 z^2 + h_3 z^3 + h_4 z^4 + h_5 z^5\right]. \tag{A6.81}$$

Hence,

$$\begin{aligned} h_0 &= \frac{\sqrt{5}+\sqrt{10}+1}{16\sqrt{2}}, \quad h_1 = \frac{3\sqrt{5}+\sqrt{10}+5}{16\sqrt{2}}, \\ h_2 &= \frac{2\sqrt{5}-2\sqrt{10}+10}{16\sqrt{2}}, \quad h_3 = \frac{-2\sqrt{5}-2\sqrt{10}+10}{16\sqrt{2}}, \\ h_4 &= \frac{-3\sqrt{5}+3\sqrt{10}+5}{16\sqrt{2}}, \quad h_5 = \frac{-\sqrt{5}+\sqrt{10}+1}{16\sqrt{2}}. \end{aligned} \tag{A6.82}$$

Consider the following two functions:

$$\begin{aligned} lclx_1(t) &= 1 - |t| \quad -1 \le t \le 1 \\ &= 0 \quad otherwise \end{aligned} \tag{A6.83}$$

$$\begin{aligned} lclx_2(t) &= e^{-t} \quad t \ge 0 \\ &= 0 \quad otherwise \end{aligned} \tag{A6.84}$$

In Section (6.2), we saw impulse response of Daubechies analysis low pass filter. We also saw why the zero inside the circle was selected during the filter design. The following section provides simulation based understanding of the same concept.

A6.4 | Impact of location of zeros

It should be noted that location of zeros impact the speed of the system. They do NOT have direct impact on the stability of the system. As can be seen from Figure A6.1, the system zeros are inside unit circle. The phase is low and hence the delay is less.

As zeros are on the unit circle as shown in Figure A6.2, the phase increases thus increasing the delay. With zeros outside the unit circle as shown in Figure A6.3, the phase further increases making the system further sluggish. Readers should note that the impulse response in converging for Figures A6.1, A6.2 and A6.3 ensuring the stability of the system. Thus, positioning of zeros does NOT impact system stability and it mainly affects the response time of the system.

The positioning of poles affect the system stability though. From the basic text on DSP we know that with poles inside unit circle systems are stable, with poles on the unit circle the systems are marginally stable (or unstable in strict sense) and for system poles outside the unit circle the systems have diverging impulse response and these are unstable systems.

Chapter 6 also discussed the importance of moving from Haar to Daub-x with added filter coefficients. Following MATLAB simulation depicts the same.

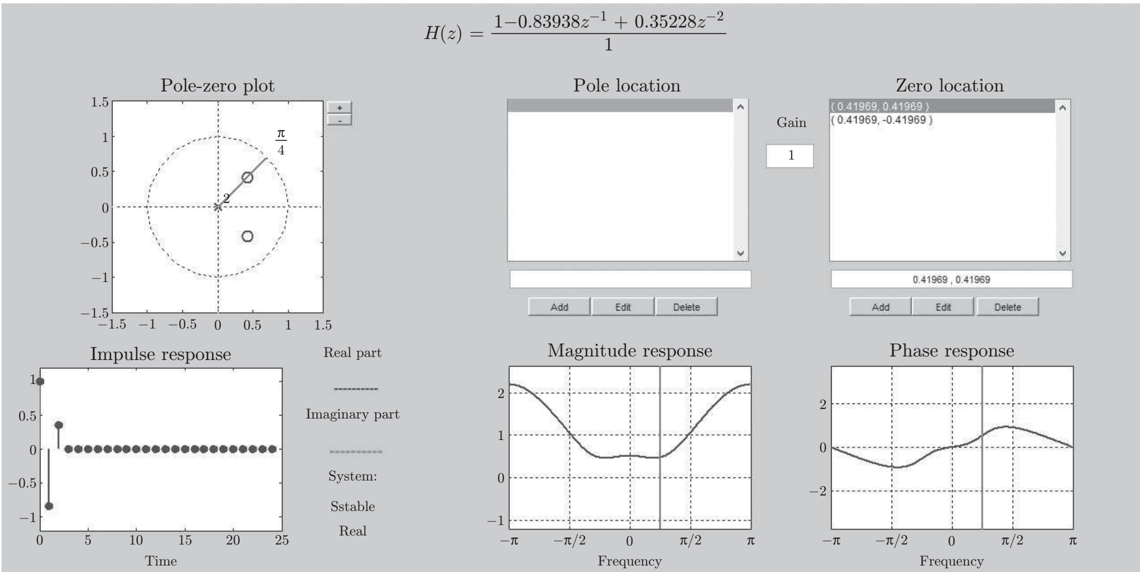

Figure A6.1 | *Impact of zeros inside unit circle*

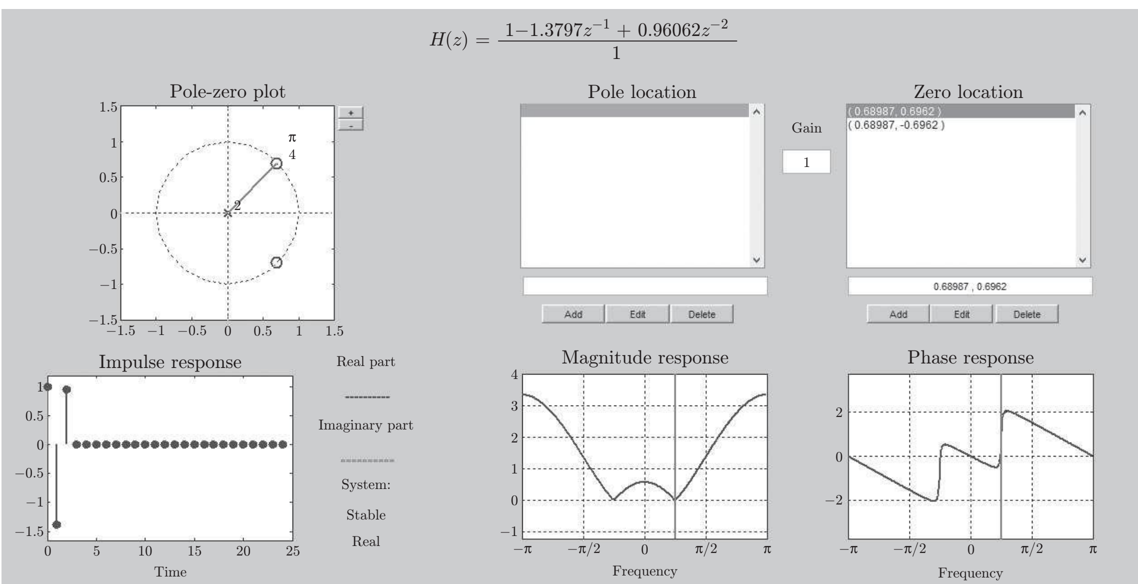

Figure A6.2 | *Impact of zeros almost on the unit circle*

A6.5 | Moving from Haar to Daub-x

Readers will remember that Haar is the only orthogonal filter with compact support and linear phase, however the frequency response of the Haar was too far away from an ideal response. That is why we wanted to add filter coefficients and hoped to improve upon the frequency response thus trying to get closer to the ideal response. We shall examine that through the following MATLAB code (Example A6.4).

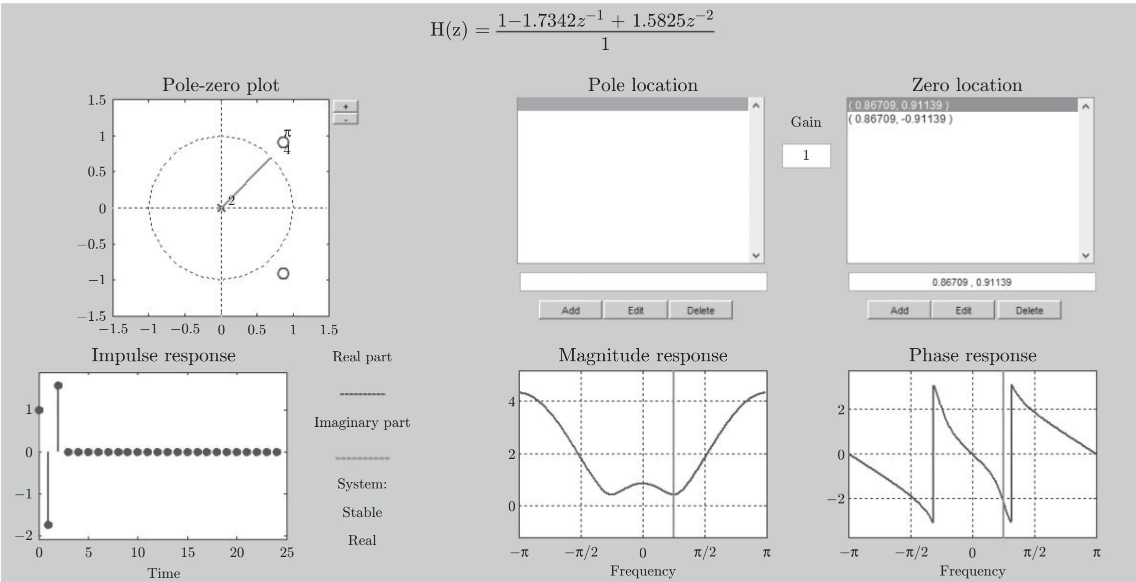

Figure A6.3 | *Impact of zeros outside unit circle*

Example A6.4 — MATLAB code: Analysis LPF responses.

```
%************************************************
%************************************************
% MATLAB code to understand Analysis LPF Response
% Haar Vs DB4: To be accompanied with book on
% Multiresolution and Multirate Signal Processing
% by Dr V M Gadre and Dr A S Abhyankar
%************************************************
%************************************************

clear all;clc;close all;
% h3=.4829;
% h2=-.8364;
% h1=.2241;
% h0=.129;

h0=.4829; h1=.8364; h2=.2241; h3=-.129;

figure(1);
%subplot(2,1,1);
for w=0:0.005:pi,
    y=abs(h0+h1*exp(-i*w)+h2*exp(-i*2*w)+h3*exp(-i*3*w));
```

```
    plot(w,y);
    hold on;
end title('MAGNITUDE RESPONSE OF ANALYSIS LPF');
%subplot(2,1,2);
for w=0:0.005:pi,
    %y=((pi/2)-(w/2));
    y=cos(w/2);
    plot(w,y);
    hold on;
end title('MAGNITUDE RESPONSE OF ANALYSIS LPF');


% subplot(3,1,3);
% for w=0:0.005:pi,
%     y1=abs(1+(-2)*exp(-i*w)+(-6)*exp(-i*2*w)+(-2)*exp(-i*3*w)+1*exp(-i*4*w));
%     plot(w,y1);
%     hold on;
% end
% title('Magnitude RESPONSE OF 5/3 ANALYSIS LPF');
```

The output produced by MATLAB code above is shown in Figure A6.4. It cab be observed that Db4 response is better than Haar and it shown pattern to move towards ideal response by adding more and more filter coefficients.

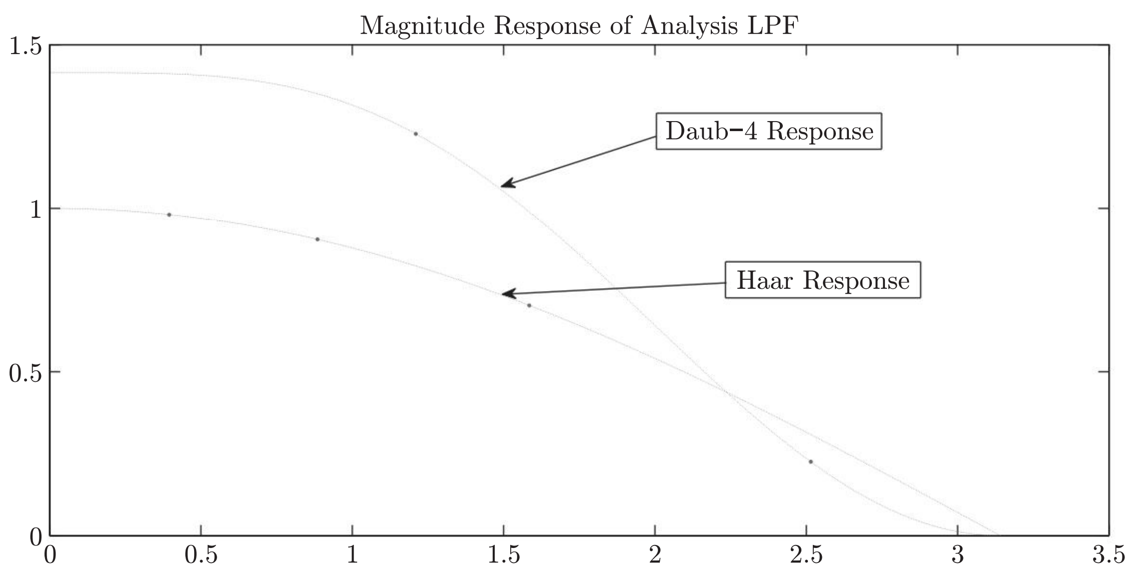

Figure A6.4 | *Comparison between Haar and Db4 Analysis LPF magnitude response*

Extended Notes for Chapter 7

A7.1 | Hybrid Filter Bank

Now lets look at some of the variants of the two-band filter bank. This time not just the two-band filter bank but also the hybrid filter bank where we have a three-band and two-band combination, as shown in Fig. A7.1.

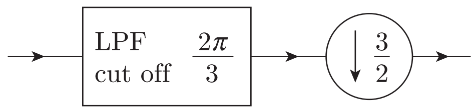

Figure A7.1 | *Hybrid filter bank*

We can interpret the operation $\downarrow \dfrac{3}{2}$ as two separate operations down-sampling by 3 and up-sampling by 2. The problem is downsampling operation is not reversible whereas upsampling operation is reversible.

Therefore we first do the upsampling by 2 and then downsampling by 3. Thus the loss is incurred at the end only. The reader can do calculations on exactly similar lines as 2-band structures.

A7.2 | Wavelet Transform Hallmarks - Tutorial

Scaling and Translation parameters of wavelet transform lead us to Multi Resolution Analysis (MRA). Firstly MRA involves Piecewise constant approximation on UNIT intervals given by scaling equation. Secondly it involves filling in details i.e. zooming in or loosing details i.e. zooming out using wavelet eqaution. In case of a signal we need to zoom in to a particular part of a signal for the purpose of analysis. For example, consider a case of ECG signal. Suppose we have a large recording of one hour and if only few samples show abnormality then we should be only able to focus on that part only. Hence the property of zooming in and zooming out is of great importance.

A7.3 | How to Realize Zoom in and Zoom out Feature?

Let us define a linear space, $V_0 = x(t)$ such that, $x(.)$ belongs to $L2(R)$.

Where,
$L2(R)$-space of square integrable functions
$x(.)$-piecewise constant on all $]n, n+1[$

For the space V0 the analysis window would be $2^0 = 1$.

Similarly let us define a space V_1 $V_1 = x(t)$ such that, x(.) belongs to $L2(R)$.

Where,
$L2(R)$-space of square integrable functions
$x(.)$-piecewise constant on all $]2^{-1}n, 2^{-1}n+1[$

As we can see for the space V_1 the analysis window is be 2^{-1}.
Similarly we can define $V_2, V_3, ...$

In general we can define, Vm=x(t) such that, x(.) belongs to L2(R).

Where,
$L2(R)$-space of square integrable functions
$X(.)$-piecewise constant on all $]2^{-}mn, 2^{-}mn+1[$

For the space V0 the analysis window would be 2^{-m}.

This leads us to a relationship called as nested subset. If we move up the window the analysis window becomes smaller and we would go on adding the detail and would eventually reach $L2(R)$. Similarly if we move down the ladder the resolution shall become coarser and coarser and we would reach a trivial subspace containing no details.
Moving up we can write,

$$\overline{\bigcup_{m\in Z} V_m = L2(R)} \tag{A7.1}$$

Moving down we can write,

$$\bigcap_{m\in Z} V_m = 0 \tag{A7.2}$$

The most important thing about wavelets is that we can be talking about a function and its projection in any subspace which can be neatly constructed using just one single function, i.e. $\psi(t)$. We can do this using hallmarks of wavelet transform i.e. scaling, translation and also dilation. This would span W subspaces but V subspaces would be spanned by scaling function $\phi(t)$ shown in Figure A7.2.

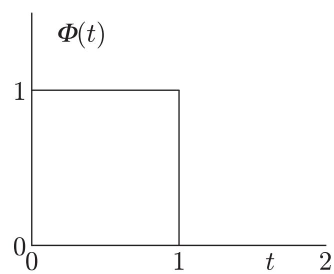

Figure A7.2 | *Haar* $\phi(t)$

The purpose of having a scaling function is to span that particular subspace V_m. This guarantees the generation of ladder of subspaces which in turn leads us to MRA.

Let's have a look at axioms of this MRA,

1. $\bigcup V_m \approx L2(R)$
2. $\bigcap_{m\in Z} V_m = 0$
3. There exists a $\phi(t)$ such that, $V_m = span_{n\in Z}\phi(2^m t - n)$.
4. $\phi(t-n)_{n\in Z}$ is an orthogonal set.
5. If, $f(t)\in V_m$, then $f(2^{-m}t)\in V_0, \forall m \in Z$
6. If, $f(t)\in V_0$, then $f(t-n)\in V_0, \forall n \in Z$

There also exists a MRA theorem which states,
Given these axioms there exists $\psi(.) \in L2(R)$, such that $\{\psi(2^{-m}t-n)\}$ span $L2(R)$
One way of realizing MRA can be a two-band filter bank shown in Figure A7.3.

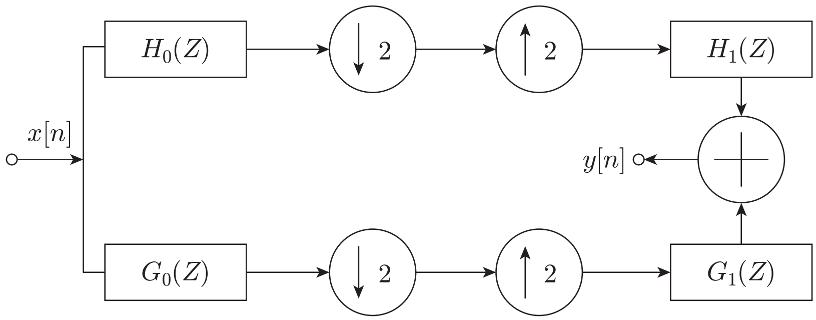

Figure A7.3 | *Two-band filter bank*

However, major drawback of two-band filter bank is that we end up moving down the ladder and loosing information. But in many application moving up ladder is required.

A7.4 | Vanishing Moments Significance - Tutorial

Now, since many a times we are interested in detecting spike or jumps discontinuities in the signal. We would like to know what kind of wavelets will be able to detect such activities. To find such wavelets which see discontinuities in linear, quadratic or higher order polynomial structures we would will first understand the concept of maximum order of vanishing moments.
Moments:
The moment of order m, M_m of f(x) on interval (a,b) is given as,

$$M_m = \int_a^b x^m f(x)dx \tag{A7.3}$$

From the above equation we can find the moment of order m, for $m = 0,1,2,...$

When these moments of higher order vanish, they convey important information regarding underlying wavelet. We would analyze this fact but before that first let's solve a problem with Haar wavelet to understand that these moments actually vanish. Let $\psi(x)$ denote Haar which is same as daub1. Its first order moment would be,

$$M_0 = \int_0^1 x^0 \psi(x)dx$$

$$M_0 = \int_0^{1/2} 1dx + \int_{1/2}^1 -1dx$$

$$M_0 = x\Big|_0^{1/2} + x\Big|_{1/2}^1$$

$$M_0 = 0$$

Thus, we can say that 0^{th} moment of the Haar mother wavelet vanishes. Let us check for 1^{st} order moment.

$$M_1 = \int_0^1 x^1 \psi(x) dx$$

$$M_1 = \int_0^{1/2} x dx + \int_{1/2}^1 - x dx$$

$$M_1 = \frac{x^2}{2}\Big|_0^{1/2} + \frac{x^2}{2}\Big|_{1/2}^1$$

$$M_1 = \frac{-1}{4} \neq 0$$

Thus, we can say that 1^{st} moment of the Haar mother wavelet does not vanish. Also as far as Haar mother wavelet is concerned it has only one moment i.e. o^{th} moment which vanishes.

Extended Notes for Chapter 8

A8.1 | Uncertainty Product

There is a bound on simultaneous time and frequency localization. So essentially one cannot localize as much as one wants simultaneously in time and frequency.

One can define for time centered function $x(t)$, time variance

$$\sigma_t^2(x) = \frac{\| tx(t) \|_2^2}{\| x(t) \|_2^2}$$

Recall meaning of time center, time center

$$t_0 = \int \frac{t \mid x(t) \mid^2}{\| x(t) \|_2^2} dt$$

By time centered, we mean $t_0 = 0$.

Similarly for frequency, frequency center or frequency mean

$$\Omega_0 = \int \frac{\Omega \mid \hat{x}(\Omega) \mid^2}{\| \hat{x}(\Omega) \|_2^2} d\Omega$$

By frequency centered, we mean $\Omega_0 = 0$.

Analogous to time variance, for frequency centered function $\hat{x}(\Omega)$ frequency variance

$$\sigma_\Omega^2(x) = \frac{\| \Omega \hat{x}(\Omega) \|_2^2}{\| \hat{x}(\Omega) \|_2^2}$$

If function is not time centered and frequency centered then one need to take second moment around respective centers.

For an $L_2(\mathbb{R})$ function the uncertainty product i.e. product of time and frequency variance is lower bounded by 0.25.

$$\sigma_t^2(x).\sigma_\Omega^2(x) \geq \frac{1}{4}$$

Example A8.1 — Calculate uncertainty product of $e^{-|t|}$ for all t.

Solution First we need to verify if the function is $L_2(\mathbb{R})$ and check if it is centered in time and frequency.

$$\| x(t) \|_2^2 = \int_{-\infty}^{+\infty} | x(t) |^2 \, dt$$

$$\| x(t) \|_2^2 = 2\int_0^{+\infty} e^{-2t} dt$$

$$\| x(t) \|_2^2 = 1$$

From Figure A8.1 one can clearly say that $x(t)$ is symmetric about $t = 0$ and is a real and even function of t. Since it real and even function in time domain it should have real and even fourier transform too. So obviously the function $x(t)$ is time and frequency centered.

Time variance σ_t^2:

$$\sigma_t^2(x) = \frac{\int_{-\infty}^{+\infty} t^2 \, | x(t) |^2 \, dt}{\int_{-\infty}^{+\infty} | x(t) |^2 \, dt} = 2\int_0^{+\infty} t^2 e^{-2t} dt = \frac{1}{2}$$

Frequency variance σ_Ω^2:

$$\sigma_\Omega^2(x) = \frac{\| \Omega \hat{x}(\Omega) \|_2^2}{\| \hat{x}(\Omega) \|_2^2}$$

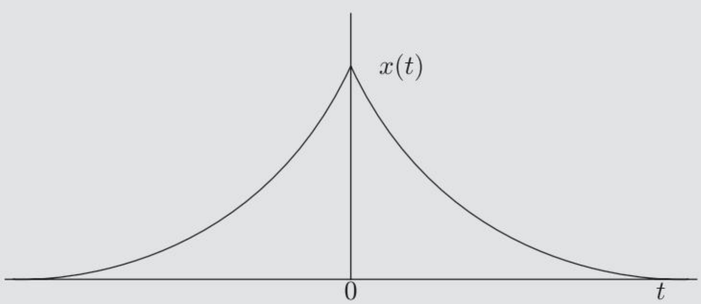

Figure A8.1 | *x(t) curve*

$$\sigma_{\Omega}^{2}(x) = \frac{\| j\Omega\hat{x}(\Omega) \|_2^2}{\| \hat{x}(\Omega) \|_2^2}$$

By applying Parseval's Theorem it becomes

$$\sigma_{\Omega}^{2}(x) = \frac{\left\| \dfrac{dx(t)}{dt} \right\|_2^2}{\| x(t) \|_2^2}$$

Now

$$x(t) = e^{-|t|}$$

So

$$\left\| \frac{dx(t)}{dt} \right\|_2^2 = \| x(t) \|_2^2$$

$$\sigma_{\Omega}^{2}(x) = 1$$

Uncetrtainty Product:

$$\sigma_t^2(x).\sigma_{\Omega}^2(x) = \frac{1}{2} * 1$$

$$\sigma_t^2(x).\sigma_{\Omega}^2(x) = 0.5(> 0.25)$$

Example A8.2 — Calculate uncertainty product of raised cosine function.

Solution

$$x(t) = 1 + \cos t \quad -\pi < t < \pi = 0 \quad \text{otherwise}$$

From Figure A8.2 it is clear that the function $x(t)$ is real and even, so it is already time and frequency centered. Since the function is real and even, hence

$$\| x(t) \|_2^2 = \int_{-\infty}^{+\infty} | x(t) |^2 \, dt$$

$$= 2\int_{0}^{+\infty} | x(t) |^2 \, dt$$

$$= 2\int_{0}^{\pi} (1 + \cos t)^2 \, dt$$

$$= 2\int_{0}^{\pi} (1 + \cos^2 t + 2\cos t) dt$$

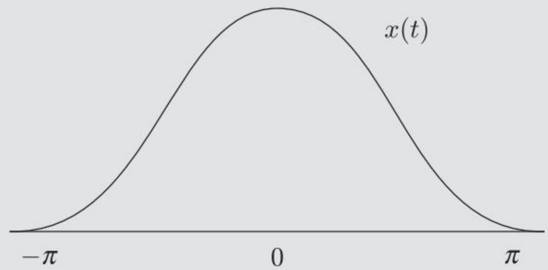

Figure A8.2 | *x(t) = 1 + cos(t)*

Consider

$$\int (1+\cos^2 t + 2\cos t)dt = \int (1 + \frac{1+\cos 2t}{2} + 2\cos t)dt$$

Now let us sketch $\cos t$ and $\cos 2t$

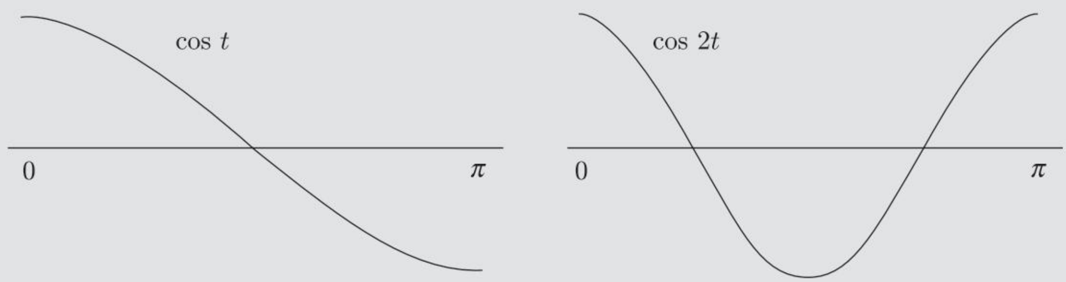

Figure A8.3 | *cos(t) and cos(2t) curves*

From Figure A8.3 it is clear that they have zero integral over $]0,\pi[$
So the above integral becomes

$$\| x(t) \|_2^2 = 2\int_0^{\pi} (1 + \frac{1}{2})dt = 3\pi$$

Frequency variance σ_Ω^2:

$$\sigma_\Omega^2(x) = \frac{\left\| \frac{dx(t)}{dt} \right\|_2^2}{\| x(t)_2^2 \|}$$

Now

$$\frac{d}{dt}x(t) = \frac{d}{dt}(1+\cos t) = -\sin t$$

$$\left\|\frac{dx(t)}{dt}\right\|_2^2 = 2\int_0^{\pi}\sin^2 t dt$$
$$= \int_0^{\pi}(1-\cos 2t)dt$$
$$= \pi$$

So frequency variance $\sigma_\Omega^2 = \frac{1}{3}$

Time variance σ_t^2:

We need

$$\int t^2 |x(t)|^2 dt = \int t^2 (1+\cos t)^2 dt$$
$$= \int t^2\left(1+\frac{1+\cos 2t}{2}+2\cos t\right)dt$$

Let us consider the term

$$\int t^2 \cos mt dt$$
$$= t^2\frac{\sin mt}{m} + 2t\frac{\cos mt}{m^2} - 2\frac{\sin mt}{m^3}$$

Now our limit is 0 to π, therefore we do not need to look at the 'sin' term which are zero at $t = 0$ and $t = \pi$. Again we do need terms containing 't' at $t = 0$. We need only consider the term $2t\frac{\cos mt}{m^2}\Big|_0^{\pi}$

For m=1, $2t\cos t|_0^{\pi} = 2\pi\cos\pi = -2\pi$

For m=2, $2t\frac{\cos t}{4}\Big|_0^{\pi} = 2\pi\frac{\cos 2\pi}{4} = 0.5\pi$

Putting these values in above equation

$$\int_0^{\pi} t^2\left(1+\frac{1+\cos 2t}{2}+2\cos t\right)dt = \int_0^{\pi}1.5t^2 dt + \int_0^{\pi} t^2\frac{\cos 2t}{2}dt + 2\int_0^{\pi} t^2\cos t dt$$
$$= \frac{\pi^3}{2} + \frac{\pi}{4} - 4\pi$$

Time variance σ_t^2

$$\sigma_t^2 = \frac{2\int_0^{\pi} t^2 |x(t)|^2 dt}{2\int_0^{\pi}(1+\cos t)^2 dt}$$

$$\sigma_t^2 = \frac{\pi^2}{3} - \frac{5}{2}$$

Uncertainty Product:

$$\sigma_t^2(x).\sigma_\Omega^2(x) = \left(\frac{\pi^2}{3} - \frac{5}{2}\right) * \frac{1}{3}$$

$$\sigma_t^2(x).\sigma_\Omega^2(x) = \frac{\pi^2}{9} - \frac{5}{6}(> 0.25)$$

Extended Notes for Chapter 9

The tiling planes on x-axis of time and y-axis of frequency (continuous or discrete) is the best way to picturise and understand the exact meaning of dealing with uncertainty principle and how the journey takes one from Fourier to Short term Fourier to Wavelets. In fact the Frequency tailings are called as 'Heisenberg Boxes' and they do not provide any time domain resolution. The Heisenberg's uncertainty principle in signal processing in captured by the the time bandwidth product and the fact that it remains greater than or equal to half for any slice of Heisenberg Box. This is shown in Figure A9.1, where (A) shows the time bandwidth product limitation and (B) depicts the Heisenberg Boxes in Fourier or Frequency domain. These boxes also indicate no resolution for from perspective of 'time'.

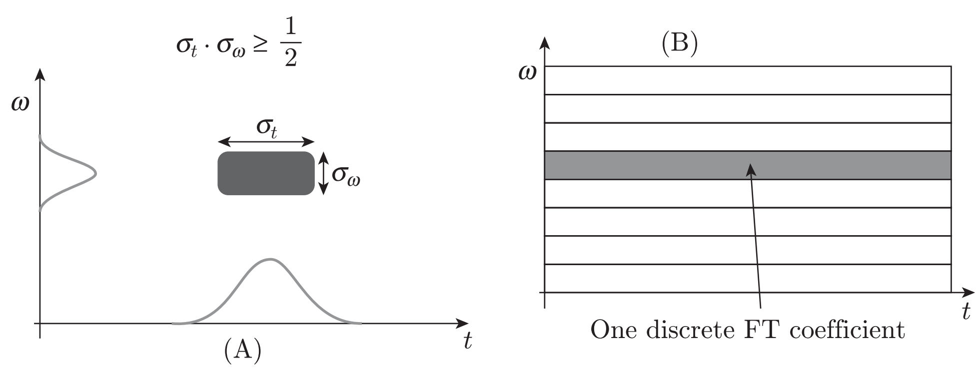

Figure A9.1 | *Time frequency tiling: heisenberg boxes*

If the DFT (Discrete Fourier Transform) of signal $x[n]$ is given as,

$$X[k] = \sum_{n=0}^{N-1} x[n]e^{\frac{-j2\pi nk}{N}} \tag{A9.1}$$

then, from the frequency perspective $\Delta\omega = \dfrac{2\pi}{N}$ and from the time perspective $\Delta t = N$. Then the product $\Delta\omega \cdot \Delta t = 2\pi$ is limiting.

Figure A9.2 shows the STFT tiling in part (A). Part (B) shows that a single resolution of wavelet (shown Haar example) gives the timing like DFT without resolution advantages for time stamps.

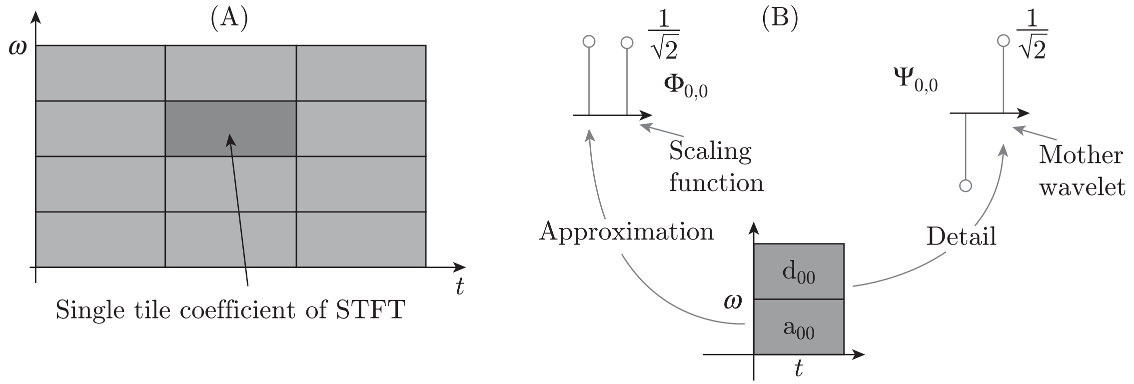

Figure A9.2 | *Time frequency tiling: STFT*

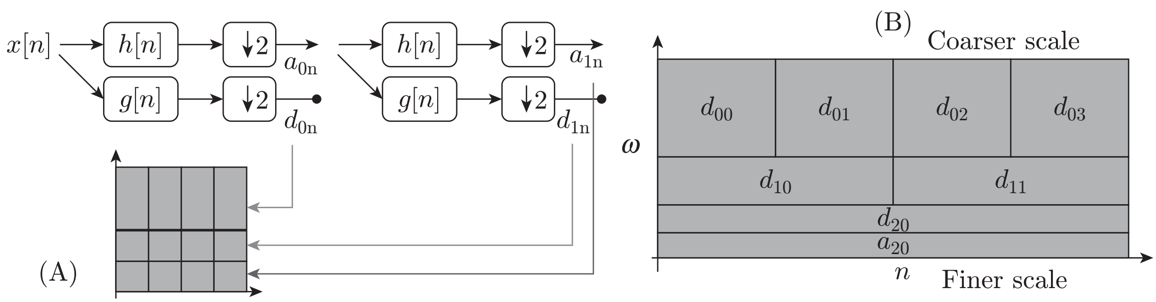

Figure A9.3 | *Time frequency tiling: wavelet style*

The wavelet style of tiling is shown in Figure A9.3. The scaling and dilation are the hallmarks of wavelet transform and they truly bring in the time resolution. The added scale brings time resolution as shown in (A) and the ladder gets formed across resolutions as shown in (B).

Extended Notes for Chapter 10

In Chapter 10 we discussed Dyadic MRA. The concept was first put forth by Stephan Mallat!

Stephane Mallat

Stephane Mallat (born 1962 in Paris France) made fundamental contributions is design and development of MRA (MultiResolution Analysis) framework in late 80's and early 90's. Particularly his association with Yves Meyer made use of wavelets practical and many fields of engineering got benefitted. Mallat is the author of A Wavelet Tour of Signal Processing. He taught course at New York University, Massachusetts Institute of Technology, etc.

Extended Notes for Chapter 11

In Chapter 11 we have discussed the bi-orthogonal filters which are faster to deploy and have become part of many standards. Dr. Charles Chui has contributed in the advancements in this part of wavelet theory.

Charles K Chui

Charles K Chui is affiliated with Stanford University and Hong Kong Baptist University currently. Charles played a leading role in technology innovations, by applying mathematics to industrial applications, with other contributions that include development of two industry standards: JPEG-2000 and MPEG-4, as well as several inventions with 38 U.S. patents. He has written more than 350 journal articles and 30 books. He co-founded ACHA with Daubechies and Coifman.

Extended Notes for Chapter 12

The B-spline complex wavelet can be a very good choice for many practical applications. The MATLAB code is modified from the toolbox and presented here:

Example 12.1 — MATLAB code for complex B-Spline wavelet.

```
%************************************************
%************************************************
% MATLAB code to generate Complex Frequency B-Spline
% Wavelet: To be accompanied with book on
% Multiresolution and Multirate Signal Processing
% by Dr V M Gadre and Dr A S Abhyankar
%************************************************
%************************************************
% This is modified from the MATLAB toolbox

% We Set order, bandwidth and center frequency parameters.
m = 3; fb = 0.5; fc = 1.5;
% The filter will have:
% Order: 3, Central Frequency: 1.5, Bandwidth: 0.5
% Set effective support and grid parameters.
lb = -20; ub = 20; n = 1000;
```

```
% Compute complex Frequency B-Spline wavelet fbsp-3-0.5-1.5.
[psi,x] = fbspwavf(lb,ub,n,m,fb,fc);

% Plot complex Frequency B-Spline wavelet.
subplot(211) plot(x,real(psi)) title('Complex Frequency B-Spline
wavelet fbsp-3-0.5-1.5') xlabel('Real part of filter
fbsp-3-0.5-1.5'), grid subplot(212) plot(x,imag(psi))
xlabel('Imaginary part of filter fbsp-3-0.5-1.5'), grid

%End
```

The generated filter is shown in Figure A12.1.

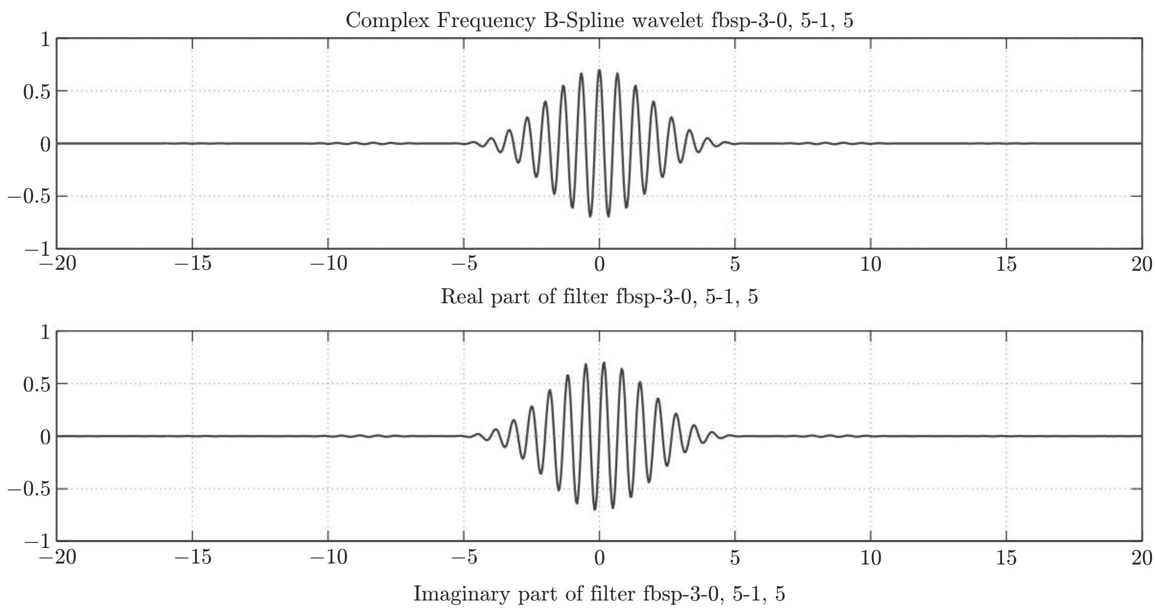

Figure A12.1 | *Complex B-spline wavelet with real and imaginary parts of the filter*

Extended Notes for Chapter 13

Wavelet packet transform gives the analyzer the flexibility to also split the signal on the high pass branch. For this to happen, however we need to evolve the basis function and the new bases do the job for us. We have discussed this in detail in Chapter 13. Splitting up on low pass as well as high pass branch may create a huge tree with many nodes not depicting the important information. This leads to redundancy and there are different criteria to select best basis to utilize the tree optimally. The one which many researchers prefer is use of Shannon entropy to decide upon the best basis.

One example of time frequency plot for the selected best basis is shown in Figure A13.1. The implementation scheme for the same selected best basis is shown in Figure A13.2.

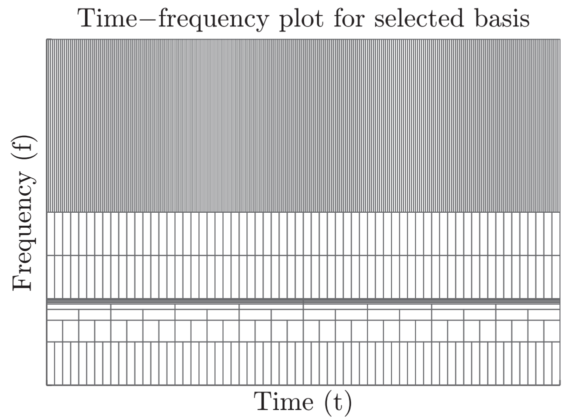

Figure A13.1 | *The time-frequency plot for the selected best basis*

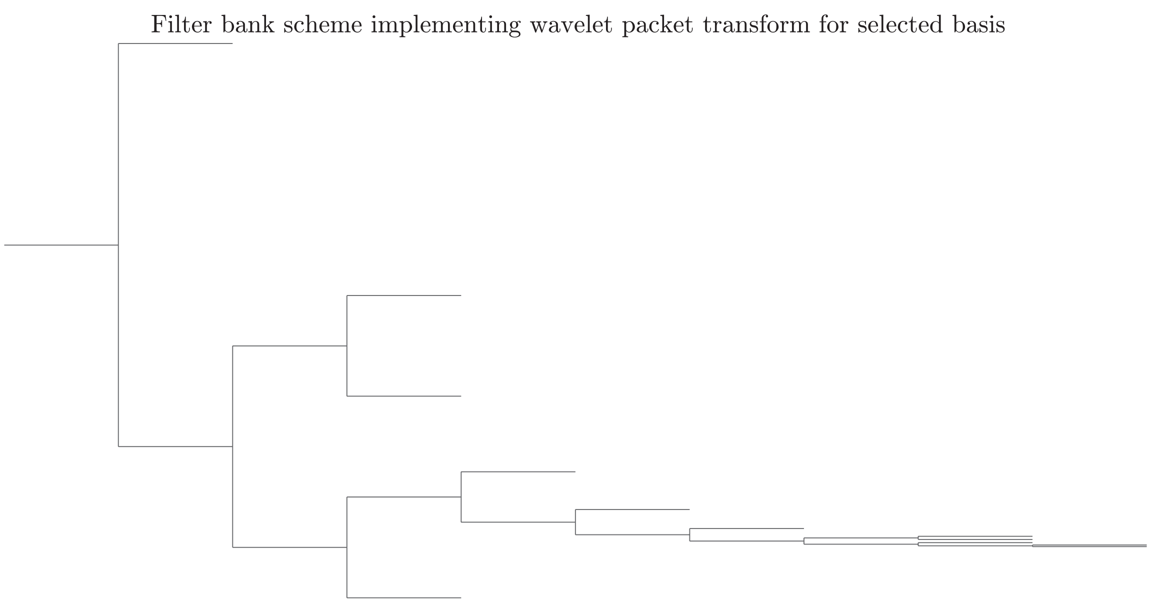

Figure A13.2 | *The filter bank implementation for the selected best basis*

Extended Notes for Chapter 14

We saw lifting scheme in Chapter 14. The in-place calculations are shown in the section below:

A14.1 | In-place Lifting Calculations

Example: Provide in-place lifting calculations for Haar decomposition and reconstruction for given signal.

$$x[n] = \{6,8,4,2\}$$

$$h_k = \{1,1\}$$

$$g_k = \left\{\frac{1}{2}, \frac{-1}{2}\right\}$$

And also shows that structure is statistically stable & Perform reverse calculations to show perfect reconstruction.

Answer:

Typical lifting scheme can be implemented as follows:

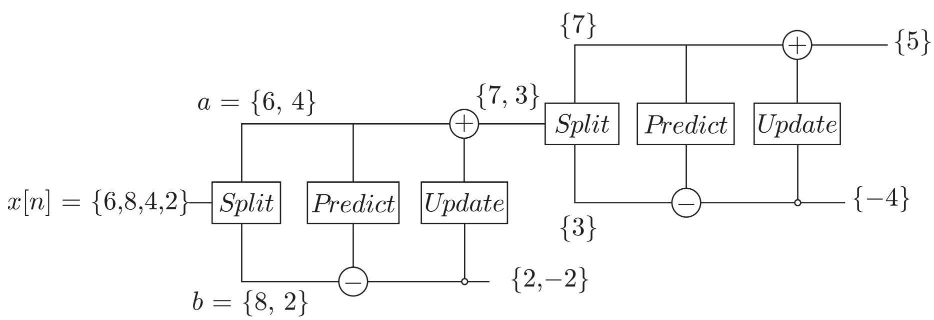

The reverse calculations are as follows:

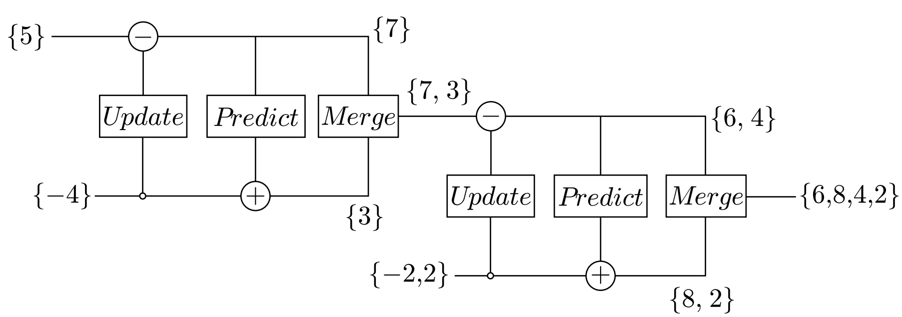

Formulae:

$$s = a + d/2 \ (LPF) \ \therefore \ \textit{replace 'a' by 's'}$$

$$d = b - a \ (HPF) \ \therefore \ \textit{replace 'b' by 'd'}$$

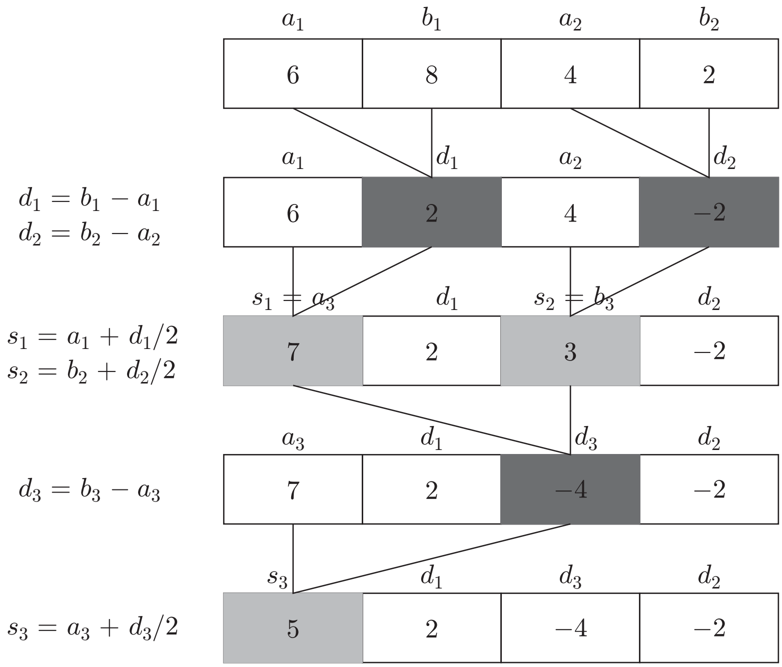

Reconstruction:

$s = a + d/2 \therefore a = s - d/2$, replace '$s$' by '$a$'
$d = b - a \therefore b = a + d$, replace '$d$' by '$b$'

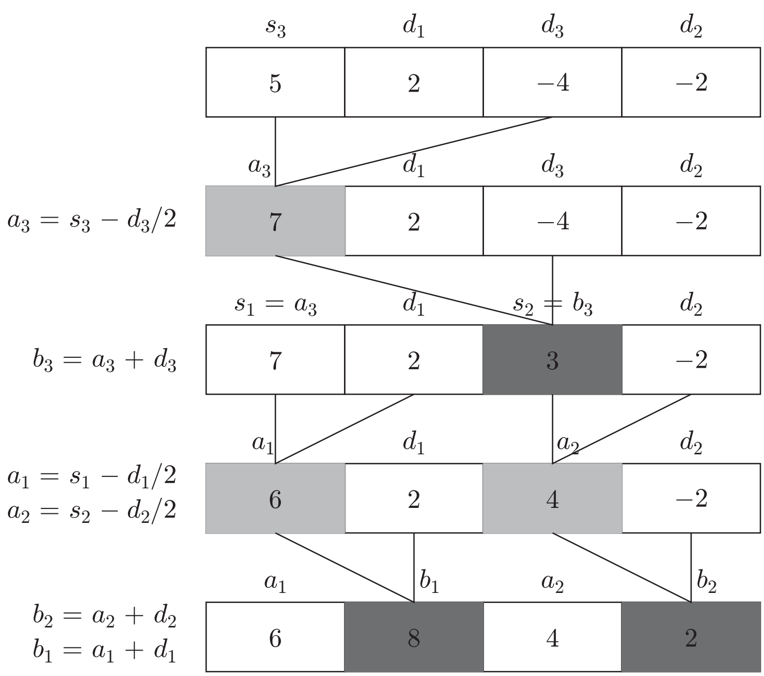

Extended Notes for Chapter 15

In Chapter 15 we saw different Wavelet families. In the following MATLAN example we shall visualize the Gabor filter.

Example A15.1 — MATLAB Code to visualize Gabor filters.

```
%************************************************
%************************************************
% MATLAB code to generate visualize Gabor
% Filters: To be accompanied with book on
% Multiresolution and Multirate Signal Processing
% by Dr V M Gadre and Dr A S Abhyankar
%************************************************
%************************************************
% This is modified from the MATLAB toolbox
% We Set wavelength and orientation of filter.
clc; clear all; close all;

g = gabor([5 10],[0 90]);

figure (1);
%subplot(2,2,1)

for p = 1:length(g)
    subplot(2,2,p);
    imshow(real(g(p).SpatialKernel),[]);
    lambda = g(p).Wavelength;
    theta  = g(p).Orientation;
    title(sprintf('Re[h(x,y)], \\lambda = %d, \\theta = %d',lambda,theta));
end
```

The filters are visualized as shown in Figure A15.1. The λ values indicate the wavelength and θ values indicate the orientation. The visualization helps us understand that Gabor filters are powerful in capturing the oriented information. θ values can vary from 0 to 180.

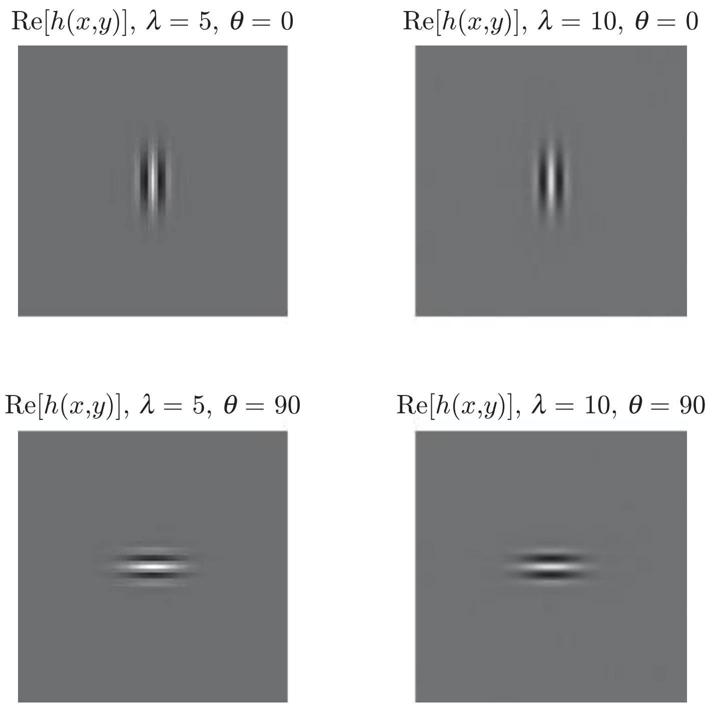

Figure A15.1 | *Gabor filter visualization*

Extended Notes for Chapter 16

In Chapter 16 we discussed many interesting points. The readers who are advanced users of wavelets techniques can explore the techniques further. For example, self-similar structures in wavelets can bring out many interesting applications. This self similarity can be observed in scaling functions $\phi(.)$ as well as wavelet functions $\psi(.)$. Interested users can create the *db*2 filter using

```
[phi,psi,t]=wavefun('db2',10);
```

and then plot the respective filters using

```
plot(t,phi);
```

and

```
plot(t,psi);
```

Then by zooming onto appropriate parts users can study the self-similarity. This is depicted in Figure A16.1 for db2 scaling function and in Figure A16.2 for db2 wavelet function.

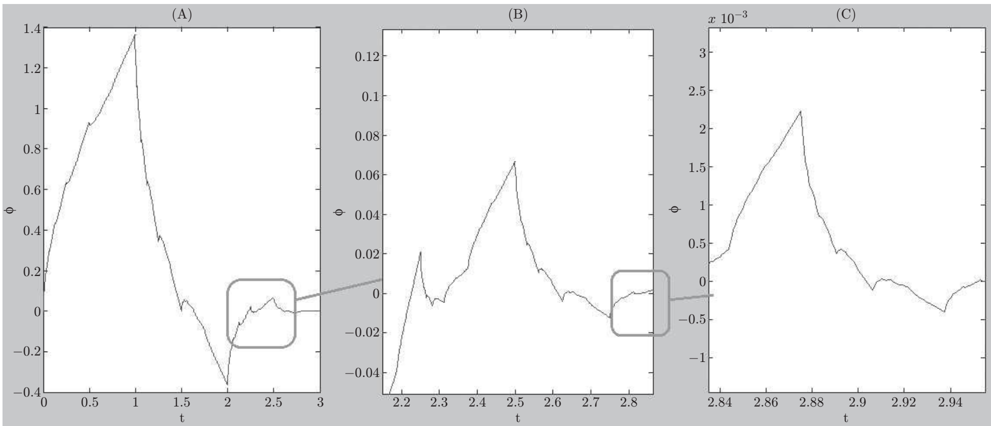

Figure A16.1 | *Self similarity in* db2 *scaling function*

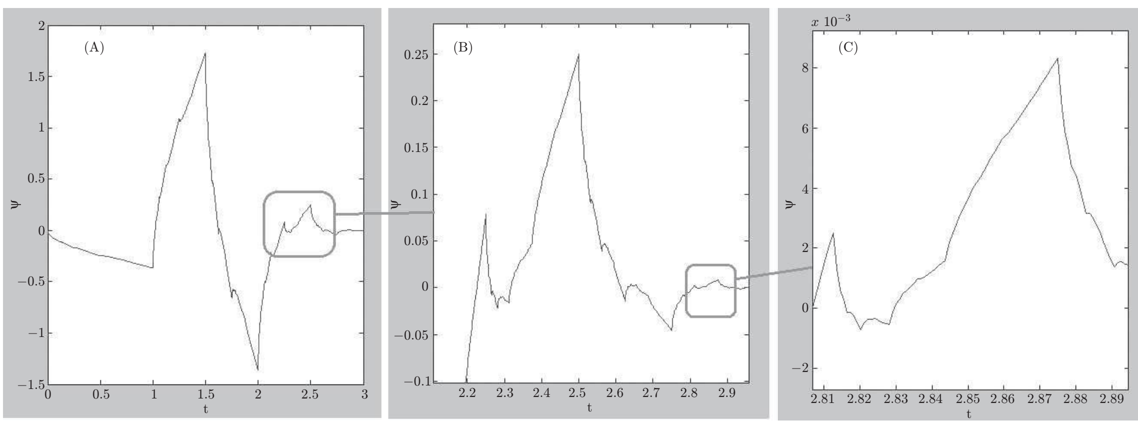

Figure A16.2 | *Self similarity in* db2 *wavelet function*

Extended Notes for Chapter 17

A17.1 | Critical Wavelet Analysis of Signal

Load the accompanying signal into the Matlab worksoace and perform proper time-frequency analysis(such as wavelet analysis) to describe the signal. Is this a stationary signal?

A17.1.1 Time Domain Presentation

The given signal in *.mat* format can be loaded in the Matlab work station, using the load command. Two matrices namely *u* and *t* each with a dimension of 401×1 cab be obtained. The *u* matrix gives the actual

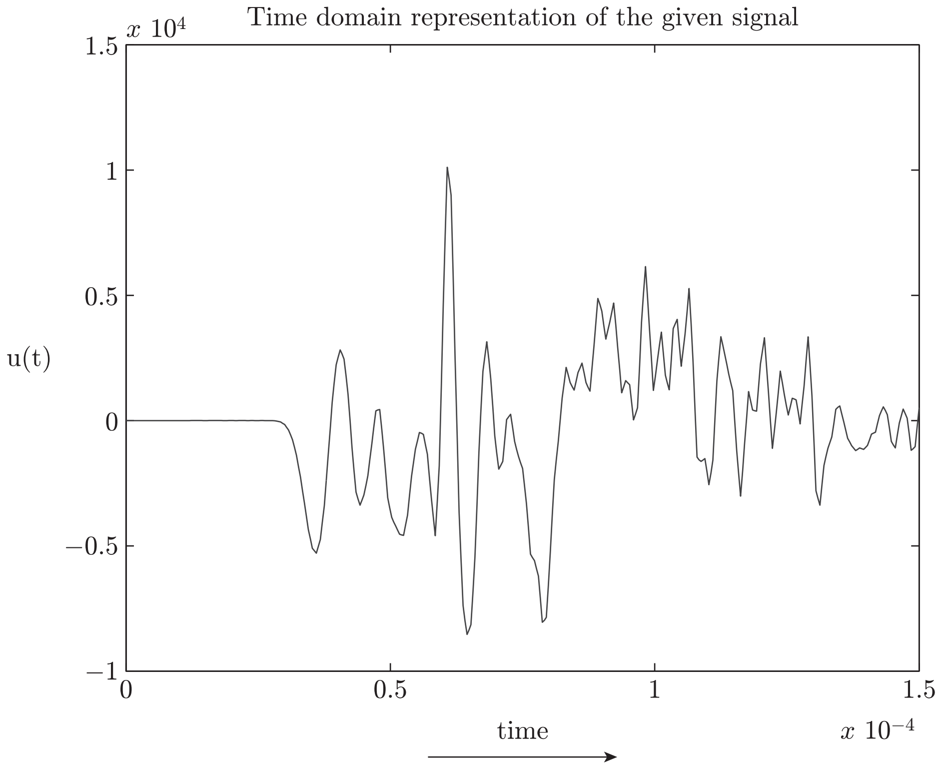

Figure A17.1 | *Signal in time domain*

signal in the time domain, while t matrix gives the time instances. So, the sampled signal $u(t)$ has been given for the analysis. The sampling needs to be uniform. Thus, sampling time is to be obtained by taking difference between any two consecutive elements of the t matrix. It's reciprocal gives the sampling period. Sampling time can be found out to be $3.7500e-007$, while the sampling period can be observed to be $2.6667e+006$.

Figure A17.1 shows the time domain representation of the signal. The signal is roughly 150μseconds long in duration.

A17.1.2 Frequency Domain Presentation

Frequency domain presentation of the signal can be obtained by using 401 points DFT. The sampling frequency should be used to calibrate the frequency axis.

Figure A17.2 shows the fourier representation of the signal. From this graph itself it can be seen that given signal is non-stationary.

A17.1.3 Time-Frequency Presentation

The scalogram of a function can be obtained by calculating a continuous wavelet transform of a given function and then sampling it at the given sampling rate. As per Morlet wavelet gives very good presentation of the signal. Hence the Morlet wavelet is used as the prototype as analyzing function.

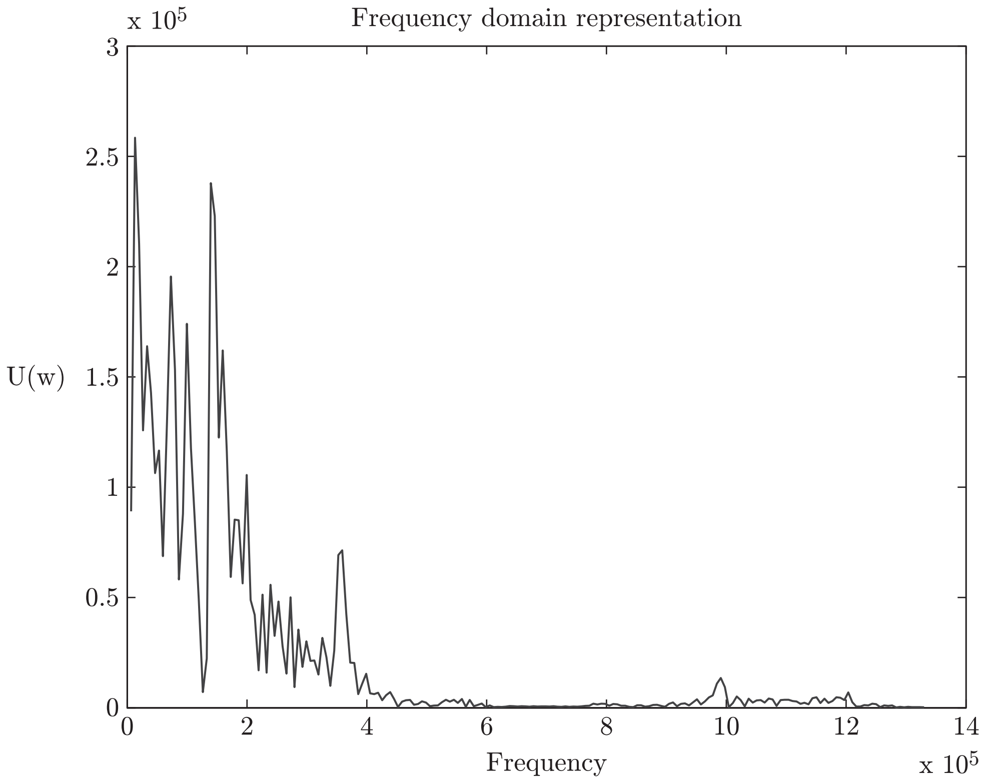

Figure A17.2 | *Signal in frequency domain*

$$\psi(t) = Ce^{jw_0 t} e^{\frac{-t^2}{2}} \tag{A17.1}$$

Windowed complex Eq. (A17.1) is used to find out its dilates and translates, thus forming Morlet family. If a is the dilation factor and b is the translation factor then

$$\psi_{a,b}(t) = \frac{1}{\sqrt{a}} \psi\left(\frac{t-b}{a}\right) \tag{A17.2}$$

To obtain the scalogram, at every scale the samples of the signal to be analyzed are convolved with the samples of the analyzing wavelet. The resulting matrix will have each row representing scale values. Too low scale and sampling frequency are avoided to avoid excessive dilations. For 0.1 scale interval the scalogram obtained is given by Figure A17.3. The 3*D* time-frequency presentation is shown in Figure A17.4. From the plots it is clear that given signal is non-stationary.

Test stationary signal

As this was my first experience to analyze signal with scalogram, I thought of designing a stationary signal and use its scalogram to compare and confirm non-stationarity of the given signal. A simple sine wave of 50Hz was designed and was analyzed in time-frequency domain. This is shown in Figure 17.5. At low scales, good time-localization of the wavelet transform is seen.

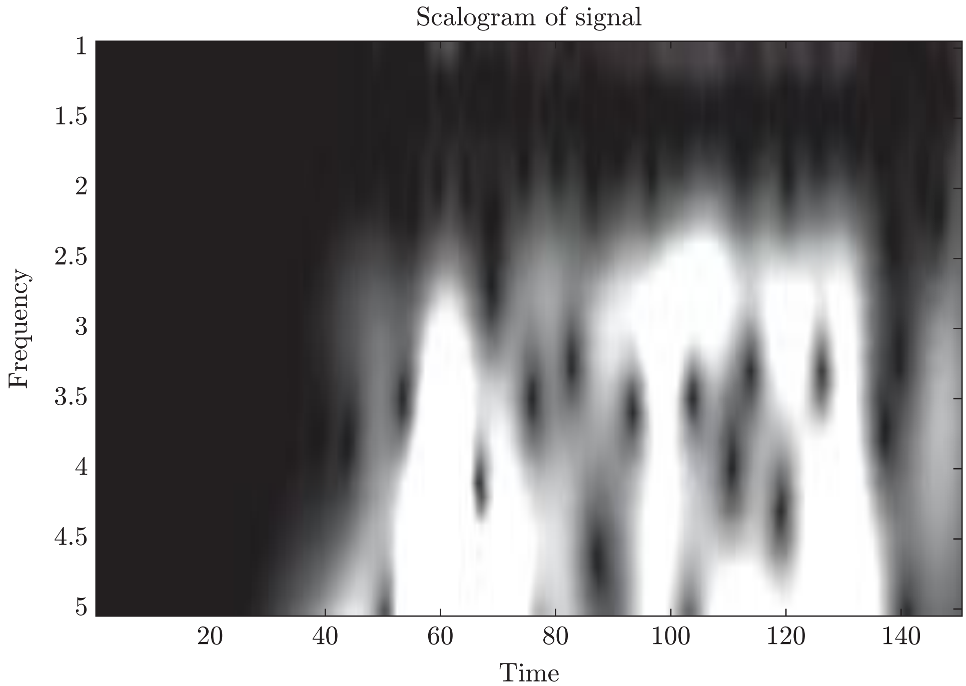

Figure A17.3 | *Scalogram of the signal*

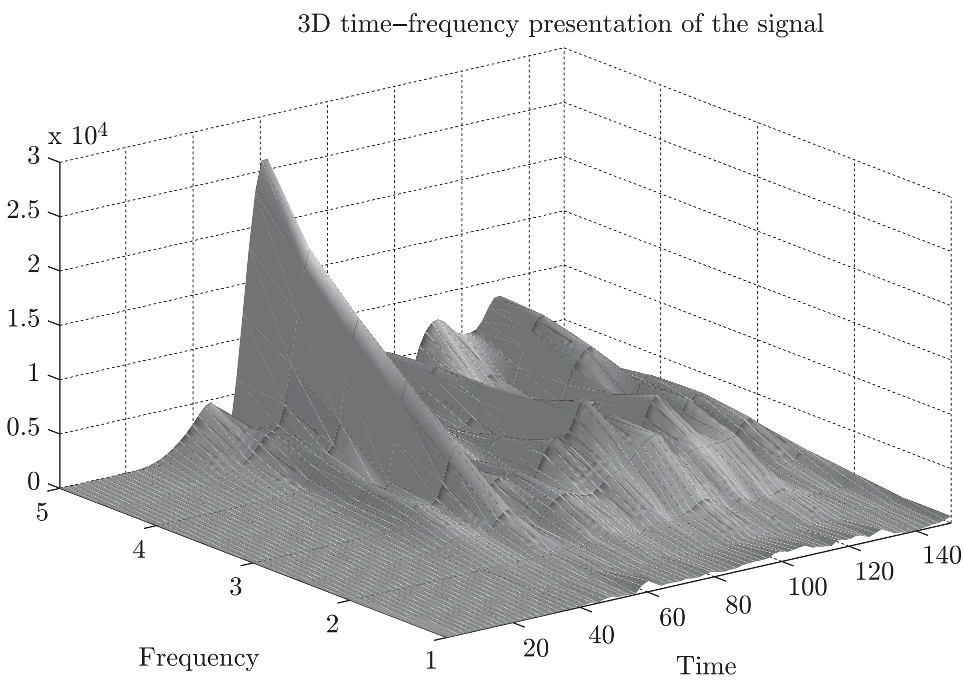

Figure A17.4 | *3D time frequency presentation*

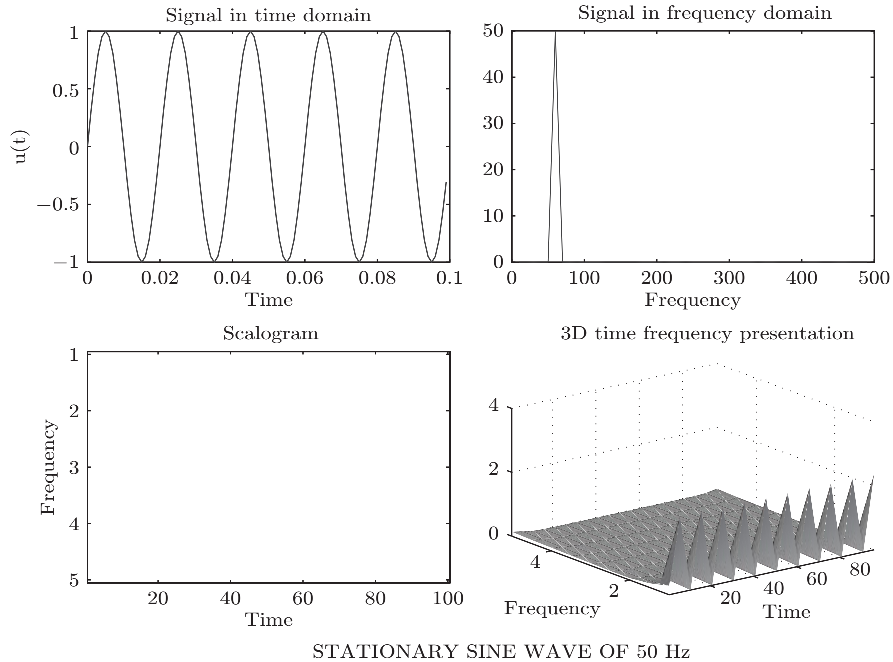

Figure A17.5 | *Analysis of a stationary signal*

A17.1.4 Fine Tuning of the Scalogram

Figure A17.6 shows the time-frequency presentation of the signal at the reduced analyzing scale. The effect of taking shorter time spans is depicted in Figure A17.7. It results in zooming out as well. The zooming in can be achieved by reducing the scale limits. This is shown in Figure A17.8. Thus it is possible to look at any specific part of the signal by zooming onto that portion. Thus, the use of the scalogram depends on what kind of analysis is to be carried out.

A17.1.5 Conclusion

- Given signal is described and analyzed in time-frequency domain.
- Exact duration of the signal is 150.375000μ seconds.
- Given signal is *non-stationary*.
- Using scalogram technique it is possible to zoom-on to any particular portion of the signal.

A17.2 | Sine Fourier Transform

Define the 'sine fourier transform' of a given signal x(t) *as*

$$C(\omega) = \int_{-\infty}^{\infty} x(t)\sin(\omega t)dt \tag{A17.3}$$

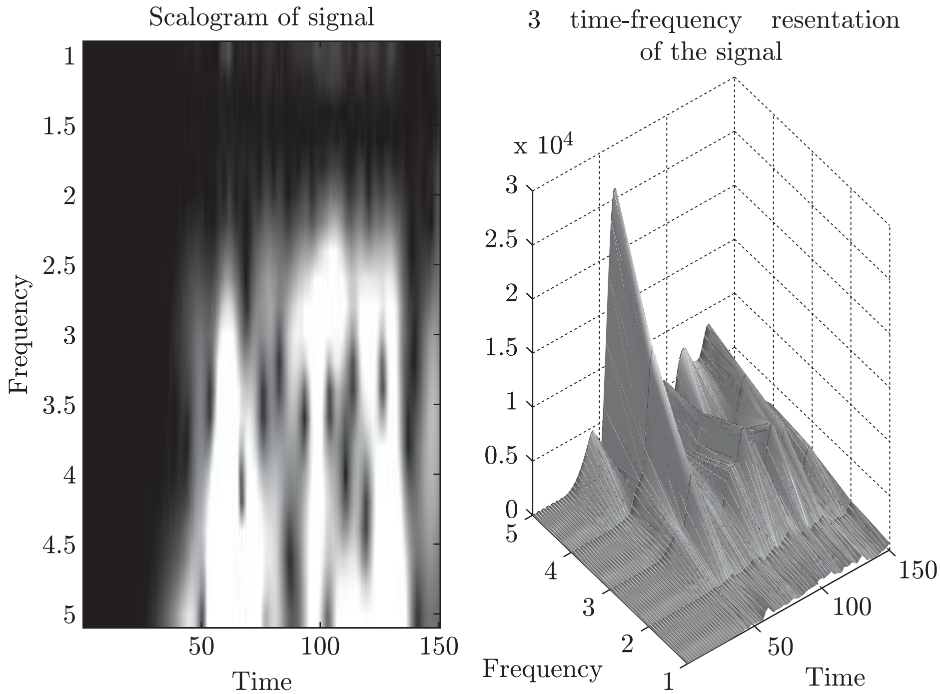

Figure A17.6 | *Time frequency analysis at reduced scale*

Determine the mathematical conditions under which this could be a well-posed definition. Under such conditions, derive an expression for the 'Inverse Sine Fourier Transform'. Establish the effect of time domain mathematical operations such as time-shift, time-scaling, differentiation, integration and multiplication in the ω-domain. Compute sine fourier transform od basic signals such as $\delta(t)$, $cos(\omega_0 t + \phi_0)$ and $e^{\alpha t}$.

A17.2.1 Sine Fourier Transform and Inverse of the Transform

The transformation definition is given as in Equation (A17.3). According to Euler's identity

$$\sin(\omega t) = \frac{e^{i\omega t} - e^{-i\omega t}}{2i} \tag{17.4}$$

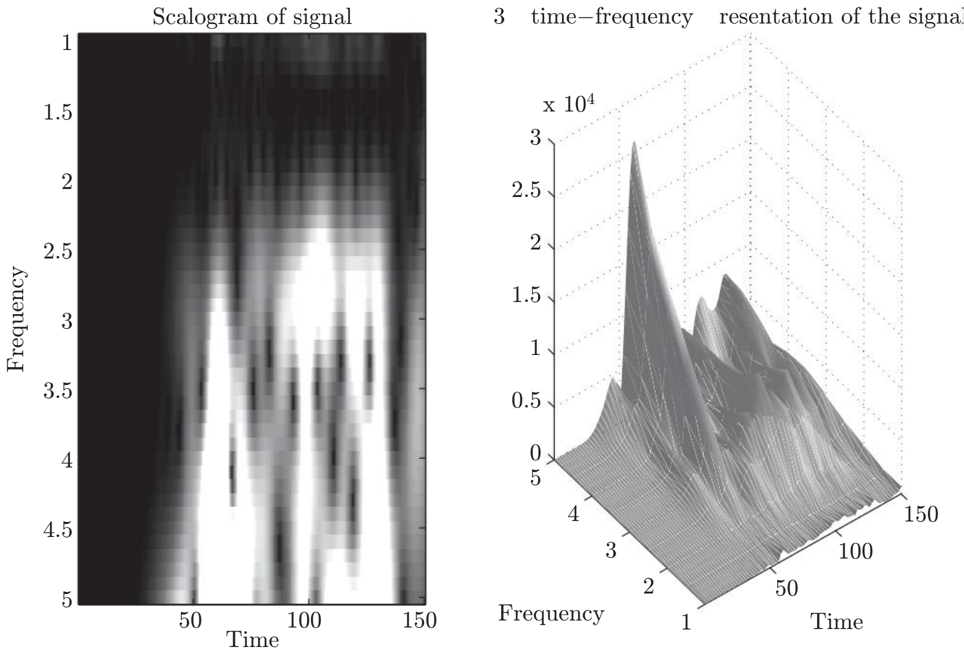

Figure A17.7 | *Time frequency analysis at shorter time span*

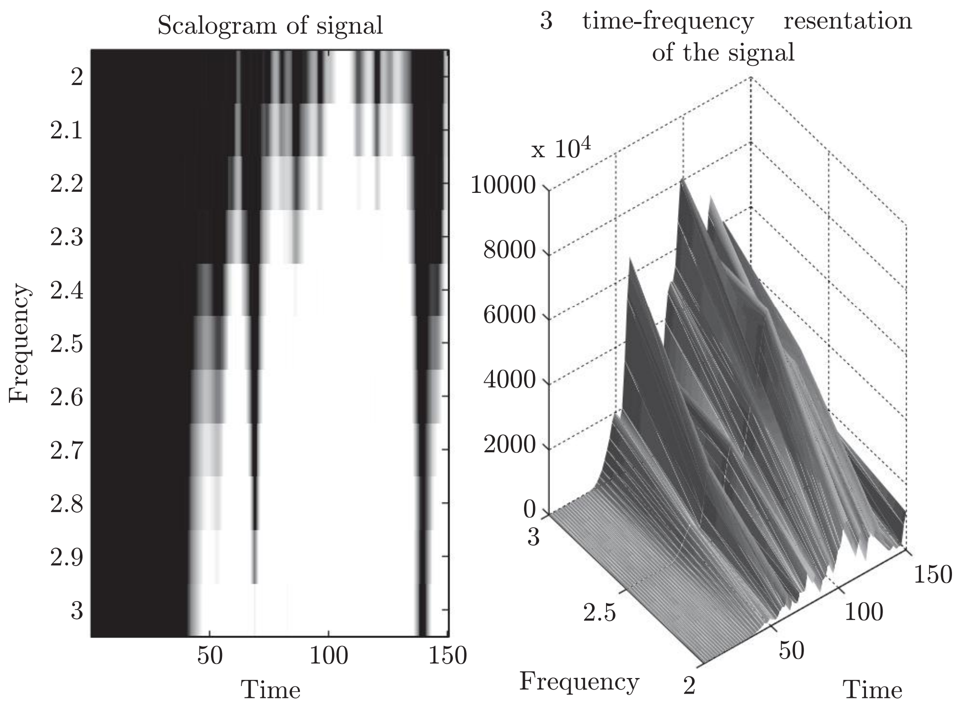

Figure A17.8 | *Time frequency analysis: zoom-in property*

So, the transform gets modified as

$$C(\omega) = \int_{-\infty}^{\infty} x(t)\left[\frac{e^{i\omega t} - e^{-i\omega t}}{2i}\right] \tag{A17.5}$$

$$C(\omega) = \frac{1}{2i}\left[\int_{-\infty}^{\infty} x(t)e^{i\omega t}\,dt - \int_{-\infty}^{\infty} x(t)e^{-i\omega t}\,dt\right] \tag{A17.6}$$

For the given definition to be a well-posed definition, the function under the consideration should follow the Dirichilet's conditions. From the Fourier series theory the function $x(t)$ follows Dirichilet's conditions in the given interval say $-a < t < a$ if

- $x(t)$ has only finite number of discontinuities in $-a < t < a$ and has no infinite discontinuities.
- In the given limits $x(t)$ has finite maxima and minima.
- The given function should be completely integrable in the given interval.

$$\int_{-a}^{a} |\, x(t) \,| < \infty \tag{A17.7}$$

From Fourier series

$$x(t) = \sum_{-\infty}^{\infty} a_n e^{\frac{int\pi}{a}} \tag{A17.8}$$

where,

$$a_n = \frac{1}{2a}\int_{-\infty}^{\infty} X(\xi)e^{\frac{-int\pi}{a}}\,d\xi \tag{A17.9}$$

Extending the limit from $a \to \infty$ we get the Fourier Integral Theorem

$$x(t) = \frac{1}{2\pi}\int_{-\infty}^{\infty} e^{ikt}\left[\int_{-\infty}^{\infty} f(\xi)e^{-ik\xi}\,d\xi\right]dk \tag{A17.10}$$

Using this theorem for the given problem

$$x(t) = \sum_{-\infty}^{\infty} a_n\left[\frac{e^{-\left(\frac{int\pi}{a}\right)} - e^{\left(\frac{int\pi}{a}\right)}}{2i}\right] \tag{A17.11}$$

$$a_n = \frac{1}{2a}\int_{-\infty}^{\infty} f(\xi)\left[\frac{e^{\frac{in\pi\xi}{a}} - e^{-\frac{in\pi\xi}{a}}}{2i}\right]d\xi \tag{A17.12}$$

So, the modified equation would be

$$x(t)=\frac{1}{2\pi}\sum_{-\infty}^{\infty}(\delta_k)\left[\int_{-a}^{a}f(\xi)\left[\frac{e^{\frac{in\pi\xi}{a}}-e^{-\frac{in\pi\xi}{a}}}{2i}\right]\right]\left[\frac{e^{-\left(\frac{ikt\pi}{a}\right)}-e^{\left(\frac{ikt\pi}{a}\right)}}{2i}\right] \tag{A17.13}$$

As $a\to\infty$ the instances become continuous and $\delta(k)$ becomes dt.

$$x(t)=\frac{1}{2\pi}\int_{-\infty}^{\infty}(dt)\left[\int_{-a}^{a}f(\xi)\left[\frac{e^{\frac{in\pi\xi}{a}}-e^{-\frac{in\pi\xi}{a}}}{2i}\right]\right]\left[\frac{e^{-\left(\frac{ikt\pi}{a}\right)}-e^{\left(\frac{ikt\pi}{a}\right)}}{2i}\right] \tag{A17.14}$$

Provided $x(t)$ is bounded

$$x(t)=\frac{2}{2\pi}\int_{0}^{\infty}dt\int_{-\infty}^{\infty}f(\xi)\frac{-1}{2}\left[e^{\frac{in\pi}{a}(\xi+t)}-e^{\frac{in\pi}{a}(\xi+t)}-e^{\frac{-in\pi}{a}(\xi+t)}+e^{\frac{in\pi}{a}(t-\xi)}\right. \tag{A17.15}$$

$$x(t)=\frac{1}{\pi}\int_{0}^{\infty}dt\int_{-\infty}^{\infty}f(\xi)[\cos(\xi+t)-\cos(\xi-t)] \tag{A17.16}$$

Now,

$$\cos(\xi+t)-\cos(\xi-t)=-2\sin(\xi)\sin(t) \tag{A17.17}$$

So, $x(t)$ is further represented as

$$x(t)=\frac{1}{\pi}\int_{0}^{\infty}dt\int_{-\infty}^{\infty}f(\xi)[-2\sin(\xi)\sin(t)] \tag{A17.18}$$

From Eq. (A17.18) it is evident that if the function $x(t)$ is an odd function then it would not have any representation. This is because the right hand side of Eq. (A17.18) will become zero.

As against this, if the given function is odd i.e. $x(-t)=-x(t)$, then it will be represented as follows:

$$x(t)=\frac{2}{\pi}\int_{0}^{\infty}\sin(kt)dt\int_{-\infty}^{\infty}f(\xi)\sin(k\xi)d\xi \tag{A17.19}$$

Also, sine function forms a complete orthogonal set over interval $[0,\pi]$.

Comparing equation (17.19) with the fourier sine series equation, we get following pair of sine fourier transform and its inverse.

$$C(\omega)=\int_{0}^{\infty}\sin(\omega t)x(t)dt \tag{A17.20}$$

$$x(t)=\frac{2}{\pi}\int_{0}^{\infty}\sin(\omega t)C(\omega)d\omega \tag{A17.21}$$

A17.2.2 Properties of the Sine Fourier Transform

Time shift property

Lets denote sine transform by F_s

$$F_s[x(t-t_0)] = \int_0^{\infty} x(t-t_0)\sin(\omega t)dt \tag{A17.22}$$

Now either by doing $t - t_0 = \xi$ substitution and then solving for $\sin(\omega\xi)\cos(\omega t_0) + \cos(\omega\xi)\sin(\omega t_0)$ or by directly doing the substitution in Eq. (A17.23) we get

$$C(\omega) = \frac{1}{2i}\left[\int_{-\infty}^{\infty} x(t)e^{i\omega(t_0+\xi)}dt - \int_{-\infty}^{\infty} x(t)e^{-i\omega(t_0+\xi)}dt\right] \tag{A17.23}$$

Time-scaling property

Let us scale the time by some factor say a. Owing to the integration of the exponentials, it can be directly observed from the transform itself that

$$F_s[x(at)] = \frac{1}{a}C\left(\frac{\omega}{a}\right) \tag{A17.24}$$

Differentiation property

$$F_s(x'(t)) = \omega F_c(x(t)) \tag{A17.25}$$

where,

$$F_c x(t) = \int_{-\infty}^{\infty} x(t)cos(\omega t)dt \tag{A17.26}$$

Integration property

$$F_s\left(\int x(t)\right) = -\omega F_c(x(t)) + \text{Const} \tag{A17.27}$$

where,

$$F_c x(t) = \int_{-\infty}^{\infty} x(t)cos(\omega t)dt \tag{A17.28}$$

Multiplication

$$F_s[f(t)g(t)] = \frac{1}{\pi}\int_0^{\infty} f(t)g(t)\sin(\omega t)dt \tag{A17.29}$$

$$F_s[f(t)g(t)] = \frac{1}{\pi}\int_0^{\infty}\left[2\int_0^{\infty}\hat{f}_s(\xi)\sin(\xi t)d\xi\,\right]g(t)\sin(\omega t)dt \tag{A17.30}$$

Using

$$\sin(a)\sin(b) = \frac{1}{2}[\cos(a-b) - \cos(a+b)] \tag{A17.31}$$

Final equation is as follows:

$$F_s[f(t)g(t)] = \int_0^\infty \hat{f}_s(t)[\hat{g}_c(|\omega - \xi|) - \hat{g}_c(\omega + \xi)]d\xi \tag{A17.32}$$

where, $\hat{g}_c$ are obtained from cosine fourier transform as given in Eq. (A17.28).

A17.2.3 Sine Transforms of Given Basic Signals

In this section, given three time domain signals are analyzed using sine transform.

Delta signal: $\delta(t)$
By definition the delta signal exists only at time $t = 0$. As $\sin(0) = 0$ the transform for this particular signal is 0.

Cosine signal: $\cos(\omega_0 t + \phi_0)$
Assuming that ϕ_0 is independent of time, cosine function is an even function. So the transform for this function also reduces to 0.

Growing exponential: $e^{\alpha t}$
As the given signal is not bounded, i.e.

$$\int_{-\infty}^{\infty} e^{\alpha t} dt \sim< \infty \tag{A17.33}$$

So, this signal can not be presented by the sine fourier transform.

A17.3 | Motion Estimation in Video Coding

Study and compare various motion estimation techniques suggested for wavelet-based video coding, including

- spatial domain
- wavelet domain
- mesh-based

Criticize these techniques along with their advantages and dis-advantages in terms of

- coding performance
- scalability
- complexity

17.3.1 Introduction

A scalable video coder is capable of producing a bit stream, such that it is decodable at different bit rates. Naturally, the encoding scheme is the most crucial one, and needs very careful designing of the parameters. This extra effort taken at the encoder side allows the decoding of the scalable video on a less powerful hardware platforms, where issues like 'memory' and 'computational time' are very critical and resources are limited. When it comes to sending the information on error-prone channels like internet, scalability can help enhance the video quality by limiting the degradation to minimum depending upon the availability of the bandwidth.

To achieve efficient compression the estimation of the motion parameters is very significant. Different motion estimation schemes are available and are used in different standards including MPEG-2, H.263, and JPEG 2000.

Given the aforementioned advantages, several scalable functionalities have been included in international image and video compression standards: JPEG contains the progressive and hierarchical modes for quality and resolution scalable coding. Using the wavelet transforms (to be discussed shortly), scalability is greatly improved and expanded in the emerging JPEG 2000 standard. However, adopting a rate-distortion (R-D) based layering structure in the JPEG 2000 code stream, encoding and decoding still can not be completely decoupled. Containing an error-feed-back loop from hybrid coding, SNR and resolution scalable video coding standardized in MPEG-2, 4 and H.263 are troubled by 'drift', and a significant loss in compression.

In recent years, wavelets have proven to be successful in compressing still images. Compared to the classical DCT approach (JPEG), the wavelet based compression schemes have the advantage of much better image quality obtained at very high compression ratios.

The very basic motivation for wavelet-based video coding is to support scalability, i.e. partial decoding of the entire sequence at various quality levels. One of the most difficult problem to be dealt with in the conventional codecs, is the problem of "drift". This problem occurs due to different resolutions. This can be addressed by using hierarchical backward motion compensation framework. But, for the practical implementation of a wavelet-based coder aliasing artifacts are needed to be dealt with. The backward/forward hybrid mode for motion compensation is suggested in. The coder adaptively regulates its motion bits investment according to motion complexity in each frame.

A17.3.2 Motion Estimation Techniques

This section describes different motion estimation techniques suggested for wavelet-based video coding. The invertibility requirement has restricted most of the approaches to either block based or global motion detection in spatial domain. Without motion estimation, temporal filtering produces visually disturbing ghosting artefacts in the low pass temporal sub bands. Such disturbances are definitely not desired where temporal scalability is of interest.

The motion estimation(ME) techniques for the wavelet-based coders can be divided into following three types

- ME in temporal domain
- ME in wavelet domain
- mesh-based ME

ME in temporal domain

As the name suggests the estimation of the motion is performed in the spatial domain. The video signal is assumed to be made up of sequence of images. The motion estimation in the spatial domain by comparing the location of a specific pixel in frame k and the next frame $k+1$. The tracking of the pixel is taken into account to formulate the motion vector. The techniques are thus dependent on the pixel resolution information. The spatial domain ME can be further divided into two clases of techniques namely, 'frame-warping techniques', and 'block-based ME'.

Frame warping techniques Invertible warping of the frames so as to align spatial features prior to application of separable Discrete wavelet transform (DWT) is known. While variety of frame operators are considered, the authors have shown that invertible warpings are unable to represent the localized expansion and contraction effects exhibited within most video sequences.

The most significant drawback of these warping techniques is that the motion stream violates the 'Nyquist rate' due to expansions and contractions. This problem gets even serious while warping back to the original pixel due to the mismatched sampling rates. This essentially creates artefacts. Some other techniques are based on non-invertible frame warping. But these techniques produce very low bit-rate video, thus applicable only for low-quality environment.

Block-based techniques This class of spatial motion estimation was originally proposed by. The video frames are divided into blocks, where each block undergoes rigid motion, usually translation. The effect of expansions and contractions in the motion filed results in 'disconnected' pixels. Naturally, these can not be coded along the motion vector, and are required to be treated separately. This affects the coding efficiency very heavily. In most of the techniques the block size is maintained fixed thus not capturing the expansive or contractive motion. The perfect reconstruction or complete invertibility is obtained only with integer block displacements, although extensions to half pixel accuracy have also been demonstrated.

While sending the motion information the 'disconnected' pixels are not encoded. They are usually send as it is. If the video contains heavy motion fields, then block based methods produce reasonable number of 'disconnected' pixels. Adaptive block varying techniques take large memory space and computational time. Encoding such a frames need better techniques to handle the motion.

Temporal transforms based on either frame-warping or block displacement generally employ only the Harr wavelet kernel. Extension to longer temporal filters have been reported, with no significant improvement in the performance. This makes sense as the motion fields are not connected to the wavelet kernels but they are related to spatial displacements. Hence to see improvement it would be needed to have kernel based ME.

ME in wavelet domain

A straightforward approach to build a wavelet based video codec, is to replace the Discrete cosine transform (DCT) in a classical video coder by the Discrete wavelet transform (DWT). A drawback of this technique is that for inter-frame coding the wavelet transform is applied to the complete error image, which contains all the artefacts. To avoid this limitation, the DWT is taken out of the prediction loop which results in video architecture. The encoder is shown in Figure (A17.9).

Both motion estimation and compensation are performed in the wavelet domain i.e. in the average image of the highest level and in the detail images. This is feasible since the wavelet transformed image

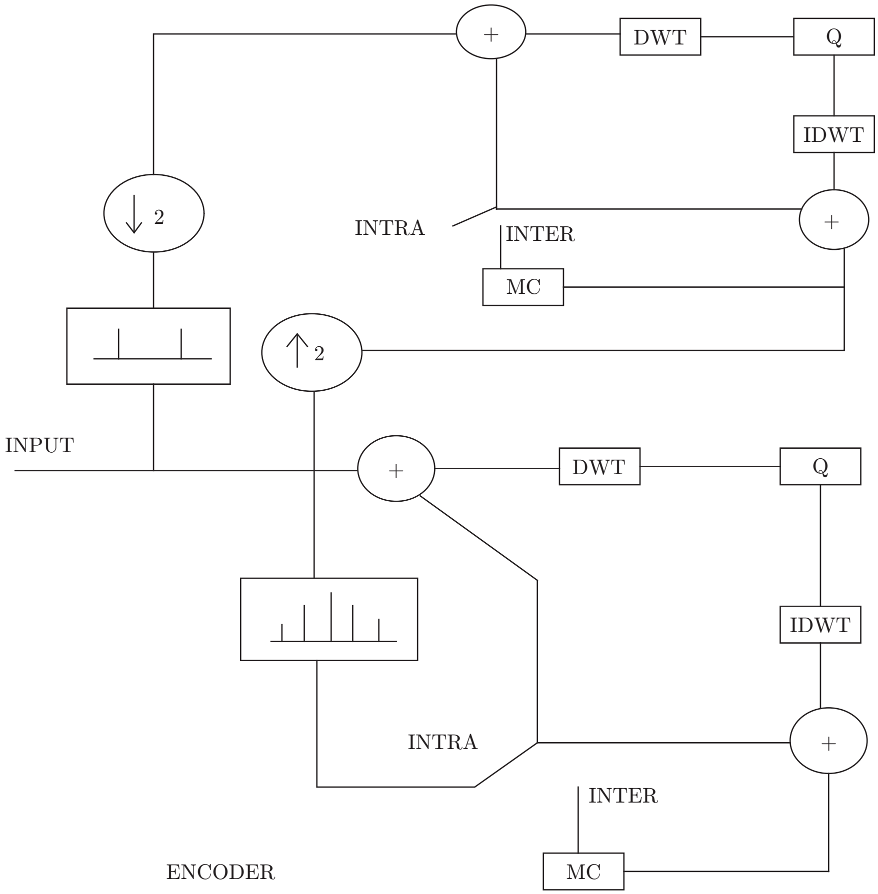

Figure A17.9 | *Wavelet based scalable video coder*

contains not only the frequency information but also spatial information, which is not in the case of DCT. The advantages of such codecs are:

- the motion field blocking artefacts are no longer transformed to wavelet domain
- inverse DWT is not always needed, so that from a hardware point of view the encoder can be simplified.

LIMAT

The Lifting based invertible motion adaptive transform (LIMAT) framework for highly scalable video compression is described in literature. The lifting technique is used to formulate wavelet filters. The lifting scheme is a novel method for constructing biorthogonal wavelets. The main difference with the classical construction is that it does not rely on the Fourier transform.

The advantages of the lifting scheme over traditional scheme are:

1. It allows faster implementation of the wavelet transform. The lifting scheme makes optimal use of similarities between high and low pass filters to speed up the calculations.

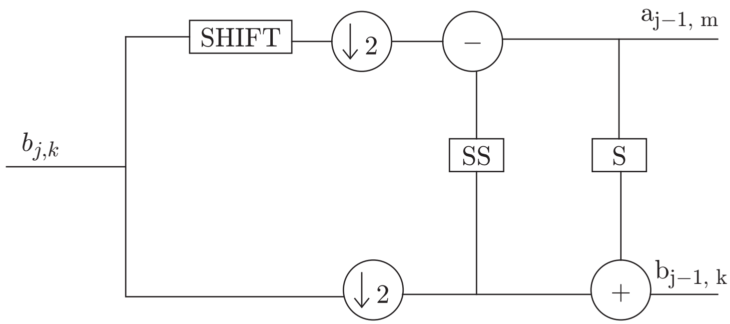

Figure A17.10 *The lifting scheme for wavelets. [It first calculates the Lazy wavelet transform, then calculates the $a_{j-1,k}$, and finally lifts the $b_{j-1,k}$]*

2. Without any auxiliary memory the original signal gets replaced wavelet transform.
3. Inverse transform can be easily found by just undoing the calculations.
4. This scheme is extremely handy in situations where Fourier transform is not available.

The basic idea behind the lifting scheme is very simple and is shown in Figure (17.10). It starts with trivial wavelet, the "Lazy wavelet"; which has the formal properties of wavelet, but is not capable of doing anything. The lifting scheme then gradually builds a new wavelet, with improved properties, by adding in new basis function. This itself is the inspiration behind the name of the scheme. The lifting scheme can be easily understood as an extension of the FIR (Finite Impulse Response) schemes.

Example: Harr wavelet

The sufficient and necessary lifting steps to conceptualize Harr wavelet transform are:

$$h_k[n] = x_{2k+1}[n] - x_{2k}[n] \tag{17.34}$$

$$l_k[n] = x_{2k}[n] + \frac{1}{2}h_k[n] \tag{17.35}$$

where $x_k[n] \equiv x_k[n1, n2]$ denotes the samples of frame k from video sequence and $h_K[n] \equiv h_k[n1, n2]$ and $l_k[n] \equiv l_k[n1, n2]$ denote the high pass and low pass sub bands frames. This decomposition of the Harr transform into the two steps is also called as the S-transform.

Now, let $v_{k1 \to k2}$ denote a motion-compensated mapping of frame $k1$ onto the co-ordinate system of $k2$. The lifting steps are modified as follows:

$$h_k[n] = x_{2k+1}[n] - v_{2k \to 2k+1}(x_{2k})[n] \tag{17.36}$$

$$l_k[n] = x_{2k}[n] + \frac{1}{2}v_{2k+1 \to 2k}(h_k)[n] \tag{17.37}$$

A17.3.3 Mesh Based ME

Drawbacks of the block based ME have already been discussed. Unlike block based ME, deformable meshes are capable of tracking complex motion, including local expansion and contraction, while maintaining continuous motion field. A regular deformable mesh is created by partitioning the current frame into the regular grid of patches, usually either triangles or quadrilaterals. The mesh node-points move to form a warped mesh on the reference frame, and the mapping is presented by the set of node displacement vectors. The motion vector at any given location within a patch is approximated by linearly interpolating the motion vectors at the patch vertices. This corresponds to an affine transformation for triangular meshes, and a bilinear transformation for quadrilateral meshes.

Following are the advantages of the deformable meshes:

- Yield motion fields that are piecewise smooth and continuous at the patch boundaries.
- These motion fields provide much better representation of the underlying motion field.
- Local searches or gradient-based methods are used, thus reducing the computational cost.
- Expansion in quantization error energy is directly related to expansion in the mesh itself.

A17.3.4 Points for Further Thinking:

- Different motion estimation techniques for wavelet-based video coders are discussed
- Different techniques are compared using coding performance, scalability and complexity.
- Coding performance of the coder improves when ME is performed in the wavelet domain as against spatial domain.
- The wavelet based coders are by default scalable. If the ME is also wavelet based it enhances the rate scalability performance.
- The complexity of the encoder increases as the wavelet kernel gets more complicates. But it reduces hardware requirements at the decoder.
- The mesh based designs do better job than block based designs, irrespective of whether ME is spatial based or wavelet based.
- Wavelet based ME provides more flexibility in providing scalability as compared to spatial domain based ME.
- If ME is wavelet based, only then improvement in the wavelet kernel improves the system performance, otherwise not.
- Mesh based wavelet motion estimators with hybrid ME directionality gives best performance and is the most modern of all the designs.

A17.4 | Wavelet Analysis Algorithm in Detail on Fingerprint Image

A17.4.1 Wavelet Analysis

The algorithm concentrates on time-frequency ‘energy localization’. This section discusses the filter design, wavelet transform implementation, maxima energy extraction, multiresolution, and wavelet packet analysis.

- Filter design
- Wavelet Transform Implementation
- Maxima Energy Extraction
- Multiresolution Analysis
- Wavelet Packet Analysis

Filter Design

For this particular exercise, Daubechies wavelet is selected as the mother wavelet. This is in accordance with the following properties of Daubechies wavelets:

- orthonormality, having finite support.
- optimal, compact representation of the original signal from a sub-band coding point of view, thus producing multiresolution effect.
- capability to select maximum vanishing moments and minimum phase, so as to extract even minute details from smoother parts.
- cascade algorithm which can zoom-in on particular features of ϕ.

Daubechies filters used for this algorithm are designed so that the phase of the filter is minimum and the number of vanishing moments are maximum. This is of particular importance as not all the images are well focused and it is crucial to extract the changing information even from the smoother parts of the images.

The main focus of the implementation is to construct compactly supported wavelets ψ. The scaling function ϕ itself is chosen to have compact support, hence it automatically ensures the compact support of wavelet ψ. Multiresolution analysis leads naturally to a hierarchial and fast scheme for the computation of the wavelet coefficients of a given function.

From the definition of h_n:

$$h_n = \sqrt{2}\int dx\phi(x)\overline{\phi(2x-n)} \tag{A17.38}$$

It can be seen that only finite number of h_n could be non-zero, so that ψ reduces to a finite linear combination of compactly supported functions. This ensures the compact support of ψ. Selecting both ψ and ϕ to have compact support, ensures that the corresponding subband filtering scheme uses only FIR type of filters.

For compactly supported ϕ, the 2π periodic function h_o becomes a trigonometric polynomial.

$$m_o(\xi) = \frac{1}{\sqrt{2}}\sum_n h_n e^{-in\xi} \tag{A17.39}$$

The orthonormality of the $\phi_{0,n}$ implies:

$$|h_o(\xi)|^2 + |h_o(\xi+\pi)|^2 = 1. \tag{A17.40}$$

The Equation (17.40) in z domain is as follows:

$$|H(z)|^2 + |H(-z)|^2 = 1 \quad \text{all } |z| = 1 \tag{A17.41}$$

Thus, the initial task is to find out the trigonometric polynomial. Then, the roots of that polynomial produce the zeros. To maintain the minimum phase only zeros inside the unit circle are to be retained. This procedure is called as 'cascade algorithm'.

Let N be the length of the filter to be designed. Then, $(N/2)-1$ degrees of freedom are used to obtain maximum vanishing moments $k = N/2$.

To design a compactly supported ϕ, the periodic function m_o in Eq. (A17.39) is, when transformed in 'z' domain, seen as trigonometric polynomial, say $H(z)$

$$H(z) = \frac{1}{2}\sum_{n=0}^{N/2} h_n z^n = \left(\frac{1+z}{2}\right)^k Q(z) \tag{A17.42}$$

where,

$$Q(z) \in \pi_{N-m},\ Q(1) = 1, \quad \text{and} \quad Q(-1) \neq 0 \tag{A17.43}$$

Since, $k = \dfrac{N}{2}$, we only need to find $Q(z)$ under constraints to formulate H(z) and ultimately $h[n]$.

$H(z) = \left(\dfrac{1+z}{2}\right)^k Q(z)$ satisfies $|H(z)|^2 + |H(-z)|^2 = 1$ only if $(|Q(e^{jw})|^2)$ can be written as

$$|Q(e^{jw})|^2 = \sum_{0}^{k-1} \binom{(N/2)-1+k}{k} \left(\frac{-1}{4}\right)^k (e^{-jw} - 2 + e^{jw})^k \tag{A17.44}$$

The filter is designed for $N = 16$ and $k = 8$.

$$(|Q(z)|)^2 = Q(z).Q(z^{-1}) = p\left(\frac{2-z-z^{-1}}{4}\right) \tag{A17.45}$$

$$p(y) = \sum_{0}^{k-1} \binom{7+k}{k} y^k \tag{A17.46}$$

where $y = \left(\dfrac{2-z-z^{-1}}{4}\right)$

$$(|Q(z)|)^2 = \sum_{0}^{k-1}\left(\binom{(N/2)-1+k}{k}\left(\frac{2-z-z^{-1}}{4}\right)^k\right) = \sum_{0}^{7}\left(\binom{15}{8}\left(\frac{2-z-z^{-1}}{4}\right)^8\right) \tag{A17.47}$$

The roots of this equation are found out to be 2.7367, 2.5296 + 0.8198i, 2.5296 – 0.8198i, 1.9388 + 1.4558i, 1.9388 – 1.4558i, 1.0380 + 1.7304i, 1.0380 – 1.7304i, 0.2549 + 0.4250i, 0.2549 – 0.4250i, 0.3298 + 0.2476i, 0.3298 - 0.2476i, 0.3577 + 0.1159i, 0.3577 – 0.1159i, 0.3654. For constructing Q from $|Q|^2$ zeros inside the unit circle are retained, which gives minimum phase solution; $z1 = 0.2549 + 0.4250i$, $z1^* = 0.2549 - 0.4250i$, $z2 = 0.3298 + 0.2476i$, $z2^* = 0.3298 - 0.2476i$, $z3 = 0.3577 + 0.1159i$, $z3^* = 0.3577 + 0.1159i$, $z4 = 0.3654$. Value of the constant is calculated using $Q(e^{jw}) = 1$ at $w = 0$ and was found to be 0.0544 after scaling. Writing $H(z)$ back and reading off the coefficients gives the $h[n]$ values.

The roots of Eq. (17.47) and the retained roots to formulate the minimum phase filter are given in Table (17.1). The value of the constant is calculated using $Q(e^{jw}) = 1$ at $w = 0$ and was found to be 0.0544 after scaling.

Table 17.1 | *Daubechies linear phase filter design*

Roots of equation 1.68	**Retained roots**	
2.7367	-	
$2.5296 + 0.8198i$	-	
$2.5296 - 0.8198i$	-	
$1.9388 + 1.4558i$	-	
$1.9388 - 1.4558i$	-	
$1.0380 + 1.7304i$	-	
$1.0380 - 1.7304i$	-	
$0.2549 + 0.4250i$	*	(z_1)
$0.2549 - 0.4250i$	*	(z_1^*)
$0.3298 + 0.2476i$	*	(z_2)
$0.3298 - 0.2476i$	*	(z_2^*)
$0.3577 + 0.1159i$	*	(z_3)
$0.3577 - 0.1159i$	*	(z_3^*)
0.3654	*	(z_4)
* = retained roots		

In formulating $S(z)$, we have freedom in choosing $r_k, k = 1,\ldots,K$, which are real non zero values, and $z_l, l = 1,\ldots,L$, which are complex values. For any such choice, $|S(e^{-jw/2})|$ is different from the result of any such choice only by some multiplicative constant that is independent of w. For example $S(z) = S_{m-1}(z)$, defined by

$$S_{m-1}(z) := C \times \prod_{k=1}^{K}(z - r_k)\prod_{l=1}^{L}(z - z_l)(z - \bar{z}_l) \tag{A17.48}$$

'C' is the constant, and the choices are made such that $S(1) = 1$. This choice of $S_{m-1}(z)$, by selecting the zeros inside the unit circle, corresponds to what is called 'minimum-phase digital filtering', with 'transfer function'

$$P_{2m-1}(z) = \frac{1}{2}\sum_{k=0}^{2m-1} p_k z^k := \left(\frac{1+z}{2}\right)^m S_{m-1}(z) \tag{A17.49}$$

Once this trigonometric polynomial is obtained, then the low pass synthesis filter coefficients are obtained by using Eq. (A17.50).

$$Nm_0(\xi) = \frac{1}{\sqrt{2}}\sum_{n=0}^{2N-1} Nh_n e^{-in\xi} \tag{A17.50}$$

$$H(z) = \left(\frac{1+z}{2}\right)^k Q(z) \tag{A17.51}$$

$Q(z)$ is substituted in Eq. (A17.51) to find $H(z)$ and ultimately $h(n)$, the analysis low pass filter. As these are the orthogonal filters, remaining filters are obtained from analysis low pass filter. For example, analysis high pass filter is obtained by inverting the analysis low pass, and negating the alternate values. Both synthesis filters are obtained by inverting the analysis filter vectors and cross labelling.

These designed filters are shown in Figure A17.11. For our algorithm, the filters are designed for the number of coefficients to be 16. This number is found to be the best trade-off between smoothness of the filters and computational time.

As stated earlier, ϕ and ψ are compactly supported L^2 functions, satisfying

$$\phi(x) = \sqrt{2}\sum_n h_n \phi(2x - n) \tag{A17.52}$$

$$\psi(x) = \sqrt{2}\sum_n (-1)^n h_{-n+1}\phi(2x - n) \tag{A17.53}$$

Designed ϕ and ψ functions are shown in Figure A17.12. The $\psi_{j,k}(x) = 2^{-\frac{j}{2}}\psi(2^{-j}x - k), j,k \in Z$ forms a tight frame of $L^2(R)$, which is an orthonormal basis.

Wavelet transform

The algorithm of wavelet transform implementation revolves around following equation,

$$f(x) = \sum_{-\infty}^{\infty}\beta_k \phi(x-k) + \sum_{I\in I,|I|\le 1}\alpha(I)\psi_I(x) \tag{A17.54}$$

$$f_j(x) = \sum_k \alpha_{i,k} 2^{\frac{j}{2}}\phi(2^j x - k) + \sum_k \beta_{i,k} 2^{\frac{j}{2}}\psi(2^j x - k) \tag{A17.55}$$

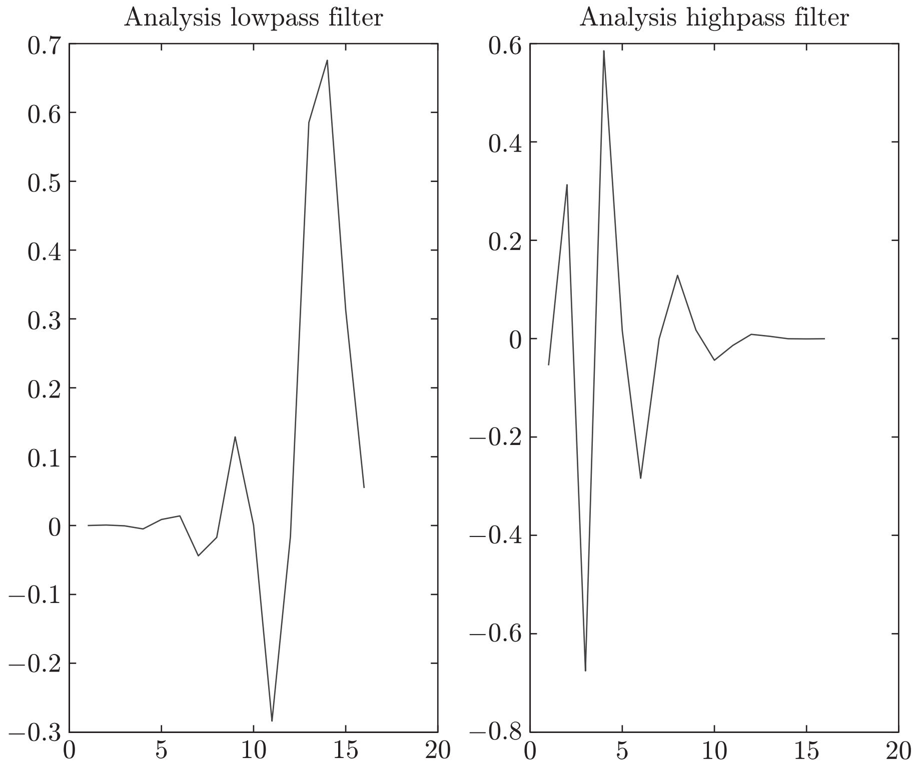

Figure A17.11 | *Daubechies analysis filters. The left figure shows the low pass filter and the right figure shows high pass filter. [The filters are designed for the number of coefficients to be 16. X axis indicates the coefficient number, while the Y axis shows the value for that coeficient number. The filter is normalized so that sum of all the filter coefficients is equal to* $\sqrt{2}$.*]*

where, $\beta_k = \int_{-\infty}^{\infty} f(t)\bar{\phi}(t-k)dt$, and $\alpha(I) =< f, \psi_I >$.

where, $\alpha_{i,k} = \int f_j(x) 2^{\frac{j}{2}} \phi(2^j x - k)dx$, and $\beta_{i,k} = \int f_j(x) 2^{\frac{j}{2}} \psi(2^j x - k)dx$.

Simpler way to see Eq. (A17.54) is that the wavelets (ψ_I) arise from an m-regular multiresolution approximation. Let V_l denote the closed subspaces of $L^2(R)$ which has the functions $2^{l/2}\phi(2^l x - k), k \in Z$, as an orthonormal basis and let W_l be the orthogonal complement of V_l in V_{l+1}. Then, Equation 17.54 expresses that the functions $2^{l/2}\phi(2^l x - k), k \in Z$, form an orthonormal basis.

Equation (17.55) expresses that the functions $2^{l/2}\phi(2^l x - k), k \in Z$, form an orthonormal basis. The decomposition of Eq. (A17.55) is very flexible and decomposition of the fingerprint images result in orthogonal sub-bands. The resulting sub-bands are processed independently.

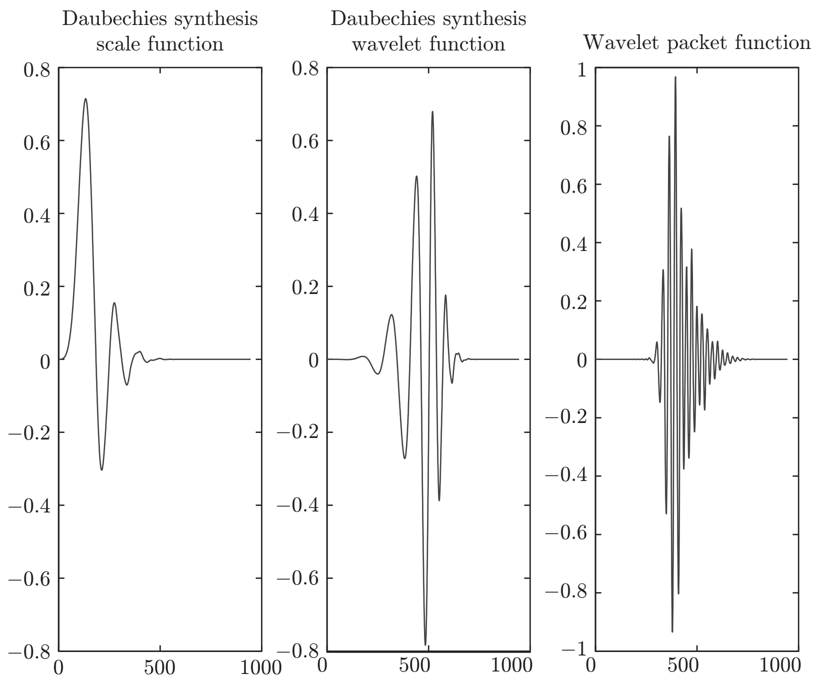

Figure A17.12 *Left figure indicates Daubechies scale function (ϕ), middle figure indicates Daubechies wavelet function (ψ), and right figure shows the wavelet packet function. For all figures, the number of iterations are selected to be 5*

If ψ and ϕ have compact support, like in case of Daubechies wavelets, then Eq.(A17.54) gives a decomposition of any distribution of order less than m. The series on the right hand side of Eq.(A17.54) converges to $f(x)$ in the sense of distributions and the scalar products β_k and $\alpha(I)$.

The 2-D wavelets are computed by applying 1-D algorithm over all the rows as well as columns of the input 2-D vector. Offsets are added and wavelet vector dimensions are adjusted. Thus, implementation of 2-D transform comes from the 1-D transform.

Maxima energy extraction

When an image is translated using these analysis wavelet filters the decomposition coefficients associated with these filters for this image get modified instead of undergoing similar translation. However, the maxima of the wavelet transform also undergoes translation, when an image is translated [?]. Because of this, the wavelet maxima energy points are capable of detecting sharp variation points, and of formulating a signal presentation that is well adapted for characterizing patterns.

So, the first step performed after transforming the images is ‘maxima energy extraction’ for each scale. Let $\psi(x) \in L^2(R)$ be a function whose average is zero and

$$\psi_{2^j}(x) = \frac{1}{2^j}\psi\left(\frac{x}{2^j}\right) \quad \text{(A17.56)}$$

The wavelet transform of a function $f(x)$ at the scale 2^j and position x can be viewed as the convolution product:

$$W_{2^j} f(x) = f * \psi_{2^j}(x) \tag{A17.57}$$

The 'dyadic wavelet transform' is the sequence of functions $(W_{2^j} f(x))_{j \in Z}$. After the transform, the sub-bands are marked, and n maxima values are retained for each scale.

Figure A17.13 shows reconstructed fingerprint images after maxima energy extraction for different values of n, including 10, 100, 1000, and 10000, where n is the number indicating the total number of top values to be retained. The figure is generated by calculating the inverse transform from only the retained top n wavelet coefficients for each scale.

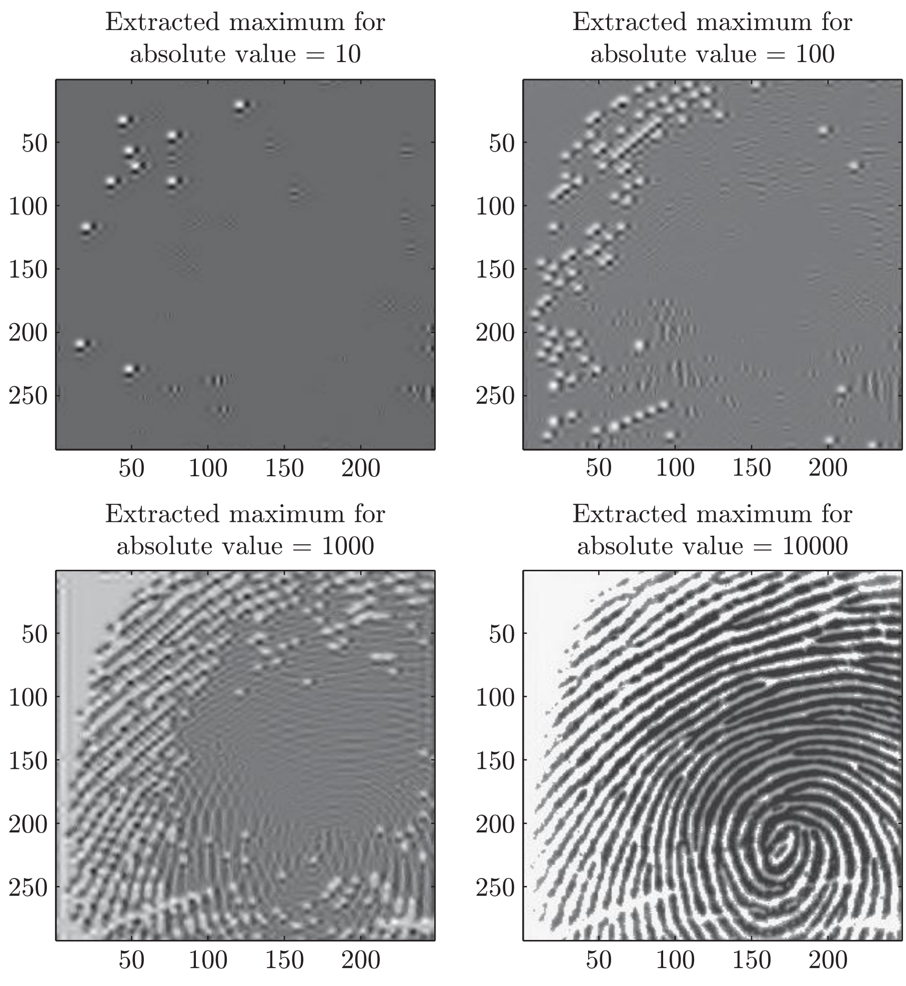

Figure A17.13 *Maxima energy extraction. The figure shows the inverse transform of sample fingerprint images after retaining the most significant 10,100,1000 and 10000 wavelet coefficients for each scale*

Multiresolution analysis

Multiresolution analysis (MRA) can analyze the image under consideration at different scales simultaneously. This analysis mainly focuses on the low-frequency content of the images. As the scale increases the image gets more blurred, adding to the low pass effect. For varying scales, by selecting the appropriate type of analysis filters, segmentation into horizontal, vertical, and diagonal directions is possible. Figure A17.14 displays the images with the details embedded for varying scales.

While analyzing $2^n \times 2^n$ images, the maximum decomposition that is possible is scale n. The basis applied for the scale selection is as follows:

- Decompose given image into sub bands.
- Calculate energy of each sub band and get maximum energy value e_{max} for that scale. For a sub band $f(x,y)$ with $1 < x < X$, and $1 < y < Y$, energy is defined as

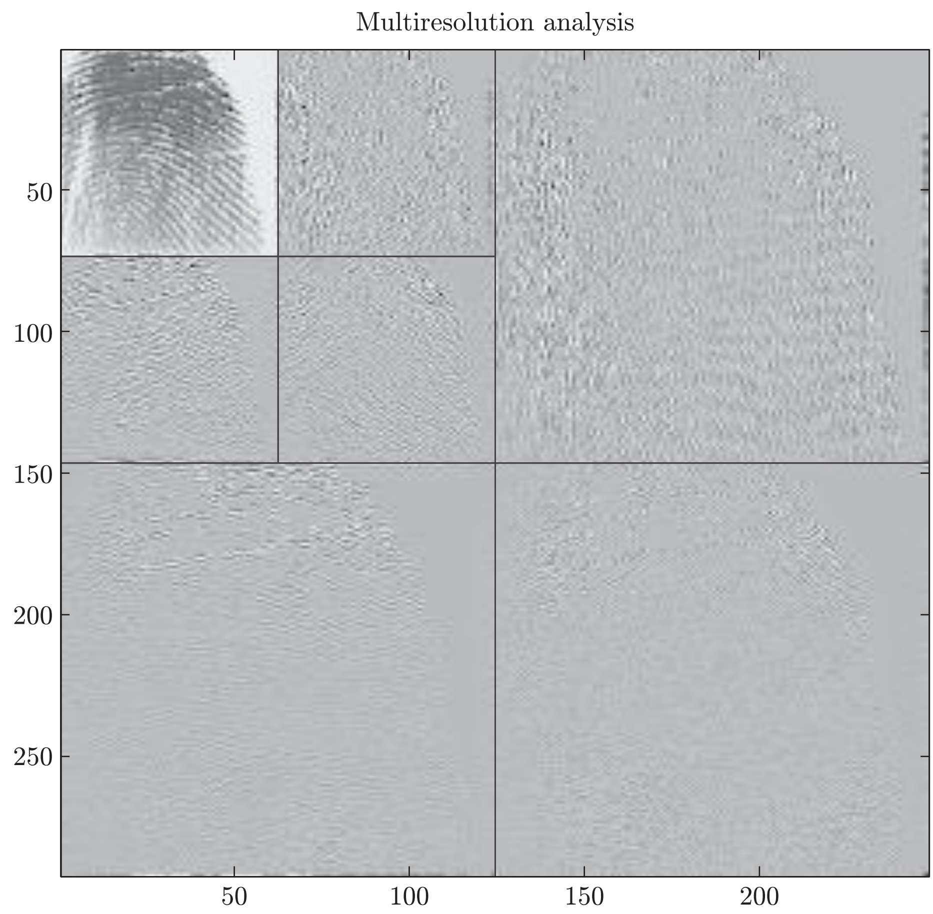

Figure A17.14 *Multiresolution analysis of a sample fingerprint image. The scale used is 2. The low pass band is seen in the left top corner. As seen, the transform steps are getting applied to the low pass data. Thus, MRA mainly analyzes low pass contents of the image*

$$e = \frac{1}{XY}\sum_{x=1}^{X}\sum_{y=1}^{Y} | f(x,y) | \tag{A17.58}$$

- If energy of a sub band is significantly small, such that $e < C \times e_{max}$, where C ranges from 0 to 1, stop the decomposition process.In this algorithm the criteria for stopping decomposition is that the energy content must be less than 40% of the total energy (C=0.4).

For this study the scale selected for MRA is 2. Within the second scale, four sub-bands are obtained, namely, low pass (LP), high pass (HP) diagonal, HP vertical and HP horizontal. These sub-bands are processed independently and are used for further analysis.

2-D wavelet packet analysis

This technique performs analysis on both high-pass as well as low-pass content. The basis selection is done in such a way so as to suppress low pass content, and to enhance and analyze high pass content. The scale selected for this analysis is 3, and the selection process is same as to one described in the last section for the case of MRA.

Wavelet packet expansion can be seen as algorithmically similar to a sub-band coding scheme. The entire collection of wavelet packets is matched effectively to the images for analysis and synthesis. An entropy based wavelet packet expansion called Coifman-Wickerhauser algorithm is used [?].

By introducing the notion of "distance", it is possible to check how good the correlation is between basis and a function in terms of the Shannon entropy of the expansion. Let H denote a Hilbert space, and let $\upsilon \in H, \| \upsilon \| = 1$ and assume that H decomposes into an orthogonal direct sum given as:

$$H = \oplus \sum H_i \tag{A17.59}$$

$$\varepsilon^2(\upsilon, \{H_i\}) = -\sum \| \upsilon_i \|^2 \, l_n \, \| \upsilon_i \|^2 \tag{A17.60}$$

Equation (A17.60) represents the measure of distance between υ and the orthogonal decomposition. In particular, if υ already lies in one of the H_i, then $\varepsilon^2(\upsilon,\{H_i\}) = 0$. This means that the decomposition is effective into 1 nonzero component, while all others are zero. For υ having nonzero components in several H_i, then $\varepsilon^2(\upsilon,\{H_i\}) > 0$. Shannon equation helps in characterizing ε^2.

If

$$H = \oplus\left(\sum H^i\right) \oplus \left(\sum H_j\right) = H_+ \oplus H_- \tag{A17.61}$$

where, H^i and H_j give orthogonal decompositions $H_+ = \sum H^i$, $H_- = \sum H_j$, then

$$\varepsilon^2(\upsilon;\{H^i, H_j\}) = \varepsilon^2(\upsilon;\{H_+, H_-\}) + \| \upsilon_+ \|^2 \, \varepsilon^2\left(\frac{\upsilon_+}{\| \upsilon_+ \|}, \{H^i\}\right) + \| \upsilon_- \|^2 \, \varepsilon^2\left(\frac{\upsilon_-}{\| \upsilon_- \|}, \{H_j\}\right) \tag{A17.62}$$

This is called as Shannon's equation for entropy. This equation is used to calculate the smallest entropy expansion of the signal.

As an example, Figure 17.15 shows the wavelet packet coefficient division, as per the log of the energy function used to calculate the weights of the nodes.

- Weight analysis using log of the energy values.
- Basis uses 202 elements of wavelet packet library.
- Original signal weight: 40476.5
- Transformed signal weight: 9932.2

As an example, Figure 17.16 shows the wavelet packet coefficient division, as per the norm values used to calculate the weights of the nodes.

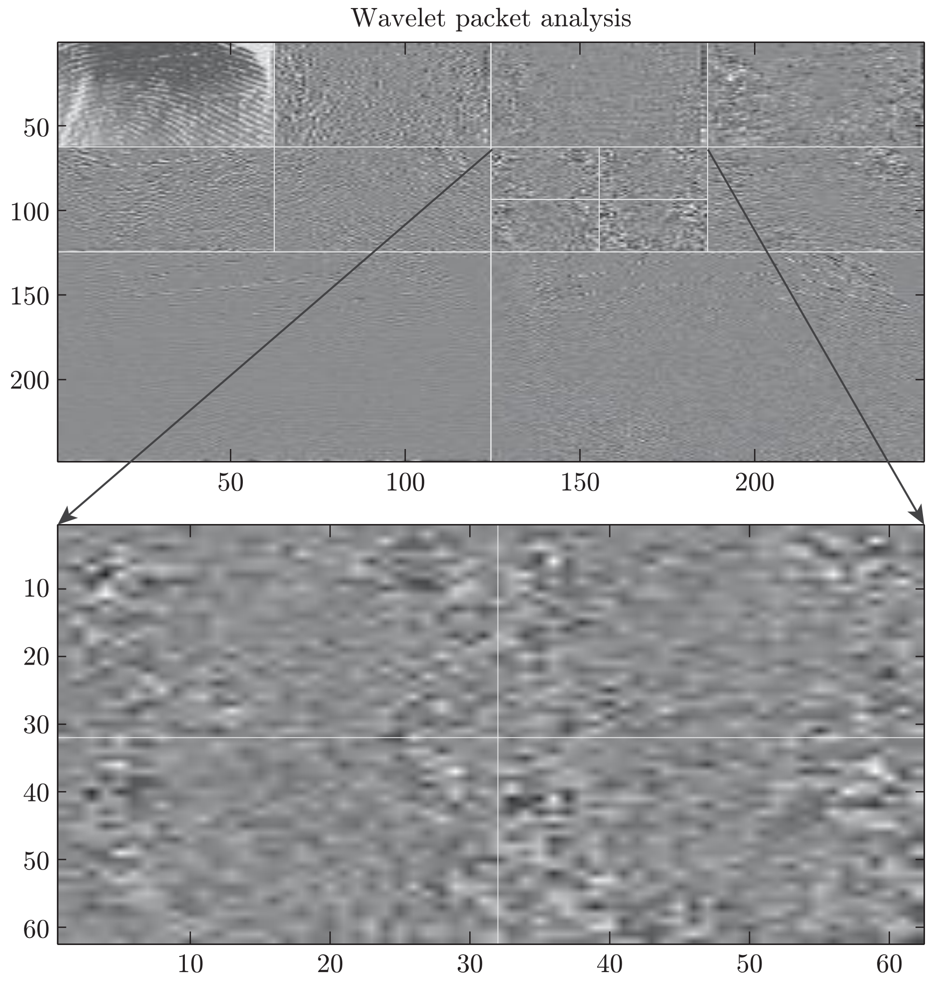

Figure A17.15 *Wavelet packet transform. The scale selected is 3, and all the sub-bands are shown. Only high pass scale 3 sub-bands are retained for further analysis. These are seen as the smallest four rectangles in the figure and magnified below*

- Weight analysis using norm values.
- Basis uses 226 elements of wavelet packet library.
- Original signal weight: 595316
- Transformed signal weight: 56715

The core wavelet packet design comes from the basic quadrature mirror filter (QMF) bank. The algorithm works as follows:

- Construct a vector containing the tree path as determined through the filter bank tree. The filter associated with the tree path is interpolated using $2^{i-1}-1$ zeros between each sample. The value of i ranges from $2^{j}-1$ and selects one node of j branch tree.
- Interpolate and iterate the filters using the selected tree path, specified zeros, and selected scale.

For the specified or calculated basis, a wavelet packet transform is implemented. The algorithm works as follows:

- Perform level analysis in the analysis tree. The weight is calculated at every node. The output at every level is divided into high pass and low pass information content. For this particular algorithm, as further iterations are to be computed on high pass data, low frequency data is suppressed.
- Calculate points of division in accordance with the basis vector tree developed.
- Zero pad the output, if necessary, to maintain the overall phase of the signal.

Wavelet packet analysis of the image under consideration using selected basis is shown in Figure A17.15. The designed tree and the corresponding wavelet packet sub bands are shown in Figure A17.16. The figure demonstrates wavelet packet transform for three scales. All the wavelet bands are seen clearly. The low pass data, seen in the top left corner is discarded. The bands of interest are the four smallest rectangles used for further analysis. Although most of the energy spectrum is observed associated with the low frequency band, the fast changing coefficients are embedded in the high frequency band.

For this algorithm, norm values are used to calculate the weights of the node, and thus to formulate the basis vector. The best basis selected for the first image is used for the second image, such that there are similar sub-band divisions, in order to avoid any miss-match during further processing.

Further, post-processing steps are needed, which are not discussed here and are left as an exploration area.

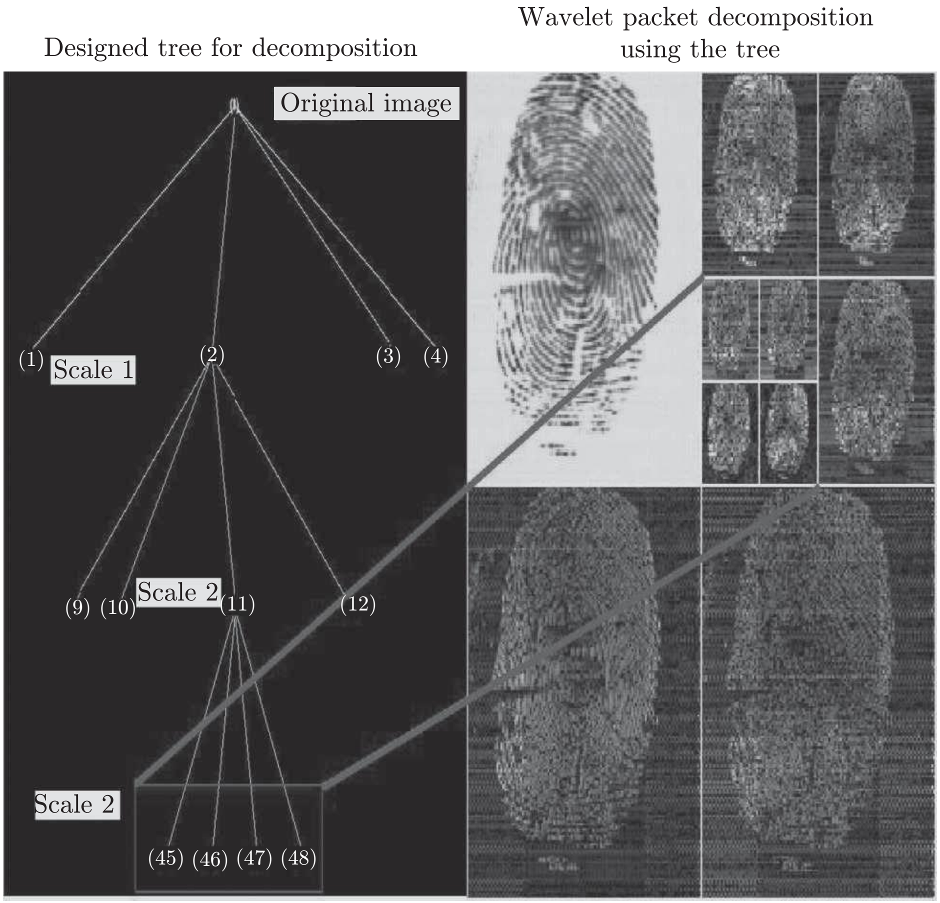

Figure A17.16 *A tree designed using the best basis search and the corresponding wavelet packet decomposition images. The four sub bands at the end of the third scale are selected for further analysis*

References and Bibliography

A. Aldroubi and E. Lin, editors, *Wavelets, Multiwavelets, and Their Applications*, AMS, 1998.

A. Aldroubi and M. Unser, editors, *Wavelets in Medicine and Biology*, CRC Press, Boca Raton, Florida, 1996.

A. Boggess and F. Narcowich, *First Course in Wavelets with Fourier Analysis, A*, Prentice Hall, 2001.

A. Bruce and H.-Y. Gao, *Applied Wavelet Analysis with S-PLUS*, Springer Verlag, 1996.

A. Cohen and R. D. Ryan, *Wavelets and Multiscale Signal Processing*, Applied Mathematics and Mathematical Computation Series, CRC Press, Boca Raton, Florida, 1995.

A. Cohen, *Numerical Analysis of Wavelet Methods*, volume 32 of *Studies in Mathematics and Its Applications*, Elsevier, 2003.

A. Damlamian and S. Jaffard, editors, *Wavelet methods in mathematical analysis and engineering*, Number 14 in Contemporary and Applied Mathematics, World Scientific, 2010.

A. Iske, E. Quak, and M. S. Floater, editors, *Tutorials on Multiresolution in Geometric Modelling*, Mathematics and Visualization, Springer-Verlag, 2002.

A. Jensen and A. la Cour-Harbo, *Ripples in Mathematics - the Discrete Wavelet Transform*, Springer-Verlag, 2001.

A. Kunoth, editor, *Wavelet Methods - Elliptic Boundary Value Problems and Control Problems*, Teubner Verlag, 2001.

A. Mertins, *Signal Analysis: Wavelets, Filter Banks, Time-Frequency Transforms and Applications*, John Wiley & Sons, 1999.

A. Teolis, *Computational signal processing with wavelets*, 1998.

A. A. Petrosian and F. G. Meyer, editors, *Wavelets in Signal and Image Analysis, From Theory to Practice*, volume 19 of *Computational imaging and vision*, Kluwer Academic Publishers, 2001.

A. I. Zayed, *Advances in Shannon's Sampling Theory*, CRC Press, 1993.

A. K. Louis, P. Maass, and A. Rieder, *Wavelets: Theory and applications*, John Wiley, 1997.

A. N. Akansu and M. J. T. Smith, editors, *Subband and Wavelet Transforms Design and Applications*, volume 40 of *The International Series in Engineering and Computer Science*, Kluwer, 1995.

A. N. Akansu and R. A. Haddad, *Multiresolution Signal Decomposition: Transforms, Subbands and Wavelets*, Academic Press/Harcourt Brace Jovanovich, 1992.

Abdul J. Jerri, editor, *Advances in The Gibbs Phenomenon*, Sampling Publishing, 2011.

Abdul J. Jerri, *Introduction to Wavelets*, Sampling Publishing, 2011.

Abdul J. Jerri, *Student's Solutions Manual to Accompany `Introduction to Wavelets'*, Sampling Publishing, 2011.

B. Burke Hubbard, *The World According to Wavelets: The Story of a Mathematical Technique in the Making*, AK Peters, Wellesley, MA, 1998.

B. Engquist, P. Löstedt, and O. Runborg, *Multiscale Methods in Science and Engineering*, volume 44, Springer, 2005.

B. Vidakovic, *Statistical Modeling by wavelets*, J. Wiley, 1999.

B. M. ter Haar Romeny, *Front-End Vision and Multi-Scale Image Analysis*, volume 27 of *Computational imaging and vision*, Kluwer, 2003.

B. W. Silverman and J. C. Vassilicos, editors, *Wavelets the key to intermittent information*, Oxford University Press, 2000.

B. W. Suter, *Multirate and Wavelet Signal Processing*, Wavelet analysis and its applications, Academic Press, 1997.

C. Bandt, M. Barnsley, R. Devaney, K. J. Falconer, V. Kannan, and V. Kumar, editors, *Fractals, Wavelets, and their Applications*, Springer, 2014.

C. Blatter, *Wavelets — A primer*, A.K. Peters, 1998.

C. Blatter, *Wavelets — Eine Einführung*, Advanced Lecture Notes in Mathematics, Vieweg, 1998.

C. Cattani and J. Rushchitsky, *Wavelet and Wave Analysis as Applied to Materials with Micro or Nanostructure*, volume 74 of *Advances in Mathematics for Applied Sciences*, World Scientific, 2007.

C. Chui, editor, *Wavelet Subdivision Methods: GEMS for Rendering Curves and Surfaces*, CRC Press, Boca Raton, 2010.

C. Gasquet, P. Witomski, and R. Ryan, *Fourier analysis and applications*, volume 30 of *Texts in Applied Mathematics*, Springer, 1999.

C. Heill, *Wavelets, Frames and Operator Theory*, AMS, 2004.

C. Rohwer, editor, *Nonlinear Smoothing and Multiresolution Analysis*, 2005.

C. Taswell, *Handbook of Wavelet Transform Algorithms*, Boston, 1997.

C. A. Cabrelli, C. Heil, and U. M. Molter, *Self-Similarity and Multiwavelets in Higher Dimensions*, volume 170 of *Memoirs of the AMS*, AMS, 2004.

C. E. D'Attelis and E. M. Fernández-Berdaguer, editors, *Wavelet Theory and Harmonic Analysis in Applied Sciences*, Applied and Numerical Harmonic Analysis. 1997.

C. K. Chui and Q. T. Jiang, *Applied Mathematics: Data Compression, Spectral Methods, Fourier Analysis, Wavelets, and Applications*, Springer / Atlantis Press, 2014.

C. K. Chui, editor, *Wavelets: A Tutorial in Theory and Applications*, volume 2 of *Wavelet Analysis and its Applications*, Academic Press, Boston, 1992.

C. K. Chui, *An Introduction to Wavelets*, volume 1 of *Wavelet Analysis and its Applications*, Academic Press, Boston, 1992.

C. K. Chui, *Wavelets: A mathematical tool for signal analysis*, volume 1 of *SIAM Monographs on Mathematical Modeling and Computation*, SIAM, 1997.

C. S. Burrus, R. A. Gopinath, and H. Guo, *Introduction to Wavelets and Wavelet Transforms: A Prime*, Prentice Hall, 1998.

D. Alpay, editor, *Wavelets, Multiscale Systems and Hypercomplex Analysis*, volume 167 of *Operator theory, Advances, Applications*, Birkhäuser, 2006.

D. Deng, D. Huang, R. Q. Jia, W. Lin, and J. Wang, editors, *Wavelet Analysis and Applications*, volume 25 of *AMS/IP Studies in Advanced Mathematics*, AMS, 2002.

D. Hong and T. X. He, editors, *Approximation Theory, Wavelets, and Numerical Analysis*, volume 155 of *J. Comput. Appl. Math*, Elsevier, 2003.

D. Kammler, *First Course in Fourier Analysis*, Prentice Hall, 2000.

D. B. Percival and A. T. Walden, *Wavelet Methods for Time Series Analysis*, volume 4 of *Cambridge Series in Statistical and Probabilistic Mathematics*, Cambridge University Press, 2000.

D. F. Mix and K. J. Olejniczak, *Elements of Wavelets for Engineers and Scientists*, Wiley-Interscience, 2003.

D. K. Ruch and P. J. Van Fleet, *Wavelet Theory: An Elementary Approach with Applications*, Wiley, 2009.

D. X. Zhou, editor, *Wavelet Analysis: Twenty Years' Developments*, volume 1 of *Series in Analysis*, World Scientific, 2002.

Desanka P. Radunovic, *Wavelets, from Math to Practice*, Springer Verlag, 2009.

Di Jizheng, *Fundamentals of Wavelets*, WIT Press, 2012.

E. Aboufadel and S. Schlicker, editors, *Discovering Wavelets*, John Wiley & Sons, September 1999.

E. Foufoula-Georgiou and P. Kumar, editors, *Wavelets in Geophysics*, Wavelet analysis and its applications, Academic Press, 1994.

E. Hernandez and G. L. Weiss, editors, *A First Course on Wavelets*, volume 26 of *Studies in Advanced Mathematics*, CRC Press, 1996.

E. Prestini, editor, *Applied harmonic analysis*, 2002.

E. J. Stollnitz, T. Derose, and D. H. Salesin, *Wavelets for Computer Graphics : Theory and Applications*, The Morgan Kaufmann Series in Computer Graphics and Geometric Modeling. Morgan Kaufman Publ., 1996.

F. Fekri, editor, *Finite Field Wavelet Transforms*, Prentice Hall, 2003.

F. Keinert, *Wavelets and Multiwavelets*, volume 42 of *Studies in Advanced Mathematics*, Chapman & Hall, 2003.

F. Walnut, editor, *An Introduction to Wavelet Analysis*, 2001.

G. Bachmann, E. Beckenstein, and L. Narici, *Fourier and Wavelet Analysis*, Springer Verlag, 1999.

G. Battle, *Wavelets and Renormalization*, volume 10 of *World Scientific Series in Approximation*, World Scientific, 2002.

G. Bi and Y. Zeng, editors, *Transforms and fast algorithms for signal analysis and representation*, Applied and Numerical Harmonic Analysis. 2002.

G. Erlebacher, M. Y. Hussaini, and L. M. Jameson, editors, *Wavelets, Theory and Applications*, Oxford University Press, 1998.

G. Kaiser, *A friendly guide to wavelets*, 1994.

G. Strang and T. Nguyen, *Wavelets and Filter Banks*, Wellesley-Cambridge Press, Box 812060, Wellesley MA 02181, fax 617-253-4358, 1996.

G. G. Walter and X. Shen, *Wavelets and Other Orthogonal Systems with Applications*, CRC Press, 2000. (second edition).

G. G. Walter, *Wavelets and Other Orthogonal Systems, Second Edition*, Studies in Advanced Mathematics, CRC Press, 2000.

Gitta Kutyniok and Demetrio Labate, editors, *Shearlets*. Applied and Numerical Harmonic Analysis, Springer, 2012.

H. Adeli and H. Kim, *Wavelet-Based Vibration Control of Smart Buildings and Bridges*, CRC Press, 2009.

H. Adeli and X. Jiang, *Intelligent Infrastructure: Neural Networks, Wavelets, and Chaos Theory for Intelligent Transportation Systems and Smart Structures*, CRC Press, 2008.

H. Führ, *Abstract Harmonic Analysis of Continuous Wavelet Transforms*, volume 1863, Springer, 2005.

H. G. Stark, *Wavelets and Signal Processing: An Application-Based Introduction*, Springer, 2005.

H. L. Chen, editor, *Complex Harmonic Splines, Periodic Quasi-Wavelets: Theory and Applications*, Kluwer Academic Publishers, January 2000.

H. L. Chen, *Complex Harmonic Splines, Periodic Quasi-Wavelets: Theory and Applications*, Springer, 2000.

H. L. Resnikoff and R.O. Wells Jr., *Wavelets, The scalable structure of information*, Springer, 1998.

I. Daubechies, editor, *Different Perspectives on Wavelets*, 1994.

I. Daubechies, *Ten lectures on wavelets*, volume 61, 1992.

I. Ya. Novikov, V. Yu. Protasov, and M. A. Skopina, *Wavelets Theory*, volume 239 of *Translations of Mathematical Monographs*, AMS, 2011.

J. Benedetto and M. Frazier, editors, *Wavelets: Mathematics and Applications*, volume 13 of *Studies in Advanced Mathematics*, CRC Press, Boca Raton, Florida, 1993.

J. Gomes and L. Velho, *From Fourier Analysis to Wavelets*, IMPA monographs. Birkhäuser, Basel, 2015.

J. Goswami and A. K. Chan, *Fundamentals of Wavelets: Theory, Algorithms, and Applications*, Wiley, 1999.

J. Heil and D. F. Walnut, editors, *Fundamental Papers in Wavelet Theory*, Princeton Univ. Press, 2006.

J. Heil, editor, *Harmonic Analysis and Applications*, Applied Numerical Harmonic Analysis. 2005.

J. A. Hogan and J. D. Lakey, *Time-Frequency and Time-Scale Methods*, Applied Numerical Harmonic Analysis, Springer Verlag, 2005.

J. C. van den Berg, editor, *Wavelets in Physics*, Cambridge University Press, 1999.

J. C. van den Berg, editor, *Wavelets in Physics*, Cambridge University Press, 2004.

J. J. Benedetto and A. I. Zayed, editors, *Sampling, Wavelets, and Tomography*, Applied and Numerical Harmonic Analysis Series, 2003.

J. J. Benedetto and P. J. S. G. Ferreira, editors, *Modern Sampling Theory: Mathematics and Applications*. Applied and Numerical Harmonic Analysis, 2001.

J. L. Starck, F. Murtagh, and J. Fadili, *Sparse Image and Signal Processing: Wavelets, Curvelets, Morphological Diversity*, Cambridge University Press, 2010.

J. L. Starck, F. Murthagh, and A. Bijaoui, *Image Processing and Data Analysis: The Multiscale Approach*, volume 177 of *Translations of mathematical Monographs*, Cambridge University Press, 1998.

J. L. Walker, *A Primer on Wavelets and their Scientific Applications*, volume 29 of *Series in Advanced Mathematics*, CRC Press, 1999, Second edition 2008.

J. P. Antoine, R. Murenzi, P. Vandergheynst, and S. Twareque Ali, *Two-Dimensional Wavelets and their Relatives*, Cambridge University Press, 2004.

J. P. Li, J. Zhao, V. Wickerhauser, Y. Y. Tang, and L. Peng, editors, *Wavelet Analysis and its Applications, Proceedings of the Third International Conference on WAA*, World Scientific, 2003, (2 volumes).

J. P. Li, *Wavelet Analysis and Signal Processing - Theory, Applications and Software Implementation*. Chongqing Publishing House, 1997.

Jonathan Cohen and Ahmed Zayed, editors, *Wavelets and Multiscale Analysis, Theory and Applications*, 2011.

K. Trimeche, editor, *Generalized Harmonic Analysis and Wavelet Packets: An Elementary Treatment of Theory and Applications*, CRC Press, 2001.

K. Trimeche, editor, *Generalized Wavelets and Hypergroups*, CRC Press, 1997.

K. Urban, editor, *Wavelets in Numerical Simulation, Problem Adapted Construction and Applications*, Lecture Notes in Computational Science and Engineering, Springer-Verlag, 2002.

K. U. Gröchering, editor, *Foundations of Time-Frequency Analysis*, 2000.

L. Debnath and F. Shah, *Wavelets Transforms and Their Applications (2nd. ed.)*, Birkhäuser, Basel, 2015.

L. Debnath, editor, *Wavelet Transforms and Time-Frequency Signal Analysis*, Applied and Numerical Harmonic Analysis, Birhhäuser Boston, 2001.

L. Debnath, editor, *Wavelets and Signal Processing*, Applied and Numerical Harmonic Analysis, Birhhäuser Boston, 2003.

L. Debnath, editor, *Wavelets and Their Applications*, Birhhäuser Boston, 2002.

L. Prasad and S.S. Iyengar, *Wavelet Analysis with Applications to Image Processing*, CRC Press, Boca Raton, Florida, 1997.

L. L. Schumacher and G. Webb, editors, *Recent Advances in Wavelet Analysis*, Academic Press, 1993.

L. W. Baggett and D.R. Larson, editors, *The Functional and Harmonic Analysis of Wavelets and Frames*, volume 247, September 1999.

M. Ainsworth, J. Levesley, M. Marletta, and W.A. Light, editors, *Wavelets, Multilevel Methods and Elliptic PDEs*, Claredon Press, 1997.

M. Bownik, *Anisotropic Hardy Spaces and Wavelets*, Oxford University Press, 2003.

M. Farge, J. C. R. Hunt, and J.C. Vassilicos, editors, *Wavelets, Fractals, and Fourier Transforms*, Claredon Press, 1993.

M. Frazier, B. Jawerth, and G. Weiss, editors, *Littlewood-Paley Theory and the Study of Function Spaces*, Oxford University Press, 1992.

M. Frazier, *An introduction to wavelets through linear algebra*, Undergraduate Texts in Mathematics, Springer Verlag, 1999.

M. Holschneider, *Wavelets: An Analysis Tool*, Oxford Mathematical Monographs. Oxford University Press, 1998.

M. Jansen and P. Oonincx, *Second Generation Wavelets and their Applications*, Springer, 2005.

M. Jansen, *Noise Reduction by Wavelet Thresholding*, volume 161 of *Lecture Notes in Statistics*, Springer Verlag, 2001.

M. Kobayashi, *Applications of Wavelets, Case studies*, SIAM, 1998.

M. Pinsky, *Introduction to Fourier Analysis and Wavelets*, Brooks-Cole, Inc., 2001.

M. Thuillard, *Wavelets in Soft Computing*, volume 25 of *World Scientific Series in Robotics and Intelligent Systems*, World Scientific, 2001.

M. Vetterli and J. Kovacevic, *Wavelets and subband coding*, Applied Mathematics and Mathematical Computation Series. Prentice Hall, Englewood Cliffs, 1995.

M. B. Ruskai, G. Beylkin, R. Coifman, I. Daubechies, S.G. Mallat, Y. Meyer, and L. Raphael, editors, *Wavelets and their Applications*, Jones and Bartlett, 1992.

M. E. H. Ismail, M. Z. Nashed, A. I. Zayed, and A.F. Ghaleb, editors, *Mathematical Analysis, Wavelets, and Signal Processing*, 1996.

M. J. Mohlenkamp and M. C. Pereyra, *Wavelet, their friends, and what they can do for you*, EMS Series of Lectures in Mathematics, EMS, 2008.

M. P. Pereyra, *Harmonic Analysis: From Fourier to Wavelets*, AMS, 2012.

M. V. Wickerhauser, *Adapted wavelet analysis from theory to software*, A. K. Peters, 289 Linden Street, Wellesley, MA 02181, 1994.

M. W. Wong, *Discrete Fourier analysis*. Number 5 in Pseudo-Differential Operators, Birkhäuser, 2011.

M. W. Wong, *Wavelet Transforms and Localization Operators*, Number 136. Birkhäuser, 2002.

N. Manganaro, R. Monaco, and S. Rionero, editors, *Wavelets and Stability in Continuous Media, Proceedings of the 14th conference on WASCOM 2007*, World Scientific, 2008.

O. Christensen and K. I. Christensen, *From Taylor polynomials to wavelets*, Applied Numerical Harmonic Analysis, 2004.

O. Christensen, *An Introduction to Frames and Riesz Bases*, Applied and Numerical Harmonic Analysis. 2003.

O. Christensen, *Frames and Bases for Mathematics and Engineering*, Applied and Numerical Harmonic Analysis. 2008.

O. Kounchev, *Multivariate Polysplines*, Academic Press, 2001.

P P Vaidyanathan, *Multirate Systems and Filter Banks,* Prentice Hall, 1993.

P. Brémaud, *Mathematical principles of signal processing*, Springer-Verlag, 2002.

P. Das, A. Abbate, and C. DeCusatis, *Wavelets and Subbands: Fundamentals and applications*, Applied and Numerical Harmonic Analysis, 2001.

P. Desanka, *Wavelets, from Math to Practice*, Springer, 2009.

P. Flandrin, *Time-Frequency / Time-Scale Analysis*, volume 10 of *Wavelet Analysis and its Applications*, Academic Press, 1998.

P. Jorgensen and O. Bratteli, *Wavelets through a looking glass*, Applied and Numerical Harmonic Analysis. Birkhäuser, 2002.

P. Wojtaszczyk, *A mathematical Introduction to Wavelets*, volume 37 of *London Mathematical Society Students Texts*, Cambridge University Press, 1997.

P. G. Casazza and G. Kutyniok, editors, *Finite Frames*, Applied and Numerical Harmonic Analysis, Springer, 2012.

P. J. Laurent, A. Le Mehaute, and L. Schumaker, editors, *Wavelets, Images, and Surface Fitting*, A.K. Peters, 1994.

P. J. Van Fleet, *Discrete Wavelet Transformations: An Elementary Approach with Applications*, Wiley, 2008.

P. K. Jain, editor, *Wavelets and Allied Topics*, CRC Press, Boca Raton, 2003.

P. K. Jain, H. N. Mhaskar, M. Krishna, J. Prestin, and D. Singh, editors, *Wavelets and Allied Topics*, Narosa, New Delhi, 2001.

P. R. Massopust, *Fractal Functions, Fractal Surfaces, and Wavelets*, Academic Press, 1995.

P. S. Addison, editor, *The Illustrated Wavelet Transform Handbook: Introductory Theory and Applications in Science, Engineering, Medicine and Finance*, CRC Press, Boca Raton, 2002.

Palle E. T. Jorgensen, Kathy D. Merrill, and Judith A. Packer, editors, *Representations, Wavelets, and Frames*, Applied and Numerical Harmonic Analysis, 2008.

PP Vaidyanathan, *Multirate digital filters, filter banks, polyphase networks, and applications: a tutorial - Proceedings of the IEEE*, 1990.

R. Carmona, W. L. Hwang, and B. Torrésani, editors, *Gabor and Wavelet Transforms with an Implementation in S*, Wavelet analysis and its applications, Academic Press, 1998.

R. Gençay, F. Selçuk, and B. Whitcher, *An Introduction to Wavelets and Other Filtering Methods in Finance and Economics*, Academic Press, 2001.

R. Klees and R. Haagmans, editors, *Wavelets in the Geosciences*, Springer Verlag, 2000.

R. Schneider. *Multiskalen-und Wavelet-Matrixkompression*, Advances in Numerical Mathematics, Teubner, 1998.

R. Shankar Pathak, *The wavelet transform*, World Scientific, 2009.

R. T. Ogden, editor, *Essential wavelets for statistical applications and data analysis*, 1996.

R. X. Gao and R. Yan, *Theory and Applications for Manufacturing*, Springer Verlag, 2011.

Robert X Gao and Ruqiang Yan, *Wavelets, Theory and Applications for Manufacturing*, Springer Verlag, 2011.

S. Basu and B. C. Levy, editors, *Multidimensional Filter Banks and Wavelets: Research Developments and Applications*, Springer, 1997.

S. Dubuc and G. Deslauriers, editors, *Spline Functions and the Theory of Wavelets, 1999*, volume 18 of *CRM Proceedings & Lecture Notes*, AMS, 1999.

S. Gopalakrishnan, editor, *Wavelet Methods for Dynamical Problems: With Application to Metallic, Composite, and Nano-Composite Structures*, CRC Press, Boca Raton, 2010.

S. Igari, *Real Analysis - with an Introduction to Wavelet Theory*, volume 177 of *Translations of mathematical Monographs*, AMS, 1998.

S. Jaffard, Y. Meyer, and R.D. Ryan, *Wavelets. Tools for Science & Technology*, SIAM, 2001, (Update of Y. Meyer: Wavelets: Algorithms & Applications).

S. Mallat, editor, *A Wavelet Tour of Signal Processing*, Academic Press, 1998.

S. S. Goh, A. Ron, and Z. Shen, editors, *Gabor and wavelet frames*, World Scientific, 2007.

S. S. Iyengar, E. C. Cho, and V. V. Phoha, *Foundations of Wavelet Networks and Applications*, Chapman & Hall, CRC Press, 2002.

S. T. Ali, J. P. Antoine, and J. P. Gazeau, *Coherent States, Wavelets, and Their Generalizations*, Springer Verlag, 2000.

T. Qain, M. I. Vai, and Y. Xu, *Wavelet Analysis and Applications*, Applied and Numerical Harmonic Analysis. 2007.

T. Strutz. *Bilddatenkompression*, Vieweg, 2000.

T. F. Chan and J. Shen, editors, *Image processing and analysis: variational PDE, wavelet, and stochastic methods*, SIAM, 2005.

T. H. Koornwinder, editor, *Wavelets: an elementary treatment of theory and applications*, volume 1 of *Series in Approximations & Decompositions*, World Scientific, 1993.

T. -X. He and E. B. Lin, *Wavelet analysis and its applications*, Numerical methods, computer graphics and economics. World Scientific, 2012.

T.-X. He, editor, *Wavelet Analysis and Multiresolution Methods*, volume 212 of *Lecture Notes in Pure and Applied Mathematics*, Marcel Dekker, 2000.

W. Baeni, *Wavelets - eine Einfuehrung fuer Ingenieure*, Oldenburg, 2001.

W. Czaja and D. Speegle, *Wave Packets and Related Transforms*, Applied and Numerical Harmonic Analysis, 2009.

W. Dahmen, *Multiscale Wavelet for Partial Differential Equations*, Wavelet analysis and its applications, Academic Press, 1997.

W. Freeden and V. Michel, *Multiscale Potential Theory With Applications to Geoscience*, Applied Numerical Harmonic Analysis, 2004.

W. Härdle, G. Kerkyacharian, D. Picard, and A. Tsybakov, *Wavelets, Approximation, and Statistical Applications*, volume 129 of *Lecture Notes in Statistics*, Springer Verlag, 1998.

X. Dai and D. R. Larson, *Wandering Vectors for Unitary Systems and Orthogonal Wavelets*, 1998.

X. Shen and A. Zayed, editors, *Multiscale Signal Analysis and Modeling*, Springer, 2012.

Y. Ishikawa, editor, *Wavelet analysis for clinical medicine*, Medical Publication, 2001.

Y. Meyer and R. Coifman, editors, *Wavelets. Calderón-Zygmund and Multilinear Operators*, Cambridge University Press, 1997.

Y. Meyer, editor, *Wavelets and applications*, volume 20 of *Research Notes in Applied Mathematics*, Springer, 1992. Proceedings Internat. Conf. Marseille, May, 1989.

Y. Meyer, *Wavelets and Operators*, volume 37 of *Cambridge Studies in Advanced Mathematics*, Cambridge University Press, 1992.

Y. Meyer, *Wavelets, Vibrations and Scalings*, 1998.

Y. Meyer, *Wavelets: Algorithms and Applications*, Philadelphia, 1993. Translated and revised by R.D. Ryan.

Y. Nievergelt, *Wavelets made easy*, Birkhäuser, 1999.

Y. Zeevi, *Signal and Image Representation in Combined Spaces*, Wavelet analysis and its applications, Academic Press, 1997.

Y. T. Chan, *Wavelet basics*, Kluwer, 1995.

Y. Y. Tang, J. Liu, L. Yang, and H. Ma, editors, *Wavelet theory and its application to pattern recognition*, World Scientific, 1999.

Y. Y. Tang, *Wavelet theory approach to pattern recognition*, World Scientific, 2009.

Index

U

V

W

Y

Z

N

O

P

Q

R

S

T